C4R

Capacity for Rail

Towards an affordable, resilient, innovative and high-capacity European Railway System for 2030/2050

Innovative designs and methods for VHST (intermediate)

Submission date: 30/09/2017

Public deliverable D 12.1

This project has received funding from the European Union's Seventh Framework Programme for research, technological development and demonstration under grant agreement n° 605650








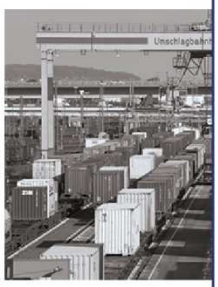

Collaborative project SCP3-GA-2013-60560
Increased Capacity 4 Rail networks through enhanced infrastructure and optimised operations
FP7-SST-2013-RTD-1

Lead contractor for this deliverable:

- CENTRO DE ESTUDIOS Y EXPERIMENTACION DE OBRAS PUBLICAS - CEDEX

Project coordinator

- International Union of Railways, UIC

www.Capacity4rail@eu

Executive Summary

The main objectives of this deliverable are a) to analyse the impact of the pass-by of Very High Speed Trains (VHST) in the dynamic response of a railway ballasted track and b) to identify improvements that are necessary to implement in the railway track design to hold the circulation of VHST.

To fulfill these objectives, the first task that was to select some of the tests performed in CEDEX Track Box (CTB) on ballasted tracks subjected to the pass-by of trains. The results obtained in those selected tests were used to calibrate and validate the numerical models developed by IST.

In this respect, Chapter 3 is devoted to describe the tests performed in CEDEX Track Box (CTB) in a 1:1 scale model of a ballasted track with granular subballast subjected to the pass-by of 1 M axle loads of a passenger train travelling at 300 km/h. This particular CTB section was considered along this subtask of the project, as the reference track case, taken as basis for further analysis and upgrade to be made. Appendix 8.1 collects a detailed description of the model tested, the instrumentation installed and the results obtained.

An intermediate task was the performance of two in-situ test campaigns in the Madrid-Barcelona High Speed Line to create a data base of the vibrations measured in a real track produced by passing-by of different trains travelling at high speeds (around 300 km/h) and to analyze the track dynamic behaviour. Chapter 4 collects all the information of these two campaigns while Appendix 8.2 shows all the results obtained.

The main core of the document is the performance of a set of numerical analysis by IST using a model validated with the CTB reference case to estimate track responses at vhs and to further apply parametric studies and optimization algorithms. The analysis made enabled to identify the potential dangers of the current railway track properties for vhs, upgrading its design. Furthermore, numerical simulations made allowed to determine the best combination of modifications, in terms of properties in the different elements of the railway section, to decrease the negative impacts of the vibrations produced by VHST.

Keywords: Very high speed, in-situ campaigns, numerical analysis, model tests.

Project team members: CEDEX, ADIF, IST, INECO, VOSSLOH

Table of content

Abbreviations and acronyms

Abbreviation / Accronym	Description
CTB	CEDEX Track Box
RP	Railpad
USP	Under Sleeper Pad
VHS	Very High Speed
VHST	Very High Speed Trains

1 Background

There is an increased demand on the railway sector and much resource is spent on increasing the capacity of the existing network as well as expanding and connecting new lines. The European Commission is working towards the creation of a Single European Railway Area and has promoted a modal shift from road to rail to achieve more competitive and resource-efficient transport system. The European Commission White Paper outlines the following targets:

- 30% of the road freight over 300 km should shift to other modes such as rail or waterborne transport by 2030 and to more than 50% by 2050.
- Aim to triple the length of the existing high-speed railway (HSR) network by 2030 and complete a European HSR rail network by 2050. By 2050, the majority of medium distance passenger transport should go by rail.
- By 2050, connect all core network airports to the rail network, preferably by HSR and ensure that all core seaports are sufficiently connected to the rail freight.

Hence, a considerable investment will be needed to expand and upgrade the capacity of the rail network infrastructure. To reach these ambitious goals, much effort must be spent on finding viable solutions. This includes:

- Finding methods to prove that a larger share of the existing infrastructure can be upgraded to future demands with sufficient safety margins.
- Finding more cost- and time efficient methods in building new railway infrastructure.
- Finding optimal solutions considering investment, whole life cycle cost and environmental impact.

One of the paths to give a satisfactory response to future demands is to increase the maximum commercial speed to values around 400 km/h. However this speed increase can produce important impacts in the current infrastructure.

Taking that into account, and within the framework of the Capacity 4 Rail European project, the first step in this SP1 subtask was to evaluate the behaviour of the current ballasted track sections when subjected to the pass-by of trains running at very high speed, up tp 400km/h. Once analysed those impacts, the second step was to determine the possible and best improvements in the different elements that compose the track section to ensure a safe use of the infrastructure, low maintenance costs and acceptable level of comfort for passengers.

These steps have been developed in this WP and delivered through three different approaches: the performance of some model tests, in-situ test campaigns and the use of numerical models.

2 Objectives

This WP will contribute to identify and investigate technical barriers and operational requirements to increase maximum speeds in commercial operation, which currently range from 300 to 350 km/h.

The main objectives of this deliverable are:

- to analyse the impact of the pass-by of Very High Speed Trains (VHST) in the current railway track sections and
- to identify those changes that are necessary to implement in the railway track design to hold the VHST pass-by.

First of all, it is important to remark that, in the context of this work, VHST are considered trains that travel at speeds greater than the current commercial speeds (between 300 and 350 km/h), so VHST speeds will be in the range of 360 to 400 km/h.

The main source of potential problems that can arise for the VHST pass-by is the increase of vibrations in the railway section that can produce, on one hand, a dramatic increase in the ballast rate degradation and, on other hand, problems of disturbance in the surroundings.

To fulfill with the objectives, the first task that was carried out was the performance of a set of numerical analysis (made by IST) to identify the potential dangers to the current railway track design and to determine the best combination of modifications, in terms of properties in the different elements of the railway section, to decrease the negative impacts of the vibrations produced by VHST. To calibrate and validate the numerical models, CEDEX sent IST the results of some tests performed on a ballasted track with a usual cross section equipped with usual track components (rail, railpad and sleepers).

Once the study was performed and the best theoretical solution was determined, the idea was to perform some additional tests in CEDEX Track Box (CTB) on some 1:1 scale models to evaluate those theoretical findings at speeds between 360 to 400 km/h.

However, unfortunately during some maintenance works carried out in CEDEX Track Box (CTB), a problem in the hydraulic system was discovered. To solve the problem, repair works were performed between September 2016 and January 2017, just the period previously scheduled for the performance of VHST tests, so the tests could not be performed. In spite of it, it is worth noting that during the time devoted to the repair works, CEDEX built the 1:1 scale model of a ballast track to perform the VHST tests, as described in Chapter 4 of this report.

An intermediate task that was performed was the data collection of the real behaviour of a high speed line in two in-situ test campaigns carried out in the Madrid-Barcelona High Speed Line using the techniques developed by CEDEX. The objective was to have real data to validate the results to be obtained in CTB.

3 Tests on 1:1 scale model in CTB

3.1 OBJECTIVES

This chapter collects the works performed by CEDEX relative to the demonstrator defined in the Sub-Task 1.2.2. "Verification by full scale models" of WP 1.2. The scope of this demonstrator is to define the possible modifications in the design and in the maintenance operations of the current high speed lines (HSL) to be able to hold very high speed trains (VHST) when travelling at speeds up to 400 km/h.

Before performing any test, it was decided that CEDEX provides data from previous tests performed in CTB on ballasted tracks to other C4R partners for them to calibrate and validate their numerical models. Chapter 3 collects all the information that was provided in February 2015.

As a starting point, the performance of an existing track system in operation will be subjected to an increase in the operation speed and then the system will be improved by adding elements to withstand the expected effects. The results will make it possible to create a matrix of data, useful to understand the performance of railways at such high speeds.

All components of the track bed and platform of the model will be fully monitored to record the variations in track stiffness, speed and accelerations. The short term and long term effects induced in the mechanical performance of the model by the passage of trains simulated under VHST conditions will be recorded.

All these tests should have been performed in CEDEX Track Box (CTB). However, unfortunately during some maintenance works carried out in CTB, a problem in the hydraulic system was discovered. To solve the problem repair works were performed between September 2016 and January 2017, just the period previously scheduled for the performance of VHST tests, so the tests could not be performed. However, it is worth noting that during the time devoted to the repair works, CEDEX built the 1:1 scale model of a ballast track to perform the VHST tests, as described below.

3.2 RESULTS OF PREVIOUS TESTS

The data of previous tests sent to calibrate the numerical models were obtained in a 1:1 scale model of a ballasted track with granular subballast tested in CTB some years ago. The model was subjected to the pass-by of 1 M axle loads of a passenger train travelling at 300 km/h.

In Appendix 8.1, there is a description of the model tested, the instrumentation installed and the results obtained.

3.3 DESCRIPTION OF THE MODEL TO BE TESTED

The structural section of CEDEX Track Box is 4 m deep and it is formed by the following elements, listed from bottom to top: Embankment, Form layer, Subballast layer, Ballast and Sleeper, rails and fastening system [1 and 2].

Figure 1 shows the schematic structural section used in the present study and Figure 2

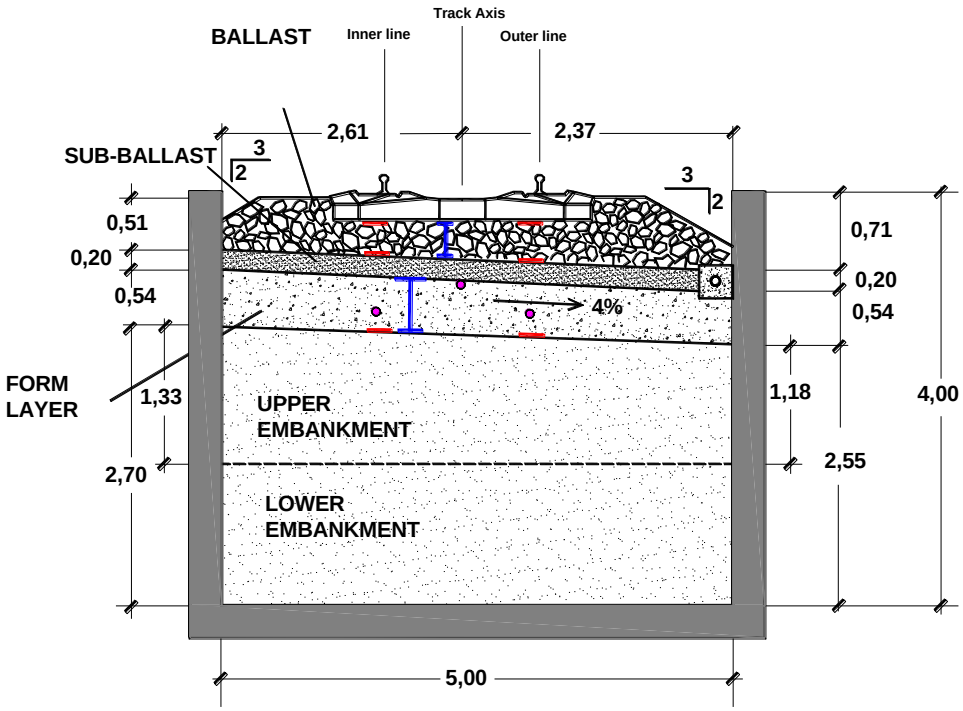

FIGURE 1: CROSS SECTION USED IN THE PRESENT STUDY

The 1:1 scale model constructed (Figure 1) is provided with: a rail gage of 1.435 m; a ballast thickness of 0.35 m under the inner rail and 0.40 m below the outside rail; a granular suballast layer of 0.20 m thickness with an inclination of 4% towards the outside and a form layer with the same inclination and a thickness close to 0.55 m. Ballast was compacted in two layers: 0.20 m thick each one under the outer rail; and 0.20 m thick the lower one and 0.15 m thick the upper one under the inner rail.

FIGURE 2: BALLASTED TRACK PREPARED FOR THE VHST TESTS

The sensors to be deployed in CTB testing zone will have been aimed to the measurement of the absolute and relative displacements of the track components in the static tests and to the evaluation of the amplitude of displacements, velocities and accelerations induced in those components by the pass-by of trains at speeds up to 400 km/h.

Two different systems will be used:

- External system: constituted by a set of around 40 sensors providing absolute and relative displacements of rails, rail-sleeper pads and sleepers in the static tests and the amplitude of displacements, velocities and accelerations of those elements under the pass-by of simulated trains in the quasi-static tests. It will consist on the following sensors:
    - Laser systems.
    - Rail-pad resistivemeters.
    - Rail 2 Hz geophones.
    - Sleeper 1 Hz geophones.
    - Rail ±50·g accelerometers.
    - Sleeper ±10·g accelerometers.

- Internal system: made up of 40 sensors placed in the track bed layers (ballast, and subballast), form layer and embankment to play the same roles that the external sensors in the track superstructure elements. Furthermore, some ballast particles instrumented with accelerometers inside will be placed in some points of the railway track to measure the accelerations in the ballast layer.

3.4 DESCRIPTION OF TESTS

The set of tests to be performed at CEDEX Track Box (CTB) began with the construction of an existing VHS track with similar characteristics to the one already in operation in the 'Madrid – Barcelona' line.

The type of train to simulate in the actuators will be the Siemens S-103 and Talgo S-102, as they are the trains whose pass-by have been recorded in the in-situ test campaigns described in Appendix 8.2.

The tests to be performed in this stage are the following:

- Test A: 300 km/h and 10^6 axles to study short and long term behaviour
- Test B: 320 km/h and 10^5 axles to study short term behaviour
- Test C: 360 km/h and 10^5 axles to study short term behaviour
- Test D: 400 km/h and 10^6 axles to study short and long term behaviour

After this, some new components will be implemented in the experimental track and the improved track will be tested in the same conditions as previous. Two setups are planned to test, as seen in Figure 3:

- Test 2: Vossloh System with nominal stiffness 60 kN/mm (the secant will be 18-68 kN according to EN standard).
- Test 3: Vossloh System with nominal stiffness 60 kN/mm (the secant will be 18-68 kN according to EN standard) and USP with 0.3 N/mm³ bedding modulus.

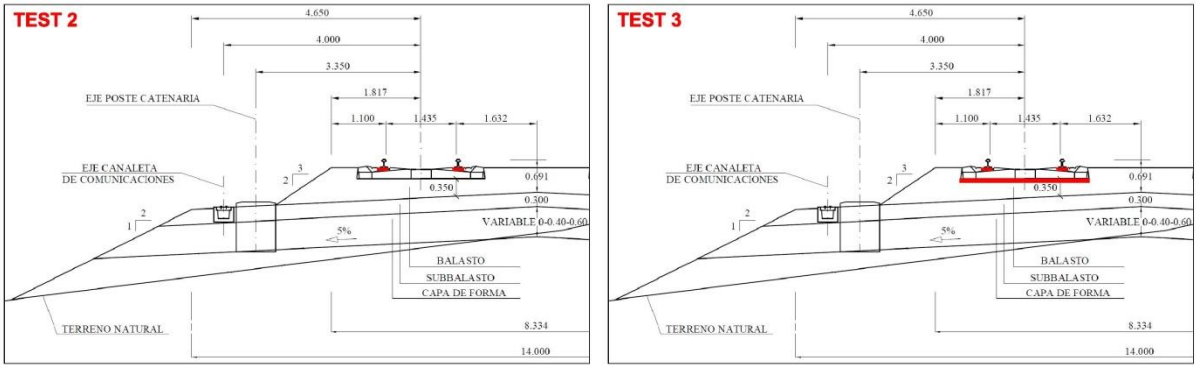

FIGURE 3: IMPROVEMENTS IN THE TRACK SECTION TO HOLD VHST

The matrix of results from the tests will be processed to obtain the variations in the main parameters. The results will lead to conclusions that will help to analyse the very high speed system.

The track response will be measured in terms of:

- Displacements, with laser system and potentiometers.
- Speeds, with 2 Hz geophones and 1 Hz geophones
- Accelerations, with ±50·g accelerometers and ±10·g accelerometers

The measurements will be made at:

- Rail: with 2 Hz geophones and ±50·g accelerometers.
- Rail pad: with rail-pad potentiometers.
- Sleeper: with 1 Hz geophones and ±10·g accelerometers.

4 Data collection during in-situ test campaigns

4.1 Objective

The general goal of the two in-situ campaigns was to create a data base of the vibrations measured in a real track produced by passing-by of different trains travelling at high speeds (around 300 km/h) and its dynamic behaviour. This data base will be used as a source to validate the test results obtained in CEDEX Track Box (CTB). To make easier the comparison, the instrumentation set used in the second campaign reproduced a typical configuration used in CTB.

4.2 Description of the works

The first campaign was performed by CEDEX on November, 2015 at PK 72+200 of the Madrid-Barcelona High Speed Line, while the second one carried out on June, 2016 at PK 74+233, a straight track section far from stations, tunnels and bridges, in which trains can travel at their maximum speed in this line (300 km/h).

Figure 4 shows a photograph of the test site of the second campaign.

Figure 4: PK 74+233 Madrid-Barcelona High Speed Line- Straight track section

More details about these in-situ campaigns can be found in Appendix 8.2.

The instrumentation installed, that can be seen in Figure 5, consisted of the following sensors to be used with techniques developed by CEDEX [3 and 4]:

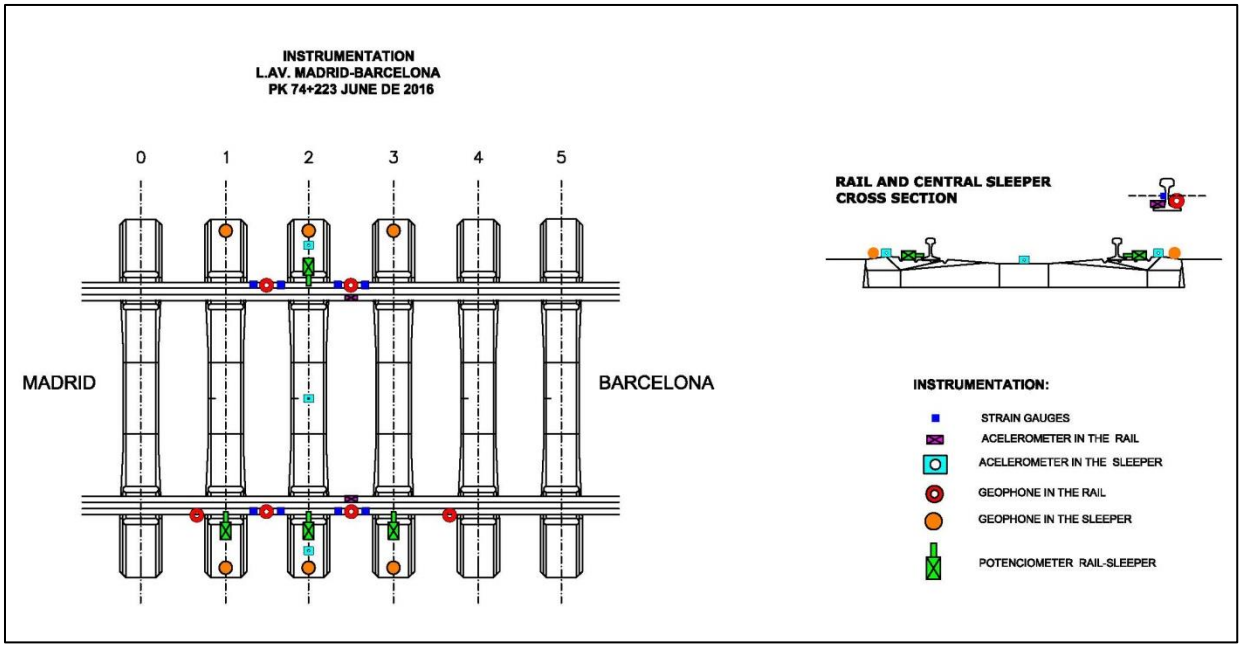

FIGURE 5: SKETCH OF THE INSTRUMENTATION INSTALLED FOR THE SECOND CAMPAIGN

- Eight strain gauges (represented by dark-blue squares): the gauges are glued at the level of the neutral fibre of the rail in order to measure only shear strains. Loads are obtained using the pair placed at the span between two sleepers.
- Seven 2 Hz geophones installed in the rail (marked with red spots): they are used to measure the vertical velocity of the vibration in the rail produced by the trains pass-by. It is also possible to obtain the rail deflections by integrating these velocity signals.
- Six 1 Hz geophones (represented by orange circles): they are stacked at both ends of the sleeper surface to measure the vertical velocity of the vibration at those points.
- Two vertical accelerometers stacked in the rail (shown with fuchsia rectangles).
- Three triaxial accelerometers stacked in the sleeper surface (represented by light-blue squares).
- Four potentiometers (presented with green rectangles): they are used to measure the rail-sleeper relative motion, from which is possible to calculate the pad deformation.

Furthermore, six ballast particles instrumented with accelerometers were placed in different positions as can be seen in Figure 6.

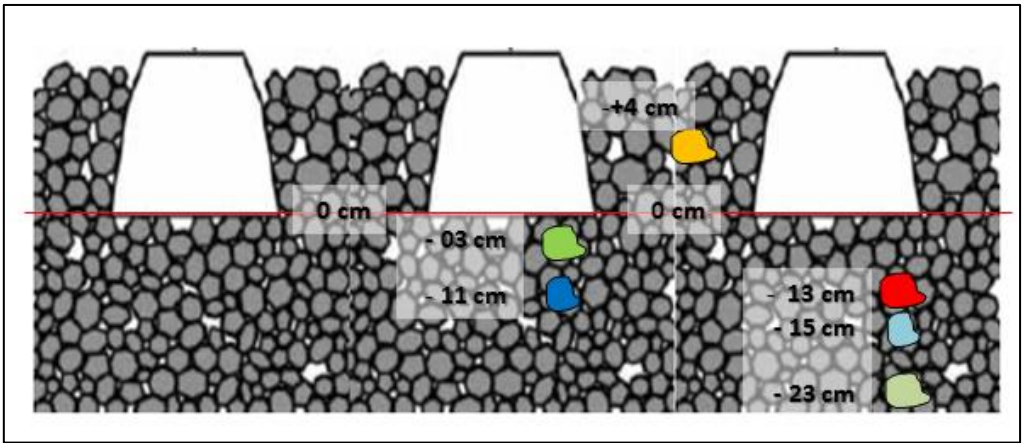

FIGURE 6: POSITION OF THE BALLAST PARTICLES INSTRUMENTED WITH ACCELEROMETERS

A total of 8 and 37 trains were recorded, respectively, in the first and second campaigns. Those trains covered five types of trains (Talgo S102, Siemens S-103, CAF S-120, Talgo AVRIL) that travel at speeds between 225 and 310 km/h.

The following step is the process of the raw data for each kind of sensor. For all the time signals obtained, the first step is to calculate the Fast Fourier Transform (FFT) to visualize the frequency domain and then to decide the filter which must be applied, in case it is necessary. In general for this kind of studies, the most used filter is the Low Pass Filter (LPF) which cuts off frequencies above the range of interest in each particular case.

4.3 RESULTS

The parameters that have been analysed are the following:

- Track stiffness, considered as the ratio between the loads applied by the train, obtained from the strain gauges, and the rail deflection obtained from the time integration of rail velocity.
- Pad vertical displacement, measured by potentiometers as the relative motion between rail and sleepers.
- Vertical rail velocity.
- Vertical sleeper velocity.
- Vertical rail acceleration
- Vertical sleeper acceleration
- Ballast particle acceleration.

More details about the results obtained in these two in-situ campaigns can be found in Appendix 8.2.

Table 1 collects the fundamental values obtained.

TABLE 1: SUMMARY OF THE RESULTS OBTAINED IN THE TEST CAMPAIGNS

Parameter	Variation with speed	Range of values
Track stiffness	No	85 – 115 kN/mm
Pad vertical displacement	No	0.35 – 0.45 mm
Rail velocity	Slight increase	30 – 75 mm/s
Sleeper velocity	Increase	10 – 25 mm/s
Rail acceleration	No	1.0 – 2.5 g
Sleeper acceleration	No	0.65 – 0.80 g

5 Track Design Optimization for Very High Speed

5.1 OBJECTIVES

This chapter summarizes the work performed by IST within SP1 in Task 1.2.2 “New track design and specifications for VHST”, more specifically in subtask 1.2.2.1 - “Track design for VHST” aiming at proposing optimized innovative track design for very high speed on the basis of numerical simulation and real scale laboratory test. The work made by IST was mainly related to the numerical simulations part, that is, the development, validation and application of a numerical train/track FE model focused on estimations of track response to very high speed trains circulations. The inter-collaboration with CEDEX partner, which dealt with laboratory experimental tests (see previous chapter 3), was mandatory and crucial to have a reference track to serve as basis for both model validation (CEDEX Track Box -CTB- data results feed the model) and predictions to support decisions of which track design alternatives should be experimentally tested in the CTB within the subtask (IST model results feed the CTB).

Mainly the work was divided into the following parts:

- Numerical model validation based on the data provided by CEDEX from the tests conducted on the physical model of a ballasted track with granular subballast, CTB reference case (see chapter 3 and Appendix 8.1).
- Evaluation of the predicted dynamic response of the reference railway track (CTB reference case) and the influence of train speed increase up until 400 km/h on its dynamic behaviour.
- Evaluation of the predicted dynamic response of different track design cases (having the CTB reference case as basis) when equipped with different combinations of railpads and undersleeper pads (USPs); evaluation of train speed increase.
- Optimization of track design (several specific combinations of railpad+USP stiffness) to improve dynamic performance at very high speeds (up to 400 km/h).

Influence of train speed increase in track performance is analysed with model simulations integrated in a multi-objective optimization algorithm (helping to wisely changing properties of railpads and under-sleeper pads). Its provided the best combinations of railpad and undersleeper pads stiffness (among several tested) in order to maintain track vibrations within acceptable levels even for 400km/h. From discussion with other partners certain track design solutions were chosen from these combinations, hence supporting CEDEX within C4R project, to prepare the following upcoming experimental tests. This study was included in the working document (Internal Report) “Task 1.2.2 New track design and specifications for VHST, Sub-Task 1.2.2.1 Track design for VHST: Track design solution for soft railpads and under sleeper pads. Parametric study on train speed increase.”

All the work made by IST in WP1.2 was reported internally into three working documents which are summarized in the Appendix 8.3 of this Final Report (Deliverable D12.1, “Innovative designs and methods for VHST - Appendix 8.3: Track Design Optimization for Very High Speed”) and briefly summarized here below, in chapter 5.

5.2 BRIEF OVERVIEW OF THE COMPUTATIONAL MODEL

The computational model used throughout the project was a 3D elasto-dynamic finite element model coupled with a multibody system representing the train [5, 6, 7, 8, 9].

The computational model was subjected to a model validation process to assess its prediction accuracy. The model validation process consisted of comparing the response outputted by the computational model with experimental measurements taken during test runs conducted by CEDEX on a physical model of a railway track subjected to high-speed traffic (see Appendix 8.1 and 8.3 for more information). The focus of the validation process was placed on peak vibration levels resulting from high-speed traffic, motivated by the interest in analysing the impact of track vibrations on track degradation rates. As example of some of the results obtained, Figure 7 shows the comparison of vertical ballast and subballast acceleration time series collected from experimental tests and outputted by the computational model (300km/h).

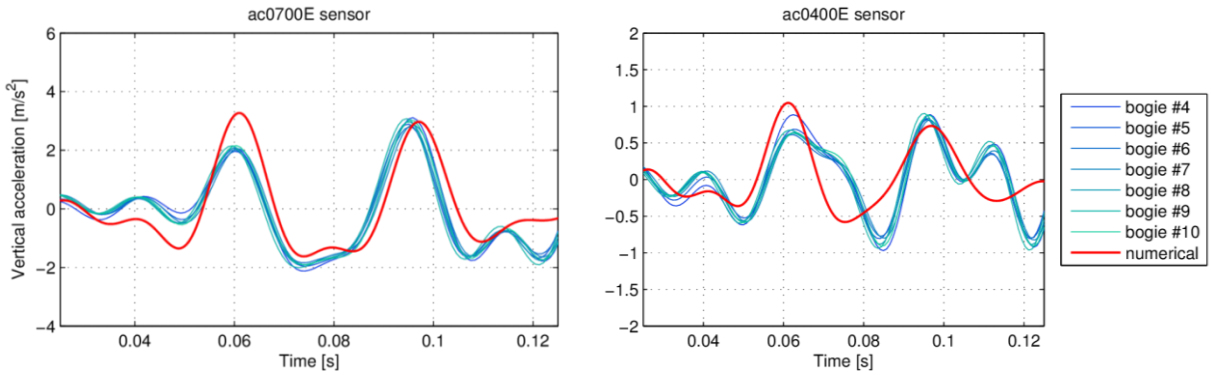

FIGURE 7: VALIDATION TESTS: COMPARISON BETWEEN EXPERIMENTAL MEASUREMENTS AND COMPUTATIONAL RESPONSE: VERTICAL BALLAST (LEFT) AND SUB-BALLAST (RIGHT) ACCELERATION TIME SERIES

From results and comparisons made, it may be state that the validation tests showed that the dynamic response outputted by the computational model agrees with laboratory measures taken on the physical model during the experimental tests conducted by CEDEX. Hence, after the validation process done within the project, computational model was considered ready and accurate to pursue with track responses estimations for different situations such as different train speeds and variations in the properties of some railway track elements, taking the track box case as reference.

5.3 OVERVIEW OF TRACK DYNAMIC RESPONSE

A general overview of the dynamic response demonstrated by the CTB reference railway track was prepared as part of the preparation stages for the track design optimization process. The goal was to obtain a preliminary description of the dynamic response across the track design space, represented by two track design parameters: nominal values of rail pad and USP vertical stiffness, to help identify potential regions of interest. In this first test analysis, these parameters were made to freely vary, respectively, within the following ranges: Kpad [20 - 200kN/mm] and K_{usp} [50 - 500kN/mm].

The multiple combinations of RP+USP were analysed in terms of the resulting estimated track dynamic responses. These were explored throughout the design space by post-processing sampling

points produced by a preliminary run of a multi-objective optimization problem analysed with a version of the DIRECT algorithm developed by IST. The contour plots of the response surfaces of the peak vertical acceleration values observed on sleepers and within the ballast layer, and the location of each sample point, are represented in Figure 8.

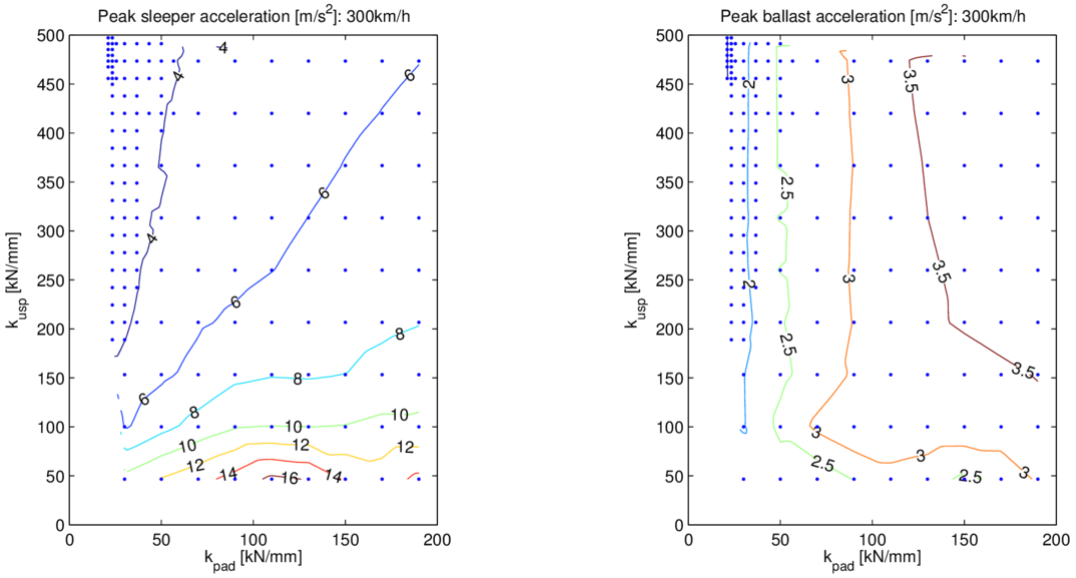

FIGURE 8: CONTOUR PLOTS OF TRACK RESPONSE QUANTITIES OF INTEREST WITH REGARDS TO RAIL PAD AND USP STIFFNESS: PEAK SLEEPER ACCELERATION LEFT AND PEAK BALLAST ACCELERATION RIGHT.

The contour plots presented in the previous figure, illustrate that there is no common global minimum within the design space. Therefore, optimal track solutions for this particular problem can be found by introducing additional constraints, such as a target value for the track's global track stiffness or establishing maximum admissible acceleration levels for a track component. It should be stressed that, due to the limited availability of in-situ measurements of railway tracks equipped with USPs, the validation process did not covered this particular track solution. Therefore, numerical results should be interpreted with care.

5.4 TRACK DESIGN OPTIMIZATION PROCESS

Motivated by the need to improve ballasted track in order to better undertake higher speeds (up to 400km/h) in an upgraded dynamic behaviour that would suppose, for instance, same level of vibrations as at 300km/h and/or same deterioration rate, a track design optimization process was pursued. Taken the best abilities of the computational model, hundreds of simulation runs were made in different parametric tests (see Appendix 8.3), so as to provide the other partners with results to enable discussion on which should be the better track solutions (combinations of RP and USP) to be subsequently tested in CEDEX Track Box.

Not having yet an established track degradation model for high-speed railway tracks (ballast fatigue law for VHS), the focus of the track design optimization process was placed on identifying track solutions that minimize both peak ballast accelerations and displacements. To meet this demand, a

track design process was conducted to identify track design solutions which improve the dynamic performance within the track (CTB reference case) for train speeds ranging from 300km/h to 400km/h. The track design variants evaluated and here presented consisted of variants of the reference track model equipped with combinations of rail pads and USPs having different stiffness. The parametric study here shown adopted the track design parameters levels summarized in Table 2.

TABLE 2: TRACK DESIGN OPTIMIZATION PROCESS: PARAMETER LEVELS.

Parameter	Levels
Rail pad stiffness k_{pad} [kN/mm]	40, 60, 80, 100
USP stiffness k_{usp} [kN/mm]	40, 60, 80, 100
Train speed v [km/h]	300, 320, 330, 350, 360, 380, 400

Due to the concerns regarding short and long-term track degradation processes, peak vertical displacements and accelerations within the ballast layer were used to compare the performance of each track design variant.

As the existence of solutions within the design space depends on the introduction of additional design constraints, track design variants were also classified based on global track stiffness. Each track stiffness class thus reflects a lower bound constraint imposed leading to reasonable and admissible global track stiffness values. To focus the analysis on variants which maximize performance improvements with regards to the reference track model, the Pareto set of each track stiffness class was identified for each train speed level, which was subsequently used to determine the best performing track design solutions throughout all circulation speeds. A list with the selected track design variants reached, is presented in Table 3.

TABLE 3: TRACK DESIGN OPTIMIZATION: SELECTED TRACK DESIGN VARIANTS.

	Track design variant		
Global track stiffness	Model variant: M(k_{pad},k_{usp})	K_{pad} [kN/mm]	K_{usp} [kN/mm]
> 50 kN/mm	M(40,60)	40	60
> 60 kN/mm	M(40,80)	40	80
> 70 kN/mm	M(60,80)	60	80
> 80 kN/mm	M(80,100)	80	100

Some of the many results obtained are shown in Figure 9 that illustrates performance of each track design variant through its response values: peak ballast displacements and accelerations, here presented for train speeds of 300, 350 and 400km/h.

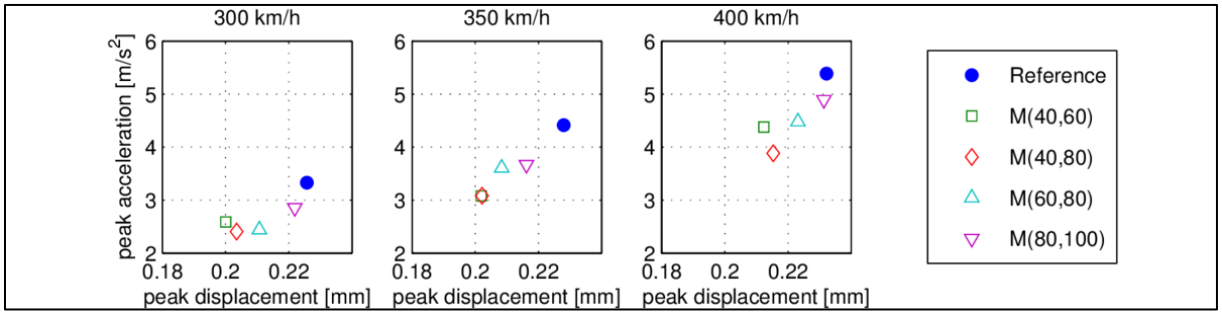

FIGURE 9: TRACK DESIGN OPTIMIZATION: PEAK RESPONSE VALUES OF SELECTED TRACK VARIANTS.

As expected, the introduction of USPs resulted in a reduction of the peak acceleration levels observed within the ballast and subballast layer. From results obtained, track vibrations underneath sleepers, outputted by selected track design variants are markedly reduced with regards to reference CTB results, for all train speeds.

To emphasize the reductions in vibration levels, peak ballast accelerations outputted by the selected track design variants are compared with the reference results in Figure 10, where the percentage of reduction in the maximum acceleration values (with respect to the reference CTB) are indicated.

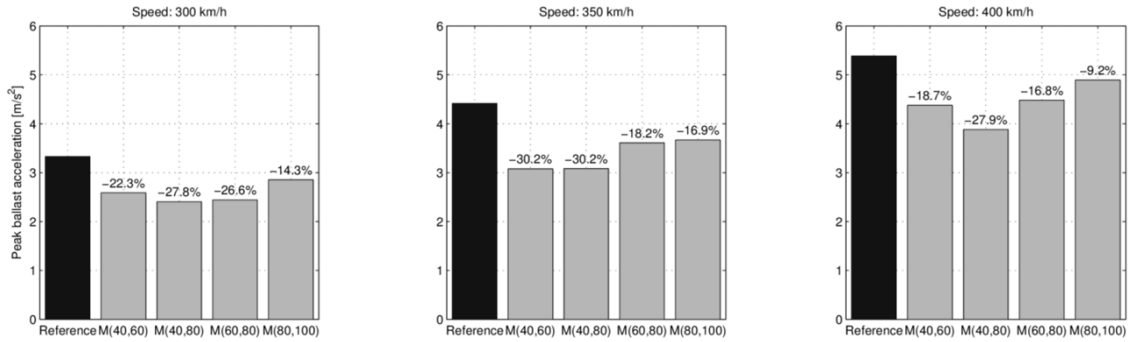

FIGURE 10: TRACK DESIGN OPTIMIZATION: RELATIVE REDUCTION IN PEAK BALLAST ACCELERATION.

All track design variants selected based on the track design optimization process improves the performance over the reference track design by significantly reducing ballast maximum acceleration values comparing to the reference CTB (see Appendix 8.3 for further results). However, the introduction of USPs has also lead to a significant increase in the vertical acceleration levels outputted by the railway components supported by USPs (rails and sleepers) in all simulations. This suggests that although USPs may improve key design aspects, such as stress and vibration levels within the track structure as well as reducing abrasion and particle breakage, these improvements may involve trade-offs between other limit states and design constraints. Moreover, the computational model does not take into account the embedding effect of the ballast stones by the USP elastic layer, which would count as another benefit for USP applications.

Once more, it should be stressed that results should be interpreted with care due to the limited availability of in-situ measurements of railway tracks equipped with USPs, as well as tracks subjected to trains circulating at speeds up to 400km/h.

Furthermore, numerical results are here analysed exclusively from instantaneous responses, so conclusions cannot be directly extrapolated with regards to long-term performance or a life cycle analysis perspective.

This should be overcome with the results obtained from experimental tests to be further made in the CTB with the chosen track solutions, wisely combining both railpads and USPs.

6 Summary and conclusions

The main objectives of this deliverable are:

- to analyse the impact of the pass-by of Very High Speed Trains (VHST) in the current railway track sections, and
- to identify changes that are necessary to implement in the railway track design in order to improve dynamic performance under VHST circulation .

To fulfill with the objectives, the following tasks were performed:

- Selection of some of the tests performed in CEDEX Track Box (CTB) on ballasted tracks subjected to the pass-by of trains. The results obtained in those selected tests were used to calibrate and validate the numerical models developed by IST.
- Performance of two in-situ test campaigns to analyse the track dynamic behaviour and to create a data base of the vibrations measured in a real track produced by passing-by of different trains travelling at high speeds (around 300 km/h). This data base will be used as a source to validate the test results obtained in CEDEX Track Box (CTB).
- Development, validation and application of a numerical train/track FEM model focused on estimations of track response to very high speed trains circulations.

  - Evaluation of the predicted dynamic response of different track design cases (having the CTB reference case as basis) when equipped with different combinations of railpads and undersleeper pads (USPs), including the study of the impact of increasing train speed;

  - Optimization of track design (several specific combinations of railpad and USP stiffness) to improve dynamic performance at very high speeds (up to 400 km/h).

The objective of the track design optimization process performed with the FEM model was placed on identifying track solutions that would minimize both peak ballast accelerations and displacements, maintaining acceptable sleepers vibrations and desirable global track vertical stiffness. After some optimization procedures, analysis came up finally with some track design solutions to be further evaluated consisting of variants of the reference track model (CTB) equipped with combinations of rail pads and USPs having different stiffness, as following:

- Rail pad stiffness: 40, 60, 80, 100 kN/mm
- USP stiffness: 40, 60, 80, 100 kN/mm
- Train speed: 300, 320, 330, 350, 360, 380, 400 km/h.

Afterwards, from results obtained, four track design solutions were selected. The main results reached for the selected design variants are shown in Figure 10 in terms of peak ballast displacements and accelerations.

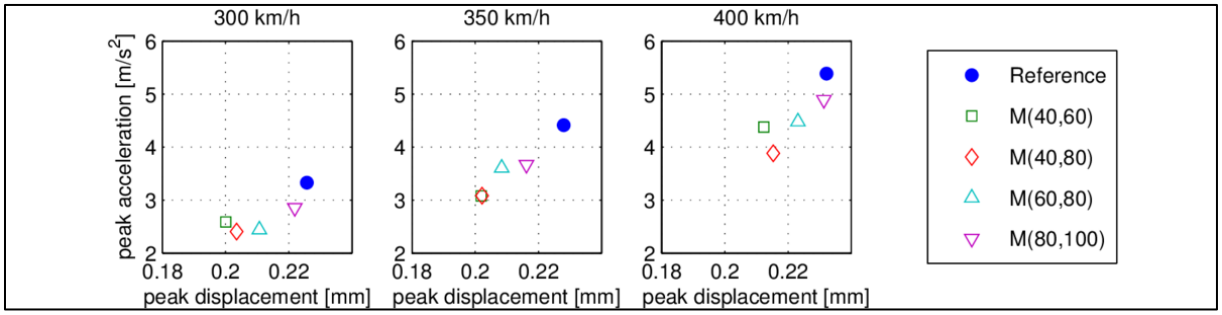

FIGURE 10: TRACK DESIGN OPTIMIZATION: PEAK RESPONSE VALUES OF SELECTED TRACK VARIANTS.

As expected, the introduction of USPs resulted in a reduction of the peak acceleration levels observed within the ballast and subballast layer. These results seem to indicate that the introduction of USPs is a good tool to allow the pass-by of trains at VHS. However other results suggest these improvements may involve trade-offs between other limit states and design constraints, namely among ballast, sleeper and rail vibration levels, and resulting degradation processes.

This imply that these results must be considered with care as the numerical results here analysed are provided exclusively from track instantaneous responses, so, conclusions cannot be directly extrapolated to track long-term performance nor within a life cycle analysis perspective.

Further experimental tests and computations to simulate cyclical effects, as repeated train passages to produce track settlement would have to be done.

Hence more research is needed in terms of the development of more complete numerical models and the performance of some tests on 1:1 scale models, namely in a long term perspective, including track deterioration prediction, before implementing some of these solutions in real tracks.

7 References

[1] CEDEX Track Box as an experimental tool to test railway tracks at 1:1 scale. J. Estaire, F. Pardo de Santayana, V. Cuéllar. In Proceedings of the 19th International Conference on Soil Mechanics and Geotechnical Engineering, Seoul 2017.

[2] Testing railway tracks at 1:1 scale at CEDEX Track Box. José Estaire, Vicente Cuéllar & María Santana. International Congress on High-Speed Rail. Ciudad Real (Spain), 4-6 October 2017

[3] Instrumentation techniques for studying the horizontal behaviour of high-speed railways. J. Moreno-Robles; I. Crespo-Chacón; J. L. García-de-la-Oliva. Procedia Engineering - Advances in Transportation Geotechnics III. 143, pp. 870 - 879. Elsevier, 2016.

[4] On the use of geophones in the low-frequency regime to study rail vibrations. I. Crespo-Chacón; J. L. García-de-la-Oliva; E. Santiago-Recuerda. Procedia Engineering - Advances in Transportation Geotechnics III. 143, pp. 782 - 794. Elsevier, 2016.

[5] Maciel, R. & Ferreira, P., 2016. Optimization algorithm applied to VHS track design towards enhanced track dynamic performance and reduced settlement, 11th World Congress on Railway Research -WCRR 2016. Milan.

[6] Ferreira, P. & López-Pita, A., 2015. Numerical modelling of high speed train/track system for the reduction of vibration levels and maintenance needs of railway tracks. Construction and Building Materials, pp. Volume 79, pages 14–21.

[7] Ferreira, P. & Maciel, R., 2014. Inverse problems applied to the optimization of numerical model validation of railway track dynamic behavior. Lisbon, 4th International Conference on Engineering Optimization - EngOpt2014, Lisbon, 8-11th September, 2014.

[8] Ferreira, P. & López-Pita, A., 2013. Numerical modeling of high-speed train/track system to assess track vibrations and settlement prediction. Journal of Transportation Engineering, Volume 139, pp. 330-337.

[9] Ferreira, P., 2010. Modelling and prediction of the dynamic behaviour of railway infrastructures at very high speeds, PhD Thesis, Instituto Superior Técnico, Lisbon.

8 Appendices

8.1 Tests on 1:1 scale model in CTB

8.2 Data collection in in-situ test campaigns

8.3 Track Design Optimization for Very High Speed

C4R
Capacity for Rail

SEVENTH FRAMEWORK PROGRAMME

Project co-funded by the European Commission

Collaborative project SCP3-GA-2013-60560

Increased Capacity 4 Rail networks through enhanced infrastructure and optimised operations

FP7-SST-2013-RTD-1

Deliverable 12.1

Innovative designs and methods for VHST (intermediate)

Appendix 8.1

Tests on 1:1 scale model in CTB

Dissemination Level		
PU	Public	**PU**
PP	Restricted to other program participants (including the Commission Services)	
RE	Restricted to a group specified by the consortium (including the Commission Services)	
CO	Confidential, only for members of the consortium (including the Commission Services)	

Lead contractor for this deliverable: ..... CEDEX

Document status		
Revision	Date	Description
1	2015/02/230	Version N°1
2	2017/09/20	Version N°2
Reviewed	YES	

Table of content

Abbreviations and acronyms

Abbreviation / Accronym	Description
CTB	CEDEX Track Box
HSL	High Speed Lines
VHST	Very High Speed Trains

1 Background and Objectives

This report collects the works performed by CEDEX relative to the demonstrator defined in the Sub-Task 1.2.2. "Verification by full scale models" of WP 1.2. The scope of this demonstrator is to define the possible modifications in the design and in the maintenance operations of the current high speed lines (HSL) to be able to hold very high speed trains (VHST) when travelling at speeds up to 400 km/h.

Before performing any test, it was decided that CEDEX provides data from previous tests performed in CTB on ballasted tracks to other C4R partners for them to calibrate and validate their numerical models. Chapter 3 collects all the information that was provided in February 2015.

As a starting point, the performance of an existing track system in operation will be subjected to an increase in the operation speed and then the system will be improved by adding elements to withstand the expected effects. The results will make it possible to create a matrix of data, useful to understand the performance of railways at such high speeds.

All components of the track bed and platform of the model will be fully monitored to record the variations in track stiffness, speed and accelerations. The short term and long term effects induced in the mechanical performance of the model by the passage of trains simulated under VHST conditions will be recorded.

All these tests should have been performed in CEDEX Track Box (CTB). However, unfortunately during some maintenance works carried out in CTB, a problem in the hydraulic system was discovered. To solve the problem repair works were performed between September 2016 and January 2017, just the period previously scheduled for the performance of VHST tests, so the tests could not be performed. However, it is worth noting that during the time devoted to the repair works, CEDEX built the 1:1 scale model of a ballast track to perform the VHST tests, as described below.

2 CEDEX Track Box (CTB)

CEDEX Track Box (CTB) is a 21 m long, 5 m wide and 4 m deep facility whose main objective is to test, at 1:1 scale, complete railway track sections of conventional and high speed lines for passenger and freight trains, at speeds up to 450km/h.

The testing facility was designed, built and developed as part of SUPERTRACK ("Sustained Performance of Railway Tracks", 2001-05) and INNOTRACK ("Innovative Track Systems", 2005-2009) projects funded by the European Union Fifth and Sixth Framework Programs, respectively. Figure 1 shows a general view of the testing facility.

Its principal advantage is the possibility of performing fatigue tests in a fast way as in one working week, the effect of the passing-by of trains during a year in a real section can be modelled.

The reproduction of the effect of the approaching, passing-by and departing of a train in a test cross-section, as it occurs in a real track section, is performed by application of loads, adequately unphased as a function of the train velocity which is being simulated, produced by three pairs of servo-hydraulic actuators (that can apply a maximum load of 250 kN at a frequency of 50 Hz), placed on each rail and 1,5 m longitudinally separated, as seen in Figure 2.

Furthermore, the reproduction of wheel and track imperfection effects that produces low amplitude high frequency dynamic loads can also be carried out by the use of two piezoelectric actuators (Figure 3) that can apply loads up to 20 kN at 300 Hz.

The railway track response, in terms of displacements, velocities, accelerations and pressures, is collected from a great number of linear variable differential transformers (LVDTs), geophones, accelerometers and pressure cells installed inside both the embankment and the bed layers (ballast, sub-ballast and form layer) of the track (Figure 5).

On the other hand, the railway superstructure response is recorded with mechanical displacement transducers, laser sensors, geophones and accelerometers installed on the different track components (rail, sleeper and railpad) (Figure 4). The acquisition data unit can receive information from 150 sensors at the same time.

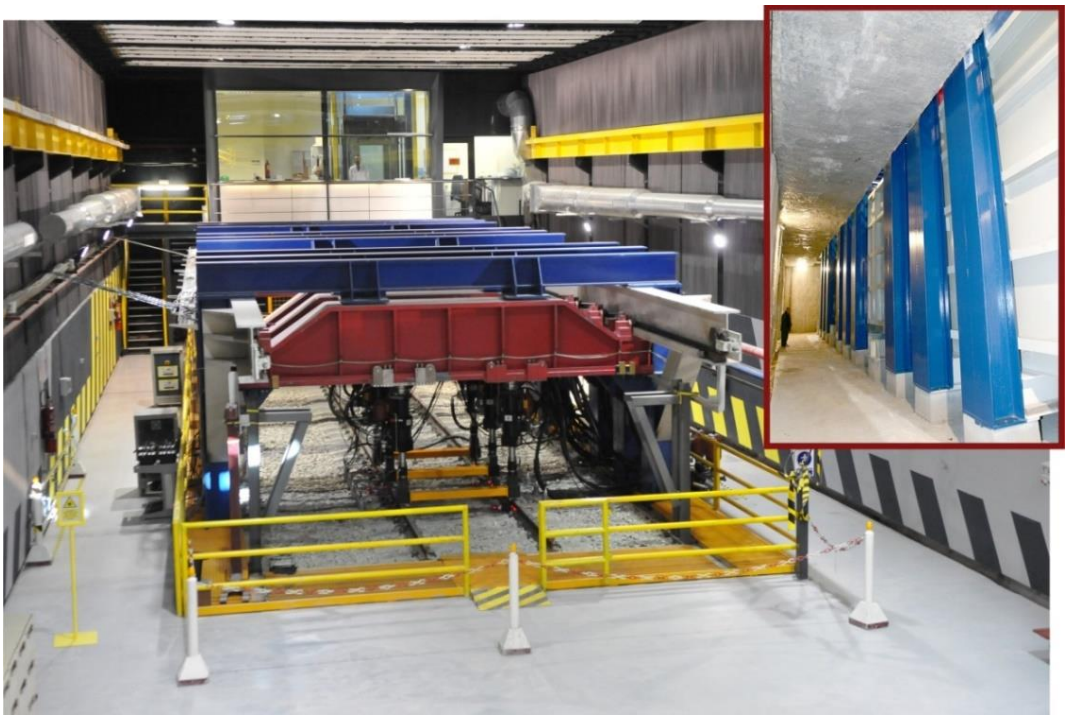

FIGURE 1 CEDEX TRACK BOX (CTB) VIEW WITH ZONE 1, TESTING ZONE, IN THE FOREGROUND AND CONTROL ROOM IN THE BACKGROUND

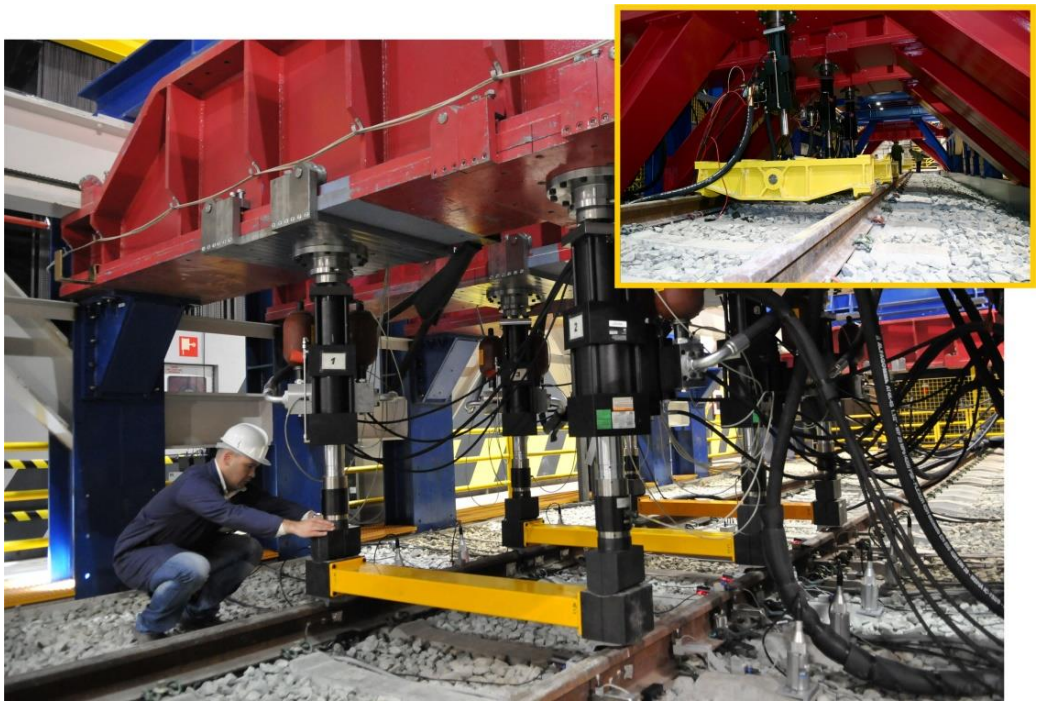

FIGURE 2 VIEW OF THE LOADING SYSTEM FORMED BY THREE PAIRS OF HYDRAULIC ACTUATORS

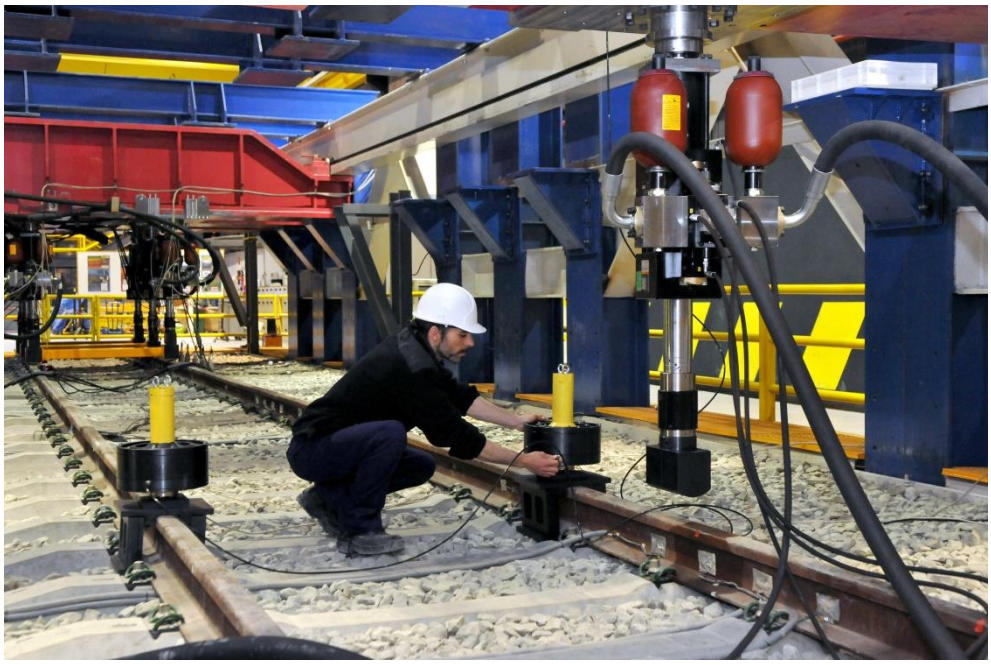

FIGURE 3 VIEW OF THE PIEZOELECTRIC ACTUATORS TO SIMULATE THE EFFECT OF TRACK IMPERFECTION

FIGURE 4 VIEW OF THE SURFACE INSTRUMENTATION INSTALLED IN ONE TEST

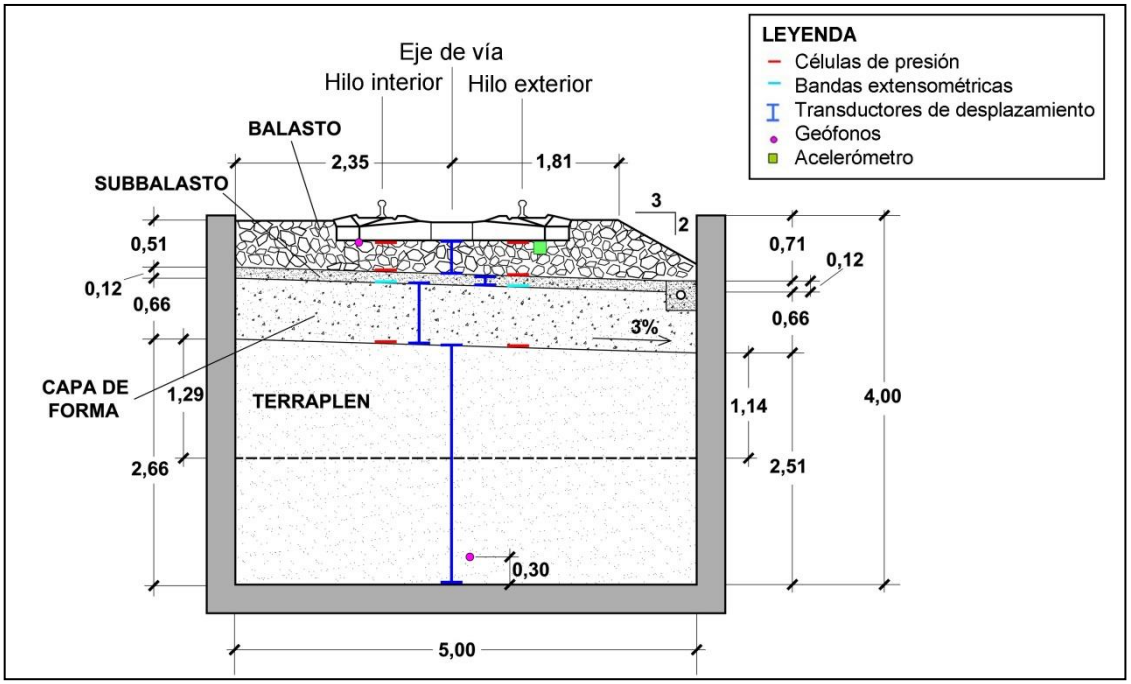

FIGURE 5 CTB CROSS-SECTION WITH SOME OF THE INTERNAL SENSORS INSTALLED FOR ONE OF THE TESTS

FIGURE 6: VIEW OF THE MOTORS OF THE HYDRAULIC SYSTEM WITH A POWER OF 350 CV EACH TO GENERATE A PRESSURE OF 210 BARS AND A FLOW OF 1800 L/MIN

3 Results of previous tests on ballasted track with granular subballast

3.1 Introduction

To fulfill the objective that IST could begin to calibrate its numerical model, it was decided that CEDEX sent them some results coming from previous tests performed in CTB in 1:1 scale models of ballasted track.

Taking that into account, this Sub-chapter collects the data provided by CEDEX to IST to calibrate its numerical models. These data come from some test results obtained in a 1:1 scale model of a ballasted track with granular subballast tested in CTB some years ago. The model was subjected to the pass-by of 1 M axle loads of a passenger train travelling at 300 km/h.

The following sections are devoted to describe the model tested, the instrumentation installed and the results obtained. These data were sent to IST for them to calibrate its numerical model in February 2015.

3.2 Description of the physical model tested

The geometric dimensions of the cross section of the 1:1 scale model of a ballasted track with granular subballast used in the tests are given in Figure 7.

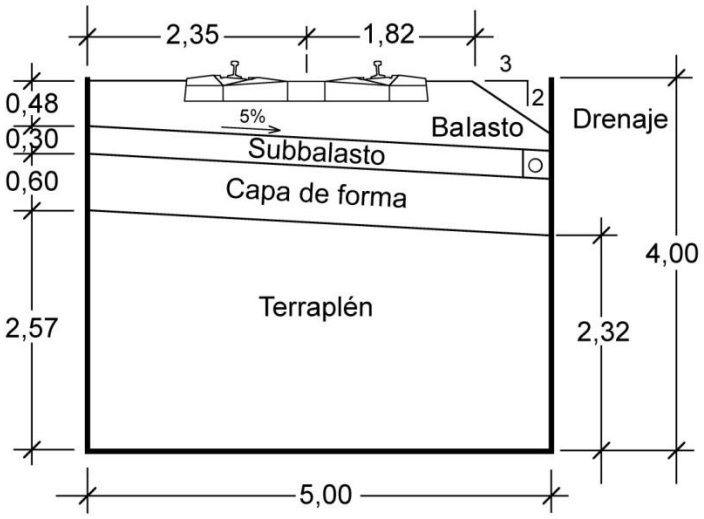

Figure 7: Dimensions (m) of the 1:1 scale model used in the tests

The track, with the international gage (1.435 m), is constituted by the following elements:

- **Rails**: They are of 60-E1 type. They have a mass per length of 60 kg/m and a flexural stiffness EI = 6.4155 MN·m2

- **Sleepers**: The sleepers are mono-block concrete pre-stressed units of AI-99 type. They have an average mass of 344 kg, a width of 0.22 m at the centre and 0.30 m at the edges and a height of 0.21 m at the centre and 0.23 m at the edges, as seen in Figure 8.

- **Fastening system**: It is fabricated by Vossloh (Figure 9), consisting on the following elements:
  - Under rail pads (URP's): They are of PAE-2 type with a thickness of 7 mm (Figure 9). Its vertical nominal stiffness is around 100 kN/mm (secant value between 20 and 95 kN as obtained in unconfined compression tests).
  - Rail clamps: They are of SKL-1 type.
  - Angular guide plates: They are of A2 type.
  - Sleeper screws: they are of Plastirail 22-115-5 type with sleeper prefabricated tracks and plastic dowels. Their clamping torque was 200 N·m.

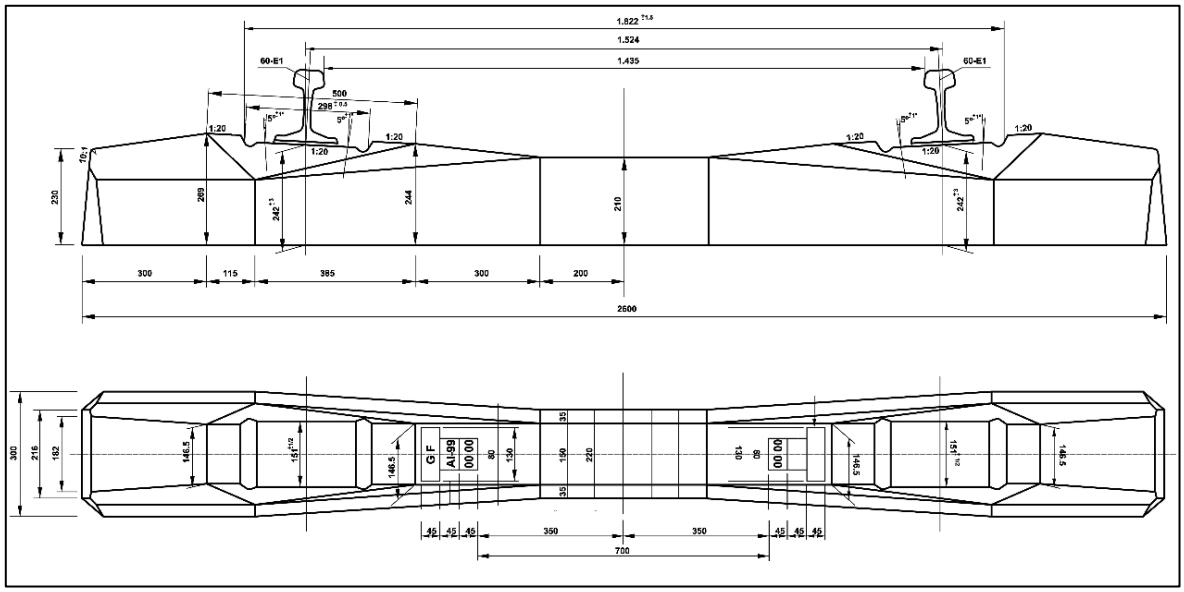

FIGURE 8: AI-99 SLEEPER (DIMENSIONS IN MM)

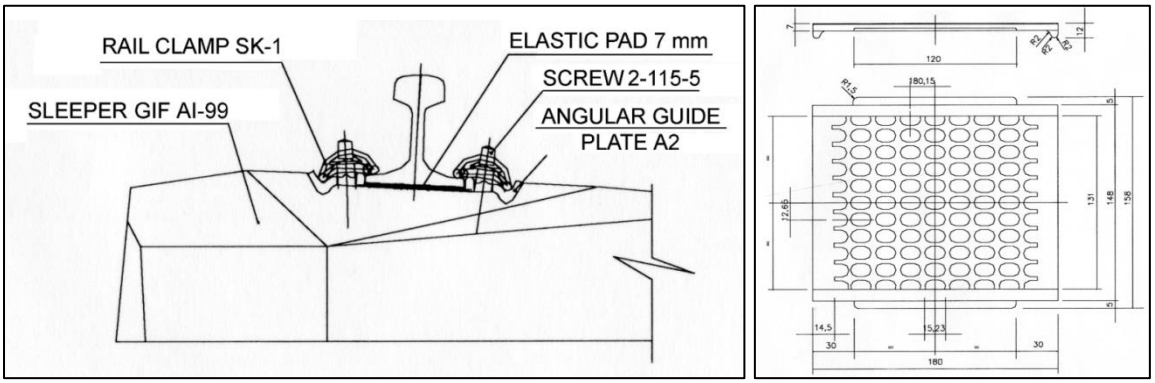

FIGURE 9: VOSSLOH FASTENING SYSTEM (RIGHT) AND PAE-2 UNDER RAIL PAD (LEFT)

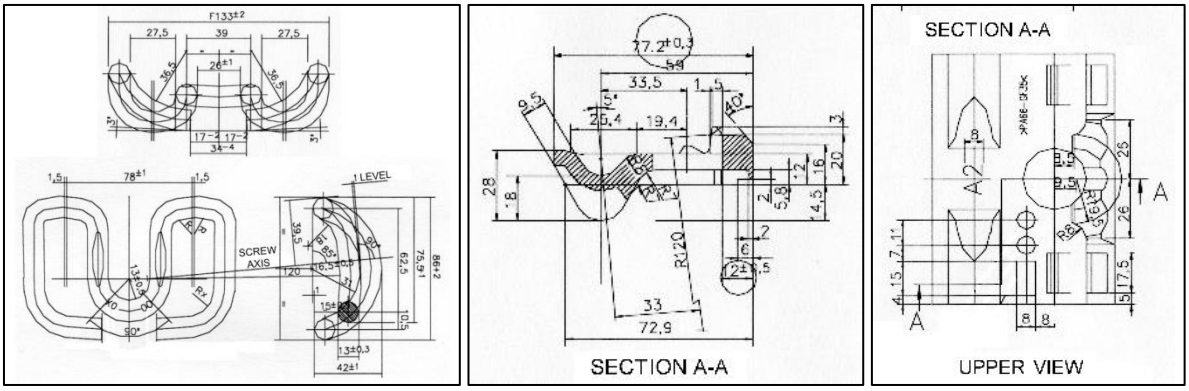

FIGURE 10: SKL-1 RAIL CLAMP (LEFT) AND A-2 ANGULAR GUIDE PLATE /CENTER AND RIGHT) [DIMENSIONS IN MM]

Figure 11 shows the grain size distribution curves of the materials that constitute the bed layers indicated in Figure 7.

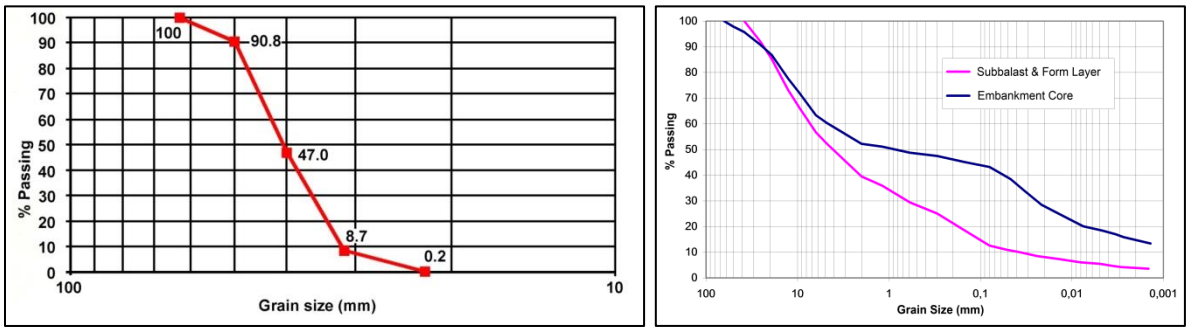

FIGURE 11: GRAIN SIZE DISTRIBUTION CURVES: BALLAST (LEFT) AND SUBBALLAST, FORM LAYER AND EMBANKMENT (RIGHT)

A summary of the mechanical properties of the bed layers materials, as determined by plate loading tests and geophysical procedures, is given in Table 1 and Table 2:

TABLE 1: PROPERTIES OF THE TRACK BED LAYERS

Properties	Embankment		Form Layer	Granular Subballast
	Upper	Lower		
Thickness	1.255 m	1.350 m	0.600 m	0.300 m
Unified Soil Classification System	SC (clayey sand)	GC (clayey gravel of low plasticity)	GW (well graded gravel with sand)	GW (well graded gravel with sand)
Liquid Limit	45.5 %	25.6 %	17.4 %	17.4 %
Plasticity Index	32.7%	7 %	2 %	2 %
Dry unit weight	17.5 kN/m^3	21.2 kN/m^3	21.5 kN/m^3	22.0 kN/m^3
Water content	10 %	2 %	4 %	3.5 %
E_{V2} modulus	---	---	165 MPa	170 MPa
Shear wave velocity	200 m/s	300 m/s	260 m/s	270 m/s
Young modulus maximum value, E_{max}	---	----	400 MPa	440 MPa
Poisson ratio	0.30	0.30	0.30	0.30

TABLE 2: PROPERTIES OF BALLAST LAYER

ADIF classification	1st class ballast
Parent rock	Andesite
Unconfined compression strength of the parent rock	230 MPa
Flakiness index (UNE – EN 933-3:1997)	7.4 %
Los Angeles coefficient (UNE-EN 1097-2:1999)	12 %
Sulfate soundness (UNE-EN 1367 2:2000)	1.85 %
Specific density(UNE-EN 1097 6:2001)	2.65 Mg/m^3
Water absortion (UNE-EN 1097 6:2001)	0.89 %

3.3 INSTRUMENTATION INSTALLED

The internal system of sensors used in the model central cross-section is indicated in Figure 12.

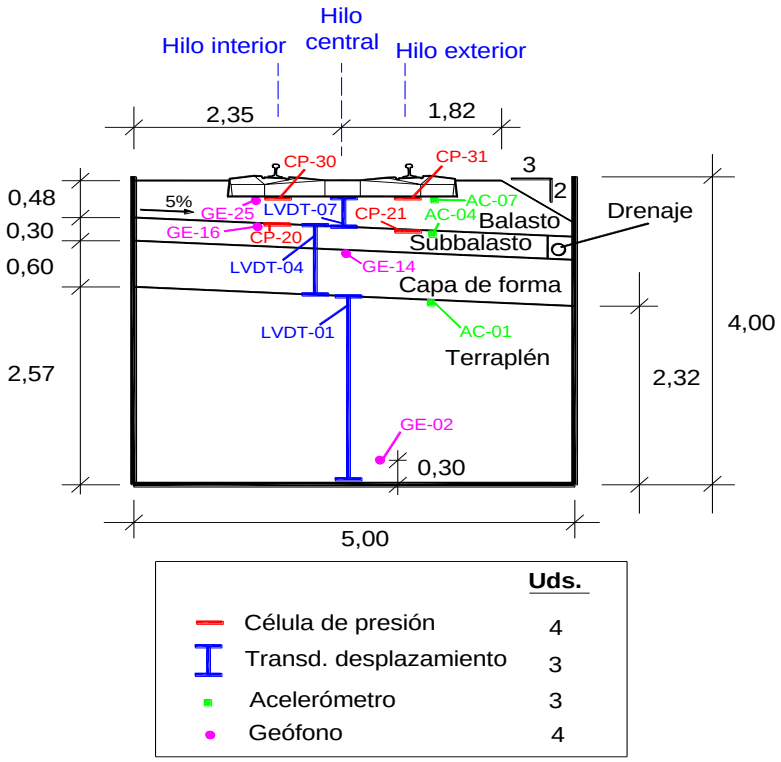

FIGURE 12: SENSORS DEPLOYED IN THE INTERNAL PART OF CENTRAL CROSS-SECTION

The geophones identified in Figure 12 are 4 Hz sensors and the accelerometers are of the ±10·g type. The LVDT sensors have a resolution of 0.001 mm and measuring ranges of ±5 mm (LVDT-07 and LVDT -04) and ±50 mm (LVDT-01).

Figure 13 illustrates the type of external sensors deployed in the track superstructure components. This external system is constituted of:

- One laser system with receiver in the outside rail, near the central sleeper (sleeper 0 in Figure 13). It has been used to measure track absolute displacements with a resolution of 0.01 mm and an estimated error of ± 0.02 mm.
- Two resistevemeters in the central sleeper to measure rail-sleeper relative displacements in both rails (see Figure 13). They have the same resolution and estimated error that the laser system.
- Two 1Hz vertical geophones in the central sleeper (see Figure 13).
- One 2 Hz geophone in the outside base of the outside rail near the laser receiver, (see Figure 13).
- One ±50·g accelerometer at the outside rail in the opposite side of the 2Hz geophone (see Figure 13).
- Two ±18·g accelerometers in the central sleeper (see Figure 13).

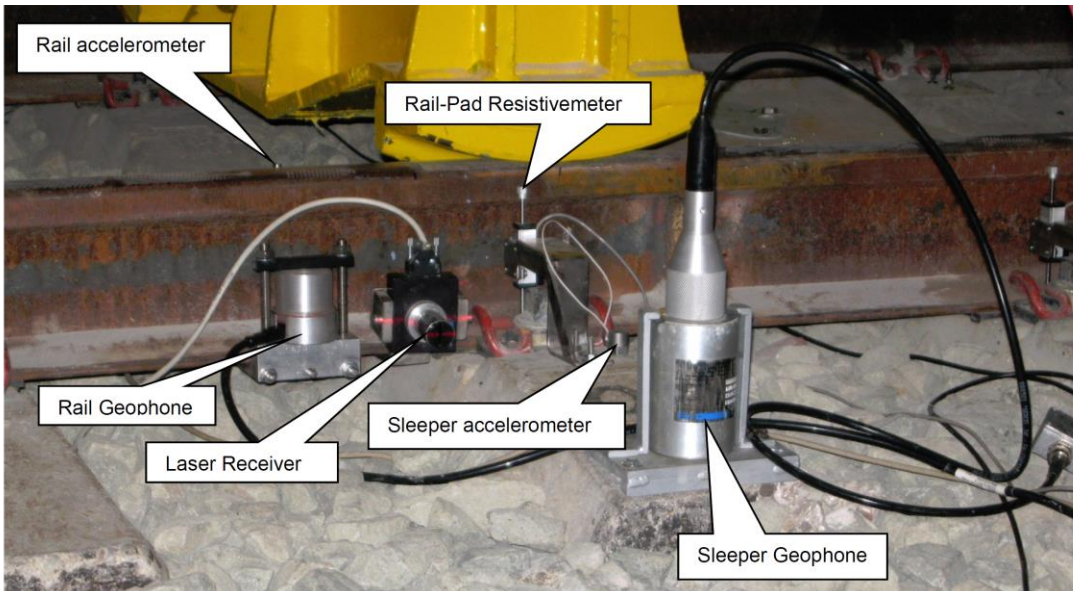

FIGURE 13: SENSORS DEPLOYED IN THE EXTERNAL PART OF CENTRAL CROSS SECTION

3.4 RESULTS OF THE STATIC TESTS

The testing routine adopted in the static test carried out at the central cross-section after tamping the ballast is illustrated in Figure 14. The test consisted of two static loading-unloading cycles with a maximum axle load of 200 kN in each one of them and a total duration of 10 minutes. The loading branches of both cycles were reached in 10 steps of 20 kN each.

The corresponding track deflections provided by the laser system are given in Figure 15. Track stiffness values of 98 kN/mm and 95 kN/mm may be derived from the data depicted in both figures for the first and second cycle, respectively. After having subjected the track to the pass-by at 300 km/h of 385.000 axle loads of the type described when discussing later on the quasi-static test, the static test was repeated and a track stiffness of 92 kN/mm was obtained.

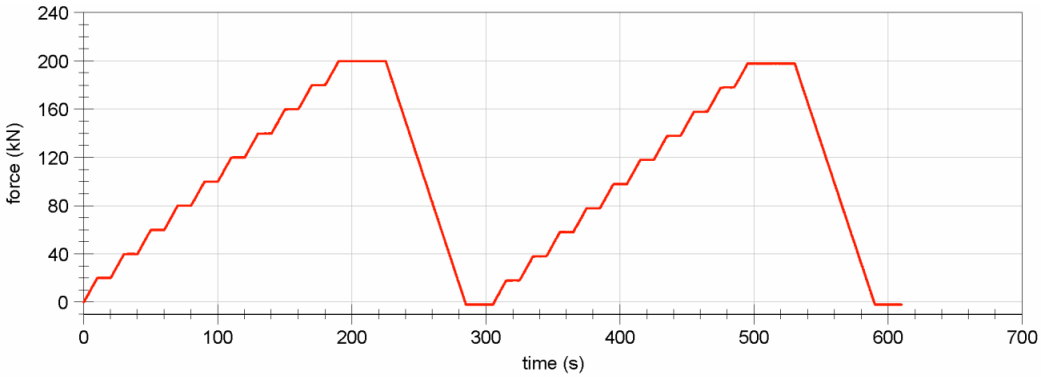

FIGURE 14: LOADING –UNLOADING ROUTINE ADOPTED IN THE STATIC TESTS

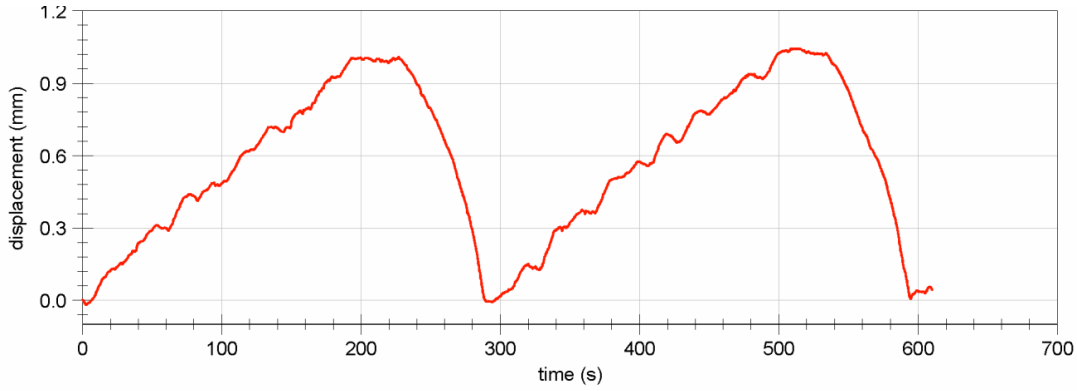

FIGURE 15: TRACK DEFLECTIONS OBTAINED IN THE STATIC TESTS

3.5 RESULTS OF THE QUASI-STATIC TESTS

To carry out the quasi-static test, the distribution of axle loads indicated in Figure 16 was selected. They represent a Eurostar train of 195.6 m with two locomotives and eight wagons having 13 bogies and 26 axles. The axle load-time signal adopted to simulate the pass-by of that type of train at 300 km/h is indicated in Figure 17.

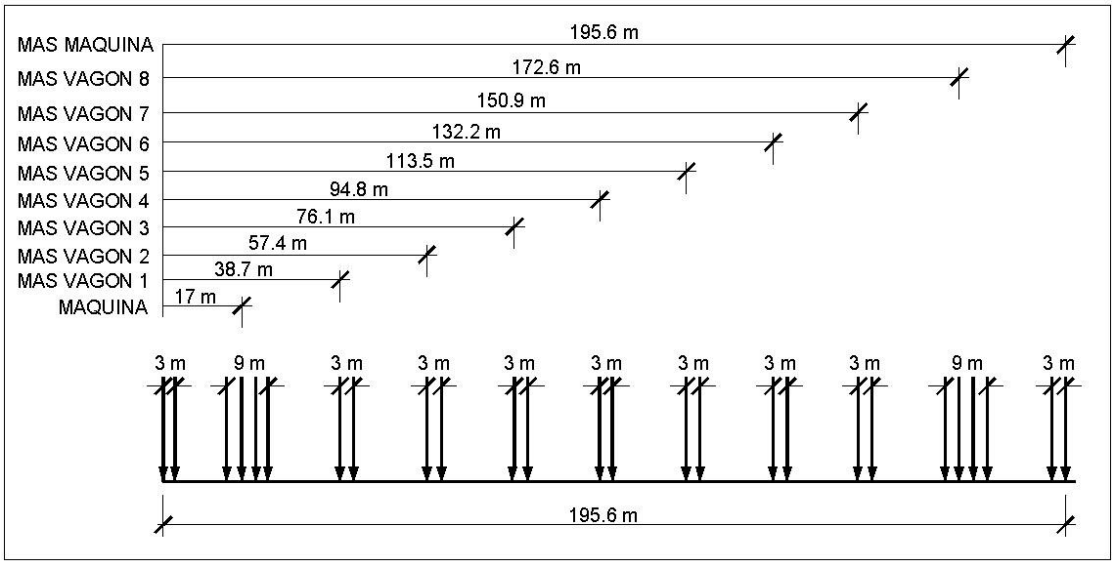

FIGURE 16: LOAD DISTRIBUTION SELECTED TO CARRY OUT THE QUASI-STATIC TEST

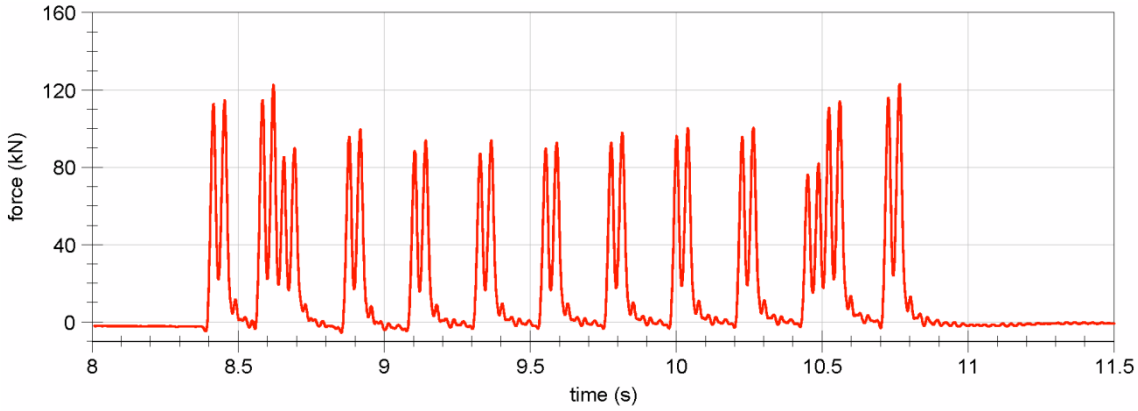

FIGURE 17: LOAD-TIME SIGNAL ADOPTED TO SIMULATE THE PASS-BY OF TRAINS AT 300 KM/H

The Fourier transform of the load time signal presented in Figure 17 is given in Figure 18.

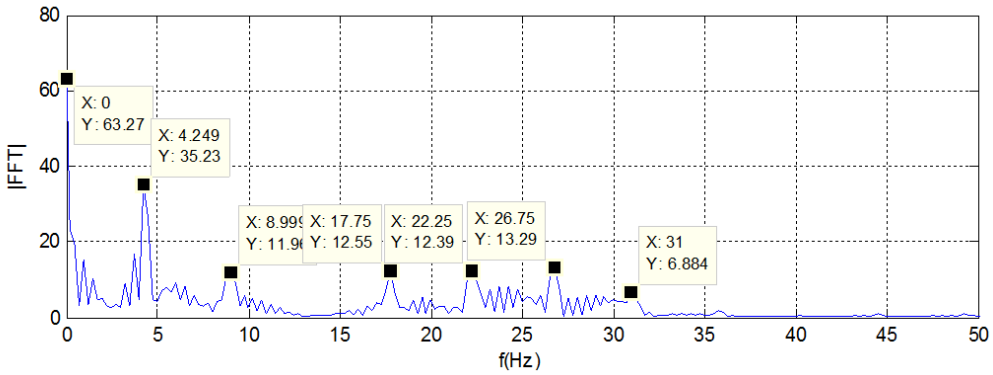

FIGURE 18: FOURIER TRANSFORM OF THE LOAD –TIME SIGNAL IN FIGURE 17

The wagon pass-by frequency 4.45 Hz (derived from the geometric data in Figure 16 and a travelling speed of 300 km/h) and its first harmonics (until the 7th one) are clearly visible in Figure 18.

To carry out the quasi-static test, the CEDEX loading system was fed with the signal represented in Figure 17 every 2.5 seconds until the pass-by of 1M axle loads was reached. Along that testing period the short–term response of all sensors under the pass-by of one train was recorded 28 times and the data obtained were very similar all the times, supporting the fact that the track stiffness obtained in one static test performed after the simulation of the pass-by of 385.242 axle loads (92 kN/mm) was practically the same that the one obtained after tamping the ballast (95 kN/mm).

To illustrate the short-term response of the track obtained in the quasi-static test, a representative signal of the track deflections experienced by the track under the pass-by of one train is provided in Figure 19.

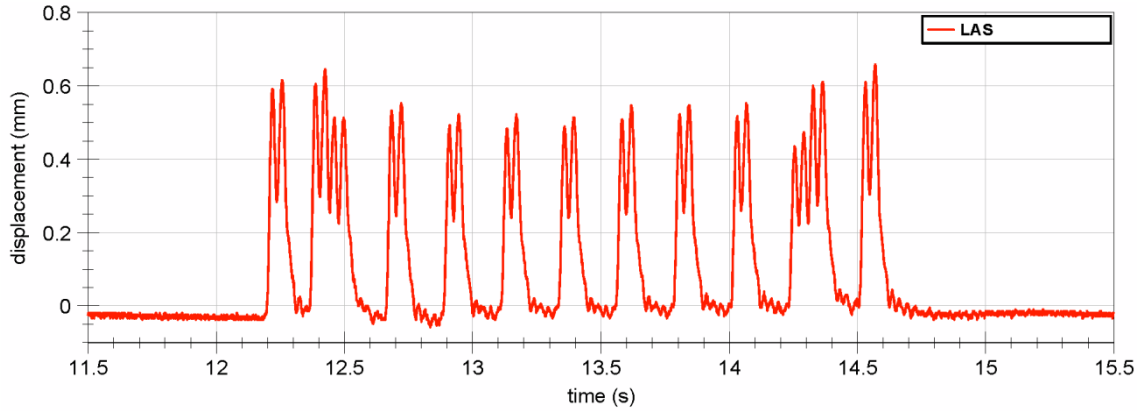

FIGURE 19: TRACK DEFLECTION-TIME SIGNAL PROVIDED BY THE LASER SYSTEM

To complete the description of the track short-term response, velocity time signals provided by the geophones installed in the different components of the track are provided in Figure 20 to Figure 25.

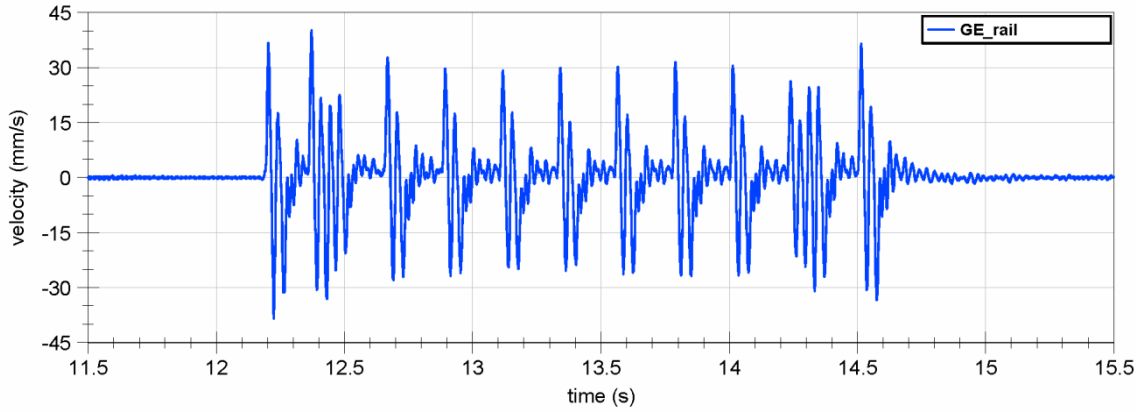

FIGURE 20: RAIL VELOCITY-TIME SIGNAL PROVIDED BY 2 HZ GEOPHONE UNDER PASS-BY OF ONE EUROSTAR TRAIN AT 300 KM/H

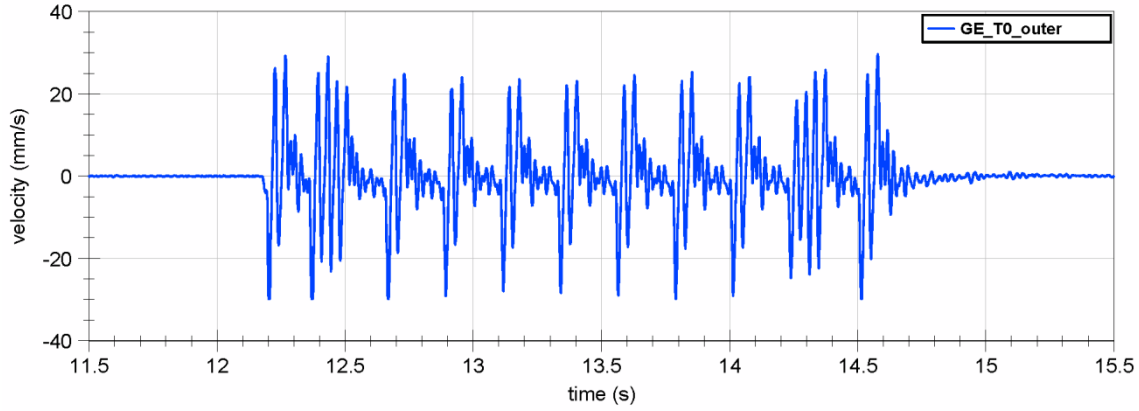

FIGURE 21: SLEEPER VELOCITY-TIME SIGNAL PROVIDED BY 1HZ GEOPHONE UNDER THE PASS-BY OF ONE EUROSTAR TRAIN AT 300 KM/H

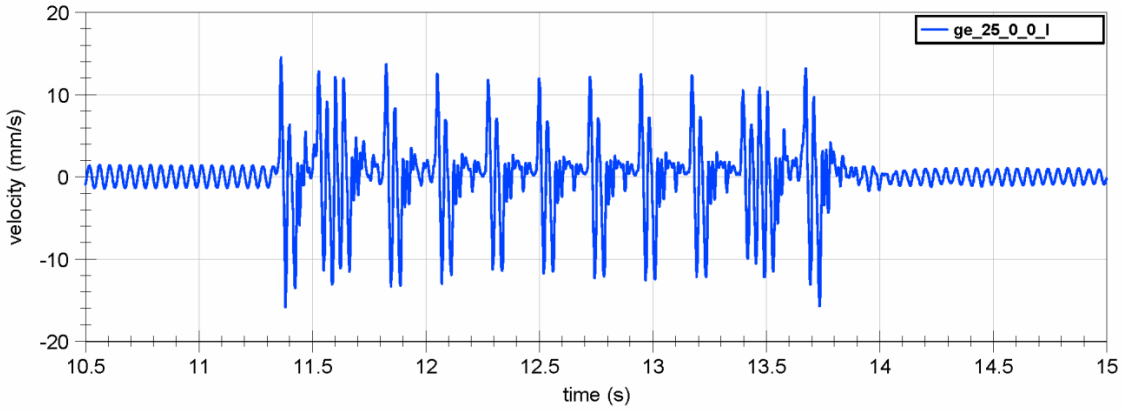

FIGURE 22: VELOCITY-TIME SIGNAL PROVIDED BY 4 HZ GEOPHONE AT THE UPPER SURFACE OF THE BALLAST LAYER UNDER THE PASS-BY OF ONE EUROSTAR TRAIN AT 300 KM/H

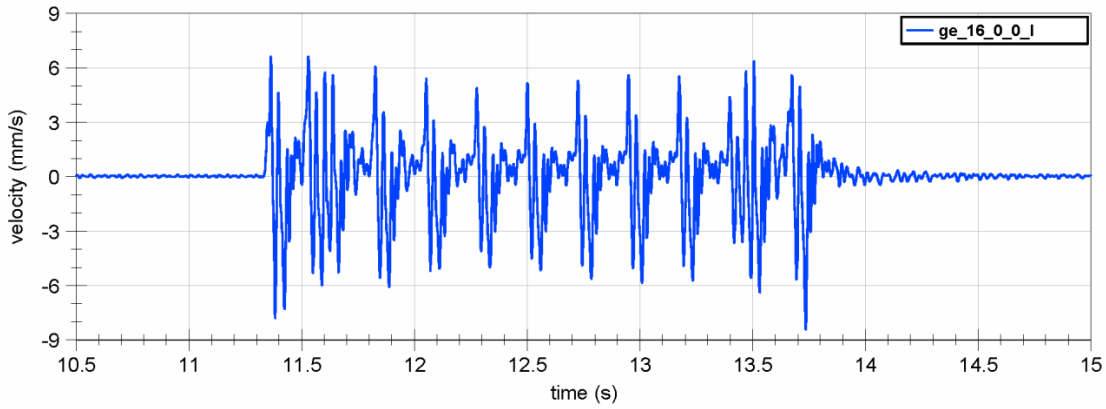

FIGURE 23: VELOCITY-TIME SIGNAL PROVIDED BY 4 HZ GEOPHONE AT THE LOWER SURFACE OF THE BALLAST LAYER UNDER THE PASS-BY OF ONE EUROSTAR TRAIN AT 300 KM/H

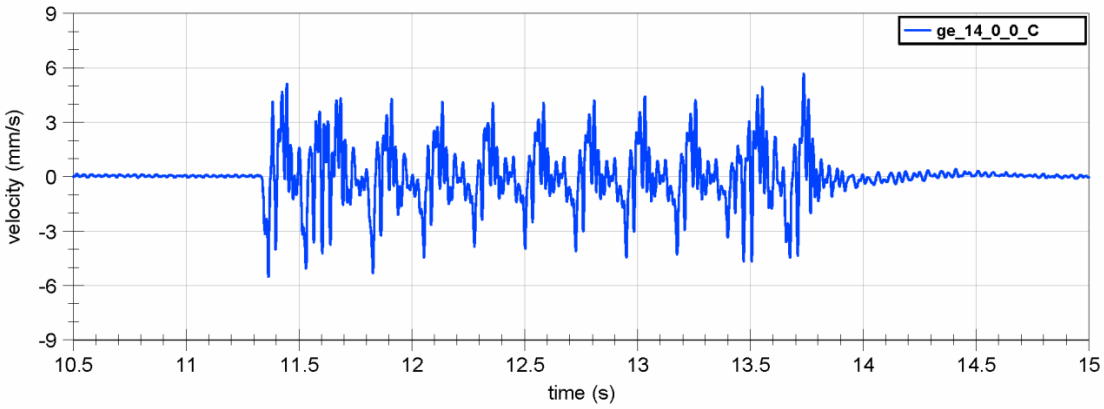

FIGURE 24: VELOCITY-TIME SIGNAL PROVIDED BY 4 HZ GEOPHONE AT THE UPPER SURFACE OF THE FORM LAYER UNDER THE PASS-BY OF ONE EUROSTAR TRAIN AT 300 KM/H

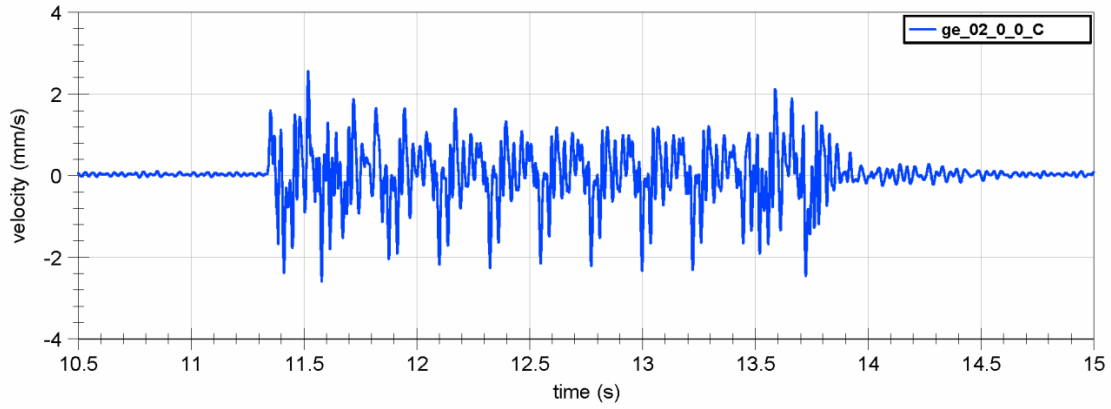

FIGURE 25: VELOCITY-TIME SIGNAL PROVIDED BY 4 HZ GEOPHONE AT THE LOWER PART OF THE EMBANKMENT UNDER THE PASS-BY OF ONE EUROSTAR TRAIN AT 300 KM/H

Unfortunately, the data provided by the accelerometers installed in the rail and in the central sleeper are not available, since at the time the test was run they did not work properly. So, in order to get the rail and sleeper acceleration-time signals and to put in perspective the data provided by the accelerometers installed in the ballast and the form layer that worked correctly, the velocity-time signals presented in Figure 20 and Figure 21 have been derived with respect time. The results obtained are provided in Figure 26 and Figure 27.

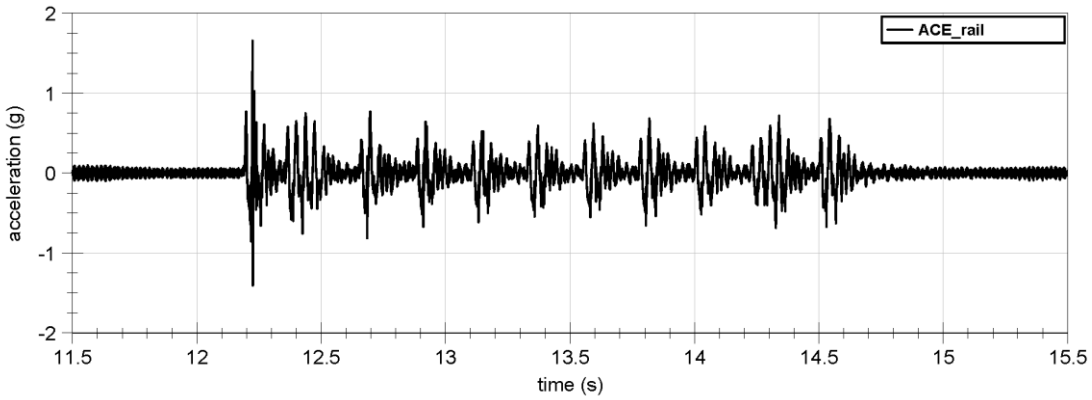

FIGURE 26: RAIL ACCELERATION-TIME SIGNAL UNDER THE PASS-BY OF ONE EUROSTAR TRAIN AT 300 KM/H

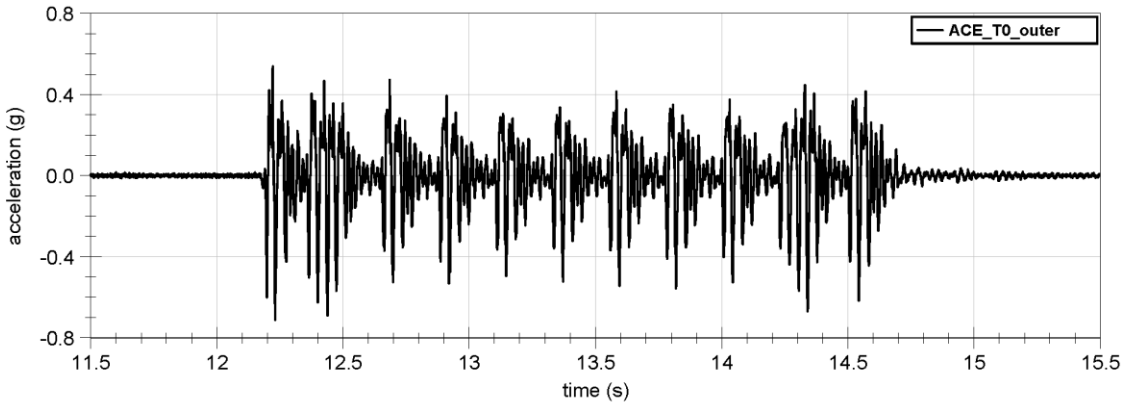

FIGURE 27: SLEEPER ACCELERATION-TIME SIGNAL UNDER THE PASS-BY OF ONE EUROSTAR TRAIN AT 300 KM/H

Finally, in Figure 28 to Figure 30 are drawn the data provided by accelerometers 07, 04, and 02 installed at the upper surfaces of ballast, subballast and embankment respectively.

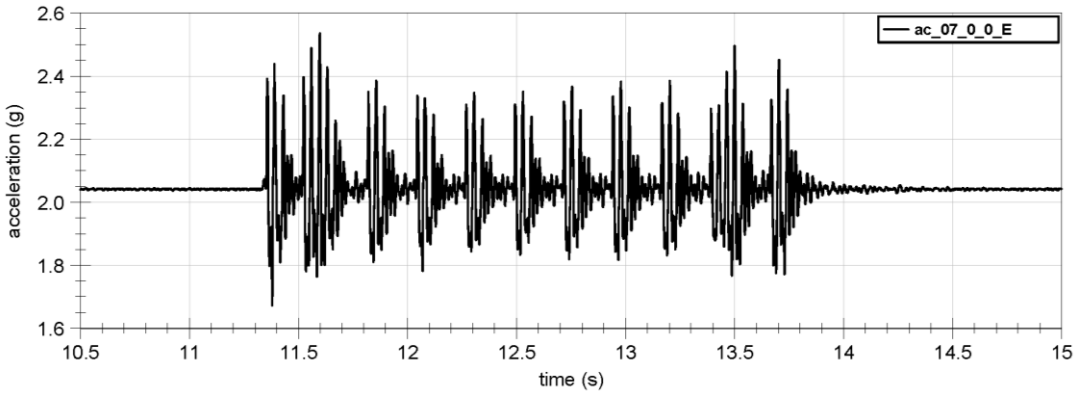

FIGURE 28: ACCELERATION-TIME SIGNAL RECORDED AT THE BALLAST UPPER SURFACE UNDER THE PASS-BY OF ONE EUROSTAR TRAIN AT 300 KM/H

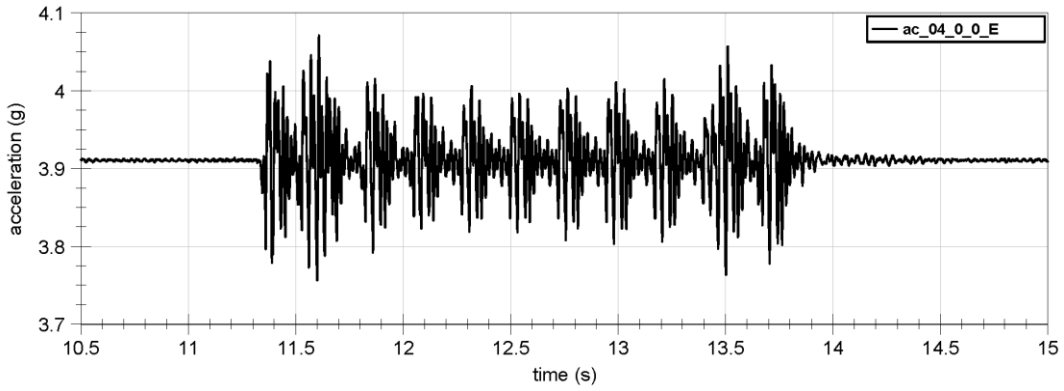

FIGURE 29: ACCELERATION-TIME SIGNAL RECORDED AT THE SUBBALLAST UPPER SURFACE UNDER THE PASS-BY OF ONE EUROSTAR TRAIN AT 300 KM/H

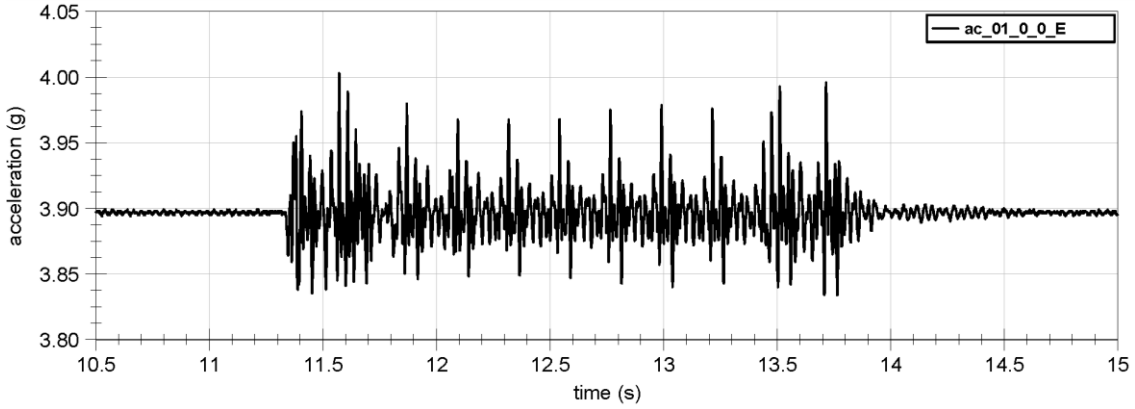

FIGURE 30: ACCELERATION-TIME SIGNAL RECORDED AT THE SURFACE OF THE EMBANKMENT UNDER THE PASS-BY OF ONE EUROSTAR TRAIN AT 300 KM/H

The track long –term response is represented by the ballast fatigue curve given in Figure 31. In that figure, the irreversible settlements (δ) of the 0.400 m thick ballast layer, recorded 28 times (with LVDT 07) along the 1M axle load quasi-static test, are plotted in the vertical coordinate axle and the number of axle load applications (N) in the horizontal coordinate axle. The empirical potential law that fits best the data plotted in that figure is also given.

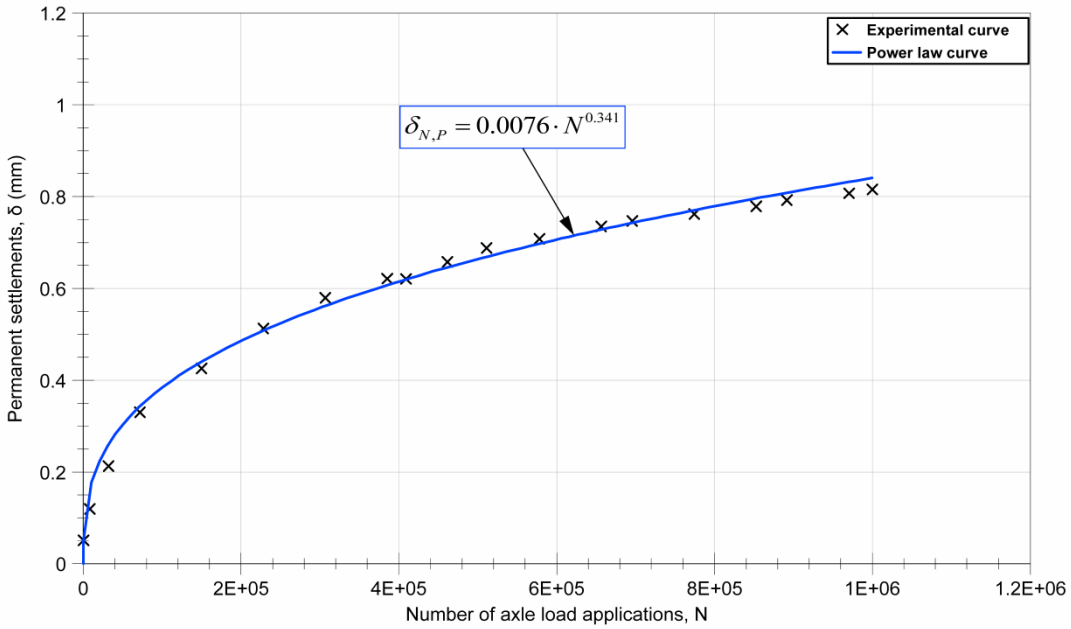

FIGURE 31: BALLAST FATIGUE CURVE FOR 1M AXLE LOAD APPLICATIONS SIMULATING THE PASS-BY OF AN EUROSTAR TRAIN AT 300 KM/H

4 Current experimental section

4.1 Cross section description

The structural section of CEDEX Track Box is 4 m deep and it is formed by the following elements, listed from bottom to top: Embankment, Form layer, Subballast layer, Ballast and Sleeper, rails and fastening system.

Figure 32 shows the schematic structural section used in the present study and Figure 33

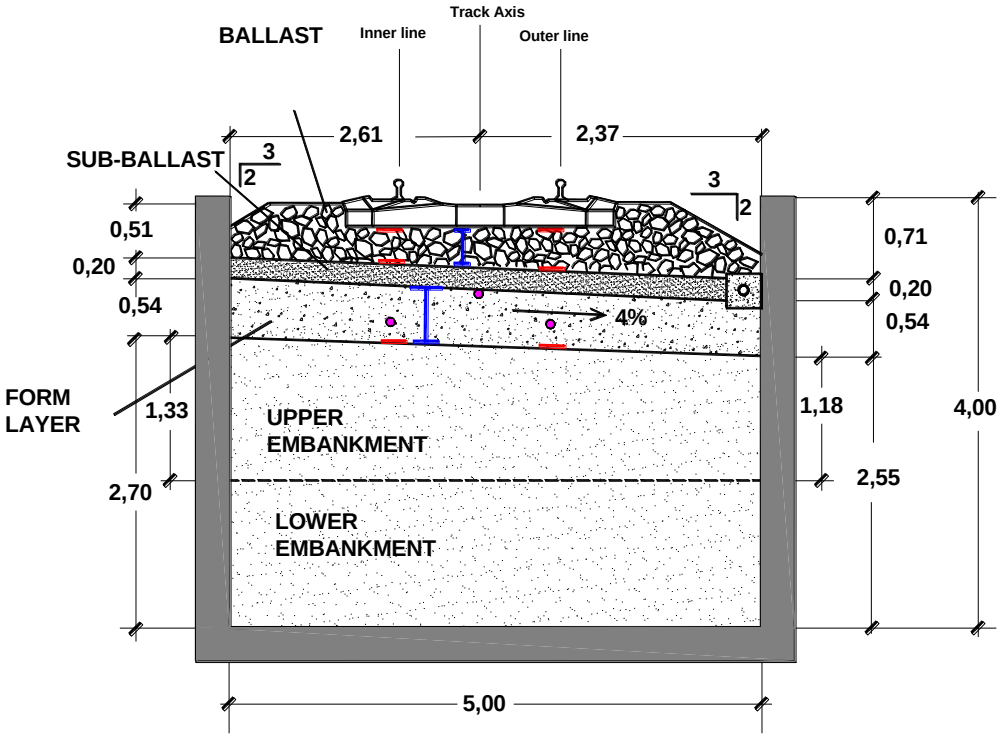

Figure 32: Cross section used in the present study

The 1:1 scale model constructed (Figure 32) is provided with: a rail gage of 1.435 m; a ballast thickness of 0.35 m under the inner rail and 0.40 m below the outside rail; a granular suballast layer of 0.20 m thickness with an inclination of 4% towards the outside and a form layer with the same inclination and a thickness close to 0.55 m. Ballast was compacted in two layers: 0.20 m thick each one under the outer rail; and 0.20 m thick the lower one and 0.15 m thick the upper one under the inner rail.

FIGURE 33: BALLASTED TRACK PREPARED FOR THE VHST TESTS

The characteristics of the different components of both the superstructure and infrastructure of the model are identified in the following paragraphs:

- Rails: They are of the 60 E1 type. They have a mass per unit length of 60 kg/m and a flexural stiffness EI of 6.4155 MN·m2.
- Sleepers: They are mono-bloc concrete pre-stressed units of the AI-04 EA UIC 60 type. Their average weight is 3.44 kN and have a length of 2.60 m, widths of 0.22 m at the centre and 0.30 m at the edges and heights of 0.21 m at the centre, 0.23 m at the edges, 0.245 m at the rail inside and 0.269 m at the rail outside.
- Fastening system: Normal Voslogh standard System with pad stiffness of 100 kN/mm with secant 20-95 kN.
- Ballast: Ballast layer is made up of andesite particles having the size distribution indicated in Figure 34.

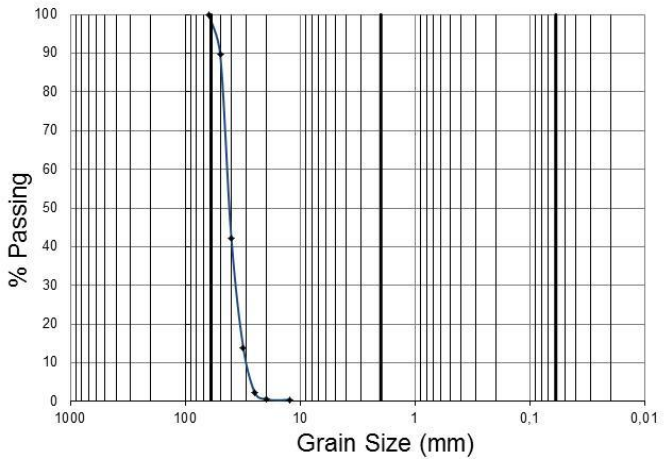

FIGURE 34: BALLAST GRAIN SIZE DISTRIBUTION CURVE

The ballast material came from the same quarry as the one described in Table 2 and it can be classified, according to EN 13450:2003, as class A (ADIF first class T1 type). From the results obtained with three ballast samples in the CGL X ray difractometer, the following mineralogical composition has been identified: 62% plagioclase (andesite); 14% quartz; 8% potasic feldespats; 6% biotite; 6% clorite; 4% hornblend and 4% others.

- Subballast: the subballast layer in CTB model has a thickness of 0.20 m and a gradient of 4% from the inner edge of the track to the outer edge as it can be observed in Figure 32. Its grain size distribution curve is given in Figure 35. It can be classified as GW (well-graded gravel with sand) according to the Unified Soil Classification System. Its maximum dry density, once corrected the Modified Proctor value to take into account the percentage of particles larger than 3/4", has been 2.18 Mg/m^3. The material was compacted to a dry density of 2.06 Mg/m^3 with a water content of 6.45%. The estimated shear wave velocity is 250 m/s.

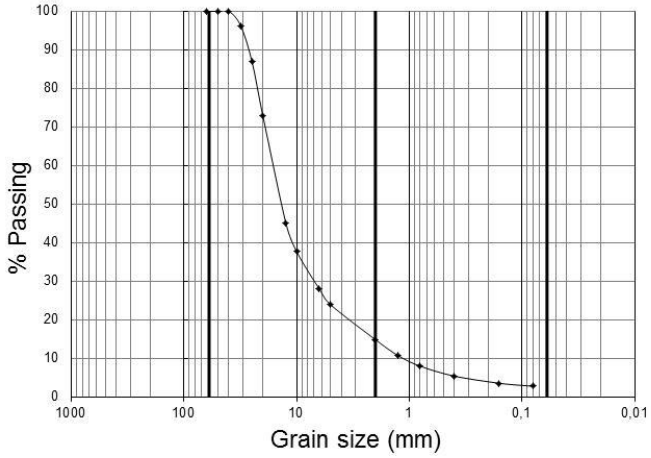

FIGURE 35: SUBBALLAST GRAIN SIZE DISTRIBUTION CURVE

- Form layer: The form layer has a mean thickness of 0.54 m. According to its grain size distribution curve (shown in Figure 36) it can be classified as GW (well-graded gravel with sand). Its dry density determined in situ by nuclear methods is 2.15 Mg/m^3. The shear wave velocity obtained by using the SASW technique is 400 m/s.

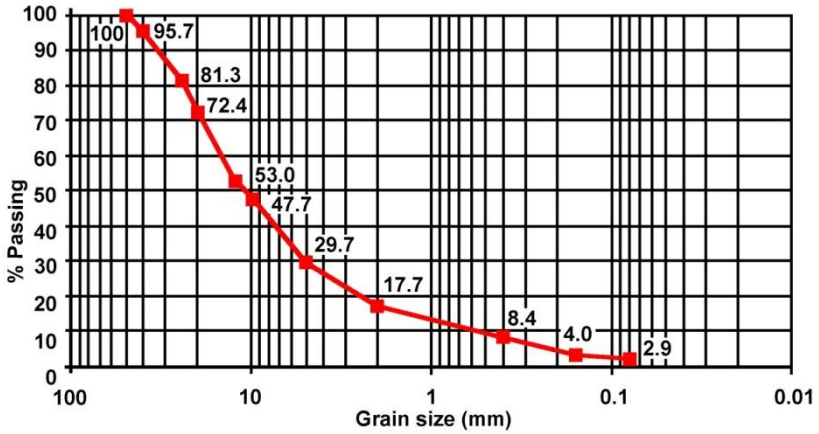

FIGURE 36: FORM LAYER GRAIN SIZE DISTRIBUTION CURVE

- Upper and lower embankment: The embankment existing in CTB model is constituted of an upper SC (clayey sand) layer with a mean thickness of 1.255 m (see Figure 32) and a lower GC (clayey gravel) layer 1.35 m thick. The grain size distribution curves of both layers are presented in Figure 37.

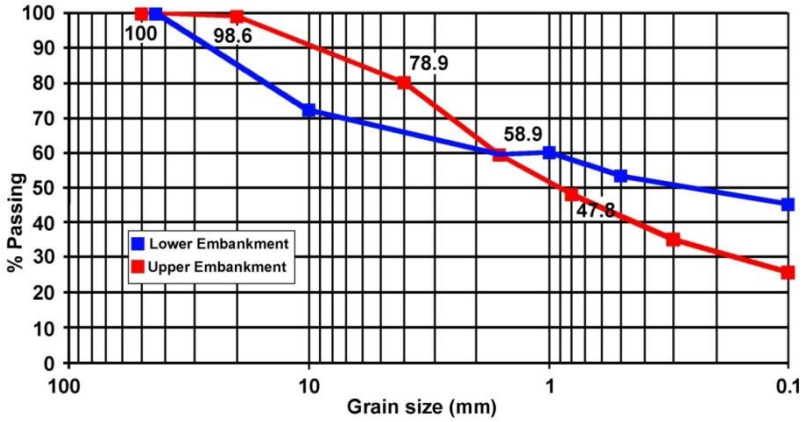

FIGURE 37: EMBANKMENT GRAIN SIZE DISTRIBUTION CURVE

The upper embankment layer is an intermediate plasticity layer with a Liquid Limit of 45.5% and a Plasticity Index of 32.7% that was compacted 5 years ago to a dry density of 17.5 Mg/m^3 with a water content of 10%. At that time a shear wave velocity of 200 m/s was found.

The lower embankment layer is a low plasticity layer with a Liquid Limit of 25.6% and a Plasticity Index of 7% in which a dry density of 21.2 Mg/m^3 and water content of 2% were determined 5 years ago. At that time a shear wave velocity of 300 m/s was determined.

Some loose of water content and an increase of the shear wave velocity can be expected in these materials, although it does not have any influence in the global mechanic behavior of the layers.

4.2 SENSOR SYSTEMS

Besides the displacement and force transducers of the CTB loading system, the rest of sensors to be deployed in CTB testing zone will have been aimed to the measurement of the absolute and relative displacements of the track components in the static tests and to the evaluation of the amplitude of displacements, velocities and accelerations induced in those components by the pass-by of trains at speeds up to 400 km/h.

Two different systems will be described:

- External system: constituted by a set of around 40 sensors providing absolute and relative displacements of rails, rail-sleeper pads and sleepers in the static tests and the amplitude of displacements, velocities and accelerations of those elements under the pass-by of simulated trains in the quasi-static tests.
- Internal system: made up of 40 sensors placed in the track bed layers (ballast, and subballast), form layer and embankment to play the same roles that the external sensors in the track superstructure elements. Furthermore, some ballast particles instrumented with accelerometers inside will be placed in some points of the railway track to measure the accelerations in the ballast layer.

4.2.1 EXTERNAL SYSTEM

The type, number and distribution of sensors to be used will be a typical distribution of the ones used in CTB in previous tests and it will be very similar to the one used in the in-situ test campaigns, described in Appendix 8.2 of Deliverable D.12.1. It will consist on the following sensors, whose photographs are collected in Figure 38:

- Laser systems.
- Rail-pad resistivemeters.
- Rail 2 Hz geophones.
- Sleeper 1 Hz geophones.
- Rail ±50·g accelerometers.
- Sleeper ±10·g accelerometers.

Laser displacement sensors

Rail pad resistivemeters

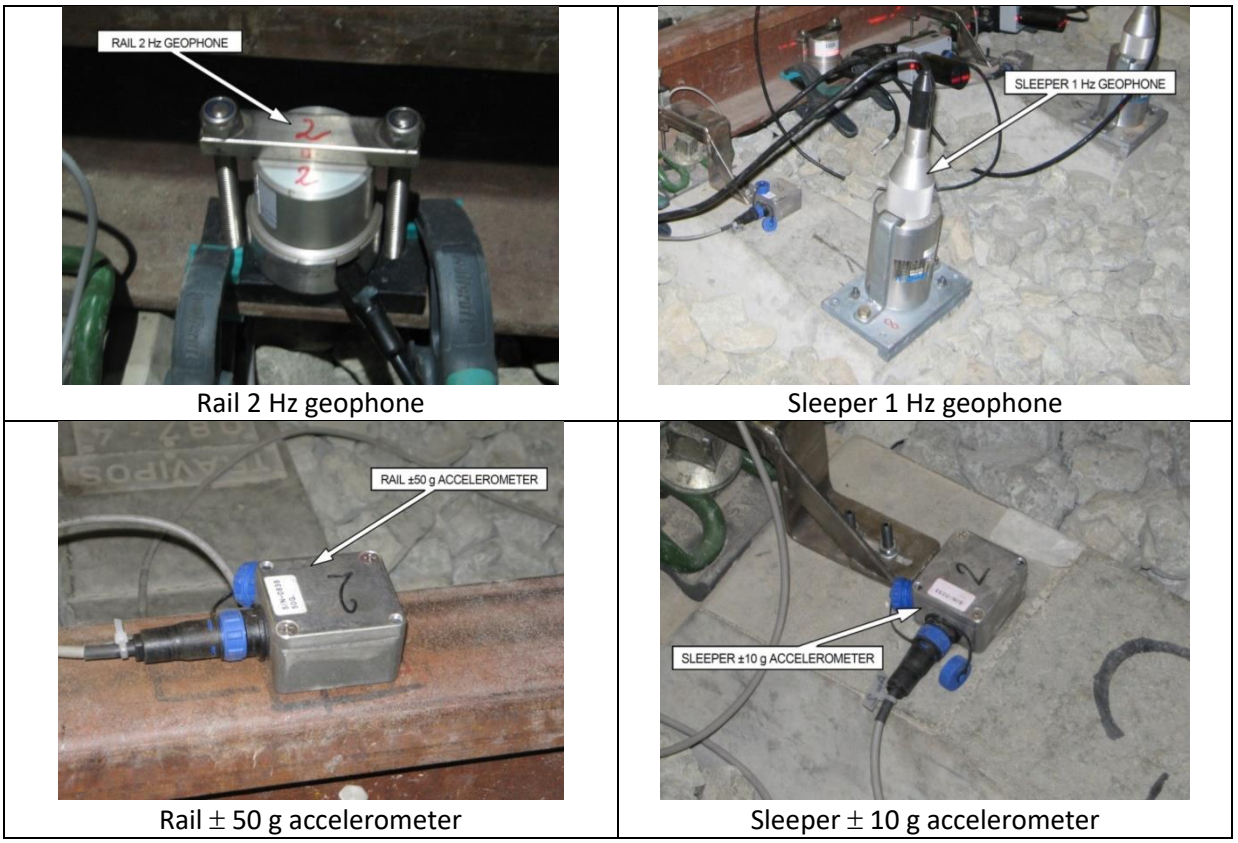

Rail 2 Hz geophone | Sleeper 1 Hz geophone

Rail ± 50 g accelerometer | Sleeper ± 10 g accelerometer

FIGURE 38: SENSORS TO BE USED IN THE MODEL INSTRUMENTATION

4.2.2 INTERNAL SYSTEM

The internal sensors have been distributed along the embankment and the other bed track layers, as shown in Figure 39.

The instrumentation installed consisted of some geophones and accelerometers. It is important to highlight the installation of some LVDT sensors to measure the ballast layer permanent settlements. The way they were mounted in ballast, attaching their heads to the sleepers and fixing their base to the top of the subballast layer can be seen in Figure 40.

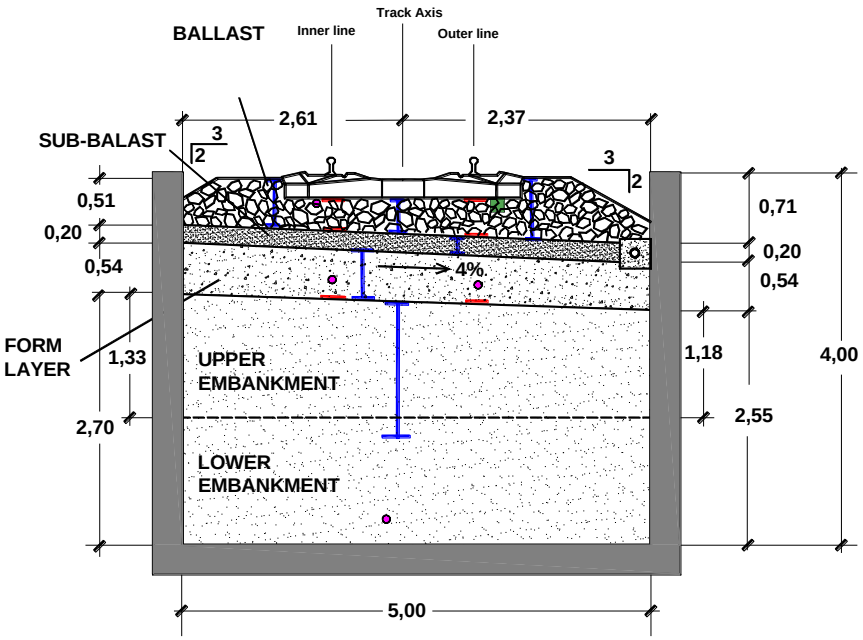

Symbol	Sensor Name
	Pressure cell
	Displacement transducer (LVDT)
	Geophone
	Acelerometer

FIGURE 39: INTERNAL SENSORS LOCATED IN THE CENTRAL CROSS SECTIONS (LENGTHS IN M)

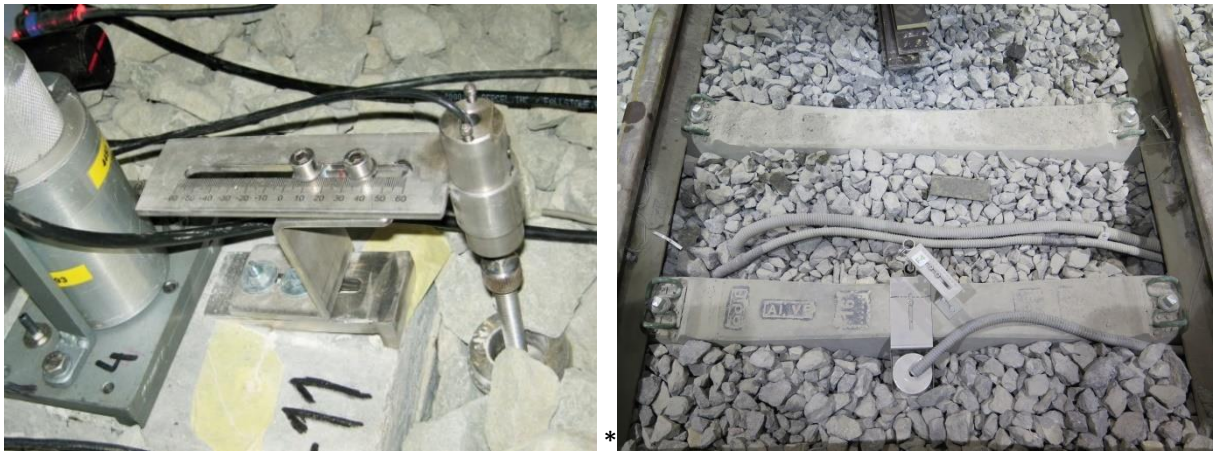

FIGURE 40: LVDT SENSOR HEAD ATTACHED TO ONE SLEEPER

5 Current test plan

5.1 Test description

The set of tests to be performed at CEDEX Track Box (CTB) began with the construction of an existing VHS track with similar characteristics to the one already in operation in the 'Madrid – Barcelona' line, as explained in Chapter 4. Figure 41 shows the existing railway track section in that line.

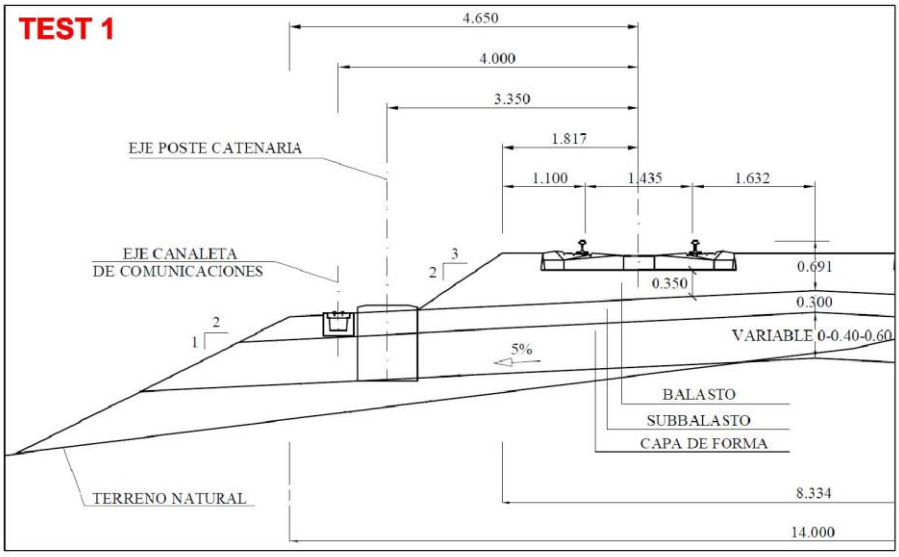

Figure 41: Existing railway configuration to be used in Test 1

The type of train to simulate in the actuators will be the Siemens S-103 and Talgo S-102, as they are the trains whose pass-by have been recorded in the in-situ test campaigns described in Appendix 8.2.

The tests to be performed in this stage will be the following:

- Test A: 300 km/h and 10^6 axles to study short and long term behaviour
- Test B: 320 km/h and 10^5 axles to study short term behaviour
- Test C: 360 km/h and 10^5 axles to study short term behaviour
- Test D: 400 km/h and 10^6 axles to study short and long term behaviour

After this, some new components will be implemented in the experimental track and the improved track will be tested in the same conditions as previous. Two setups are planned to test, as seen in Figure 42 and Figure 43:

- Test 2: Vossloh System with nominal stiffness 60 kN/mm (the secant will be 18-68 kN according to EN standard).
- Test 3: Vossloh System with nominal stiffness 60 kN/mm (the secant will be 18-68 kN according to EN standard) and USP with 0.3 N/mm³ bedding modulus.

Test 2: Implementation of a new rail pad (1st improved design)

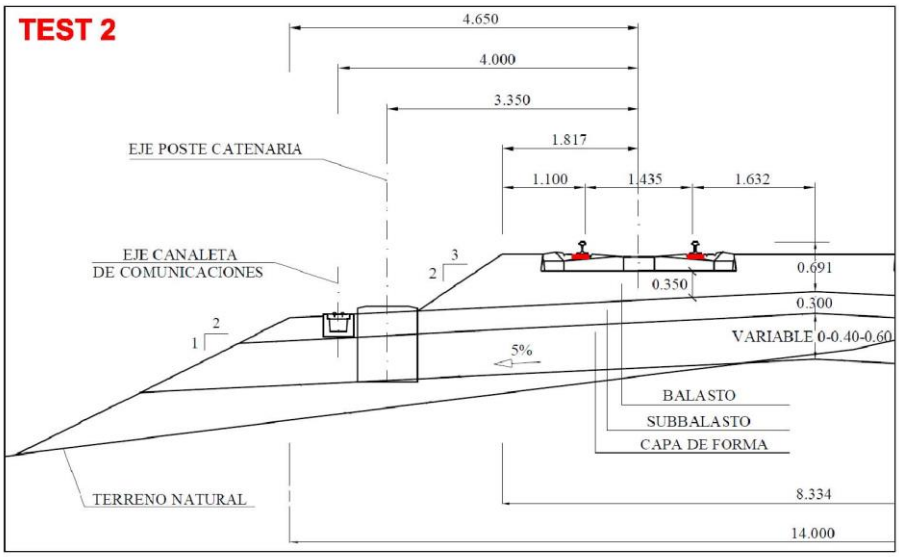

FIGURE 42: IMPLEMENTATION OF A NEW RAIL PAD (1ST IMPROVED DESIGN) TO BE USED IN TEST 2

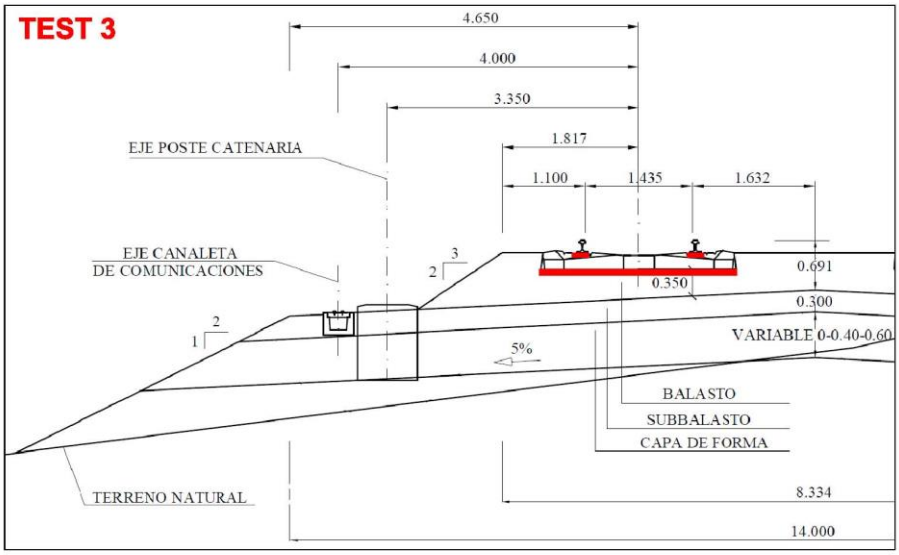

FIGURE 43: IMPLEMENTATION OF A NEW RAIL PAD AND UNDERSLEEPER PAD (2ND IMPROVED DESIGN) TO BE USED IN TEST 3

5.2 TEST RESULTS

The matrix of results from the tests will be processed to obtain the variations in the main parameters. The results will lead to conclusions that will help to analyse the very high speed system.

The track response will be measured in terms of:

- Displacements, with laser system and potentiometers.
- Speeds, with 2 Hz geophones and 1 Hz geophones
- Accelerations, with ±50·g accelerometers and ±10·g accelerometers

The measurements will be made at:

- Rail: with 2 Hz geophones and ±50·g accelerometers.
- Rail pad: with rail-pad potentiometers.
- Sleeper: with 1 Hz geophones and ±10·g accelerometers.

6 Summary

This report collects all the tasks carried out by CEDEX in the frame of Demonstrator 5.5 that was going to be performed in CEDEX Track Box (CTB) to analyze the railway track behaviour when subjected to the pass-by of VHST, at speeds up to 400 km/h, focusing the attention in the ballast degradation and in the design measurement to avoid that problem.

However, unfortunately during some maintenance works carried out in CTB, a problem in the hydraulic system was discovered. To solve the problem repair works were performed between September 2016 and January 2017, just the period previously scheduled for the performance of VHST tests, so the tests could not be performed.

During the time devoted to the repair works, CEDEX built the 1:1 scale model of a ballast track to perform the VHST tests. In a near future, CEDEX will perform the tests scheduled and distribute the results among the C4R community.

Collaborative project SCP3-GA-2013-60560

Increased Capacity 4 Rail networks through enhanced infrastructure and optimised operations

FP7-SST-2013-RTD-1

Deliverable 12.1

Innovative designs and methods for VHST (intermediate)

Appendix 8.2

In-situ test campaigns in Madrid-Barcelona HSL

Dissemination Level		
PU	Public	**PU**
PP	Restricted to other programme participants (including the Commission Services)	
RE	Restricted to a group specified by the consortium (including the Commission Services)	
CO	Confidential, only for members of the consortium (including the Commission Services)	

Lead contractor for this deliverable: ……CEDEX

Document status		
Revision	Date	Description
1	2016/03/15	First campaign
2	2017/09/20	Final Report
Reviewed	YES	

Table of contents

Abbreviations and acronyms

Abbreviation / Accronym	Description

1. Introduction

This document has been prepared in the frame of Task 1.2.2 “New track design and specifications for VHST (over 350 kph)” for the European collaborative project CAPACITY4RAIL of the 7th Framework Programme.

Task 1.2.2 is divided into two sub-tasks:

- Sub-Task 1.2.2.1. “Track design for VHST, transition zones, damping considerations and track irregularities”.
- Sub-Task 1.2.2.2. “Verification by full scale tests”.

In order to support these sub-tasks, two different field campaigns were carried out by CEDEX in two different sites of the High Speed Line Madrid-Barcelona:

- The first campaign was performed by CEDEX and ADIF on 1st and 2nd of November, 2015 at PK 72+200 of the abovementioned line and it is related with Sub-Task 1.2.2.1. The instrumentation was placed in the transition zone between the embankment and a short span bridge.
- The second campaign was made by CEDEX and ADIF to support Sub-Task 1.2.2.2 with real data. Data were collected on 1st of June, 2016 in the High Speed Line Madrid-Barcelona PK 74+233, a straight track section far from stations, tunnels and bridges, in which trains can travel at their maximum speed in this line (300 km/h).

Figure 1 and Figure 2 show photographs of the test site of first and second campaign, respectively.

The main objective of these in-situ campaigns was to create a database of the dynamic performance of the track when different trains pass by at high speed.

All the raw data recorded in this campaign are collected in Annex A.

This report performs an overview of the in-situ test campaigns carried out by CEDEX. Second chapter presents the general objectives of the work; third and fourth focus on the first and second campaign, respectively. These two chapters contain information related with the position of the installed sensors, the recorded trains, a description of the protocol used to analyze the signals as well as some examples of the results that can be obtained. Finally, a summary of the main results of both works are shown in Chapter 5.

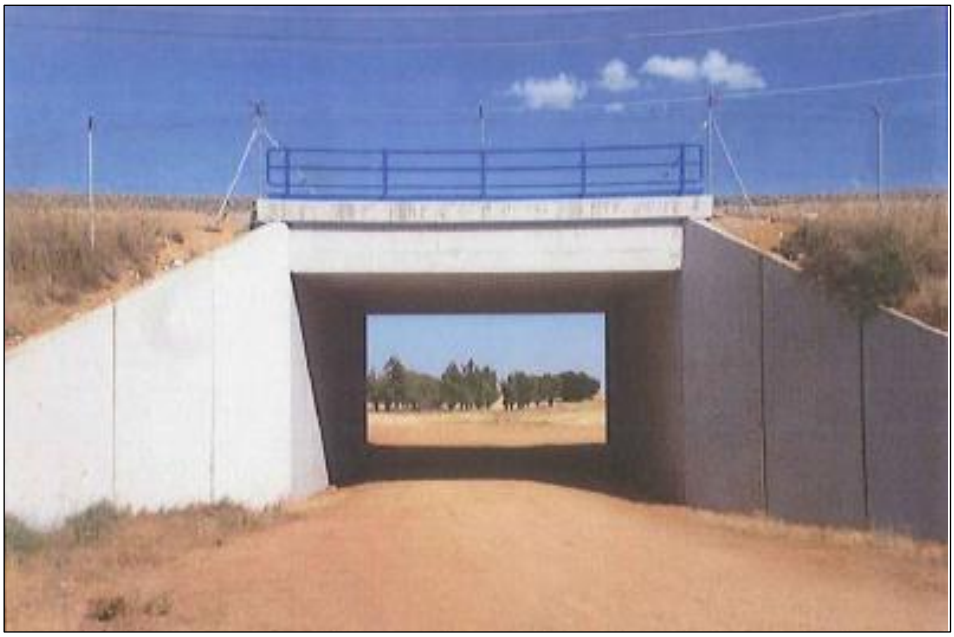

FIGURE 1: PK 72+200 - TRANSITION ZONE BETWEEN EMBANKMENT AND BRIDGE

FIGURE 2: PK74+233 - STRAIGHT TRACK SECTION

The characteristics of some of the track elements are given below:

Rail

- Profile Type: 60 E1.
- Grade: R260.
- Resistance: 880 N/mm2.
- Hardness: 260-300 hbw.
- Elemental rail bars length: 72 / 90 m.
- CWR (Thermit or Flash-butt welding)

Elastic Fastenings

- SKL-1 Tension Clamp
- Lightweight Angled Plate A-2 GFPR
- 7 mm Elastic Rail Pad (TPE, Stiffness k=100 kN/mm.).
- Anchor Dowel GFPR 6.6

Sleepers

- Prestressed/Poststressed Monoblock Concrete
- 2.600 x 300 x 242 mm.
- Weight: 315 kg per unit (with fastenings)
- Sleepers Spacing: 0,6 m.

Ballast (Type 1)

- 30-35 cm under bottom of the sleeper
- Size of particles: 32-50 mm diameter
- Los Angeles Wear Coefficient: 9-15%.

2. Objectives

The general goal of the in-situ campaigns, performed by CEDEX and ADIF, was to create a data base of the vibration measured in the track produced by trains passing-by.

The main specific objectives related with Task 1.2.2 are described in more detail below:

- Analyze the behavior of the transition between the structure and the embankment from the results obtained in the first campaign (PK 72+200, Nov.2015).
- Create a data base of different trains travelling at high speeds that can be used as a source to validate test results obtained in CEDEX Track Box. Instrumentation set used in the second campaign (PK 74+233, June 2016) is a typical configuration used in the Track Box.

3. First campaign (PK 72+00 / Nov. 2015)

3.1 INSTRUMENTATION

CEDEX´s principal objective in this field test campaign was to study the transition zone between the structure and the embankment. However, despite it is not the aim of this report, it must be mentioned that CEDEX also worked together with ADIF and INECO to install sensors in the bridge to study the dynamical effects in the structure due to the pass by of the trains. CEDEX has presented a report of this work in the frame of Task 1.2.3.

The sensors installed, whose positions are shown in Figure 3, Figure 4 and Figure 5, are the following:

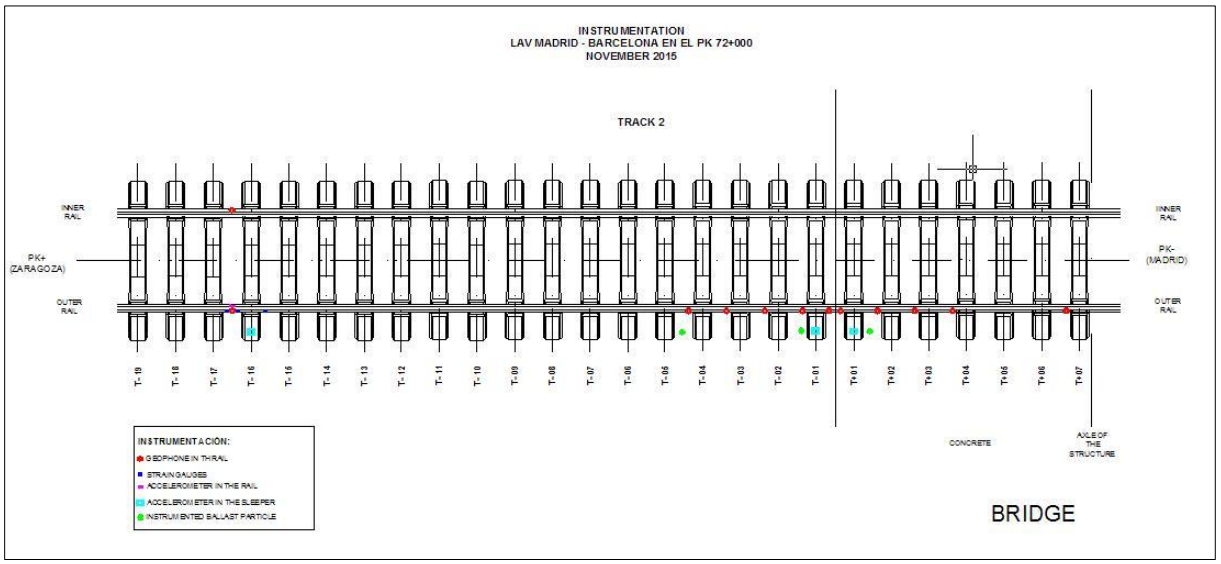

FIGURE 3: SKETCH OF THE INSTRUMENTATED SECTION

- Strain gauges (represented by dark-blue squares): the gauges were glued at the level of the neutral fibre of the rail in order to measure only shear strain. Loads were obtained using the pair placed at the span between two sleepers. The pair located at both sides of the sleeper can be used to calculate the reaction of the sleeper.
- 2Hz geophones (marked with red spots): they were installed in the rail and used to measure the velocity of the vibration in the rail produced by the trains pass-by. It is also possible to obtain the deflections by the integration of these velocity signals.
- Vertical accelerometer (shown with a fuchsia rectangle): they were stacked in the rail.
- Accelerometers (represented by light-blue squares): they were stacked in the outer side of the sleeper.

- Triaxial accelerometers installed inside different ballast particles (represented by green spots): these sensors were installed to analyse the behaviour of the structure and will not be discussed in this report.

Figure 4 and Figure 5 are zooms of the left and right side of Figure 3, respectively. Figure 4 shows the sensors installed at 10 m from the beginning of the bridge and Figure 5 shows the sleepers involved in the transition zone between the structure and the embankment. In both figures, the configuration of the instrumentation installed can be observed more clearly.

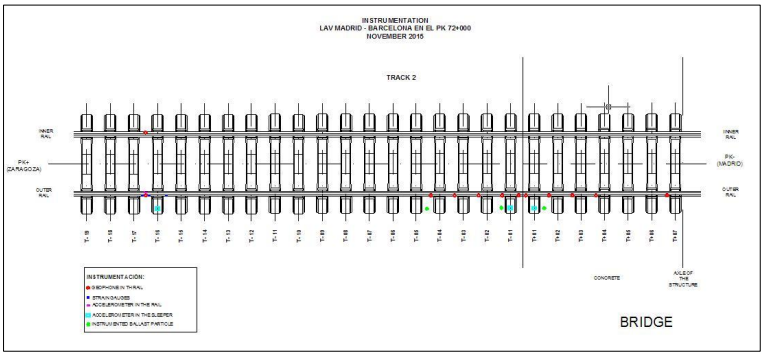

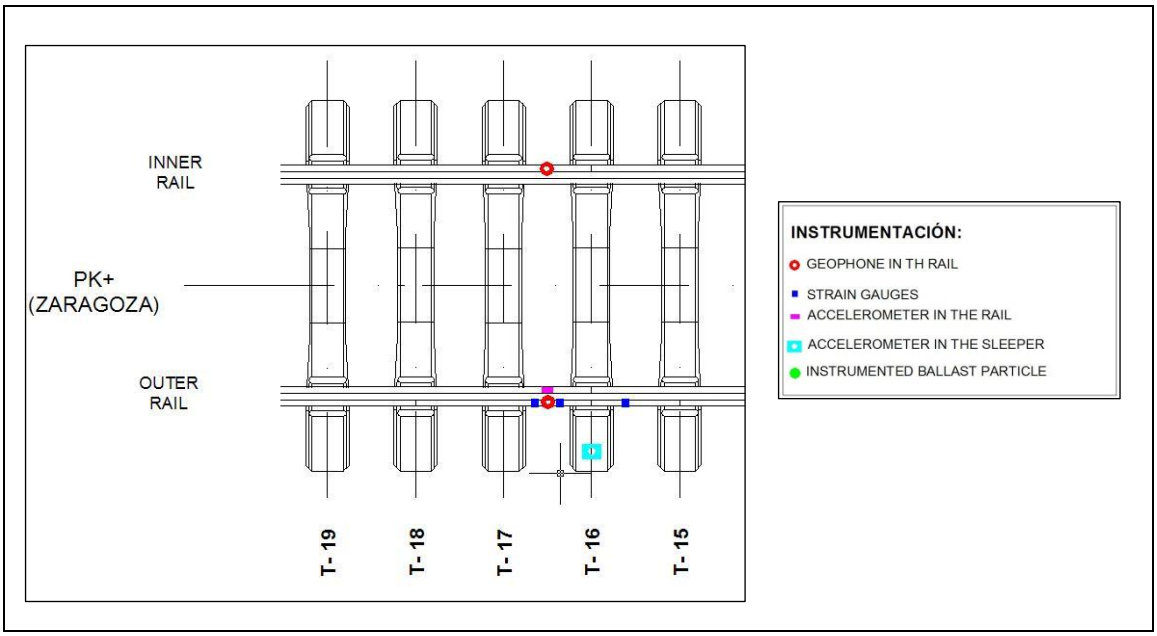

FIGURE 4: SKETCH OF THE INSTRUMENTED SECTION LOCATED AT 10 M FROM THE BRIDGE

Sleepers T-16 and T-17 are placed at the embankment, 10 m far away from the beginning of the bridge which begins between sleepers T+1 and T-1.

The instrumentation installed in this section of the test site consisted on:

- One accelerometer in the sleeper T-16.
- Another accelerometer stacked at the rail between sleepers T-16 and T-17.

- Three strain gauges and two geophones between T-16 and T-17, in the inner and outer rail. It was decided to measure the loads at that position in order to be a bit far away from the transition zone between the embankment and the bridge, trying to avoid possible anomalous effects due to the transition zone.

The deflection of the rail was obtained by the integration of the signal of the geophone placed between the strain gauges what makes it easy to calculate the track stiffness at that site. This measurement makes it possible to compare these results with others obtained in other sites studied before. The two geophones were installed, one in each rail, to determine the influence of the small curve existing at that point. The accelerometer in the rail offers redundant information as it is used to confirm the geophone measurements. The accelerometer in sleeper T-16 can be used to compare the accelerations measured in the bridge area.

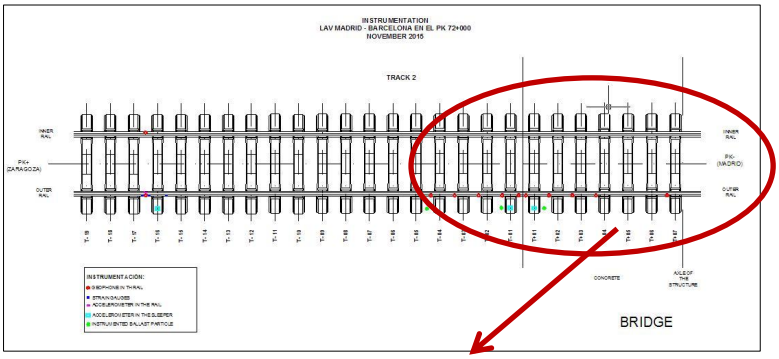

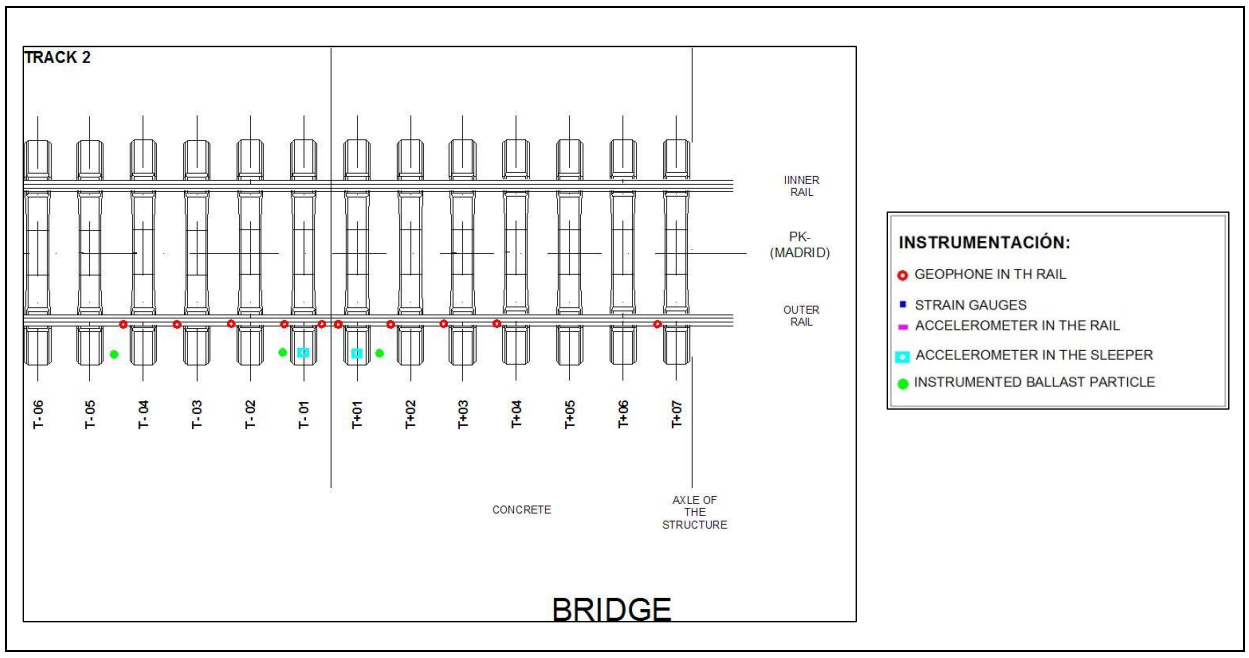

FIGURE 5: SKETCH OF THE INSTRUMENTED SECTION SITUATED IN THE TRANSITION ZONE AND ON THE BRIDGE

This sub-section contains the transition zone and the bridge. The bridge begins between T-1 and T+1, so sleepers at the right side are over the structure. The sleeper T+7 is situated at the central axle of the bridge.

The instrumentation installed consisted on:

- Ten geophones to study the vertical rail velocities and their variation along the transition zone and the bridge.
- Two accelerometers stacked at sleepers T-1 and T+1.
- Triaxial accelerometers installed inside different ballast particles. Those sensors were installed to analyse the behaviour of the structure and will not be discussed in this report.

In photographs of Figure 6 and Figure 7, the distribution of the sensors in each sub-section can be observed.

FIGURE 6: PHOTOGRAPH OF THE INSTRUMENTATION INSTALLED IN SLEEPERS T-16 AND T-17: SOME STRAIN GAUGES AND A GEOPHONE IN THE RAIL AND ONE ACCELEROMETER, IN THE LEFT SLEEPER

FIGURE 7: PHOTOGRAPH OF THE INSTRUMENTATION BETWEEN SLEEPERS T-5 AND T+7. GEOPHONE SPREAD IN THE RAIL CAN BE OBSERVED

3.2 RECORDED TRAINS

During the test campaign, eight trains were recorded:

- during the afternoon, six commercial trains that were currently operating in this track and
- during the night, two passes of a test train (AVRIL) that is able to reach velocities up to 350km/h.

Table 1 compiles information regarding the registered trains:

- The date and time (which is also the name of the file),
- the train type,
- the passing-by direction, and
- the speed.

As it can be observed in Figure 3, all the sensors were installed at Track 2, used by the trains travelling with direction to Madrid, because it was thought that the test train could reach the highest speed in that track, but unfortunately for different reasons it did not happen. It is important to take into account that, during the AVRIL test train passed-by in the two different directions, the general track behaviour can be different when the train passes from the bridge to the embankment than from the embankment to the bridge.

TABLE 1: RECORDED TRAINS

DATE & TIME	TRAIN TYPE	DIRECTION	SPEED (km/h) (±10km/h)
01/11/2015_17:20	Siemens S-103	Madrid	295
01/11/2015_18:07	S-120	Madrid	240
01/11/2015_18:31	Talgo S-102	Madrid	295
01/11/2015_18:34	Siemens S-103	Madrid	255
01/11/2015_18:46	Siemens S-103	Madrid	290
01/11/2015_19:19	Siemens S-103	Madrid	300
02/11/2015_02:12	Talgo AVRIL	Barcelona	310
02/11/2015_03:17	Talgo AVRIL	Madrid	310

3.3 SIGNAL ANALYSIS PROCEDURE

This subchapter describes the way to process the raw data for each kind of sensor. For all the time signals obtained, the first step is to calculate the Fast Fourier Transform (FFT) to visualize the frequency domain and then to decide the filter which must be applied in case it is necessary. In general for this kind of studies, the most used filter is the Low Pass Filter (LPF) which cuts off frequencies above the range of interest in each particular case.

3.3.1 VERTICAL ACCELEROMETERS

Four vertical accelerometers were installed: three stacked at different sleepers and one in the rail between the strain gauges, as seen in Figure 5 and Figure 4. FFT is calculated for each signal and then applied the appropriate LPF.

At a first sight, when looking at raw accelerograms, it was not possible to see the influence of the wheel loads in the rail or in the sleeper due to the presence of a high noise, but using a 250 Hz Low Pass Filter (LPF) the signals revealed that influence. As examples, Figure 8 shows the signal of the accelerometer placed in the rail and Figure 9 the one placed in a sleeper, for the second pass of the AVRIL test train. The peaks in the green lines represent the accelerations produced by the wheel passing-by.

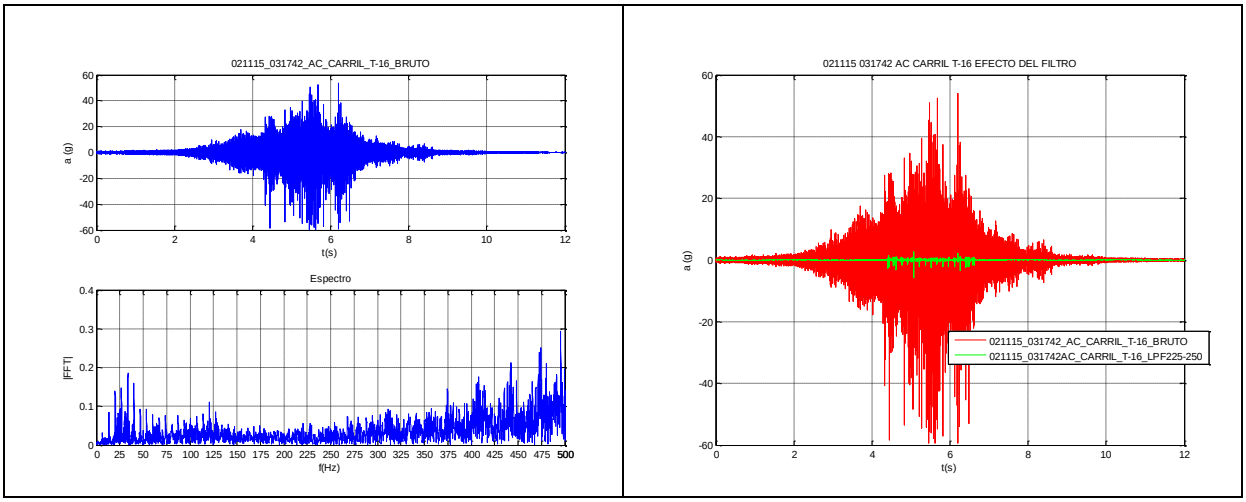

FIGURE 8: RAIL ACCELERATION FOR THE AVRIL TRAIN AT 03:17. LEFT: RAW SIGNAL AND SPECTRUM. RIGHT: EFFECT OF APPLYING A 225 HZ LPF

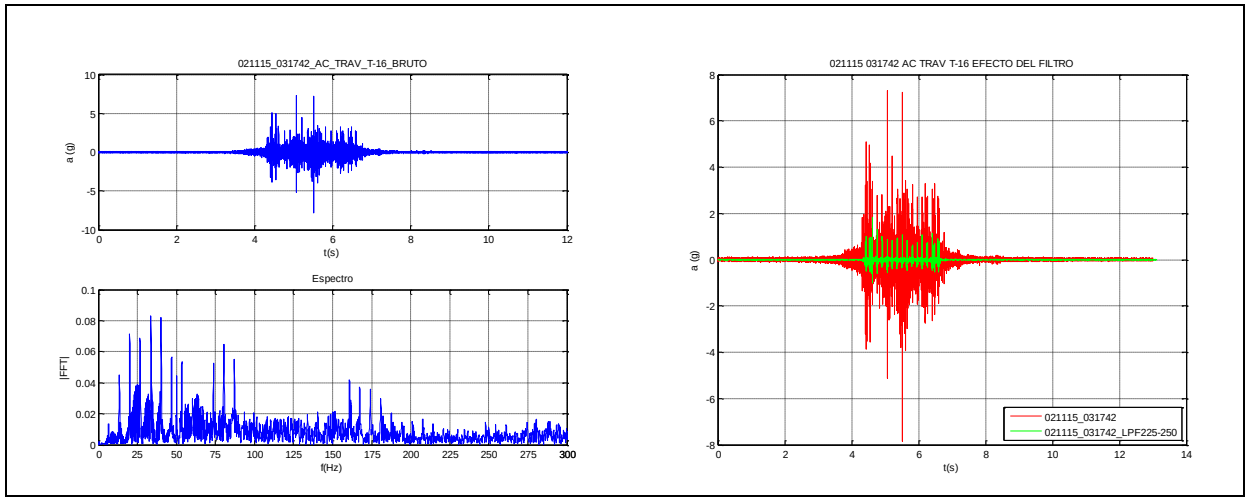

FIGURE 9: T-15 SLEEPER ACCELERATION FOR THE AVRIL TRAIN AT 03:17. LEFT: RAW SIGNAL AND SPECTRUM. RIGHT: EFFECT OF APPLYING A 225 HZ LPF

Once filtered, Figure 10 and Figure 11 show, respectively, the data of the accelerometer placed in the rail for the AVRIL test train that passed at 02:12 and the different filtered signals obtained with the accelerometers placed in the sleepers.

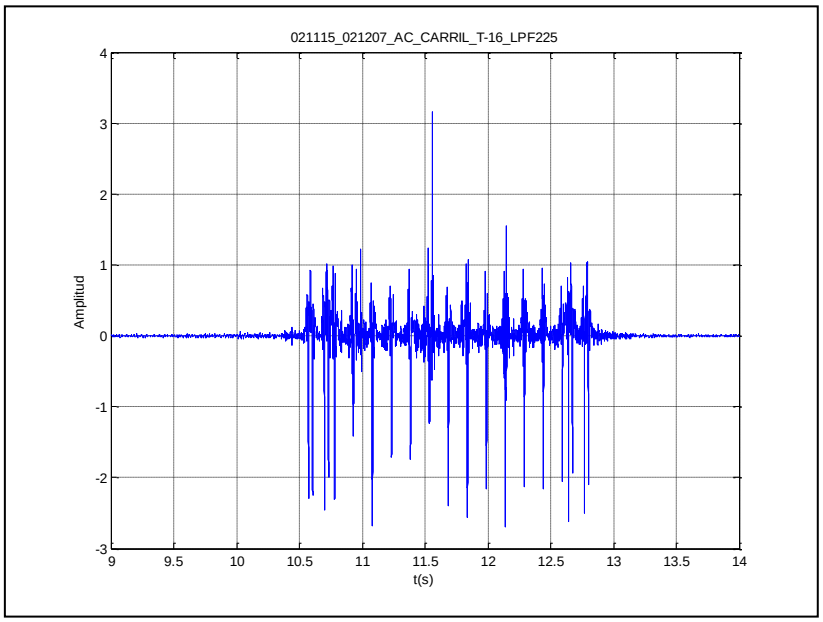

FIGURE 10: FILTERED SIGNAL OF THE VERTICAL ACCELEROMETER IN THE RAIL (TEST TRAIN AT 02:12)

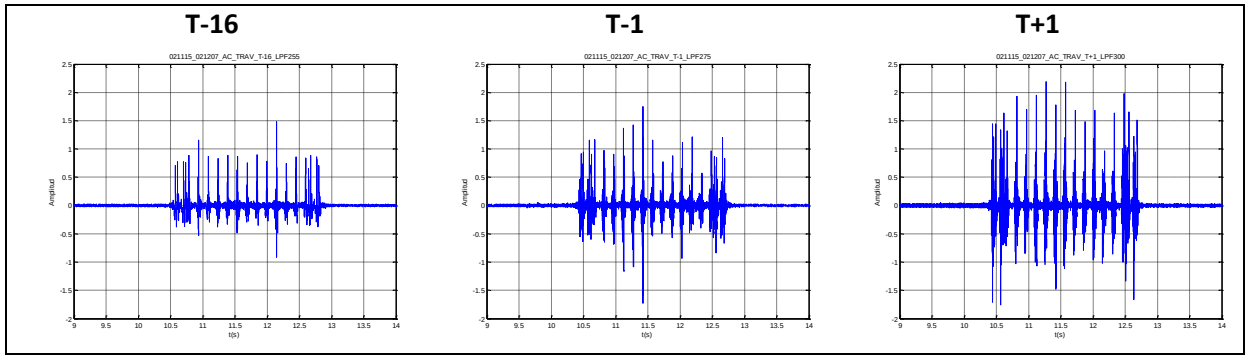

FIGURE 11: FILTERED SIGNALS OF VERTICAL ACCELEROMETERS INSTALLED IN DIFFERENT SLEEPERS (TEST TRAIN AT 02:12)

As it will be shown later, the rail acceleration can be integrated to obtain the rail velocity and then compared it with the velocity signal obtained with the geophone placed at the same position (Figure 13).

3.3.2 GEOPHONES

The same procedure applied to the accelerometers was used to analyse the geophones. First FFT was calculated for each signal and then the appropriate LPF was applied. Furthermore it was possible to integrate the geophone signals to obtain rail deflections. This is particularly important for the geophone placed in the outer rail between the strain gauges in T-16 - T-15, because it will be used to obtain the track stiffness.

Figure 12 shows an example of the velocity values obtained in different positions: in the first row the geophones situated in sleeper T-16 (10 m from the bridge) are displayed; in the second row those placed in the embankment and in the third one, those installed on the structure. Same scale has been used in all graphs.

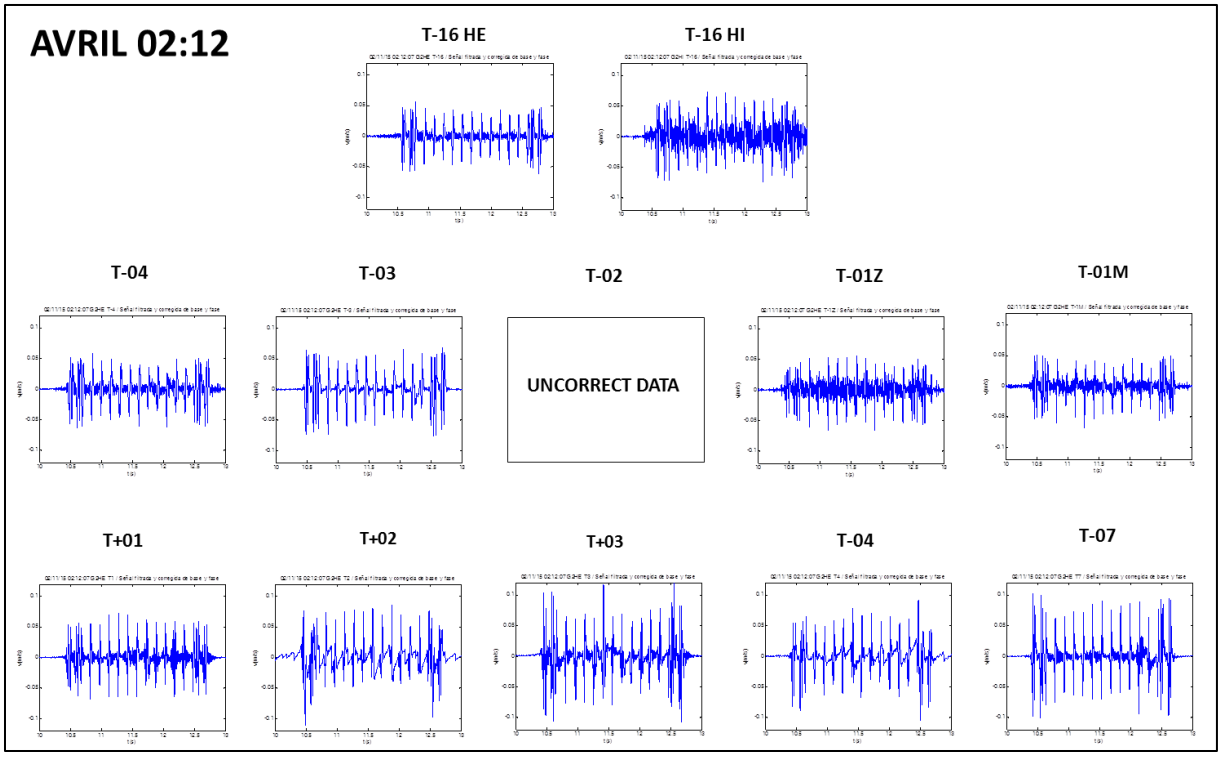

FIGURE 12: VELOCITIES REGISTERED WITH GEOPHONES SITUATED IN DIFFERENT POSITIONS (AVRIL TEST TRAIN AT 02:12

Figure 13 shows the velocity signal obtained directly with a geophone and the calculated one by the integration of the acceleration obtained with an accelerometer placed at same site. Once compared, it can be seen that both signals are quite similar.

On other hand, the deflection obtained integrating the geophone velocity signal can be observed in Figure 14.

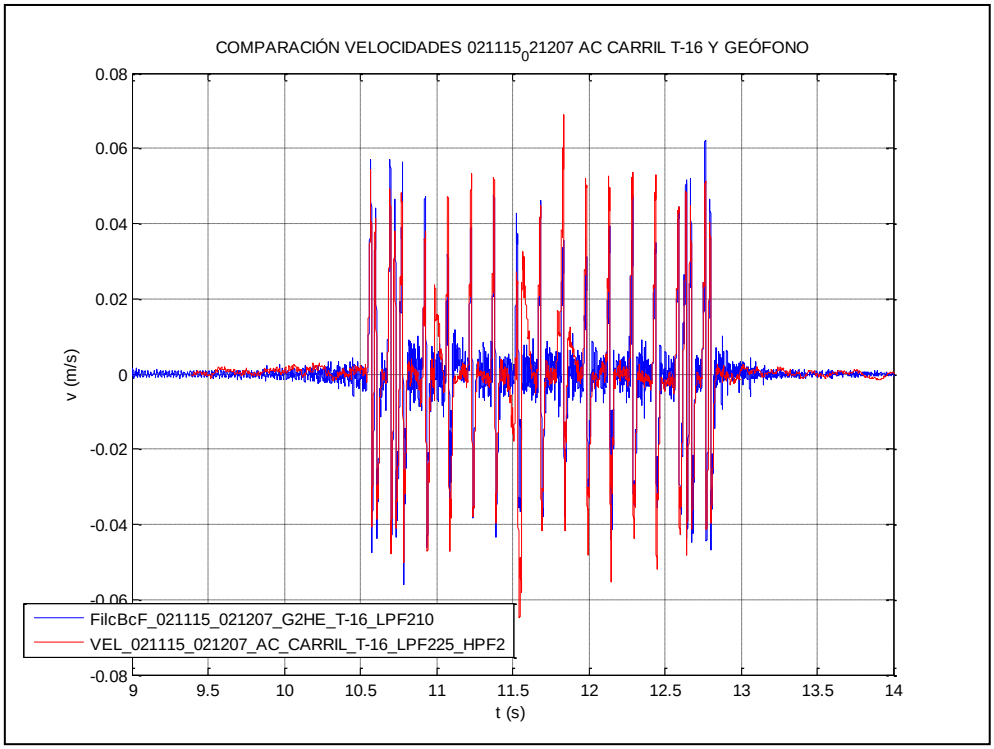

FIGURE 13: COMPARISON OF THE VELOCITIES OBTAINED DIRECTLY BY THE GEOPHONE AND THE INTEGRATED SIGNAL OF THE ACCELEROMETER; BOTH SENSORS PLACED BETWEEN THE STRAIN GAUGES IN THE OUTER RAIL T-16 T-15 (AVRIL TRAIN AT 02:12)

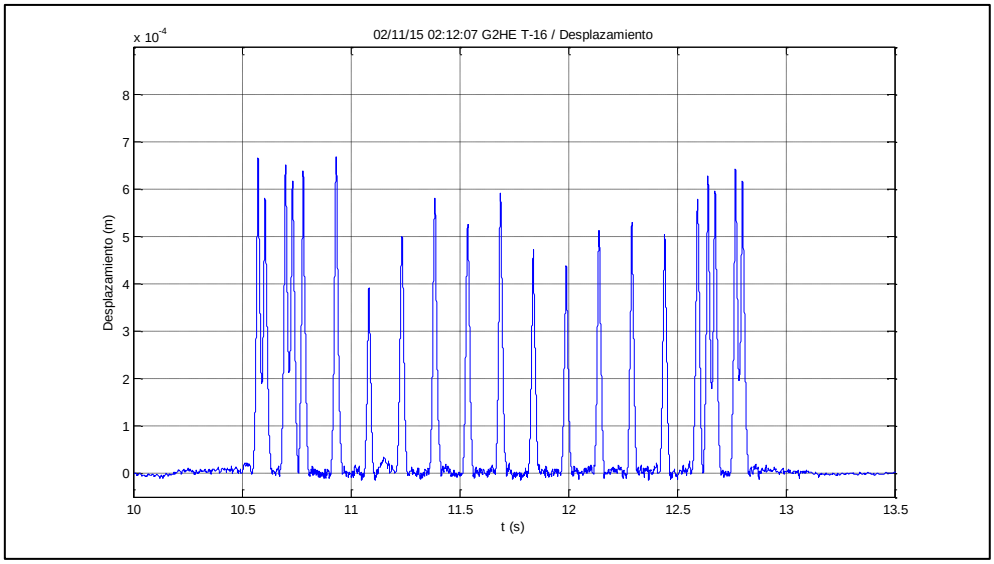

FIGURE 14: RAIL DEFLECTIONS OBTAINED FROM THE INTEGRATION OF THE VELOCITY REGISTERED BY THE GEOPHONE PLACED BETWEEN T-16 T-15 IN THE OUTER RAIL (AVRIL TRAIN AT 02:12). DESPITE RAIL MOVEMENT IS DOWNWARDS, THE PEAKS ARE PRESENTED AS POSITIVE

3.3.3 LOADS

The measurement of wheel loads were made, as sketched in Figure 15, by finding the difference between the two shear forces induced in two points of the rail, situated 0.30 m apart between two consecutive sleepers, by a travelling wheel passing over them.

First the shear stress is calculated multiplying the microstrain values recorded by the strain gauges by a constant that depends on the geometry of the rail. In this case the constant is:

$$k = (2 * 10^6 * 0.17344)\frac{kN}{\mu\varepsilon} = 346880\ \frac{kN}{\mu\varepsilon}$$

After that, the FFT of the signal is calculated and the appropriate filter is applied. Finally, the shear forces values are subtracted to obtain the load. The process to obtain the load values is described in INNOTRACK project report 1 and more detailed in Moreno, J, et al.2.

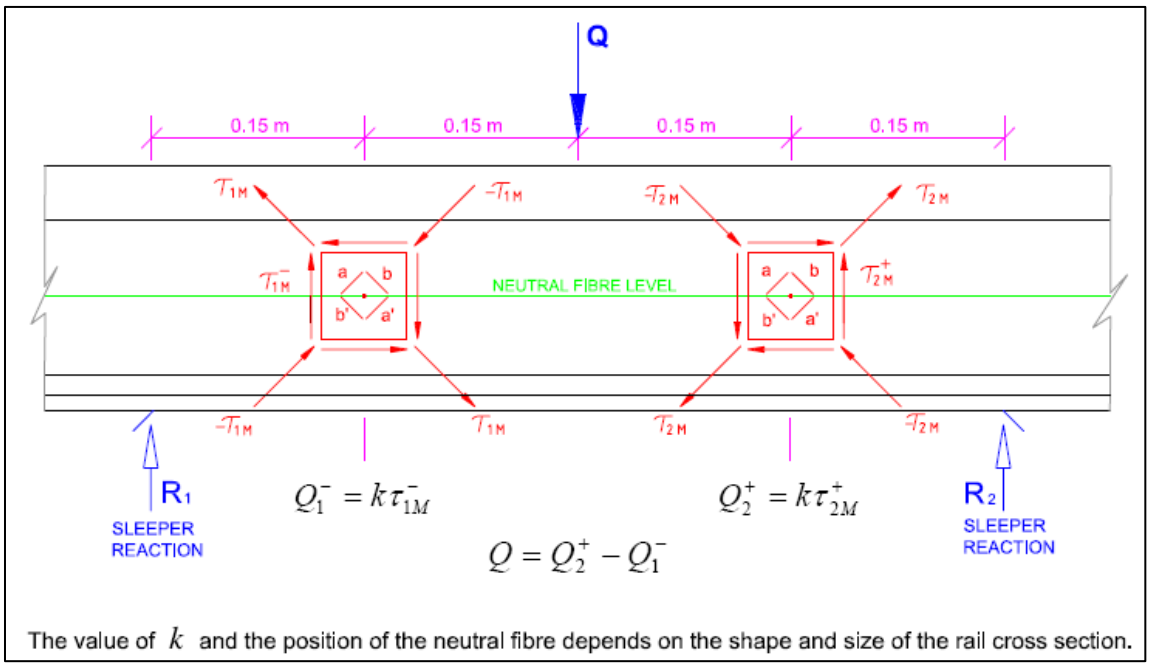

FIGURE 15: SCHEMATIC ARRANGEMENT OF STRAIN GAUGE GRIDLINES FOR MEASURING WHEEL LOADS

Figure 16 is an example of the load time history obtained for the AVRIL test train that passed at 02:12.

[1] INNOTRACK (2009). Study of variation of vertical stiffness in transition zone. Final Report coordinated by UIC under contract TIP-CT-2006-031415 for the 6th Framework Programme of the European Commission, CEDEX, Madrid.
[2] Moreno, J., Garcia de la Oliva, J.L. (2012). Determinación de las cargas aplicadas al carril mediante bandas extensométricas. Ingeniería Civil, 165, pp. 123-129.

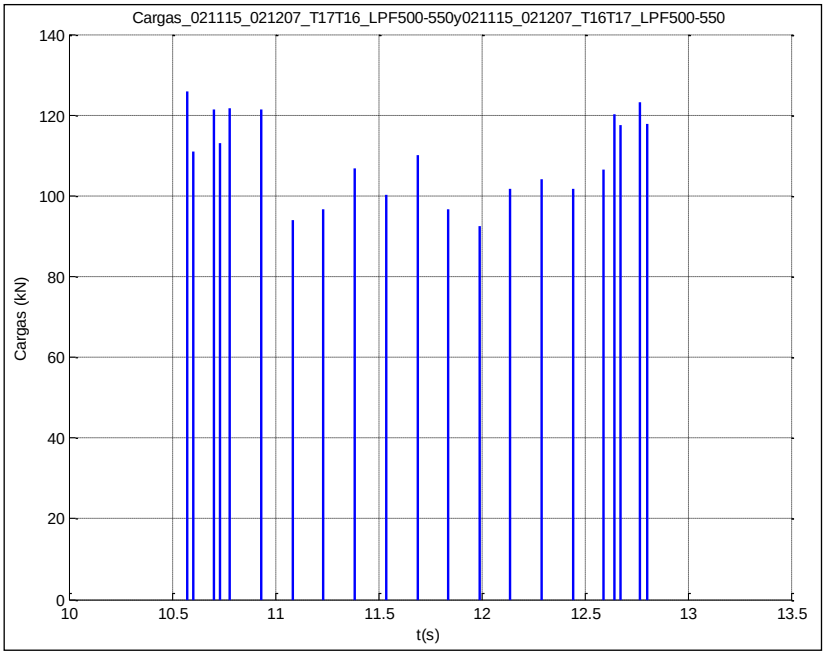

FIGURE 16: LOAD CALCULATED SIGNAL (AVRIL TEST TRAIN AT 02:12)

Another important aspect to comment is that sometimes, in the calculation of the deflection values (according to 3.3.4), only some displacement picks are considered. This is due to, that at the end of the integration process, some picks corresponding to some axles are clearly distorted so they should be disregarded in the track stiffness calculation.

Figure 17 shows two cases: first a deflection graph with a very good result; and below another deflection graph that presents anomalous picks (the picks considered in track stiffness calculations are marked in red).

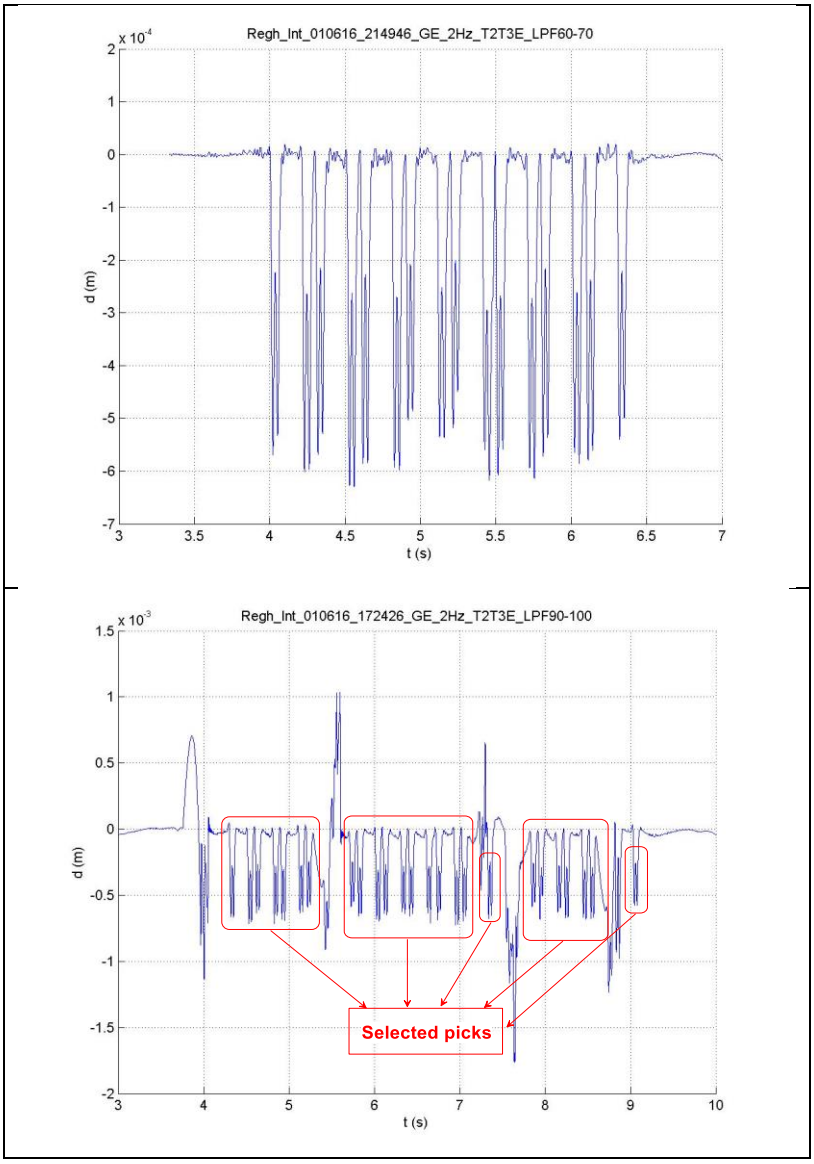

FIGURE 17: RAIL DEFLECTION OBTAINED FOR TWO DIFFERENT CASES: IN THE GRAPH ON THE TOP ALL THE PICKS CAN BE USED IN THE CALCULATIONS WHILE, IN THE BOTTOM GRAPH, ONLY THOSE MARKED IN RED AS THE REST APPEAR DISTORTED

Finally, with the results of loads and rail displacement, the values of track stiffness are calculated for the trains analysed.

3.3.4 TRACK STIFFNESS

Railway track stiffness (understood as vertical track load divided by track deflection) is a basic parameter of track design which influences, inter alia, the dynamic behavior of passing vehicles, the track geometry quality and the life of track components. In a nutshell, the vertical track stiffness is a very important indicator of track condition.

One of the methods usually used to determine the railway track stiffness requires simultaneous measurements of the maximum vertical deflection of the rail under traffic loads and the corresponding loads. The procedure for measuring both the vertical rail deflection and the wheel load has been described above. Thus, the track stiffness is simply obtained as the rate between the calculated wheel load and the maximum vertical deflection induced in the rail, as shown in Figure 18.

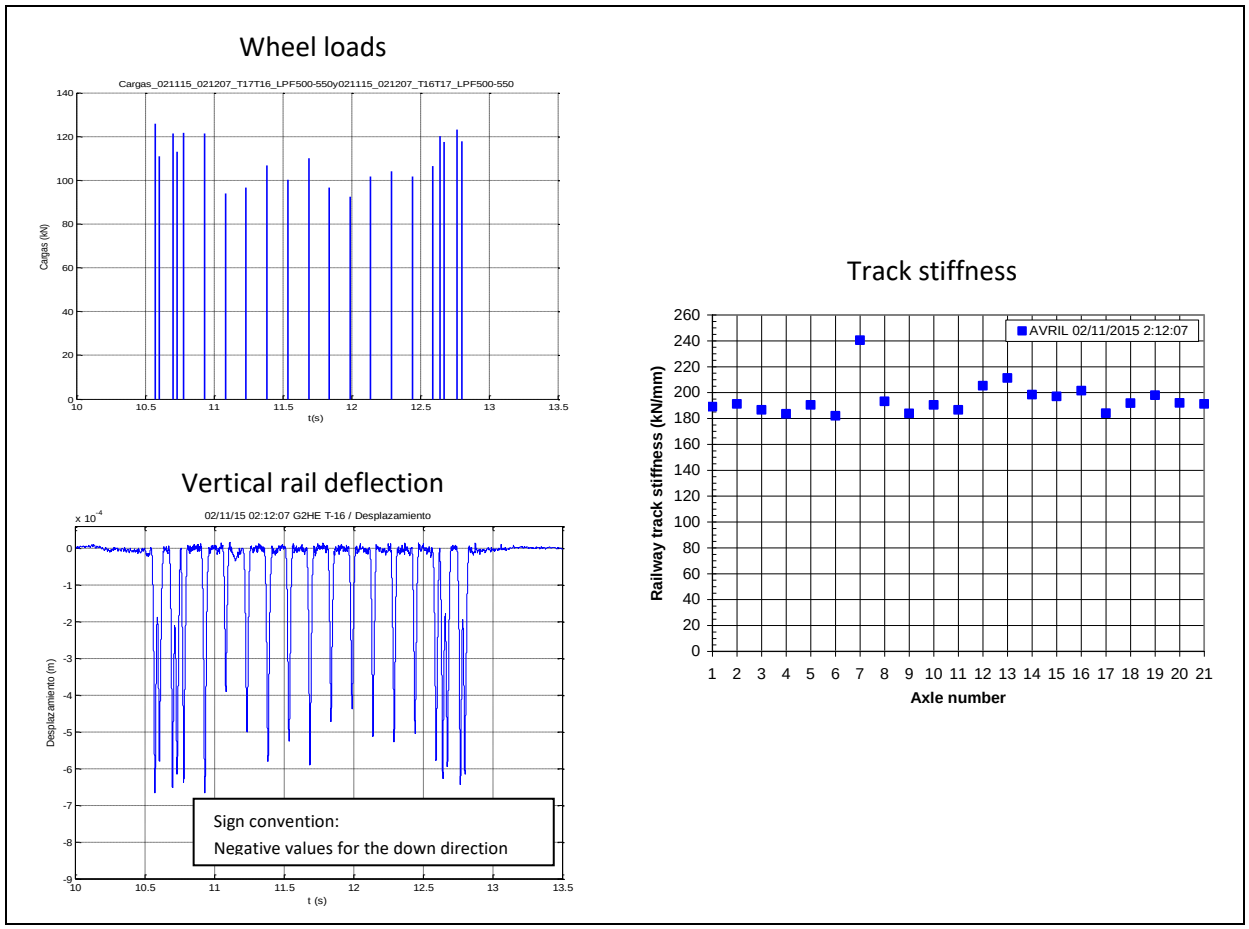

FIGURE 18: TRACK STIFFNESS (AVRIL TEST TRAIN AT 02:12) CALCULATED FOR EACH WHEEL. THE MEAN VALUE AND THE STANDARD DEVIATION HAVE ALSO BEEN OBTAINED

3.4 RESULTS

3.4.1 INTRODUCTION

This subsection contains a brief summary of the vibrations measured in the change between the bridge and the embankment and the ones measured at 10 m from the structure, as presented in Figure 3 to Figure 5. A more extended analysis is included in the report delivered by CEDEX in the frame of Task 1.2.3.

Results for vertical sleeper acceleration, vertical rail velocity and vertical rail deflection are summarized in the following sections 3.3.2 to 3.4.5. Table 2 and Table 3 collect the mean values and standard deviations of the maximum vertical peaks, and Figure 19 to Figure 23 show a representation of these values as a function of their location in the transition zone. Error bars in these figures are given by the standard deviations.

3.4.2 VERTICAL SLEEPER ACCELERATION

Table 2 shows the mean and standar deviation of the maximum vertical sleeper acceleration caused by the analyzed trains at sleepers T-16, T-01 and T+01.

TABLE 2: MEAN AND STANDARD DEVIATION OF THE MAXIMUM VERTICAL SLEEPER ACCELERATION CAUSED BY THE ANALYZED TRAINS AT SLEEPERS T-16, T-01 AND T+01

	Maximun peaks of sleeper acceleration (g)									
	TRAIN S-120 01/11/2015 18:07:06		TRAIN S-102 01/11/2015 18:31:57		TRAIN S-103 01/11/2015 18:34:53		TRAIN AVRIL 1 02/11/2015 2:12:07		TRAIN AVRIL 2 02/11/2015 3:17:42	
Outer rail, in region:	Mean	SD	Mean	SD	Mean	SD	Mean	SD	Mean	SD
Sleeper T+01	0,593	0,140	1,427	0,471	0,684	0,147	1,608	0,330	1,146	0,307
Sleeper T-01	0,650	0,163	0,901	0,092	0,726	0,165	1,043	0,261	1,052	0,193
Sleeper T-16	0,580	0,106	1,150	0,253	0,626	0,152	0,855	0,177	0,938	0,270

Table 3 shows the mean and standar deviation of the minimum vertical sleeper acceleration caused by the analyzed trains at sleepers T-16, T-01 and T+01.

TABLE 3: MEAN AND STANDARD DEVIATION OF THE MINIMUM VERTICAL SLEEPER ACCELERATION CAUSED BY THE ANALYZED TRAINS AT SLEEPERS T-16, T-01 AND T+01

	Manimun peaks of the vertical rail velocity (m/s)									
	TRAIN S-120 01/11/2015 18:07:06		TRAIN S-102 01/11/2015 18:31:57		TRAIN S-103 01/11/2015 18:34:53		TRAIN AVRIL 1 02/11/2015 2:12:07		TRAIN AVRIL 2 02/11/2015 3:17:42	
Outer rail, in region:	Mean	SD	Mean	SD	Mean	SD	Mean	SD	Mean	SD
Sleeper T+01	-0,366	0,085	-0,625	0,339	-0,426	0,133	-1,041	0,348	-0,575	0,178
Sleeper T-01	-0,314	0,104	-0,429	0,196	-0,274	0,071	-0,686	0,317	-0,425	0,104
Sleeper T-16	-0,301	0,069	-0,450	0,129	-0,284	0,067	-0,363	0,145	-0,429	0,164

Furthermore, Figure 19 and Figure 20 show the graphical representation of sleeper accelerations given in previous tables, for each sleeper.

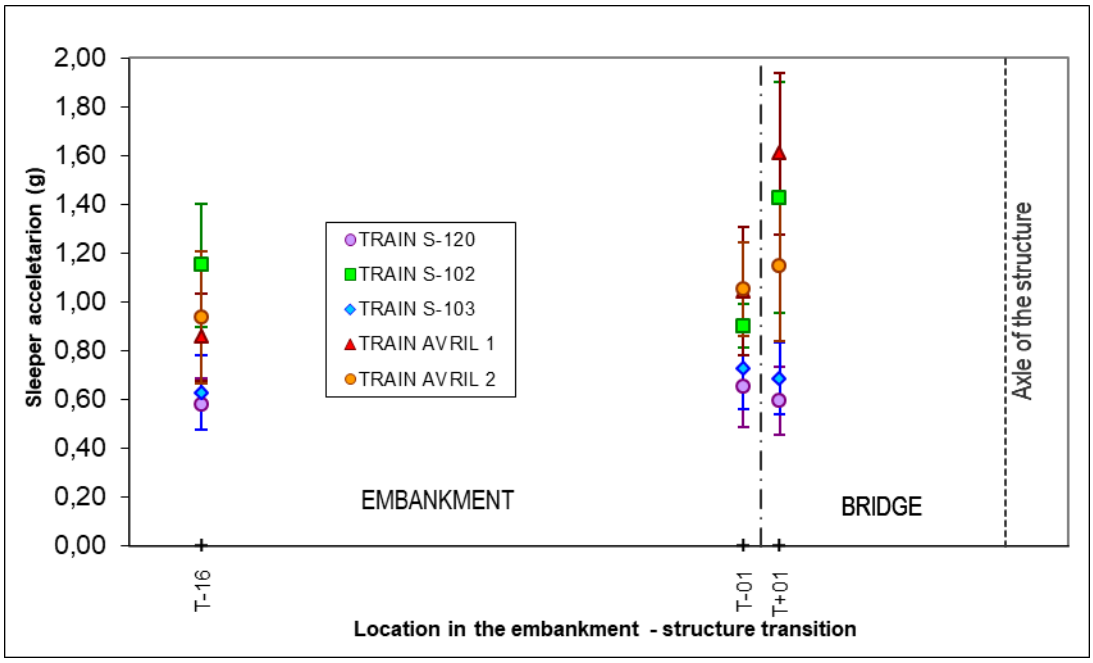

FIGURE 19: COMPARISON BETWEEN MEAN VALUES OF THE MAXIMUM VERTICAL SLEEPER ACCELERATION CAUSED BY THE ANALYZED TRAINS AT THE DIFFERENT INSTRUMENTED SLEEPERS: T-16, T-01, T+01

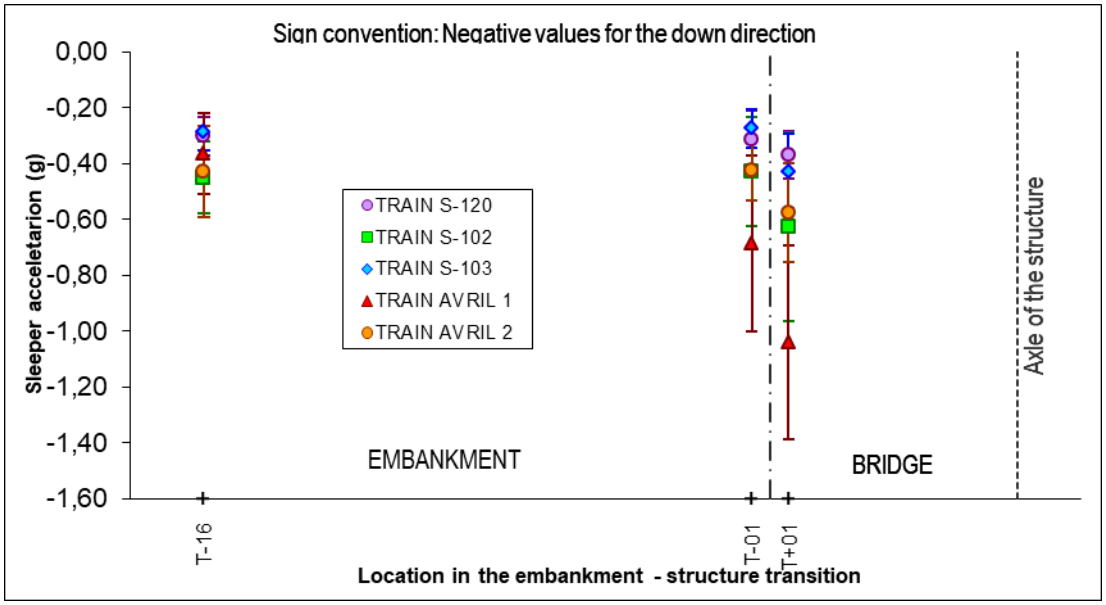

FIGURE 20: COMPARISON BETWEEN MEAN VALUES OF THE MINIMUM VERTICAL SLEEPER ACCELERATION CAUSED BY THE ANALYZED TRAINS AT THE DIFFERENT INSTRUMENTED SLEEPERS: T-16, T-01, T+01

3.4.3 VERTICAL RAIL VELOCITY

Table 4 shows the mean and standar deviation of the maximum vertical sleeper velocities caused by the analyzed trains in different regions of the embankment – structure transition.

TABLE 4: MEAN AND STANDARD DEVIATION OF THE MAXIMUM VERTICAL RAIL VELOCITIES CAUSED BY THE ANALYZED TRAINS IN DIFFERENT REGIONS OF THE EMBANKMENT – STRUCTURE TRANSITION

	Maximun peaks of the vertical rail velocity (m/s)									
	TRAIN S-120		TRAIN S-102		TRAIN S-103		TRAIN AVRIL 1		TRAIN AVRIL 2	
	01/11/2015	18:07:06	01/11/2015	18:31:57	01/11/2015	18:34:53	02/11/2015	2:12:07	02/11/2015	3:17:42
Outer rail, in region:	**Mean**	**SD**	**Mean**	**SD**	**Mean**	**SD**	**Mean**	**SD**	**Mean**	**SD**
Between T-17 and T-16	0,035	0,005	0,046	0,010	0,036	0,004	0,042	0,006	0,051	0,010
Between T-01 and T+01 (closer to T-01)	0,044	0,008	0,059	0,011	0,044	0,009	0,042	0,008	0,060	0,011
Between T-01 and T+01 (closer to T+01)	0,035	0,005	0,046	0,014	0,033	0,005	0,042	0,008	0,048	0,012
Between T+01 and T+02	0,036	0,005	0,046	0,012	0,030	0,006	0,057	0,007	0,046	0,013
Between T+06 and T+07	0,042	0,005	0,051	0,010	0,042	0,005	0,082	0,011	0,050	0,008

Table 5 shows the mean and standar deviation of the minimun vertical sleeper velocities caused by the analyzed trains in different regions of the embankment – structure transition.

TABLE 5: MEAN AND STANDARD DEVIATION OF THE MINIMUM VERTICAL RAIL VELOCITIES CAUSED BY THE ANALYZED TRAINS IN DIFFERENT REGIONS OF THE EMBANKMENT – STRUCTURE TRANSITION

	Manimun peaks of the vertical rail velocity (m/s)									
	TRAIN S-120		TRAIN S-102		TRAIN S-103		TRAIN AVRIL 1		TRAIN AVRIL 2	
	01/11/2015	18:07:06	01/11/2015	18:31:57	01/11/2015	18:34:53	02/11/2015	2:12:07	02/11/2015	3:17:42
Outer rail, in region:	**Mean**	**SD**	**Mean**	**SD**	**Mean**	**SD**	**Mean**	**SD**	**Mean**	**SD**
Between T-17 and T-16	-0,038	0,004	-0,051	0,010	-0,036	0,005	-0,046	0,008	-0,051	0,008
Between T-01 and T+01 (closer to T-01)	-0,041	0,006	-0,052	0,009	-0,040	0,006	-0,051	0,008	-0,056	0,009
Between T-01 and T+01 (closer to T+01)	-0,034	0,004	-0,041	0,009	-0,034	0,005	-0,047	0,009	-0,044	0,007
Between T+01 and T+02	-0,038	0,004	-0,046	0,013	-0,033	0,005	-0,054	0,009	-0,048	0,007
Between T+06 and T+07	-0,052	0,007	-0,059	0,008	-0,040	0,007	-0,073	0,014	-0,066	0,009

Furthermore, Figure 21 and Figure 22 show the graphical representation of sleeper accelerations given in previous tables, for each sleeper.

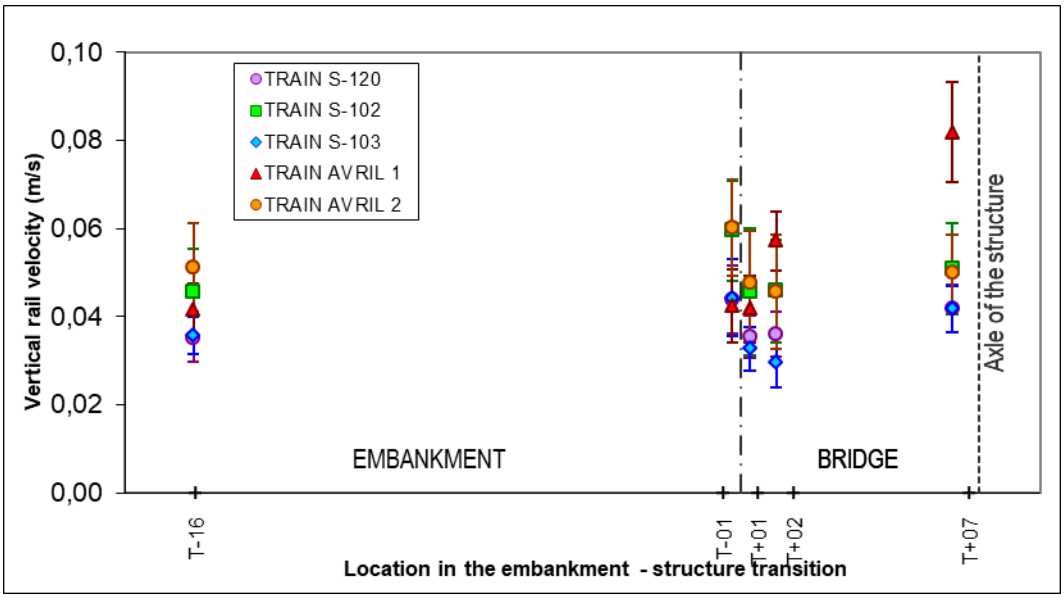

FIGURE 21: COMPARISON BETWEEN MEAN VALUES OF THE MAXIMUM VERTICAL RAIL VELOCITIES CAUSED BY THE ANALYZED TRAINS IN DIFFERENT REGIONS OF THE EMBANKMENT – STRUCTURE TRANSITION

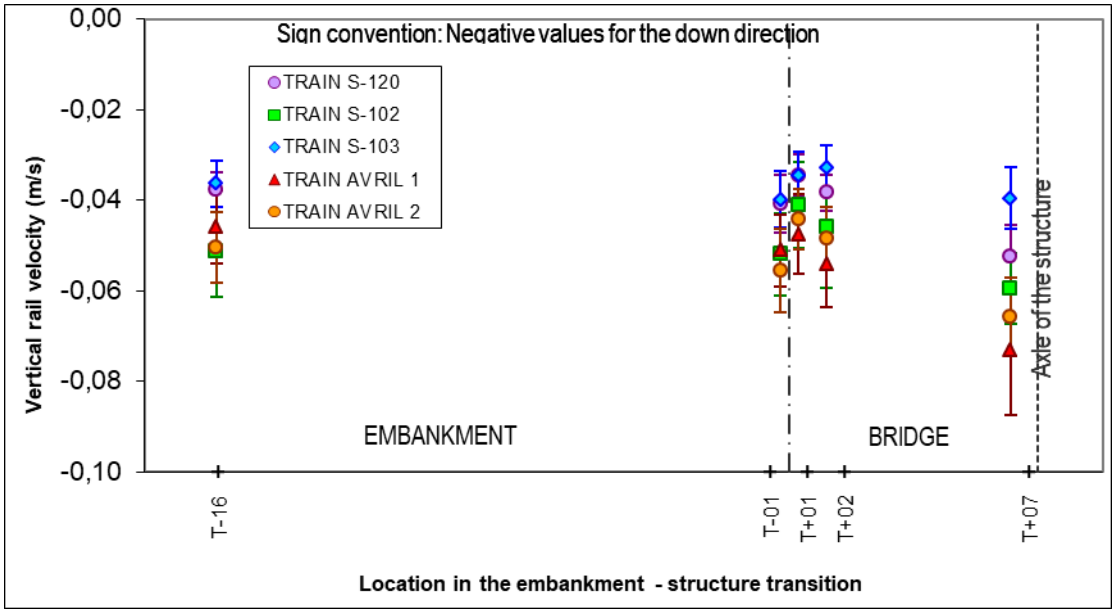

FIGURE 22: COMPARISON BETWEEN MEAN VALUES OF THE MINIMUM VERTICAL RAIL VELOCITIES CAUSED BY THE ANALYZED TRAINS IN DIFFERENT REGIONS OF THE EMBANKMENT – STRUCTURE TRANSITION

The vertical velocity seems to be similar in the embankment and in the edge of the bridge, while in the axle structure tends to be greater.

3.4.4 VERTICAL RAIL DEFLECTION

Table 6 shows the mean and standar deviation of the maximum vertical rail deflections caused by the analyzed trains in different regions of the embankment – structure transition.

TABLE 6: MEAN AND STANDARD DEVIATION OF THE MAXIMUM VERTICAL RAIL DEFLECTIONS CAUSED BY THE ANALYZED TRAINS IN DIFFERENT REGIONS OF THE EMBANKMENT – STRUCTURE TRANSITION

	Vertical rail deflection (mm)									
	TRAIN S-120 01/11/2015 18:07:06		TRAIN S-102 01/11/2015 18:31:57		TRAIN S-103 01/11/2015 18:34:53		TRAIN AVRIL 02/11/2015 2:12:07		TRAIN AVRIL 02/11/2015 3:17:42	
Outer rail, in region:	Mean	SD	Mean	SD	Mean	SD	Mean	SD	Mean	SD
Between T-17 and T-16	-0.60	0.04	-0.65	0.09	-0.57	0.05	-0.57	0.08	-0.65	0.09
Between T-01 and T+01 (closer to T-01)	-0.47	0.04	-0.51	0.07	-0.44	0.04	-0.42	0.05	-0.51	0.07
Between T-01 and T+01 (closer to T+01)	-0.45	0.04	-0.45	0.08	-0.42	0.04	-0.40	0.08	-0.48	0.06
Between T+01 and T+02	-0.47	0.04	-0.48	0.07	-0.44	0.04	-0.47	0.06	-0.47	0.06
Between T+06 and T+07	-0.58	0.07	-0.59	0.08	-0.48	0.05	-0.65	0.14	-0.59	0.07

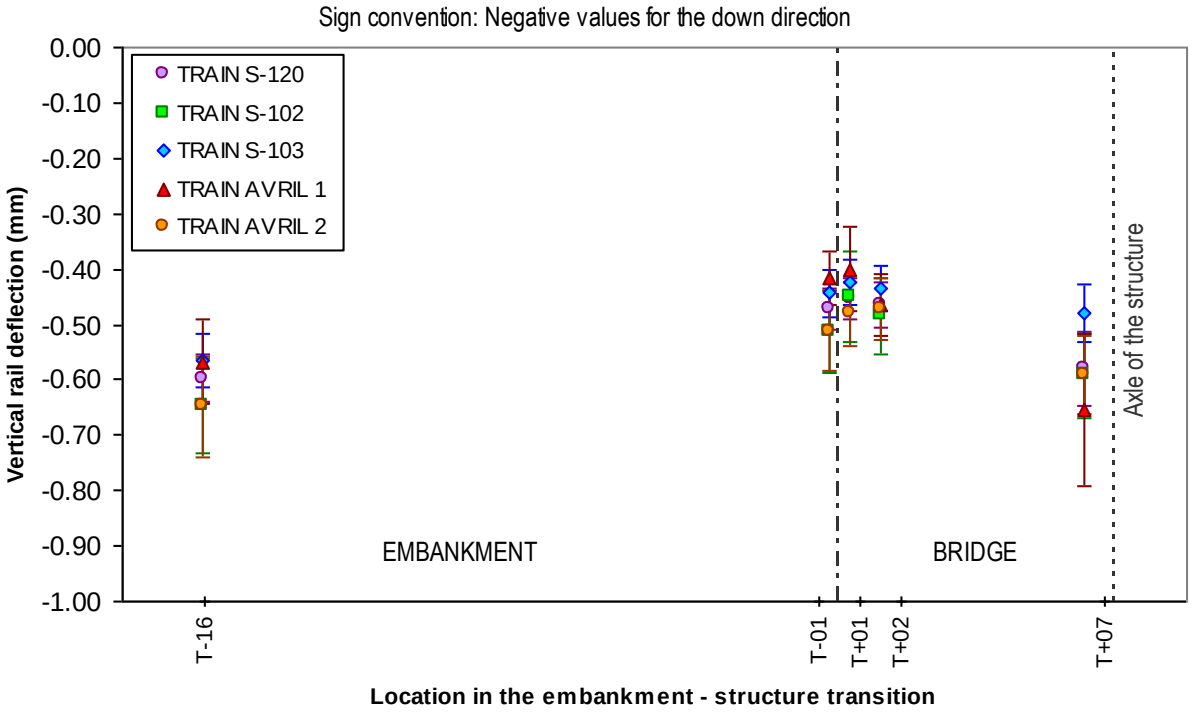

FIGURE 23: COMPARISON BETWEEN MEAN VALUES OF THE MAXIMUM VERTICAL RAIL DEFLECTIONS CAUSED BY THE ANALYZED TRAINS IN DIFFERENT REGIONS OF THE EMBANKMENT – STRUCTURE TRANSITION

The vertical deflection seems to decrease when approaching the bridge from the embankment while the value in the axle of the structure is larger than that measured in the edge of the bridge.

3.4.5 TRACK STIFNESS

Following the procedure described previously, first of all, the dynamic load measured for each one of the wheels by using the strain gauges in the zone between sleepers T-17 and T-16 of the outer rail was calculated. Table 7 lists the mean wheel load for each train and their corresponding standard deviation. For each train, these values were obtained from the curves similar to the one shown in Figure 16. The S-120, S-103 and first AVRIL trains show similar wheel loads with typical values around 110 kN and standard deviations of about 10 kN, while the wheel loads and standard deviations found for the S-102 and last AVRIL trains were slightly larger (~ 122-124 kN and 14-17 kN, respectively).

TABLE 7: MEAN AND STANDARD DEVIATION OF THE TRAINS' WHEEL LOADS IN THE OUTER RAIL

			Wheel loads (kN)	
			Outer rail (HE)	
Train type	Date	Time	Mean	SD
S-120	01/11/2015	18:07:06	113	9
S-102	01/11/2015	18:31:57	122	14
S-103	01/11/2015	18:34:53	107	9
AVRIL	02/11/2015	2:12:07	110	11
AVRIL	02/11/2015	3:17:42	124	17

Once the loads were obtained, the next step was to calculate the maximum vertical rail deflection: in this case, the deflection of the outer and inner rails, respectively, caused by the pass of the different train wheels in the zone between the sleepers T-17 and T-16. These measures were obtained by time-integration of the corresponding vertical rail velocity. As expected, once again, the S-120, S-103 and first AVRIL trains cause similar peak vertical deflections in each one of the rails with values slightly smaller than those caused by the S-102 and last AVRIL trainsTable 8 lists the mean values and standard deviation for each train. The peak values of vertical deflection show no difference between the inner and outer rails.

TABLE 8: MEAN AND STANDARD DEVIATION OF THE MAXIMUM VERTICAL RAIL DEFLECTIONS CAUSED BY THE ANALYZED TRAINS IN BOTH INNER AND OUTER RAILS BETWEEN T-17 AND T-16

			Maximum vertical rail deflection (mm) between T-17 and T-16			
			Outer rail (HE)		Inner rail (HI)	
Train type	Date	Time	Mean	SD	Mean	SD
S-120	01/11/2015	18:07:06	-0.60	0.04	-0.62	0.06
S-102	01/11/2015	18:31:57	-0.65	0.09	-0.63	0.11
S-103	01/11/2015	18:34:53	-0.57	0.05	-0.57	0.04
AVRIL	02/11/2015	2:12:07	-0.57	0.08	-0.57	0.10
AVRIL	02/11/2015	3:17:42	-0.65	0.09	-	-

Finally, track stiffness was obtained by dividing the calculated wheel load by the maximum vertical deflection induced in the rail. In this case, the deflection values of the outer rail were chosen. The division was made for each wheel and a mean value and its standard deviation is given for each train. In this procedure, the appearance of some spurious values is common, so it is recommended to remove them to have a more reliable mean value. Table 9 shows the results for each train. This table is only done to check if similar values are obtained for the different trains, but being track stiffness a characteristic track parameter it only has sense to present a general mean value for the whole data set. Its calculation is described next.

TABLE 9: MEAN AND STANDARD DEVIATION OF TRACK STIFFNESS OBTAINED BETWEEN SLEEPERS T-17 AND T-16

			Track Stiffness (kN/mm)	
			Outer rail (HE)	
Train type	Date	Time	Mean	SD
S-120	01/11/2015	18:07:06	188	17
S-102	01/11/2015	18:31:57	188	15
S-103	01/11/2015	18:34:53	188	12
AVRIL	02/11/2015	2:12:07	193	20
AVRIL	02/11/2015	3:17:42	191	17

In Figure 24 the wheel loads vs. the corresponding maximum vertical deflection caused in the rail (only for those pairs of values that provide reliable results for the railway track stiffness) have been plotted. In the range of analysed loads both parameters are clearly correlated by a simple linear relationship. The regression has been forced through the origin given the fact that no load implies no rail deflection. The linear fit provides a high absolute Pearson correlation factor ($|R| \approx -0.96$). Hence, the best value for the railway track stiffness (K) is estimated as the slope[3] of the simple linear fit shown in Figure 24:

$$K = 189.7 \pm 1.5\,\mathrm{kN/mm}$$

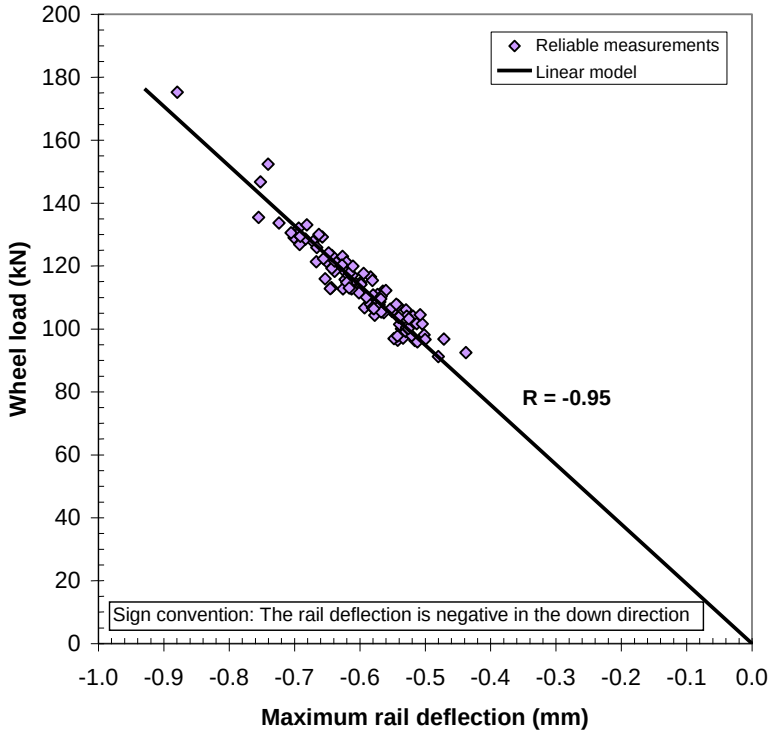

FIGURE 24: WHEEL LOAD VS. VERTICAL RAIL DEFLECTION MEASURED BY USING THE SENSORS PLACED BETWEEN SLEEPERS T-17HE AND T-16HE. NOTE THAT ONLY RELIABLE VALUES ARE PLOTTED. THE BEST VALUE FOR THE TRACK STIFFNESS HAS BEEN ESTIMATED AS THE SLOPE OF THE LINEAR FIT

The obtained track stiffness seems to be higher than that measured in regular tracks far away from bridges. The deflection values are similar to those obtained in other in situ test campaigns however load peaks measures in this test site are higher than those calculated in other campaigns for the same trains travelling at about the same speeds. As a result of that, track stiffness seems to be higher than in other study sites. Maybe the proximity of the bridge influences in this performance. The existing strain gauges are 10 m far from the beginning of the structure and there the embankment is still affected by the transition zone (see Figure 2) and the materials used are stiffer than in conventional embankments far from transition zones.

4. Second campaign (PK 74+233 / June 2016)

4.1 Instrumentation

The aim of this field campaign was to generate a data base of trains travelling at high speed that can be used to validate test results obtained in CEDEX Track Box. The selected site was a straight track section in which trains can travel at their maximum speed (around 300 km/h). Figure 25 is a general view of the site: HSL Madrid-Barcelona PK 74+233 and Figure 26 is a picture taken from the track to stand out that this section is a straight stretch without any curve and lateral slope.

Figure 25: General view of the selected site

FIGURE 26: VIEW FROM THE TRACK. THE SECTION IS STRAIGHT IN SOME KILOMETERS BEFORE AND AFTER THE SELECTED POINT

As the aim of this field campaign is to validate test results obtained in CEDEX Track Box, the instrumentation set was the typical configuration used in the Track Box. All sensors were installed in Track 1, the one used by trains traveling from Madrid to Barcelona.

Figure 27 and Figure 28 are a picture and a sketch, respectively, of the position of the sensors in the track.

FIGURE 27: SENSORS INSTALLED ON TRACK 1, USED BY THE TRAINS TRAVELLING FROM THE LEFT (MADRID) TO RIGHT (BARCELONA)

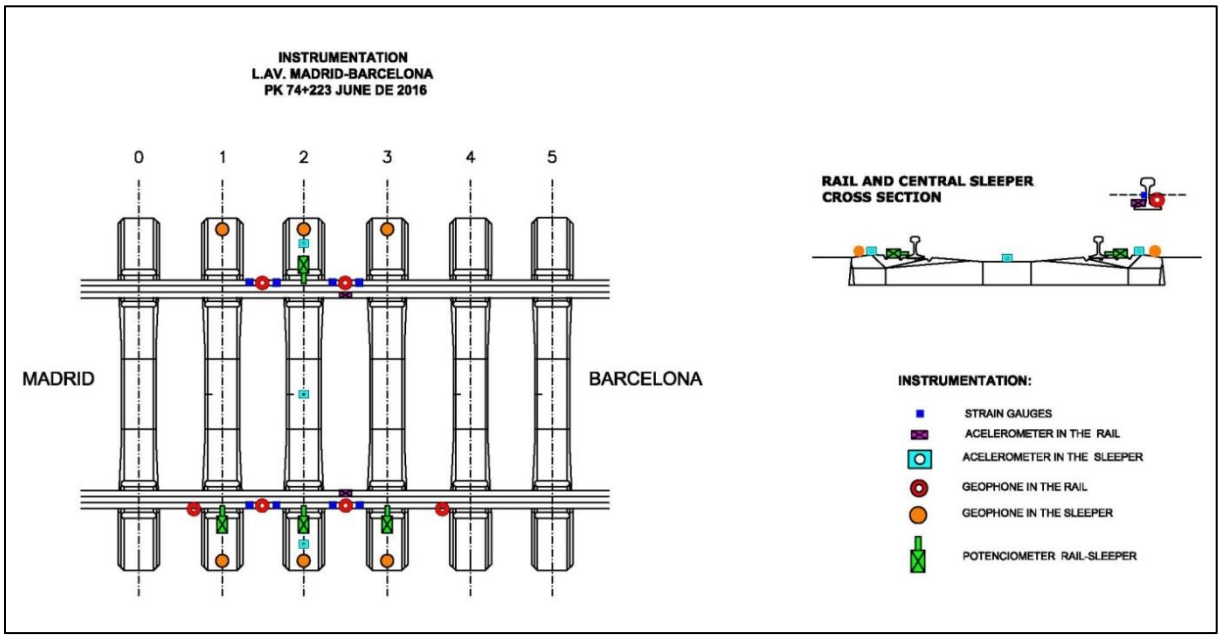

FIGURE 28: SKETCH OF THE INSTRUMENTED SECTION

The instrumentation installed consisted of the following sensors:

- Eight (8) strain gauges (represented by dark-blue squares): the gauges are glued at the level of the neutral fibre of the rail in order to measure only shear strains. Loads are obtained using the pair placed at the span between two sleepers. So loads can be obtained at four different points. The pair located at both sides of one sleeper can be used to calculate the reaction of the sleeper.
- Seven (7) 2 Hz geophones installed in the rail (marked with red spots): they are used to measure the vertical velocity of the vibration in the rail produced by the trains pass-by. It is also possible to obtain the rail deflections by integrating these velocity signals.
- Six (6) 1 Hz geophones (represented by orange circles): they are stacked at both ends of the sleeper surface to measure the vertical velocity of the vibration at those points.
- Two (2) vertical accelerometers stacked in the rail (shown with fuchsia rectangles).
- Three (3) triaxial accelerometers stacked in the sleeper surface (represented by light-blue squares).

Four (4) potentiometers (presented with green rectangles): they are used to measure the rail-sleeper relative motion. From this displacement it is possible to calculate the pad deformation.

4.2 BALLAST PARTICLE INSTRUMENTATION

The purpose of this part of the work, performed by ADIF, was to measure the ballast particle vibration levels at the pass-by of different high speed trains to determine the behaviour of the ballast layer. It is known that the accelerations of ballast particles in a High Speed Line are directly related with the dynamic train axle load and the impact force of the wheel-rail contact. On other hand, to measure the ballast particle acceleration is important as this parameter is directly related with the ballast degradation rate.

The first ballast acceleration measures were taken in Japan for speeds of 210 km/h where values of 0.3 and 0.6 g were measured. In other hand, from a study in different French lines, acceleration values on the ballast layer between 0.88 g at 140 km/h and 1.40 g at 300 km/h were determined.

Later studies determined that beyond 0.7 g the vertical displacements suffered by the ballast layer were notably increased after a certain number of load cycles. Other authors mention values of 1.2 g for the same process.

The measurements were taken firstly with an aluminium block shaped in the form of a ballast particle, as shown in Figure 29. It was designed with a hollow space to house the accelerometer and a piece of steel to change the density of the whole. Thus, the density can vary from 20 kN/m3 to 2.7 kN/m^3 with the piece of steel inside, being those values the typical ones for ballast.

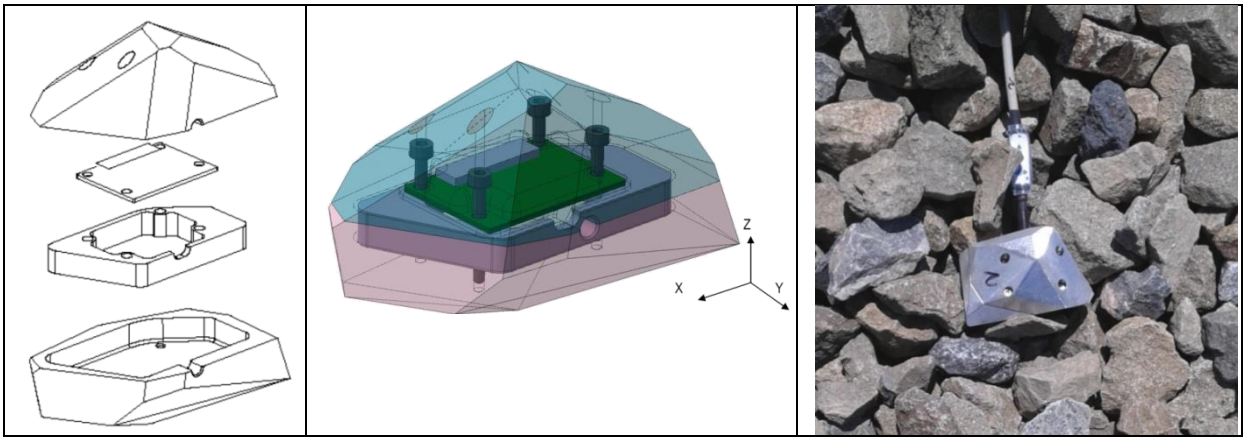

FIGURE 29: ALUMINUM BLOCK WITH THE SHAPE OF A BALLAST PARTICLE

Later on, real ballast particles were cut in two parts to house the accelerometers. A special adhesive filled the empty spaces and gave a finish with a roughness similar to ballast, as shown in Figure 30. The accelerometers used were Kionix KXD94-2802 +/-10g.

FIGURE 30: BALLAST PARTICLES INSTRUMENTED WITH ACCELEROMETERS

The measurements were taken using different layouts of accelerometers and positions: instrumented ballast particles were buried at different depths and positions, as shown in Figure 31.

A data acquisition system was connected to the accelerometers together with a wheel pass detector that acted as trigger and wheel counter. Thus, the system registered time, accelerations of each accelerometer and the pass of each wheel.

Working out that information it can be found the type of train, its speed, and the accelerations on each axis x, y and z

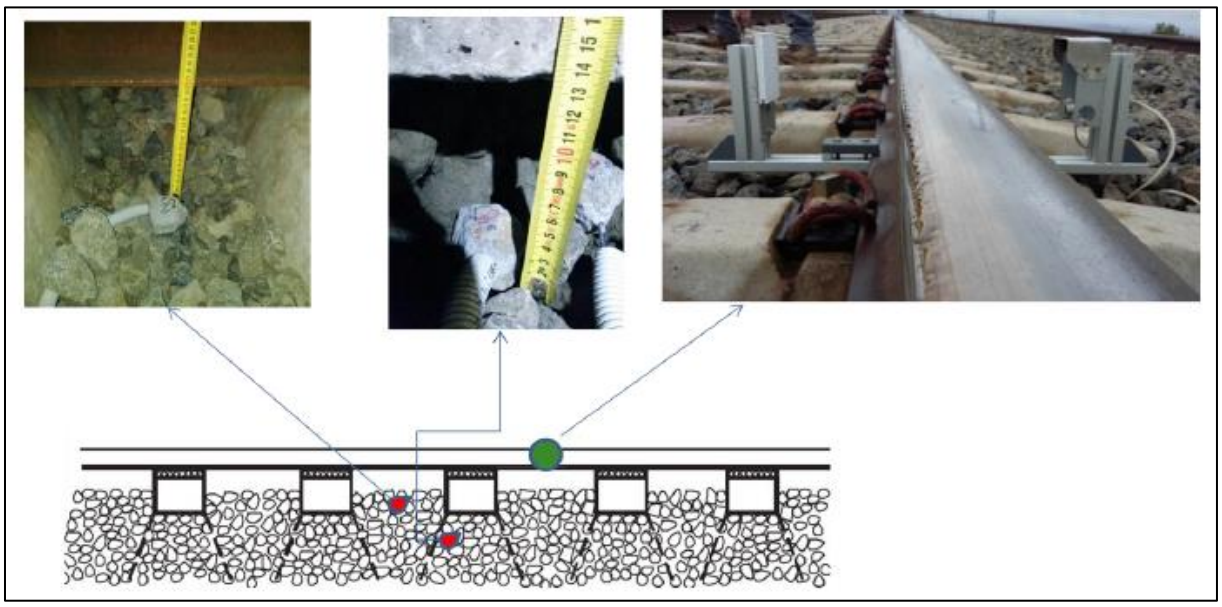

FIGURE 31: LAYOUT OF INSTRUMENTED BALLAST PARTICLES

Figure 32 represents the different positions where the ballast particles with accelerometers were placed

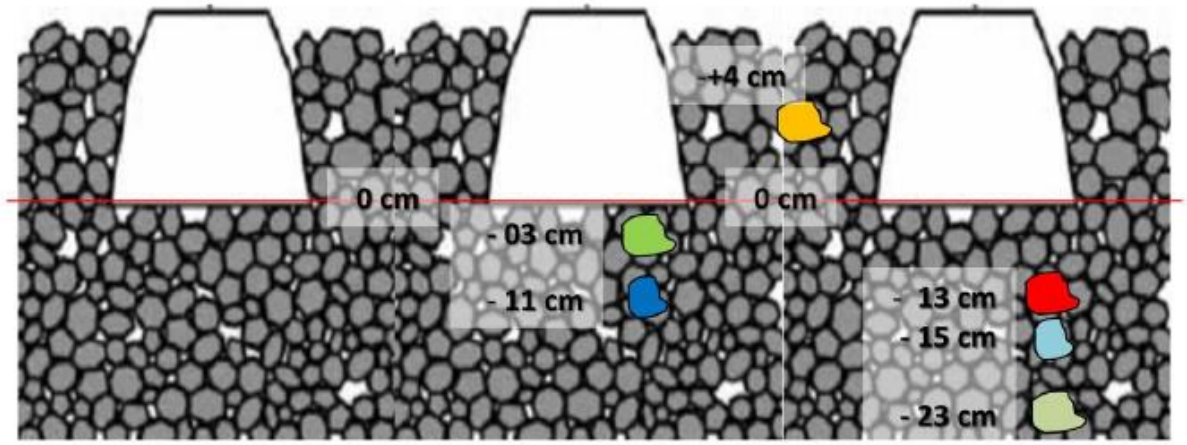

FIGURE 32: POSITION OF THE BALLAST PARTICLES INSTRUMENTED WITH ACCELEROMETERS

Additionally, in the same area where the accelerometers were placed, four penetrometer tests were performed to have a better knowledge of the ballast layer conditions in the surroundings. Figure 33 shows the position in which they were performed and the system used.

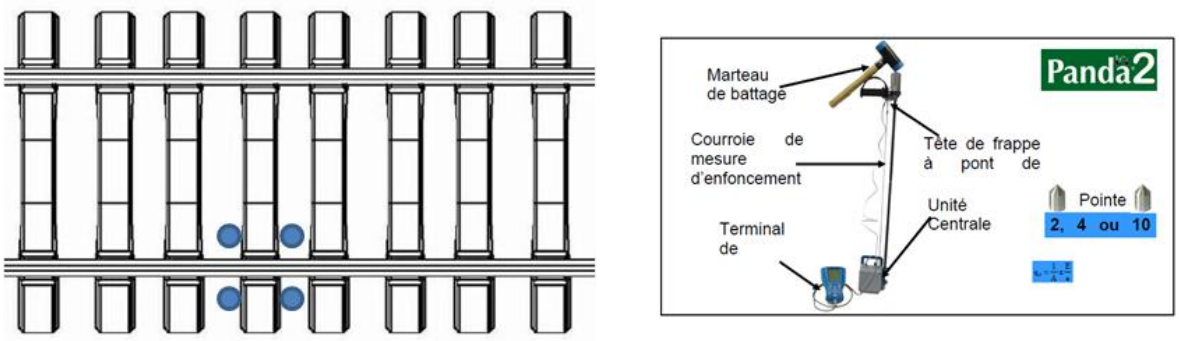

FIGURE 33: POSITION OF THE PENETROMETER TESTS AND SYSTEM USED

4.3 RECORDED TRAINS

The installation of the sensors was done during the nights of May 30th and 31th and all measures were carried out on June 1st 2016. All the trains that passed-by the track that day were recorded, being a total of 37 trains. Table 10 compiles the information regarding the registered trains:

TABLE 10: RECORDED TRAINS

TIME	TRAIN TYPE	SPEED (km/h) (±10 km/h)	COMMENTS
6:31:45	SIEMENS S103	300	(1)
6:52:39	SIEMENS S103	298	---
7:21:52	SIEMENS S103	300	---
7:41:25	TALGO S102	300	---
7:56:37	SIEMENS S103	248	---
8:01:29	CAF S120	239	---
8:21:04	SIEMENS S103	301	---
8:42:39	SIEMENS S103	297	---
8:52:26	SIEMENS S103	300	---
9:23:16	SIEMENS S103	299	---
9:52:01	SIEMENS S103	299	---
10:53:28	SIEMENS S103	299	---
11:35:54	**TALGO S102** (2)	**299**	**Double**(3)
11:53:47	SIEMENS S103	293	---
12:07:44	**CAF S120**	**226**	---
12:51:19	SIEMENS S103	297	---
13:55:11	TGV	225	---
14:21:06	SIEMENS S103	298	---
14:52:22	SIEMENS S103	300	---
15:21:31	SIEMENS S103	297	---
15:34:49	CAF S120	229	---
15:54:57	SIEMENS S103	300	---
16:22:21	TALGO S102	295	---
16:54:24	SIEMENS S103	299	---
17:24:26	**SIEMENS S103**	**298**	**Double**(3)
17:38:59	TALGO S102	299	Double(3)
17:59:25	SIEMENS S103	224	
18:22:52	SIEMENS S103	302	---
18:59:06	SIEMENS S103	299	---
19:21:34	SIEMENS S103	220	---
19:23:31	SIEMENS S103	235	---
19:32:45	**TALGO S102**	**257**	---
19:53:03	SIEMENS S103	298	---
19:59:42	SIEMENS S103	239	---
20:21:57	**TALGO S102**	**300**	---
20:57:58	**SIEMENS S103**	**250**	---
21:49:46	**SIEMENS S103**	**299**	---

(1) Noise in sleeper accelerometer signals until 12:07:44
(2) Trains highlighted in bold have been chosen for the analysis.
(3) Double" means that the train is composed by two trains of the same type

4.4 SIGNAL ANALYSIS PROCEDURE

This section summarizes the method to process the raw data obtained in the different sensors. Due to the large amount of information collected, it was decided to focus in the values of accelerations, velocities, displacements and loads obtained in the sensors placed in the central part of the instrumented section (sensors installed on sleeper T-2 and on the rails between T-2 and T-3 sleepers), as shown in Figure 34.

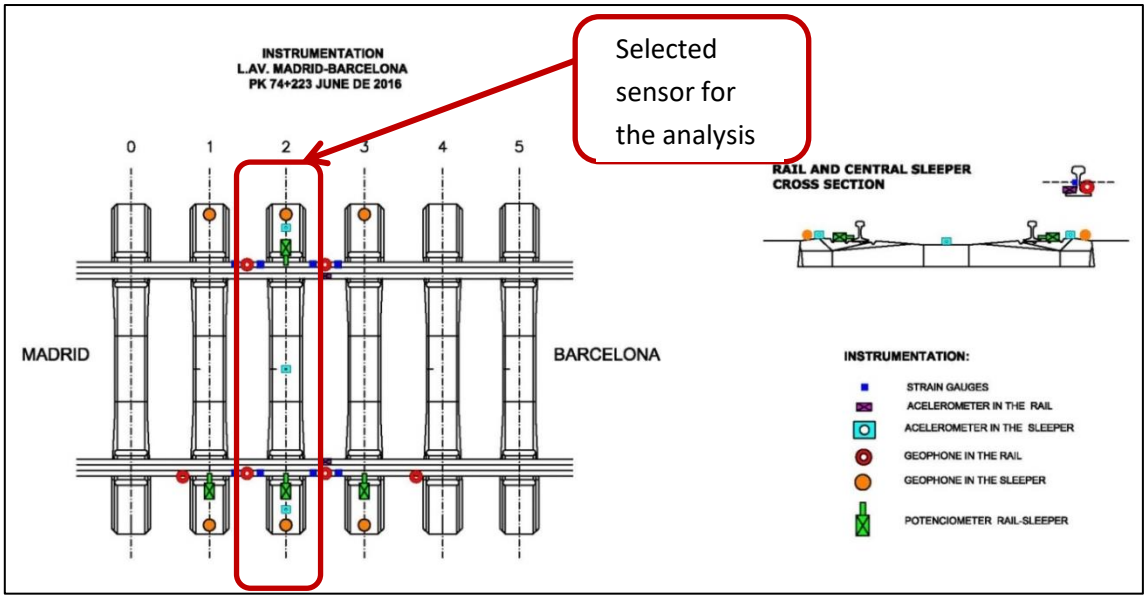

FIGURE 34: INSTRUMENTED SECTION, HIGHLIGHTING THE SENSOR SELECTED FOR THE ANALYSIS

The analysis was performed in two steps. Firstly, all the time signals obtained in the central section were filtered to delete undesirable noise, using the Low Pass Filters (LPF) indicated in Table 11, which cut off the frequencies above the value chosen in each case.

TABLE 11: LOW PASS FILTERS USED TO ANALYSE THE SIGNALS RECORDED

Parameter	Sensor	Low Pass Filter used	Position
Pad vertical displacement	Potentiometers	90 Hz	- Between outer rail and sleeper T2 - Between inner rail and sleeper T2
Rail velocity	2 Hz geophone	90 Hz	- In the outer rail between T2 and T3 - In the inner rail between T2 and T3
Sleeper velocity	1 Hz geophone	150 Hz	- In the outer side of sleeper T2 - In the inner side of sleeper T2
Rail acceleration	Accelerometer	250 Hz	- In the outer rail between T2 and T3 - In the inner rail between T2 and T3
Sleeper acceleration	Accelerometer	250 Hz	- In the outer side of sleeper T2 - In the inner side of sleeper T2 - In the center of sleeper T2
Wheel loads	Strain gauges	500 Hz	- In the outer rail between T2 and T3 - In the inner rail between T2 and T3

All the time signals obtained in the central section once filtered are collected in Annex A. The name of the sensor that appears in each figure is coincident with the name given in Figure 35.

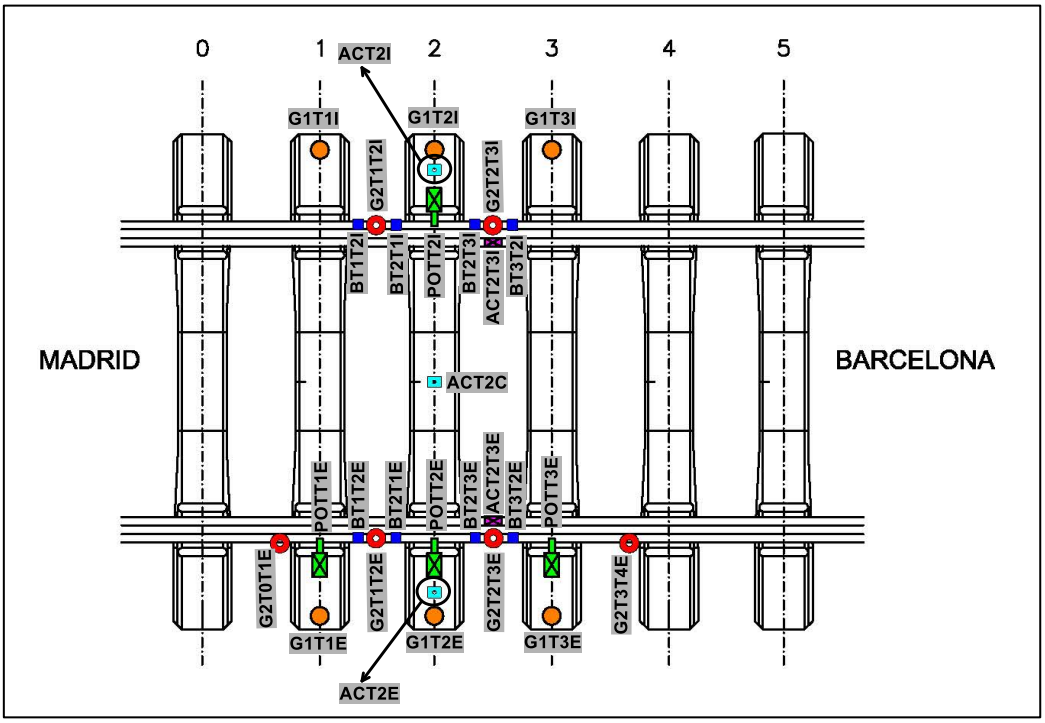

FIGURE 35: NAME USED FOR EACH SENSOR

Secondly, to be sure that the Low Pass Filters used were correct, seven different trains were chosen to perform a more careful interpretation. Two criteria were followed for the train selection: type of train and velocity. As S-103 and S-102 trains were the most common trains traveling in this track, three trains of each type were selected:

- Single formation traveling at about 300 km/h.
- Single formation traveling at about 250 km/h.
- Double formation traveling at about 300 km/h.

In addition of those six trains, a S-120 train traveling at 225 km/h was also selected for the careful analysis.

For the time signals obtained with these seven trains, the Fast Fourier Transform (FFT) was firstly calculated to visualize the frequency domain and then to decide the best values of the Low Pass Filters which should be used. The signal of each sensor was then filtered to represent only the train influence and to eliminate noise. In addition, the time axle limits were fixed to center the graph on the pass train signal.

The procedure used in this second step was the same than the one described in Chapter 3.3. It is only necessary to remark that the signal analysis procedure followed for the 1 Hz geophones and the potentiometers is very similar to the one applied for the accelerometers and the 2Hz geophones.

All the time signals processed in this second step for the seven trains selected are collected in Annex B.

4.5 RESULTS

4.5.1 INTRODUCTION

The parameters that have been analysed are the following:

- Track stiffness, considered as the ratio between the load applied by the train, obtained from the strain gauges, and the rail deflection obtained from the time integration of rail velocity.
- Pad vertical displacement, measured by potentiometers as the relative motion between rail and sleepers.
- Vertical rail velocity.
- Vertical sleeper velocity.
- Vertical rail acceleration
- Vertical sleeper acceleration
- Ballast particle acceleration.

For each of those parameters, the signals processed in the second step of the analysis for the Siemens S-103 train that passed-by at 21:19:46 are shown and a figure with a summary of the results obtained from all signals obtained in the 37 trains analysed.

4.5.2 TRACK STIFFNESS

In this chapter the track stiffness is calculated following the procedure described in 3.3.4. These values are obtained for the zone between T-2 and T-3 sleepers in inner and outer rails.

Table 12 lists the mean wheel load for each train obtained from the value of all peaks of the corresponding time history load graph. Once the load value is obtained, the vertical rail deflection is determined. Table 13 collects the mean value of the maximum rail deflection for each train obtained, as the mean value of all peaks of the corresponding time deflection graph. Finally, track stiffness is obtained by dividing the load values by the vertical deflections. This operation is made for each wheel and then the mean value of the track stiffness is calculated. The results are listed in Table 14.

TABLE 12: MEAN AND STANDARD DEVIATION OF TRAIN WHEEL LOADS IN BOTH INNER AND OUTER RAILS BETWEEN SLEEPERS T-2 AND T-3

			Wheel loads (kN) between T-2 and T-3			
			Outer rail (HE)		Inner rail (HI)	
Train type	Time	Speed (km/h)	Mean	Stand. Desv.	Mean	Stand. Desv.
S-103	21:49:46	299	58.40	6.36	67.16	7.20
S-103	20:57:58	250	65.13	4.82	71.43	4.57
S-102	20:21:57	300	73.30	7.32	81.69	7.65
S-102	19:32:45	257	73.17	8.61	75.40	10.53
S-103	17:24:26	298	60.13	7.21	65.89	6.36
S-120	12:07:44	226	70.92	6.26	75.59	5.89
S-102	11:35:54	299	74.70	8.03	78.96	10.54

TABLE 13: MEAN AND STANDARD DEVIATION OF THE MAXIMUM VERTICAL RAIL DEFLECTIONS CAUSED BY THE ANALYZED TRAINS IN BOTH INNER AND OUTER RAILS BETWEEN SLEEPERS T-2 AND T-3

			Maximum vertical rail deflection (mm) between T-2 and T-3			
			Outer rail (HE)		Inner rail (HI)	
Train type	Time	Speed (km/h)	Mean	Stand. Desv.	Mean	Stand. Desv.
S-103	21:49:46	299	-0.56	0.04	-0.63	0.04
S-103	20:57:58	250	-0.61	0.00	-0.67	0.06
S-102	20:21:57	300	-0.66	0.10	-0.73	0.09
S-102	19:32:45	257	-0.74	0.09	-0.72	0.07
S-103	17:24:26	298	-0.65	0.05	-0.75	0.09
S-120	12:07:44	226	-0.69	0.06	-0.75	0.05
S-102	11:35:54	299	-0.77	0.09	-0.80	0.05

The maximum vertical rail deflections are in the range between 0.56 mm and 0.80 mm, being the average value about 0.70 mm.

TABLE 14: MEAN AND STANDARD DEVIATION OF TRACK STIFFNESS OBTAINED IN BOTH INNER AND OUTER RAILS BETWEEN SLEEPERS T-2 AND T-3

			Stiffness between T-2 and T-3 (kN/mm)			
			Outer rail (HE)		Inner rail (HI)	
Train type	Time	Speed (km/h)	Mean	Stand. Desv.	Mean	Stand. Desv.
S-103	21:49:46	299	103.70	8.70	106.33	7.22
S-103	20:57:58	250	107.89	6.43	107.02	5.76
S-102	20:21:57	300	111.46	9.42	113.05	8.23
S-102	19:32:45	257	105.66	10.26	109.09	8.90
S-103	17:24:26	298	93.84	5.65	88.23	7.99
S-120	12:07:44	226	102.33	7.70	101.39	3.88
S-102	11:35:54	299	99.86	9.42	101.26	7.29

The calculated stiffness varies between 88 and 113 kN/mm, being the average value around 103 kN/mm. Logically, as track stiffness is a track parameter, it seems those values are quite independent of the type of train and of the train speed

Another way to obtain the track stiffness is to calculate the slope of the line that best fits the pairs of wheel load - corresponding maximum vertical deflection values, as plotted in Figure 36. With this procedure, the railway track stiffness (K) is estimated as 102.3 ±8.2 kN/mm, very similar to the one mentioned above.

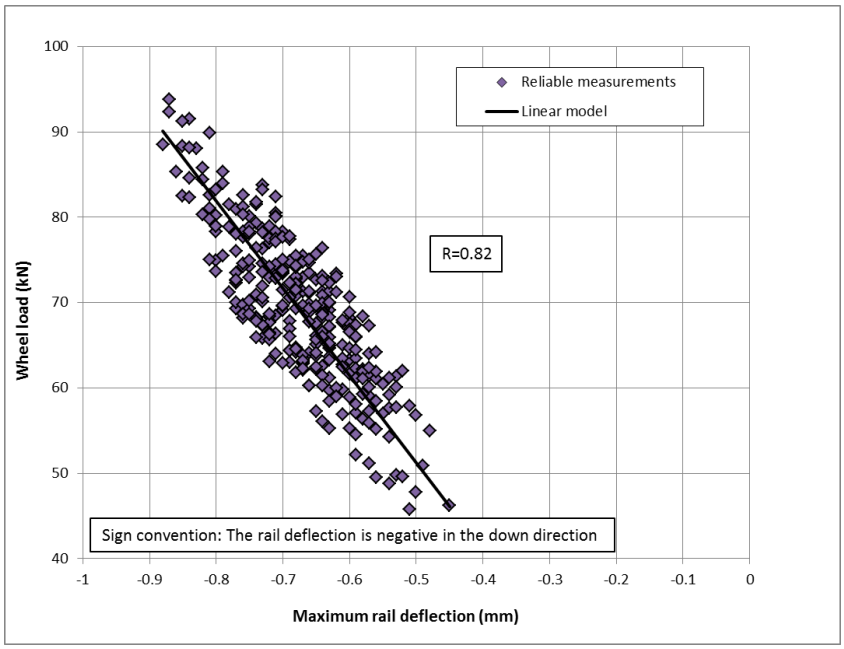

FIGURE 36: WHEEL LOAD VS. VERTICAL RAIL DEFLECTION MEASURED BY USING THE SENSORS PLACED BETWEEN T-2 AND T-3 IN BOTH INNER AND OUTER RAILS. NOTE THAT ONLY RELIABLE VALUES ARE PLOTTED

4.5.3 PAD VERTICAL DISPLACEMENT

The pad vertical displacement (also interpreted as relative displacement between rail and sleeper), is measured by the potentiometers installed. This instrumentation is located at inner and outer rail of sleeper T2. Figure 37 shows an example of measures obtained with those devices.

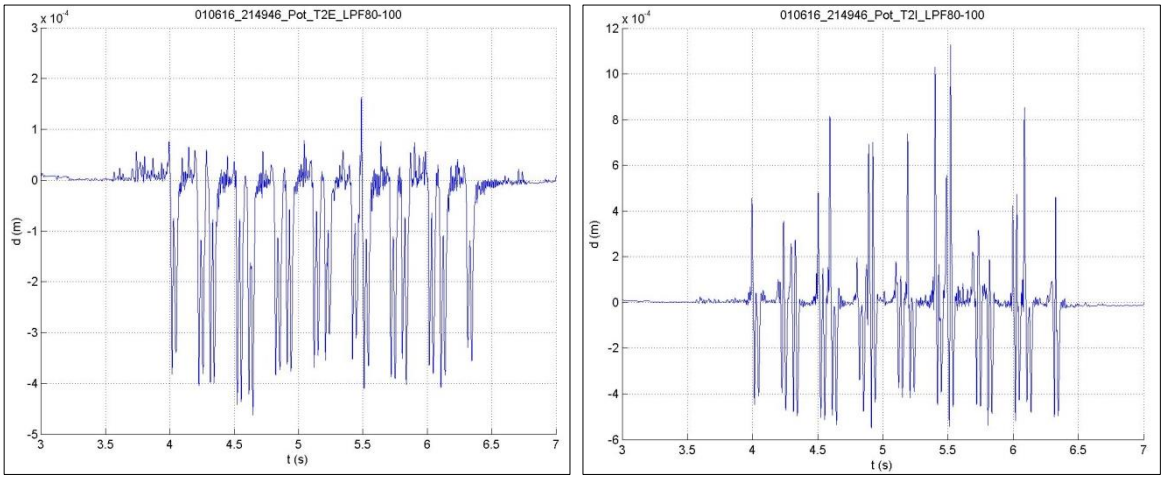

FIGURE 37: RELATIVE DISPLACEMENT BETWEEN OUTER (LEFT) AND INNER (RIGHT) RAIL AND SLEEPER T2 INDUCED BY 21:49:46 TRAIN (S-103 AT 299 KM/H).

As the displacements have been recorded for different train speeds it allows representing the variation of pad displacement with this parameter (Figure 38), and the type of train.

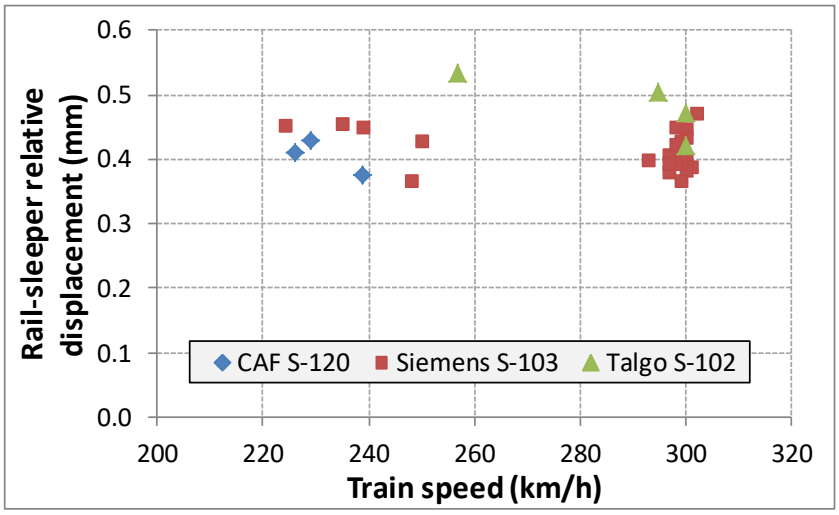

FIGURE 38: RELATIVE DISPLACEMENT BETWEEN RAIL AND SLEEPER AS FUNCTION OF TRAIN TYPE AND SPEED

Figure 38 shows that relative displacement between rail and sleepers are mainly in the range between from 0.38 and 0.45 mm for all type of trains and speeds. The maximum value (0,53 mm) recorded came from a Talgo S-102 train at 257 km/h, while minimum value (0,37 mm) is for Siemens S-103 train at 300 km/h. The results obtained seem to be independent of the train type and speed.

4.5.4 Rail velocity

Vertical rail velocity was measure by 2 Hz geophones located between sleepers T2 and T3, in the outer and inner rail. Figure 39 shows an example of records registered by this instrumentation for a S-103 train at 299 km/h.

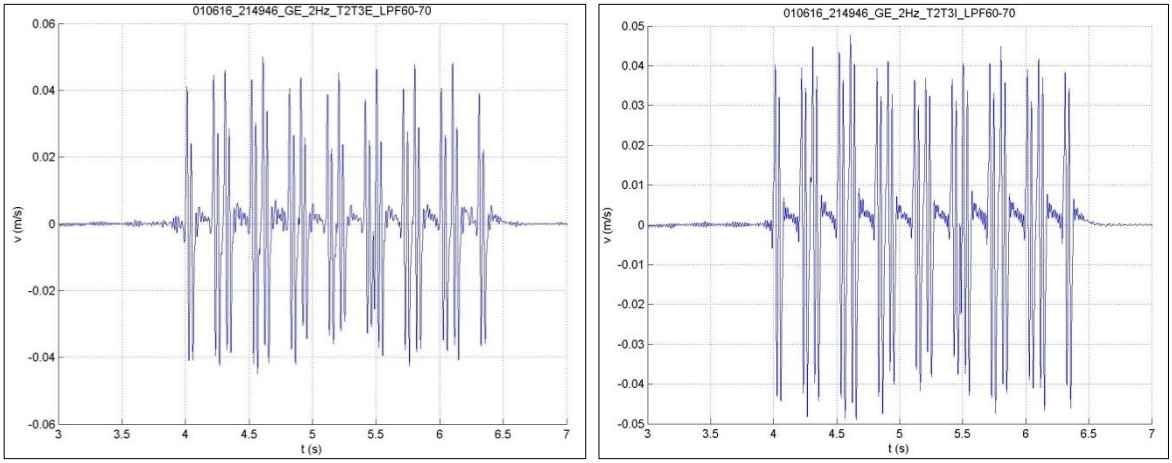

Figure 39: Rail velocity signal in the outer (left) and inner (right) rail between T2 and T3 induced by 21:49:46 train.

Figure 40 shows the rail velocities obtained for each type of train and for each passing-by speed.

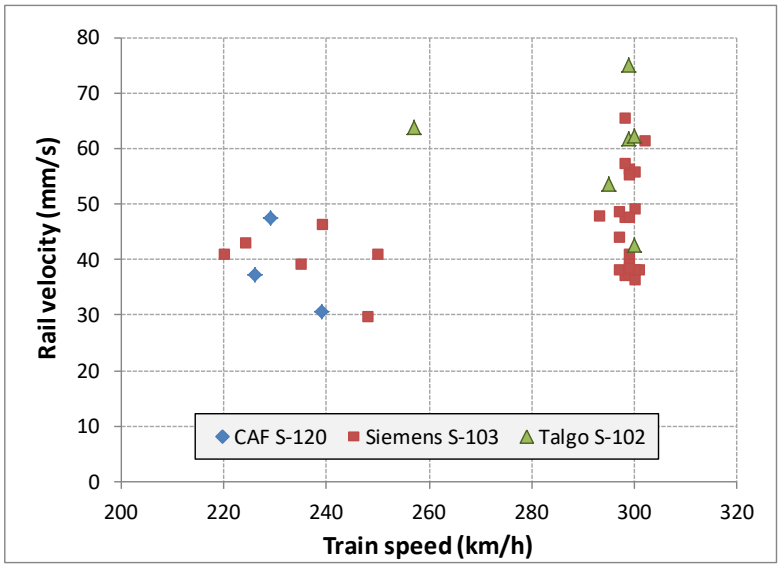

Figure 40: Rail velocity as function of train type and speed

The vertical rail velocities obtained oscillate between 30 and 75 mm/s. The minimum value is recorded for a Siemens S-103 train at 250 km/h, and maximum value is for a Talgo S-102 train at 299 km/h. It seems no correlation between rail velocities obtained and passing-by train speeds.

It can be deduced a quite light increment of the rail velocity with the train speed as for speeds between 220 and 250 km/h the mean value is around 42 mm/s while for speeds around 300 km/h that mean value increases to 49 mm/s.

4.5.5 SLEEPER VELOCITY

Vertical sleeper velocity was measured by 1 Hz geophones located at sleepers T2 at outer and inner rails. Figure 41 shows an example of data registered with this instrumentation for a S-103 train travelling at 299 km/h.

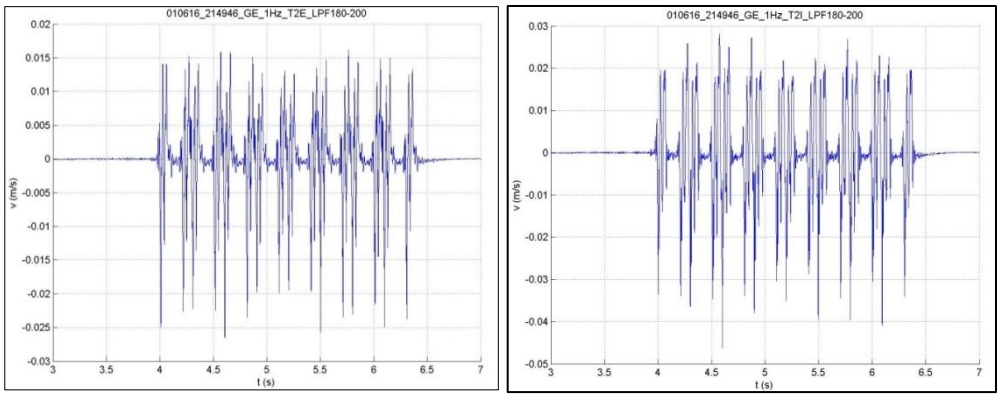

FIGURE 41: SLEEPER VELOCITY SIGNAL IN THE OUTER (LEFT) AND INNER (RIGHT) SIDE OF SLEEPER T2 INDUCED BY 21:49:46 TRAIN.

Figure 42 shows the sleeper velocities obtained for each type of train and for each passing-by speed.

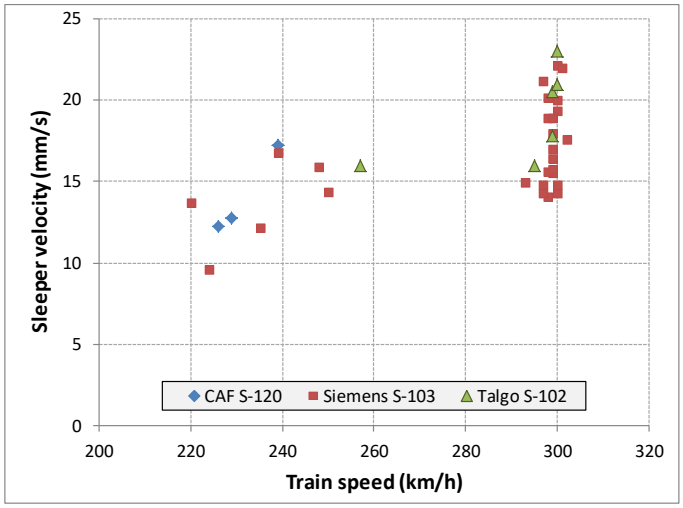

FIGURE 42: SLEEPER VELOCITY AS FUNCTION OF TRAIN TYPE AND SPEED

The vertical sleeper velocities obtained range between 10 and 23 mm/s. The minimum value was recorded for a Siemens S-103 train at 225 km/h, and maximum value was obtained for a Talgo S-102 train at 300 km/h. The sleeper velocity mean values obtained in different train speed ranges might suggest a correlation between train speed and sleeper velocities.

- Range 1 (220 - 235 km/h) with a mean value of 12 mm/s,
- Range 2 (240 – 260 km/h) with a mean value of 16 mm/s and
- Range 3 (270 – 310 km/h) with a mean value of 18 m/s

4.5.6 Rail acceleration

Vertical rail acceleration was measured by accelerometers located between sleepers T2 and T3 at outer and inner rails. Figure 43 shows an example of the measurements recorded by this kind of instrumentation for a S-103 train at 299 km/h.

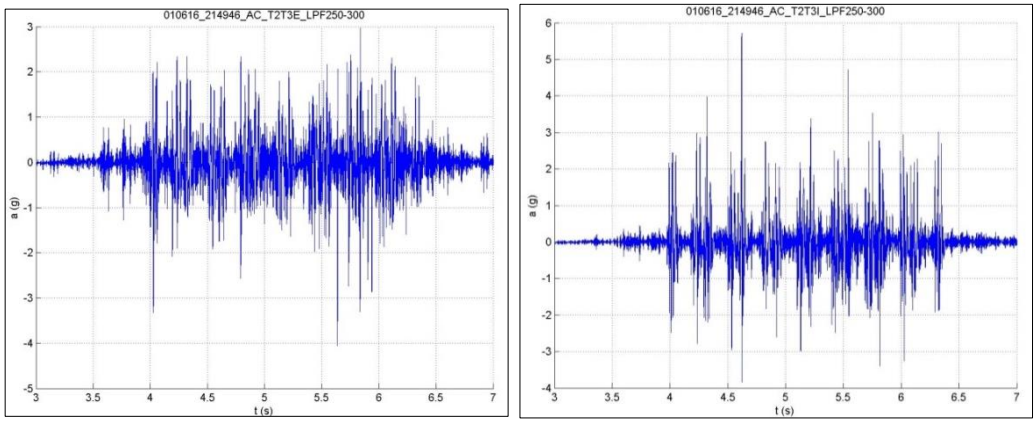

Figure 43: Rail acceleration signal in the outer (left) and inner (right) rail between T2 and T3 induced by 21:49:46 train.

Figure 44 shows the rail accelerations obtained for each type of train and for each passing-by speed.

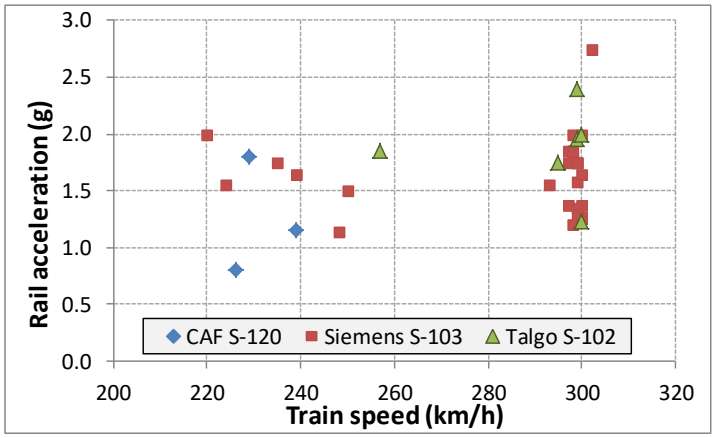

Figure 44: Rail acceleration as function of train type and speed

The rail accelerations obtained are mainly between 1.0 and 2.5 g. The minimum value (0.80 g) was recorded for a CAF S-120 train at 225 km/h while the maximum value (2.75 g) was for a Siemens S-103 train at 302 km/h. It cannot be deduced a good correlation between rail accelerations and passing-by train speeds.

4.5.7 SLEEPER ACCELERATION

Vertical sleeper acceleration was measured by accelerometers located at sleepers T2, near the outer and inner rails and in the centre of the sleeper. Figure 45 shows an example of records registered by this instrumentation for a S-103 train at 299 km/h.

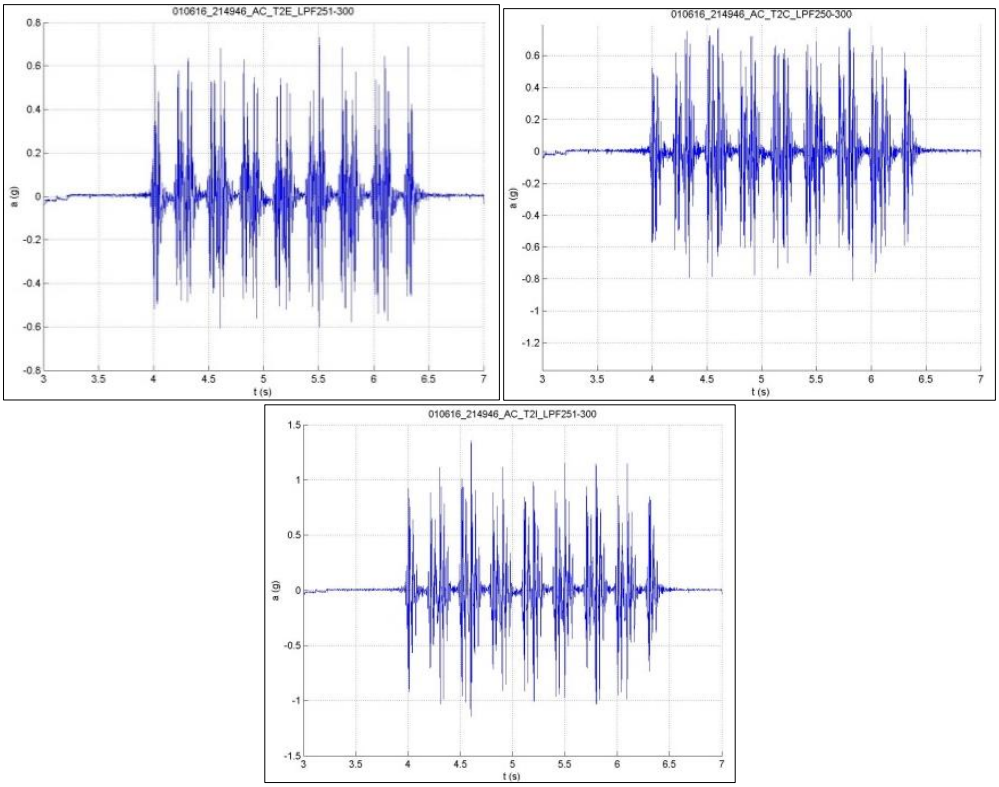

FIGURE 45: SLEEPER ACCELERATION SIGNAL IN THE OUTER (LEFT), CENTER (CENTER) AND INNER (RIGHT) SIDE OF SLEEPER T2 INDUCED BY 21:49:46 TRAIN.

Figure 46 shows the sleeper accelerations obtained for each type of train and for each passing-by speed.

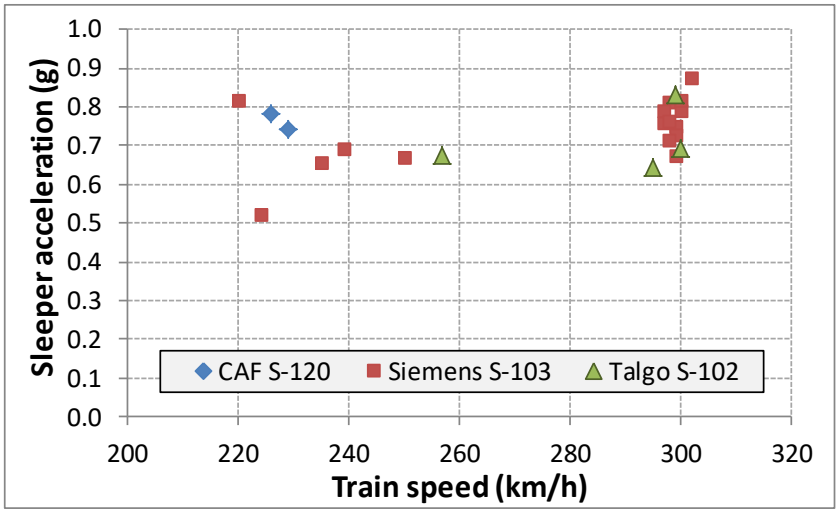

FIGURE 46: SLEEPER ACCELERATION AS FUNCTION OF TRAIN TYPE AND SPEED

The sleeper accelerations obtained are mainly in the range between 0.65 and 0.80 g. The minimum value (0.52 g) was recorded for a Siemens S-103 train at 220 km/h, and the maximum value (0.88 g) was for the same type but travelling at 302 km/h. There is not good correlation between sleeper accelerations and passing-by train speeds.

4.5.8 BALLAST PARTICLE ACCELERATION

4.5.8.1 FIRST RESULTS

The first tests were run with two aluminium ballast particles that were placed at the spot between sleepers and rails, one on the surface and another buried at the depth of the sleeper base. The train that passed during the record was a Siemens Velaro 350 running at 285 km/h (Figure 47).

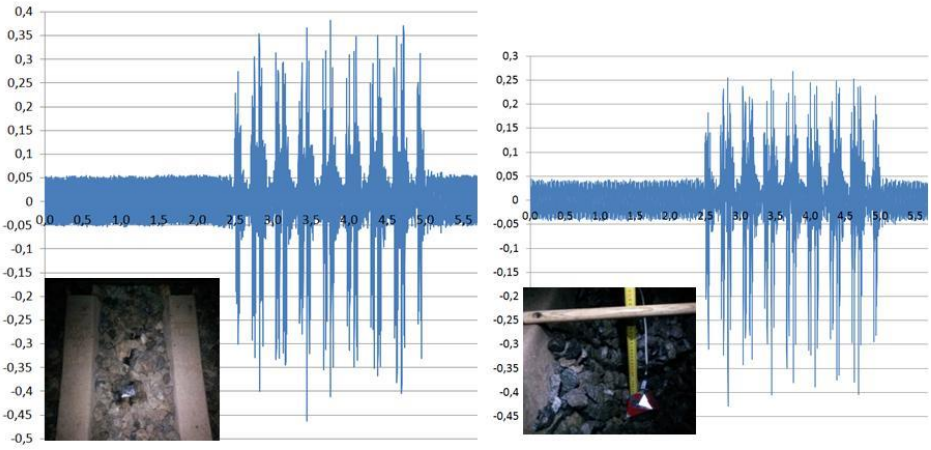

(Positive values of accelerations are represented in the same direction as gravity)

FIGURE 47: BALLAST ACCELERATION MEASURED WITH AN ALUMINUM PARTICLE

The graphs show the differences between the records obtained in the two positions: the peak accelerations are about 30% lower in the buried position for the up vertical accelerations while the down vertical accelerations are very similar (5% lower for the buried).

The next step was to use real ballast particle instrumented with accelerometers inside. In this case, the objective was to have data of ballast acceleration. To do so, after working out the raw data acquired to transform the values of (x,y,z) based on the accelerometer coordinate system to the values of (x,y,z) based on the track coordinate system, only the track z values were considered.

The following graph (Figure 48) represents the vertical accelerations when a Siemens Velaro train runs at 300 km/h with a sampling frequency of 1.6 kHz followed by a graph of its frequency spectrum.

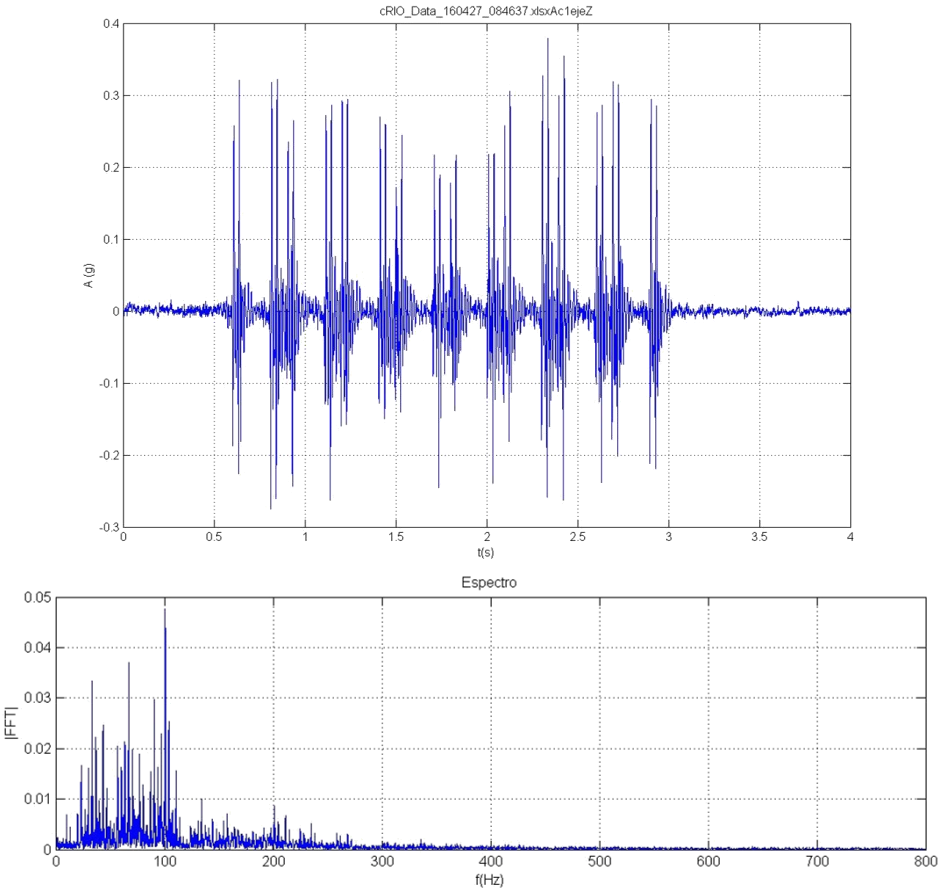

FIGURE 48: VERTICAL BALLAST PARTICLE ACCELERATIONS FOR A SIEMENS VELARO TRAIN RUNNING AT 300 KM/H AND ITS FREQUENCY SPECTRUM

Figure 49 represents the values of some expected frequencies for the same train running at 300 km/h according to the distances of some of the train and the track elements.

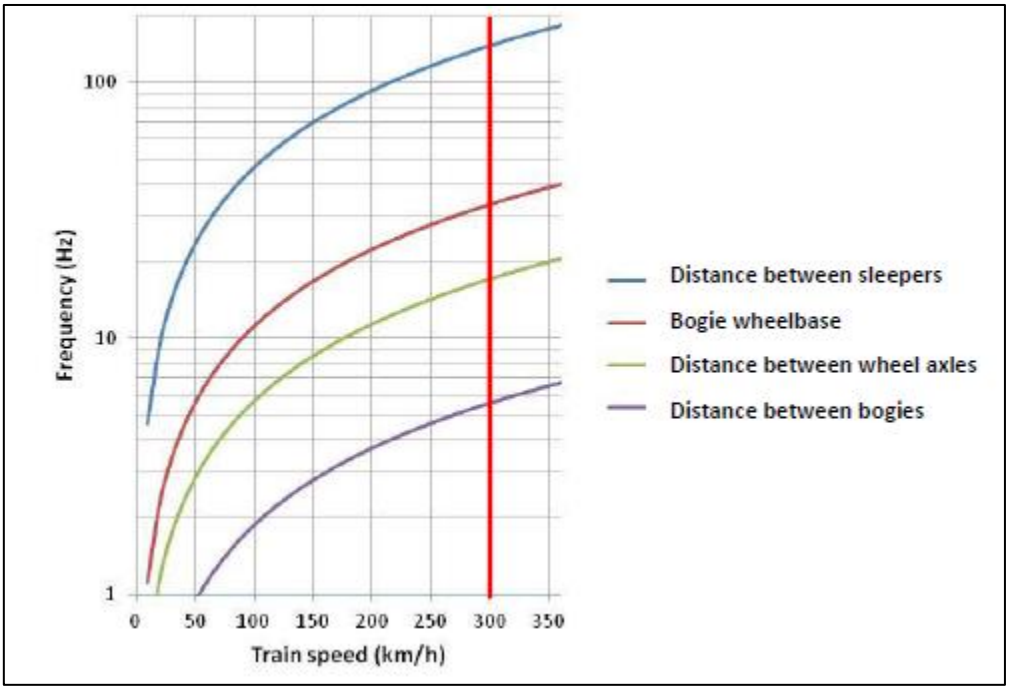

FIGURE 49: EXPECTED FREQUENCIES FOR THE SAME TRAIN RUNNING AT 300 KM/H ACCORDING TO THE DISTANCES OF SOME OF THE TRAIN AND THE TRACK ELEMENTS

In order to remove noise from the acceleration's graph, a low pass filter (275-300 Hz) was applied. Figure 50 represents a superposition of the same graph before and after applying the low pass filter (red without and green with filter).

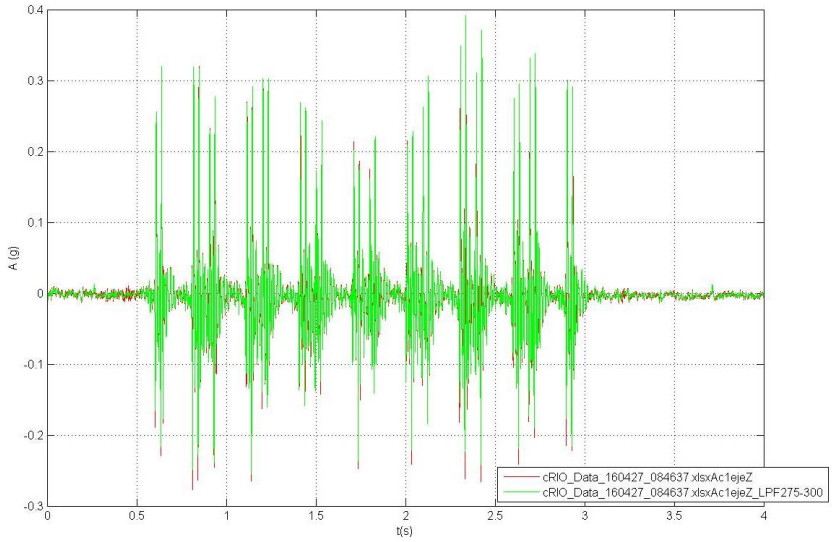

FIGURE 50: VERTICAL BALLAST PARTICLE ACCELERATIONS FOR A SIEMENS VELARO TRAIN RUNNING AT 300 KM/H AND THE SAME DATA FILTERED WITH A LOW PASS FILTER (275-300 HZ)

As it can be seen, there are just slight differences between both graphs, thus and after filtering different files it was concluded that for the purpose the project there was no need to include the filtering process.

4.5.8.2 STABILIZATION OF VALUES

For the next campaigns it was taken into consideration the fact that digging into the ballast layer to place a ballast particle is modifying the equilibrium of that area, even if it is done carefully trying to affect the minimum number of ballast particles and to maintain the sleeper-ballast contact.

A test was run to find out the moment when the acceleration values are reliable after the placement of the instrumented ballast particles. This test was run with real ballast particles with accelerometers inside, buried at 3 and 11 cm under the sleeper base.

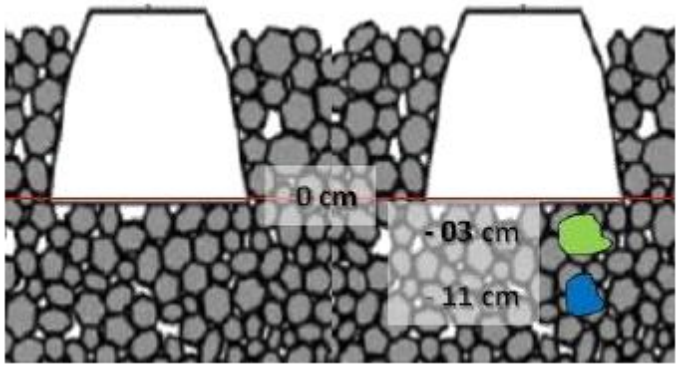

FIGURE 51: POSITION OF THE INSTRUMENTED BALLAST PARTICLE IN ONE OF THE TESTS

A daily average of 1072 axles and 16085 tons passed over the ballast particle position during the test, and 65% of the trains ran at 300 km/h. Figure 51 shows the evolution of the accelerations detected for only a specific kind of train running at 300 km/h, each graph represents the RMS values of the peak accelerations of a single day.

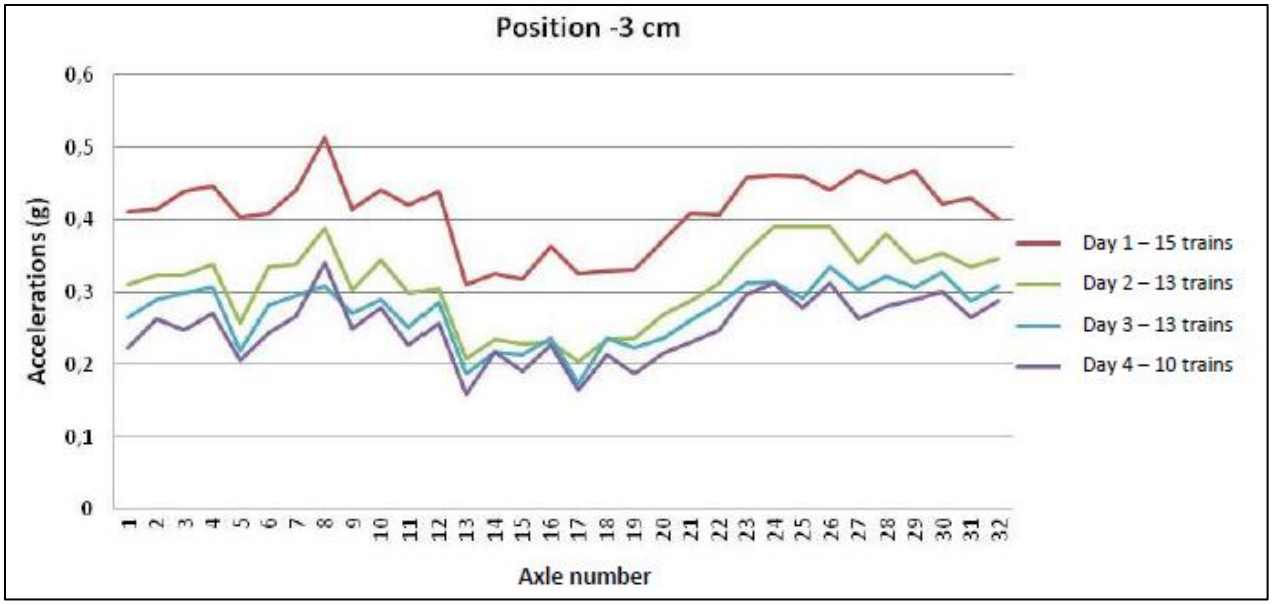

FIGURE 52: BALLAST PARTICLE ACCELERATION AS A FUNCTION OF THE DAYS PASSED SINCE THE PARTICLE PLACEMENT

The results show that after the third day, and for the traffic conditions mentioned above, the results begin to be stabilized. Note that these values of accelerations are in the opposite direction to gravity. For the accelerometer placed at -11 cm, the values show that even the second day results are stable.

4.5.8.3 BALLAST ACCELERATIONS AND AXLE LOAD

As expected, there is a clear relation between ballast accelerations and the axle load of the train. In the next graph (Figure 53) representing the positive and negative peak accelerations caused by a 32 axles train at 3 and 11 cm under the sleeper, the yellow graph represents the tons for each axle. Note that the positive values of the acceleration are in the opposite direction to gravity.

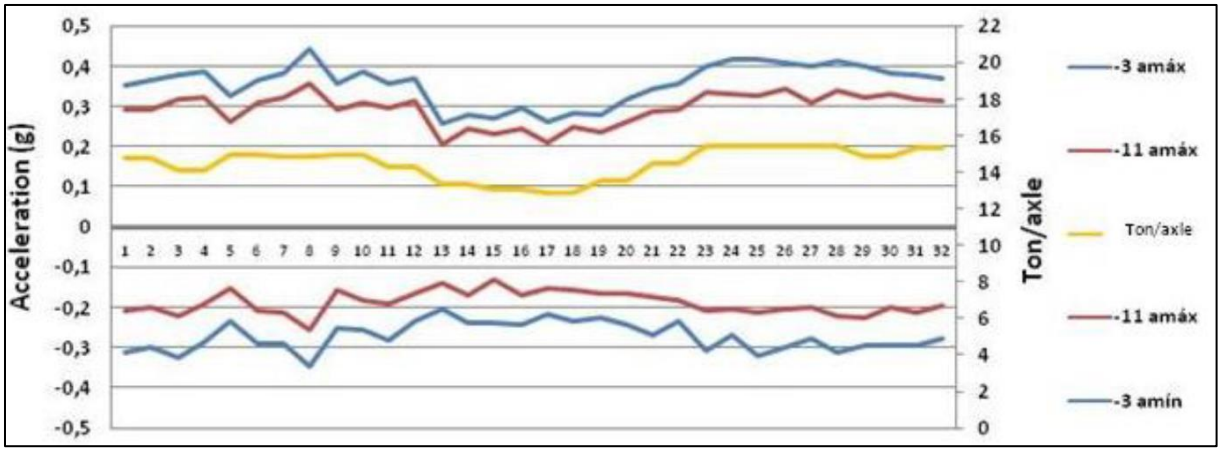

FIGURE 53: BALLAST PARTICLE ACCELERATION AS A FUNCTION OF THE AXLE LOAD

4.5.8.4 TRAIN COMPARATIVE

In Figure 54 it can be seen that each brand of train has a different acceleration "footprint", in this case the comparative is done between two groups of trains running at 300 km/h with an accelerometer placed 3 cm below the sleeper. The graphs show the positive and negative peak accelerations of each group.

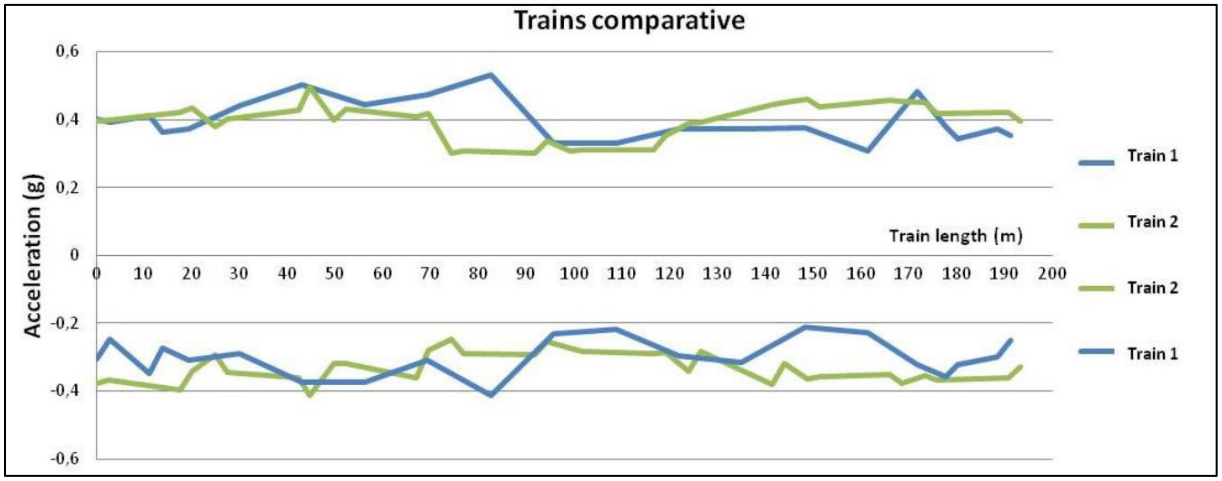

FIGURE 54: BALLAST PARTICLE ACCELERATION AS A FUNCTION OF THE PASSED-BY TRAIN

4.5.8.5 ACCELERATIONS AT DIFFERENT DEPTHS

Figure 55 shows a comparative of the accelerations at the depths and positions represented in the scheme below. The values were taken from ten Siemens Velaro trains running at 300 km/h.

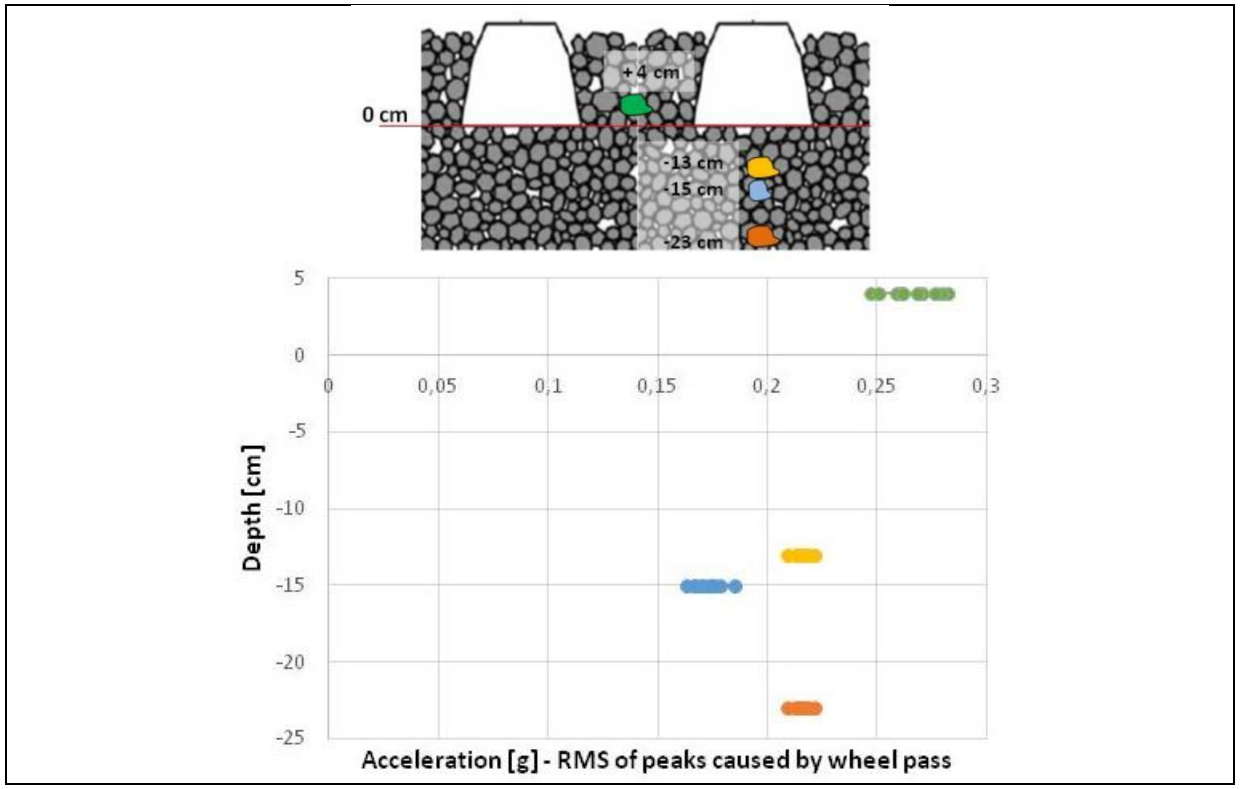

FIGURE 55: BALLAST PARTICLE ACCELERATION AS A FUNCTION OF THE DEPHT

The results show that accelerations are reduced with depth, but even at a depth of 23 cm below the sleeper base the accelerations are similar to those obtained at 13 cm. Those results will leave to future test campaigns and computer simulations the determination of the values at deeper positions.

The information obtained in this kind of tests will let us know deeper the behavior of the ballast bed, thus will be useful to determine the mass of ballast affected by the train pass, being that mass “m” one of the variables needed to find the Critical Speed.

$$v_{cr} = \frac{2}{L}\sqrt{\frac{EI}{m}} \quad \Leftrightarrow \quad v_{cr} = \sqrt[4]{\frac{4kEI}{m^2}} \quad \Leftrightarrow \quad v_{cr} = \sqrt[6]{\frac{K^2EI}{m^3}}$$

4.5.8.6 TEST CAMPAIGN OF PENETROMETER TESTS

In the same area where the accelerometers were placed, four penetrometer tests were performed to have a better knowledge of the ballast layer conditions in the surroundings (Figure 56).

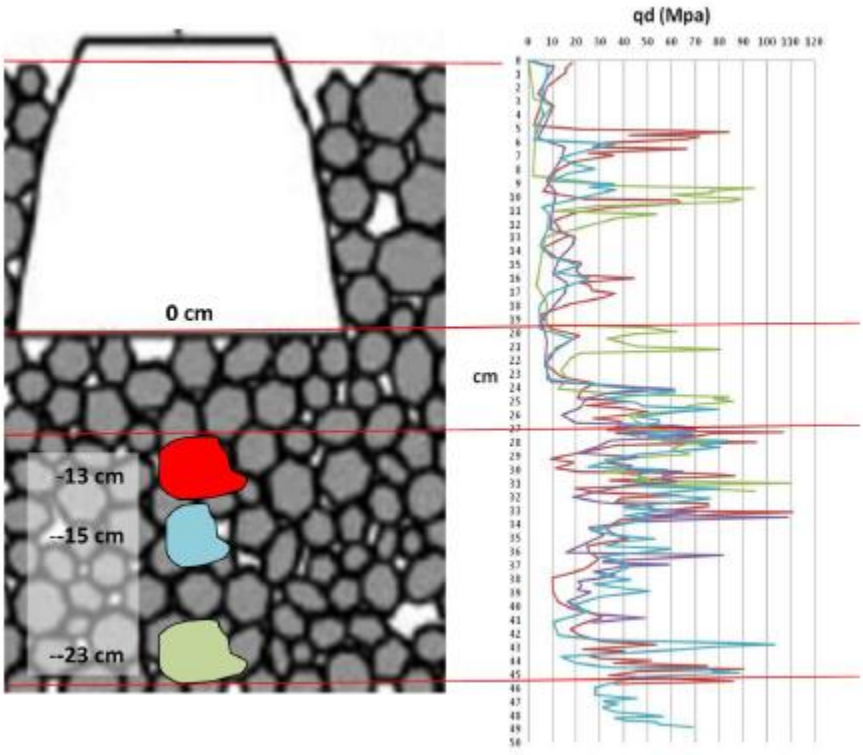

FIGURE 56: PENETROMETER TEST RESULTS

The results showed that from -23 cm to -40 cm (-3 cm to -20 cm considering the base of the sleeper as zero position) the ballast layer strength is several times higher than in the first 20 cm of the test.

5. Summary

This Appendix collects the data obtained in two in-situ test campaigns performed by CEDEX and ADIF, in two different places of Madrid-Barcelona High Speed Line.

The objective of these two campaigns was to create a data base of the railway track behaviour when subjected to the loads imposed by pass-by of trains. This data base can be used to calibrate numerical models and to compare with the results obtained in 1:1 scale models of railway track sections tested in CEDEX Track Box.

The instrumentation installed consisted of:

- Strain gauges to determine the loads imposed by the trains
- 2 Hz geophones to measure the vertical velocity of the vibration in the rail. It is also possible to obtain the rail deflections by integrating these velocity signals.
- 1 Hz geophones to measure the vertical velocity of the sleeper vibration.
- Accelerometers to measure the rail and sleepers accelerations.
- Potentiometers to measure the rail-sleeper relative motion, from which it is possible to calculate the pad deformation.

Additionally, some ballast particles were instrumented with accelerometer to measure the ballast layer accelerations.

The signal analysis procedure is explained with some examples. Once analysed all the data according to the procedure, Table 15 shows the main results obtained.

TABLE 15: SUMMARY OF THE RESULTS OBTAINED IN THE TEST CAMPAIGNS

Parameter	Variation with speed	Range of values
Track stiffness	No	88 – 113 kN/mm
Pad vertical displacement	No	0.38 – 0.45 mm
Rail velocity	Slight increase	30 – 75 mm/s
Sleeper velocity	Increase	10 – 23 mm/s
Rail acceleration	No	1.0 – 2.5 g
Sleeper acceleration	No	0.65 – 0.80 g

6. Anexxes

ANNEX A RAW DATA OBTAINED IN THE SECOND CAMPAIGN

ANNEX B DATA FROM TRAINS ANALYSED

Collaborative project SCP3-GA-2013-60560

Increased Capacity 4 Rail networks through enhanced infrastructure and optimised operations

FP7-SST-2013-RTD-1

Deliverable 12.1

Innovative designs and methods for VHST (intermediate)

Appendix 8.2

Annex A

Raw data obtained in the second campaign

This Annex collects the time signals obtained for all the trains recorded in the second campaign, collected in Table 1.

Table 1: Recorded trains

TIME	TRAIN TYPE	SPEED (km/h) (±10 km/h)	COMMENTS
6:31:45	SIEMENS S103	300	(1)
6:52:39	SIEMENS S103	298	---
7:21:52	SIEMENS S103	300	---
7:41:25	TALGO S102	300	---
7:56:37	SIEMENS S103	248	---
8:01:29	CAF S120	239	---
8:21:04	SIEMENS S103	301	---
8:42:39	SIEMENS S103	297	---
8:52:26	SIEMENS S103	300	---
9:23:16	SIEMENS S103	299	---
9:52:01	SIEMENS S103	299	---
10:53:28	SIEMENS S103	299	---
11:35:54	**TALGO S102 (2)**	**299**	**Double(2)**
11:53:47	SIEMENS S103	293	---
12:07:44	**CAF S120**	**226**	---
12:51:19	SIEMENS S103	297	---
13:55:11	TGV	225	---
14:21:06	SIEMENS S103	298	---
14:52:22	SIEMENS S103	300	---
15:21:31	SIEMENS S103	297	---
15:34:49	CAF S120	229	---
15:54:57	SIEMENS S103	300	---
16:22:21	TALGO S102	295	---
16:54:24	SIEMENS S103	299	---
17:24:26	**SIEMENS S103**	**298**	**Double(2)**
17:38:59	TALGO S102	299	Double(2)
17:59:25	SIEMENS S103	224	
18:22:52	SIEMENS S103	302	---
18:59:06	SIEMENS S103	299	---
19:21:34	SIEMENS S103	220	---
19:23:31	SIEMENS S103	235	---
19:32:45	**TALGO S102**	**257**	---
19:53:03	SIEMENS S103	298	---
19:59:42	SIEMENS S103	239	---
20:21:57	**TALGO S102**	**300**	---
20:57:58	**SIEMENS S103**	**250**	---
21:49:46	**SIEMENS S103**	**299**	---

(1) Noise in sleeper accelerometer signals until 12:07:44;
(2) Double" means that the train is composed by two trains of the same type

The recorded parameters in all the trains are the following:

- Wheel loads (from strain gauges)
- Sleeper velocity (from sleeper geophones)
- Rail velocity (from rail geophones)
- Rail and sleeper accelerations (from accelerometers)
- Rail-sleeper relative motion (from potentiometers)

NAMING USED FOR EACH SENSOR

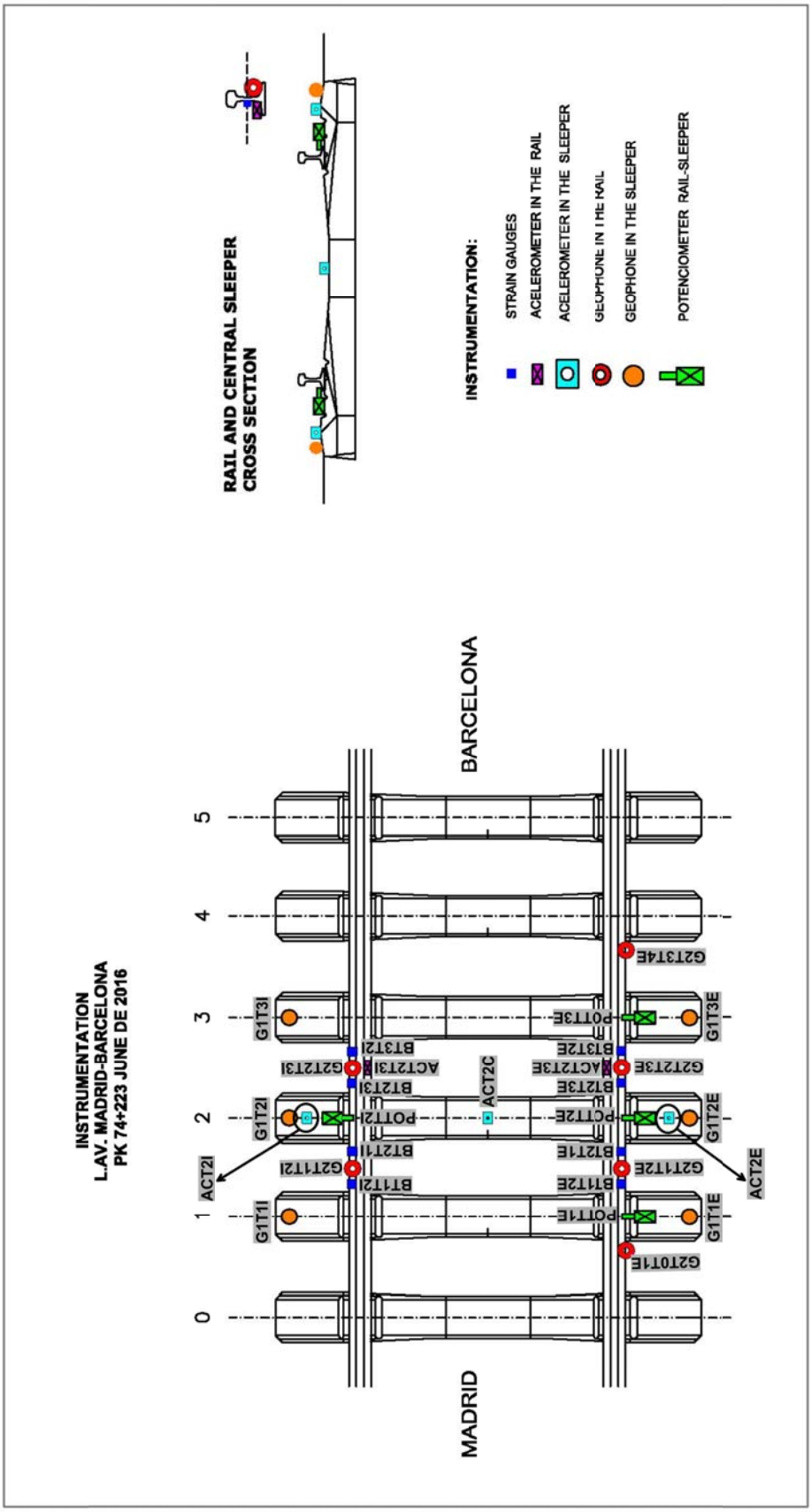

WHEEL LOADS

FROM STRAIN GAUGUES

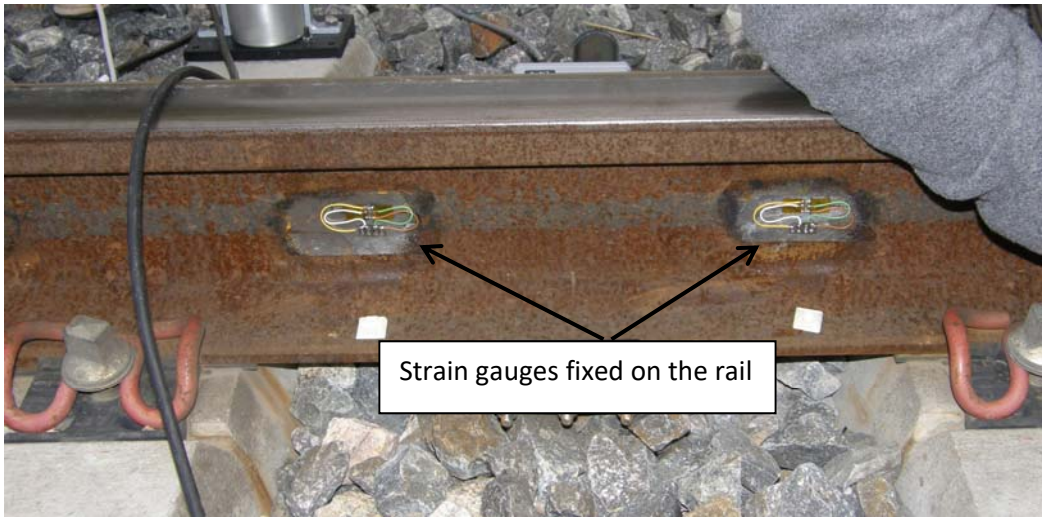

NOTES:

Units of Y axle are kilonewtons “kN” for all the plots belonging to Loads.

Units of Y axle are microstrain “με” for all the plots belonging to strain gauges.

A Low Pass Filter of 500 Hz has been applied to all raw signals.

Strain gauges
LPF 500Hz

01\06\16 06:31:45

Loads; LPF 500Hz

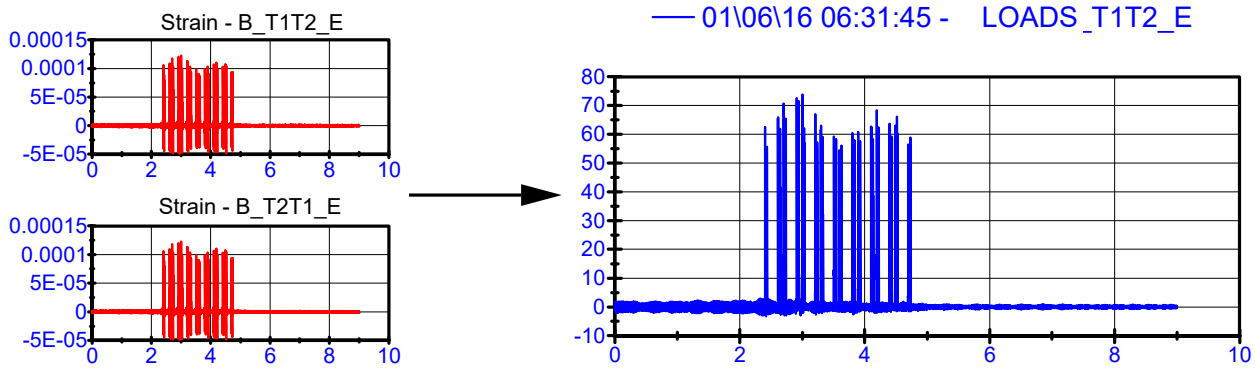

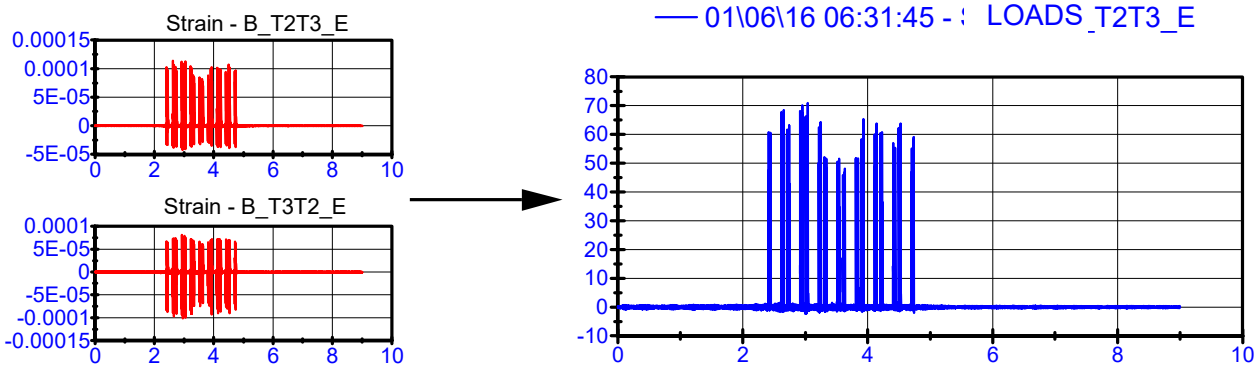

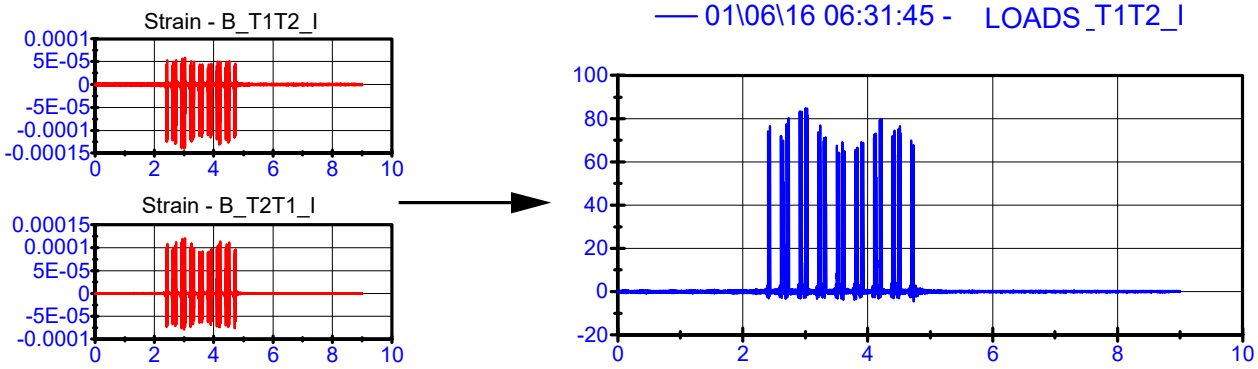

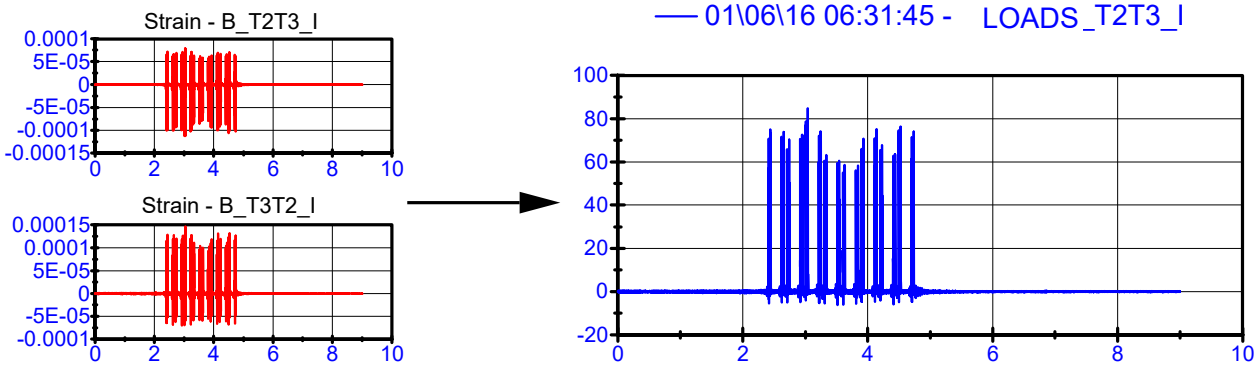

Strain gauges
LPF 500Hz

01\06\16 06:52:39

Loads; LPF 500Hz

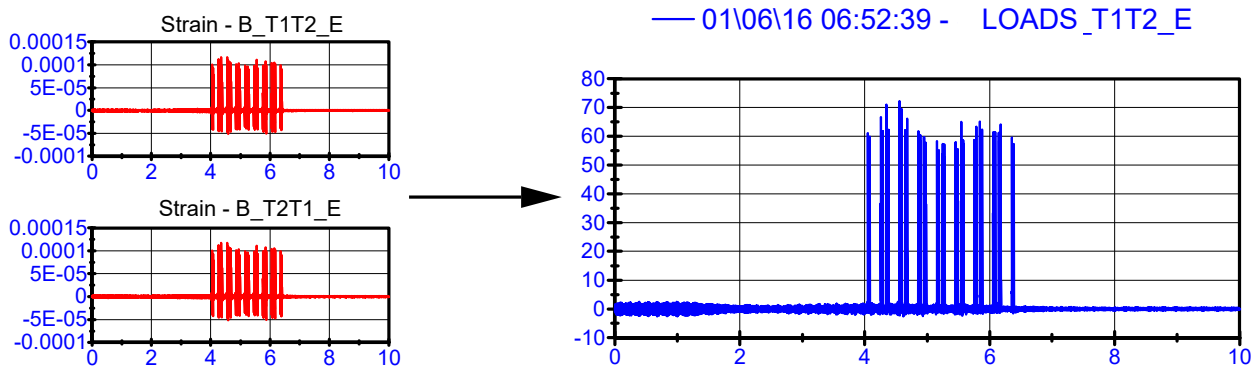

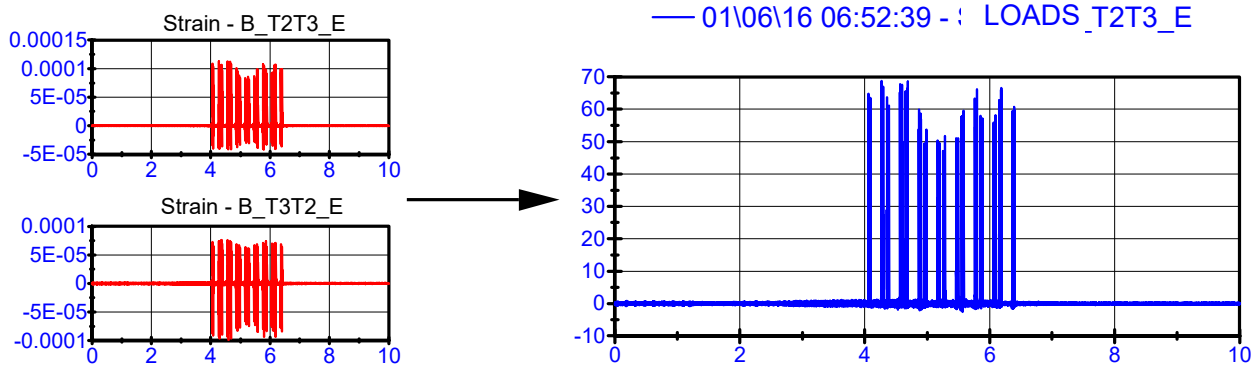

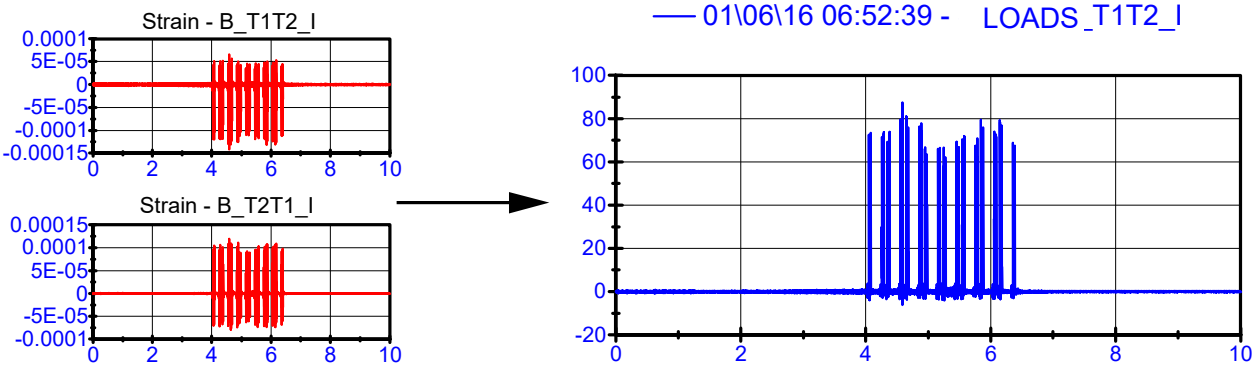

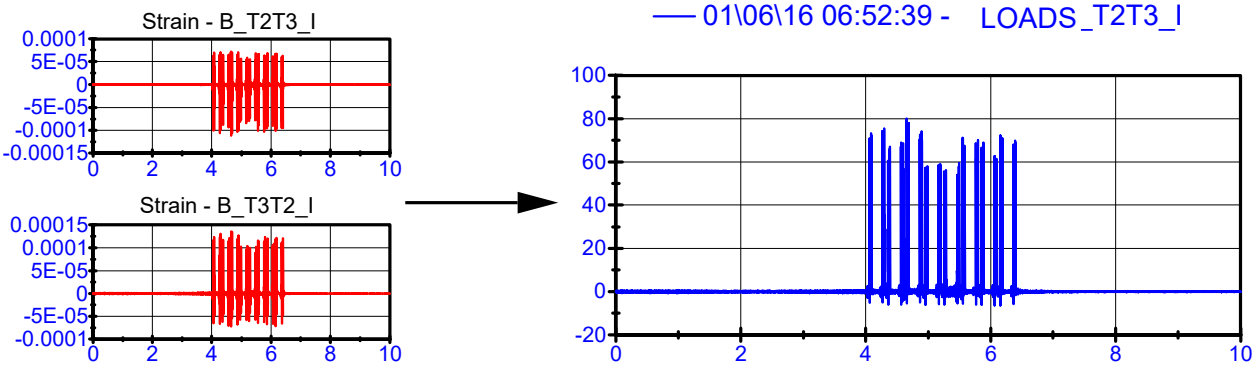

Strain gauges
LPF 500Hz

01\06\16 07:21:52

Loads; LPF 500Hz

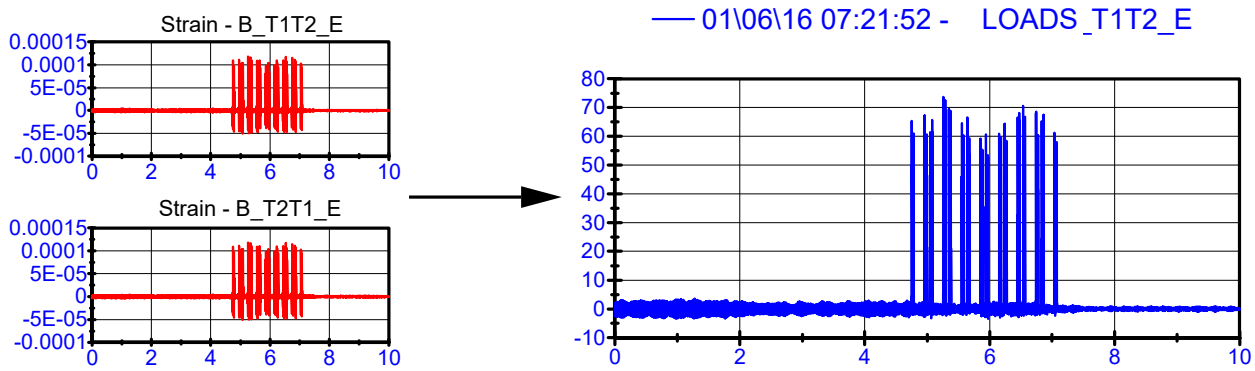

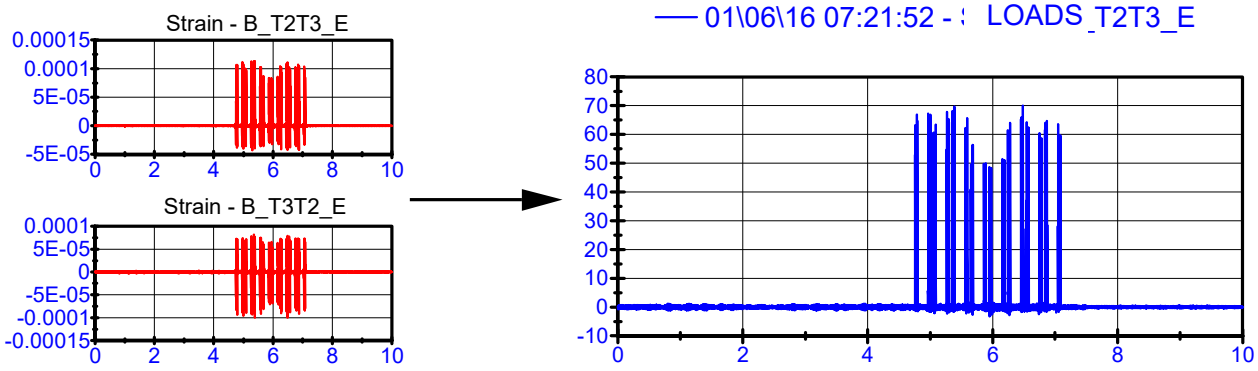

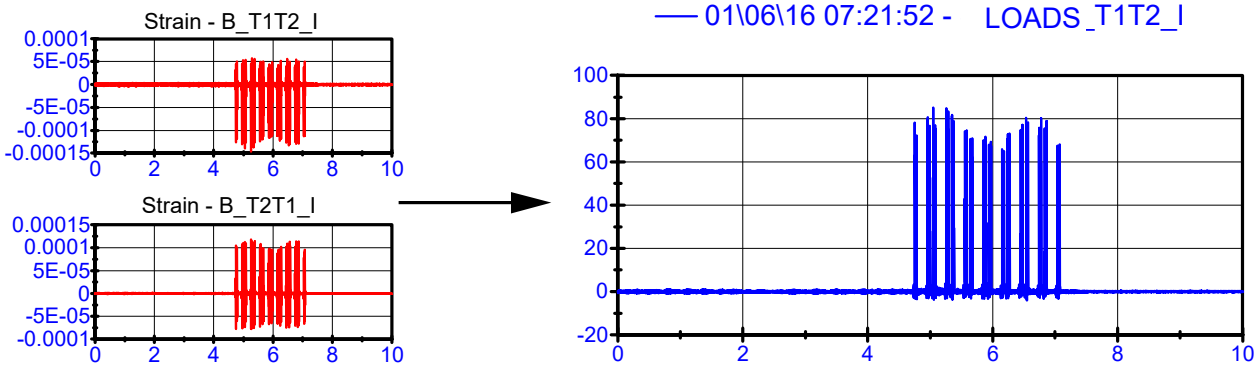

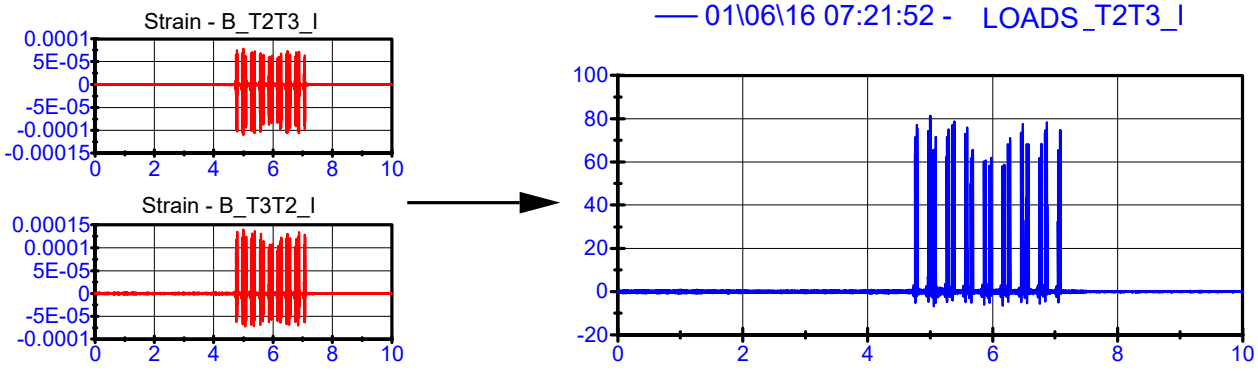

Strain gauges
LPF 500Hz

01\06\16 07:41:25

Loads; LPF 500Hz

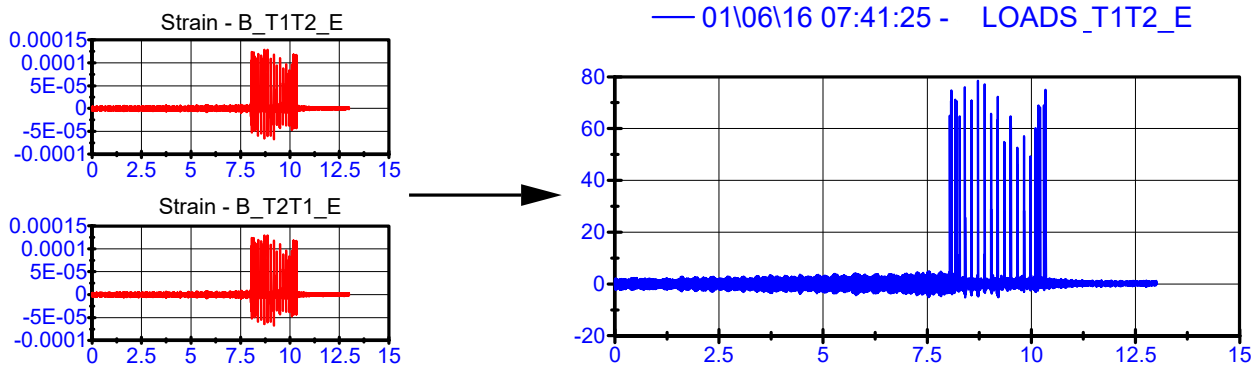

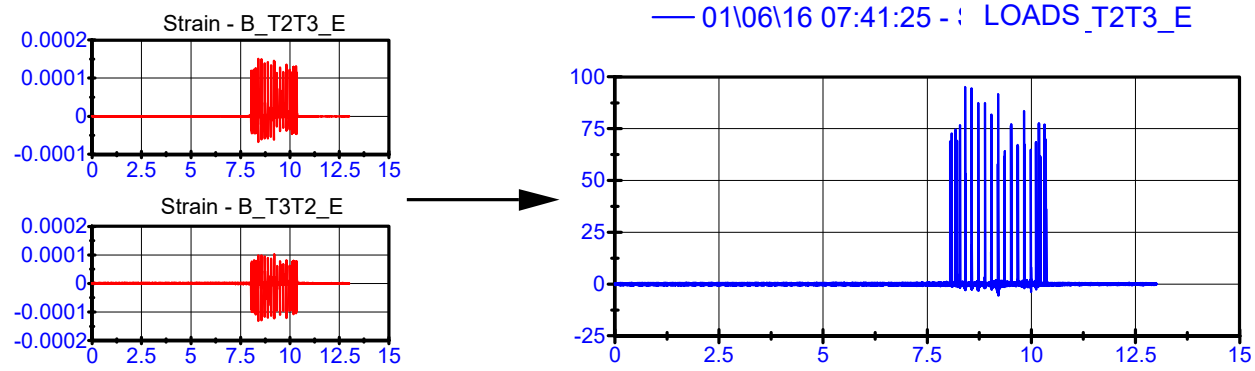

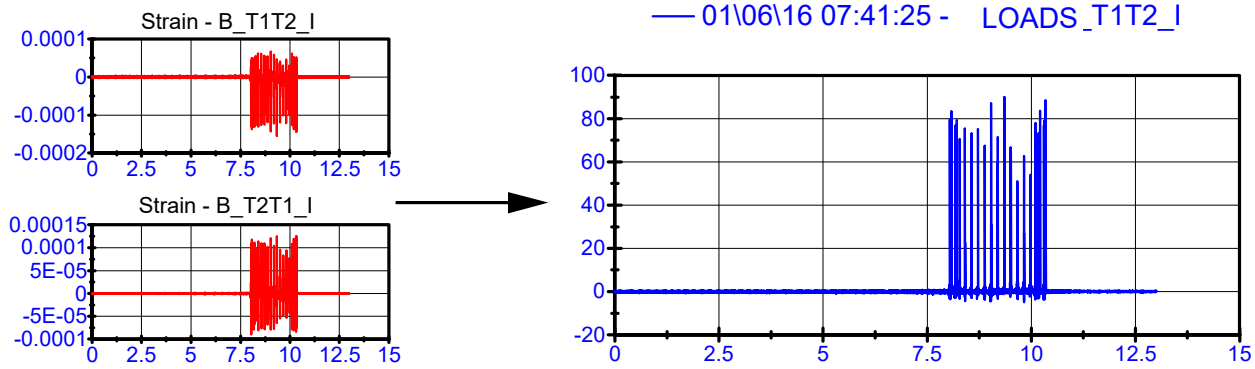

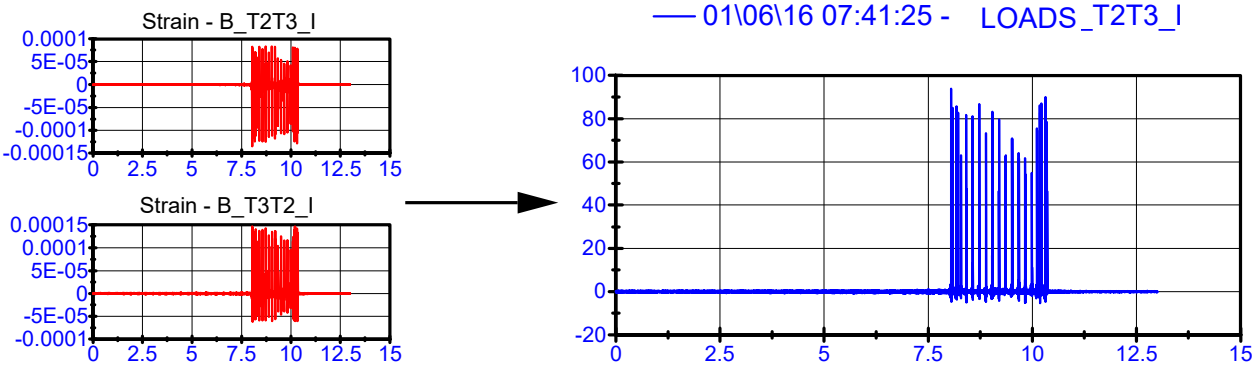

Strain gauges
LPF 500Hz

01\06\16 07:56:37

Loads; LPF 500Hz

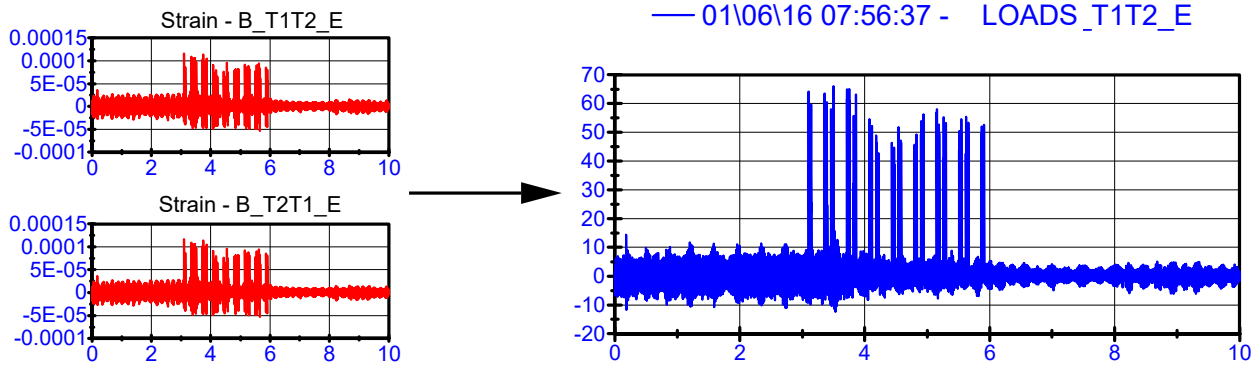

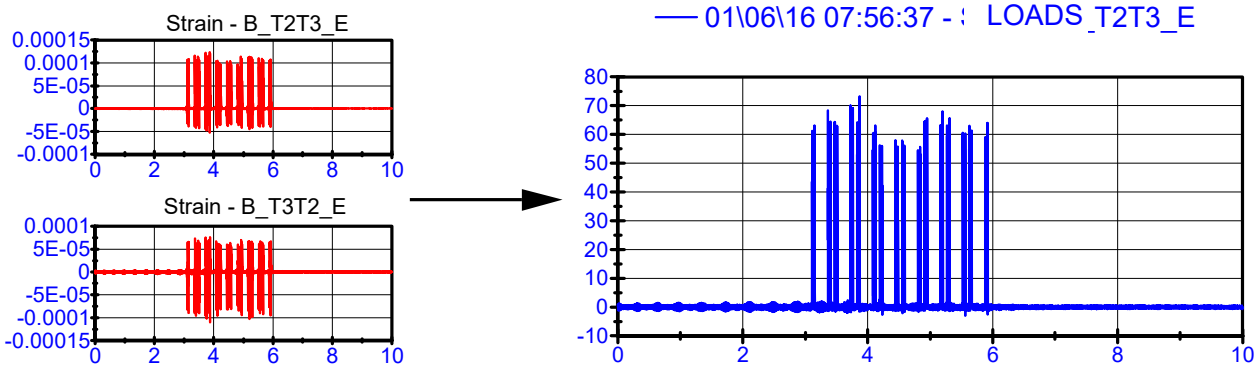

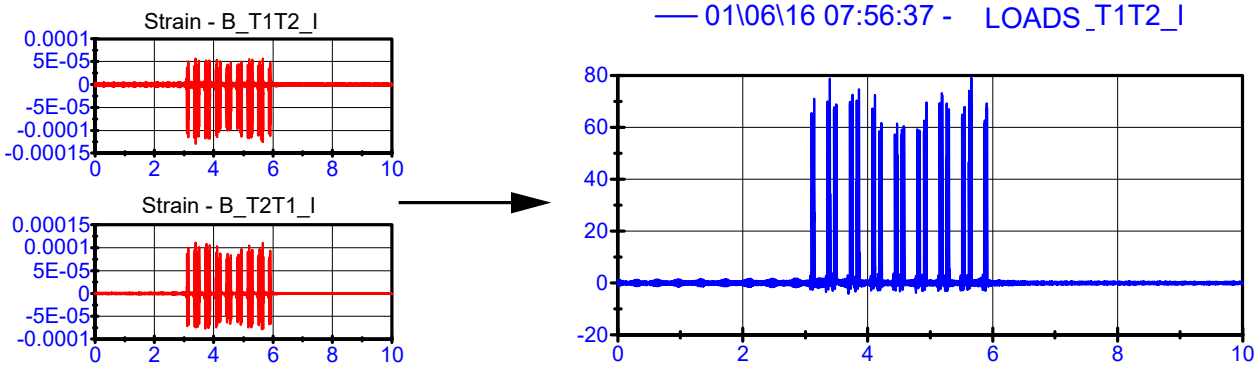

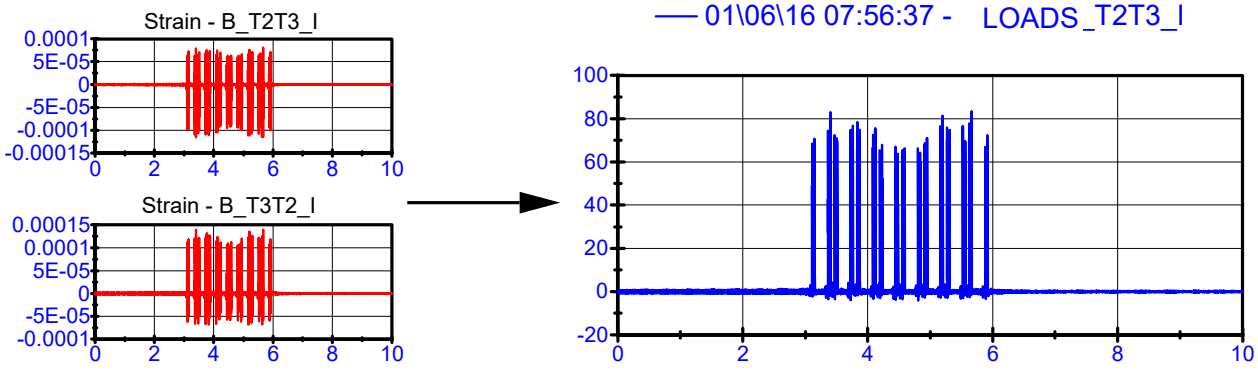

Strain gauges
LPF 500Hz

01\06\16 08:01:29

Loads; LPF 500Hz

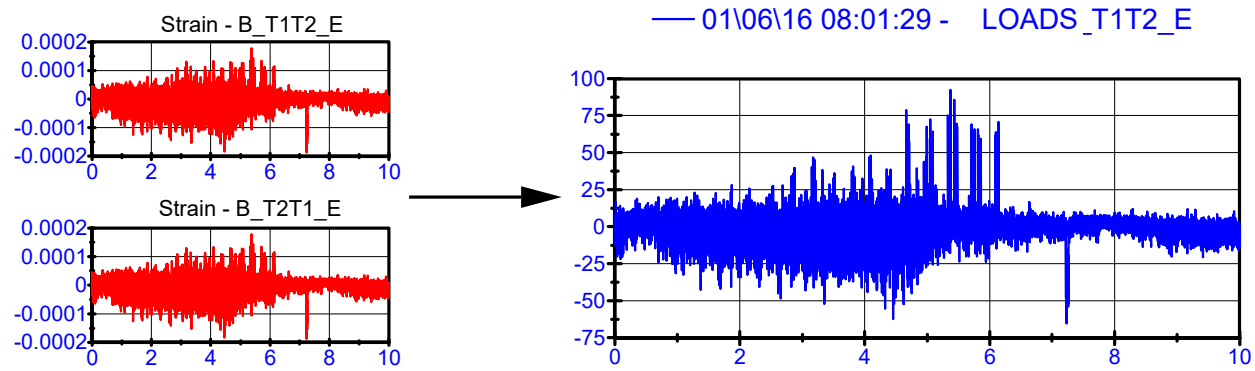

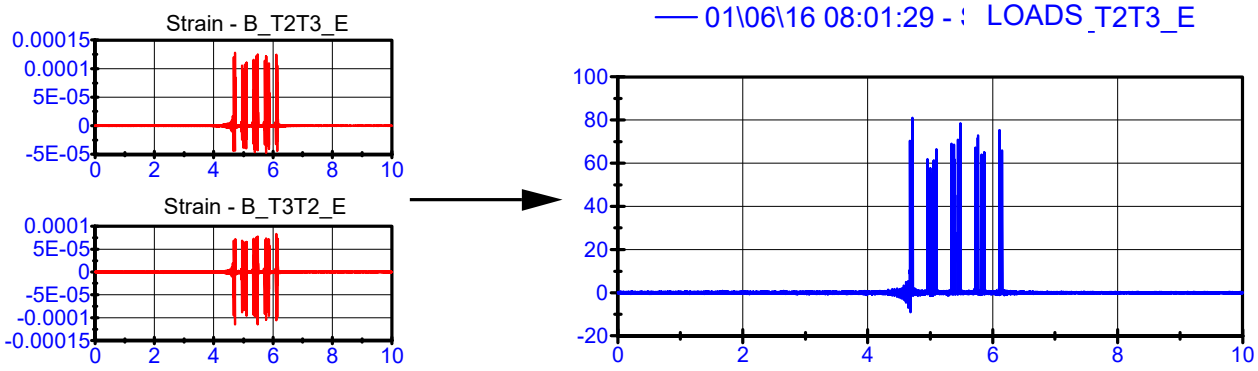

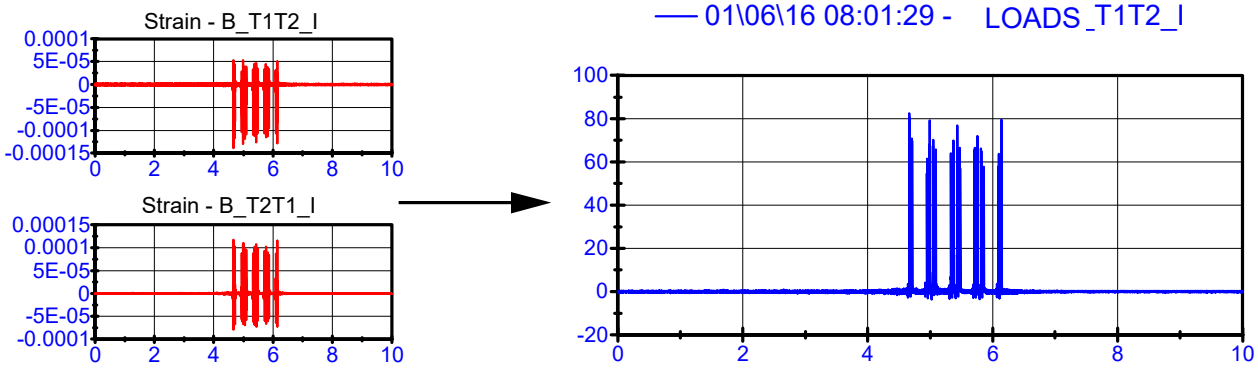

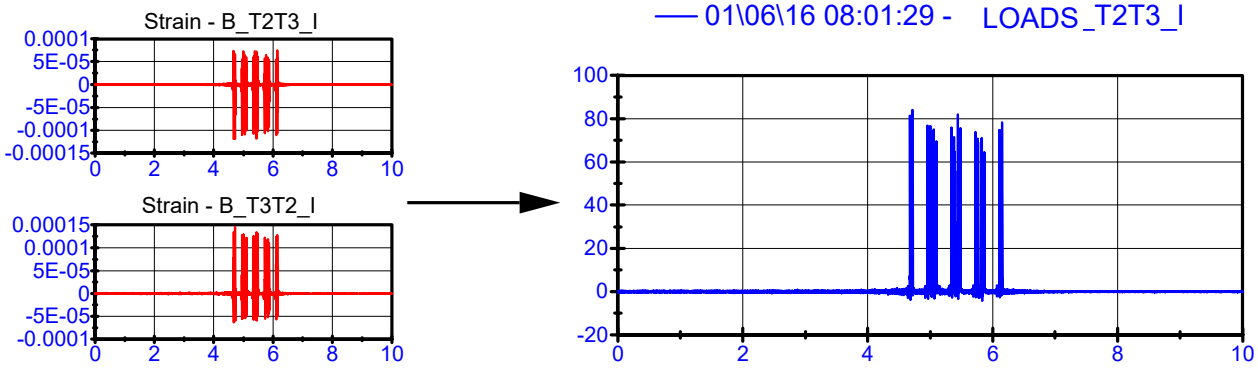

Strain gauges
LPF 500Hz

01\06\16 08:21:04

Loads; LPF 500Hz

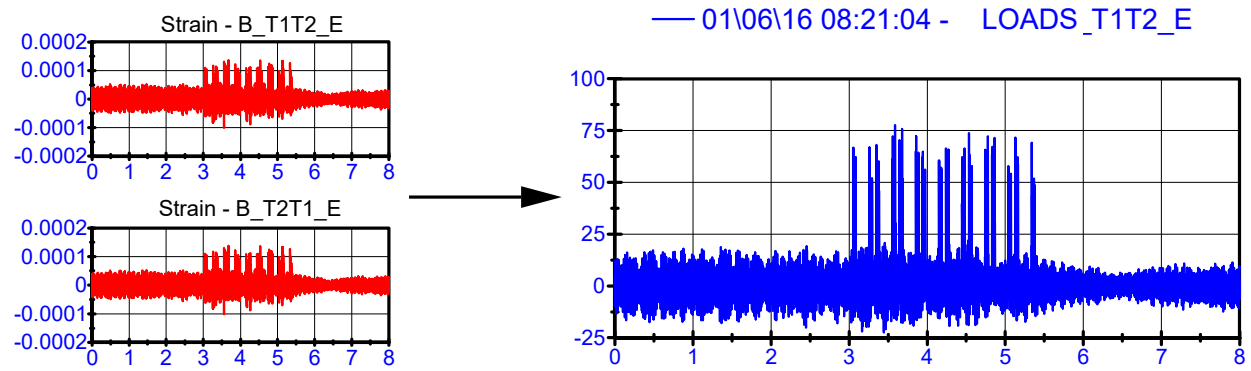

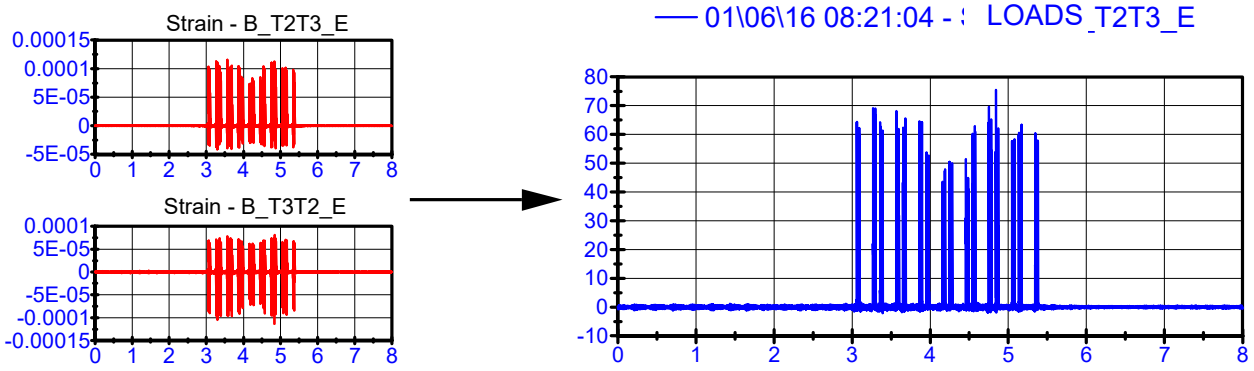

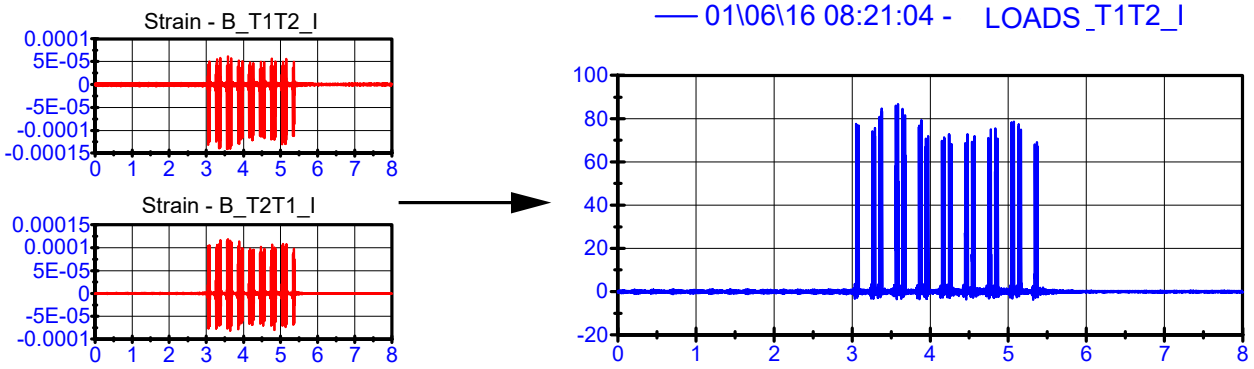

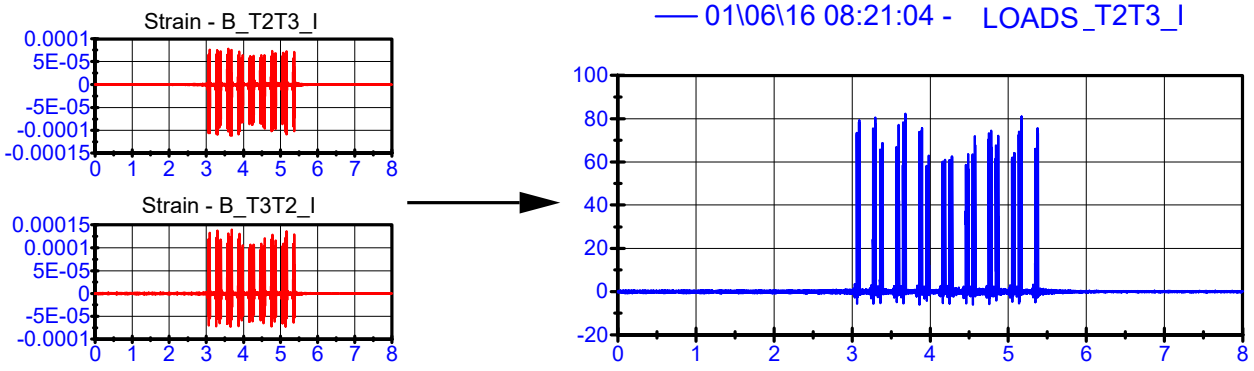

Strain gauges
LPF 500Hz

01\06\16 08:42:39

Loads; LPF 500Hz

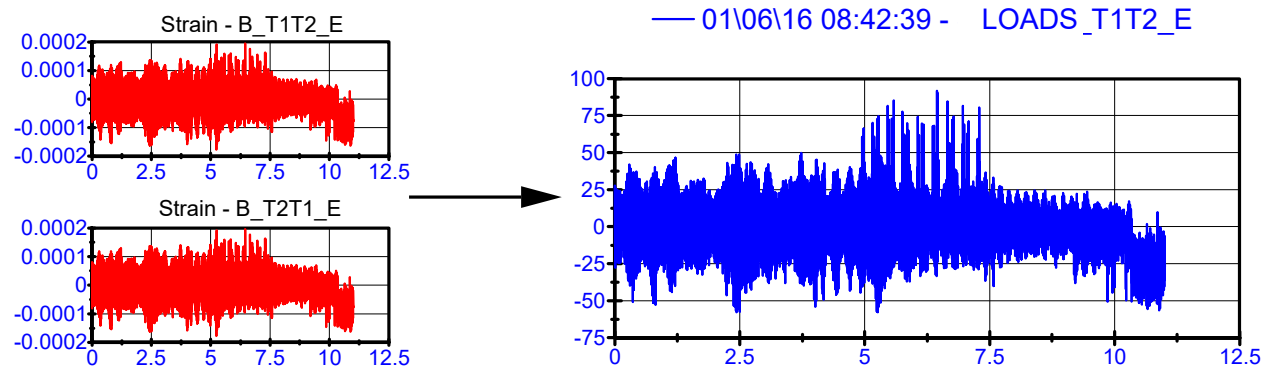

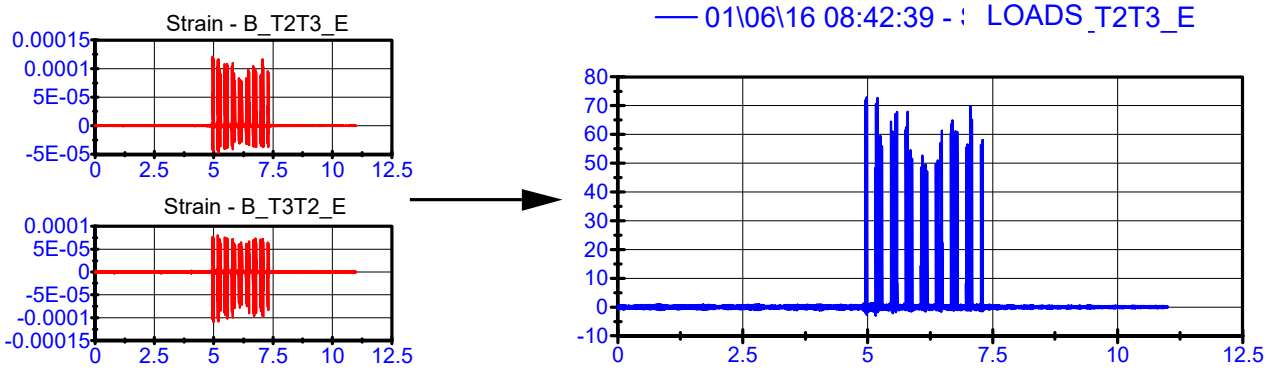

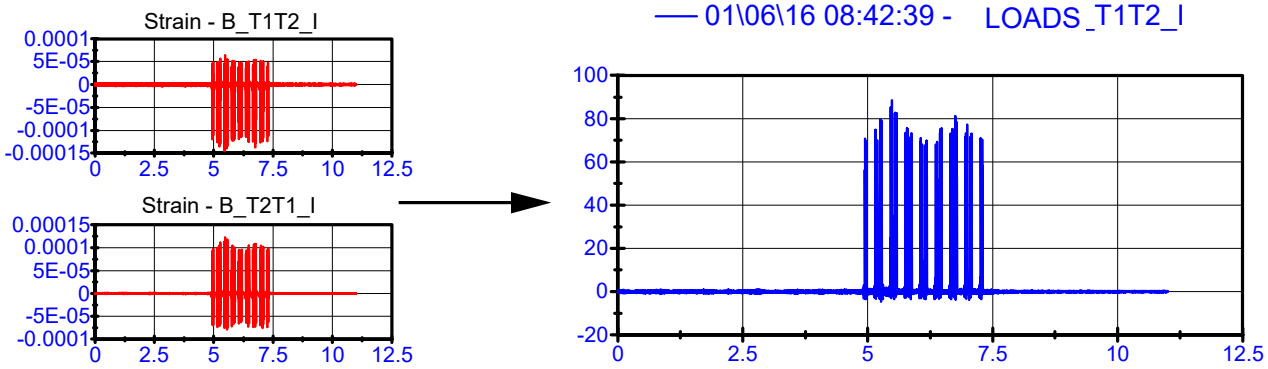

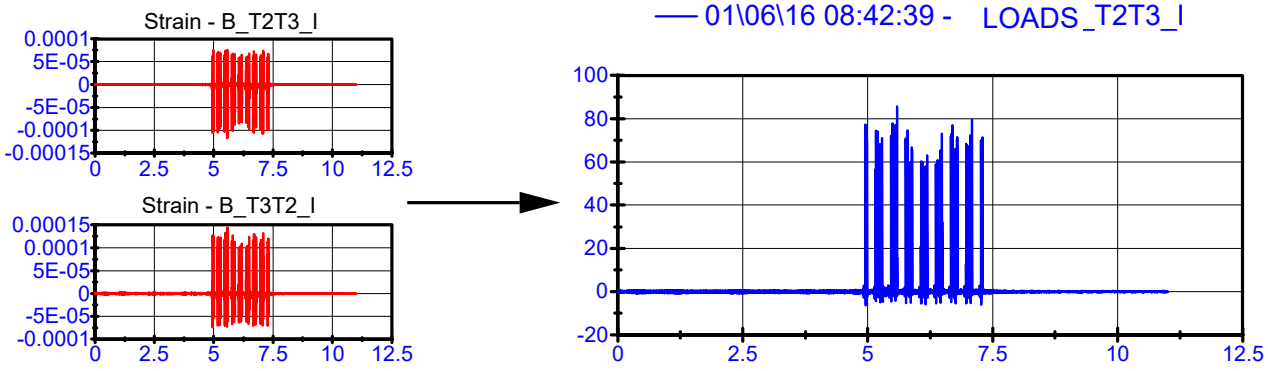

Strain gauges
LPF 500Hz

01\06\16 08:52:26

Loads; LPF 500Hz

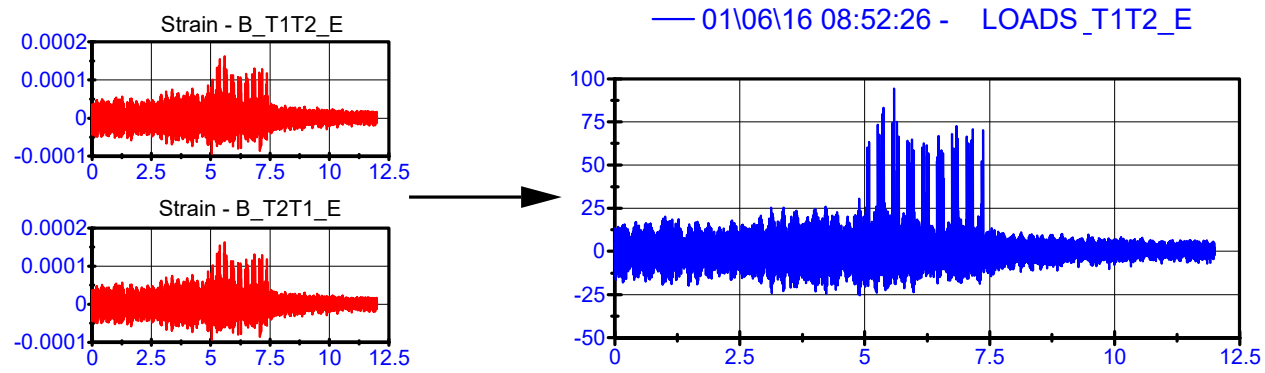

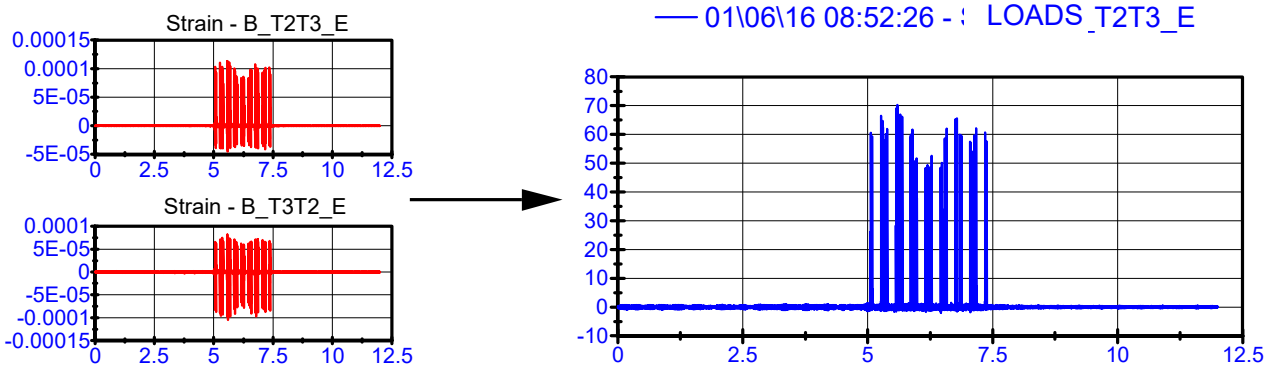

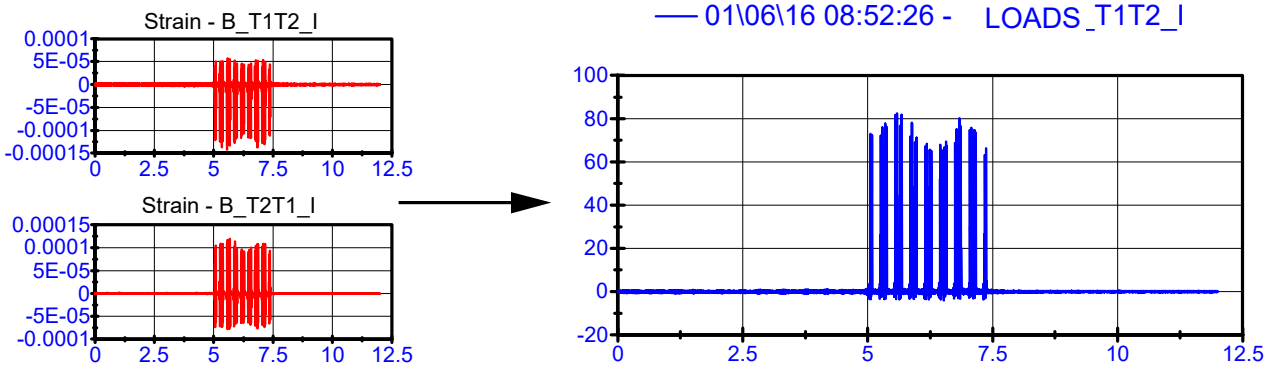

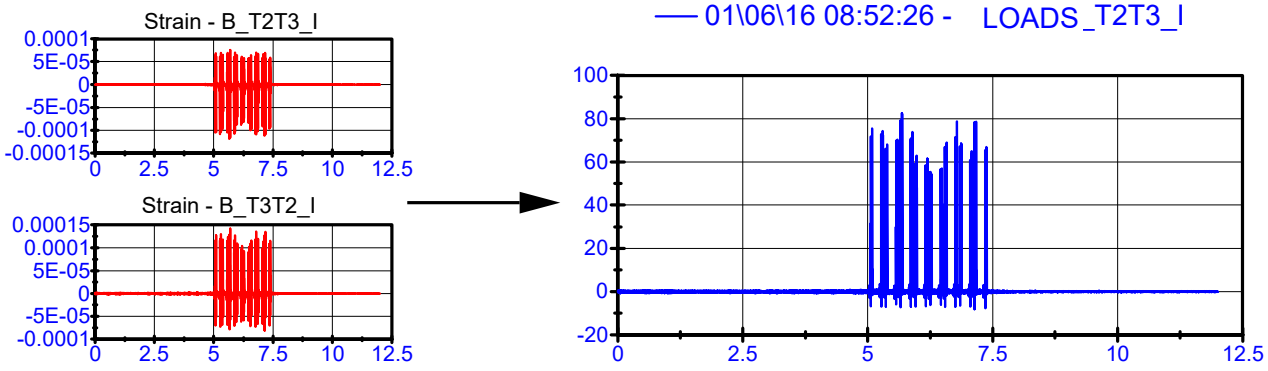

Strain gauges
LPF 500Hz

01\06\16 09:23:16

Loads; LPF 500Hz

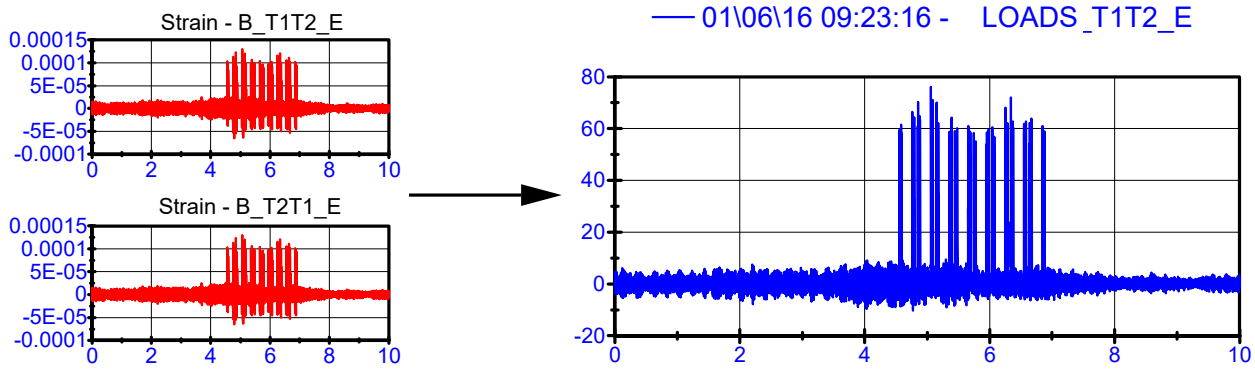

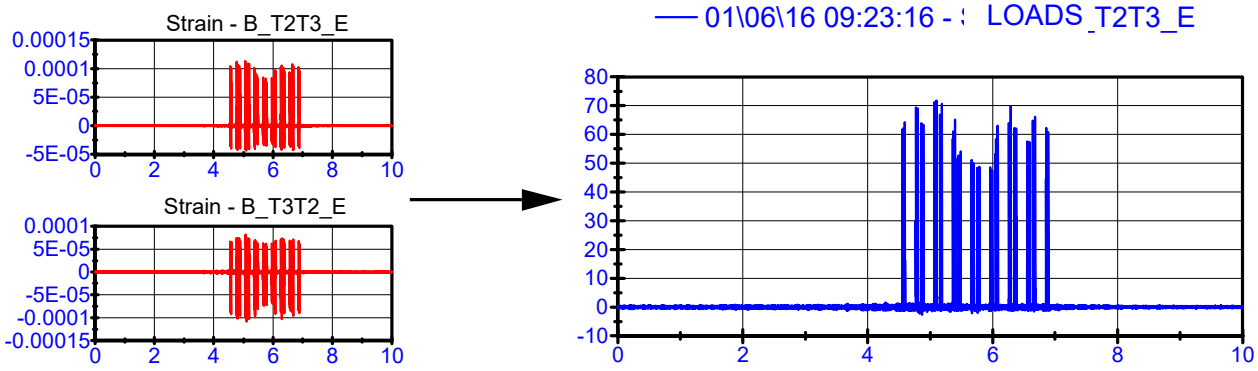

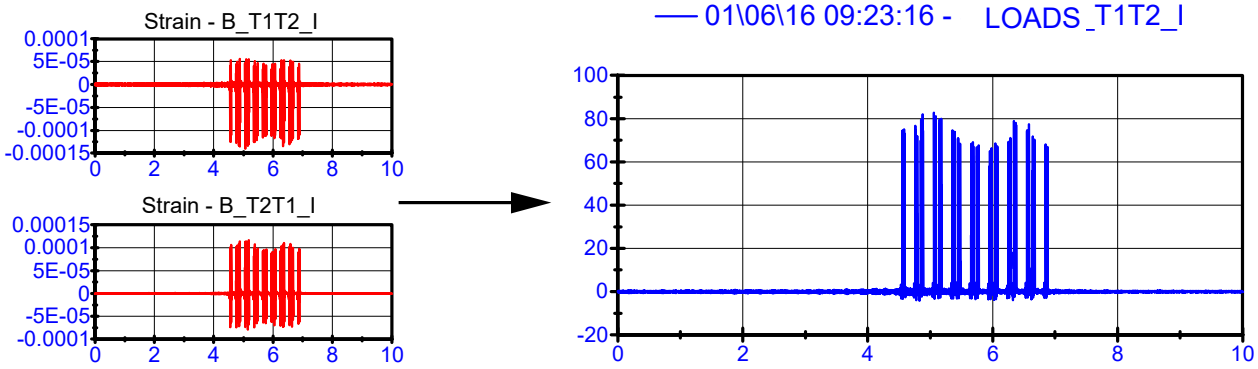

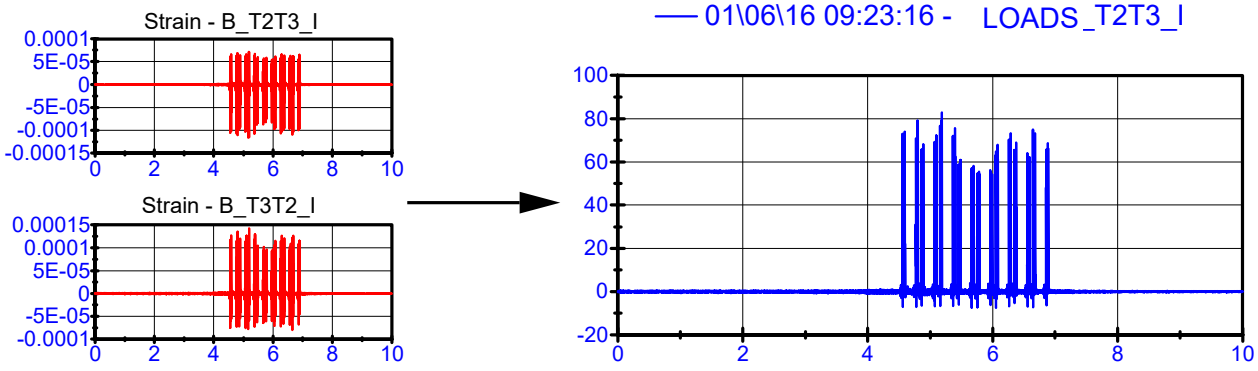

Strain gauges
LPF 500Hz

01\06\16 09:52:01

Loads; LPF 500Hz

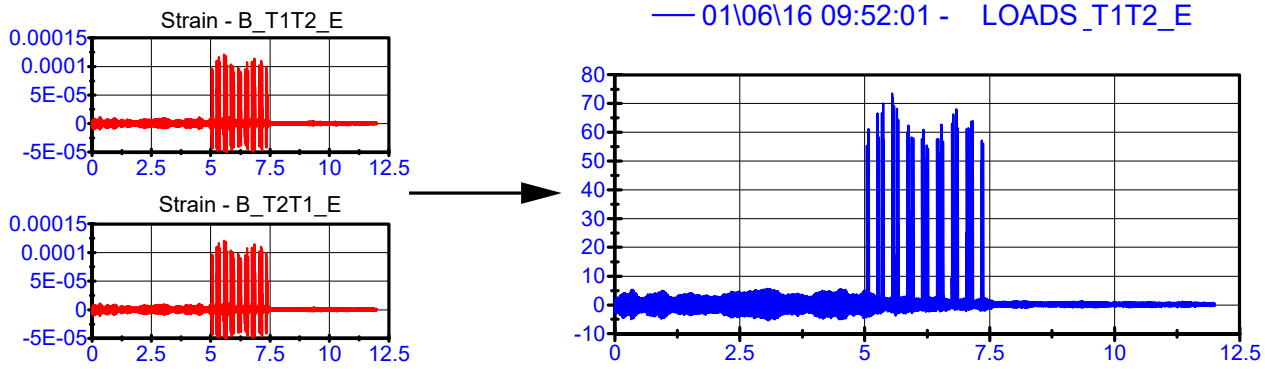

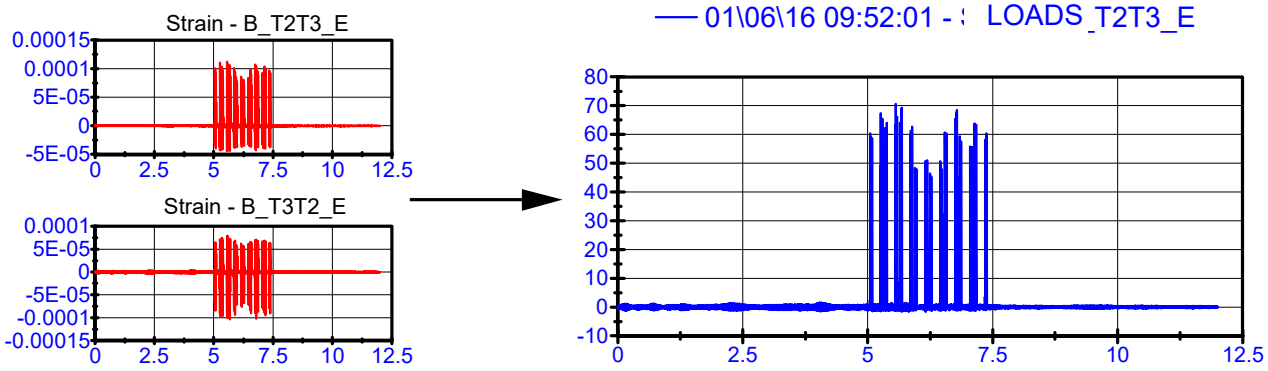

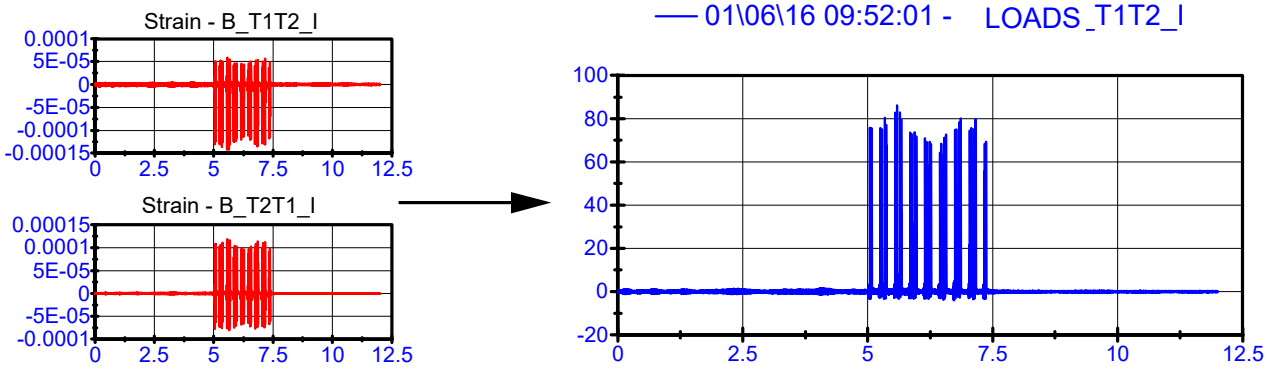

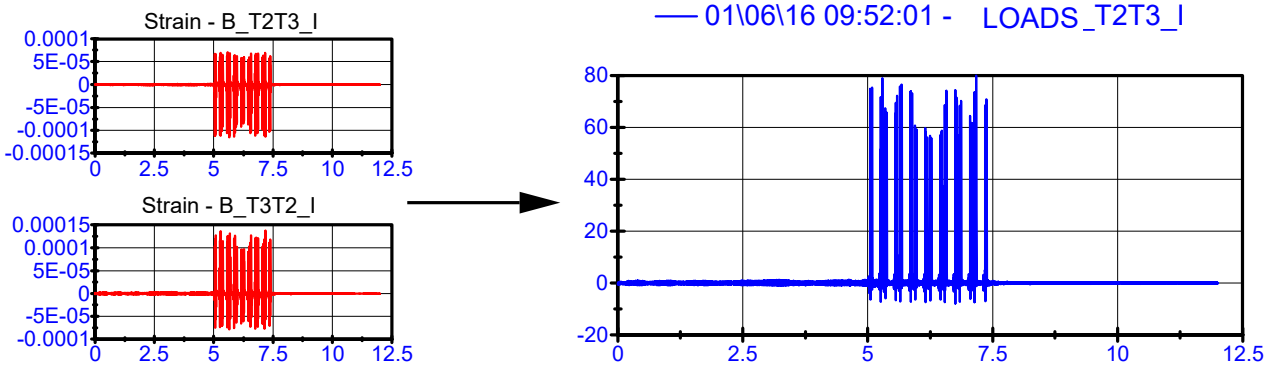

Strain gauges
LPF 500Hz

01\06\16 10:53:28

Loads; LPF 500Hz

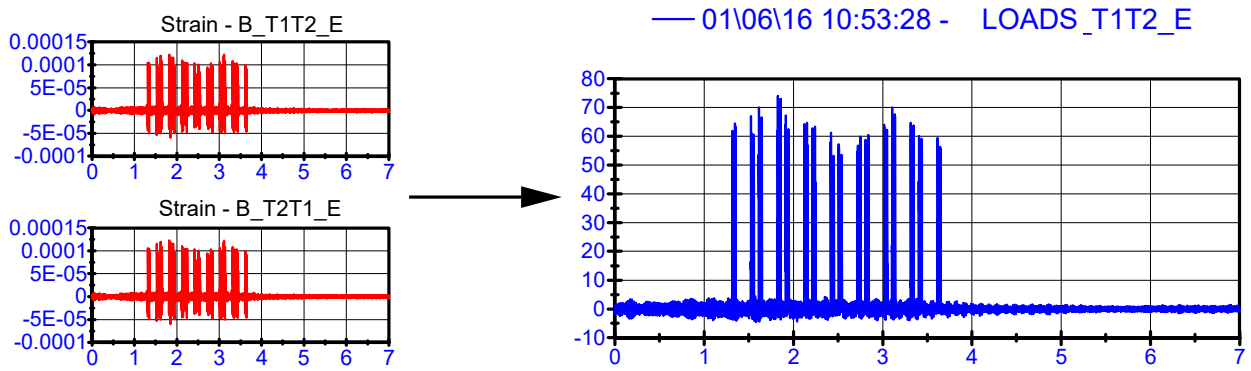

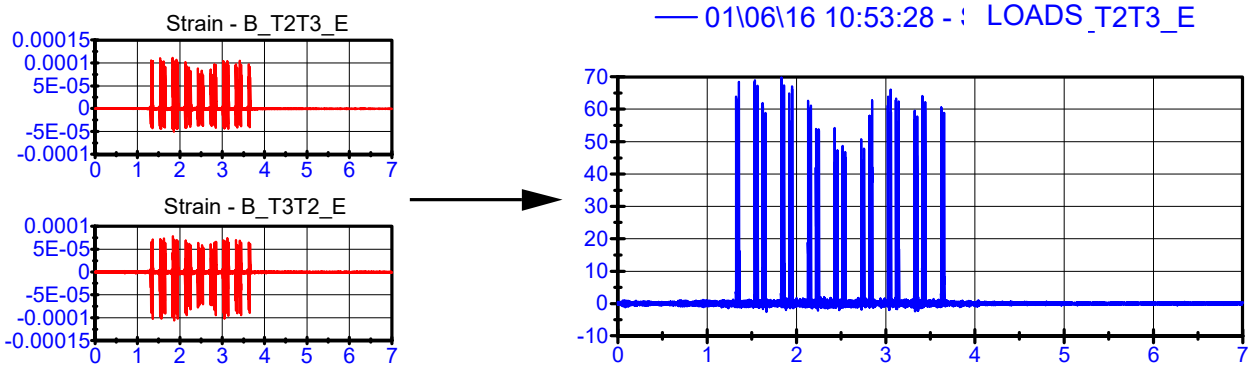

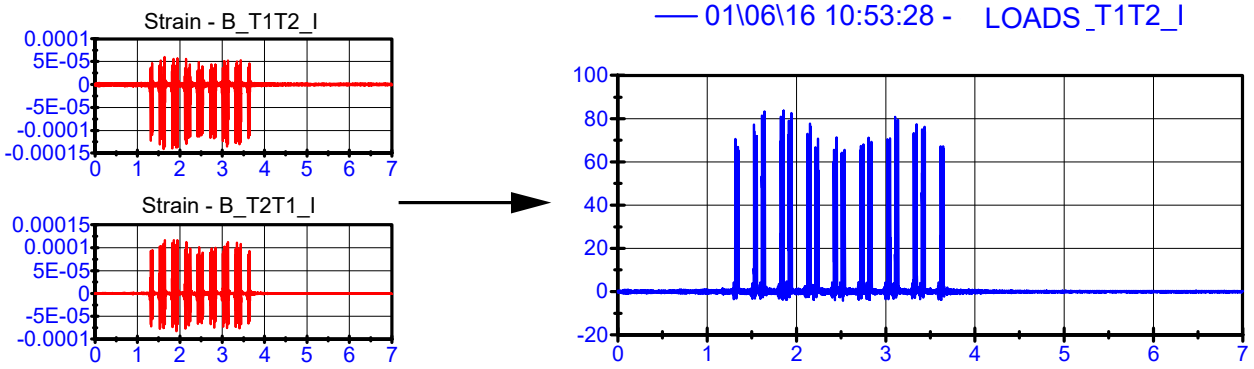

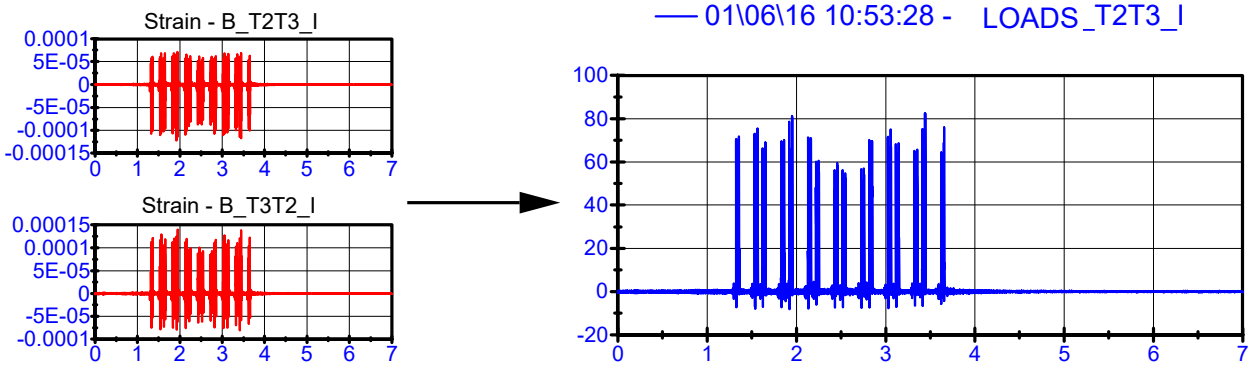

Strain gauges
LPF 500Hz

01\06\16 11:35:54

Loads; LPF 500Hz

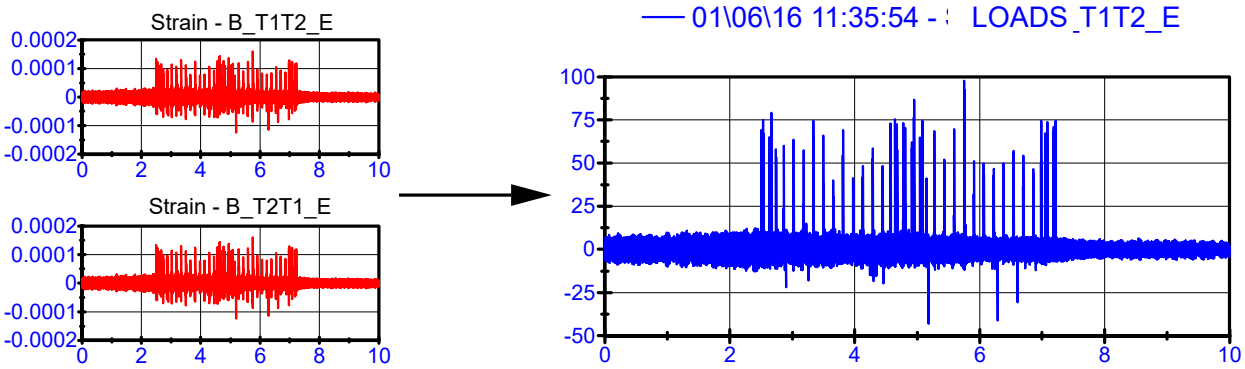

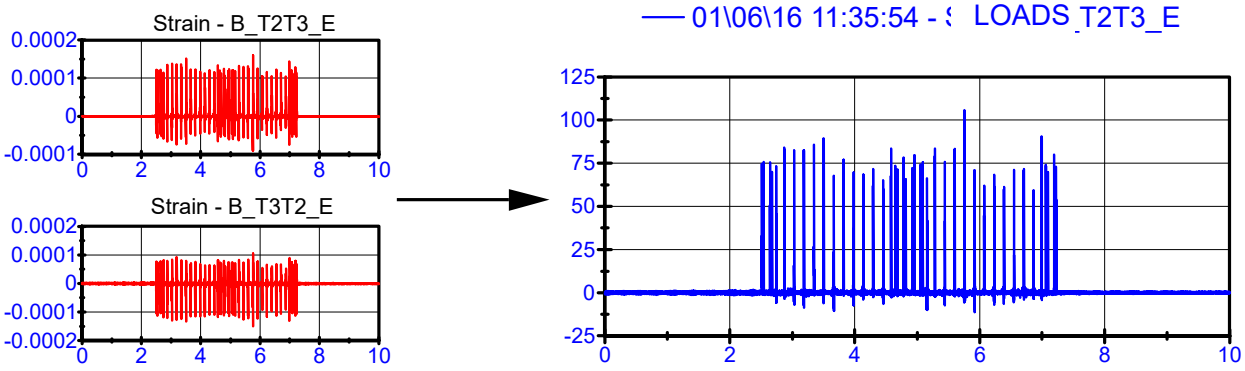

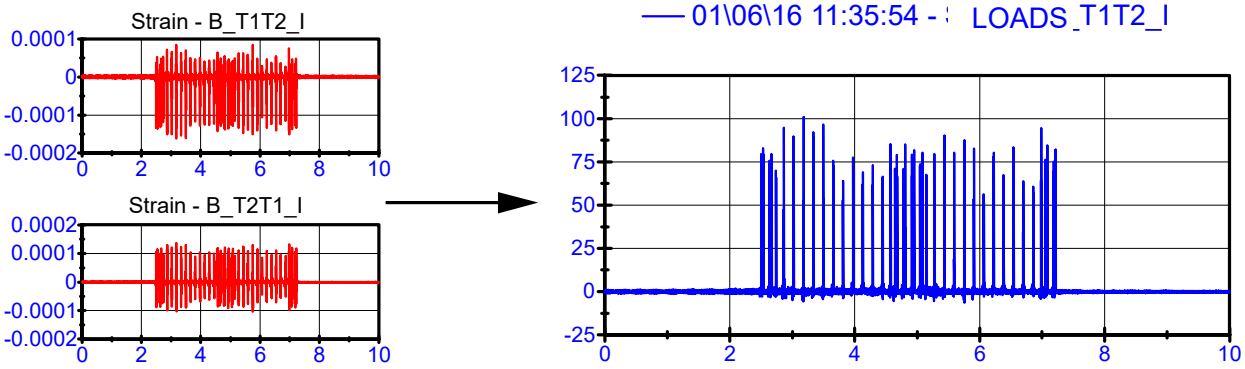

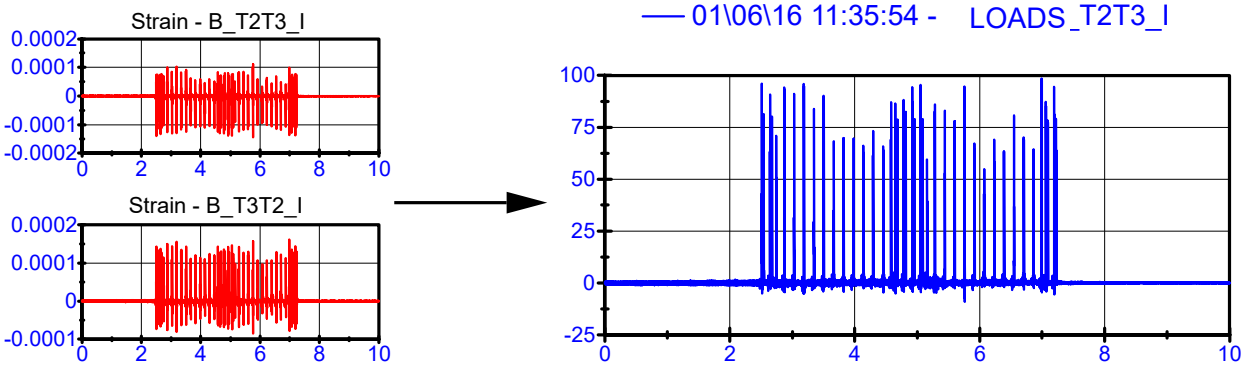

Strain gauges
LPF 500Hz

01\06\16 11:53:47

Loads; LPF 500Hz

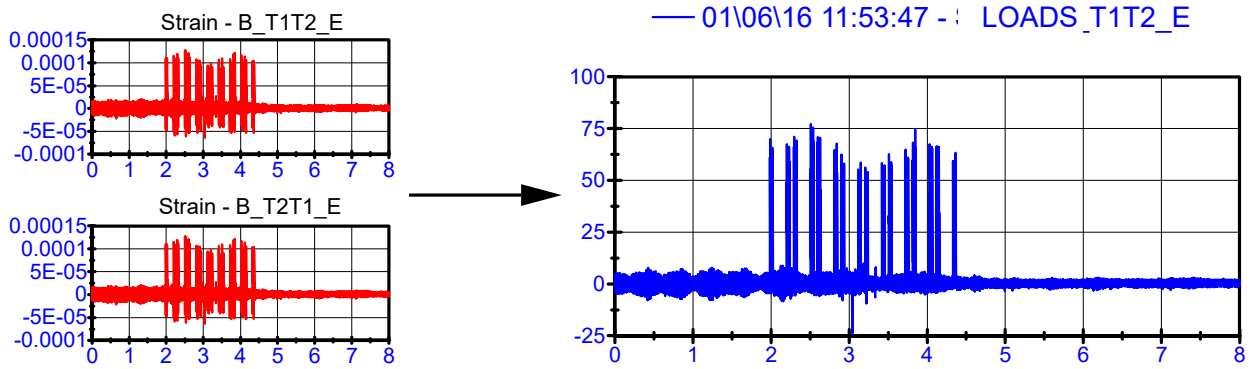

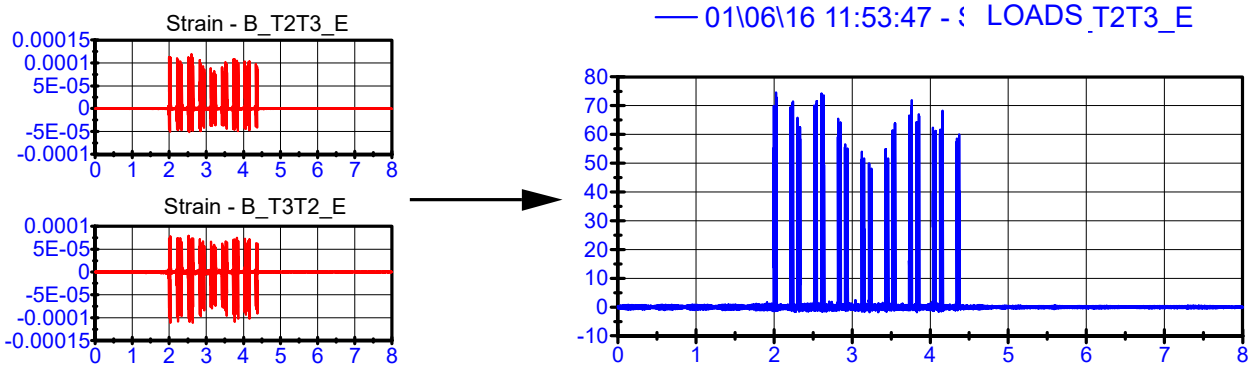

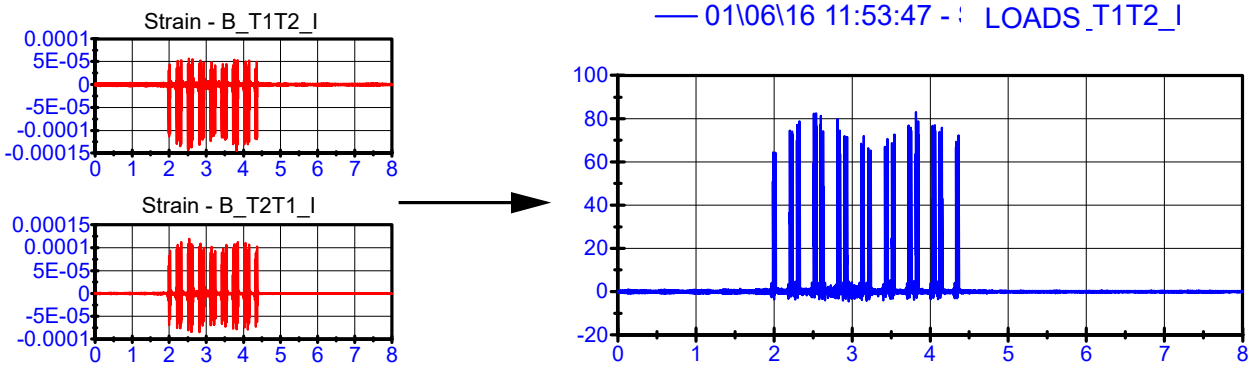

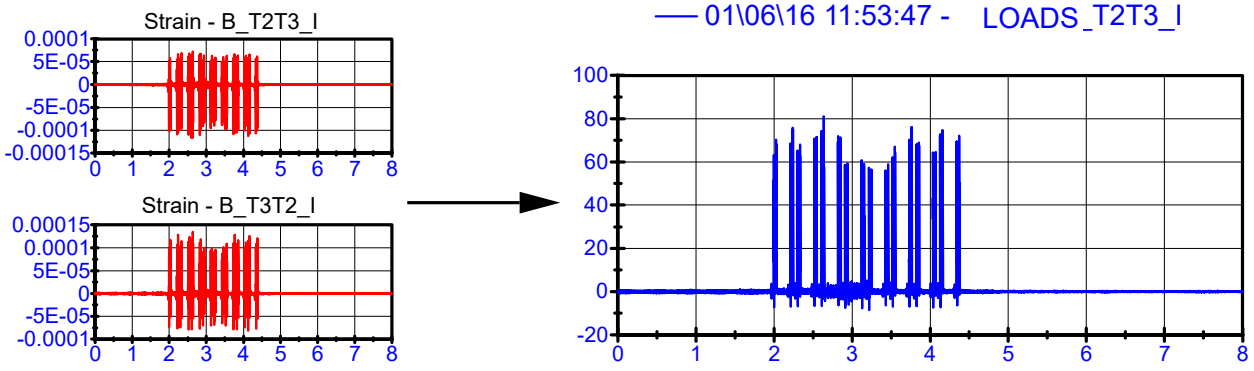

Strain gauges
LPF 500Hz

01\06\16 12:07:44

Loads; LPF 500Hz

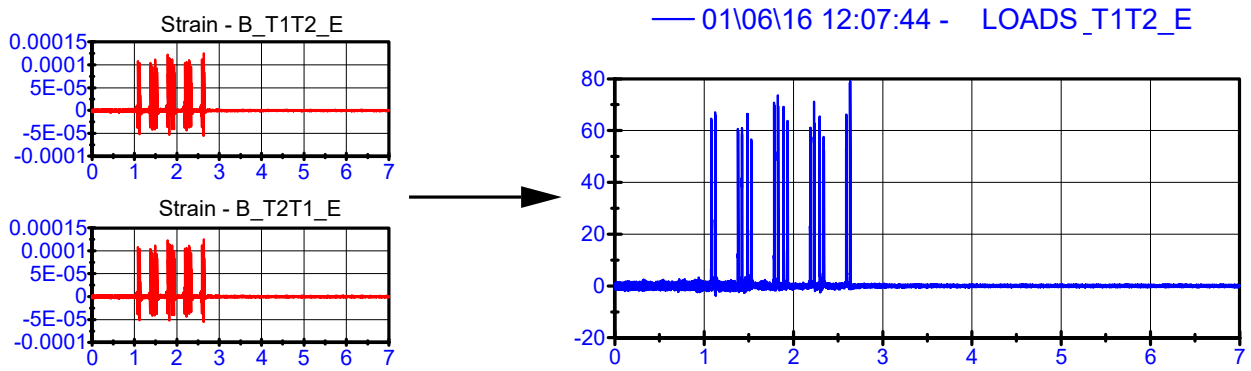

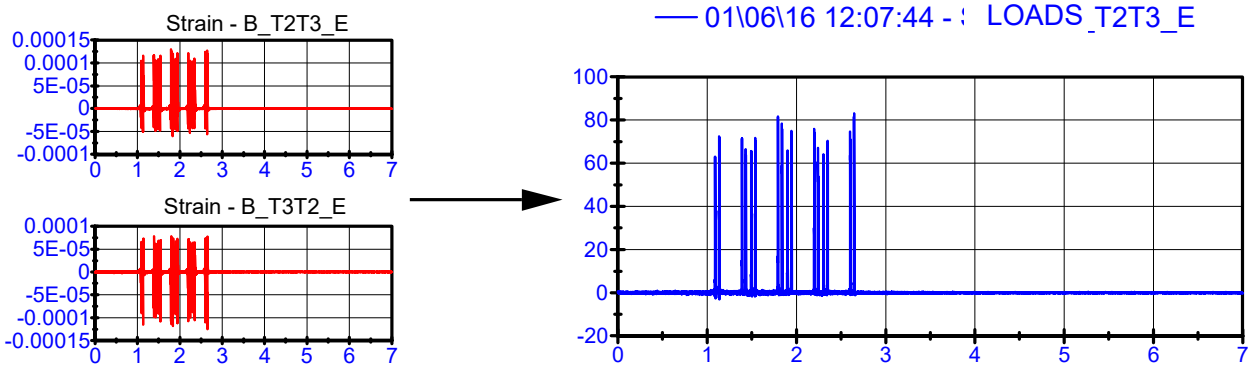

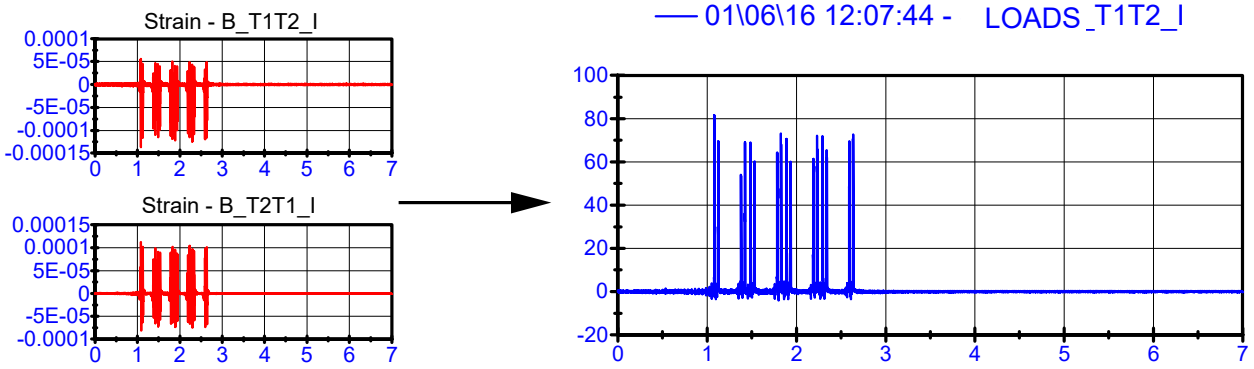

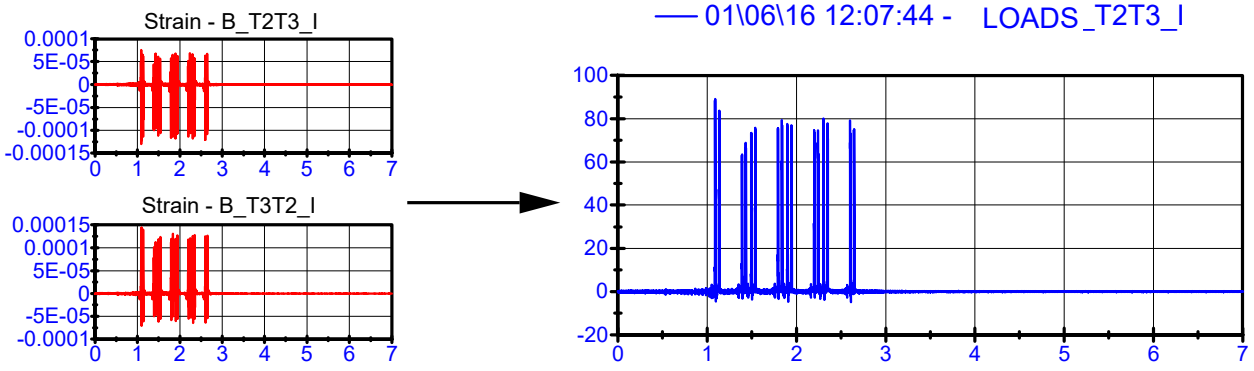

Strain gauges
LPF 500Hz

01\06\16 12:51:19

Loads; LPF 500Hz

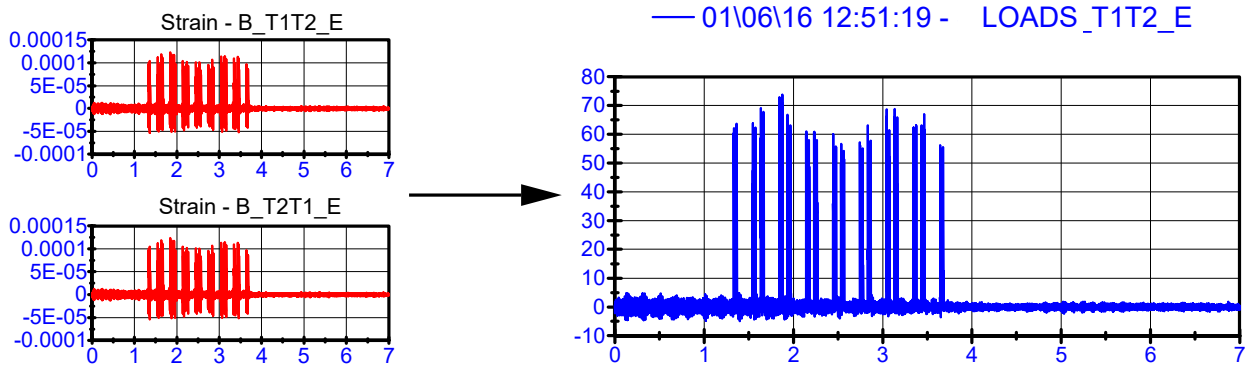

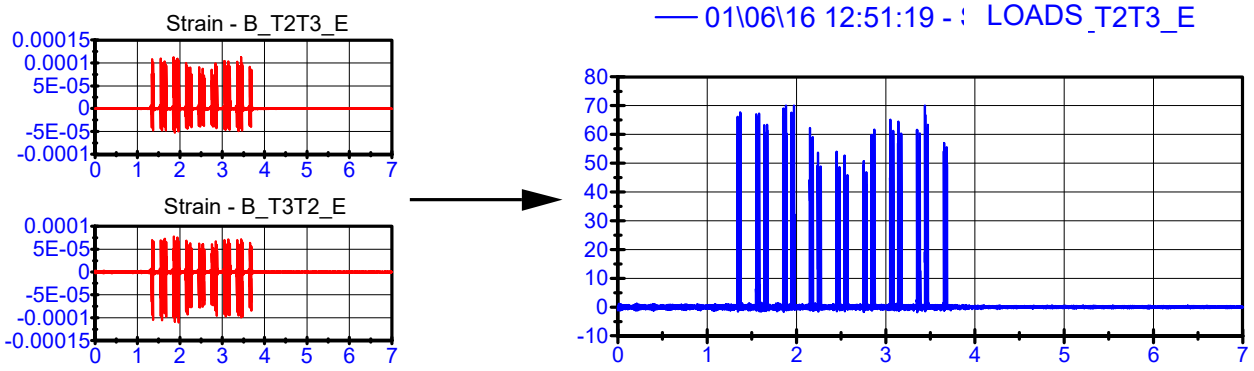

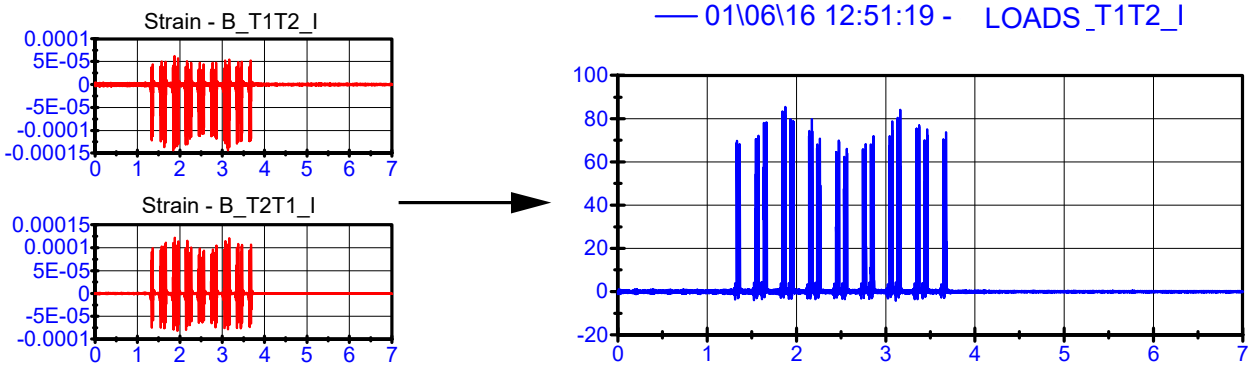

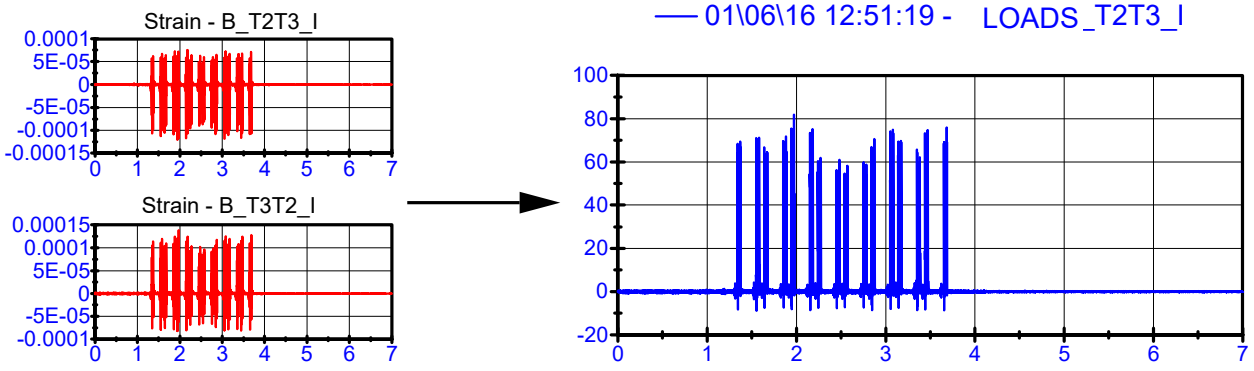

Strain gauges
LPF 500Hz

01\06\16 13:55:11

Loads; LPF 500Hz

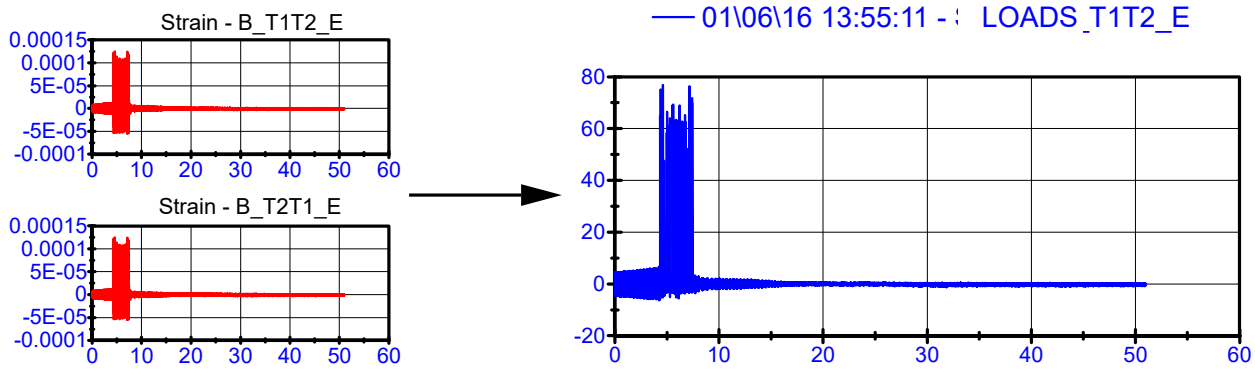

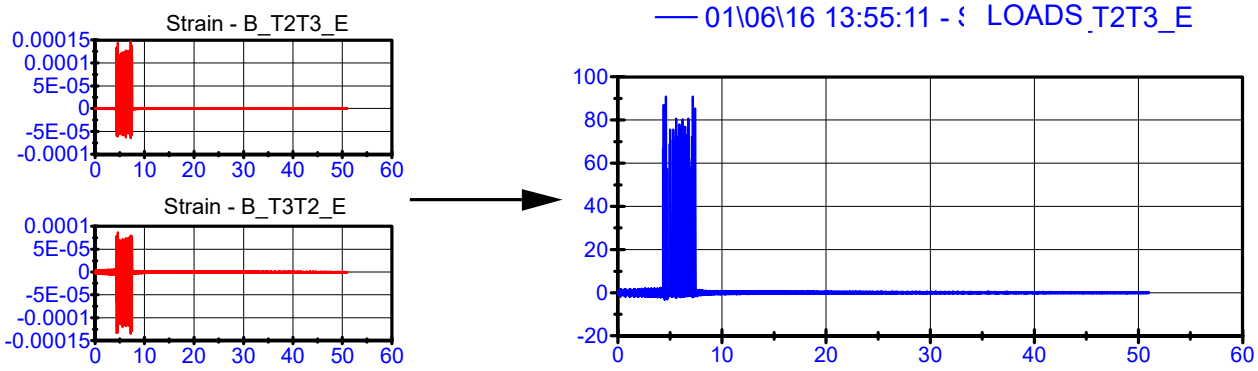

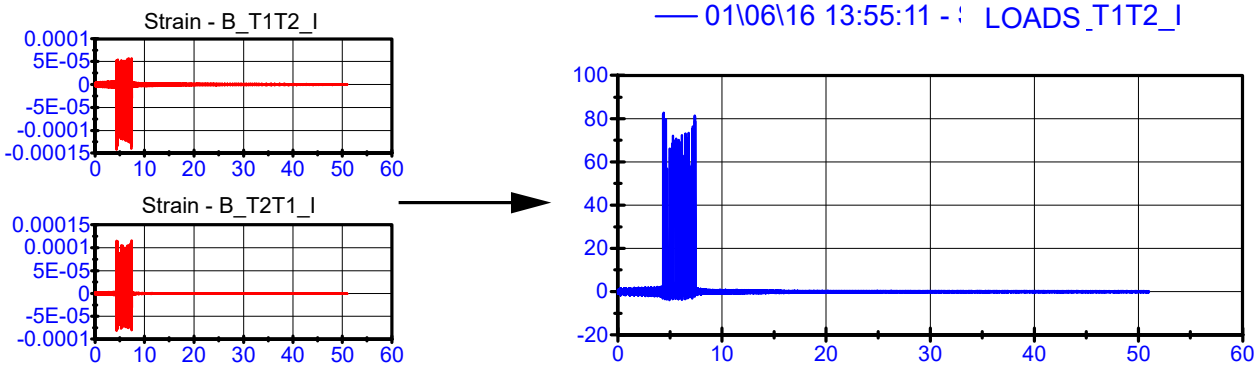

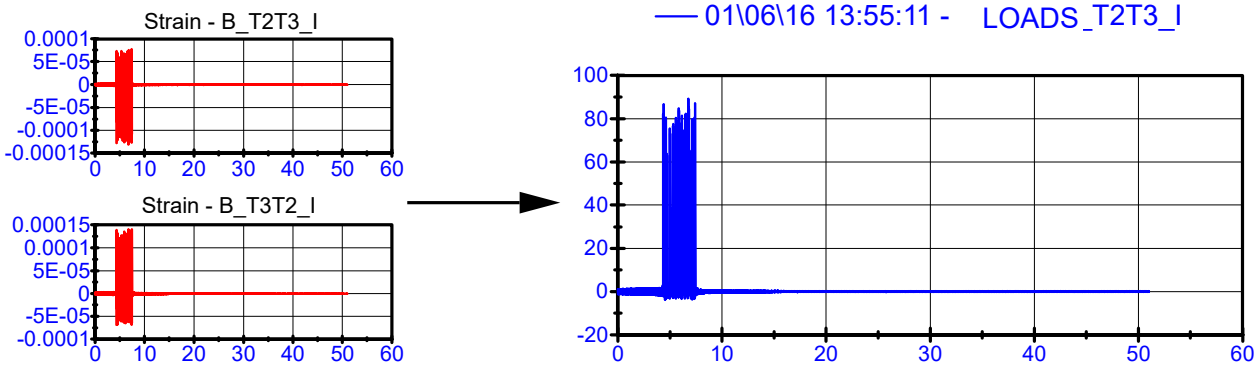

Strain gauges
LPF 500Hz

01\06\16 14:21:06

Loads; LPF 500Hz

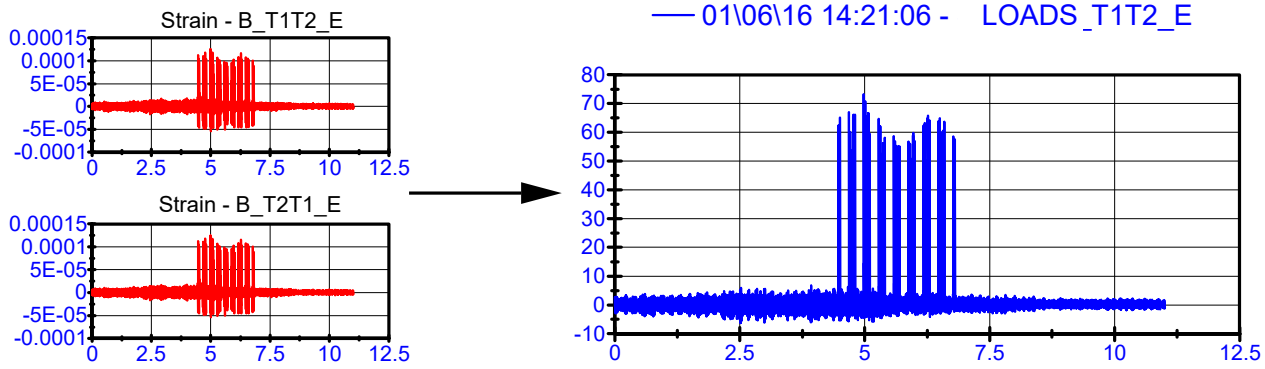

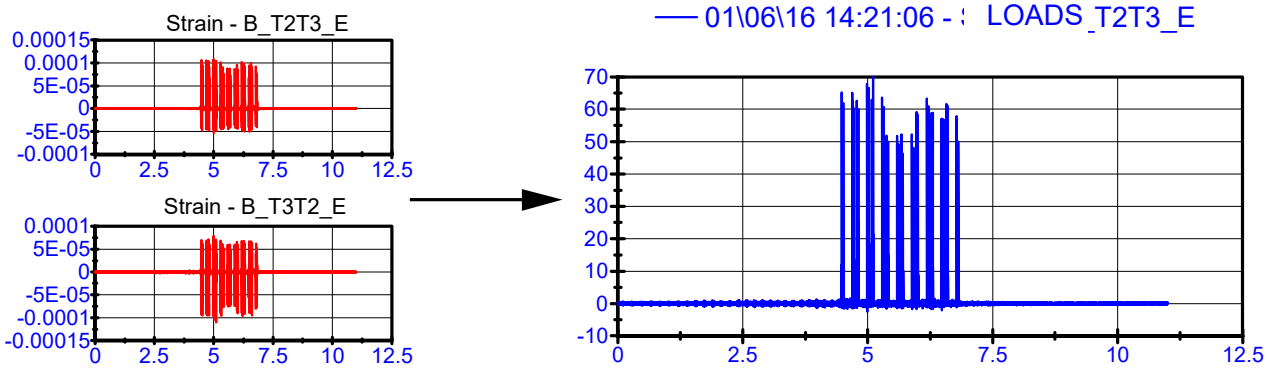

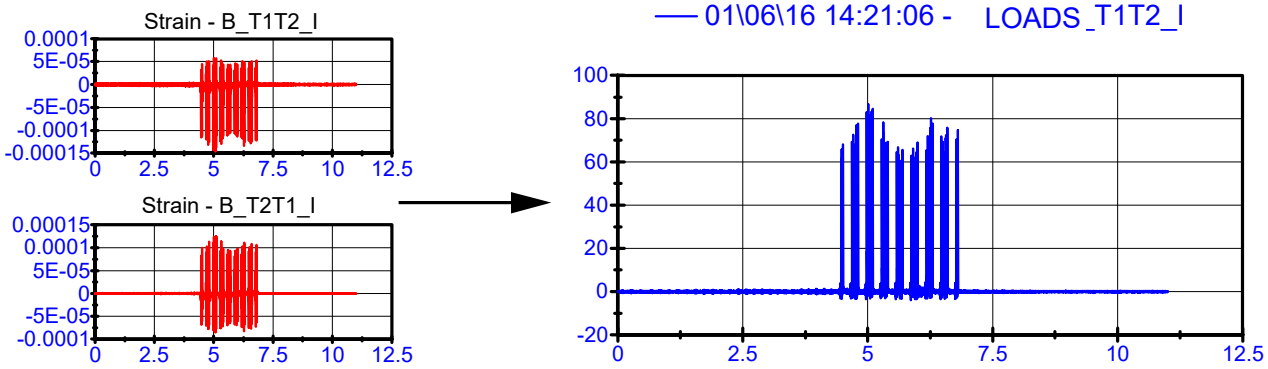

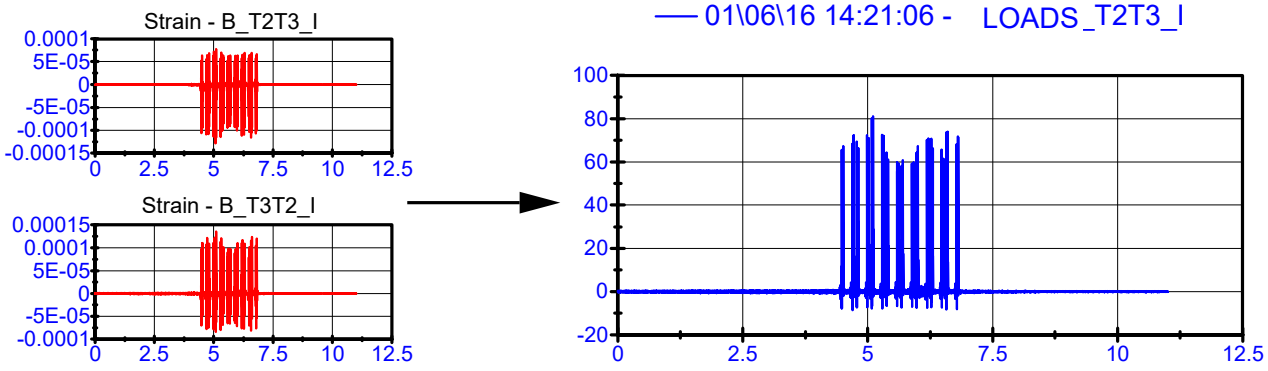

Strain gauges
LPF 500Hz

01\06\16 14:52:22

Loads; LPF 500Hz

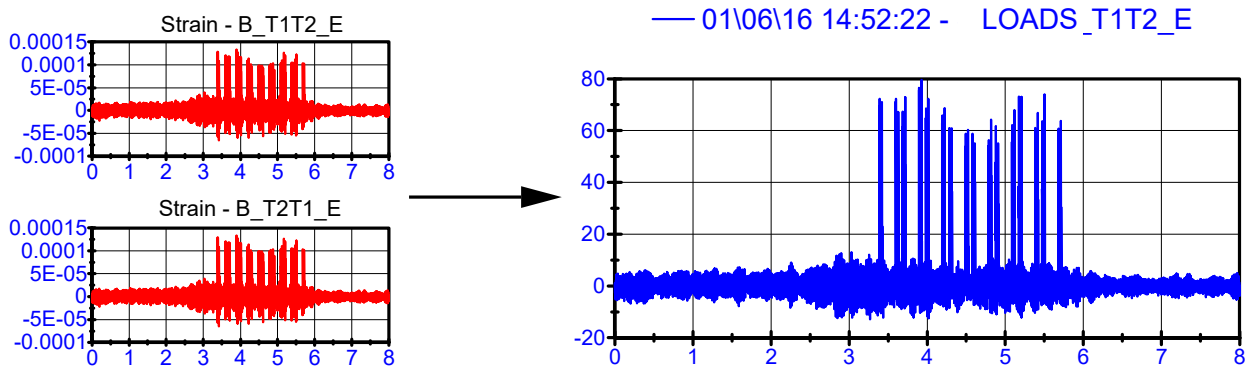

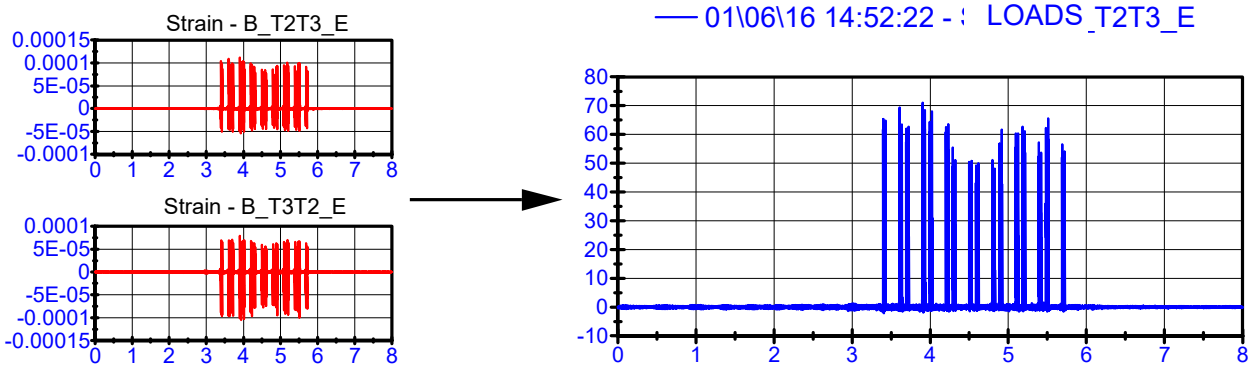

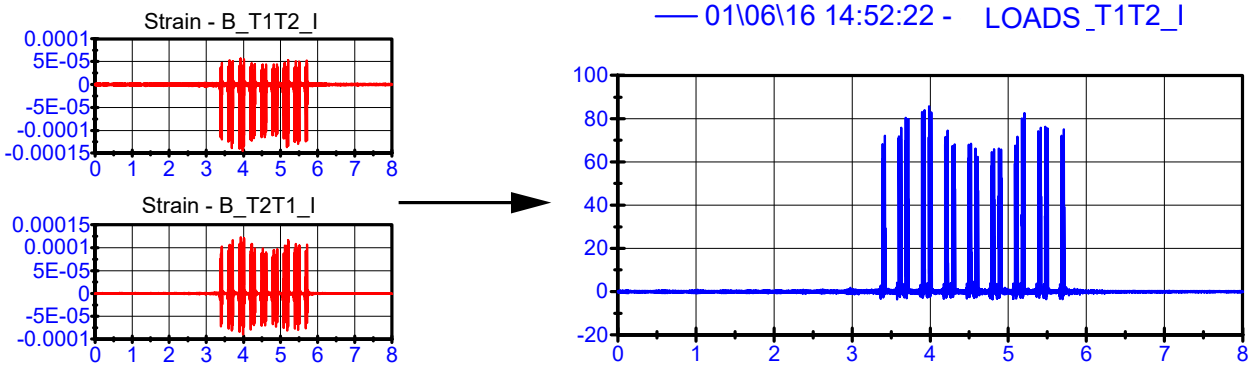

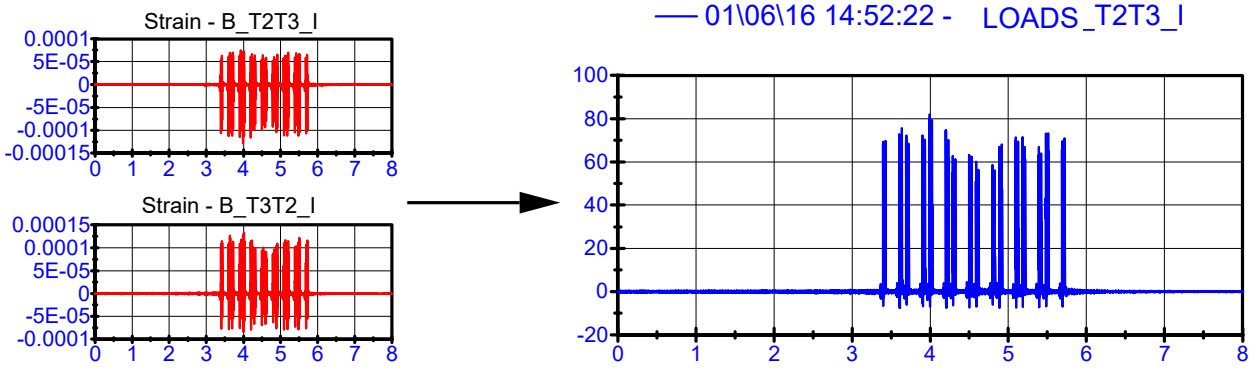

Strain gauges
LPF 500Hz

01\06\16 15:21:31

Loads; LPF 500Hz

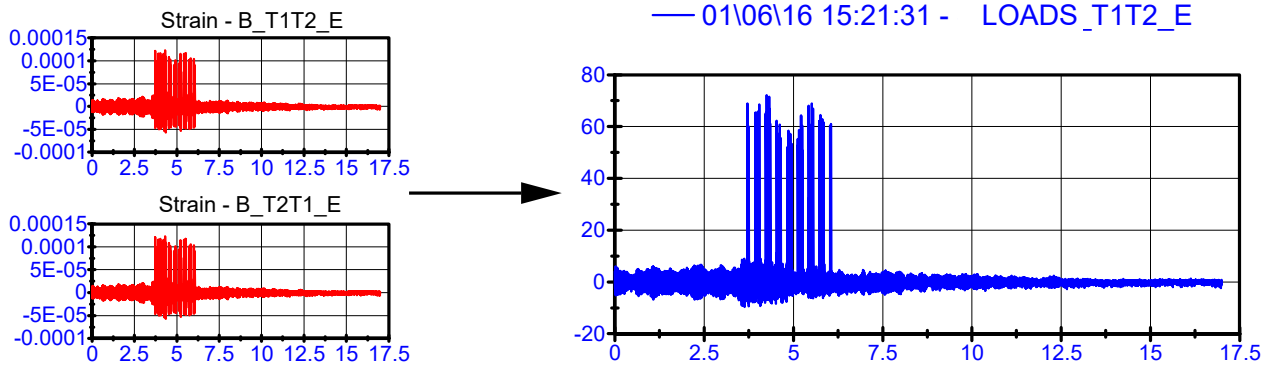

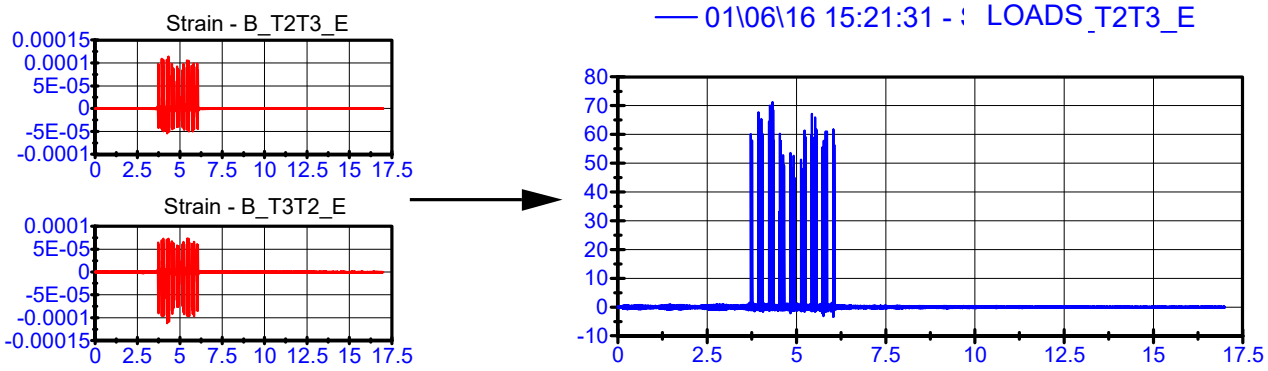

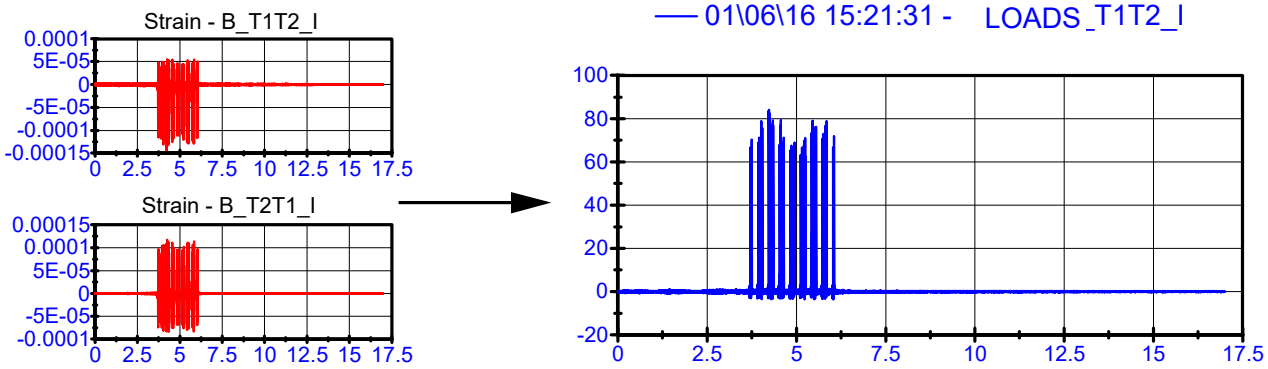

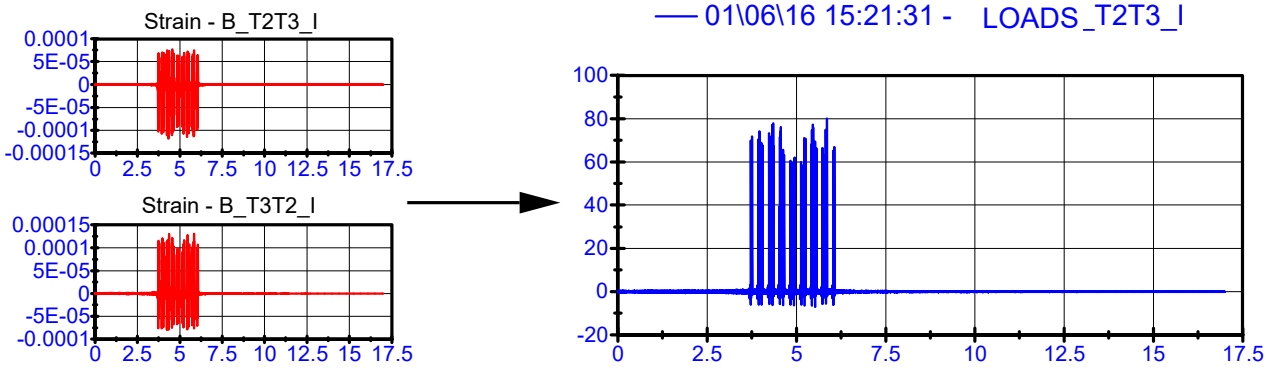

Strain gauges
LPF 500Hz

01\06\16 15:34:49

Loads; LPF 500Hz

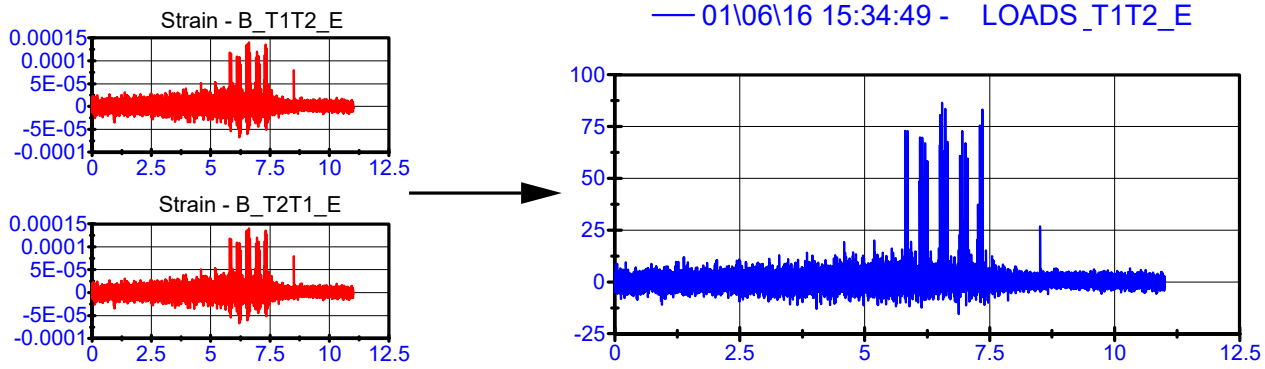

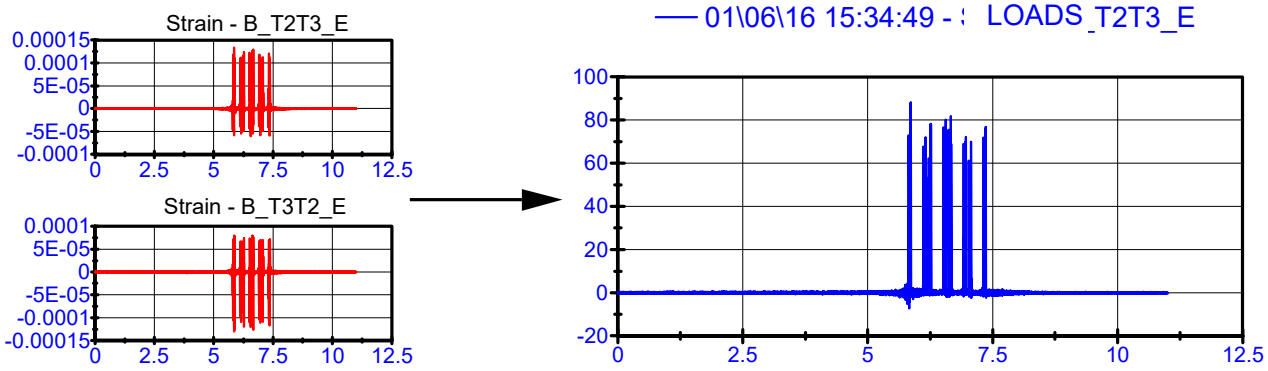

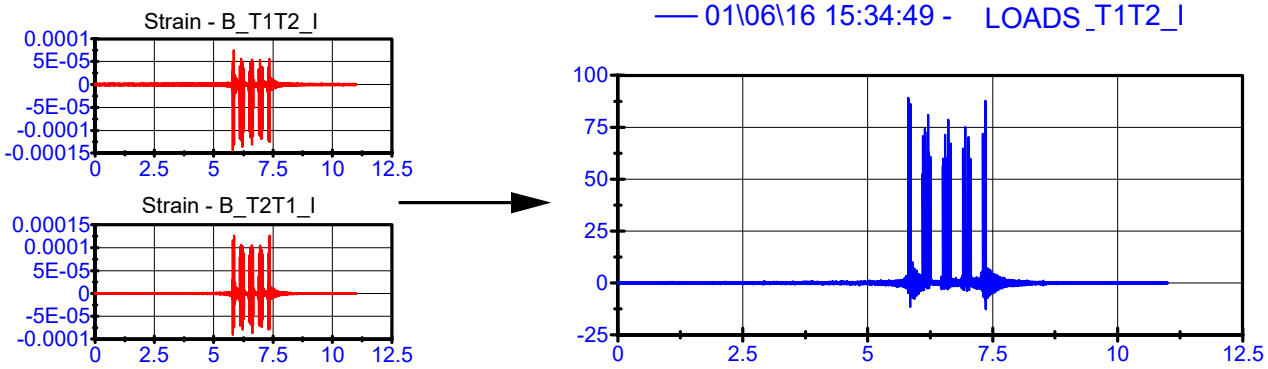

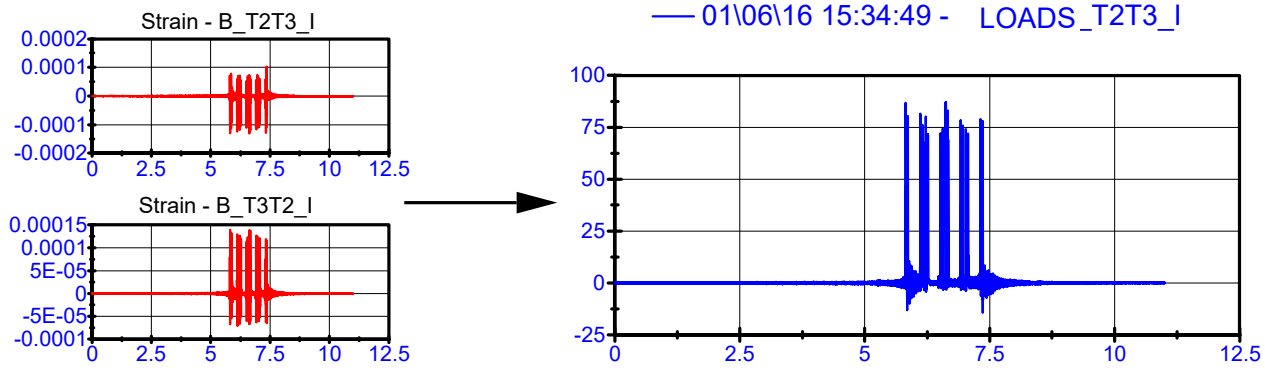

Strain gauges
LPF 500Hz

01\06\16 15:54:57

Loads; LPF 500Hz

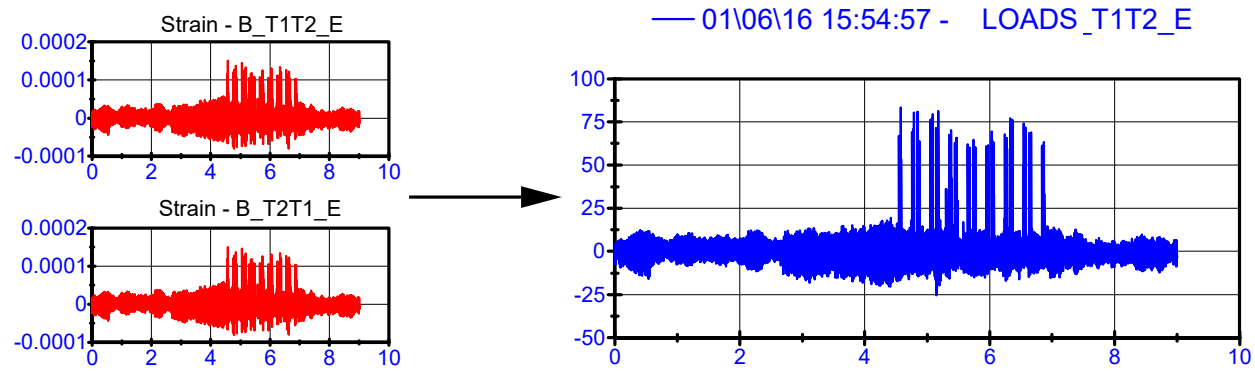

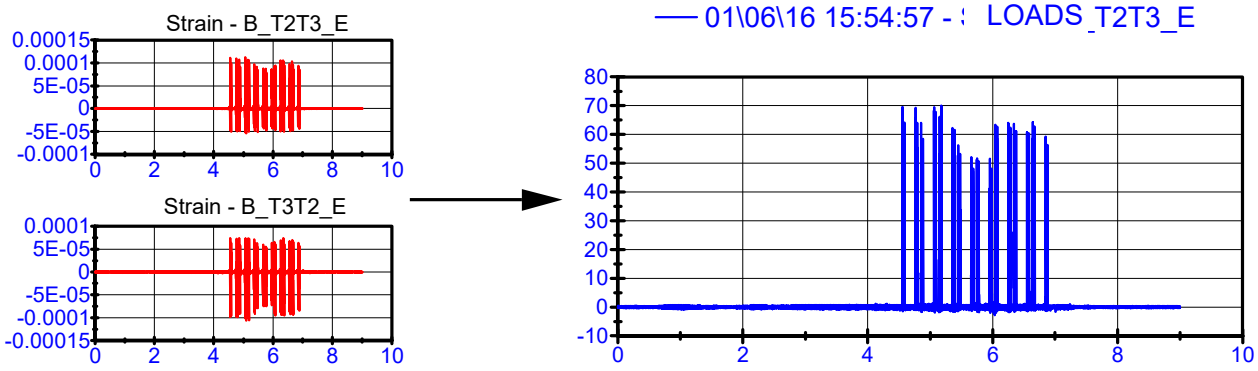

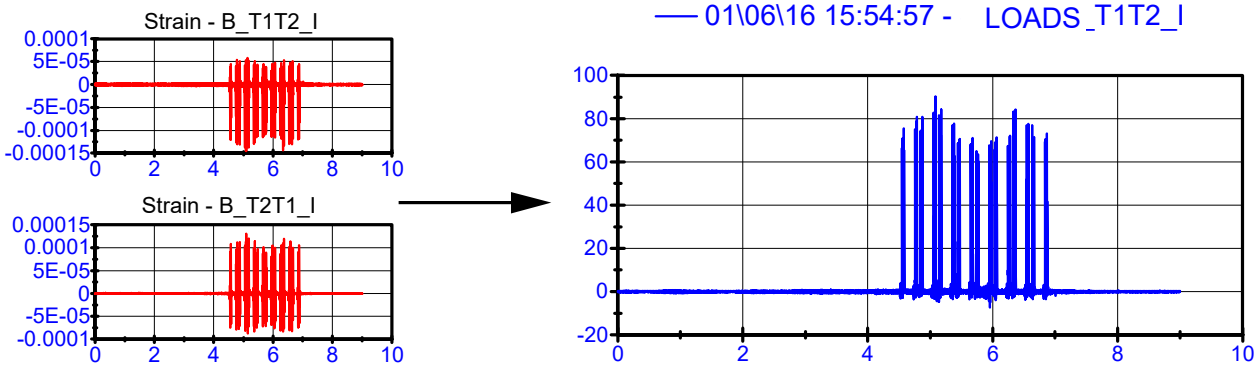

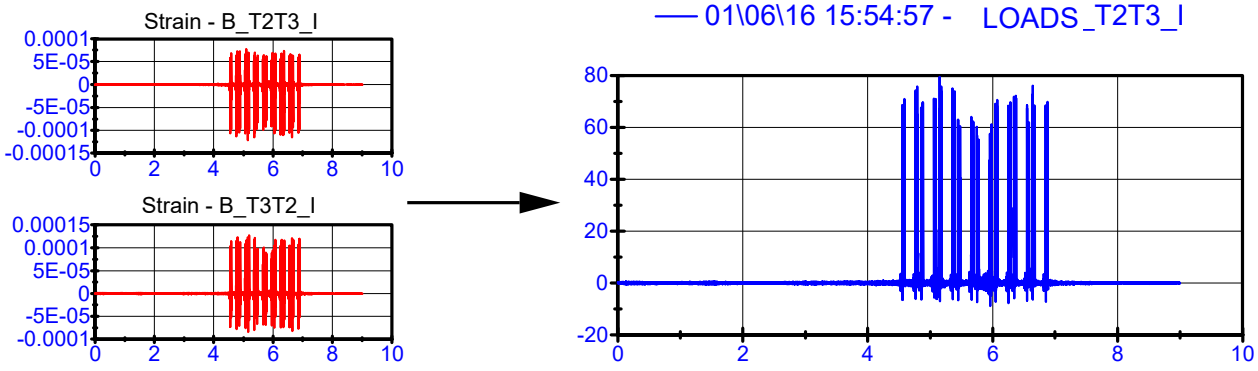

Strain gauges
LPF 500Hz

01\06\16 16:22:21

Loads; LPF 500Hz

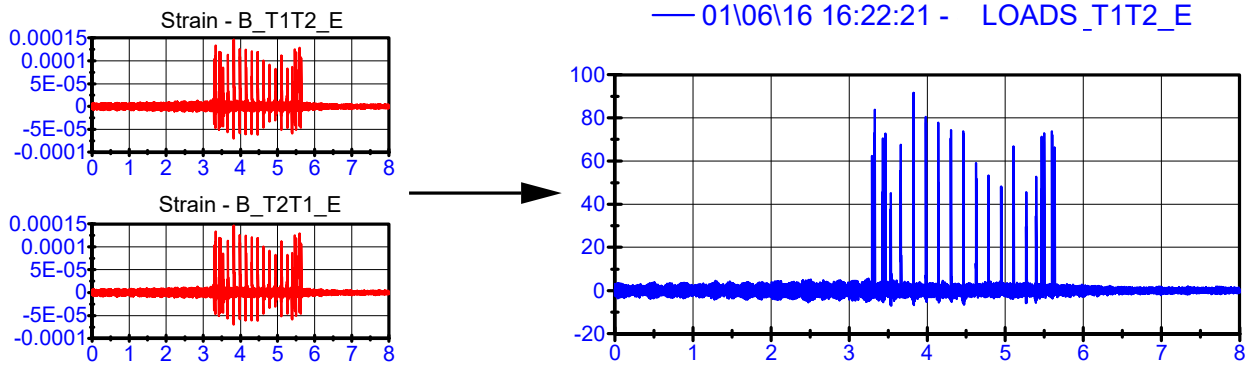

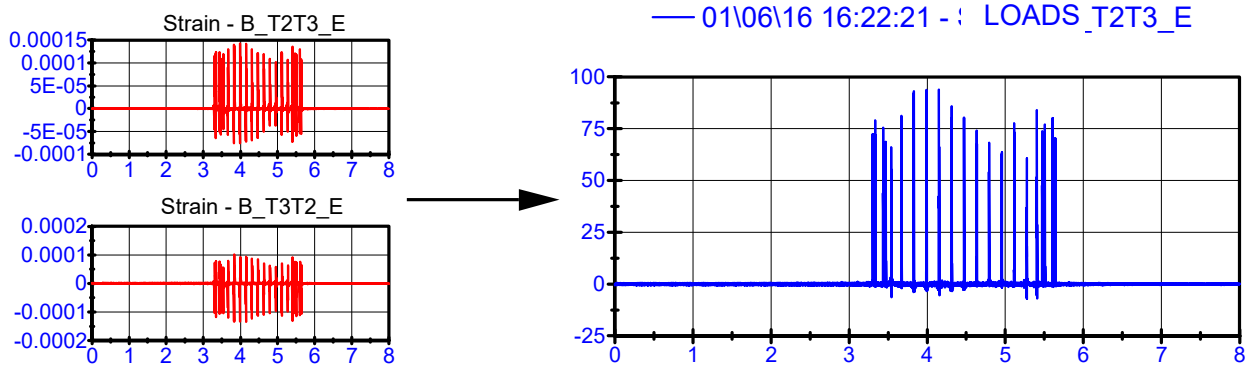

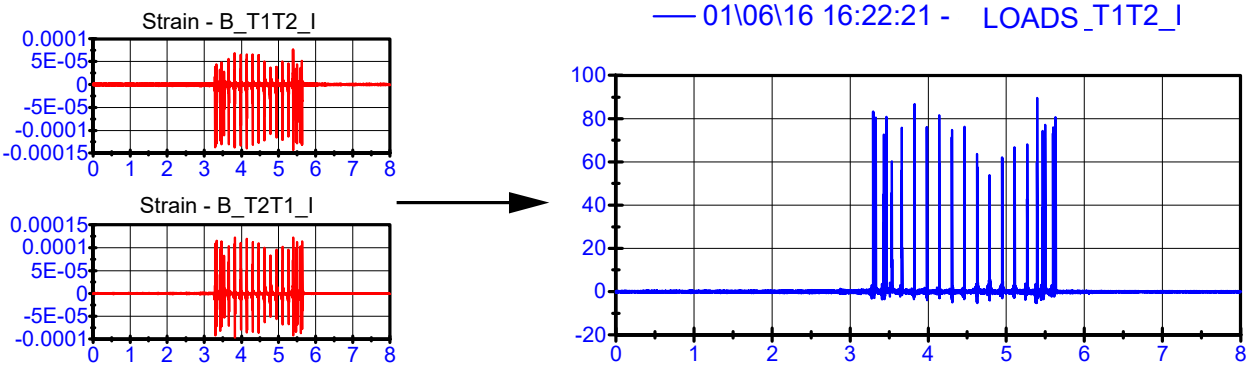

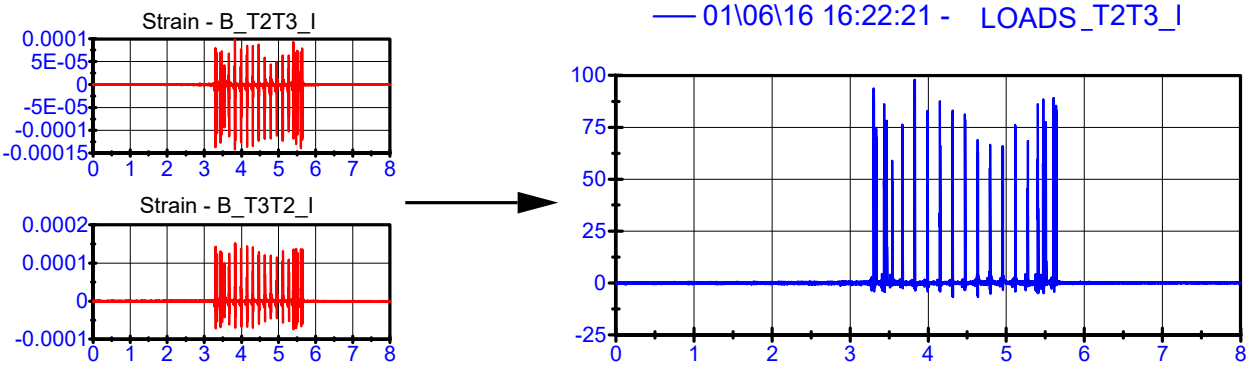

Strain gauges
LPF 500Hz

01\06\16 16:54:24

Loads; LPF 500Hz

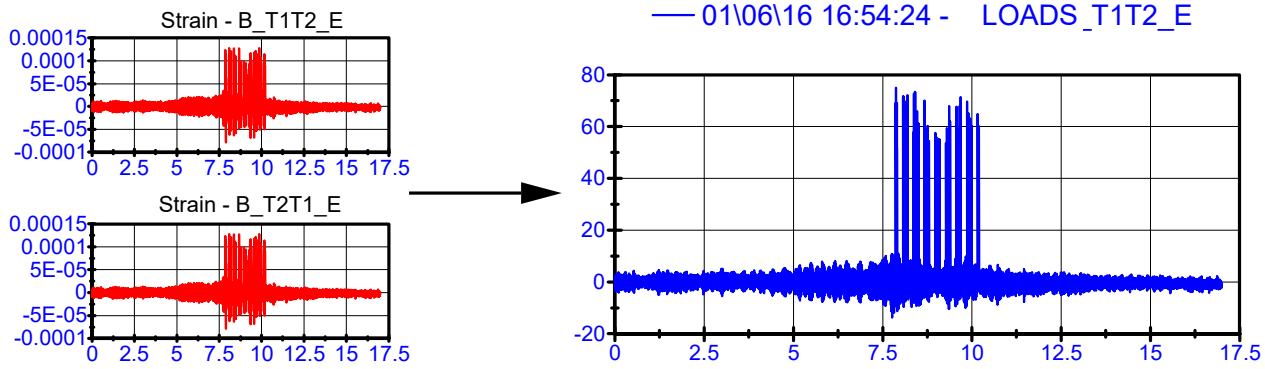

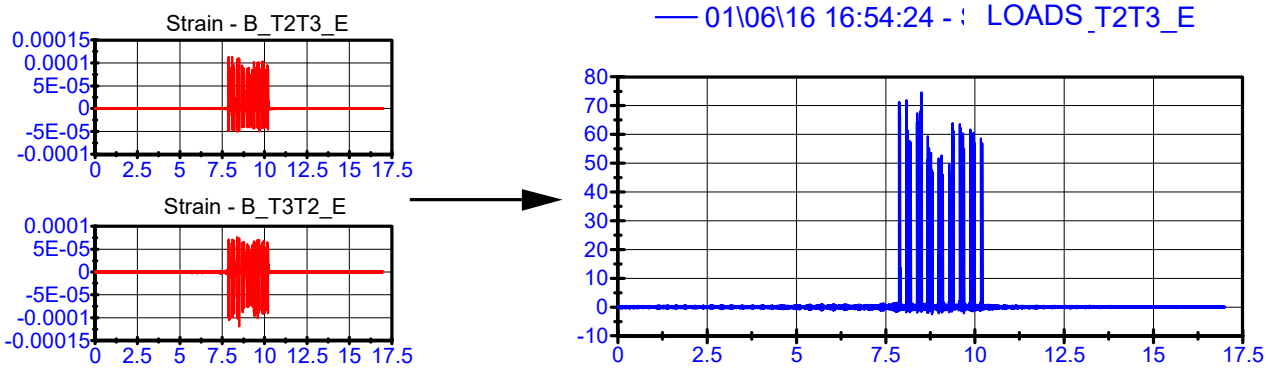

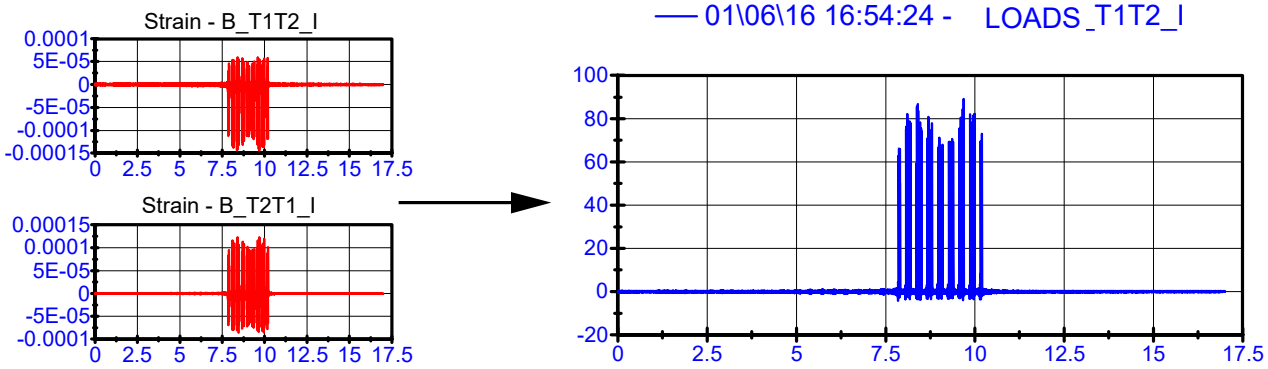

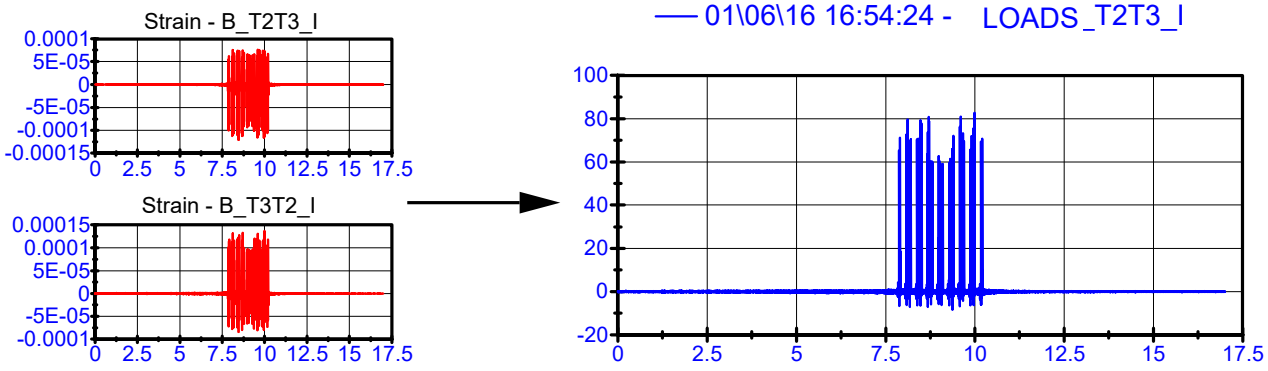

Strain gauges
LPF 500Hz

01\06\16 17:24:26

Loads; LPF 500Hz

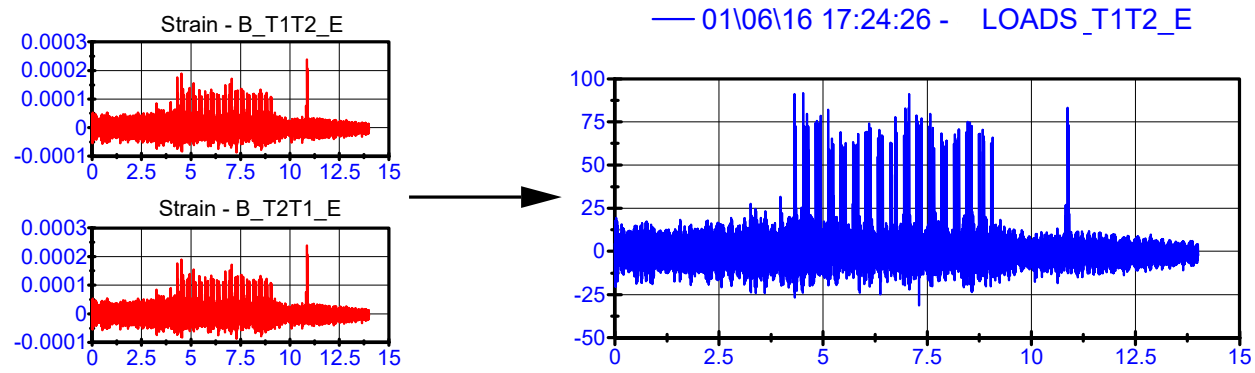

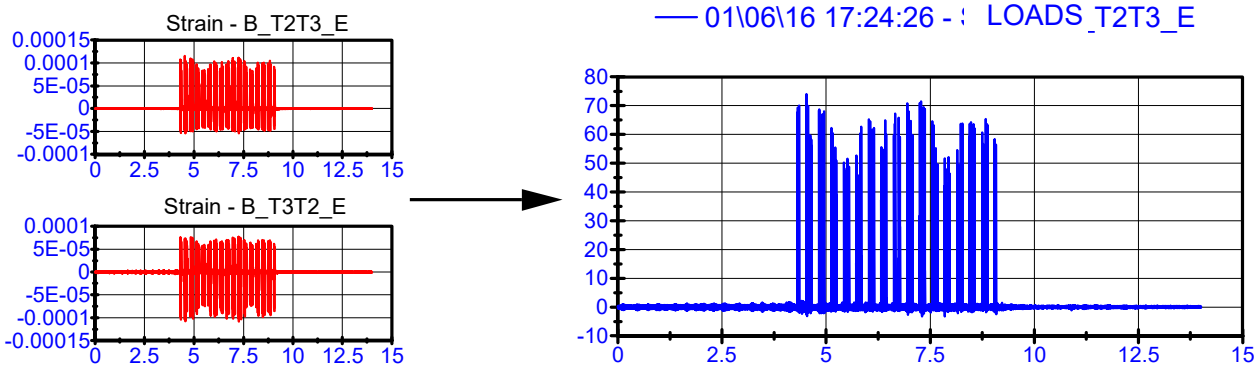

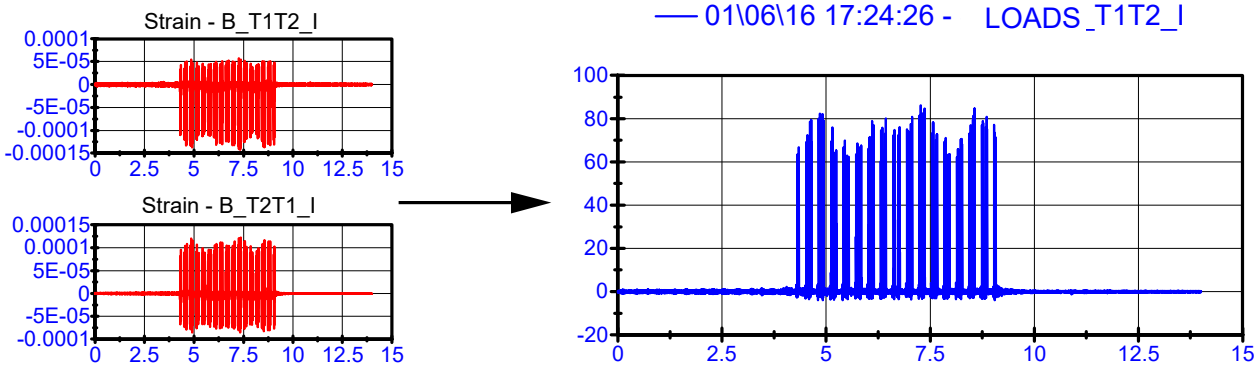

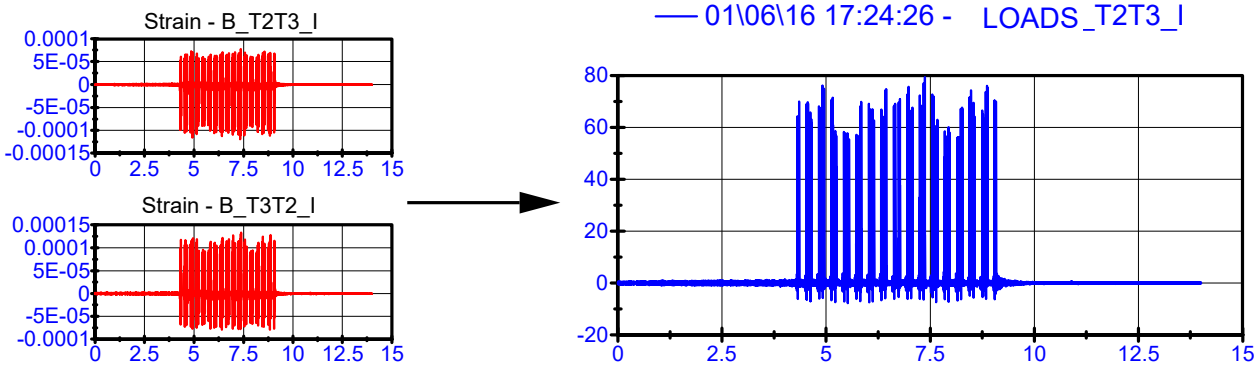

Strain gauges
LPF 500Hz

01\06\16 17:38:59

Loads; LPF 500Hz

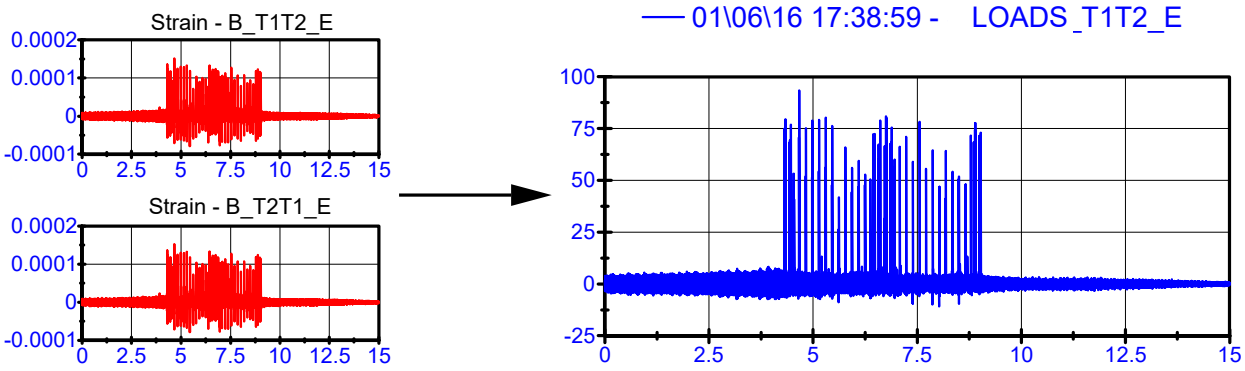

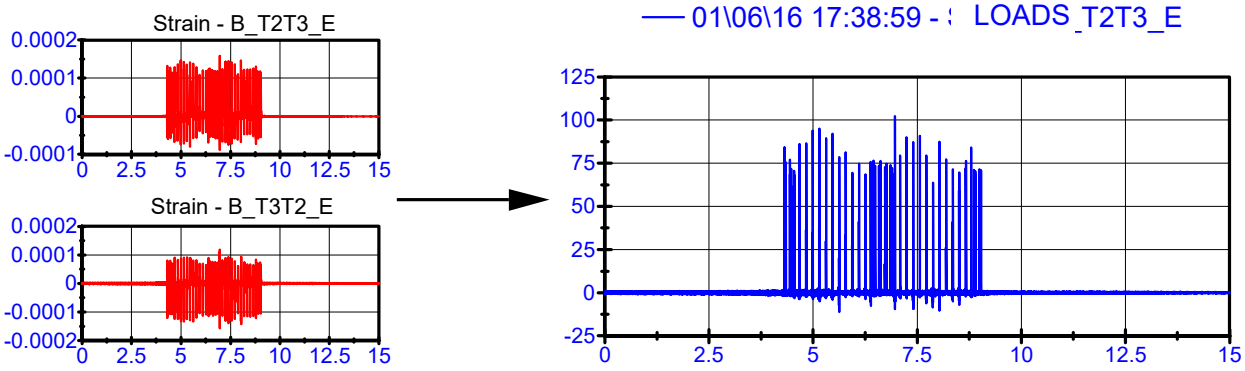

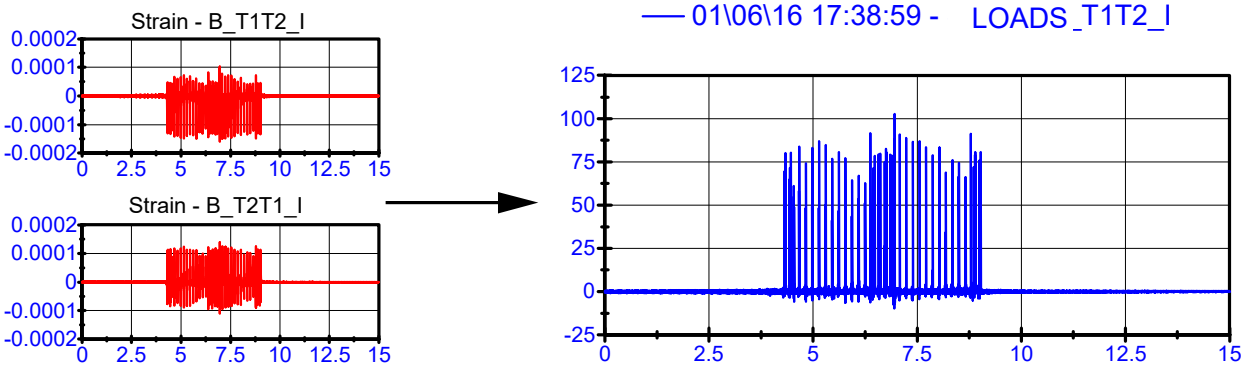

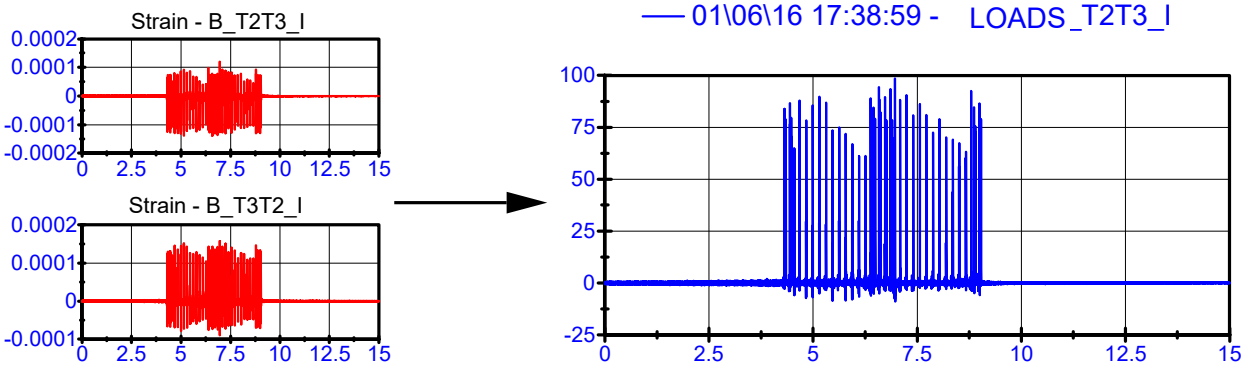

Strain gauges
LPF 500Hz

01\06\16 17:59:25

Loads; LPF 500Hz

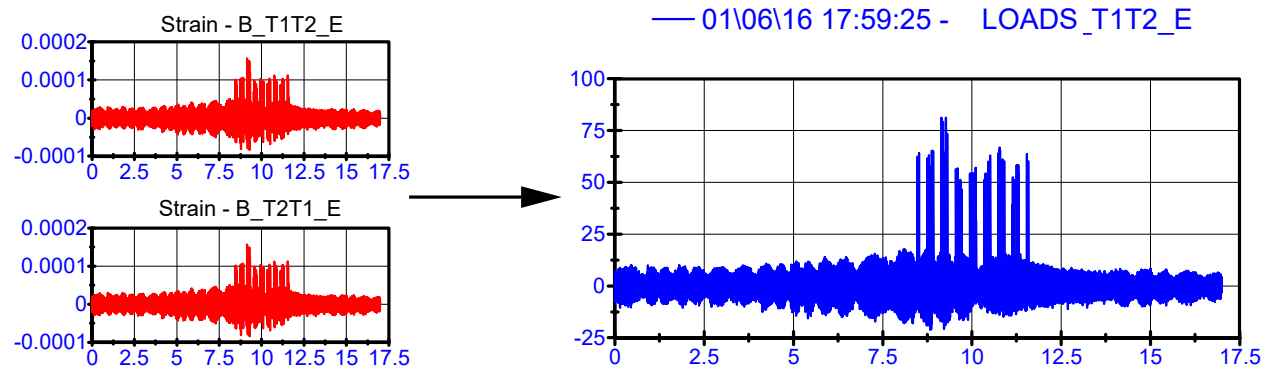

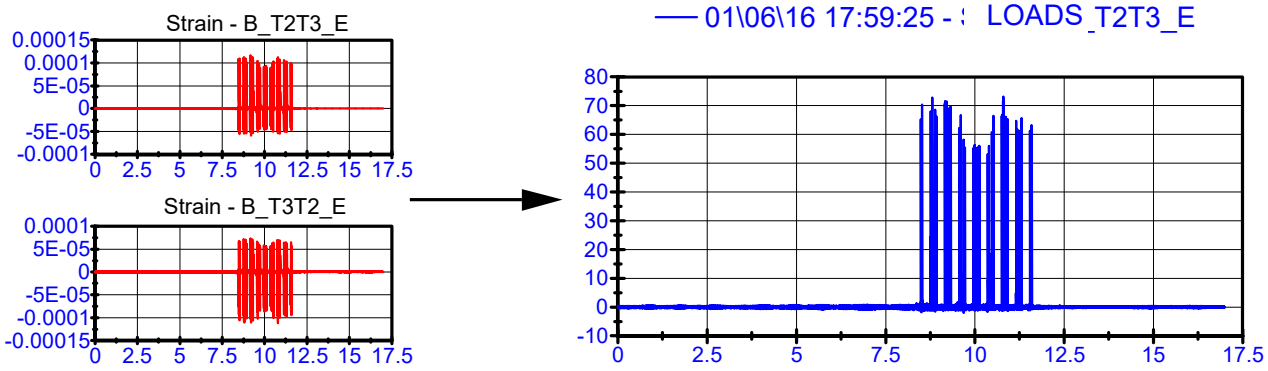

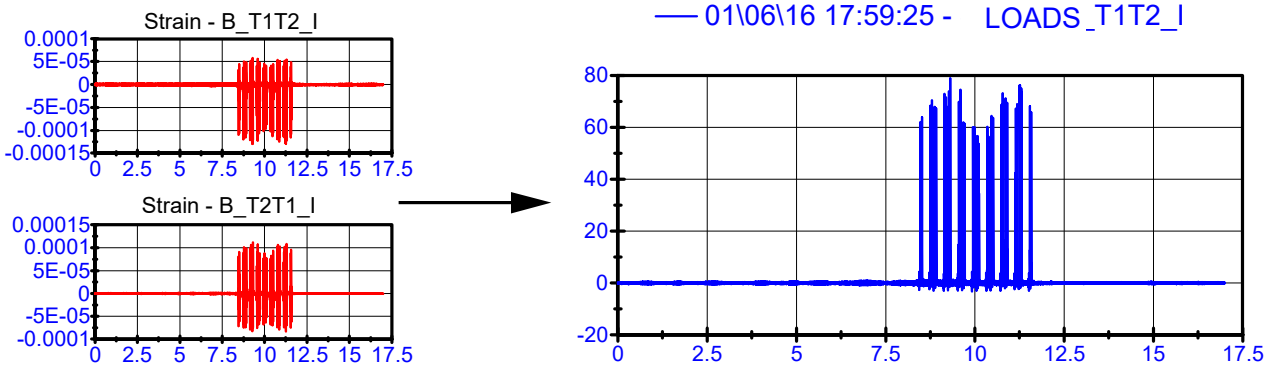

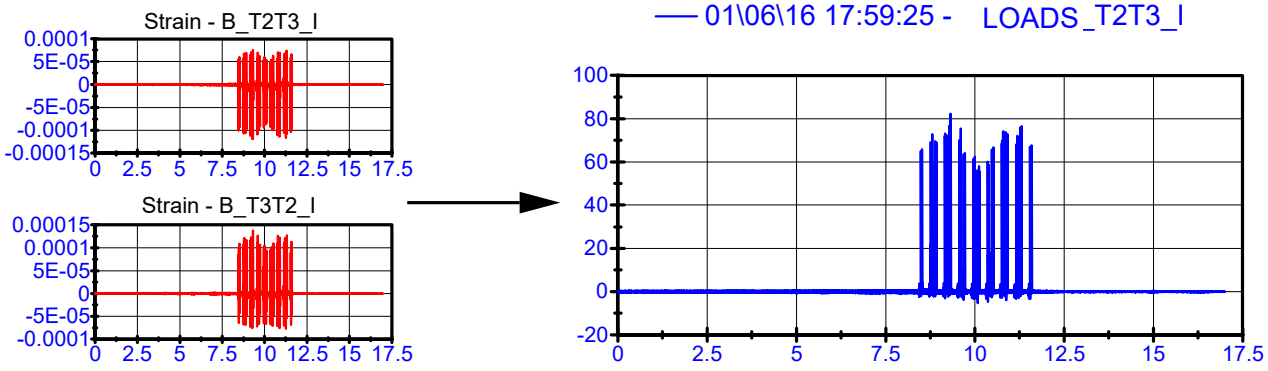

Strain gauges
LPF 500Hz

01\06\16 18:22:52

Loads; LPF 500Hz

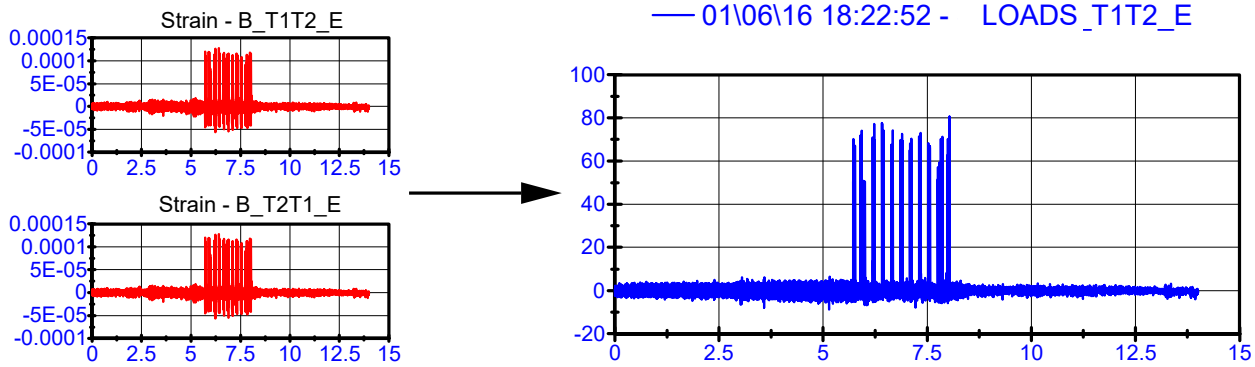

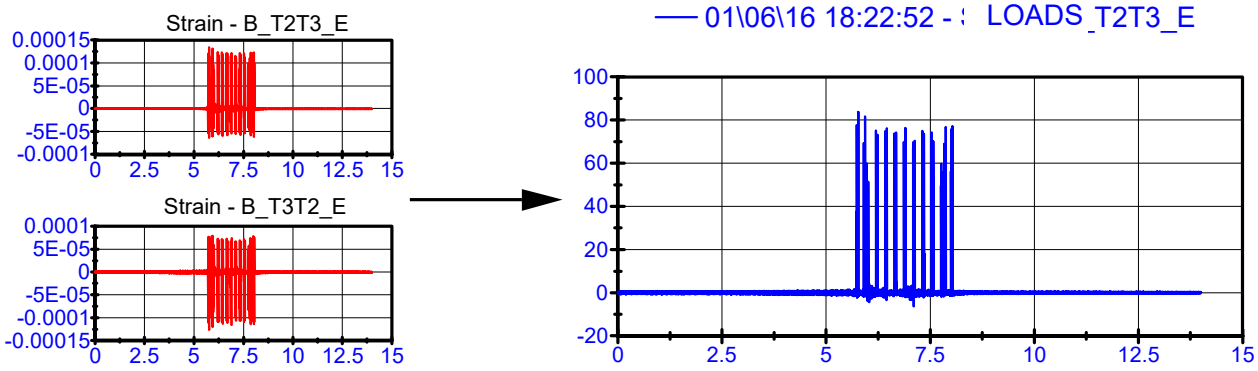

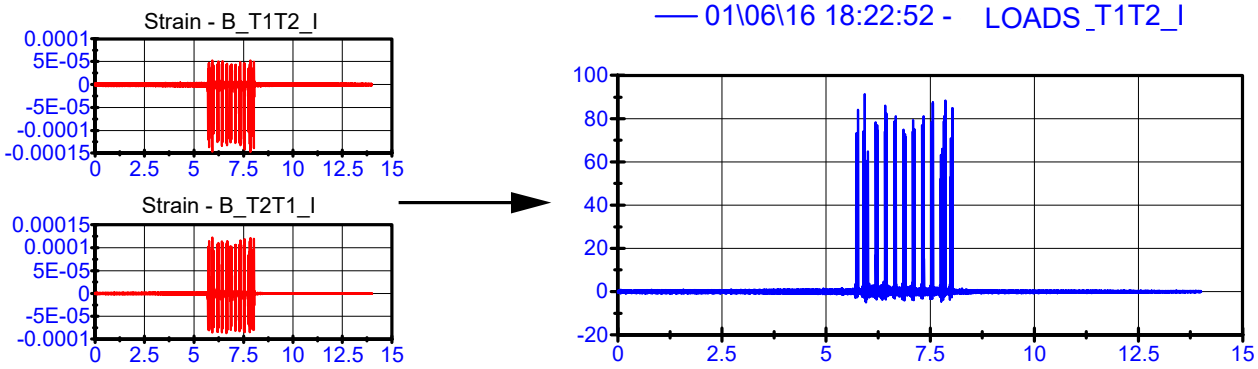

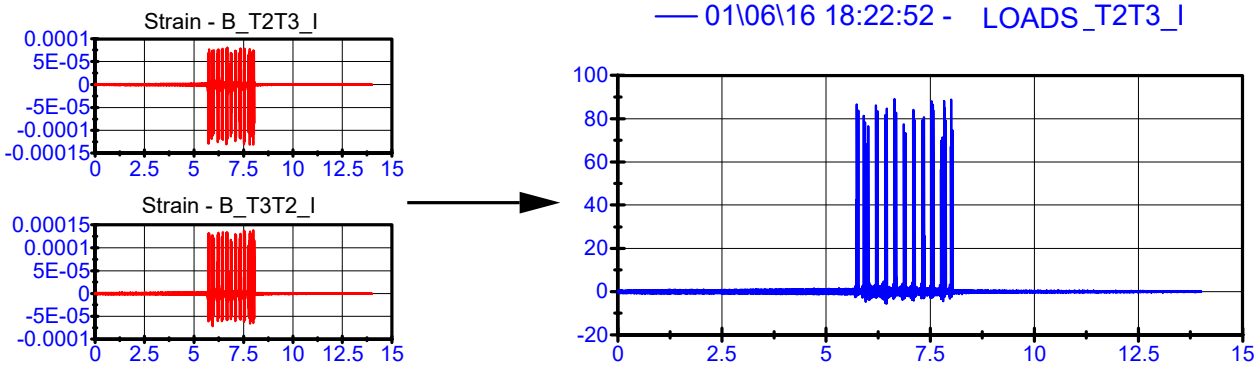

Strain gauges
LPF 500Hz

01\06\16 18:59:06

Loads; LPF 500Hz

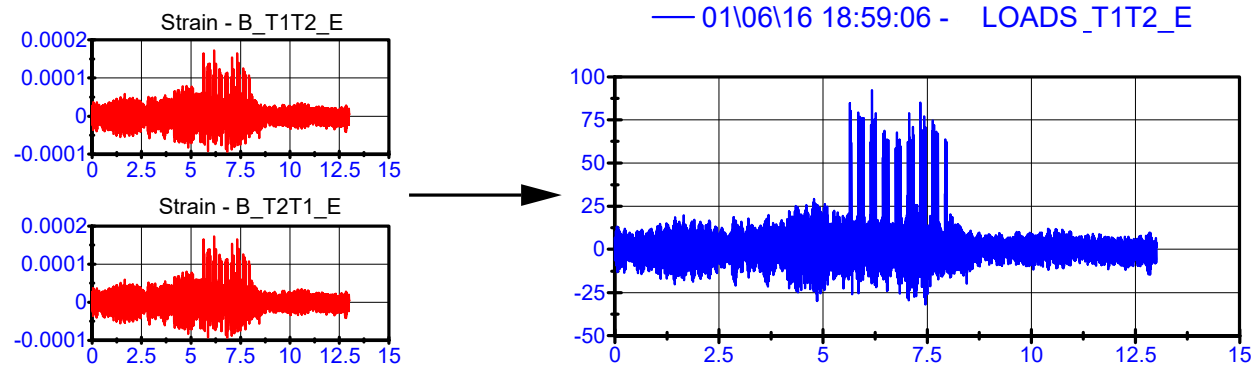

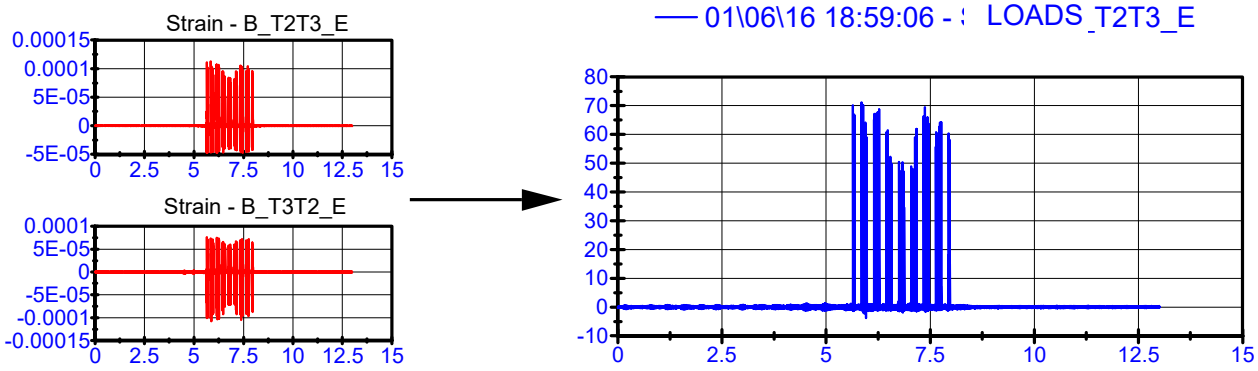

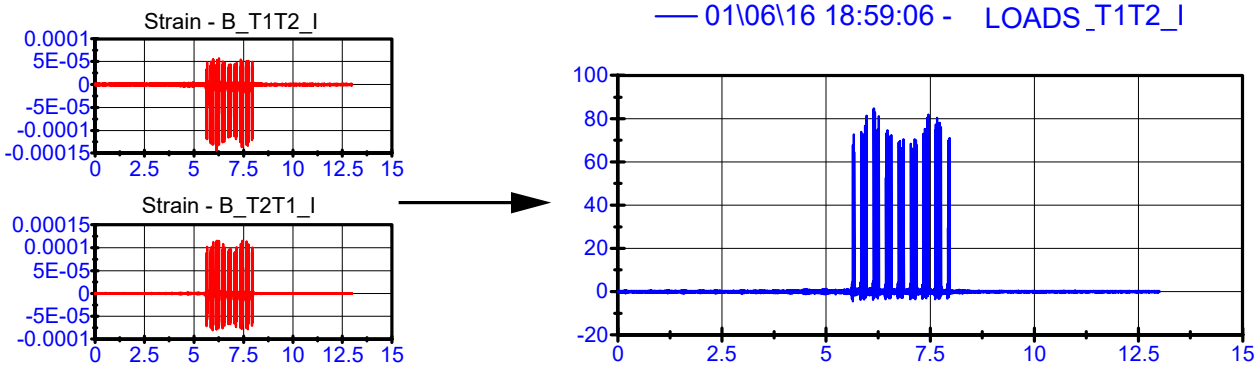

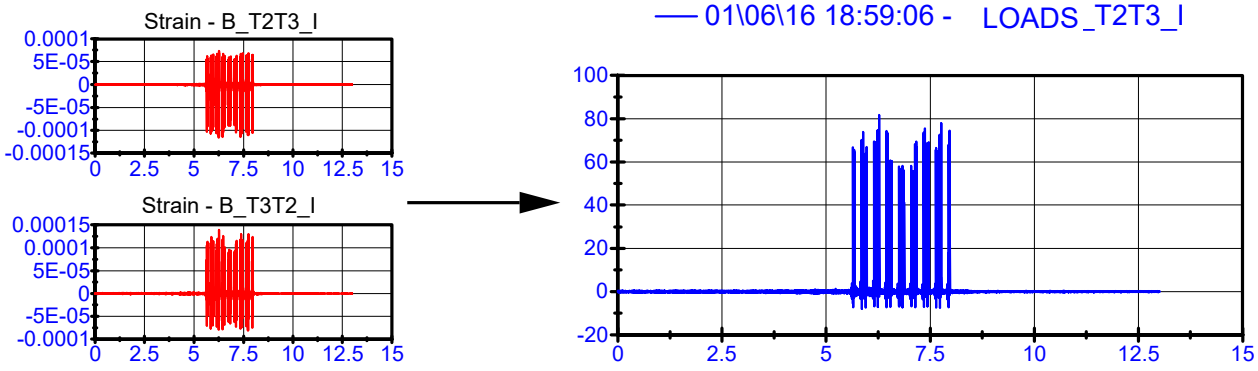

Strain gauges
LPF 500Hz

01\06\16 19:21:34

Loads; LPF 500Hz

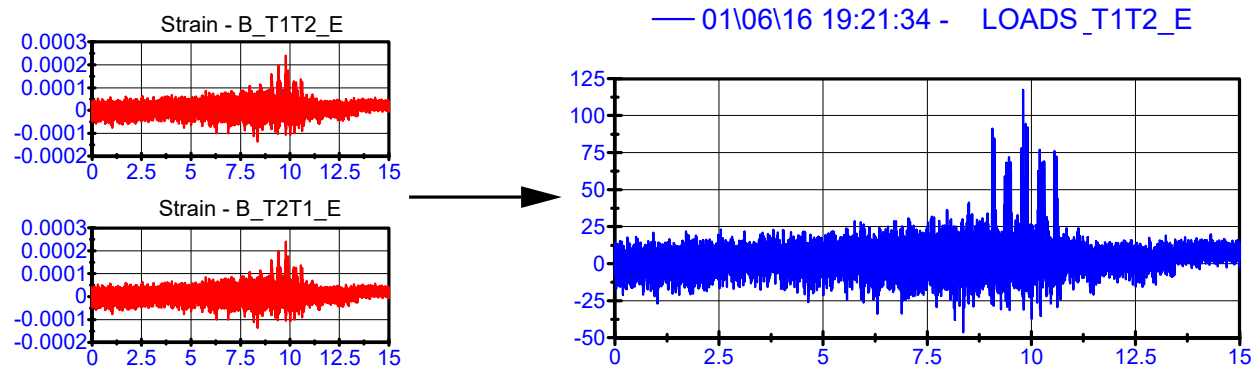

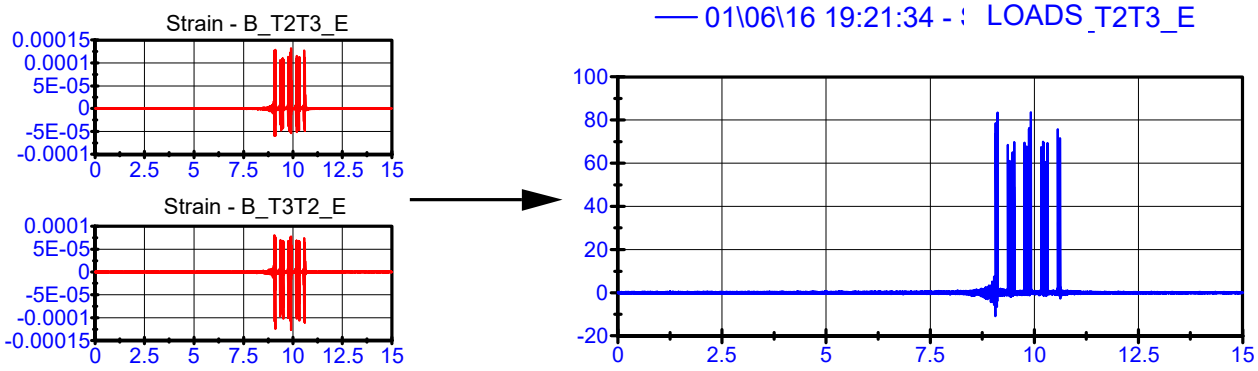

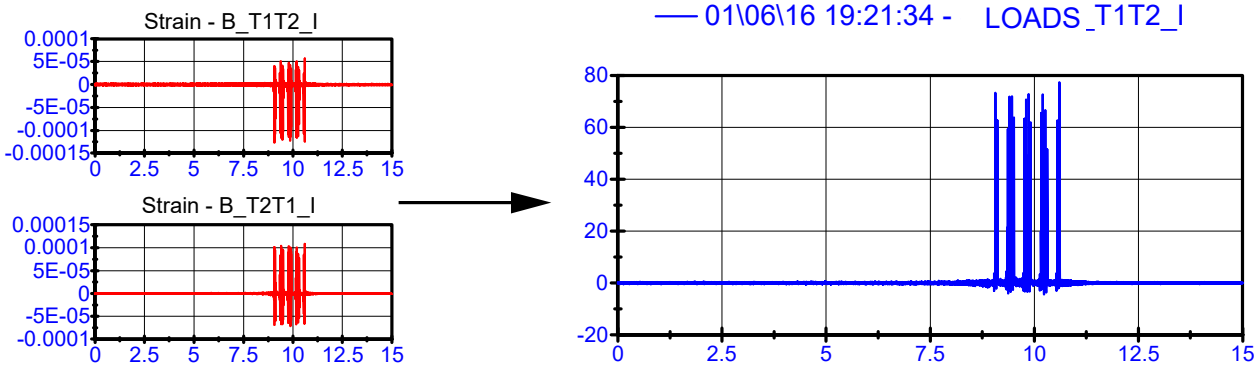

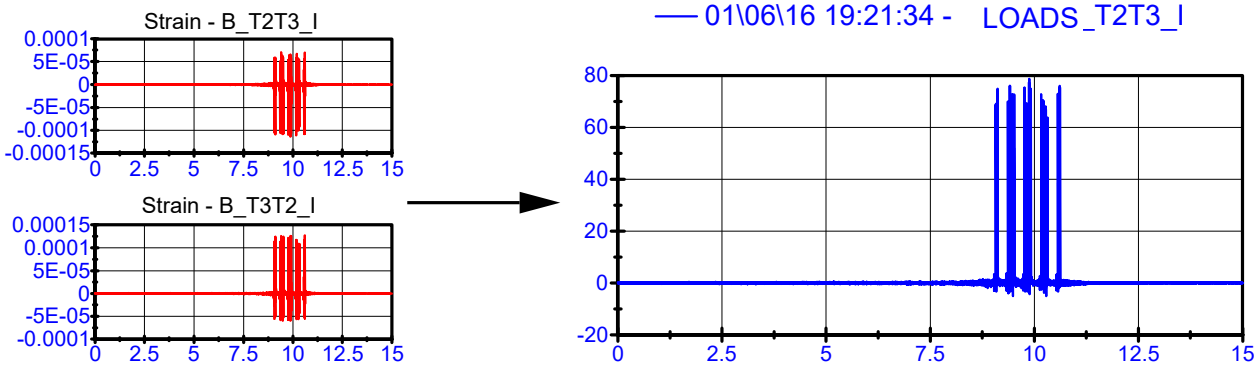

Strain gauges
LPF 500Hz

01\06\16 19:23:31

Loads; LPF 500Hz

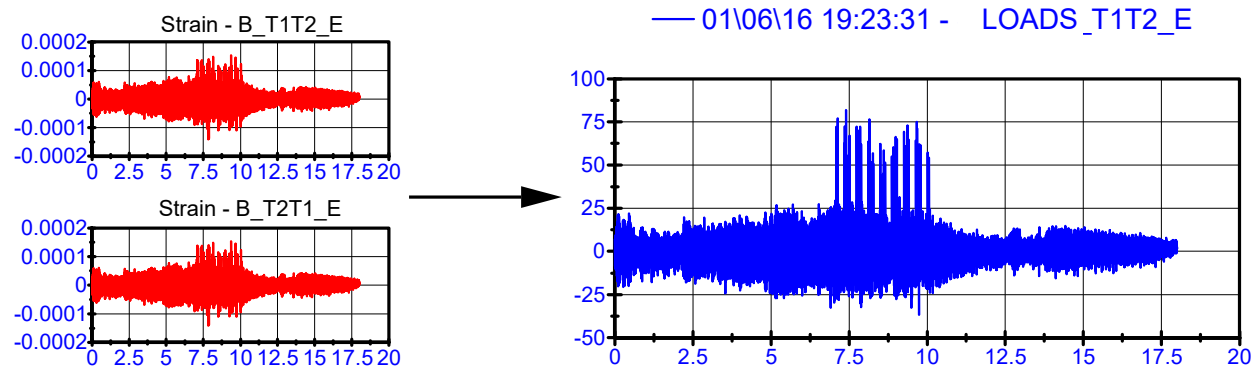

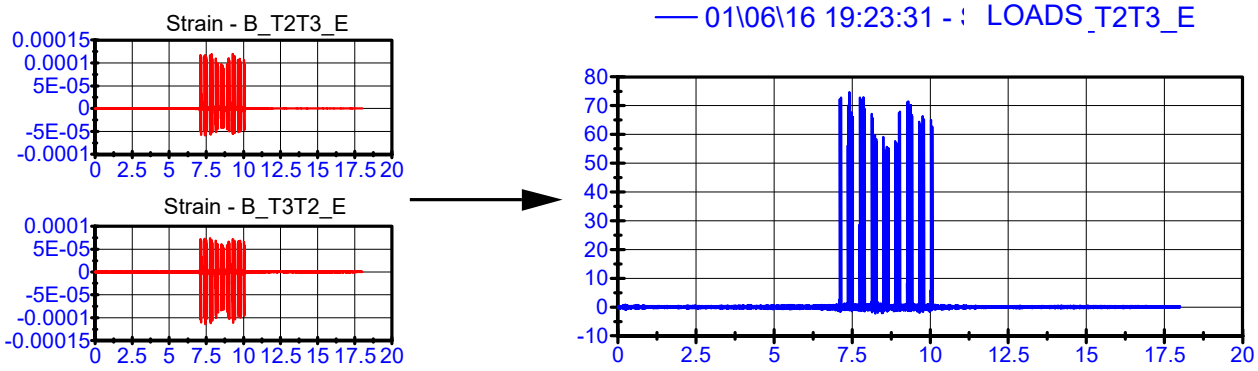

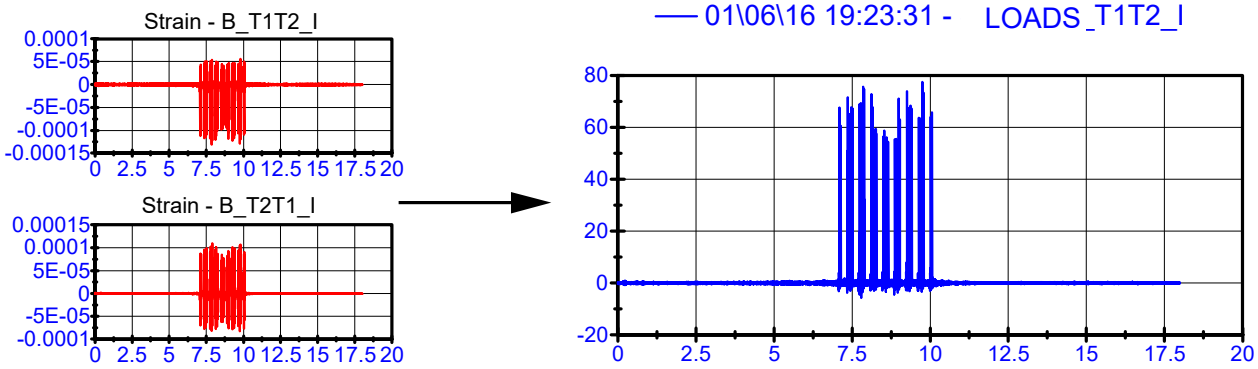

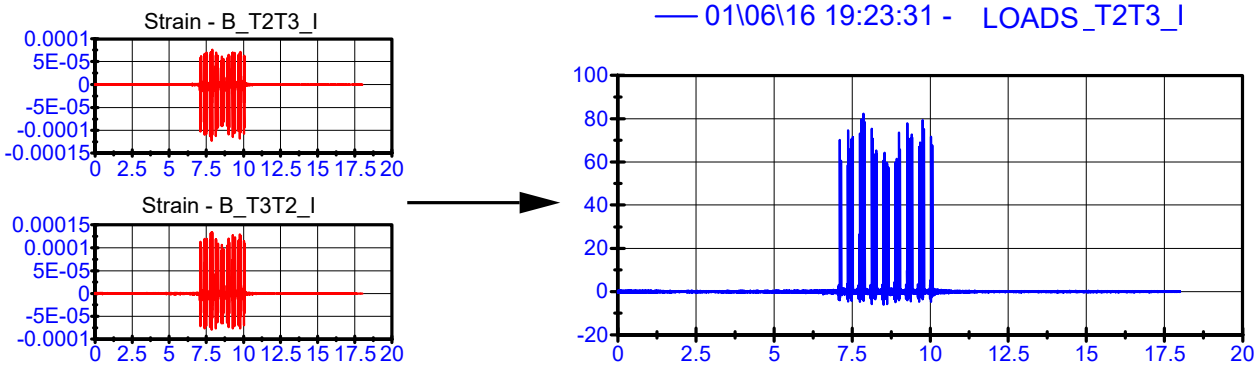

Strain gauges
LPF 500Hz

01\06\16 19:32:45

Loads; LPF 500Hz

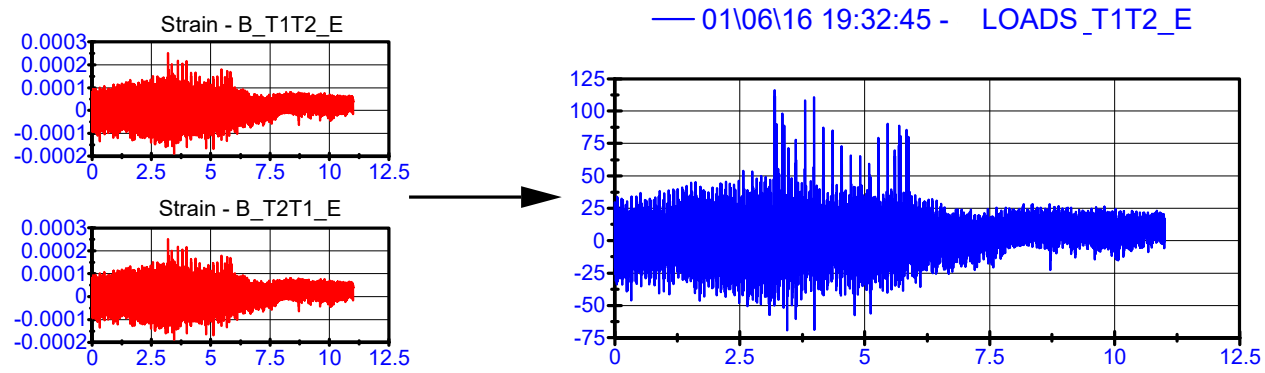

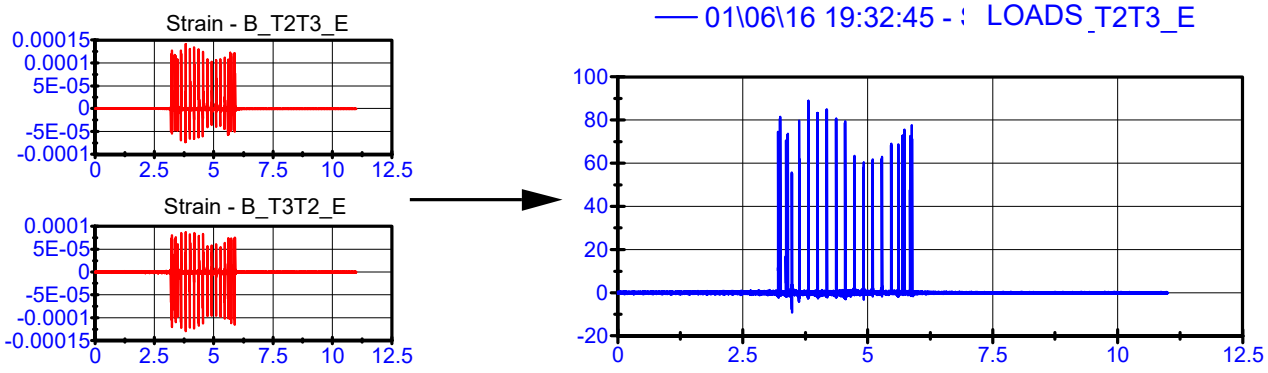

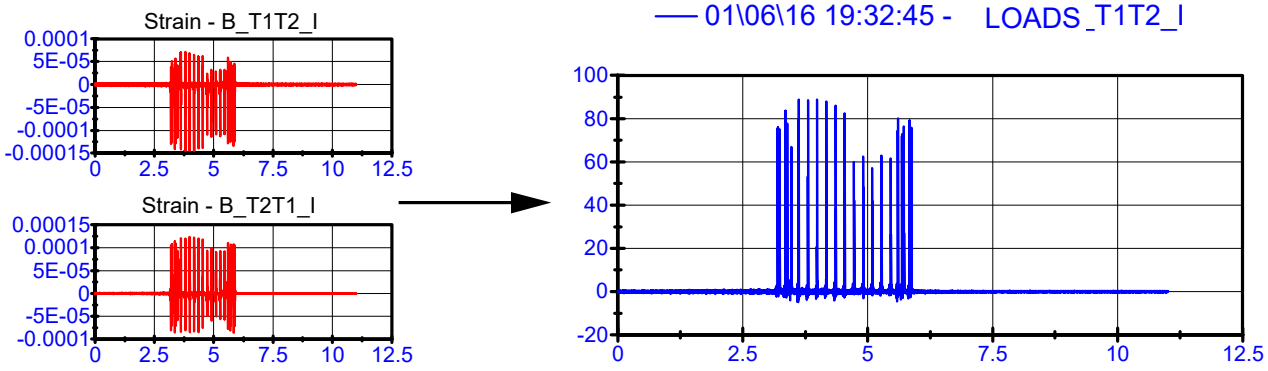

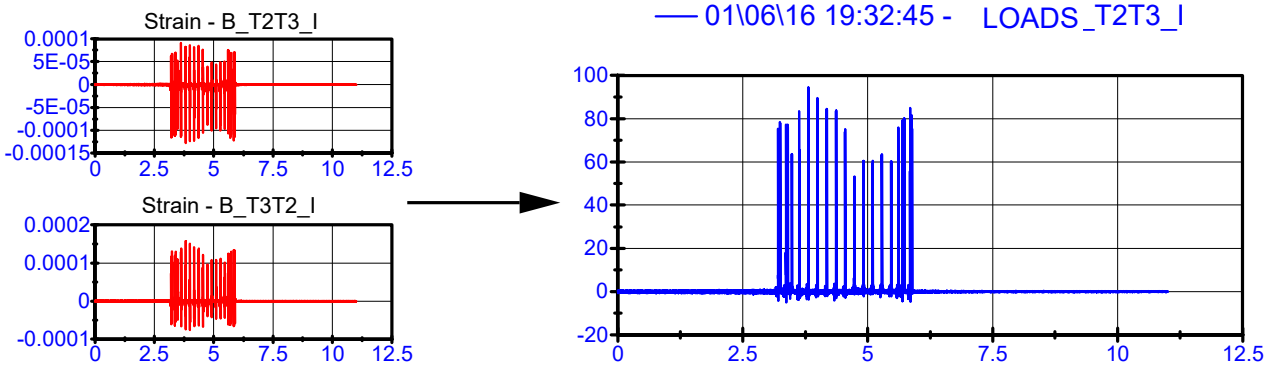

Strain gauges
LPF 500Hz

01\06\16 19:53:03

Loads; LPF 500Hz

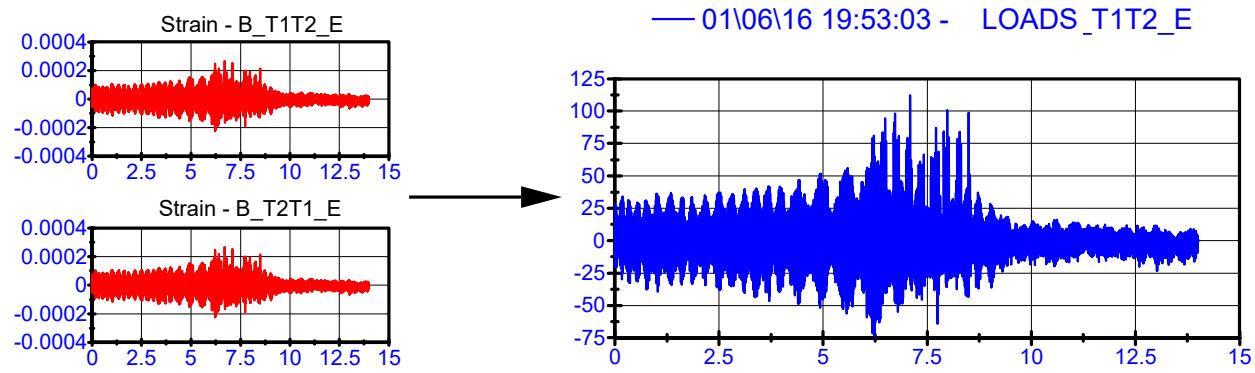

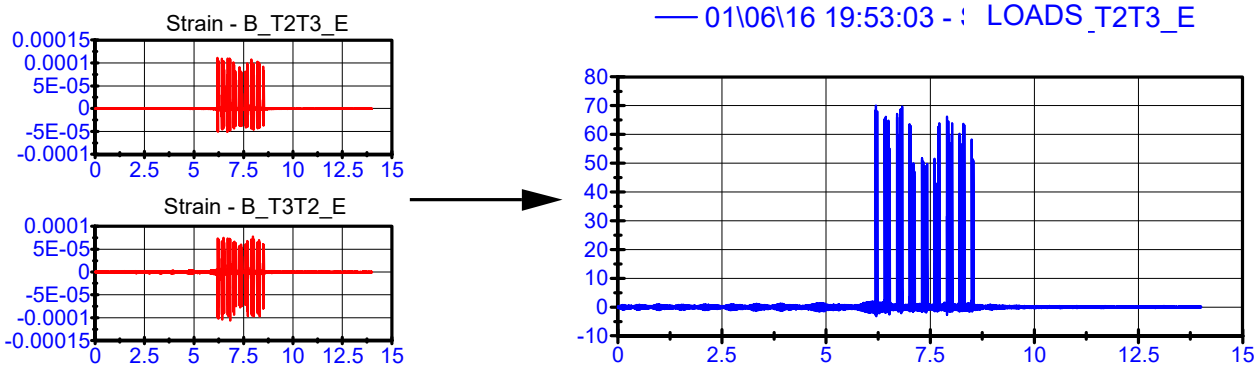

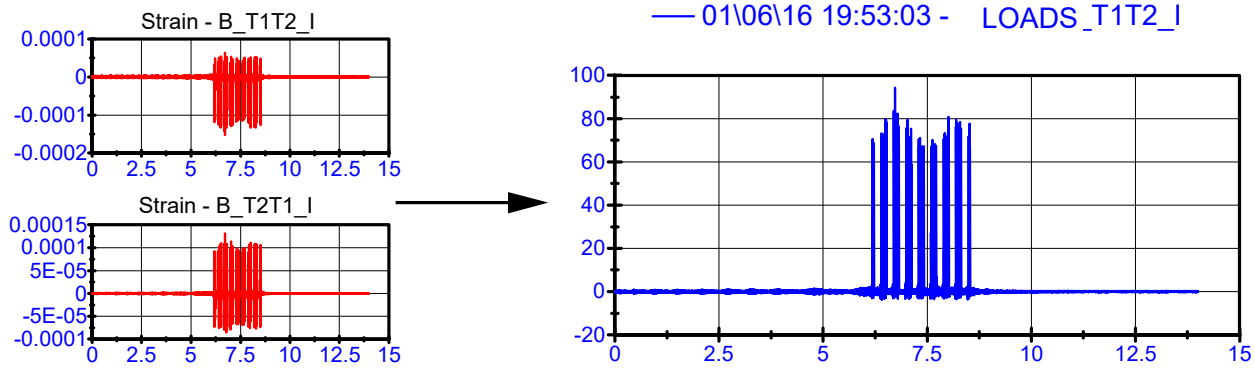

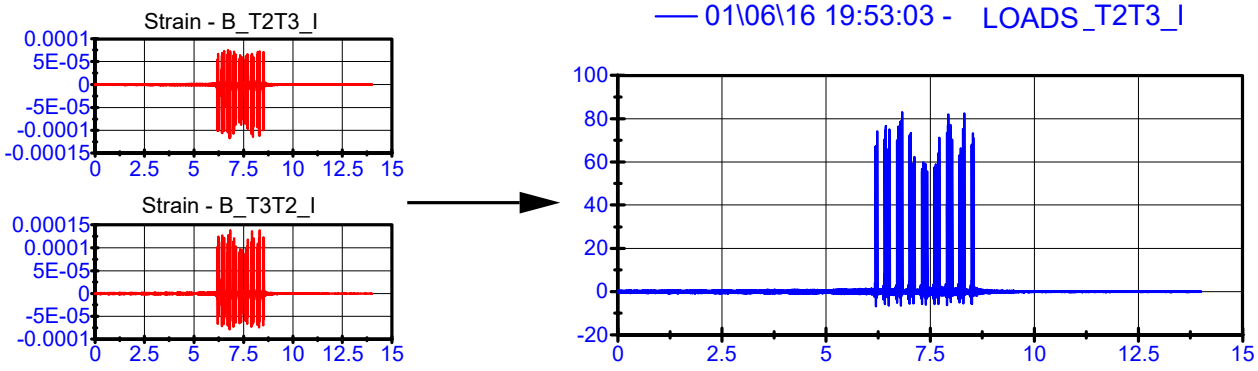

Strain gauges
LPF 500Hz

01\06\16 19:59:42

Loads; LPF 500Hz

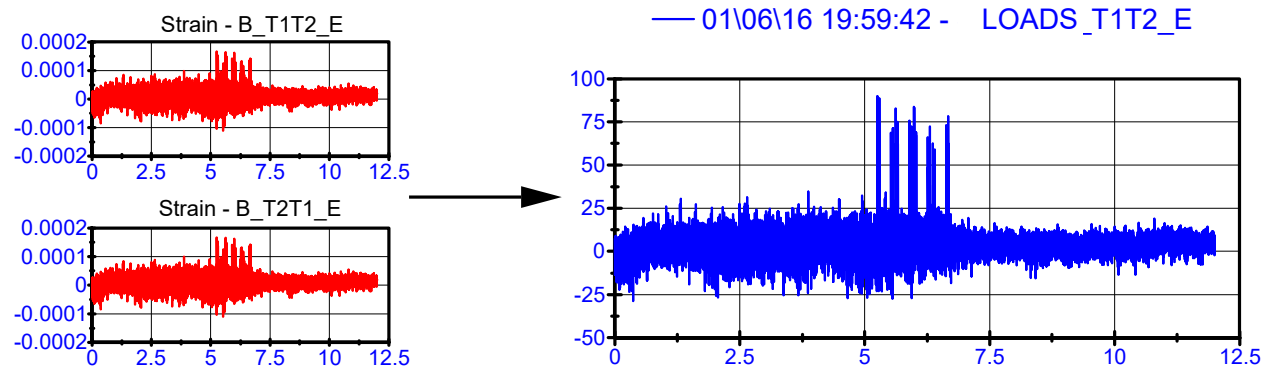

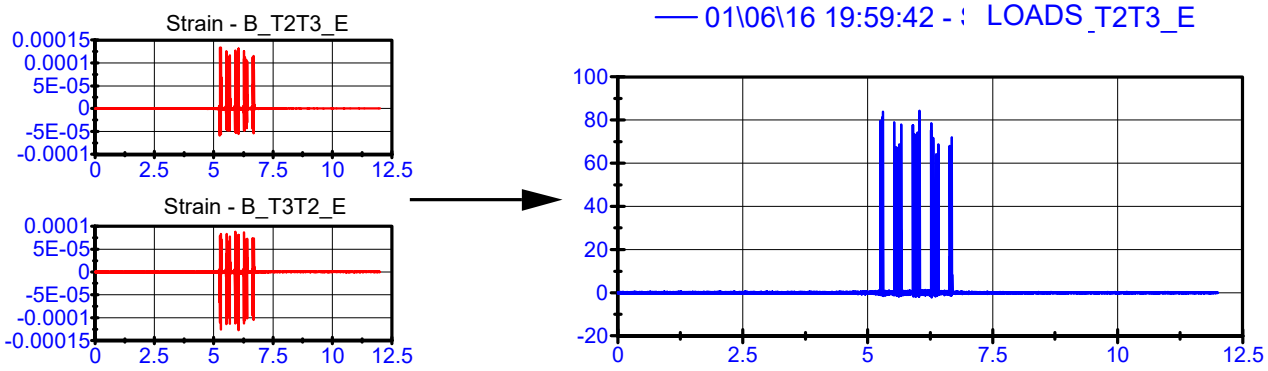

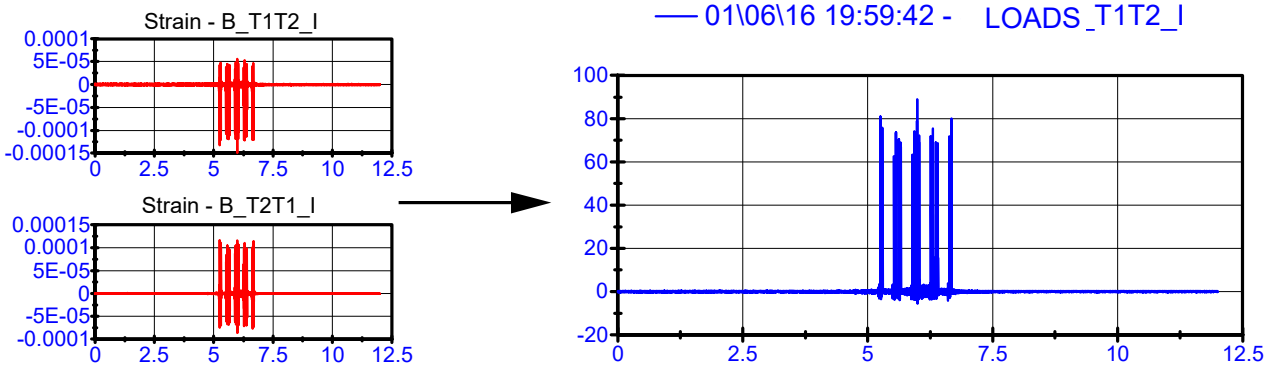

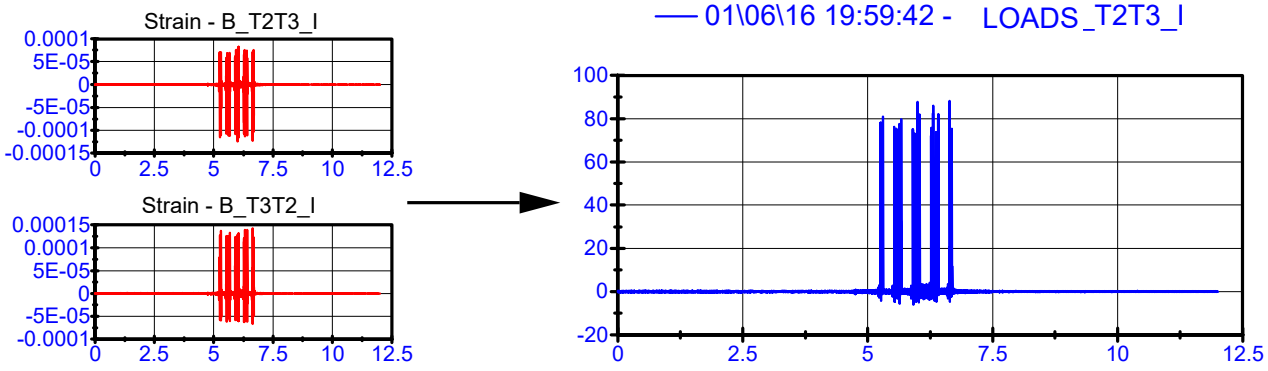

Strain gauges
LPF 500Hz

01\06\16 20:21:57

Loads; LPF 500Hz

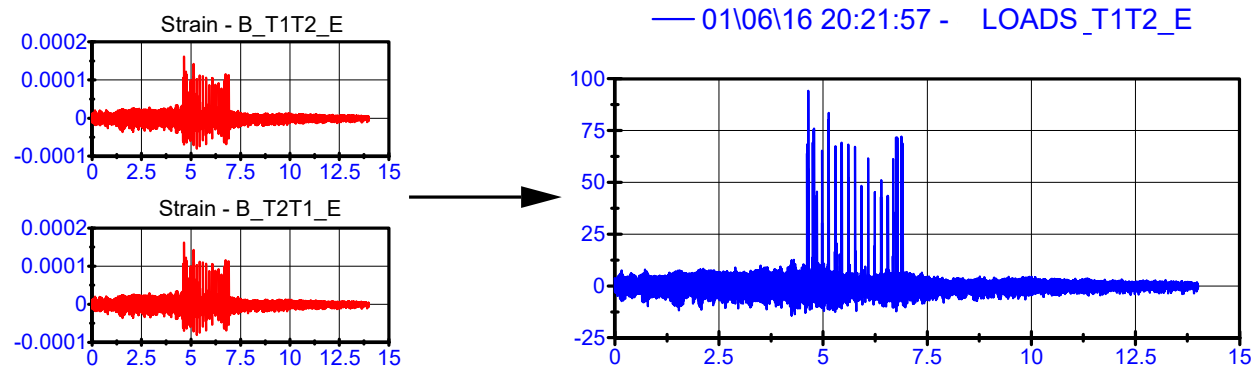

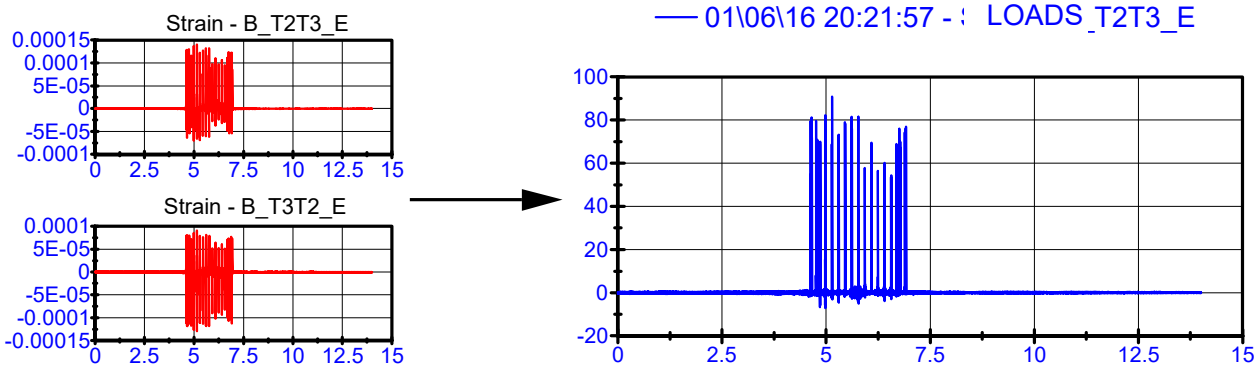

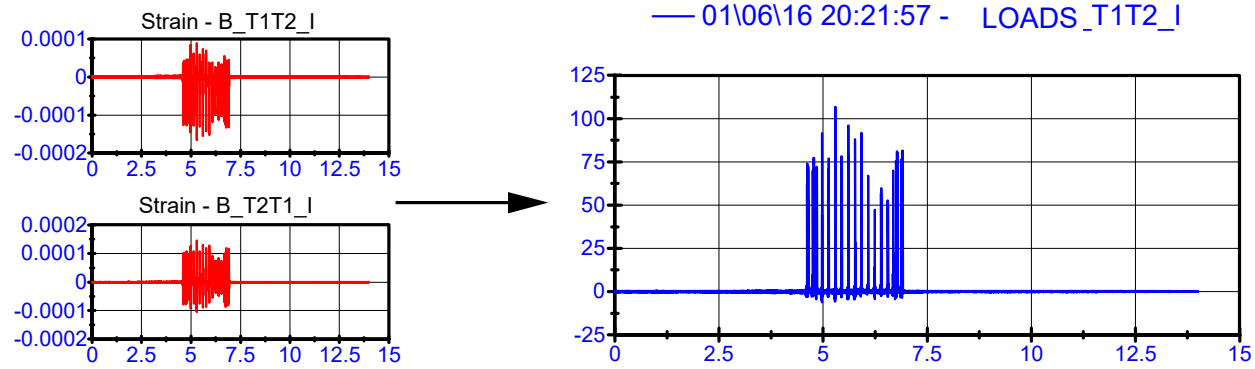

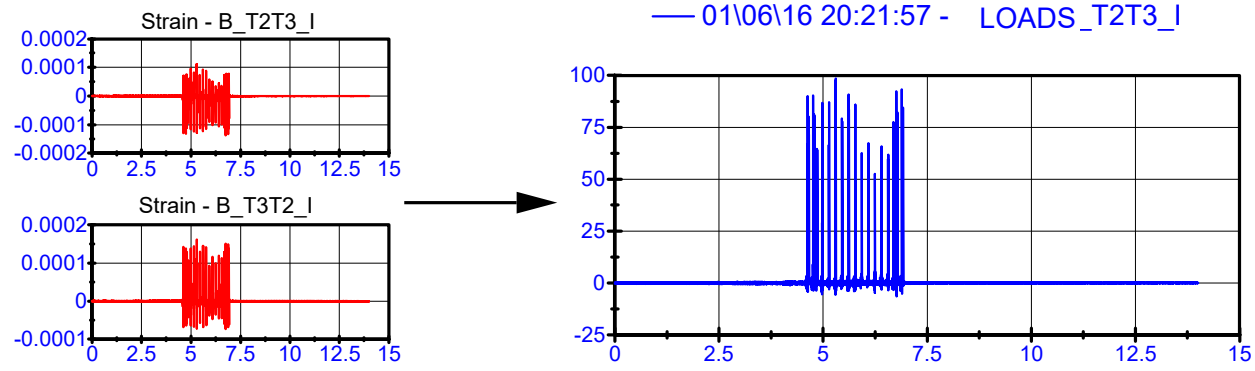

Strain gauges
LPF 500Hz

01\06\16 20:57:58

Loads; LPF 500Hz

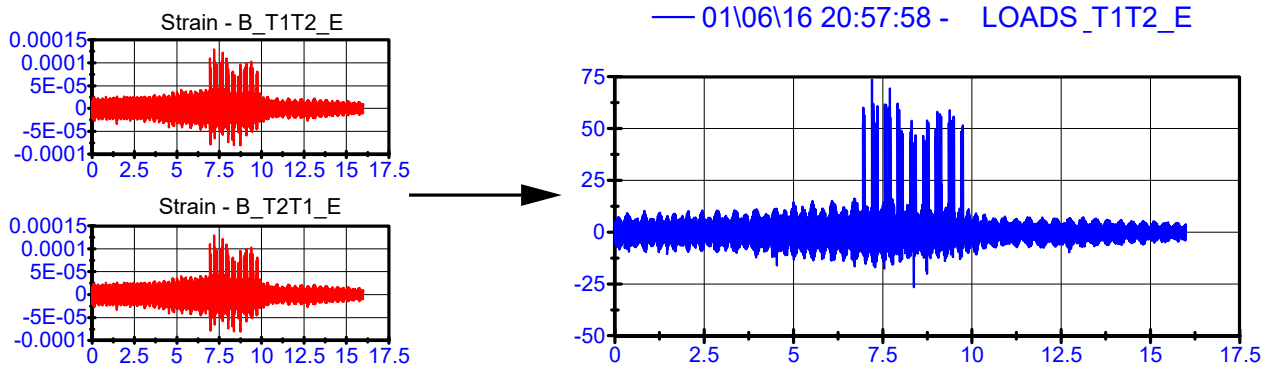

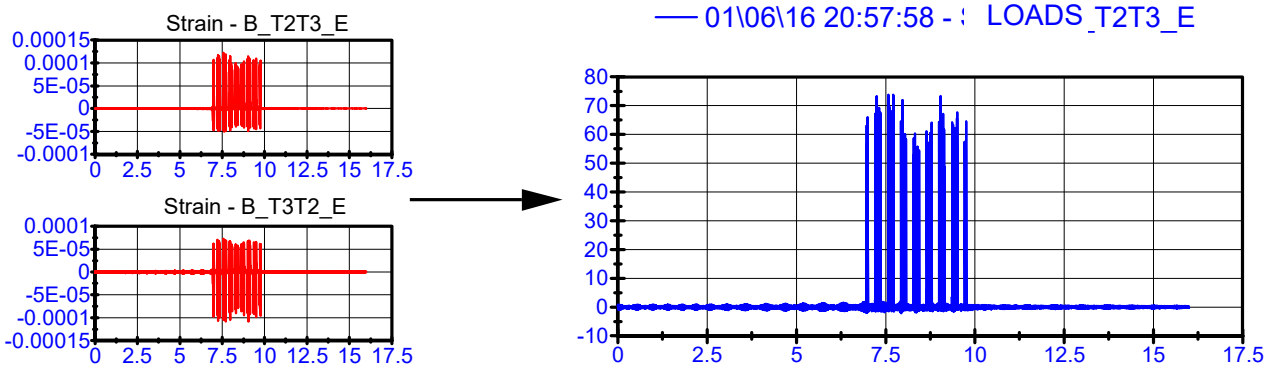

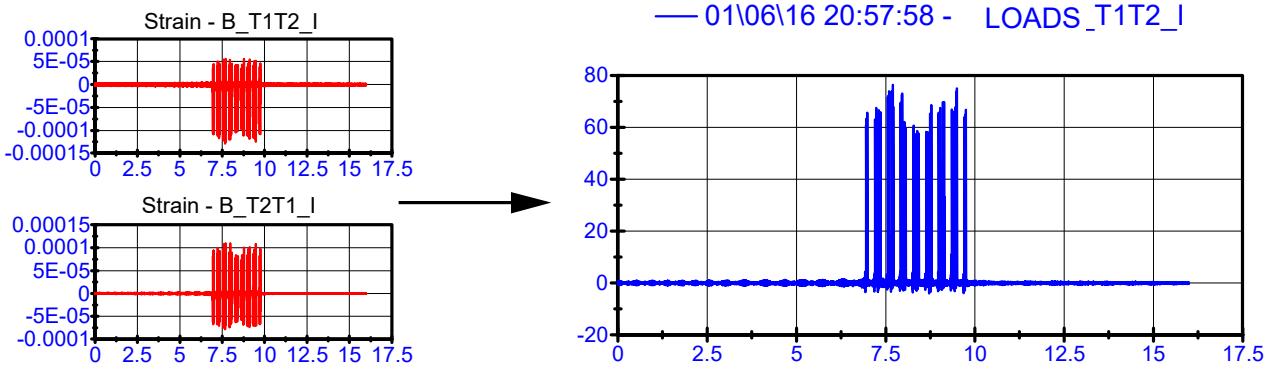

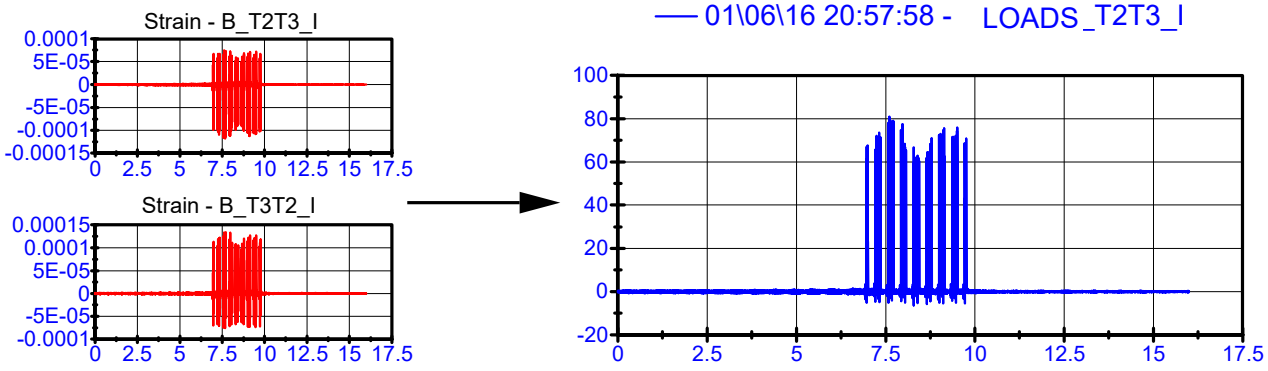

Strain gauges
LPF 500Hz

01\06\16 21:49:46

Loads; LPF 500Hz

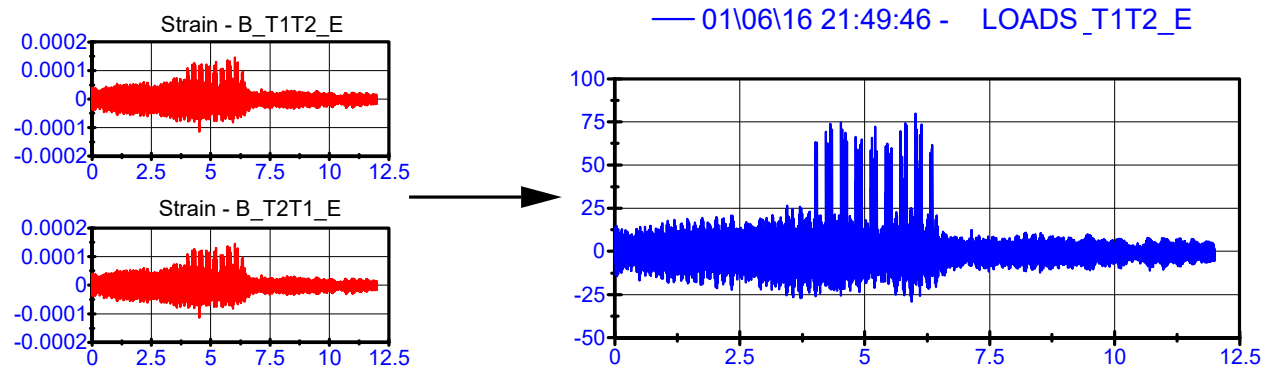

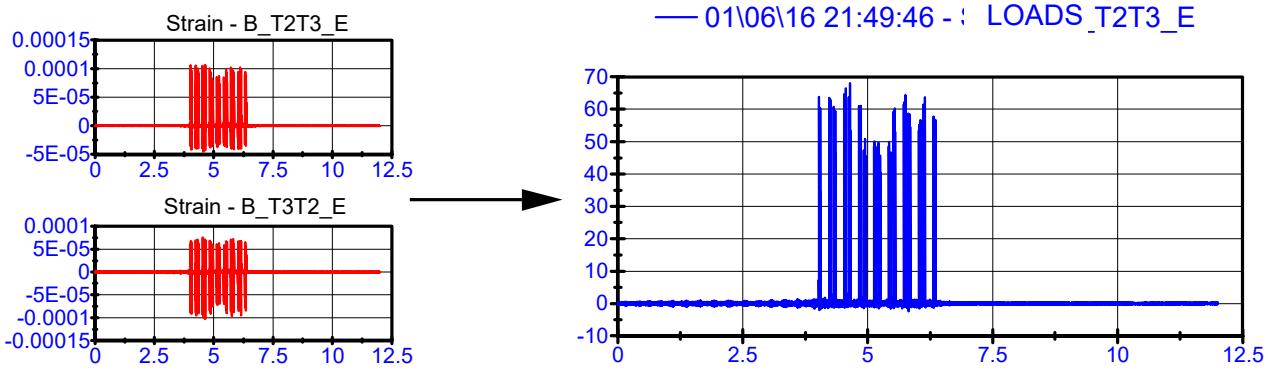

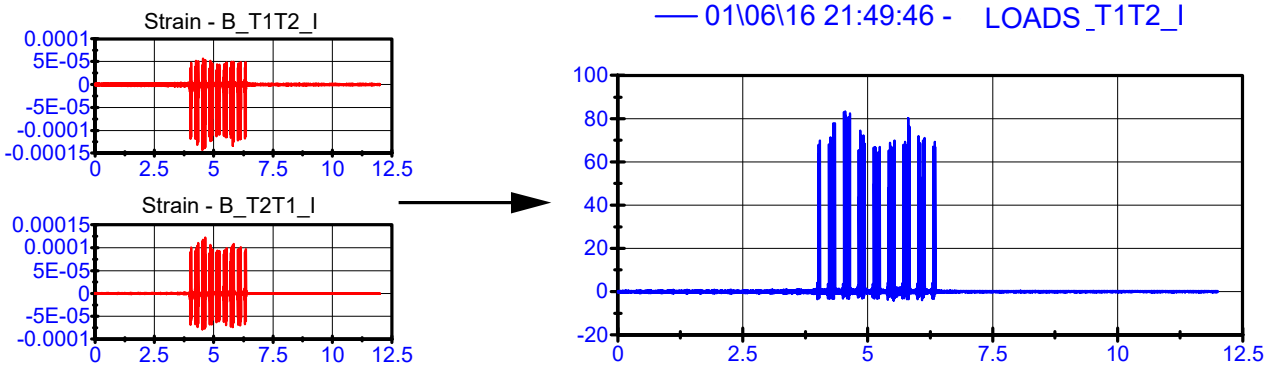

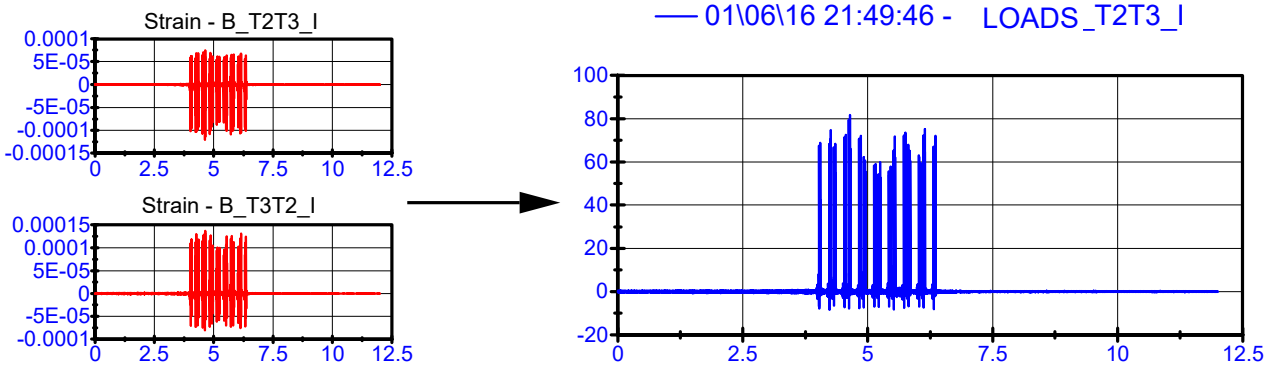

SLEEPER VELOCITY

SLEEPER GEOPHONES

NOTES:

Units of Y axle are “m/s” for all the plots belonging to sleeper velocity.

A Low Pass Filter of 150 has been applied to all raw signals.

01\06\16 06:31:45

Sleeper Geophones
LPF 150Hz

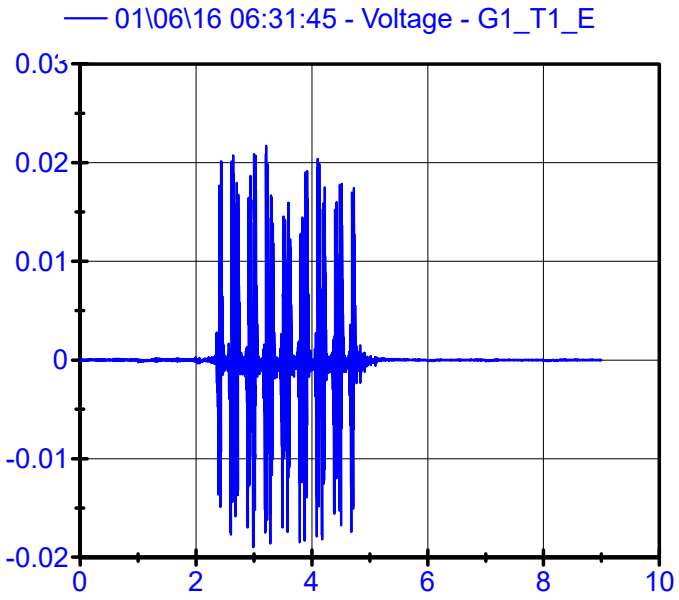

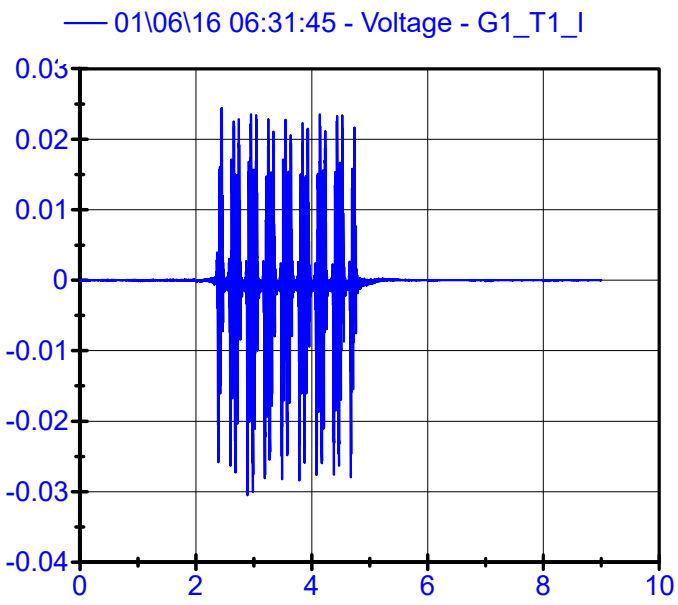

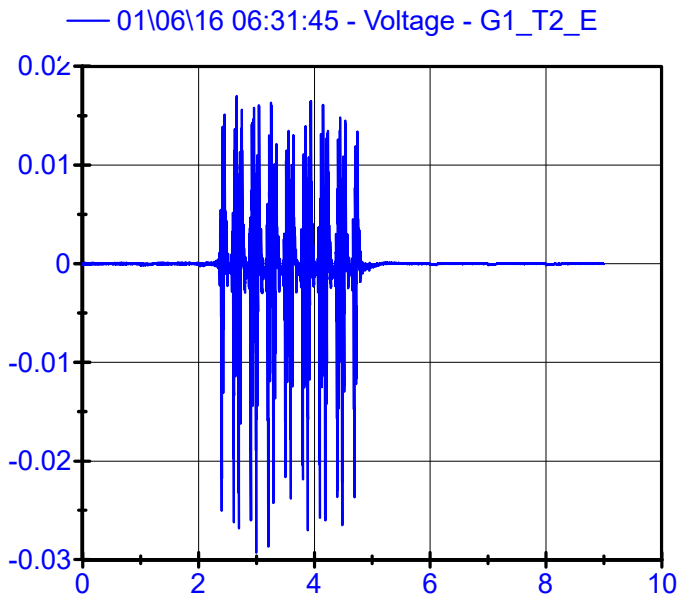

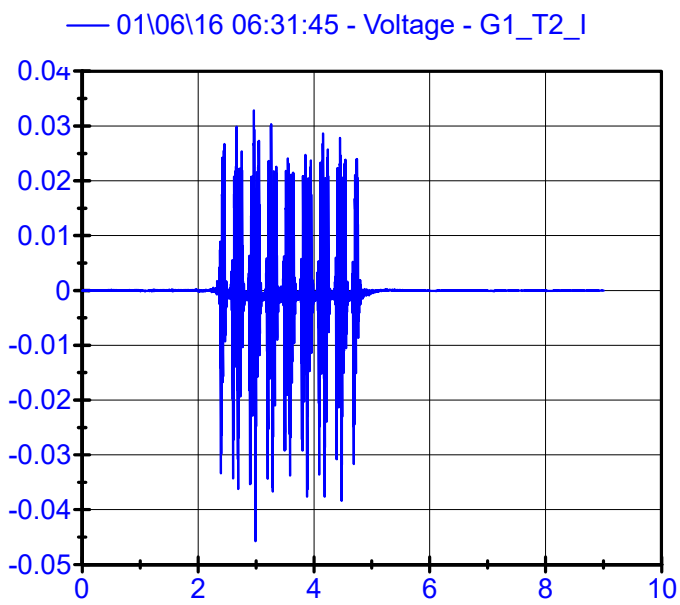

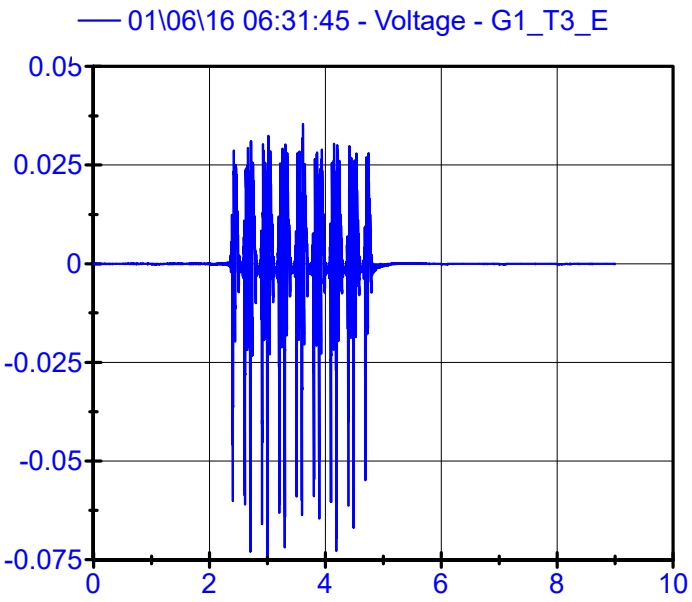

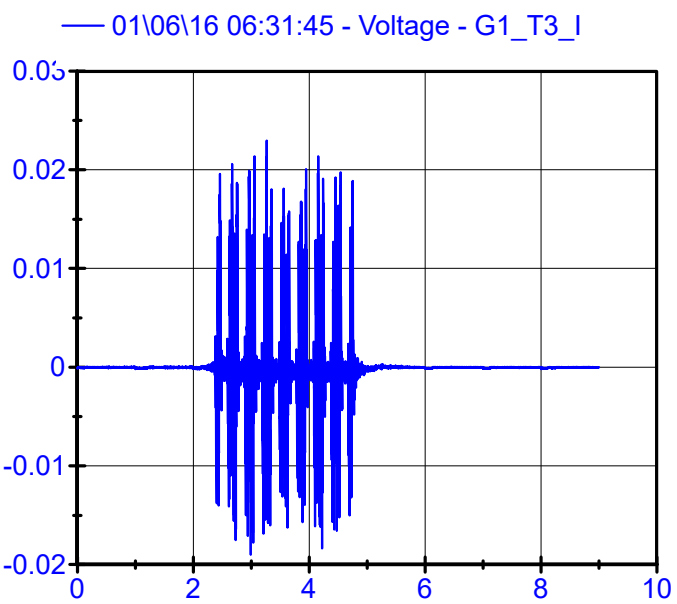

01\06\16 06:52:39

Sleeper Geophones
LPF 150Hz

01\06\16 06:52:39 - Voltage - G1_T1_E

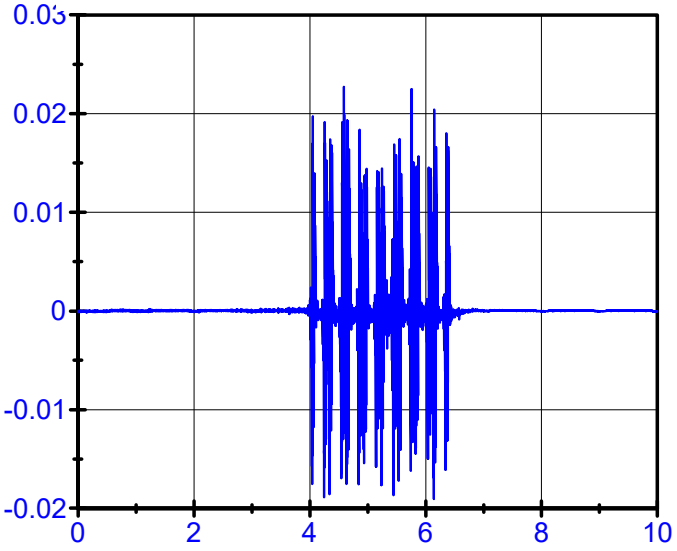

01\06\16 06:52:39 - Voltage - G1_T1_I

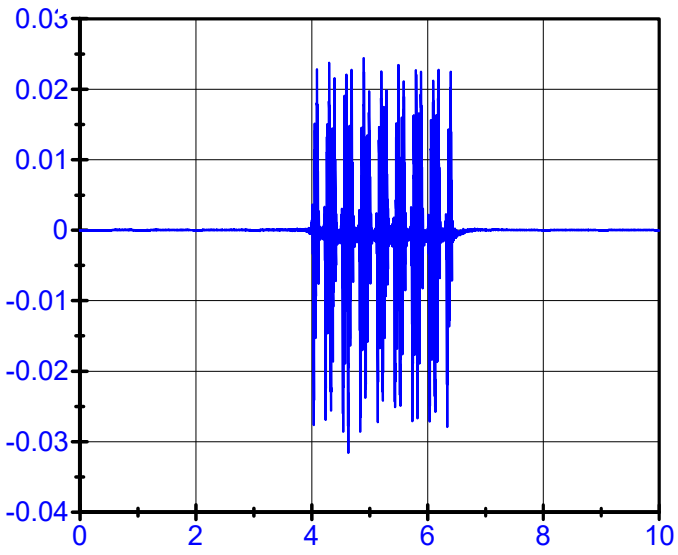

01\06\16 06:52:39 - Voltage - G1_T2_E

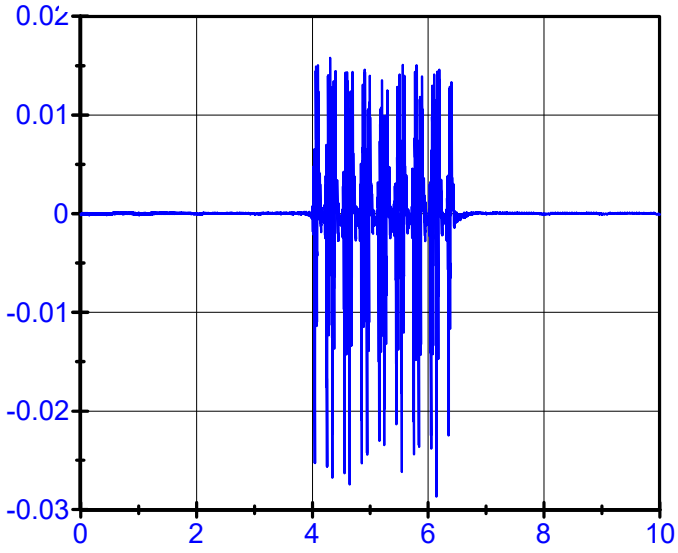

01\06\16 06:52:39 - Voltage - G1_T2_I

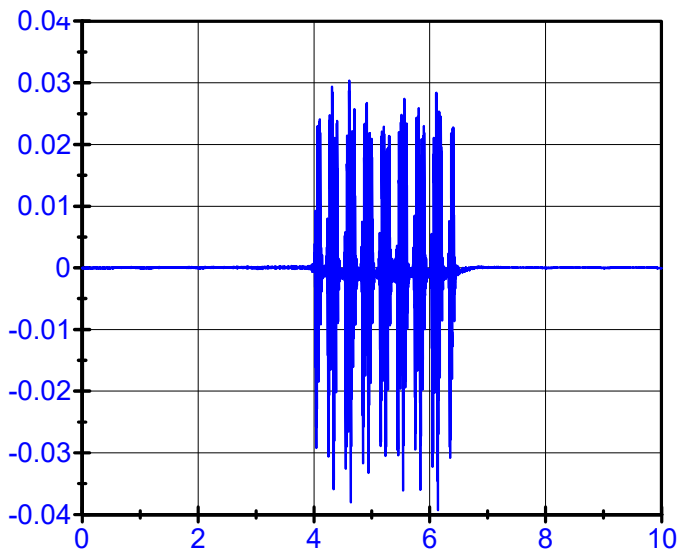

01\06\16 06:52:39 - Voltage - G1_T3_E

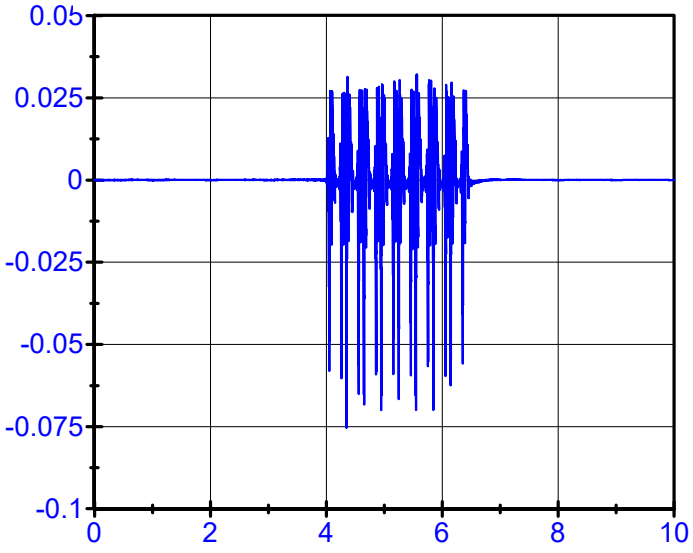

01\06\16 06:52:39 - Voltage - G1_T3_I

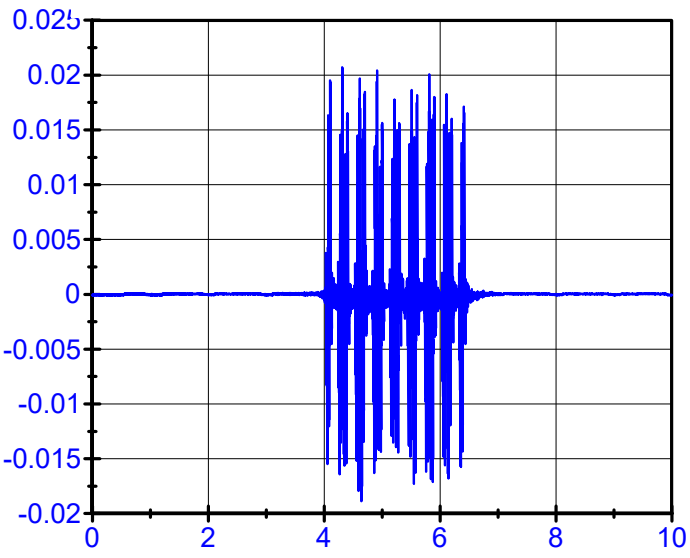

01\06\16 07:21:52

Sleeper Geophones
LPF 150Hz

01\06\16 07:21:52 - Voltage - G1_T1_E

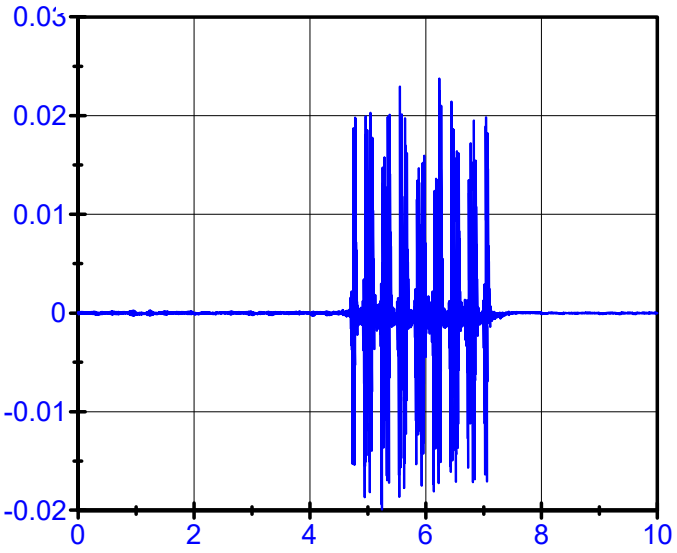

01\06\16 07:21:52 - Voltage - G1_T1_I

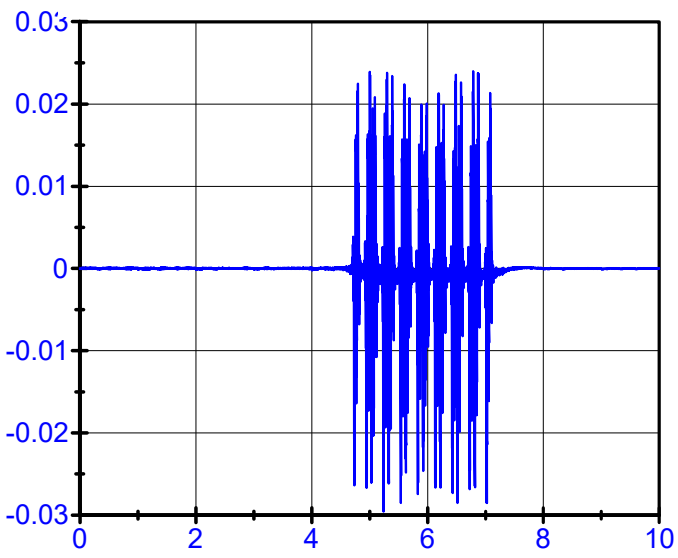

01\06\16 07:21:52 - Voltage - G1_T2_E

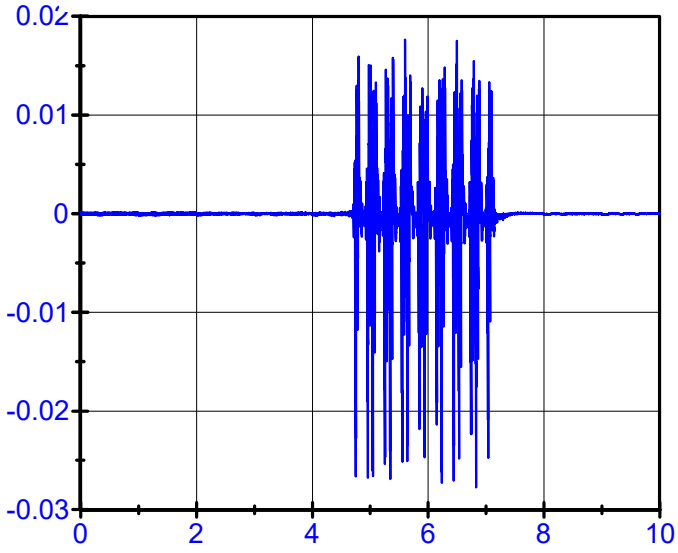

01\06\16 07:21:52 - Voltage - G1_T2_I

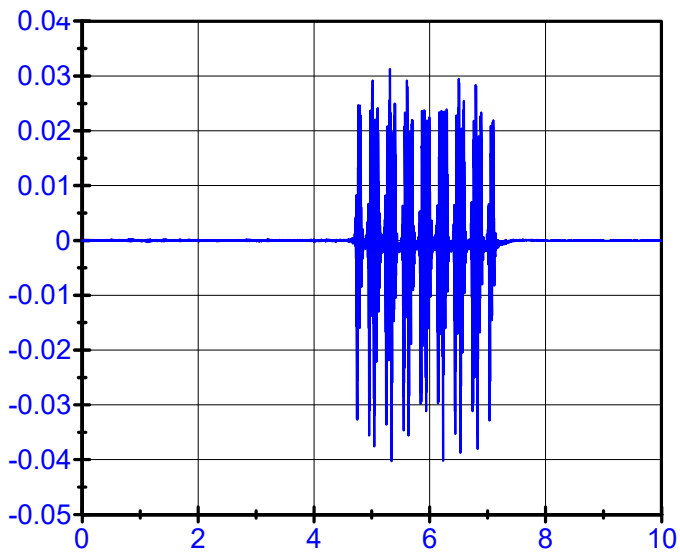

01\06\16 07:21:52 - Voltage - G1_T3_E

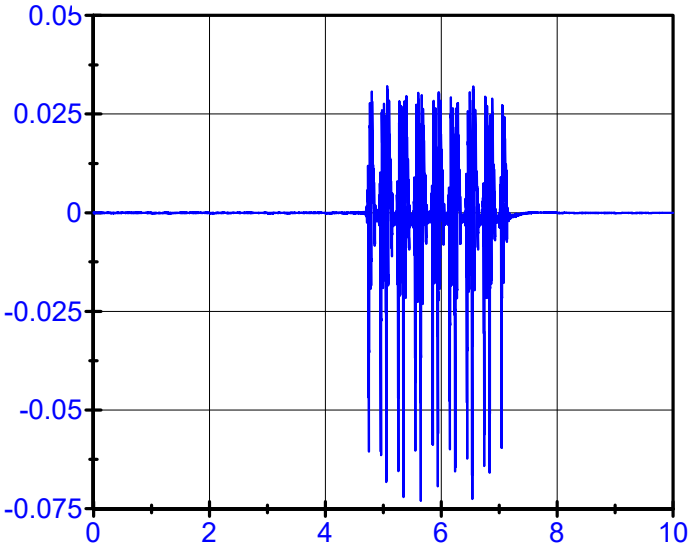

01\06\16 07:21:52 - Voltage - G1_T3_I

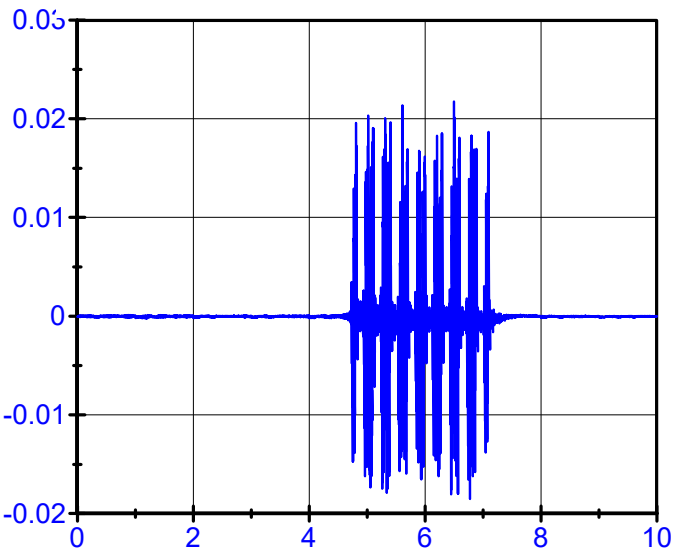

01\06\16 07:41:25

Sleeper Geophones
LPF 150Hz

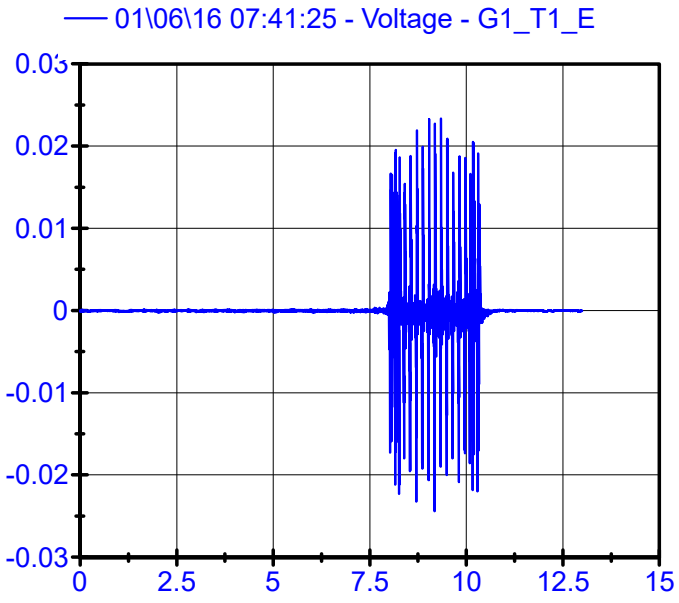

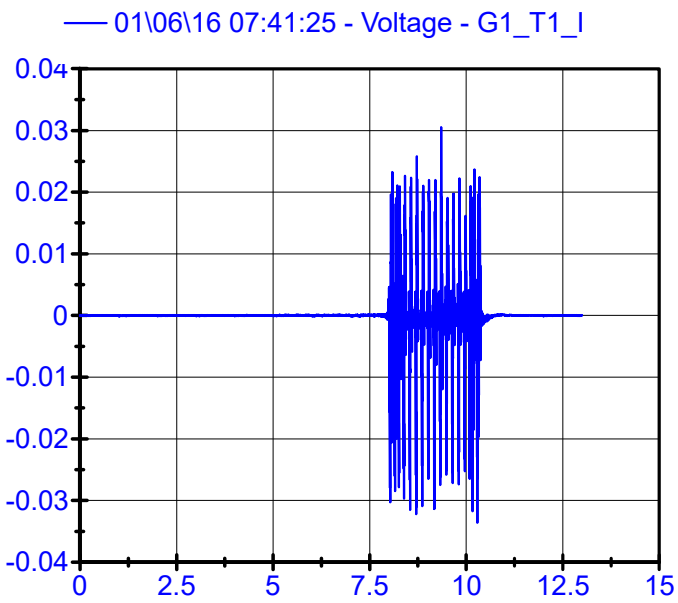

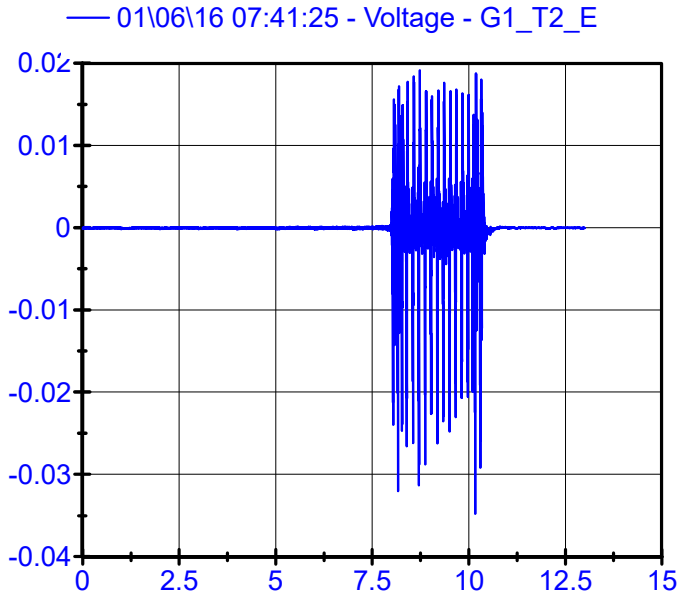

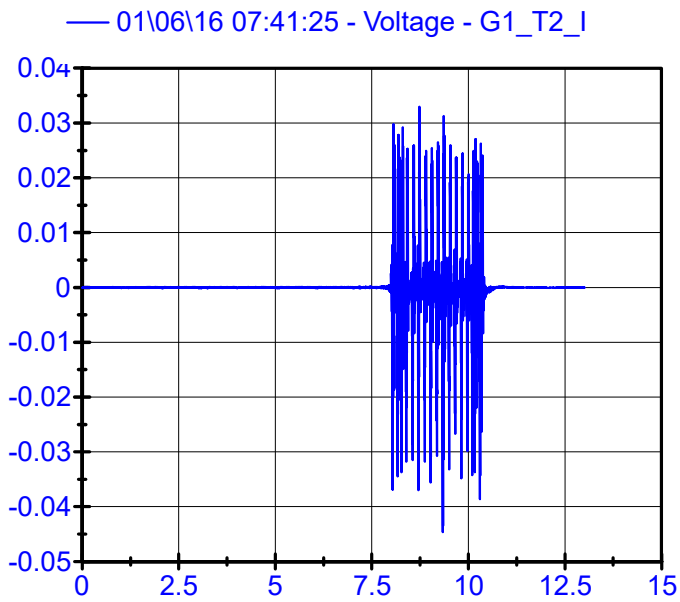

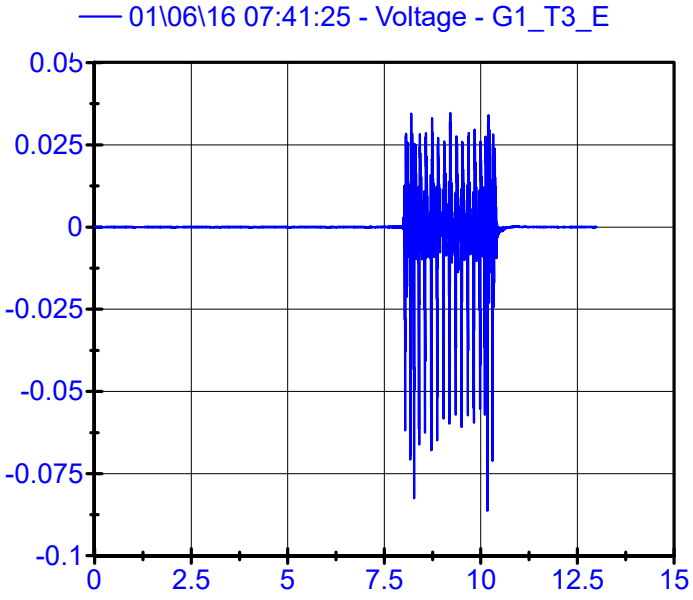

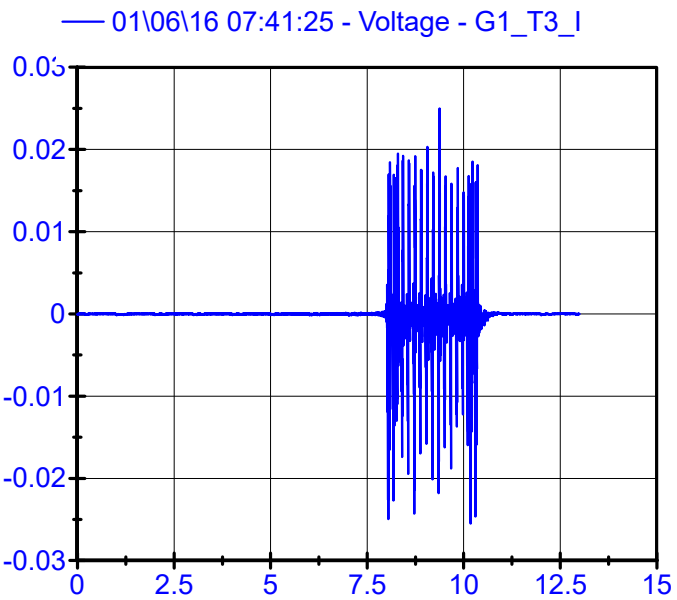

01\06\16 07:56:37

Sleeper Geophones
LPF 150Hz

01\06\16 07:56:37 - Voltage - G1_T1_E

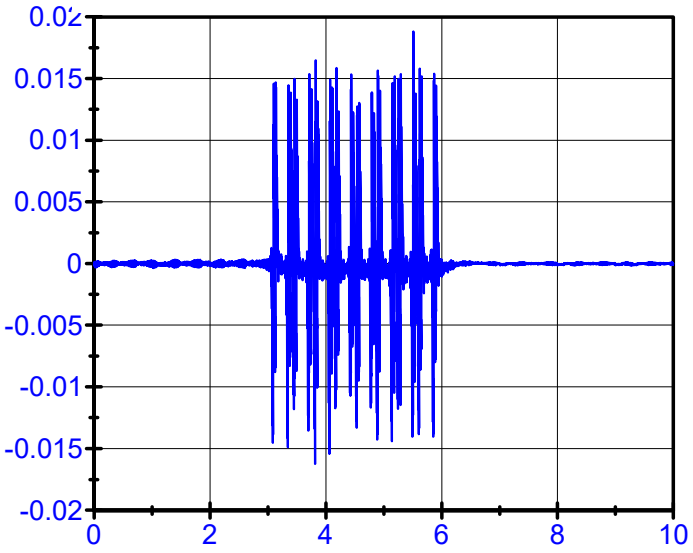

01\06\16 07:56:37 - Voltage - G1_T1_I

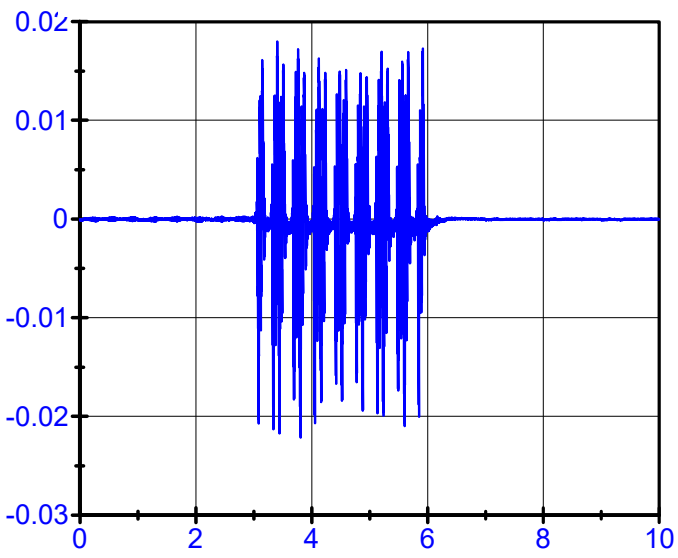

01\06\16 07:56:37 - Voltage - G1_T2_E

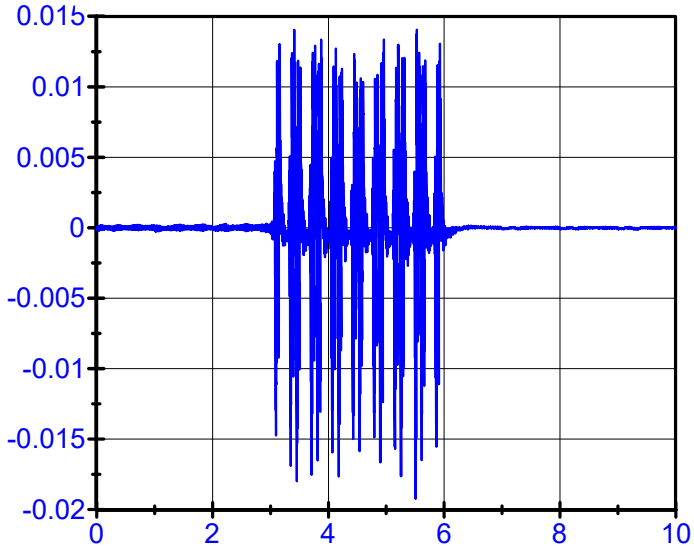

01\06\16 07:56:37 - Voltage - G1_T2_I

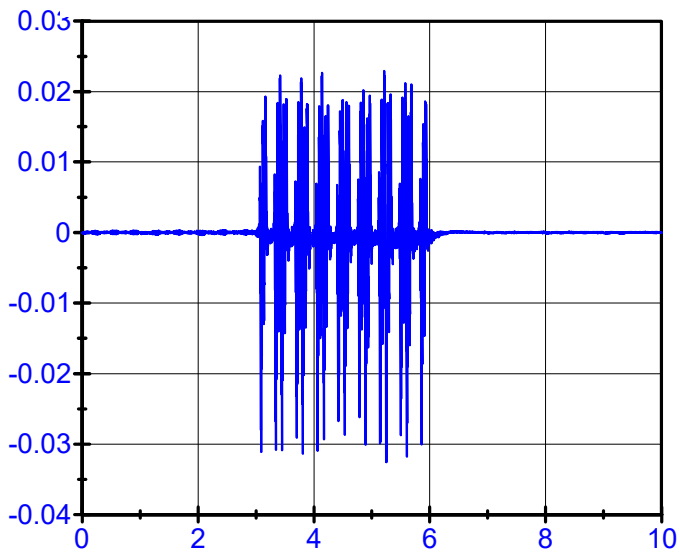

01\06\16 07:56:37 - Voltage - G1_T3_E

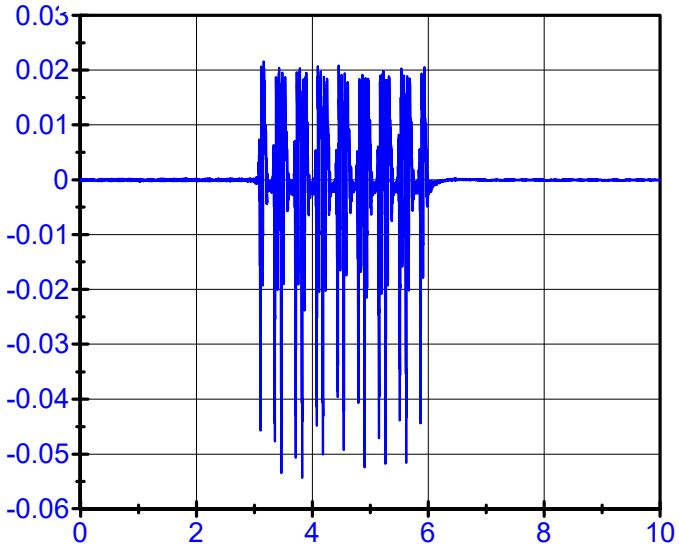

01\06\16 07:56:37 - Voltage - G1_T3_I

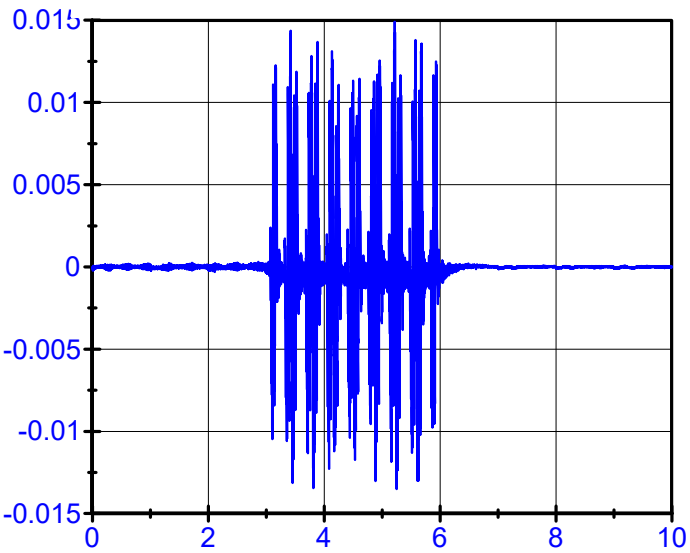

01\06\16 08:01:29

Sleeper Geophones
LPF 150Hz

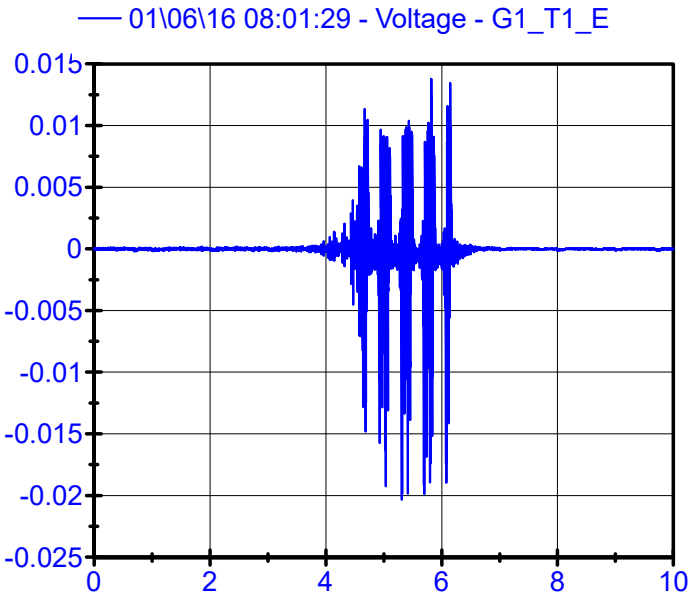

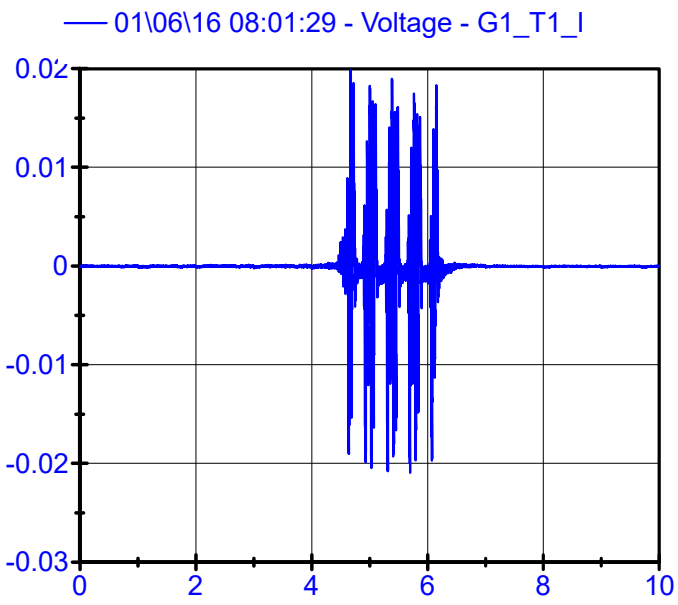

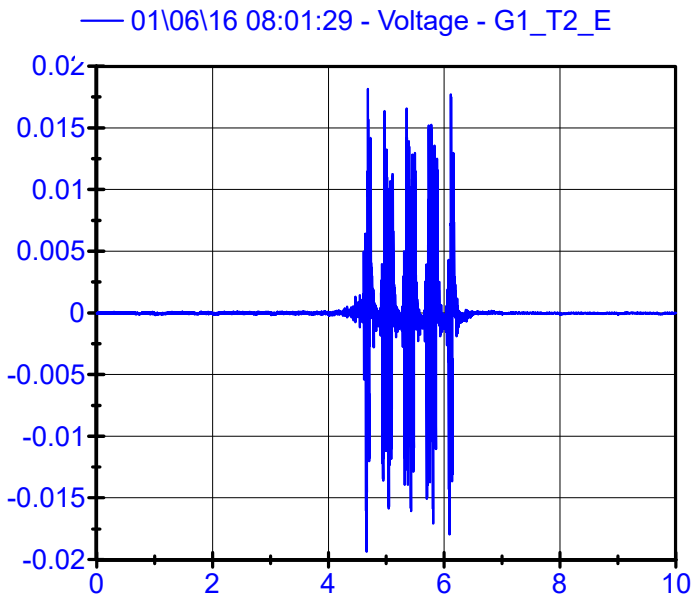

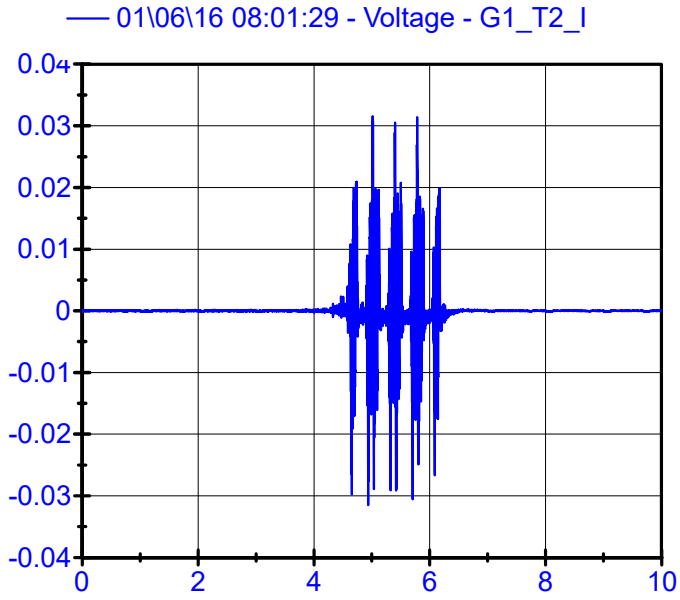

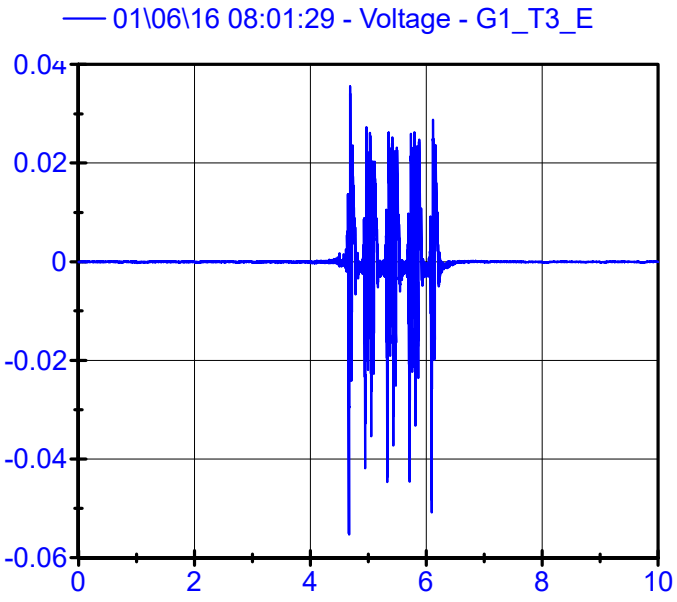

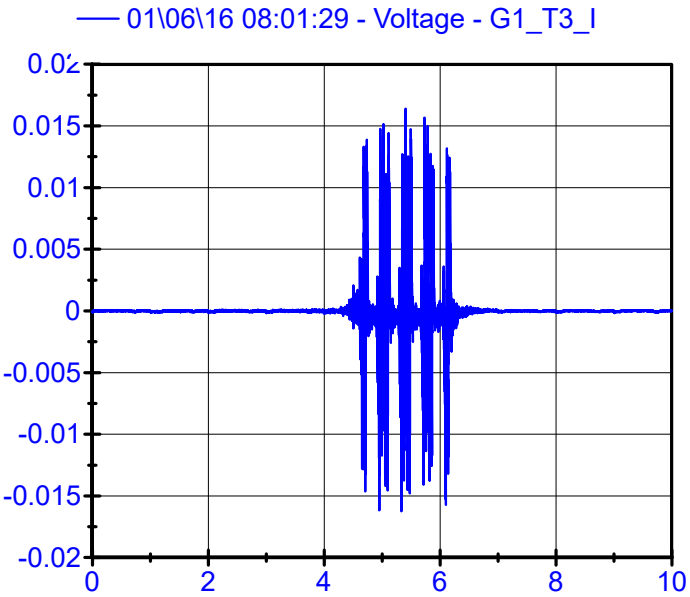

01\06\16 08:21:04

Sleeper Geophones
LPF 150Hz

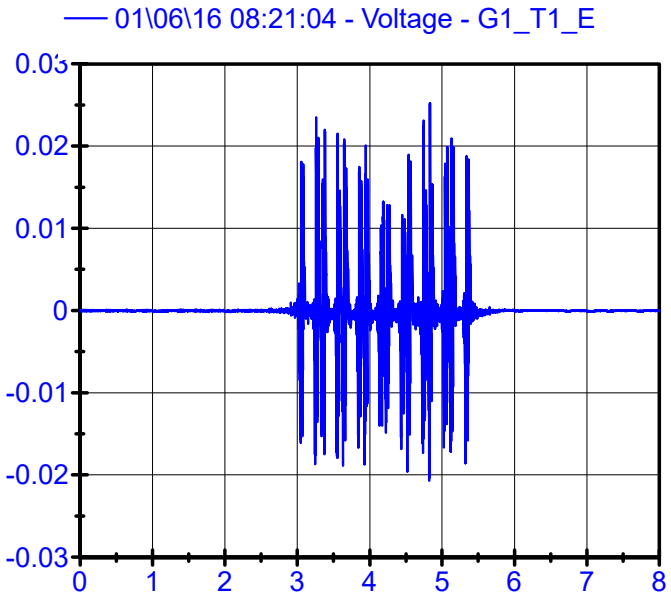

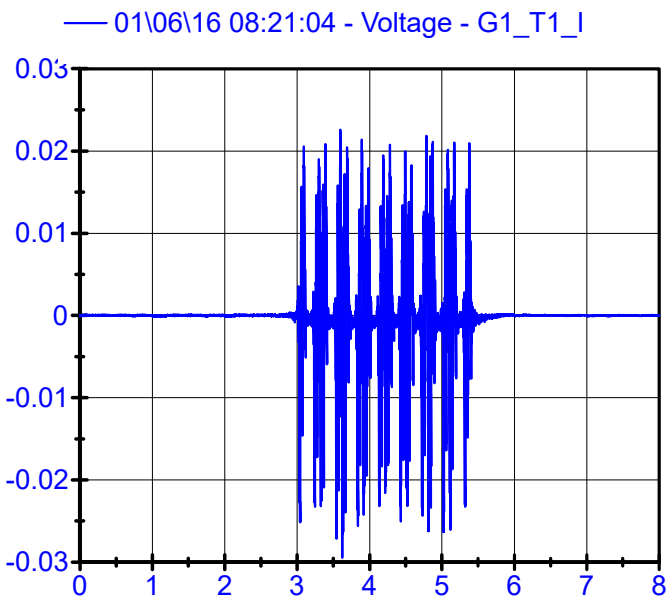

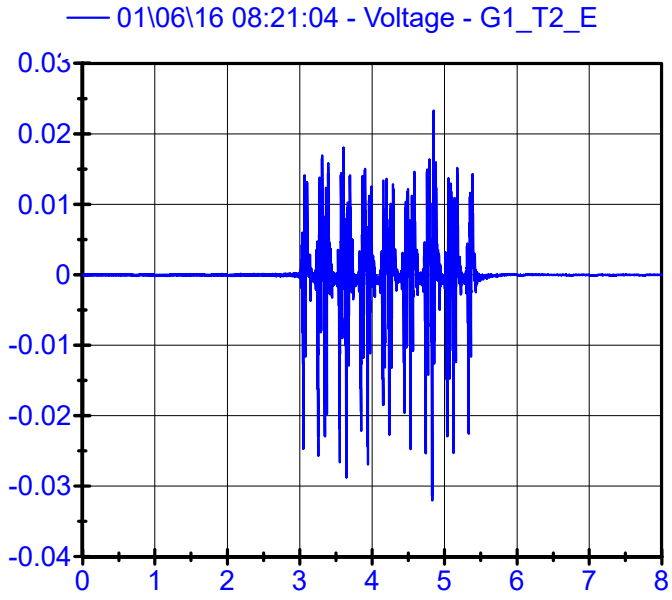

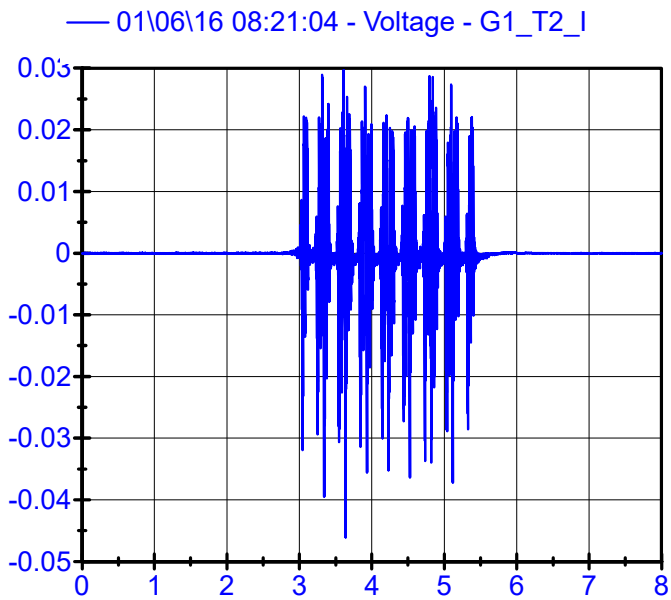

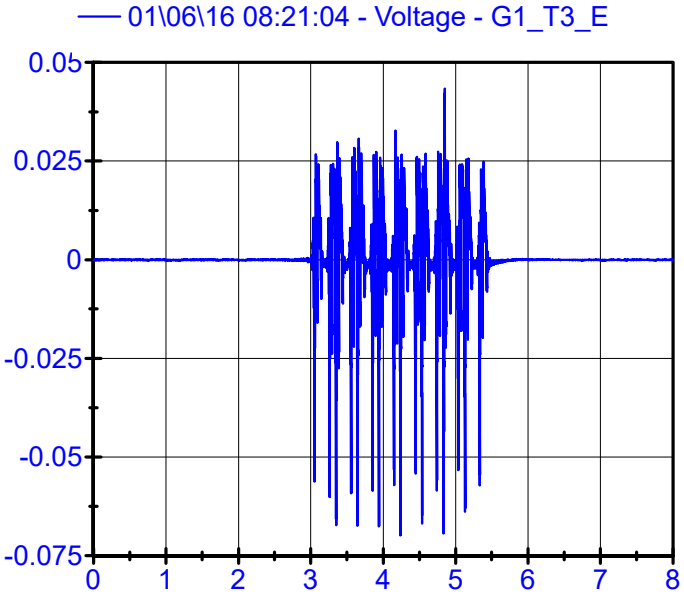

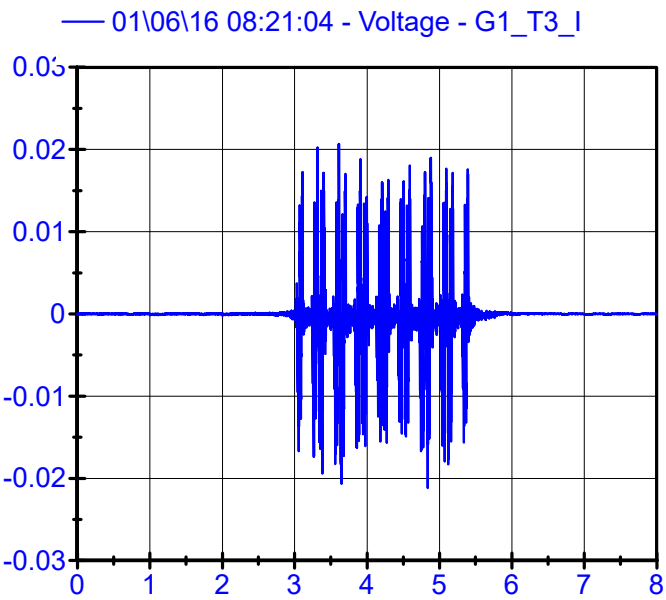

01\06\16 08:42:39

Sleeper Geophones
LPF 150Hz

01\06\16 08:42:39 - Voltage - G1_T1_E

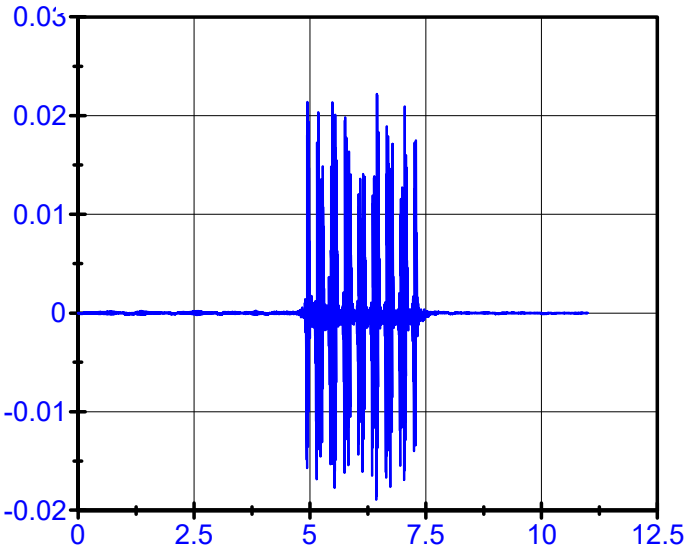

01\06\16 08:42:39 - Voltage - G1_T1_I

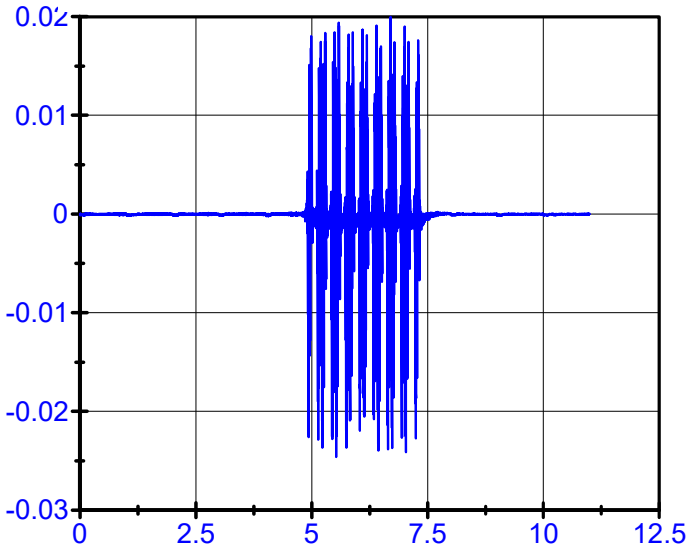

01\06\16 08:42:39 - Voltage - G1_T2_E

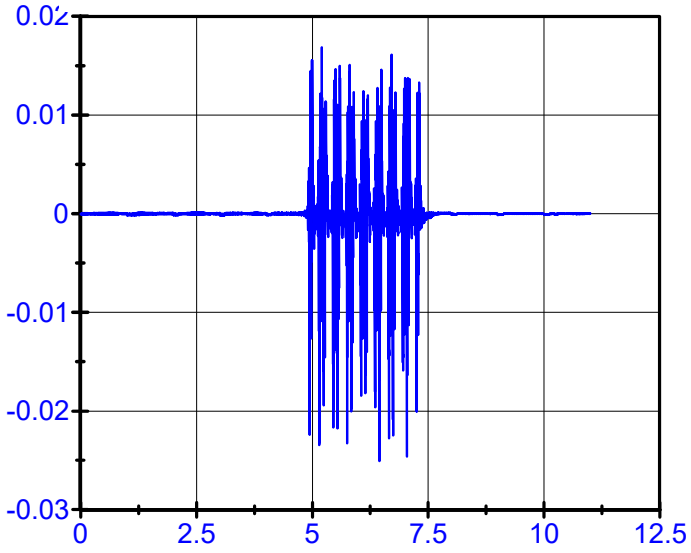

01\06\16 08:42:39 - Voltage - G1_T2_I

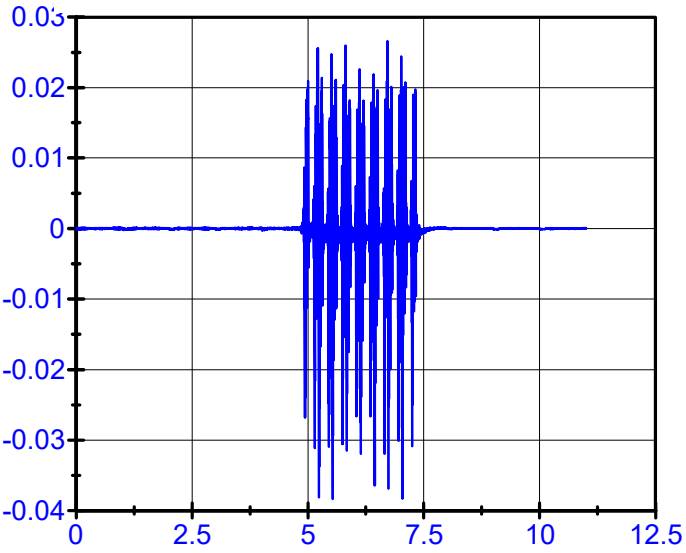

01\06\16 08:42:39 - Voltage - G1_T3_E

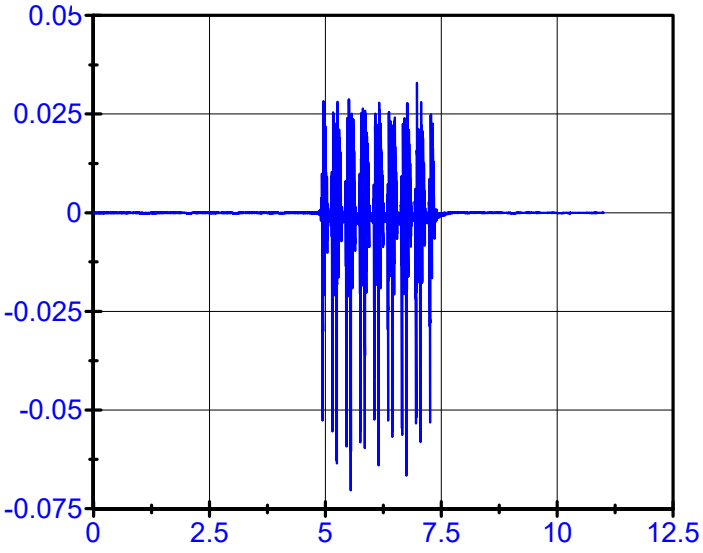

01\06\16 08:42:39 - Voltage - G1_T3_I

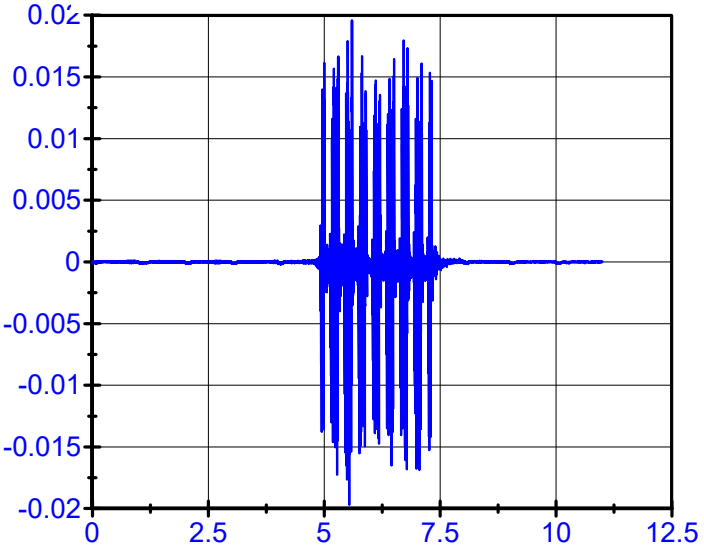

01\06\16 08:52:26

Sleeper Geophones
LPF 150Hz

01\06\16 08:52:26 - Voltage - G1_T1_E

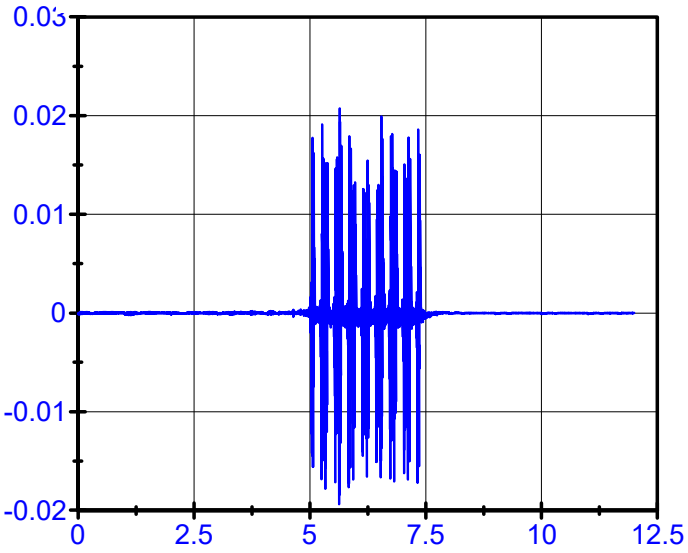

01\06\16 08:52:26 - Voltage - G1_T1_I

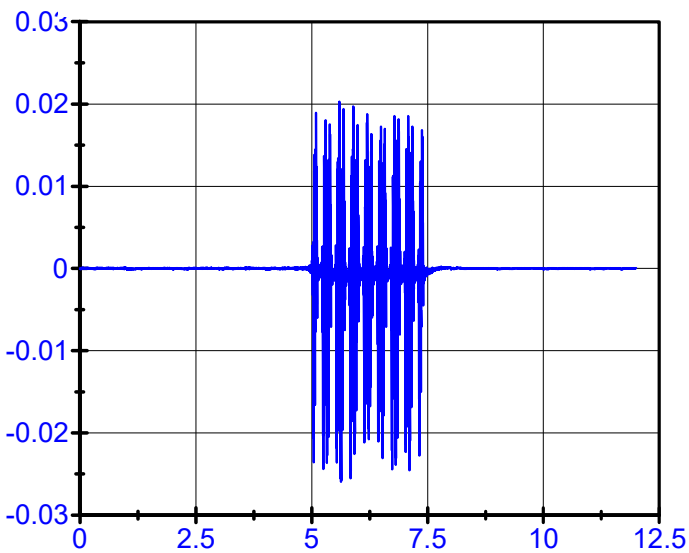

01\06\16 08:52:26 - Voltage - G1_T2_E

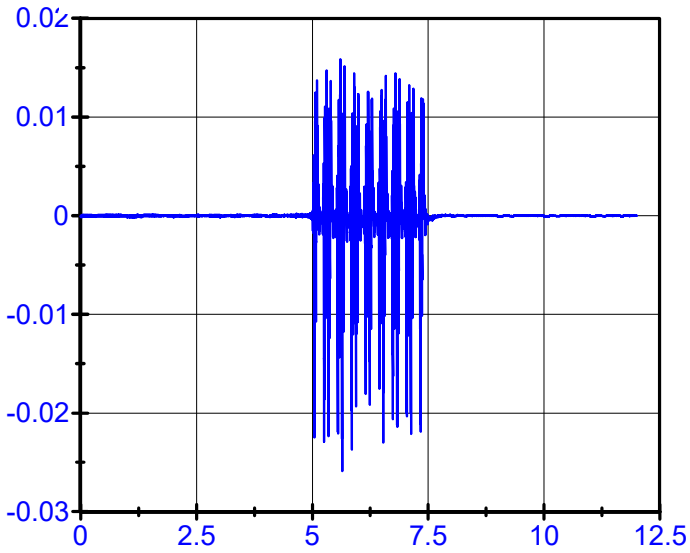

01\06\16 08:52:26 - Voltage - G1_T2_I

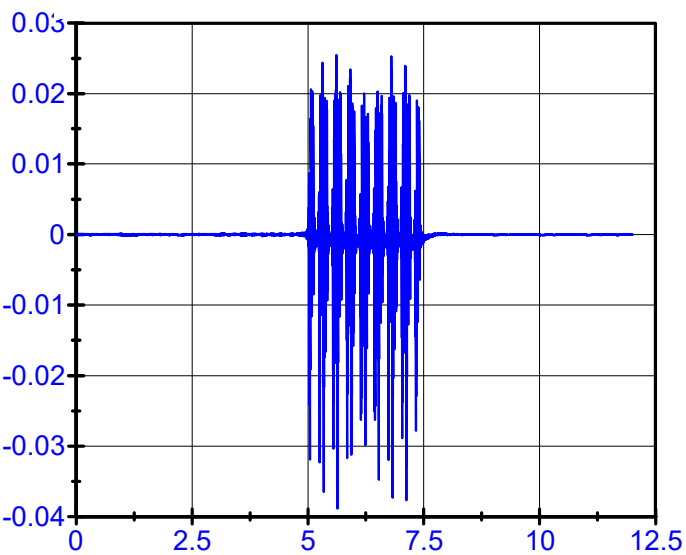

01\06\16 08:52:26 - Voltage - G1_T3_E

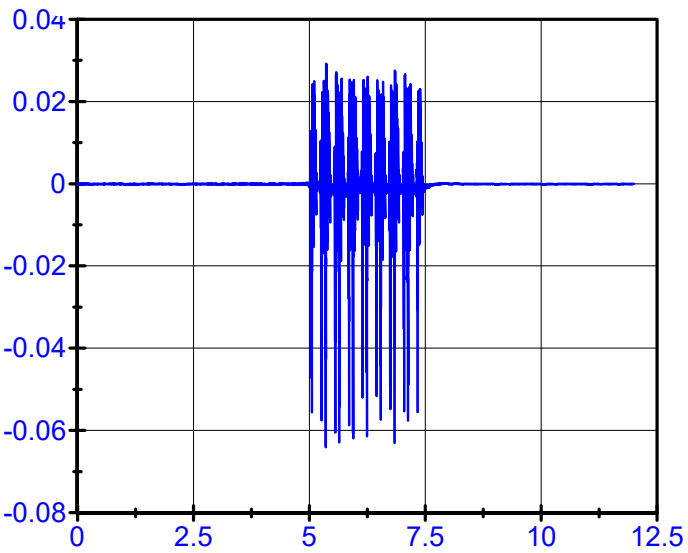

01\06\16 08:52:26 - Voltage - G1_T3_I

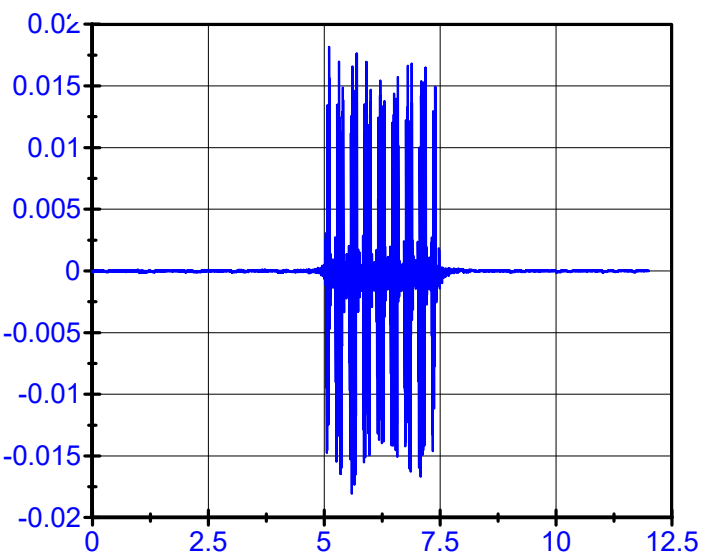

01\06\16 09:23:16

Sleeper Geophones
LPF 150Hz

01\06\16 09:23:16 - Voltage - G1_T1_E

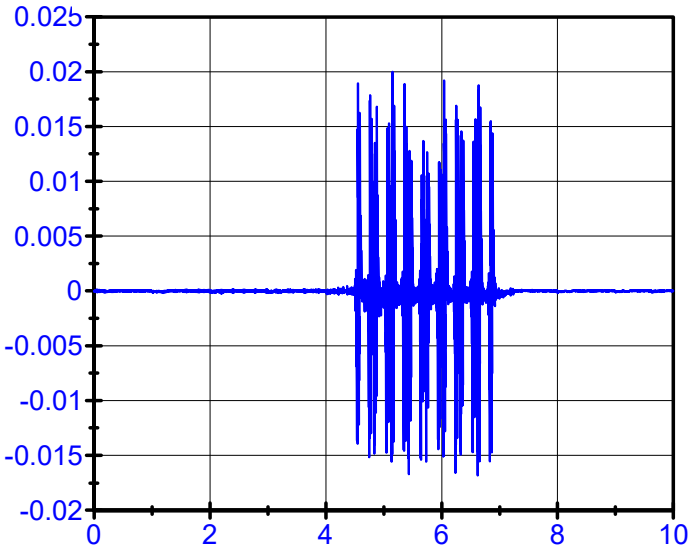

01\06\16 09:23:16 - Voltage - G1_T1_I

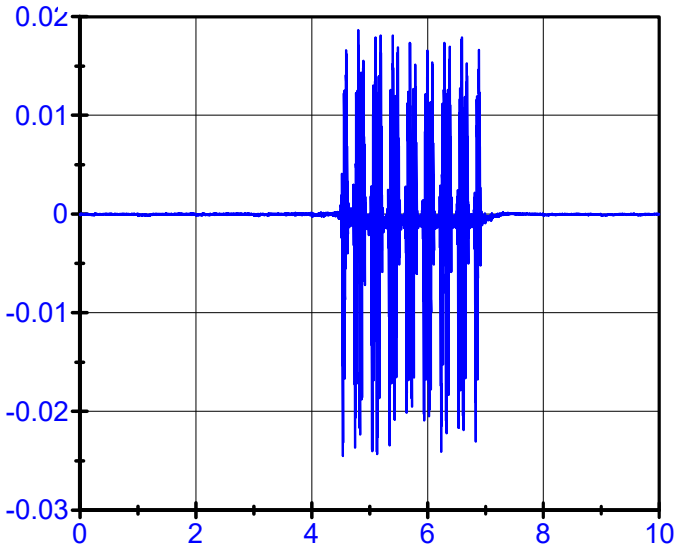

01\06\16 09:23:16 - Voltage - G1_T2_E

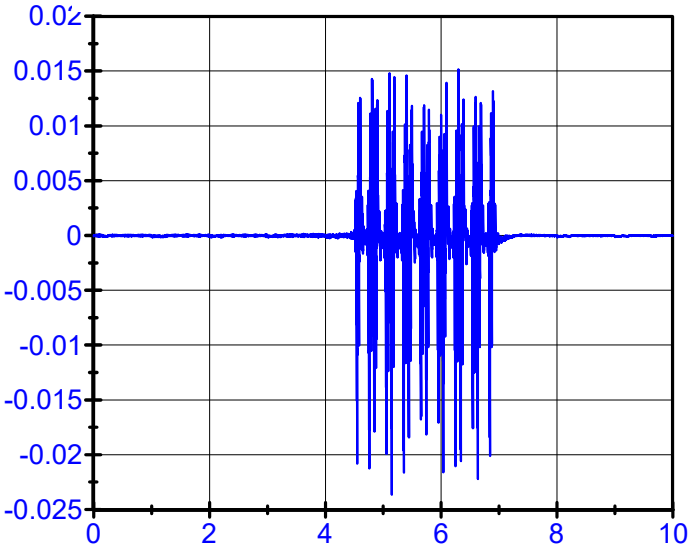

01\06\16 09:23:16 - Voltage - G1_T2_I

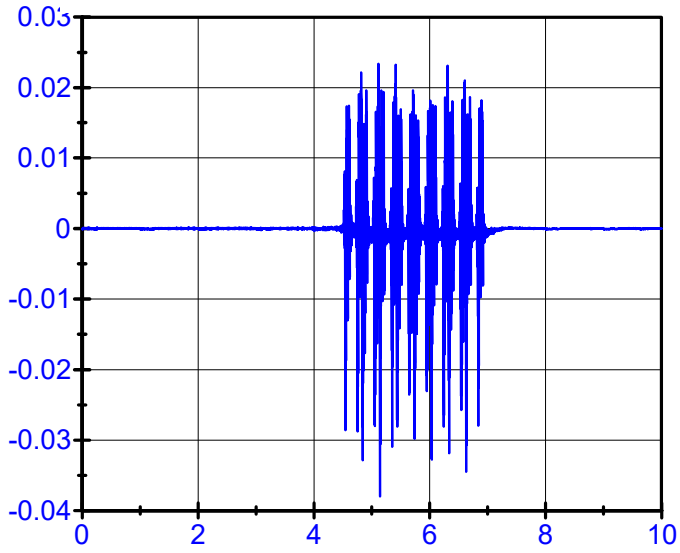

01\06\16 09:23:16 - Voltage - G1_T3_E

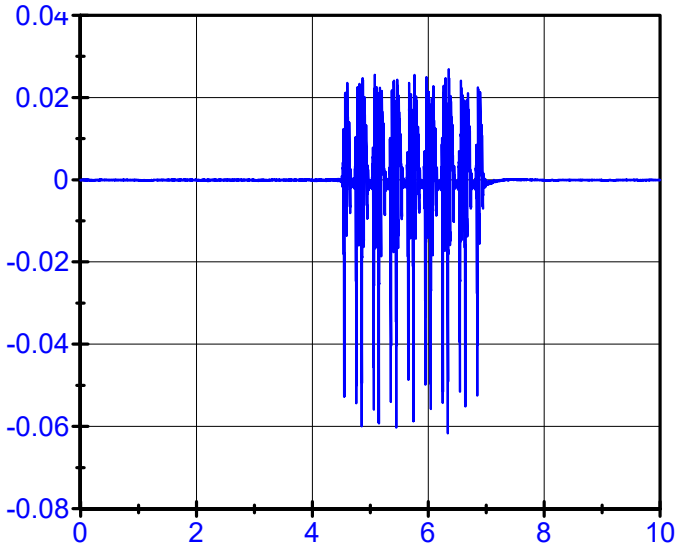

01\06\16 09:23:16 - Voltage - G1_T3_I

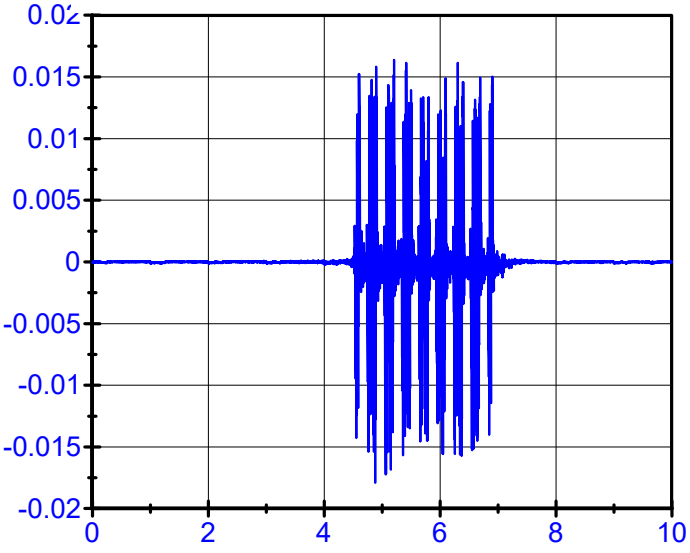

01\06\16 09:52:01

Sleeper Geophones
LPF 150Hz

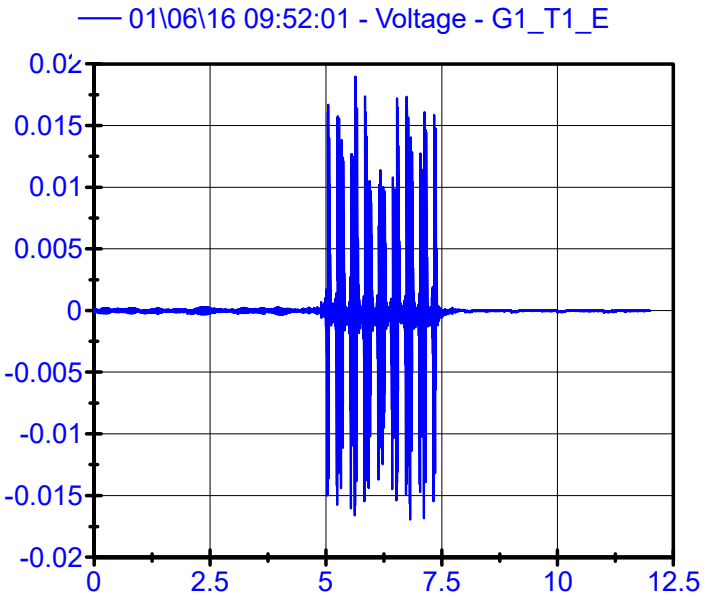

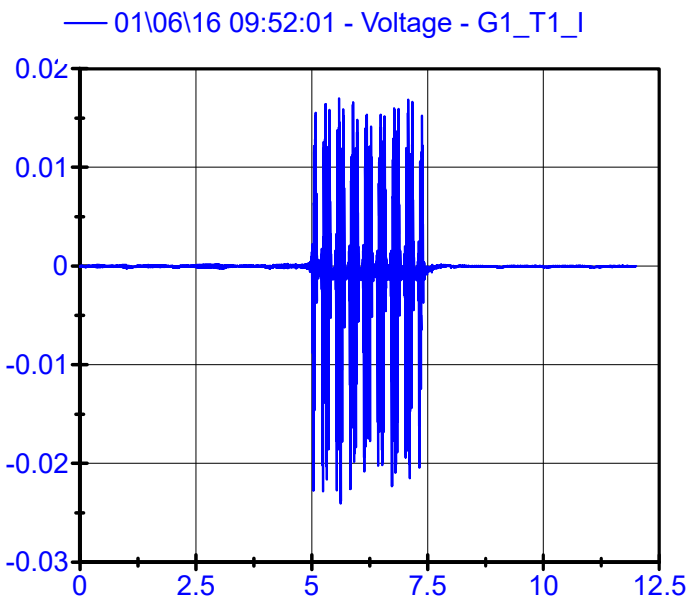

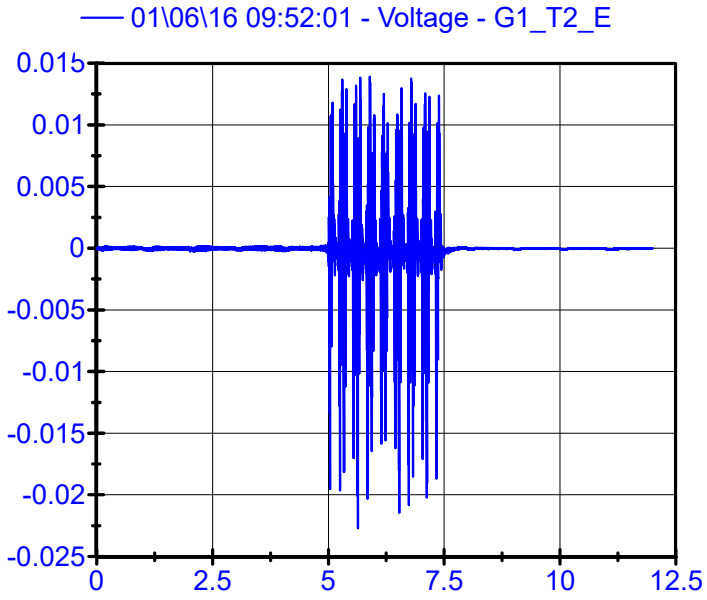

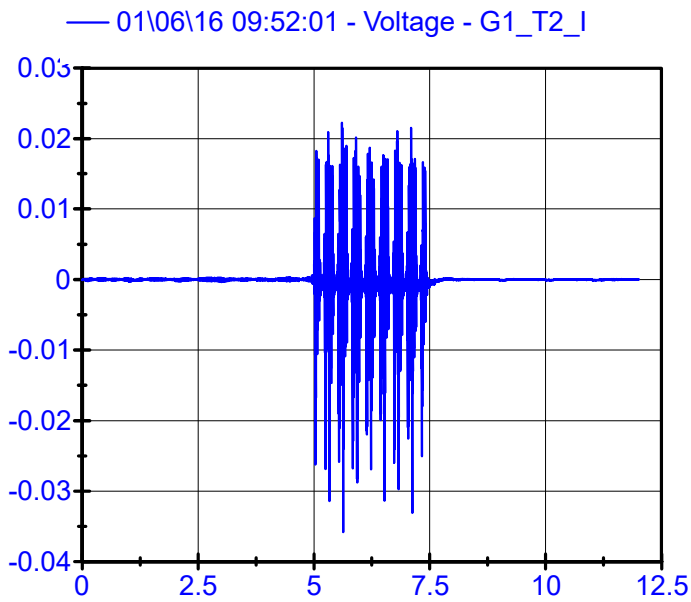

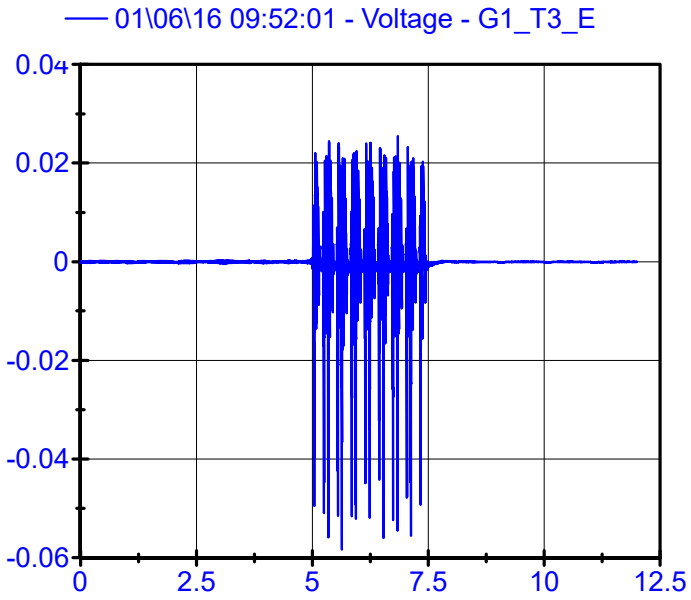

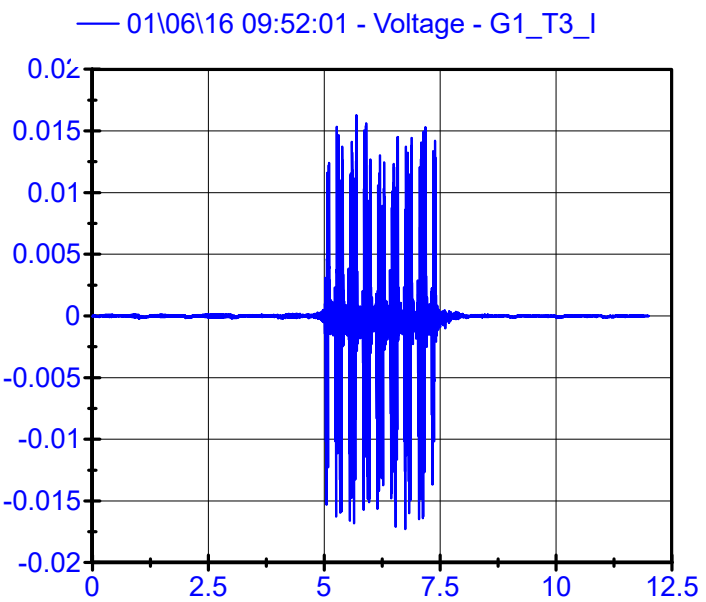

01\06\16 10:53:28

Sleeper Geophones
LPF 150Hz

01\06\16 10:53:28 - Voltage - G1_T1_E

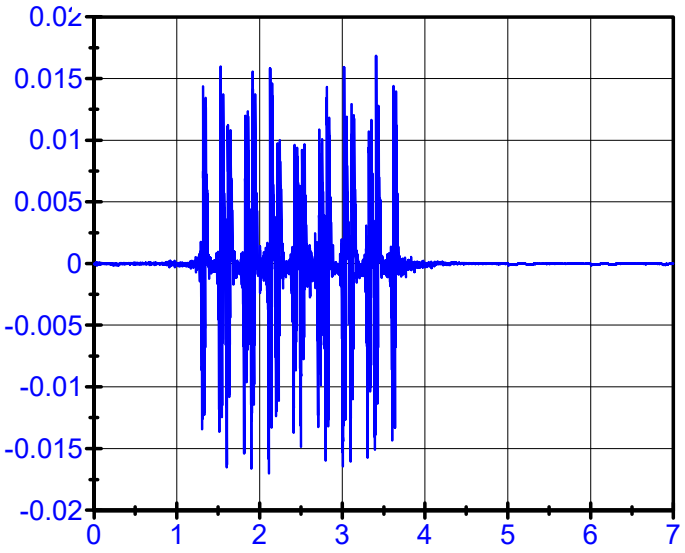

01\06\16 10:53:28 - Voltage - G1_T1_I

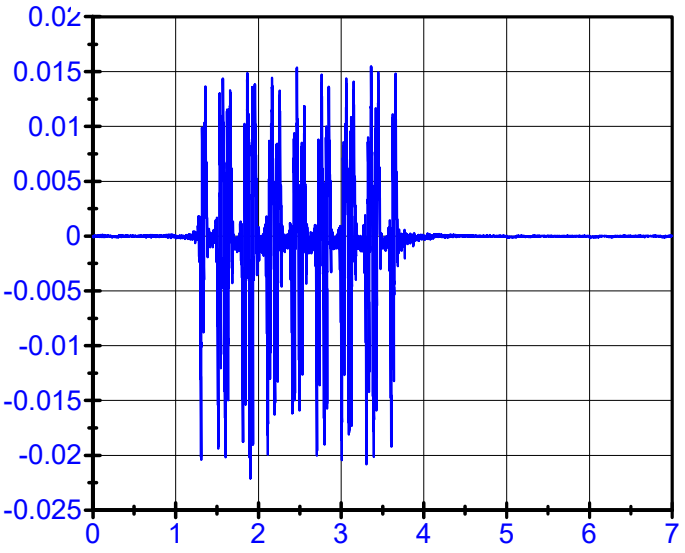

01\06\16 10:53:28 - Voltage - G1_T2_E

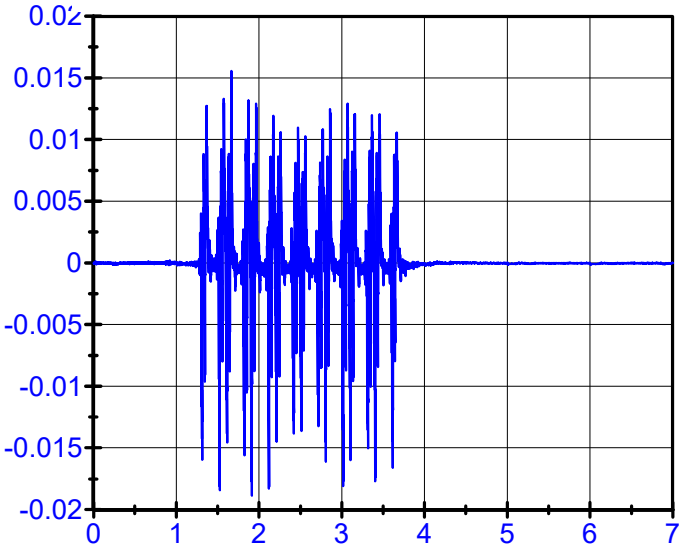

01\06\16 10:53:28 - Voltage - G1_T2_I

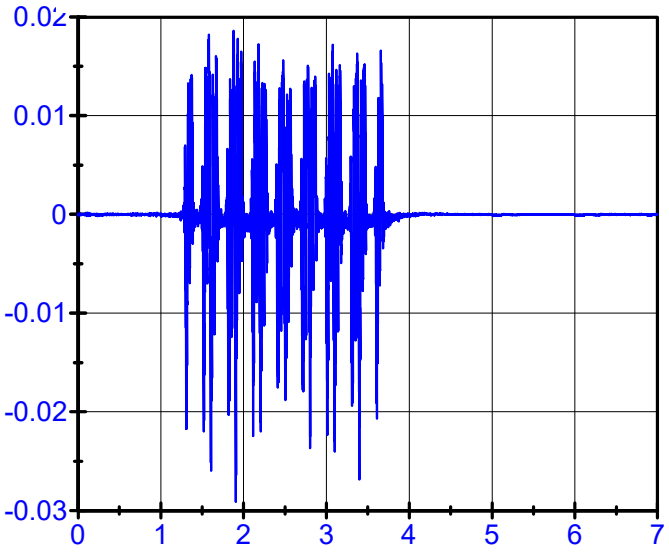

01\06\16 10:53:28 - Voltage - G1_T3_E

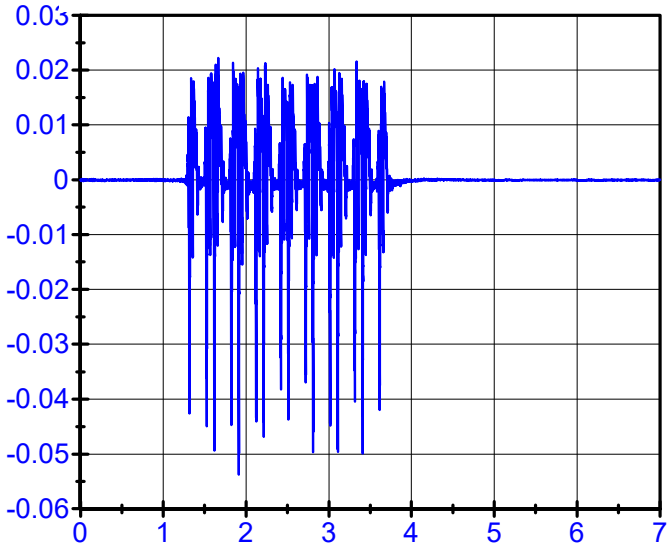

01\06\16 10:53:28 - Voltage - G1_T3_I

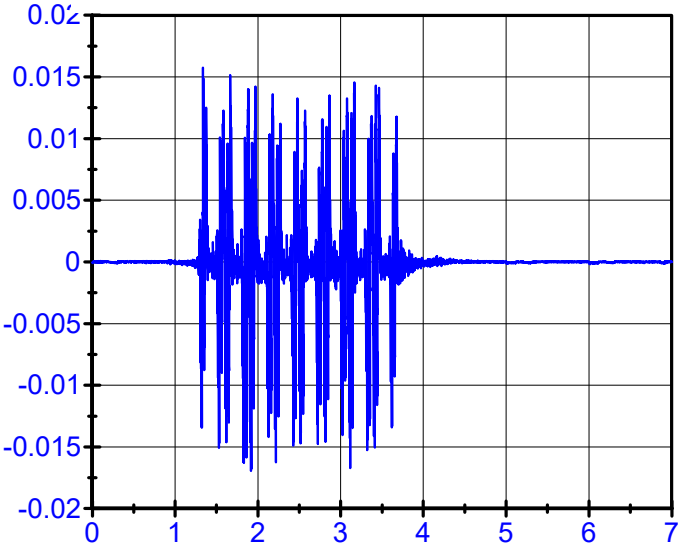

01\06\16 11:35:54

Sleeper Geophones
LPF 150Hz

01\06\16 11:35:54 - Voltage - G1_T1_E

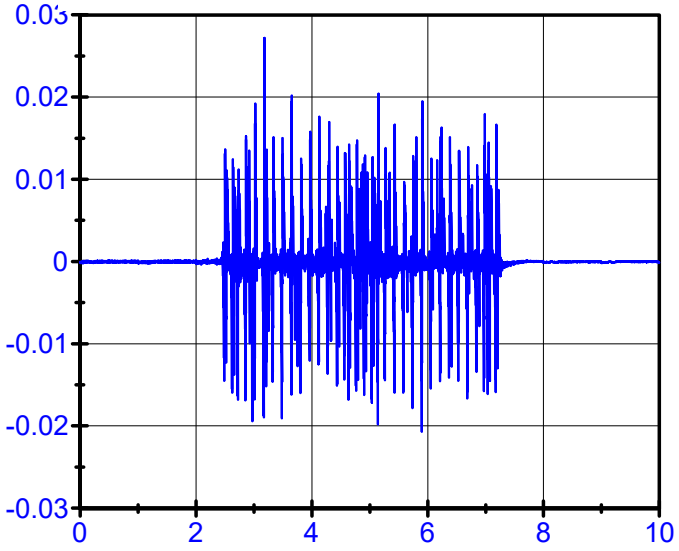

01\06\16 11:35:54 - Voltage - G1_T1_I

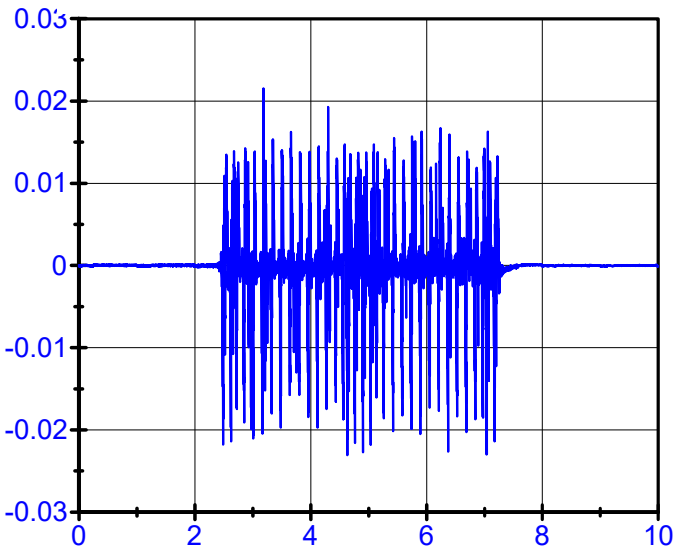

01\06\16 11:35:54 - Voltage - G1_T2_E

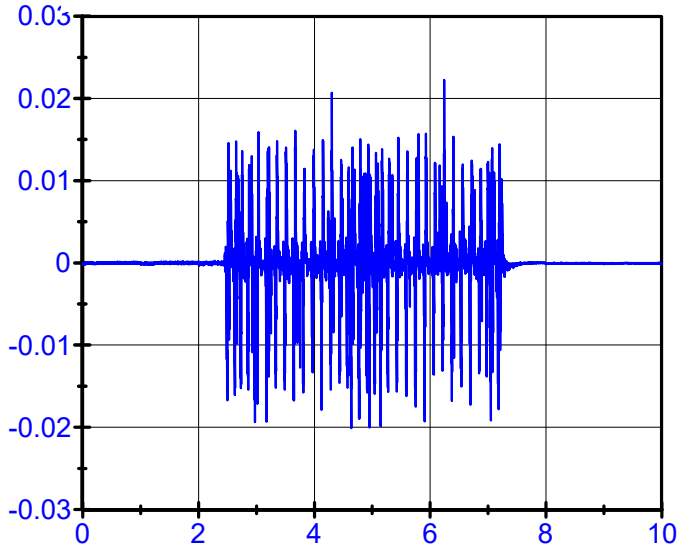

01\06\16 11:35:54 - Voltage - G1_T2_I

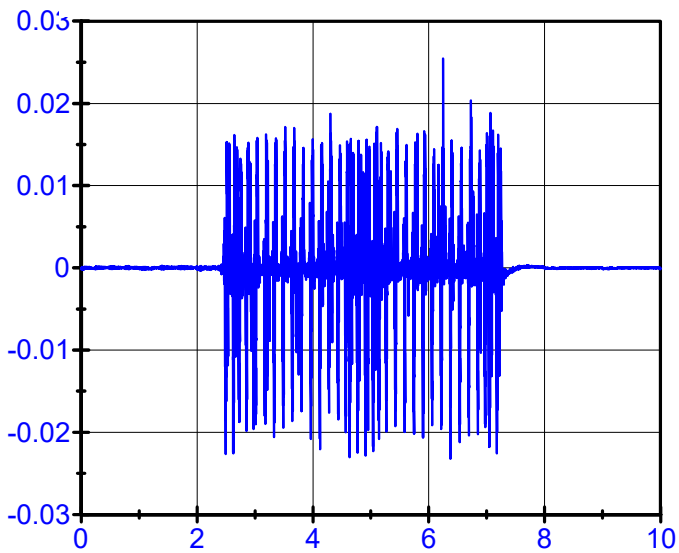

01\06\16 11:35:54 - Voltage - G1_T3_E

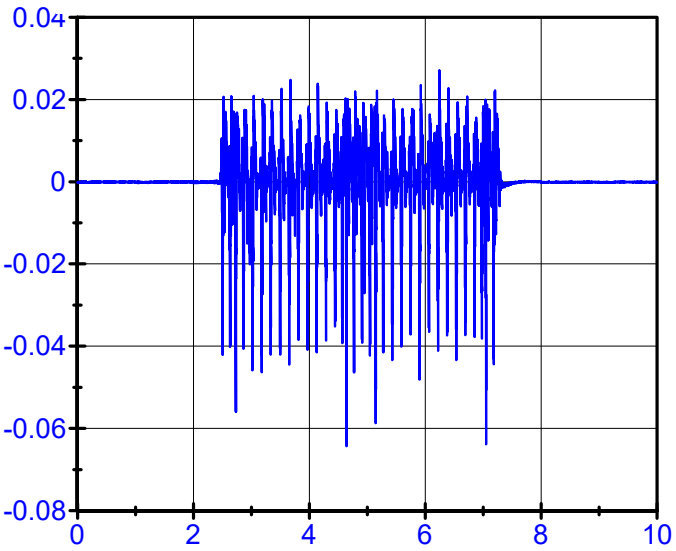

01\06\16 11:35:54 - Voltage - G1_T3_I

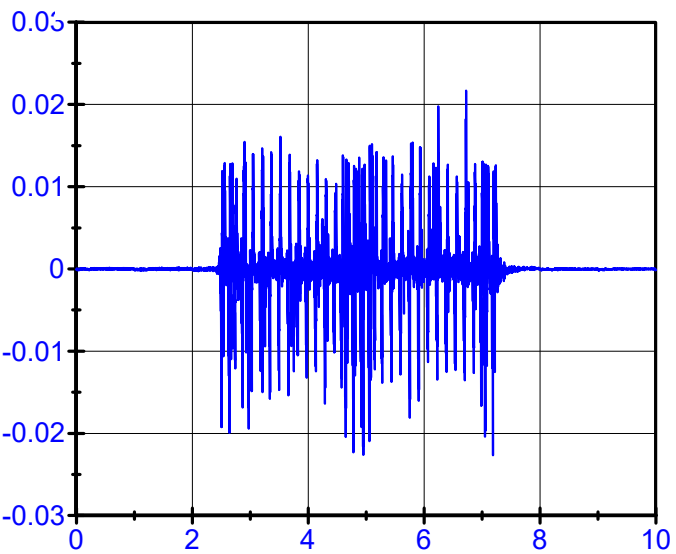

01\06\16 11:53:47

Sleeper Geophones
LPF 150Hz

01\06\16 11:53:47 - Voltage - G1_T1_E

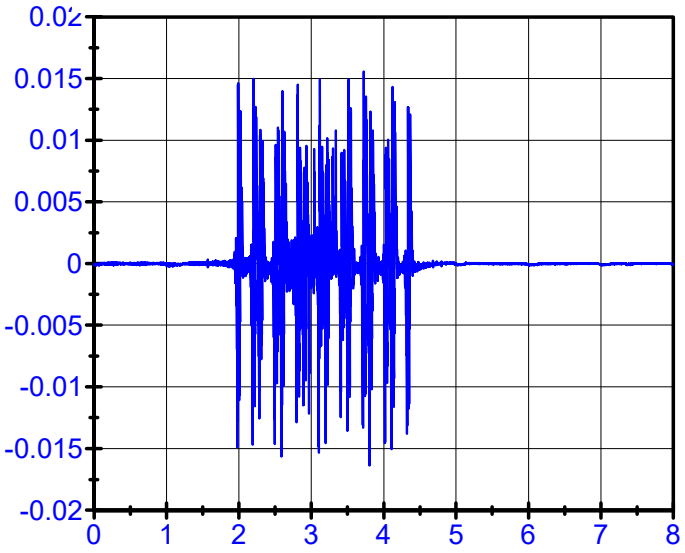

01\06\16 11:53:47 - Voltage - G1_T1_I

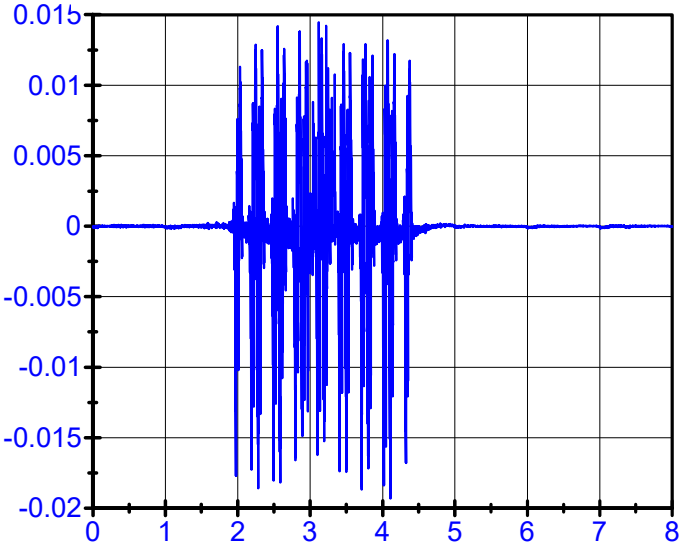

01\06\16 11:53:47 - Voltage - G1_T2_E

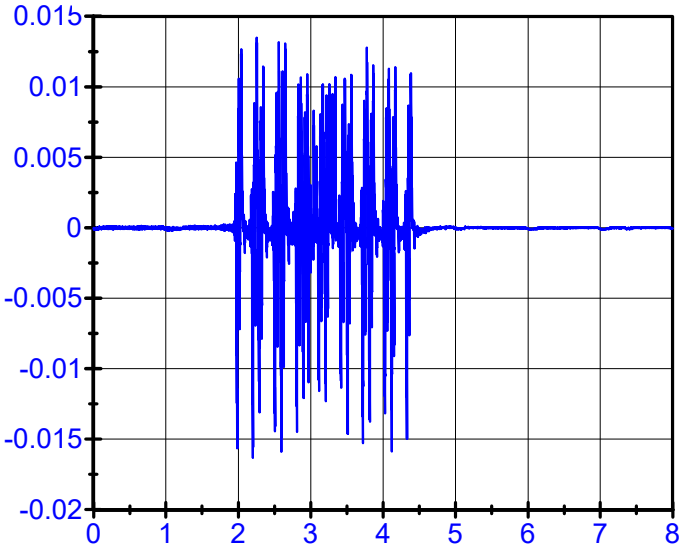

01\06\16 11:53:47 - Voltage - G1_T2_I

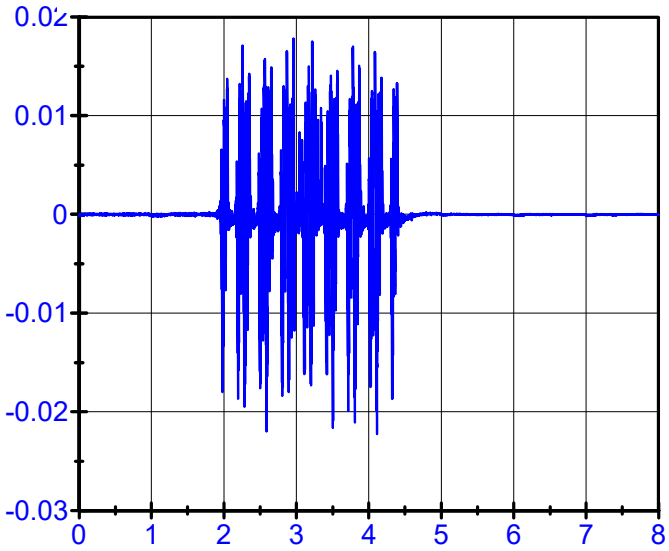

01\06\16 11:53:47 - Voltage - G1_T3_E

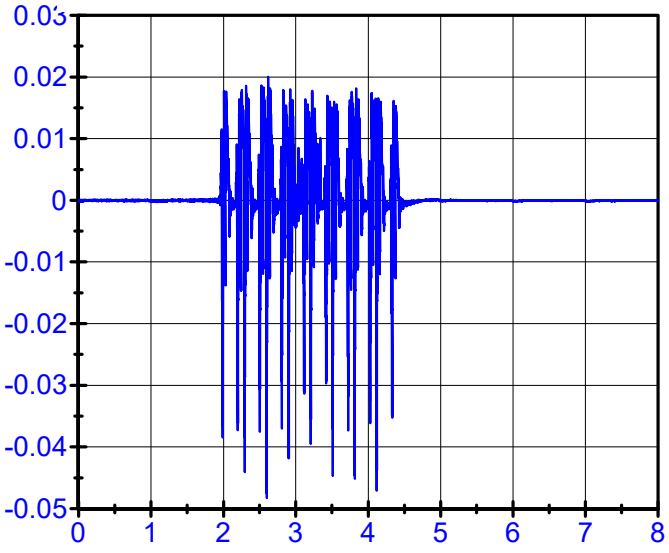

01\06\16 11:53:47 - Voltage - G1_T3_I

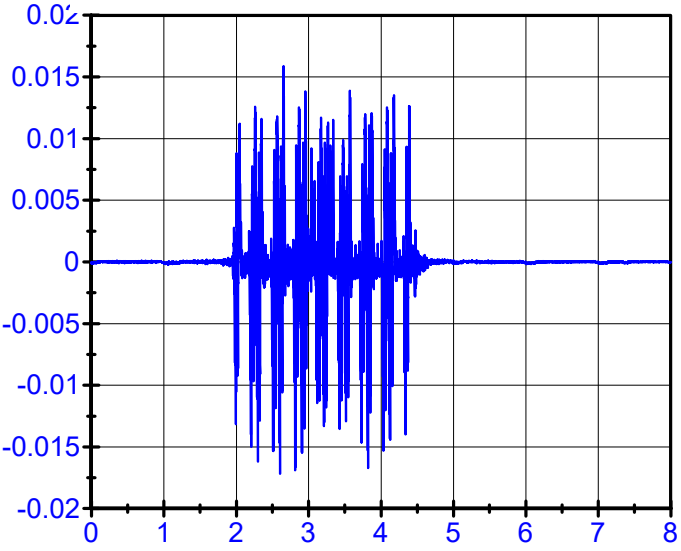

01\06\16 12:07:44

Sleeper Geophones
LPF 150Hz

01\06\16 12:07:44 - Voltage - G1_T1_E

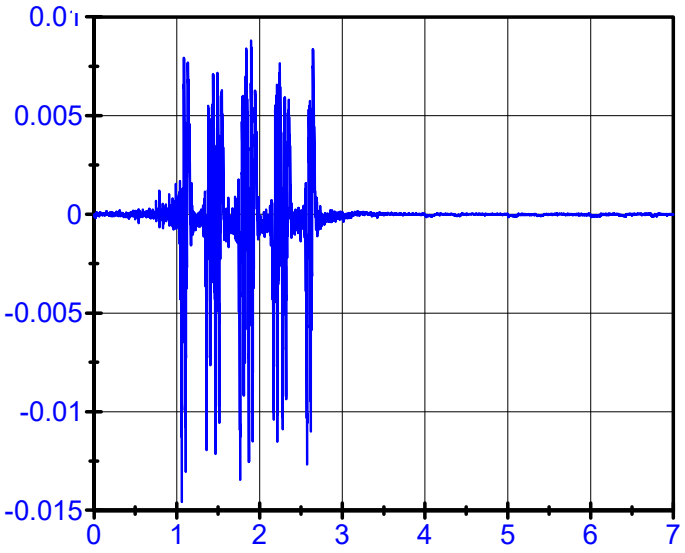

01\06\16 12:07:44 - Voltage - G1_T1_I

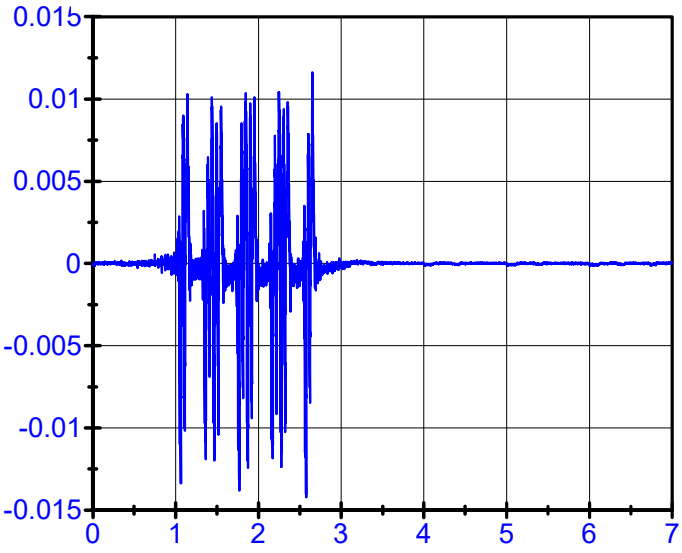

01\06\16 12:07:44 - Voltage - G1_T2_E

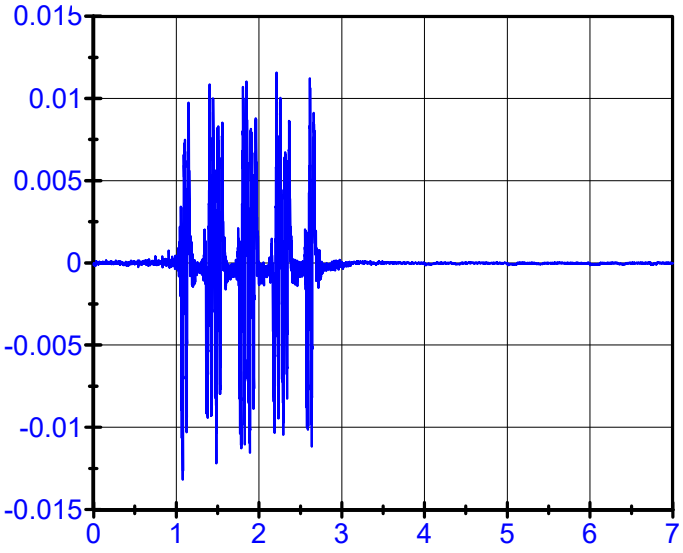

01\06\16 12:07:44 - Voltage - G1_T2_I

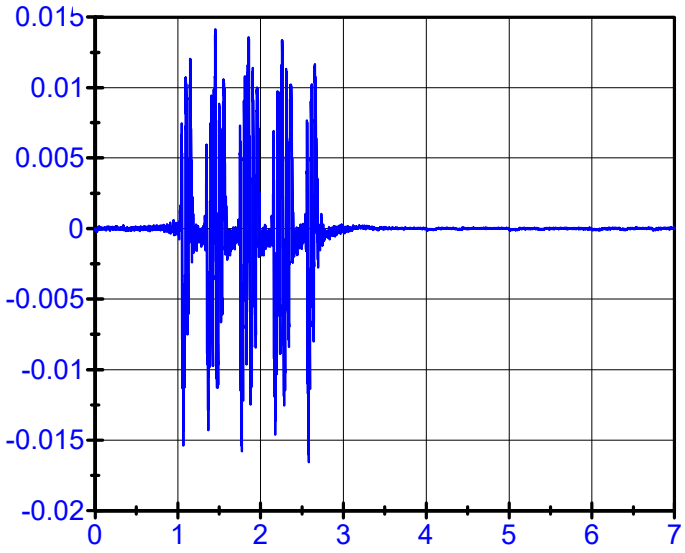

01\06\16 12:07:44 - Voltage - G1_T3_E

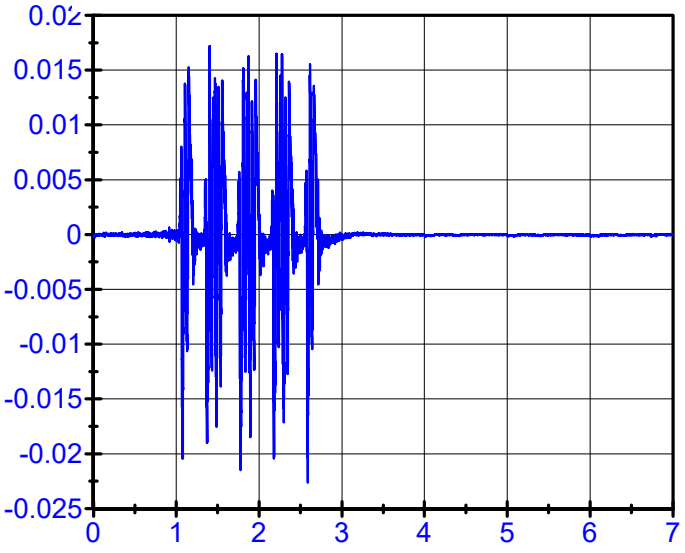

01\06\16 12:07:44 - Voltage - G1_T3_I

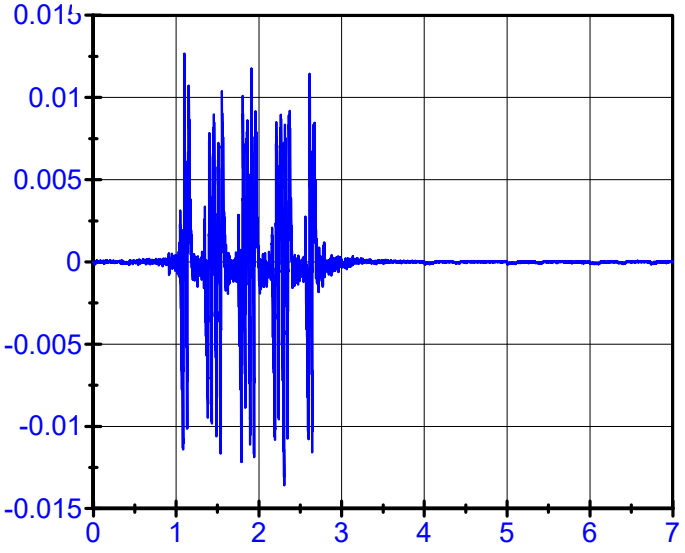

01\06\16 12:51:19

Sleeper Geophones
LPF 150Hz

01\06\16 12:51:19 - Voltage - G1_T1_E

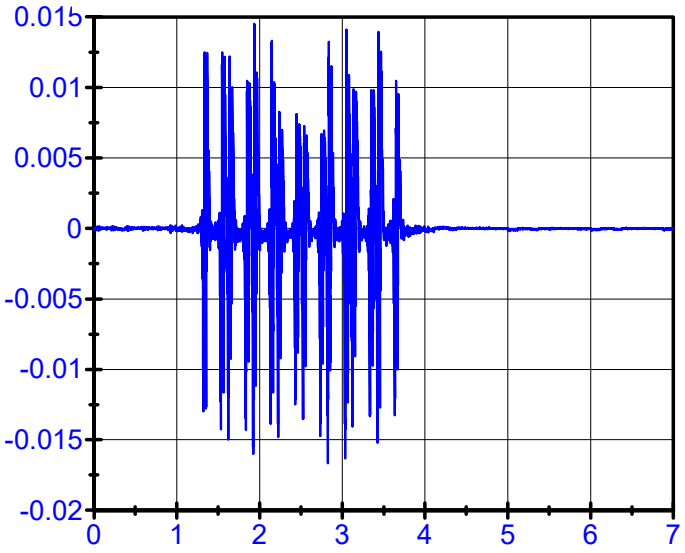

01\06\16 12:51:19 - Voltage - G1_T1_I

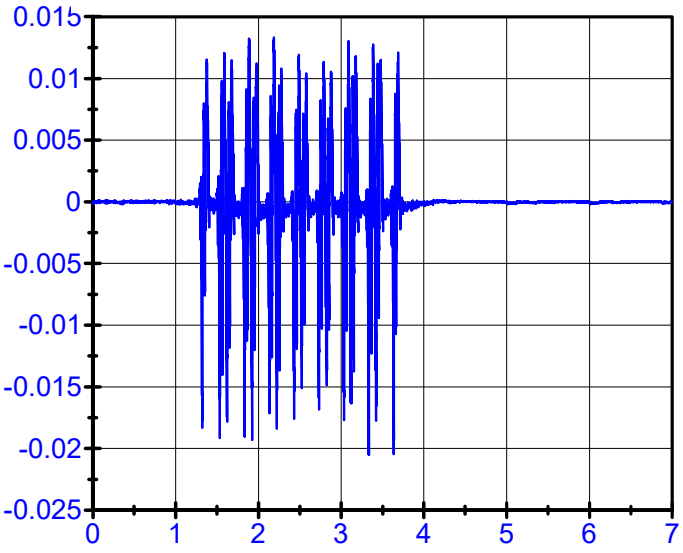

01\06\16 12:51:19 - Voltage - G1_T2_E

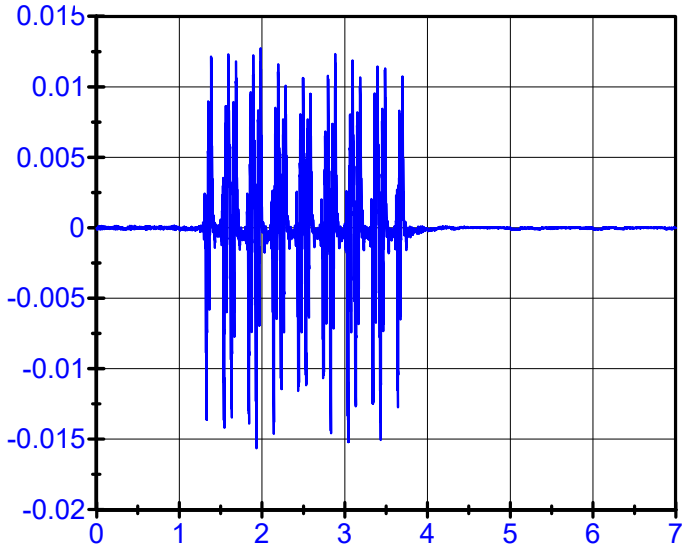

01\06\16 12:51:19 - Voltage - G1_T2_I

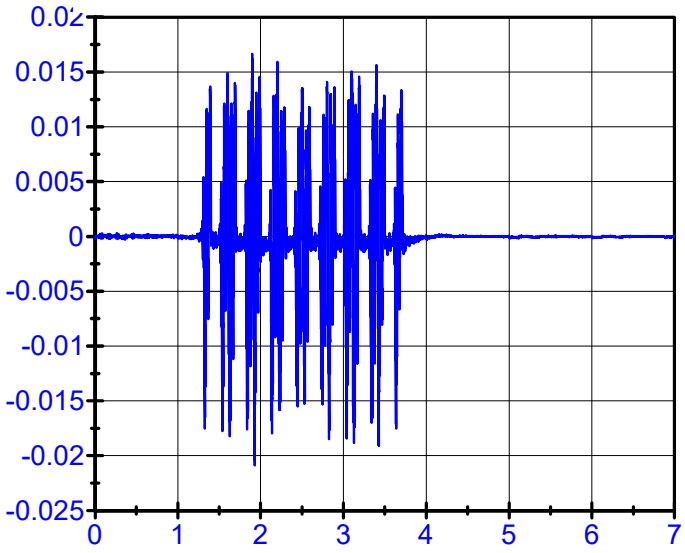

01\06\16 12:51:19 - Voltage - G1_T3_E

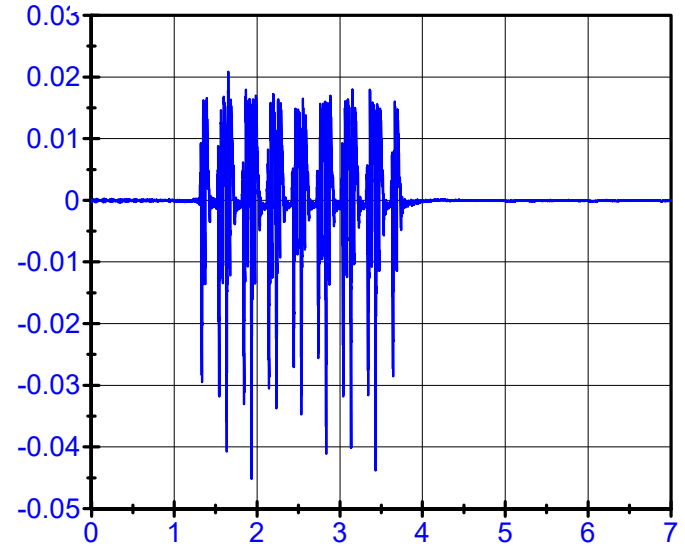

01\06\16 12:51:19 - Voltage - G1_T3_I

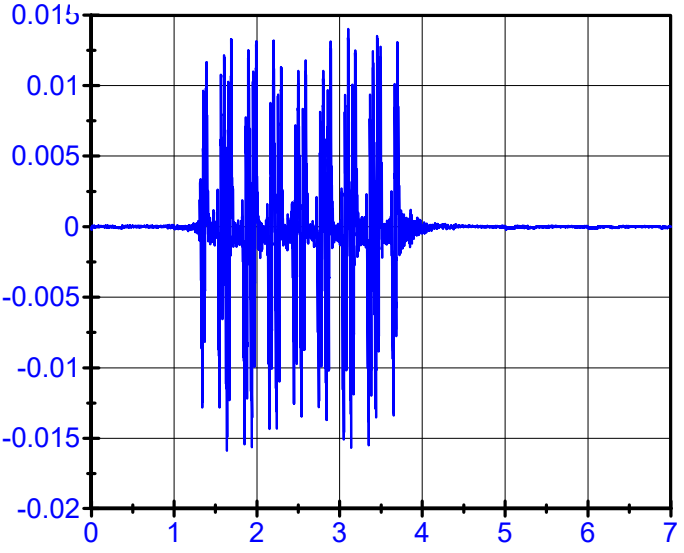

01\06\16 13:55:11

Sleeper Geophones
LPF 150Hz

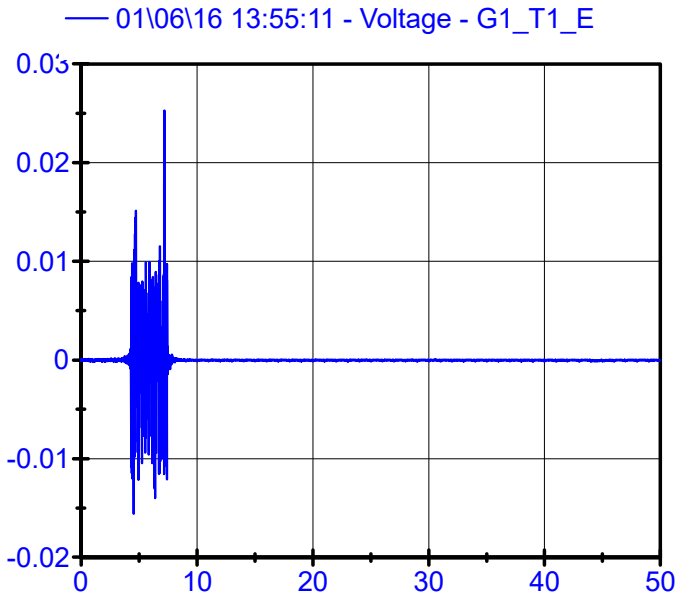

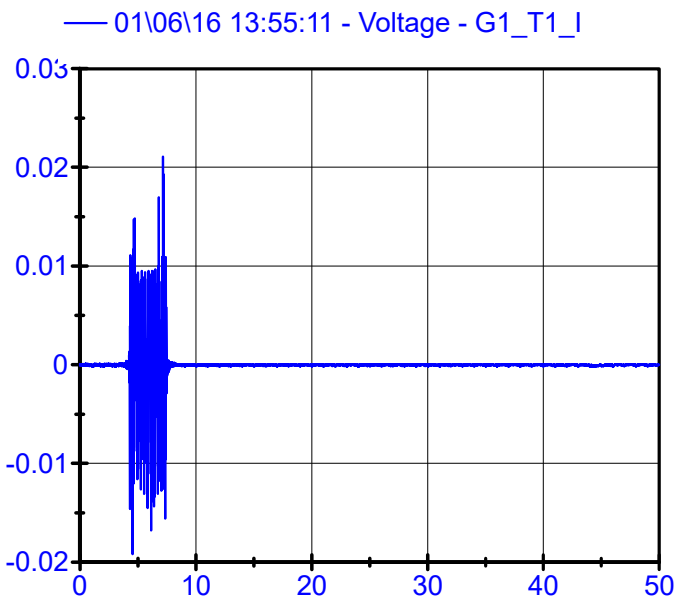

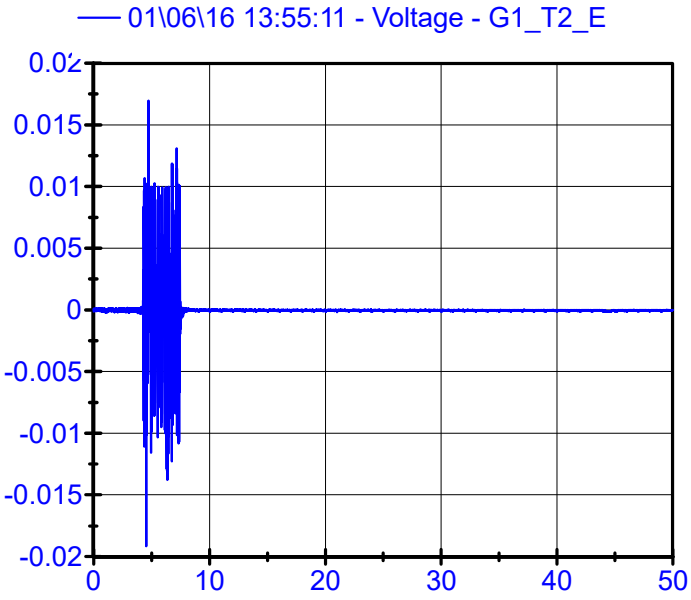

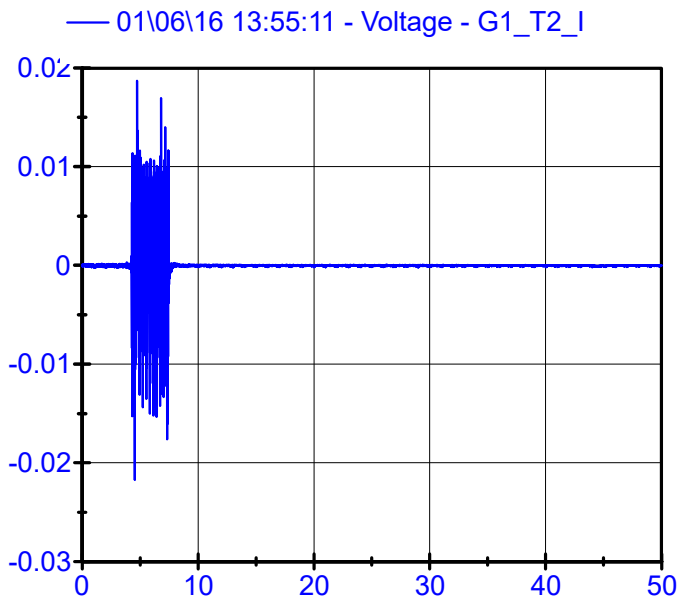

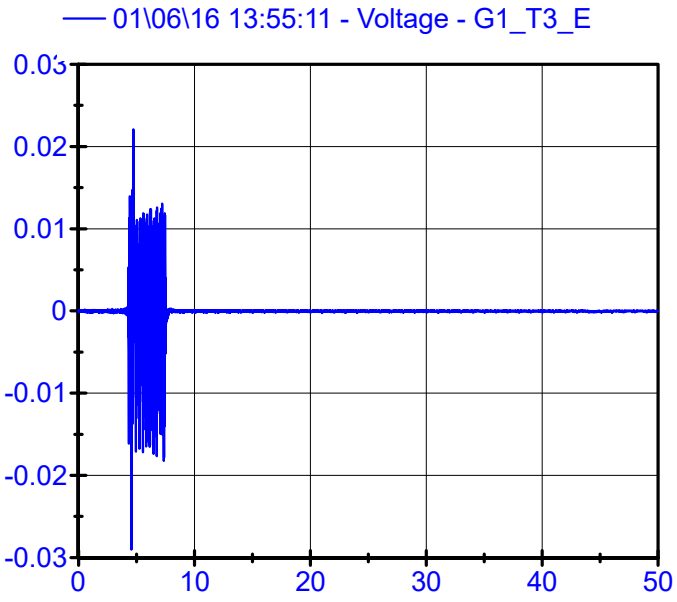

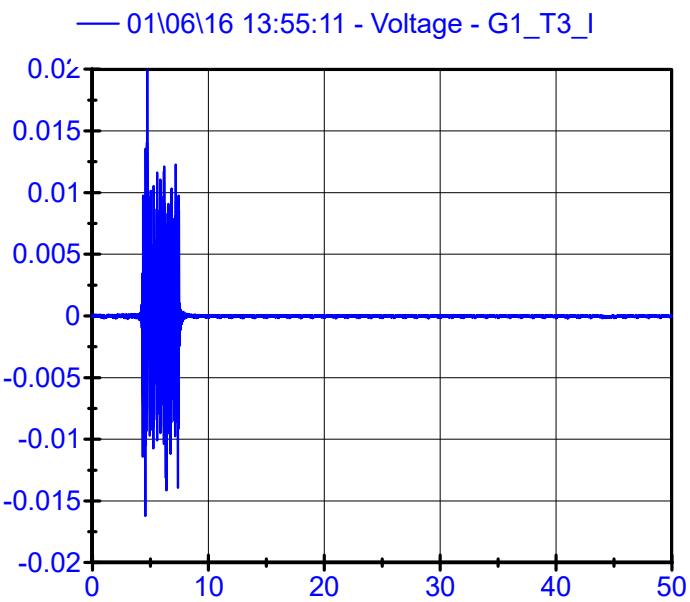

01\06\16 14:21:06

Sleeper Geophones
LPF 150Hz

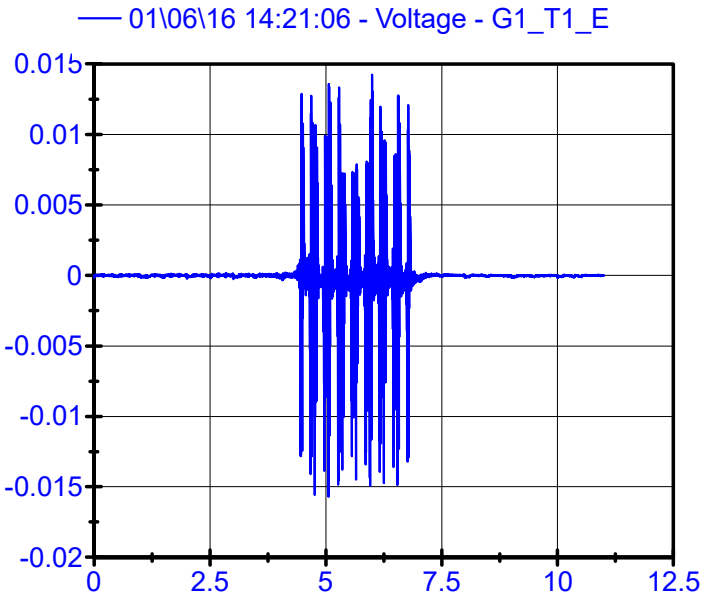

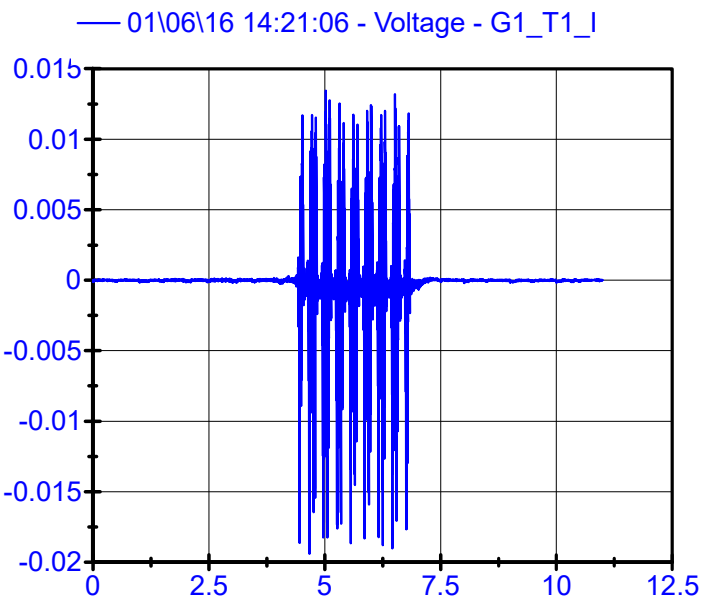

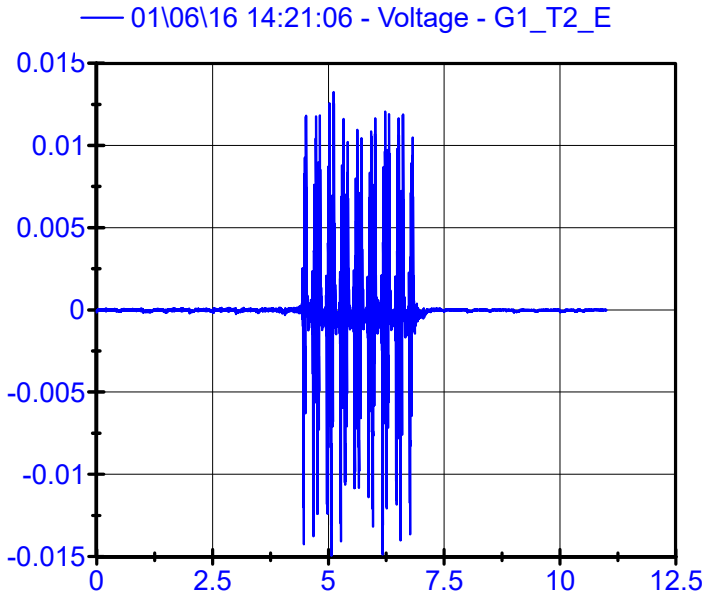

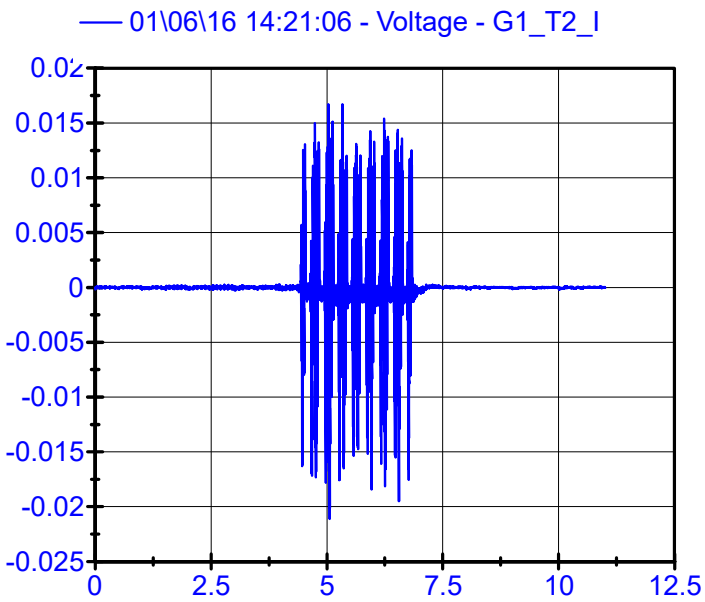

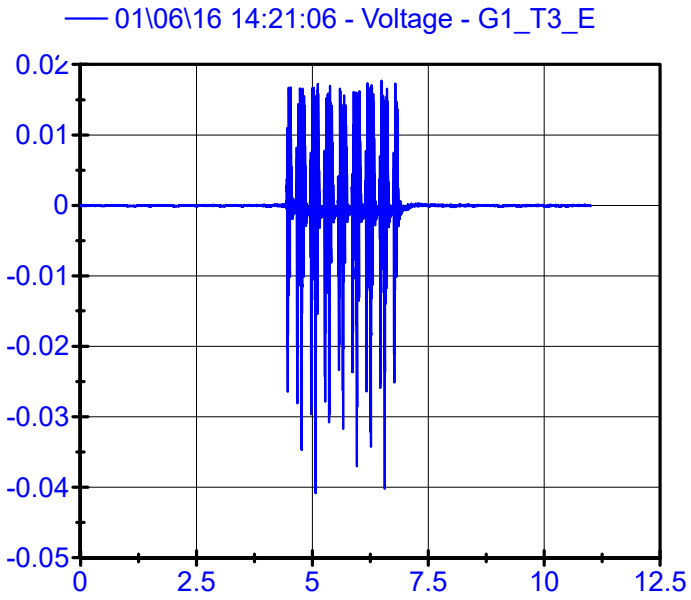

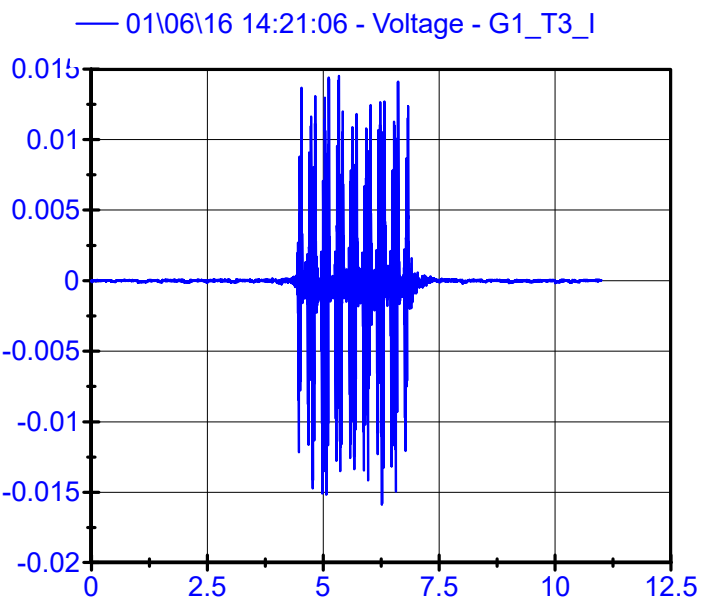

01\06\16 14:52:22

Sleeper Geophones
LPF 150Hz

01\06\16 14:52:22 - Voltage - G1_T1_E

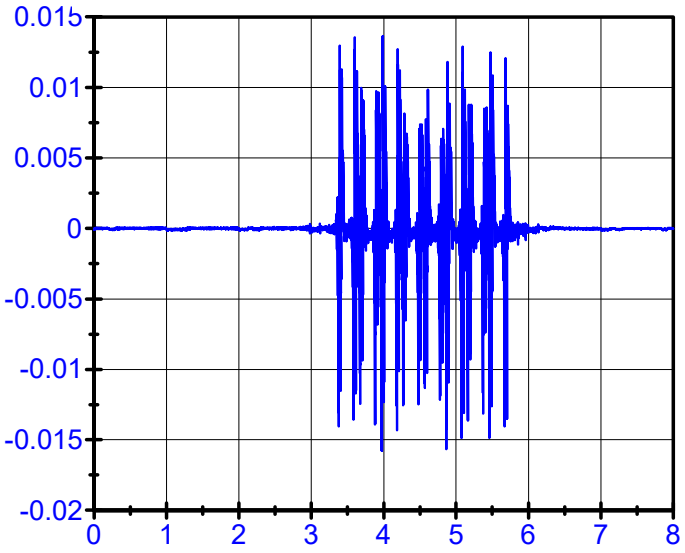

01\06\16 14:52:22 - Voltage - G1_T1_I

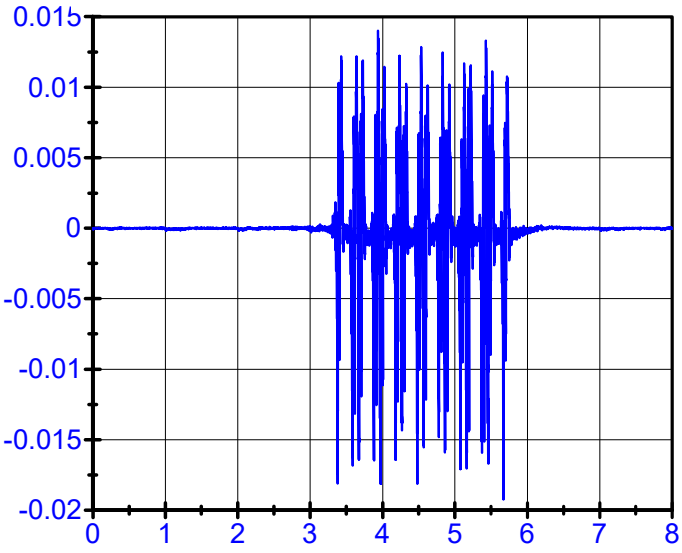

01\06\16 14:52:22 - Voltage - G1_T2_E

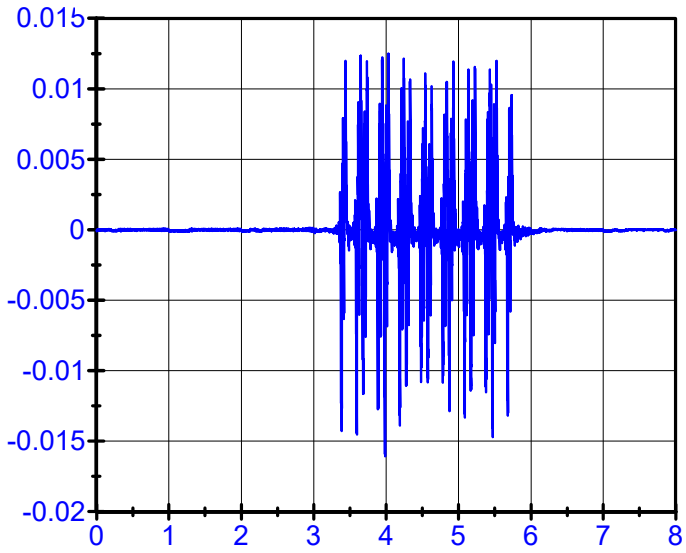

01\06\16 14:52:22 - Voltage - G1_T2_I

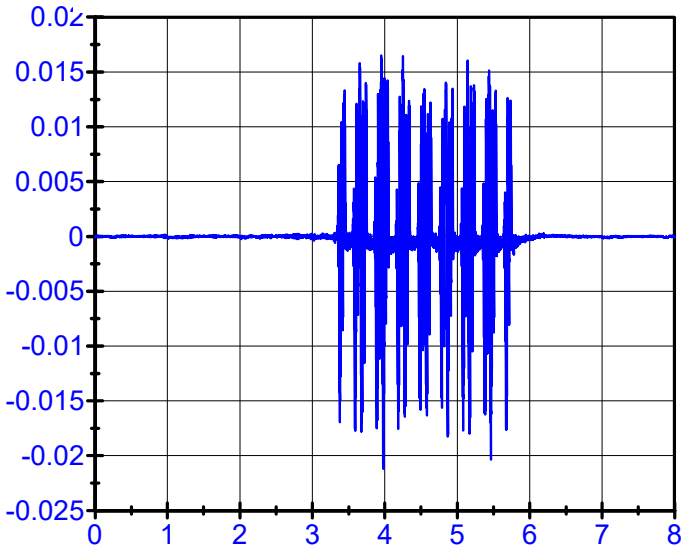

01\06\16 14:52:22 - Voltage - G1_T3_E

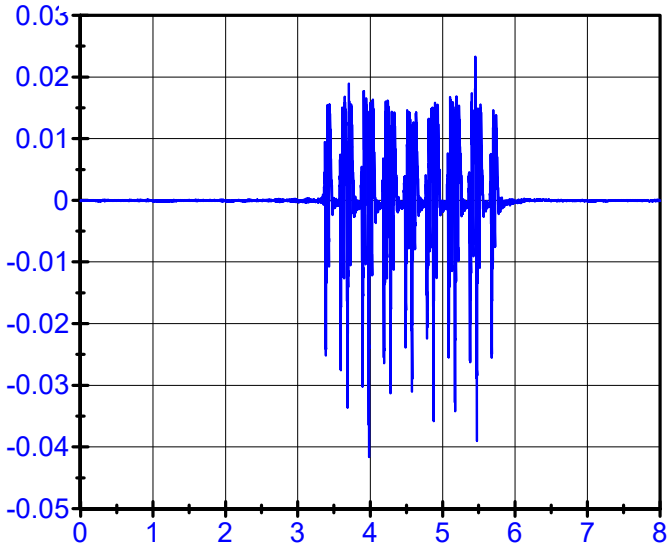

01\06\16 14:52:22 - Voltage - G1_T3_I

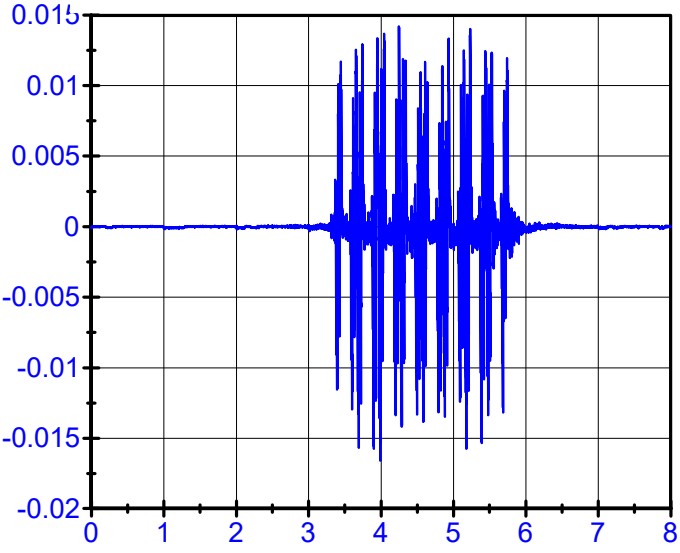

01\06\16 15:21:31

Sleeper Geophones
LPF 150Hz

01\06\16 15:21:31 - Voltage - G1_T1_E

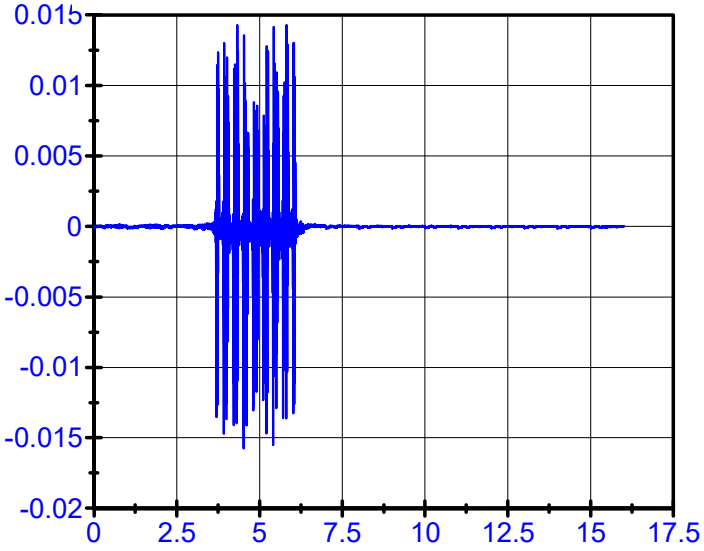

01\06\16 15:21:31 - Voltage - G1_T1_I

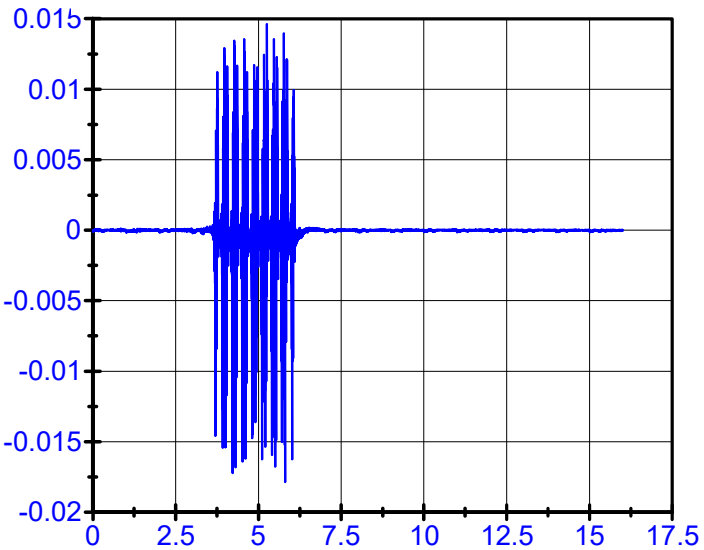

01\06\16 15:21:31 - Voltage - G1_T2_E

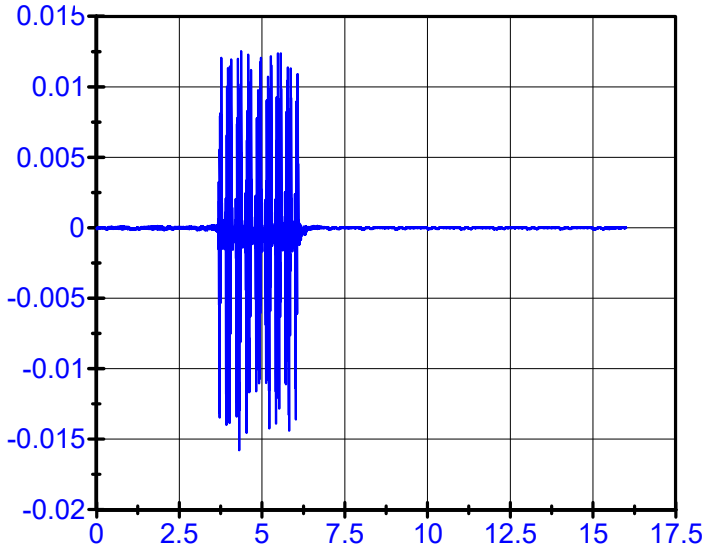

01\06\16 15:21:31 - Voltage - G1_T2_I

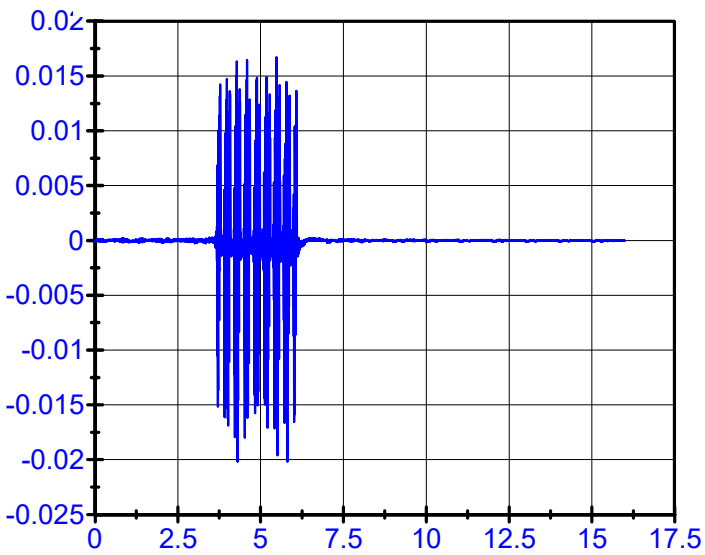

01\06\16 15:21:31 - Voltage - G1_T3_E

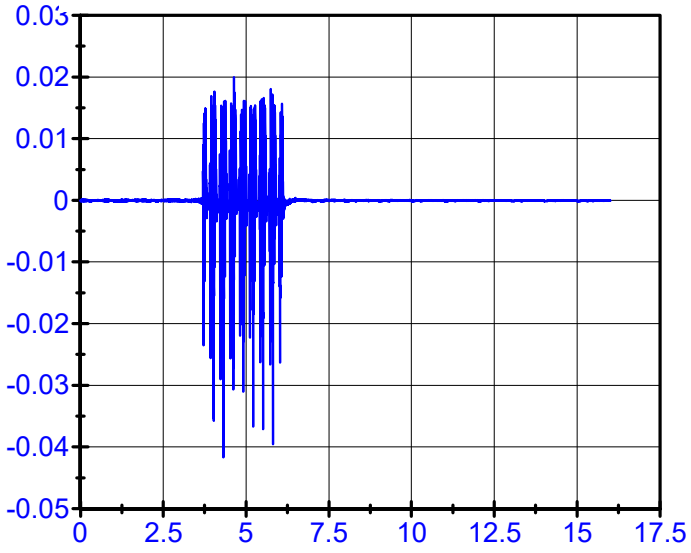

01\06\16 15:21:31 - Voltage - G1_T3_I

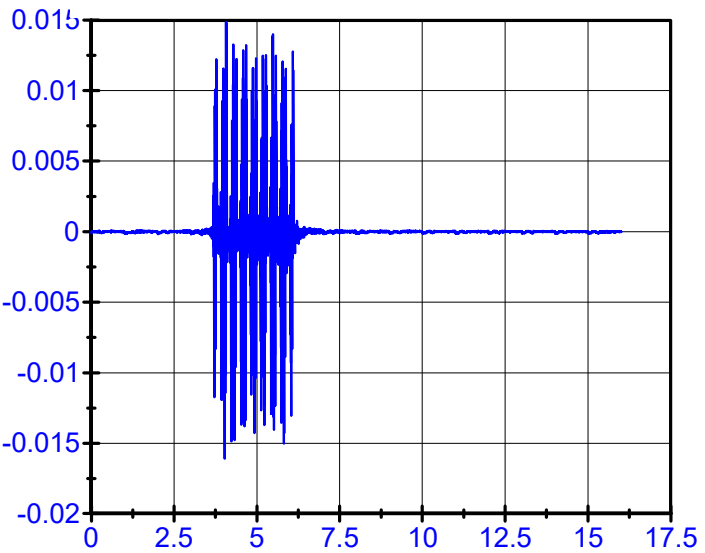

01\06\16 15:34:49

Sleeper Geophones
LPF 150Hz

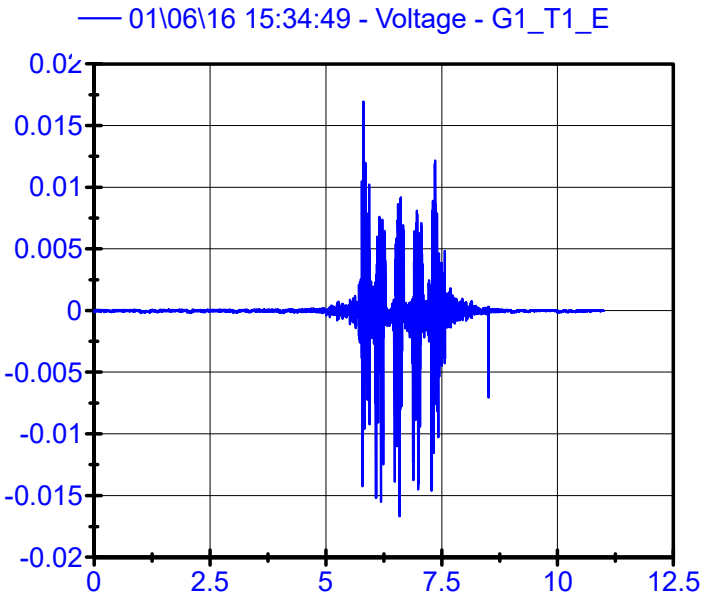

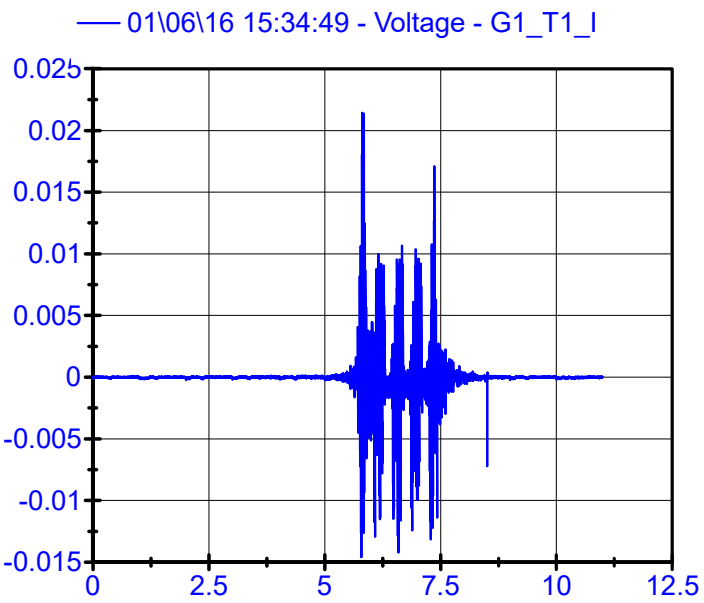

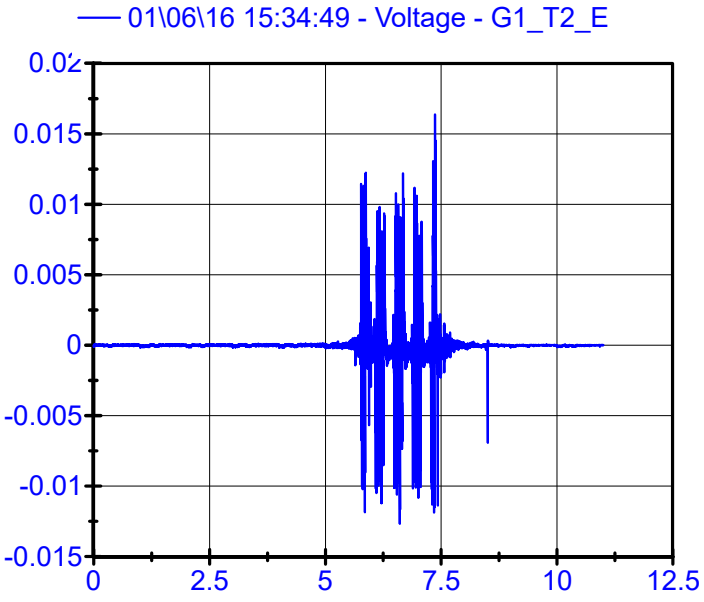

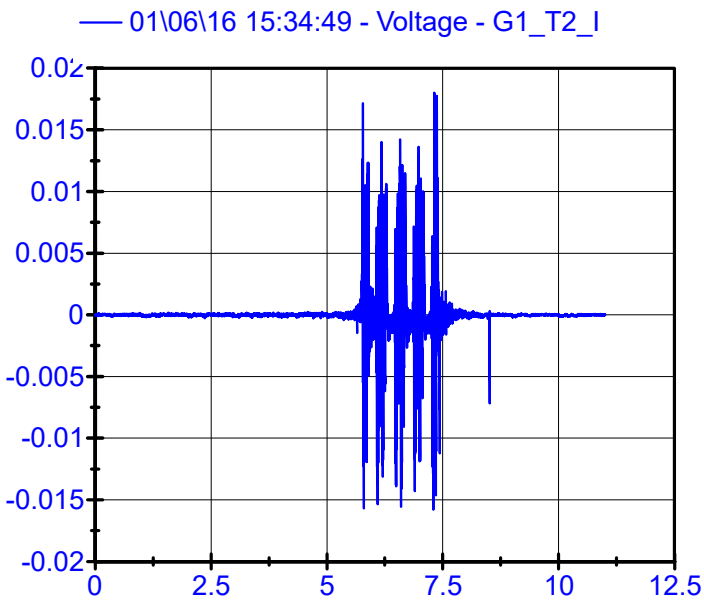

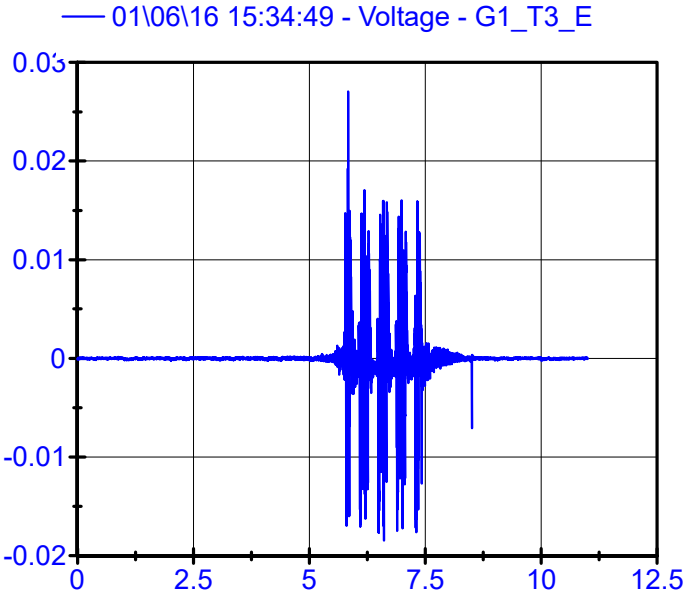

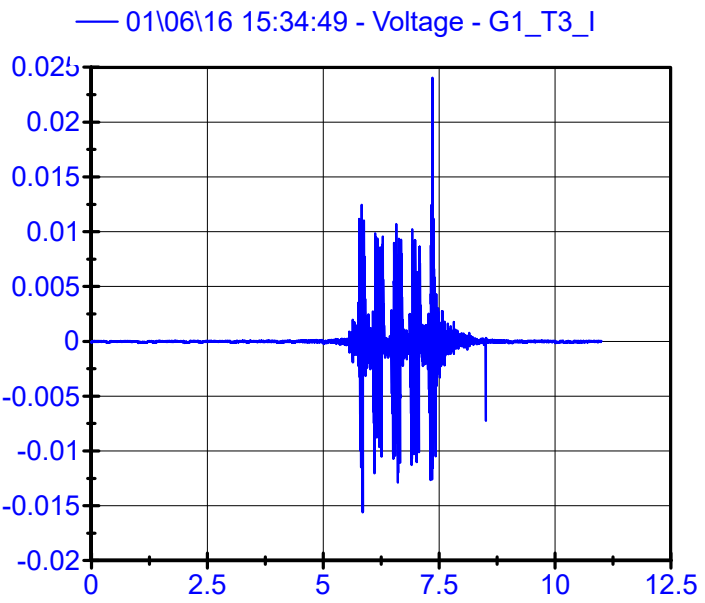

01\06\16 15:54:57

Sleeper Geophones
LPF 150Hz

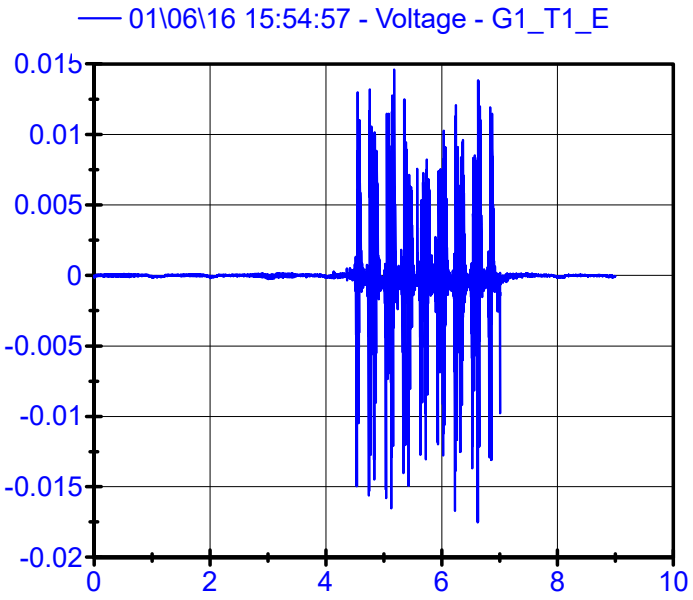

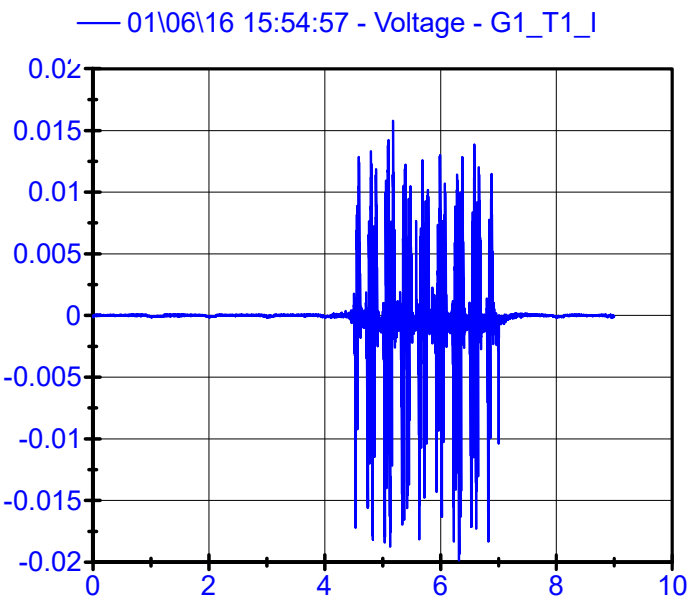

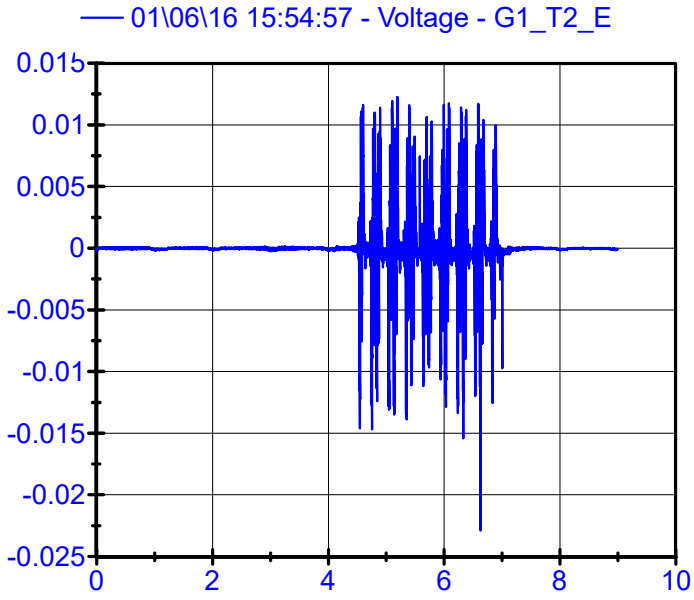

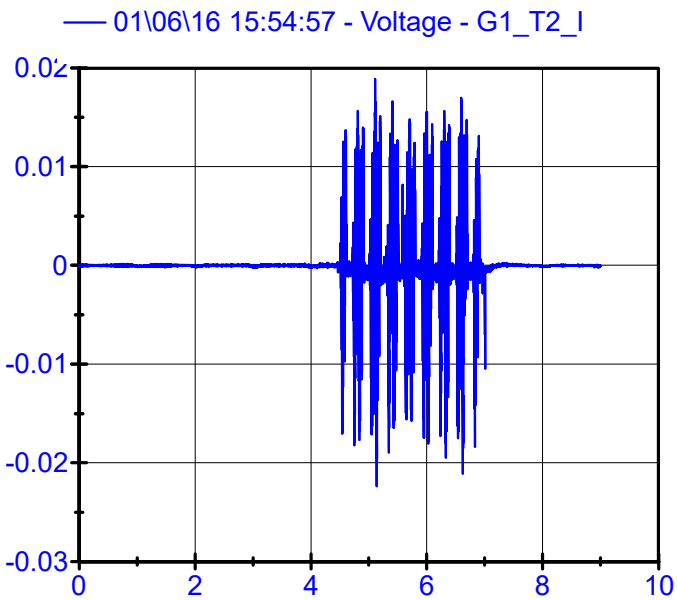

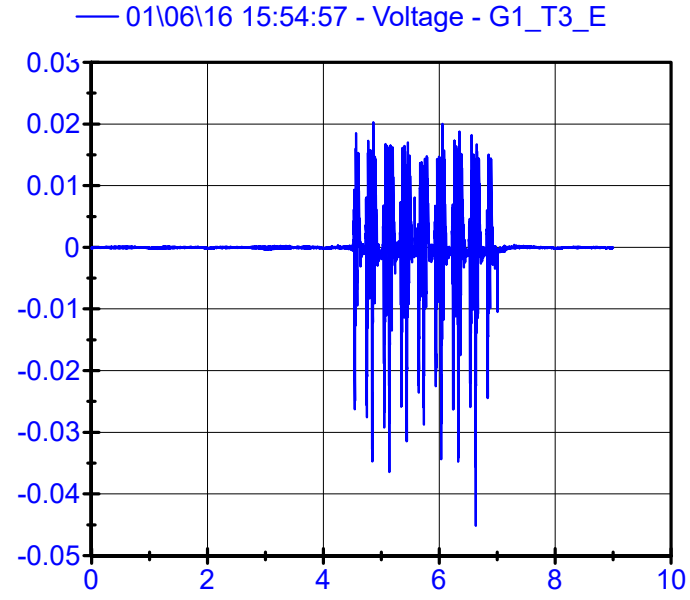

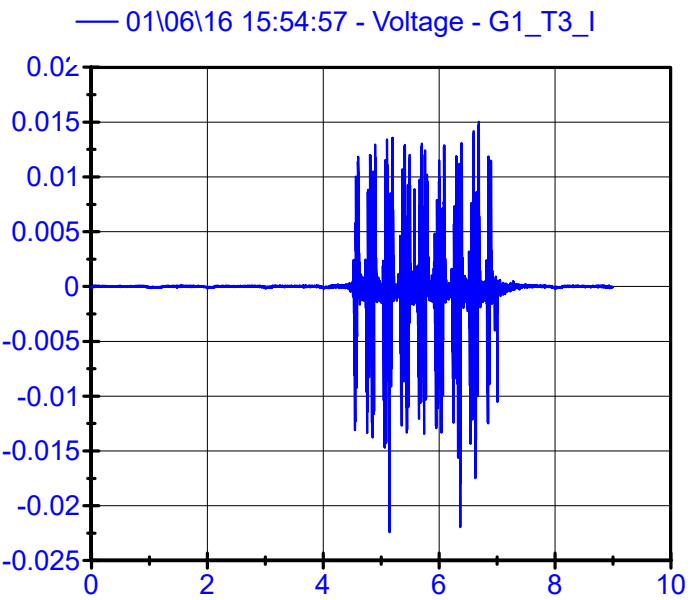

01\06\16 16:22:21

Sleeper Geophones
LPF 150Hz

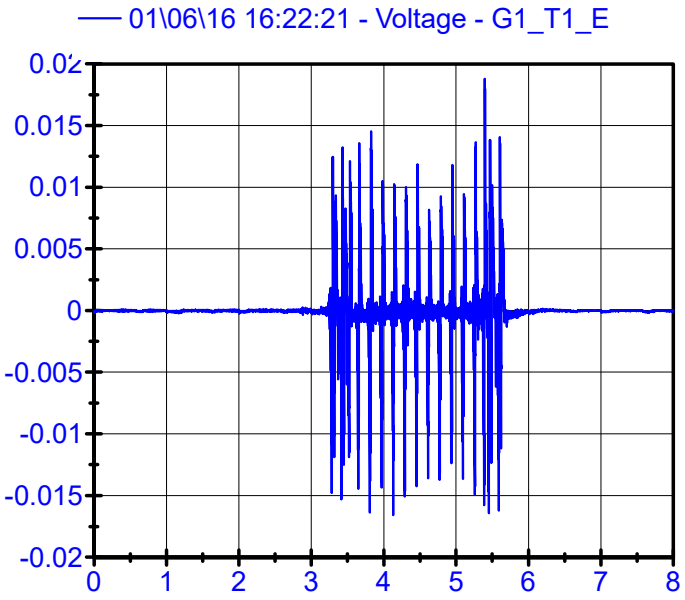

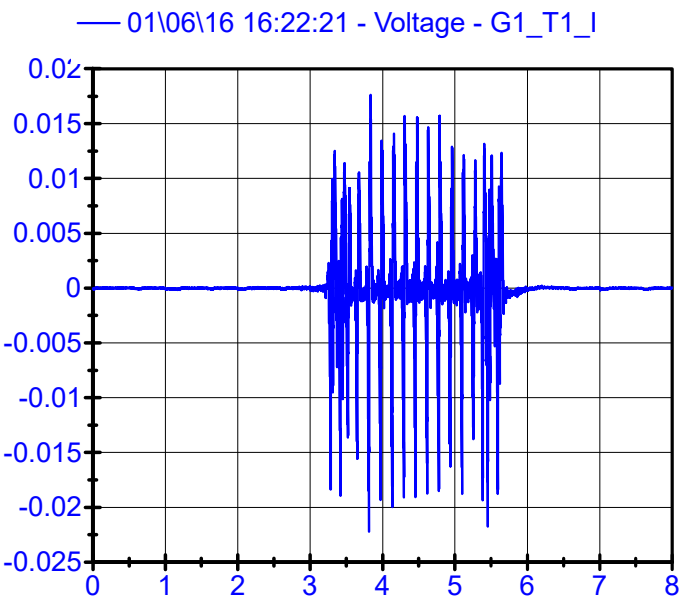

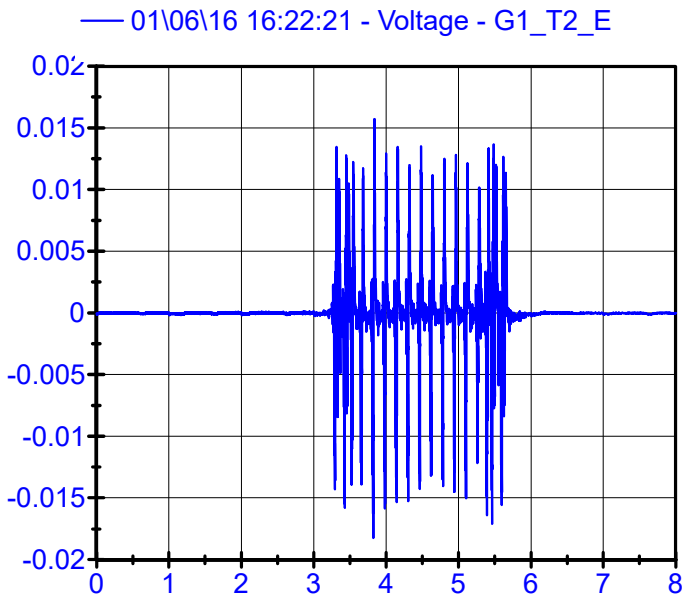

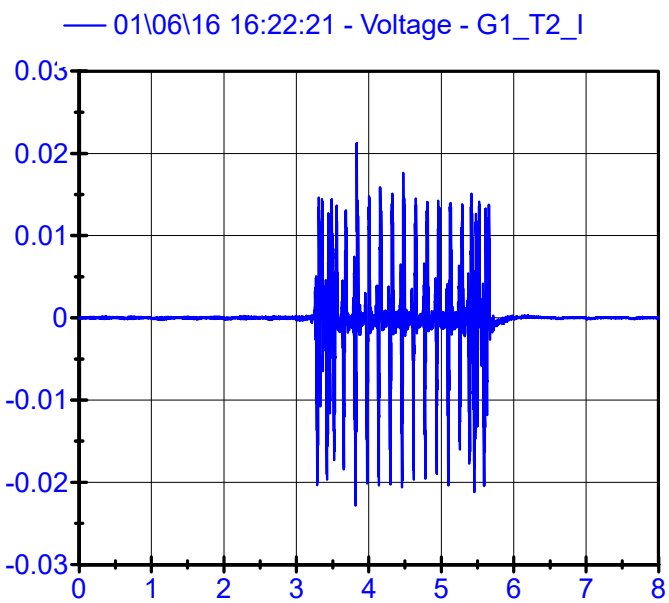

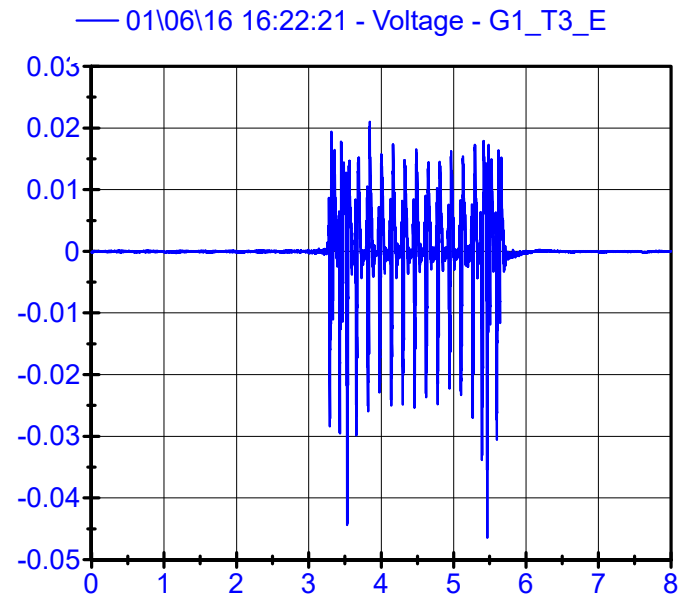

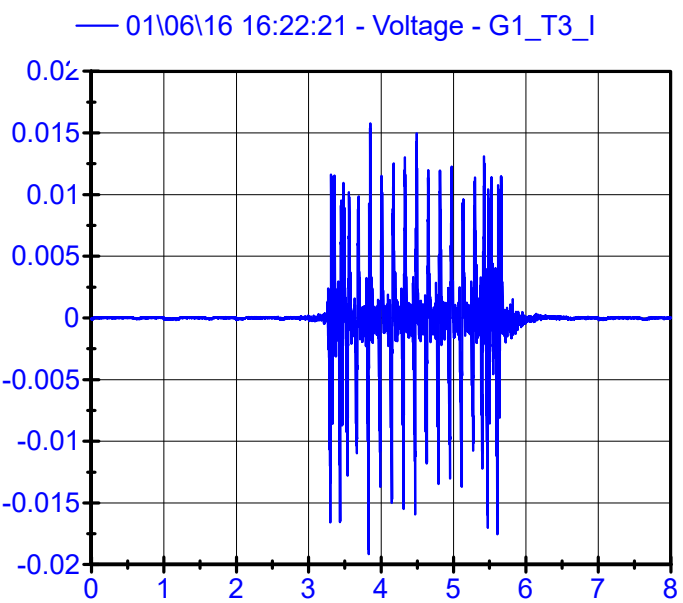

01\06\16 16:54:24

Sleeper Geophones
LPF 150Hz

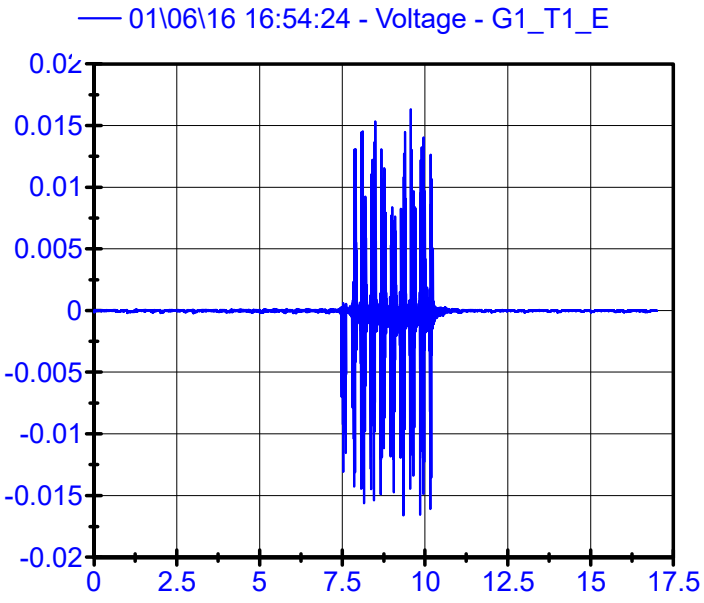

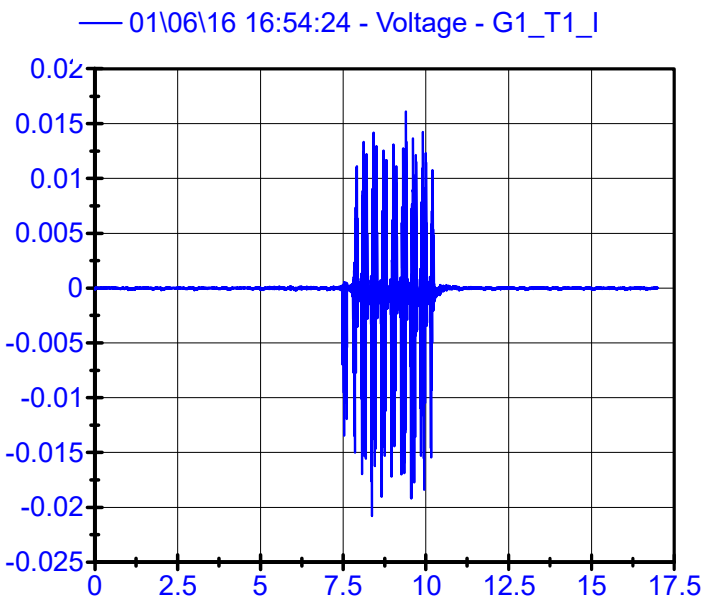

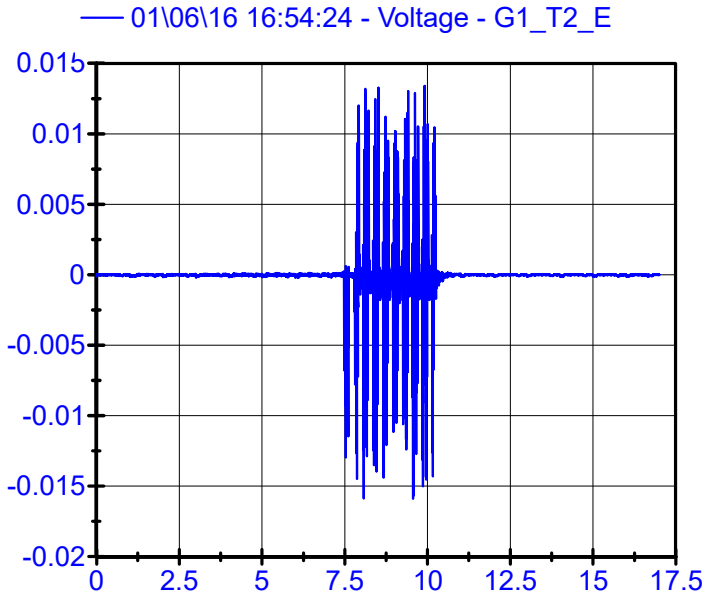

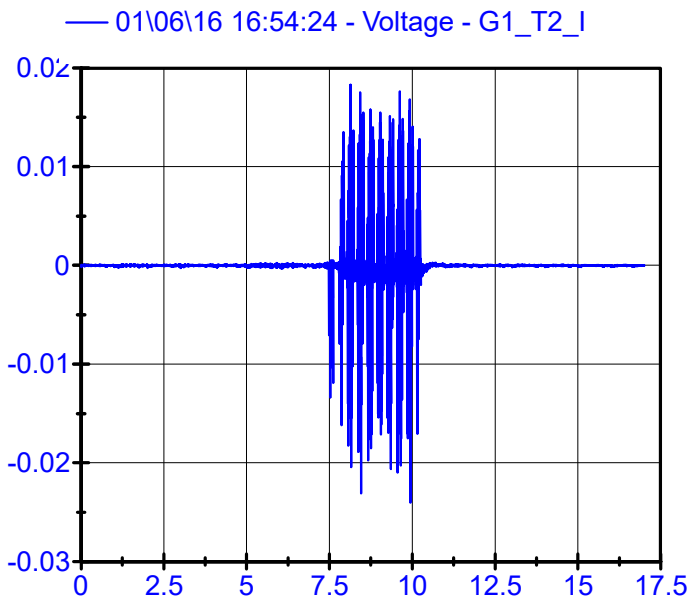

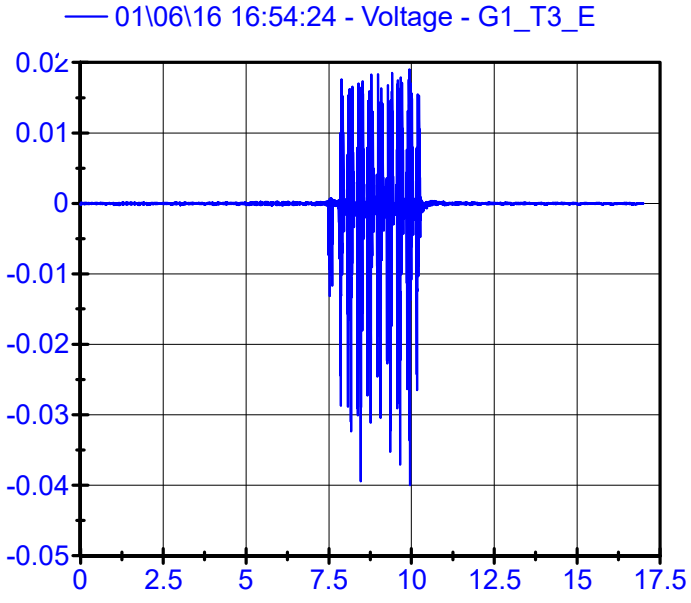

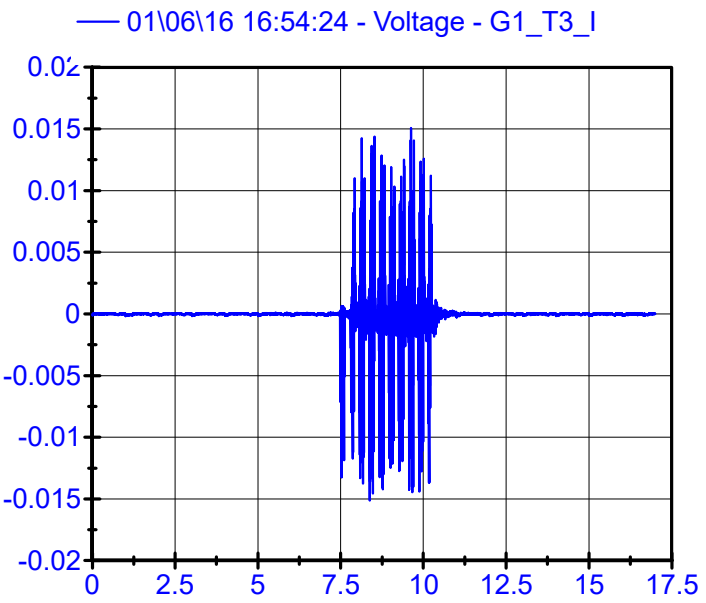

01\06\16 17:24:26

Sleeper Geophones
LPF 150Hz

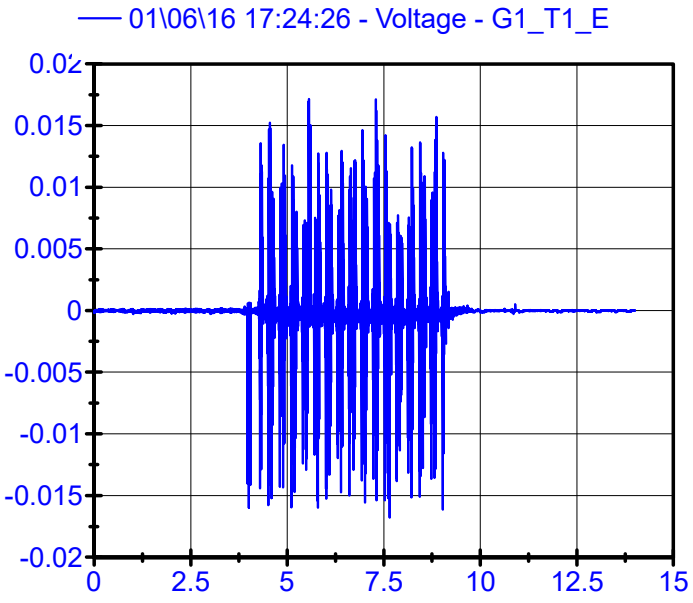

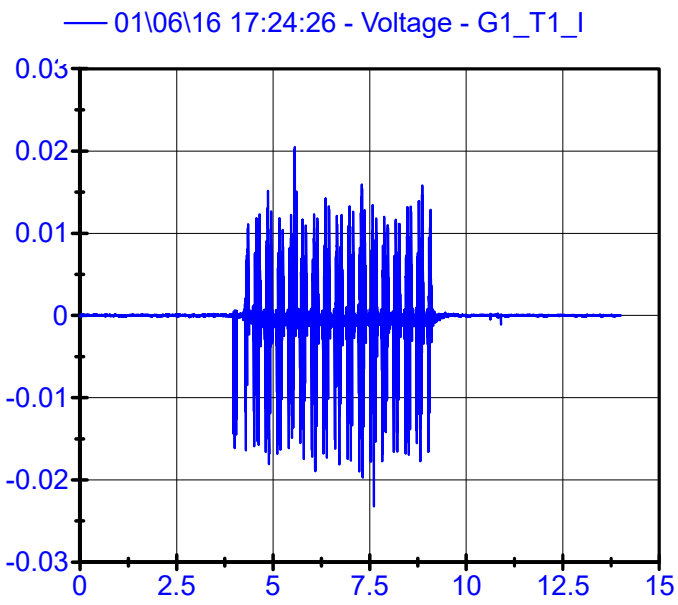

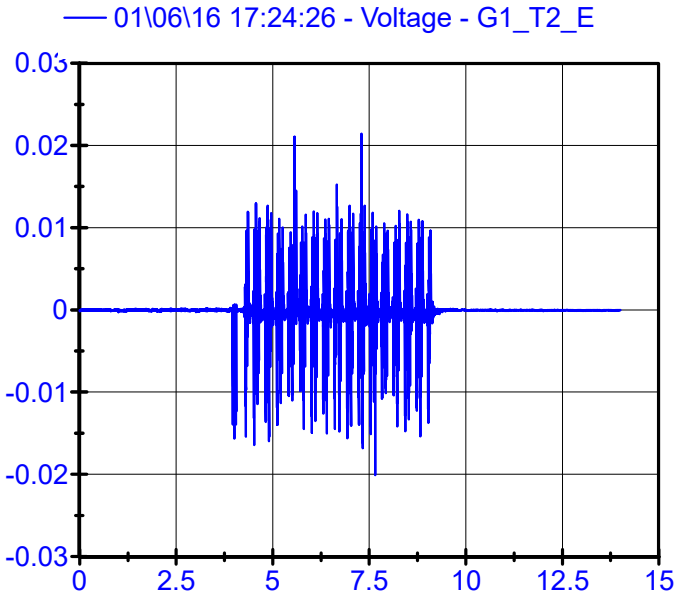

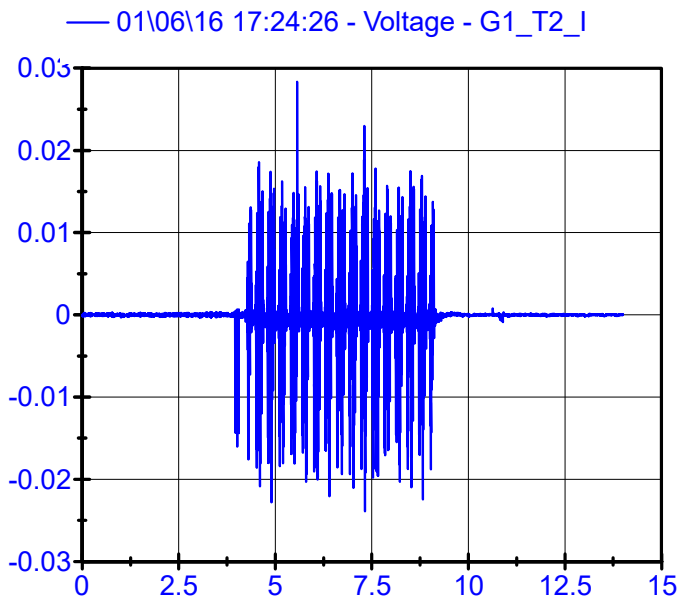

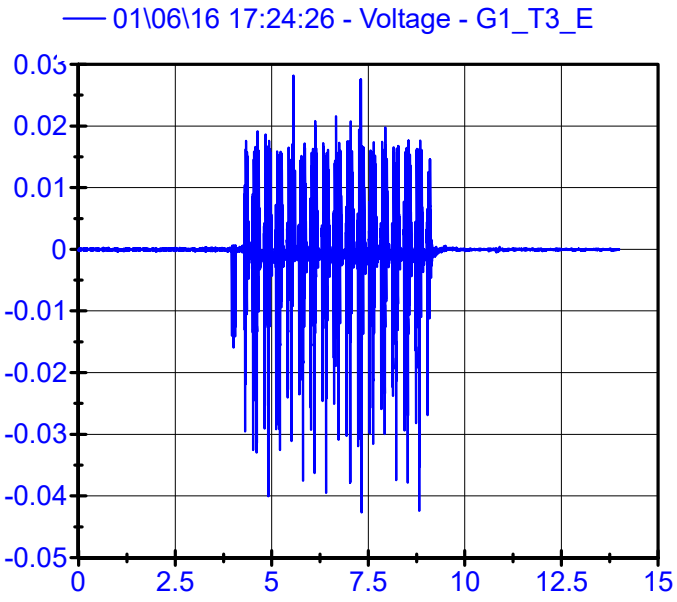

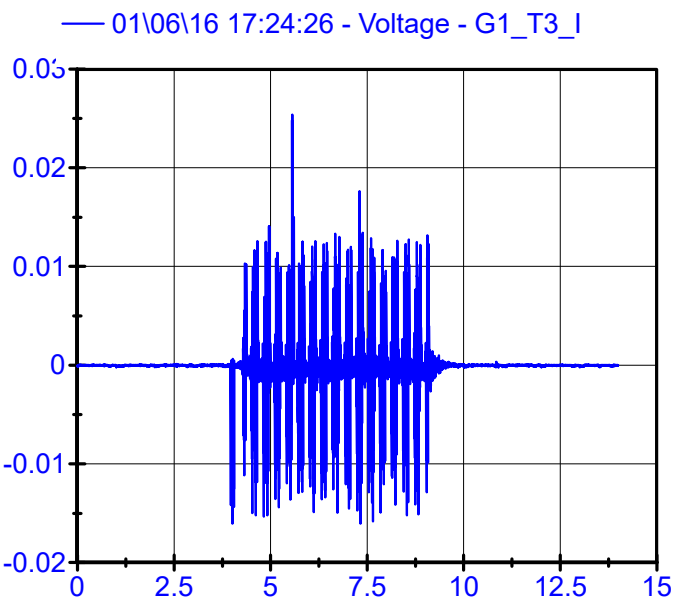

01\06\16 17:38:59

Sleeper Geophones
LPF 150Hz

01\06\16 17:38:59 - Voltage - G1_T1_E

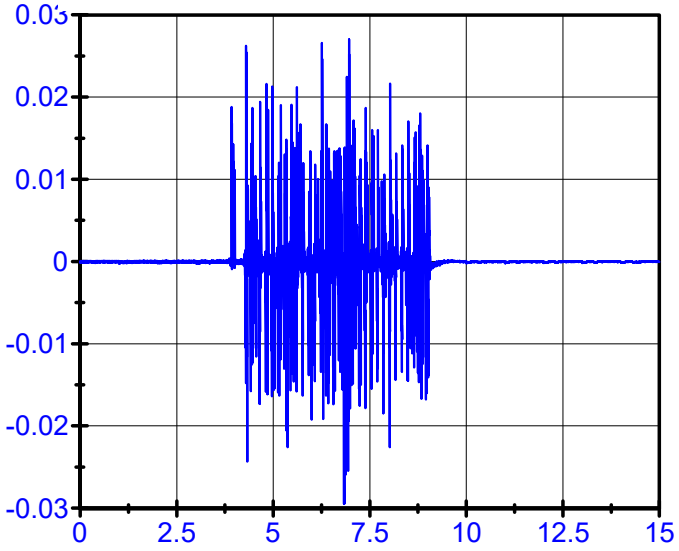

01\06\16 17:38:59 - Voltage - G1_T1_I

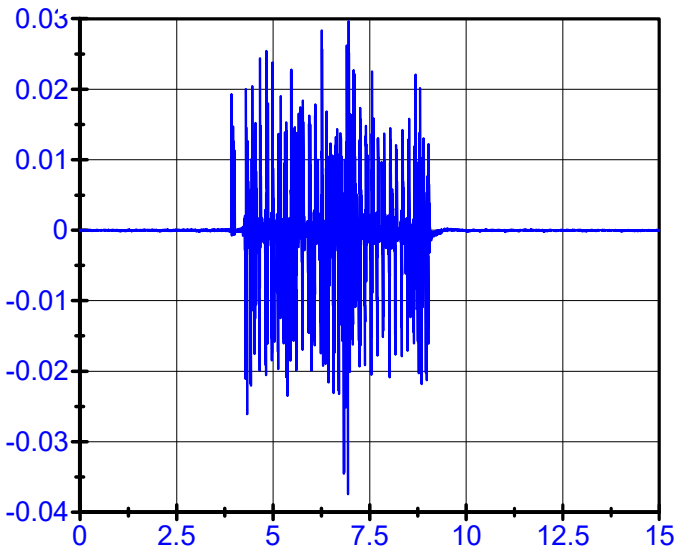

01\06\16 17:38:59 - Voltage - G1_T2_E

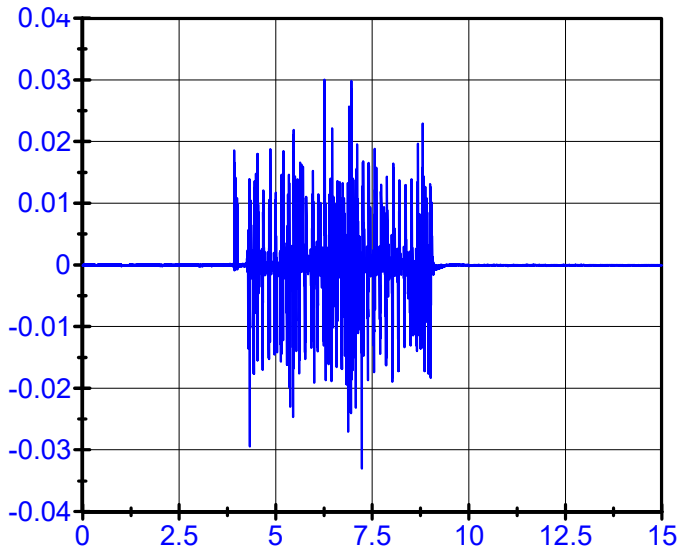

01\06\16 17:38:59 - Voltage - G1_T2_I

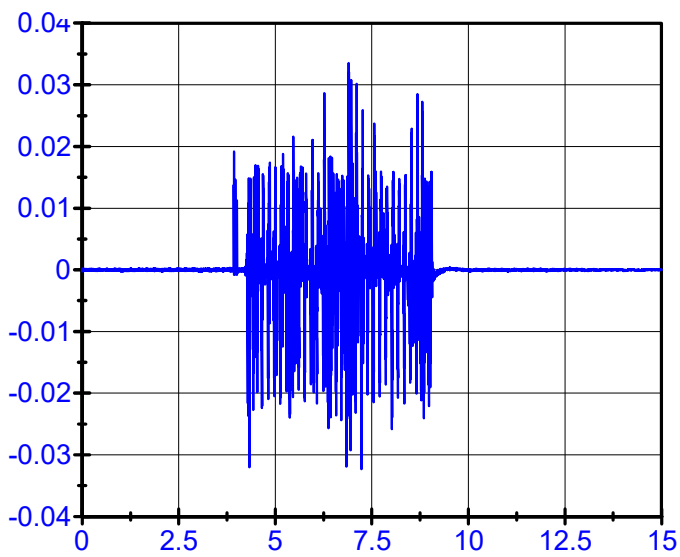

01\06\16 17:38:59 - Voltage - G1_T3_E

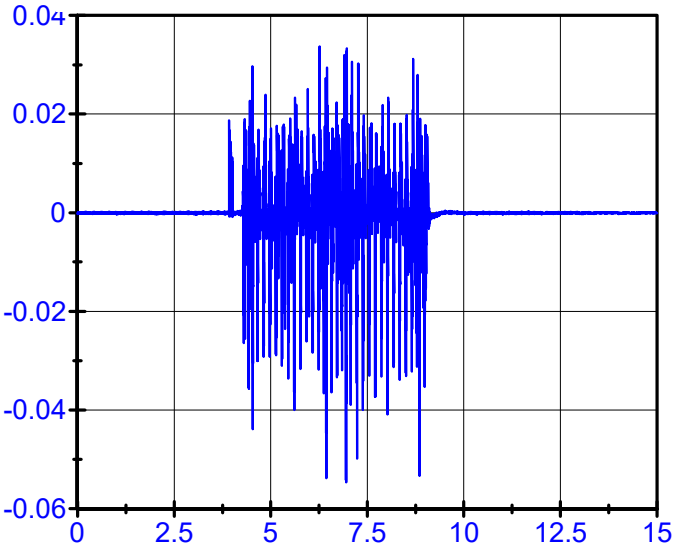

01\06\16 17:38:59 - Voltage - G1_T3_I

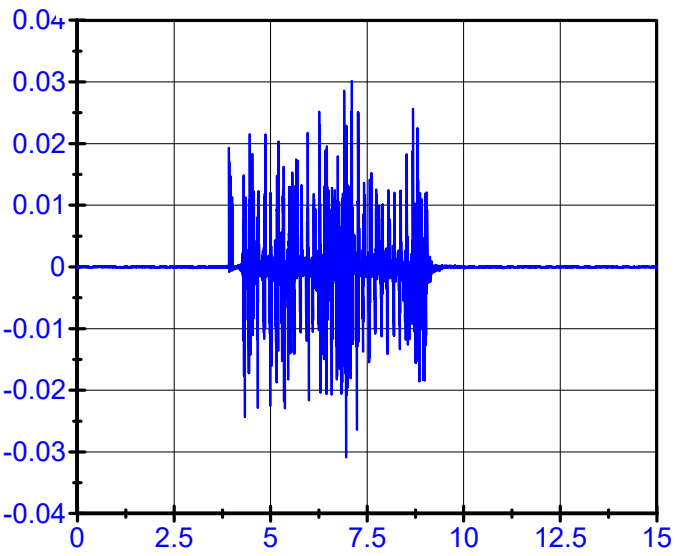

01\06\16 17:59:25

Sleeper Geophones
LPF 150Hz

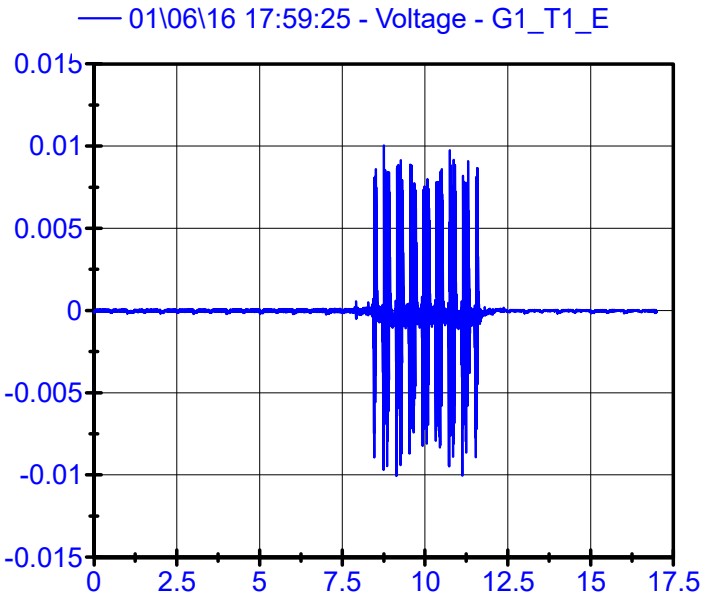

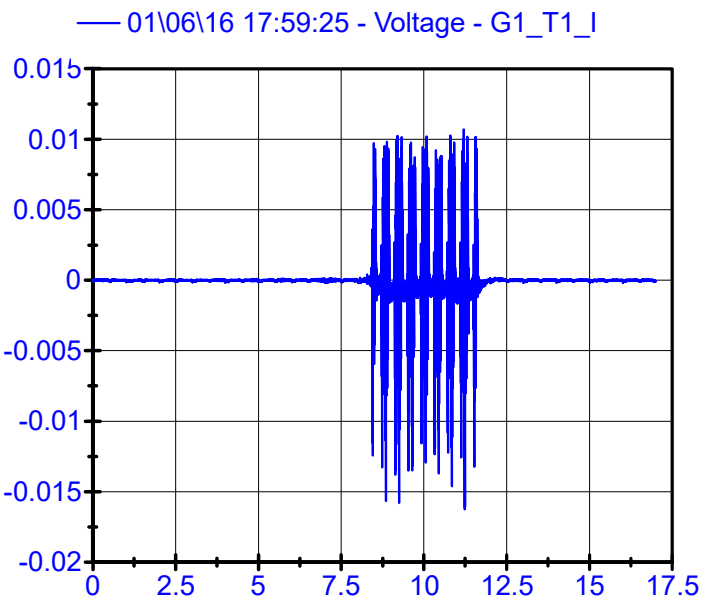

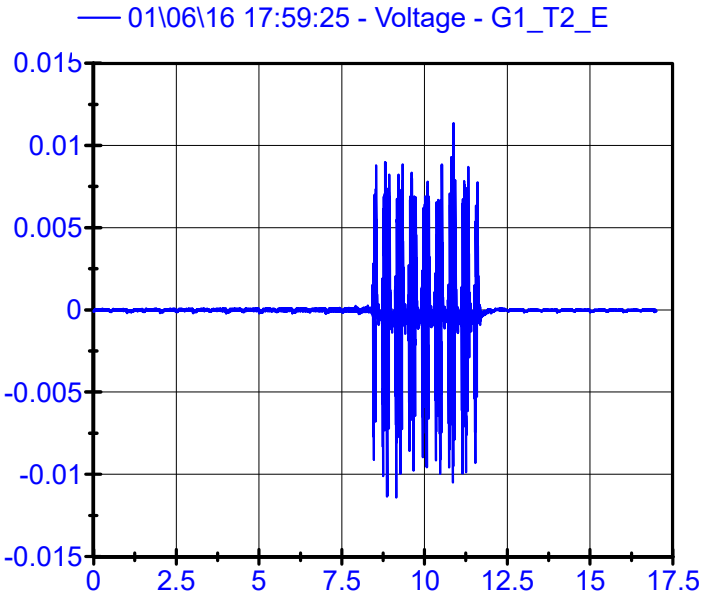

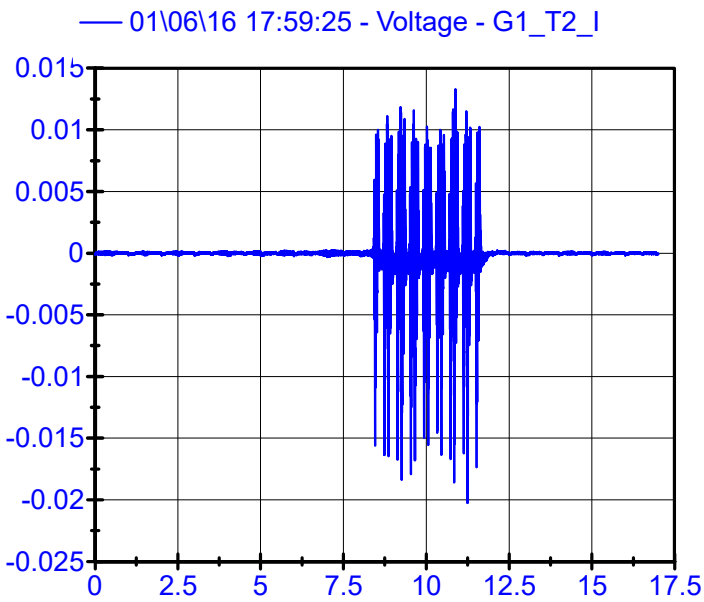

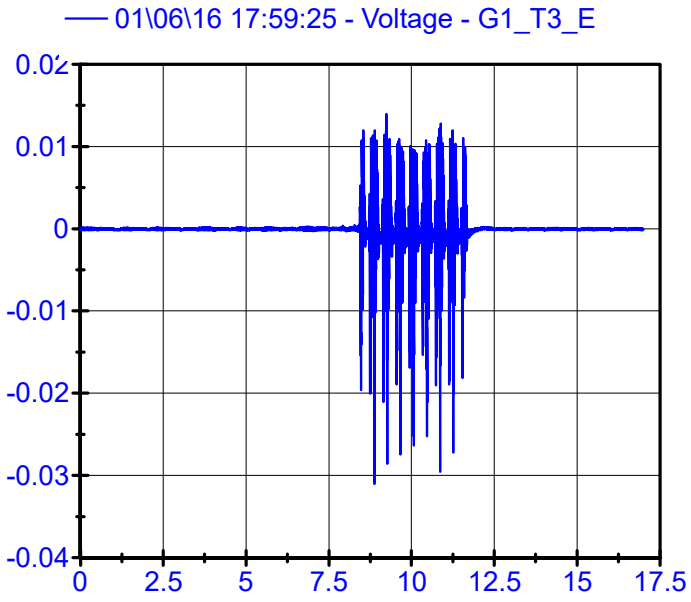

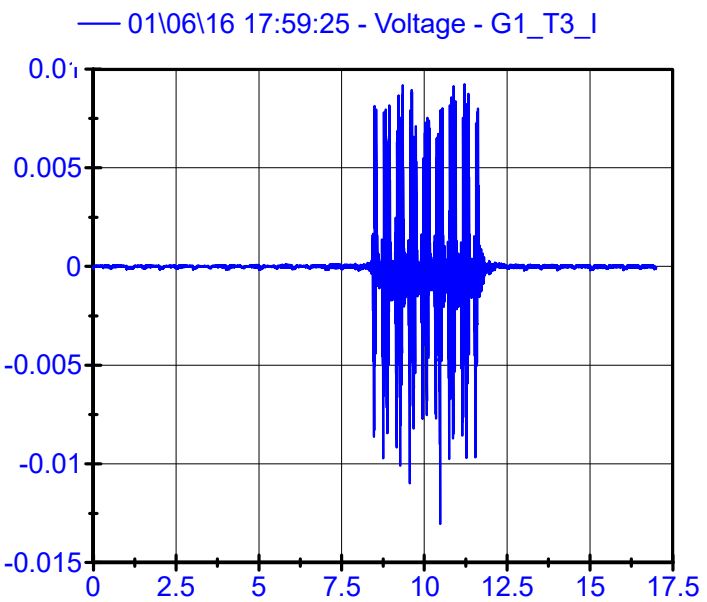

01\06\16 18:22:52

Sleeper Geophones
LPF 150Hz

01\06\16 18:22:52 - Voltage - G1_T1_E

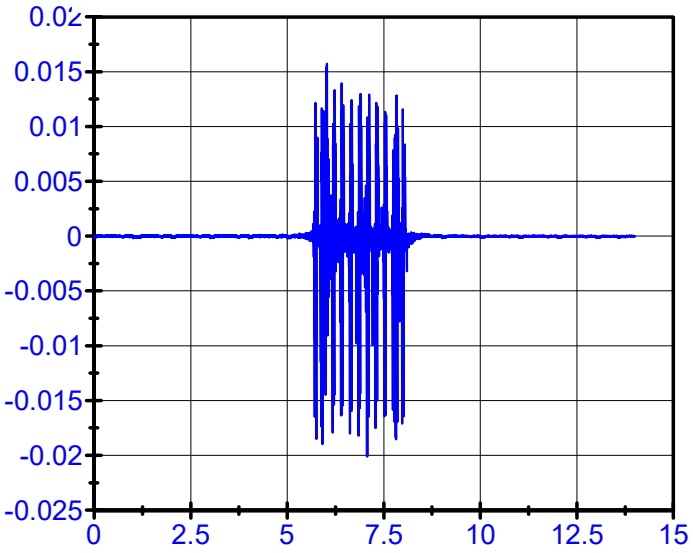

01\06\16 18:22:52 - Voltage - G1_T1_I

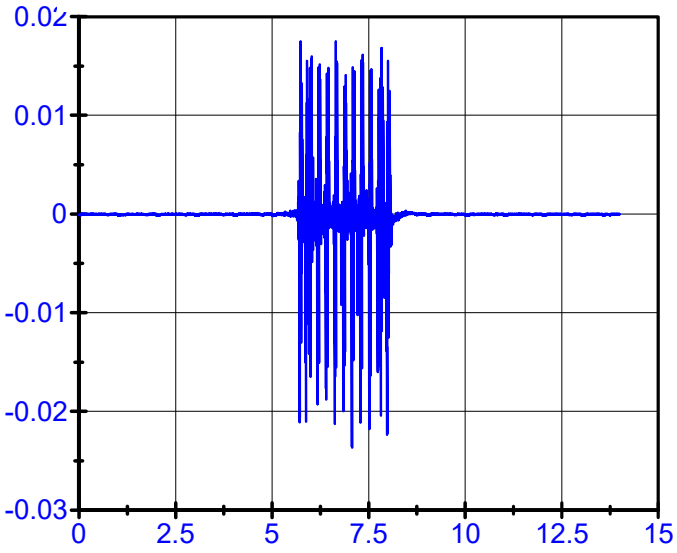

01\06\16 18:22:52 - Voltage - G1_T2_E

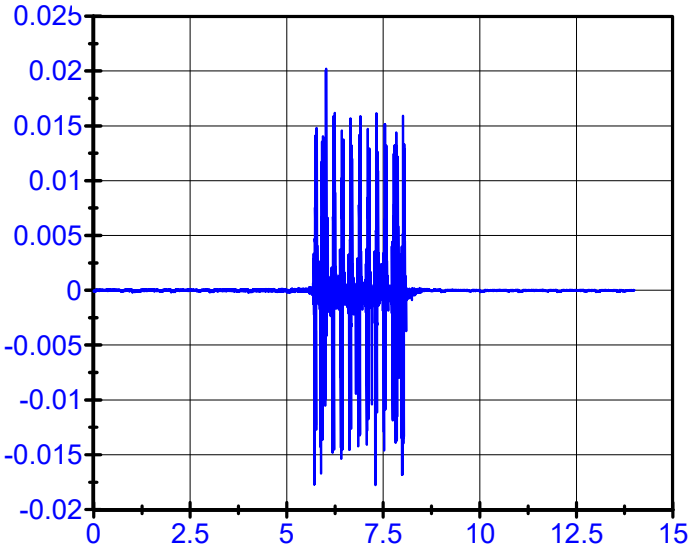

01\06\16 18:22:52 - Voltage - G1_T2_I

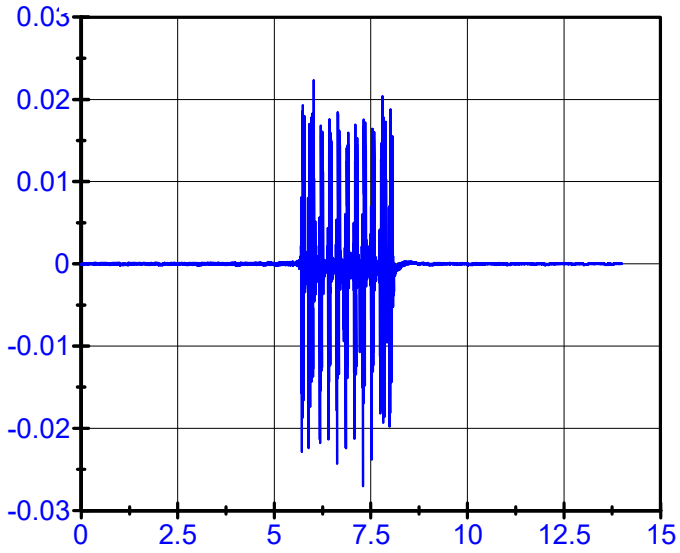

01\06\16 18:22:52 - Voltage - G1_T3_E

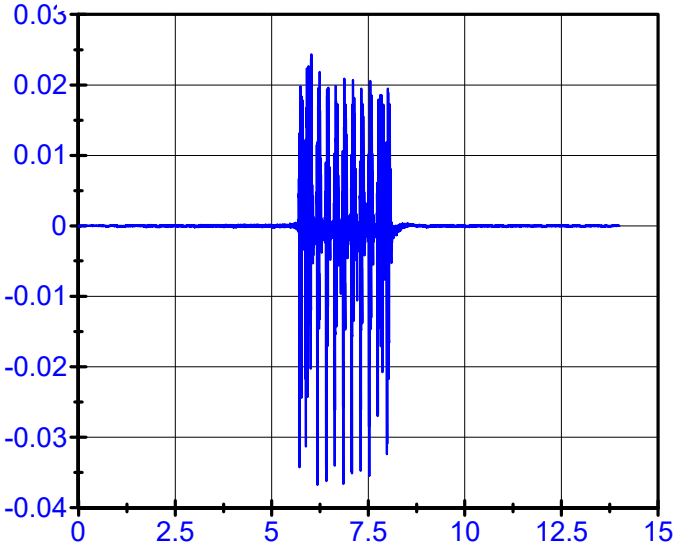

01\06\16 18:22:52 - Voltage - G1_T3_I

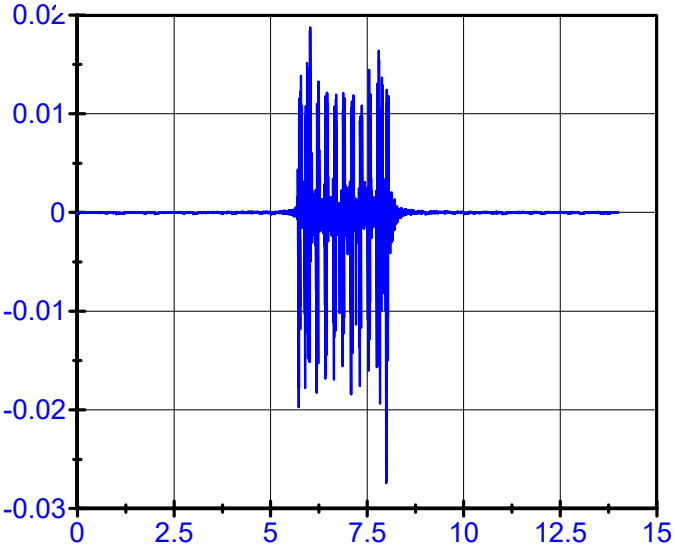

01\06\16 18:59:06

Sleeper Geophones
LPF 150Hz

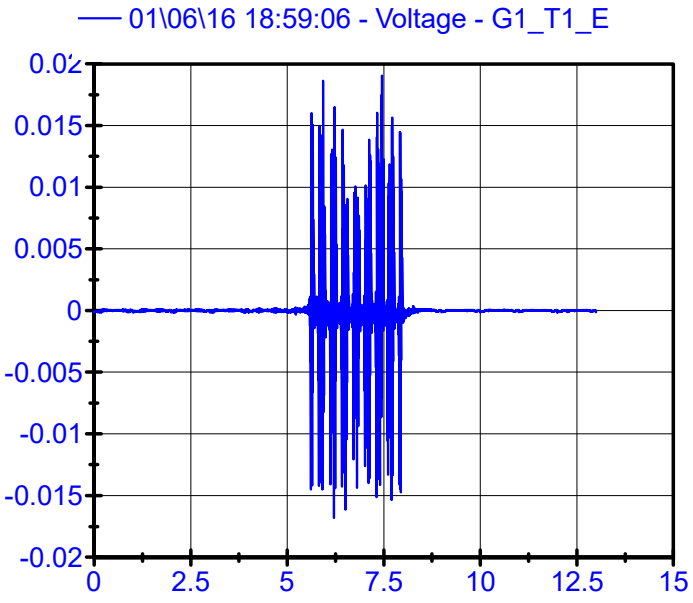

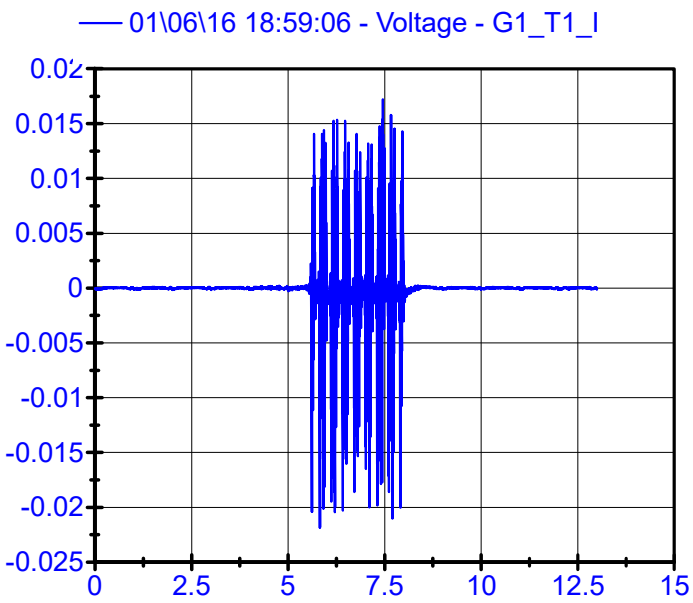

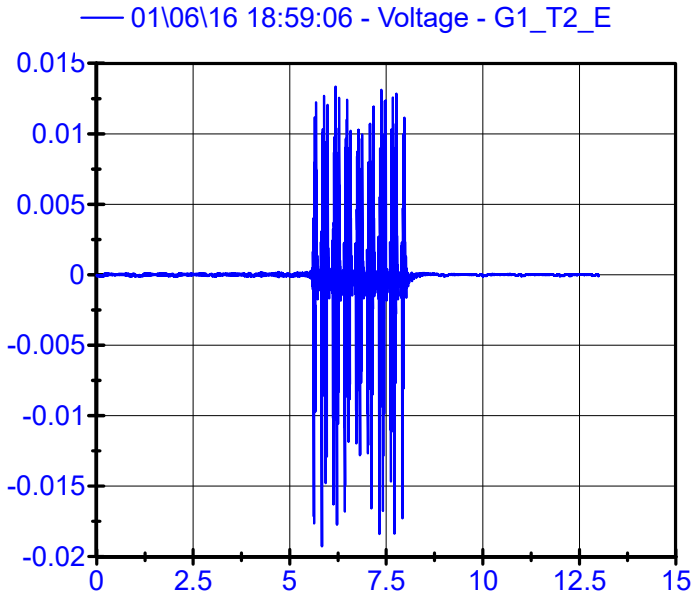

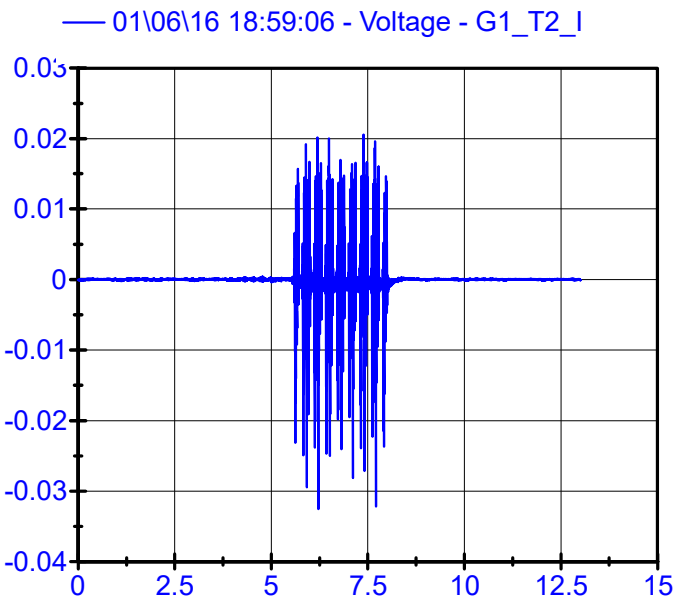

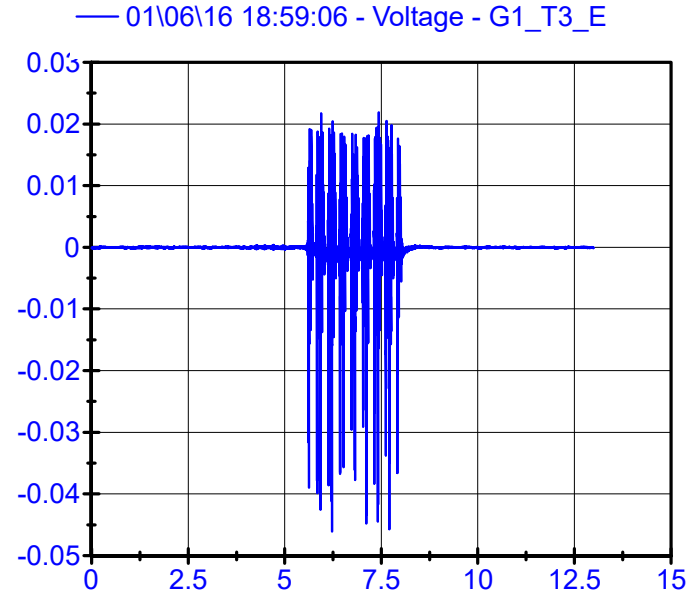

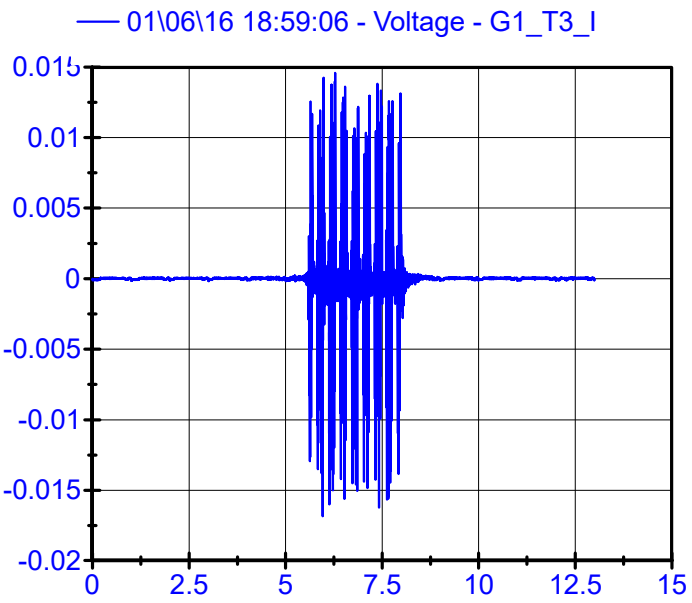

01\06\16 19:21:34

Sleeper Geophones
LPF 150Hz

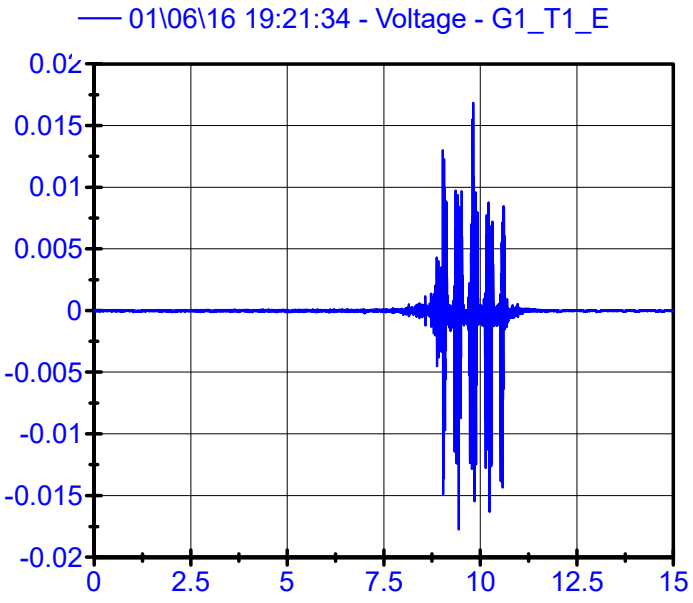

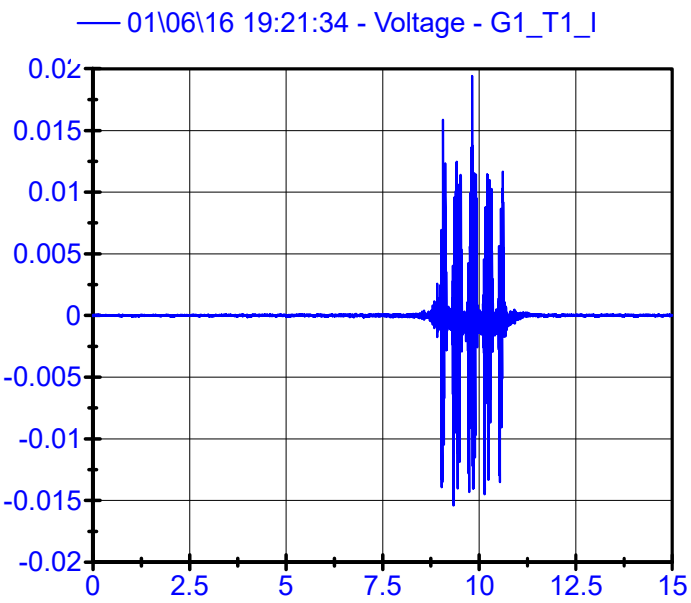

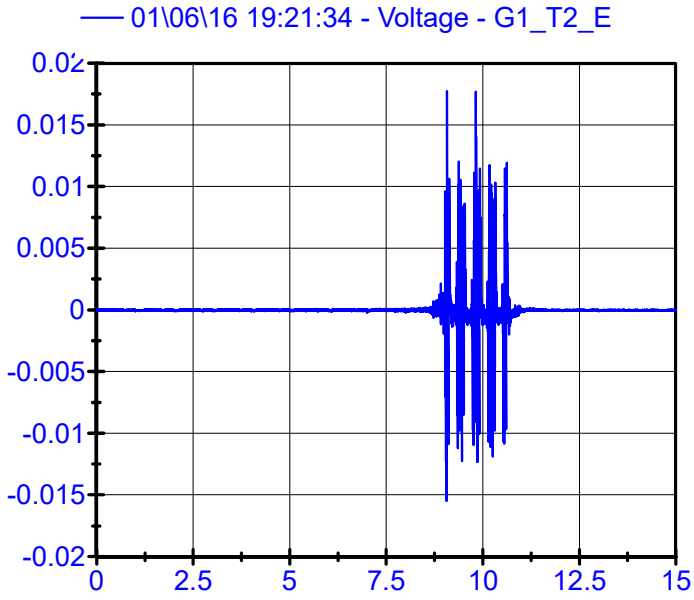

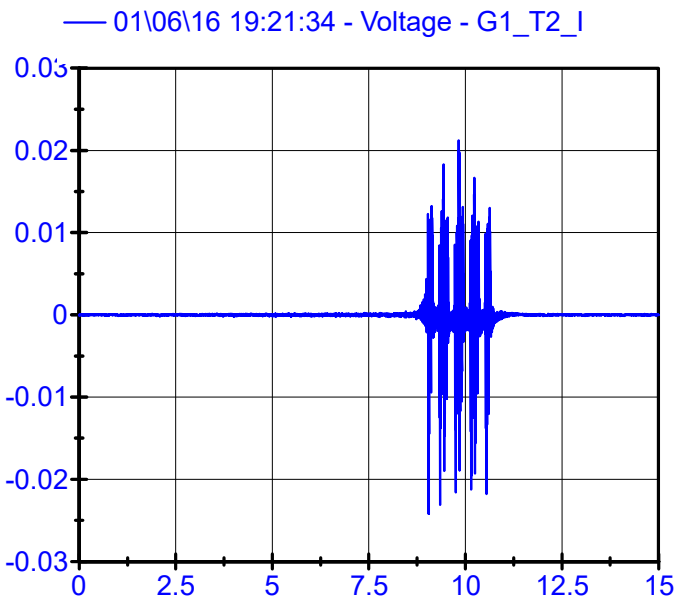

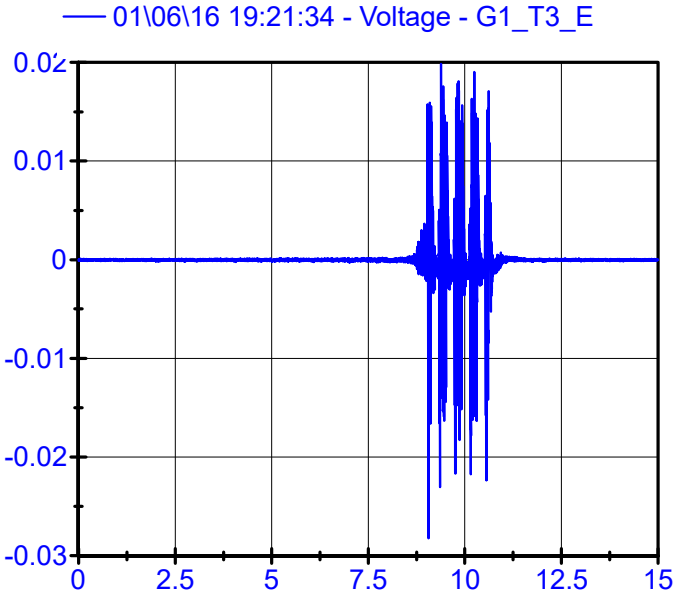

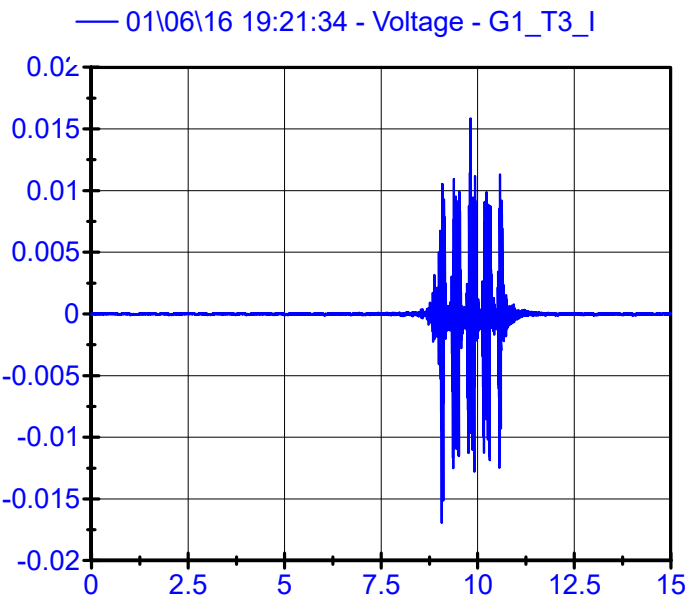

01\06\16 19:23:31

Sleeper Geophones
LPF 150Hz

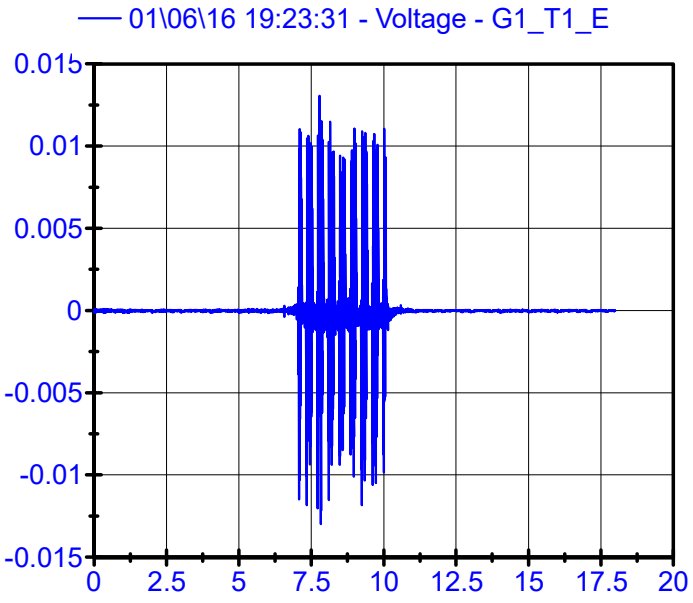

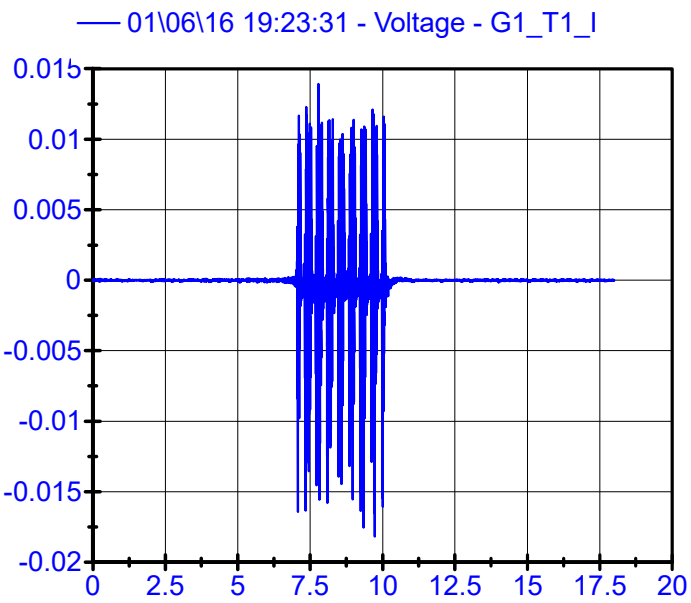

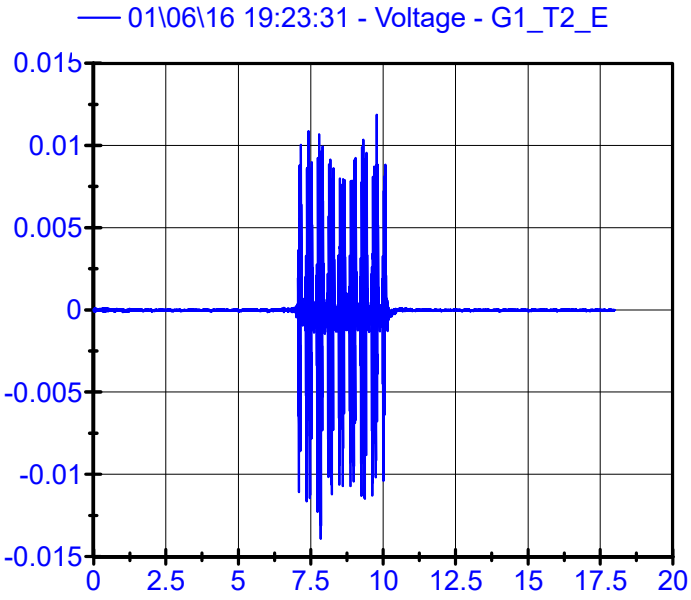

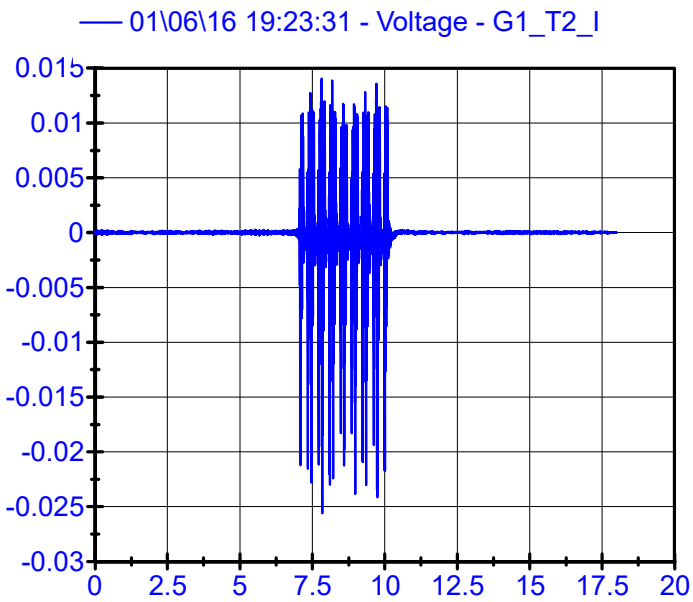

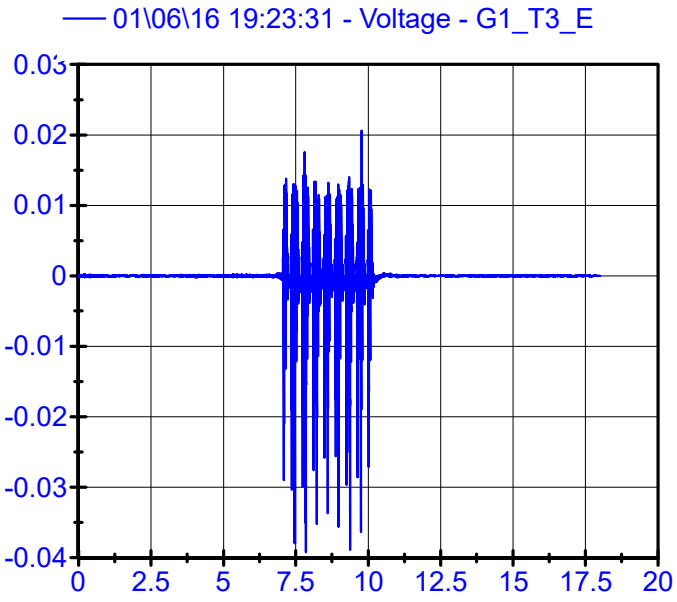

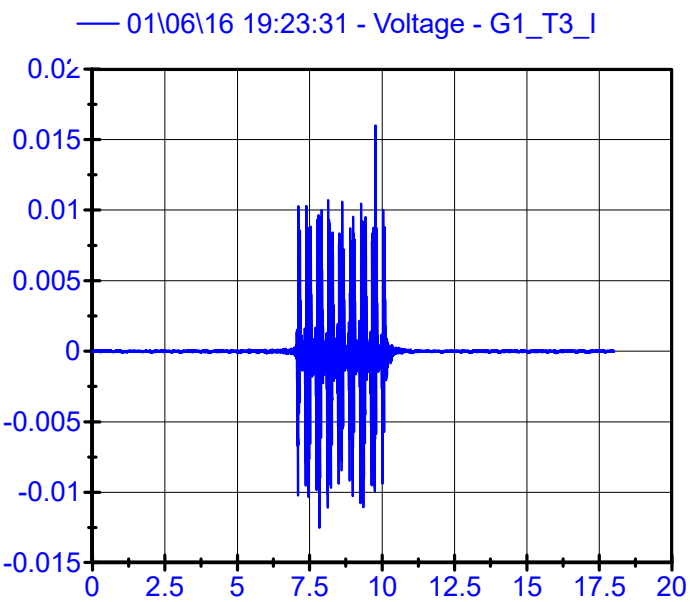

01\06\16 19:32:45

Sleeper Geophones
LPF 150Hz

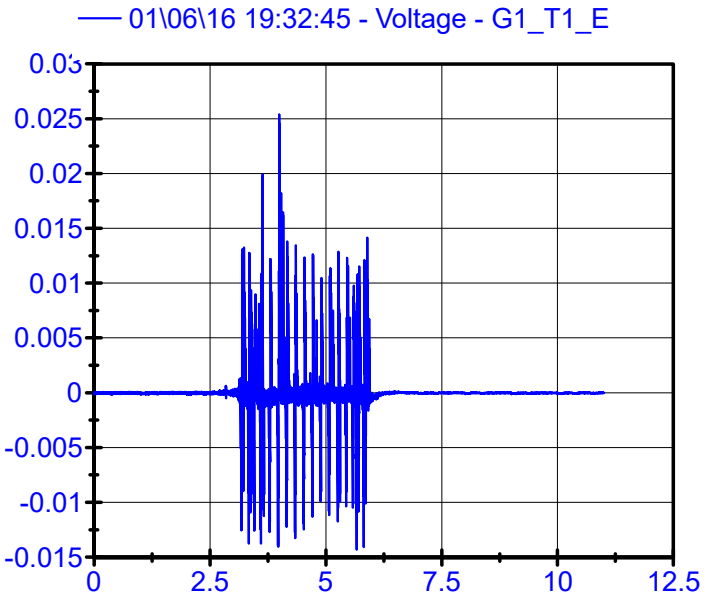

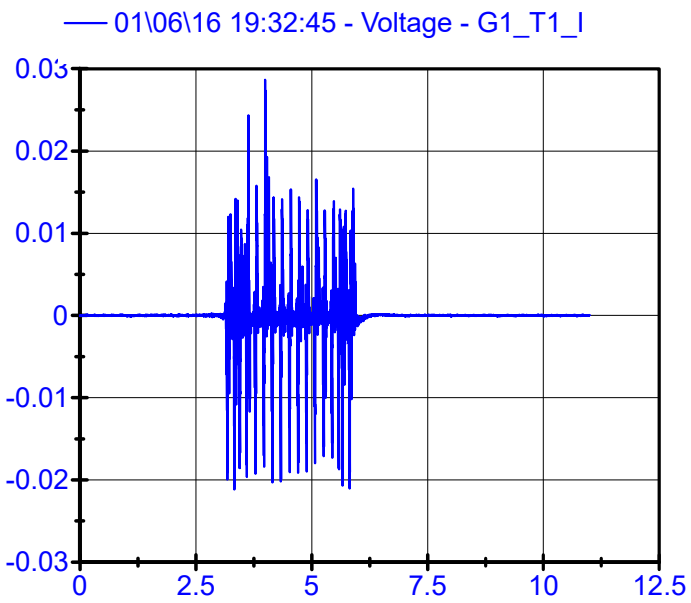

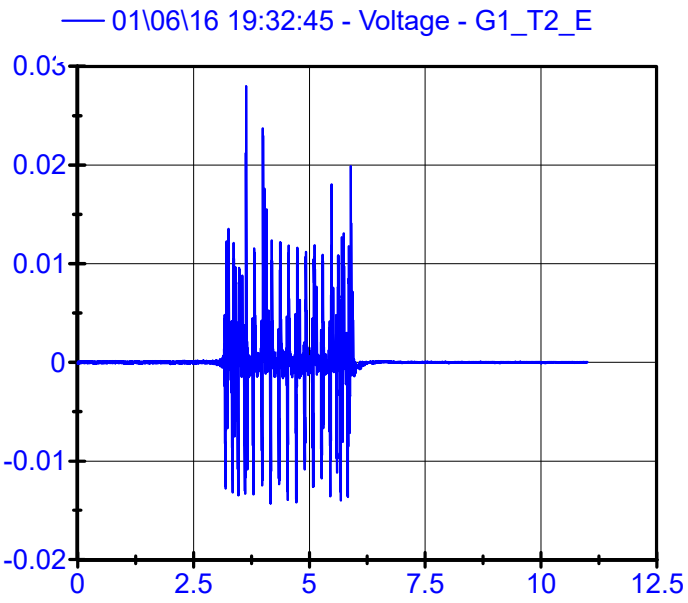

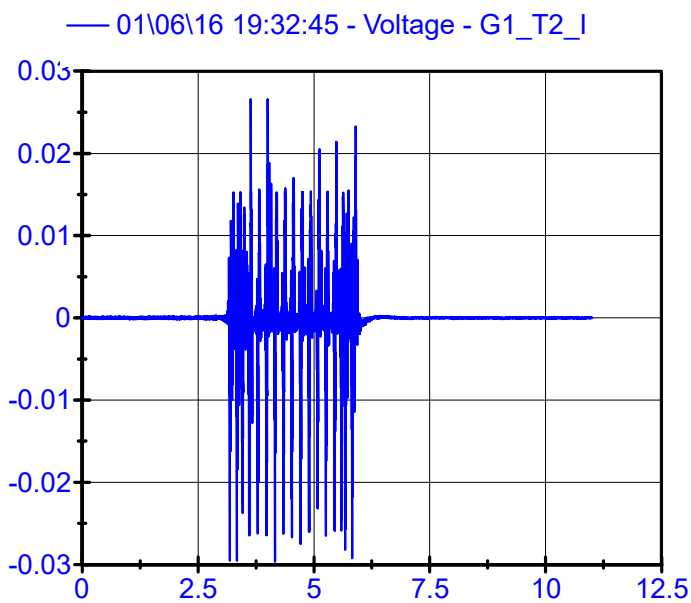

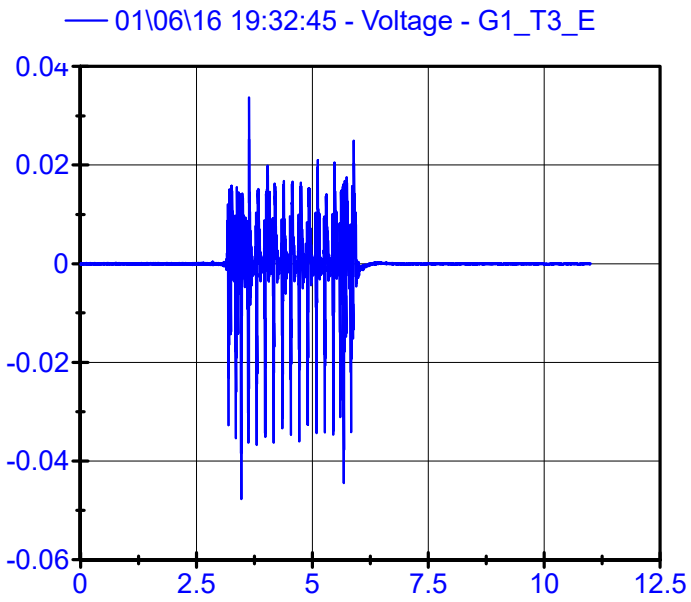

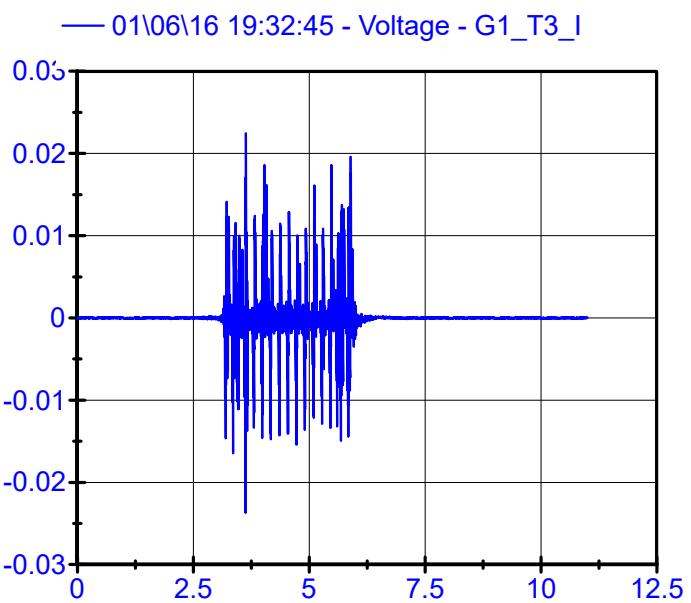

01\06\16 19:53:03

Sleeper Geophones
LPF 150Hz

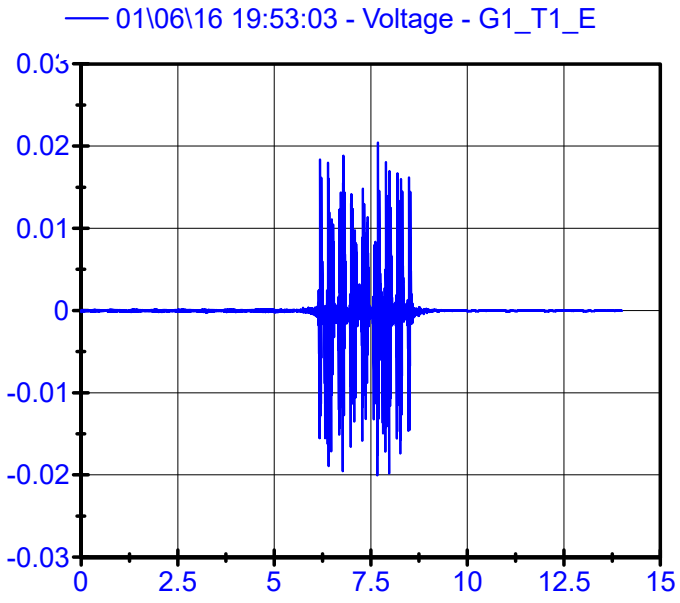

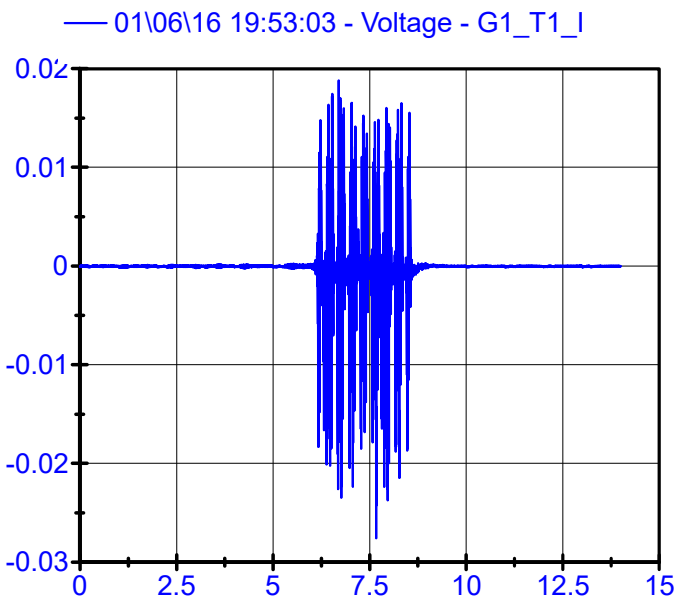

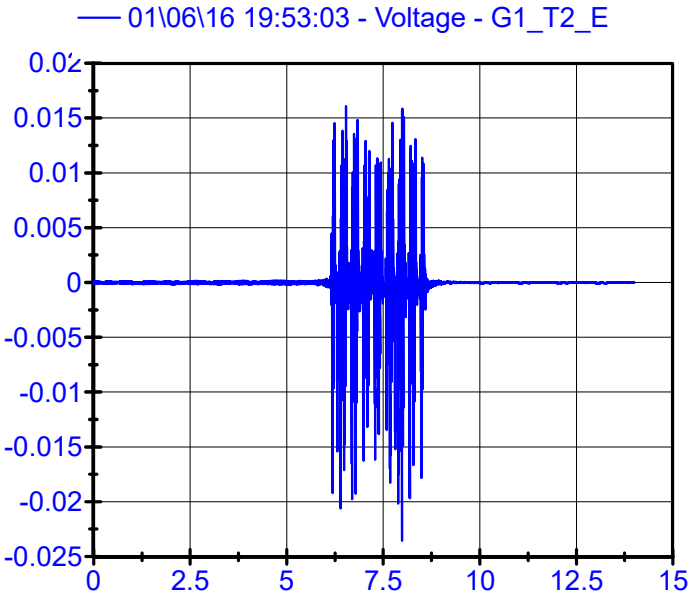

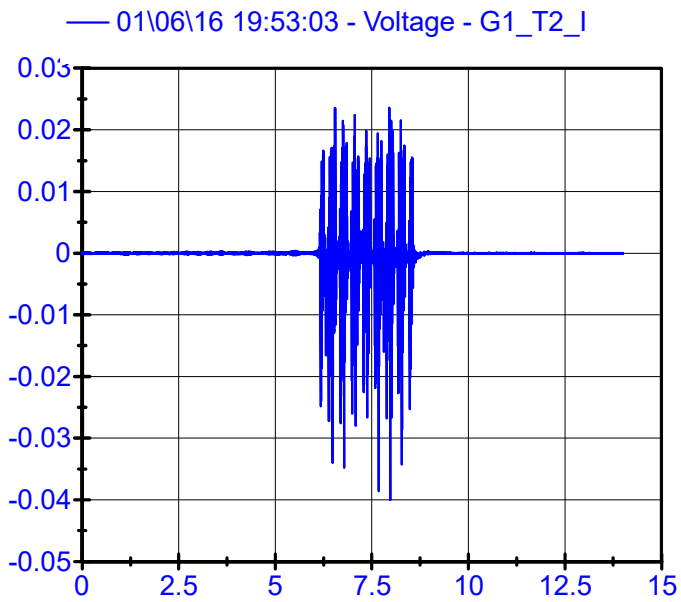

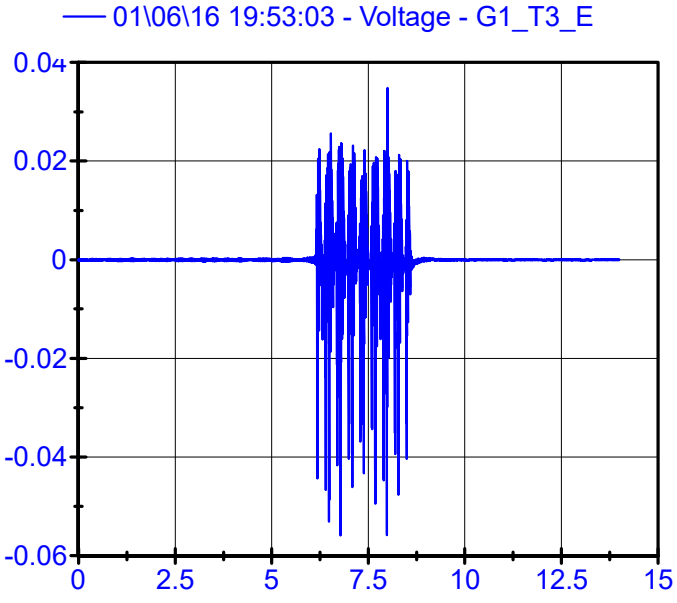

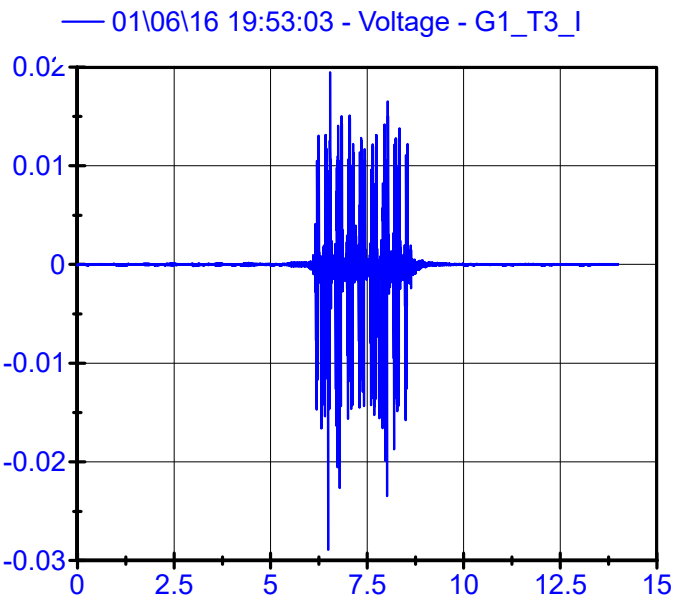

01\06\16 19:59:42

Sleeper Geophones
LPF 150Hz

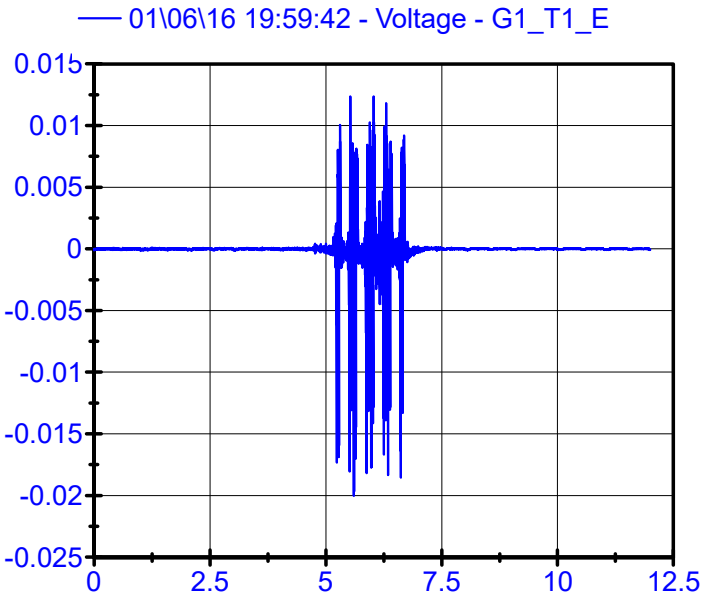

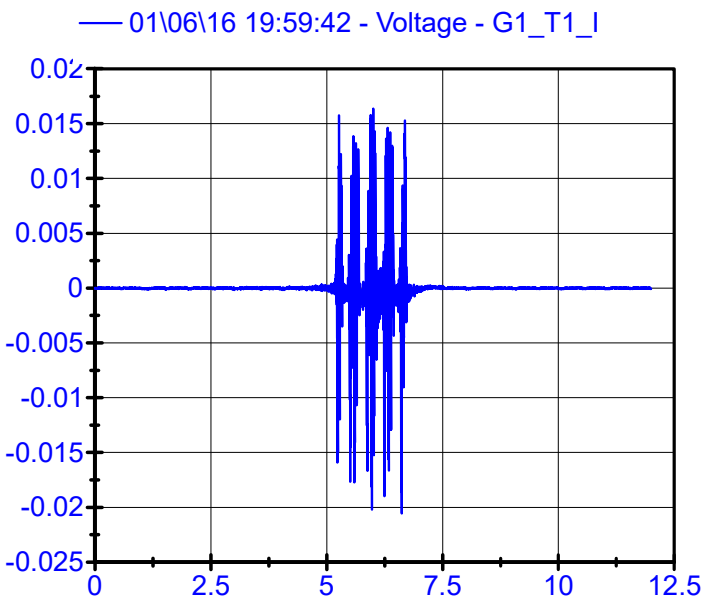

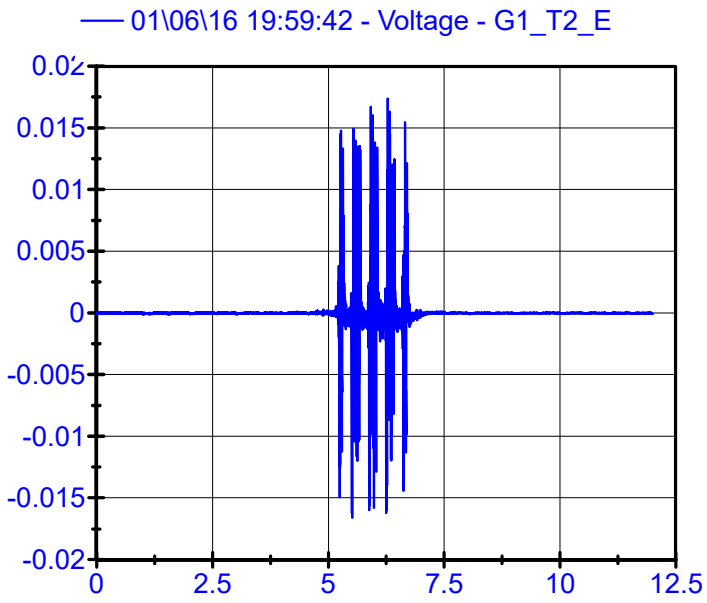

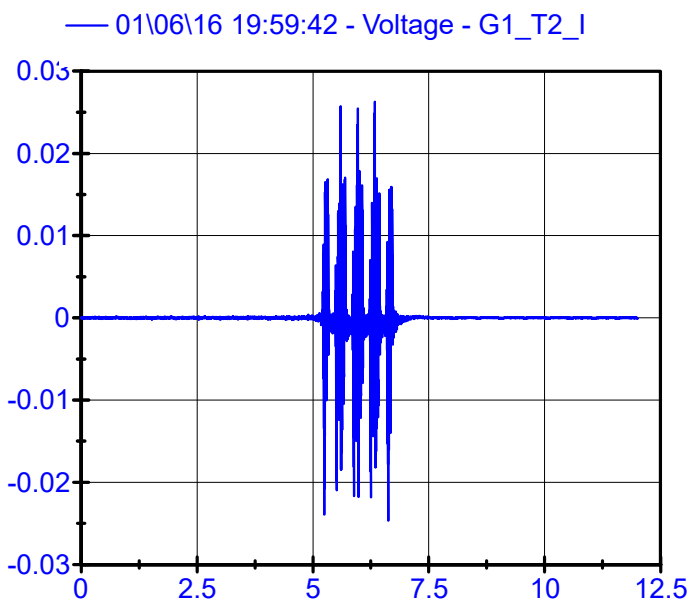

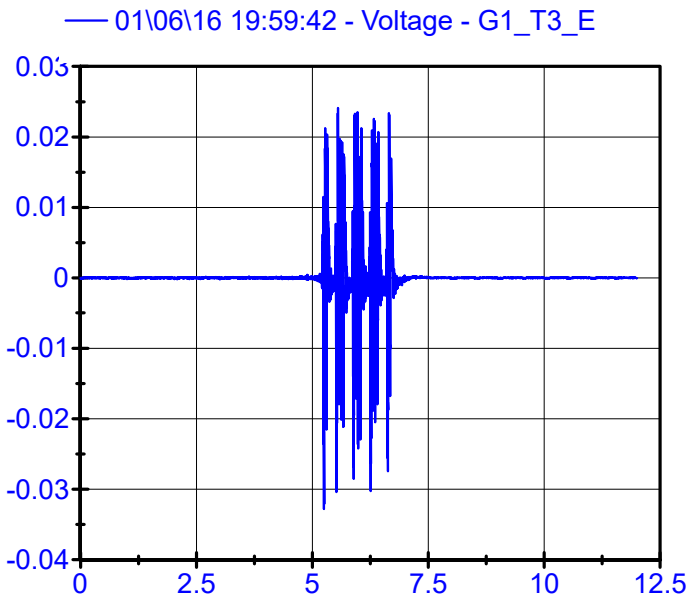

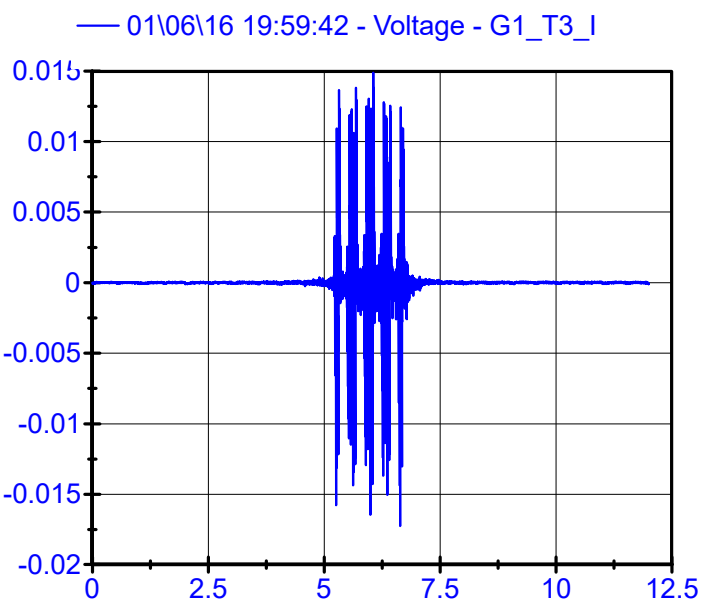

01\06\16 20:21:57

Sleeper Geophones
LPF 150Hz

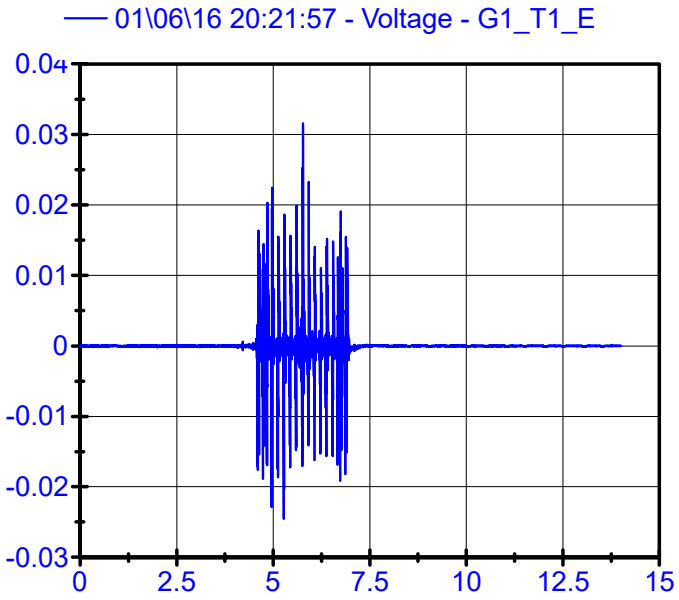

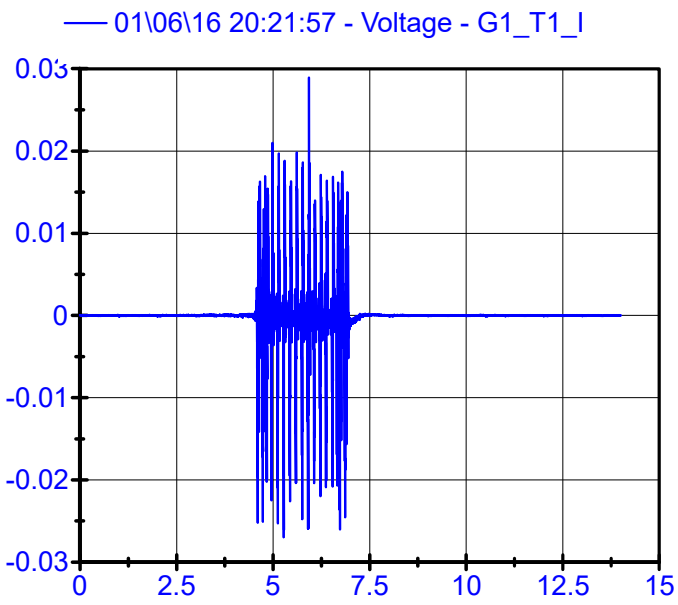

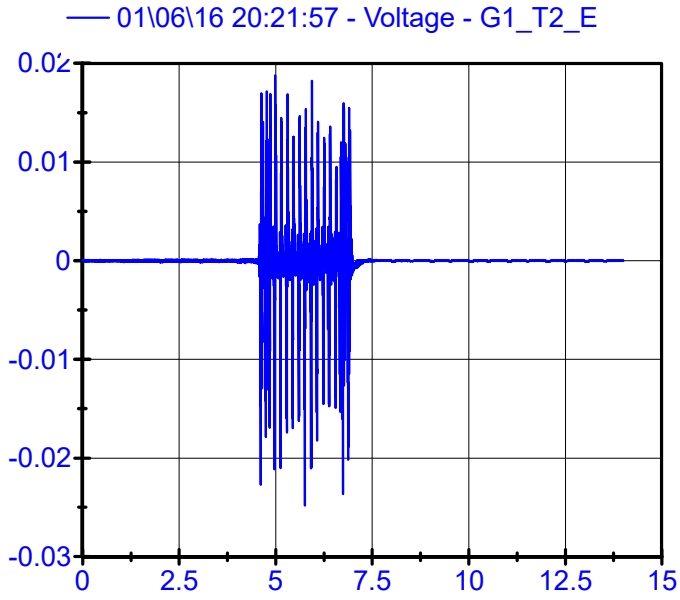

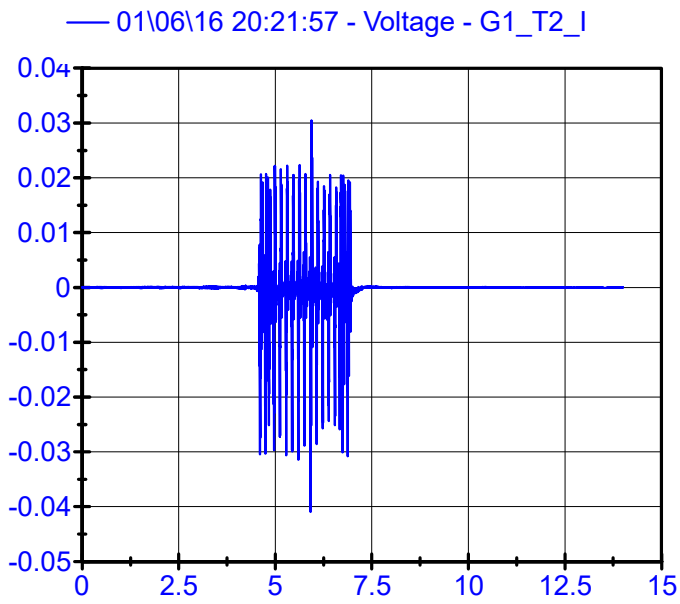

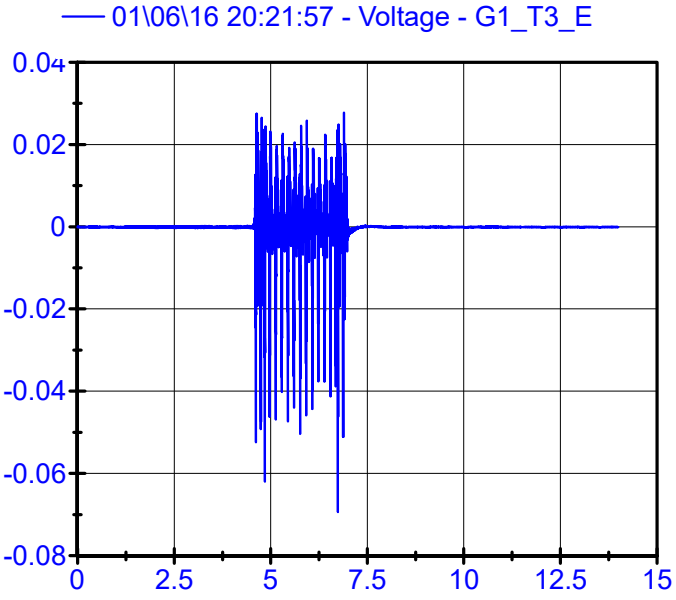

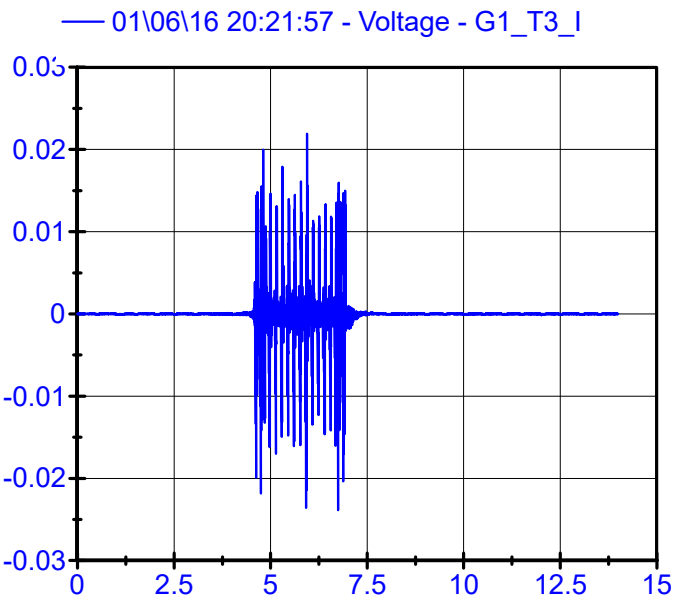

01\06\16 20:57:58

Sleeper Geophones
LPF 150Hz

01\06\16 20:57:58 - Voltage - G1_T1_E

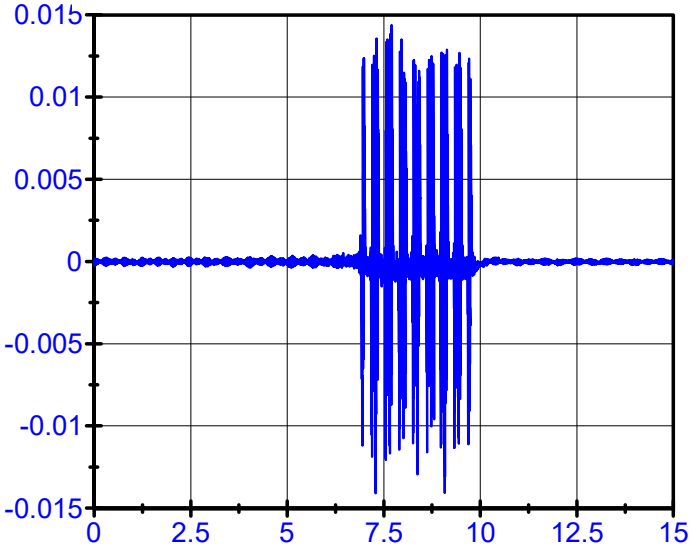

01\06\16 20:57:58 - Voltage - G1_T1_I

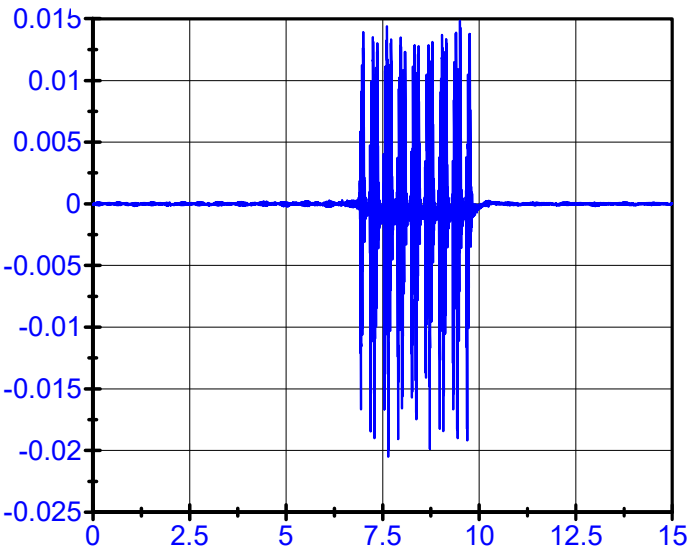

01\06\16 20:57:58 - Voltage - G1_T2_E

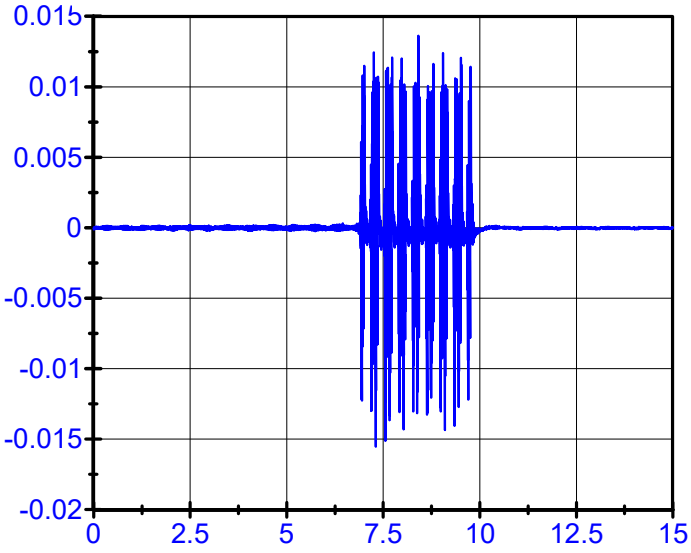

01\06\16 20:57:58 - Voltage - G1_T2_I

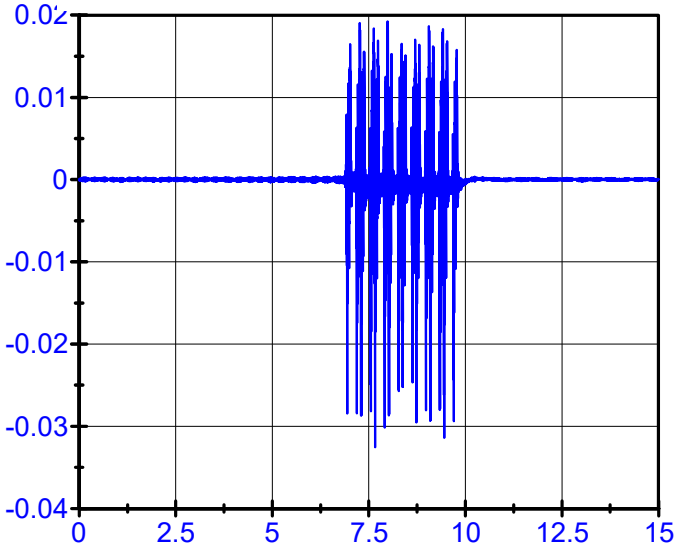

01\06\16 20:57:58 - Voltage - G1_T3_E

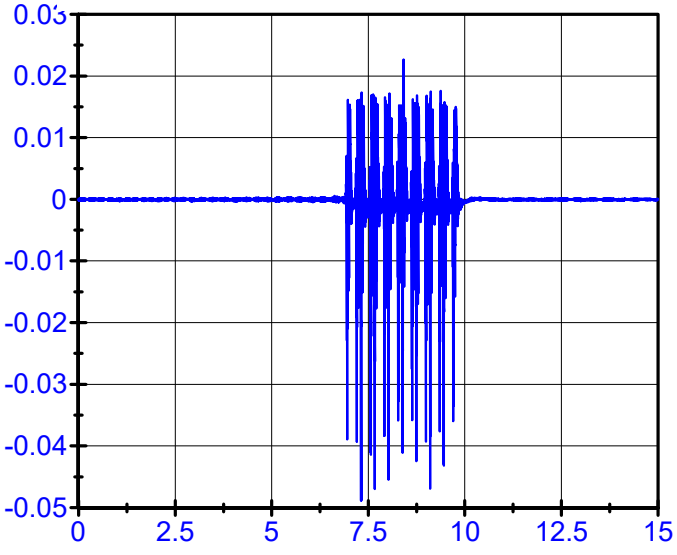

01\06\16 20:57:58 - Voltage - G1_T3_I

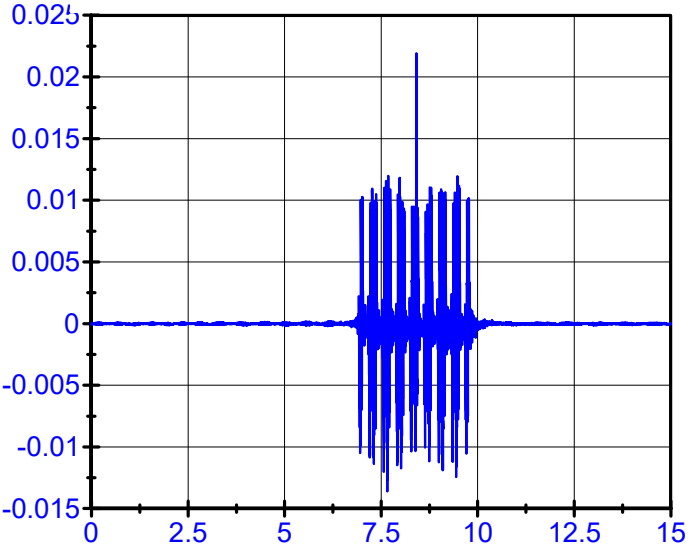

01\06\16 21:49:46

Sleeper Geophones
LPF 150Hz

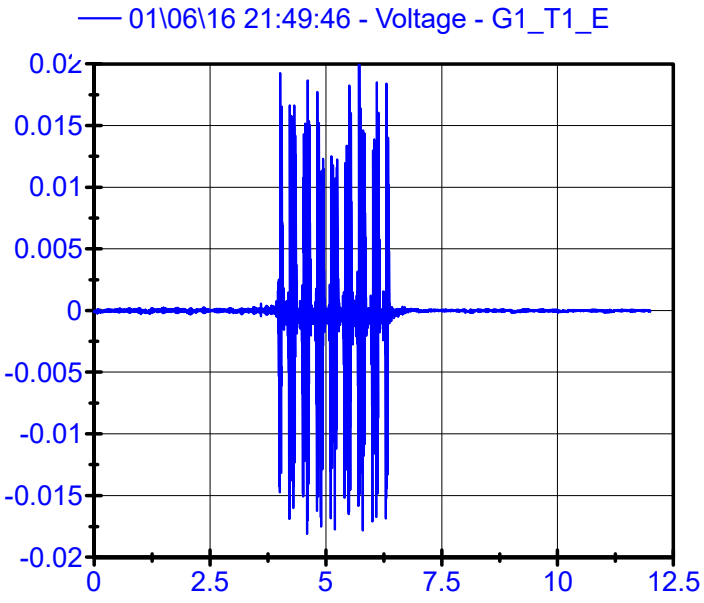

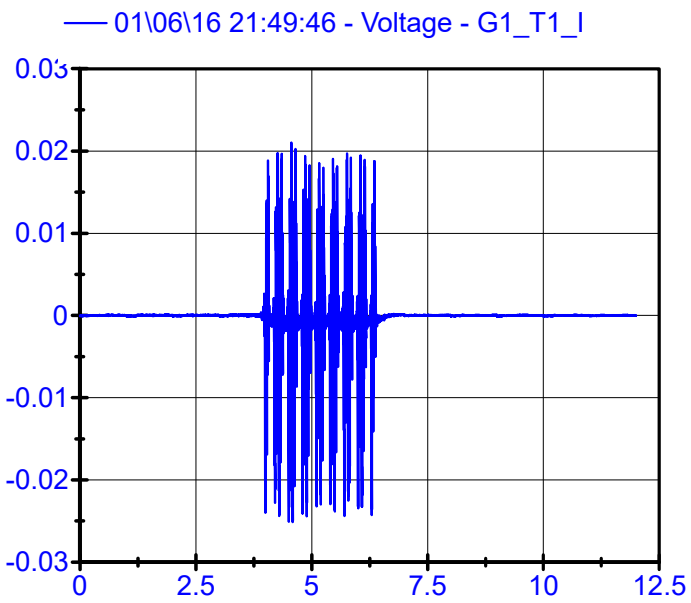

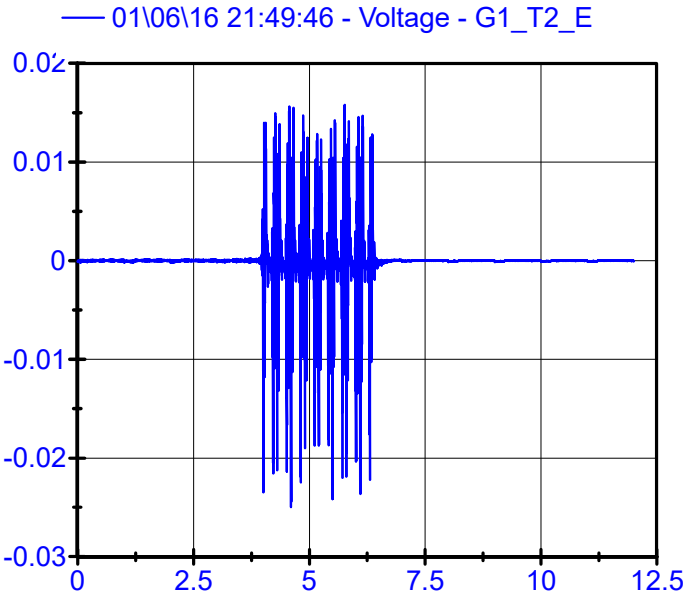

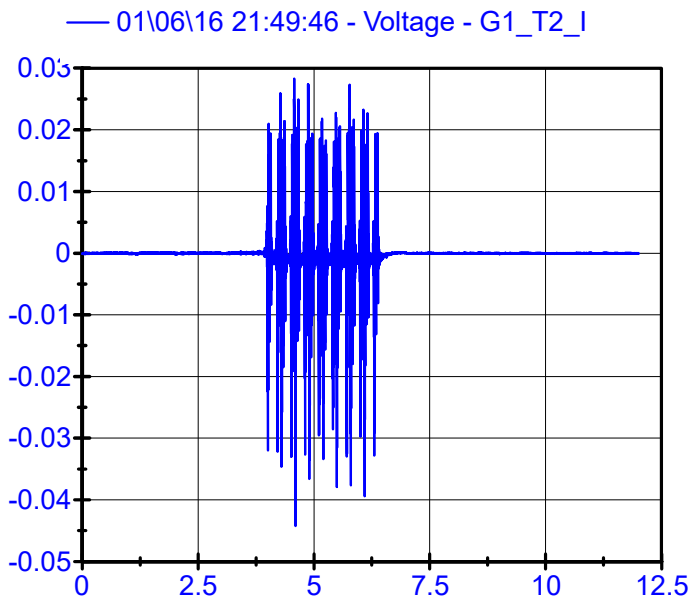

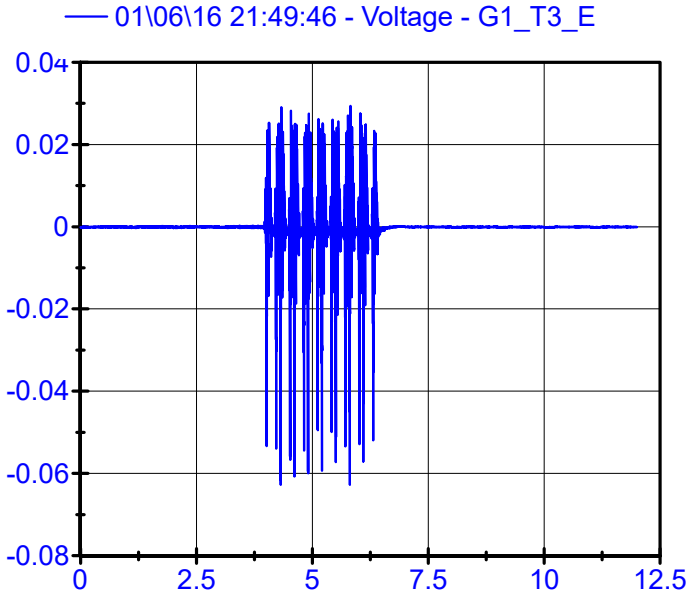

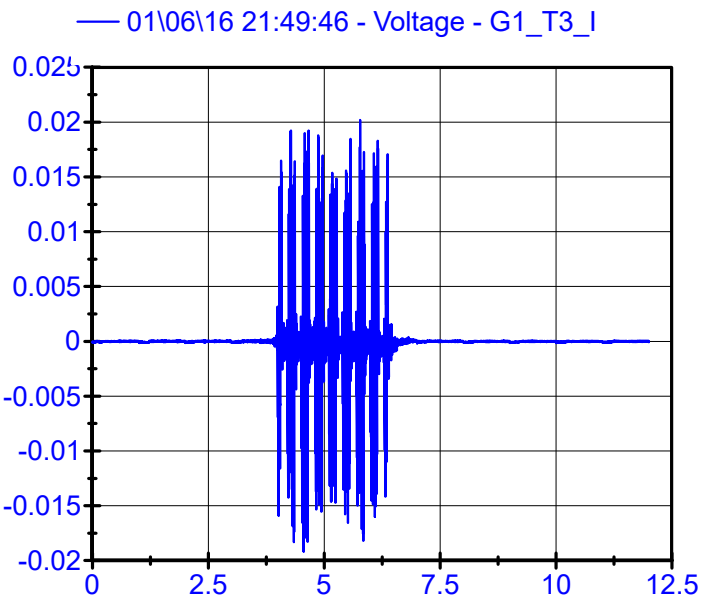

RAIL VELOCITY

RAIL GEOPHONES

NOTES:

Units of Y axle are “m/s” for all the plots belonging to rail velocity.

A Low Pass Filter of 90Hz has been applied to all raw signals.

01\06\16 06:31:45

Rail Geophones
LPF 90Hz

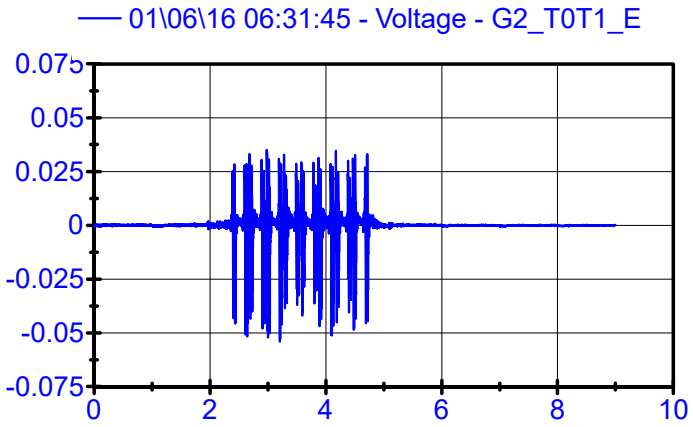

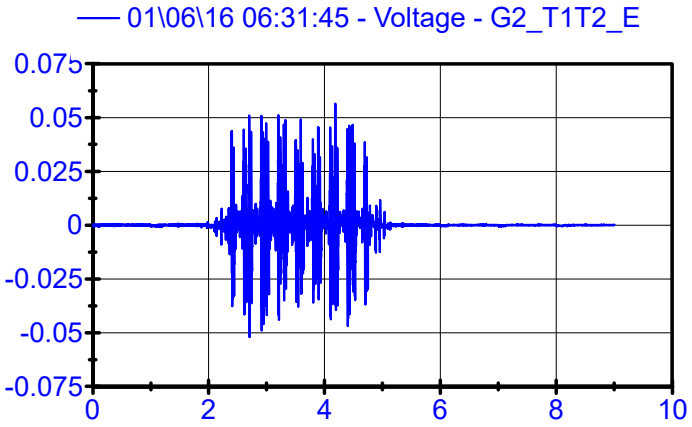

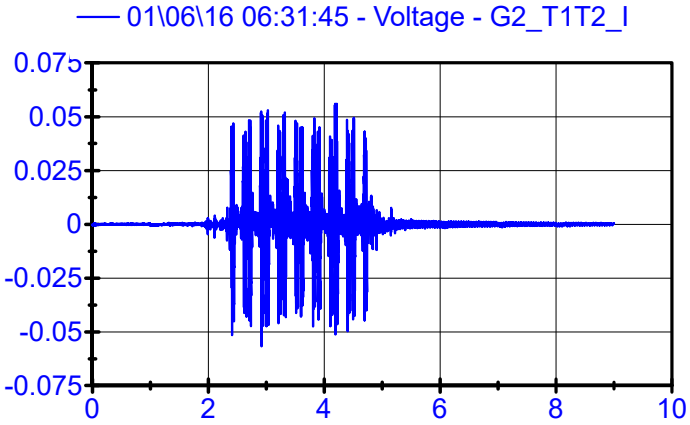

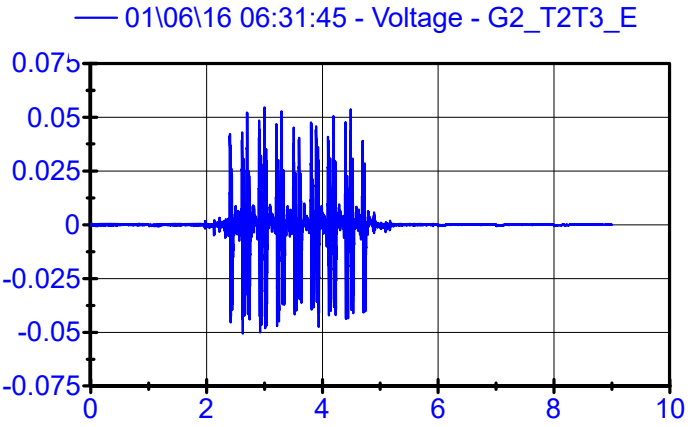

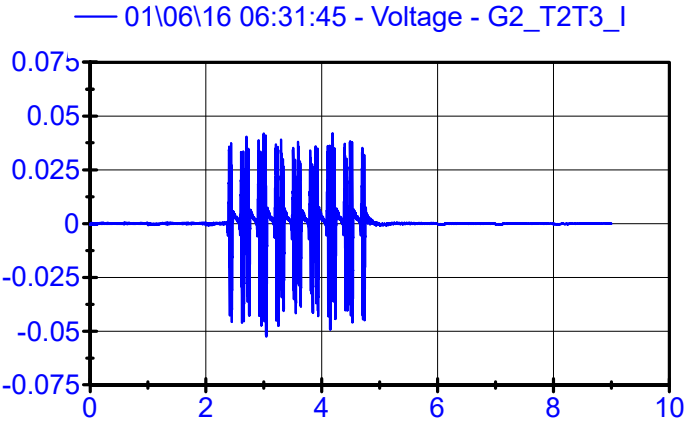

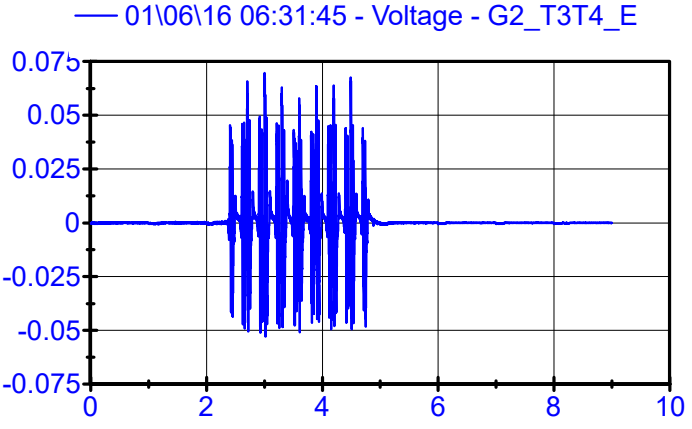

01\06\16 06:52:39

Rail Geophones
LPF 90Hz

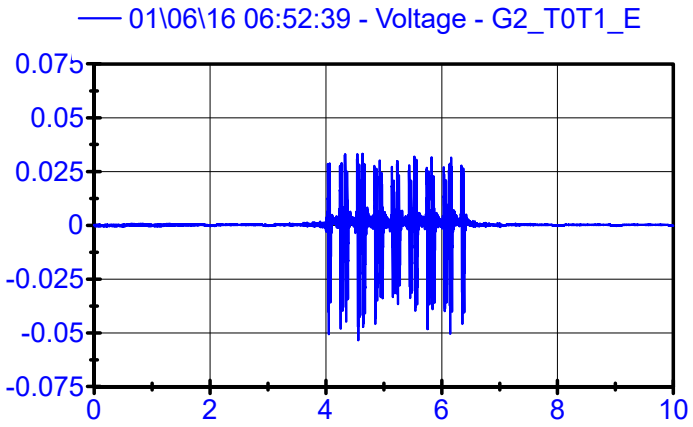

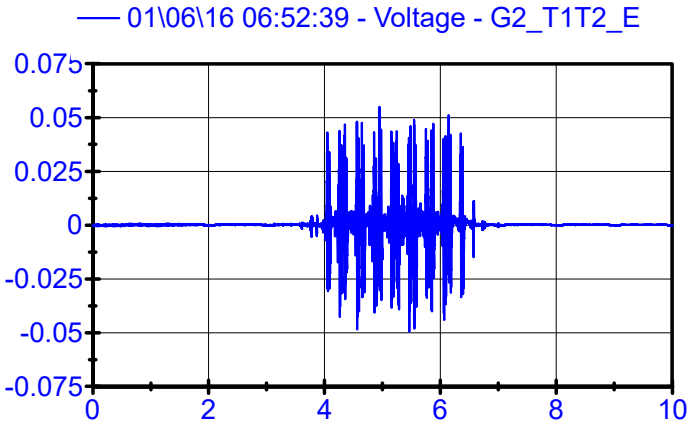

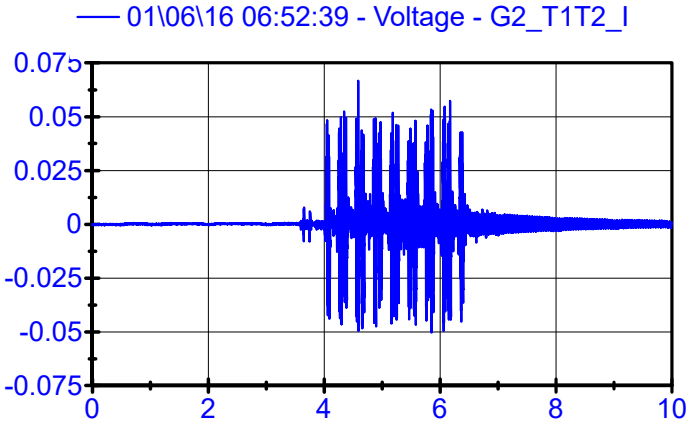

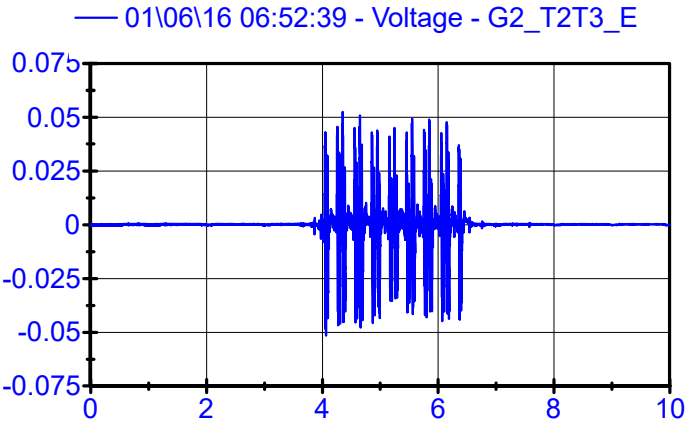

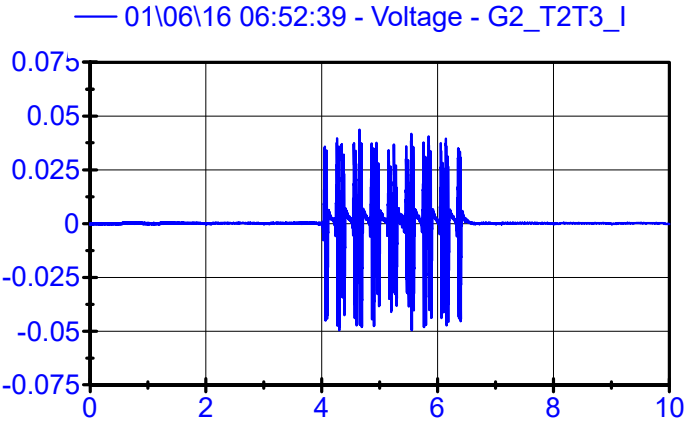

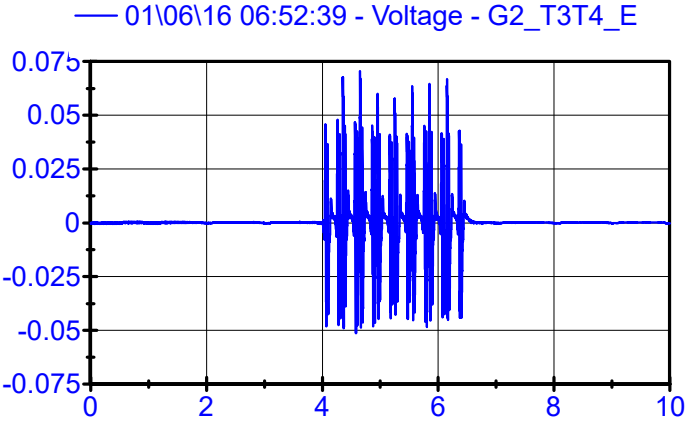

01\06\16 07:21:52

Rail Geophones
LPF 90Hz

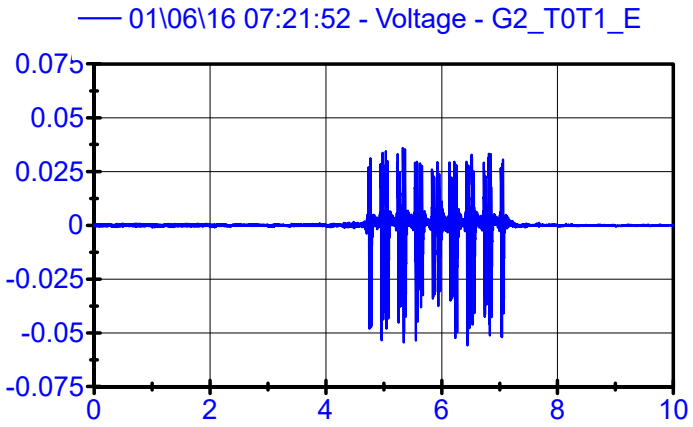

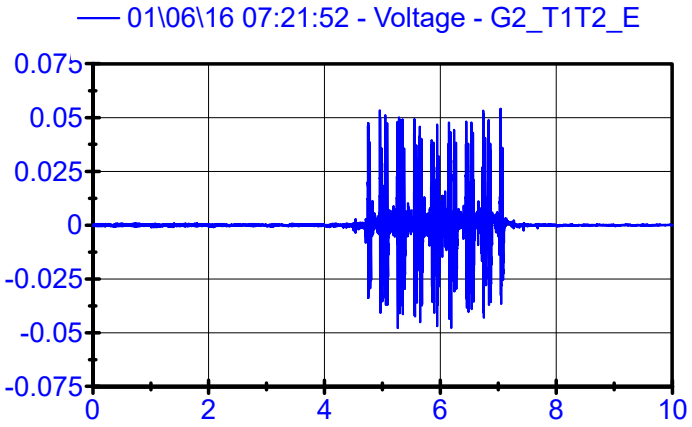

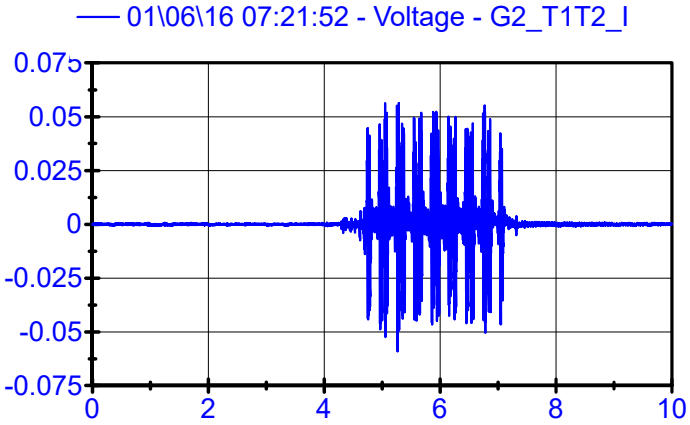

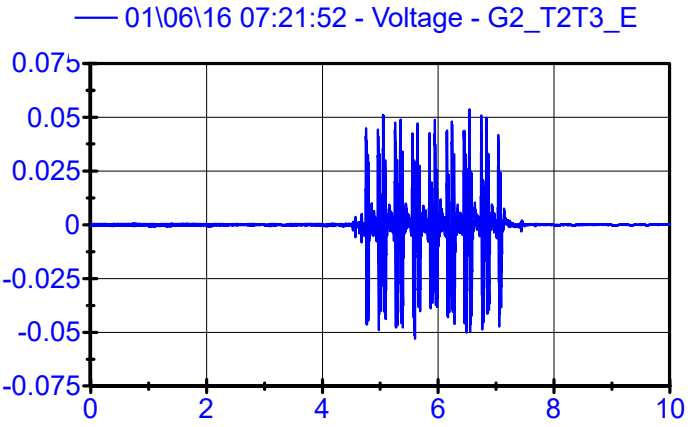

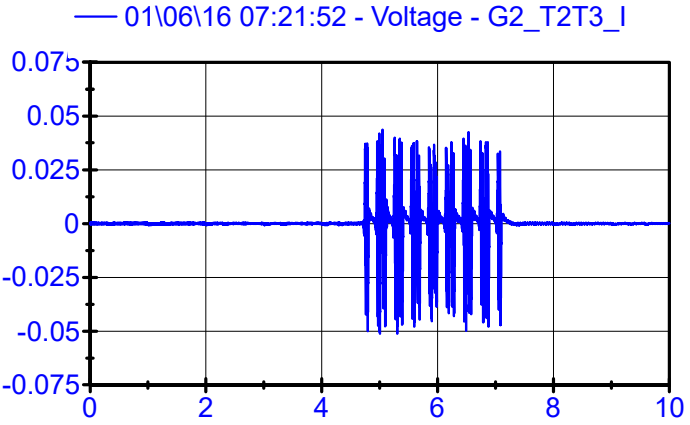

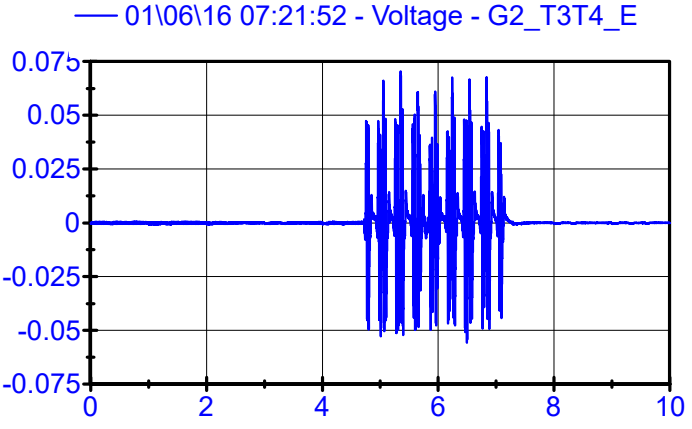

01\06\16 07:41:25

Rail Geophones
LPF 90Hz

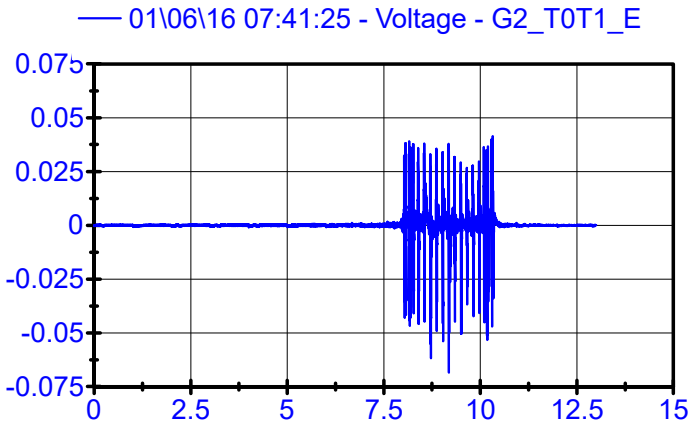

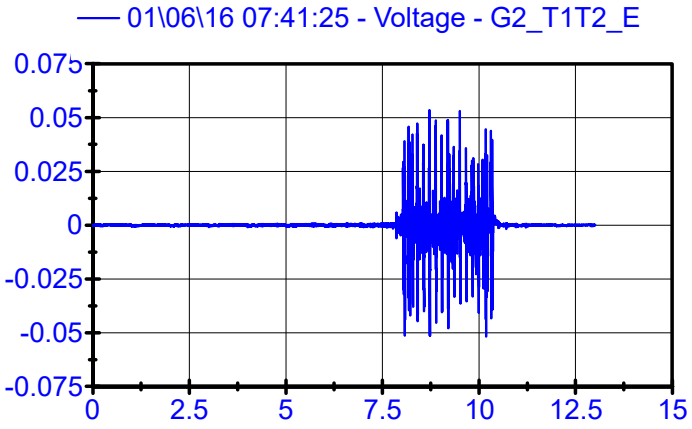

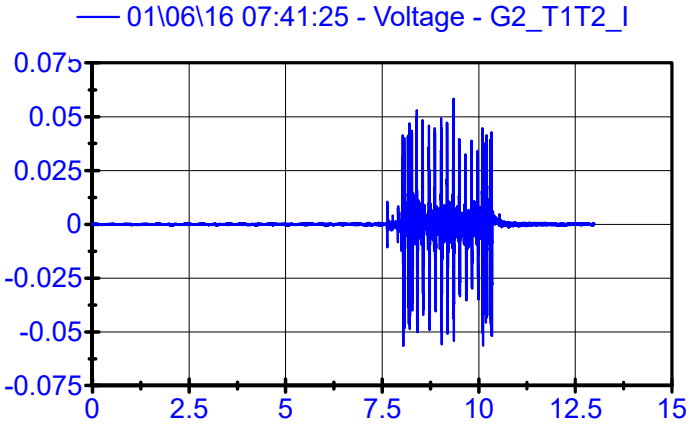

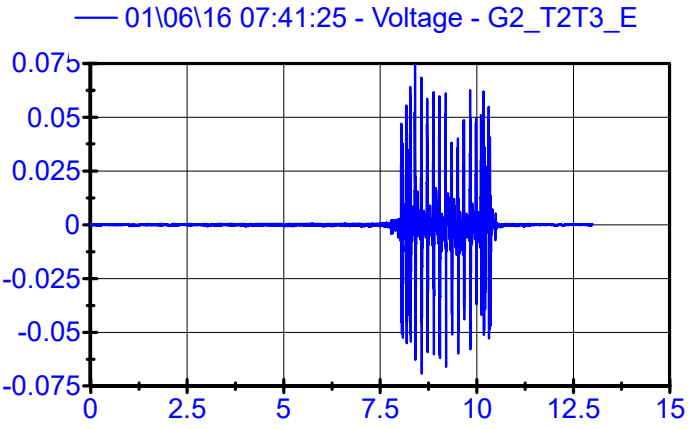

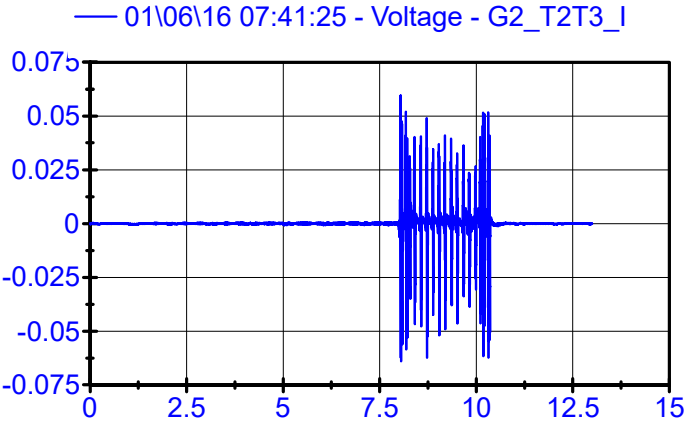

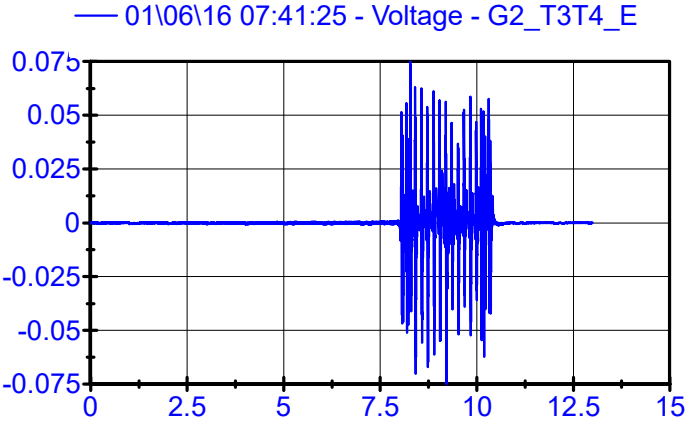

01\06\16 07:56:37

Rail Geophones
LPF 90Hz

01\06\16 07:56:37 - Voltage - G2_T0T1_E

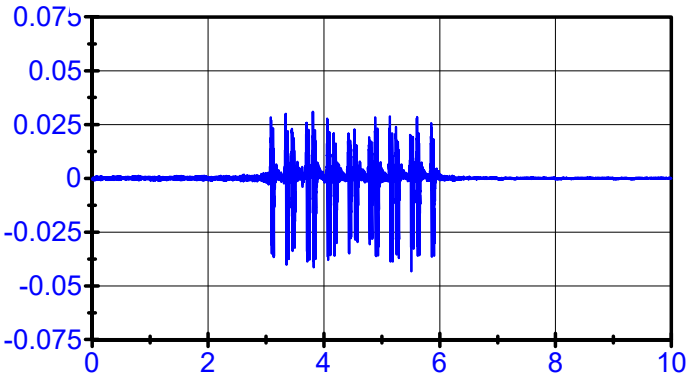

01\06\16 07:56:37 - Voltage - G2_T1T2_E

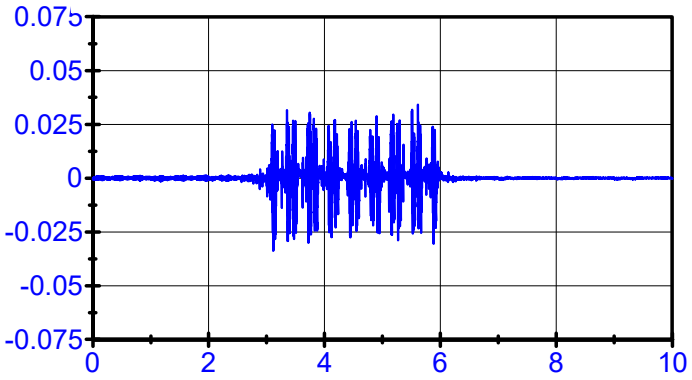

01\06\16 07:56:37 - Voltage - G2_T1T2_I

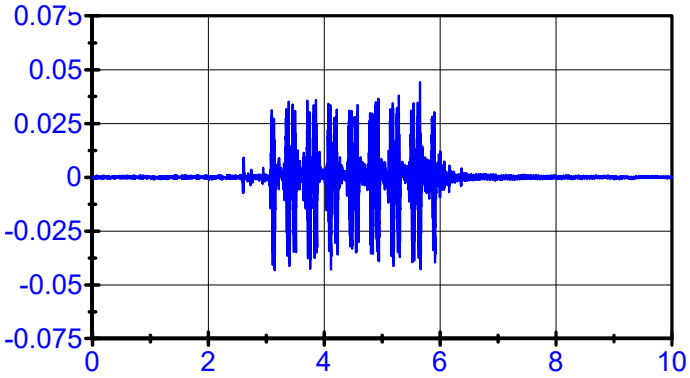

01\06\16 07:56:37 - Voltage - G2_T2T3_E

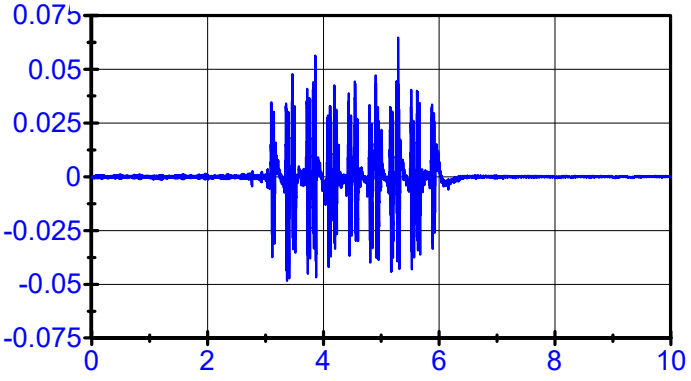

01\06\16 07:56:37 - Voltage - G2_T2T3_I

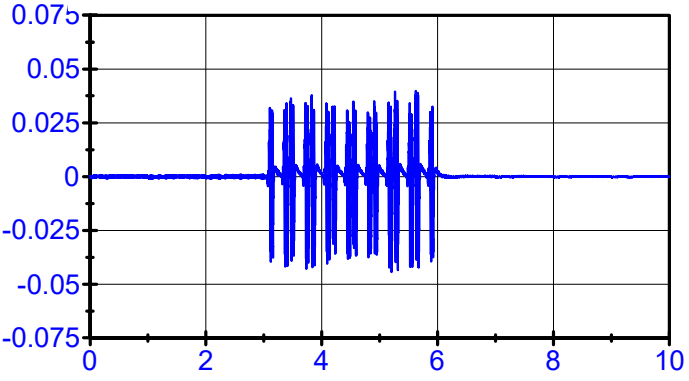

01\06\16 07:56:37 - Voltage - G2_T3T4_E

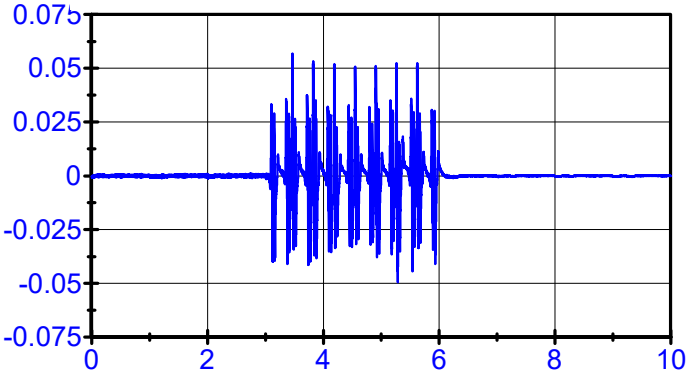

01\06\16 08:01:29

Rail Geophones
LPF 90Hz

01\06\16 08:01:29 - Voltage - G2_T0T1_E

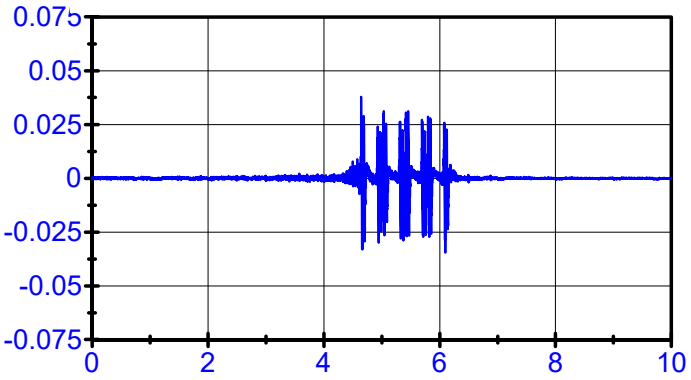

01\06\16 08:01:29 - Voltage - G2_T1T2_E

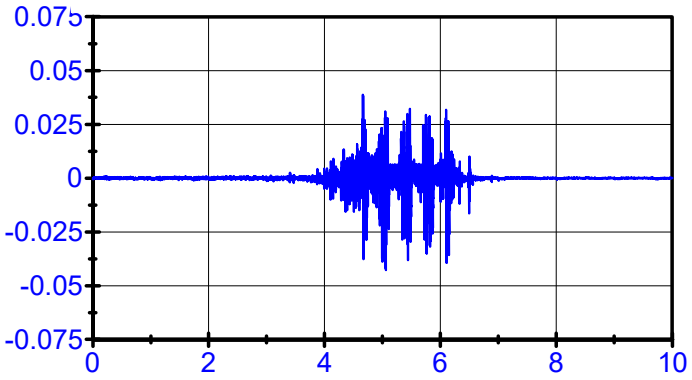

01\06\16 08:01:29 - Voltage - G2_T1T2_I

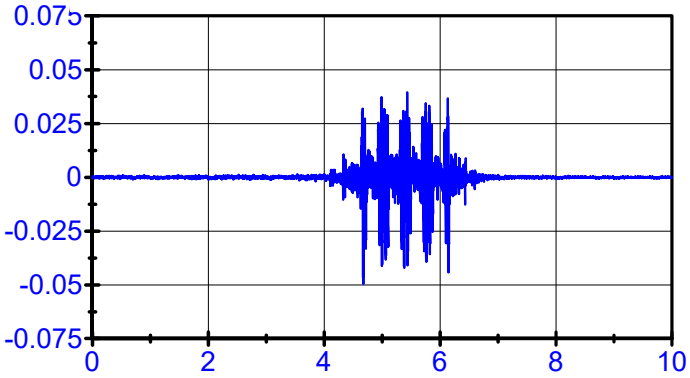

01\06\16 08:01:29 - Voltage - G2_T2T3_E

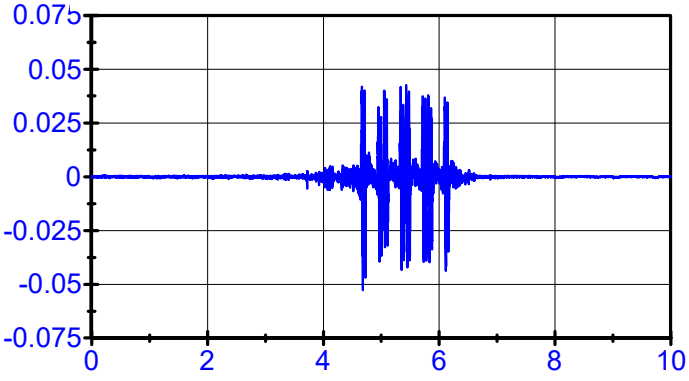

01\06\16 08:01:29 - Voltage - G2_T2T3_I

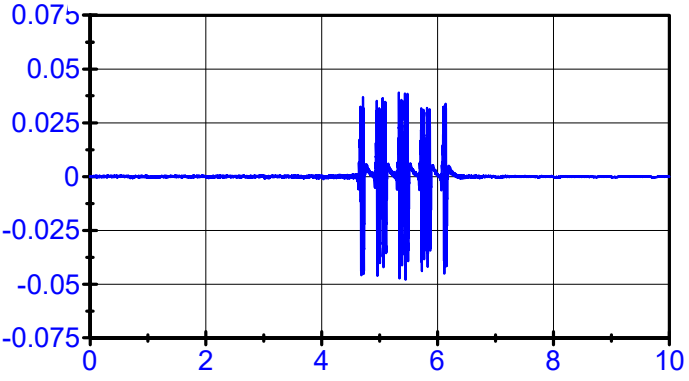

01\06\16 08:01:29 - Voltage - G2_T3T4_E

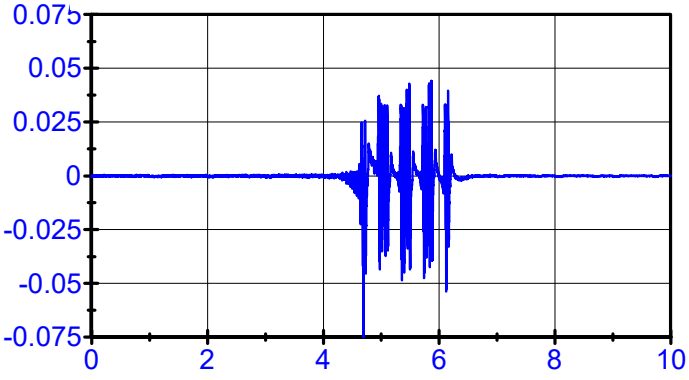

01\06\16 08:21:04

Rail Geophones
LPF 90Hz

01\06\16 08:21:04 - Voltage - G2_T0T1_E

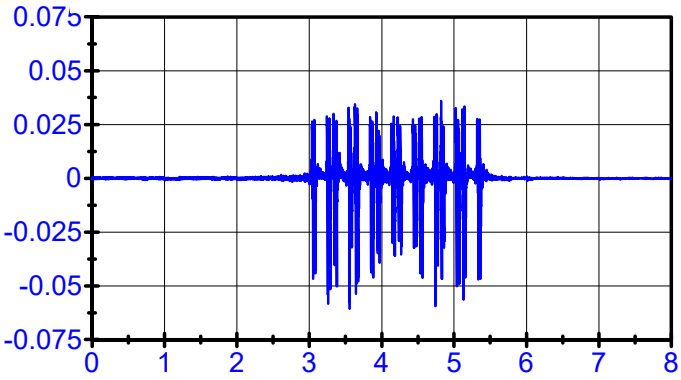

01\06\16 08:21:04 - Voltage - G2_T1T2_E

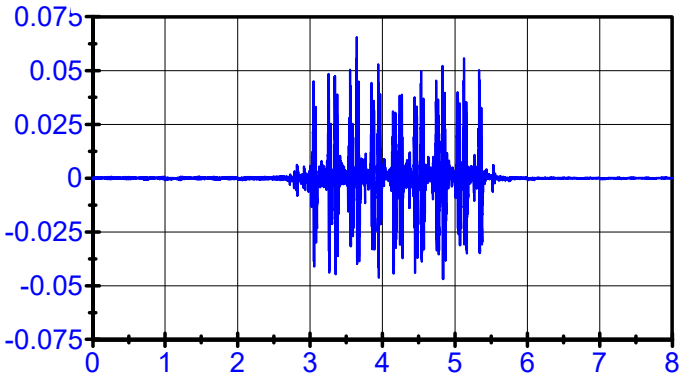

01\06\16 08:21:04 - Voltage - G2_T1T2_I

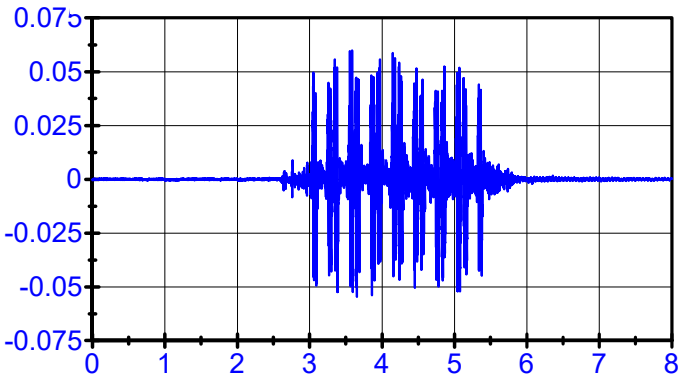

01\06\16 08:21:04 - Voltage - G2_T2T3_E

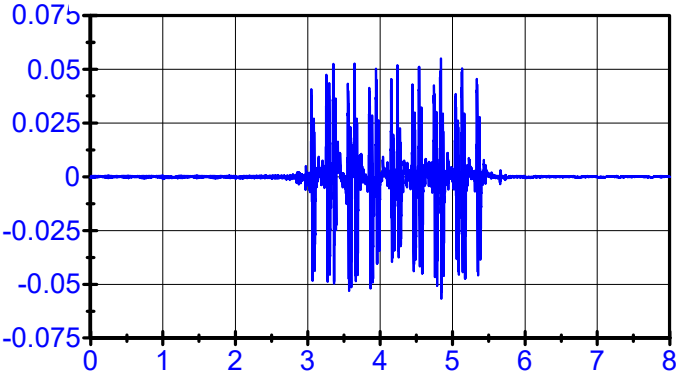

01\06\16 08:21:04 - Voltage - G2_T2T3_I

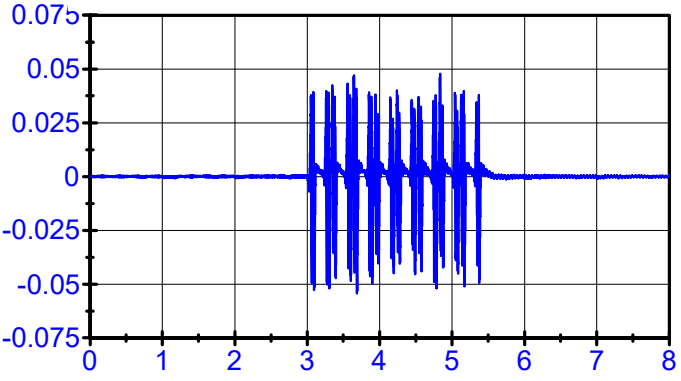

01\06\16 08:21:04 - Voltage - G2_T3T4_E

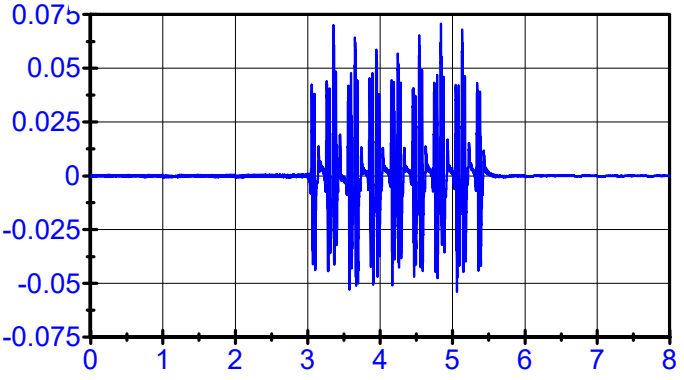

01\06\16 08:42:39

Rail Geophones
LPF 90Hz

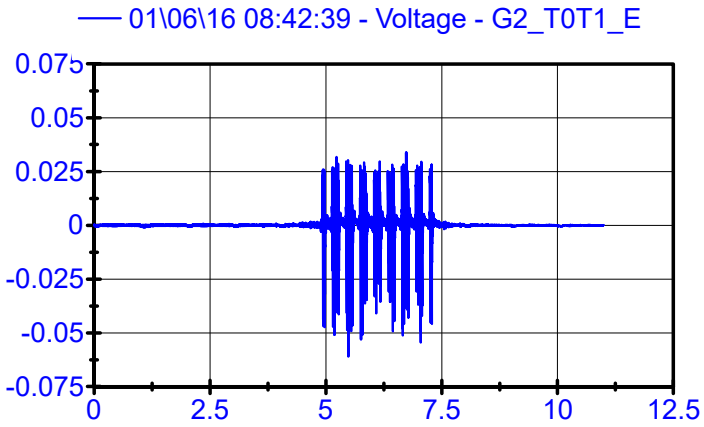

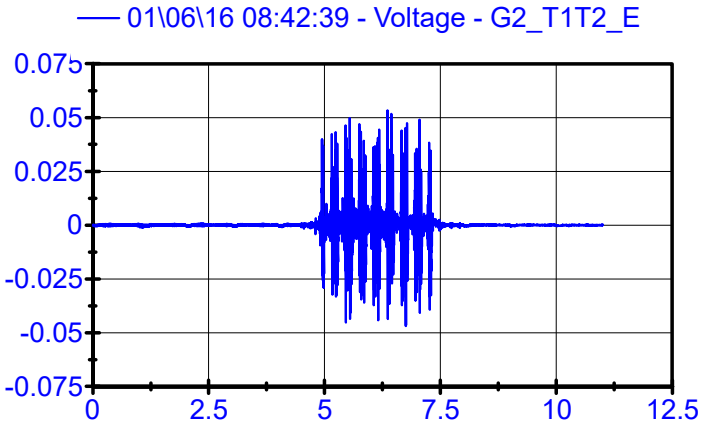

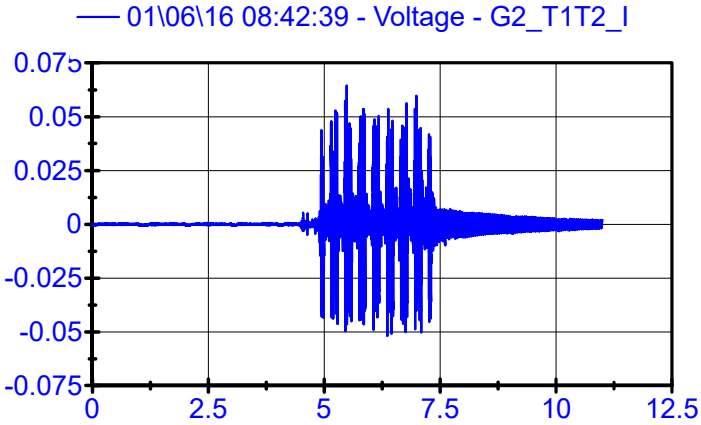

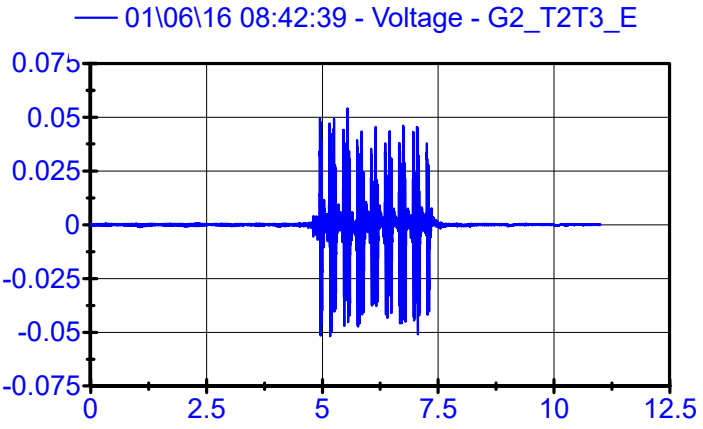

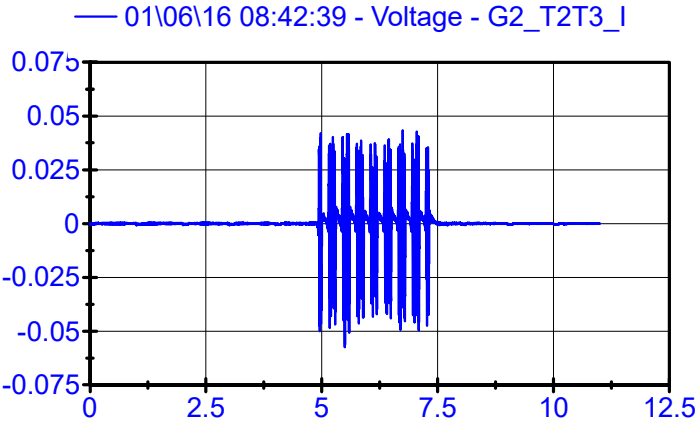

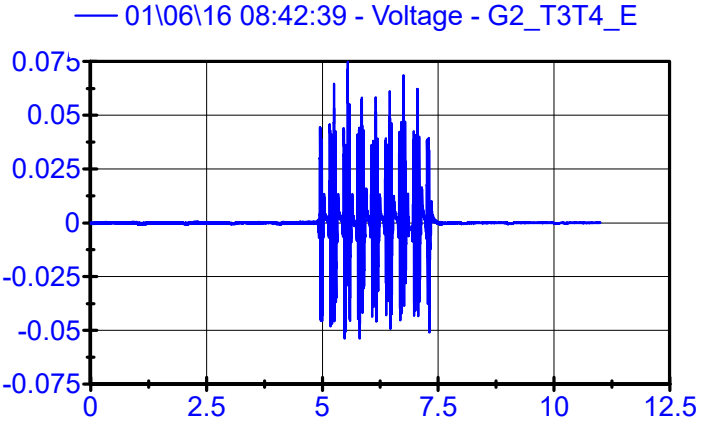

01\06\16 08:52:26

Rail Geophones
LPF 90Hz

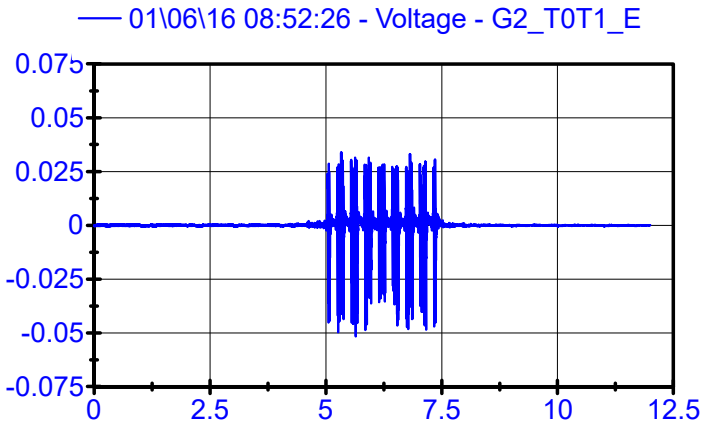

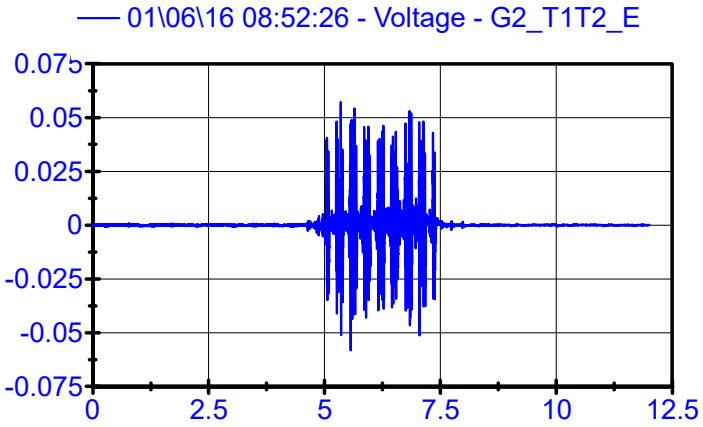

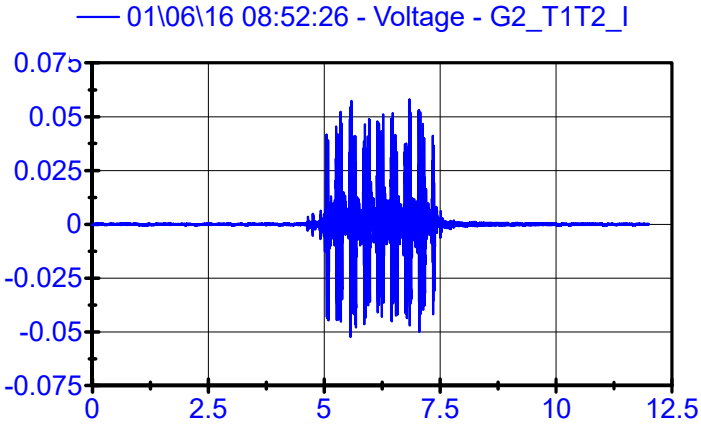

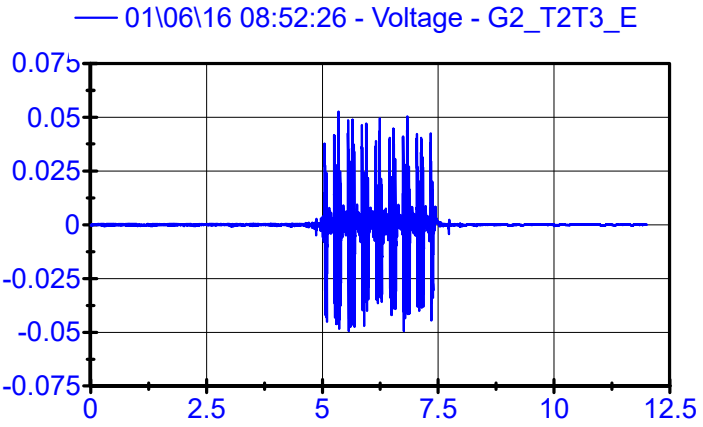

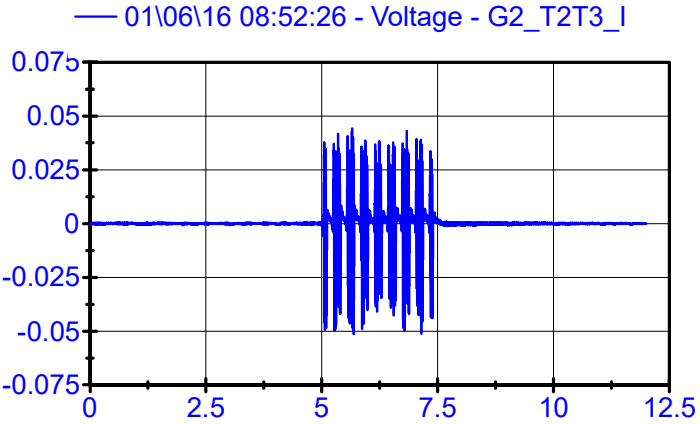

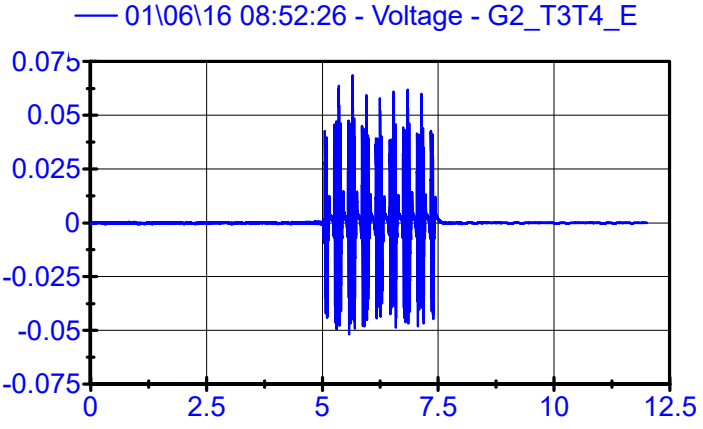

01\06\16 09:23:16

Rail Geophones
LPF 90Hz

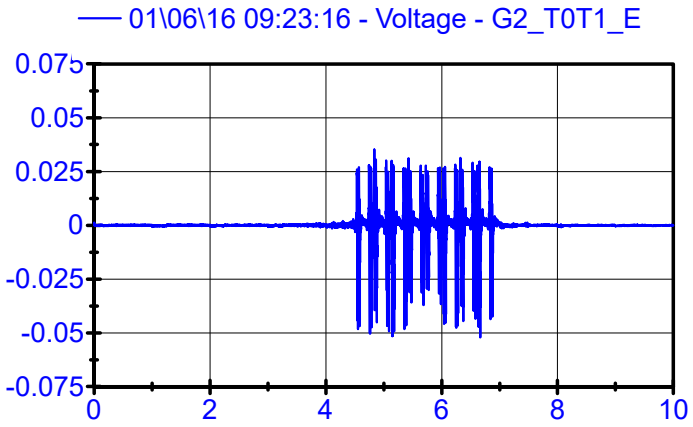

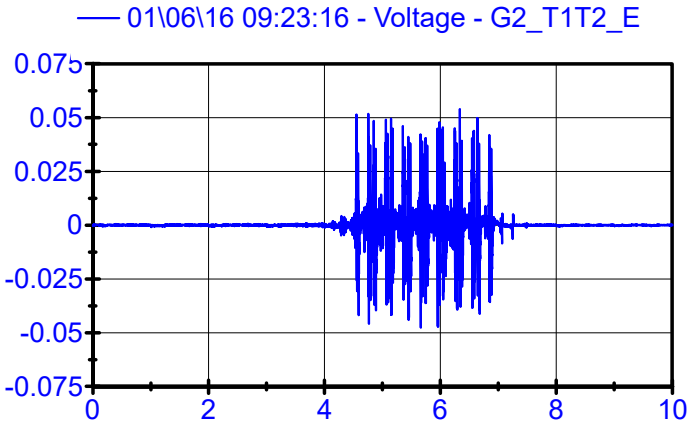

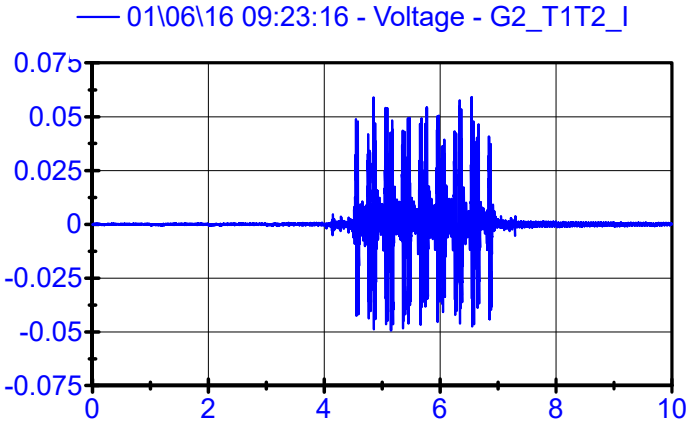

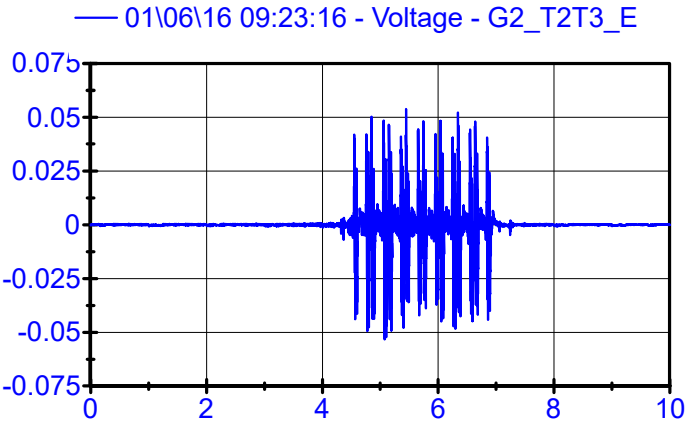

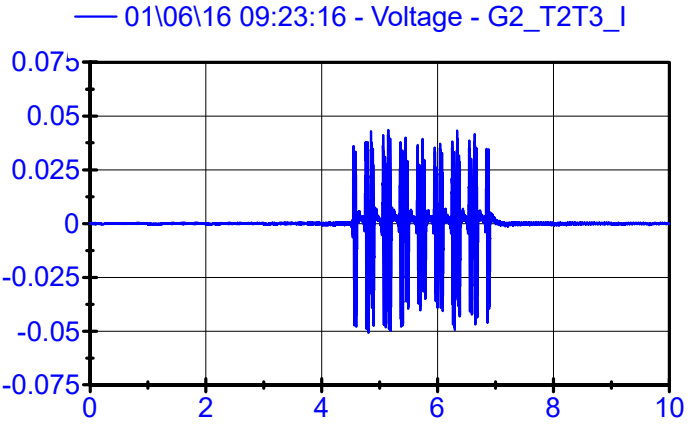

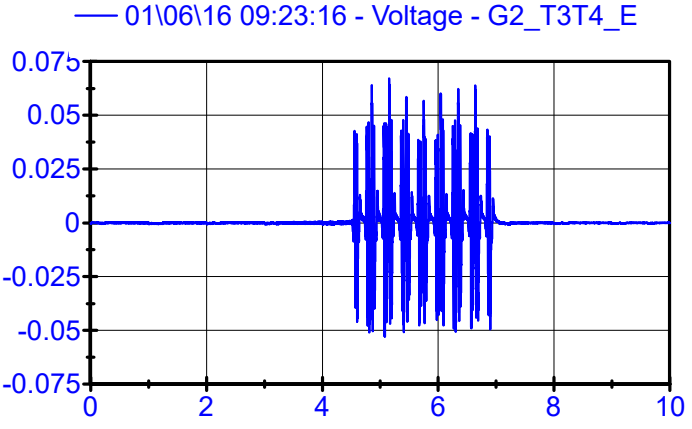

01\06\16 09:52:01

Rail Geophones
LPF 90Hz

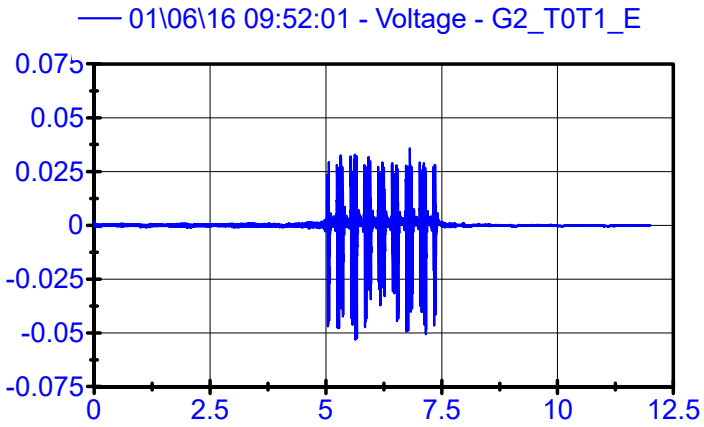

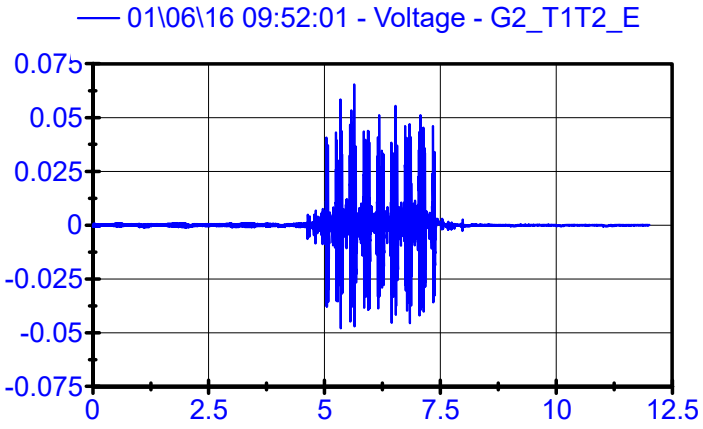

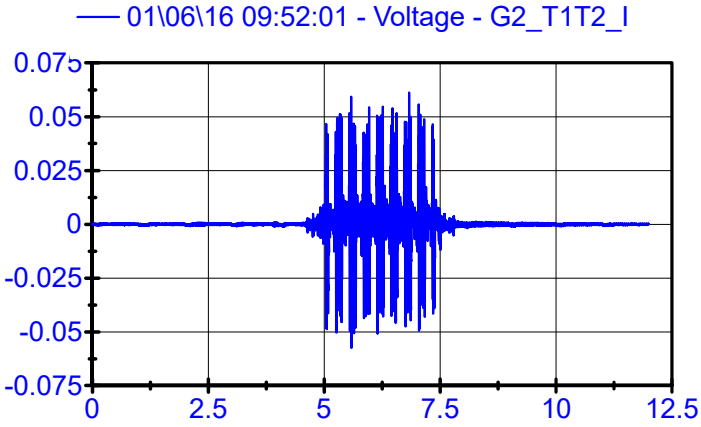

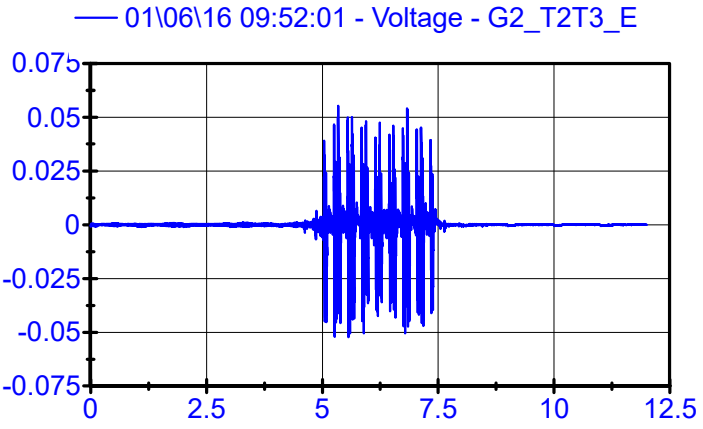

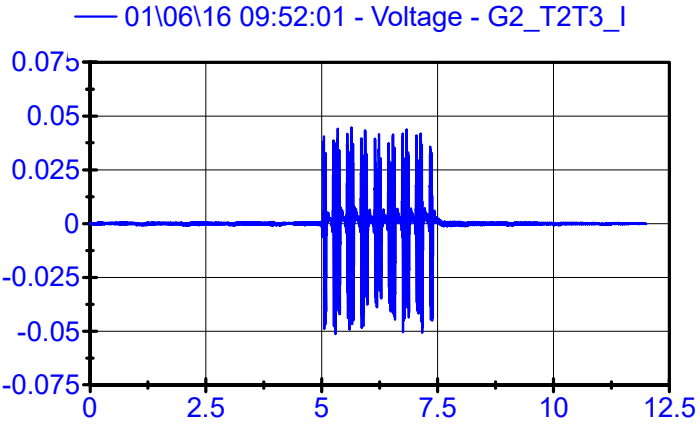

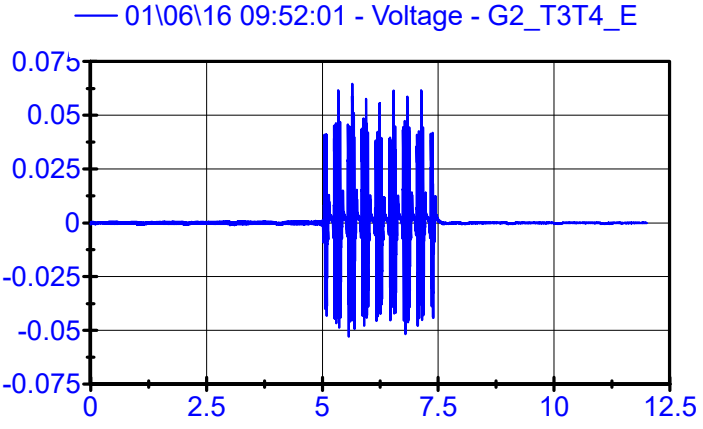

01\06\16 10:53:28

Rail Geophones
LPF 90Hz

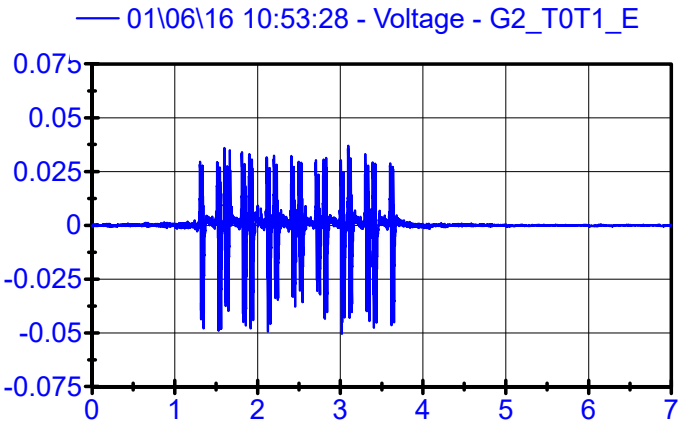

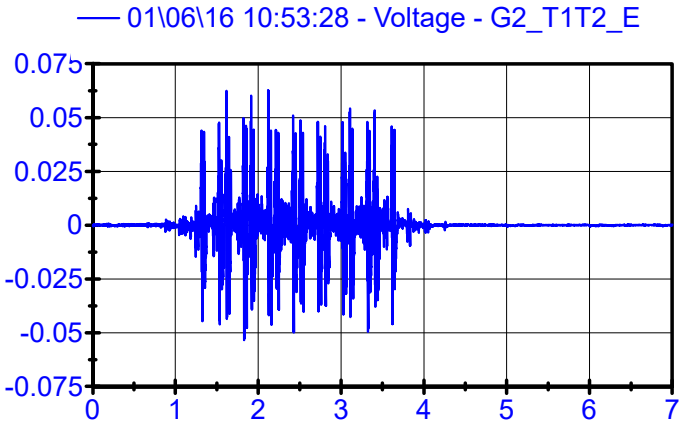

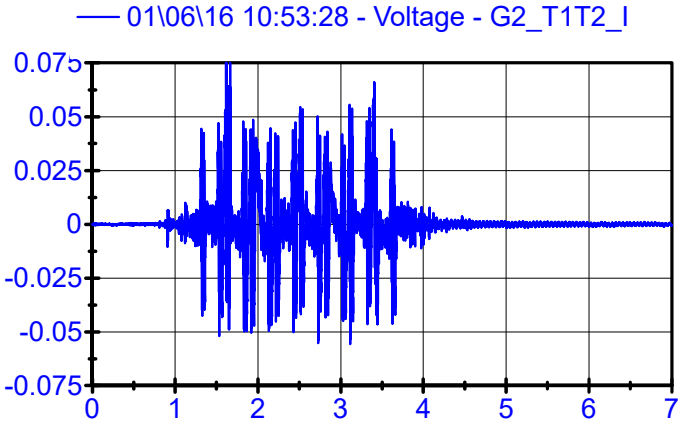

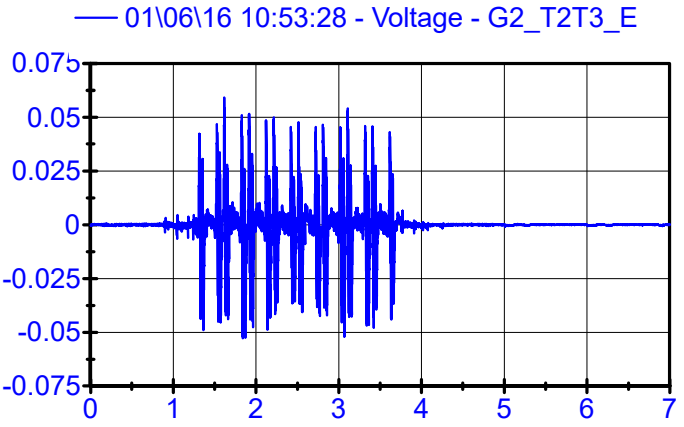

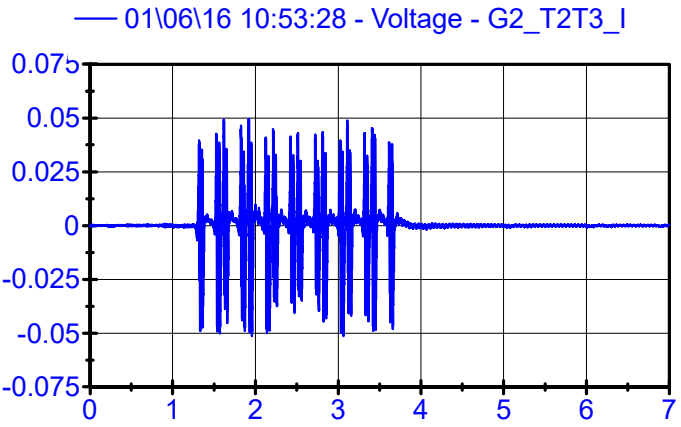

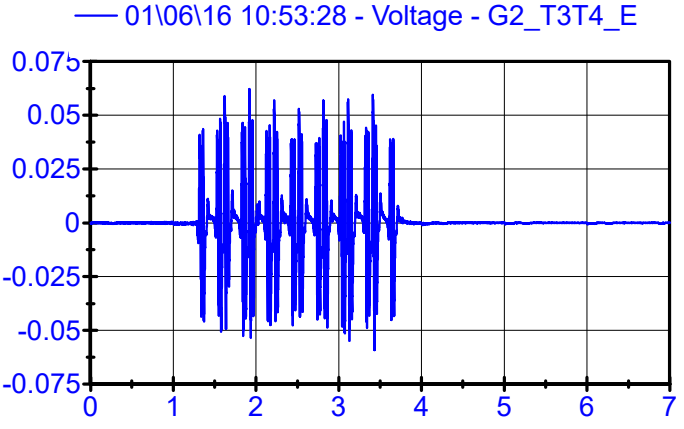

01\06\16 11:35:54

Rail Geophones
LPF 90Hz

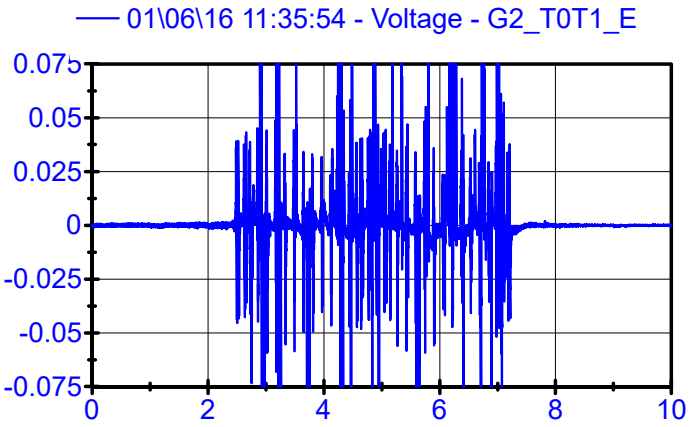

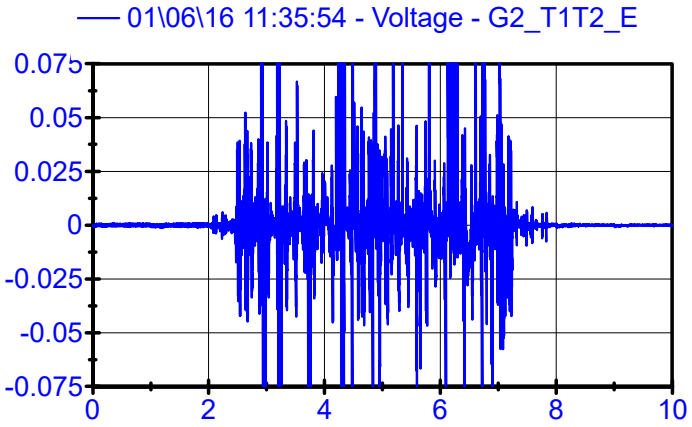

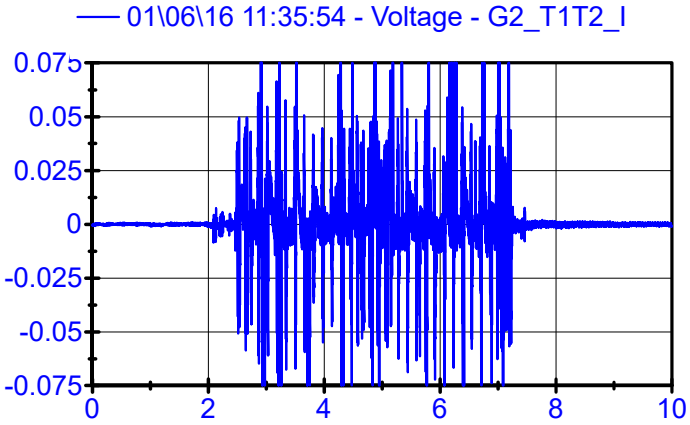

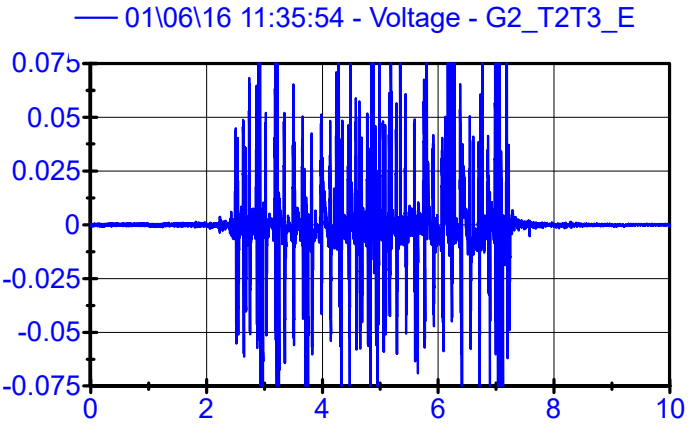

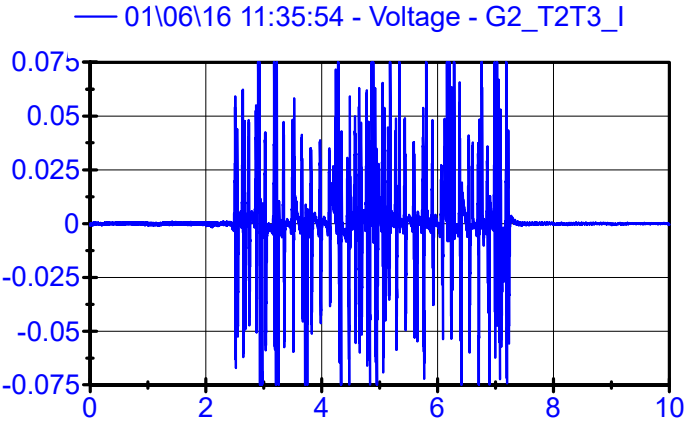

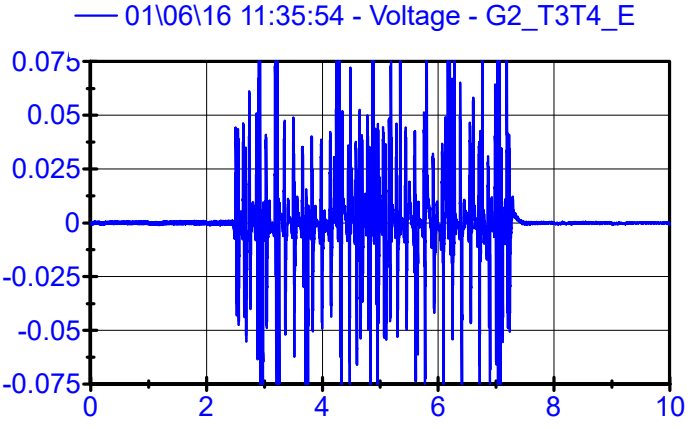

01\06\16 11:53:47

Rail Geophones
LPF 90Hz

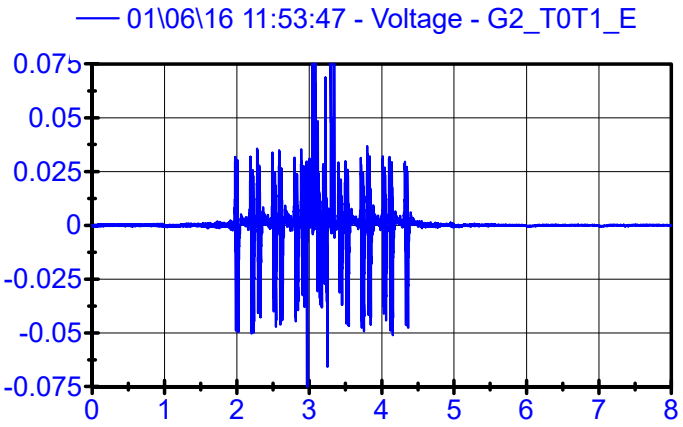

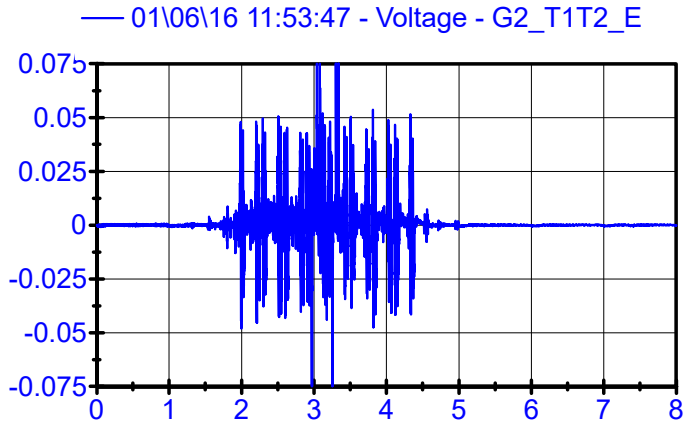

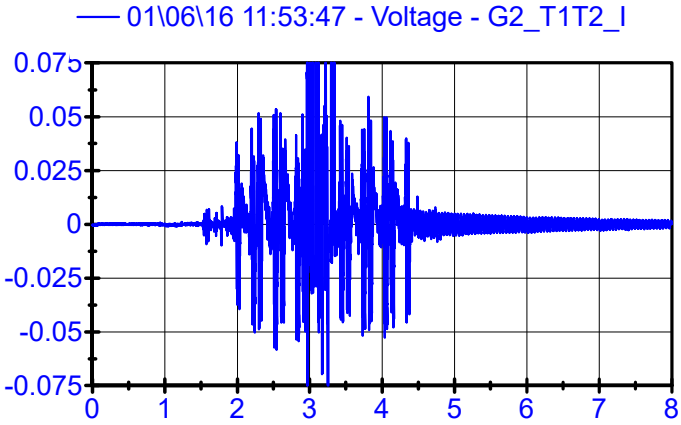

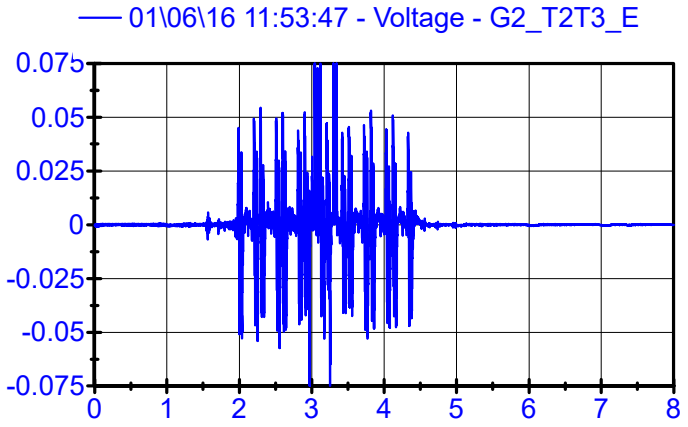

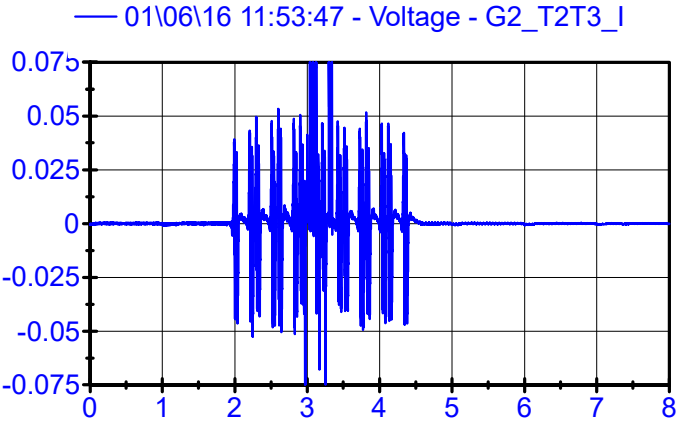

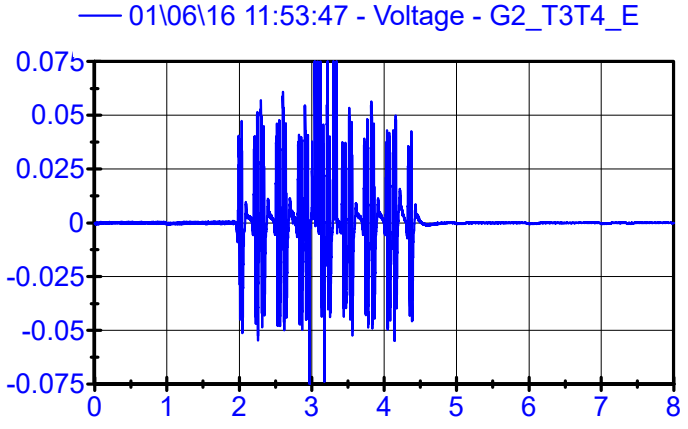

01\06\16 12:07:44

Rail Geophones
LPF 90Hz

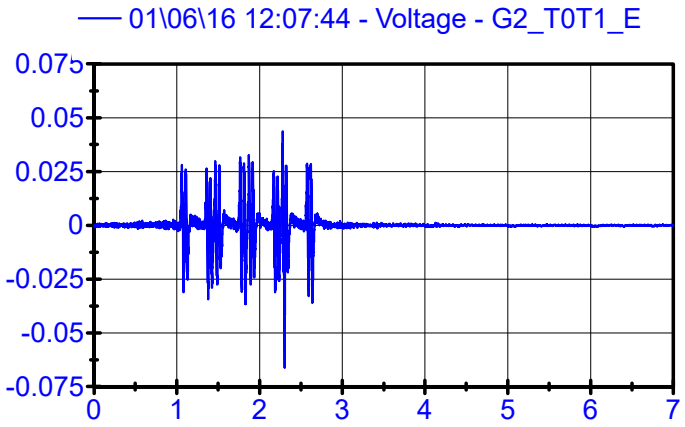

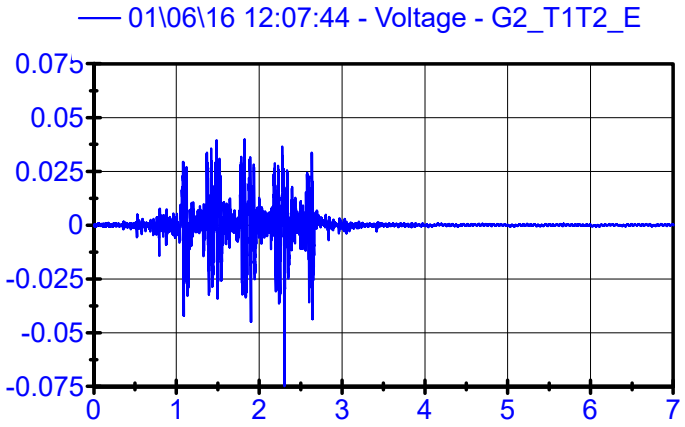

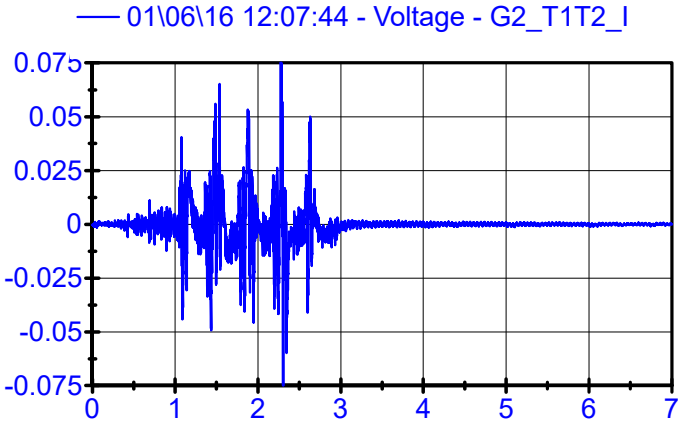

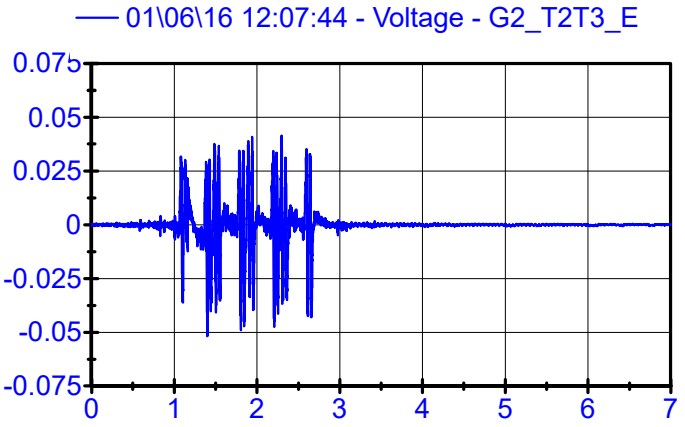

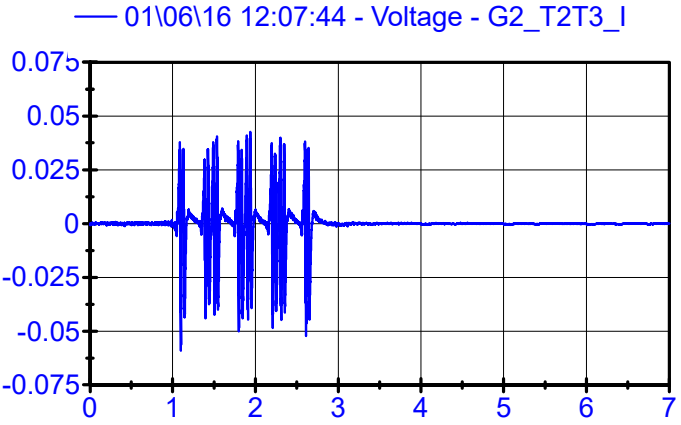

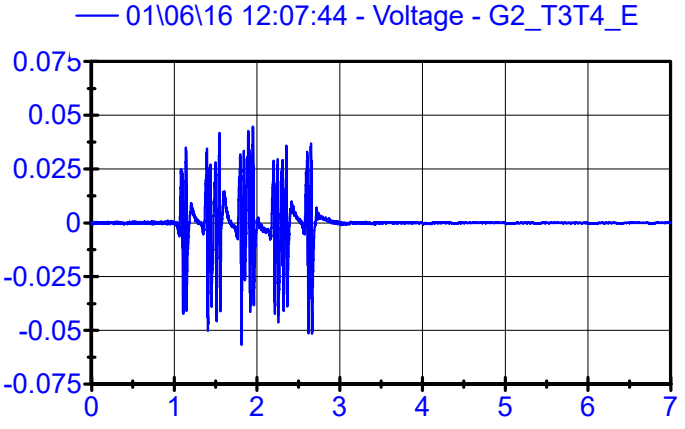

01\06\16 12:51:19

Rail Geophones
LPF 90Hz

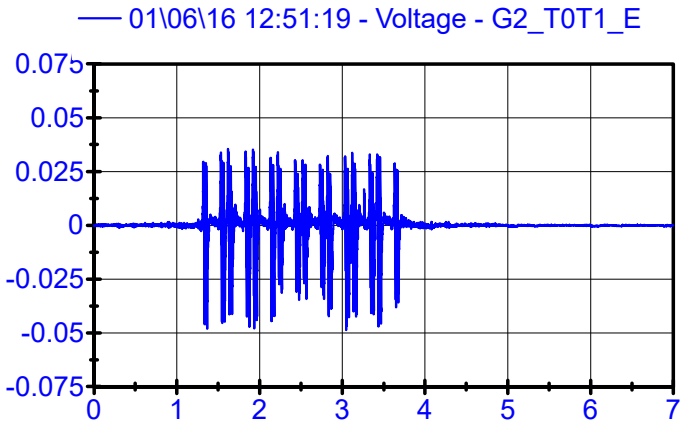

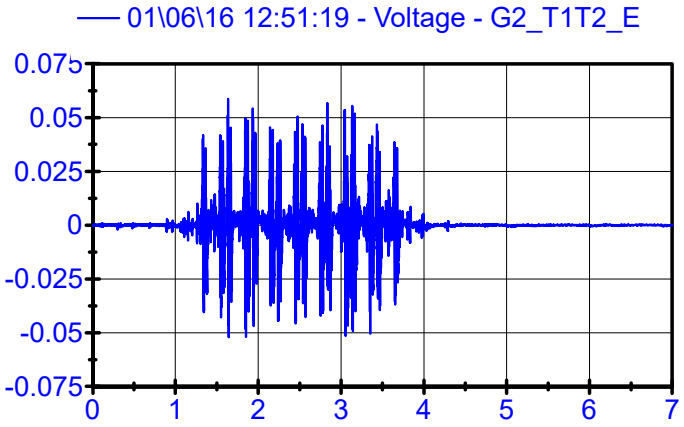

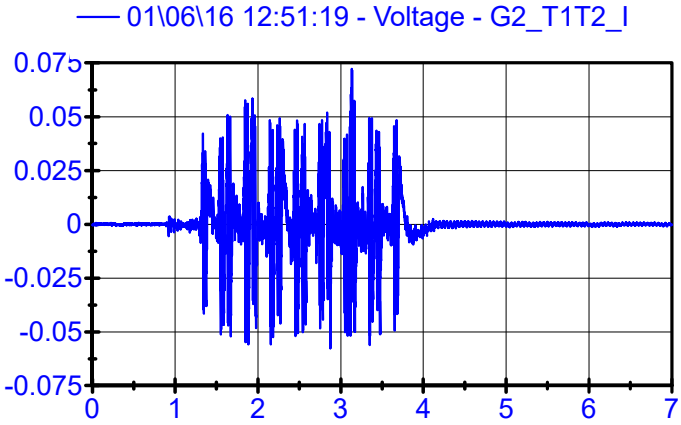

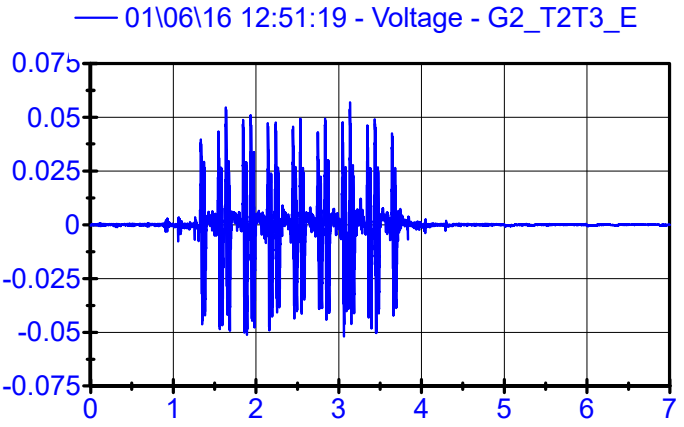

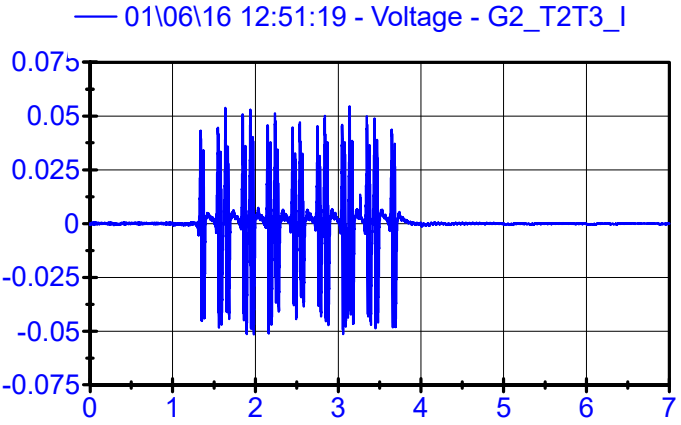

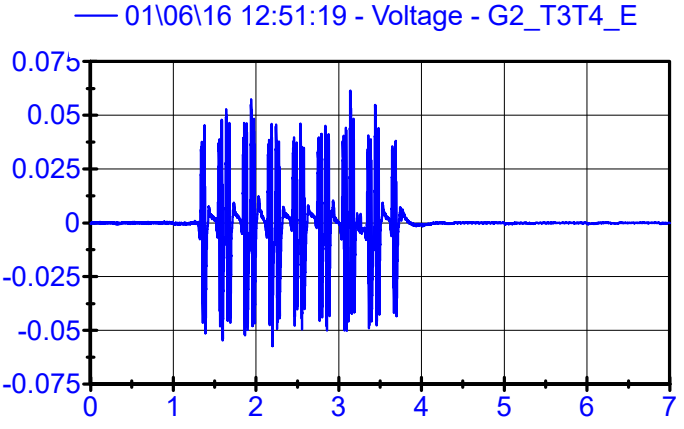

01\06\16 13:55:11

Rail Geophones
LPF 90Hz

01\06\16 13:55:11 - Voltage - G2_T0T1_E

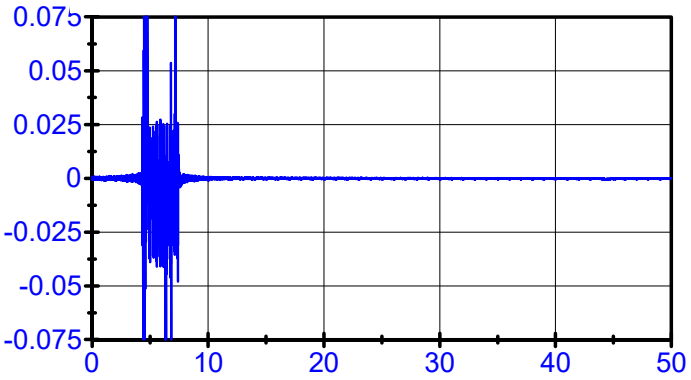

01\06\16 13:55:11 - Voltage - G2_T1T2_E

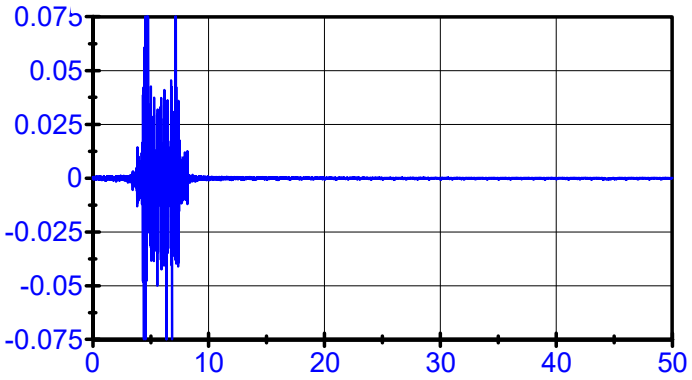

01\06\16 13:55:11 - Voltage - G2_T1T2_I

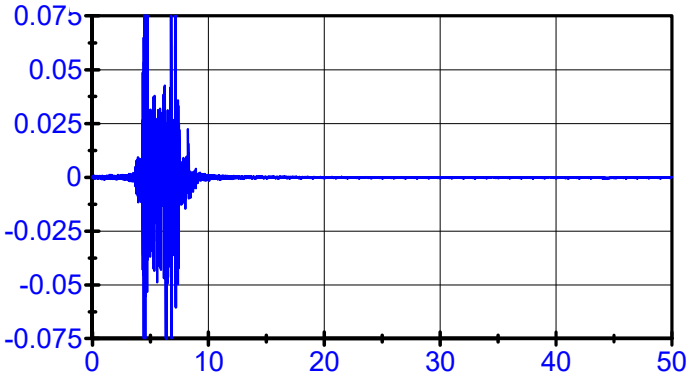

01\06\16 13:55:11 - Voltage - G2_T2T3_E

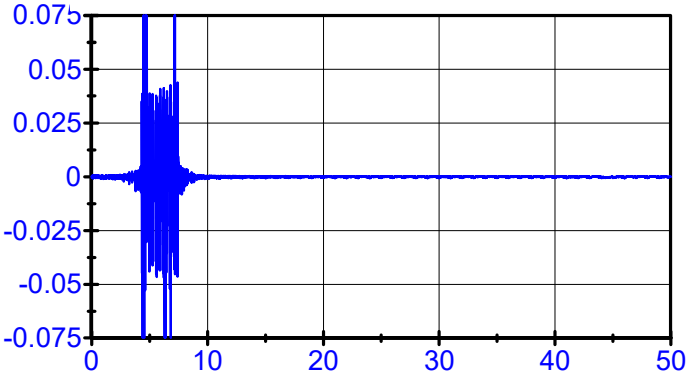

01\06\16 13:55:11 - Voltage - G2_T2T3_I

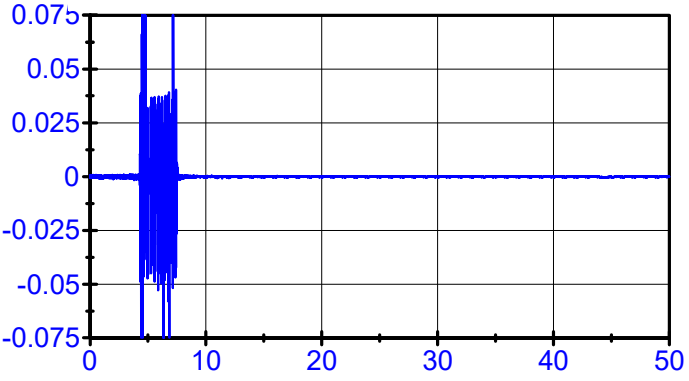

01\06\16 13:55:11 - Voltage - G2_T3T4_E

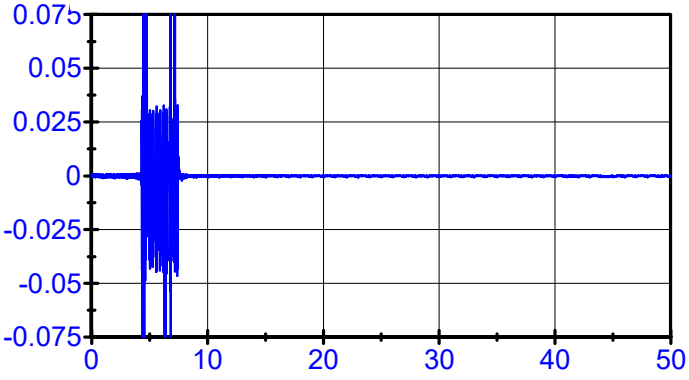

01\06\16 14:21:06

Rail Geophones
LPF 90Hz

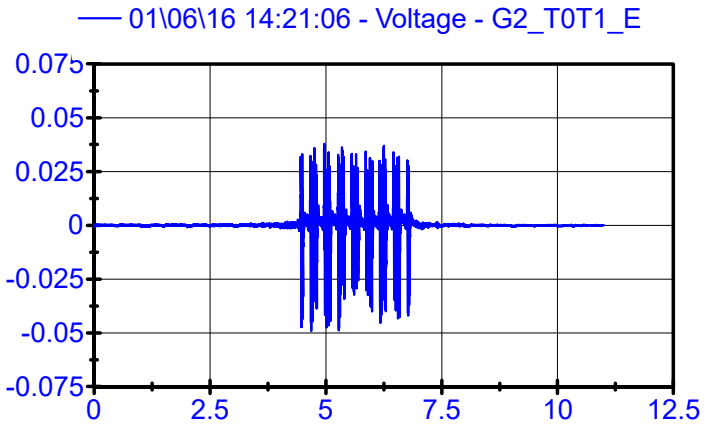

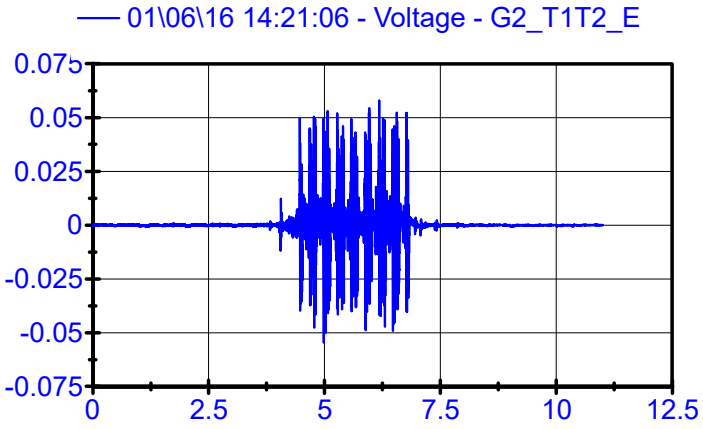

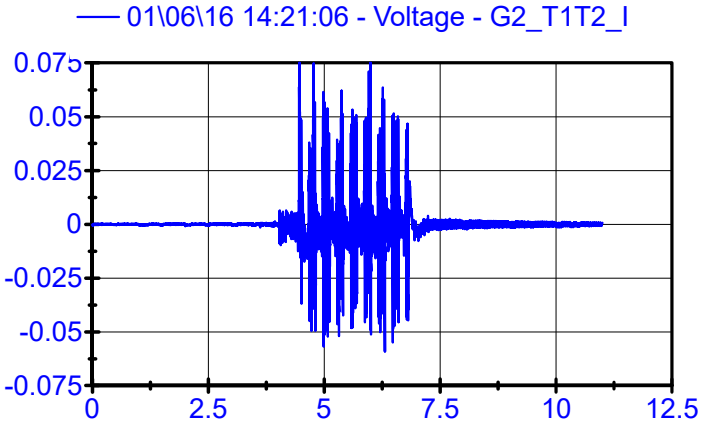

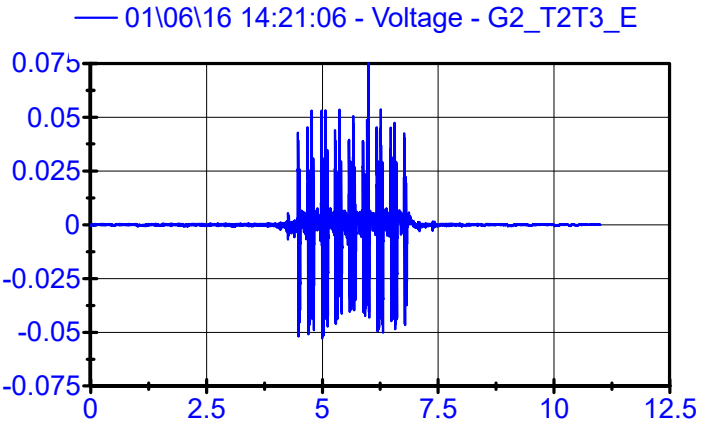

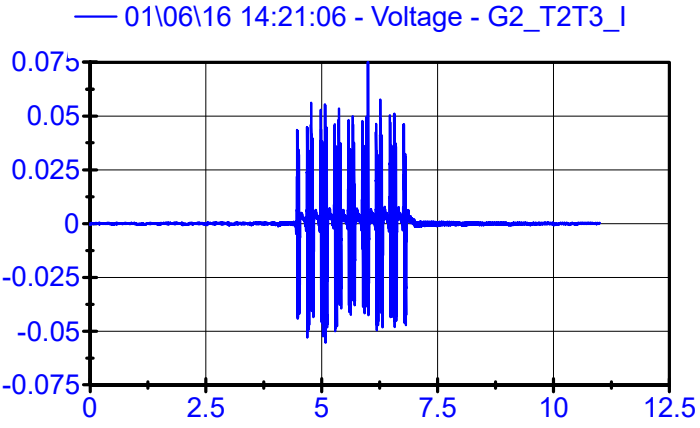

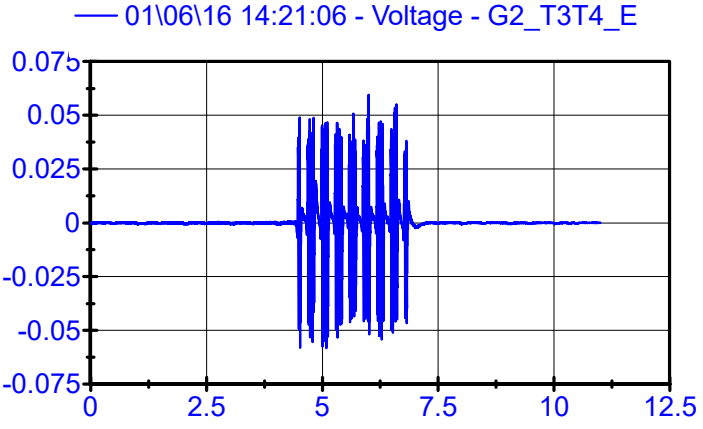

01\06\16 14:52:22

Rail Geophones
LPF 90Hz

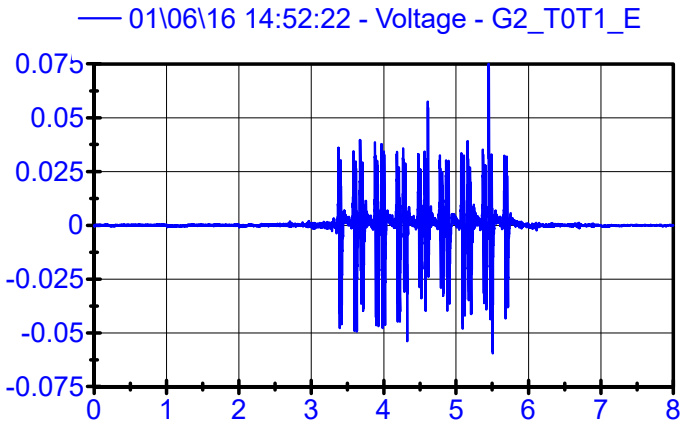

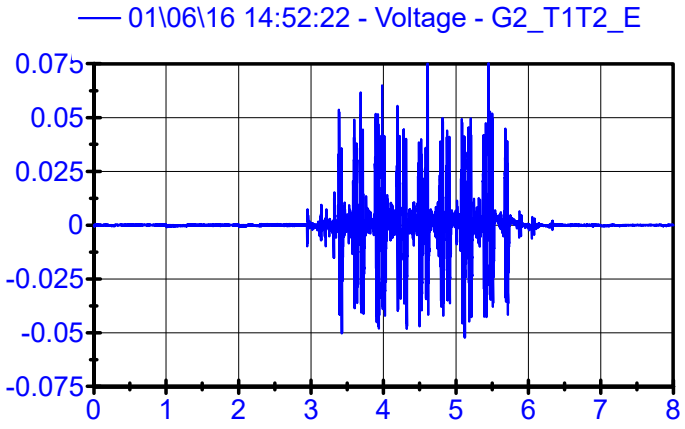

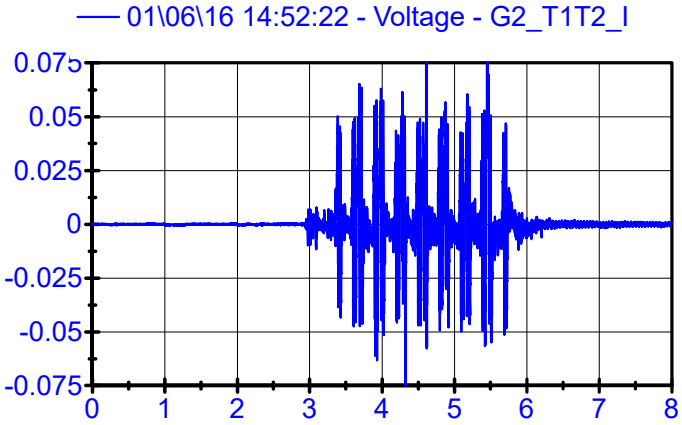

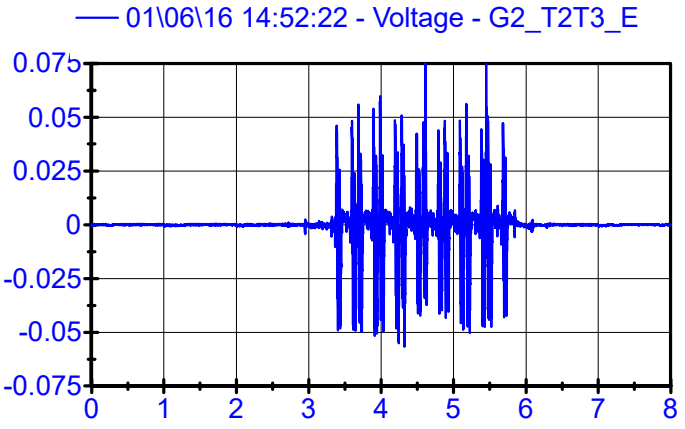

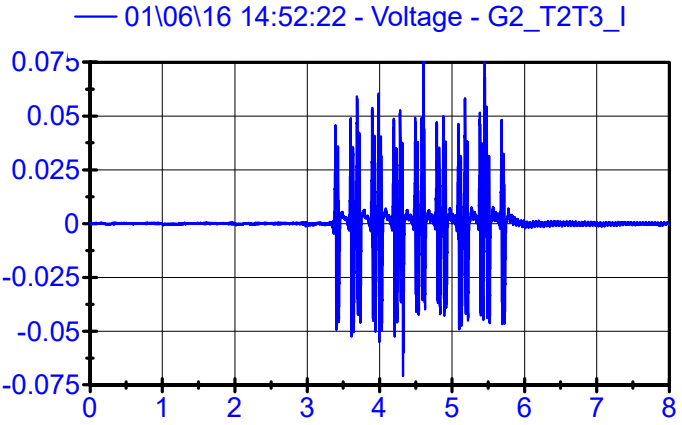

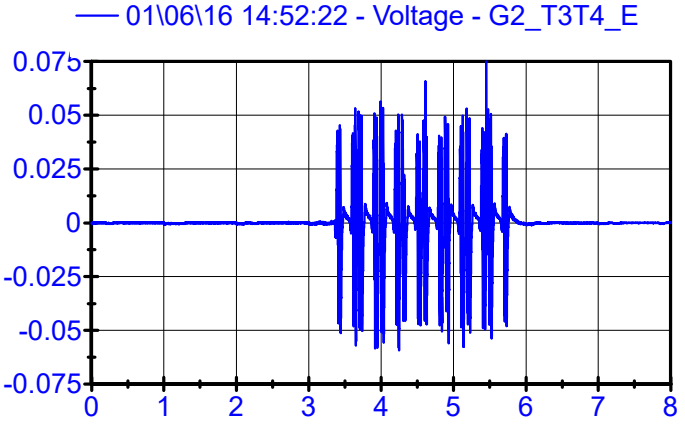

01\06\16 15:21:31

Rail Geophones
LPF 90Hz

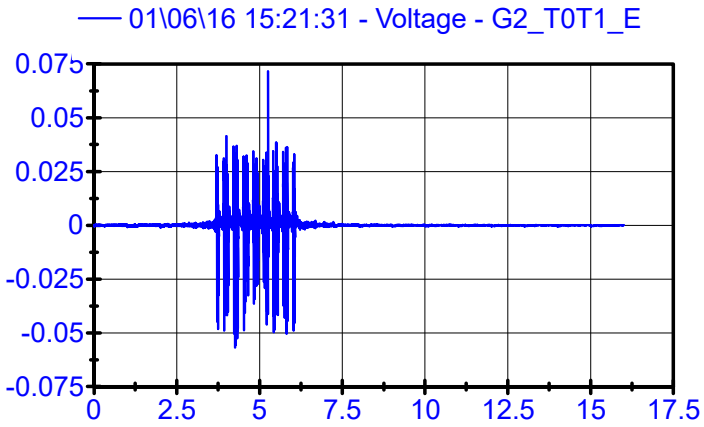

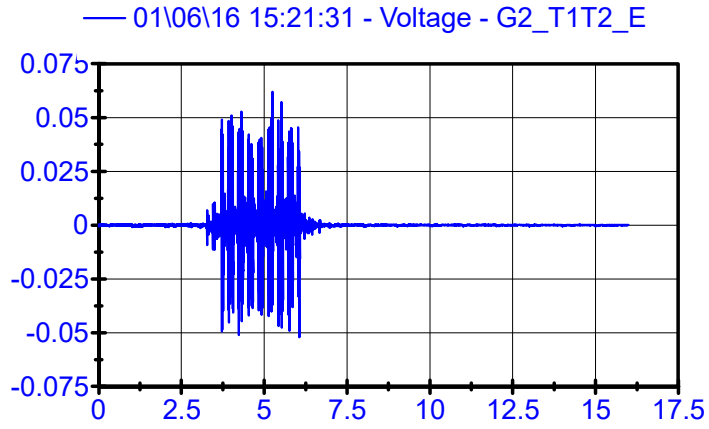

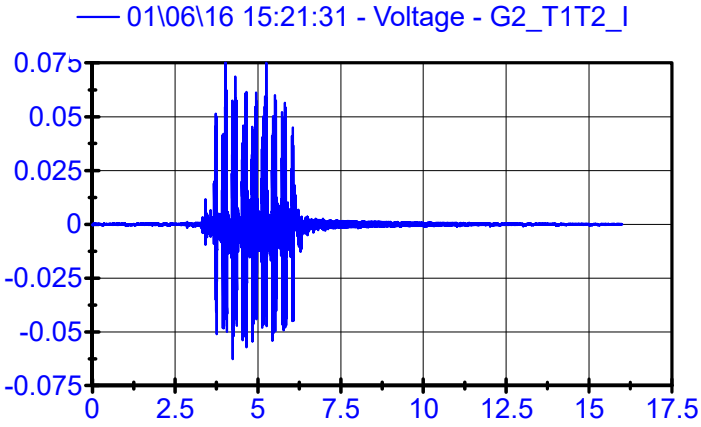

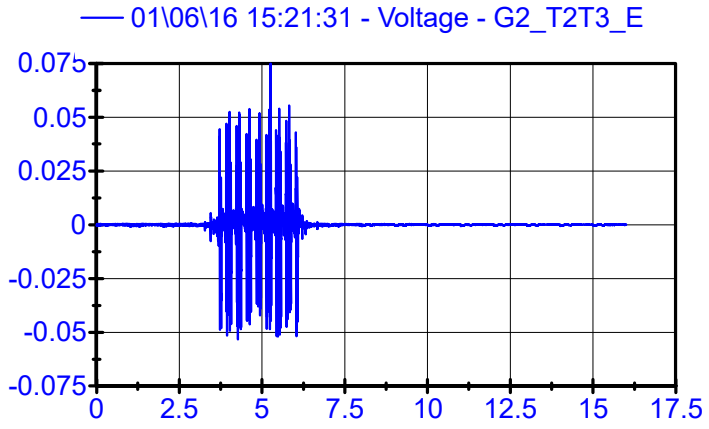

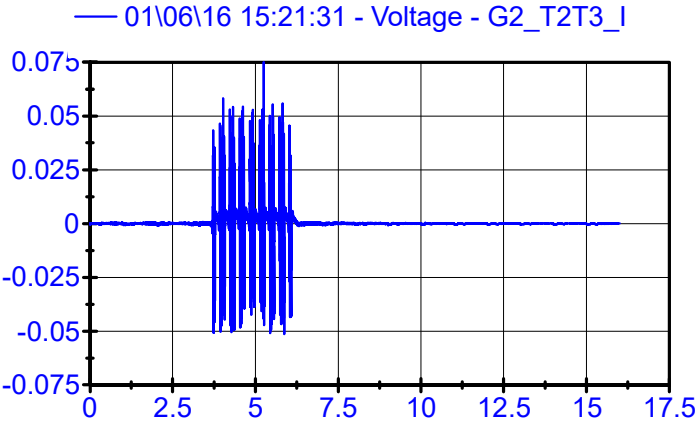

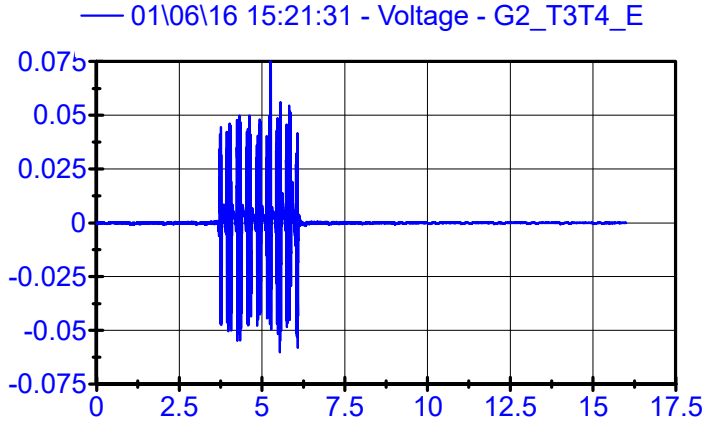

01\06\16 15:34:49

Rail Geophones
LPF 90Hz

01\06\16 15:34:49 - Voltage - G2_T0T1_E

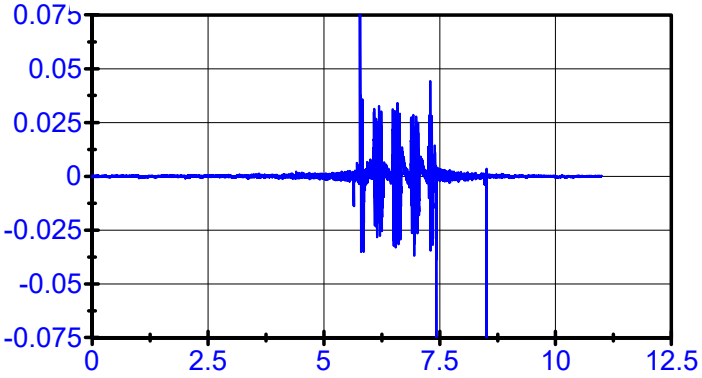

01\06\16 15:34:49 - Voltage - G2_T1T2_E

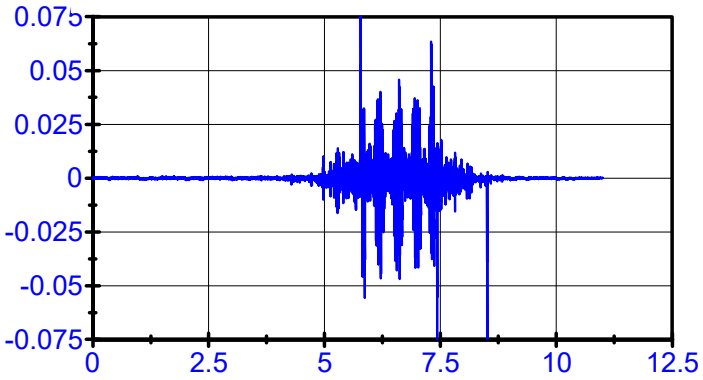

01\06\16 15:34:49 - Voltage - G2_T1T2_I

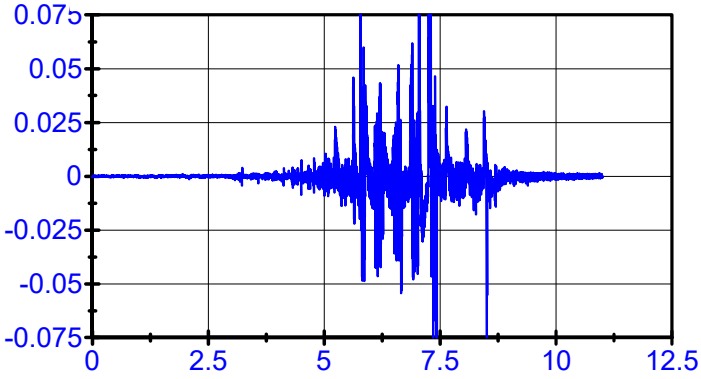

01\06\16 15:34:49 - Voltage - G2_T2T3_E

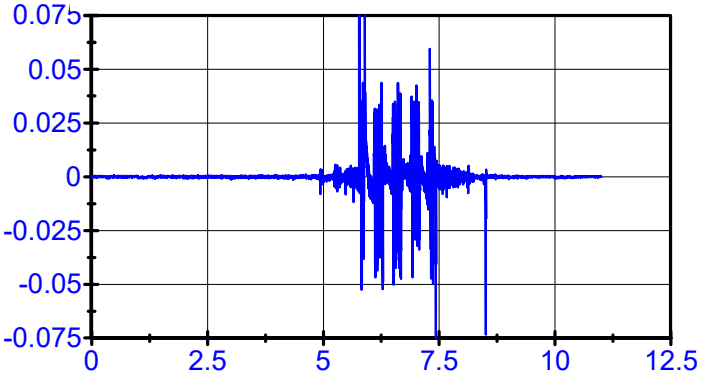

01\06\16 15:34:49 - Voltage - G2_T2T3_I

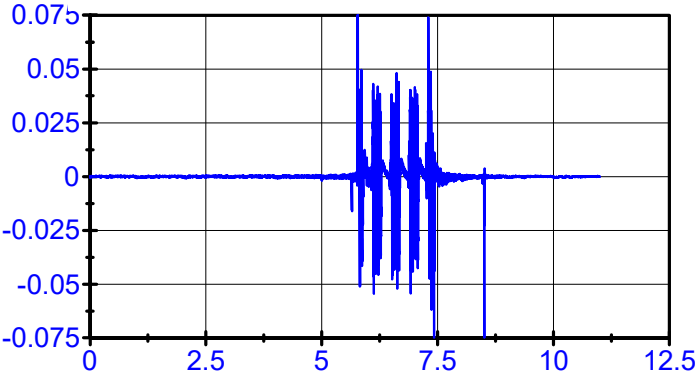

01\06\16 15:34:49 - Voltage - G2_T3T4_E

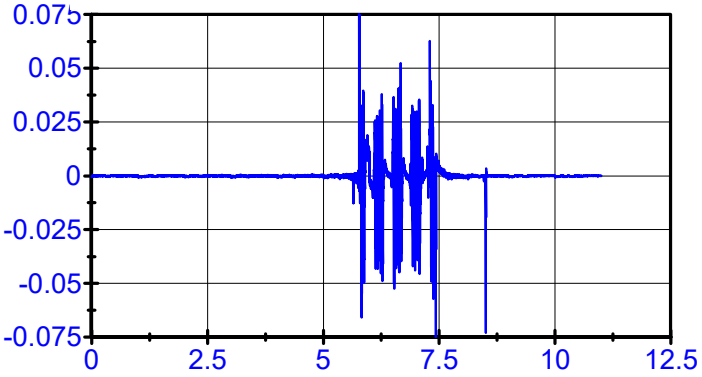

01\06\16 15:54:57

Rail Geophones
LPF 90Hz

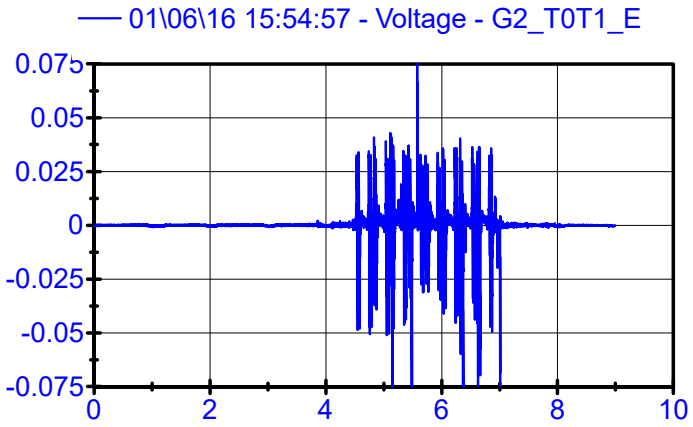

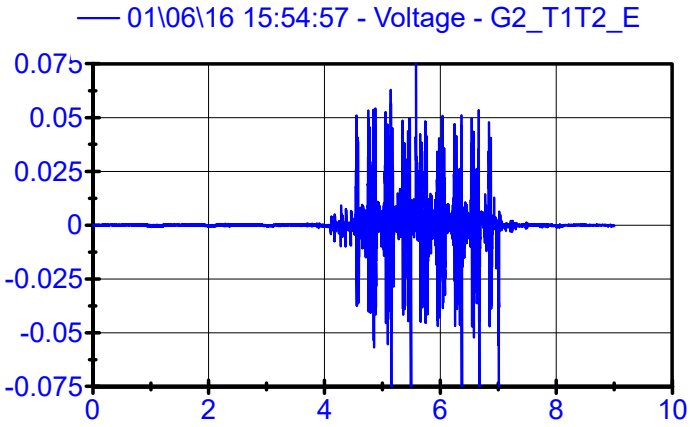

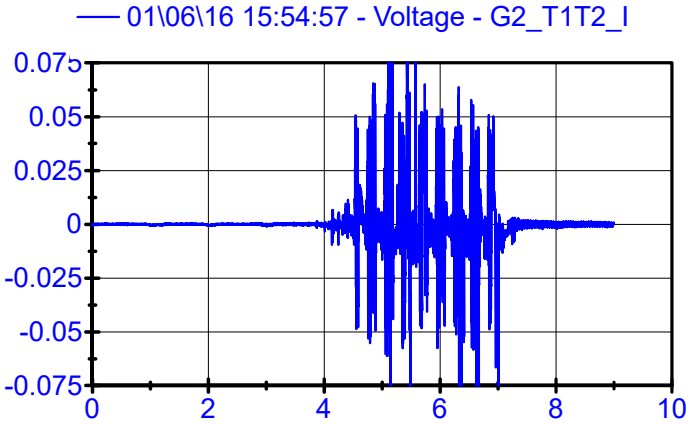

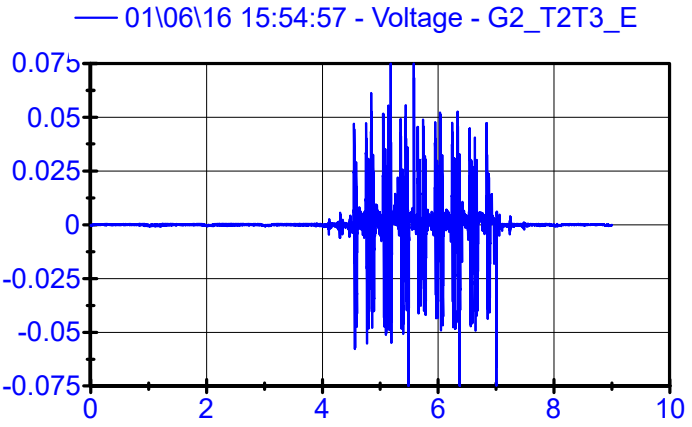

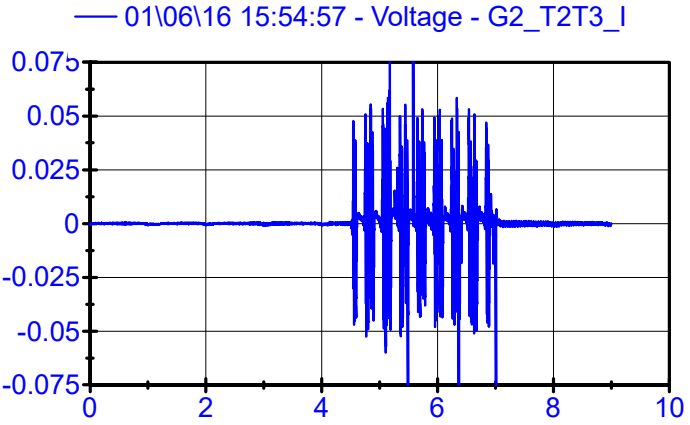

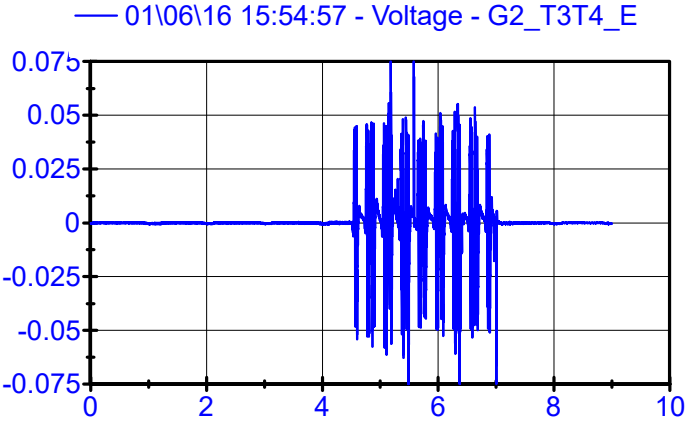

01\06\16 16:22:21

Rail Geophones
LPF 90Hz

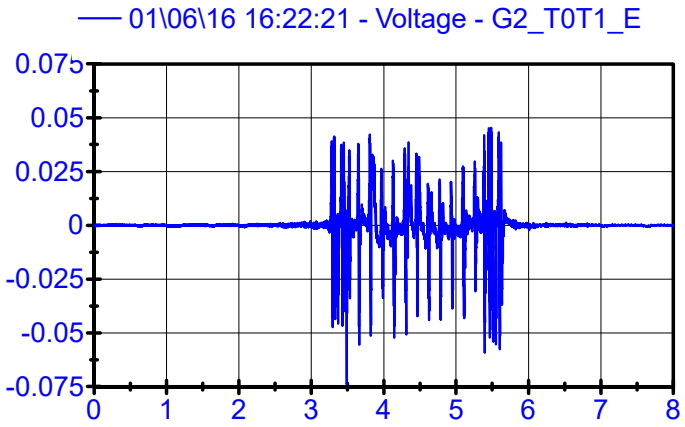

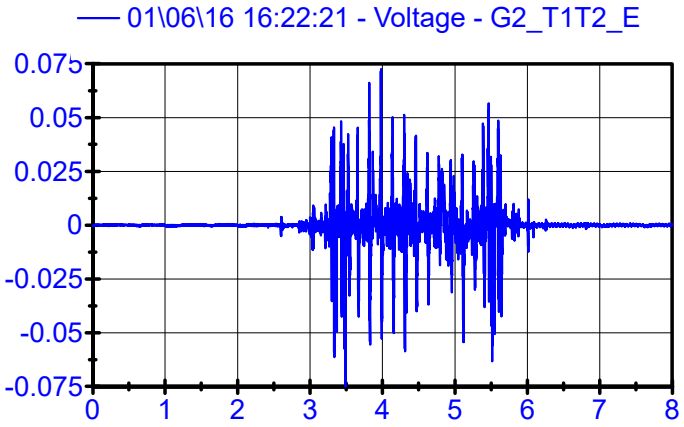

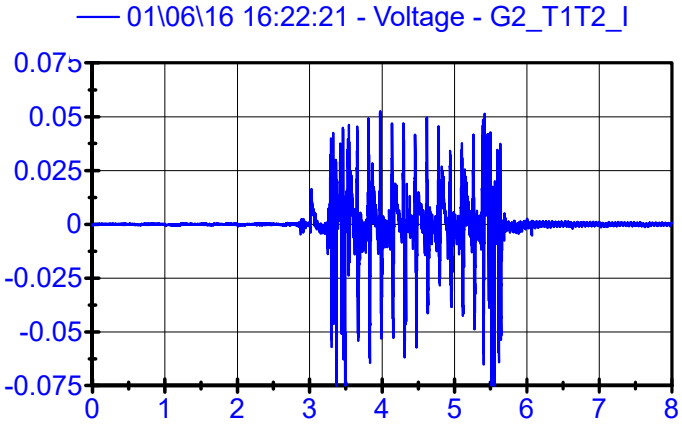

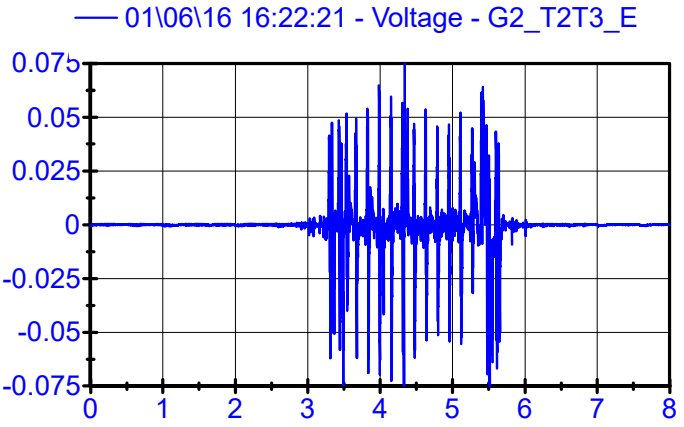

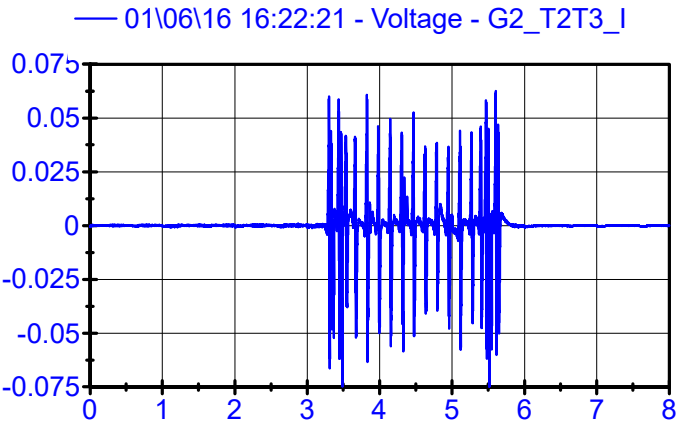

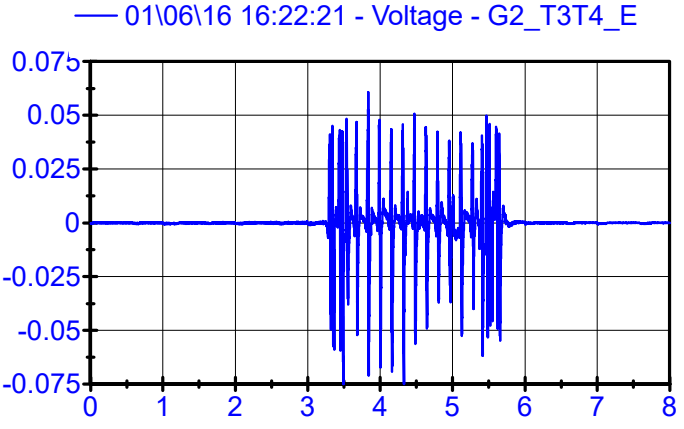

01\06\16 16:54:24

Rail Geophones
LPF 90Hz

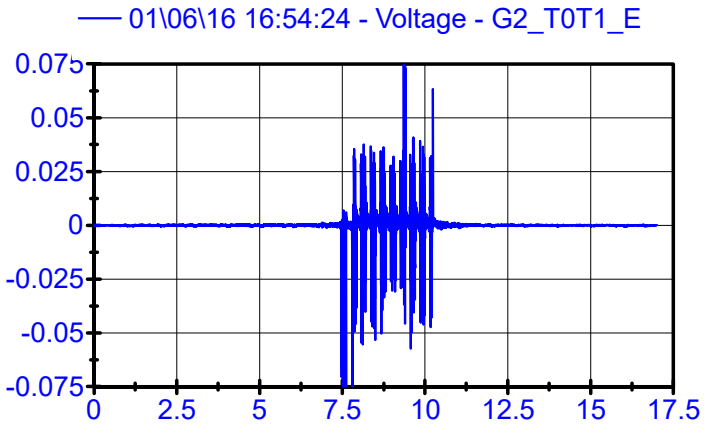

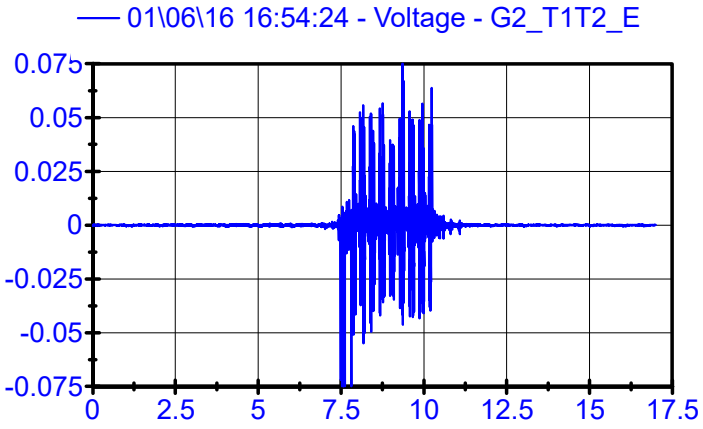

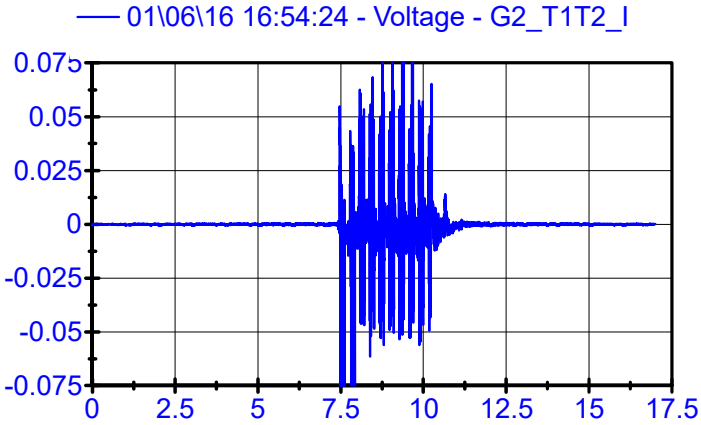

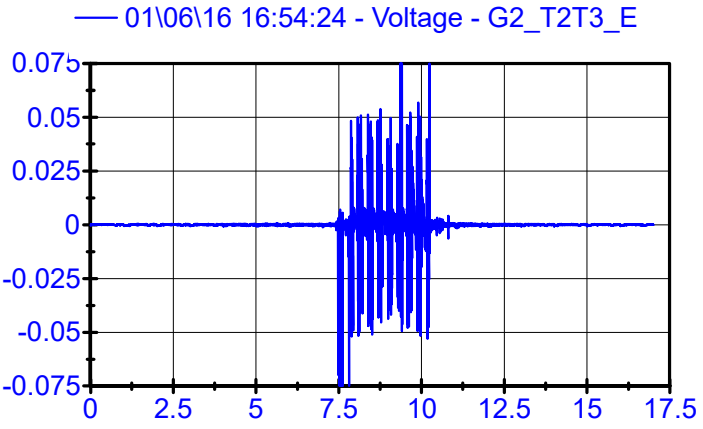

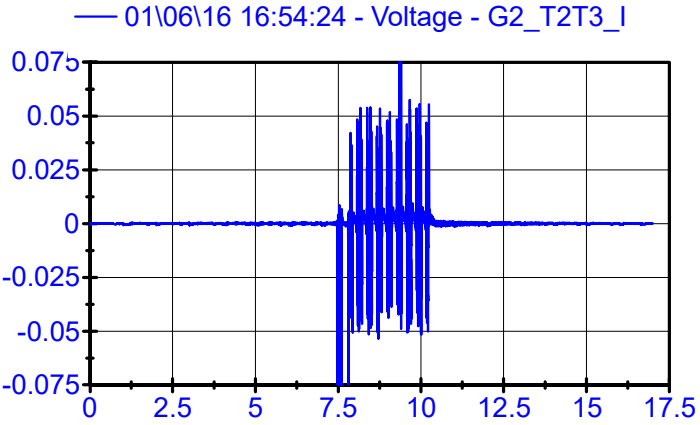

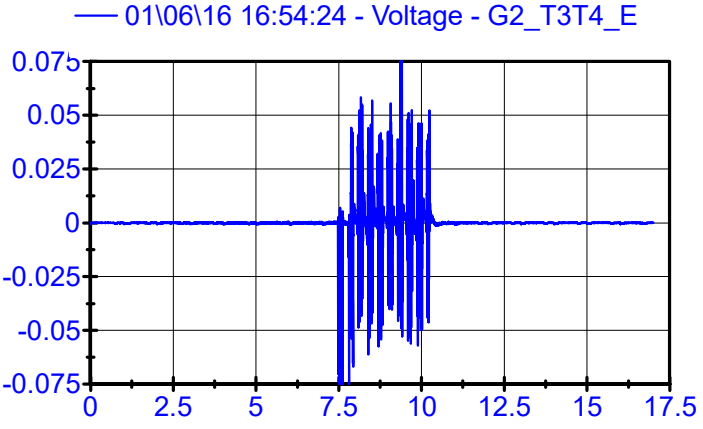

01\06\16 17:24:26

Rail Geophones
LPF 90Hz

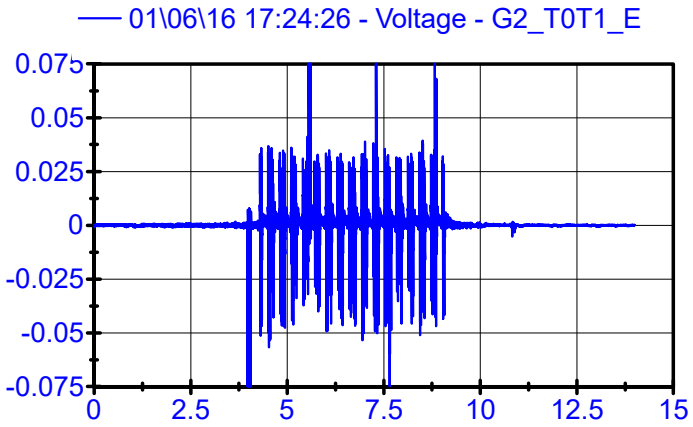

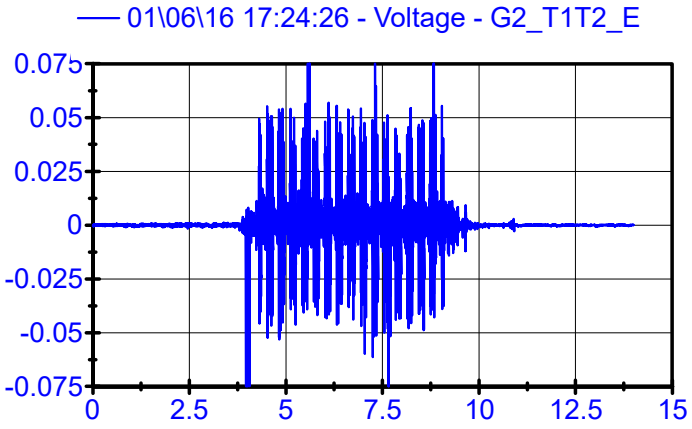

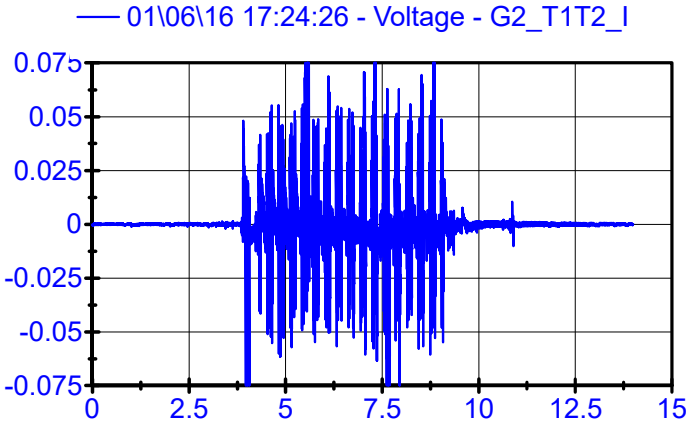

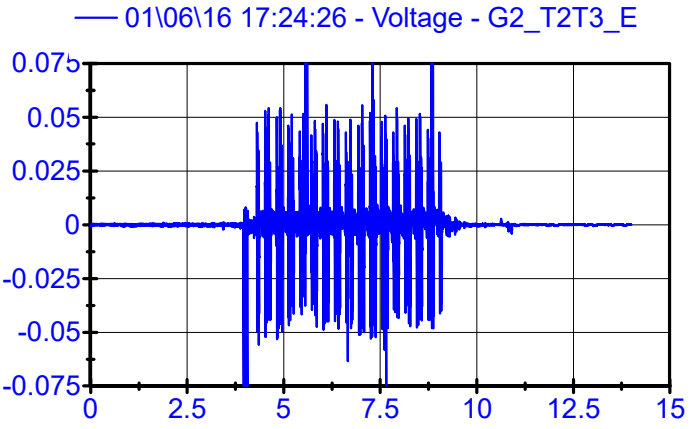

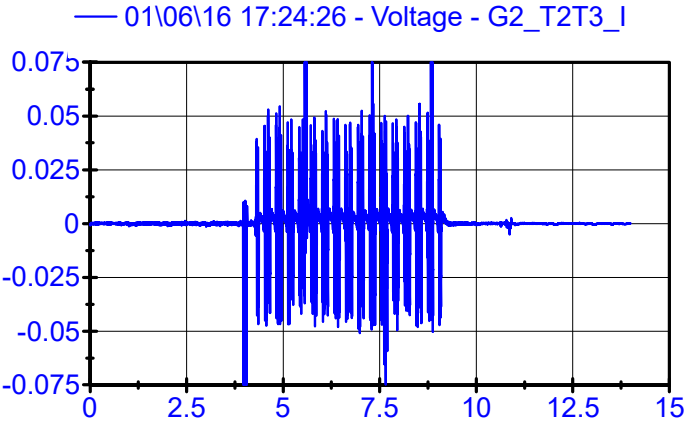

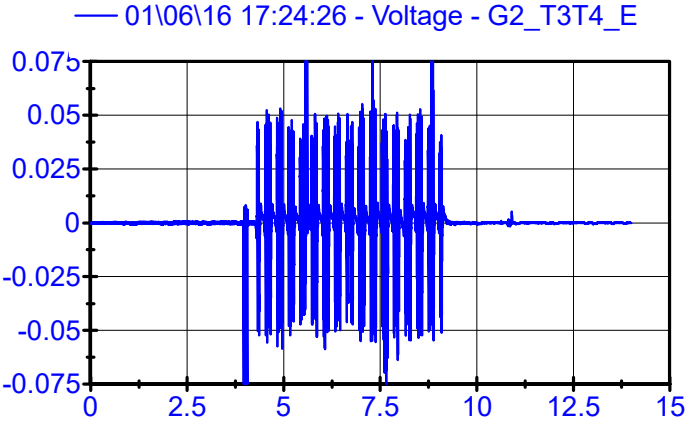

01\06\16 17:38:59

Rail Geophones
LPF 90Hz

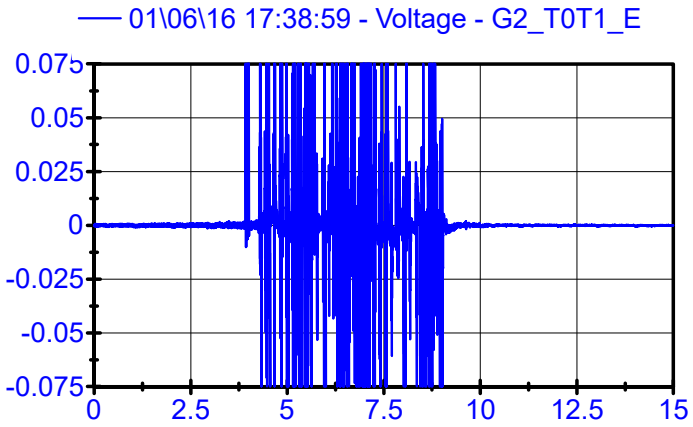

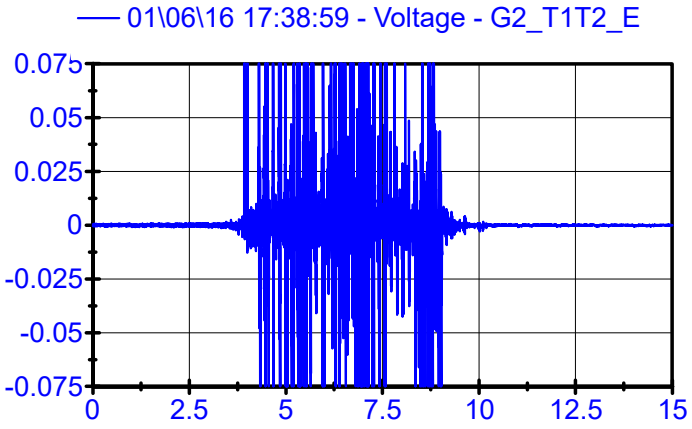

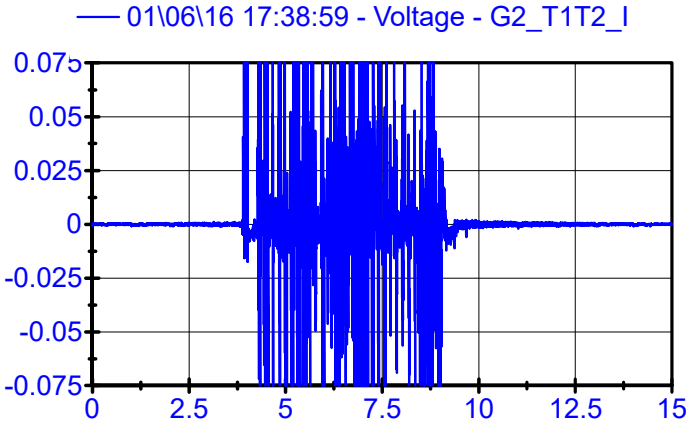

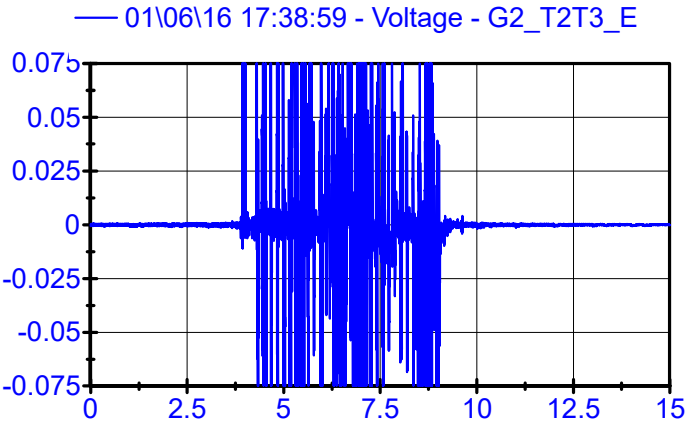

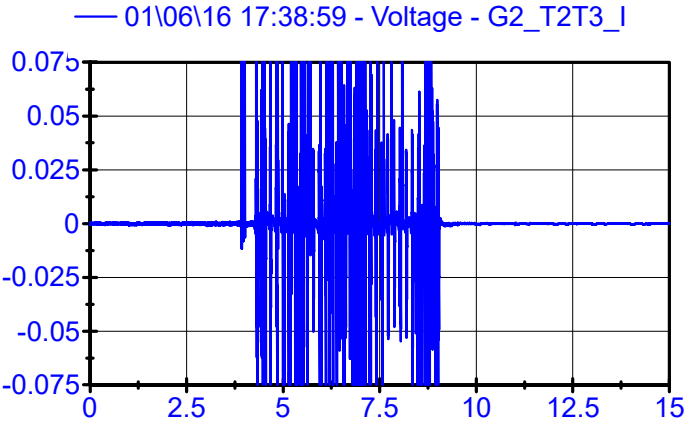

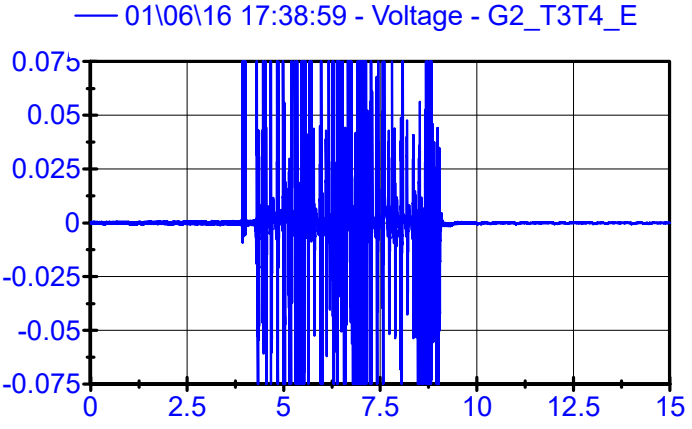

01\06\16 17:59:25

Rail Geophones
LPF 90Hz

01\06\16 17:59:25 - Voltage - G2_T0T1_E

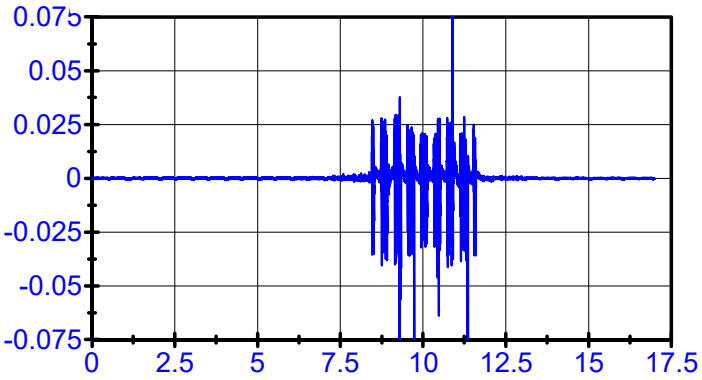

01\06\16 17:59:25 - Voltage - G2_T1T2_E

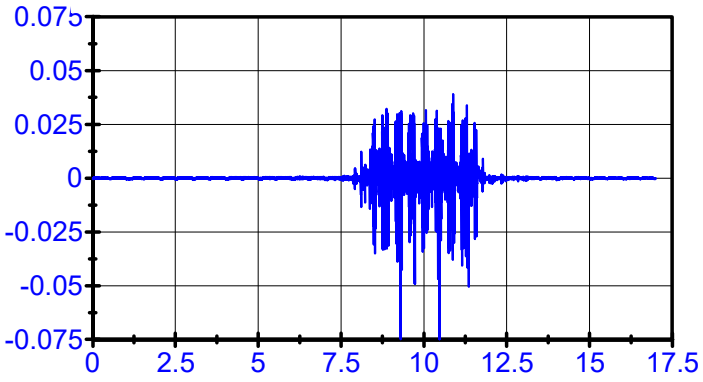

01\06\16 17:59:25 - Voltage - G2_T1T2_I

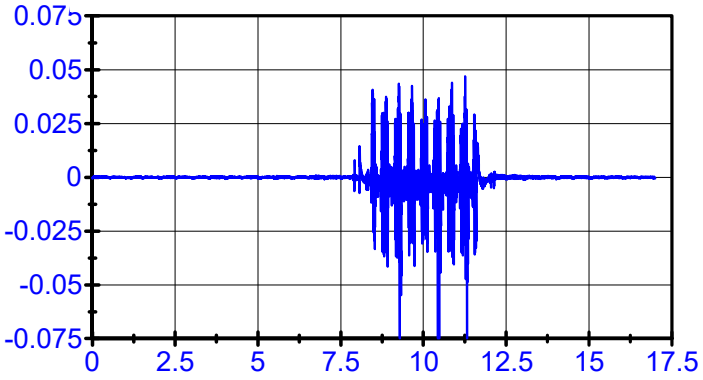

01\06\16 17:59:25 - Voltage - G2_T2T3_E

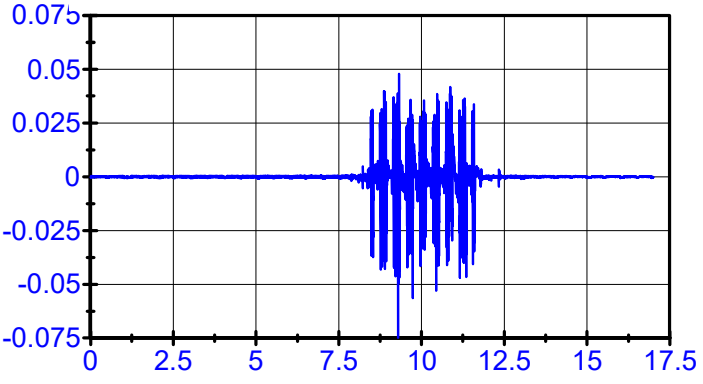

01\06\16 17:59:25 - Voltage - G2_T2T3_I

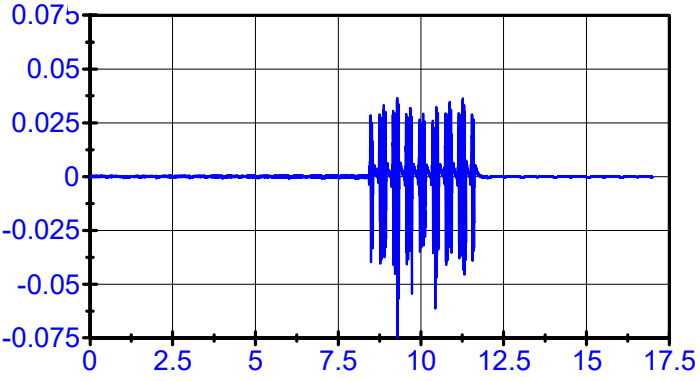

01\06\16 17:59:25 - Voltage - G2_T3T4_E

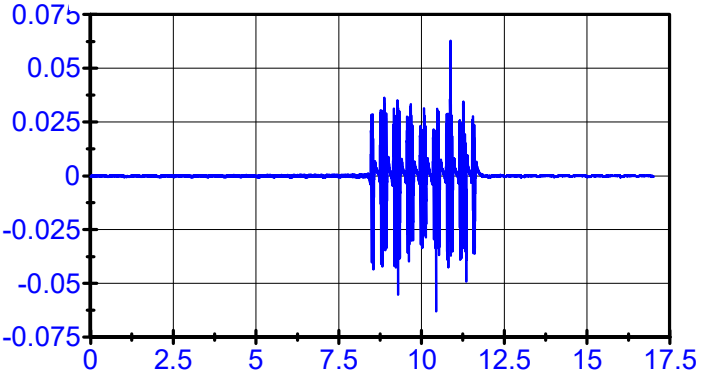

01\06\16 18:22:52

Rail Geophones
LPF 90Hz

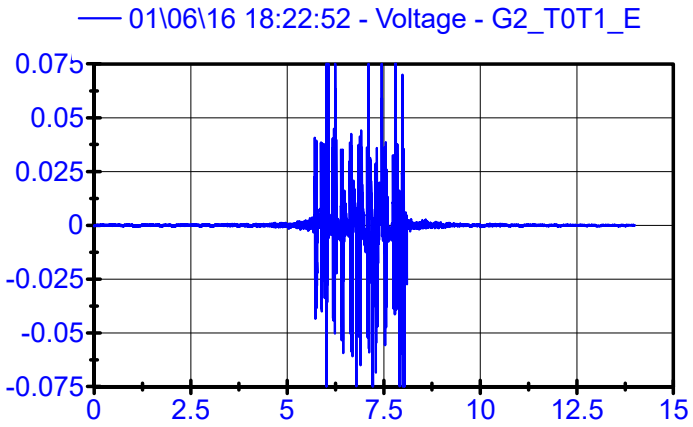

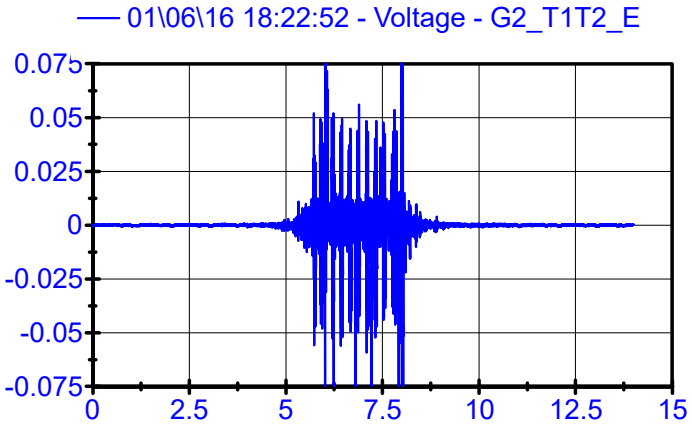

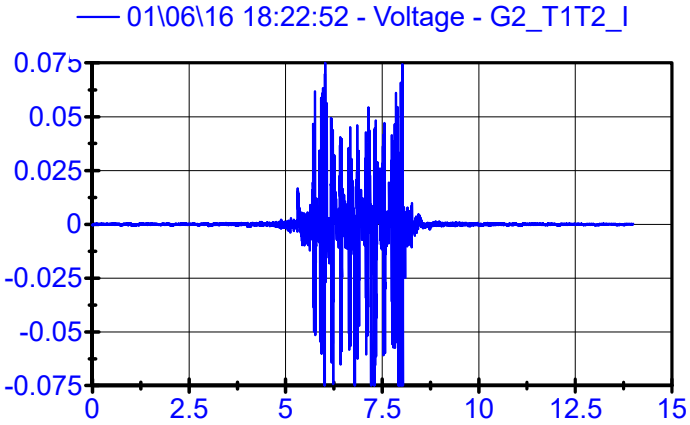

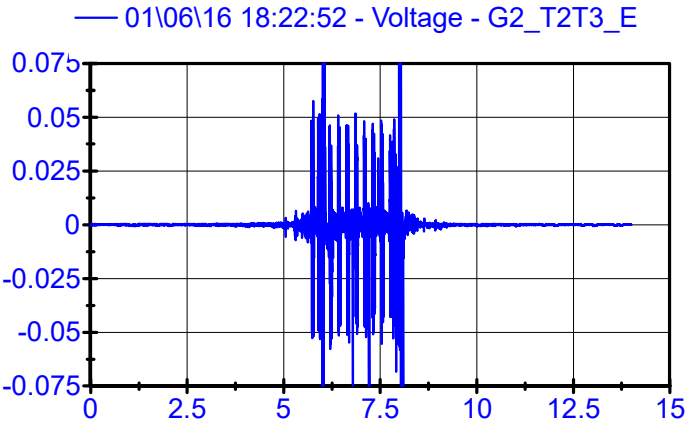

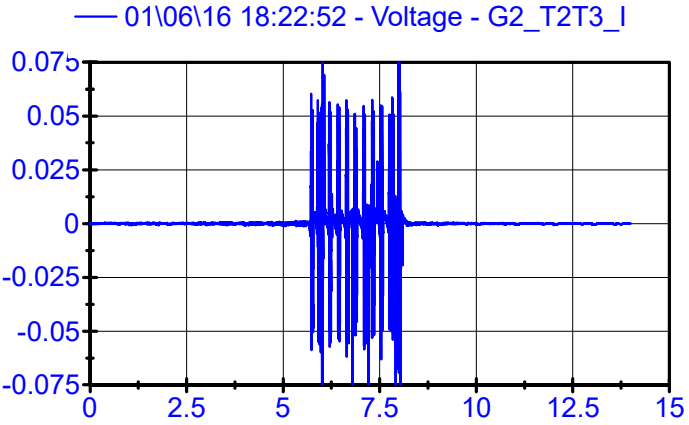

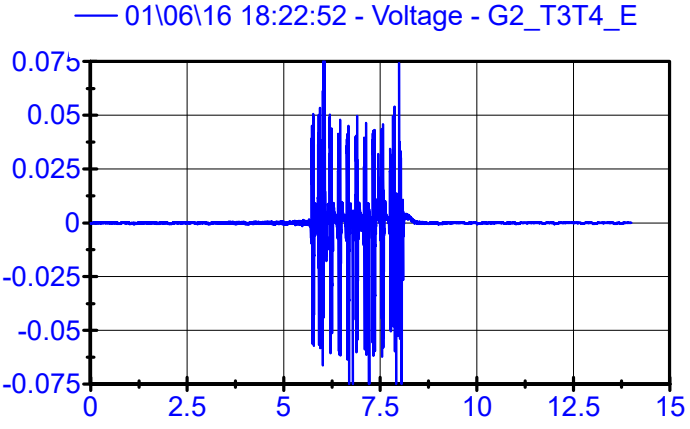

01\06\16 18:59:06

Rail Geophones
LPF 90Hz

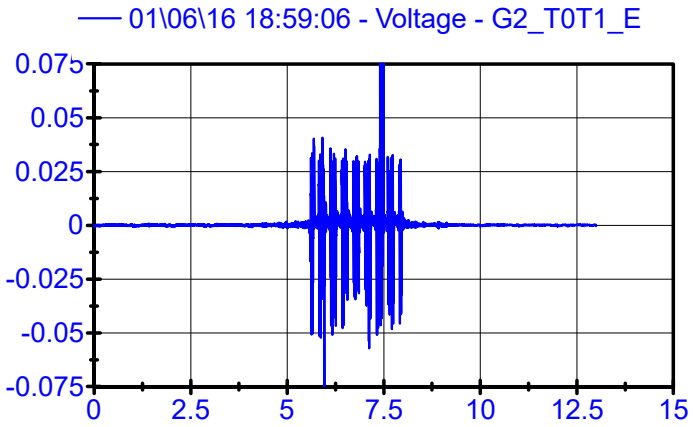

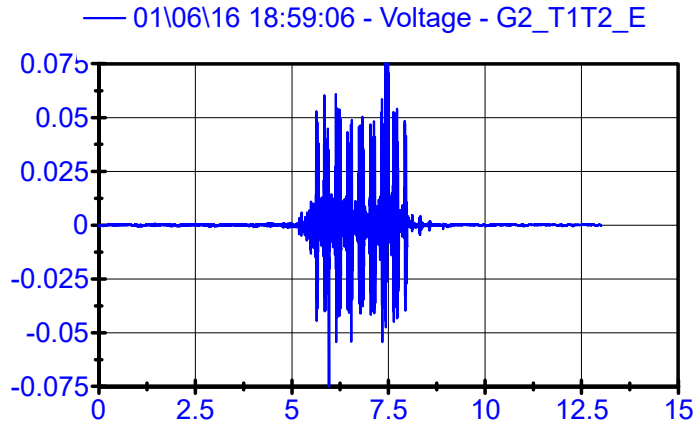

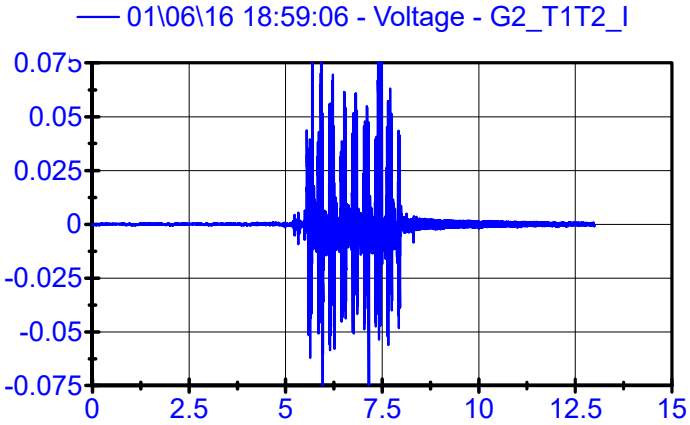

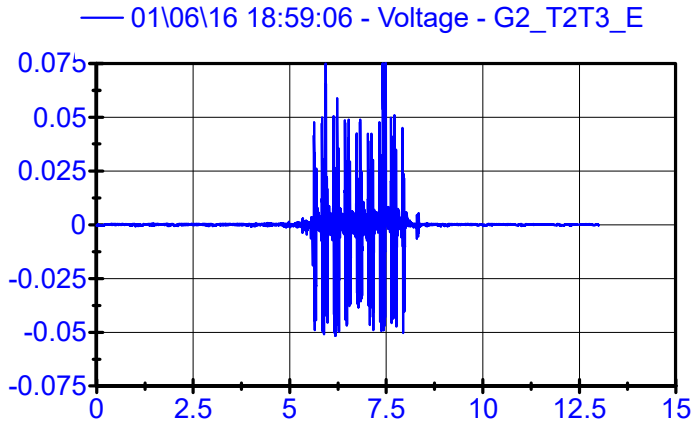

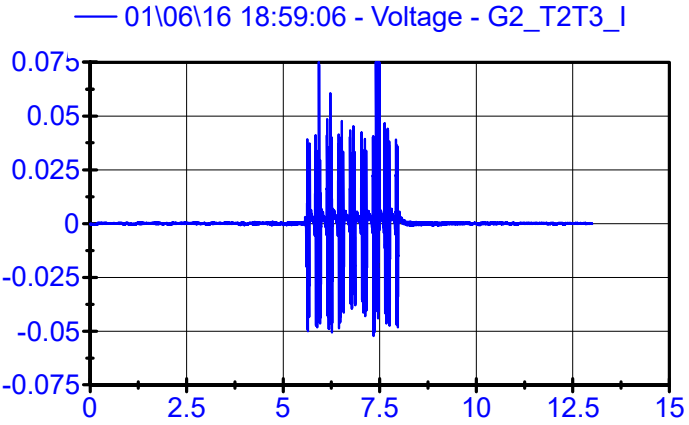

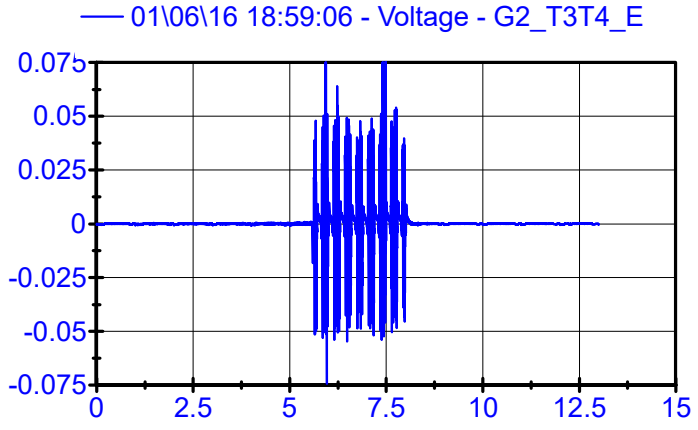

01\06\16 19:21:34

Rail Geophones
LPF 90Hz

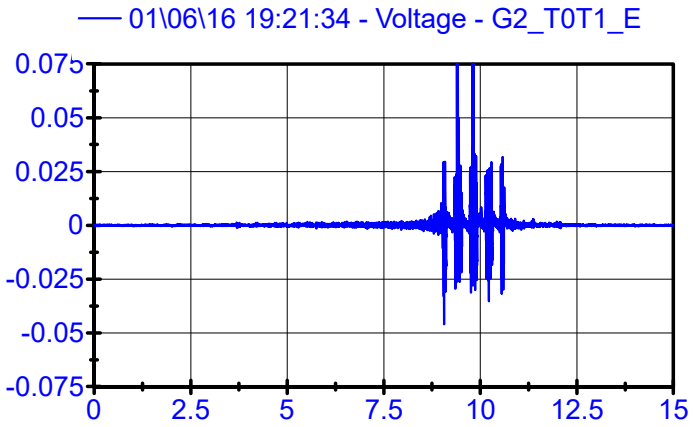

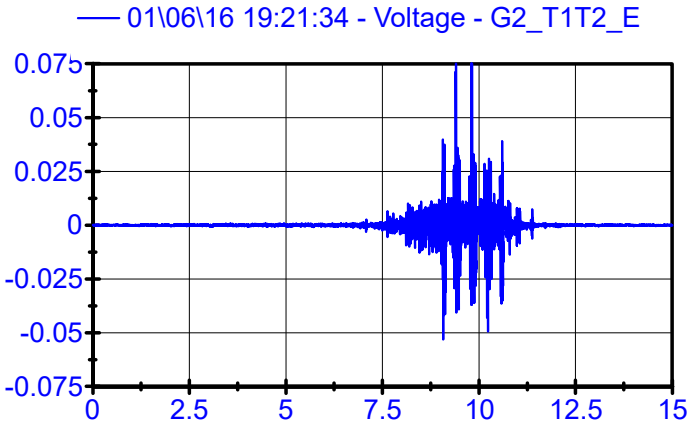

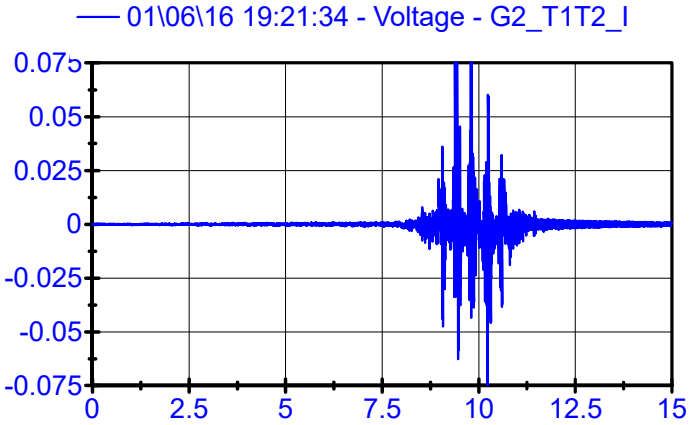

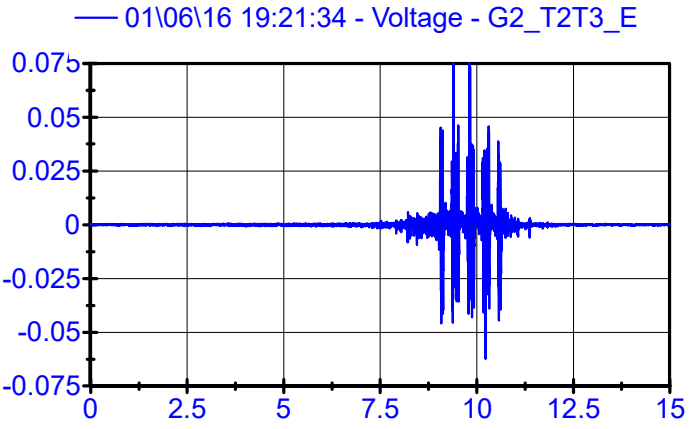

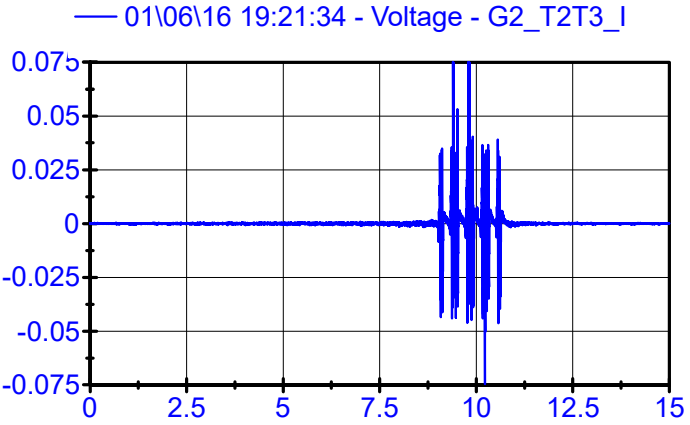

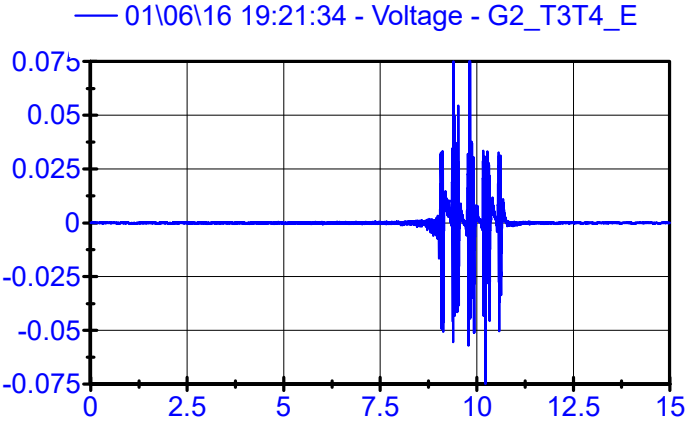

01\06\16 19:23:31

Rail Geophones
LPF 90Hz

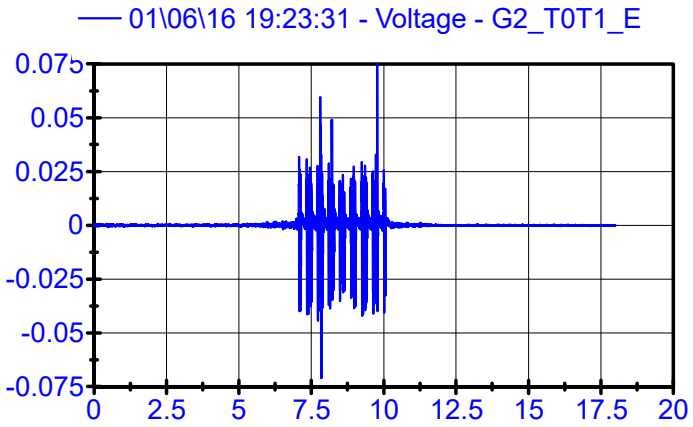

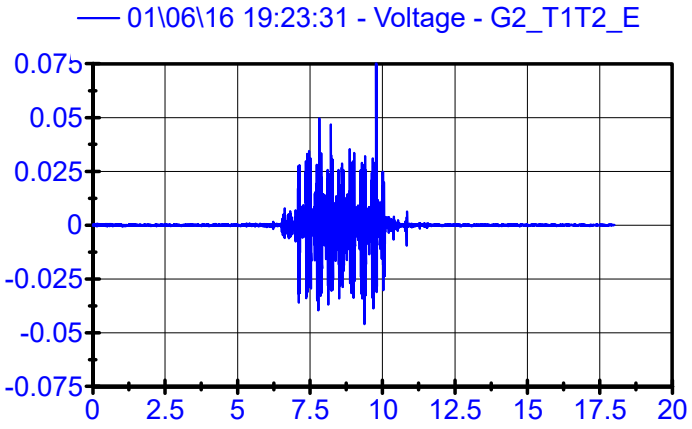

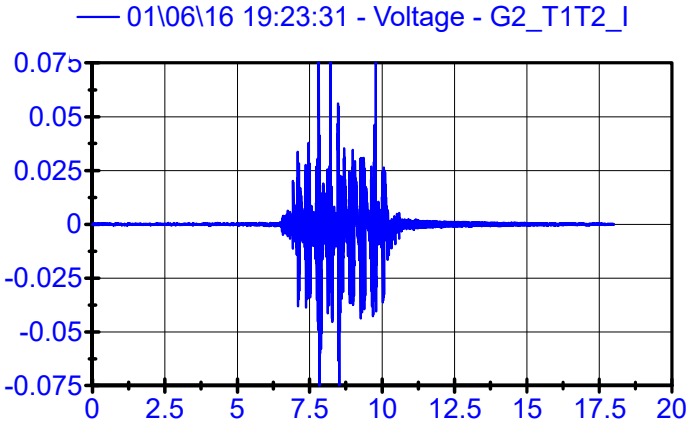

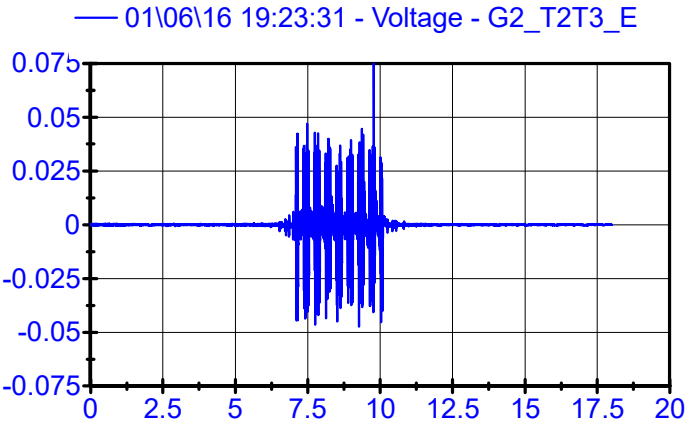

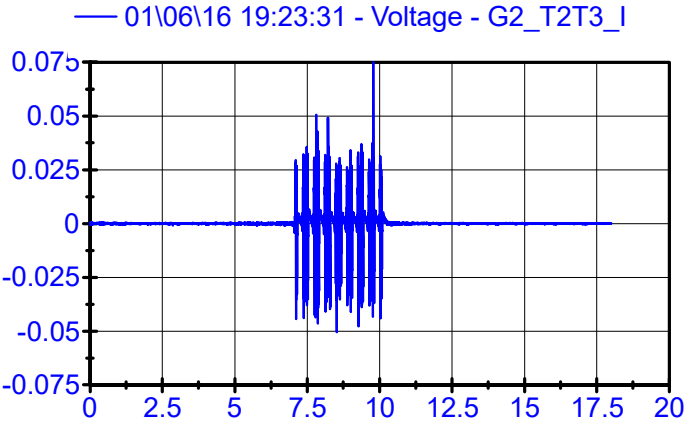

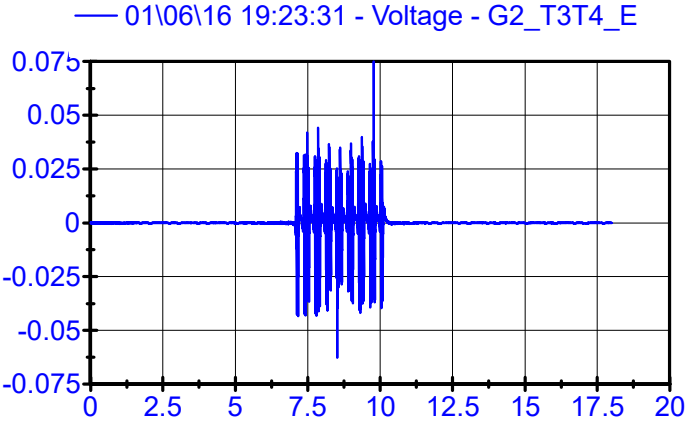

01\06\16 19:32:45

Rail Geophones
LPF 90Hz

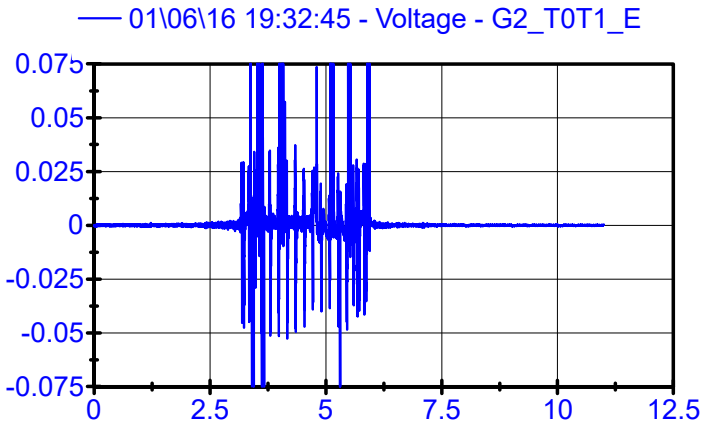

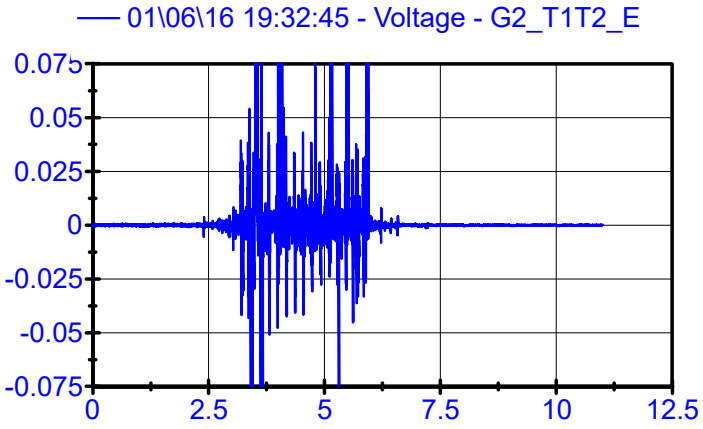

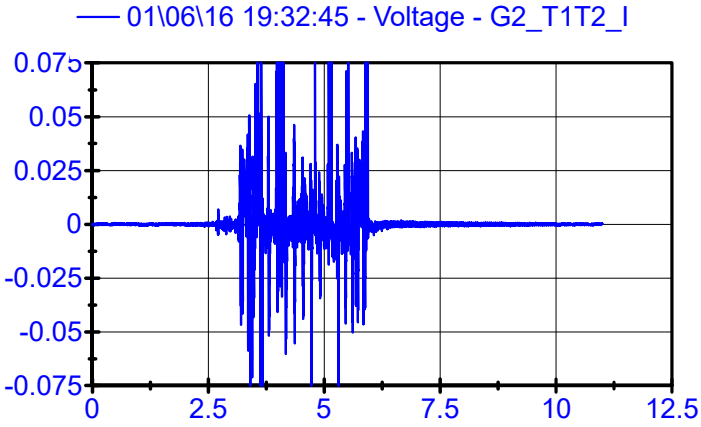

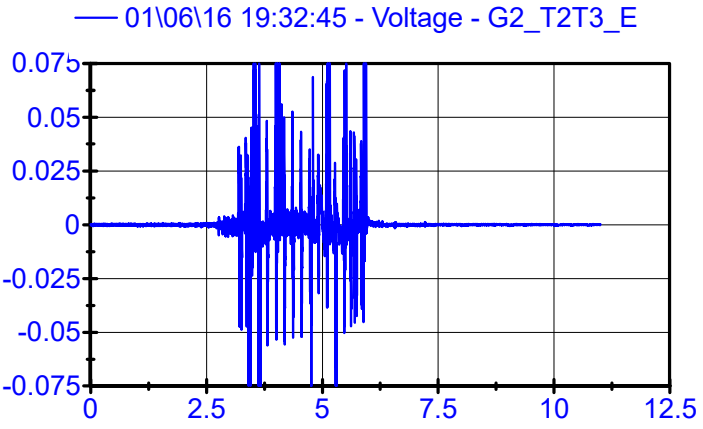

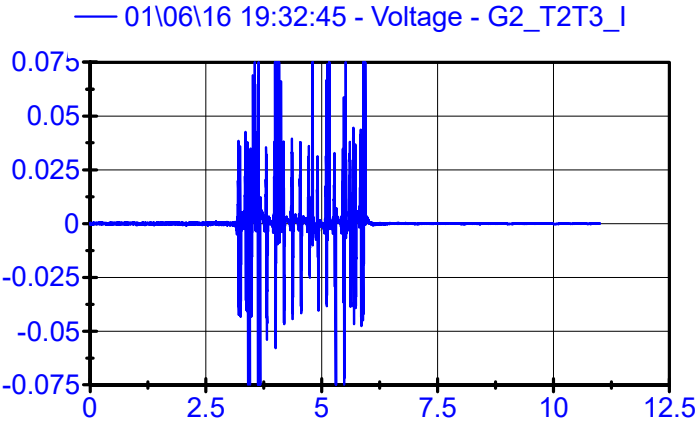

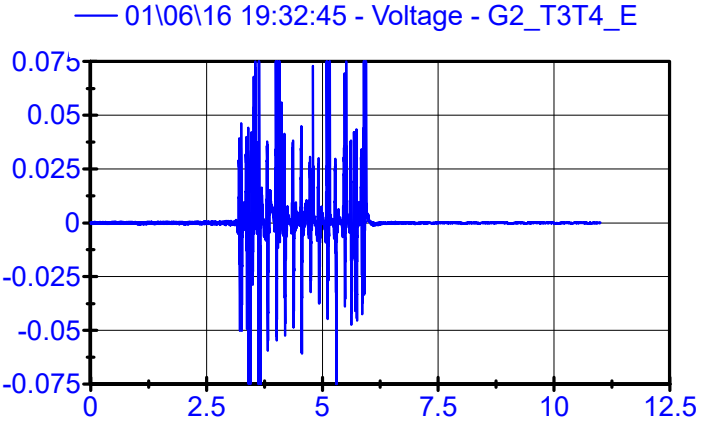

01\06\16 19:53:03

Rail Geophones
LPF 90Hz

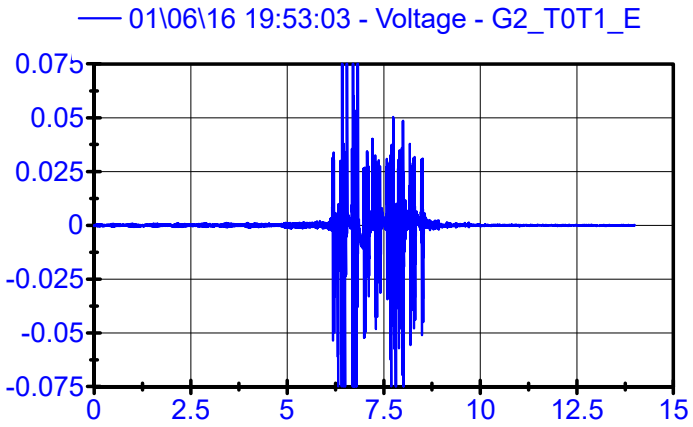

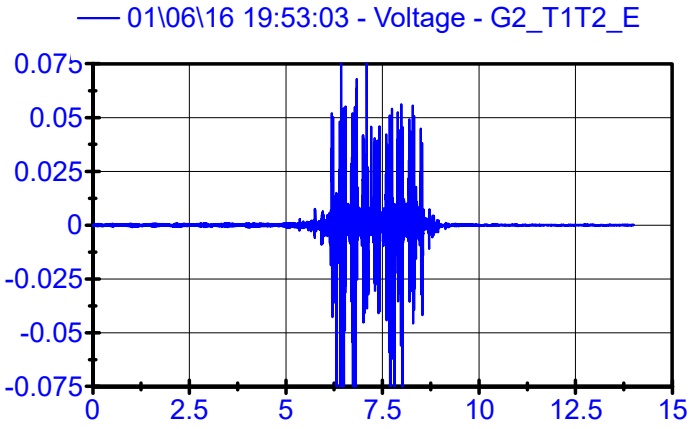

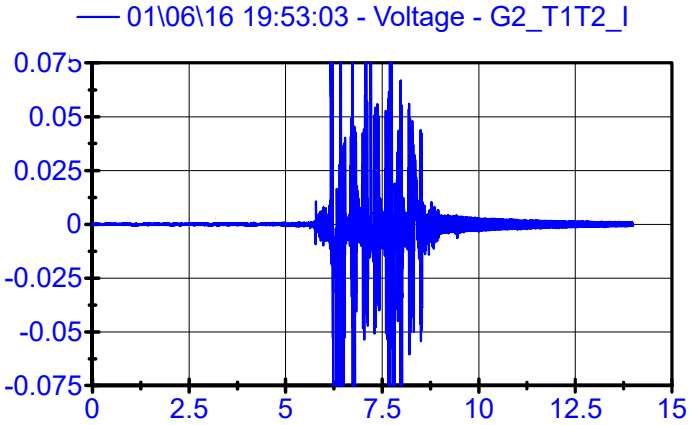

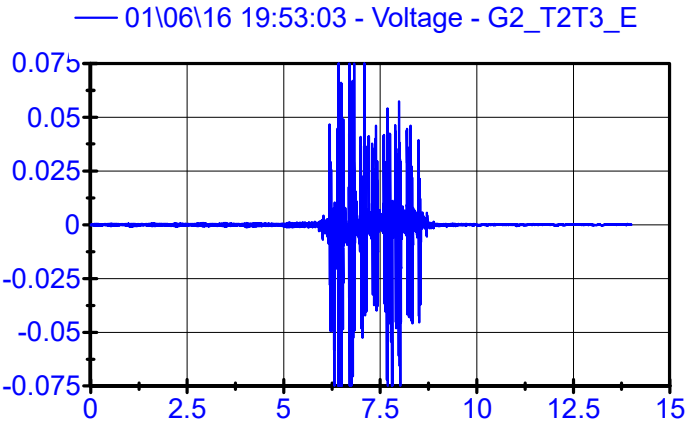

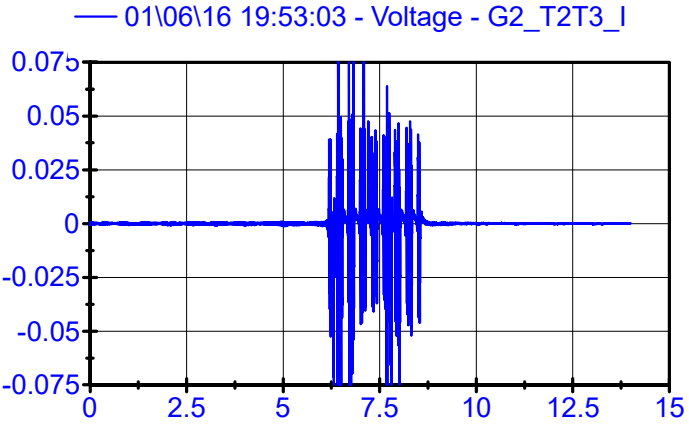

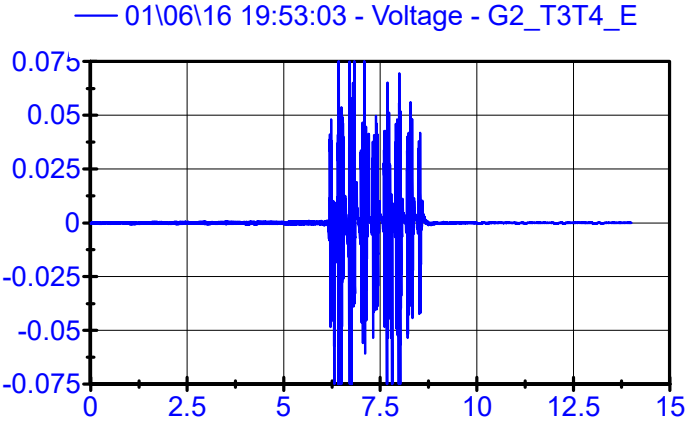

01\06\16 19:59:42

Rail Geophones
LPF 90Hz

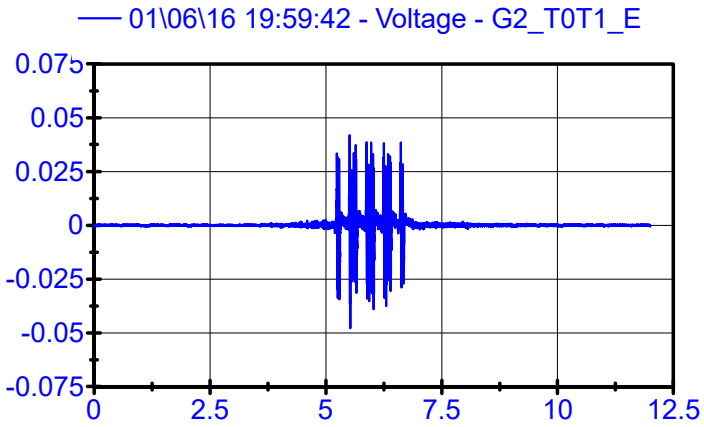

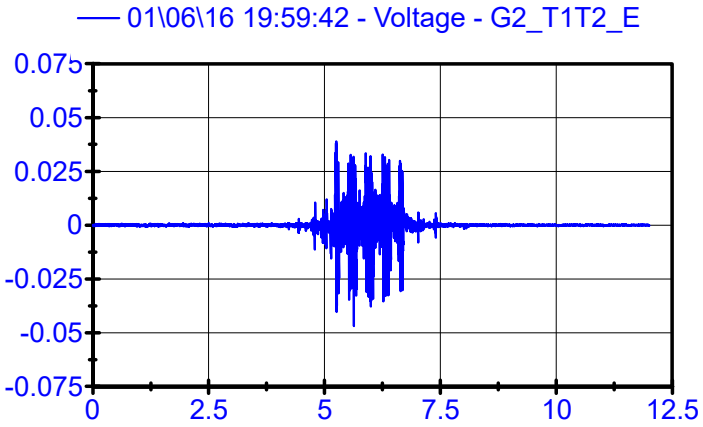

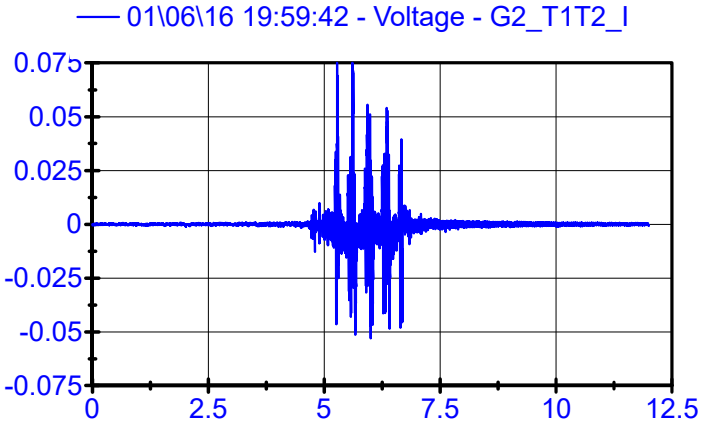

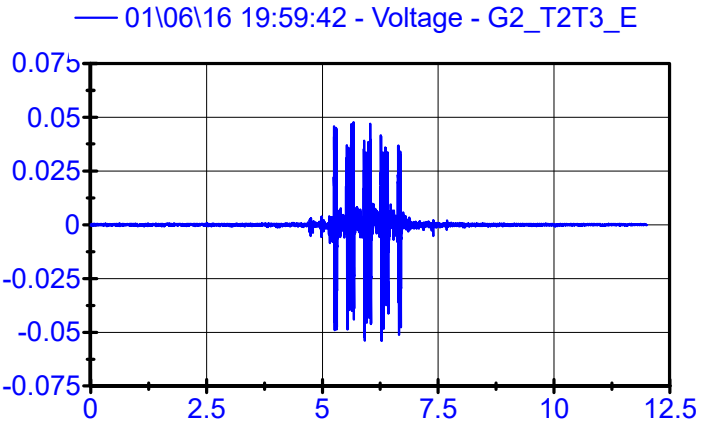

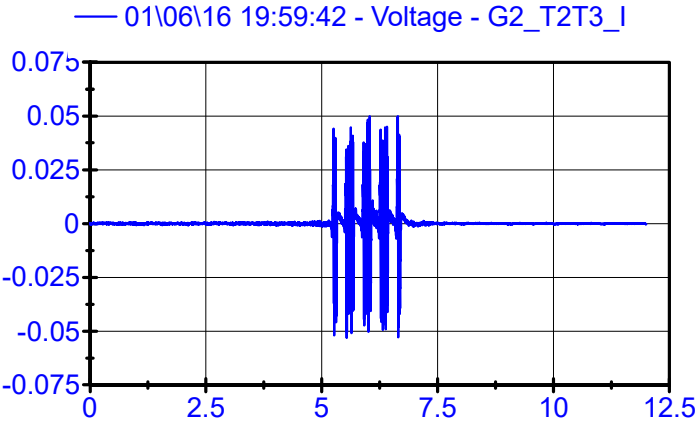

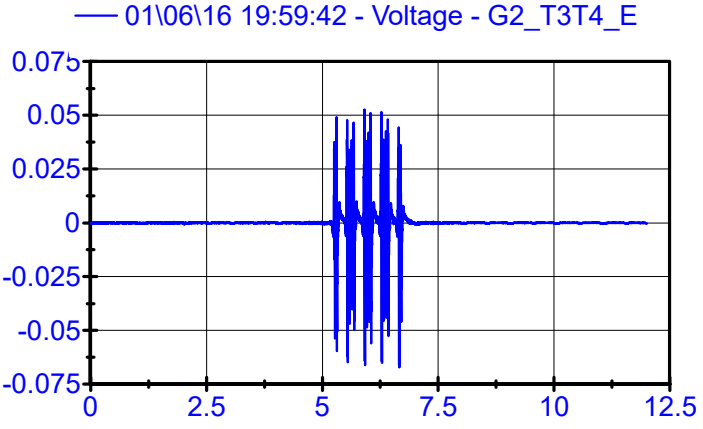

01\06\16 20:21:57

Rail Geophones
LPF 90Hz

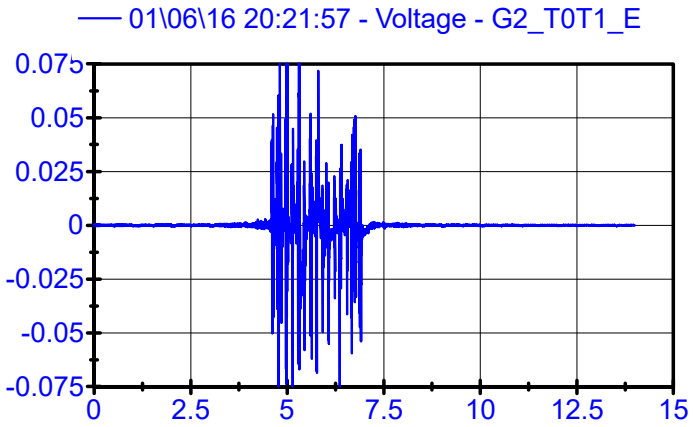

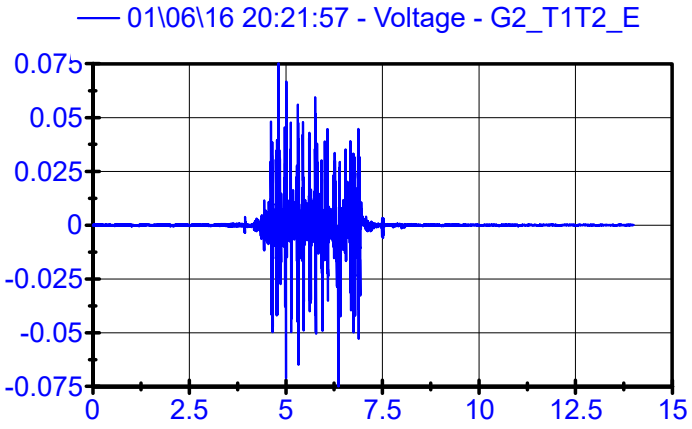

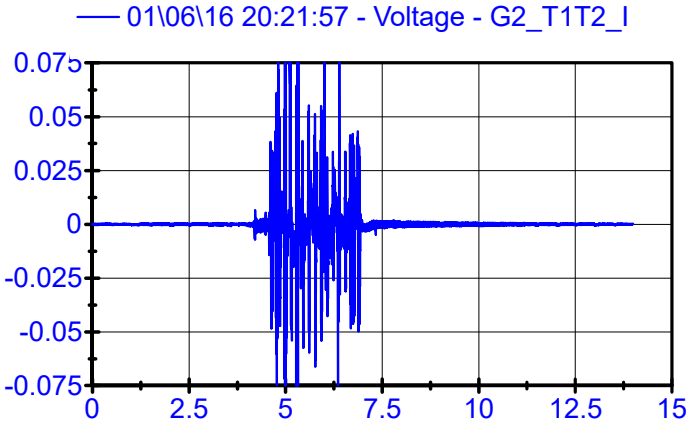

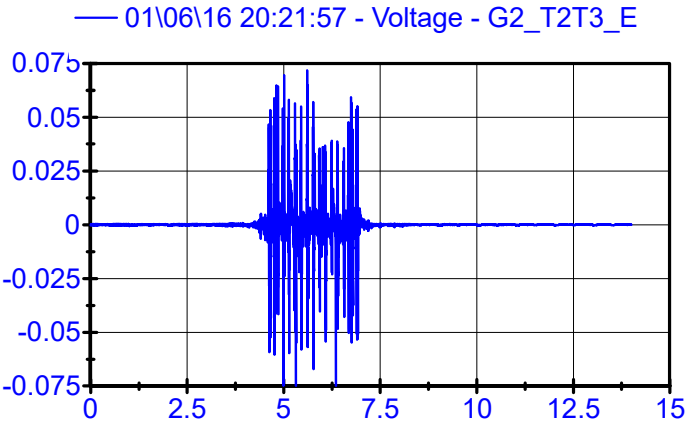

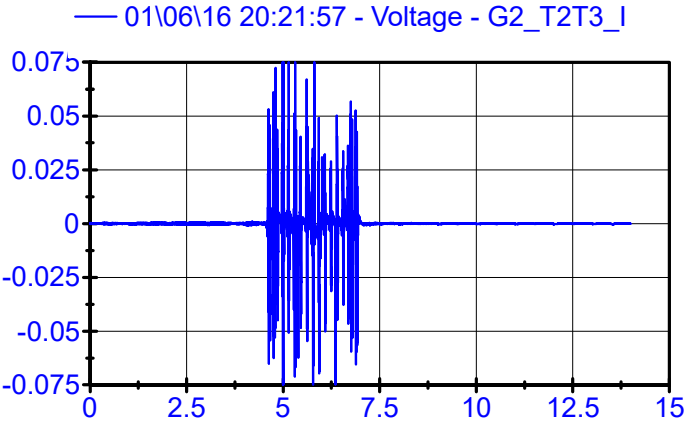

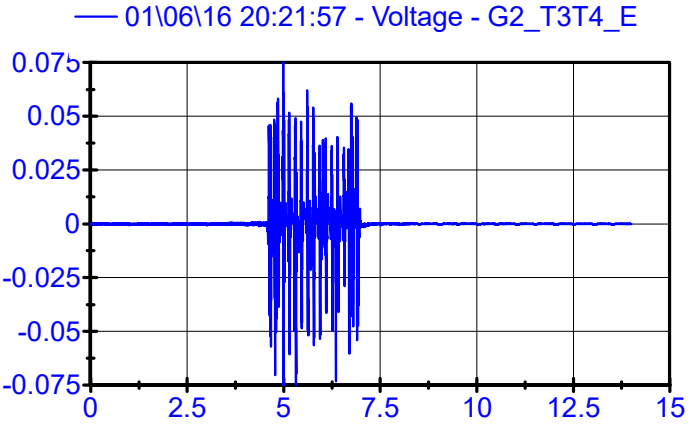

01\06\16 20:57:58

Rail Geophones
LPF 90Hz

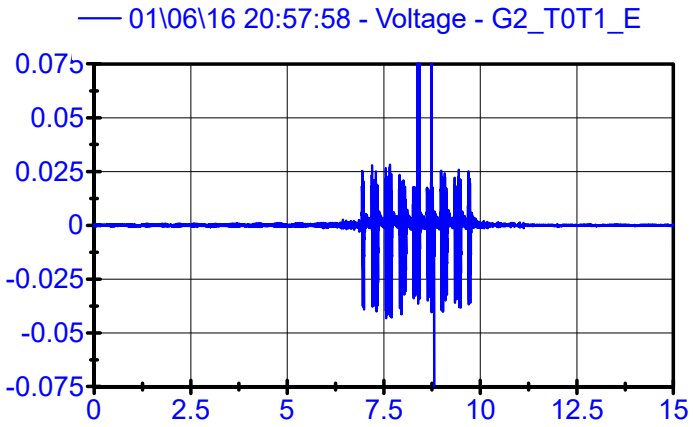

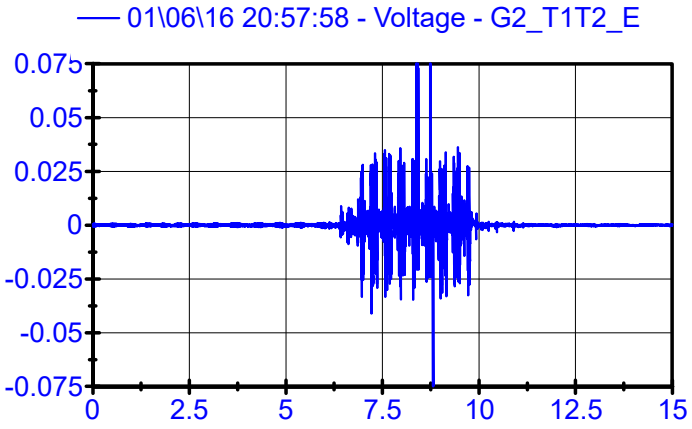

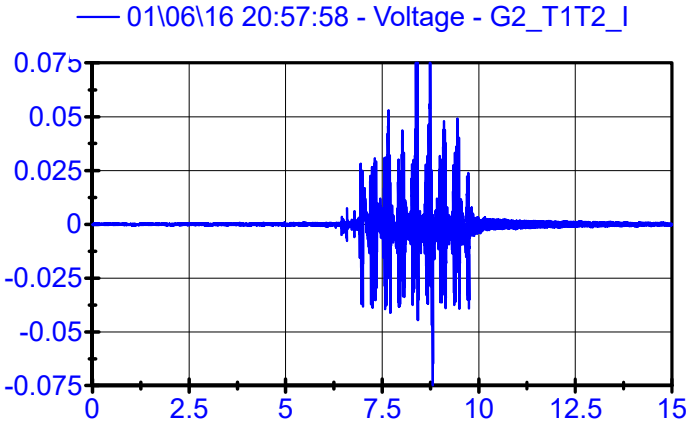

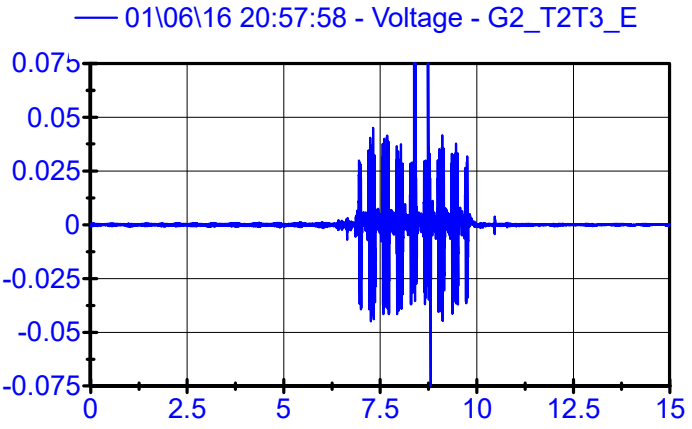

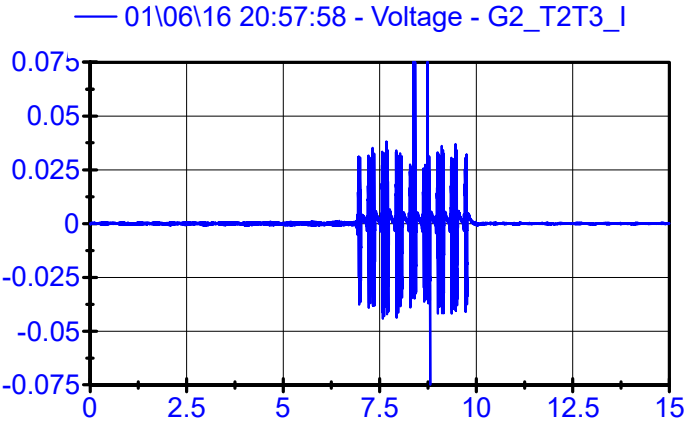

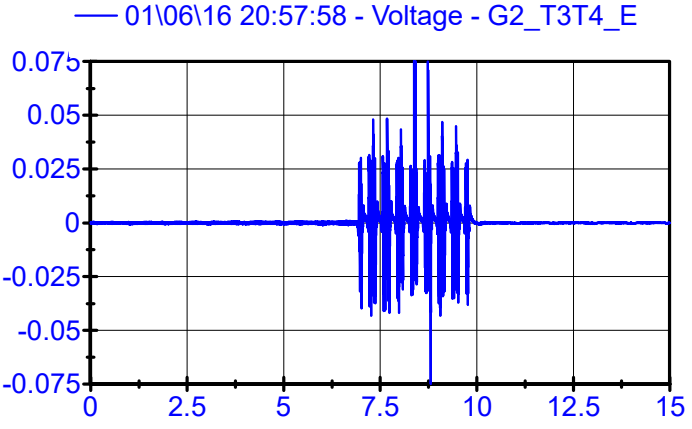

01\06\16 21:49:46

Rail Geophones
LPF 90Hz

01\06\16 21:49:46 - Voltage - G2_T0T1_E

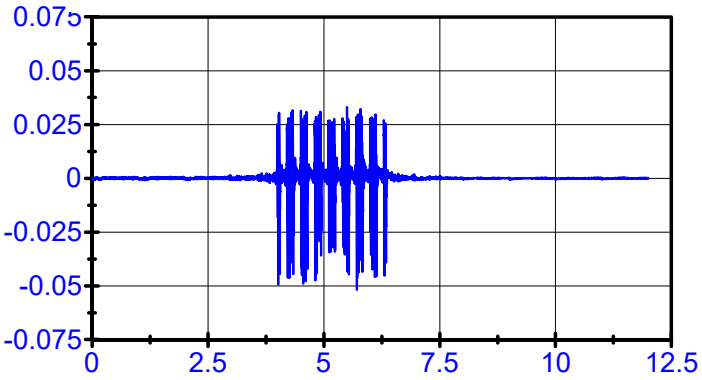

01\06\16 21:49:46 - Voltage - G2_T1T2_E

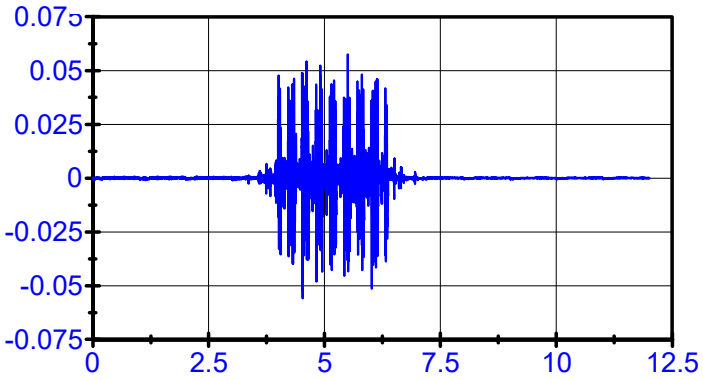

01\06\16 21:49:46 - Voltage - G2_T1T2_I

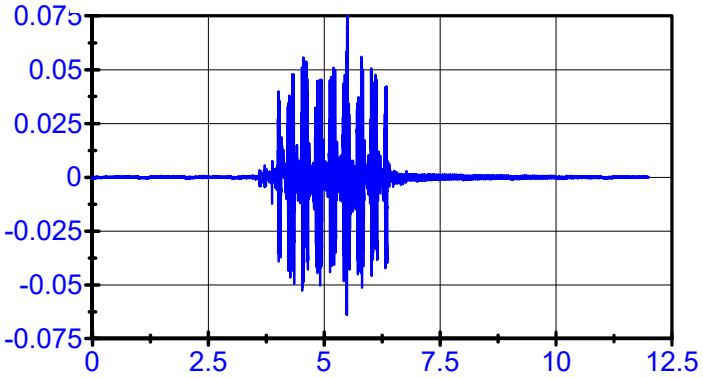

01\06\16 21:49:46 - Voltage - G2_T2T3_E

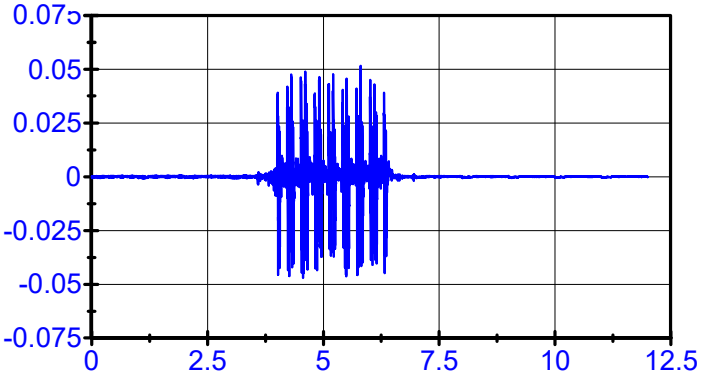

01\06\16 21:49:46 - Voltage - G2_T2T3_I

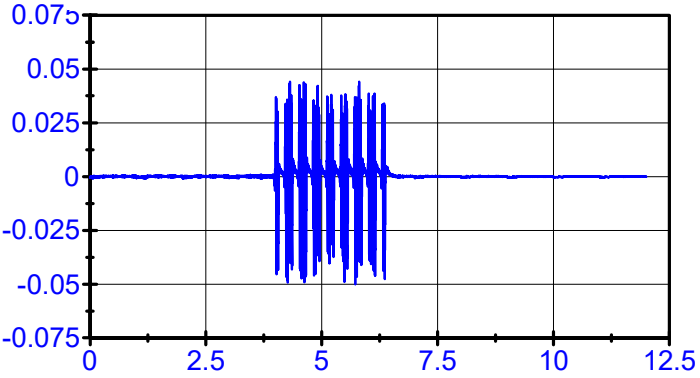

01\06\16 21:49:46 - Voltage - G2_T3T4_E

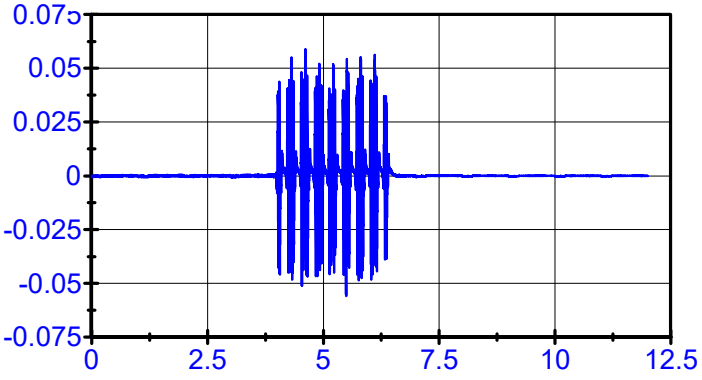

RAIL & SLEEPER ACCELERATIONS

ACCELEROMETERS

NOTES:

Units of Y axle are “g” for all the plots belonging to both rail and sleeper acceleration.

A Low Pass Filter of 250 Hz has been applied to all raw signals of sleeper acceleration.

A Low Pass Filter of 200 Hz has been applied to all raw signals of rail acceleration.

01\06\16 06:31:45

Sleeper Accelerometers
LPF 250Hz

01\06\16 06:31:45 - Voltage - AC_T2_E

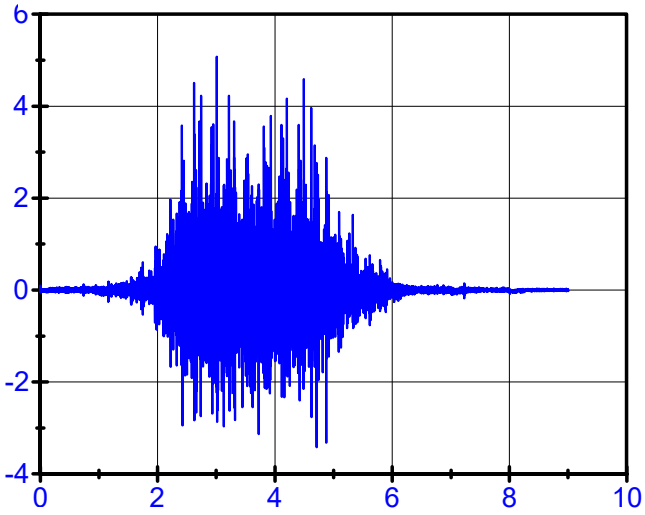

01\06\16 06:31:45 - Voltage - AC_T2_C

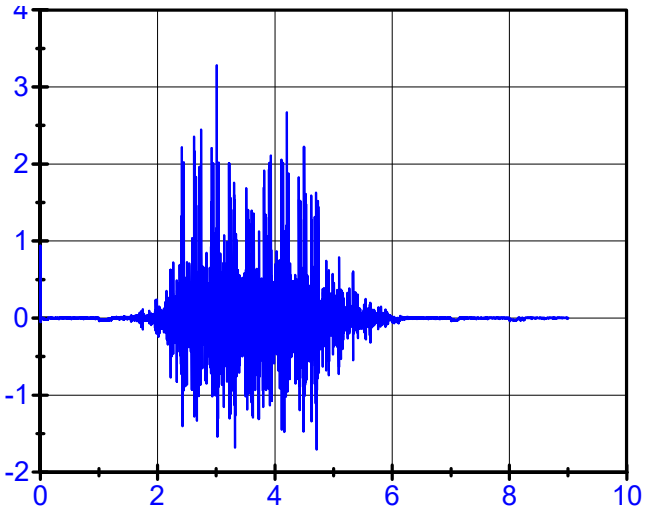

01\06\16 06:31:45 - Voltage - AC_T2_I

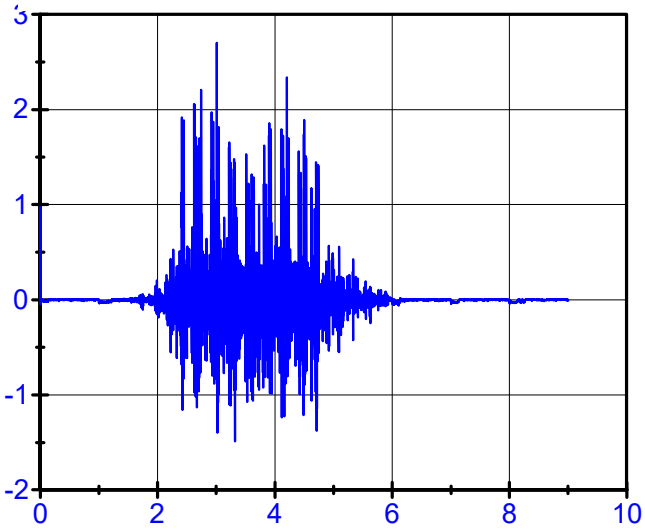

Rail Accelerometers
LPF 200Hz

01\06\16 06:31:45 - Voltage - AC_T2T3_E

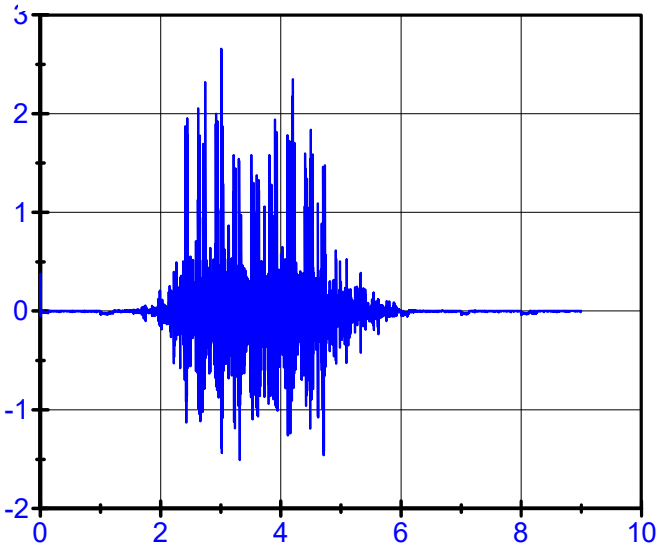

01\06\16 06:31:45 - Voltage - AC_T2T3_I

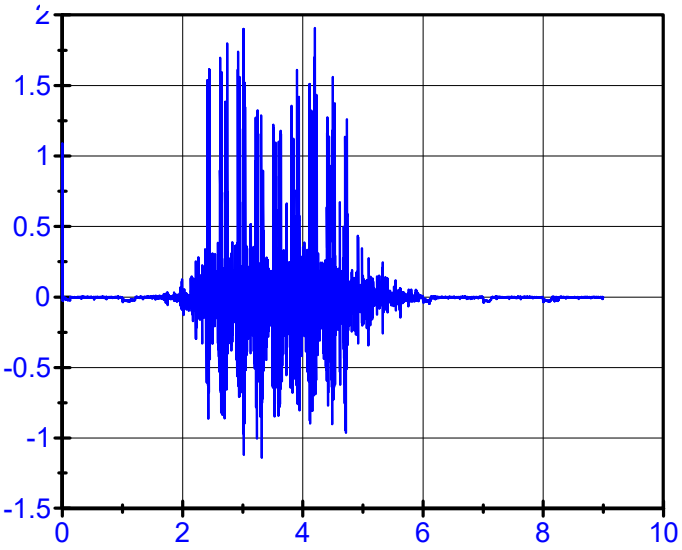

01\06\16 06:52:39

Sleeper Accelerometers
LPF 250Hz

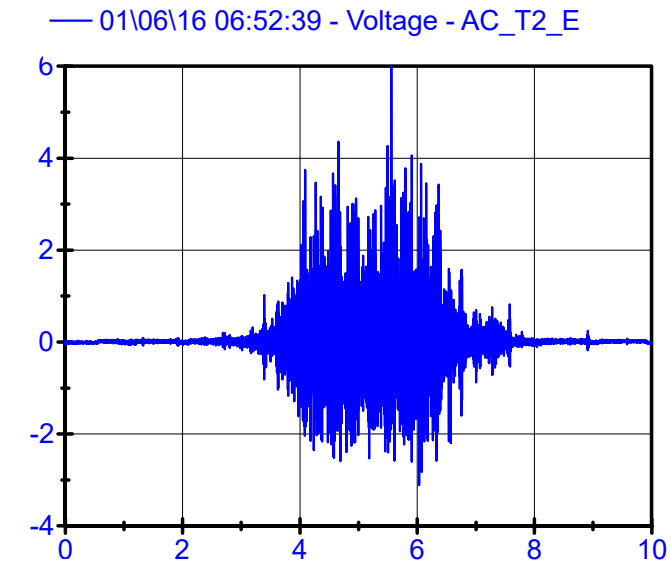

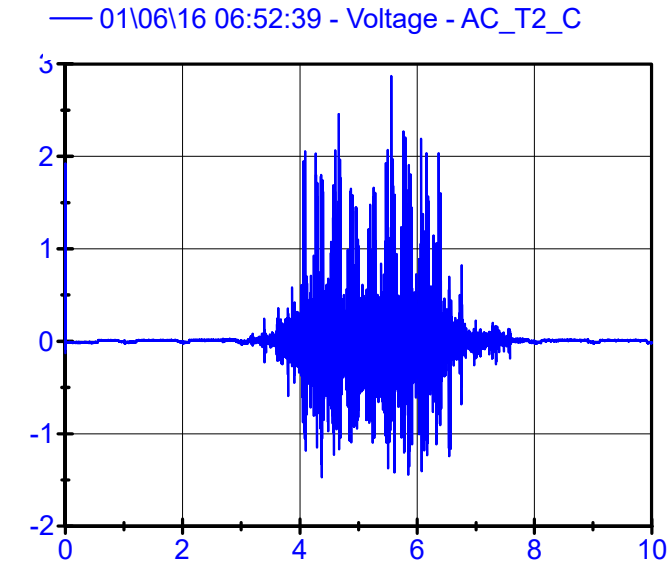

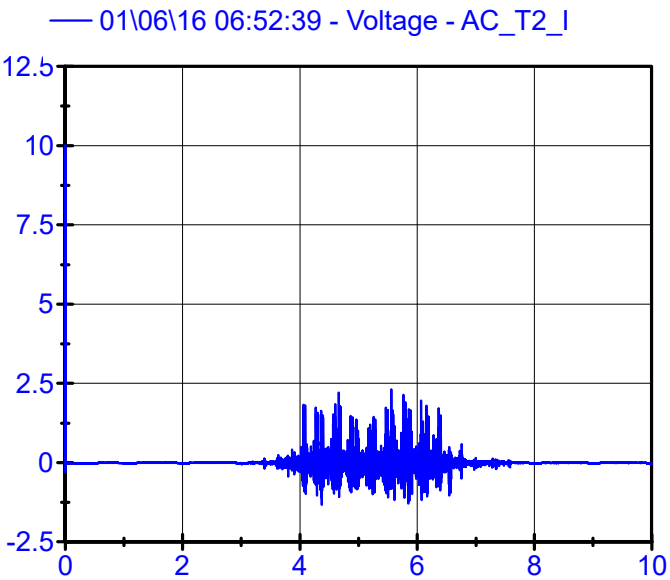

Rail Accelerometers
LPF 200Hz

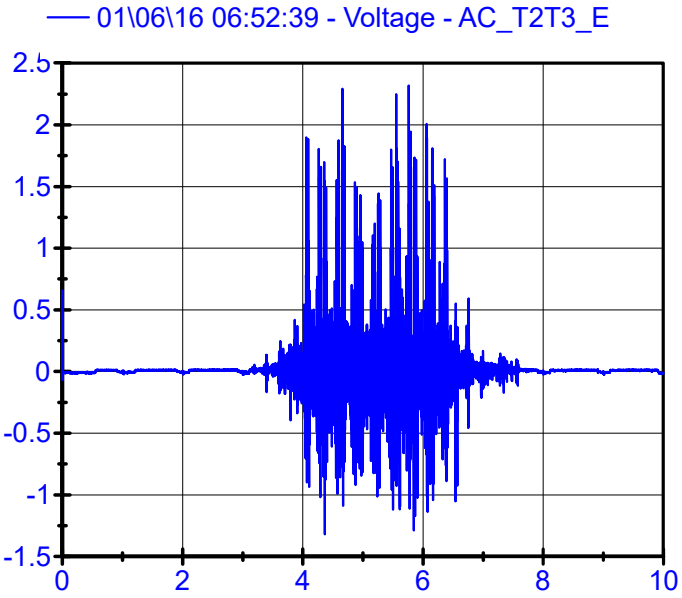

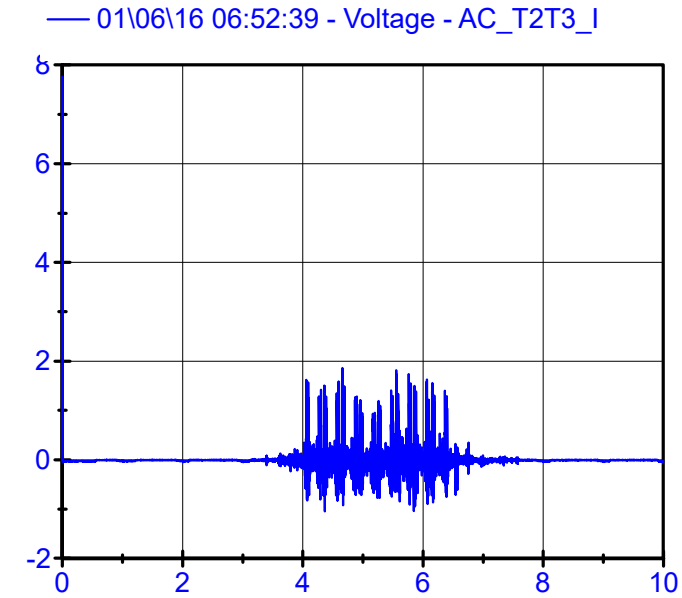

01\06\16 07:21:52

Sleeper Accelerometers
LPF 250Hz

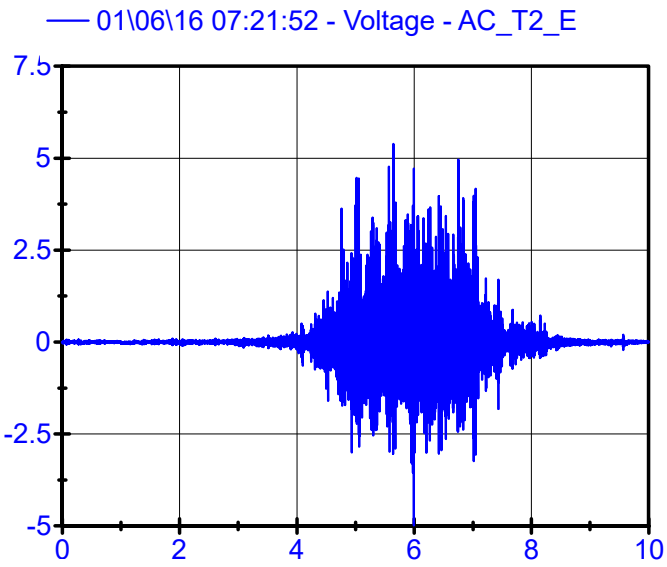

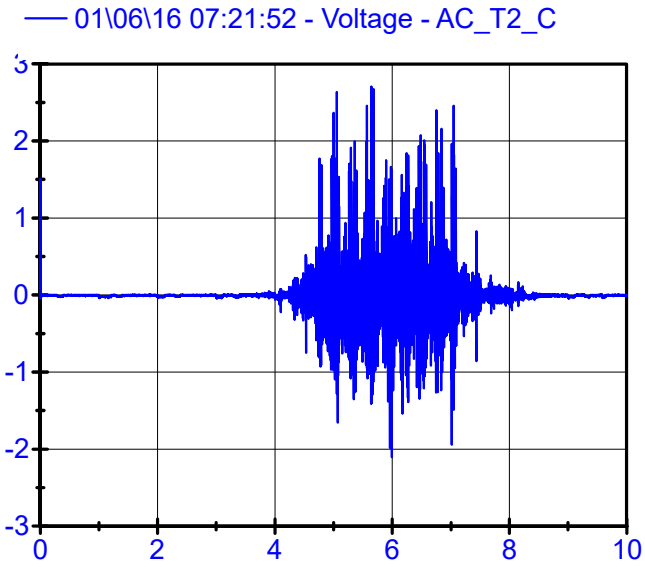

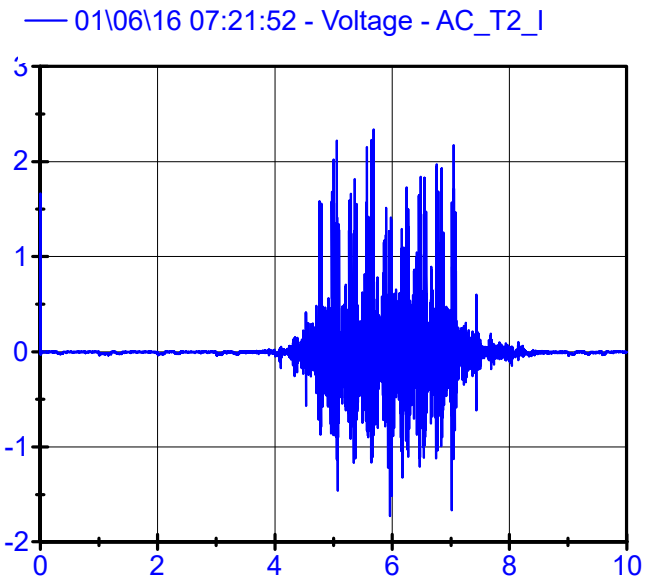

Rail Accelerometers
LPF 200Hz

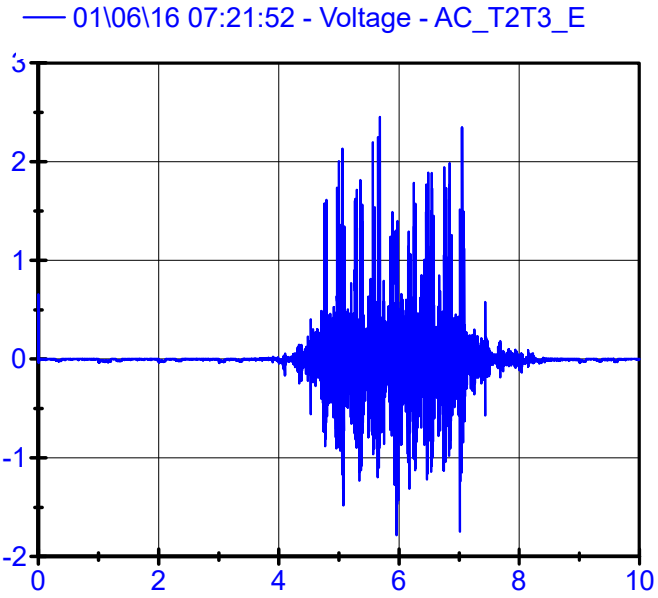

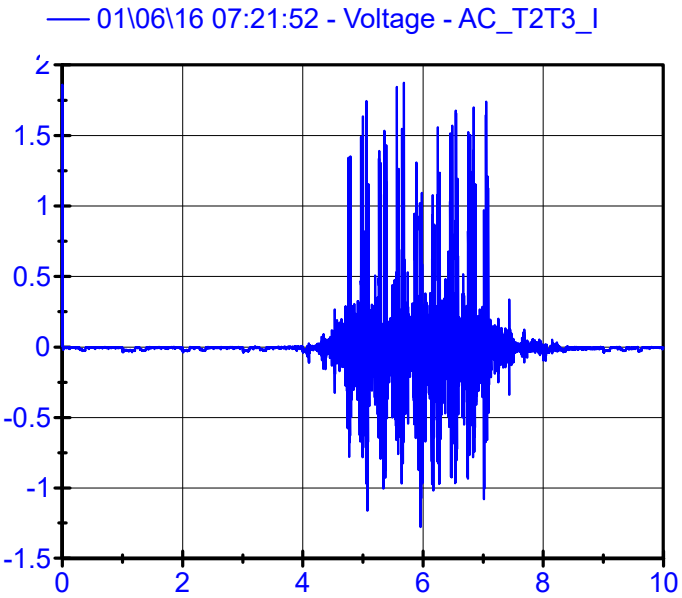

01\06\16 07:41:25

Sleeper Accelerometers
LPF 250Hz

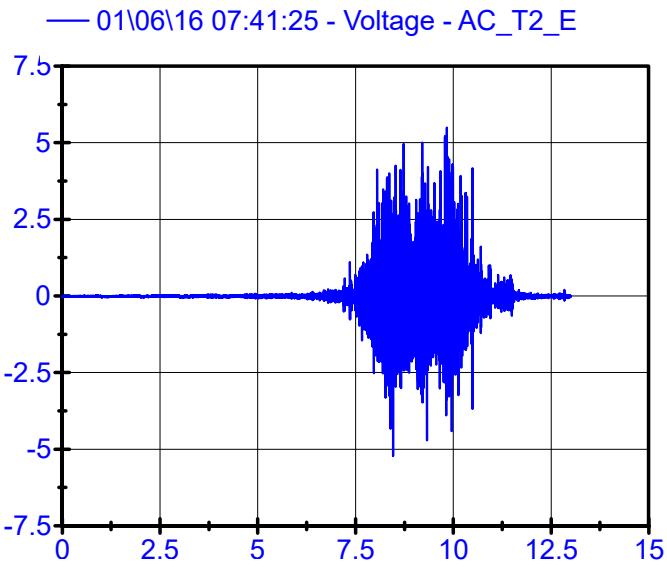

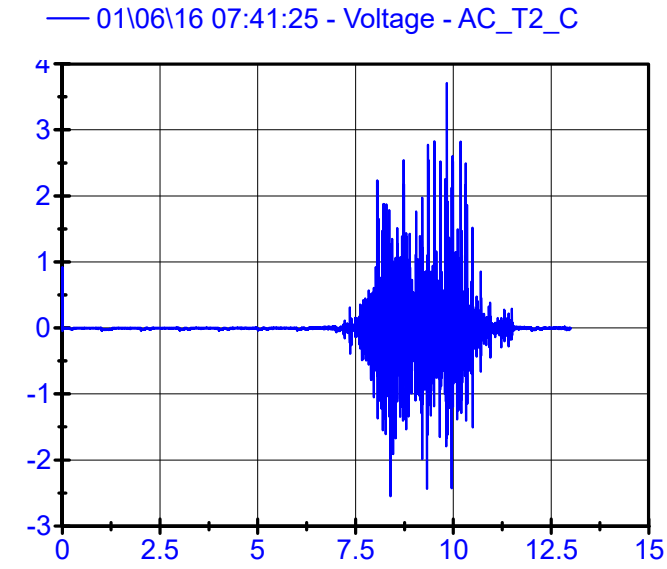

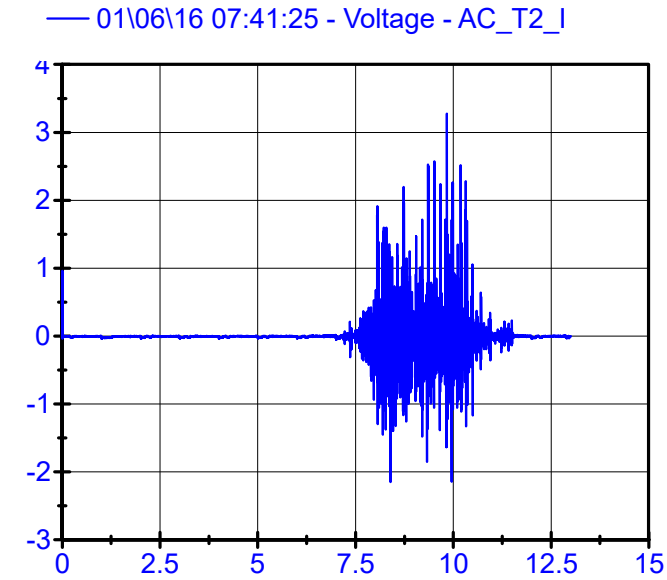

Rail Accelerometers
LPF 200Hz

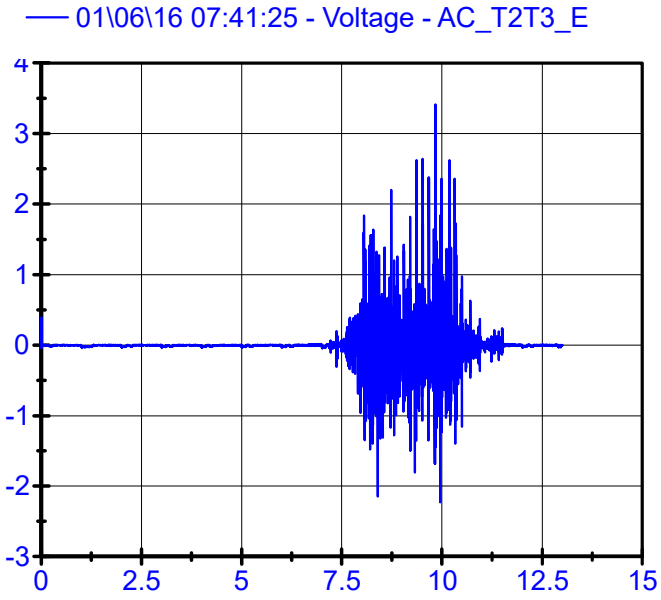

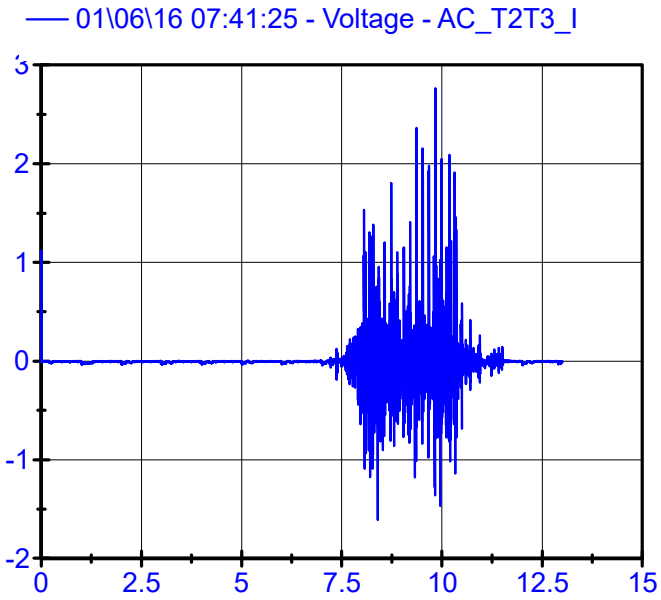

01\06\16 07:56:37

Sleeper Accelerometers
LPF 250Hz

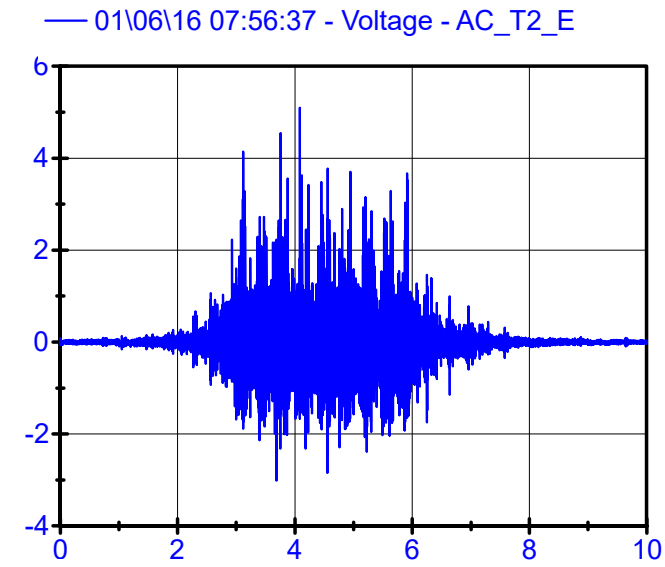

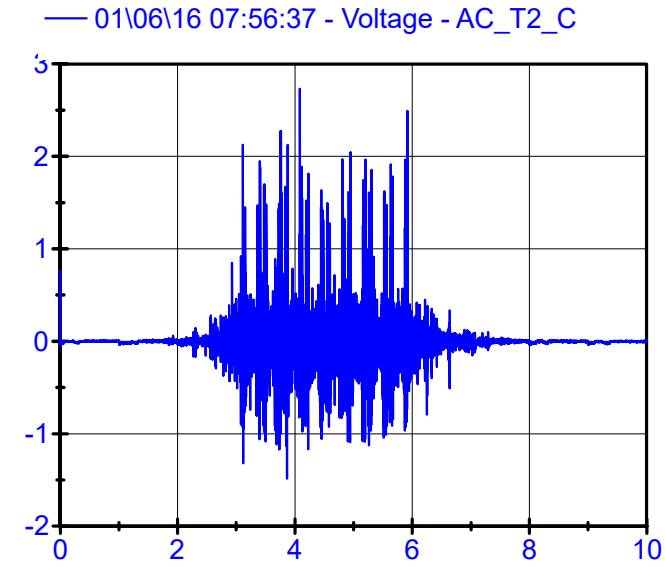

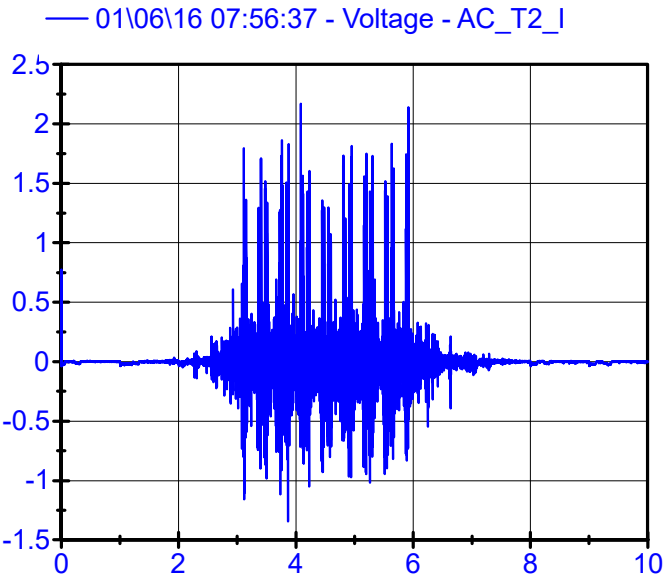

Rail Accelerometers
LPF 200Hz

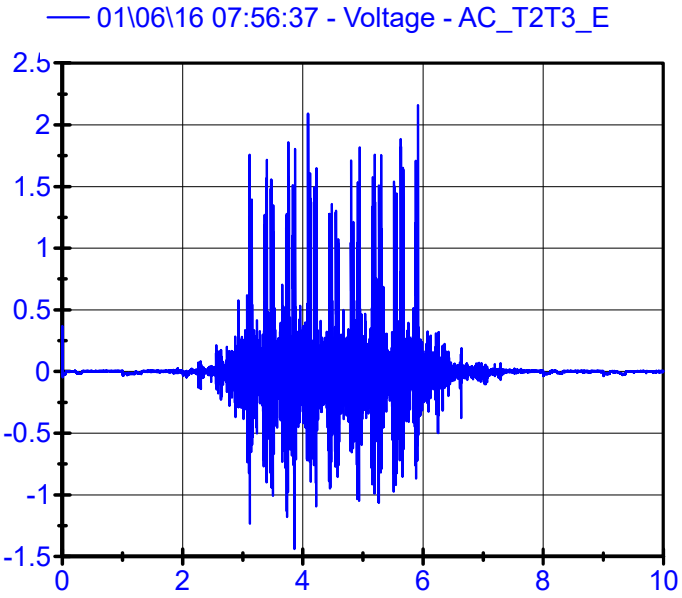

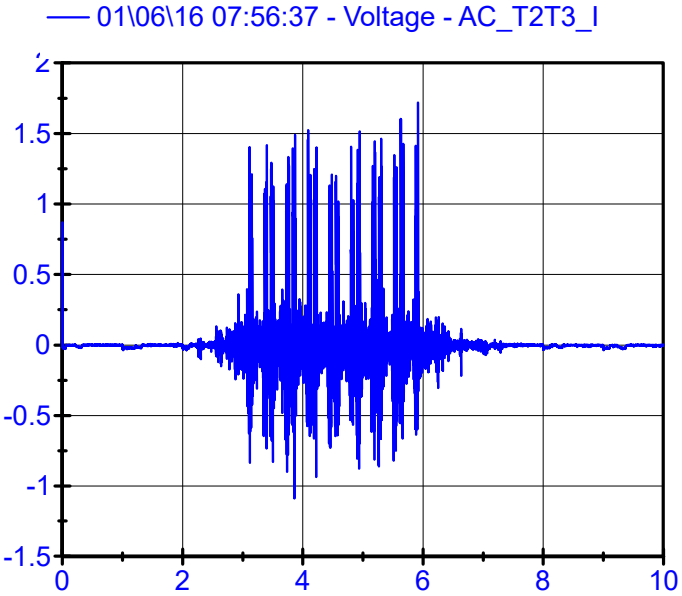

01\06\16 08:01:29

Sleeper Accelerometers
LPF 250Hz

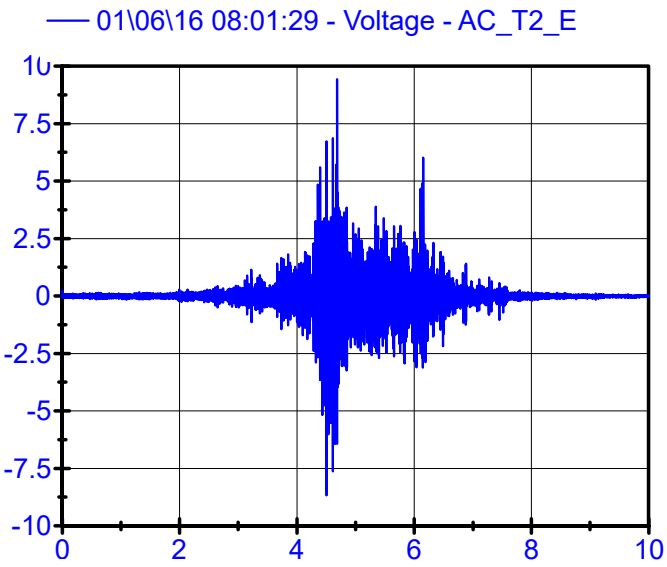

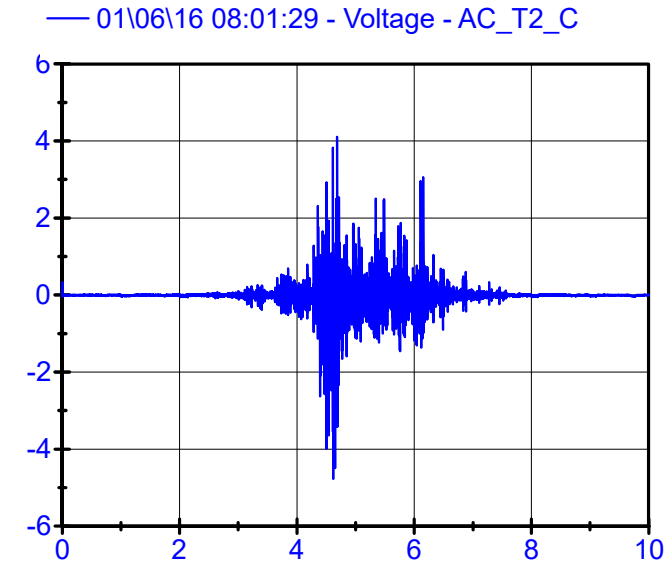

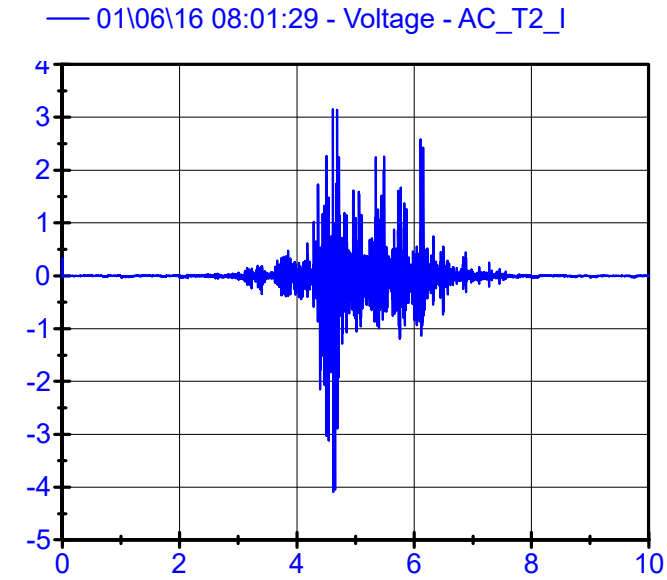

Rail Accelerometers
LPF 200Hz

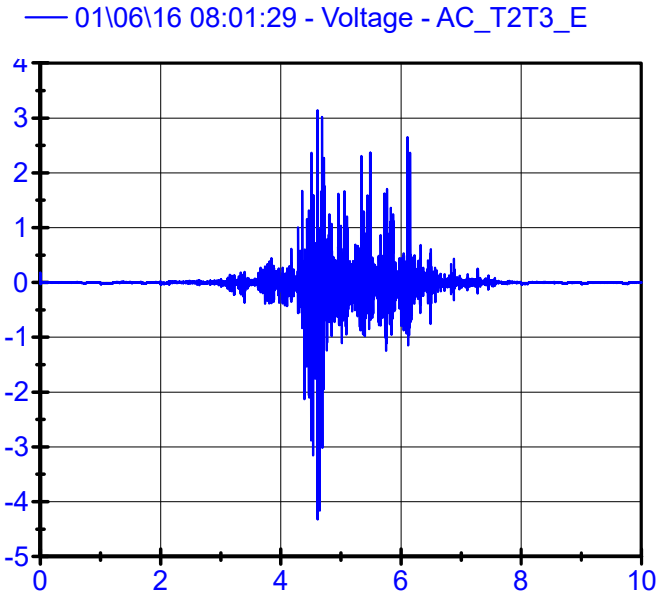

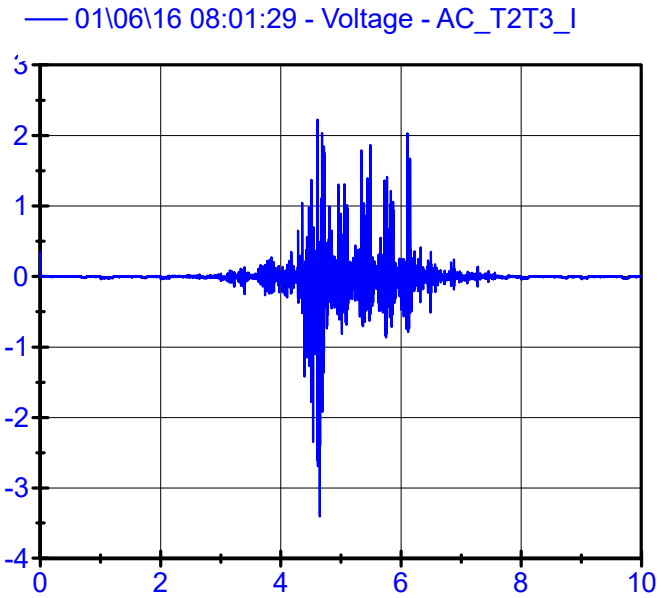

01\06\16 08:21:04

Sleeper Accelerometers
LPF 250Hz

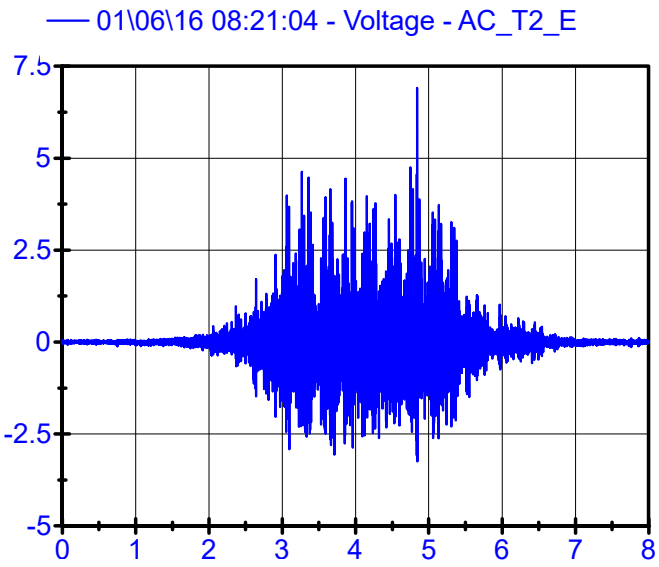

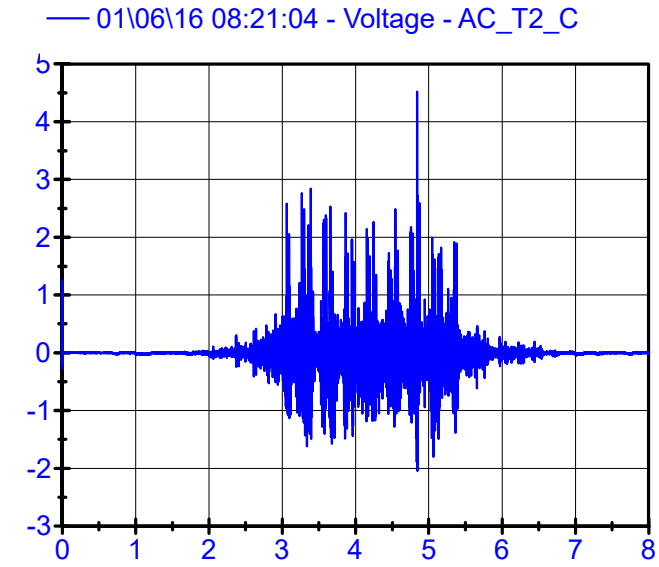

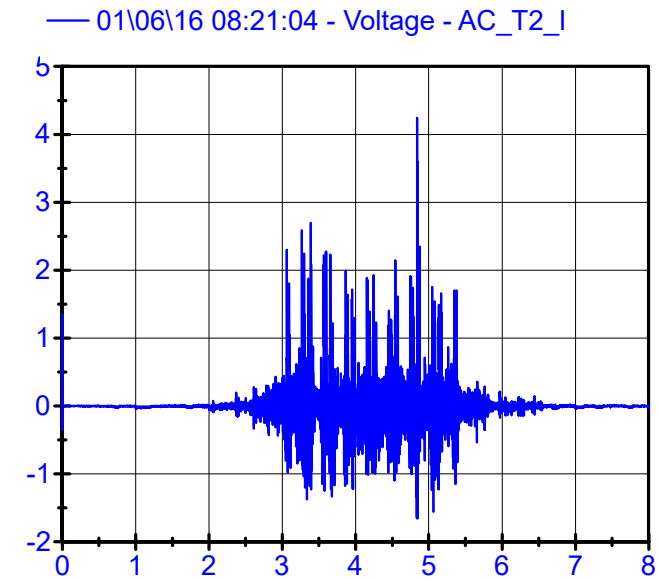

Rail Accelerometers
LPF 200Hz

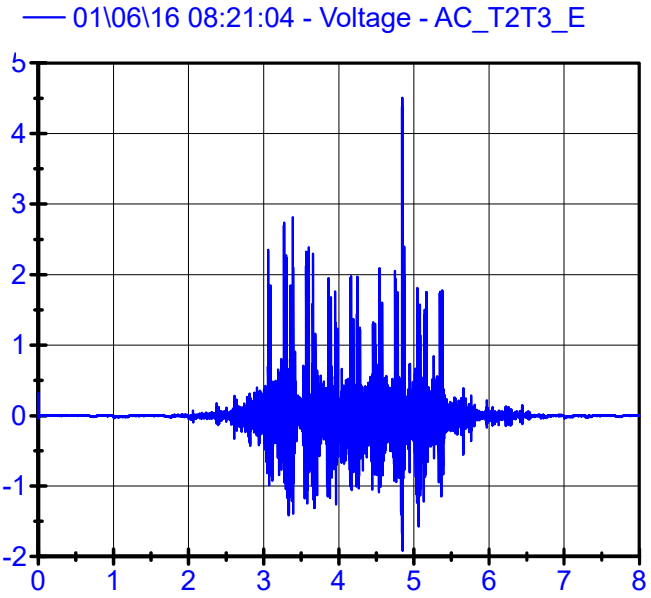

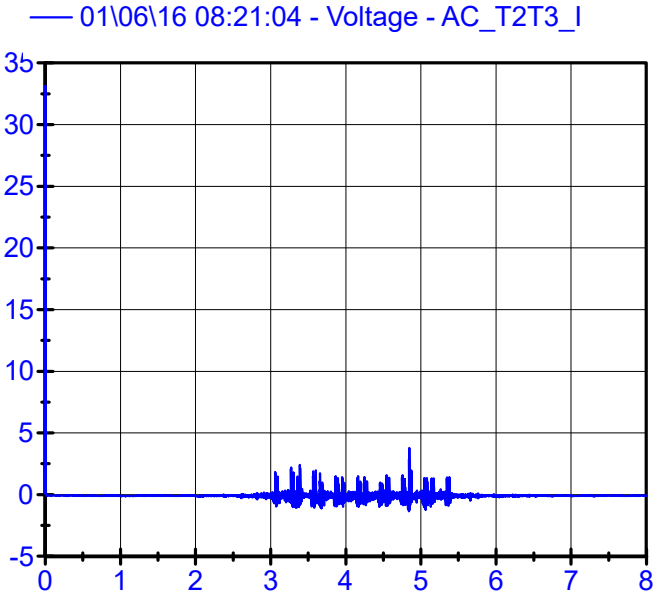

01\06\16 08:42:39

Sleeper Accelerometers
LPF 250Hz

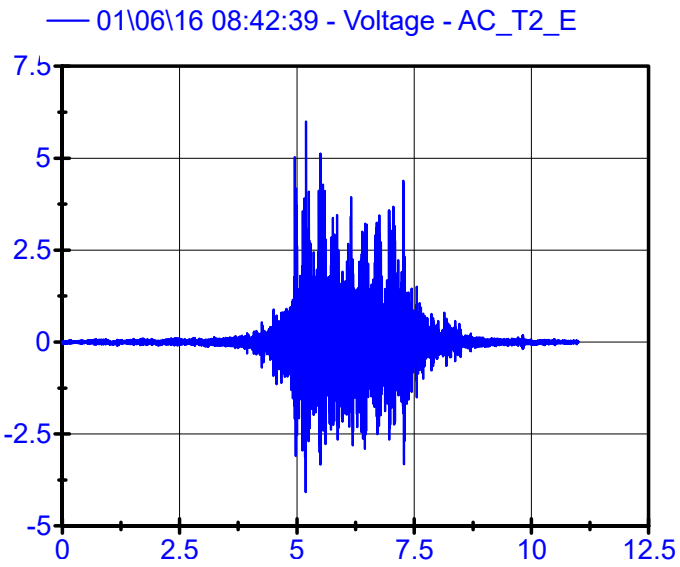

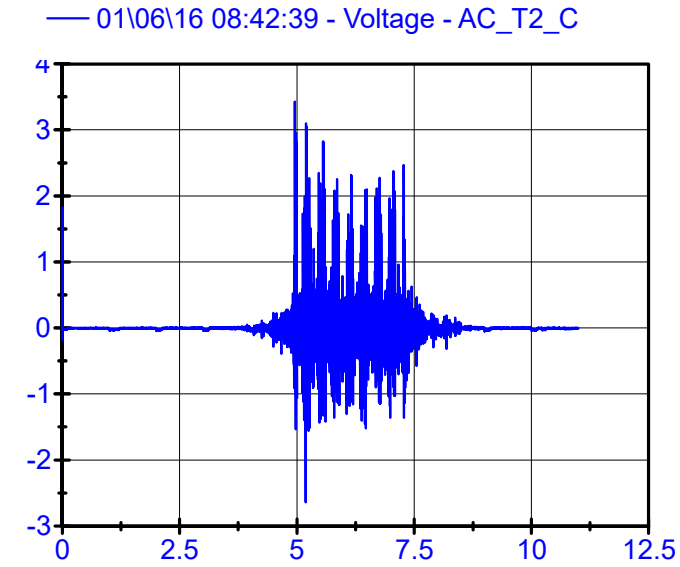

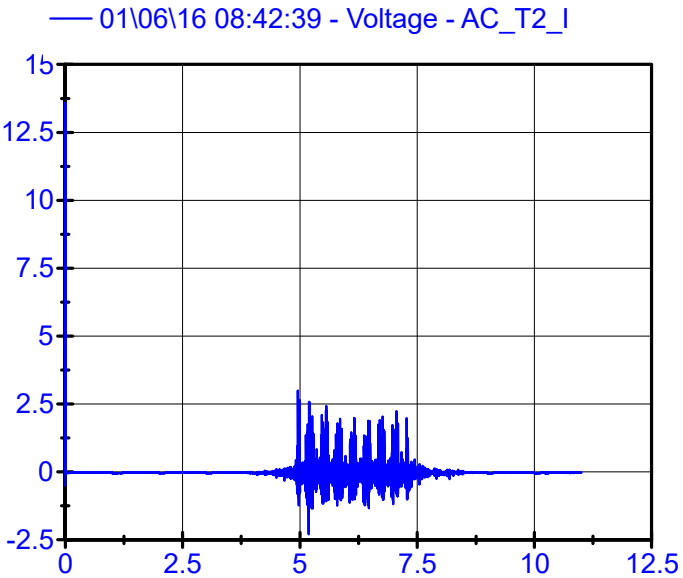

Rail Accelerometers
LPF 200Hz

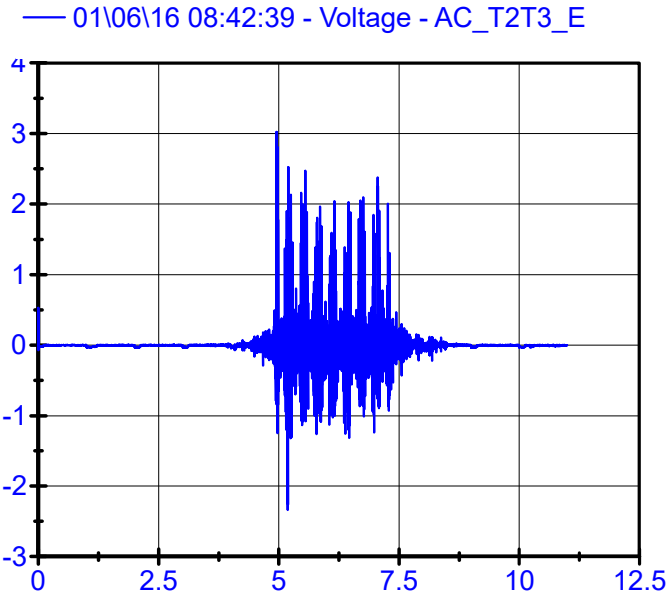

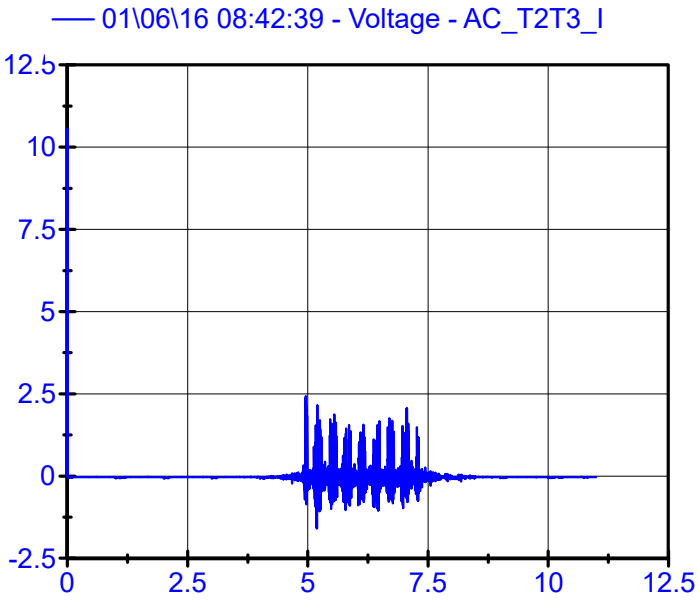

01\06\16 08:52:26

Sleeper Accelerometers
LPF 250Hz

01\06\16 08:52:26 - Voltage - AC_T2_E

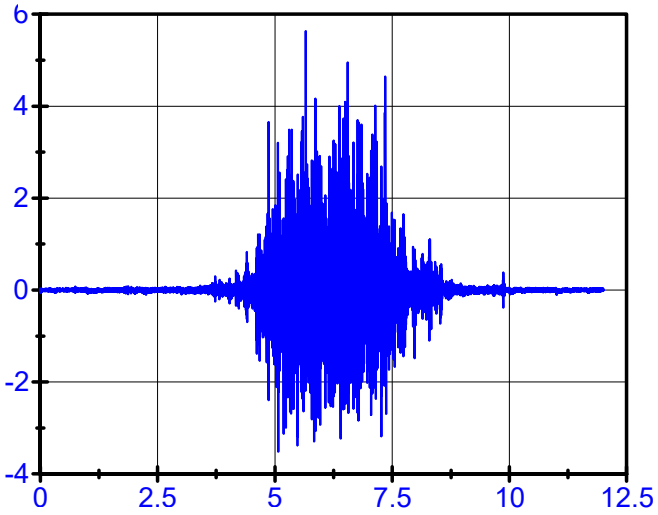

01\06\16 08:52:26 - Voltage - AC_T2_C

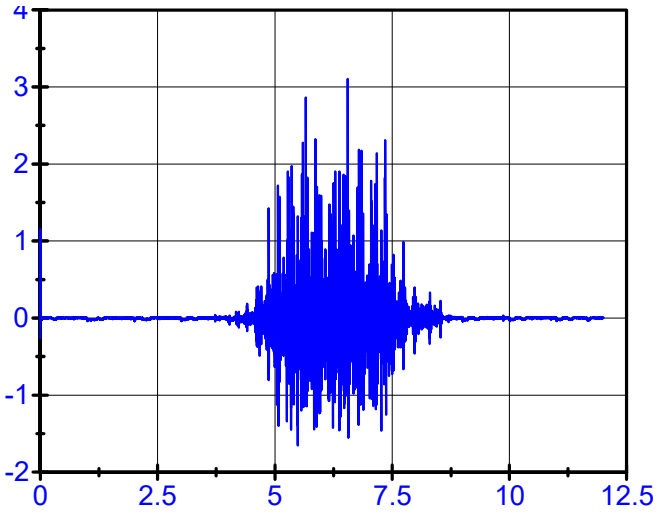

01\06\16 08:52:26 - Voltage - AC_T2_I

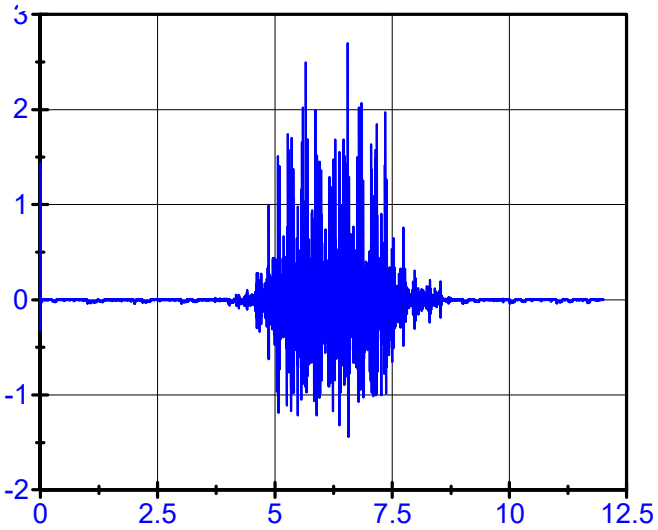

Rail Accelerometers
LPF 200Hz

01\06\16 08:52:26 - Voltage - AC_T2T3_E

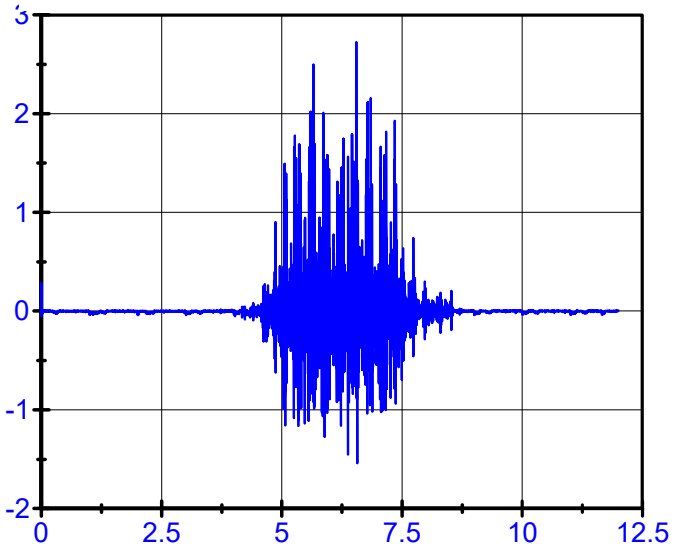

01\06\16 08:52:26 - Voltage - AC_T2T3_I

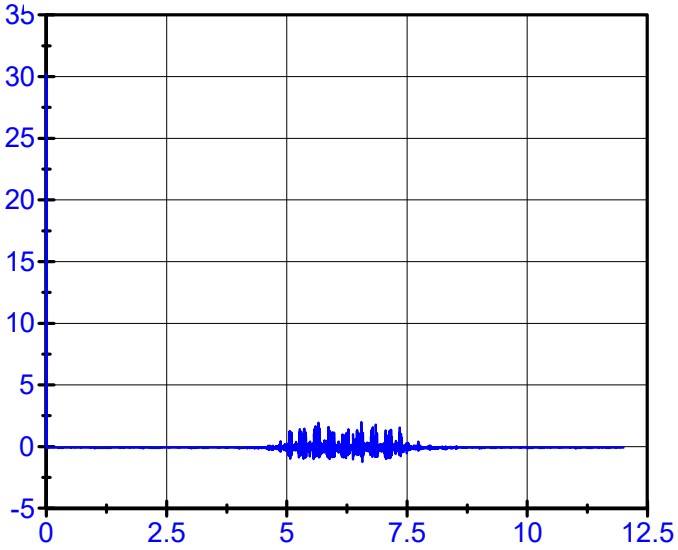

01\06\16 09:23:16

Sleeper Accelerometers
LPF 250Hz

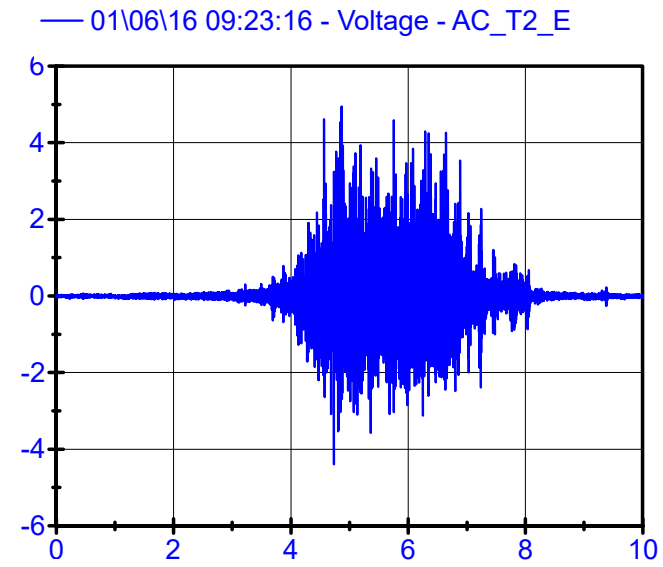

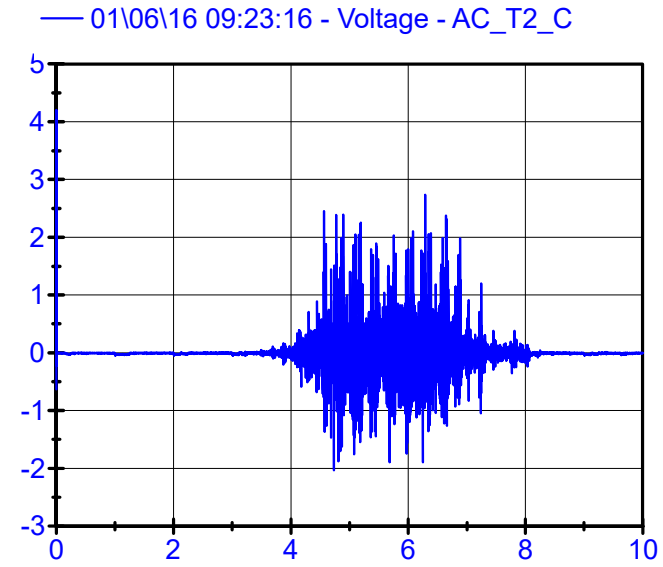

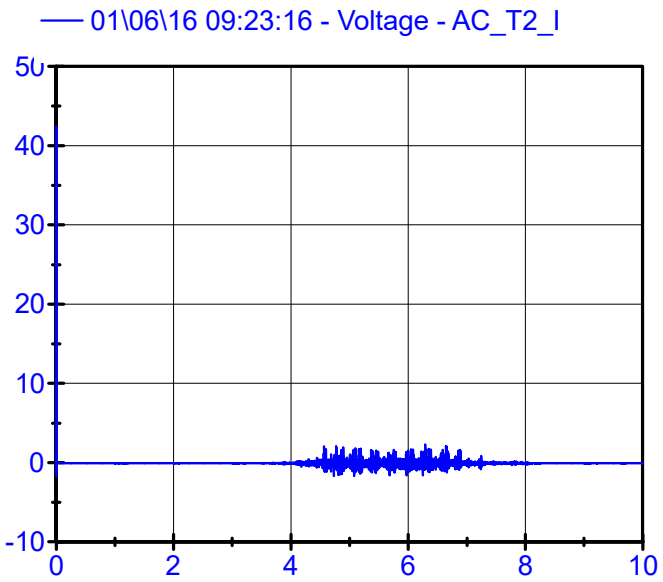

Rail Accelerometers
LPF 200Hz

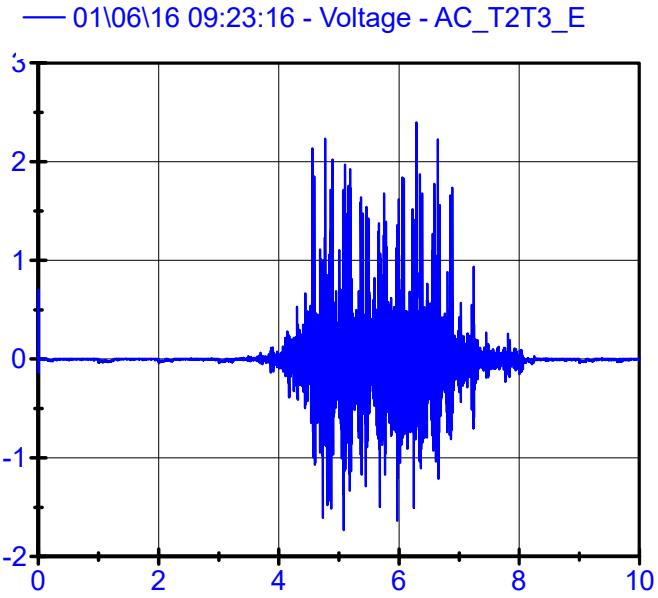

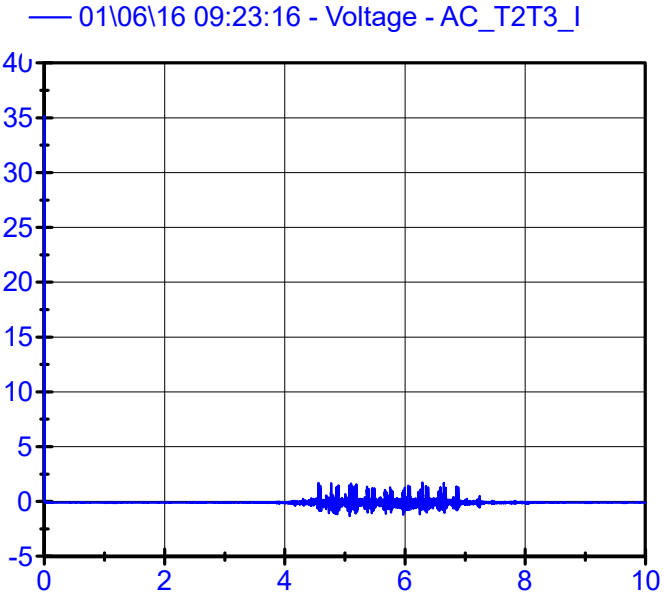

01\06\16 09:52:01

Sleeper Accelerometers
LPF 250Hz

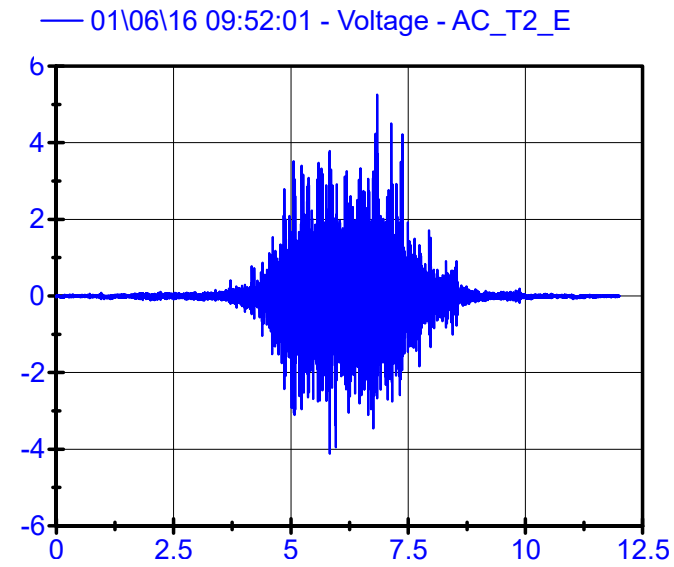

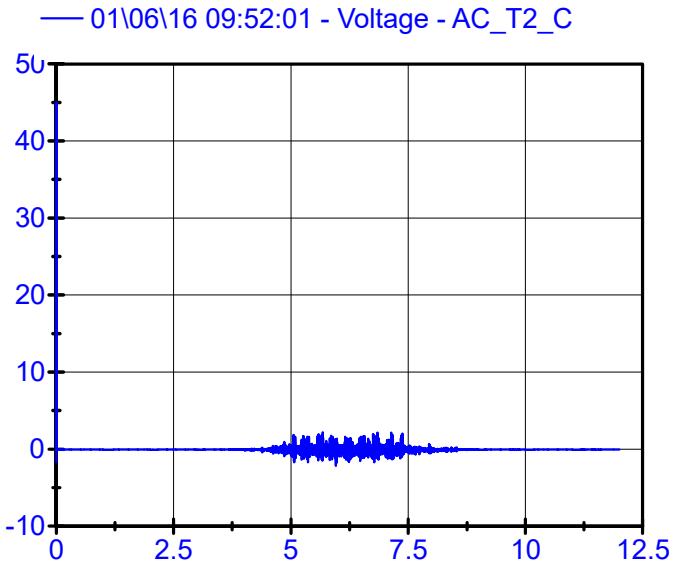

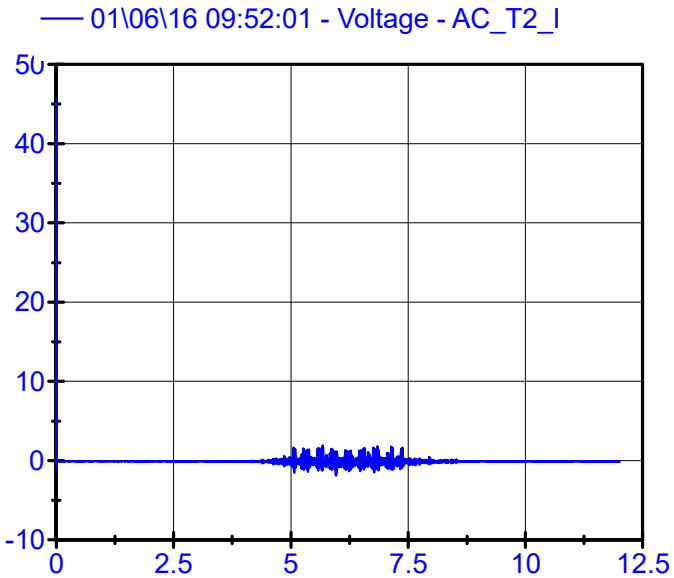

Rail Accelerometers
LPF 200Hz

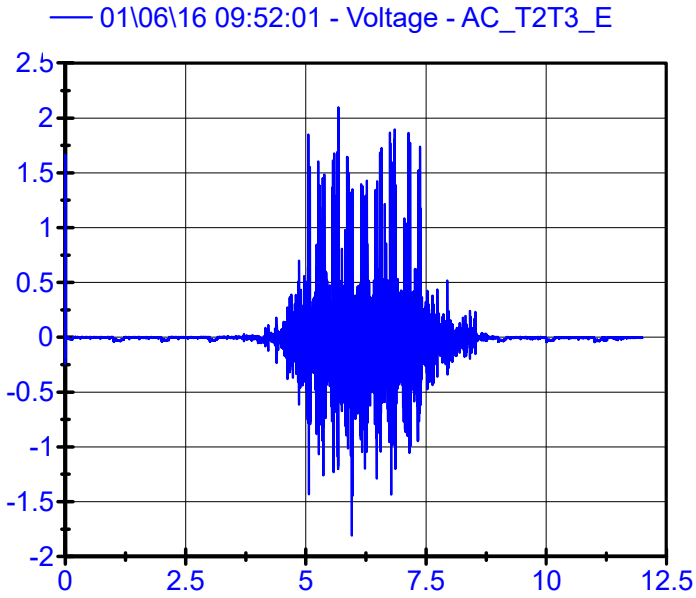

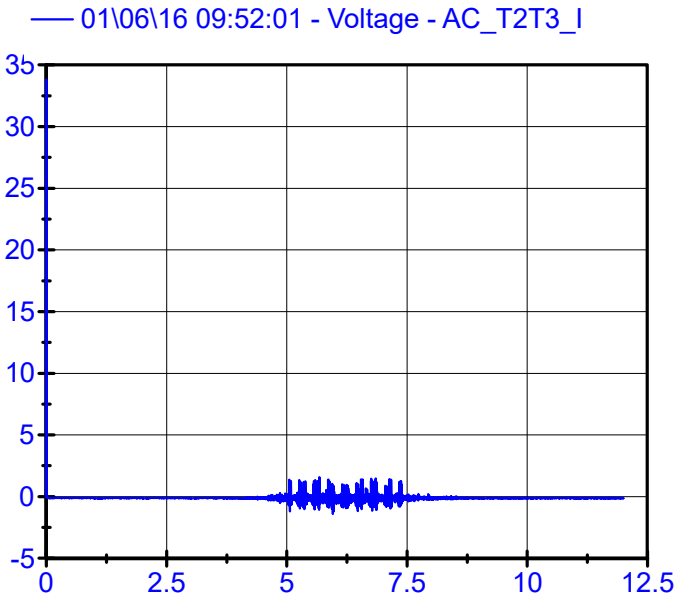

01\06\16 10:53:28

Sleeper Accelerometers
LPF 250Hz

01\06\16 10:53:28 - Voltage - AC_T2_E

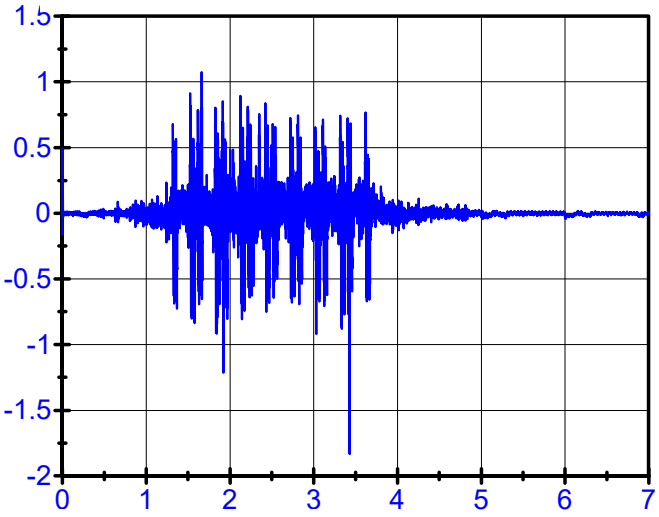

01\06\16 10:53:28 - Voltage - AC_T2_C

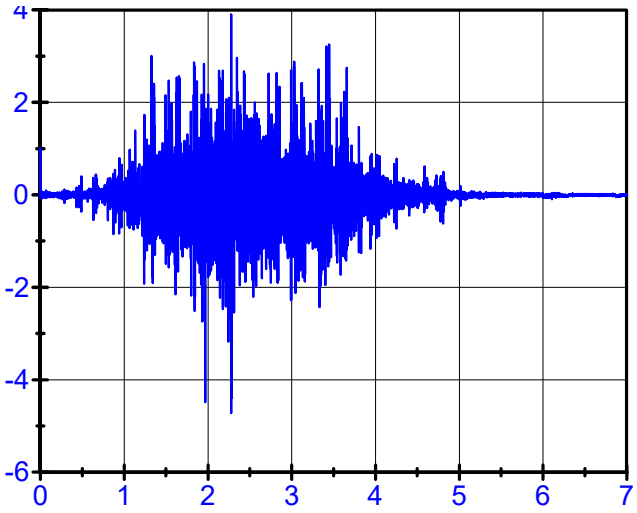

01\06\16 10:53:28 - Voltage - AC_T2_I

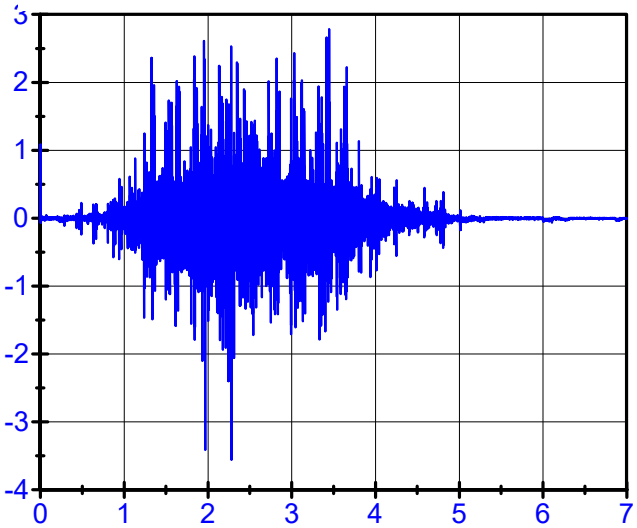

Rail Accelerometers
LPF 200Hz

01\06\16 10:53:28 - Voltage - AC_T2T3_E

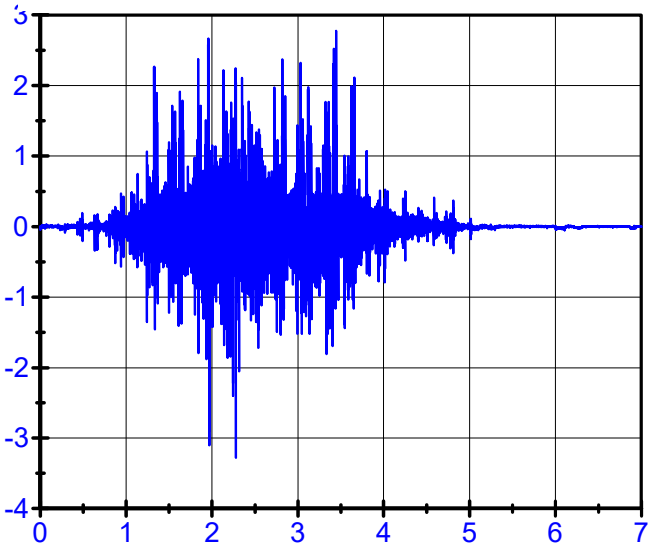

01\06\16 10:53:28 - Voltage - AC_T2T3_I

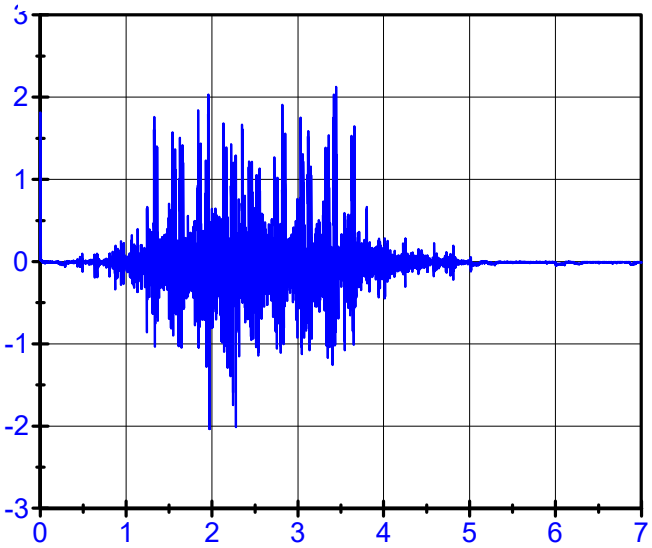

01\06\16 11:35:54 ·

Sleeper Accelerometers
LPF 250Hz

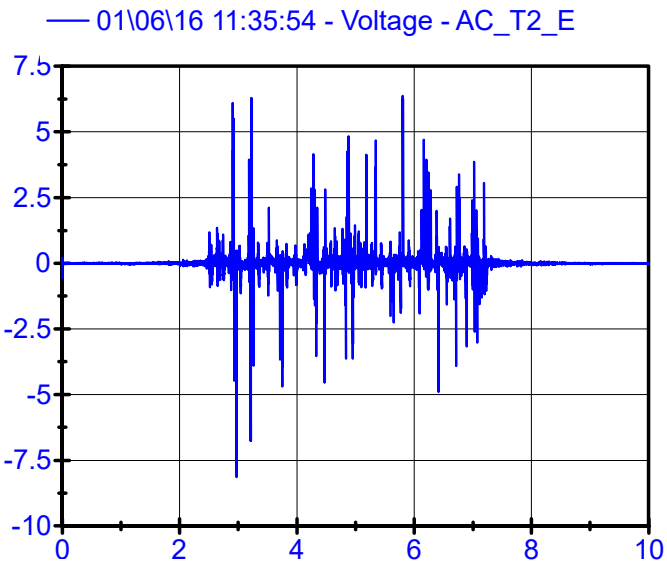

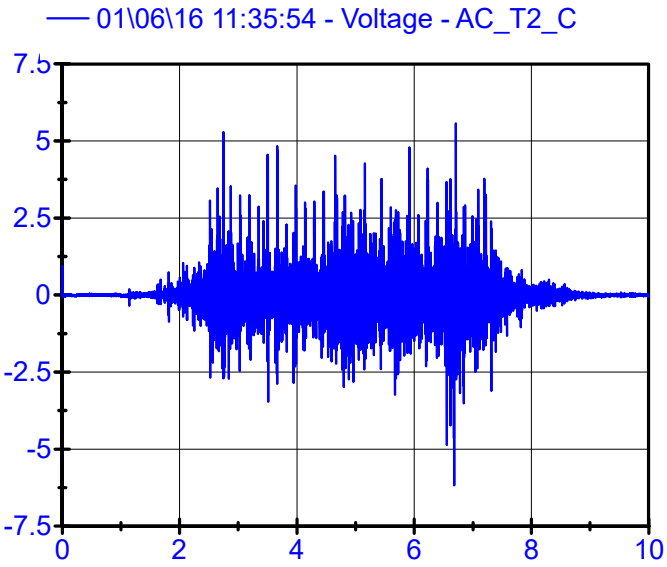

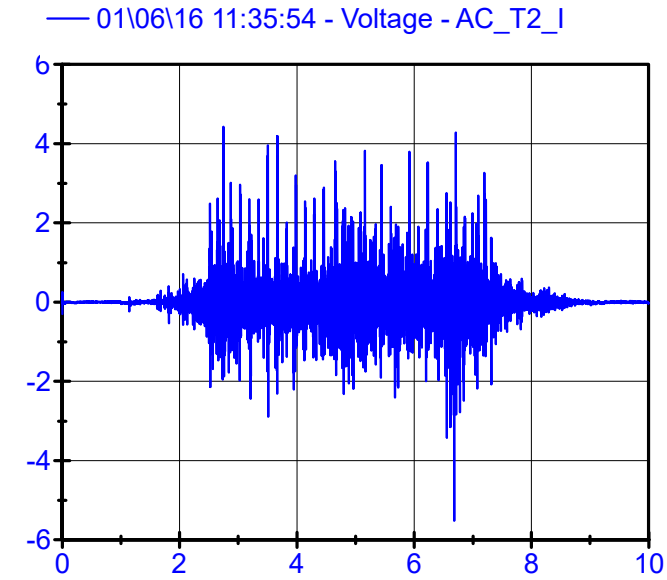

Rail Accelerometers
LPF 200Hz

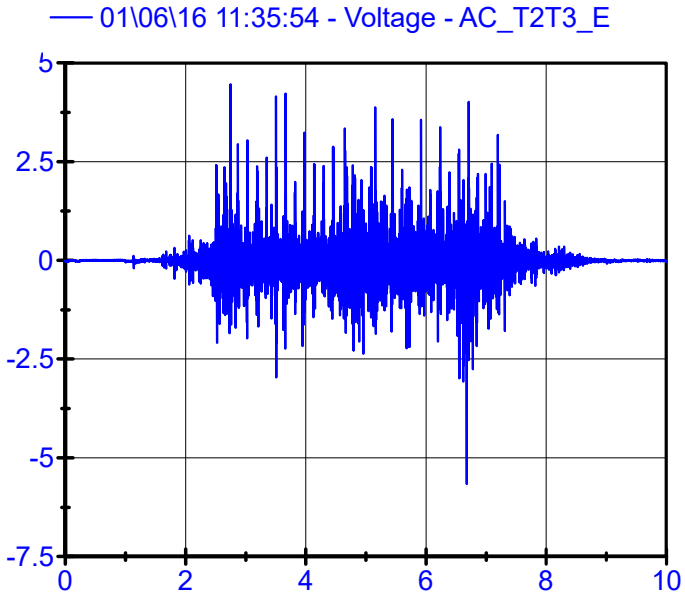

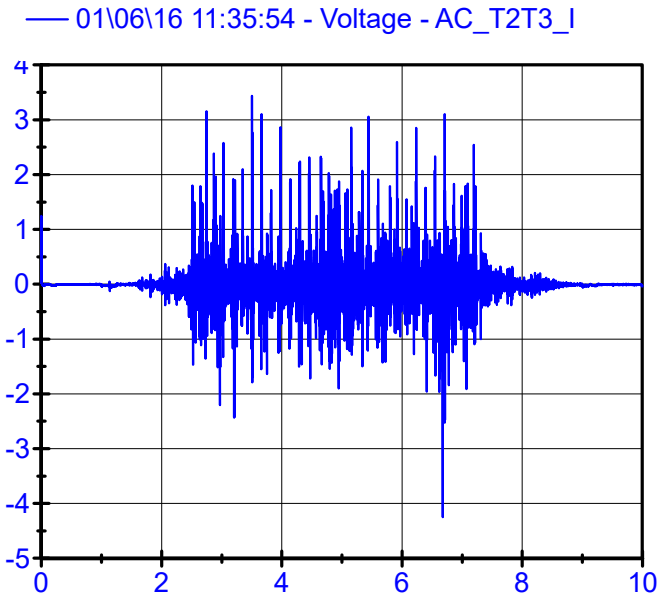

01\06\16 11:53:47 ·

Sleeper Accelerometers
LPF 250Hz

01\06\16 11:53:47 - Voltage - AC_T2_E

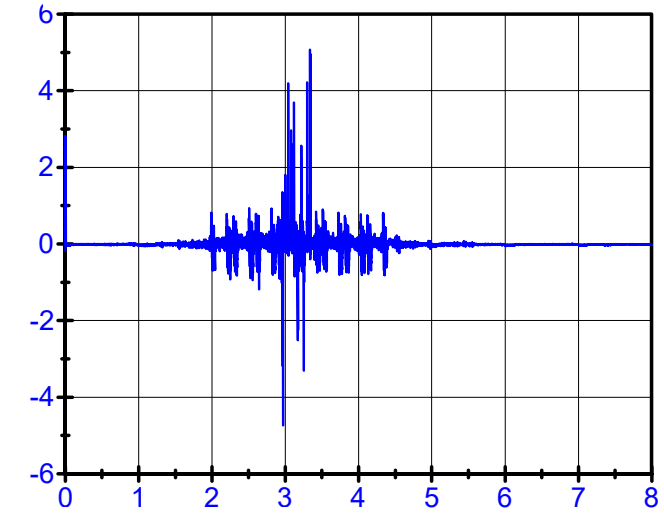

01\06\16 11:53:47 - Voltage - AC_T2_C

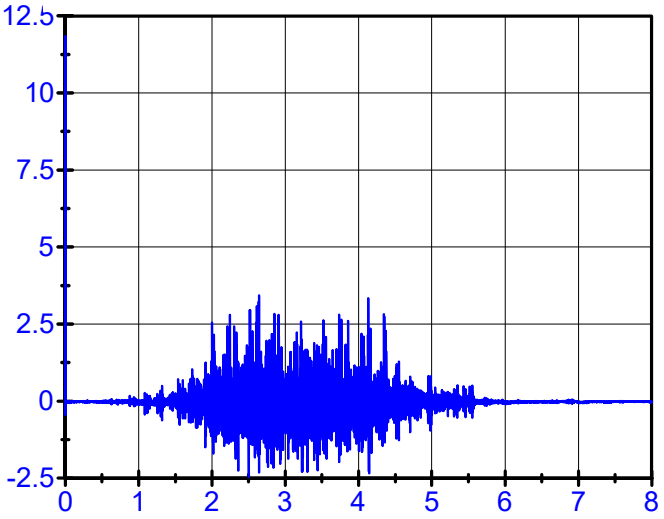

01\06\16 11:53:47 - Voltage - AC_T2_I

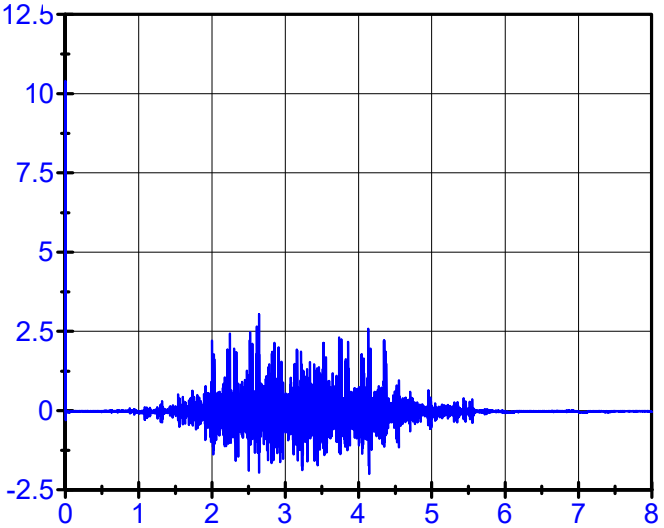

Rail Accelerometers
LPF 200Hz

01\06\16 11:53:47 - Voltage - AC_T2T3_E

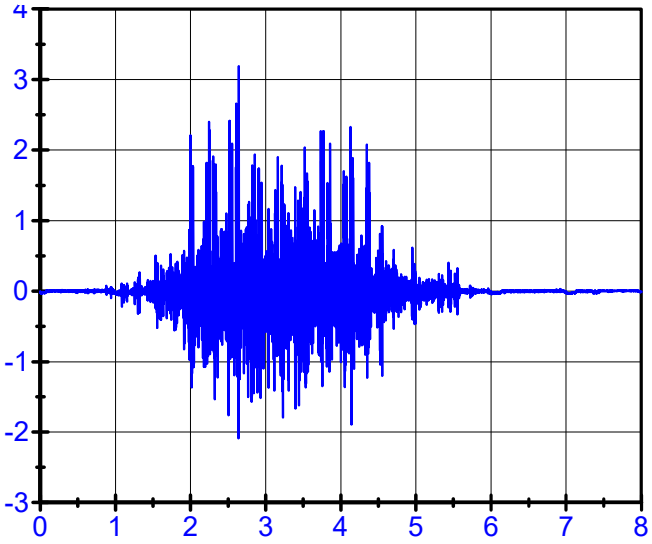

01\06\16 11:53:47 - Voltage - AC_T2T3_I

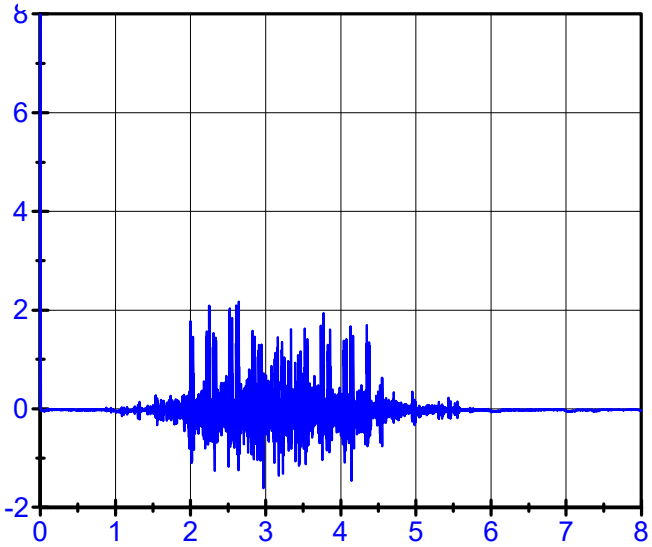

01\06\16 12:07:44

Sleeper Accelerometers
LPF 250Hz

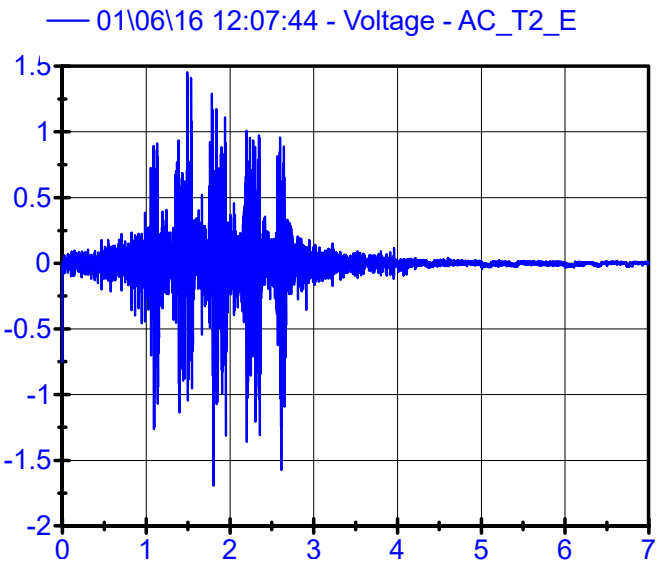

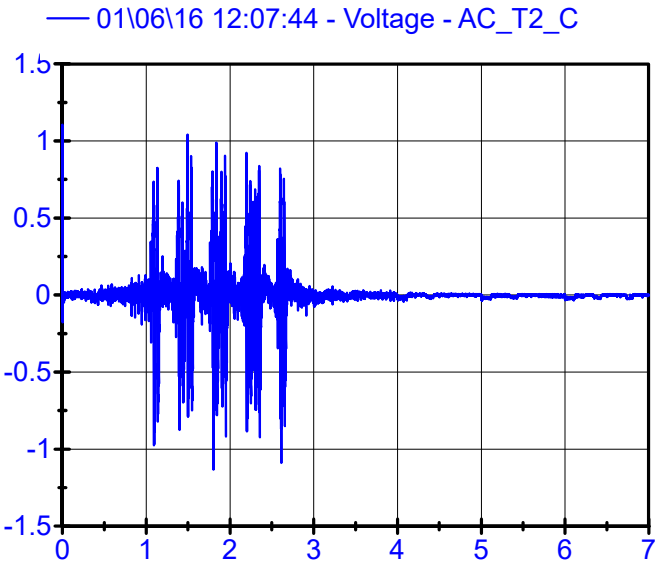

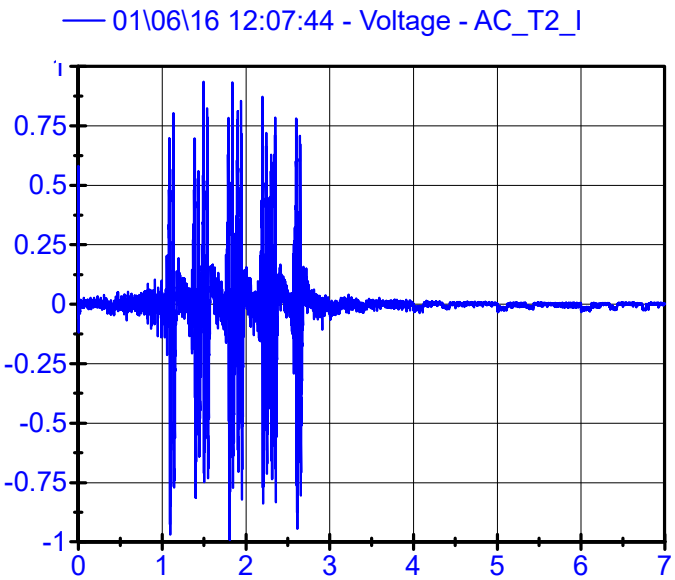

Rail Accelerometers
LPF 200Hz

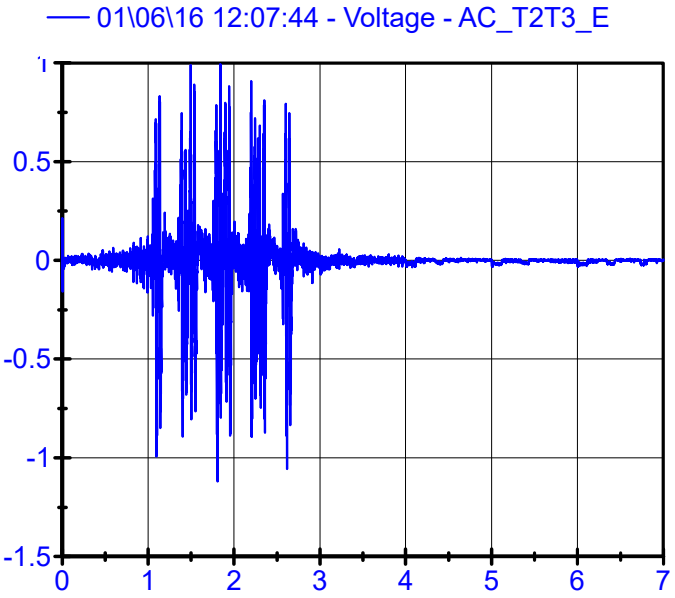

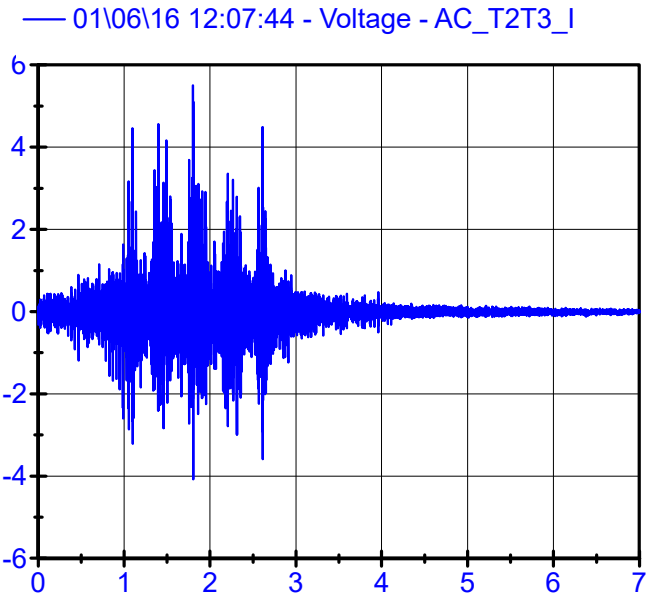

01\06\16 12:51:19

Sleeper Accelerometers
LPF 250Hz

01\06\16 12:51:19 - Voltage - AC_T2_E

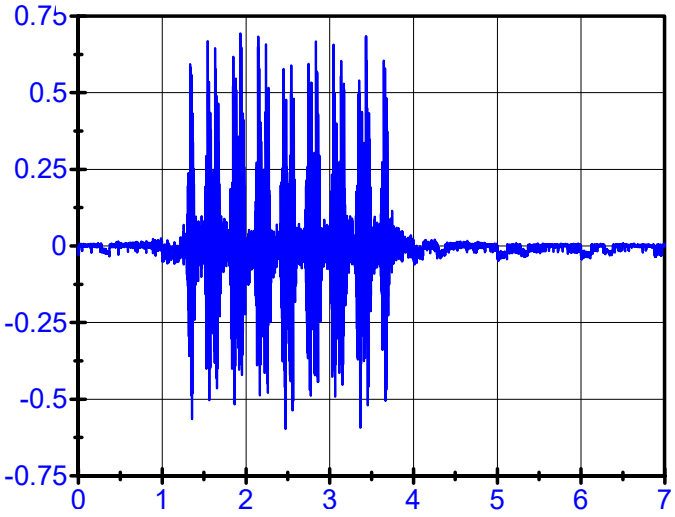

01\06\16 12:51:19 - Voltage - AC_T2_C

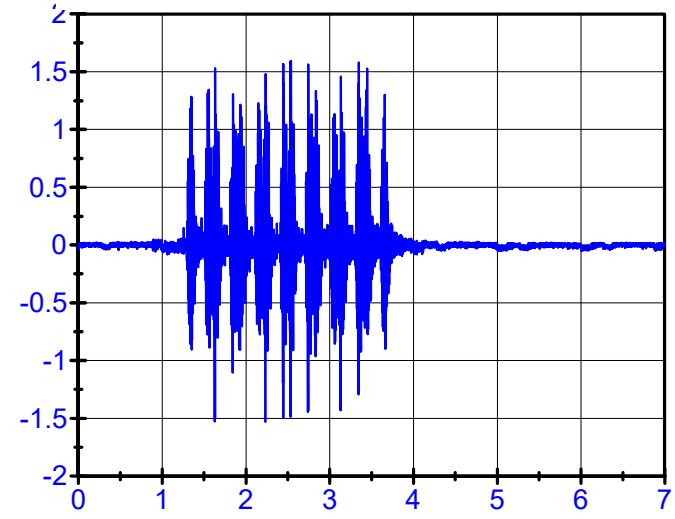

01\06\16 12:51:19 - Voltage - AC_T2_I

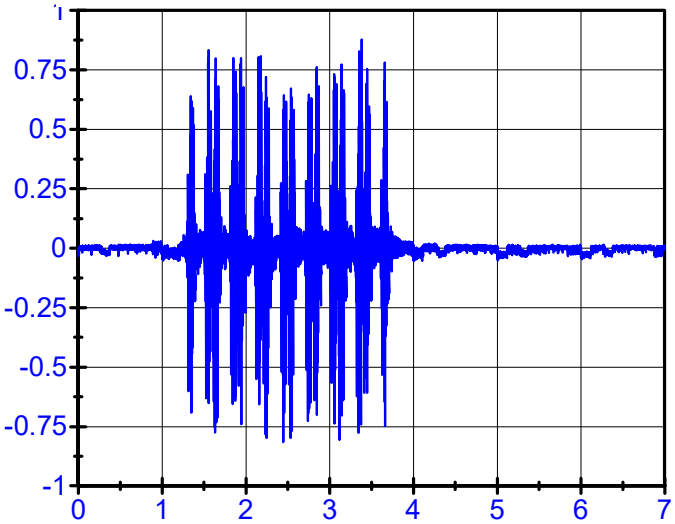

Rail Accelerometers
LPF 200Hz

01\06\16 12:51:19 - Voltage - AC_T2T3_E

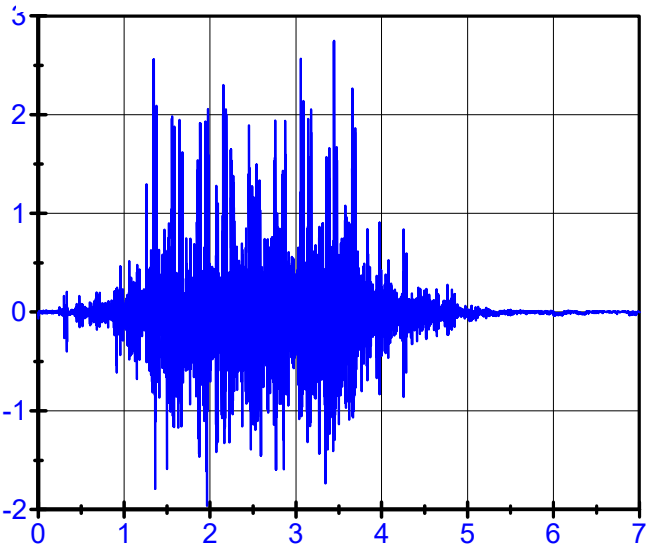

01\06\16 12:51:19 - Voltage - AC_T2T3_I

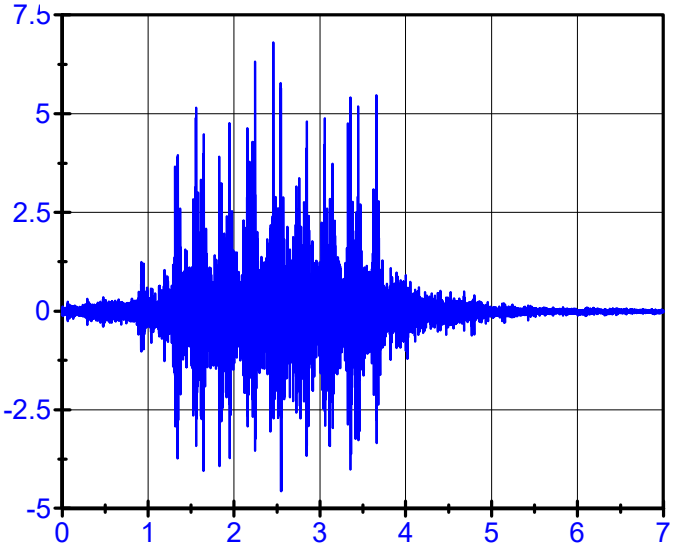

01\06\16 13:55:11 ·

Sleeper Accelerometers
LPF 250Hz

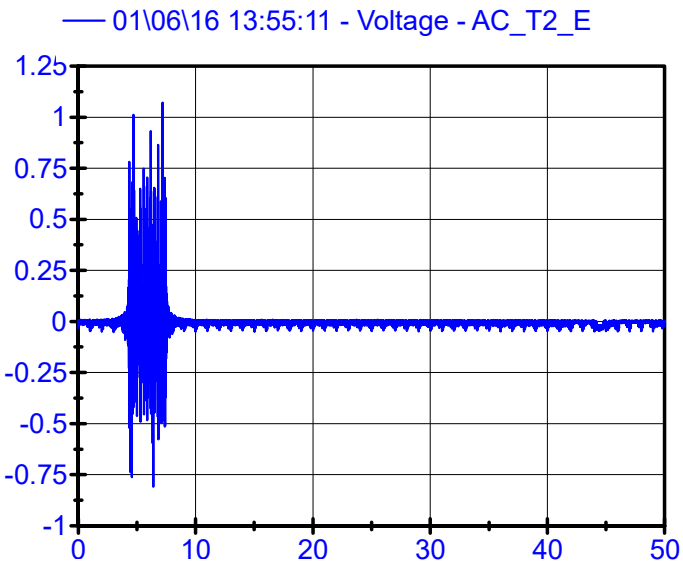

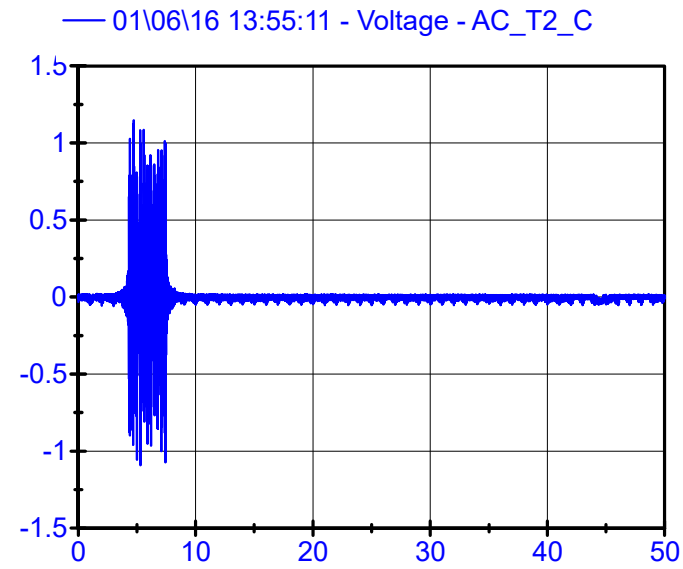

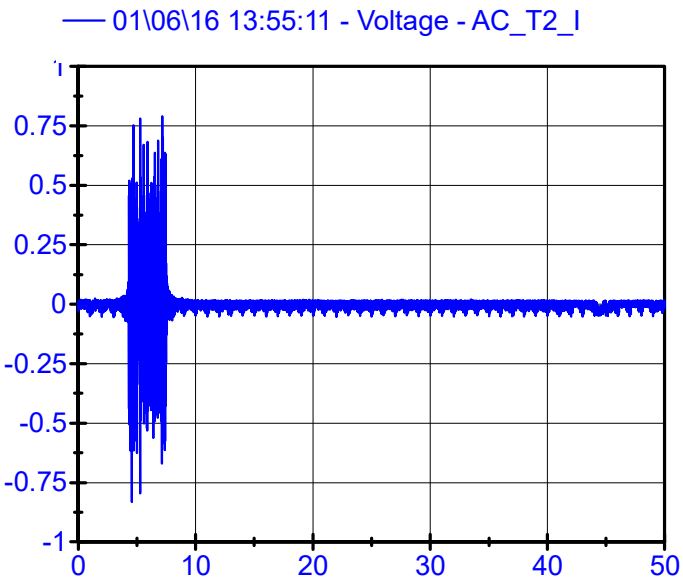

Rail Accelerometers
LPF 200Hz

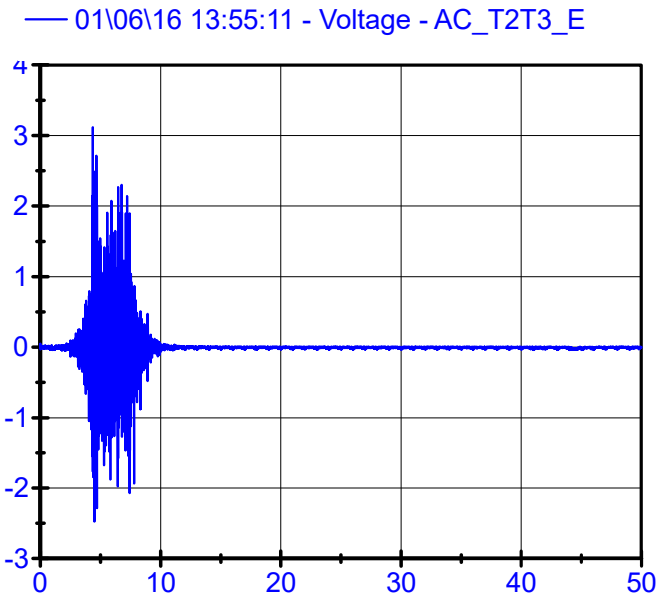

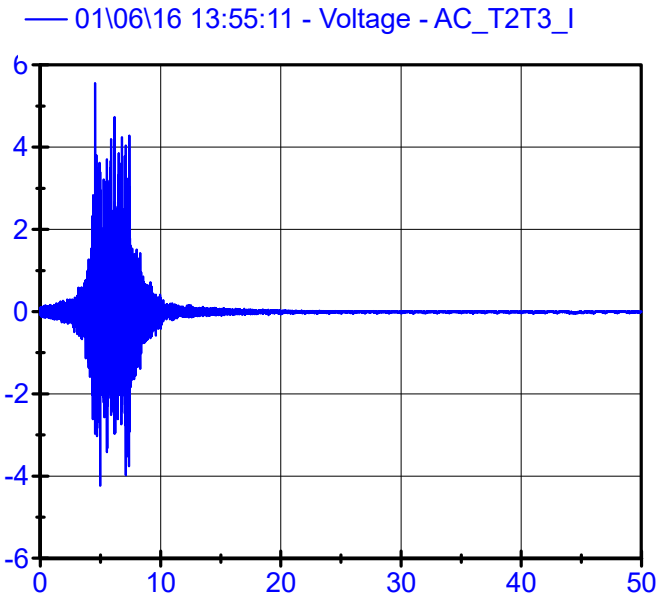

01\06\16 14:21:06

Sleeper Accelerometers
LPF 250Hz

01\06\16 14:21:06 - Voltage - AC_T2_E

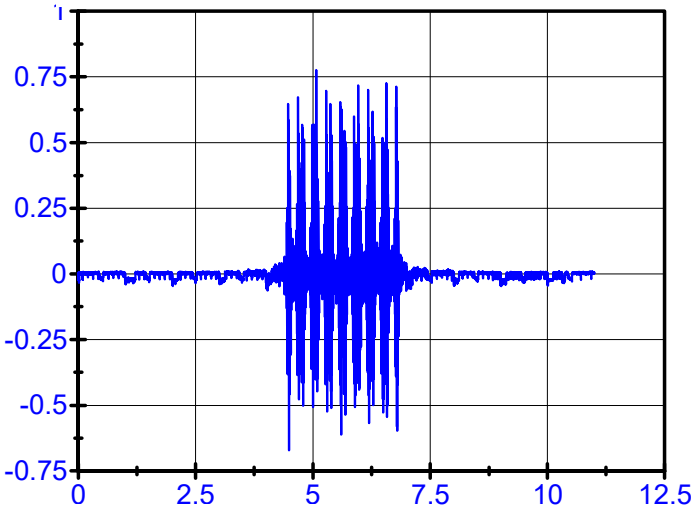

01\06\16 14:21:06 - Voltage - AC_T2_C

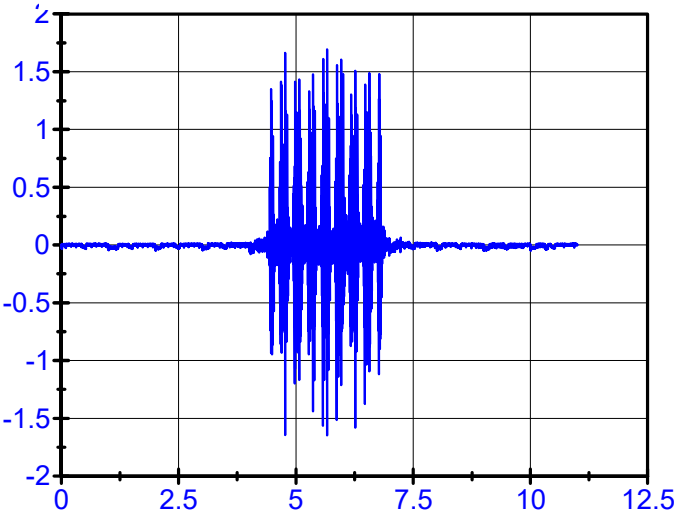

01\06\16 14:21:06 - Voltage - AC_T2_I

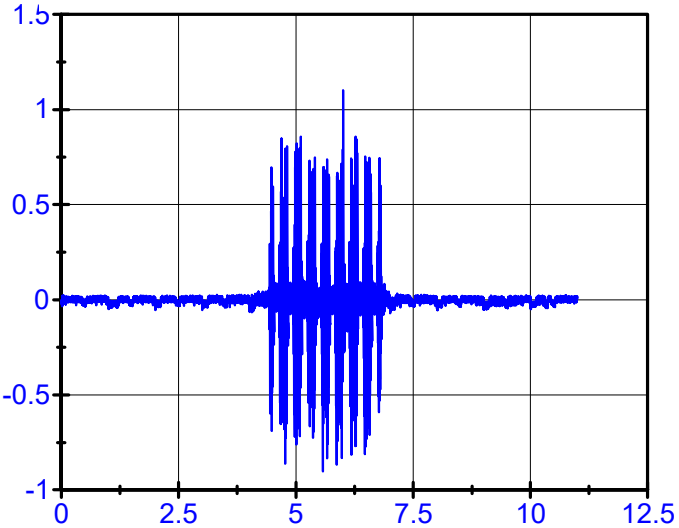

Rail Accelerometers
LPF 200Hz

01\06\16 14:21:06 - Voltage - AC_T2T3_E

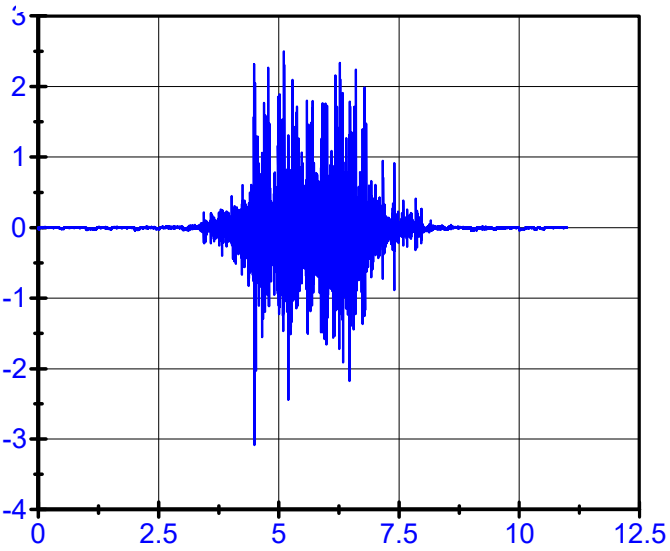

01\06\16 14:21:06 - Voltage - AC_T2T3_I

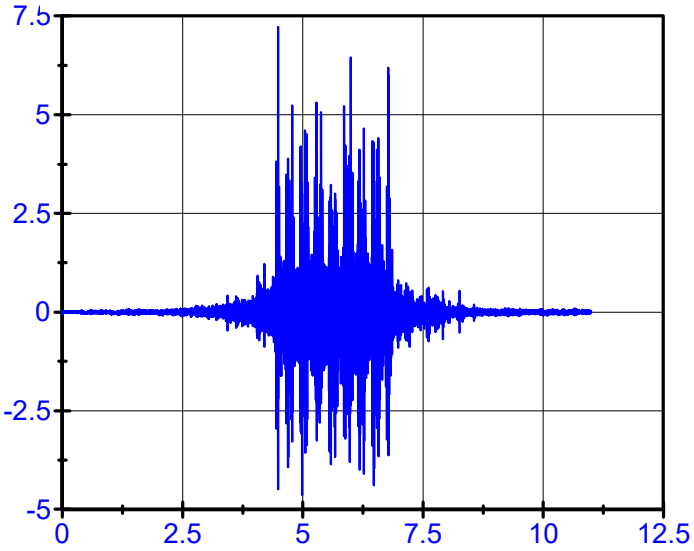

01\06\16 14:52:22

Sleeper Accelerometers
LPF 250Hz

01\06\16 14:52:22 - Voltage - AC_T2_E

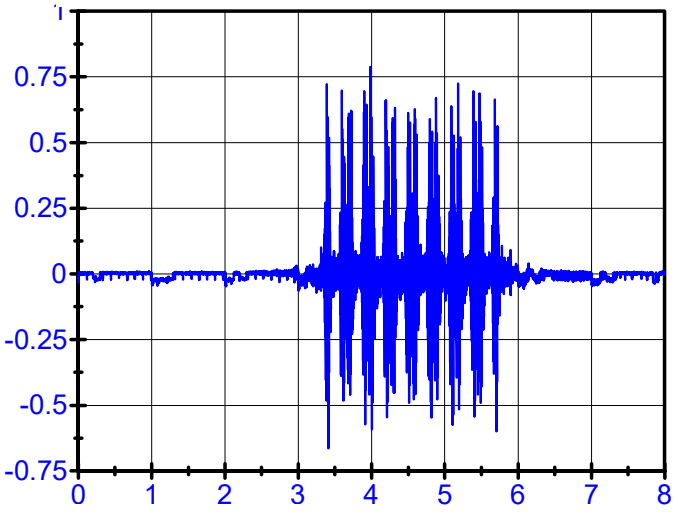

01\06\16 14:52:22 - Voltage - AC_T2_C

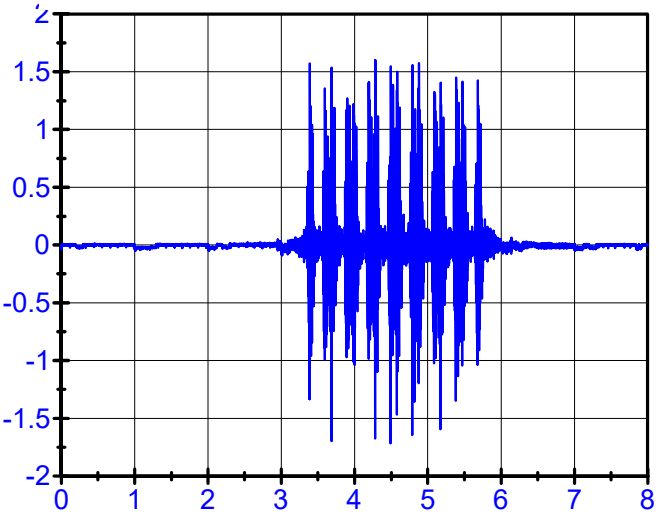

01\06\16 14:52:22 - Voltage - AC_T2_I

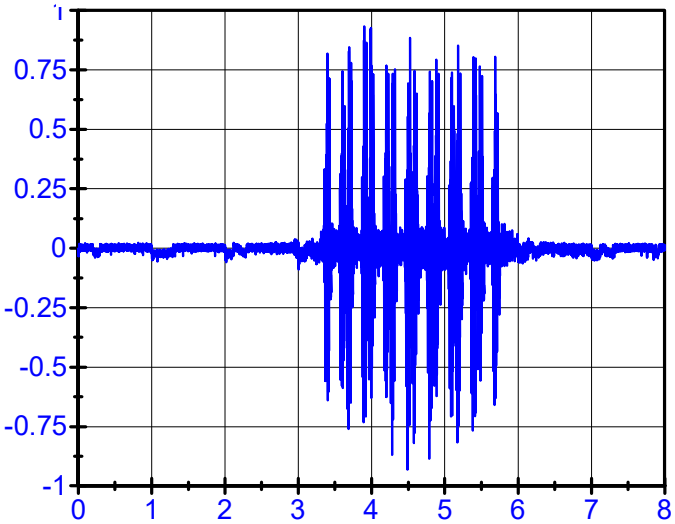

Rail Accelerometers
LPF 200Hz

01\06\16 14:52:22 - Voltage - AC_T2T3_E

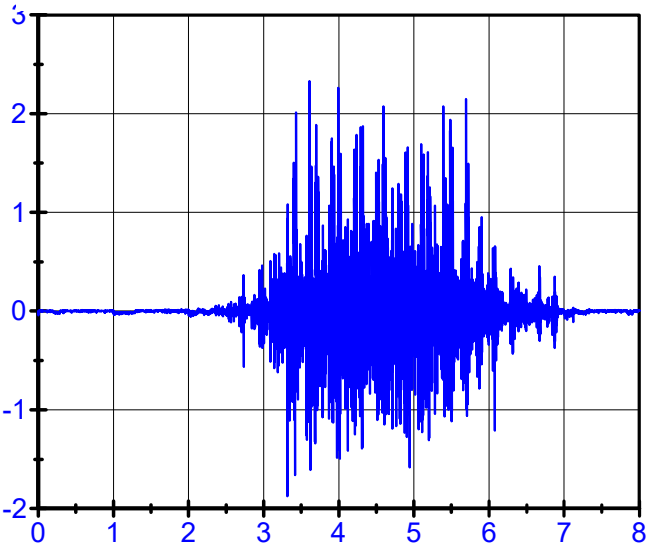

01\06\16 14:52:22 - Voltage - AC_T2T3_I

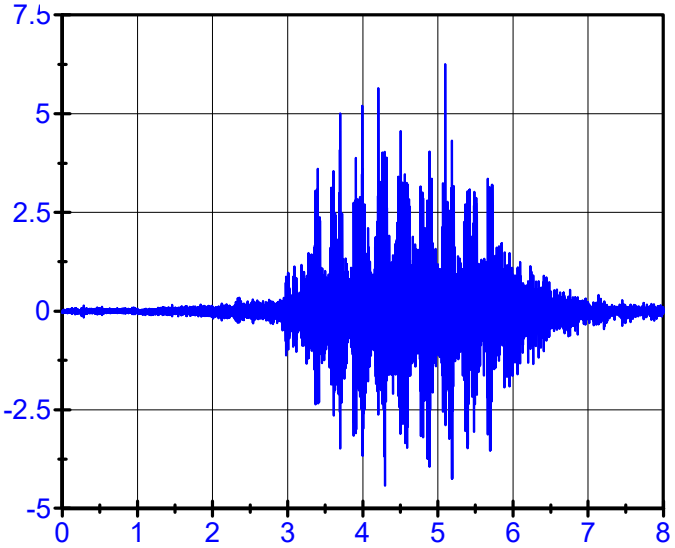

01\06\16 15:21:31

Sleeper Accelerometers
LPF 250Hz

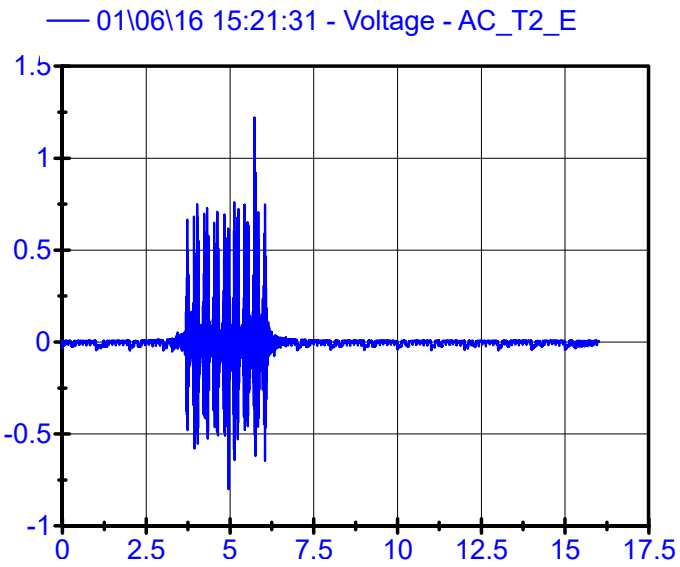

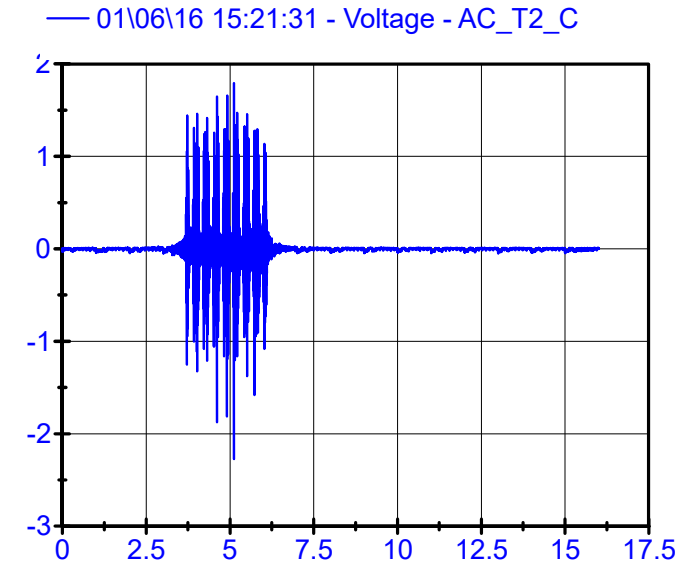

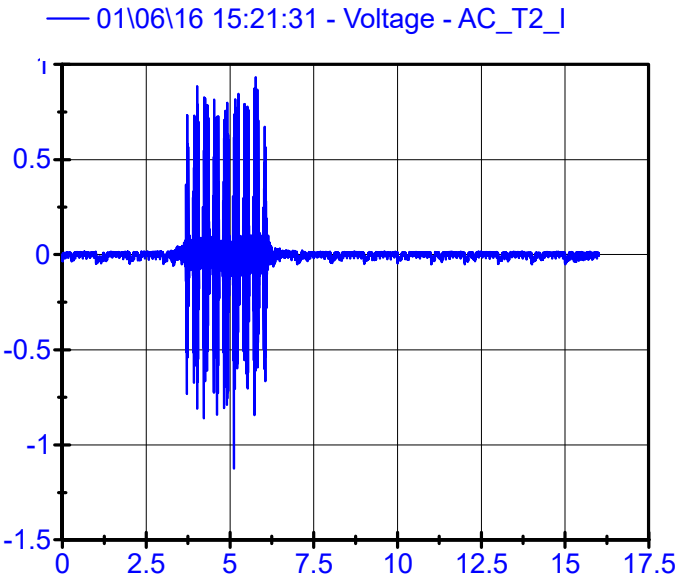

Rail Accelerometers
LPF 200Hz

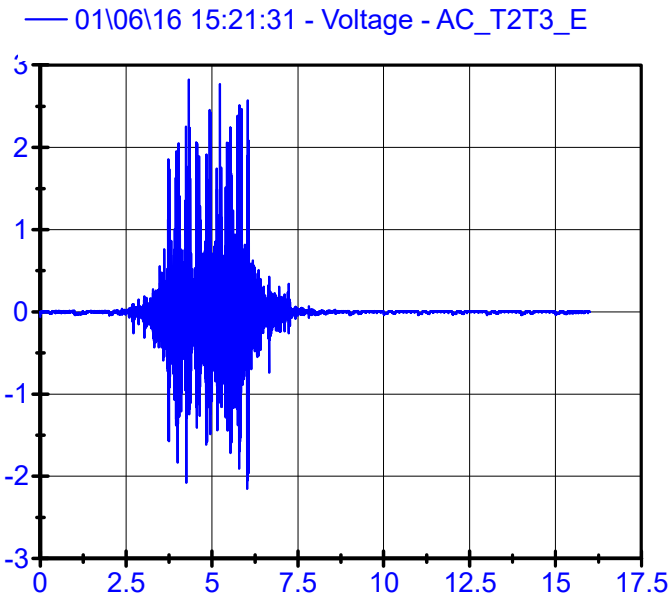

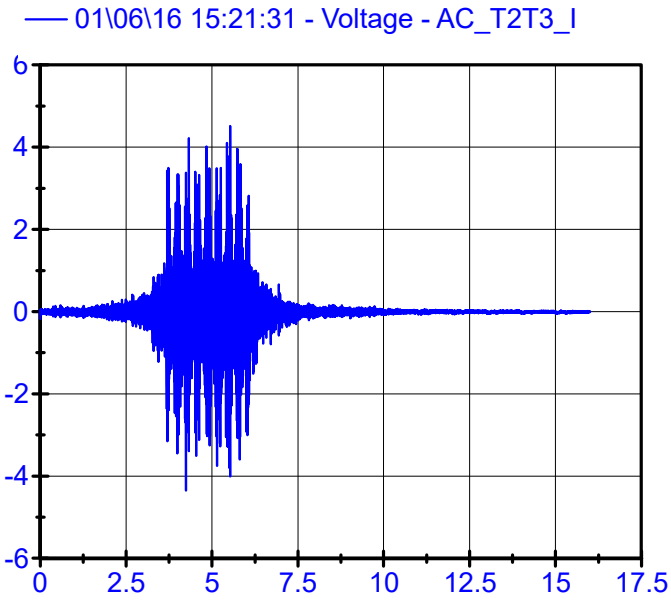

01\06\16 15:34:49

Sleeper Accelerometers
LPF 250Hz

01\06\16 15:34:49 - Voltage - AC_T2_E

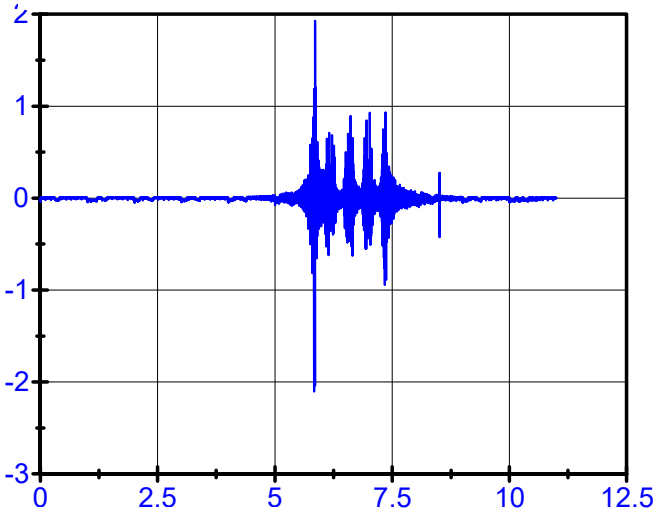

01\06\16 15:34:49 - Voltage - AC_T2_C

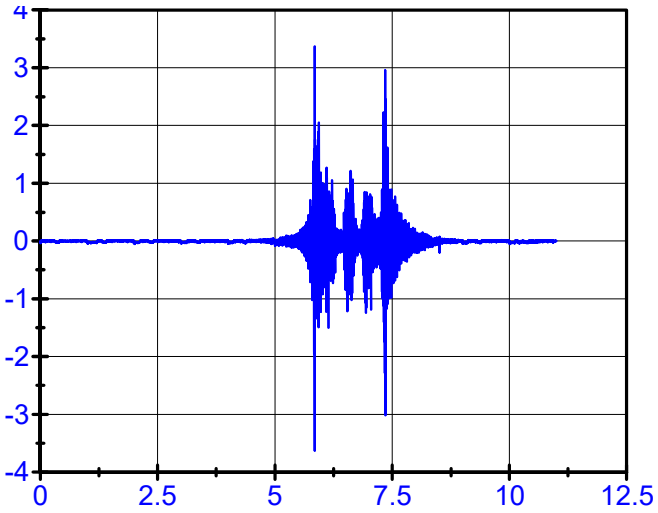

01\06\16 15:34:49 - Voltage - AC_T2_I

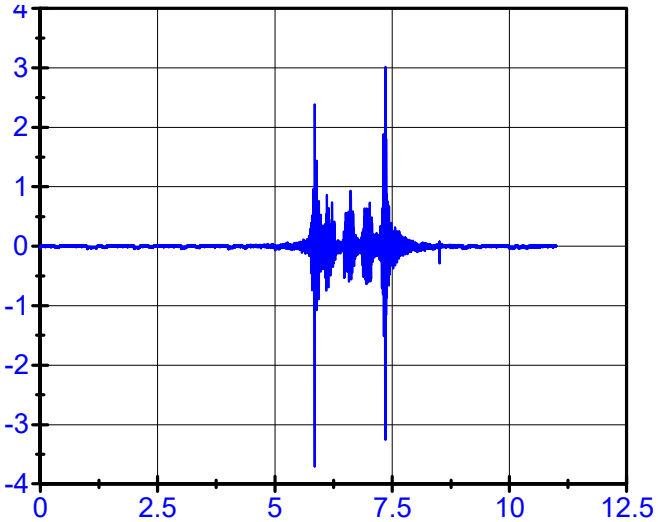

Rail Accelerometers
LPF 200Hz

01\06\16 15:34:49 - Voltage - AC_T2T3_E

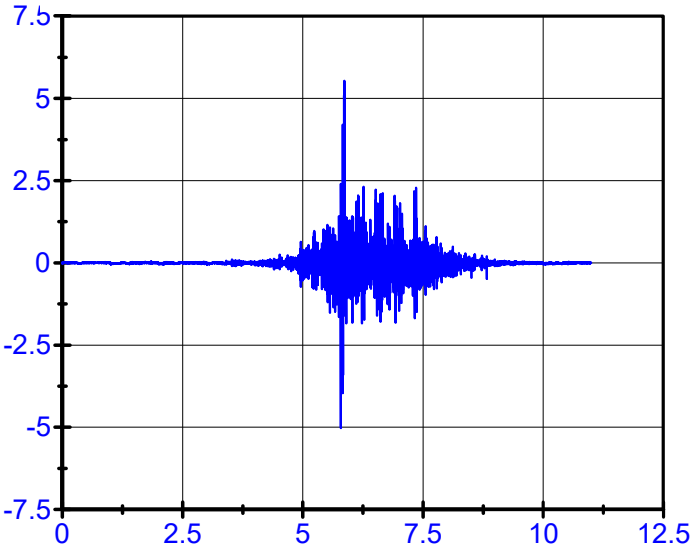

01\06\16 15:34:49 - Voltage - AC_T2T3_I

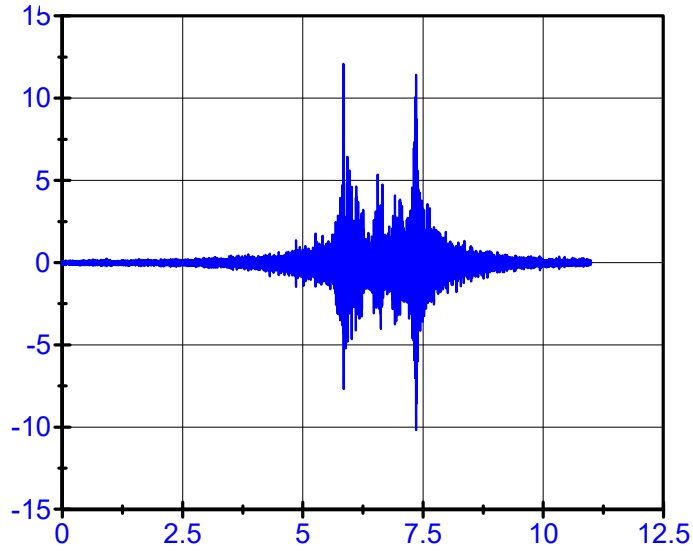

01\06\16 15:54:57

Sleeper Accelerometers
LPF 250Hz

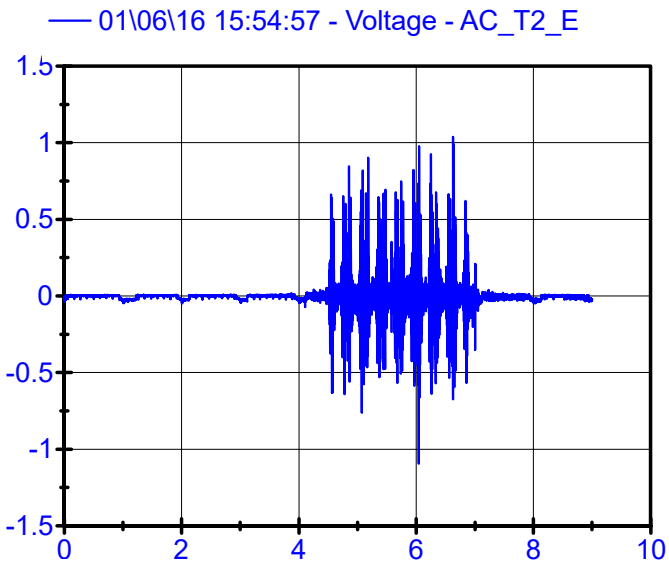

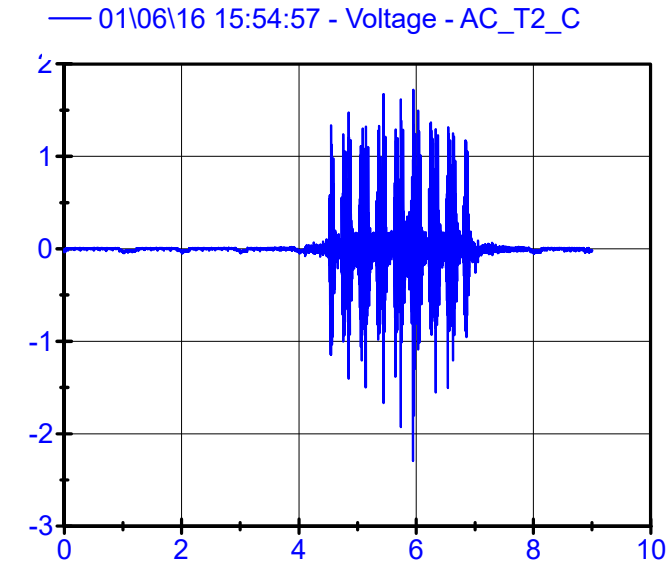

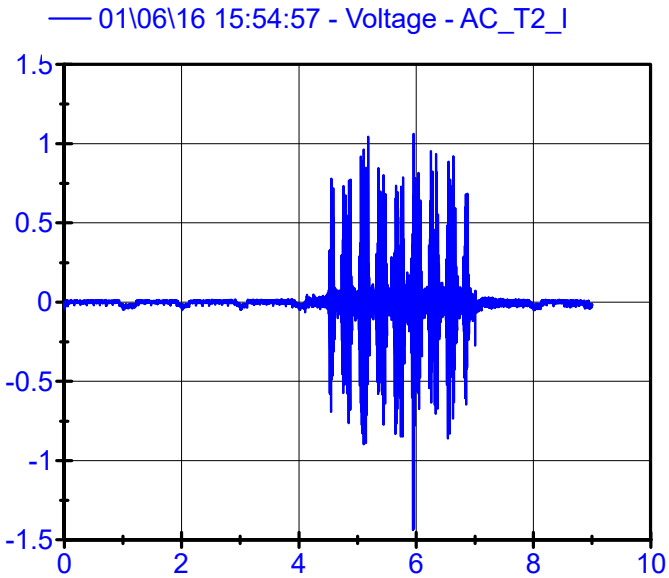

Rail Accelerometers
LPF 200Hz

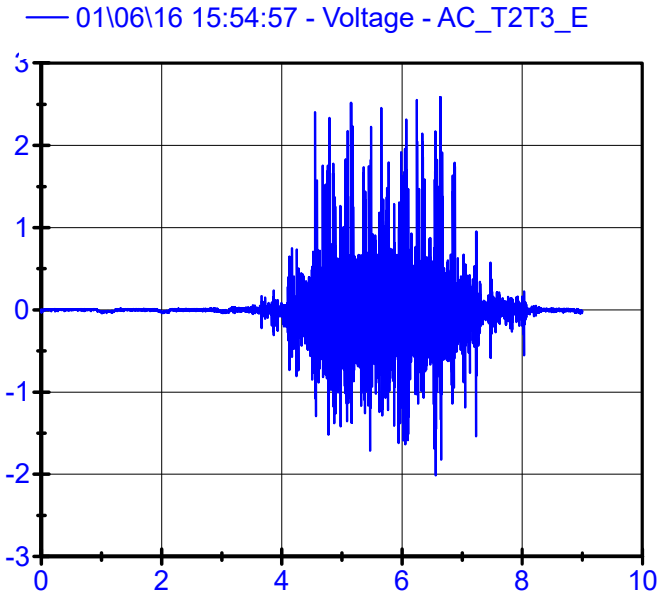

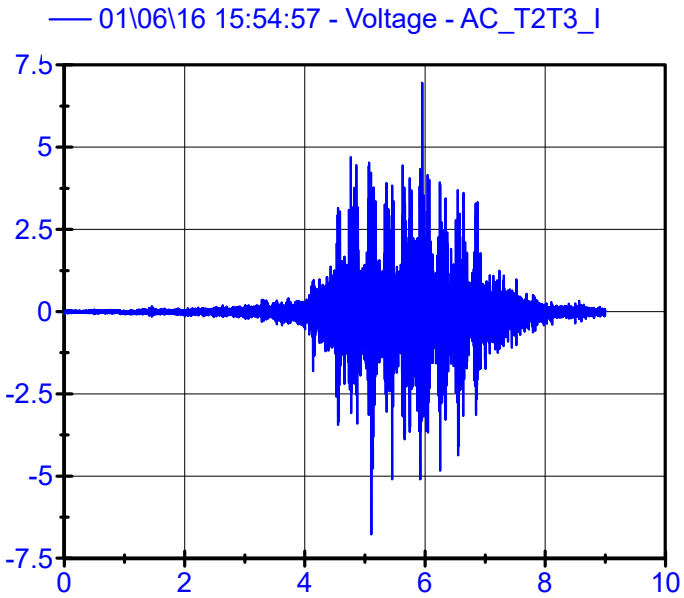

01\06\16 16:22:21

Sleeper Accelerometers
LPF 250Hz

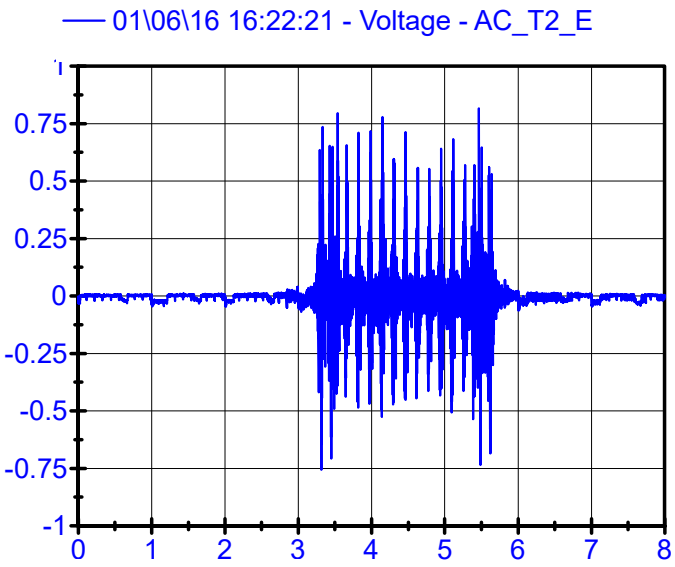

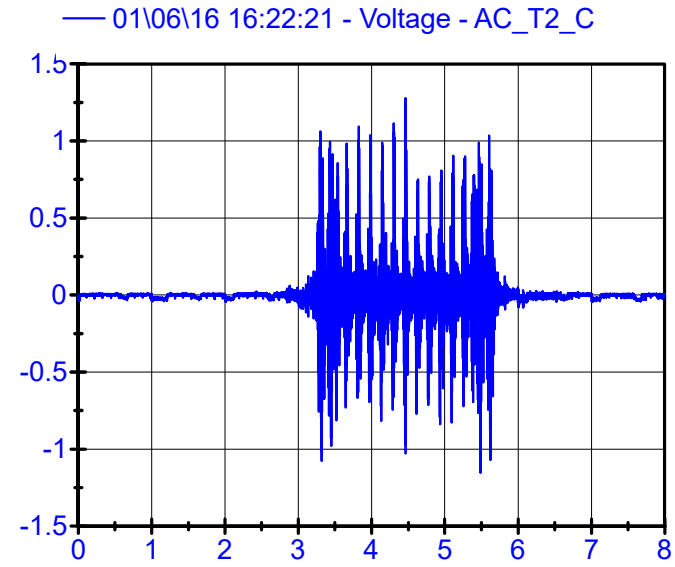

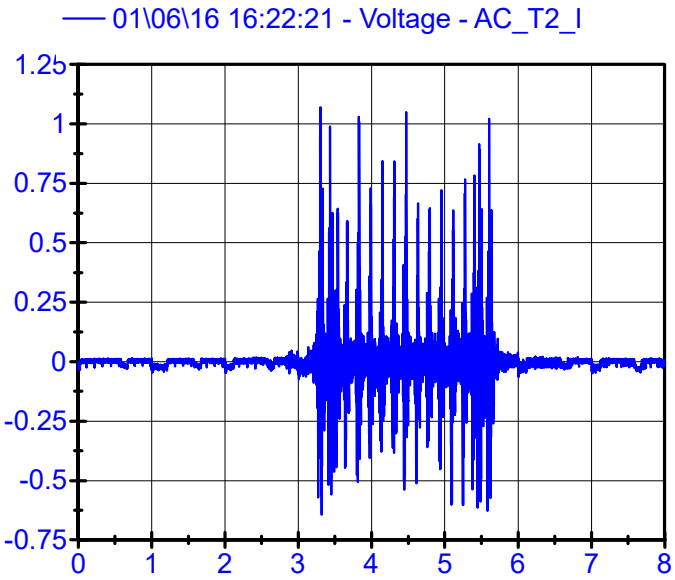

Rail Accelerometers
LPF 200Hz

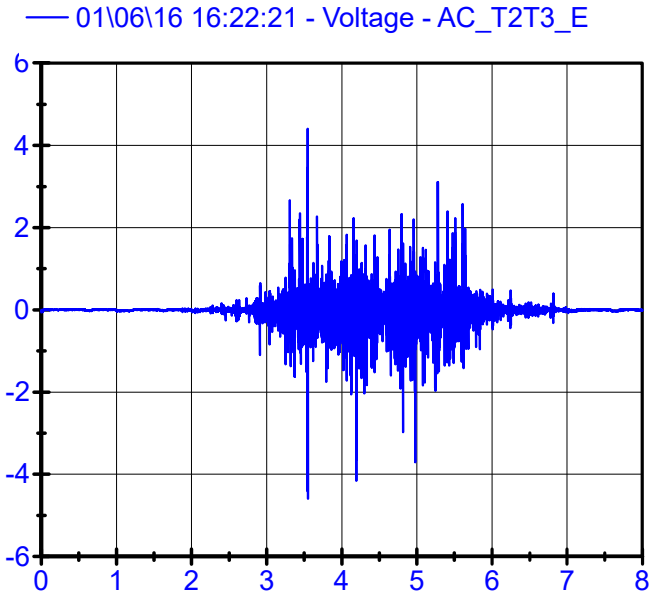

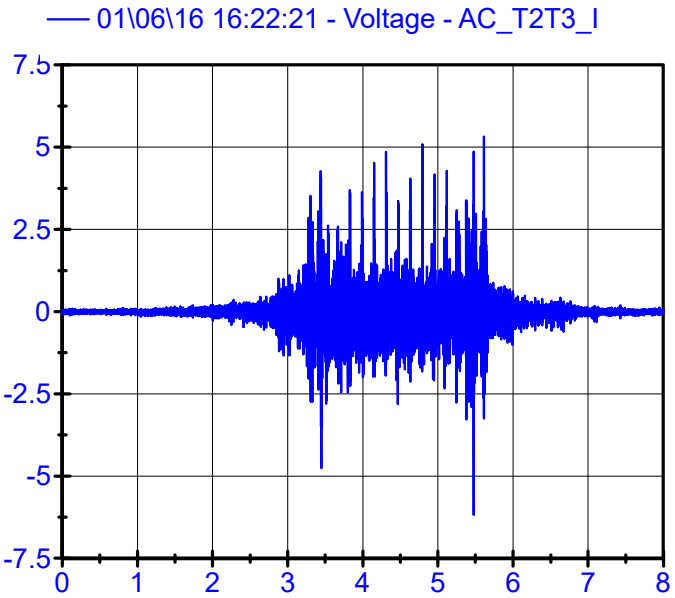

01\06\16 16:54:24

Sleeper Accelerometers
LPF 250Hz

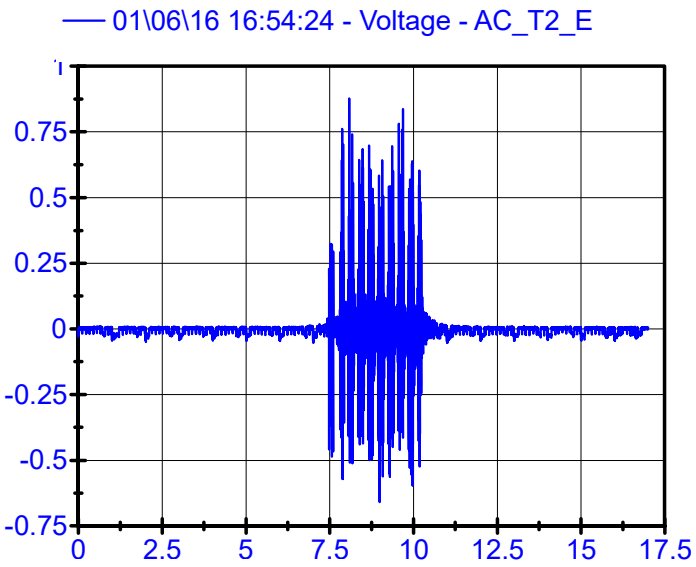

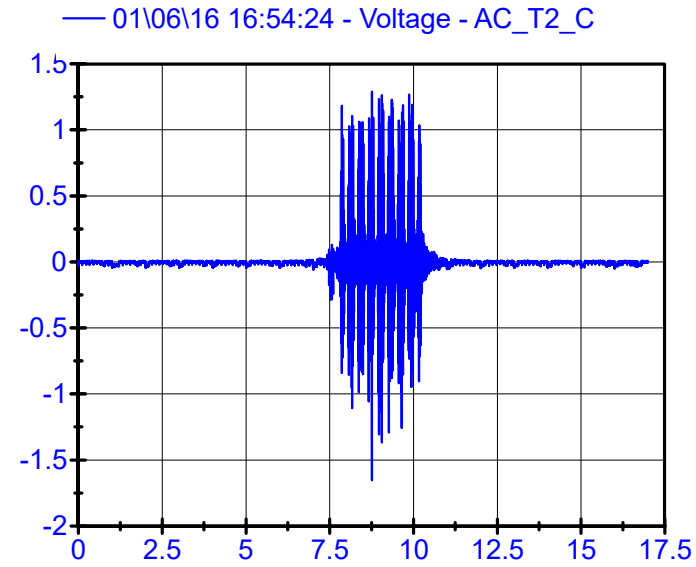

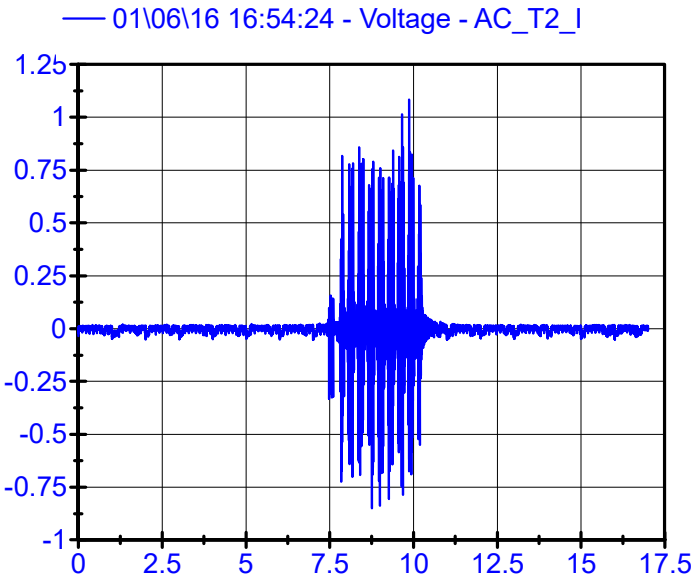

Rail Accelerometers
LPF 200Hz

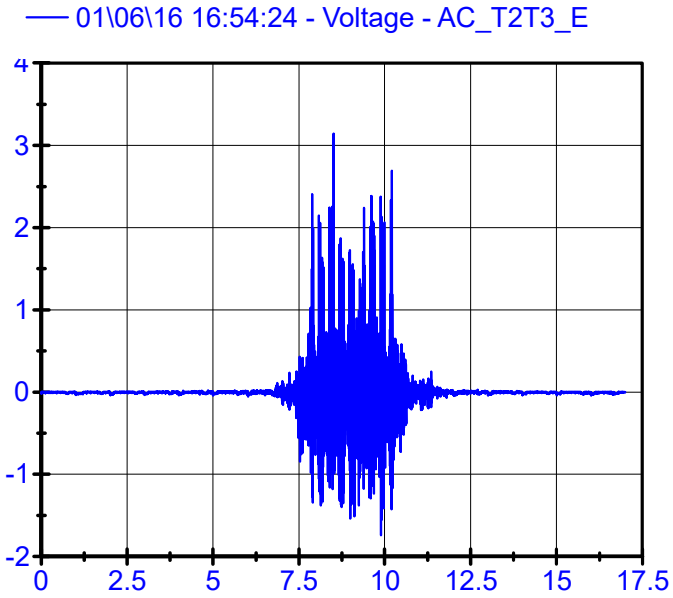

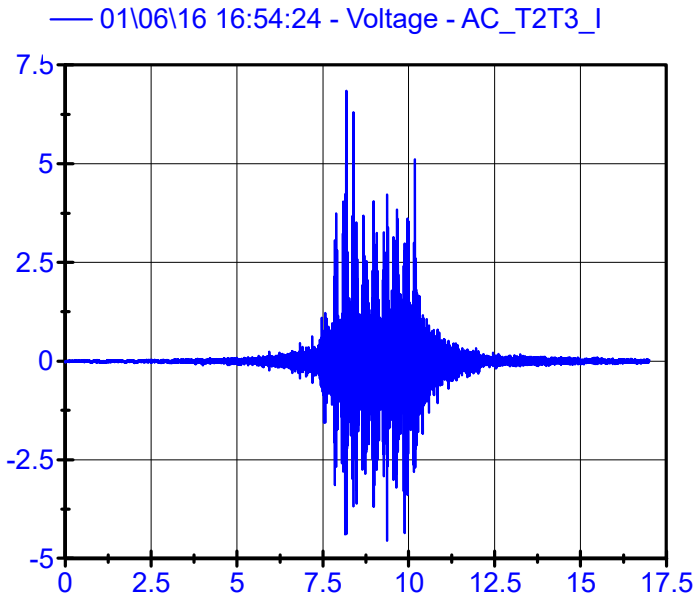

01\06\16 17:24:26

Sleeper Accelerometers
LPF 250Hz

01\06\16 17:24:26 - Voltage - AC_T2_E

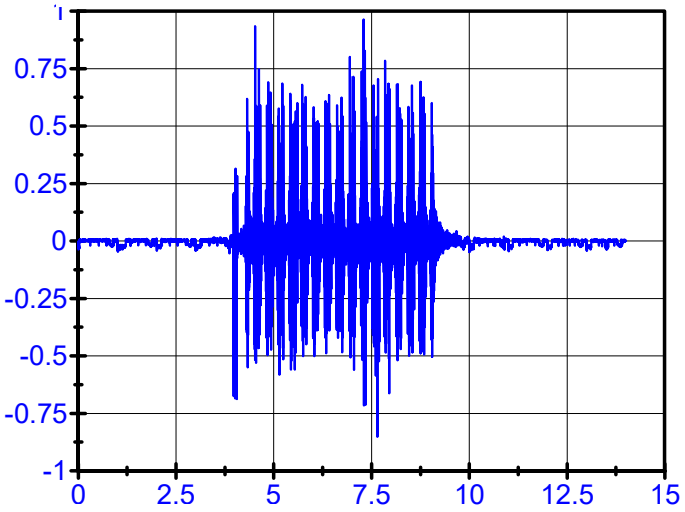

01\06\16 17:24:26 - Voltage - AC_T2_C

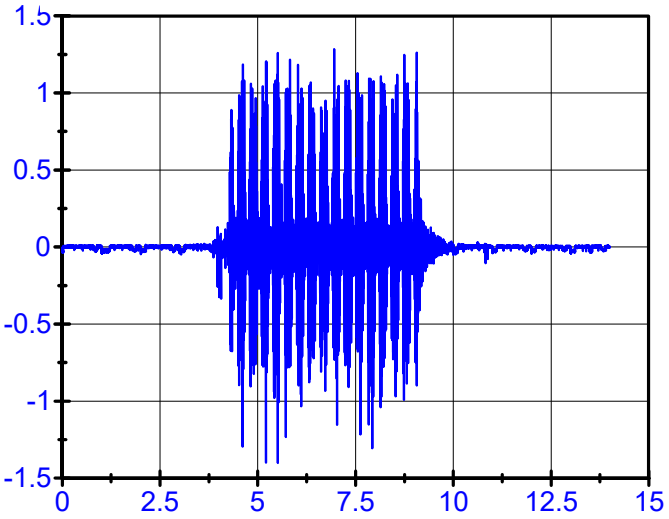

01\06\16 17:24:26 - Voltage - AC_T2_I

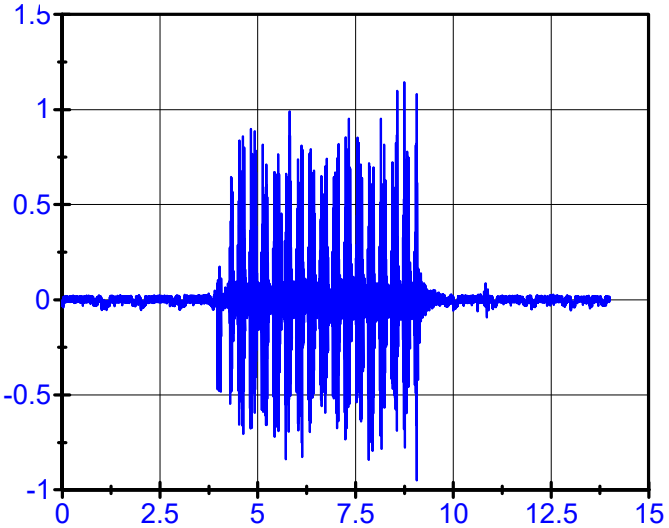

Rail Accelerometers
LPF 200Hz

01\06\16 17:24:26 - Voltage - AC_T2T3_E

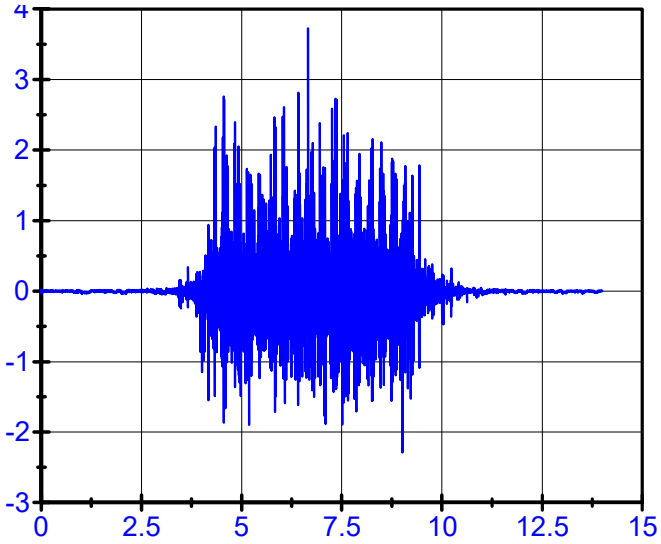

01\06\16 17:24:26 - Voltage - AC_T2T3_I

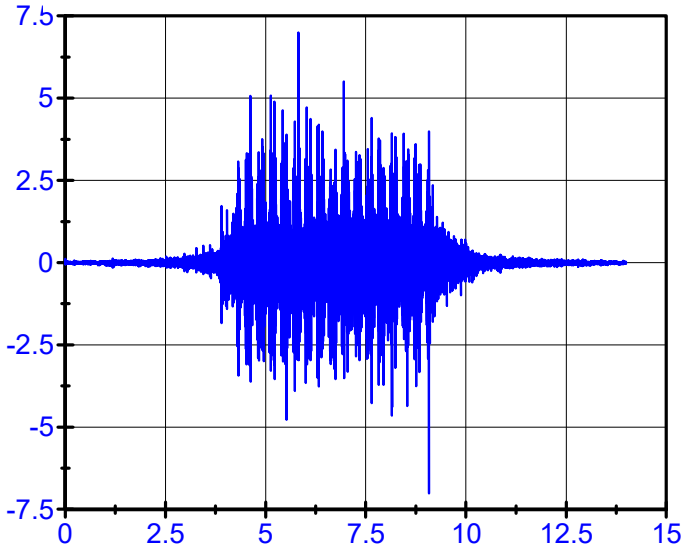

01\06\16 17:38:59

Sleeper Accelerometers
LPF 250Hz

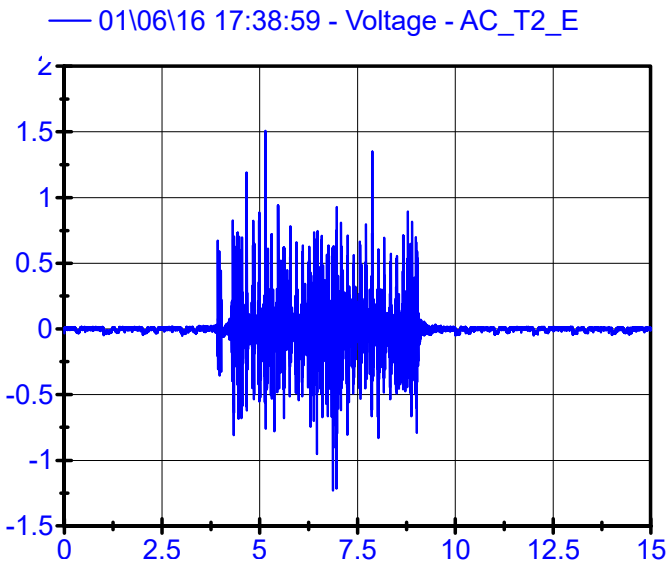

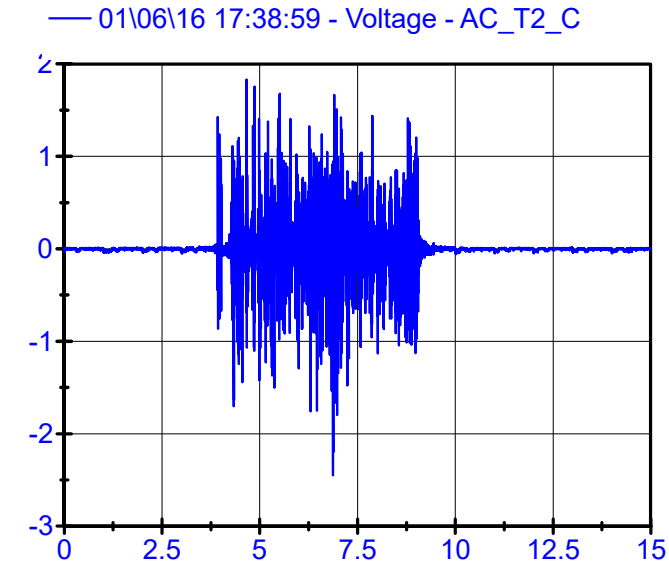

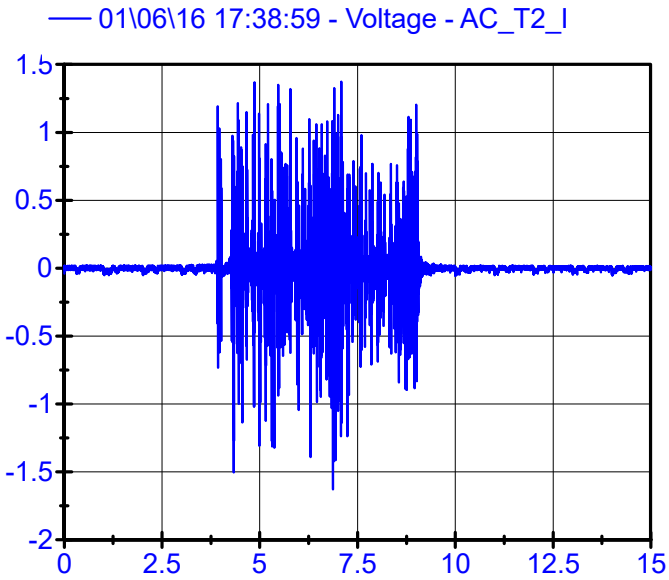

Rail Accelerometers
LPF 200Hz

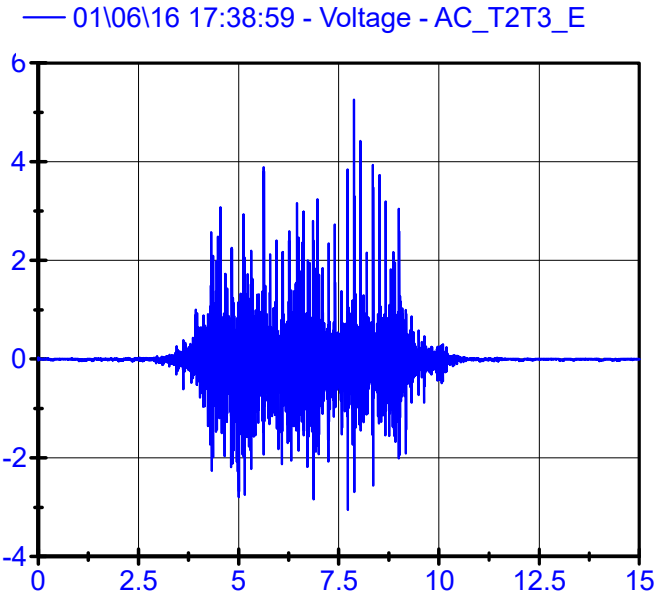

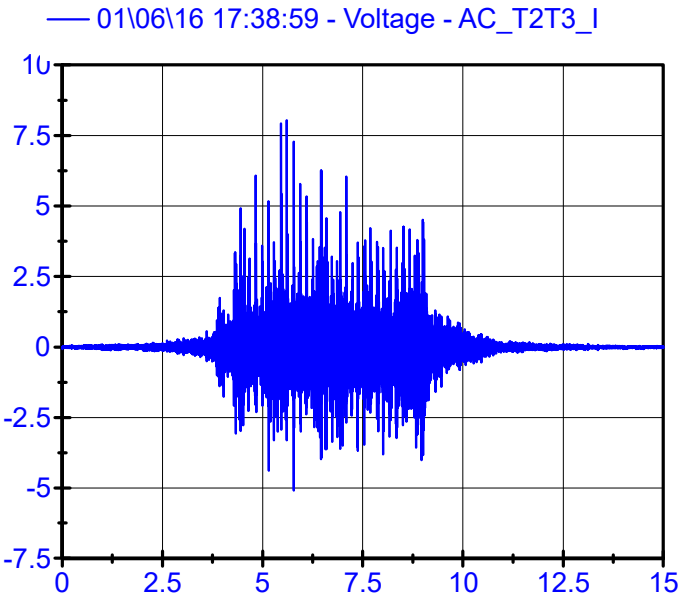

01\06\16 17:59:25

Sleeper Accelerometers
LPF 250Hz

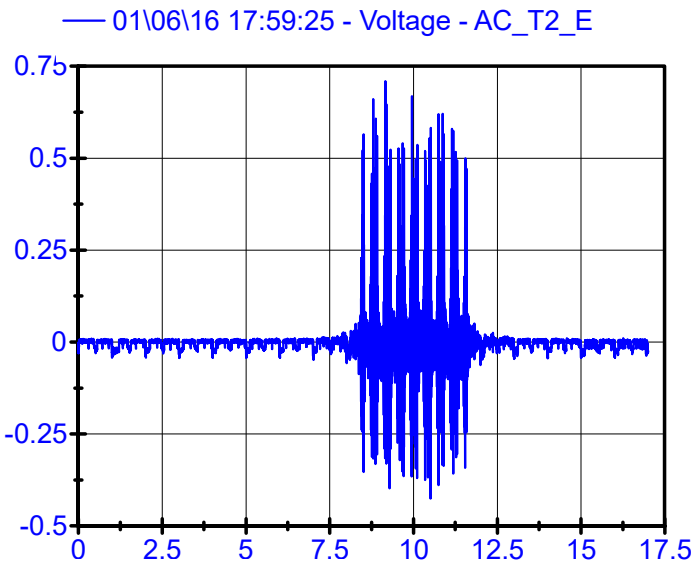

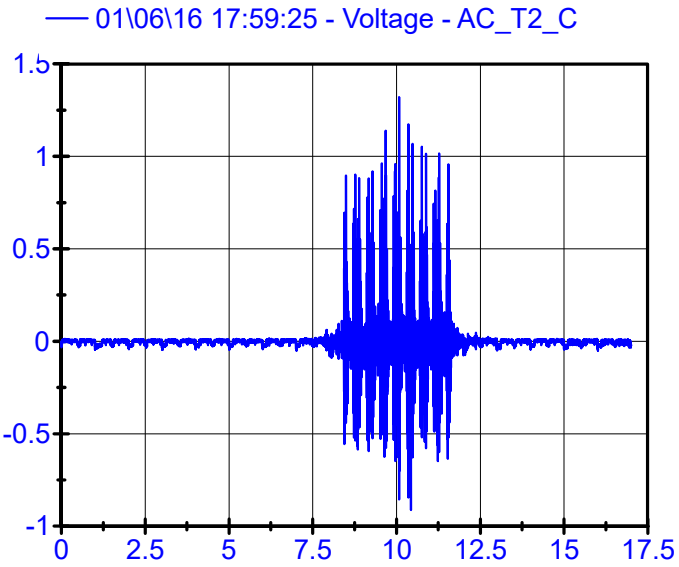

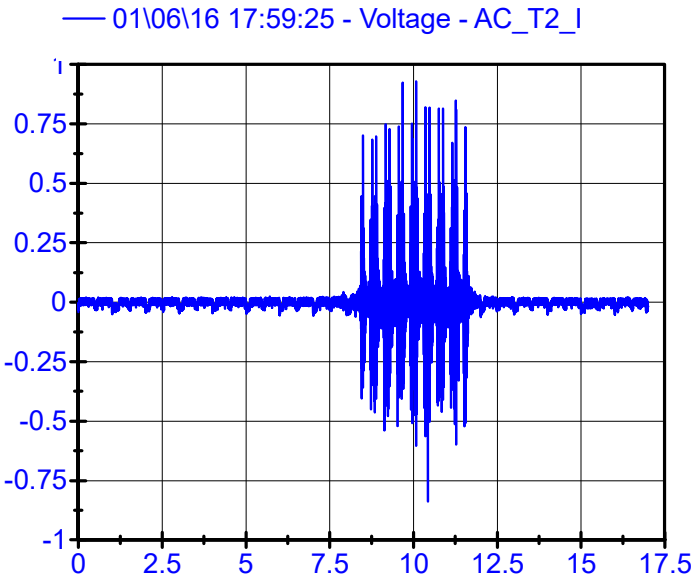

Rail Accelerometers
LPF 200Hz

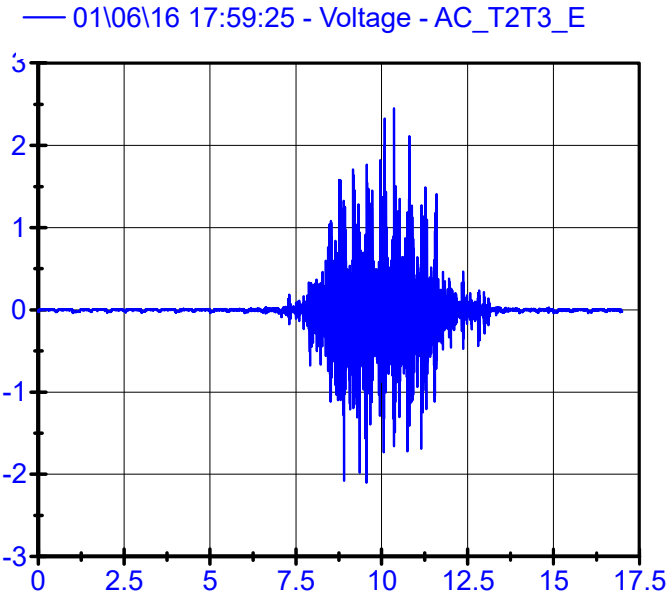

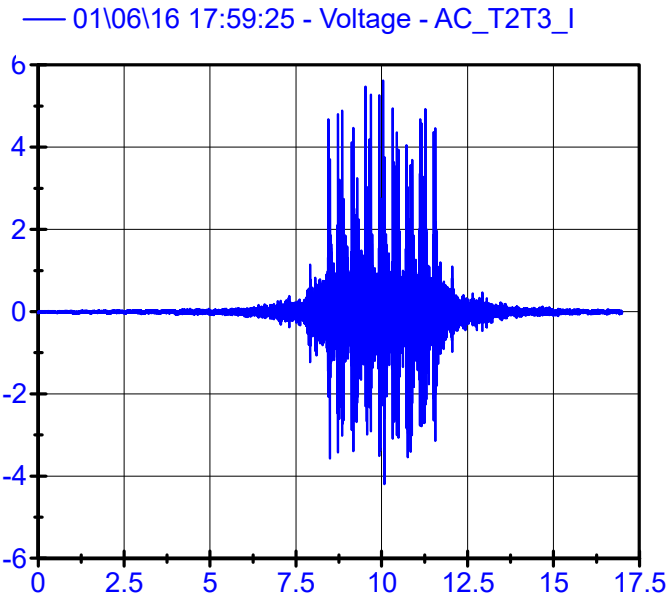

01\06\16 18:22:52

Sleeper Accelerometers
LPF 250Hz

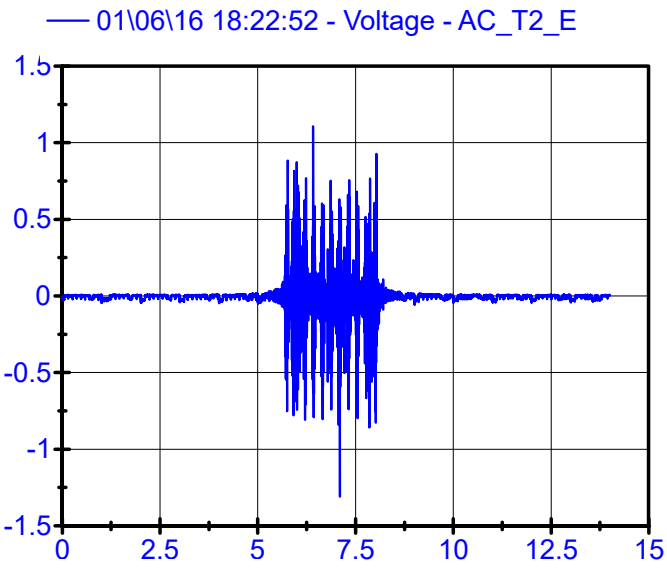

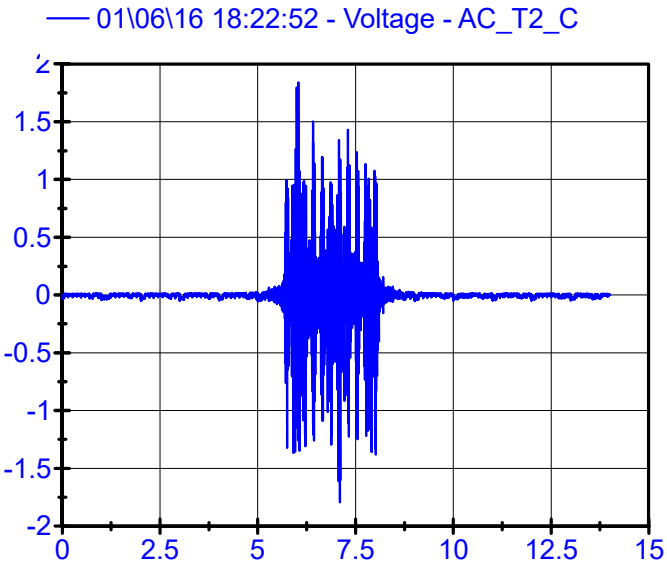

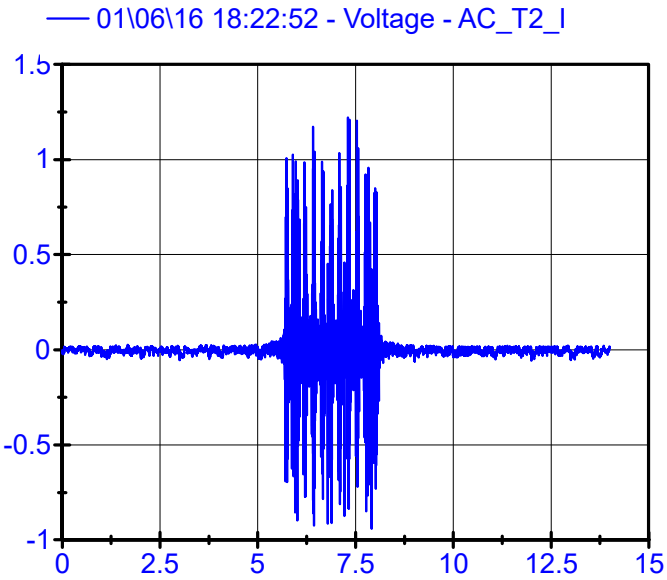

Rail Accelerometers
LPF 200Hz

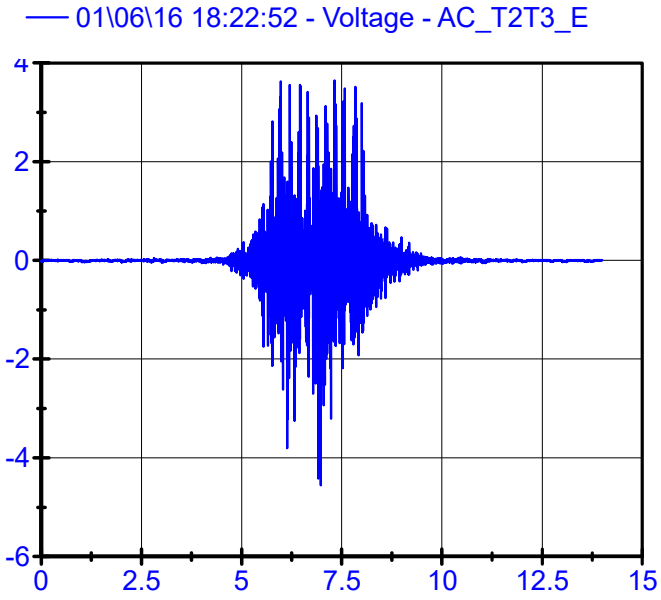

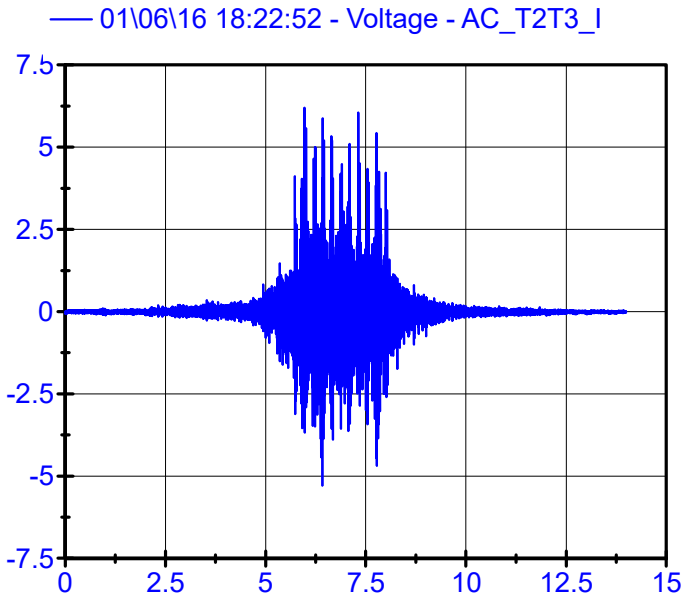

01\06\16 18:59:06

Sleeper Accelerometers
LPF 250Hz

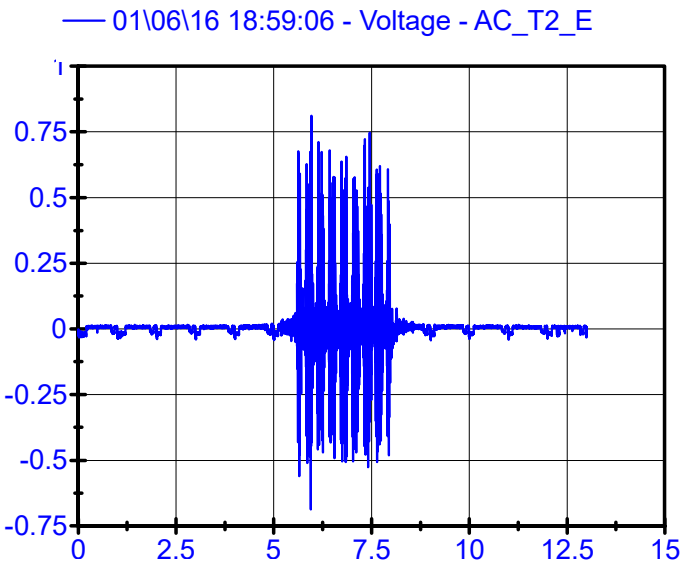

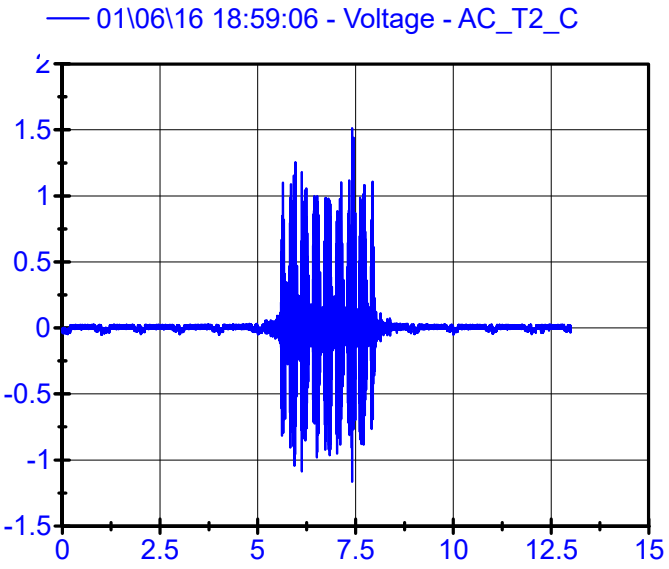

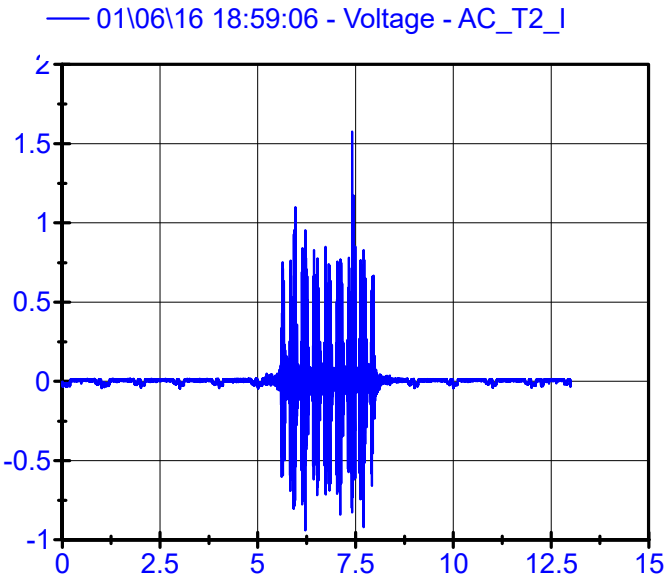

Rail Accelerometers
LPF 200Hz

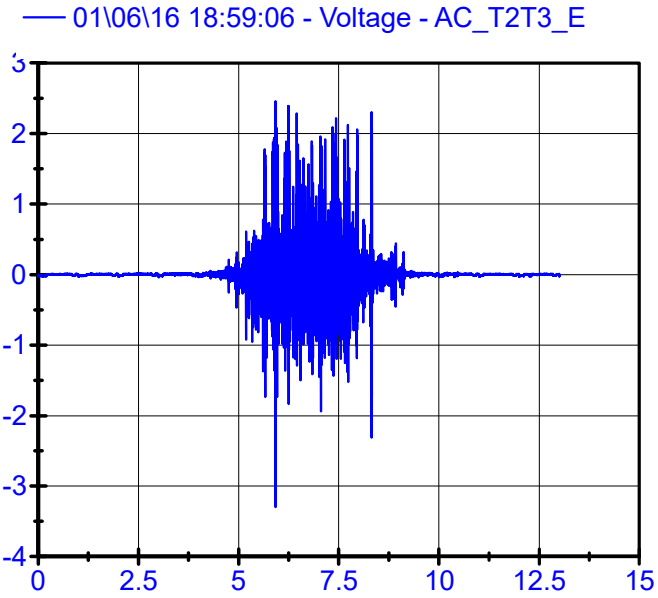

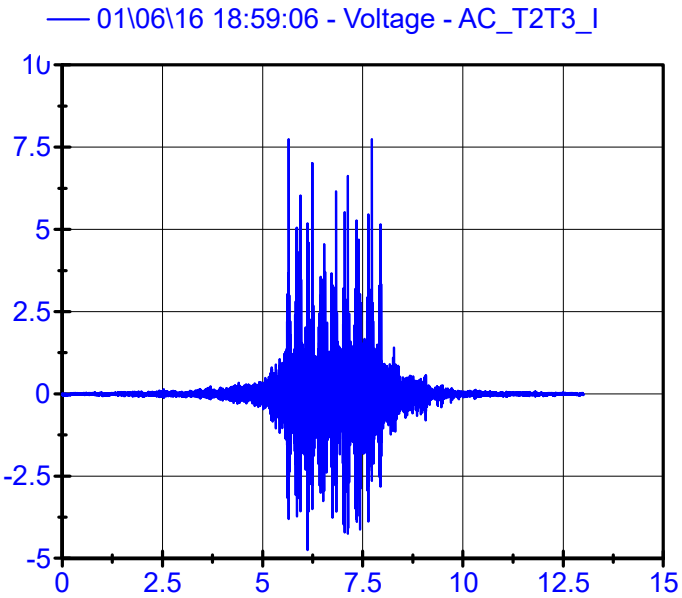

01\06\16 19:21:34

Sleeper Accelerometers
LPF 250Hz

01\06\16 19:21:34 - Voltage - AC_T2_E

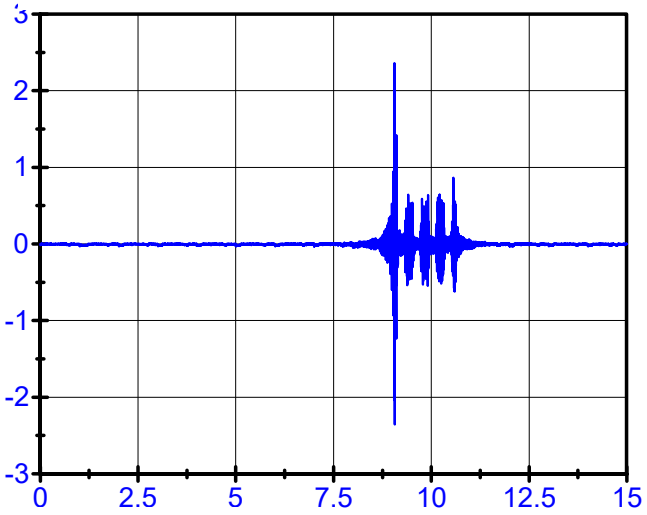

01\06\16 19:21:34 - Voltage - AC_T2_C

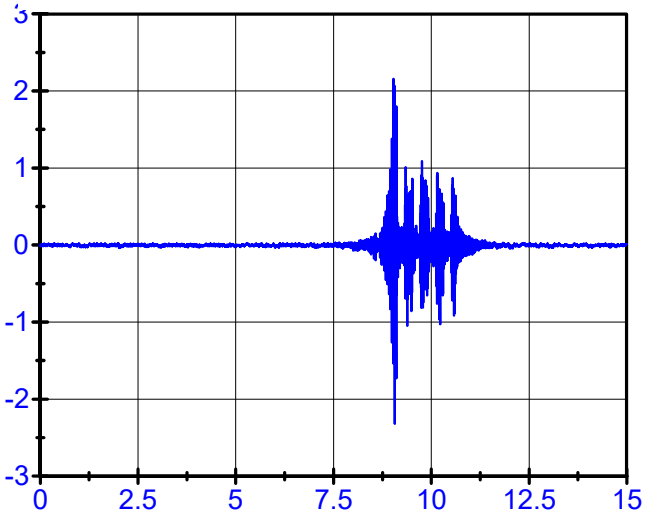

01\06\16 19:21:34 - Voltage - AC_T2_I

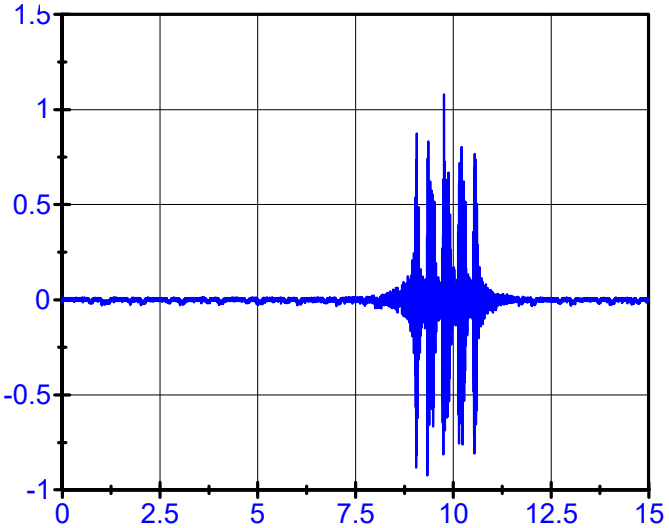

Rail Accelerometers
LPF 200Hz

01\06\16 19:21:34 - Voltage - AC_T2T3_E

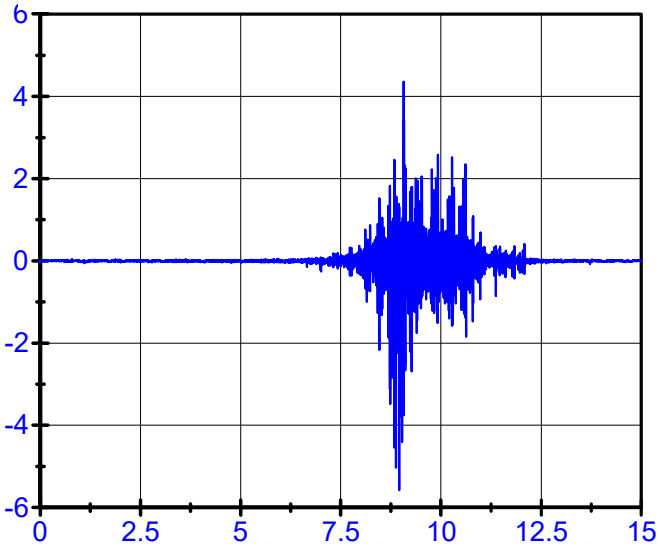

01\06\16 19:21:34 - Voltage - AC_T2T3_I

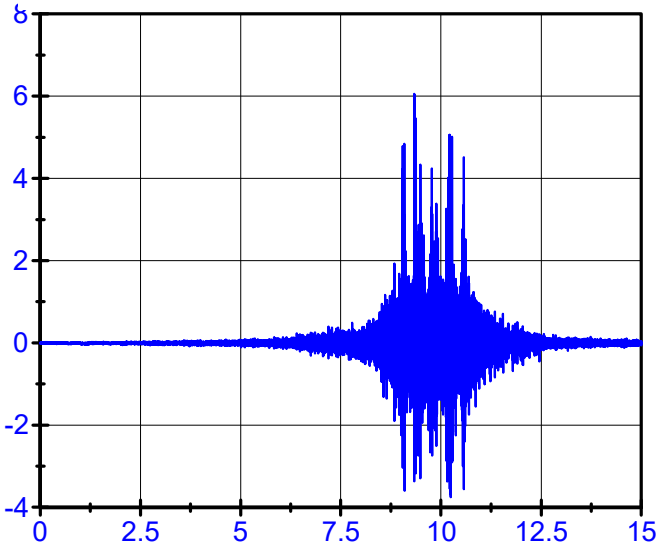

01\06\16 19:23:31

Sleeper Accelerometers
LPF 250Hz

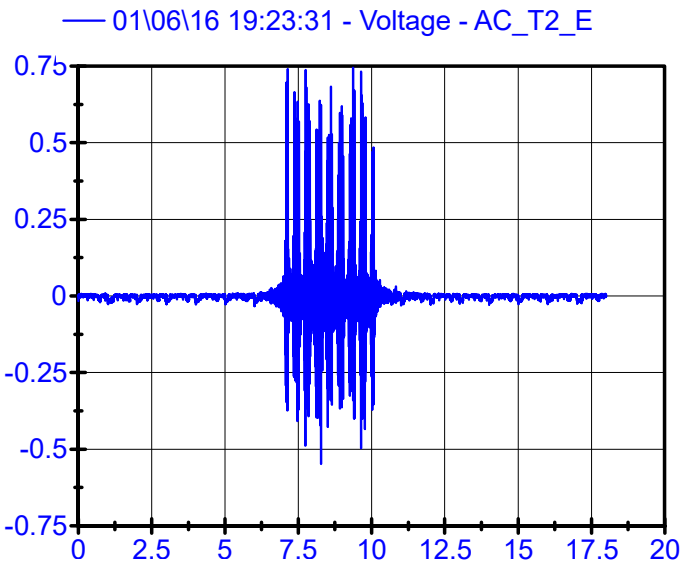

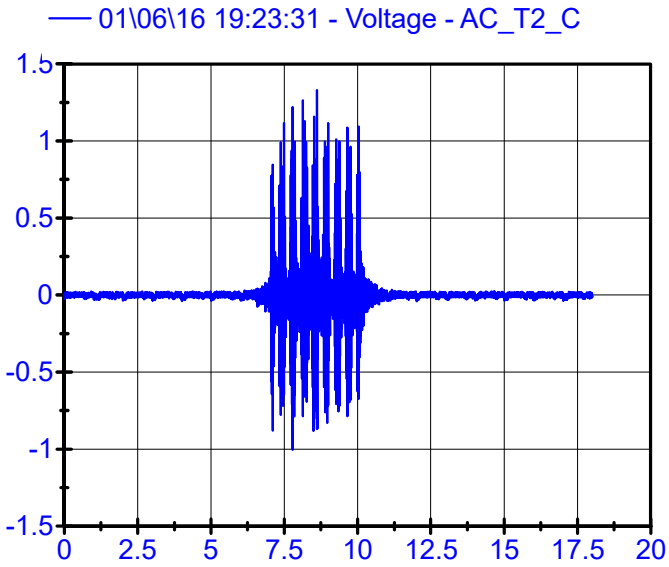

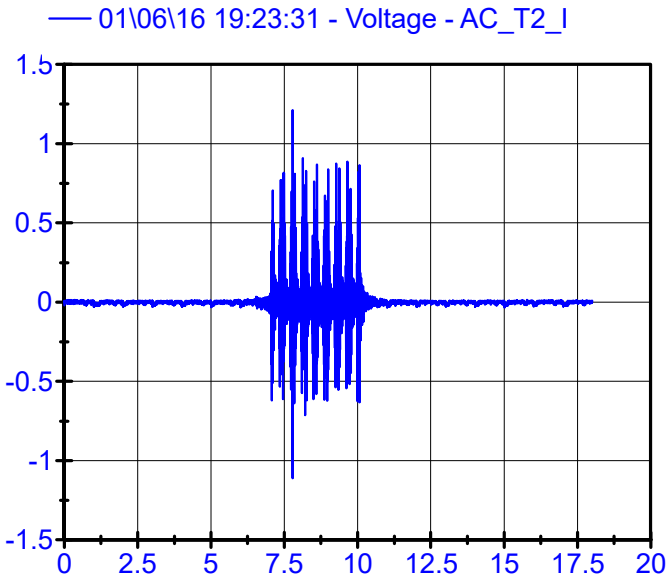

Rail Accelerometers
LPF 200Hz

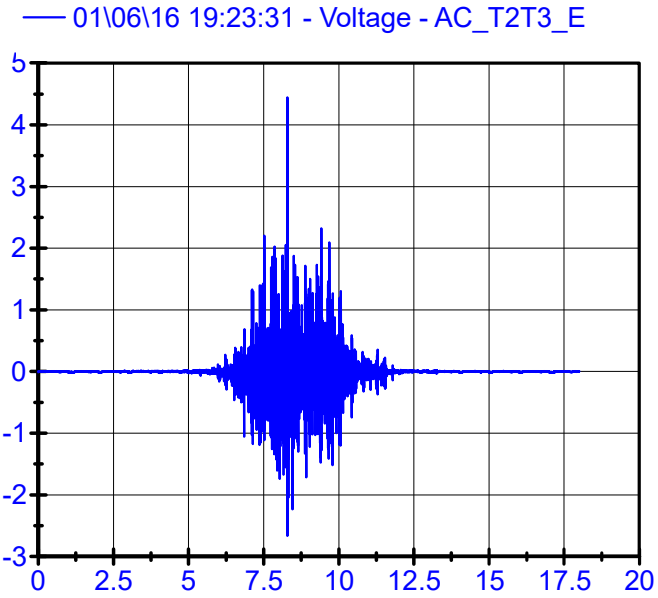

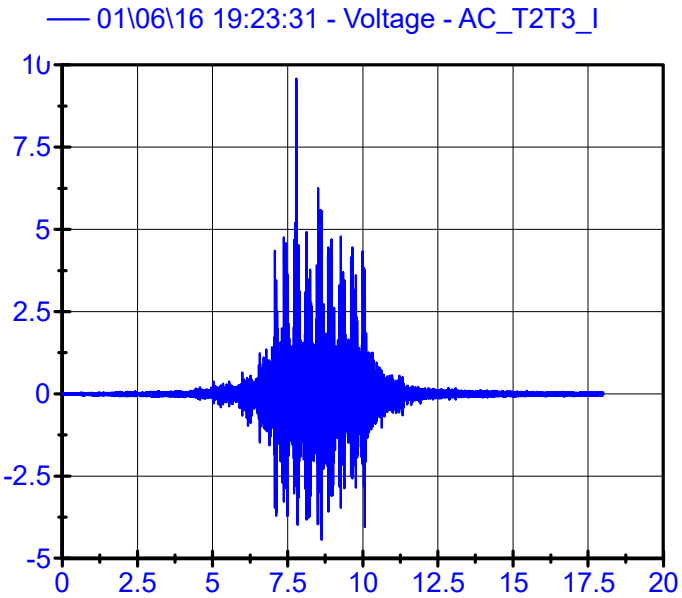

01\06\16 19:32:45

Sleeper Accelerometers
LPF 250Hz

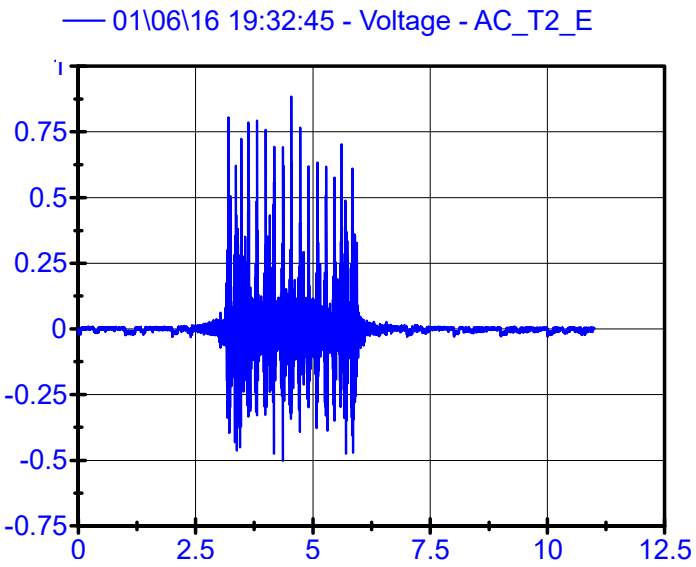

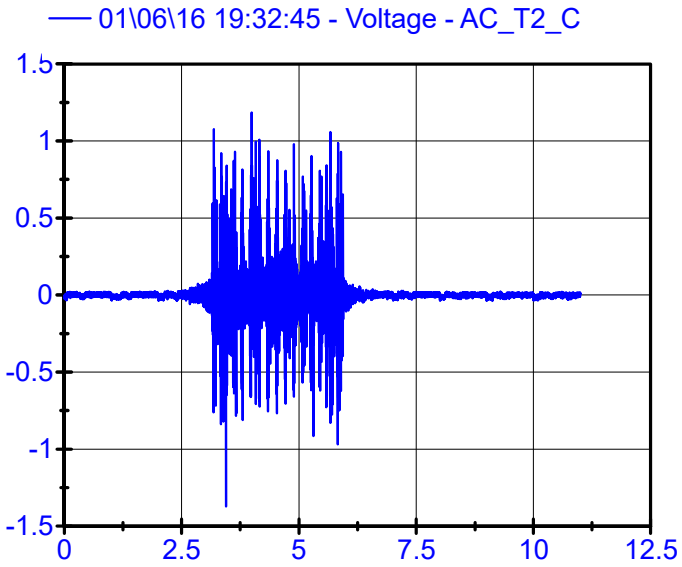

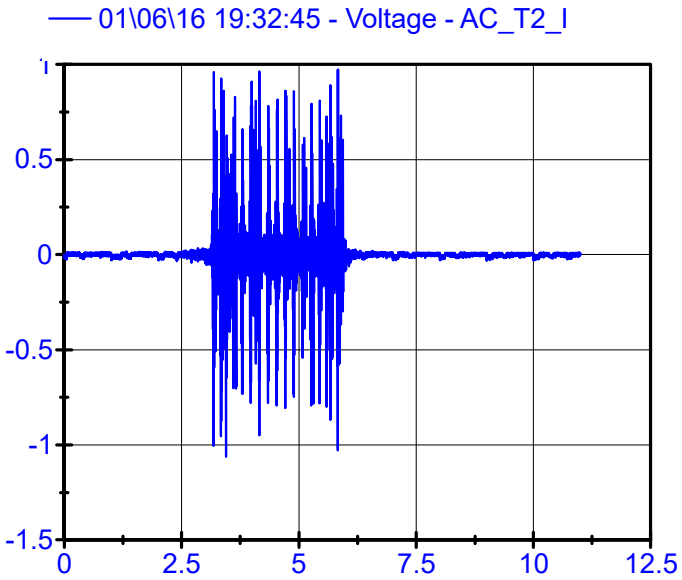

Rail Accelerometers
LPF 200Hz

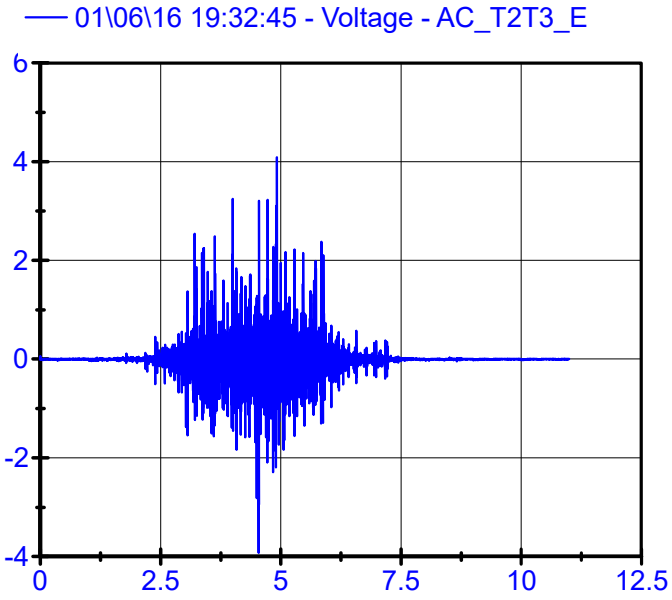

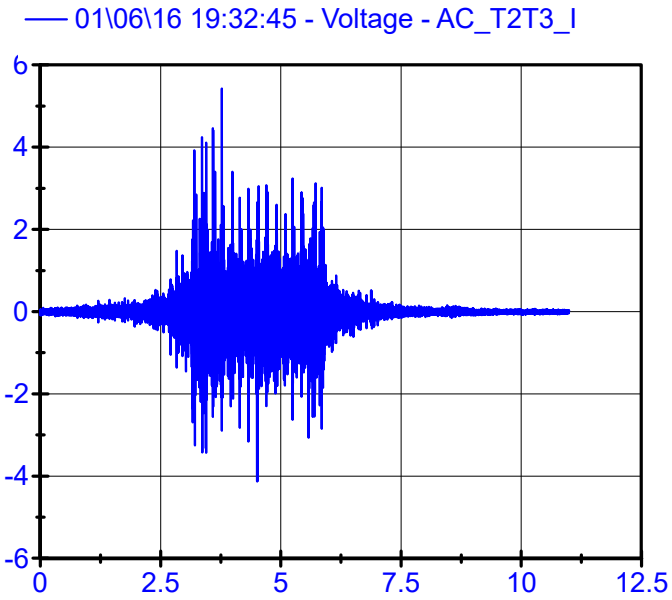

01\06\16 19:53:03

Sleeper Accelerometers
LPF 250Hz

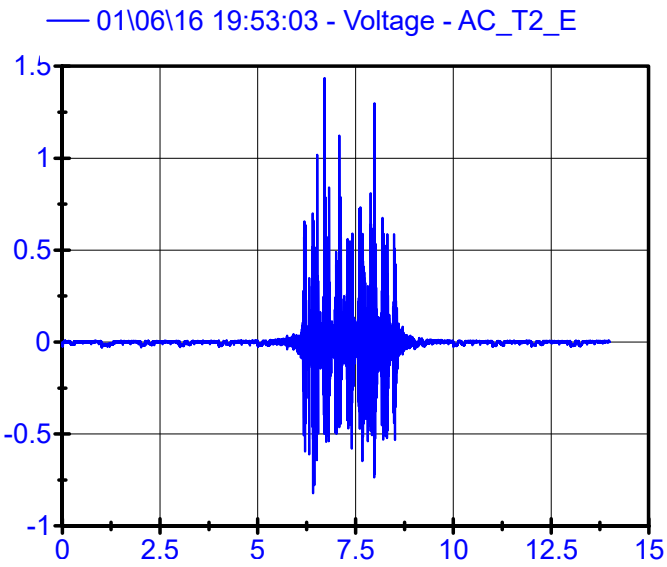

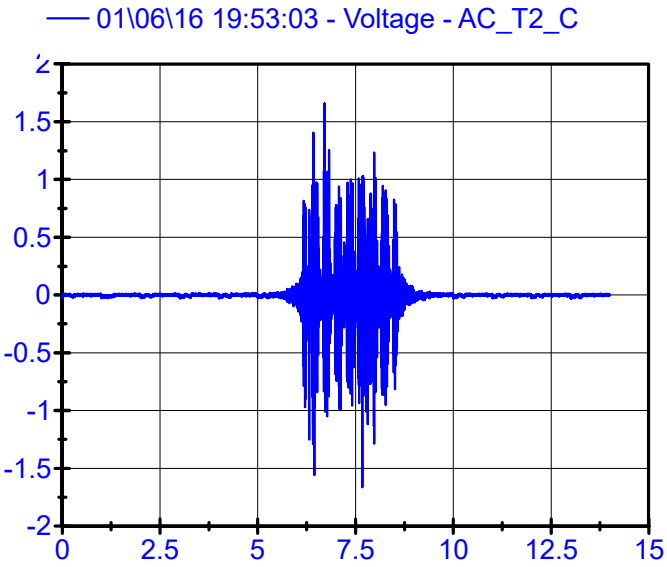

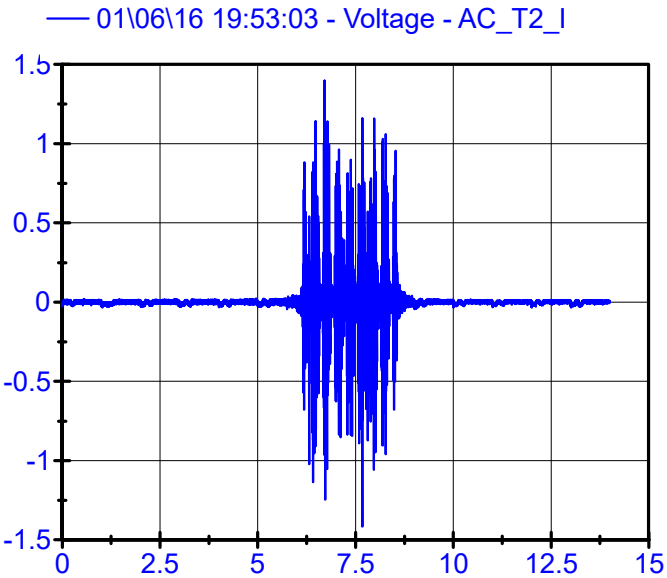

Rail Accelerometers
LPF 200Hz

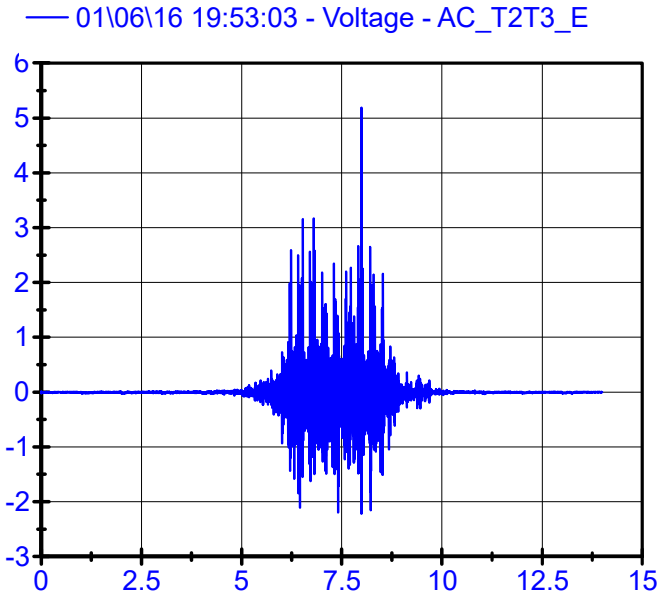

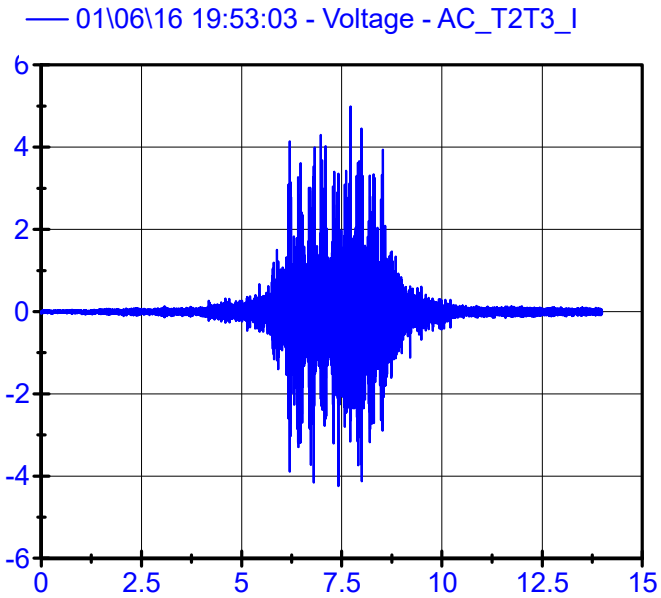

01\06\16 19:59:42

Sleeper Accelerometers
LPF 250Hz

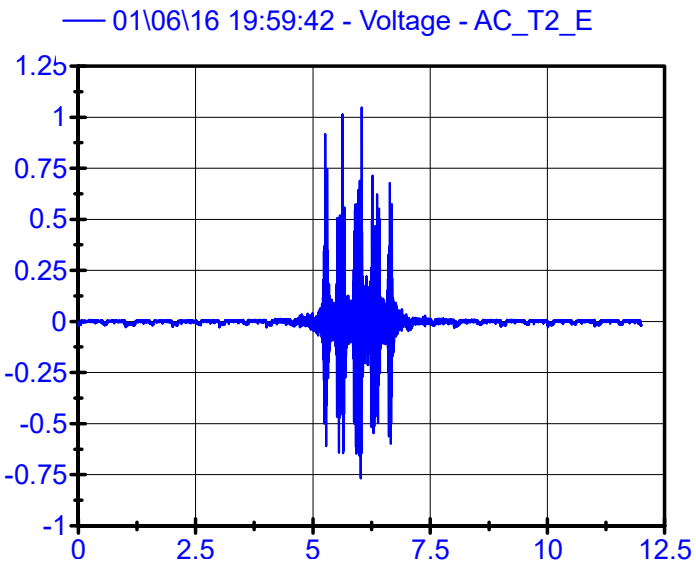

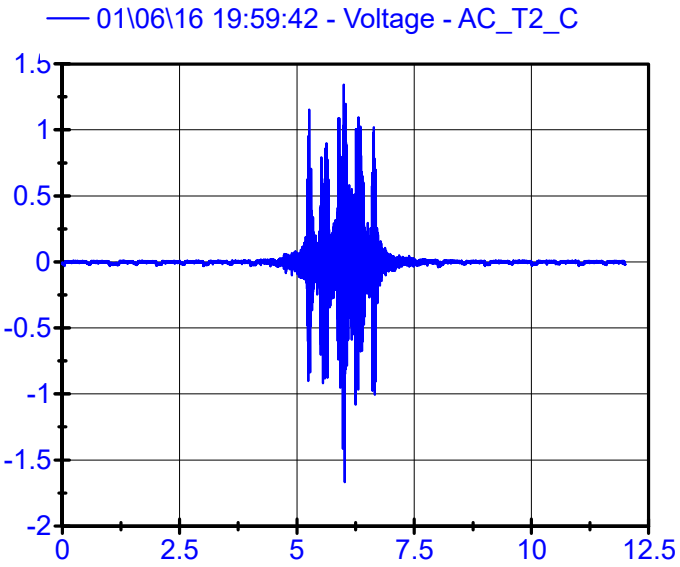

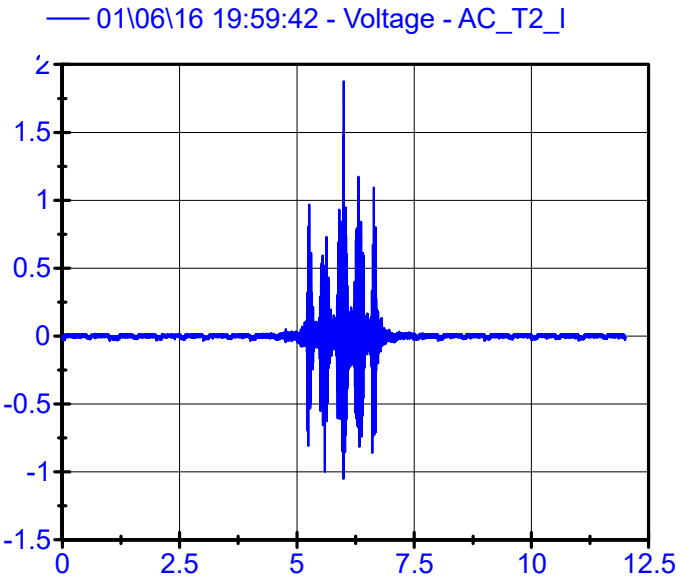

Rail Accelerometers
LPF 200Hz

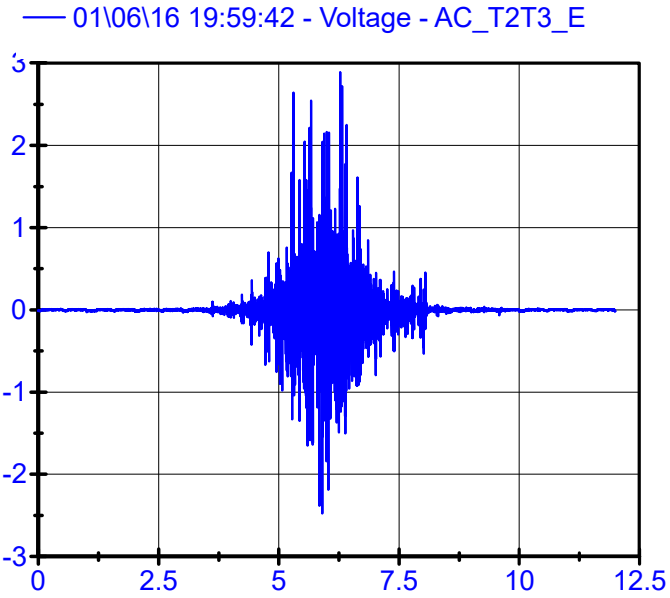

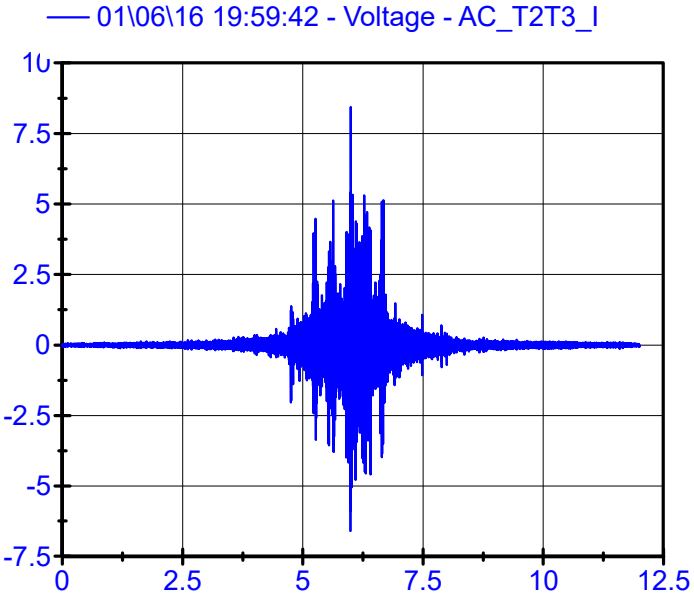

01\06\16 20:21:57

Sleeper Accelerometers
LPF 250Hz

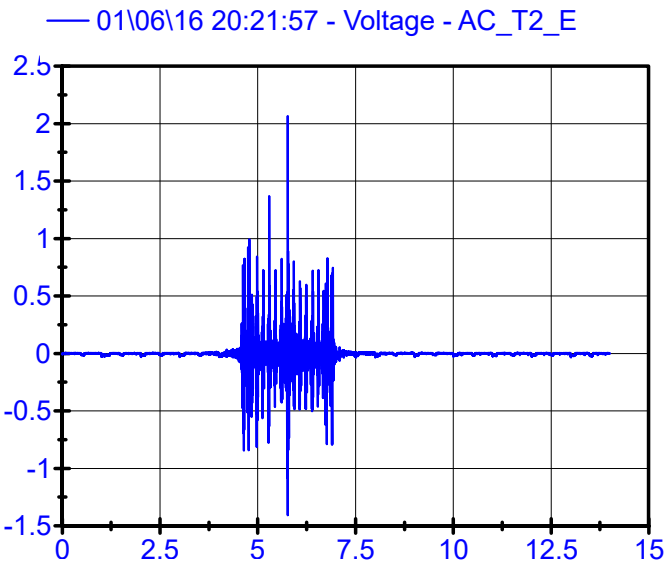

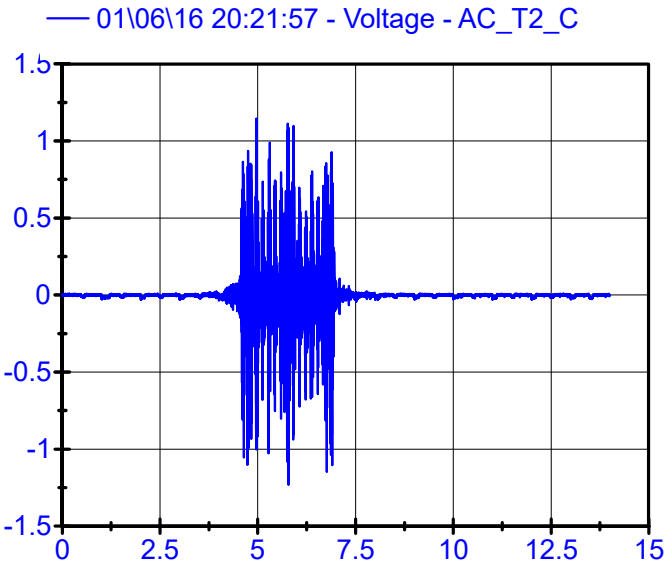

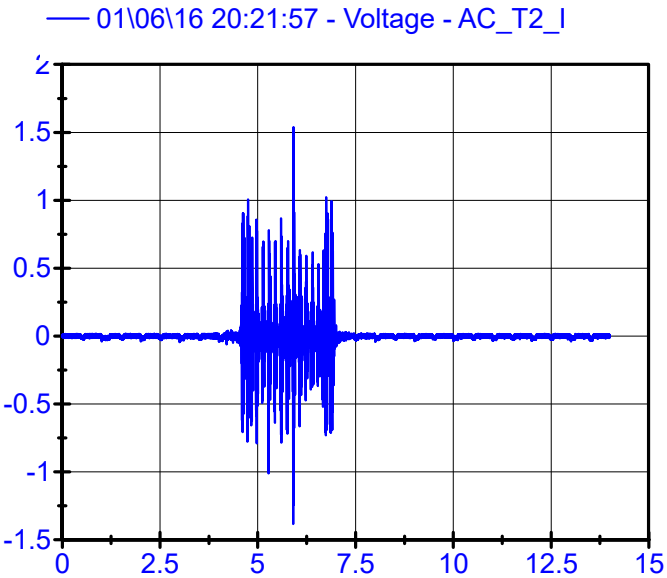

Rail Accelerometers
LPF 200Hz

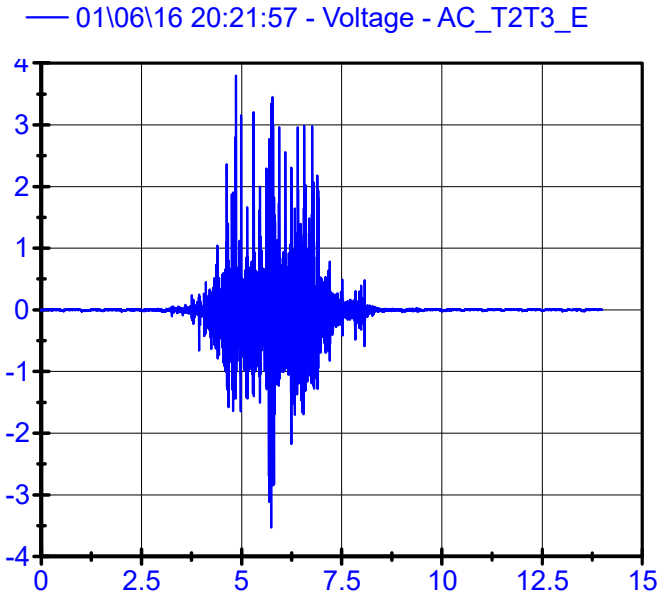

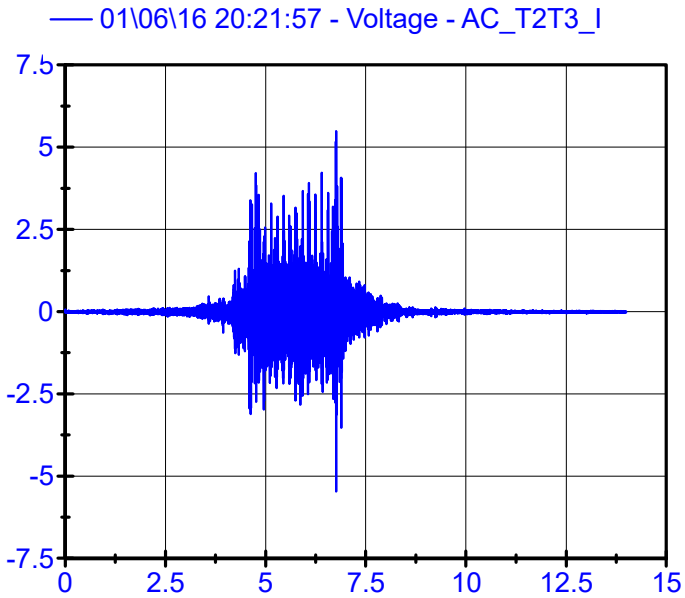

01\06\16 20:57:58

Sleeper Accelerometers
LPF 250Hz

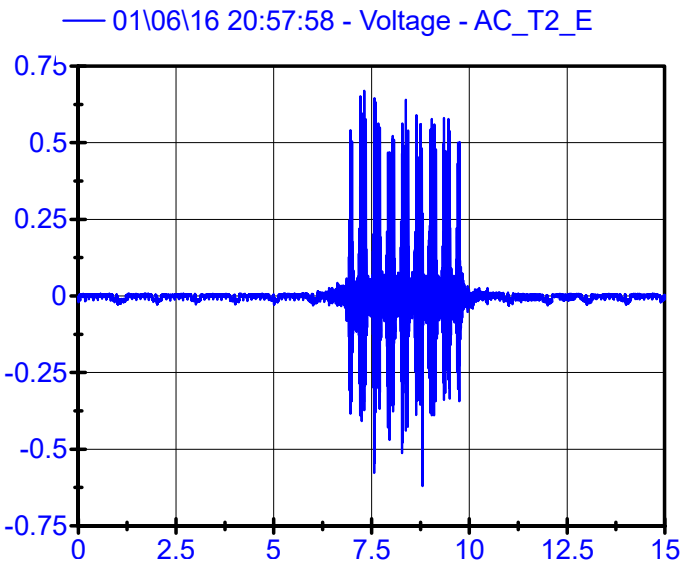

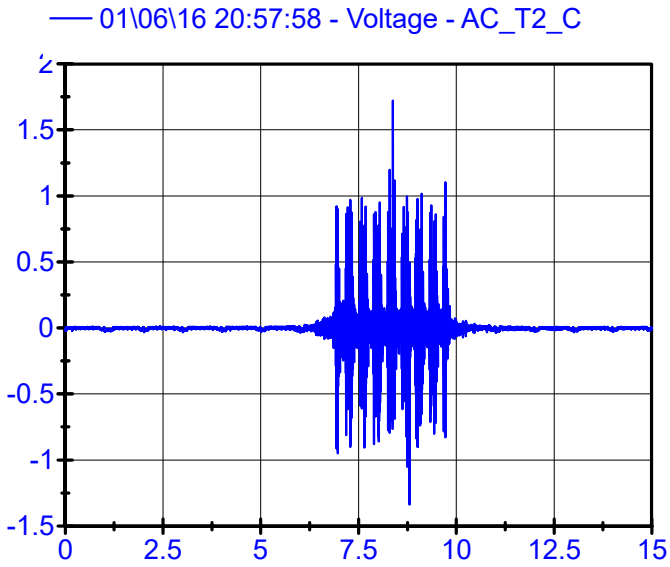

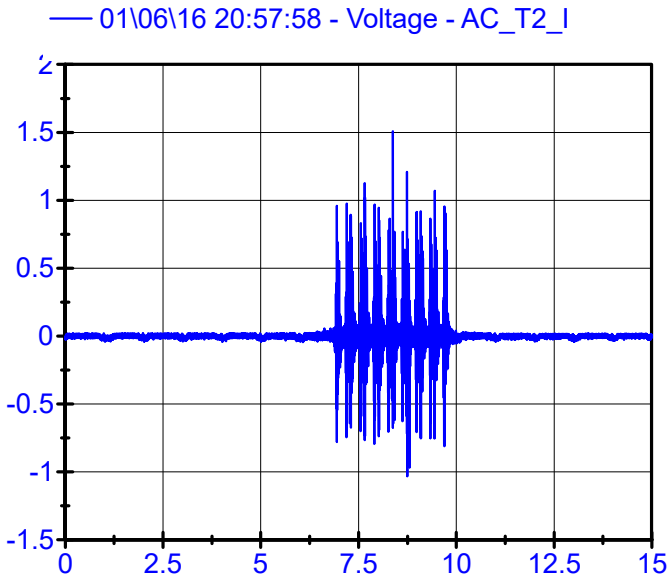

Rail Accelerometers
LPF 200Hz

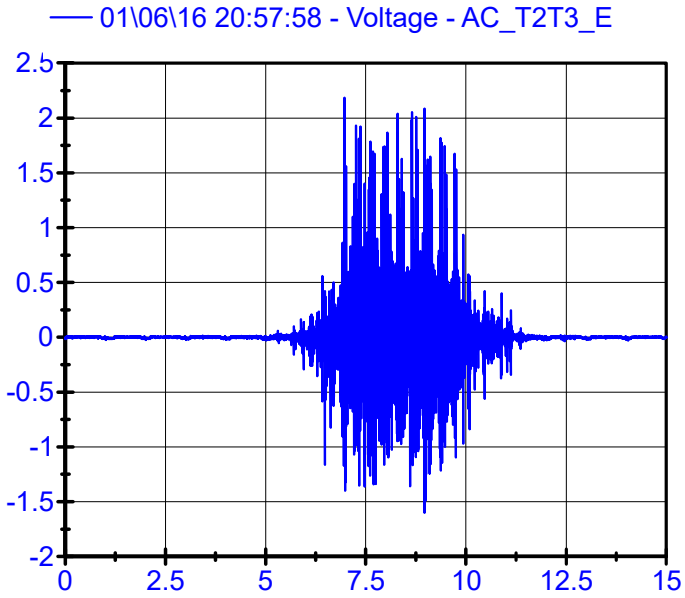

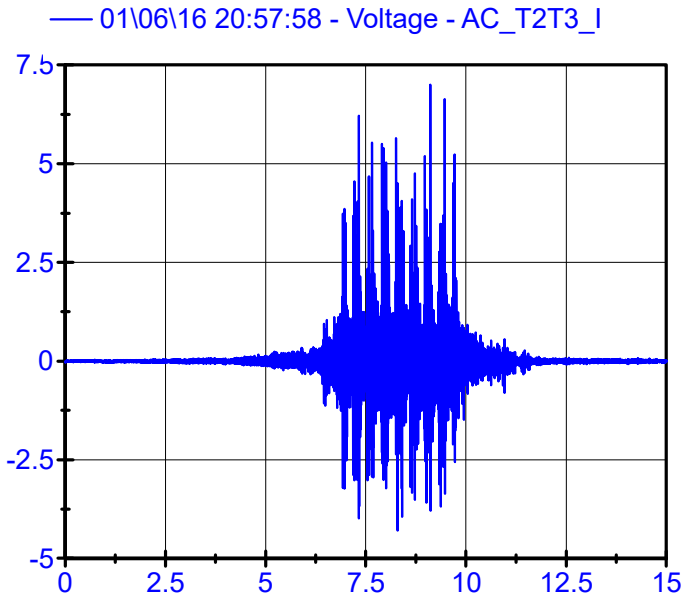

01\06\16 21:49:46

Sleeper Accelerometers
LPF 250Hz

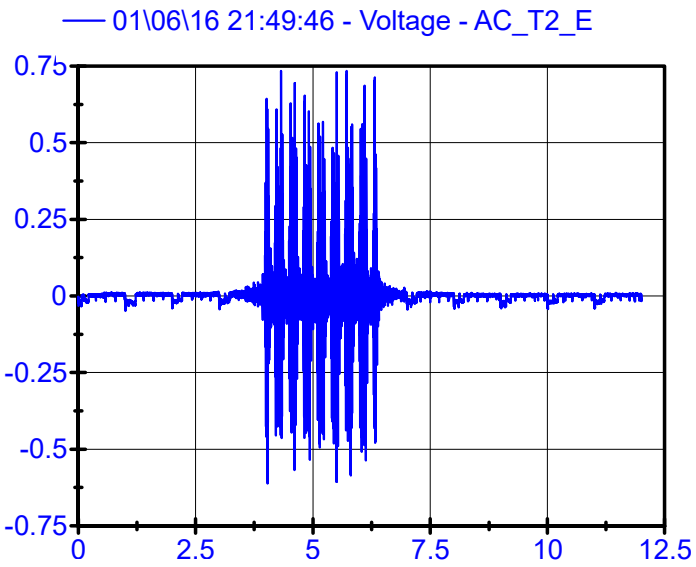

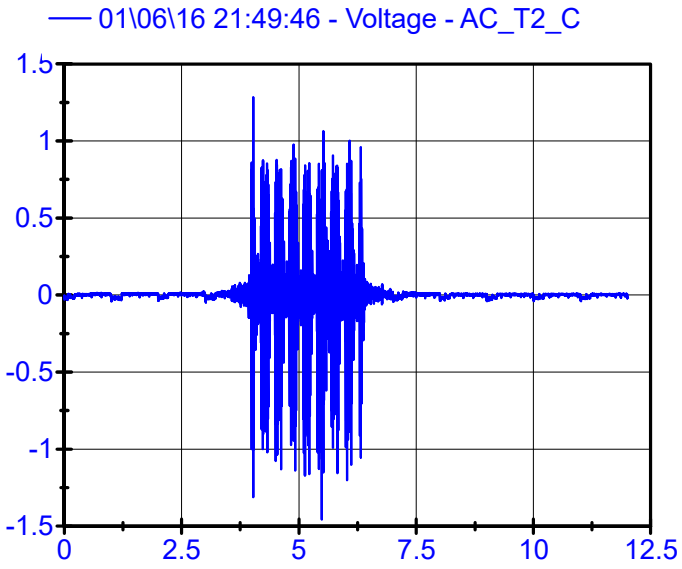

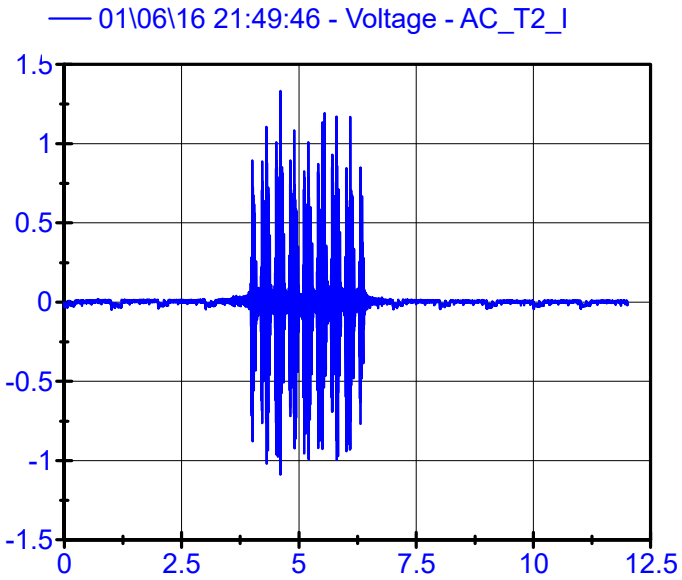

Rail Accelerometers
LPF 200Hz

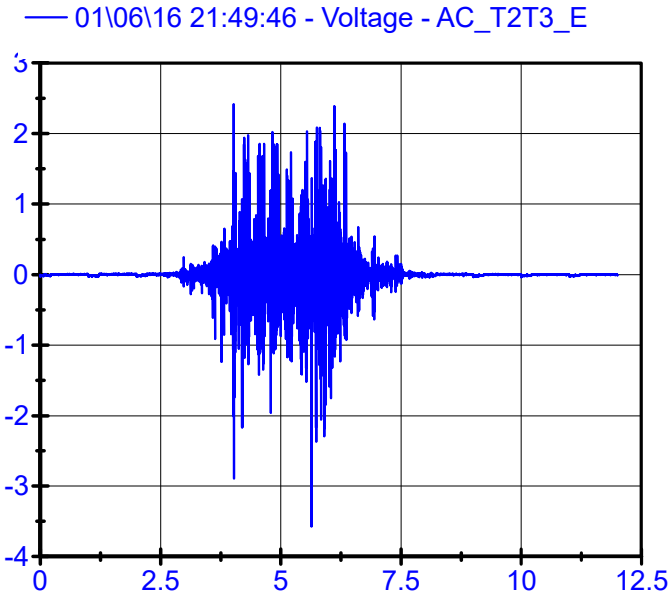

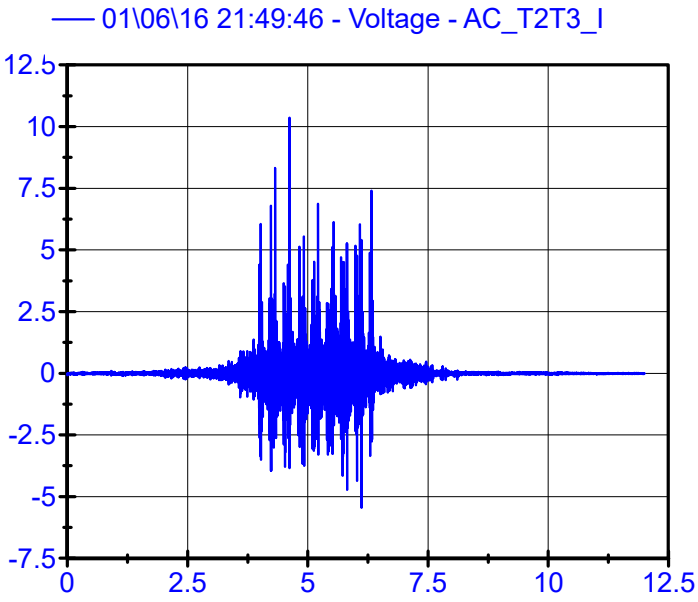

RAIL-SLEEPER RELATIVE MOTION

POTENTIOMETERS

NOTES:

Units of Y axle are “m” for all the plots belonging to rail-sleeper relative motion.

A Low Pass Filter of 90 Hz has been applied to all raw signals.

01\06\16 06:31:45

Potentiometers
LPF 80Hz

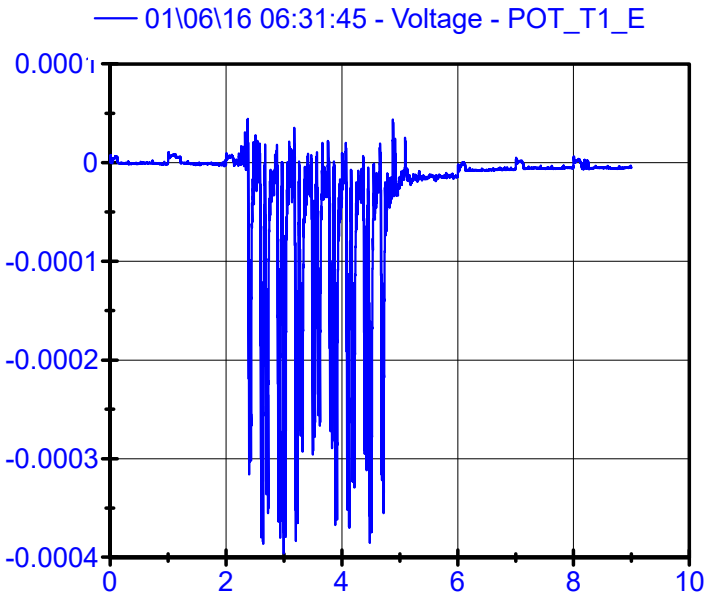

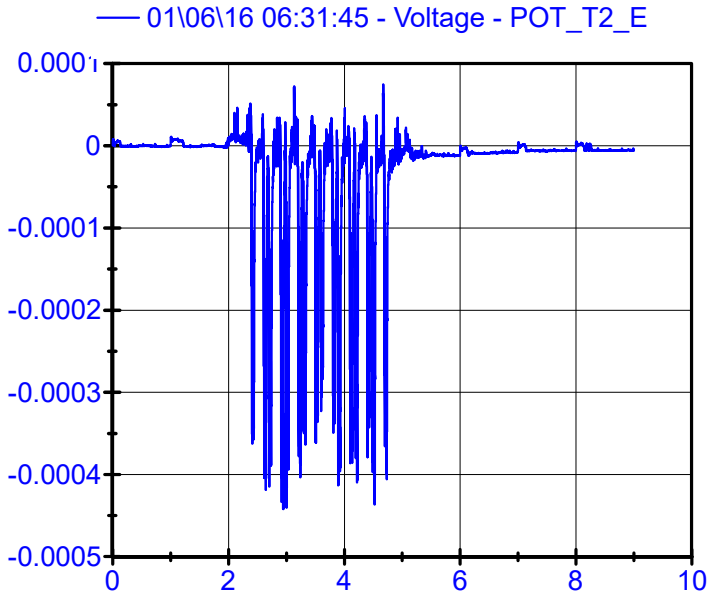

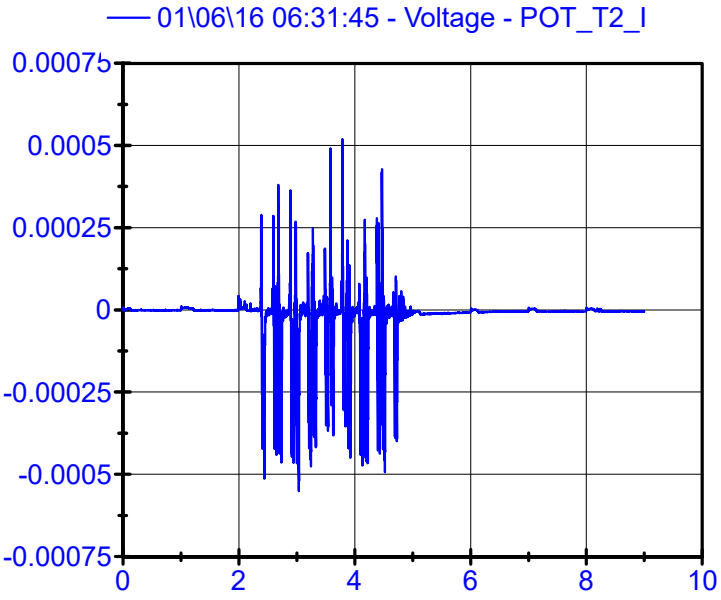

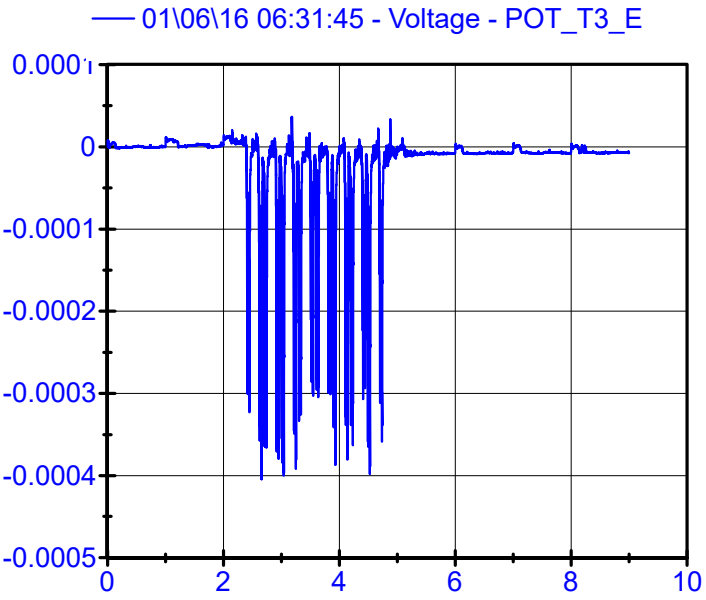

01\06\16 06:52:39

Potentiometers
LPF 80Hz

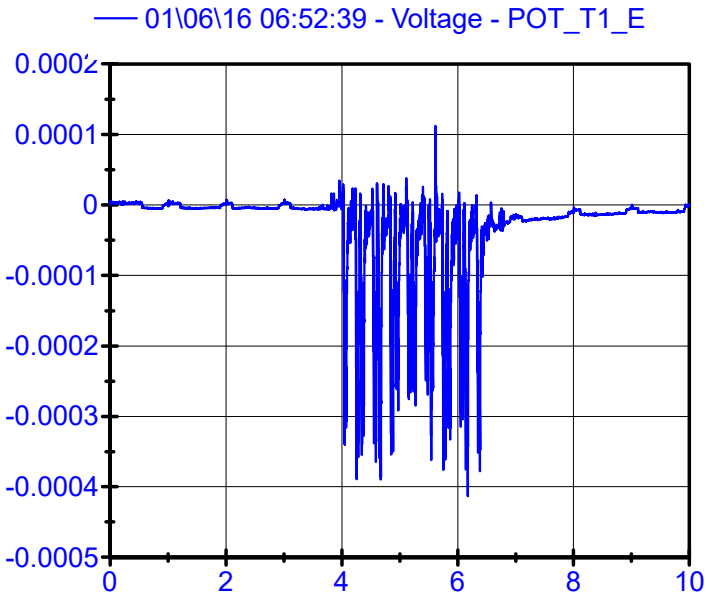

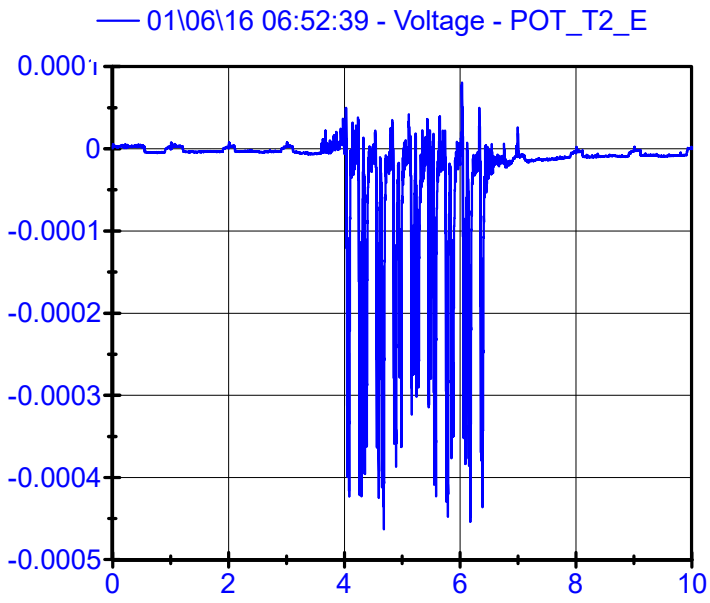

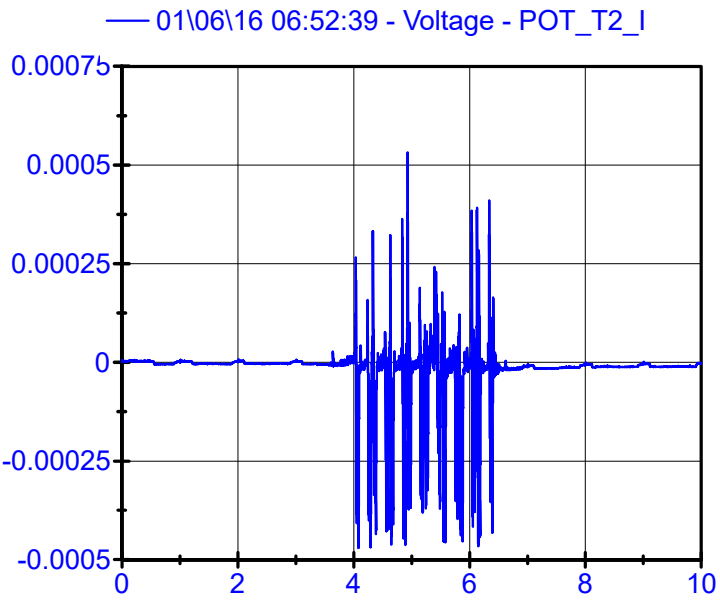

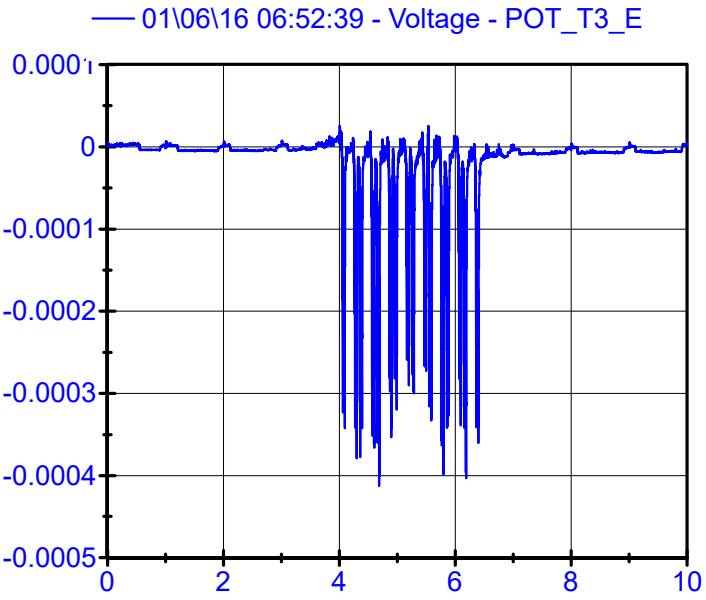

01\06\16 07:21:52

Potentiometers
LPF 80Hz

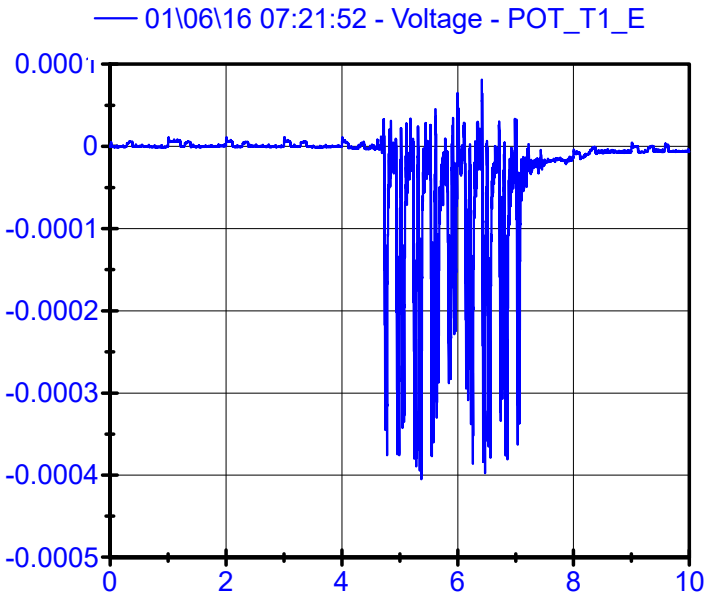

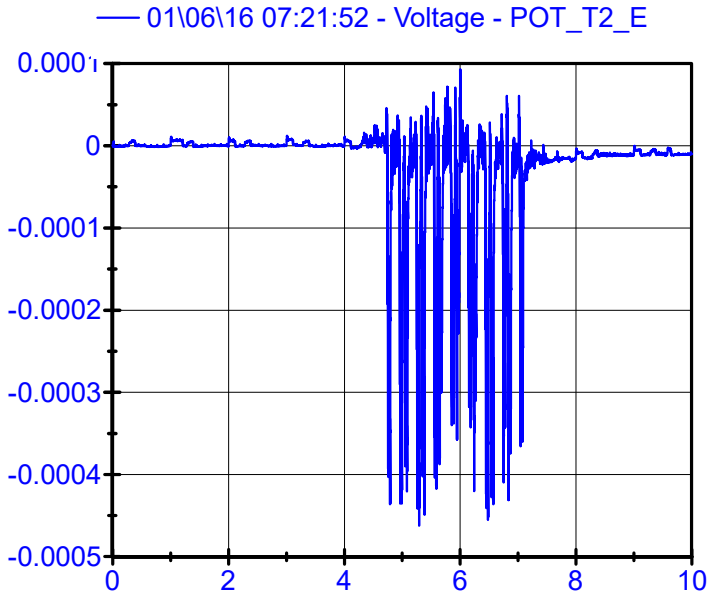

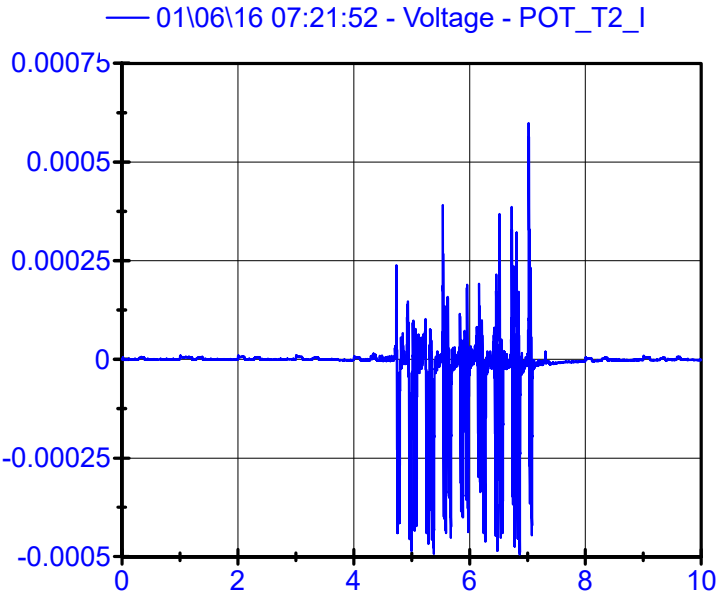

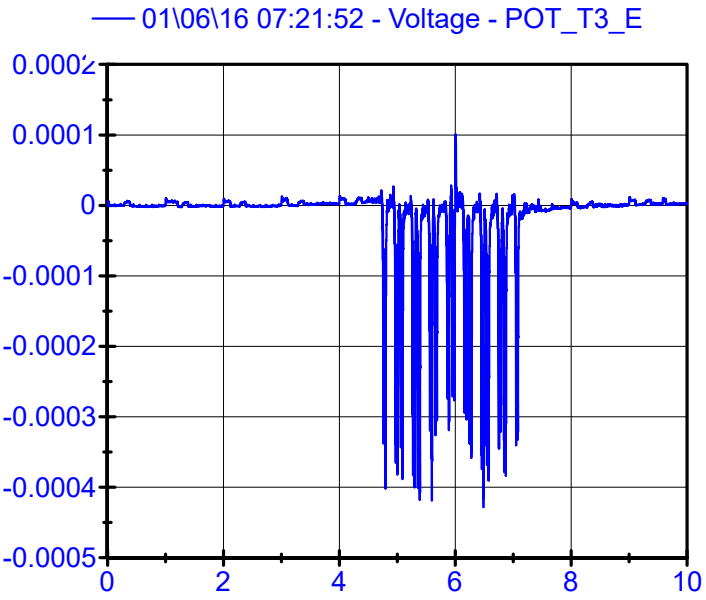

01\06\16 07:41:25

Potentiometers
LPF 80Hz

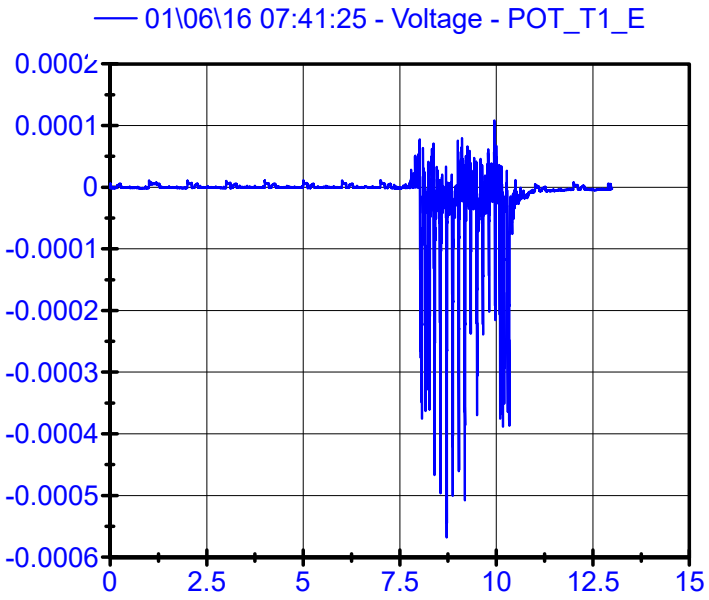

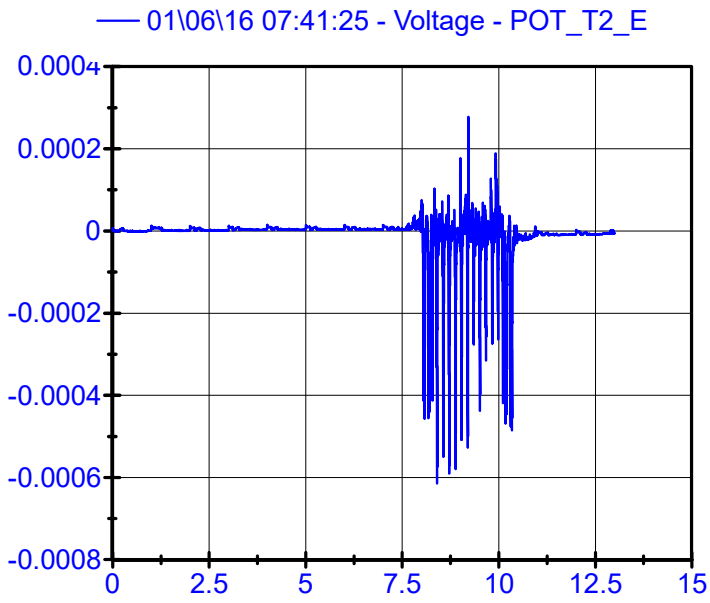

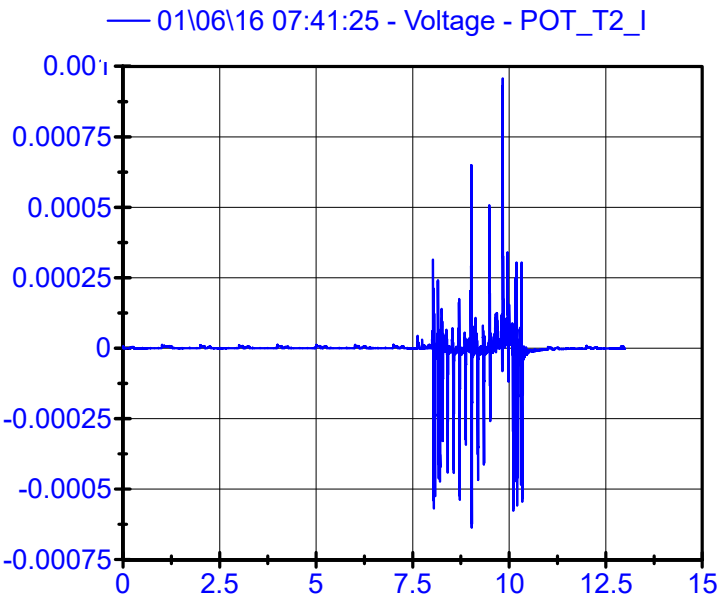

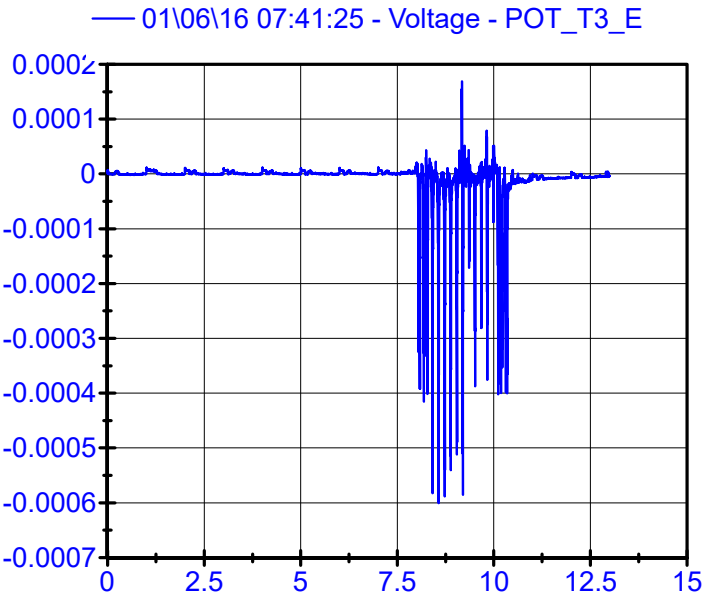

01\06\16 07:56:37

Potentiometers
LPF 80Hz

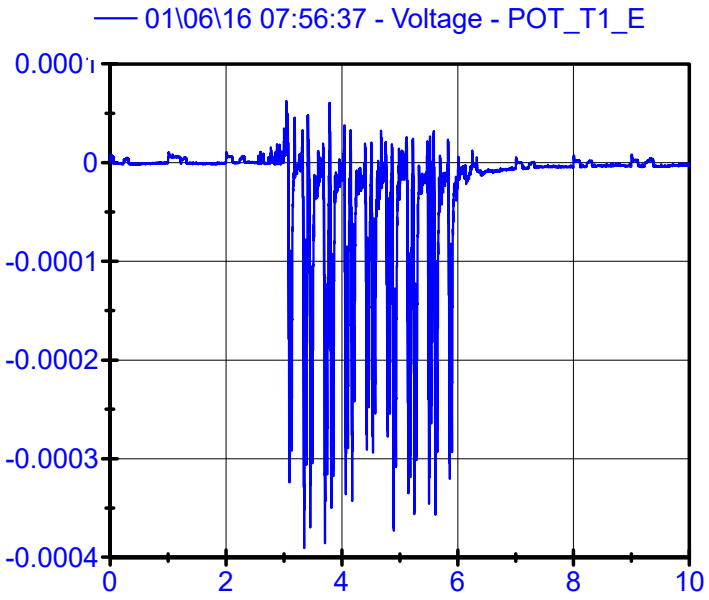

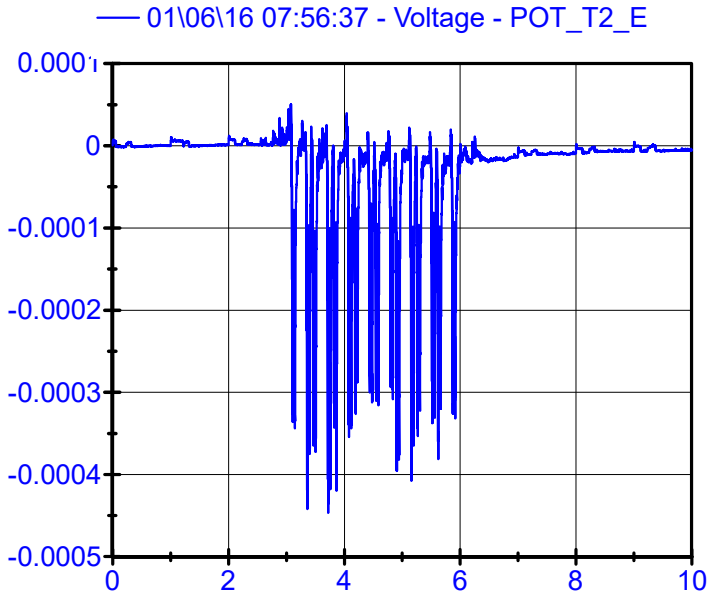

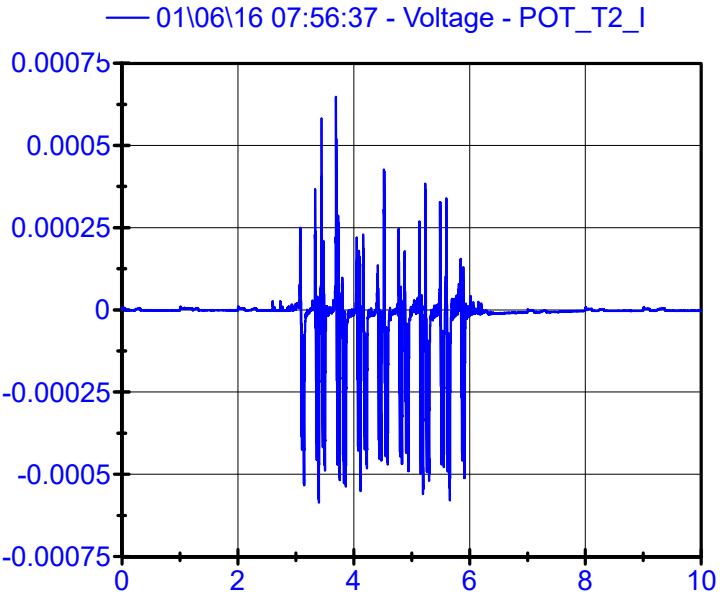

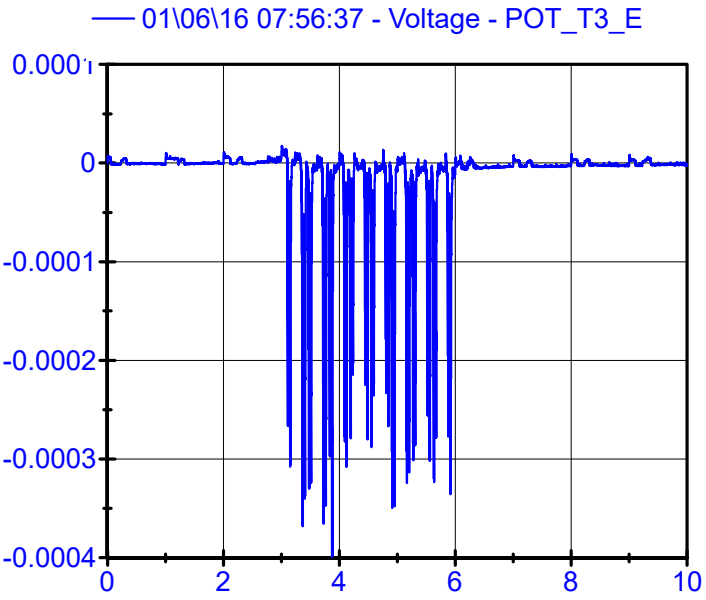

01\06\16 08:01:29

Potentiometers
LPF 80Hz

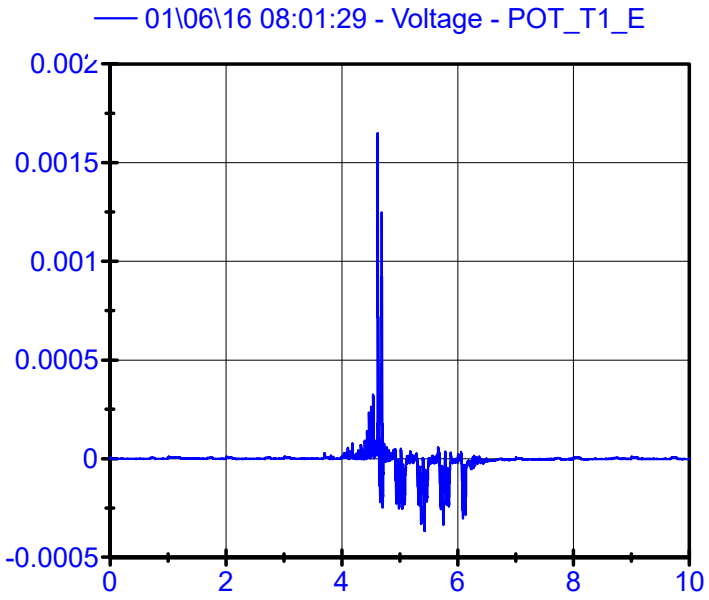

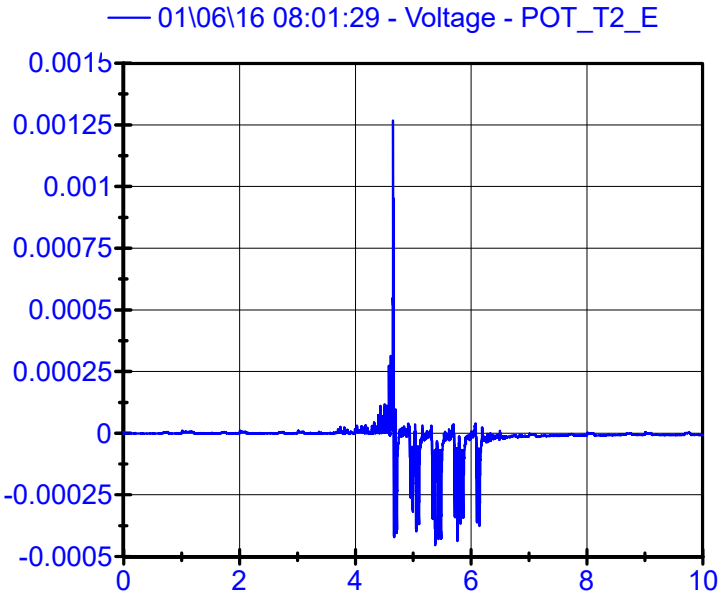

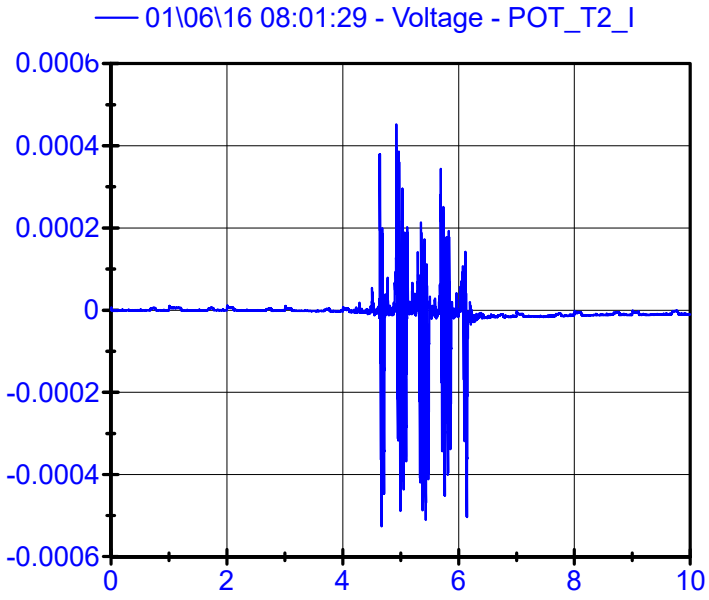

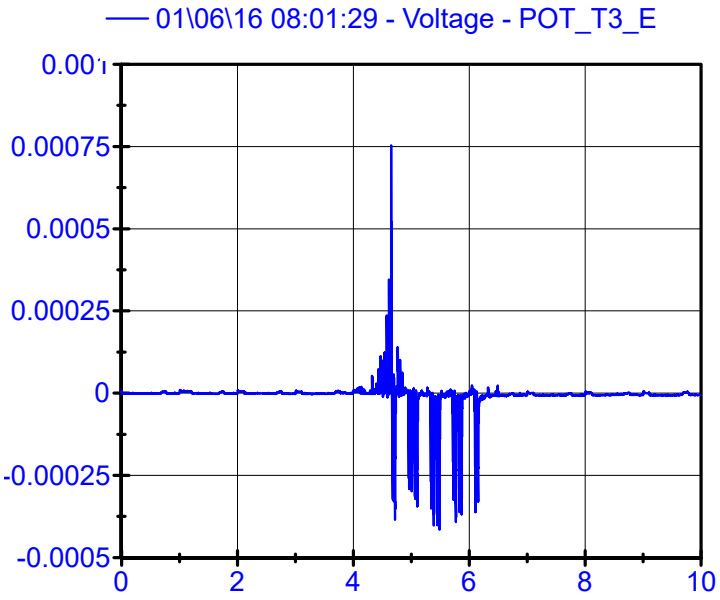

01\06\16 08:21:04

Potentiometers
LPF 80Hz

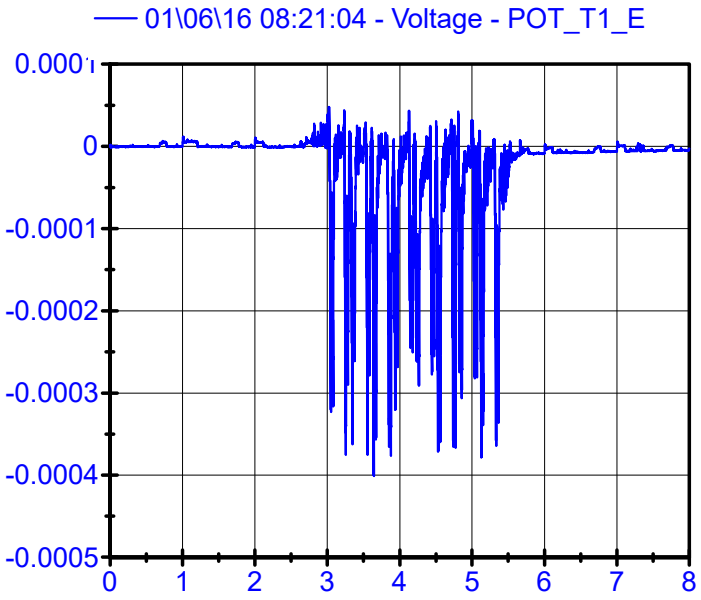

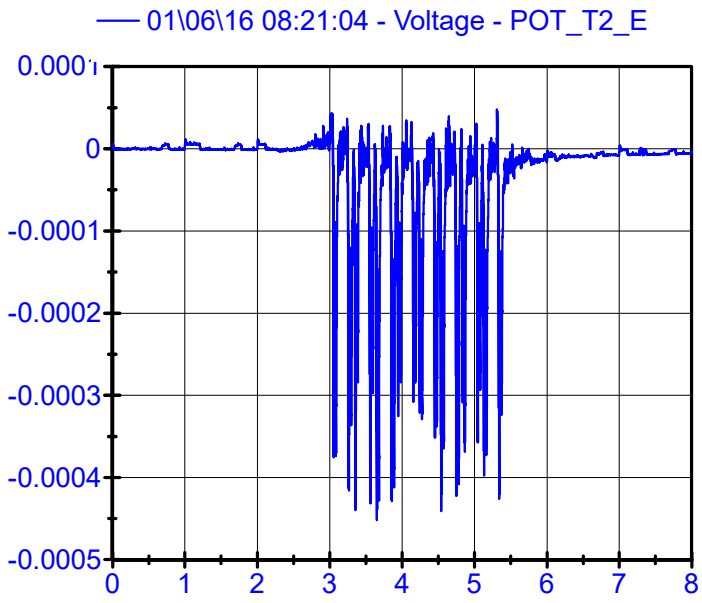

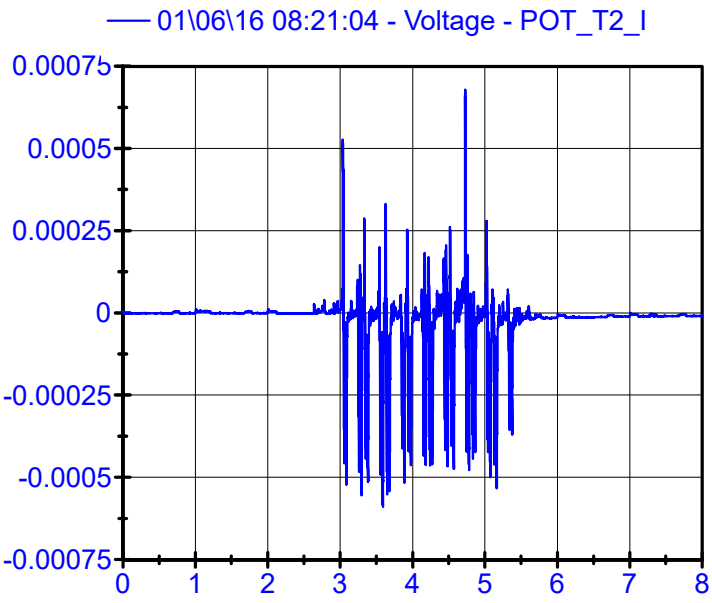

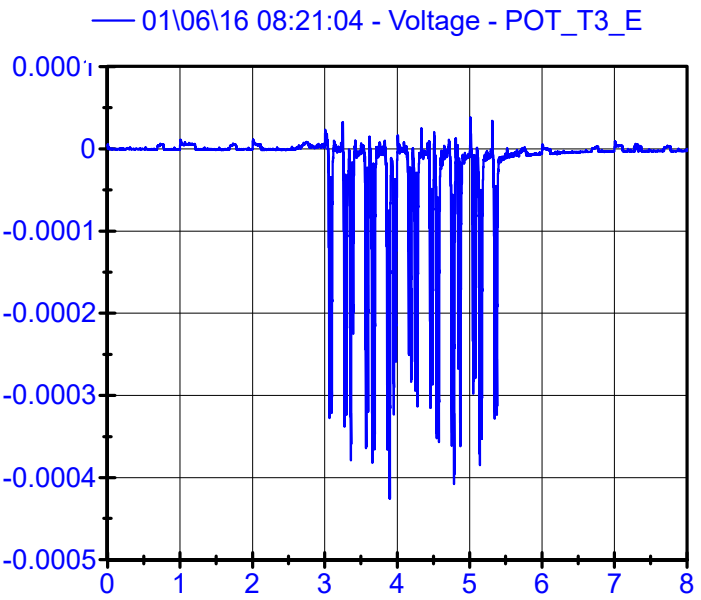

01\06\16 08:42:39

Potentiometers
LPF 80Hz

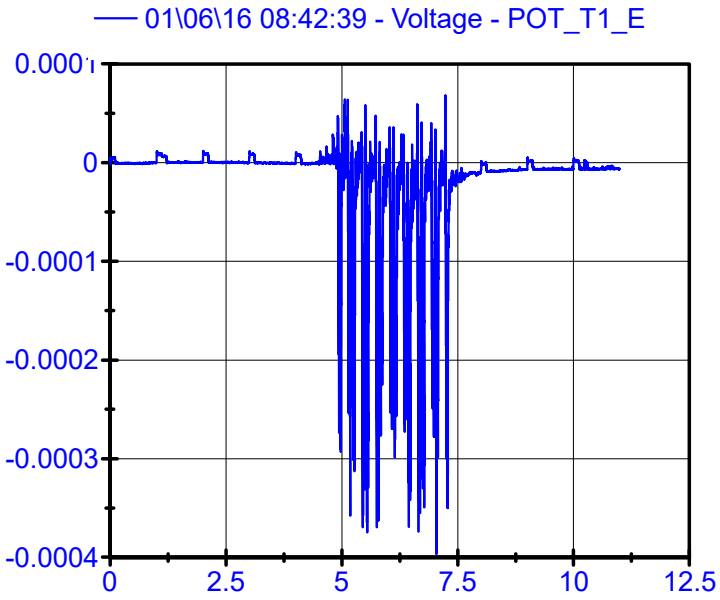

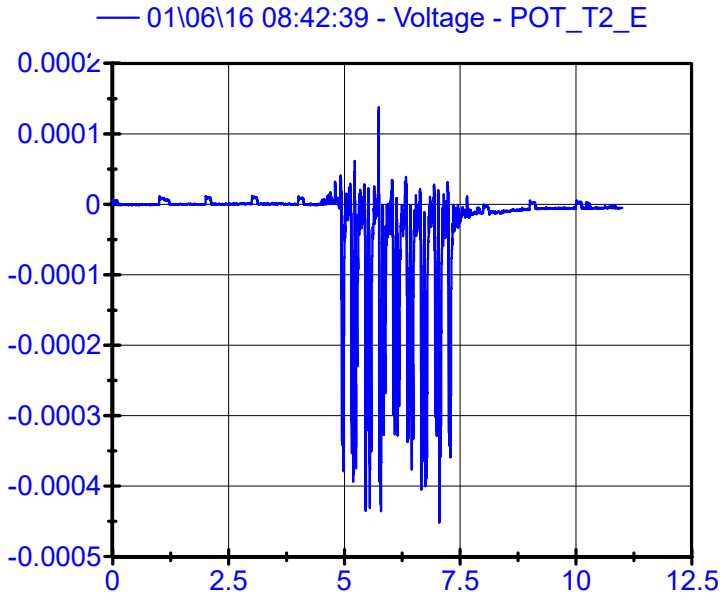

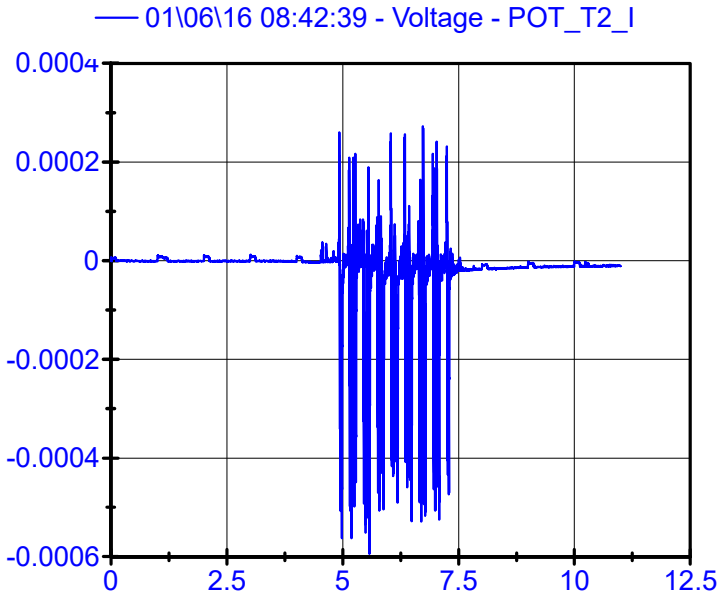

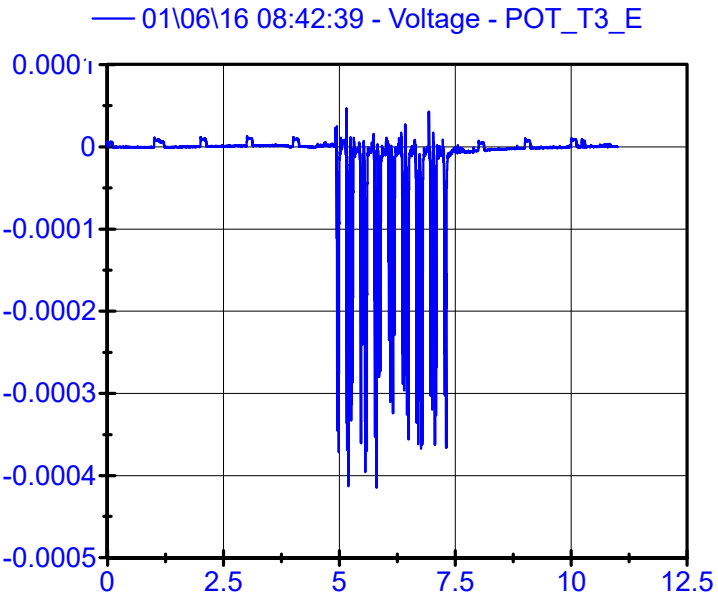

01\06\16 08:52:26

Potentiometers
LPF 80Hz

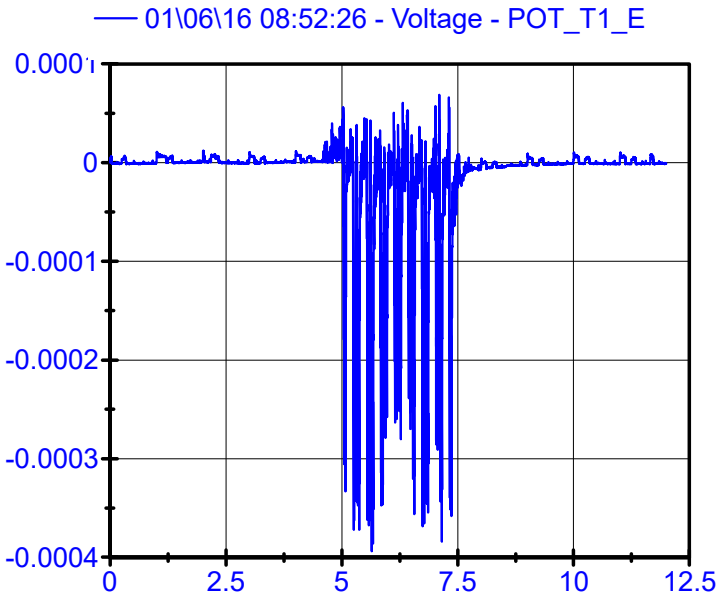

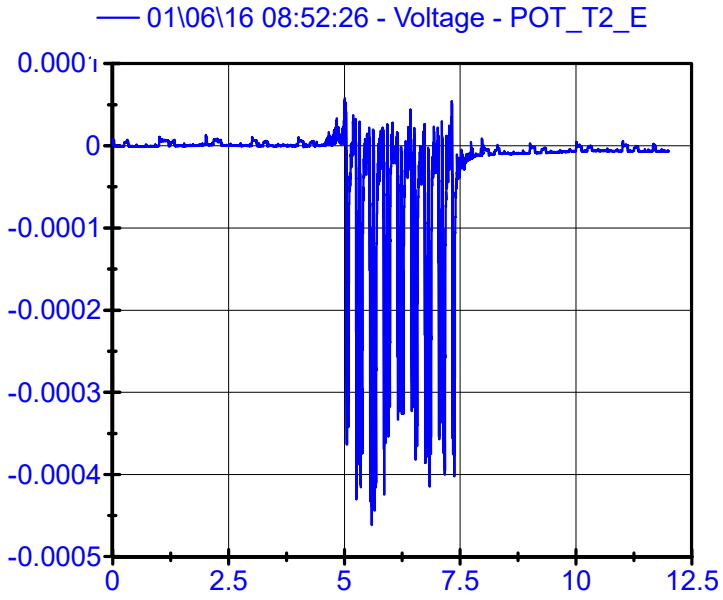

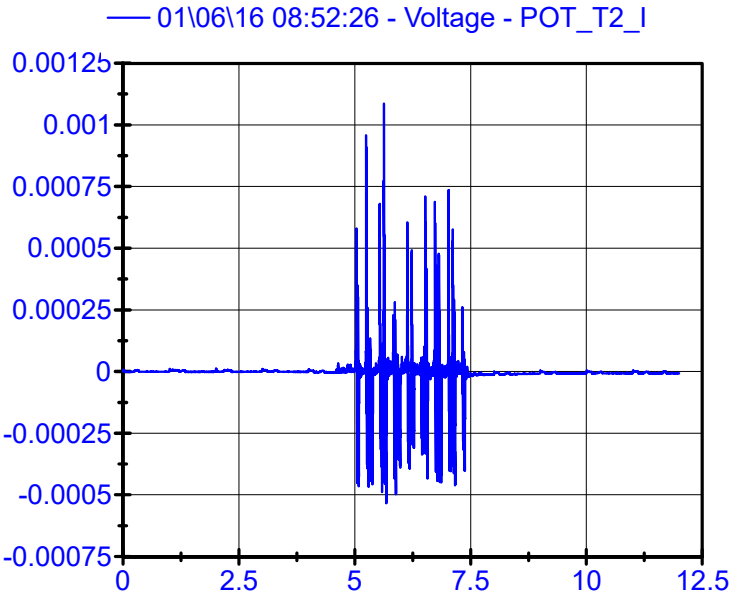

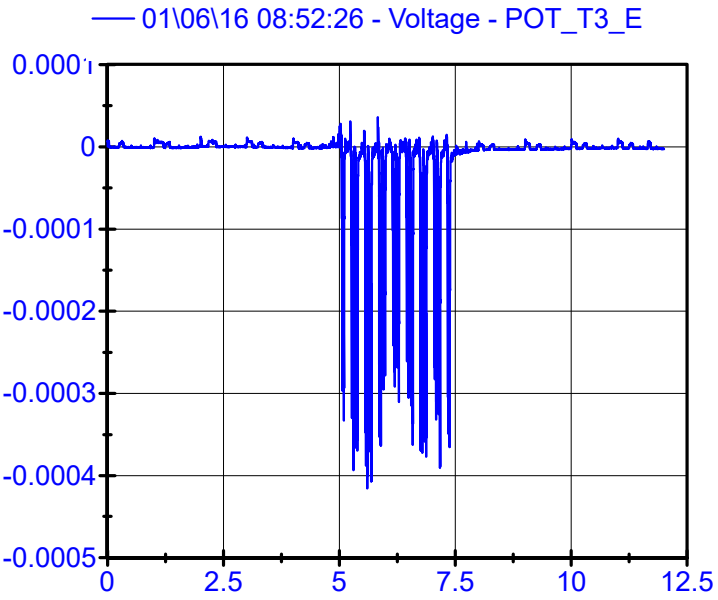

01\06\16 09:23:16

Potentiometers
LPF 80Hz

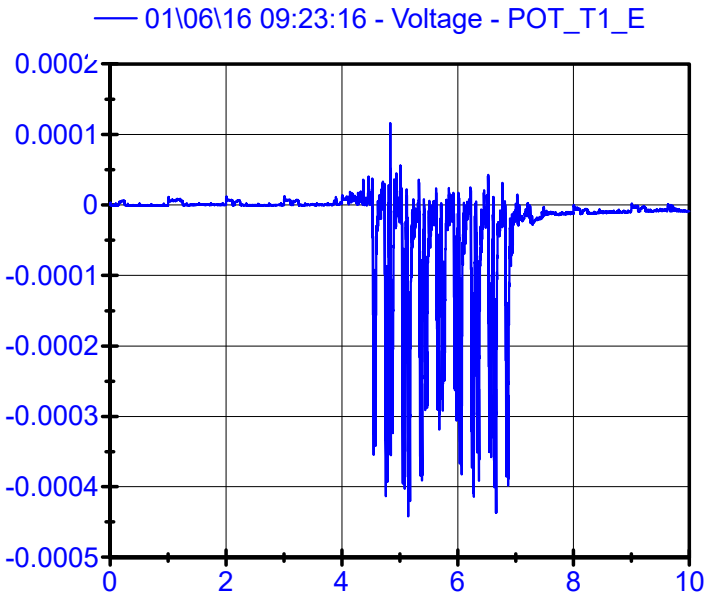

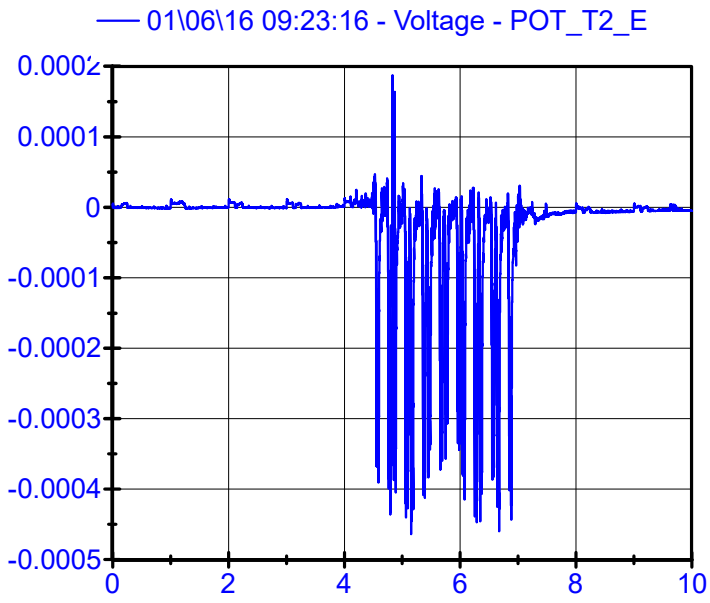

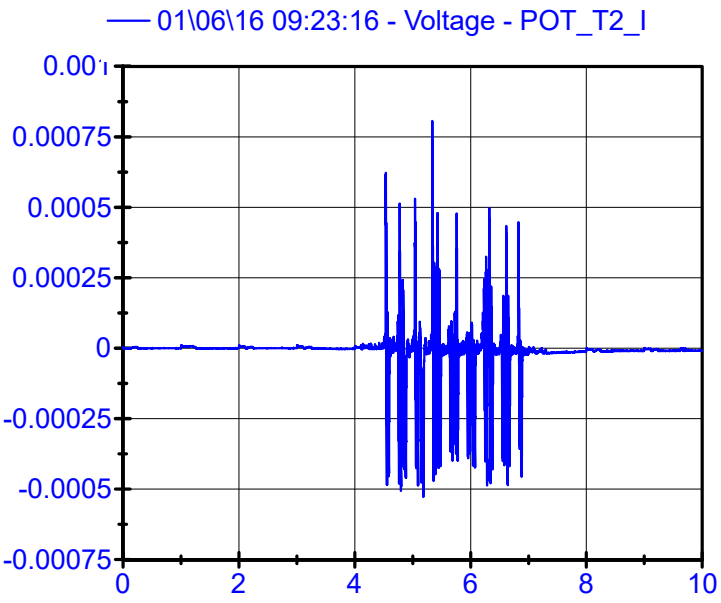

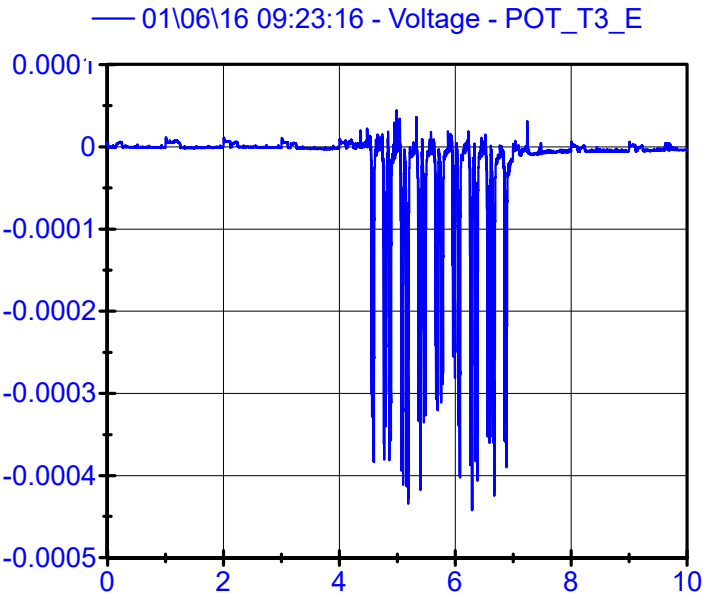

01\06\16 09:52:01

Potentiometers
LPF 80Hz

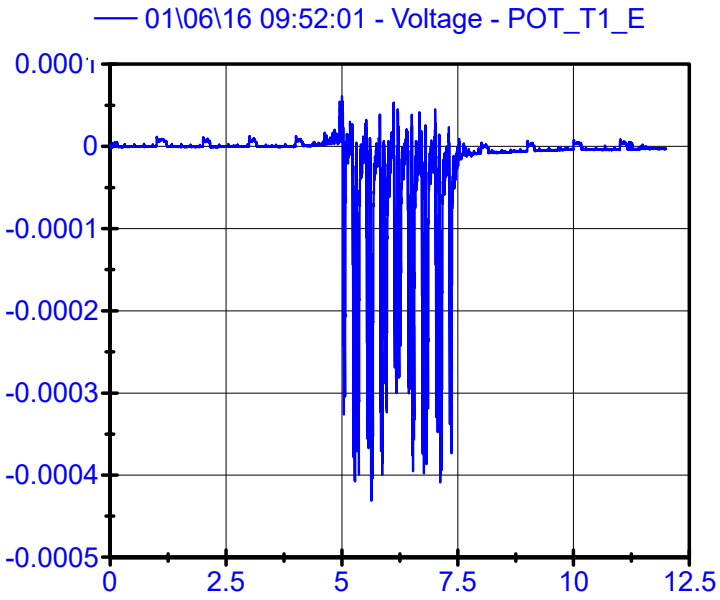

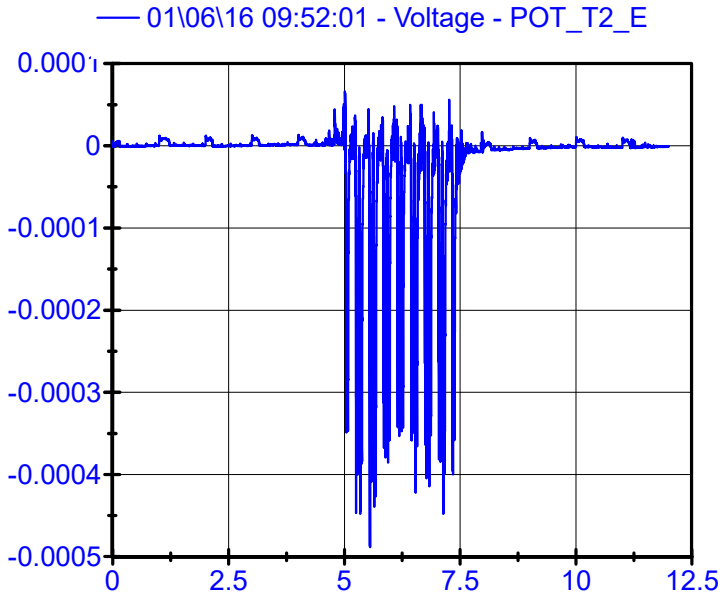

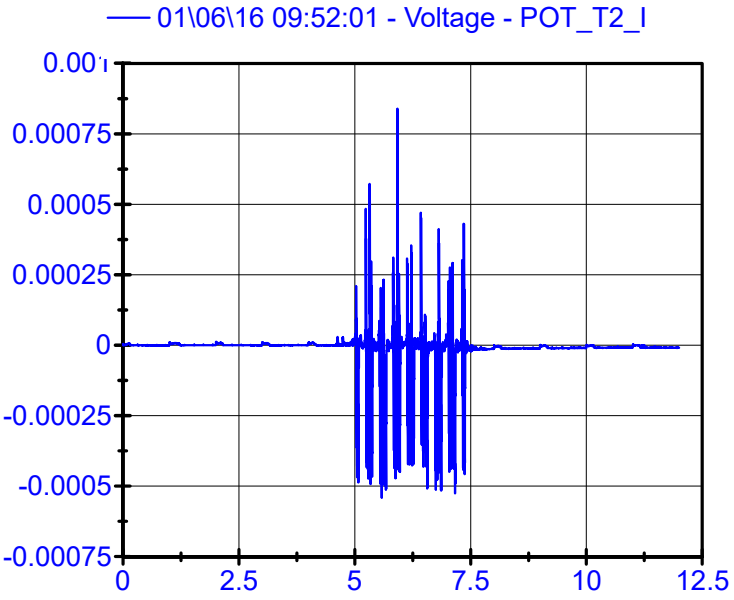

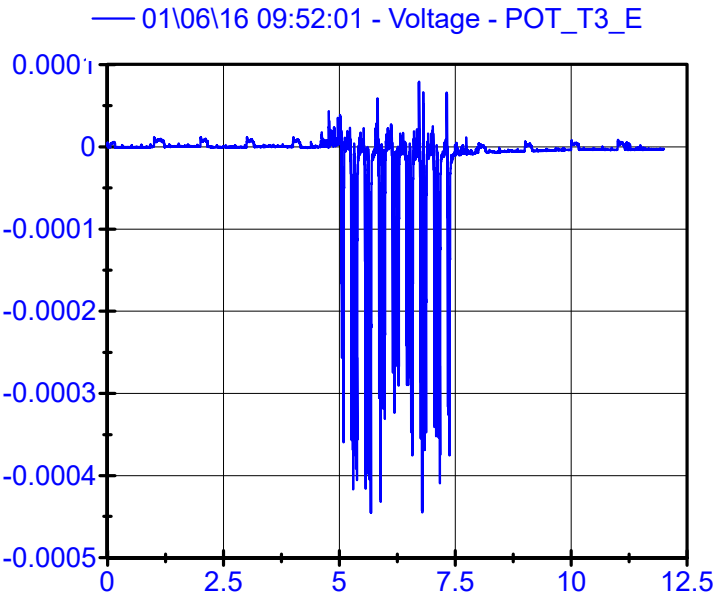

01\06\16 10:53:28

Potentiometers
LPF 80Hz

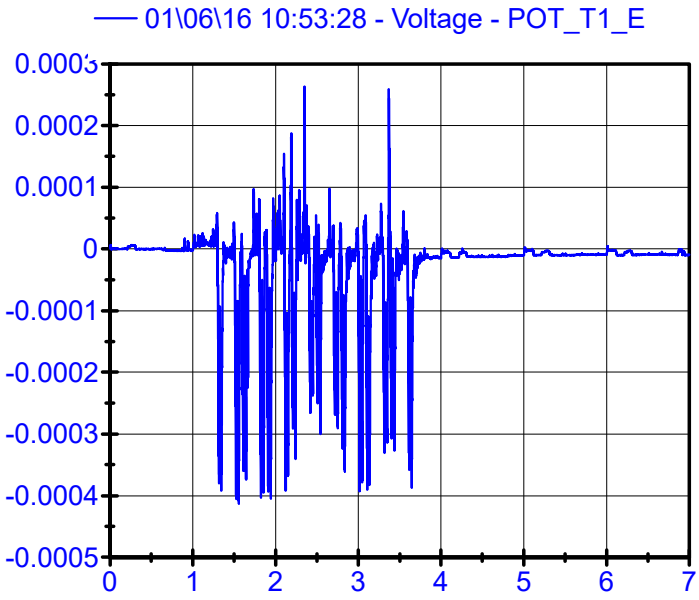

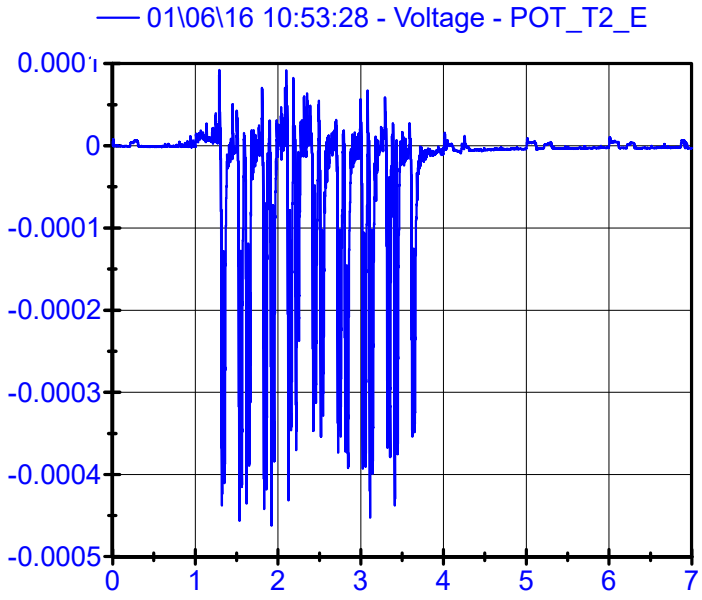

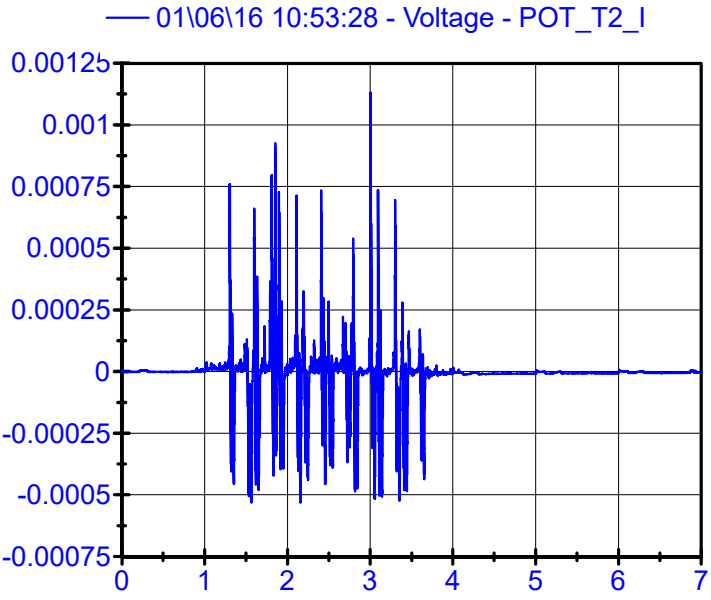

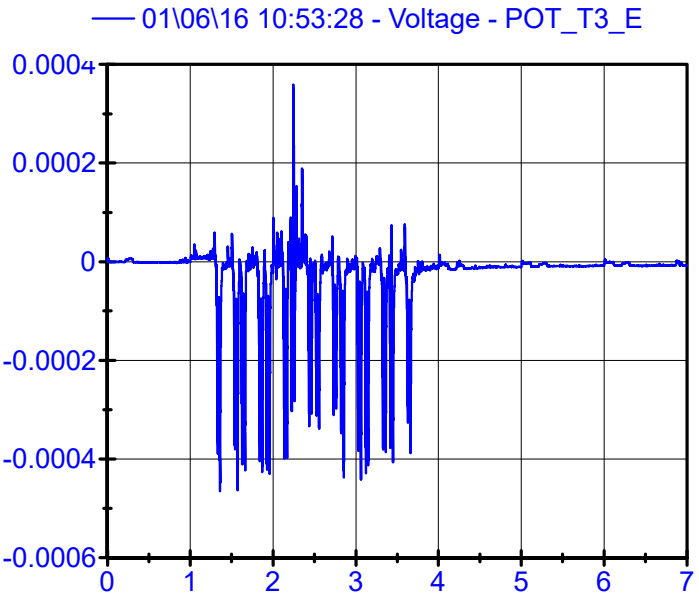

01\06\16 11:35:54

Potentiometers
LPF 80Hz

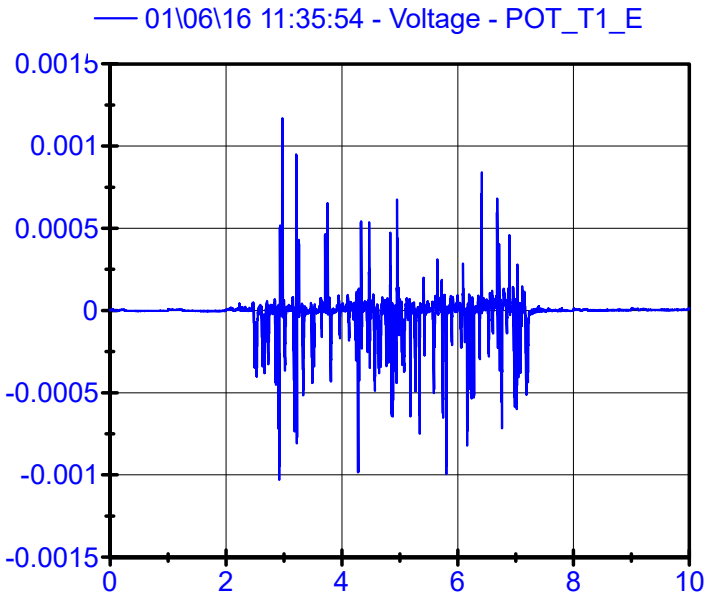

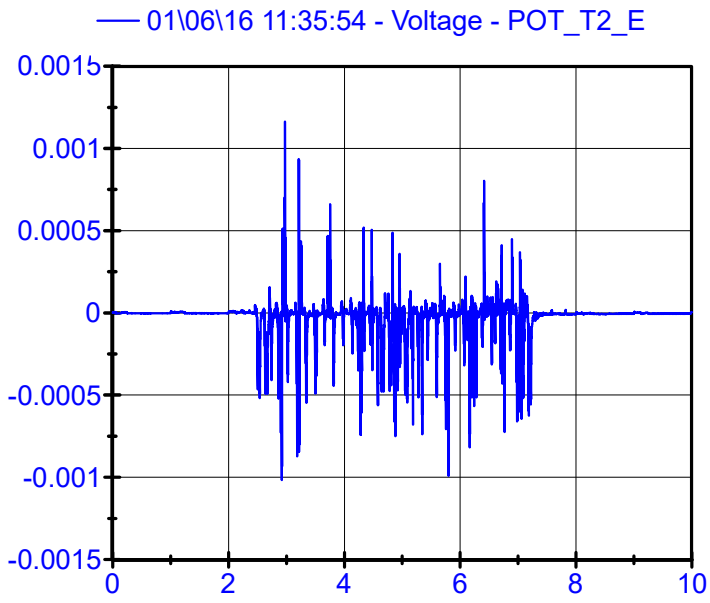

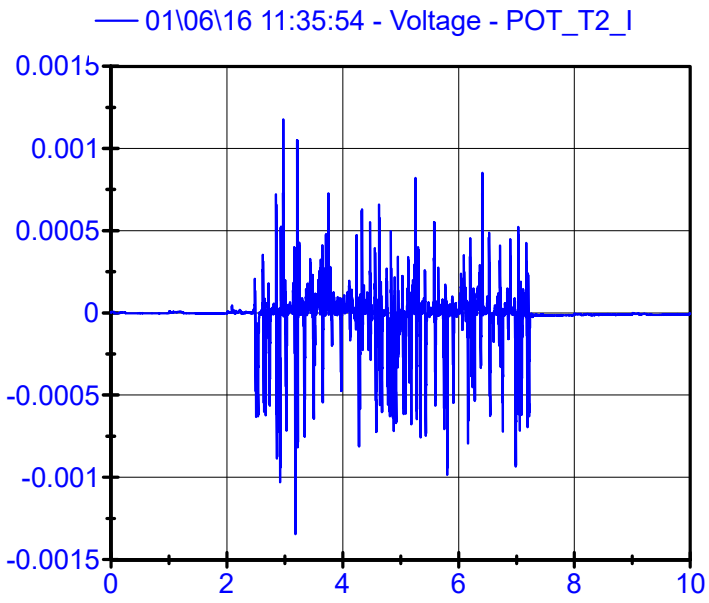

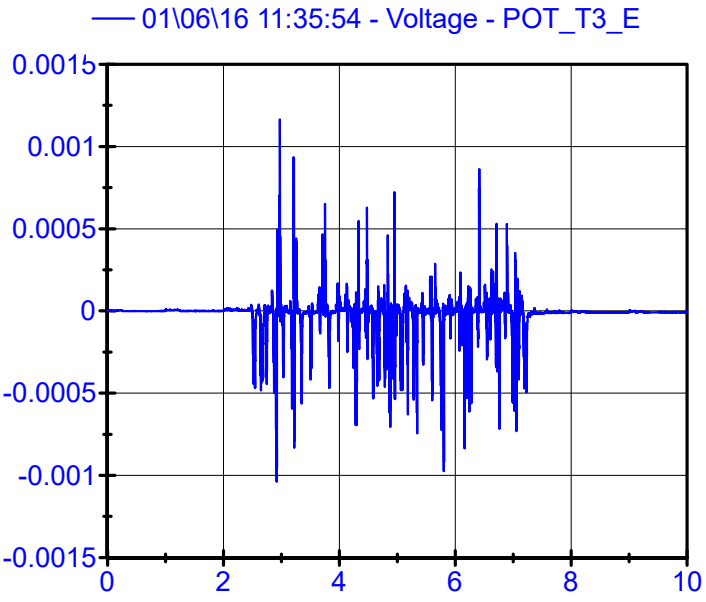

01\06\16 11:53:47

Potentiometers
LPF 80Hz

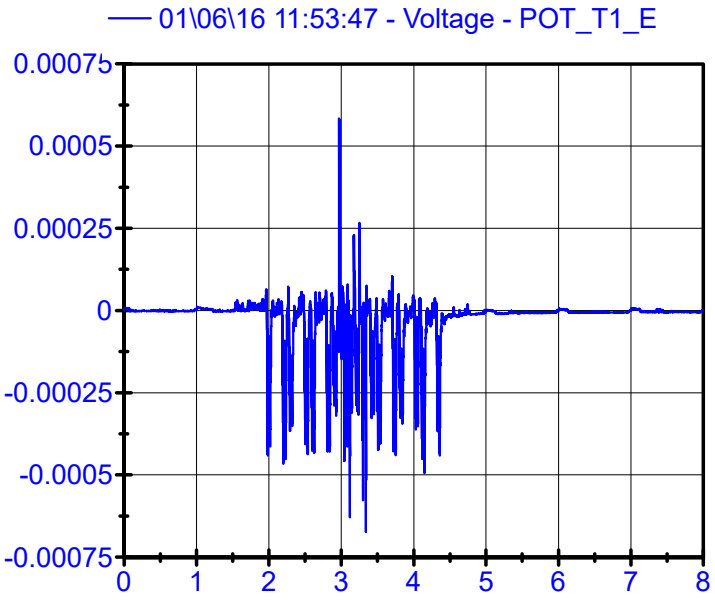

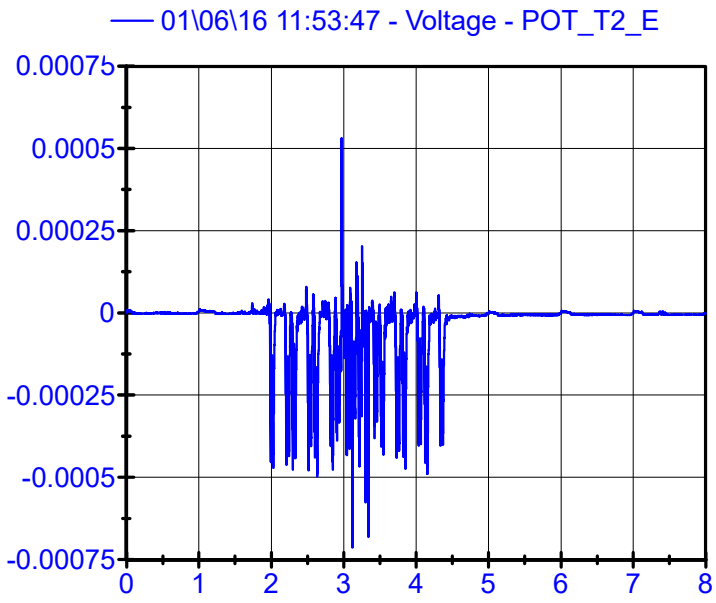

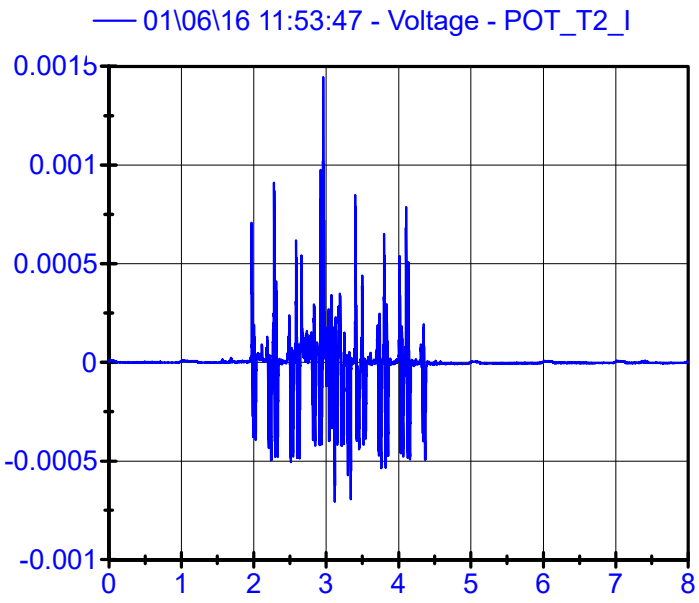

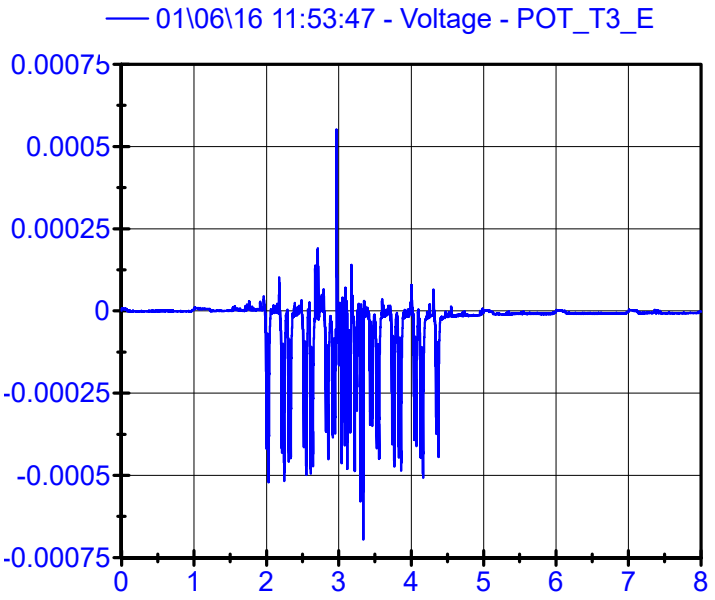

01\06\16 12:07:44

Potentiometers
LPF 80Hz

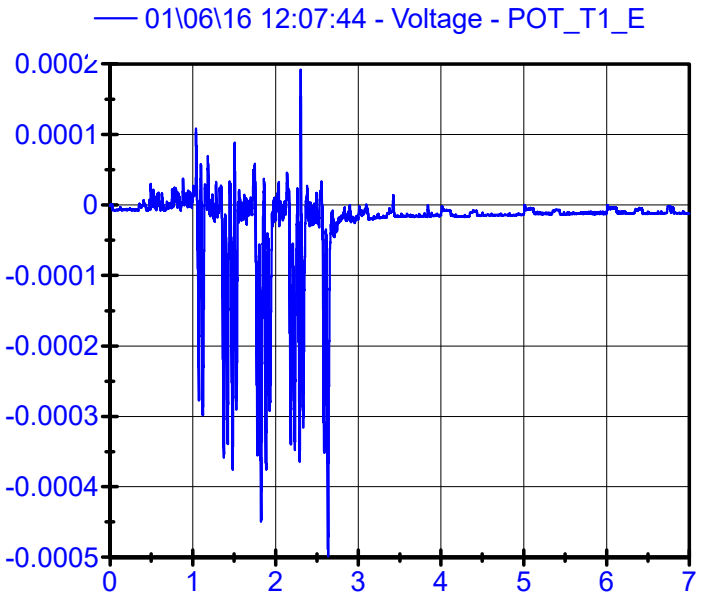

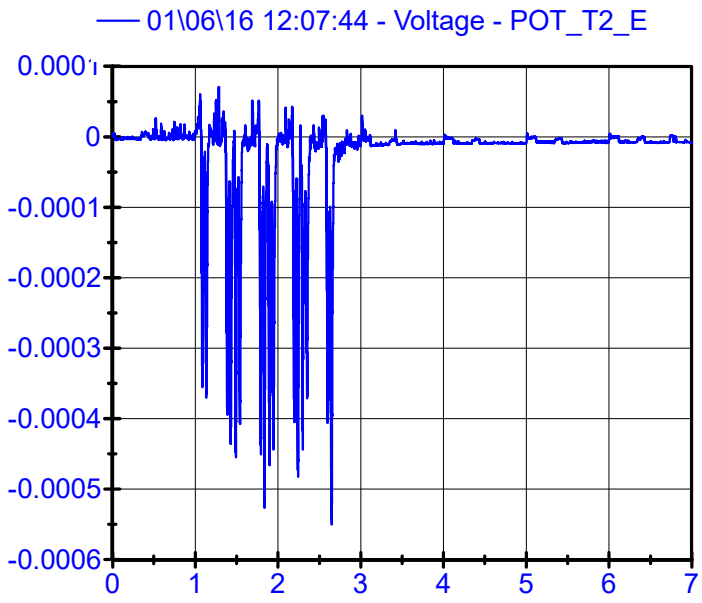

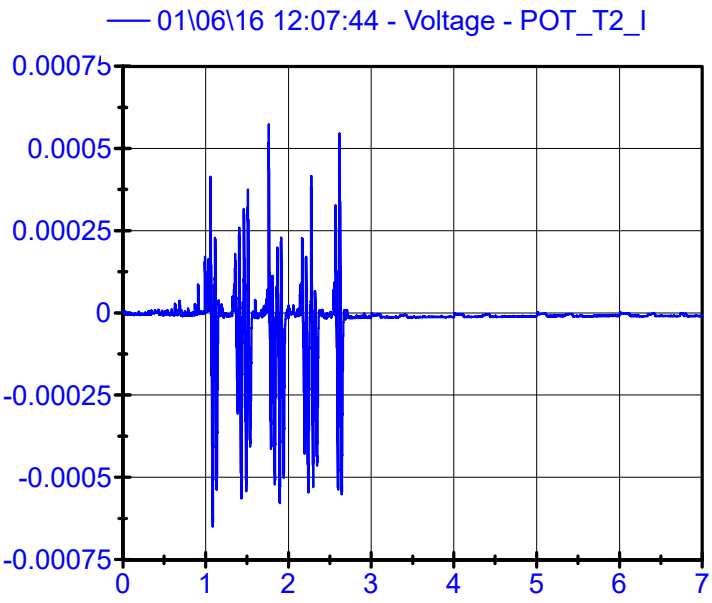

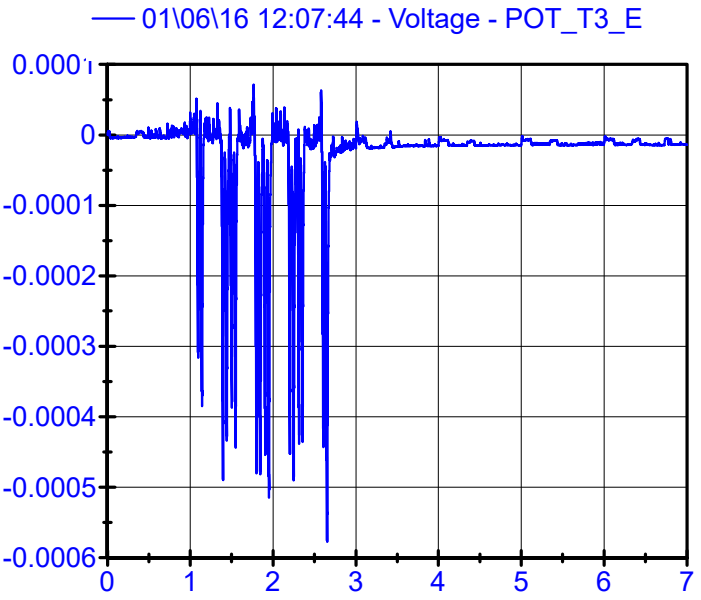

01\06\16 12:51:19

Potentiometers
LPF 80Hz

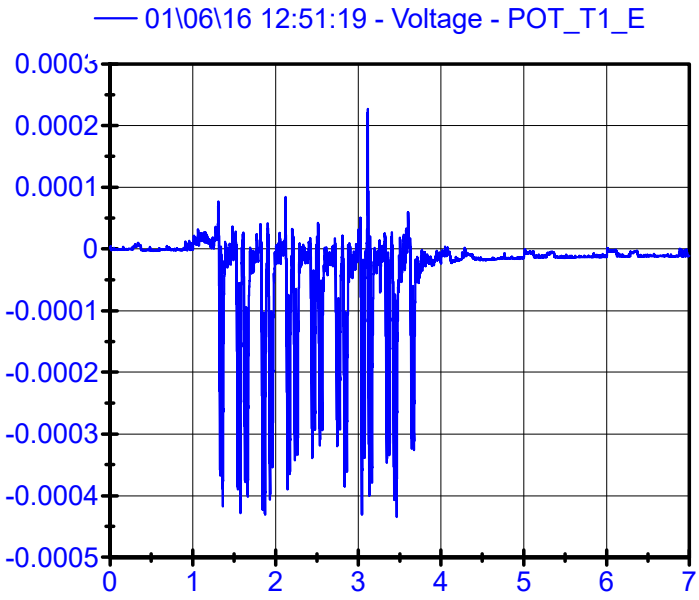

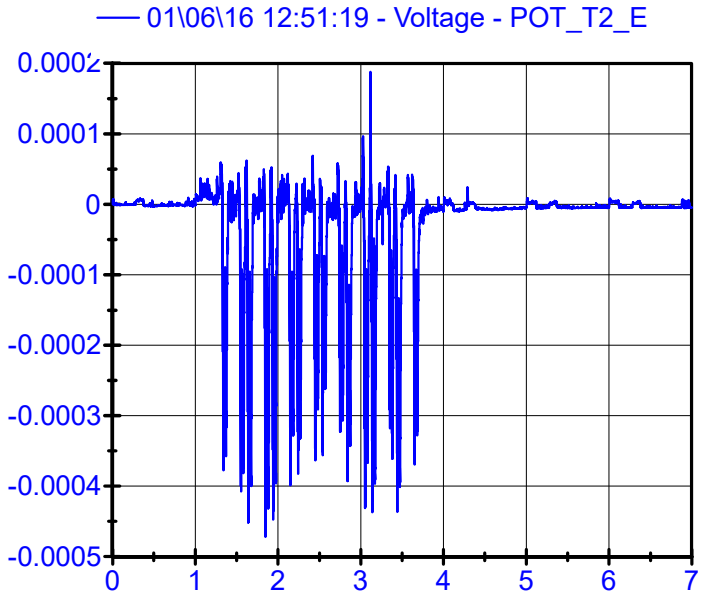

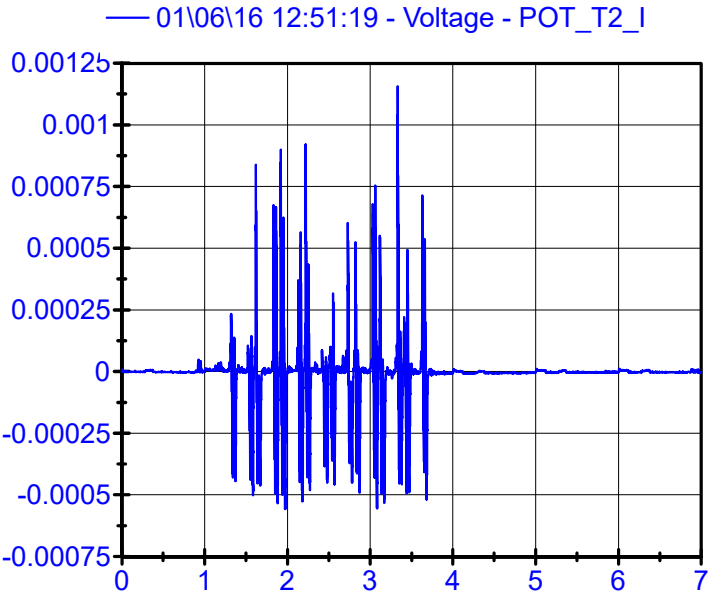

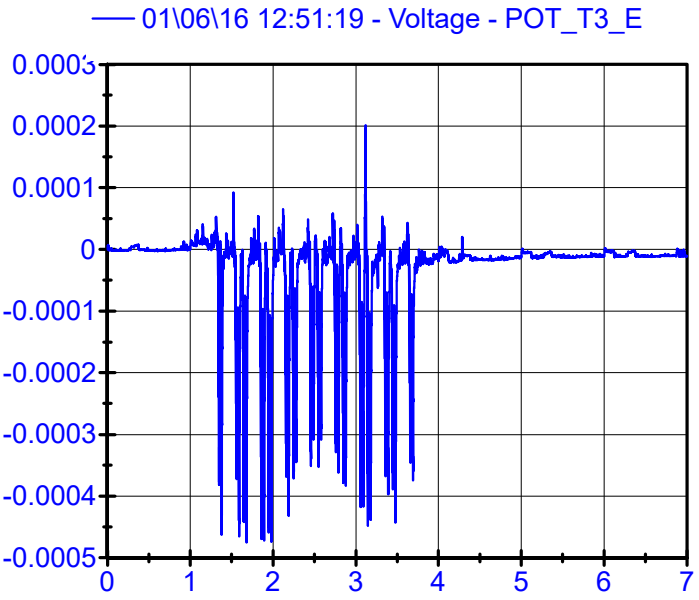

01\06\16 13:55:11

Potentiometers
LPF 80Hz

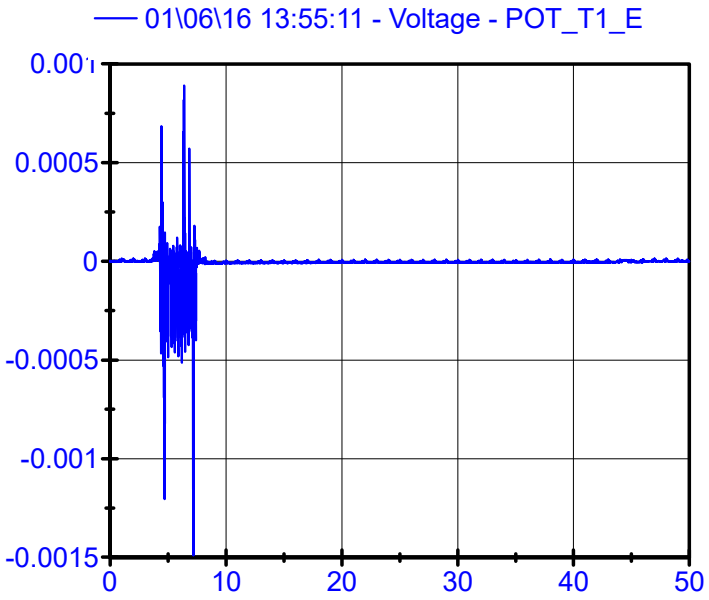

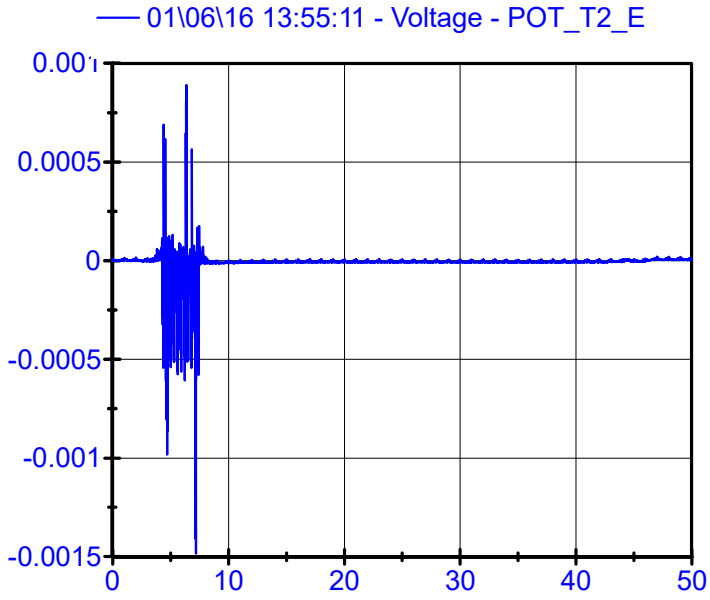

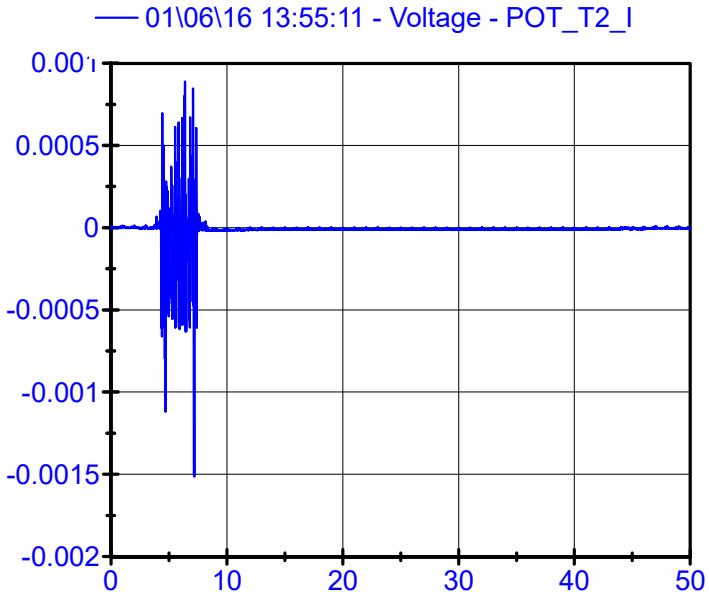

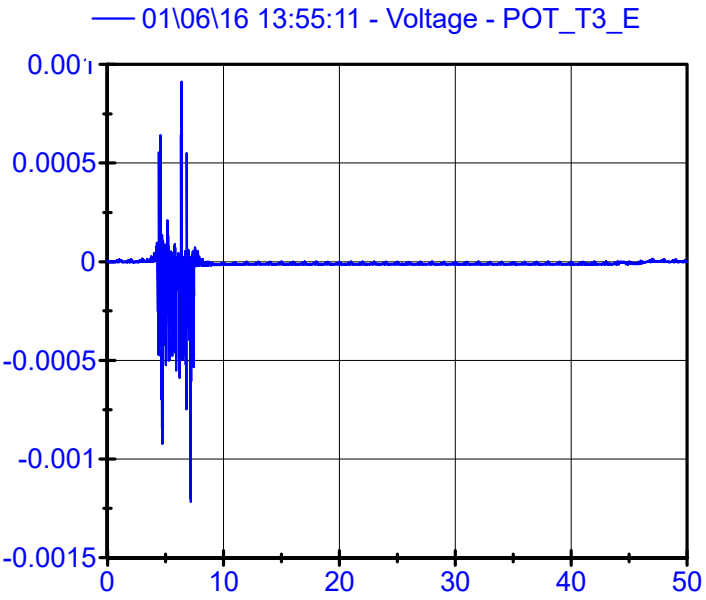

01\06\16 14:21:06

Potentiometers
LPF 80Hz

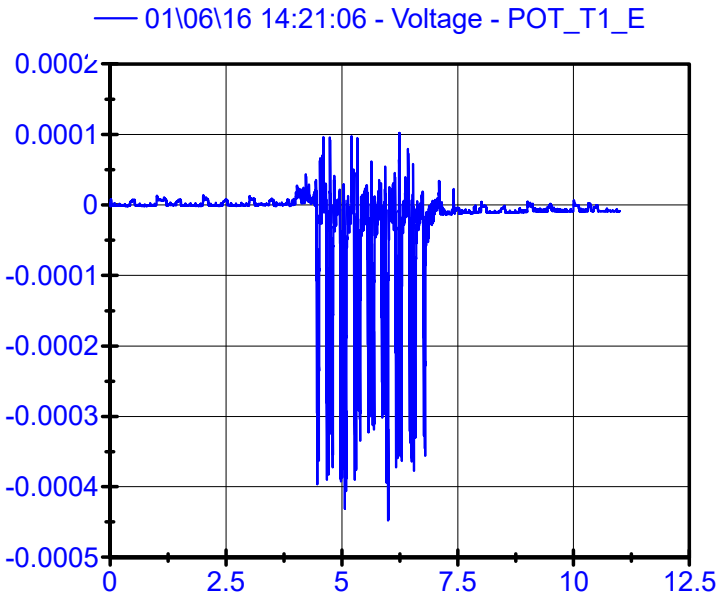

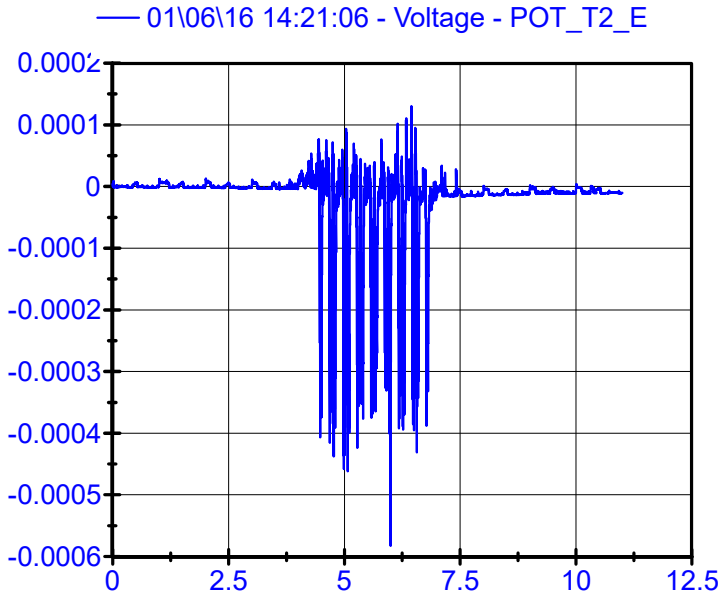

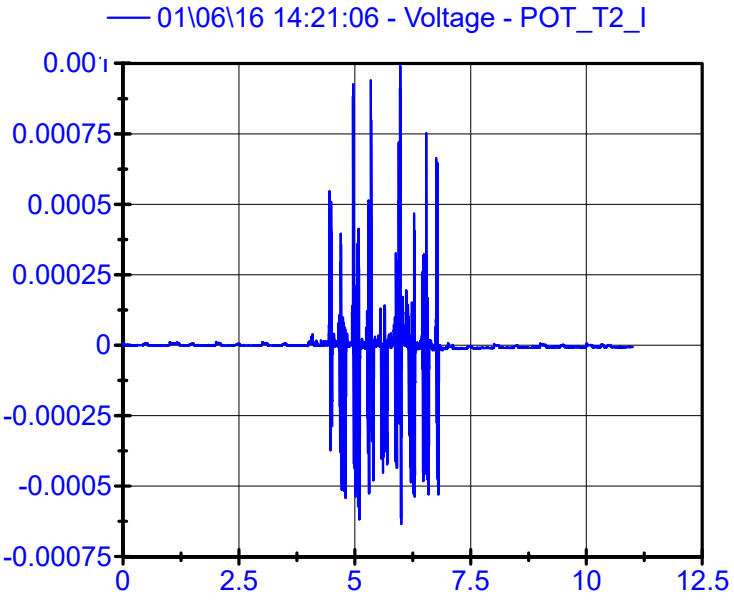

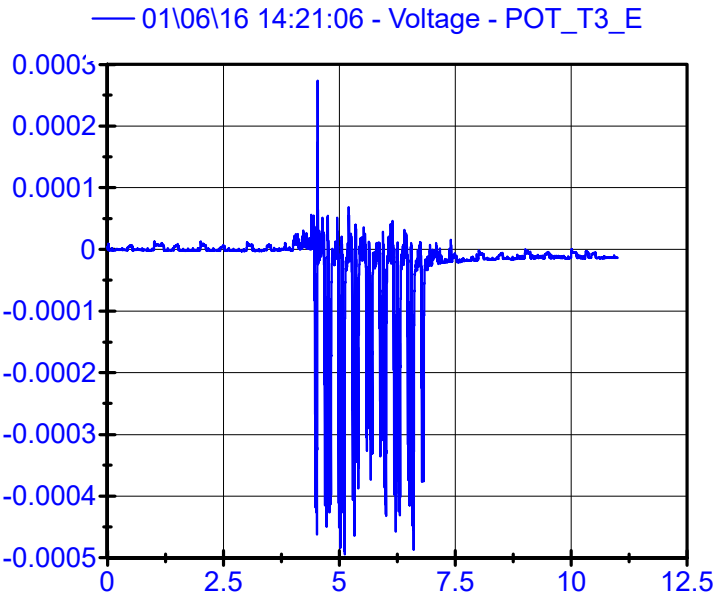

01\06\16 14:52:22

Potentiometers
LPF 80Hz

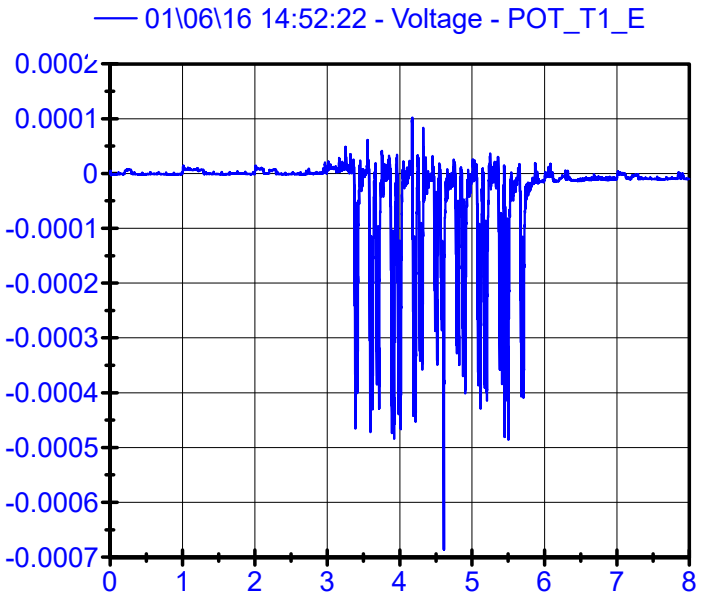

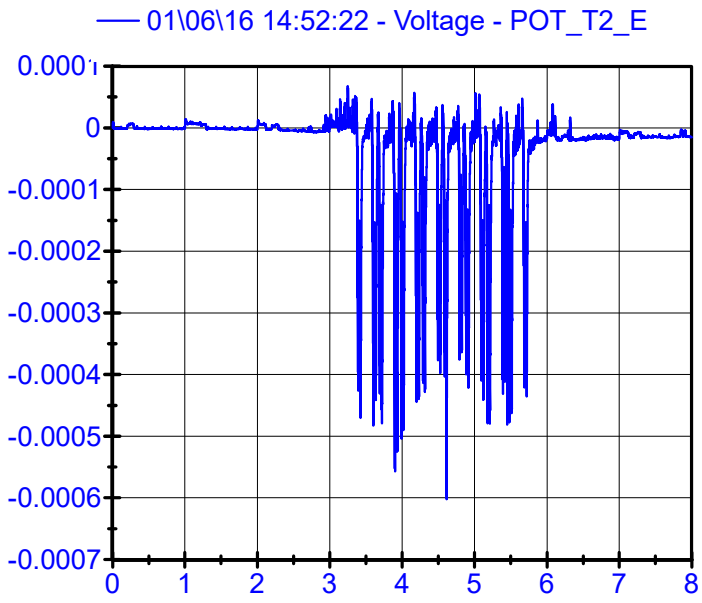

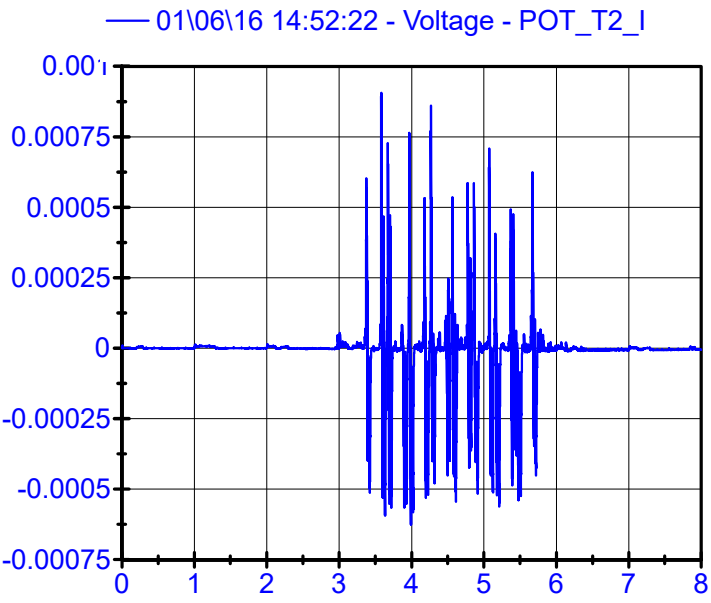

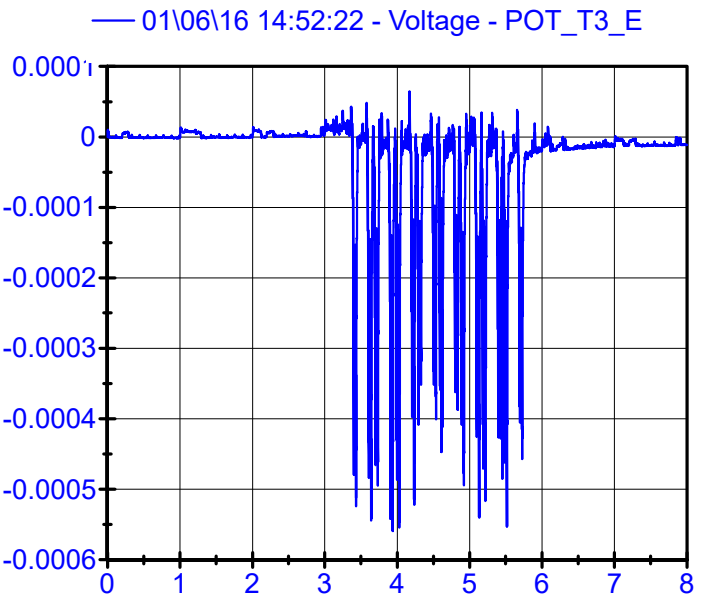

01\06\16 15:21:31

Potentiometers
LPF 80Hz

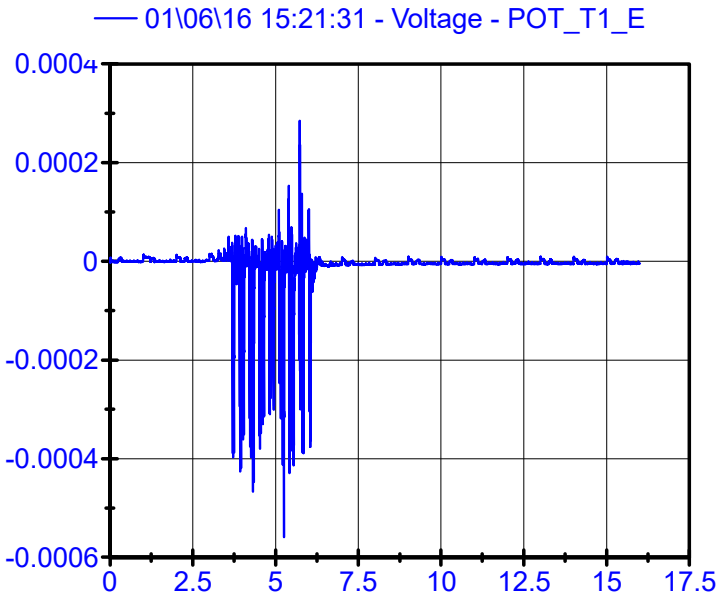

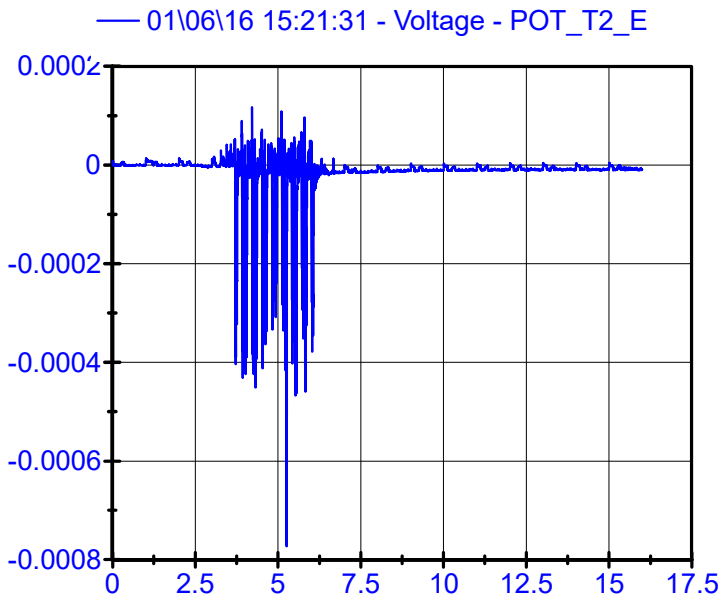

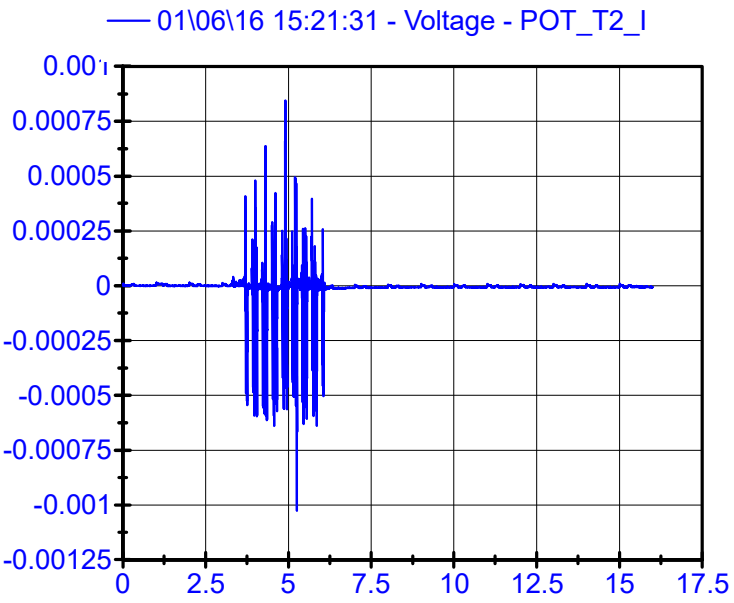

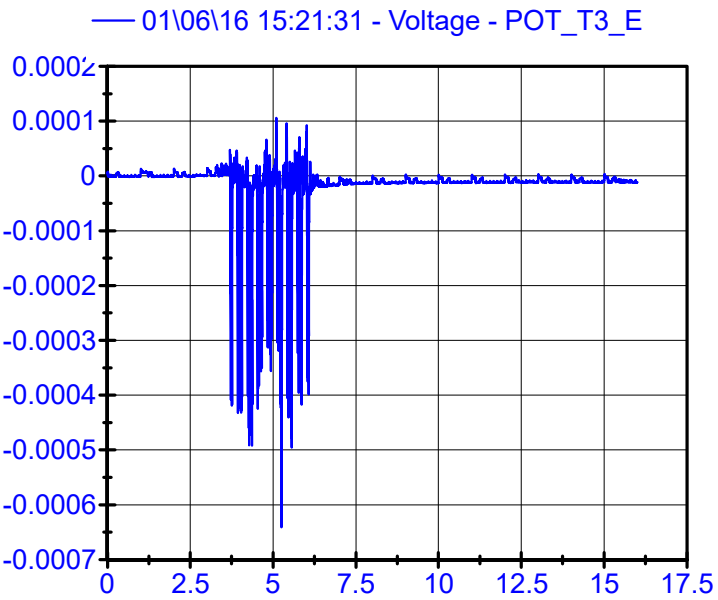

01\06\16 15:34:49

Potentiometers
LPF 80Hz

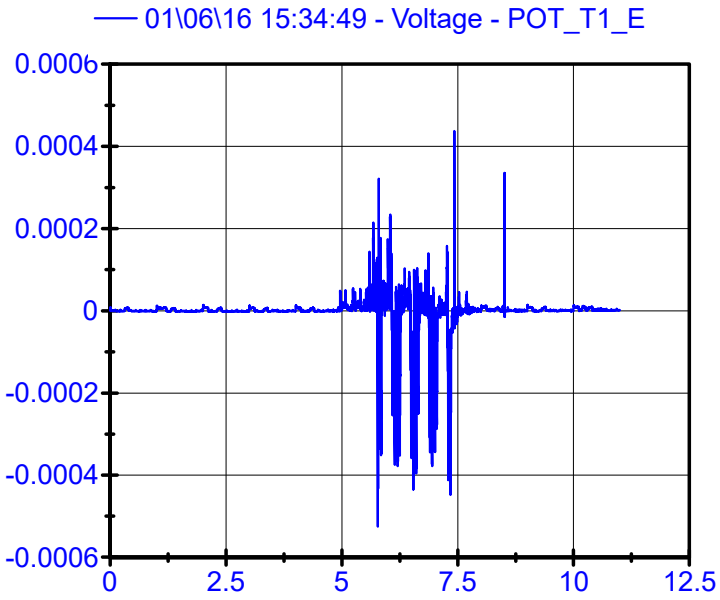

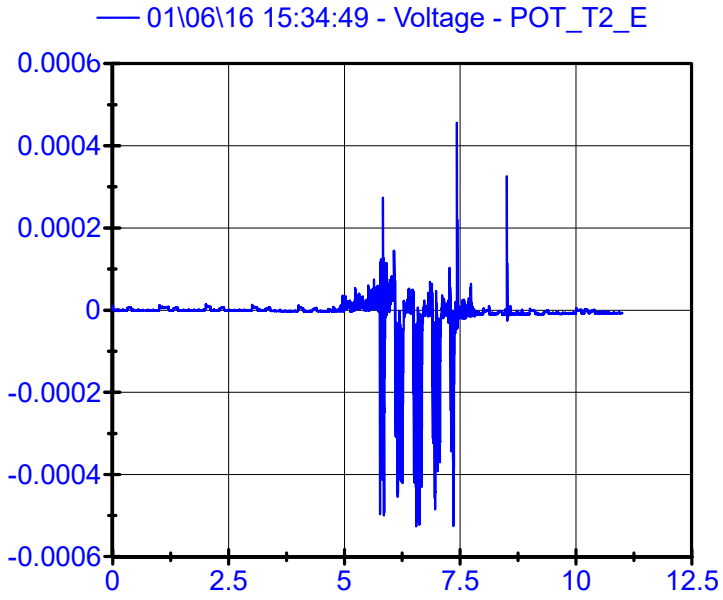

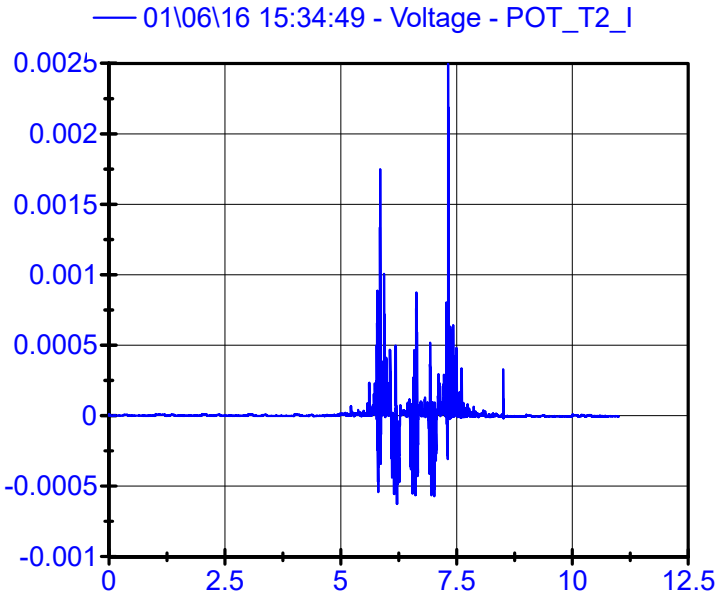

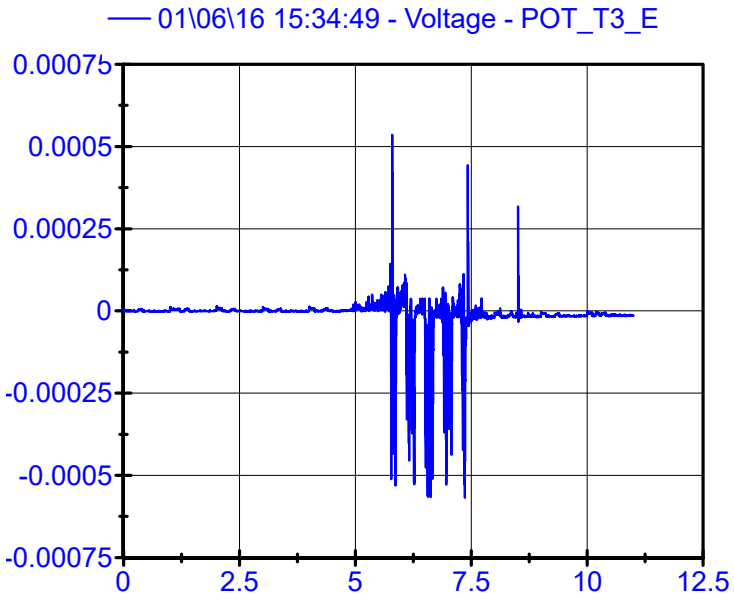

01\06\16 15:54:57

Potentiometers
LPF 80Hz

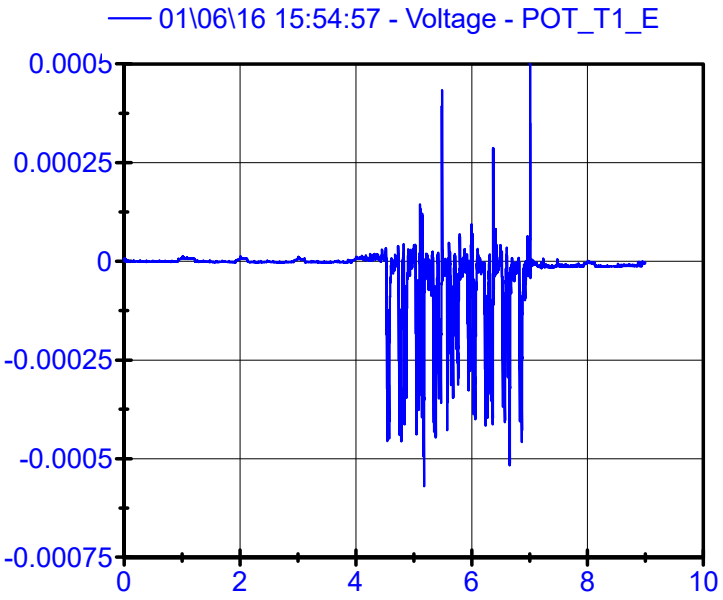

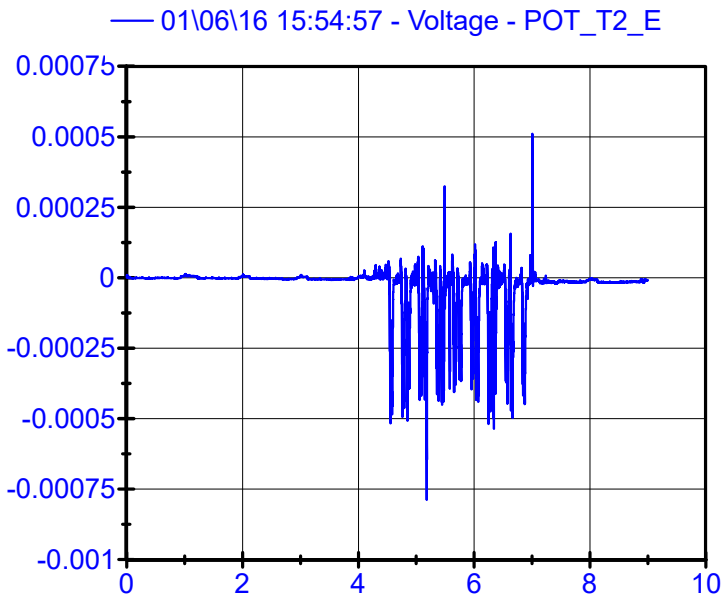

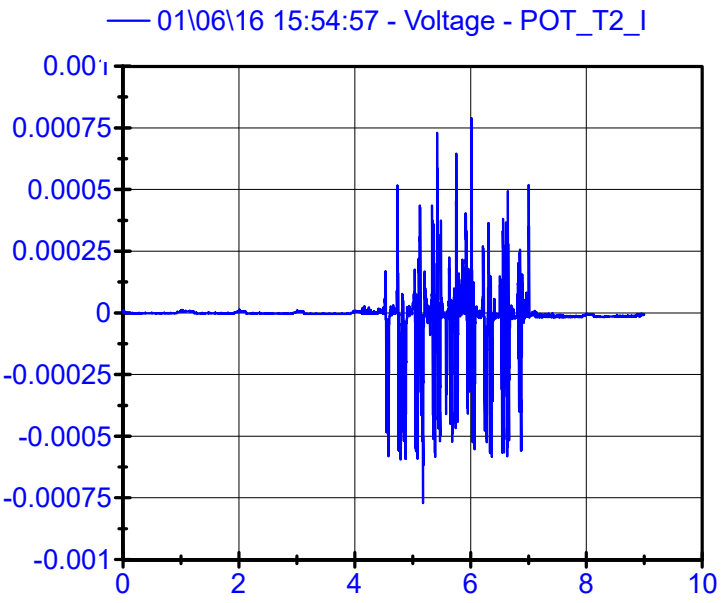

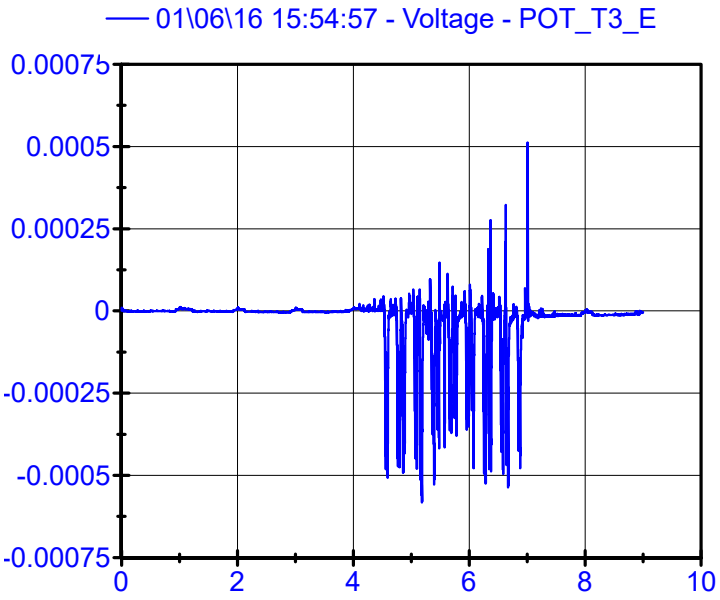

01\06\16 16:22:21

Potentiometers
LPF 80Hz

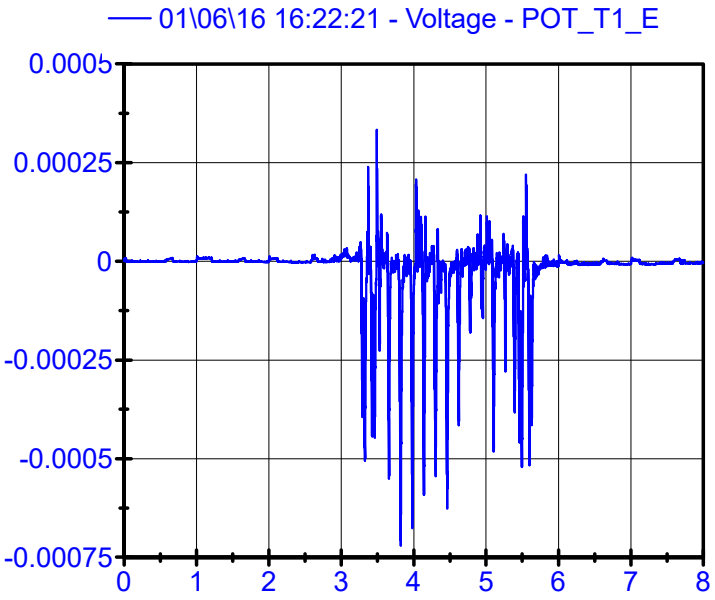

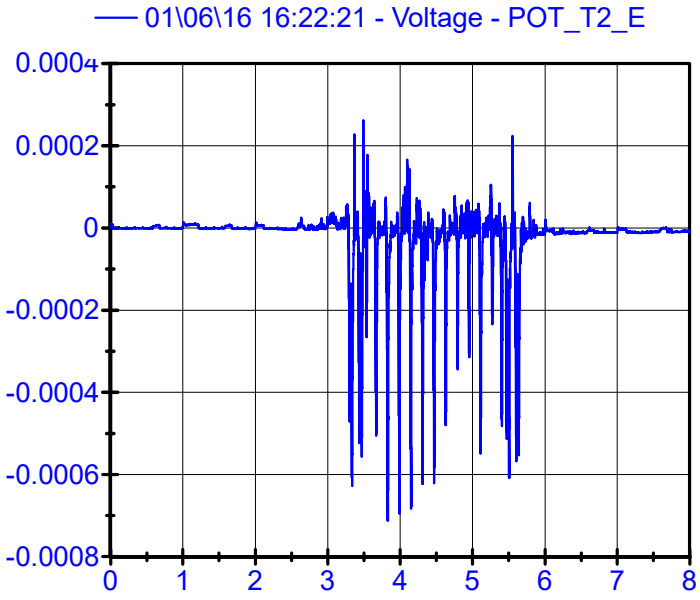

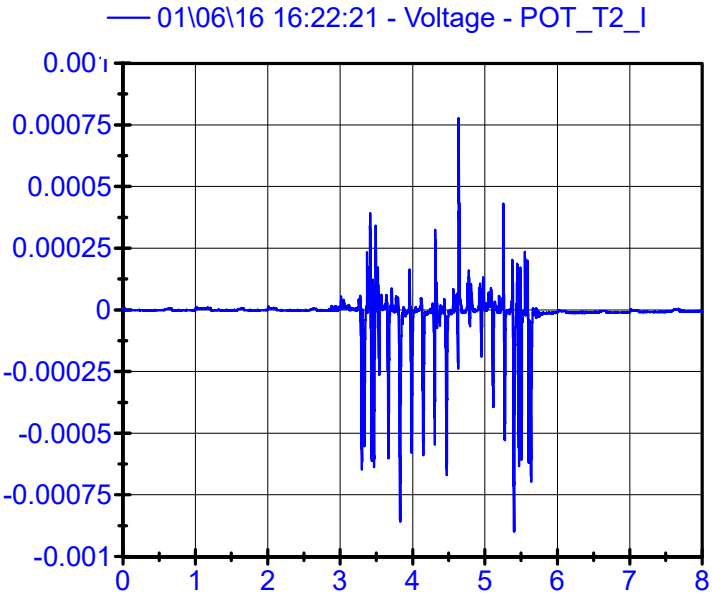

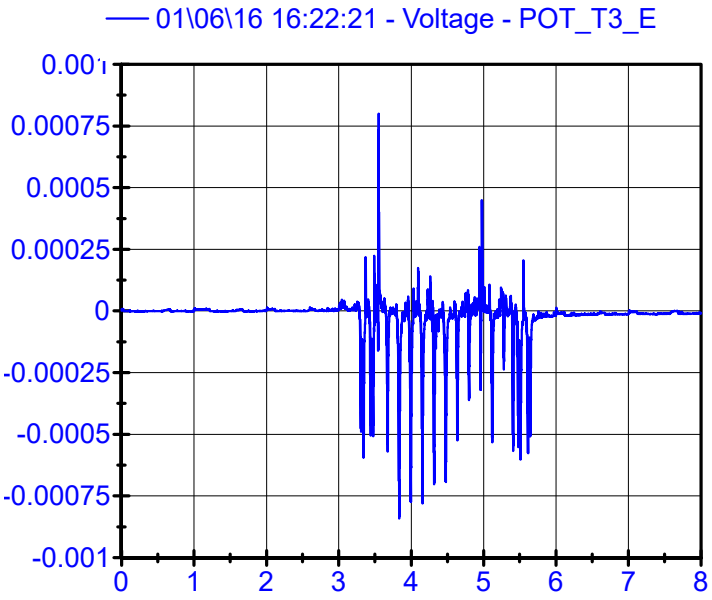

01\06\16 16:54:24

Potentiometers
LPF 80Hz

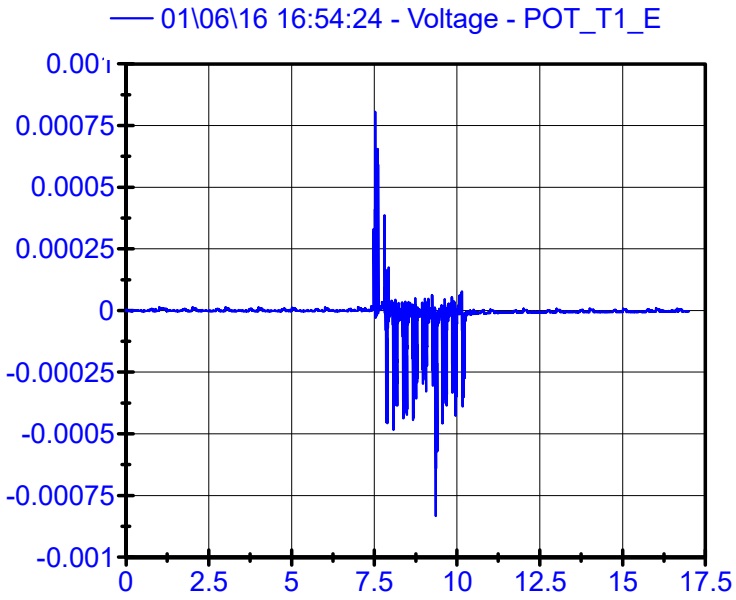

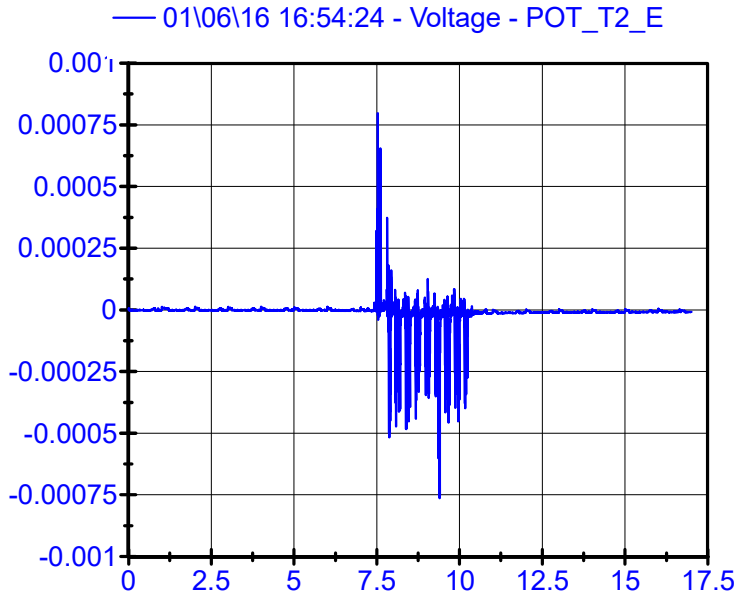

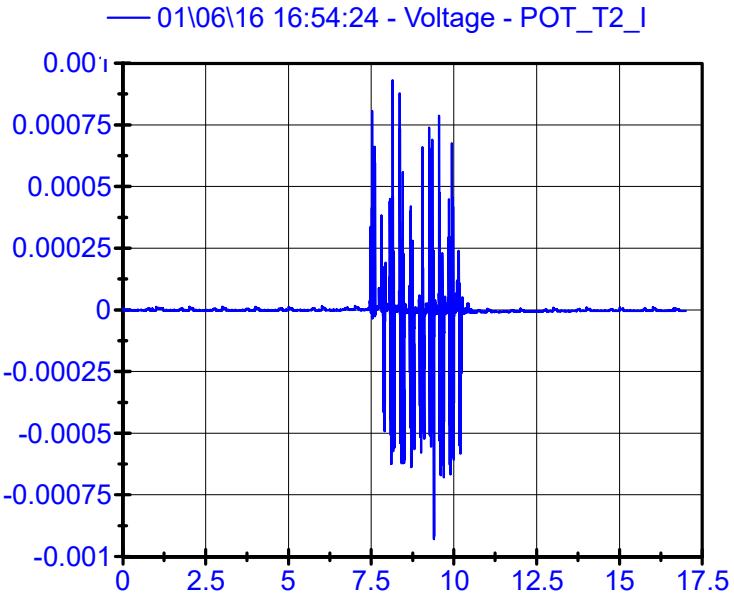

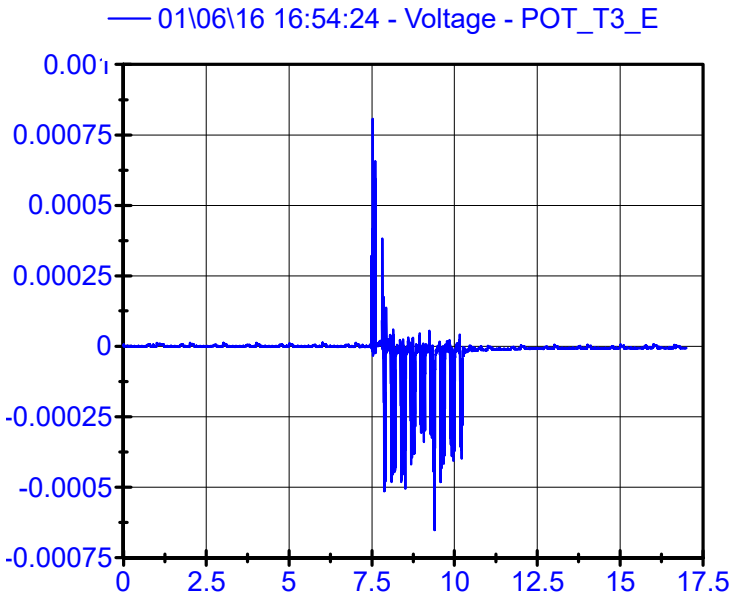

01\06\16 17:24:26

Potentiometers
LPF 80Hz

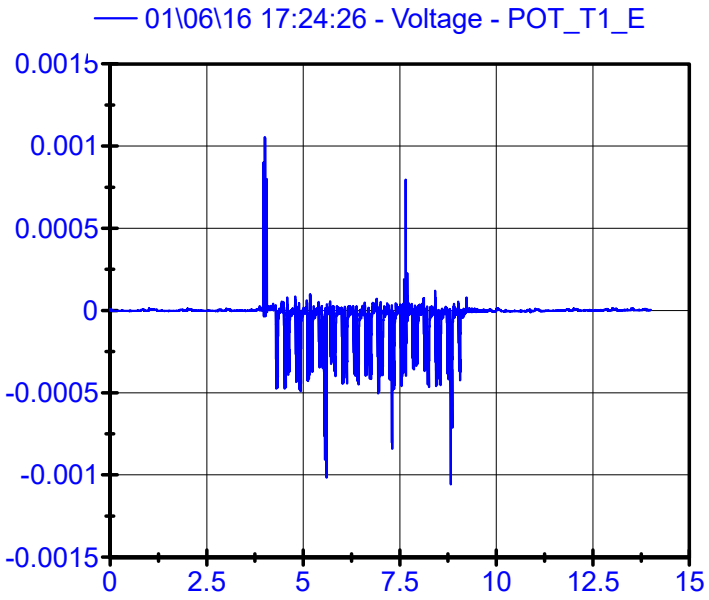

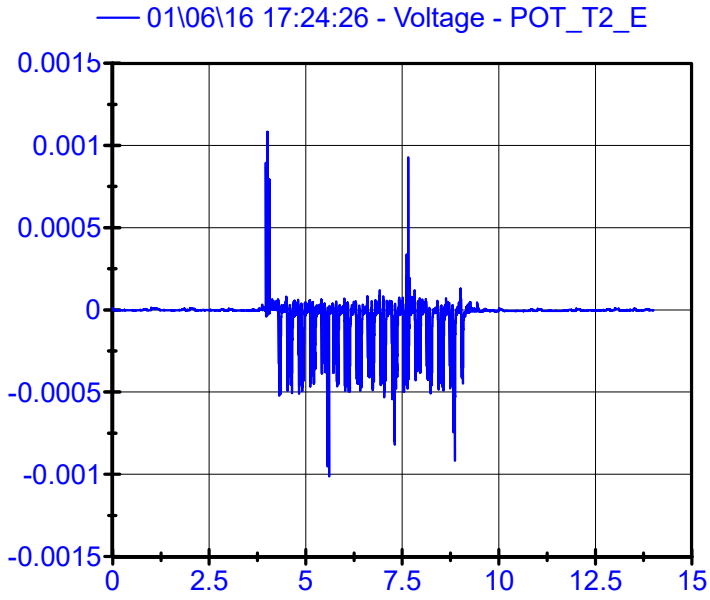

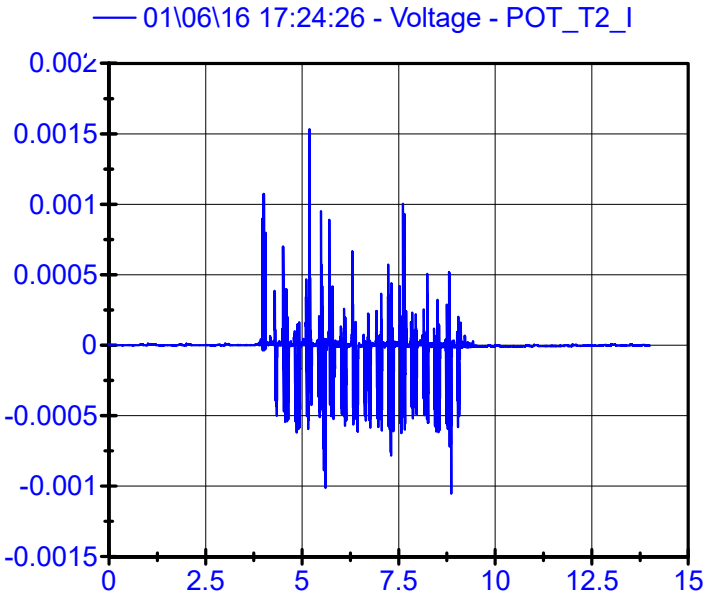

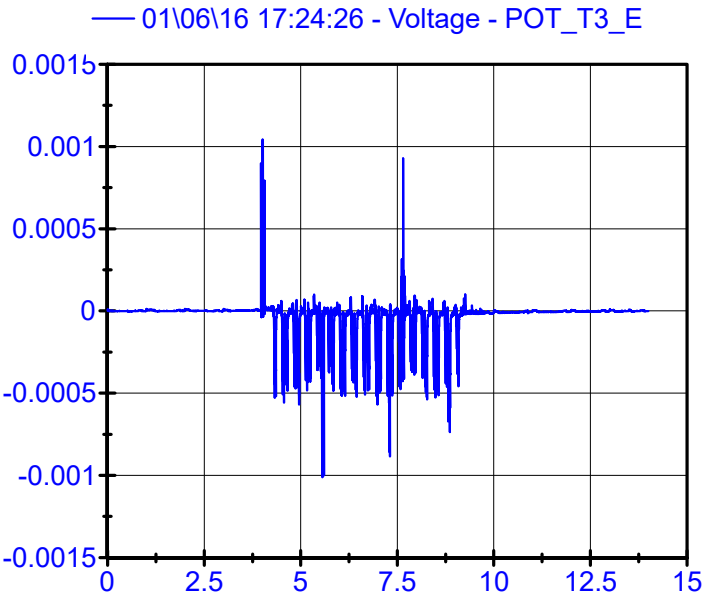

01\06\16 17:38:59

Potentiometers
LPF 80Hz

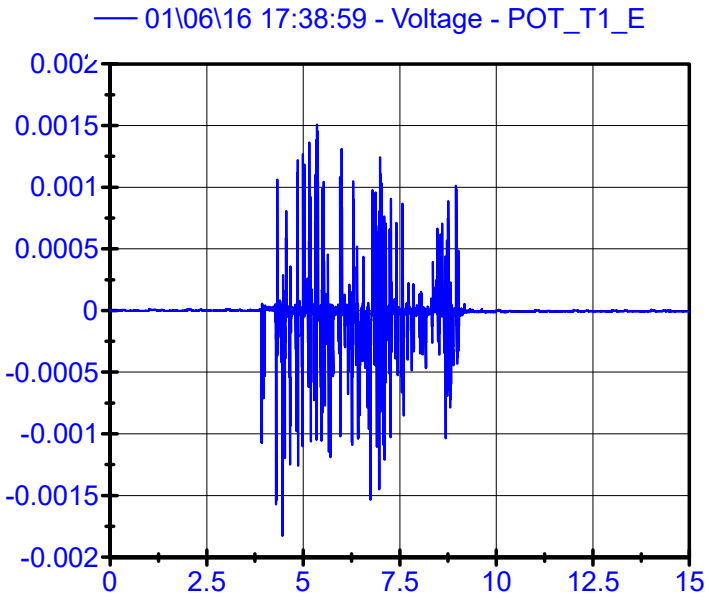

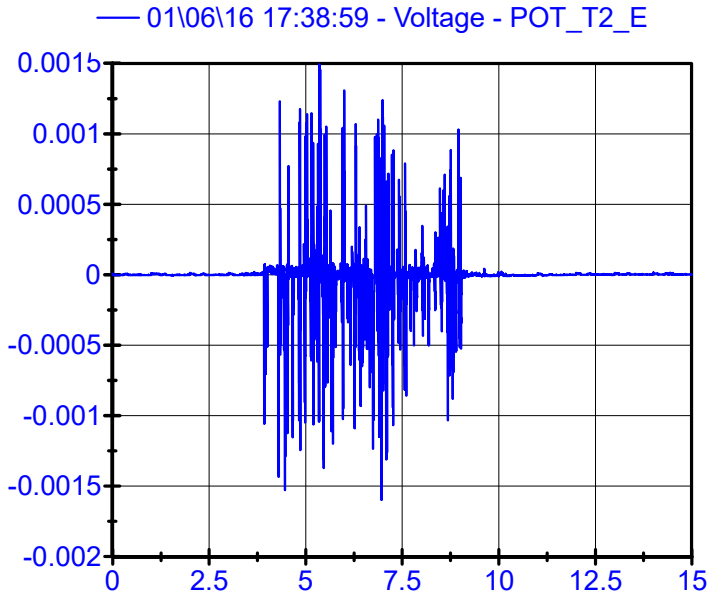

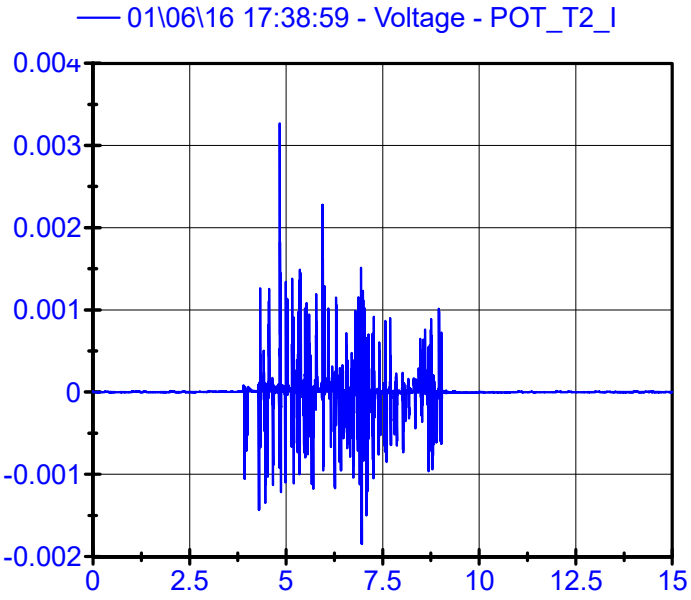

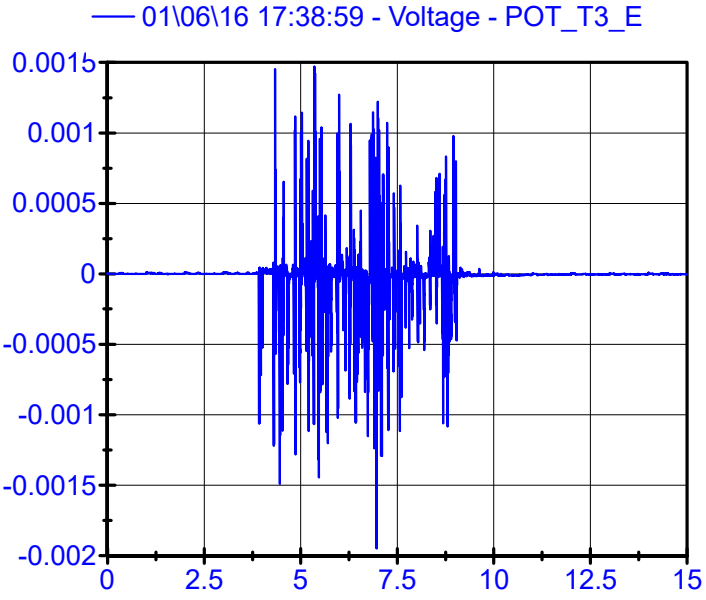

01\06\16 17:59:25

Potentiometers
LPF 80Hz

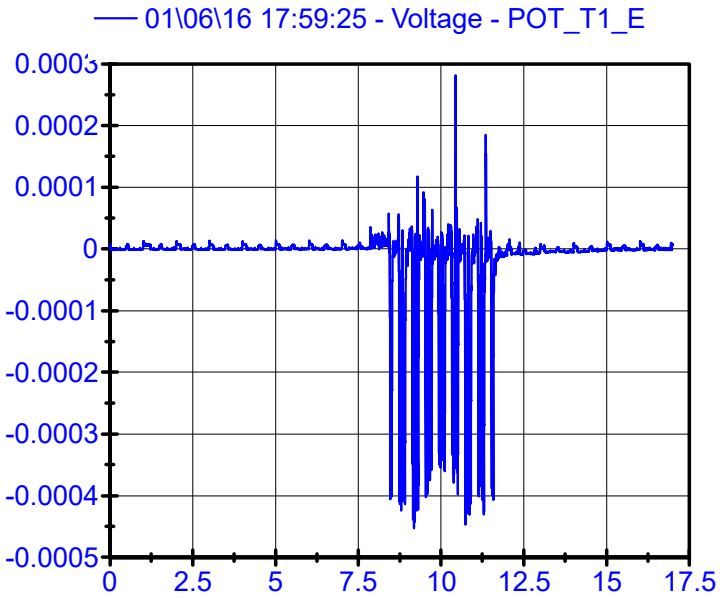

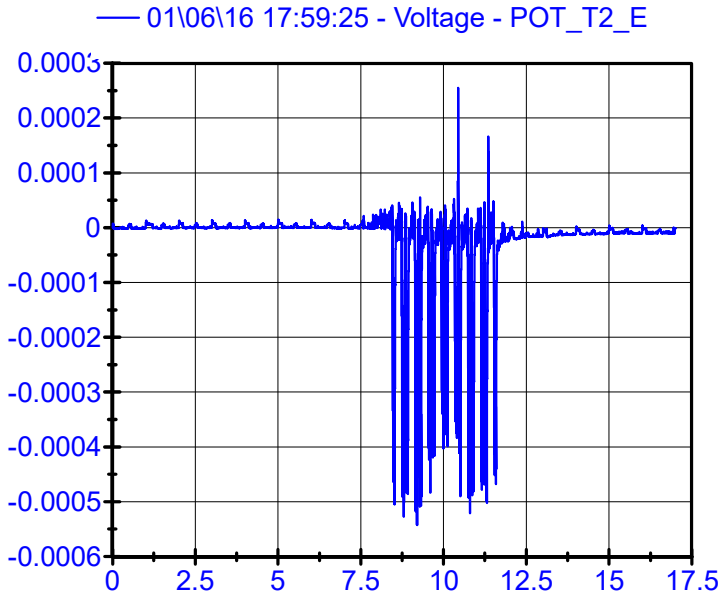

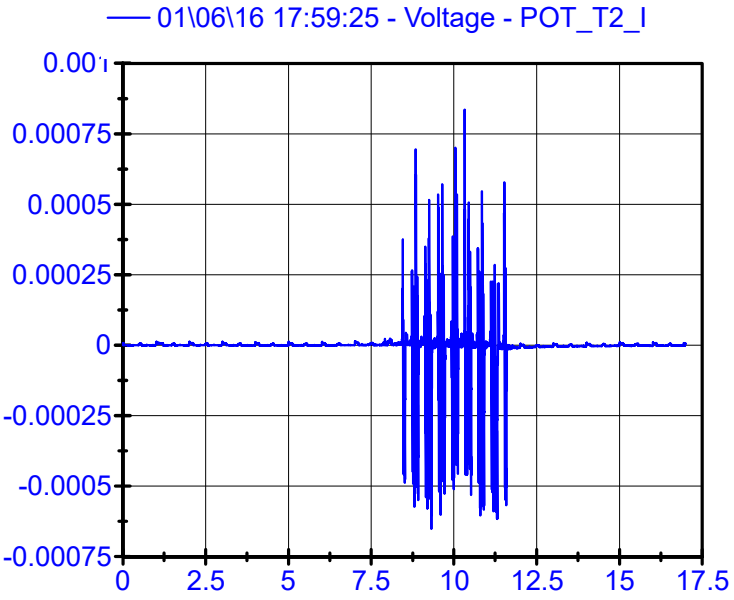

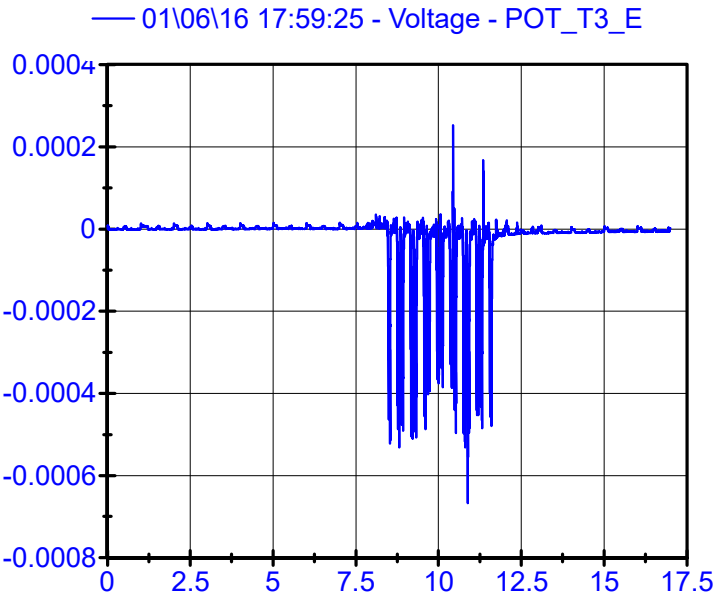

01\06\16 18:22:52

Potentiometers
LPF 80Hz

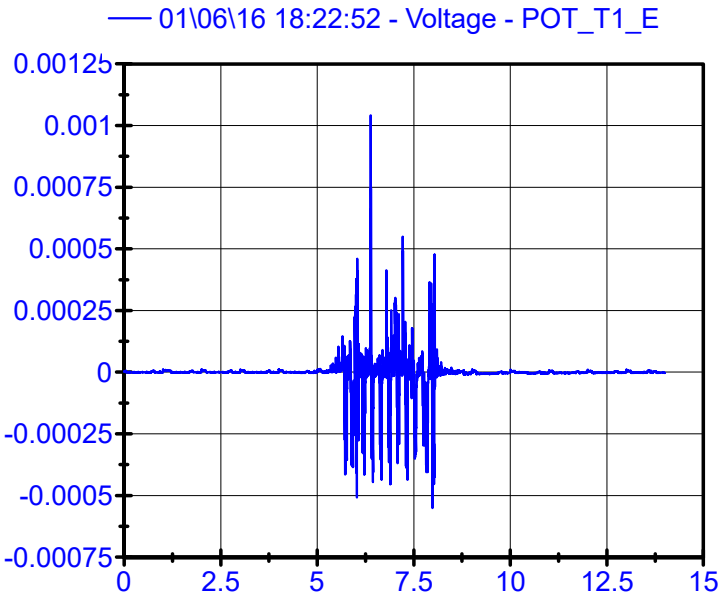

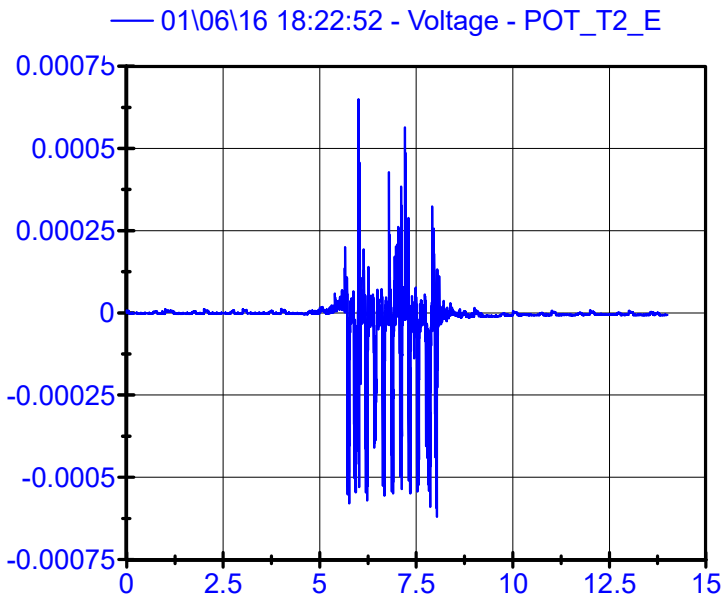

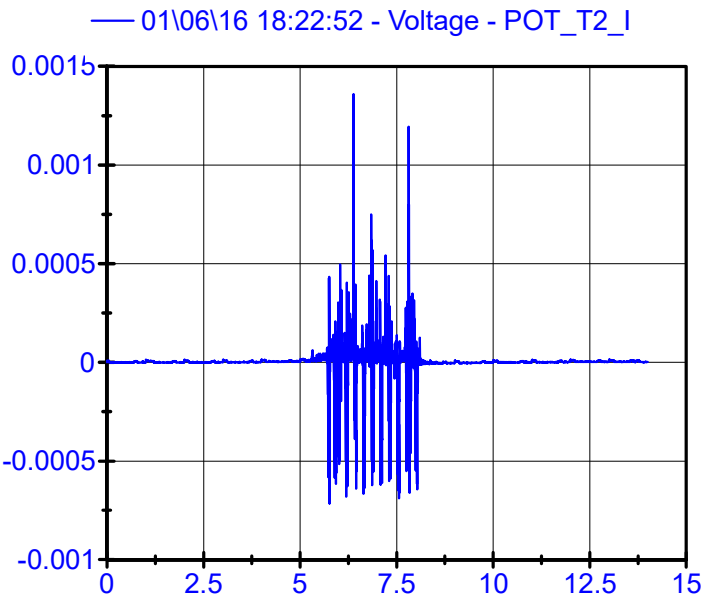

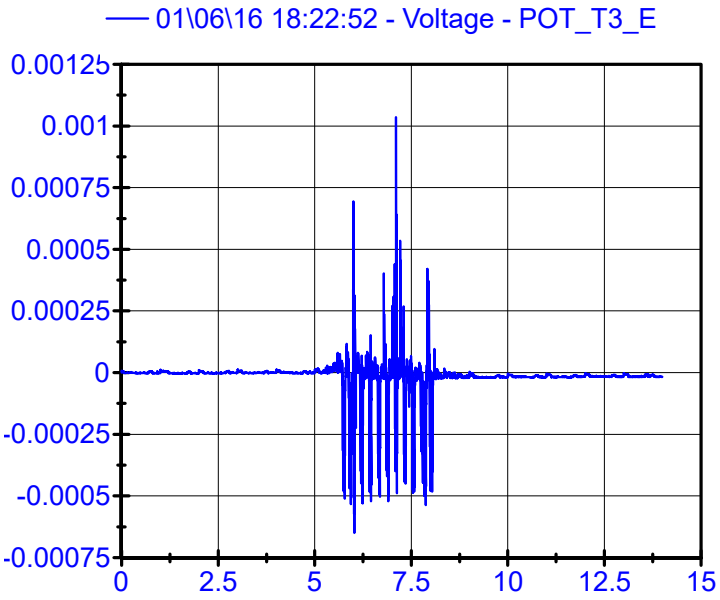

01\06\16 18:59:06

Potentiometers
LPF 80Hz

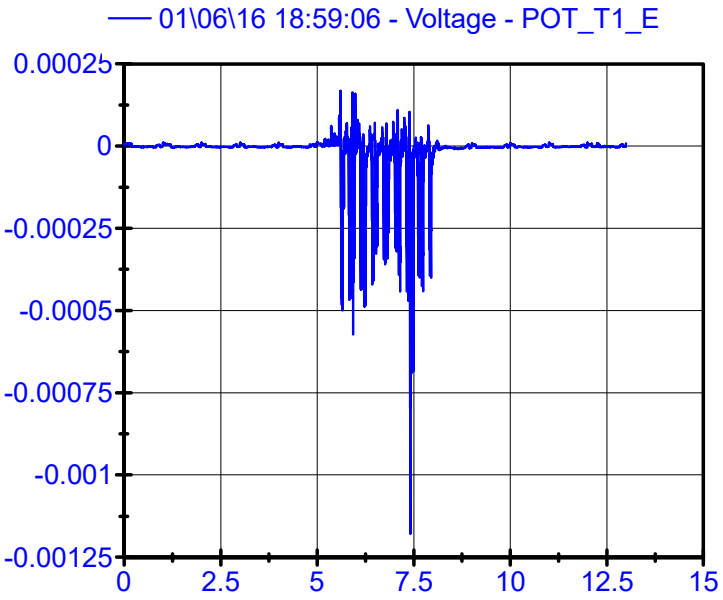

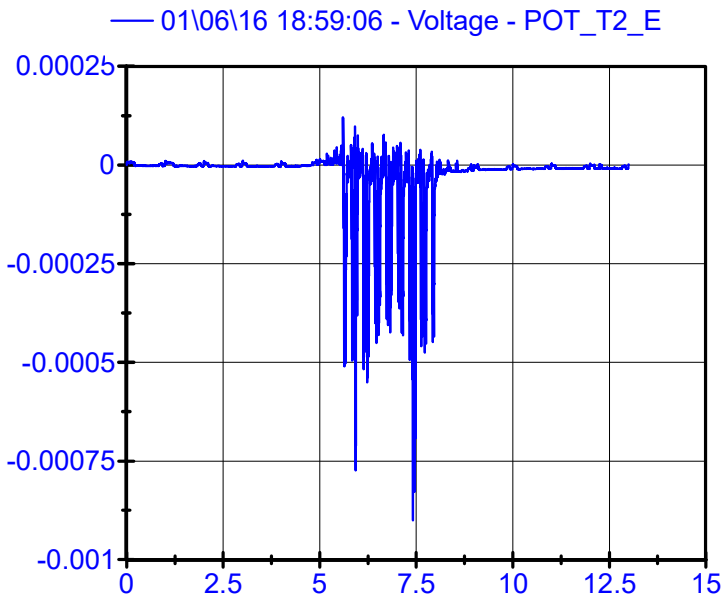

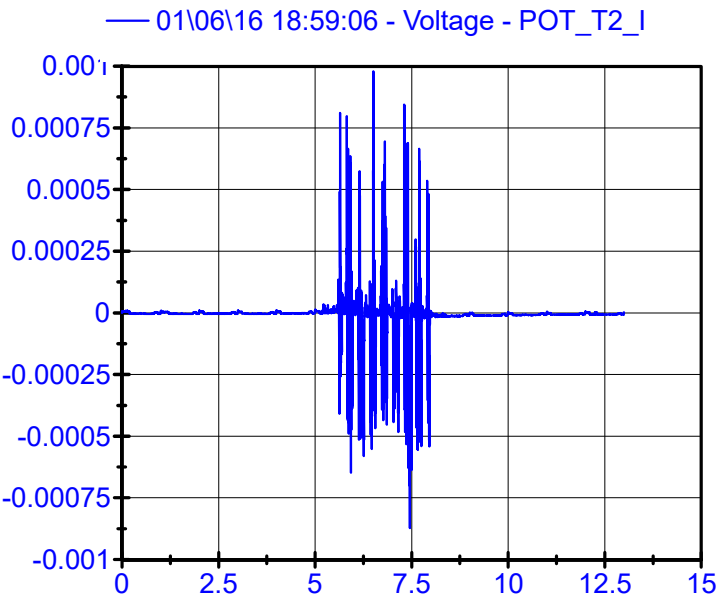

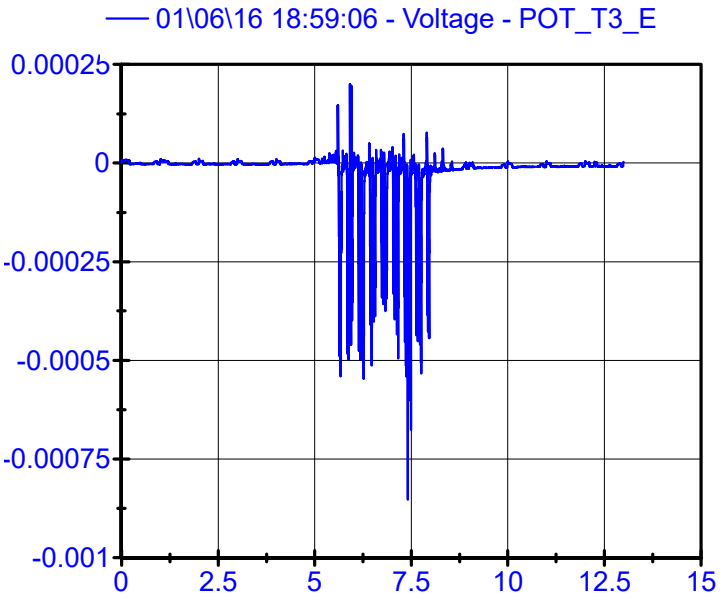

01\06\16 19:21:34

Potentiometers
LPF 80Hz

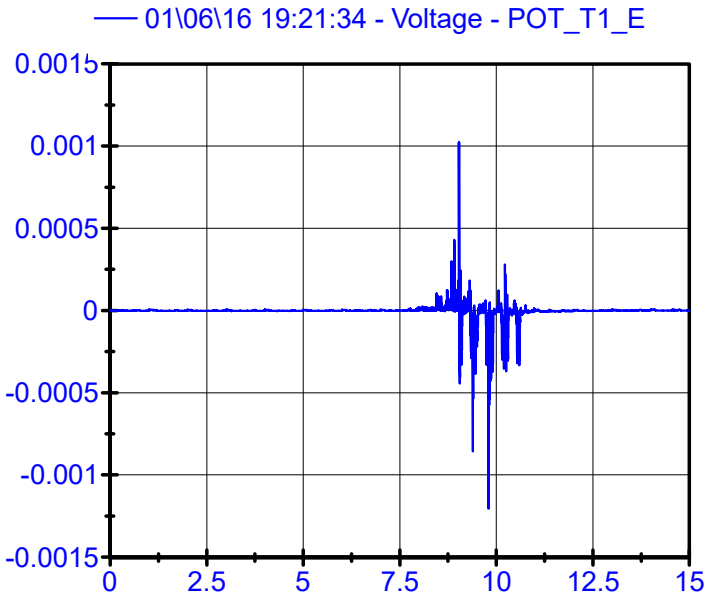

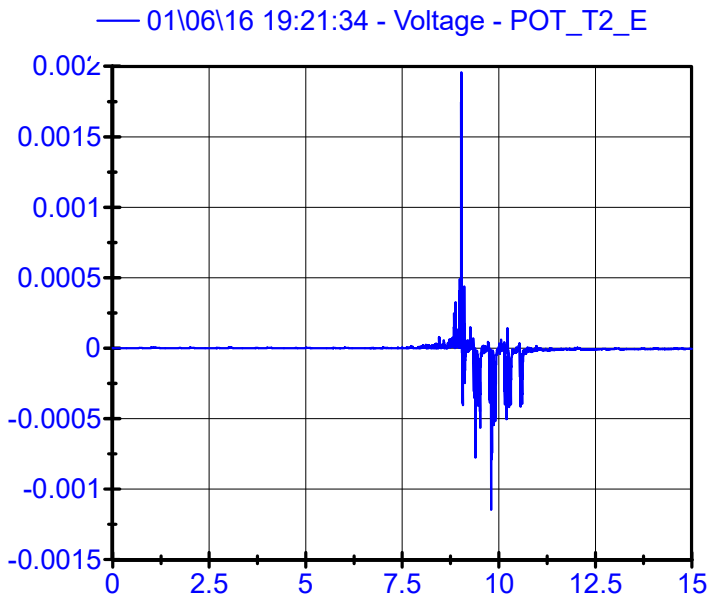

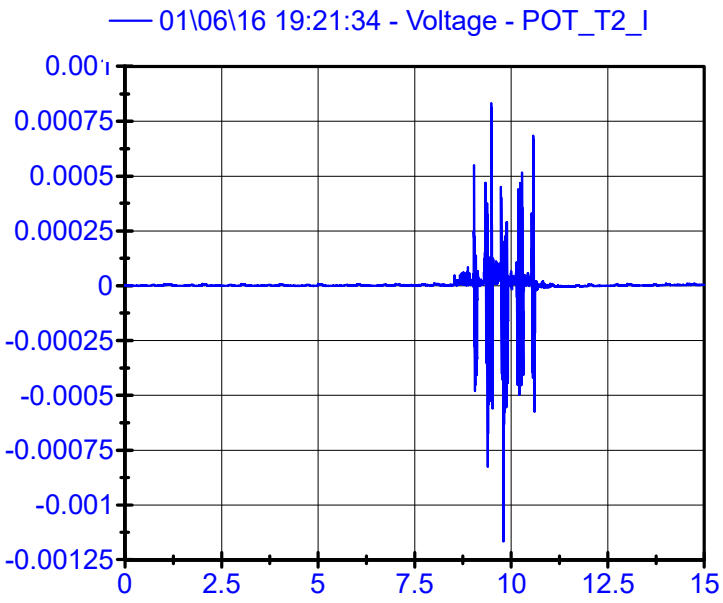

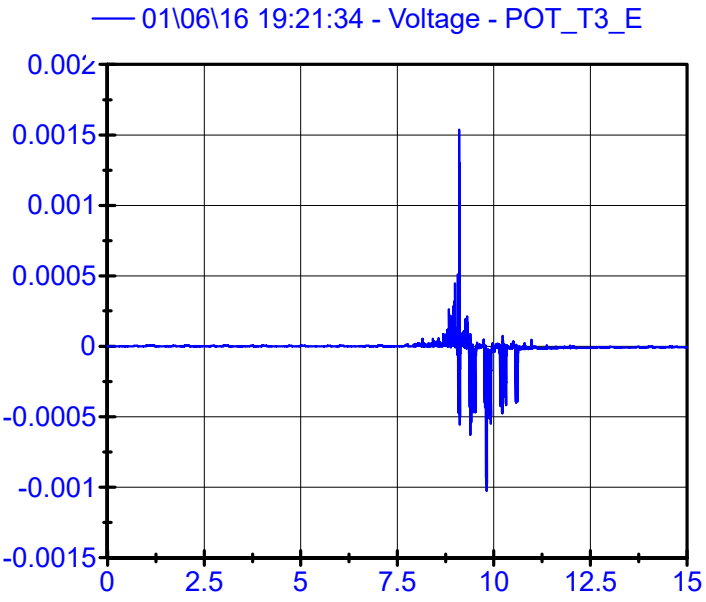

01\06\16 19:23:31

Potentiometers
LPF 80Hz

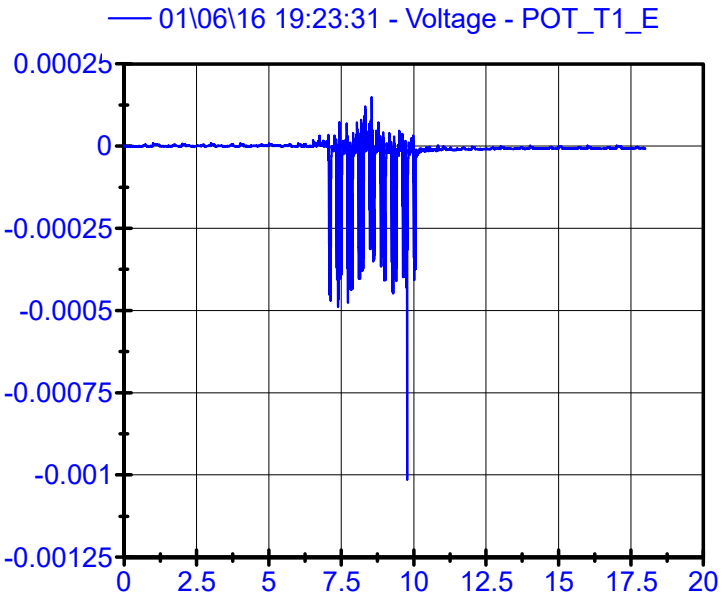

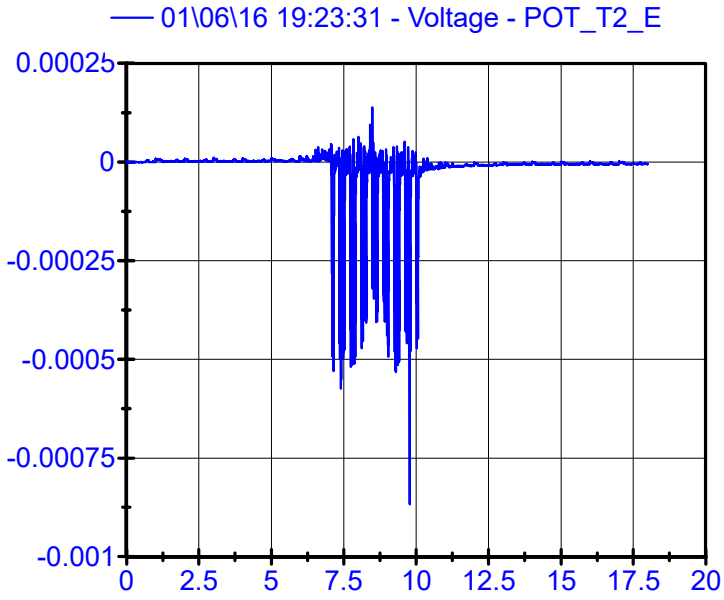

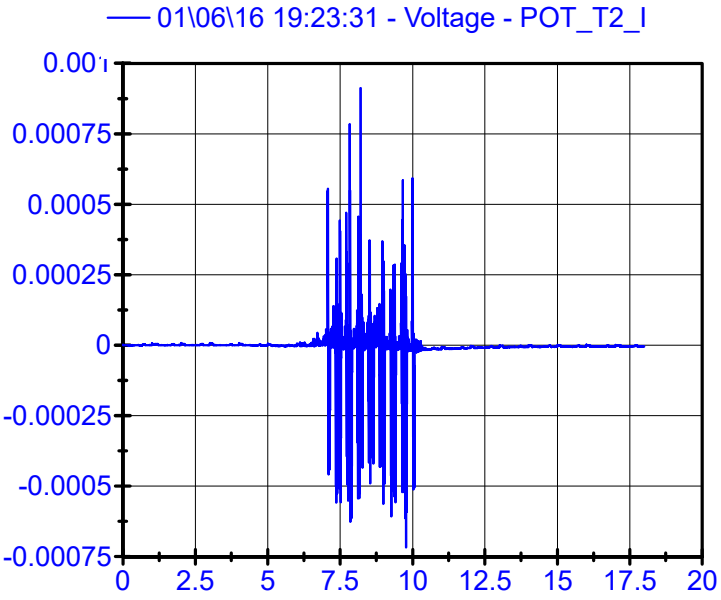

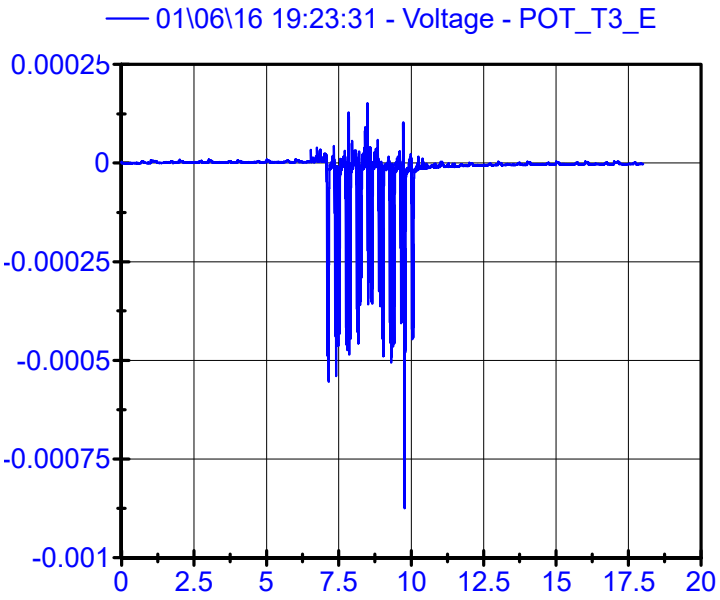

01\06\16 19:32:45

Potentiometers
LPF 80Hz

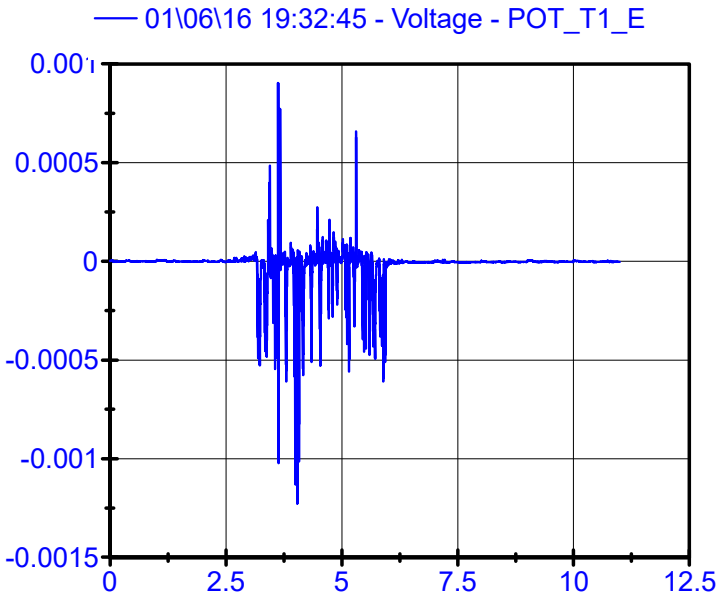

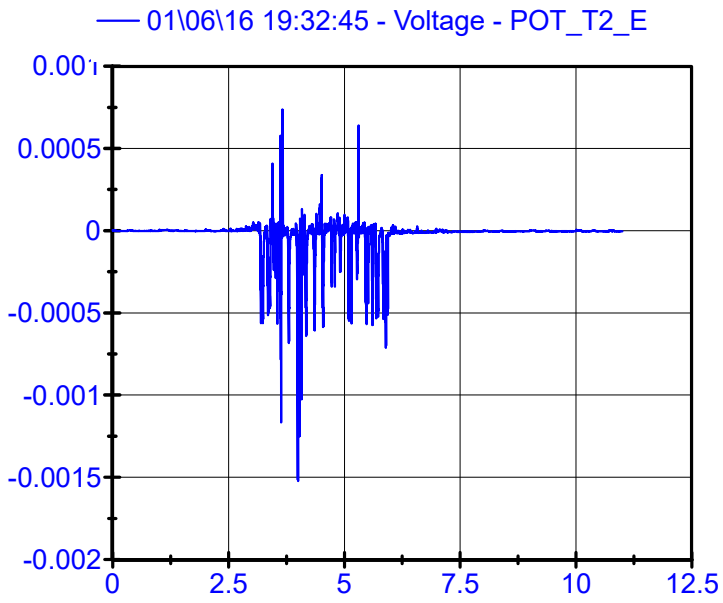

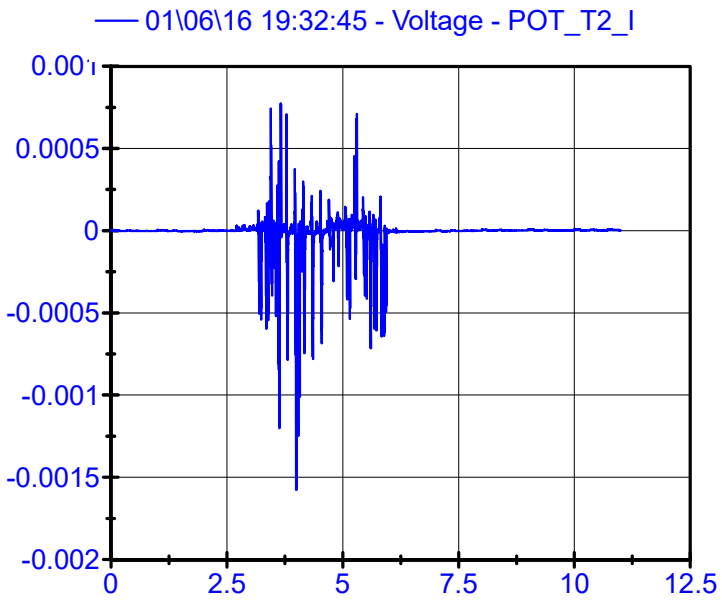

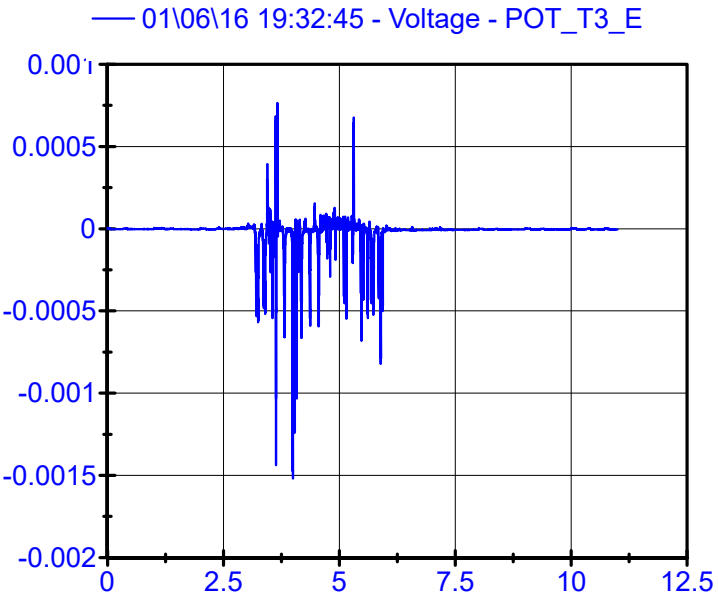

01\06\16 19:53:03

Potentiometers
LPF 80Hz

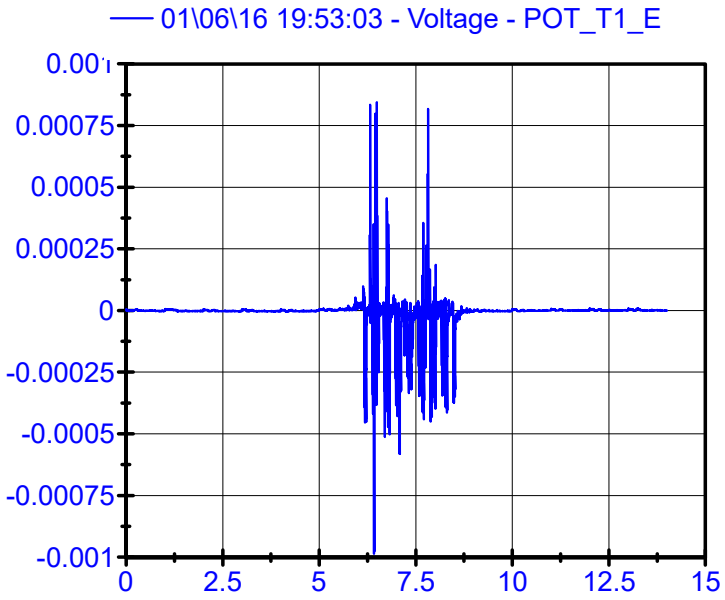

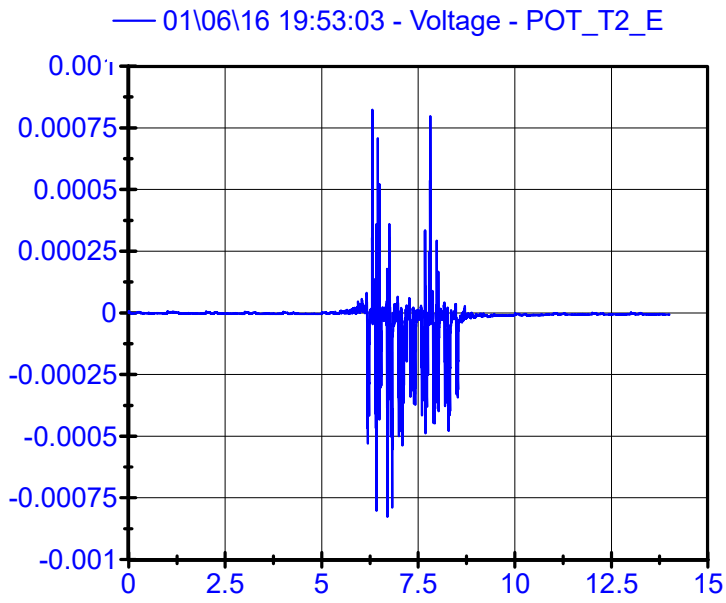

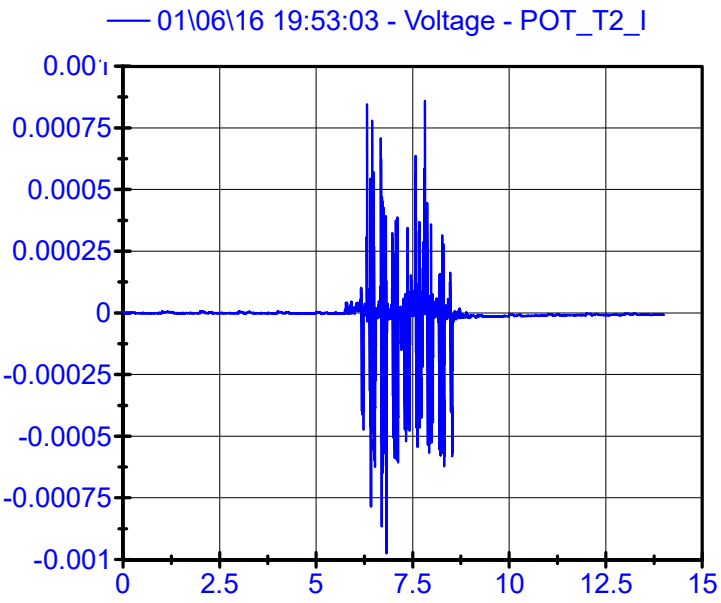

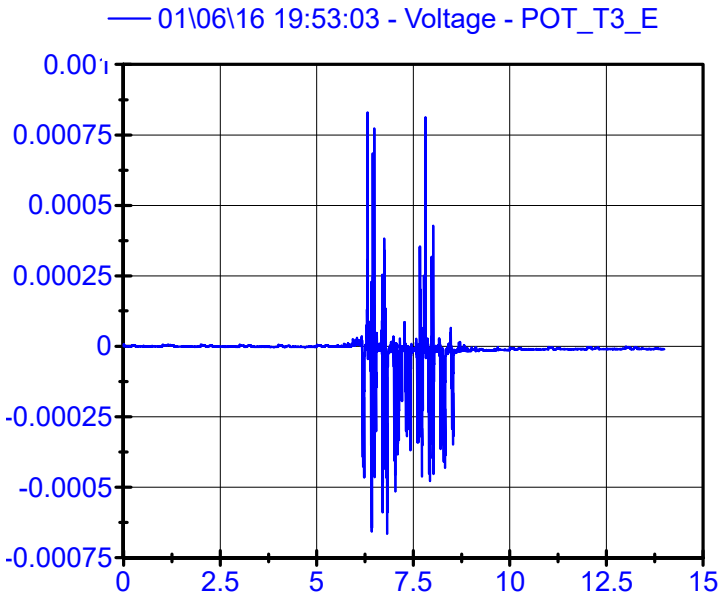

01\06\16 19:59:42

Potentiometers
LPF 80Hz

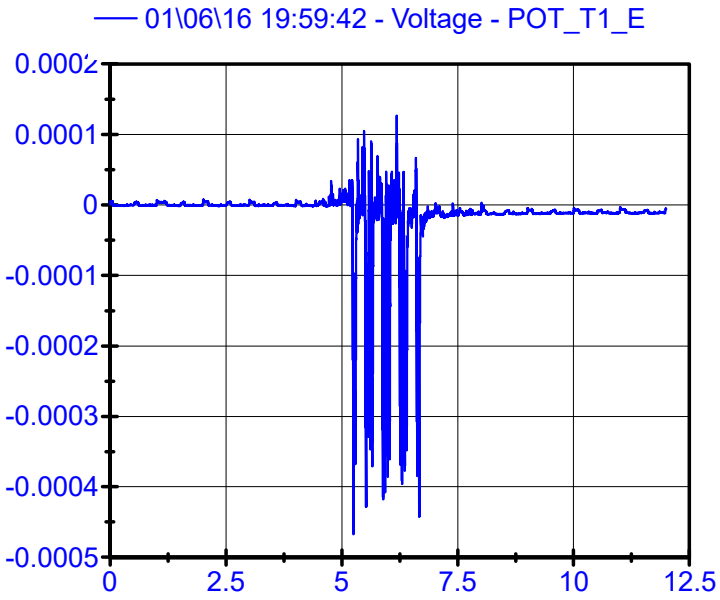

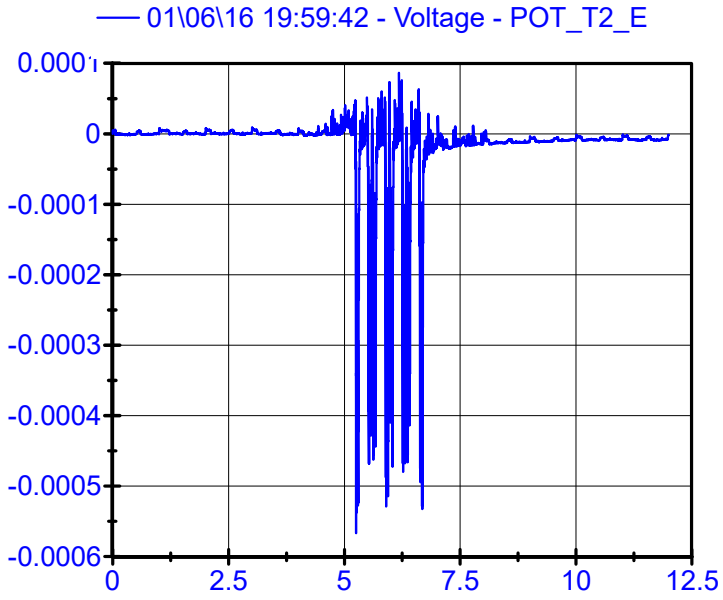

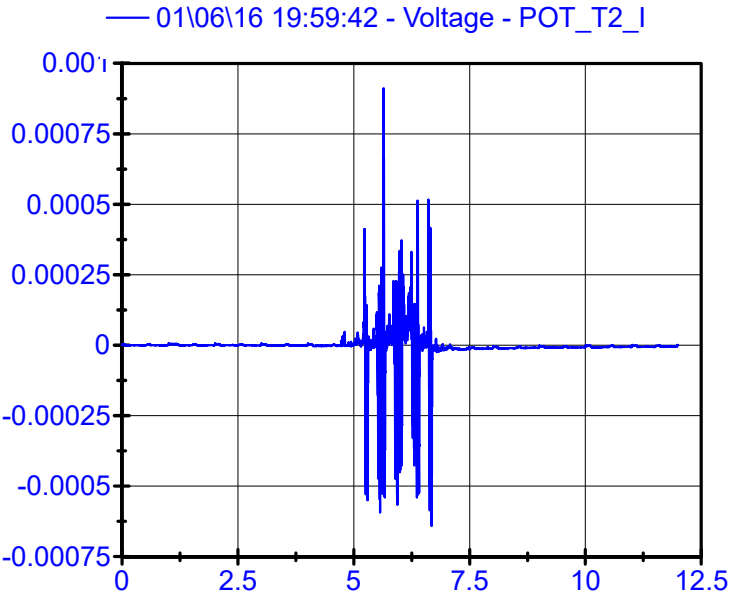

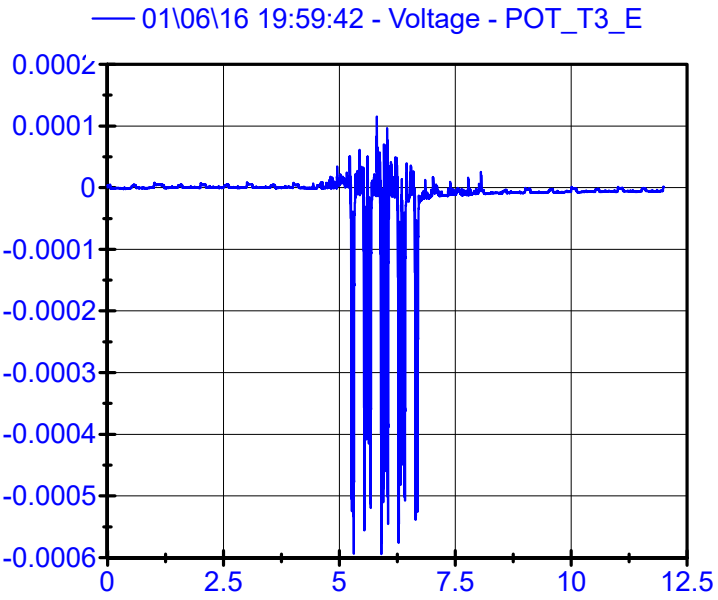

01\06\16 20:21:57

Potentiometers
LPF 80Hz

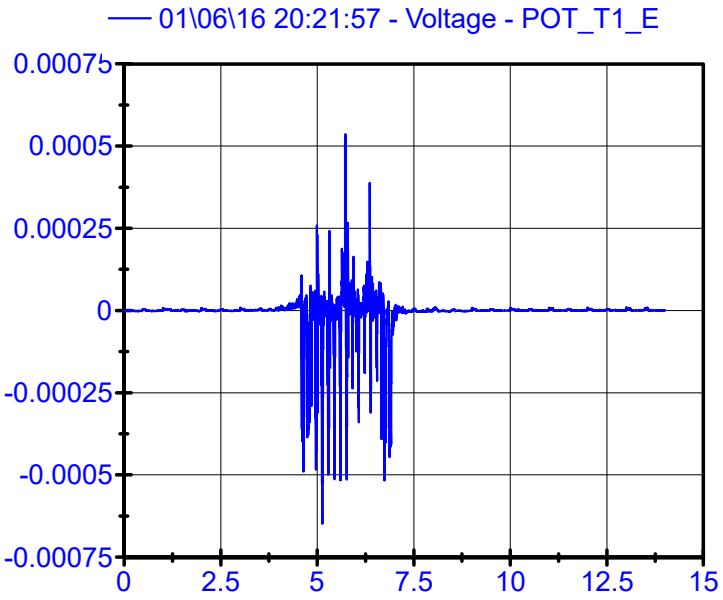

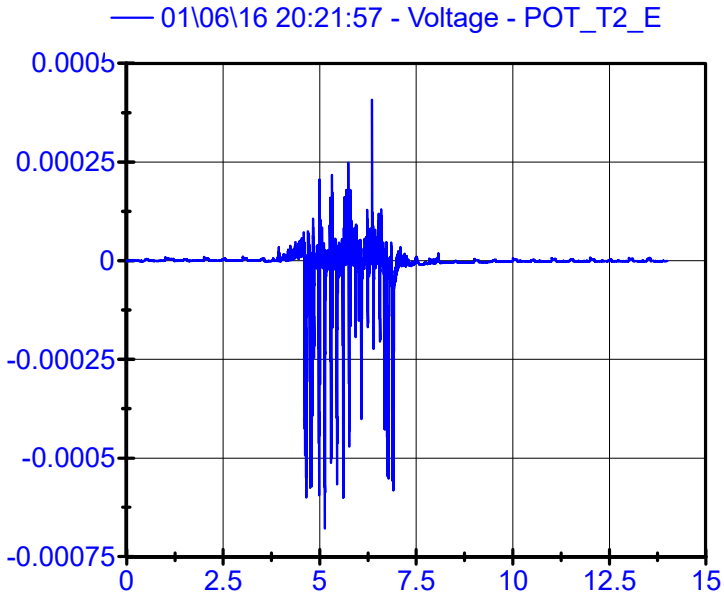

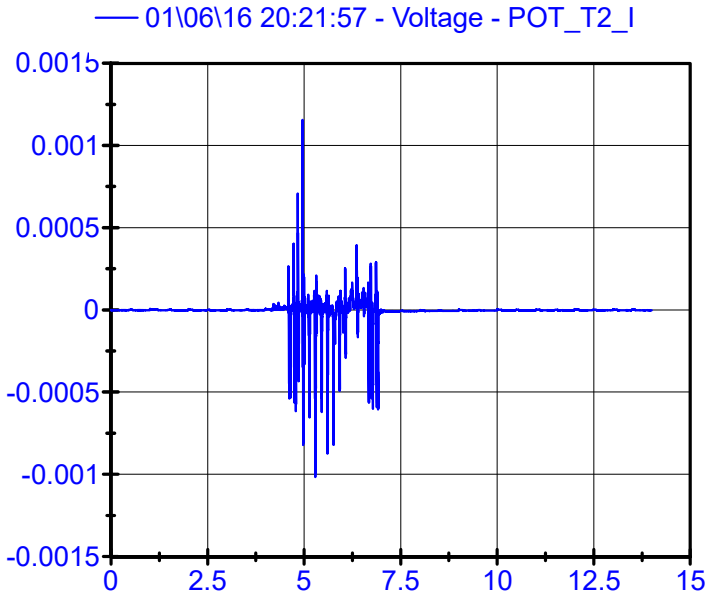

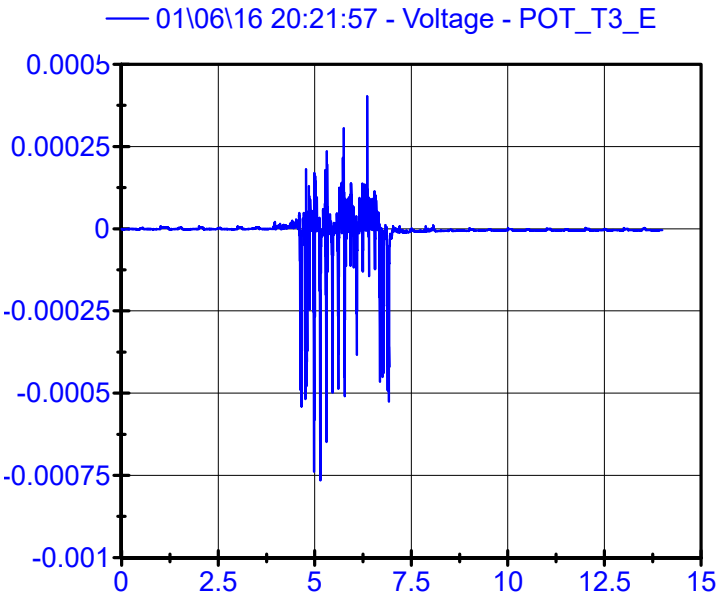

01\06\16 20:57:58

Potentiometers
LPF 80Hz

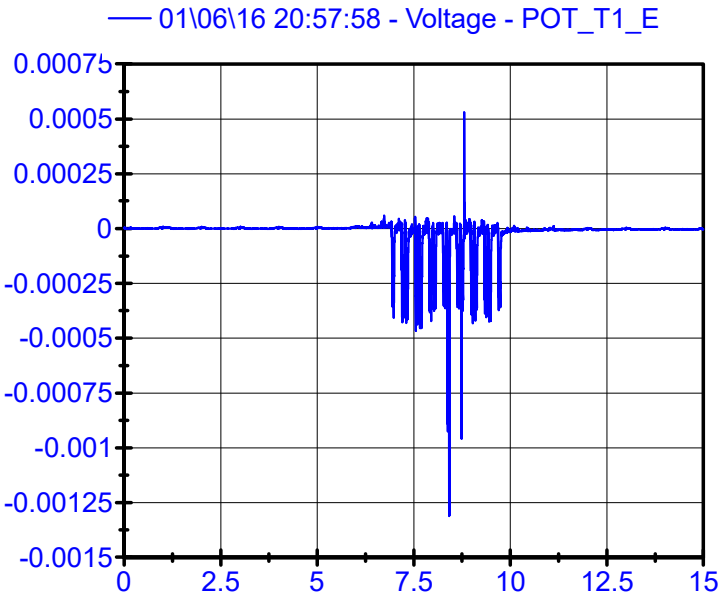

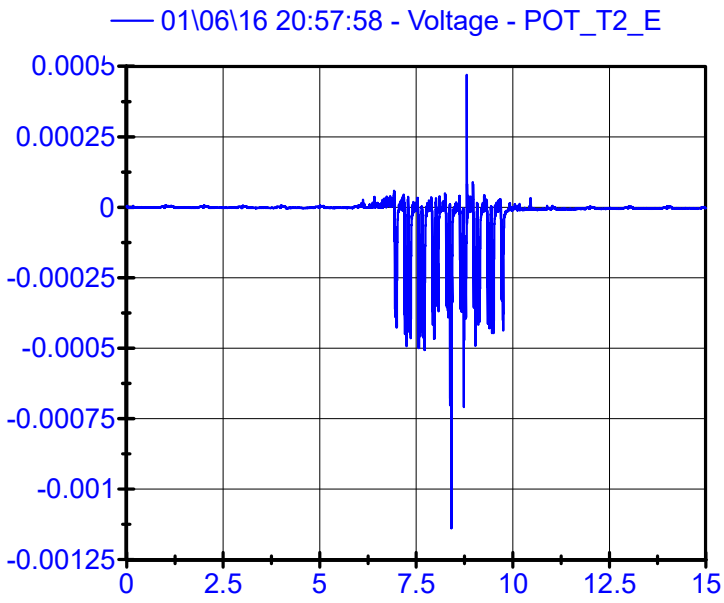

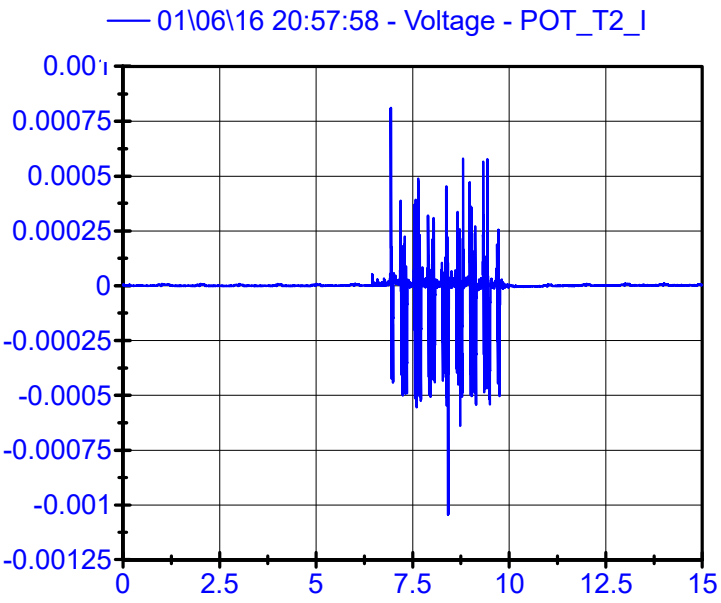

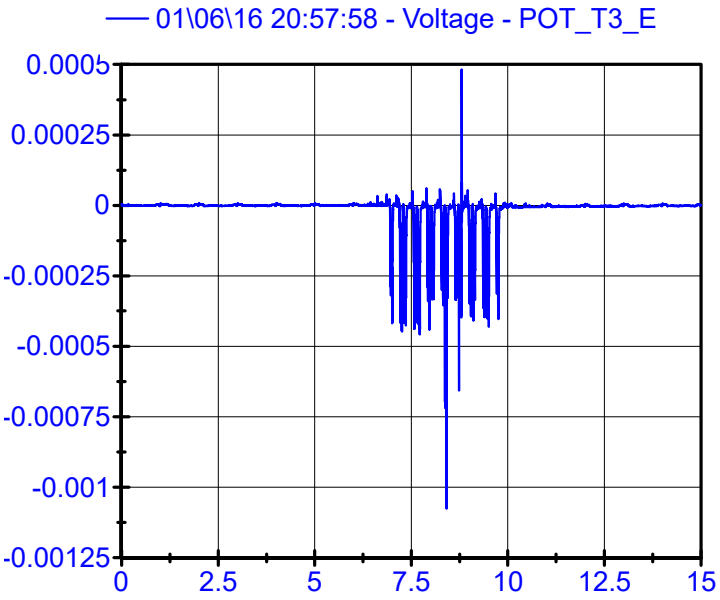

01\06\16 21:49:46

Potentiometers
LPF 80Hz

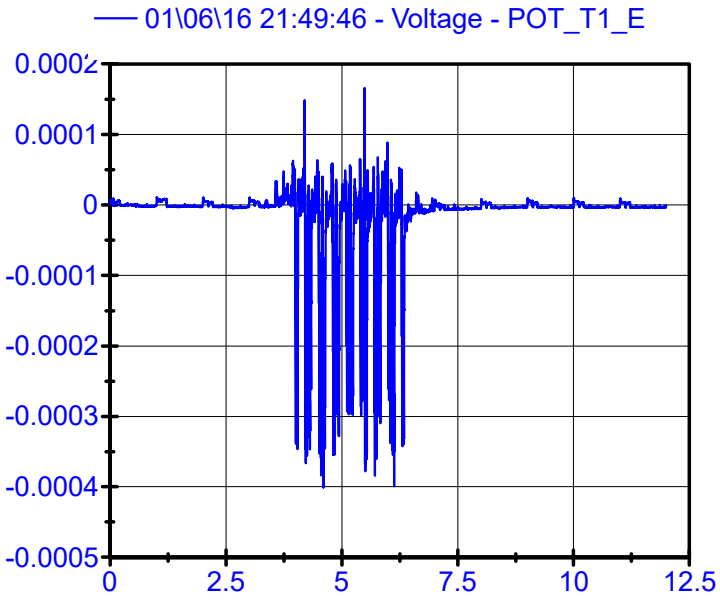

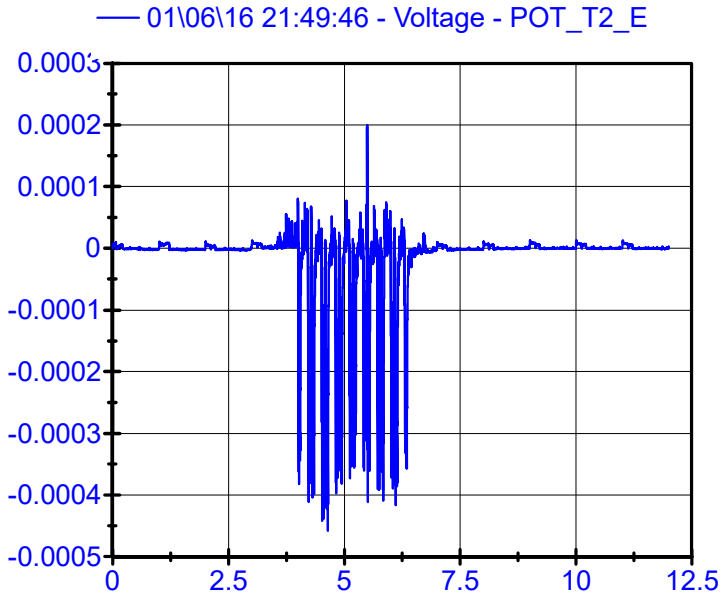

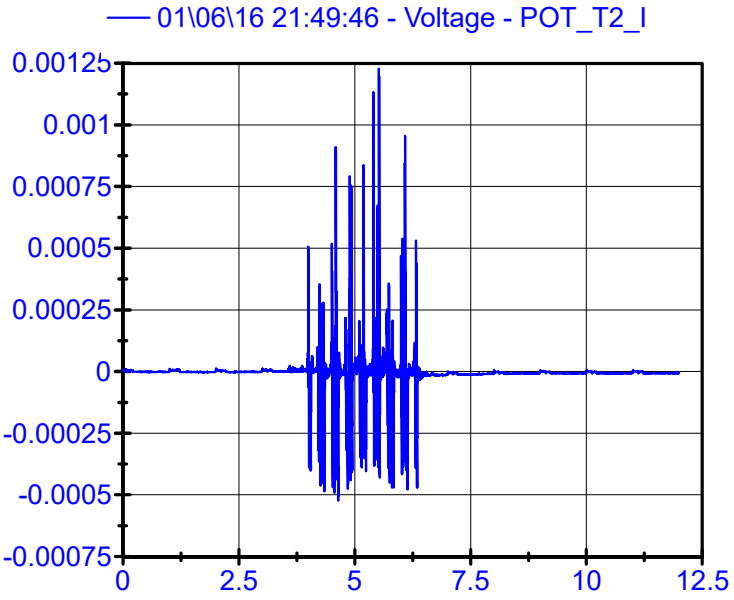

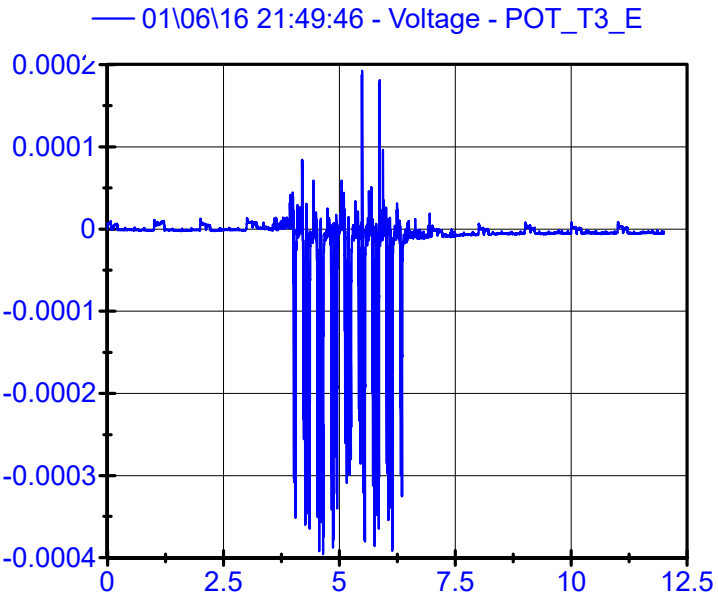

Collaborative project SCP3-GA-2013-60560

Increased Capacity 4 Rail networks through enhanced infrastructure and optimised operations

FP7-SST-2013-RTD-1

Deliverable 12.1

Innovative designs and methods for VHST (intermediate)

Appendix 8.2

Annex B: Data from trains analysed

Table of content

1 Introduction

This Annex collects the time signals obtained for the seven trains, collected in Table 1, selected from the 47 recorded.

Table 1: Recorded trains

TIME	TRAIN TYPE	SPEED (km/h) (±10 km/h)
11:35:54	TALGO S102	299
12:07:44	CAF S120	226
17:24:26	SIEMENS S103	298
19:32:45	TALGO S102	257
20:21:57	TALGO S102	300
20:57:58	SIEMENS S103	250
21:49:46	SIEMENS S103	299

These time signals were processed according to the following procedure: the Fast Fourier Transform (FFT) was firstly calculated to visualize the frequency domain and then to decide the best values of the Low Pass Filters which should be used. The signal of each sensor was then filtered to represent only the train influence and to eliminate noise. In addition, the time axle limits were fixed to center the graph on the pass train signal.

The signals that are shown for each train are the following:

- Sleeper velocity signal in the outer side of sleeper T2
- Sleeper velocity signal in the inner side of sleeper T2
- Rail velocity signal in the outer rail between T2 and T3
- Rail velocity signal in the inner rail between T2 and T3
- Sleeper acceleration signal in the outer side of sleeper T2
- Sleeper acceleration signal in the inner side of sleeper T2
- Sleeper acceleration signal in the center of sleeper T2
- Rail acceleration signal in the outer rail between T2 and T3
- Rail acceleration signal in the inner rail between T2 and T3
- Relative displacement between outer rail and sleeper T2
- Relative displacement between inner rail and sleeper T2
- Rail deflection in the outer rail between T2 and T3
- Rail deflection in the inner rail between T2 and T3
- Loads in the outer rail between T2 and T3
- Loads in the inner rail between T2 and T3

2 Train S103 (Time 21:49:46 /32 axles / 299 km/h)

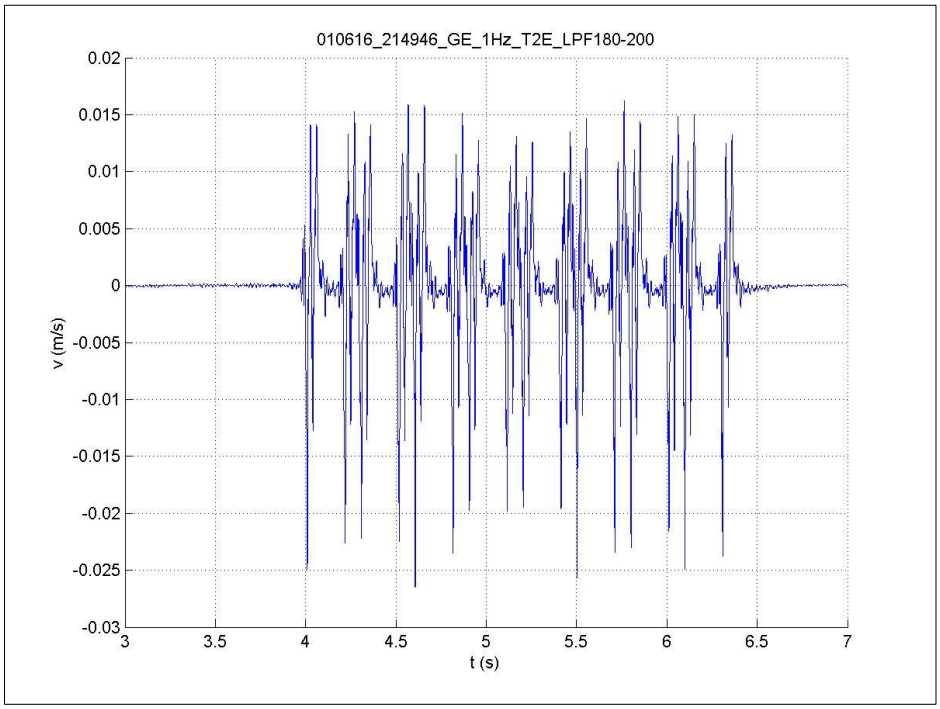

Figure 1: Sleeper velocity signal in the outer side of sleeper T2 induced by 21:49:46 train.

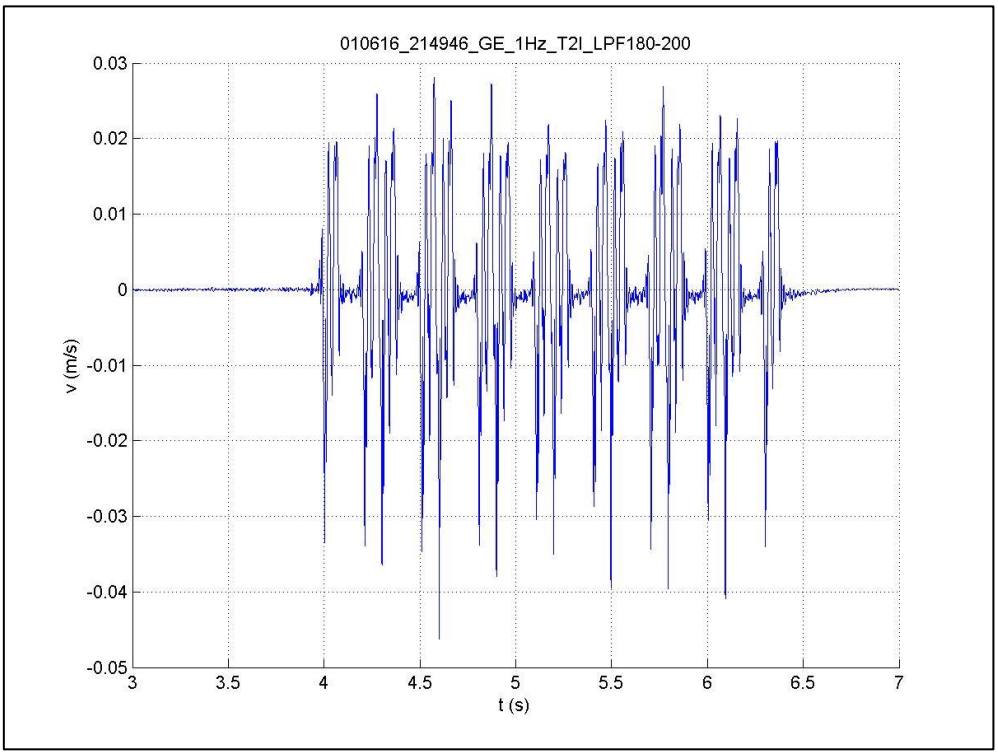

Figure 2: Sleeper velocity signal in the inner side of sleeper T2 induced by 21:49:46 train.

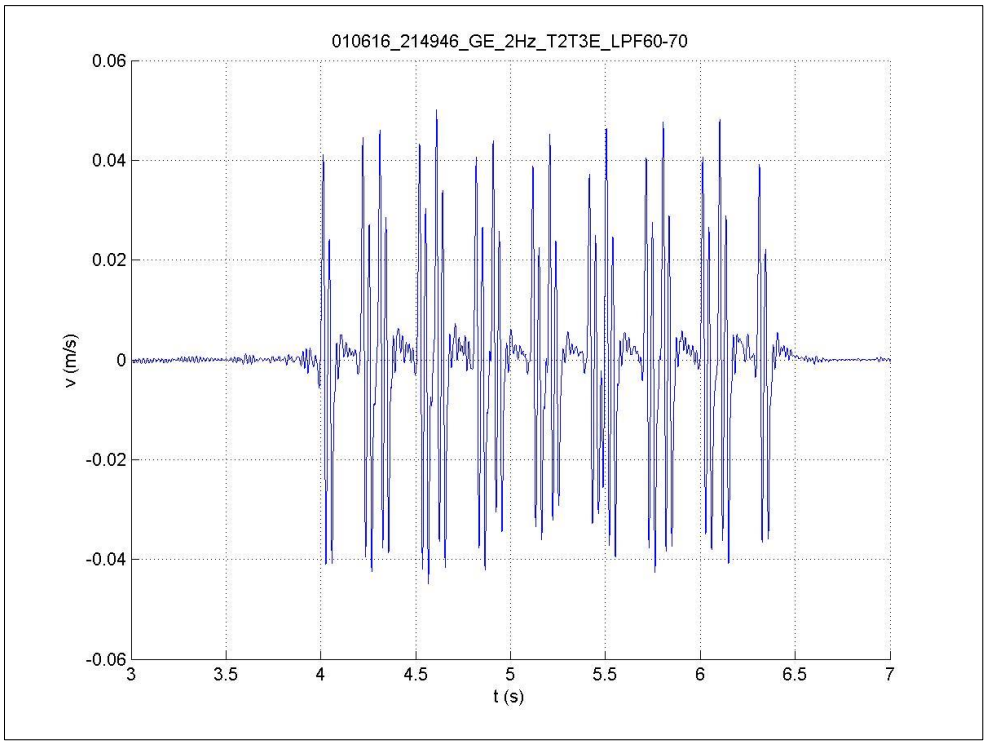

Figure 3: Rail velocity signal in the outer rail between T2 and T3 induced by 21:49:46 train.

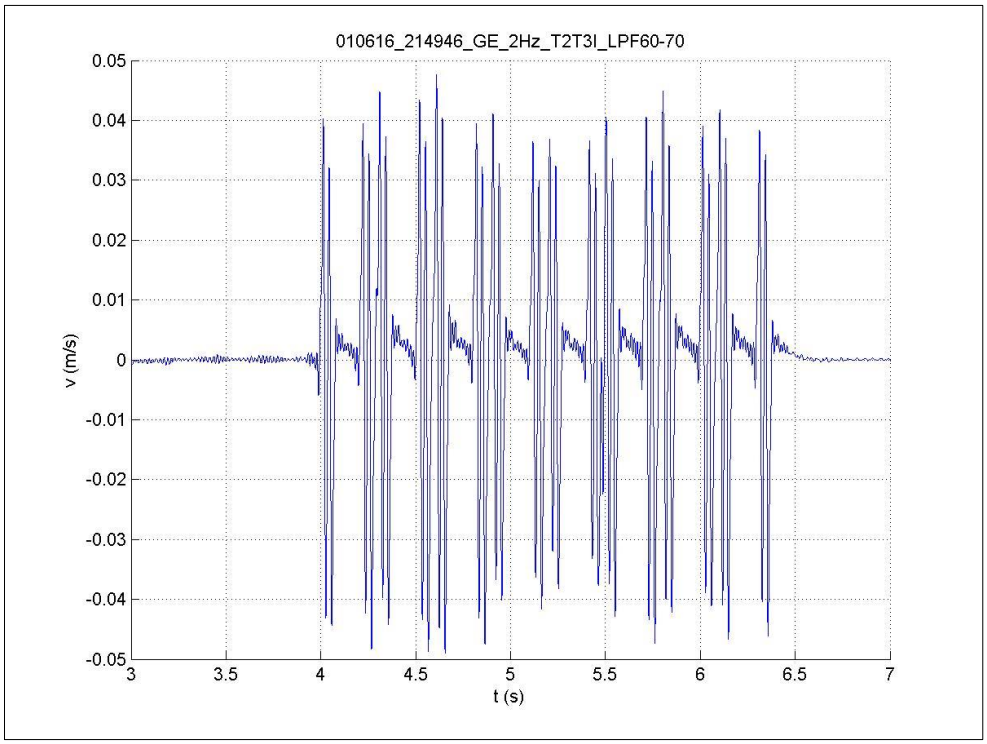

Figure 4: Rail velocity signal in the inner rail between T2 and T3 induced by 21:49:46 train.

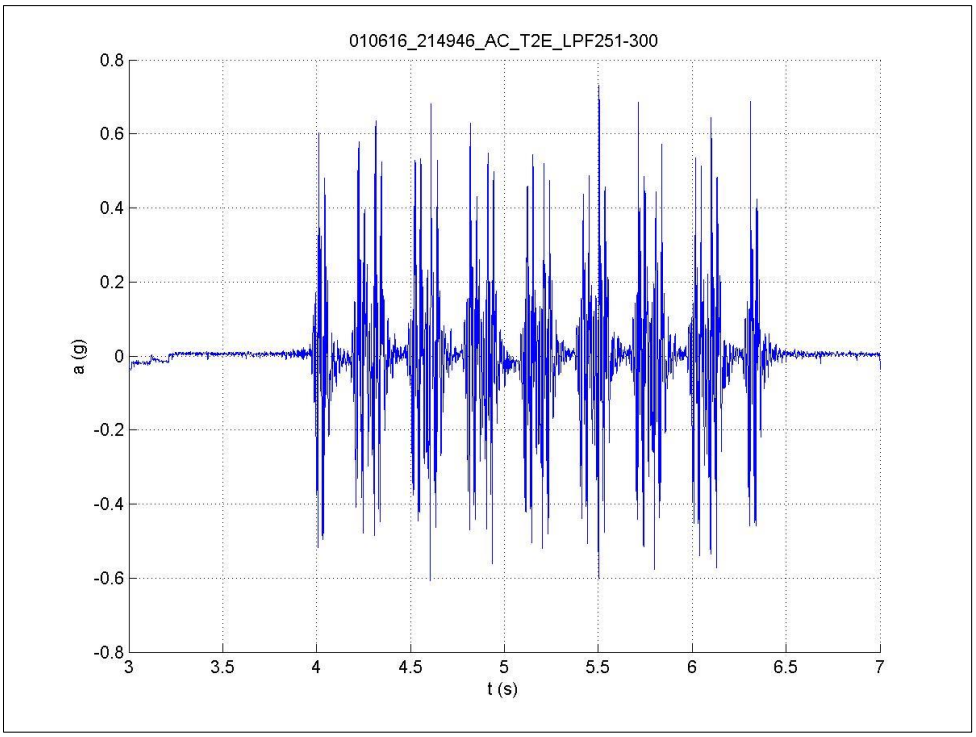

Figure 5: Sleeper acceleration signal in the outer side of sleeper T2 induced by 21:49:46 train.

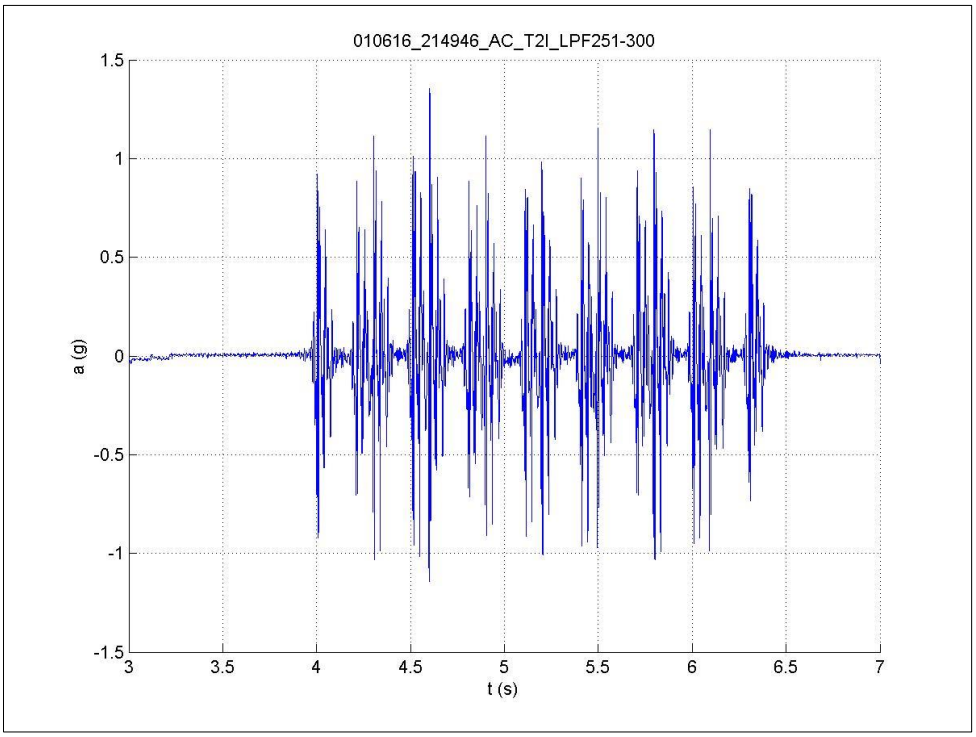

Figure 6: Sleeper acceleration signal in the inner side of sleeper T2 induced by 21:49:46 train.

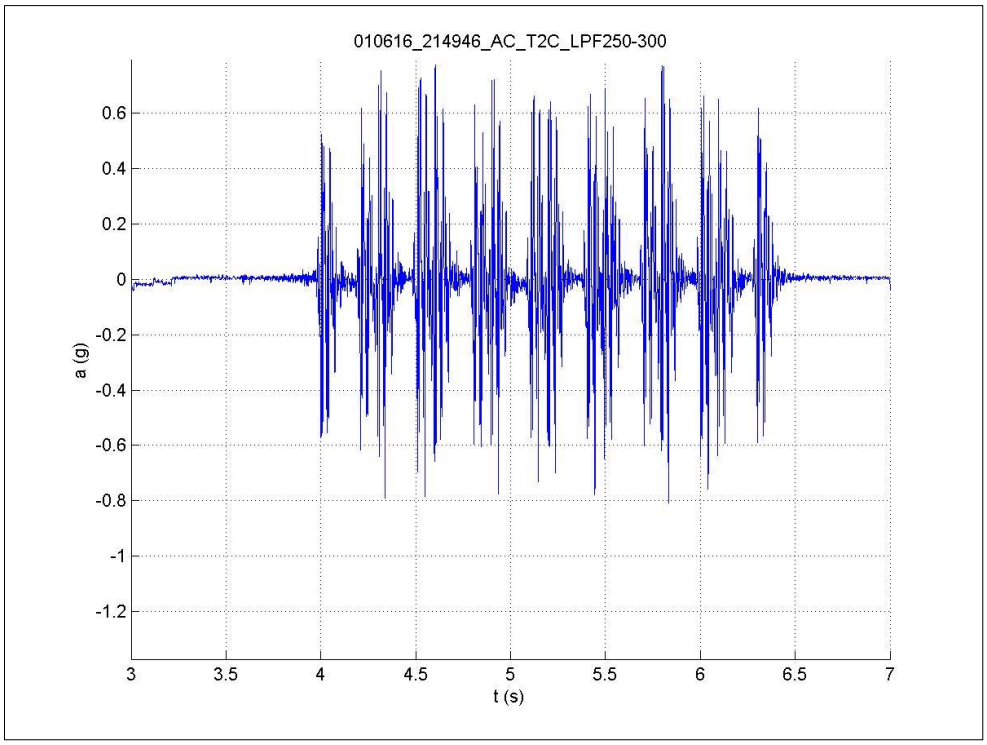

Figure 7: Sleeper acceleration signal in the center of sleeper T2 induced by 21:49:46 train.

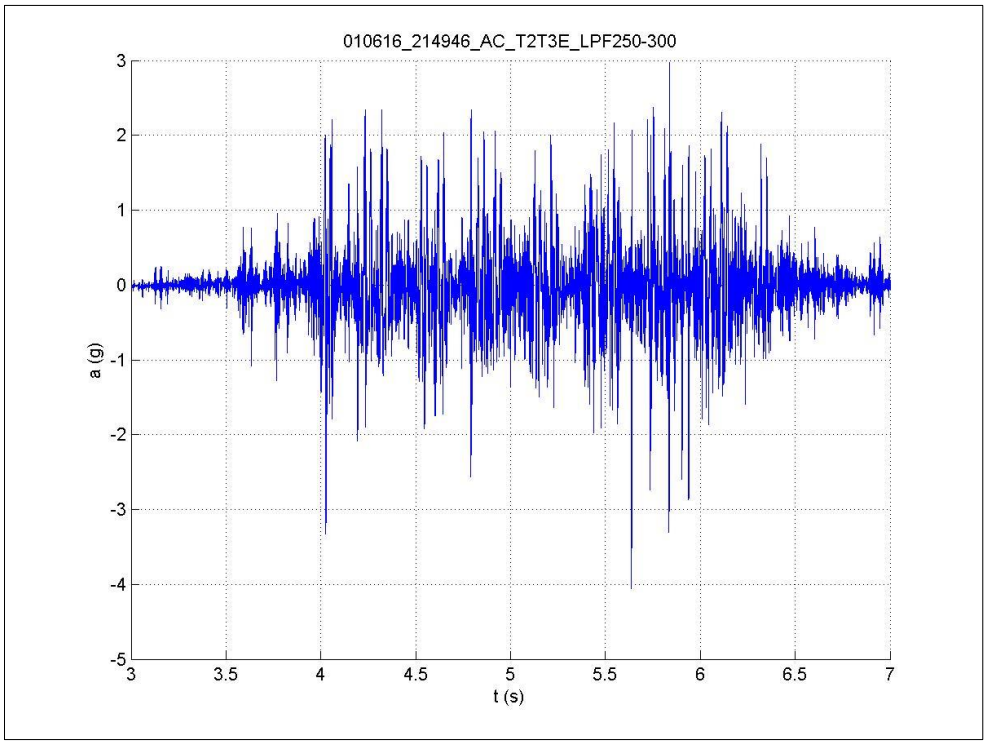

Figure 8: Rail acceleration signal in the outer rail between T2 and T3 induced by 21:49:46 train.

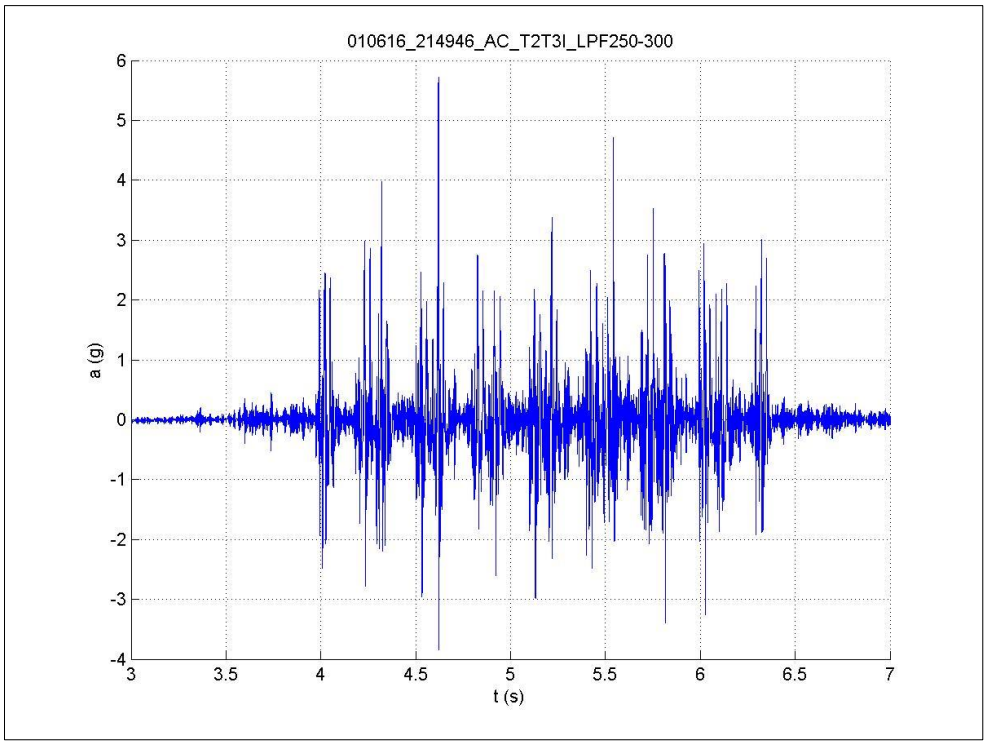

Figure 9: Rail acceleration signal in the inner rail between T2 and T3 induced by 21:49:46 train.

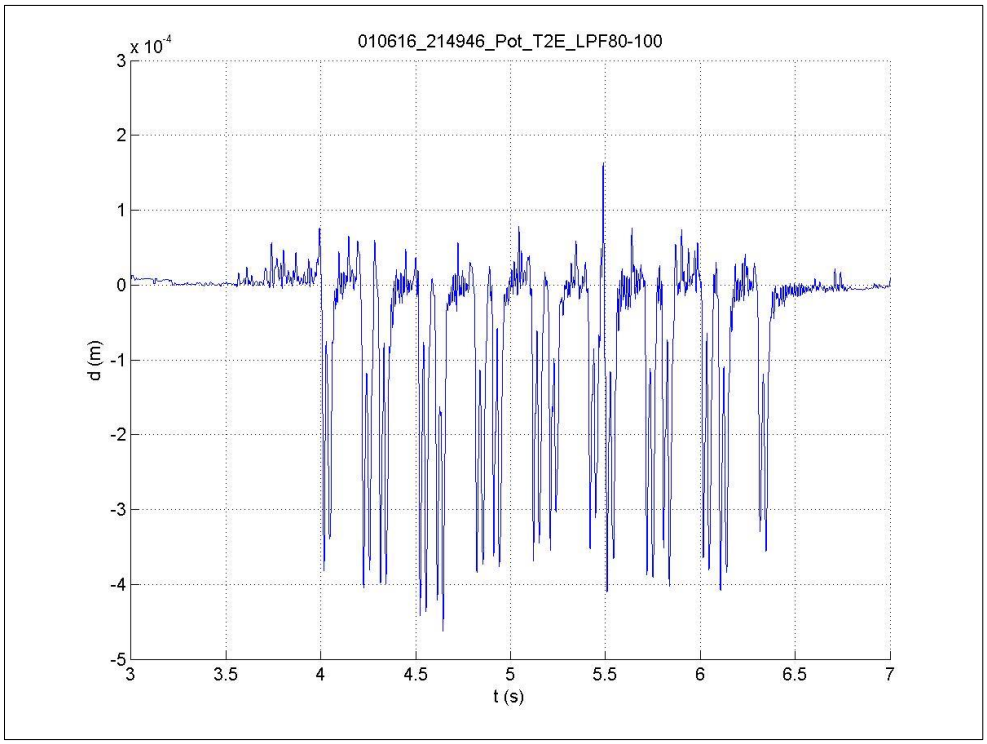

Figure 10: Relative displacement between outer rail and sleeper T2 induced by 21:49:46 train.

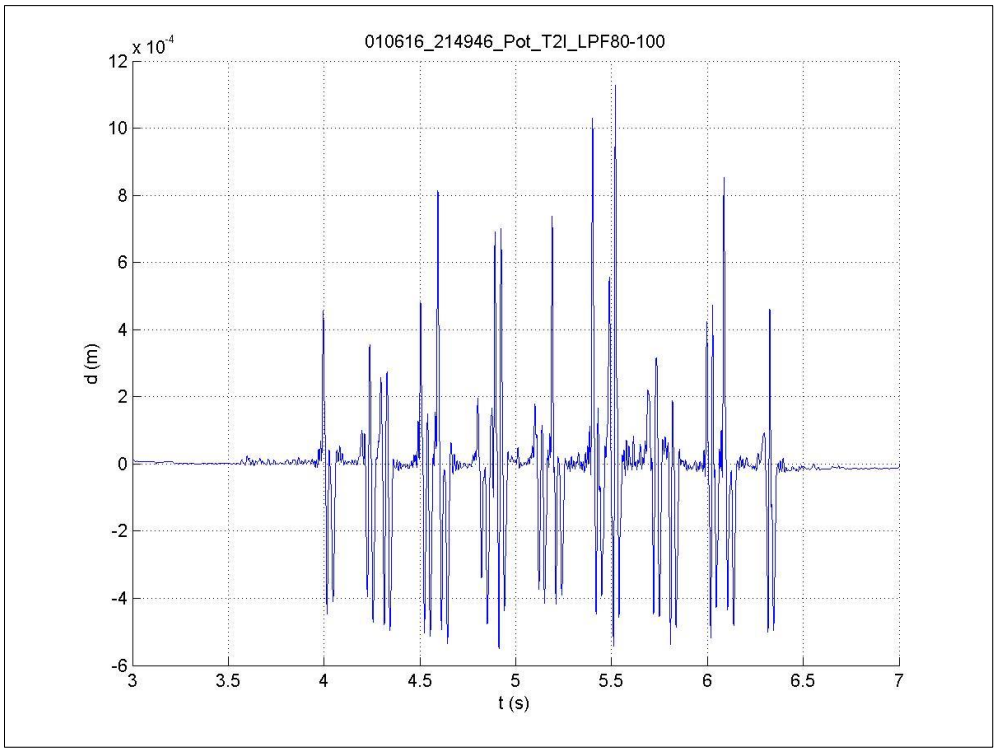

Figure 11: Relative displacement between inner rail and sleeper T2 induced by 21:49:46 train.

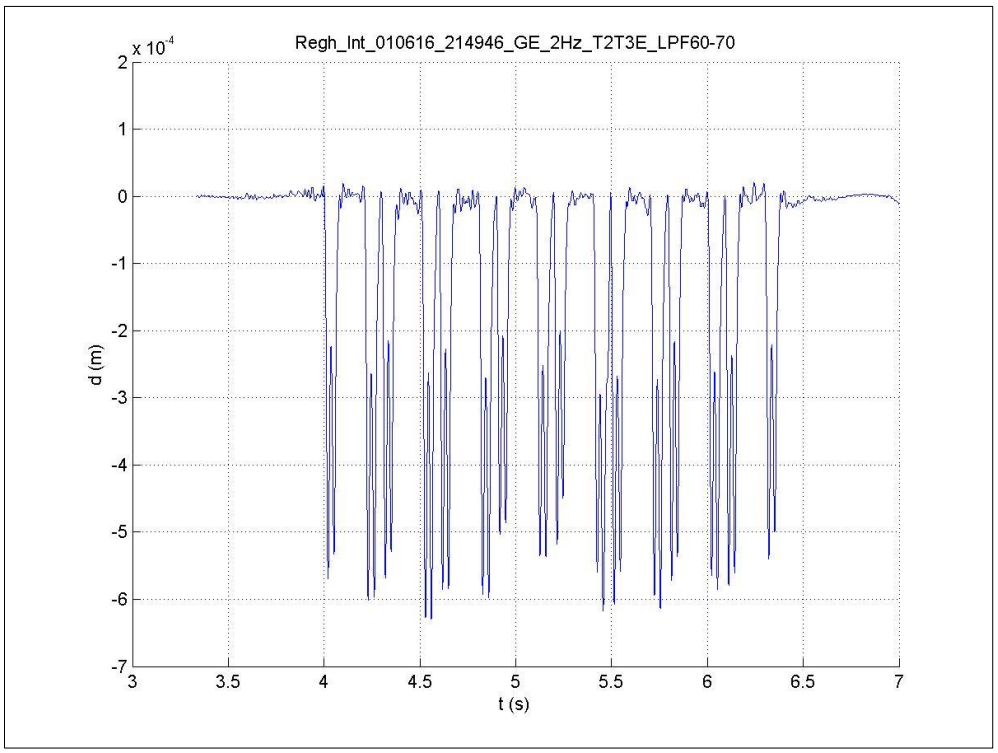

Figure 12: Rail deflection in the outer rail between T2 and T3 induced by 21:49:46 train.

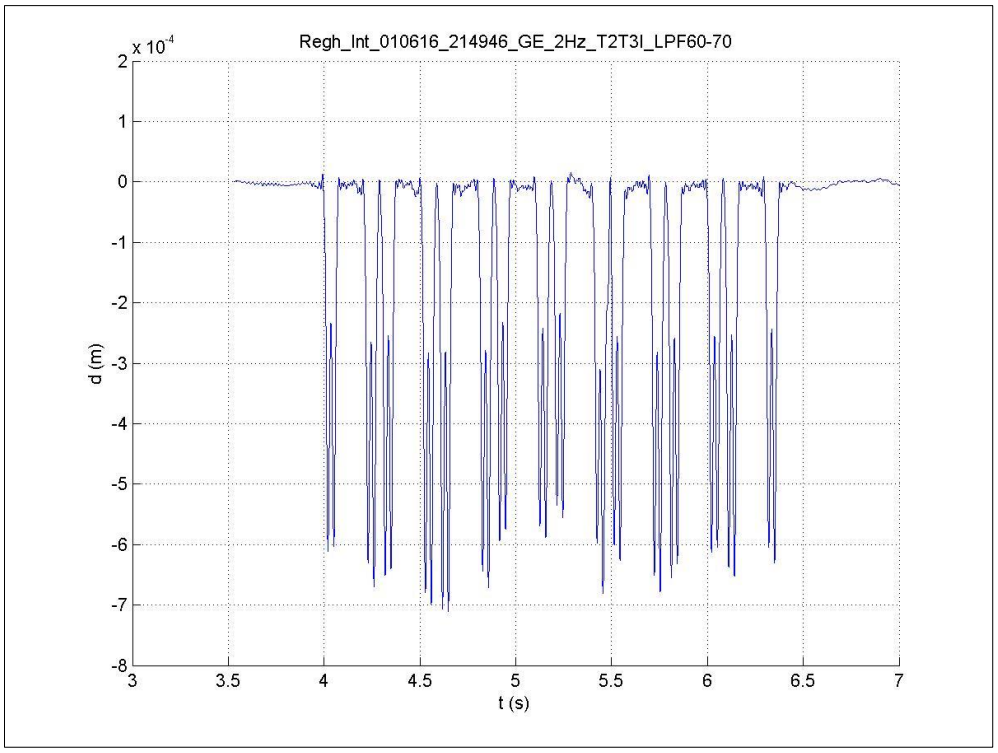

Figure 13: Rail deflection in the inner rail between T2 and T3 induced by 21:49:46 train.

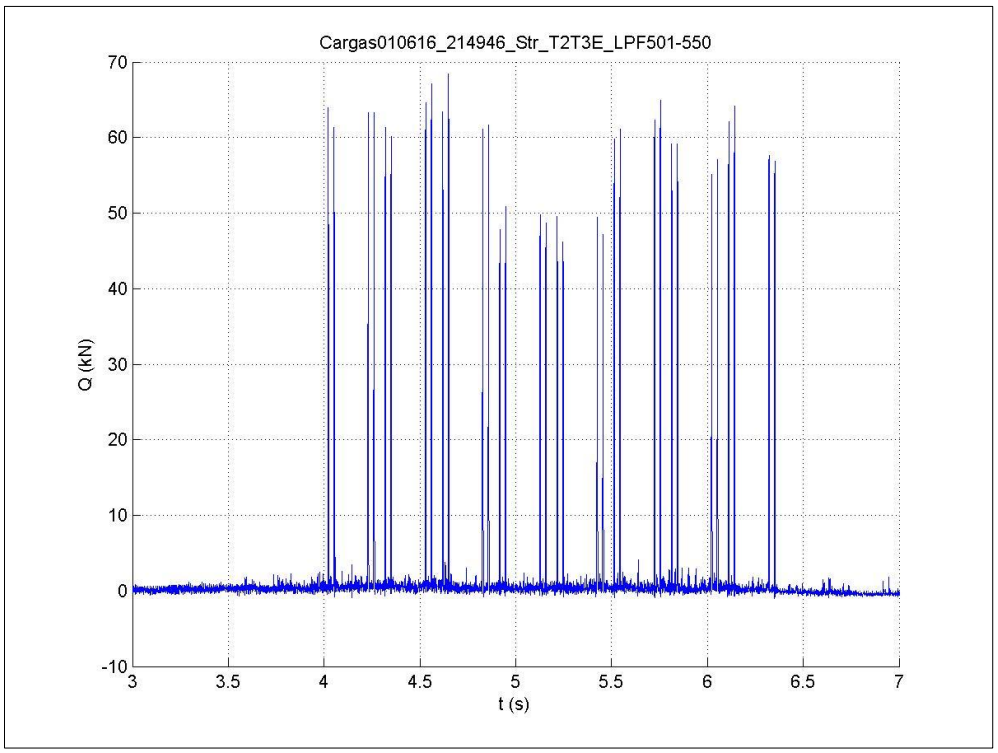

Figure 14: Loads in the outer rail between T2 and T3 induced by 21:49:46 train.

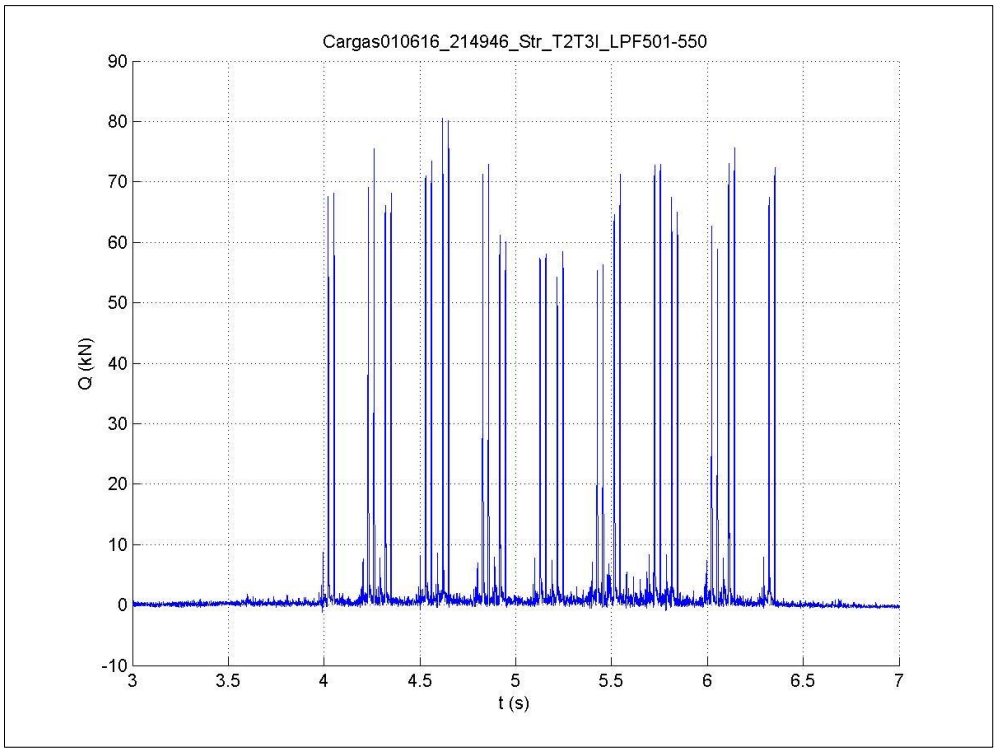

Figure 15: Loads in the inner rail between T2 and T3 induced by 21:49:46 train.

3 Train S103 (Time 20:57:58 / 32 axles / 250 km/h)

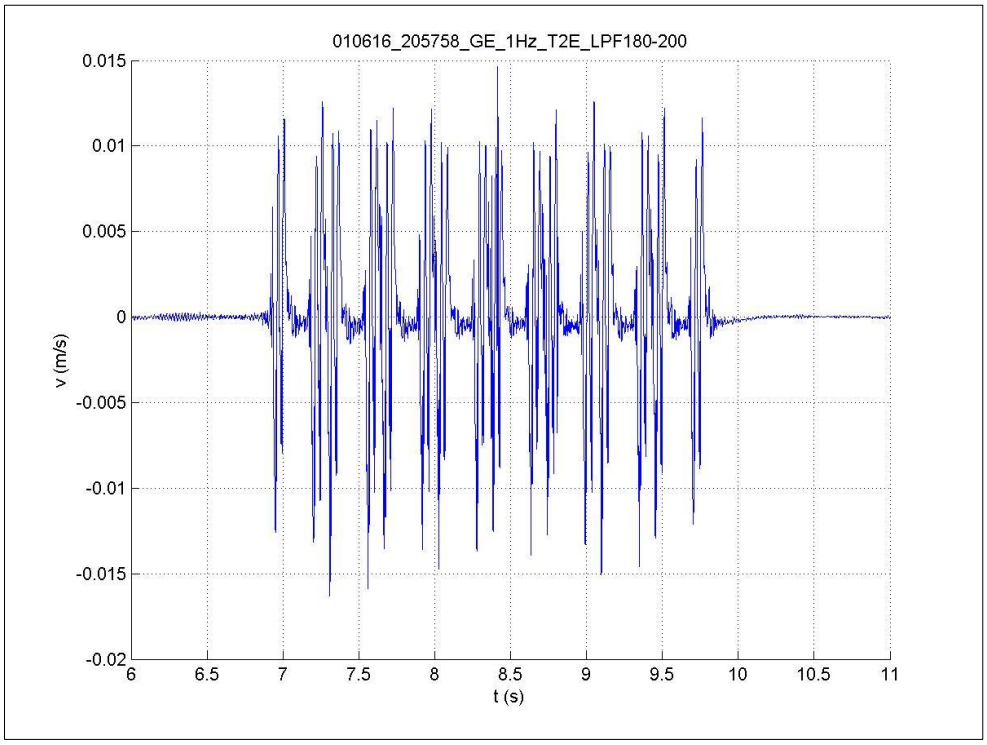

Figure 16: Sleeper velocity signal in the outer side of sleeper T2 induced by 20:57:58 train.

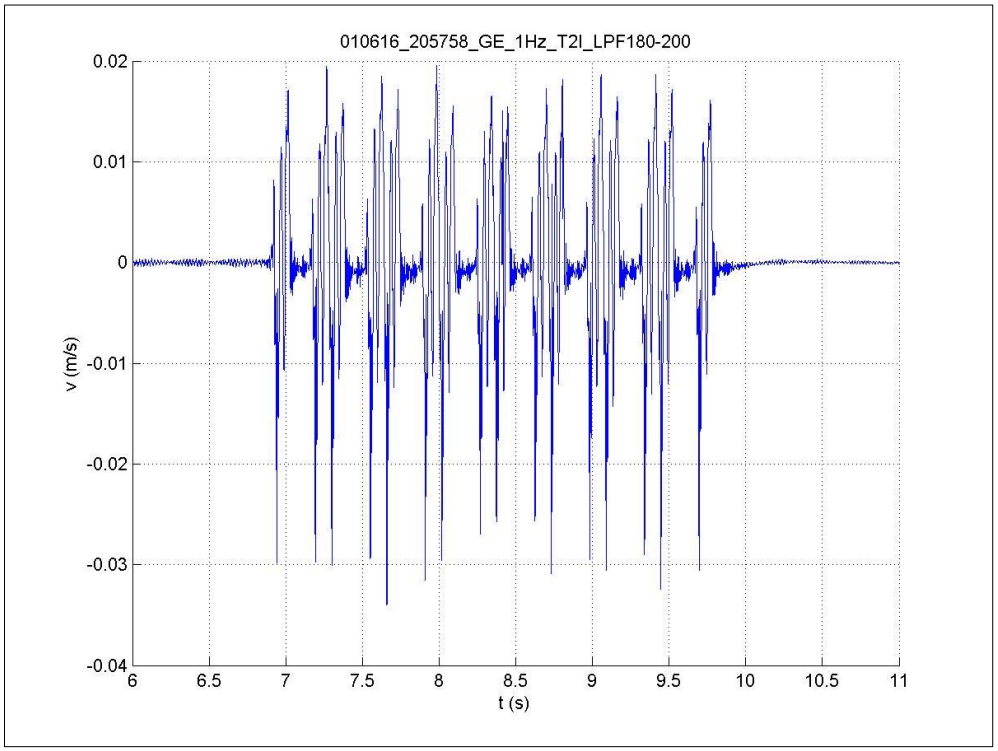

Figure 17: Sleeper velocity signal in the inner side of sleeper T2 induced by 20:57:58 train.

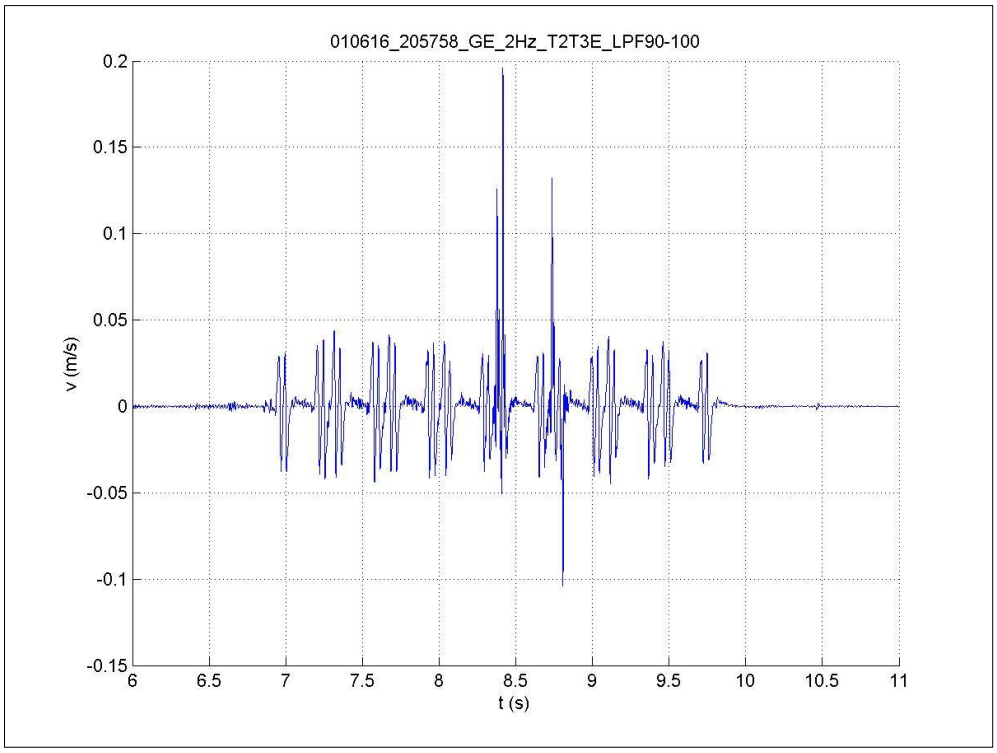

Figure 18: Rail velocity signal in the outer rail between T2 and T3 induced by 20:57:58 train.

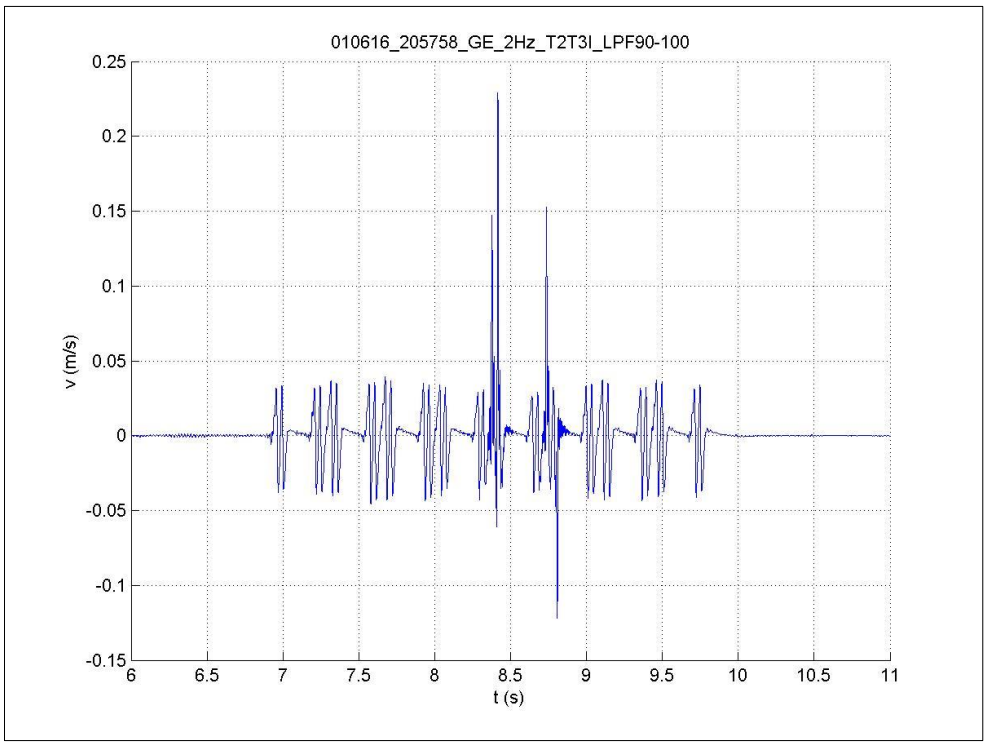

Figure 19: Rail velocity signal in the inner rail between T2 and T3 induced by 20:57:58 train.

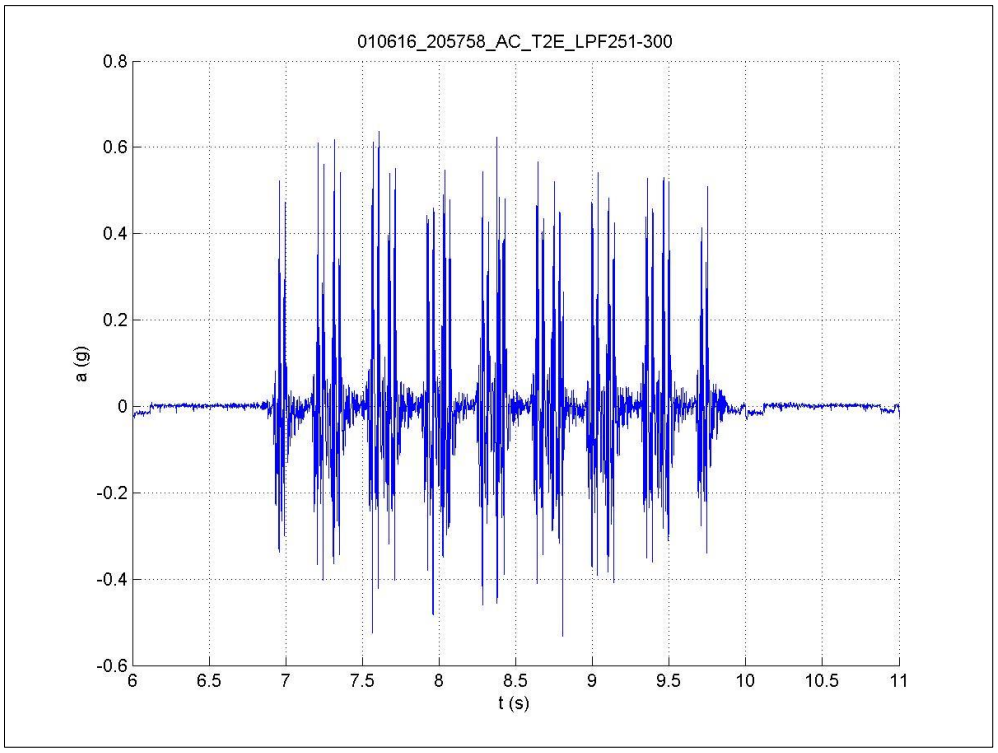

Figure 20: Sleeper acceleration signal in the outer side of sleeper T2 induced by 20:57:58 train.

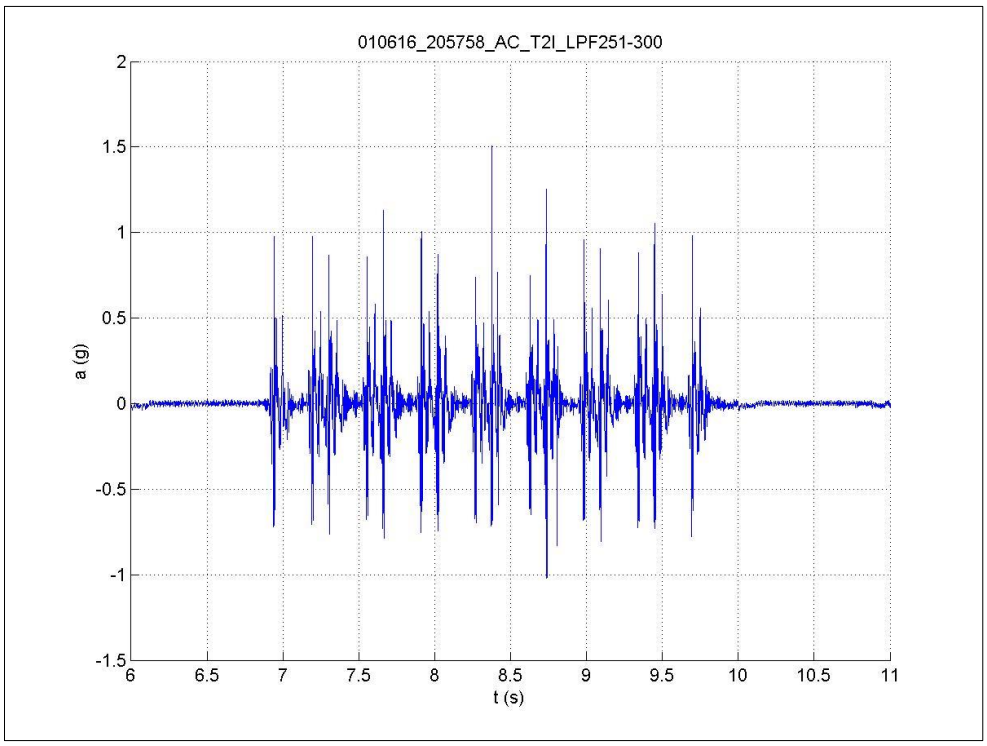

Figure 21: Sleeper acceleration signal in the inner side of sleeper T2 induced by 20:57:58 train.

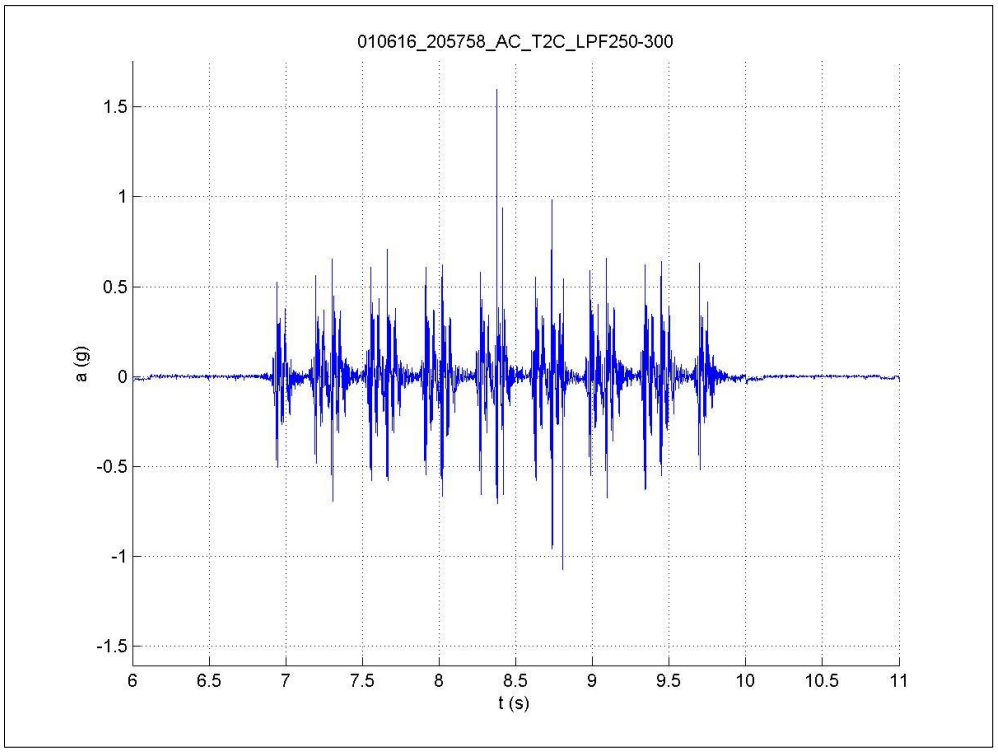

Figure 22: Sleeper acceleration signal in the center of sleeper T2 induced by 20:57:58 train.

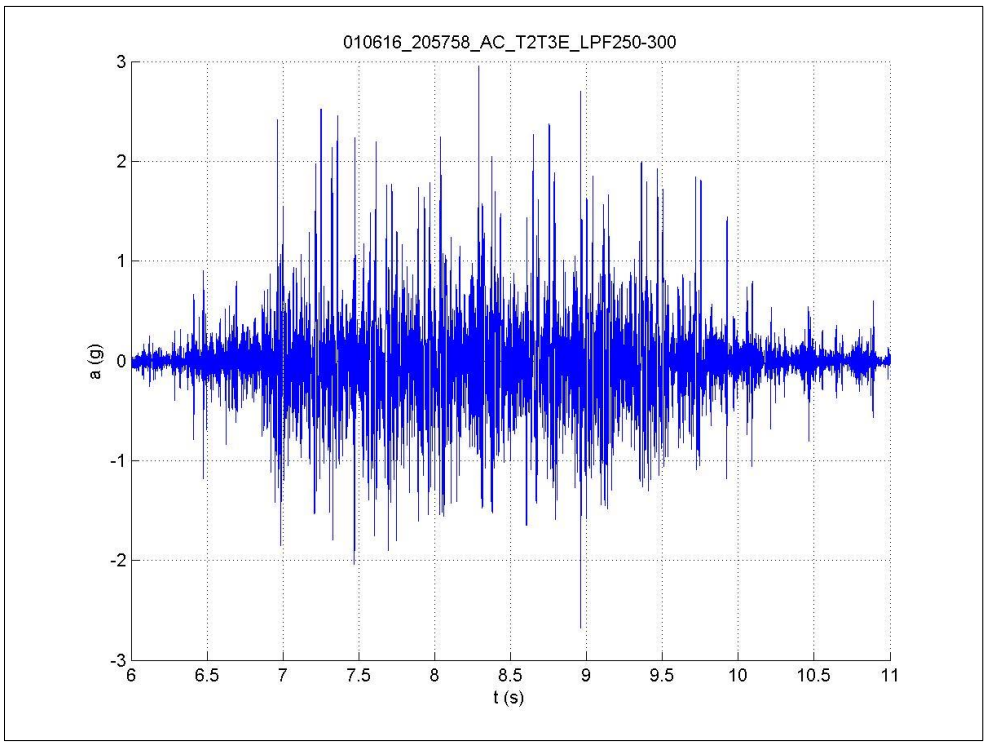

Figure 23: Rail acceleration signal in the outer rail between T2 and T3 induced by 20:57:58 train.

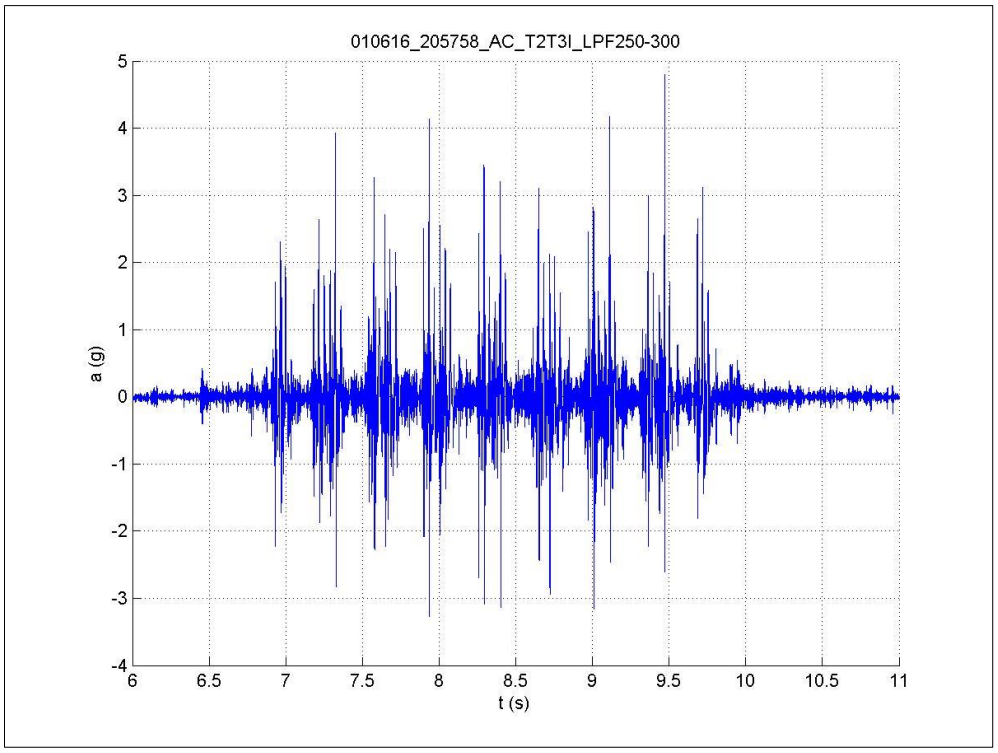

Figure 24: Rail acceleration signal in the inner rail between T2 and T3 induced by 20:57:58 train.

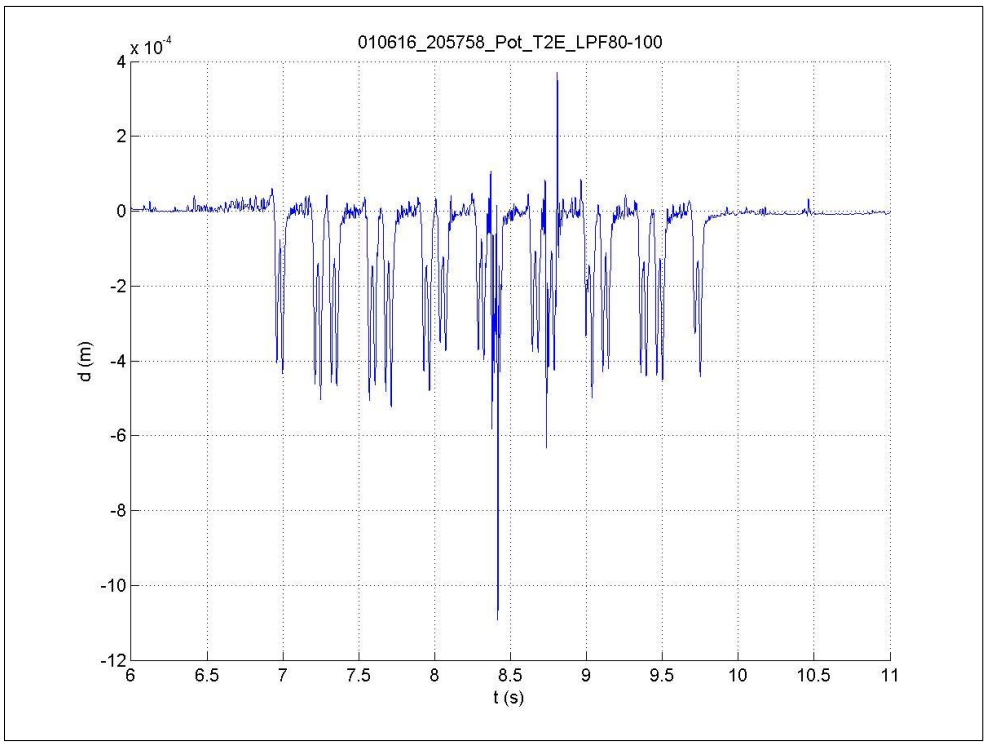

Figure 25: Relative displacement between outer rail and sleeper T2 induced by 20:57:58 train.

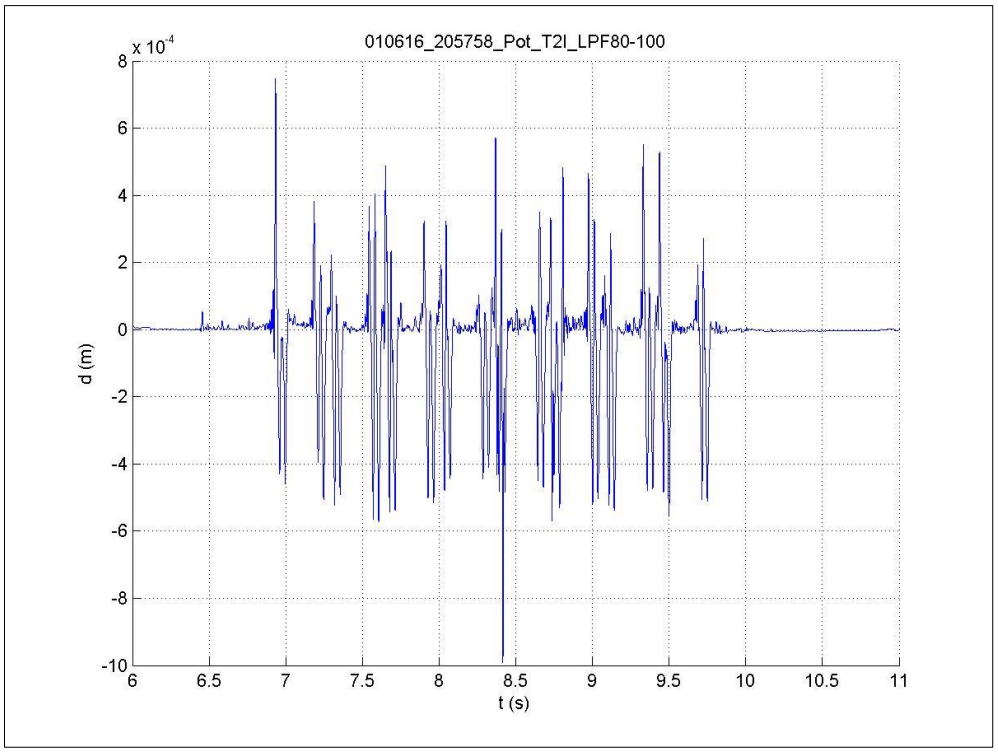

Figure 26: Relative displacement between inner rail and sleeper T2 induced by 20:57:58 train.

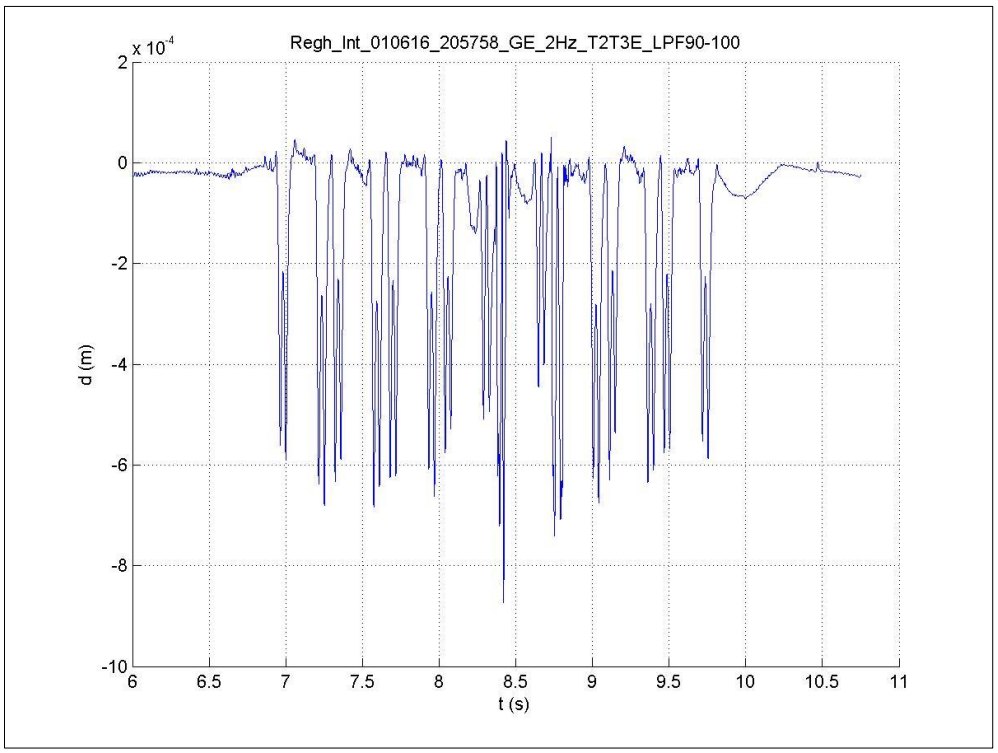

Figure 27: Rail deflection in the outer rail between T2 and T3 induced by 20:57:58 train.

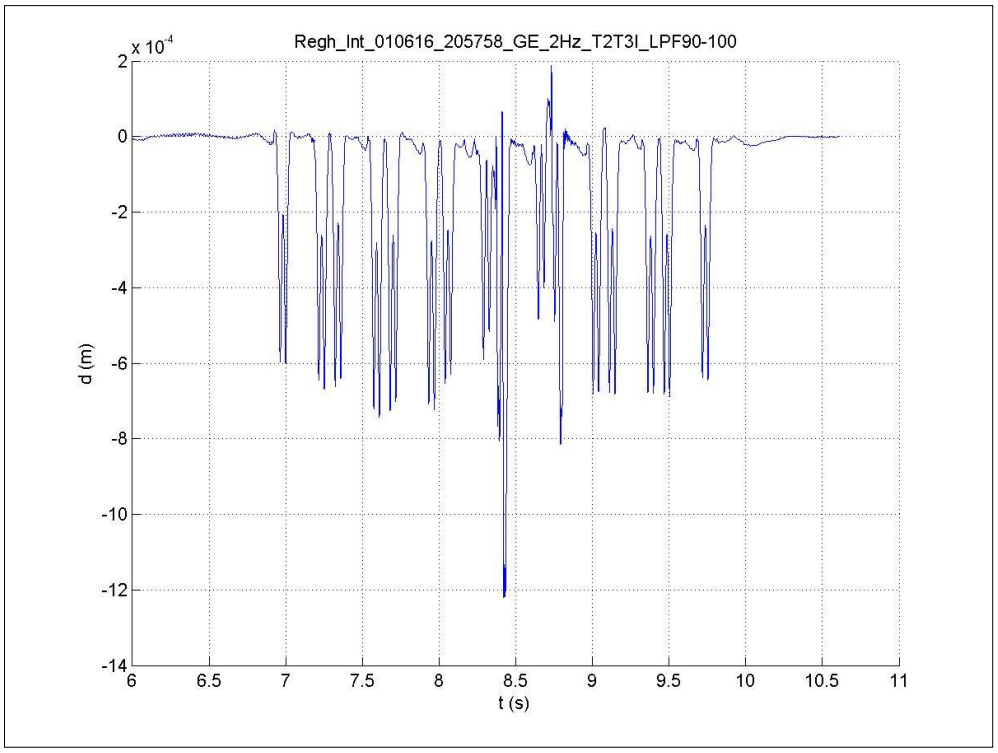

Figure 28: Rail deflection in the inner rail between T2 and T3 induced by 20:57:58 train.

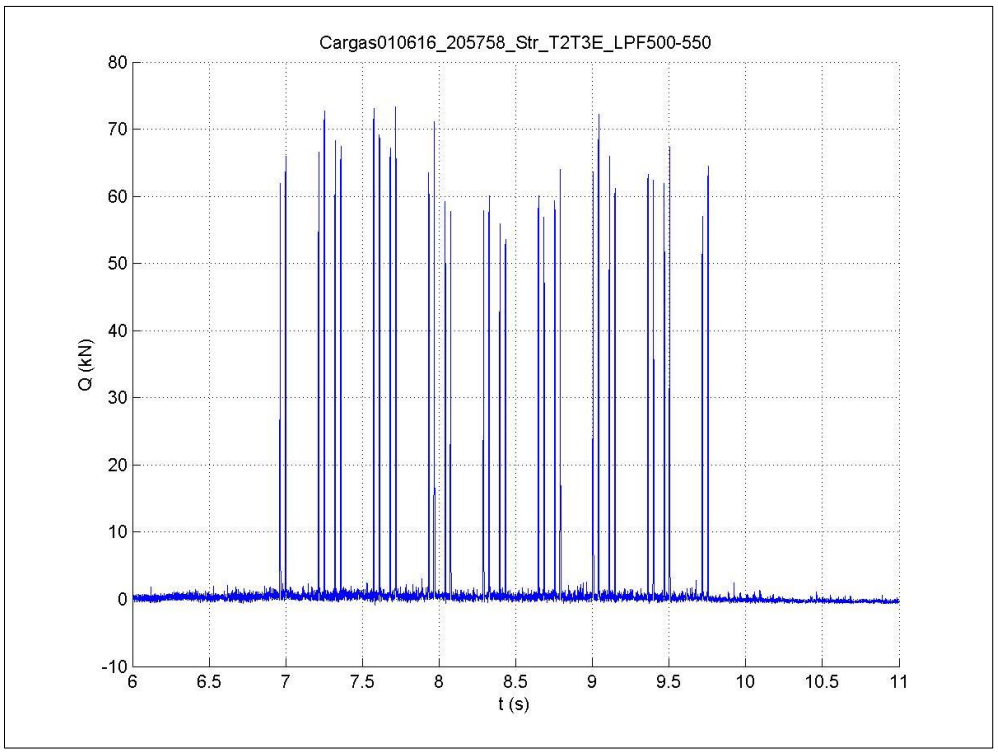

Figure 29: Loads in the outer rail between T2 and T3 induced by 20:57:58 train.

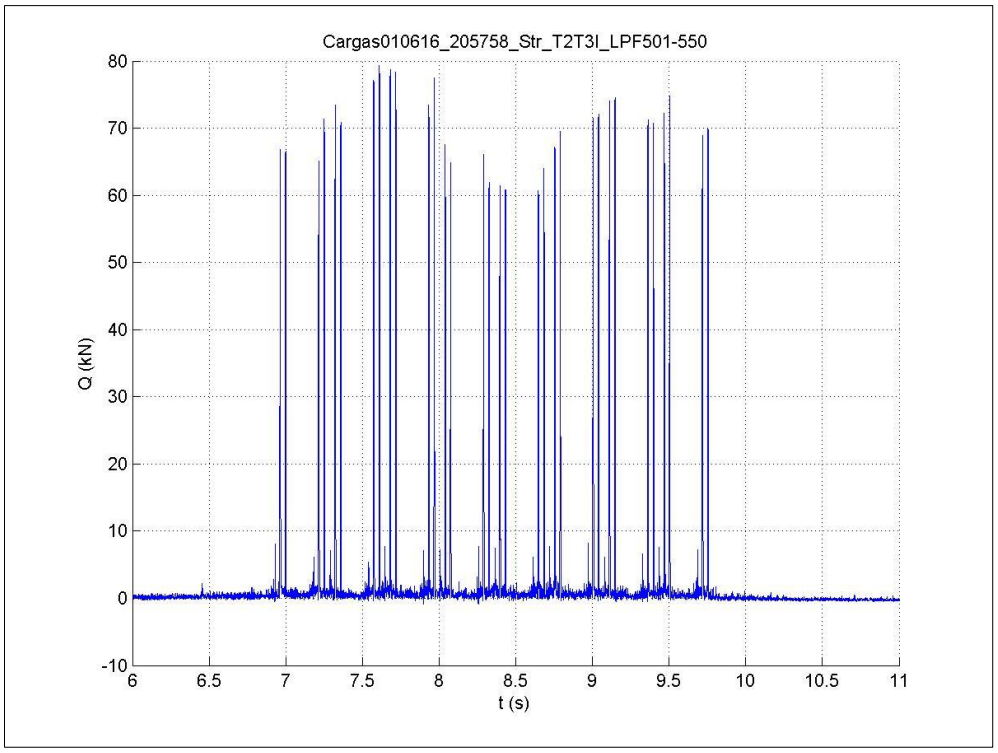

Figure 30: Loads in the inner rail between T2 and T3 induced by 20:57:58 train.

4 Train S102 (Time 20:21:57 / 21 axles / 300 km/h)

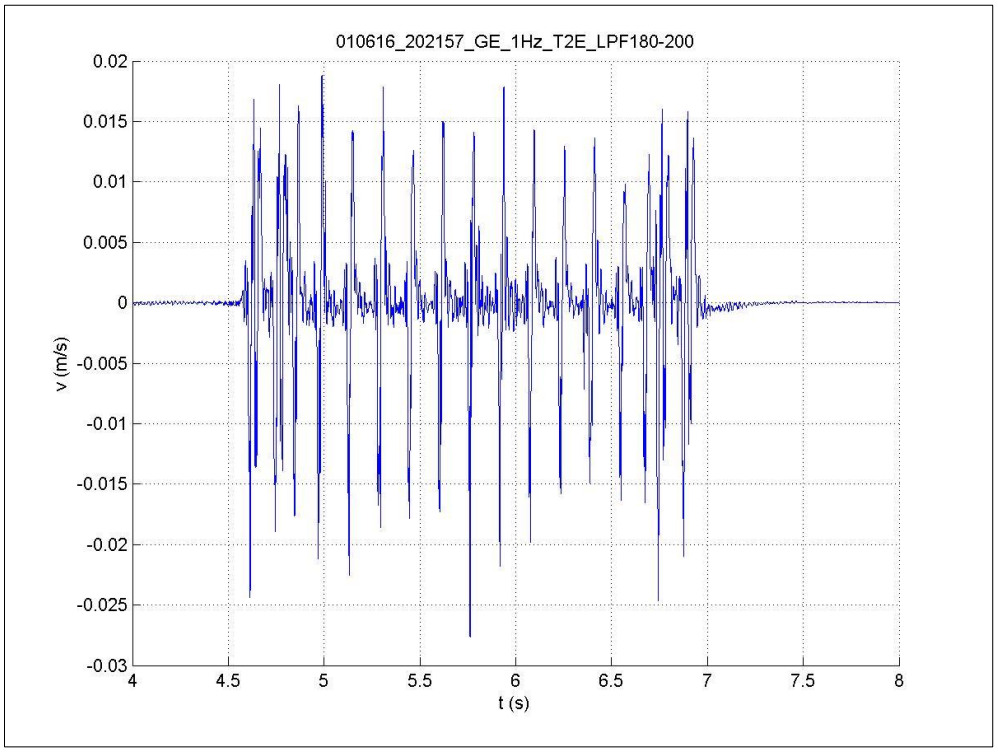

Figure 31: Sleeper velocity signal in the outer side of sleeper T2 induced by 20:21:57 train.

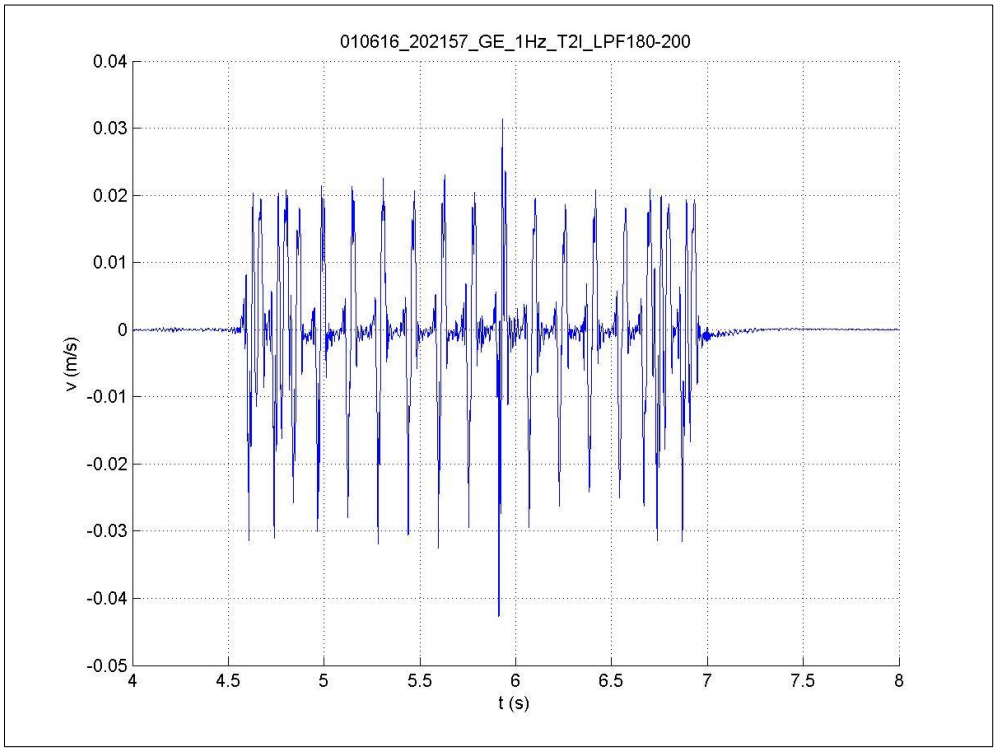

Figure 32: Sleeper velocity signal in the inner side of sleeper T2 induced by 20:21:57 train.

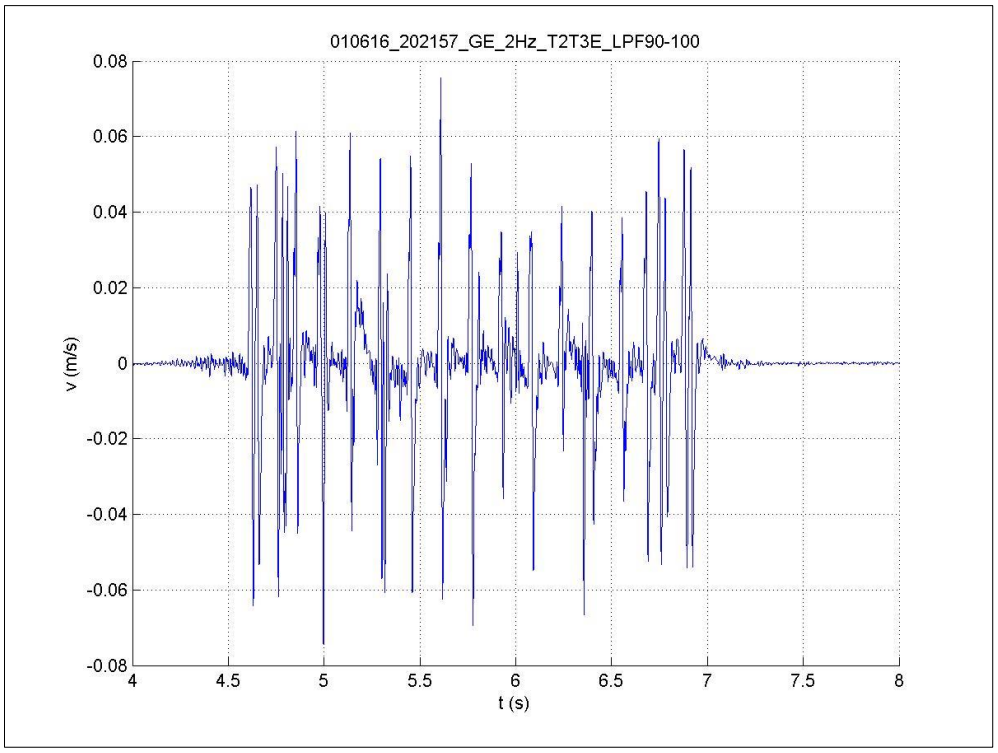

Figure 33: Rail velocity signal in the outer rail between T2 and T3 induced by 20:21:57 train.

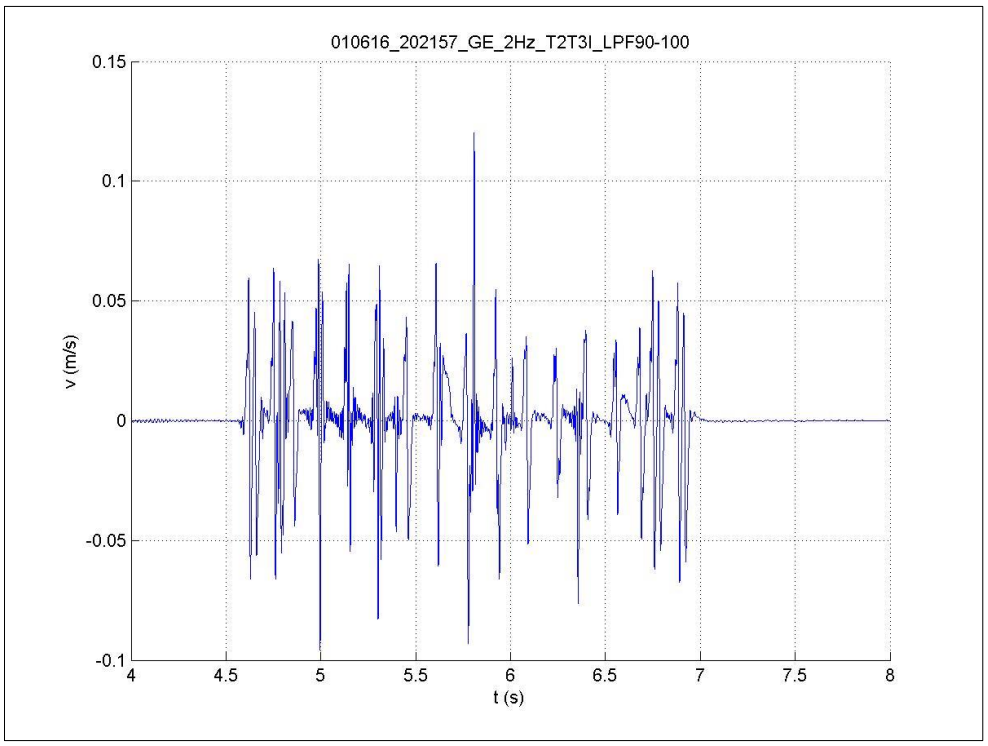

Figure 34: Rail velocity signal in the inner rail between T2 and T3 induced by 20:21:57 train.

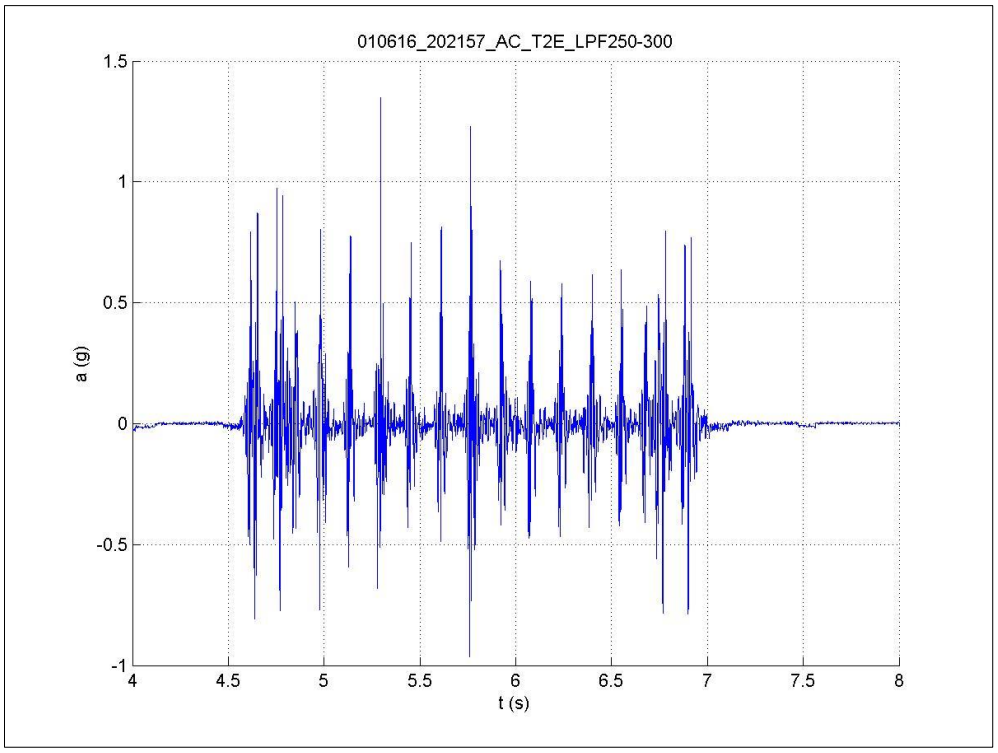

Figure 35: Sleeper acceleration signal in the outer side of sleeper T2 induced by 20:21:57 train.

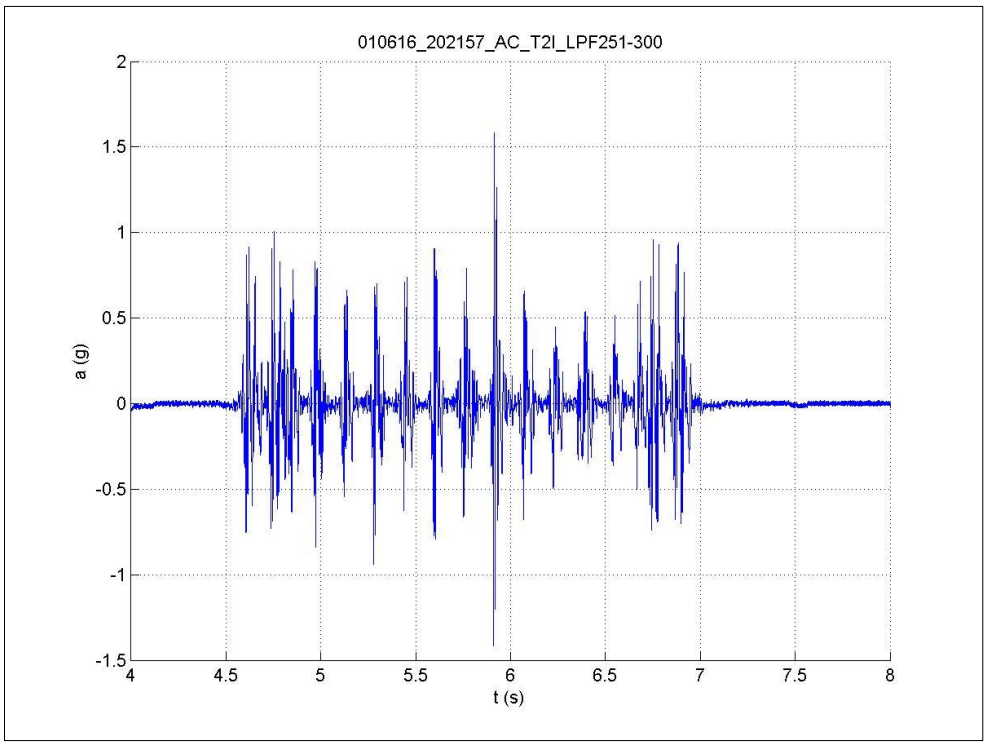

Figure 36: Sleeper acceleration signal in the inner side of sleeper T2 induced by 20:21:57 train.

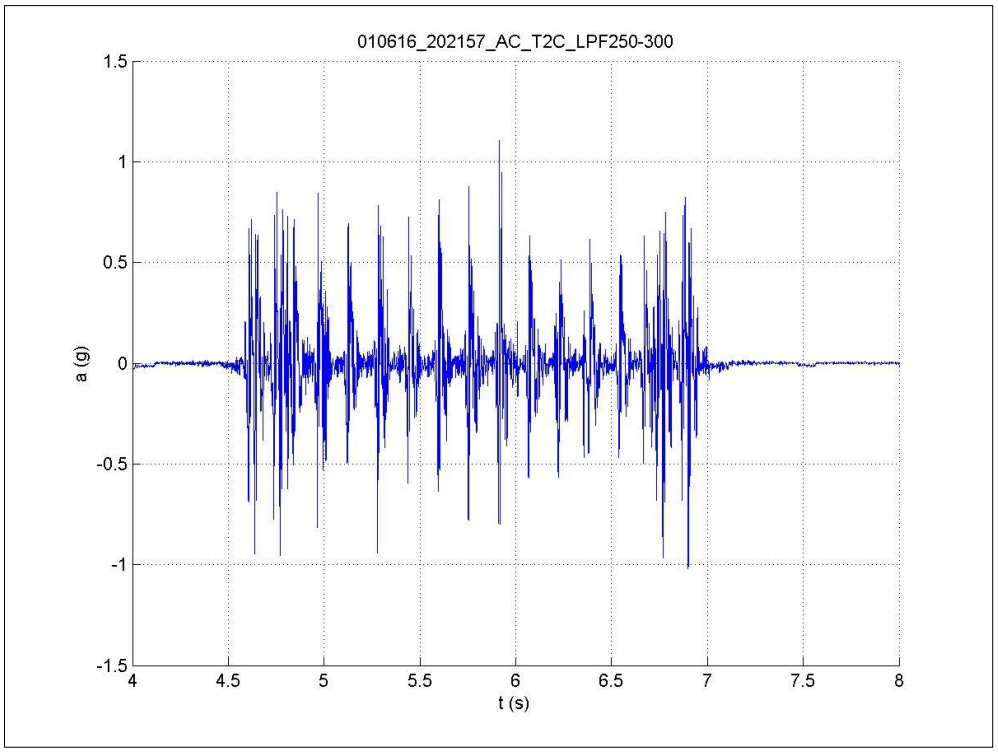

Figure 37: Sleeper acceleration signal in the center of sleeper T2 induced by 20:21:57 train.

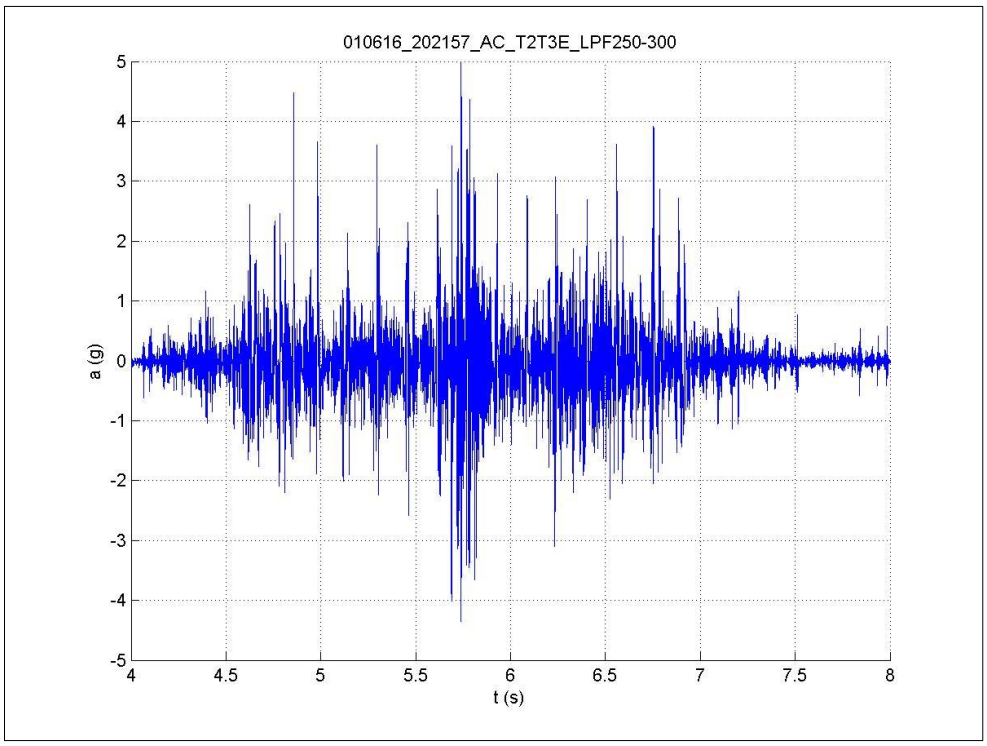

Figure 38: Rail acceleration signal in the outer rail between T2 and T3 induced by 20:21:57 train.

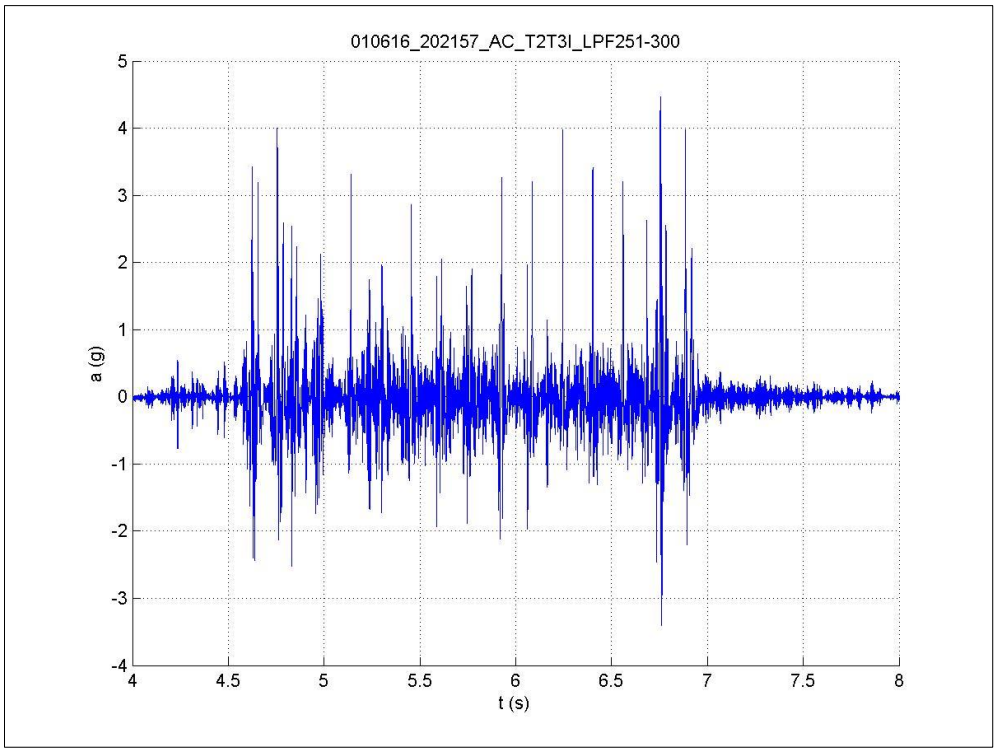

Figure 39: Rail acceleration signal in the inner rail between T2 and T3 induced by 20:21:57 train.

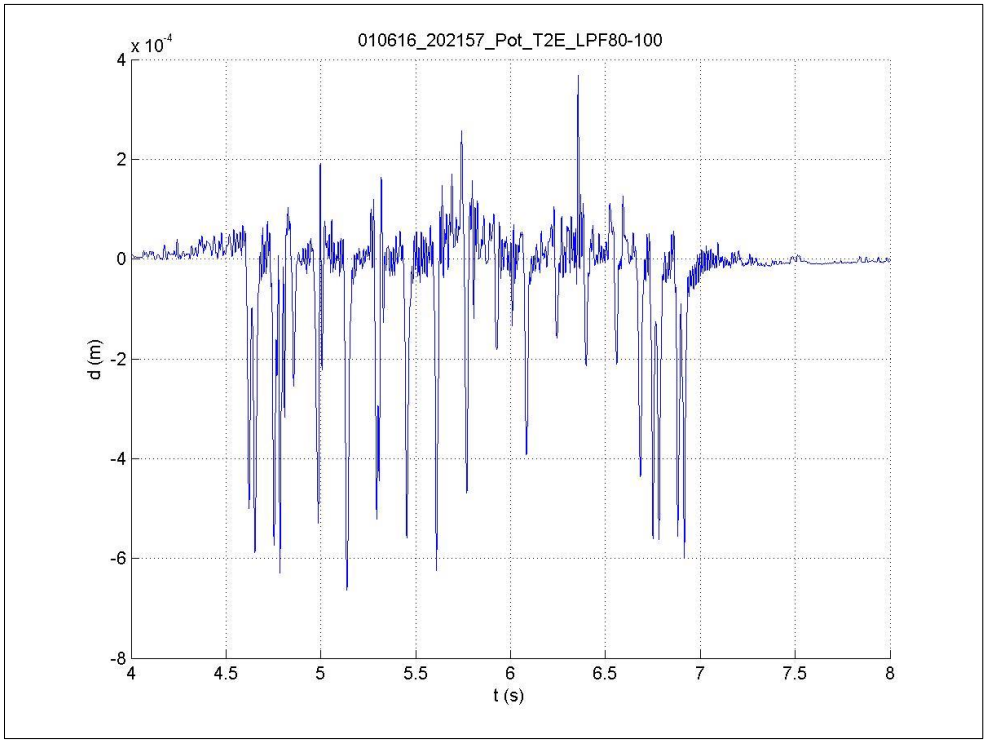

Figure 40: Relative displacement between outer rail and sleeper T2 induced by 20:21:57 train.

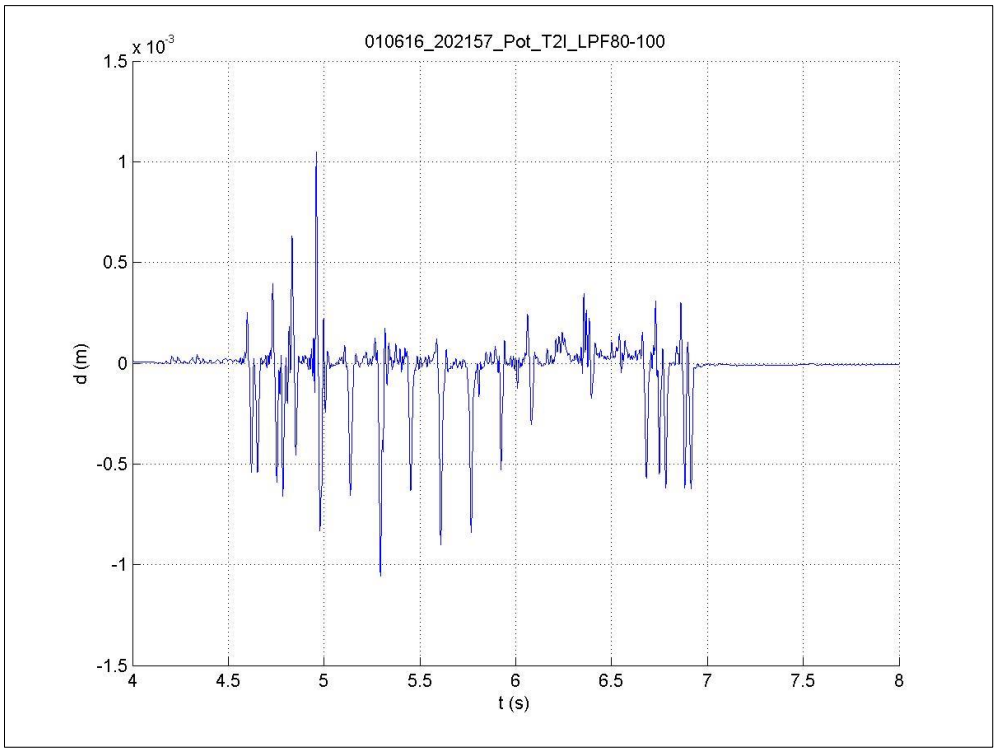

Figure 41: Relative displacement between inner rail and sleeper T2 induced by 20:21:57 train.

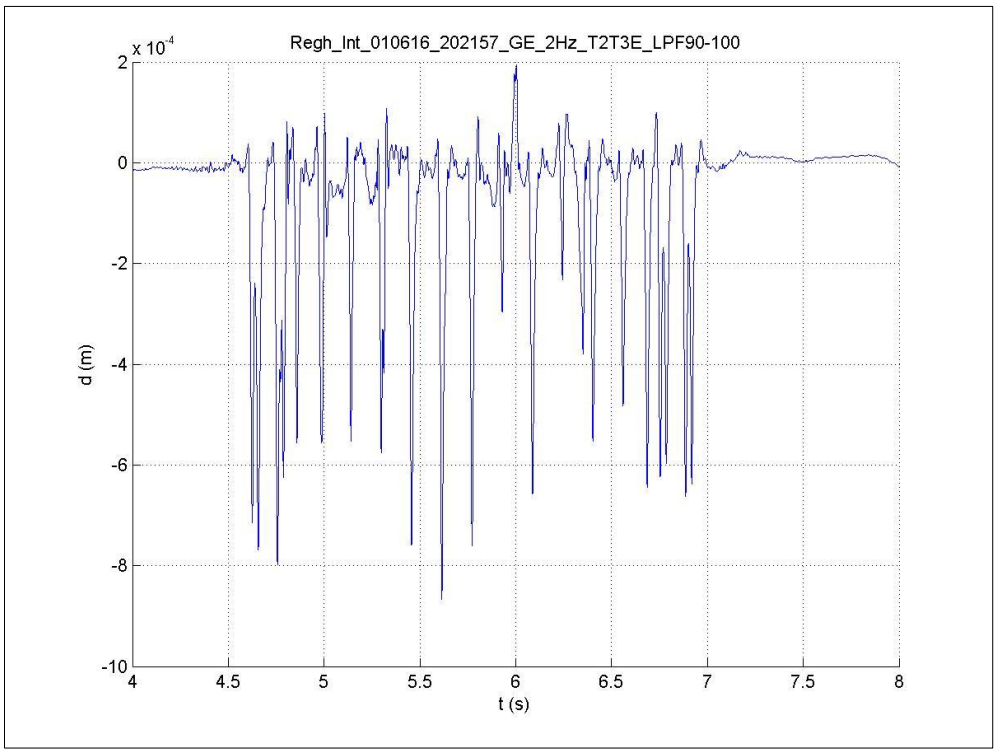

Figure 42: Rail deflection in the outer rail between T2 and T3 induced by 20:21:57 train.

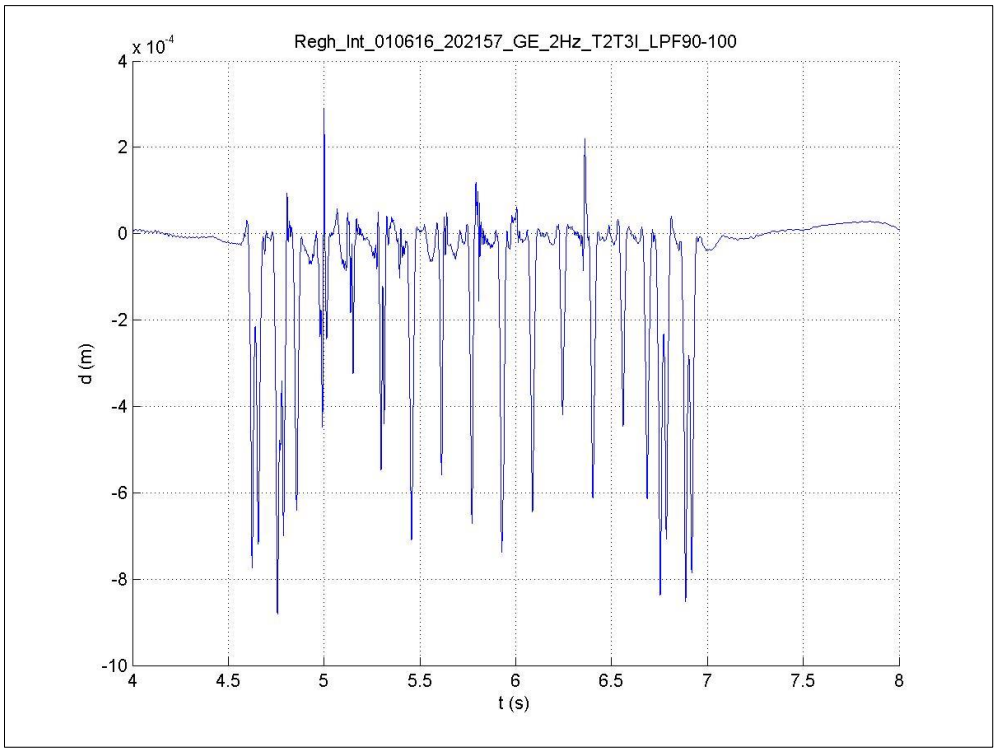

Figure 43: Rail deflection in the inner rail between T2 and T3 induced by 20:21:57 train.

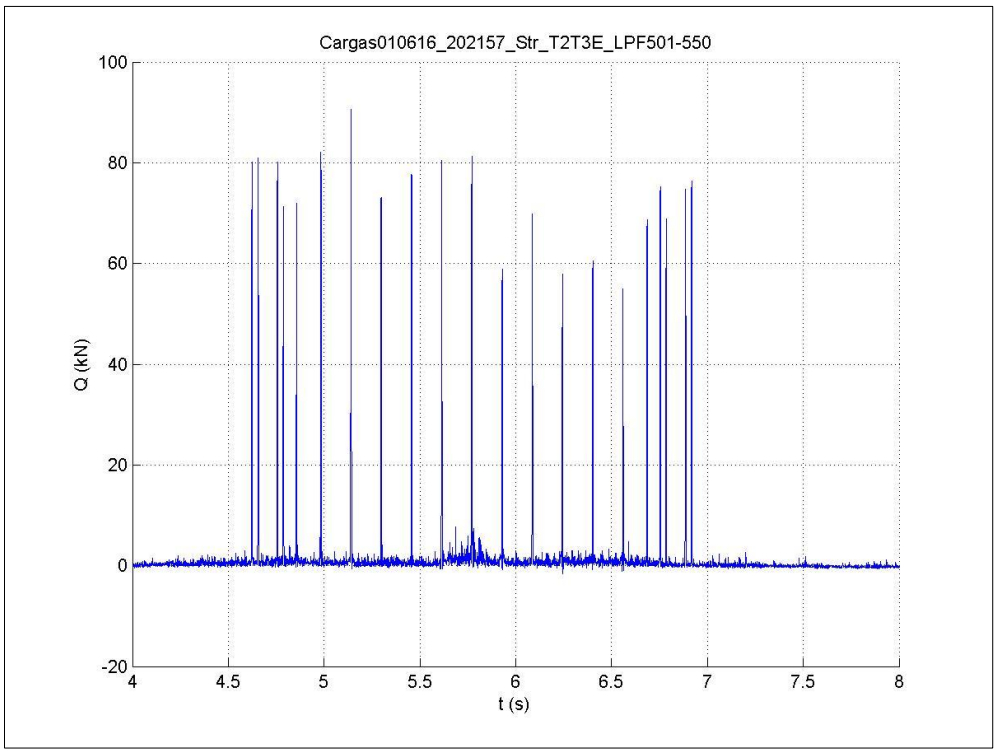

Figure 44: Loads in the outer rail between T2 and T3 induced by 20:21:57 train.

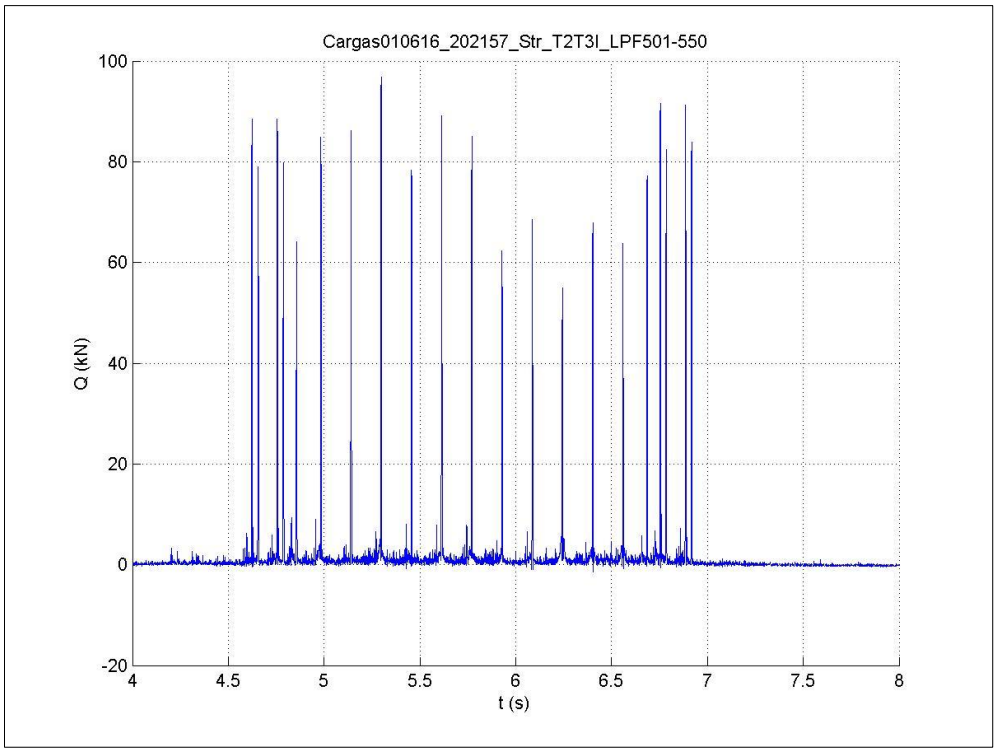

Figure 45: Loads in the inner rail between T2 and T3 induced by 20:21:57 train.

5 Train S102 (Time 19:32:45 / 21 axles / 257 km/h)

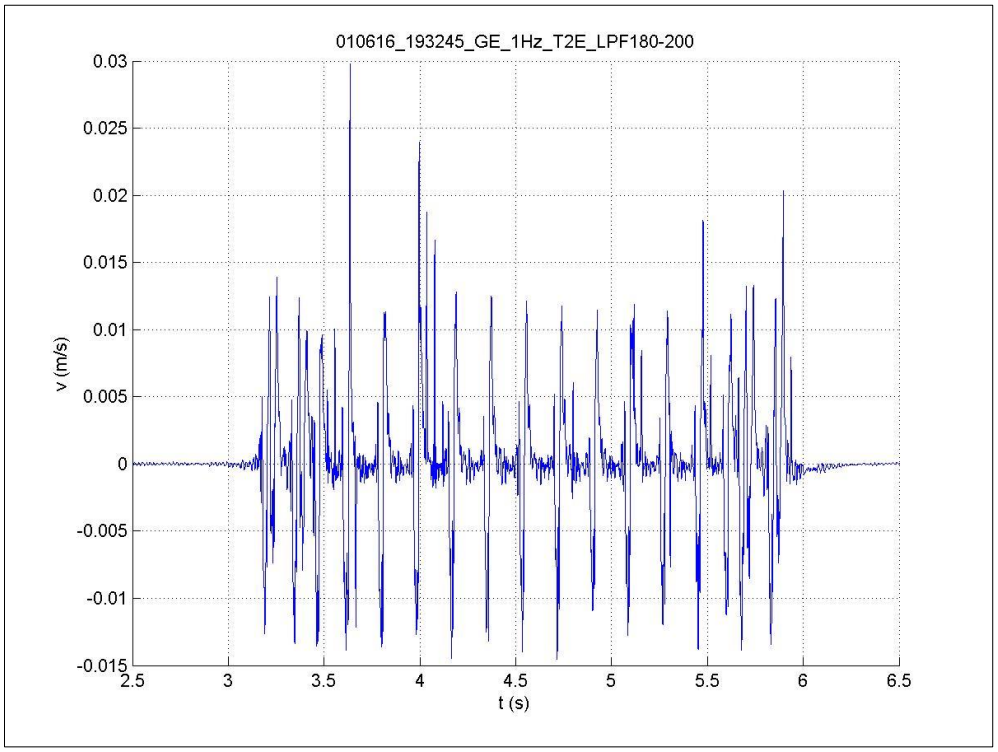

Figure 46: Sleeper velocity signal in the outer side of sleeper T2 induced by 19:32:45 train.

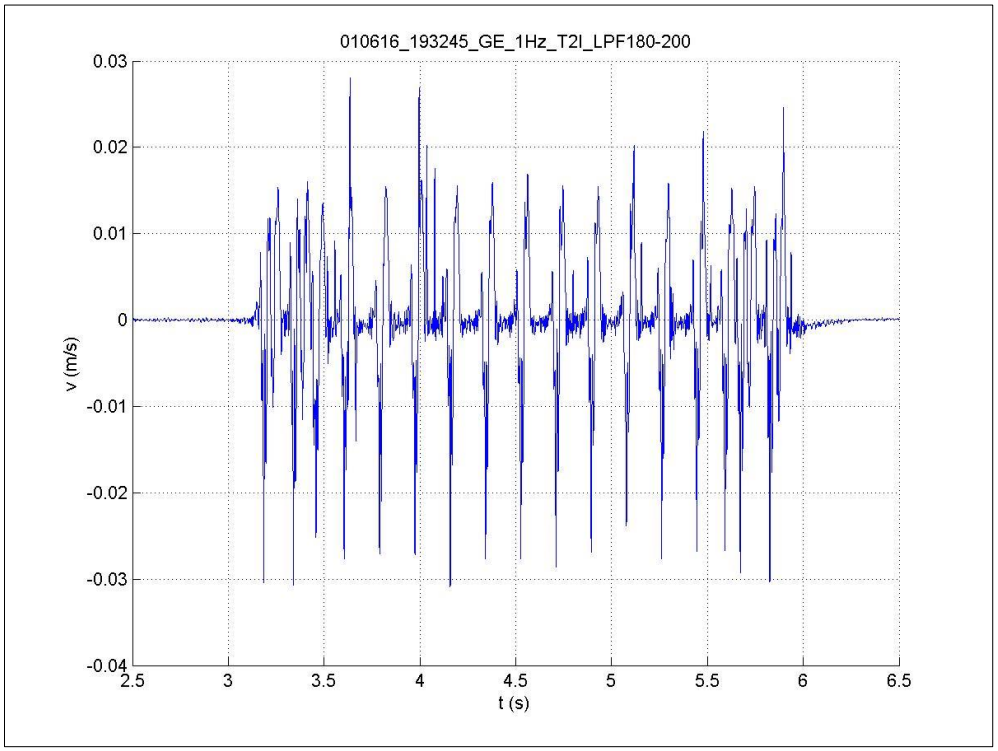

Figure 47: Sleeper velocity signal in the inner side of sleeper T2 induced by 19:32:45 train.

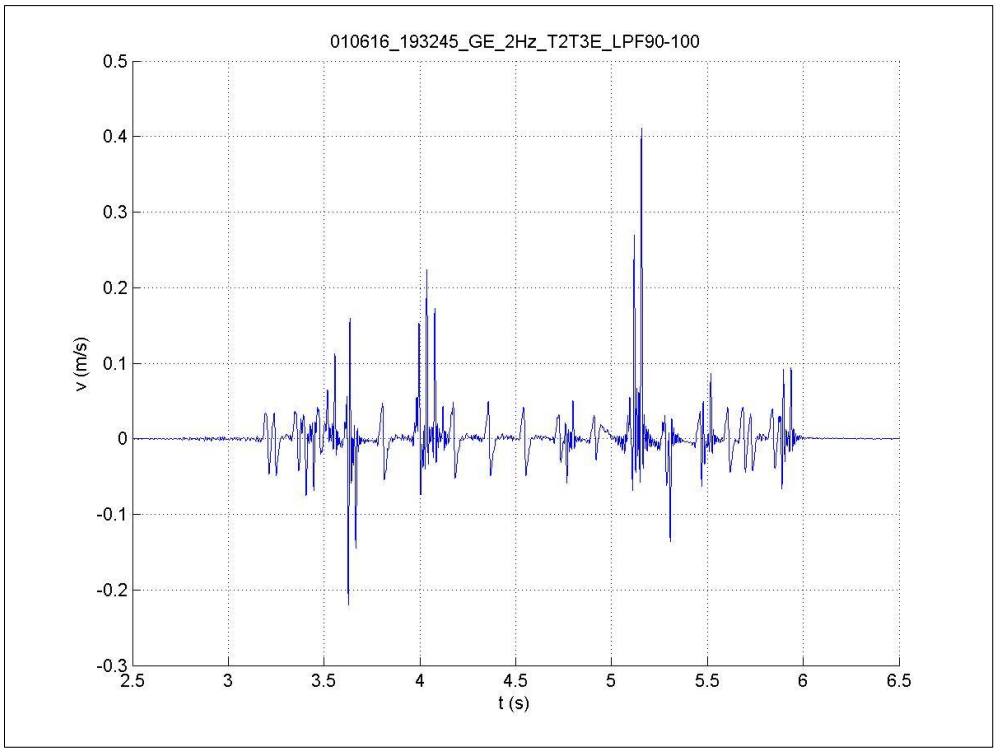

Figure 48: Rail velocity signal in the outer rail between T2 and T3 induced by 19:32:45 train.

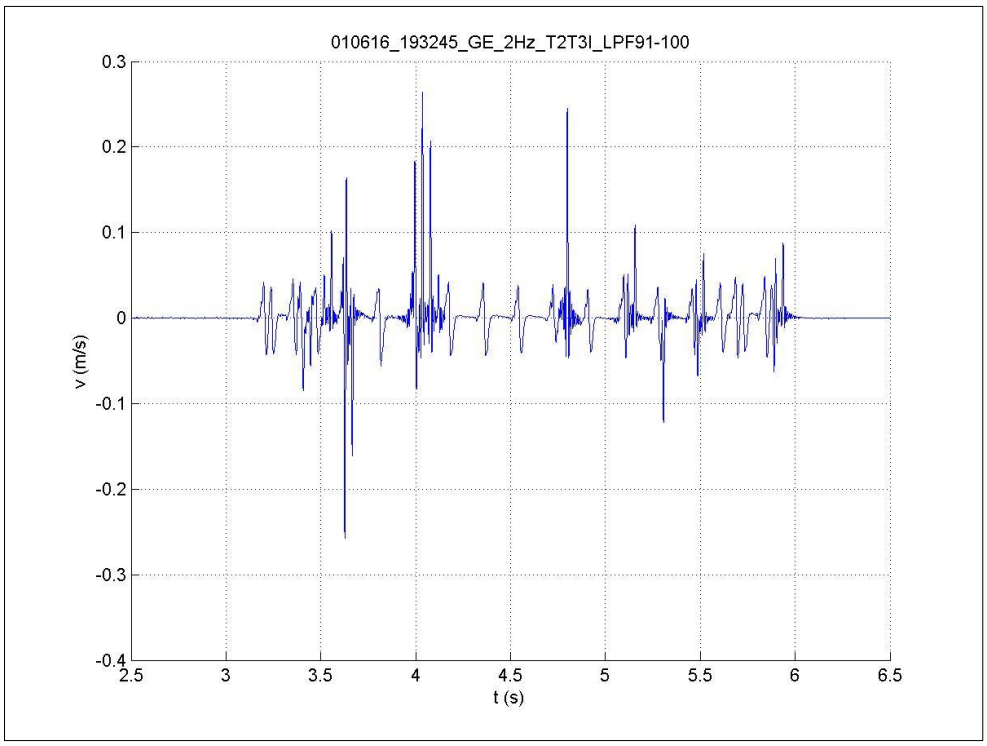

Figure 49: Rail velocity signal in the inner rail between T2 and T3 induced by 19:32:45 train.

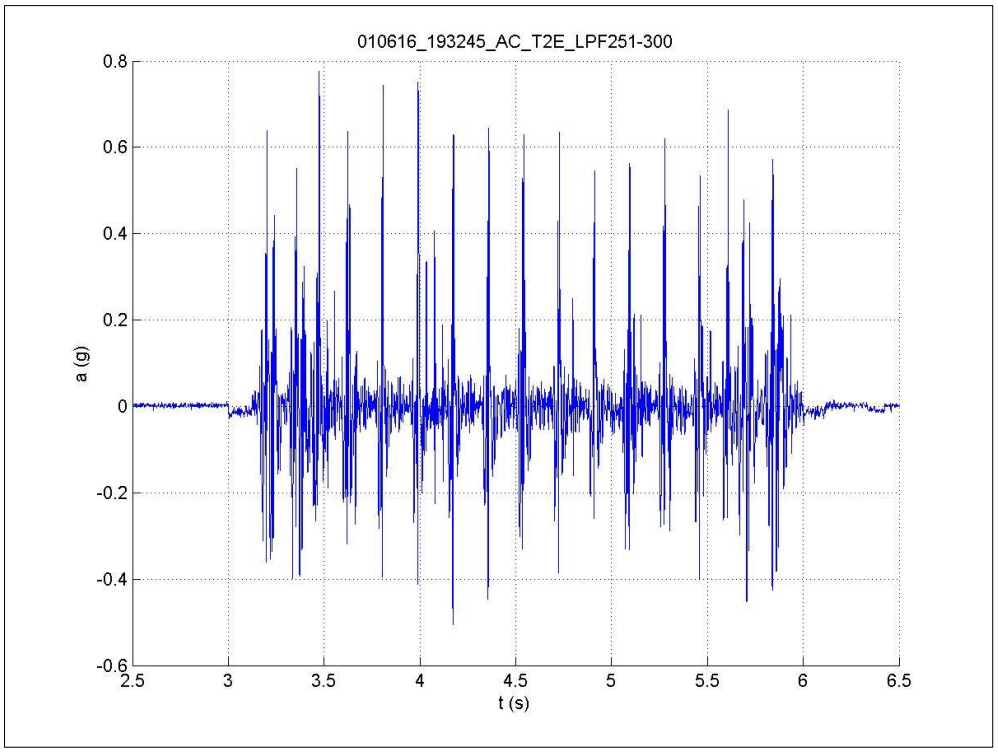

Figure 50: Sleeper acceleration signal in the outer side of sleeper T2 induced by 19:32:45 train.

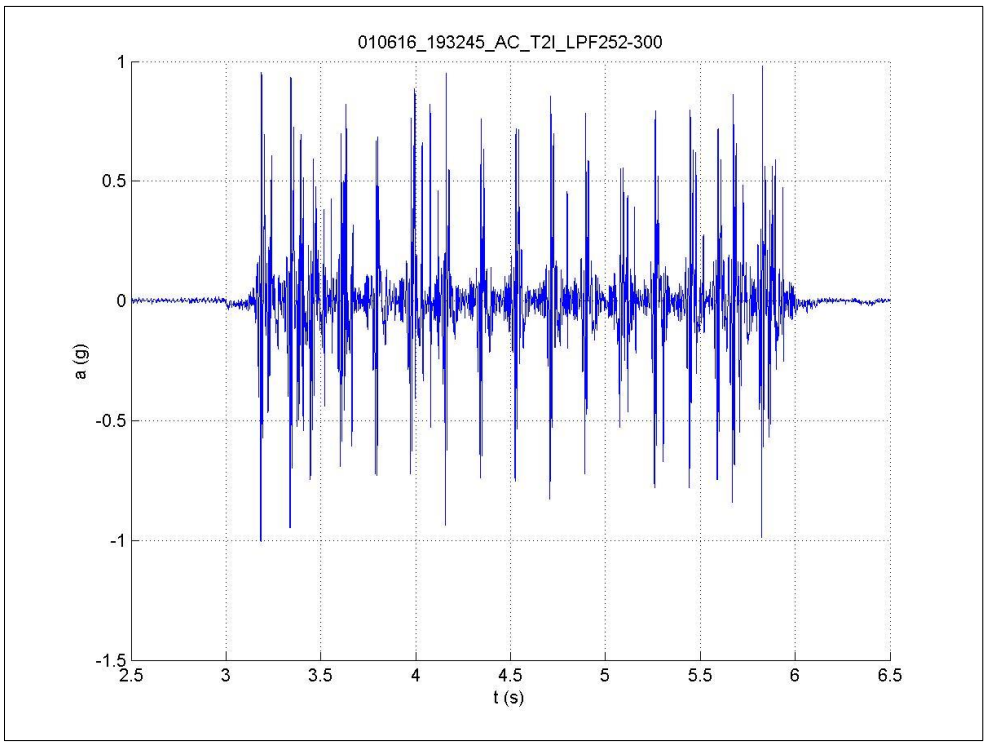

Figure 51: Sleeper acceleration signal in the inner side of sleeper T2 induced by 19:32:45 train.

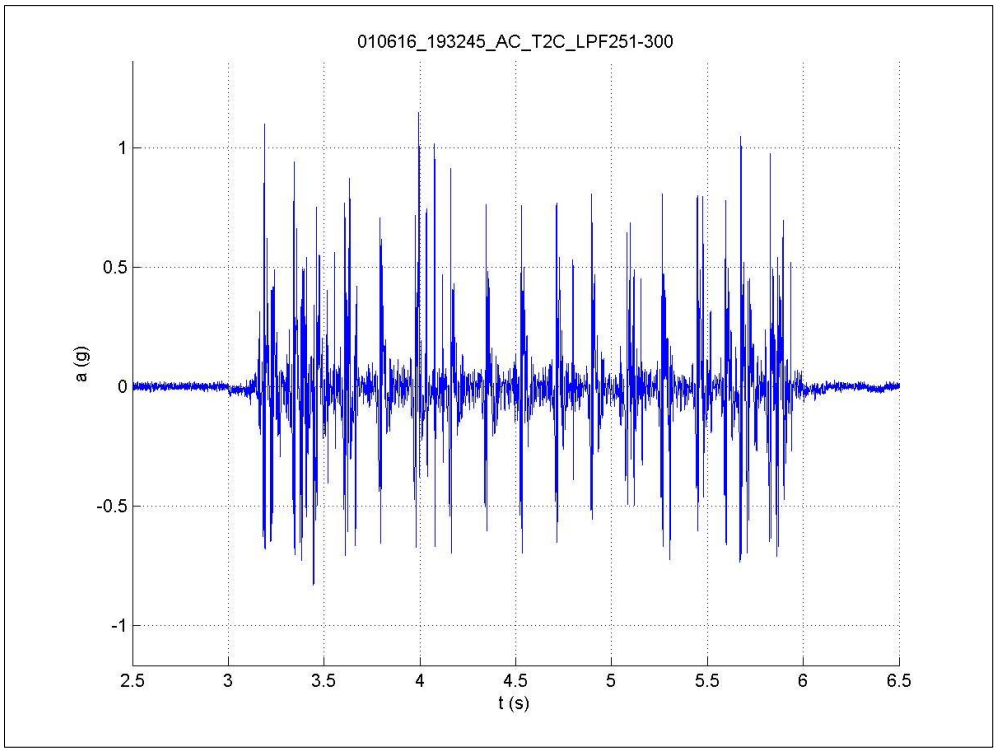

Figure 52: Sleeper acceleration signal in the center of sleeper T2 induced by 19:32:45 train.

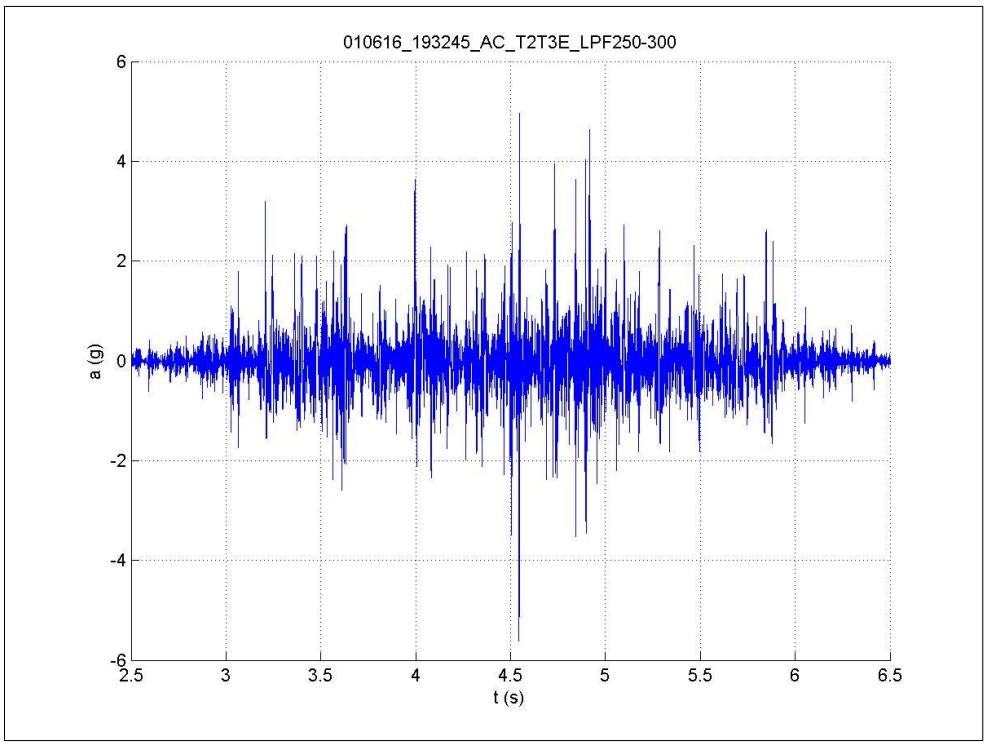

Figure 53: Rail acceleration signal in the outer rail between T2 and T3 induced by 19:32:45 train.

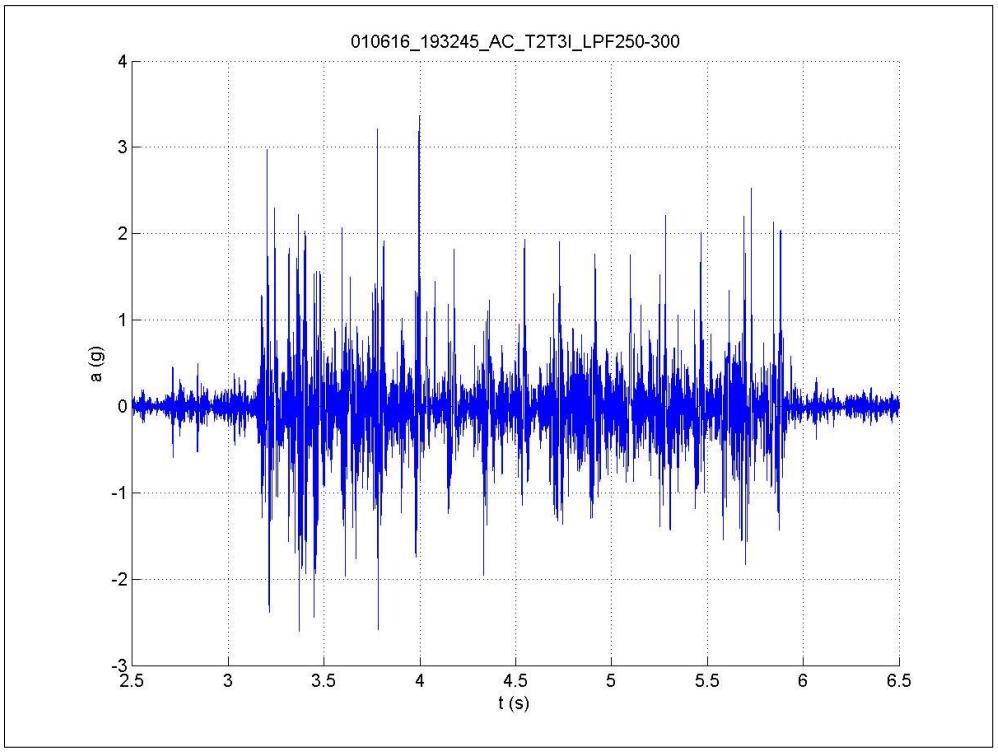

Figure 54: Rail acceleration signal in the inner rail between T2 and T3 induced by 19:32:45 train.

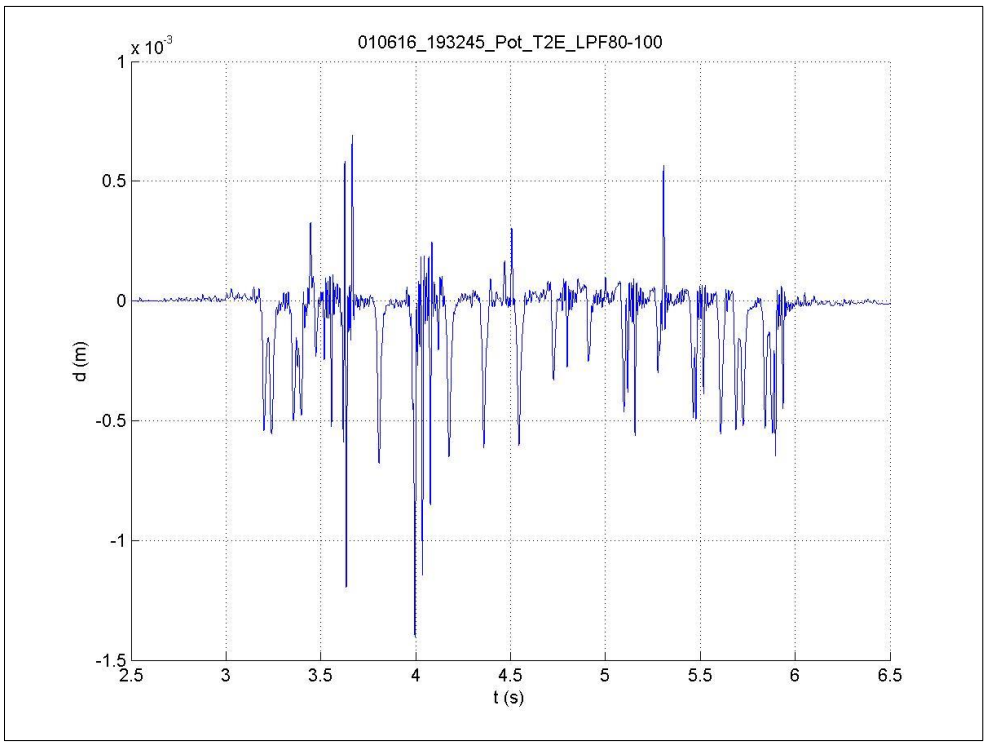

Figure 55: Relative displacement between outer rail and sleeper T2 induced by 19:32:45 train.

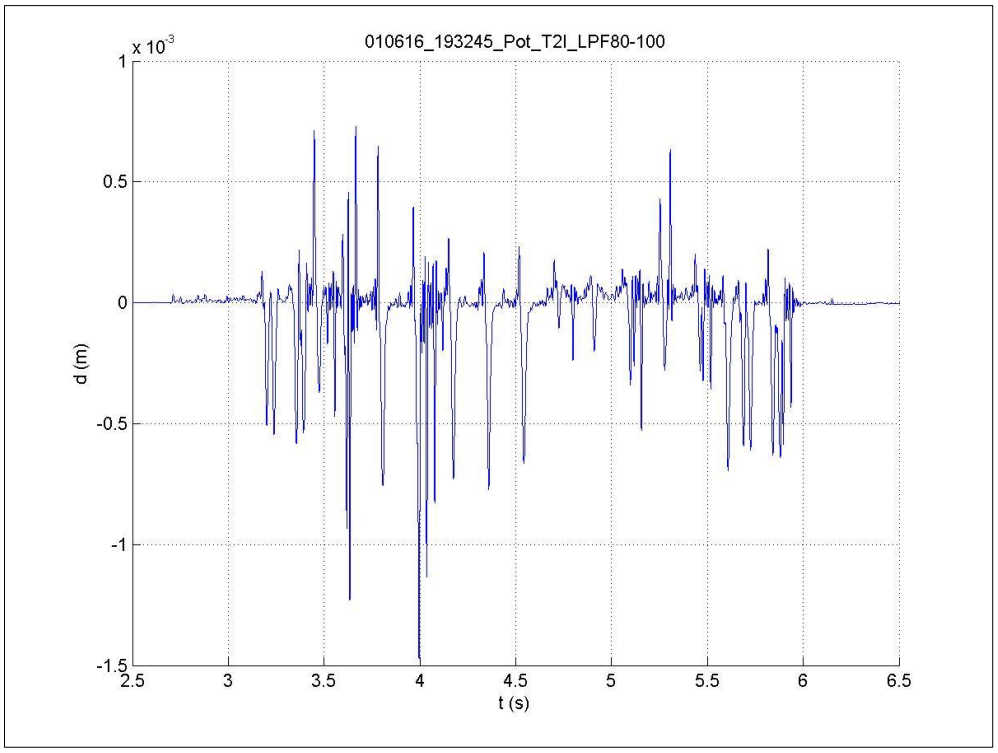

Figure 56: Relative displacement between inner rail and sleeper T2 induced by 19:32:45 train.

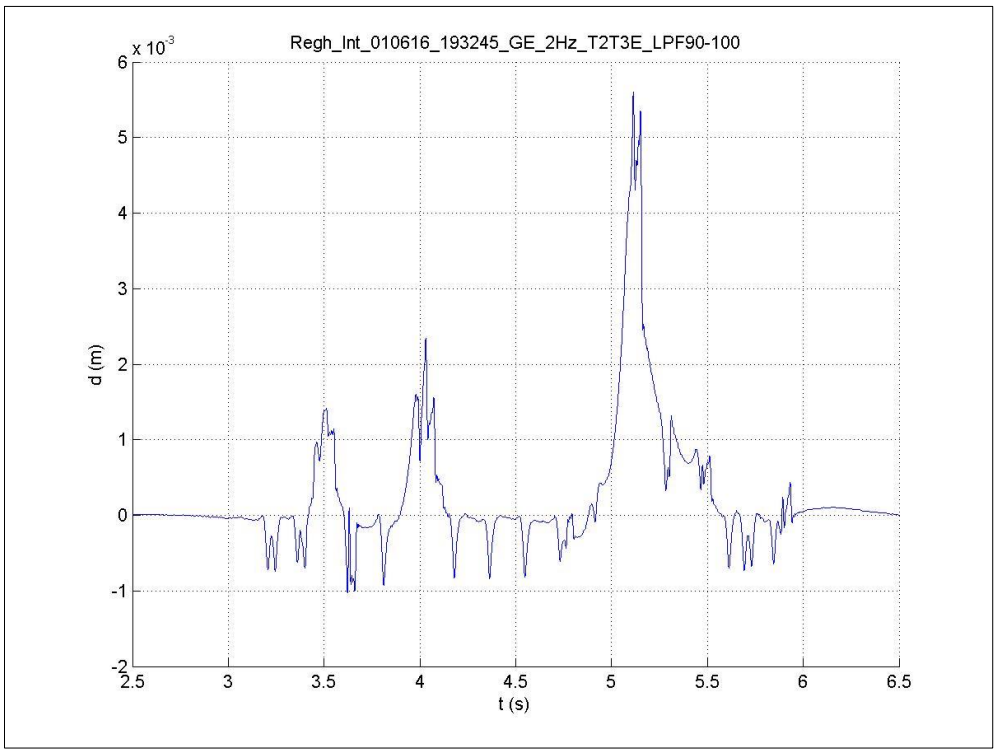

Figure 57: Rail deflection in the outer rail between T2 and T3 induced by 19:32:45 train.

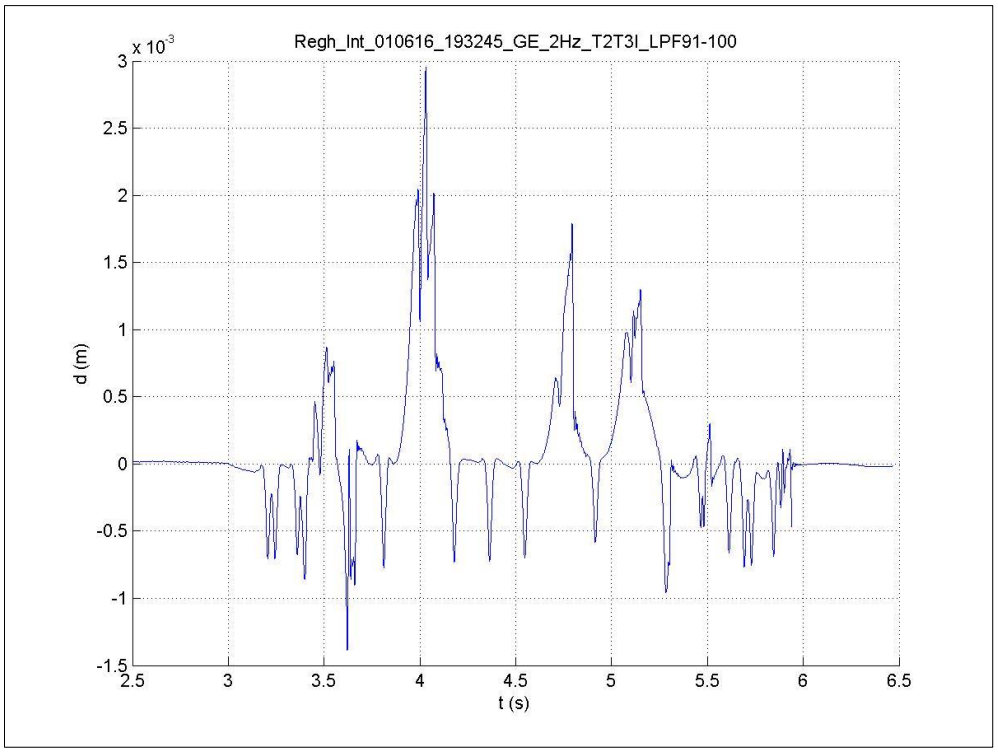

Figure 58: Rail deflection in the inner rail between T2 and T3 induced by 19:32:45 train.

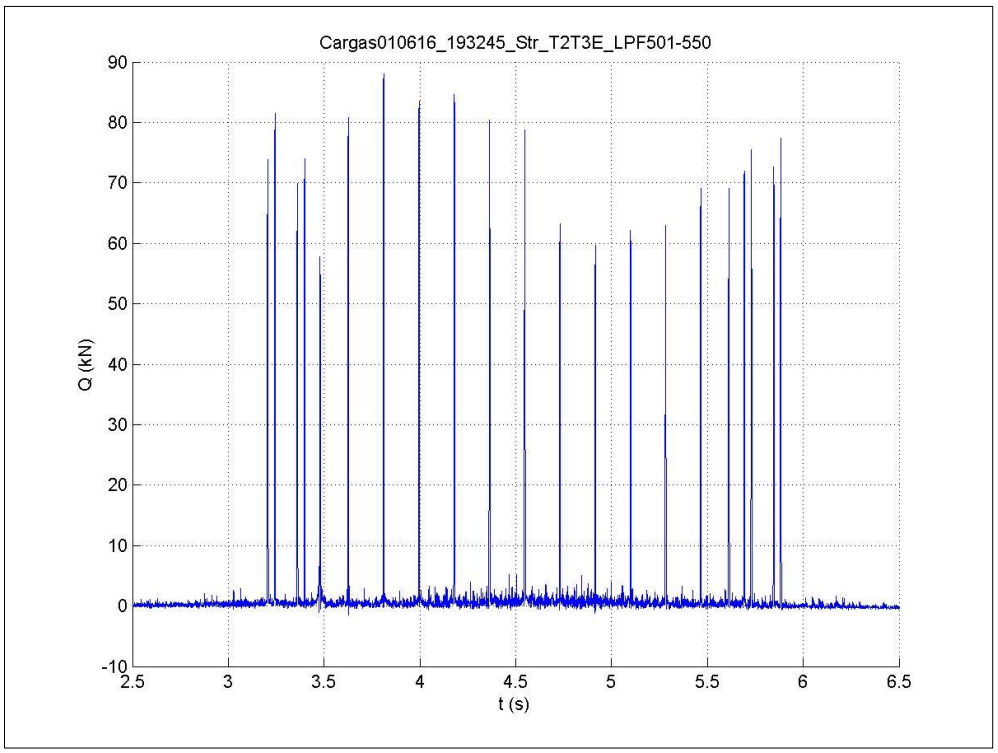

Figure 59: Loads in the outer rail between T2 and T3 induced by 19:32:45 train.

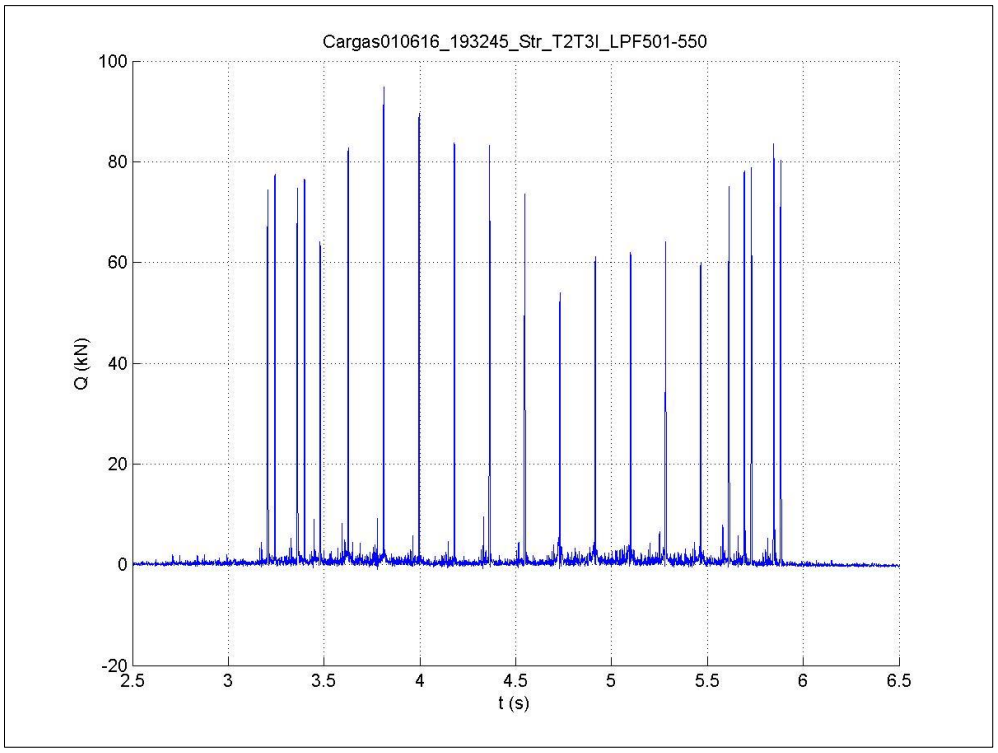

Figure 60: Loads in the inner rail between T2 and T3 induced by 19:32:45 train.

6 Train S103 (Time 17:24:26 / 64 axles / 298 km/h)

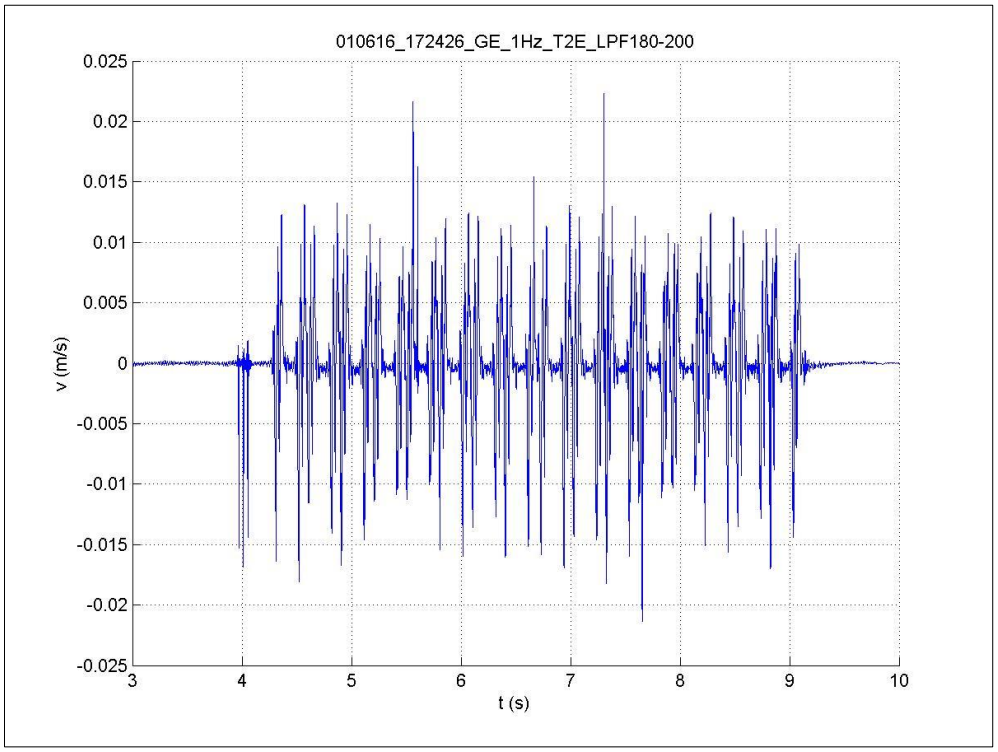

Figure 61: Sleeper velocity signal in the outer side of sleeper T2 induced by 17:24:26 train.

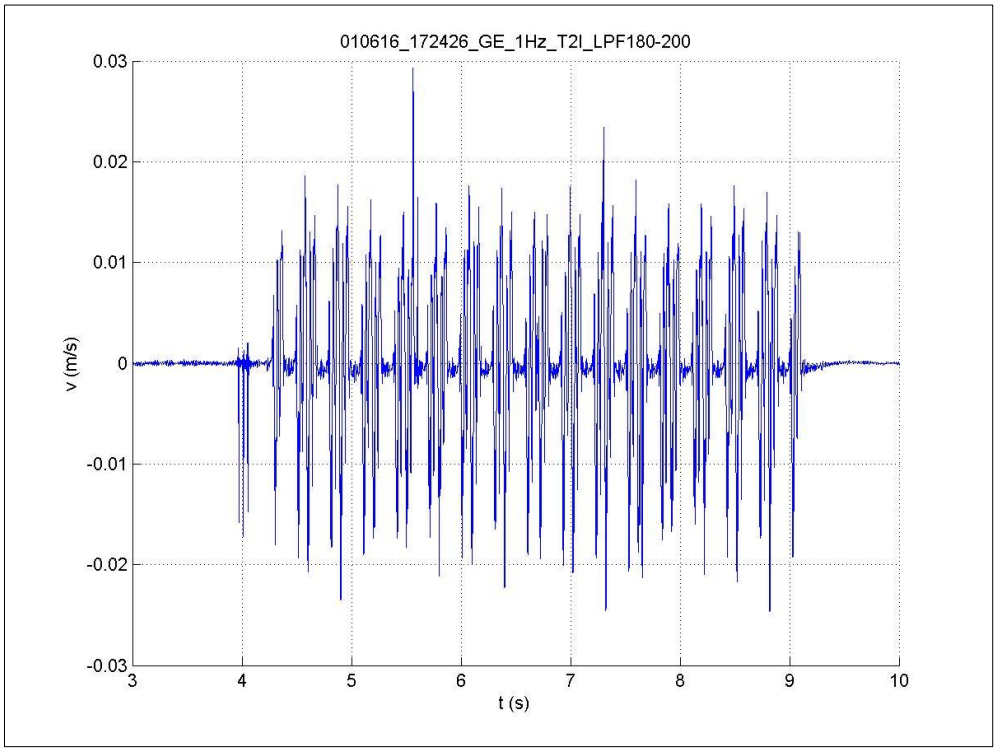

Figure 62: Sleeper velocity signal in the inner side of sleeper T2 induced by 17:24:26 train.

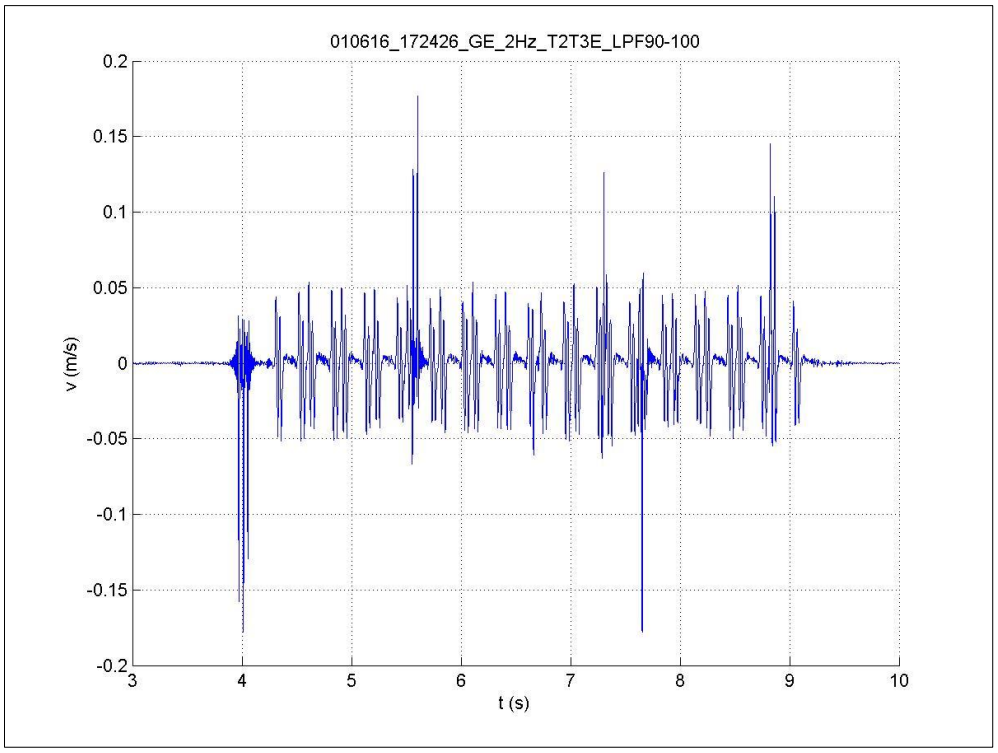

Figure 63: Rail velocity signal in the outer rail between T2 and T3 induced by 17:24:26 train.

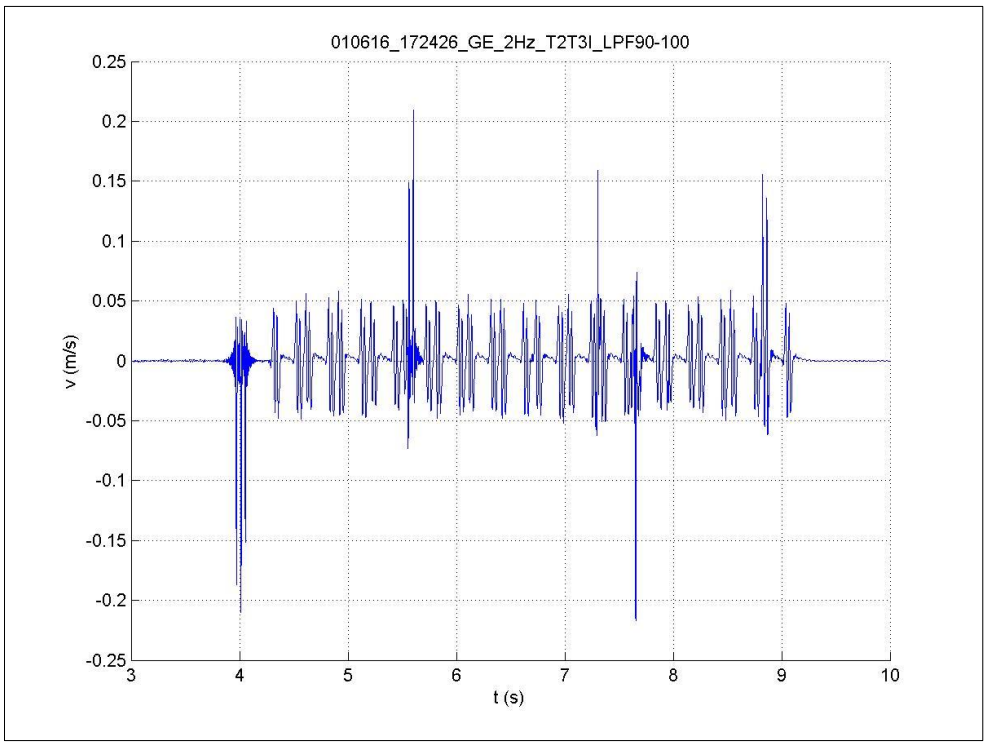

Figure 64: Rail velocity signal in the inner rail between T2 and T3 induced by 17:24:26 train.

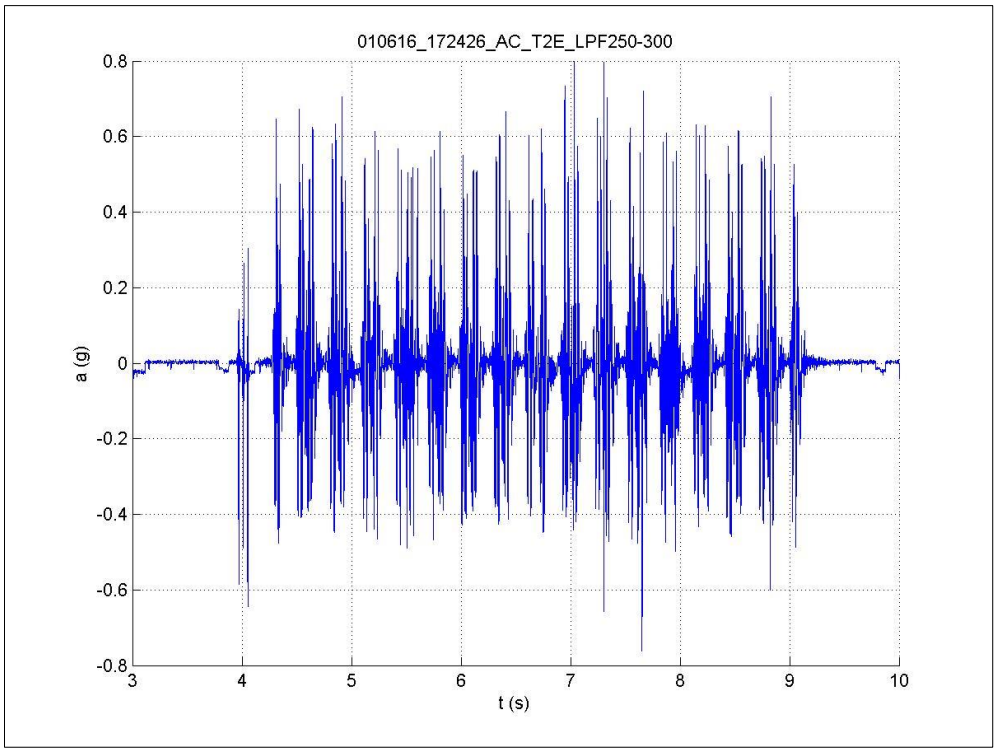

Figure 65: Sleeper acceleration signal in the outer side of sleeper T2 induced by 17:24:26 train.

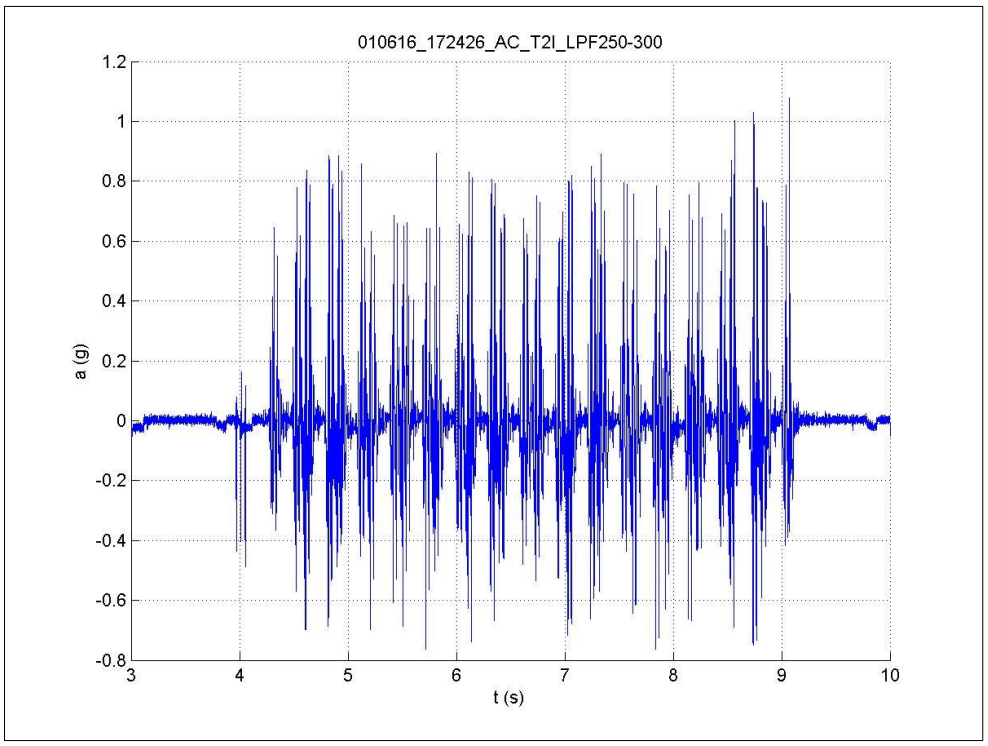

Figure 66: Sleeper acceleration signal in the inner side of sleeper T2 induced by 17:24:26 train.

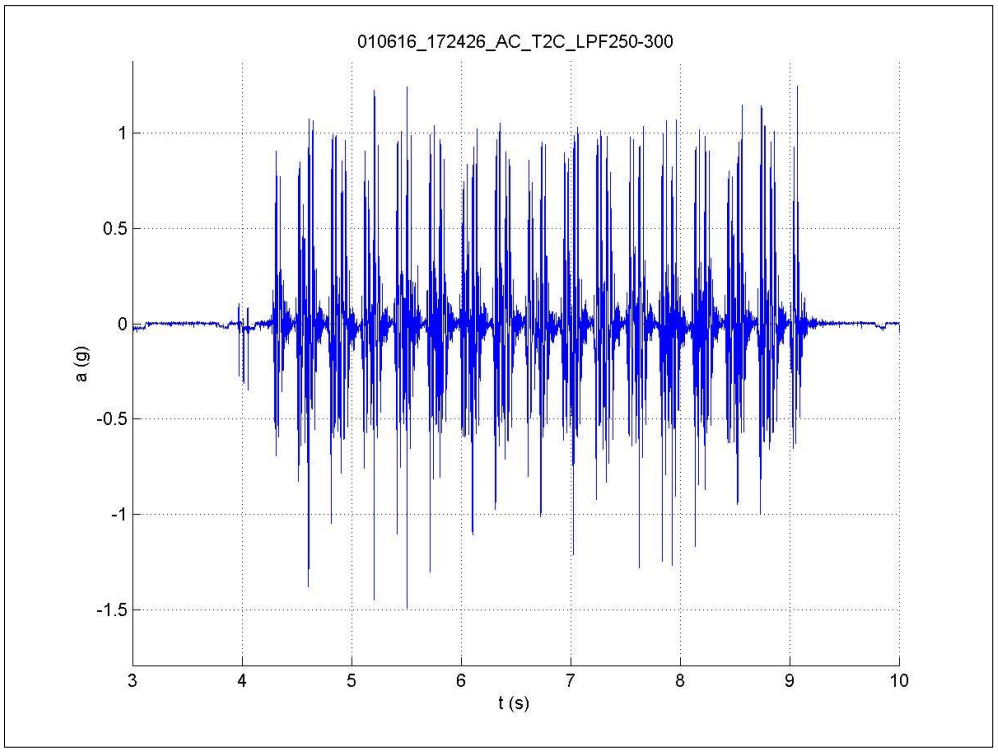

Figure 67: Sleeper acceleration signal in the center of sleeper T2 induced by 17:24:26 train.

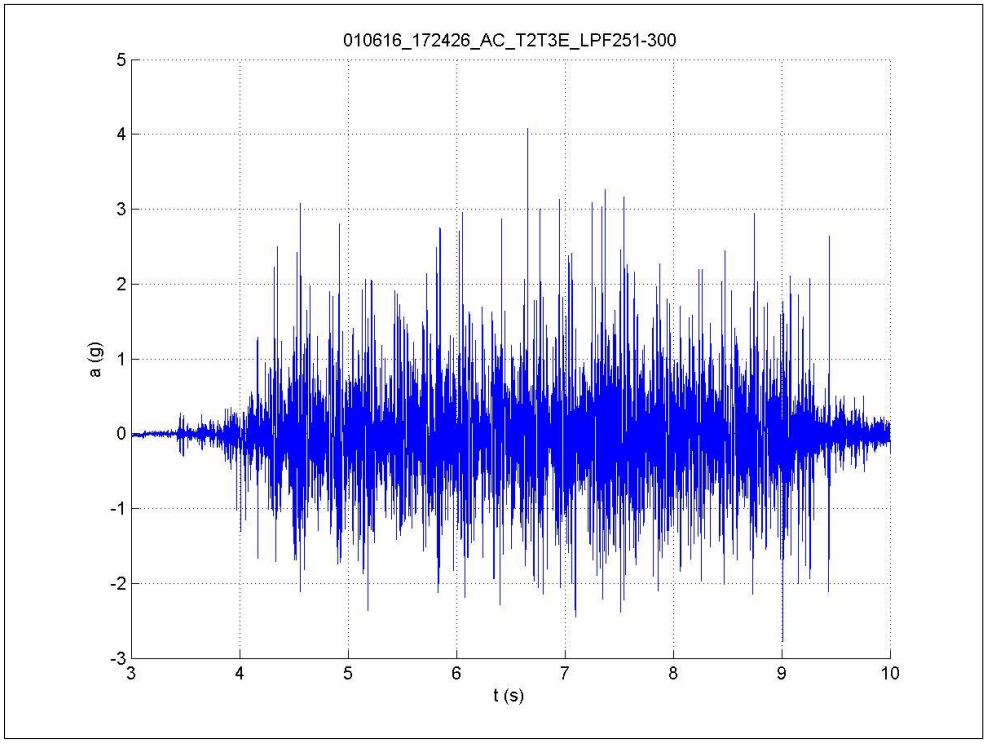

Figure 68: Rail acceleration signal in the outer rail between T2 and T3 induced by 17:24:26 train.

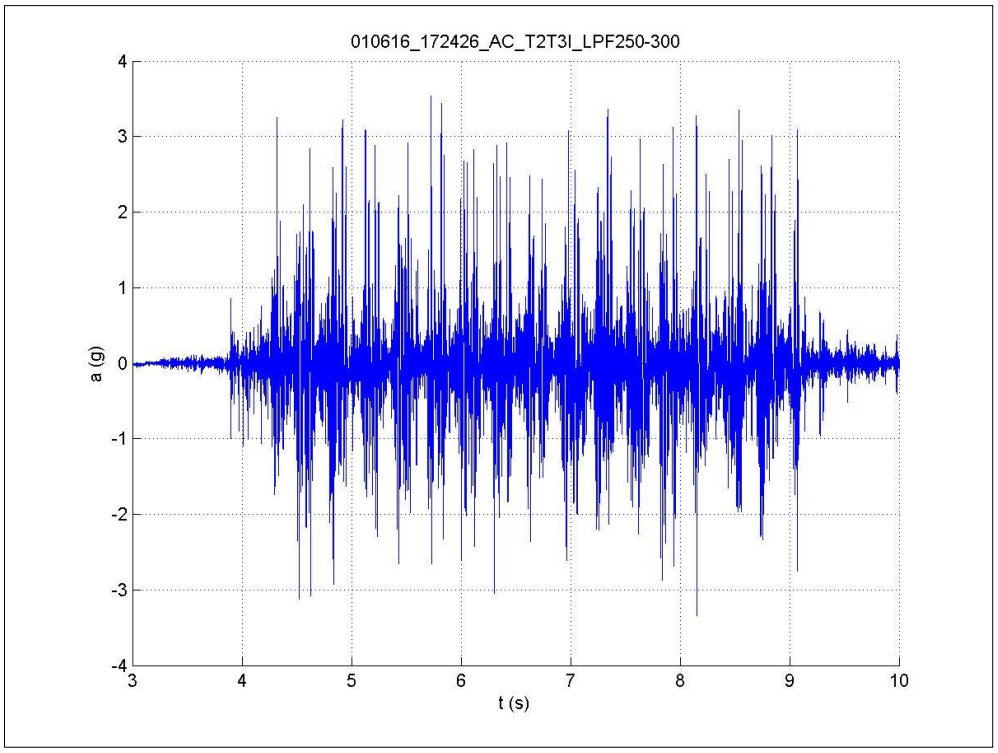

Figure 69: Rail acceleration signal in the inner rail between T2 and T3 induced by 17:24:26 train.

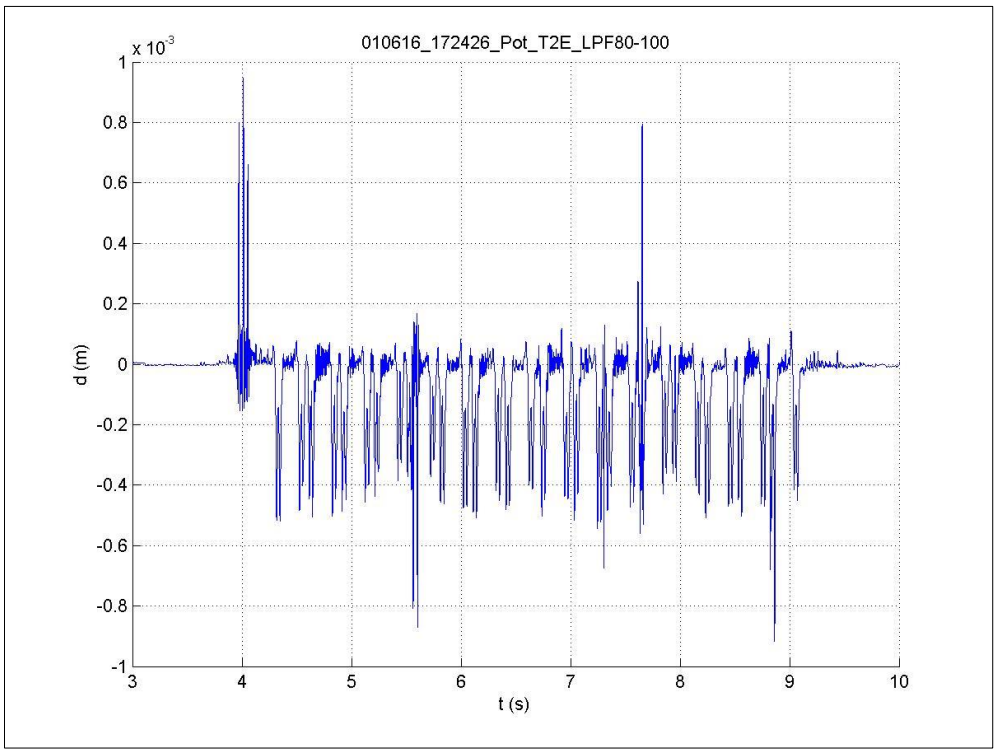

Figure 70: Relative displacement between outer rail and sleeper T2 induced by 17:24:26 train.

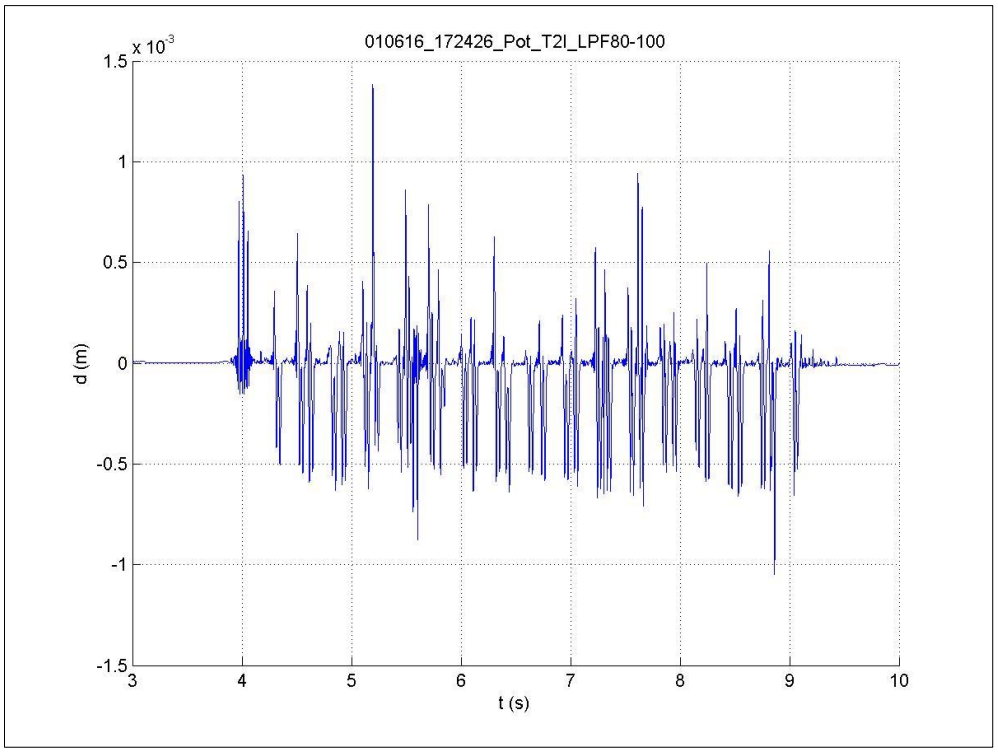

Figure 71: Relative displacement between inner rail and sleeper T2 induced by 17:24:26 train.

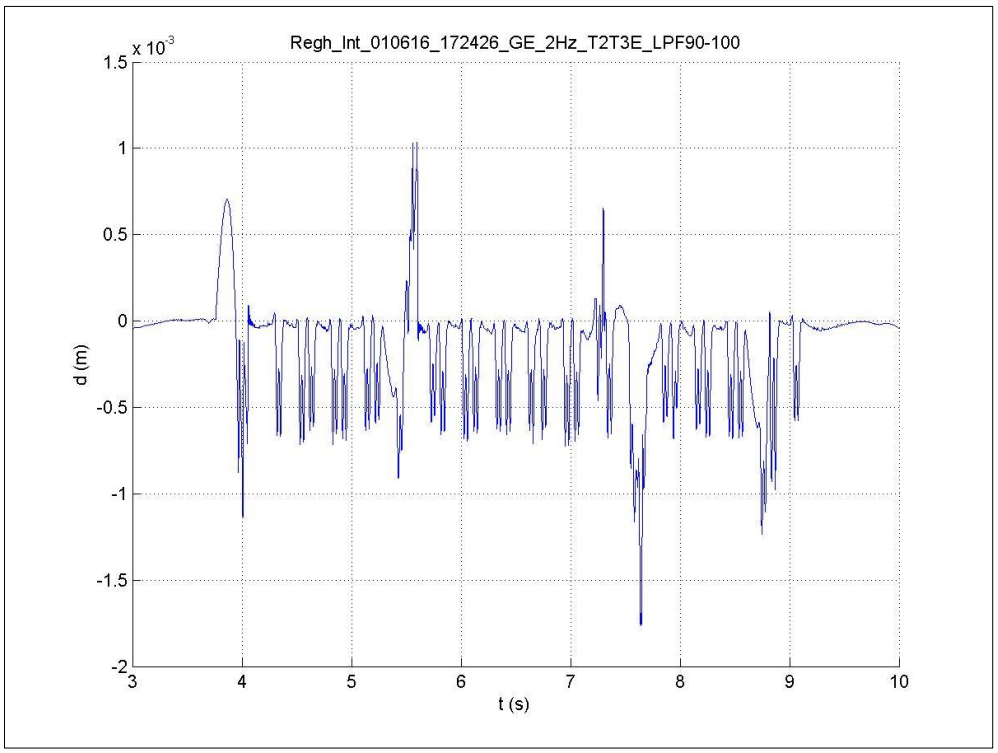

Figure 72: Rail deflection in the outer rail between T2 and T3 induced by 17:24:26 train.

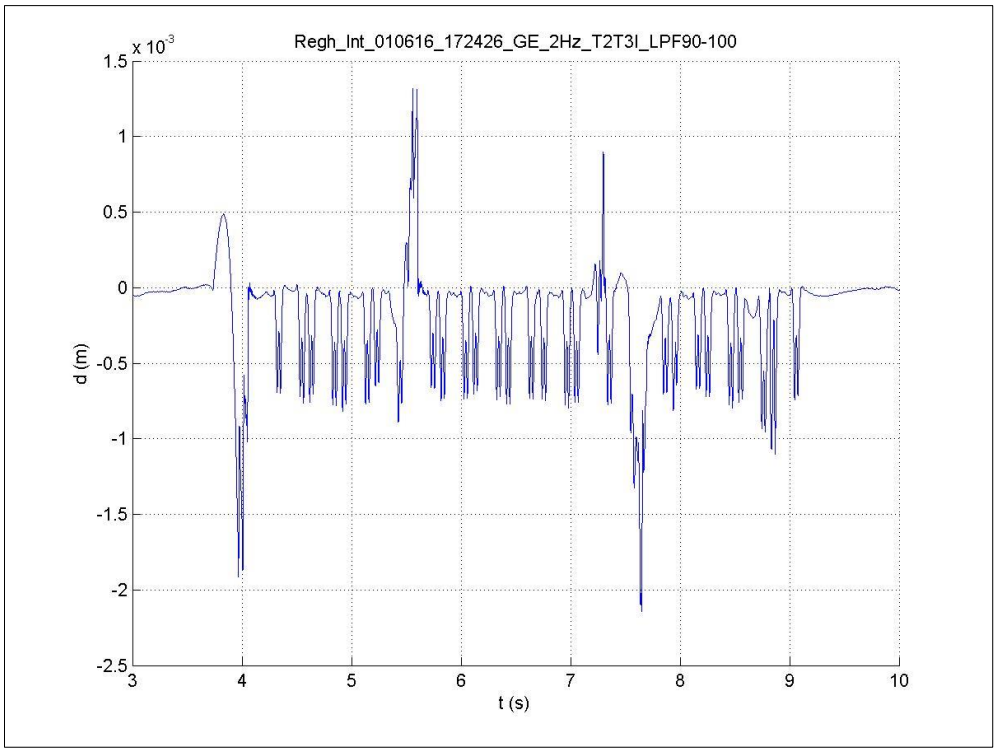

Figure 73: Rail deflection in the inner rail between T2 and T3 induced by 17:24:26 train.

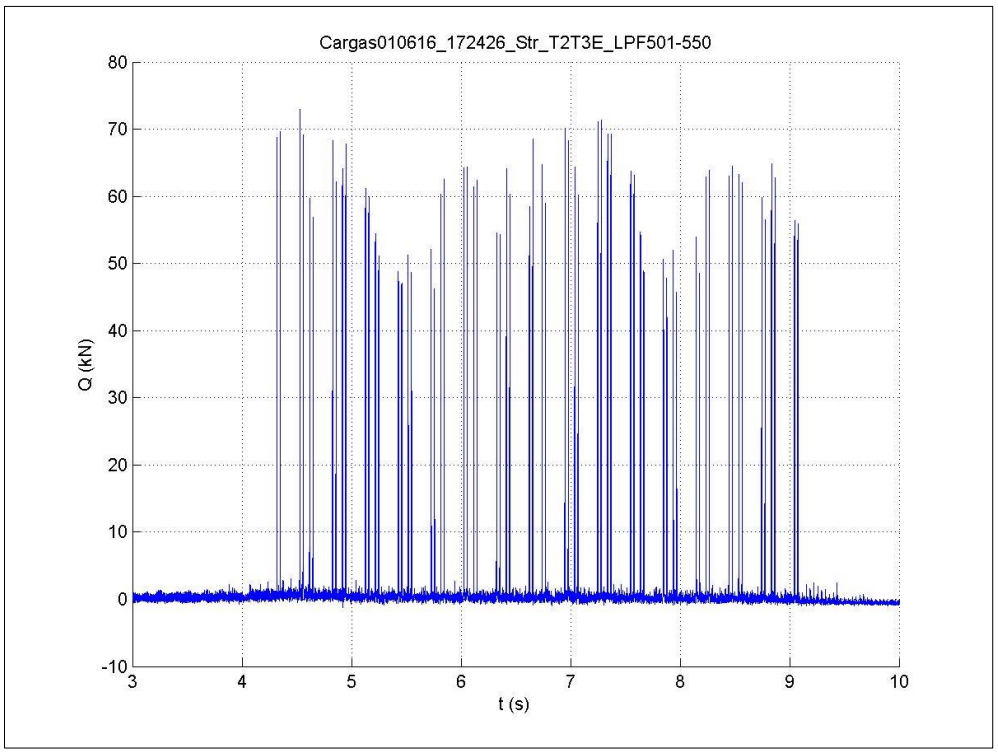

Figure 74: Loads in the outer rail between T2 and T3 induced by 17:24:26 train.

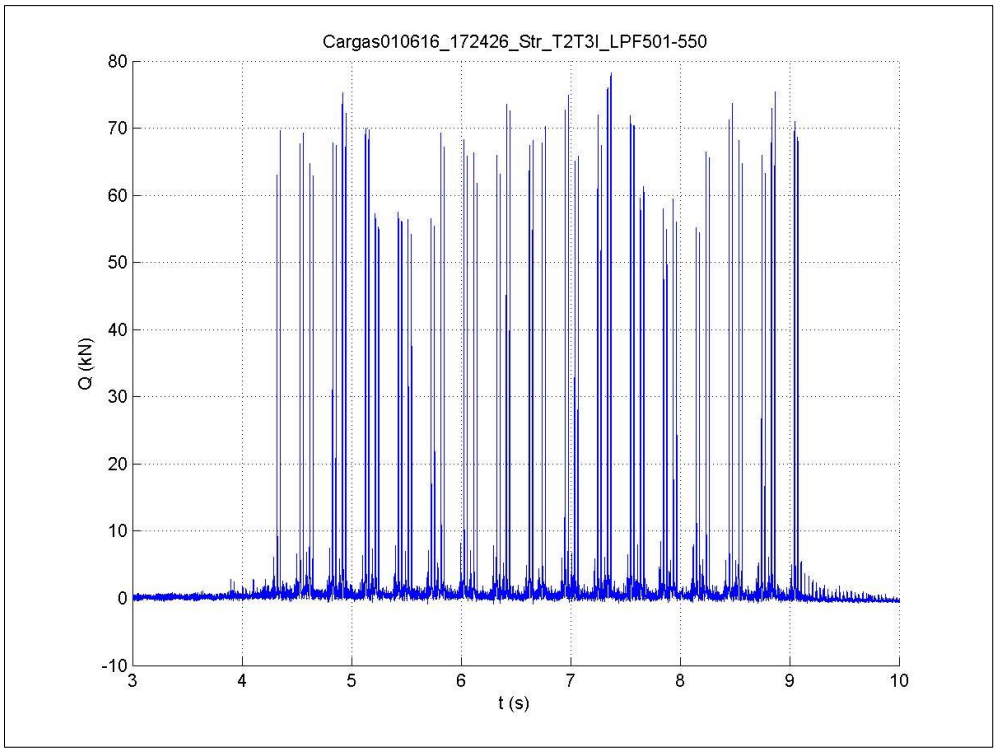

Figure 75: Loads in the inner rail between T2 and T3 induced by 17:24:26 train.

7 Train S102 (Time 11:35:54 / 42 axles / 299 km/h)

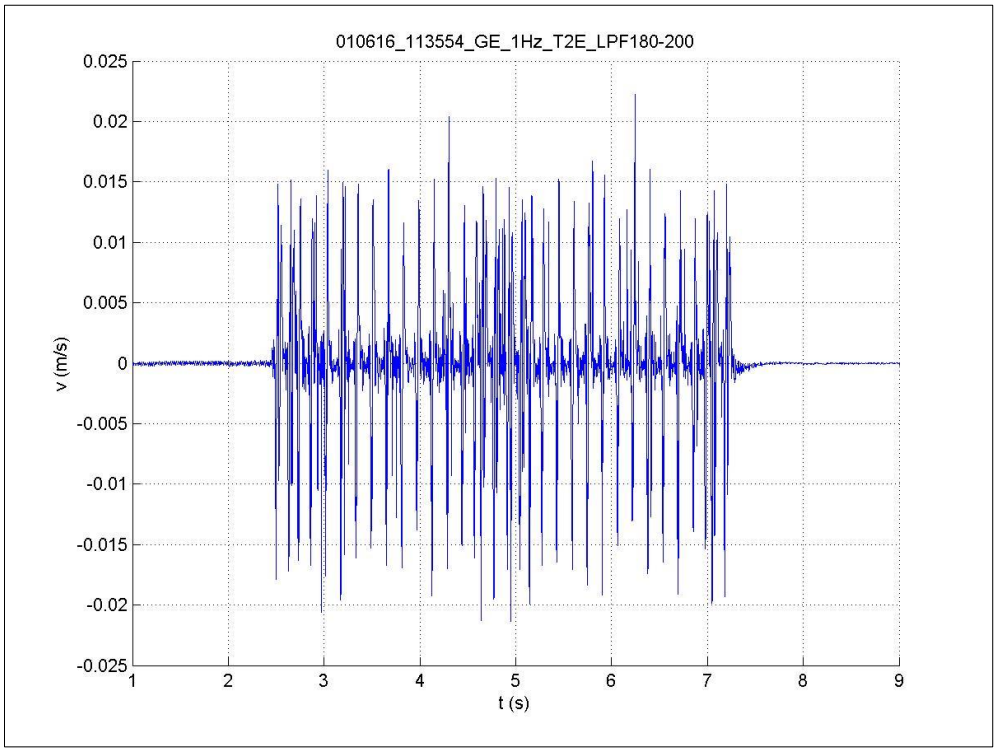

Figure 76: Sleeper velocity signal in the outer side of sleeper T2 induced by 11:35:54 train.

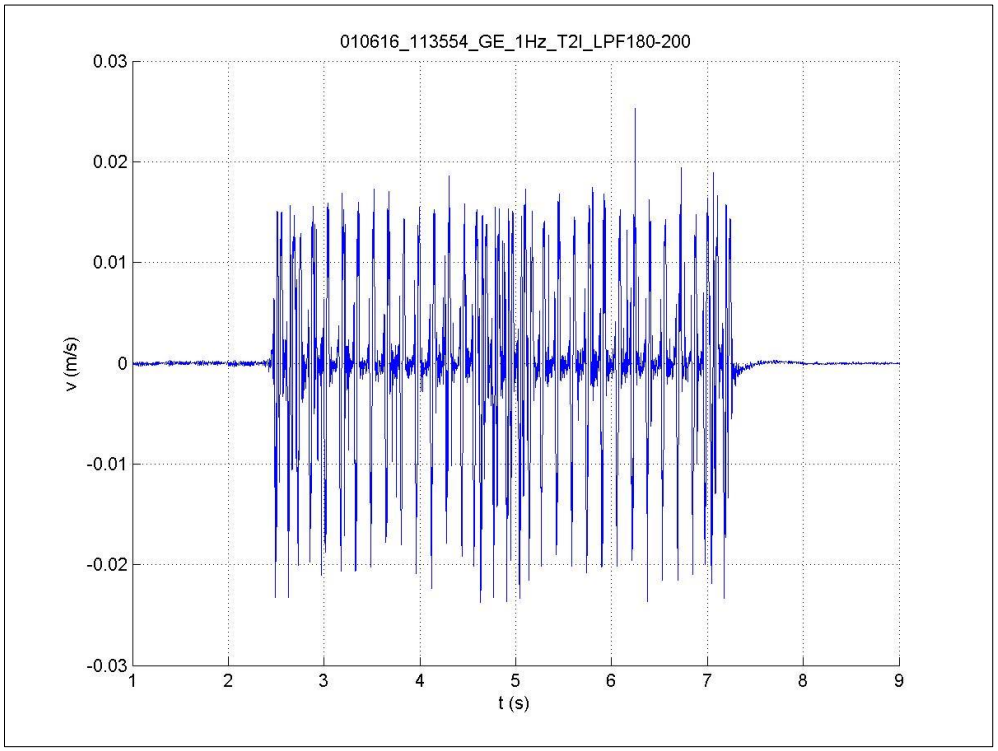

Figure 77: Sleeper velocity signal in the inner side of sleeper T2 induced by 11:35:54 train.

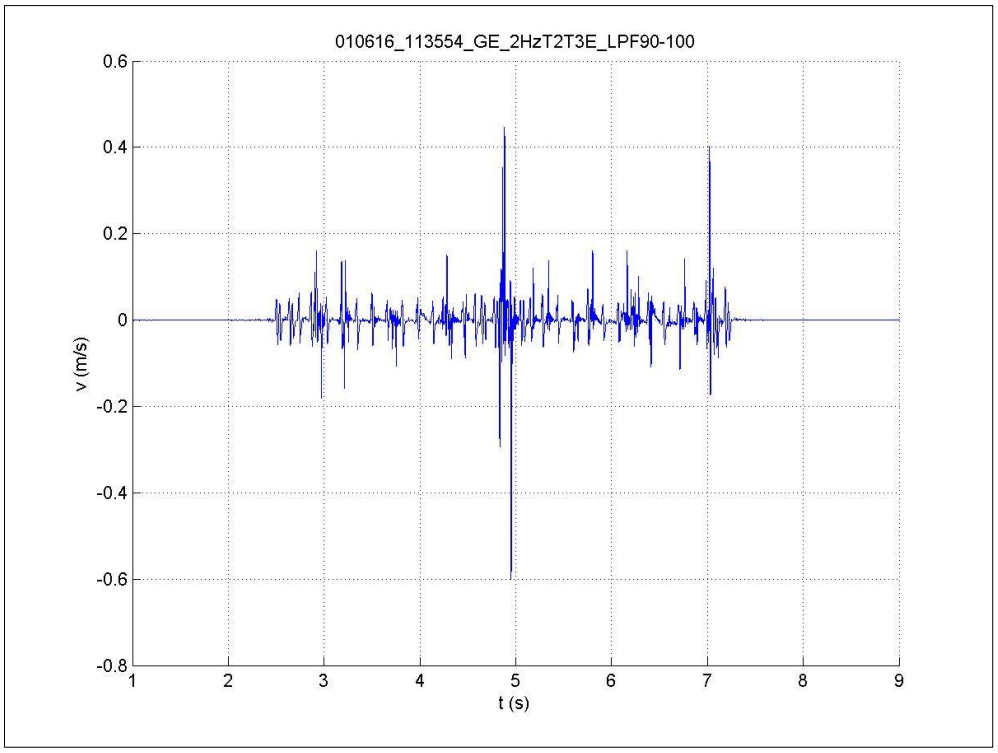

Figure 78: Rail velocity signal in the outer rail between T2 and T3 induced by 11:35:54 train.

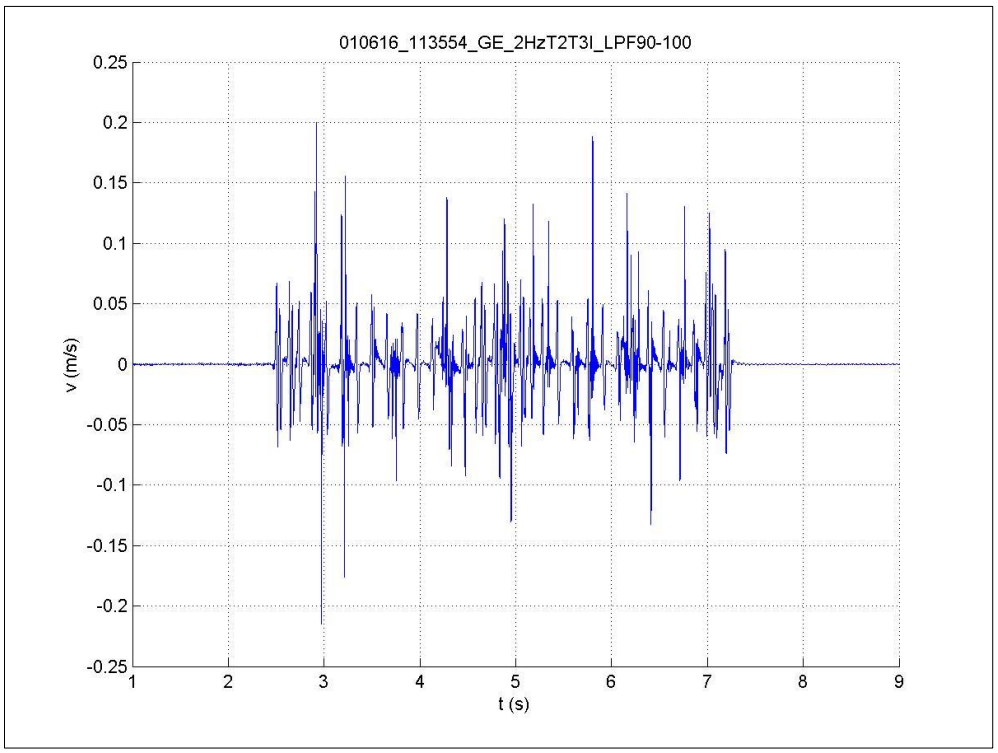

Figure 79: Rail velocity signal in the inner rail between T2 and T3 induced by 11:35:54 train.

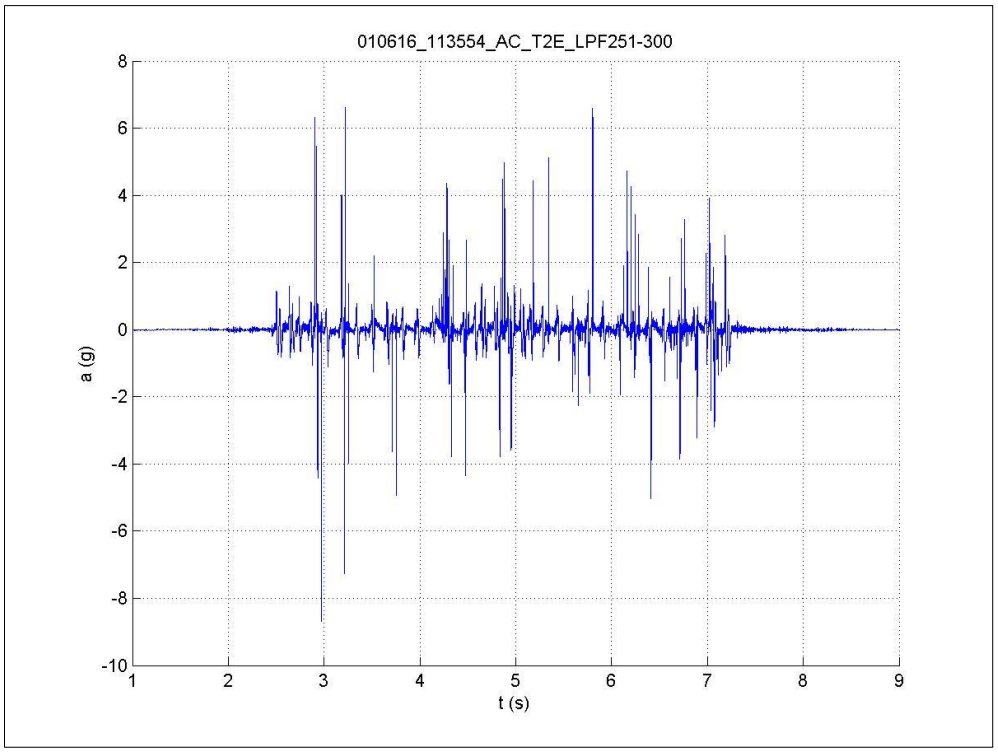

Figure 80: Sleeper acceleration signal in the outer side of sleeper T2 induced by 11:35:54 train.

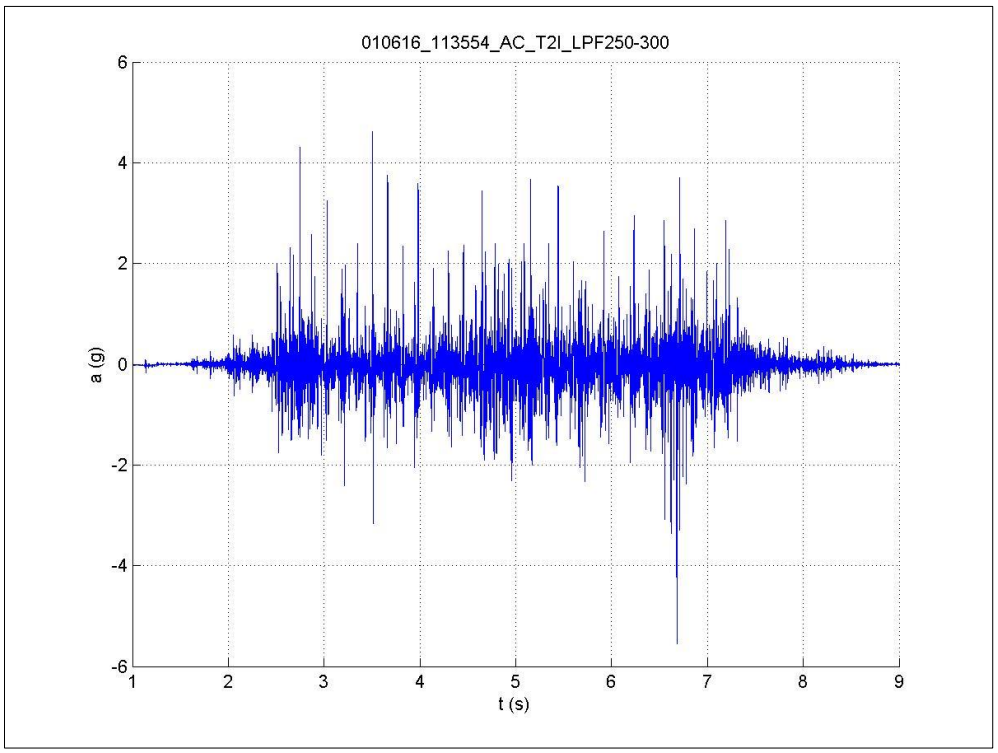

Figure 81: Sleeper acceleration signal in the inner side of sleeper T2 induced by 11:35:54 train.

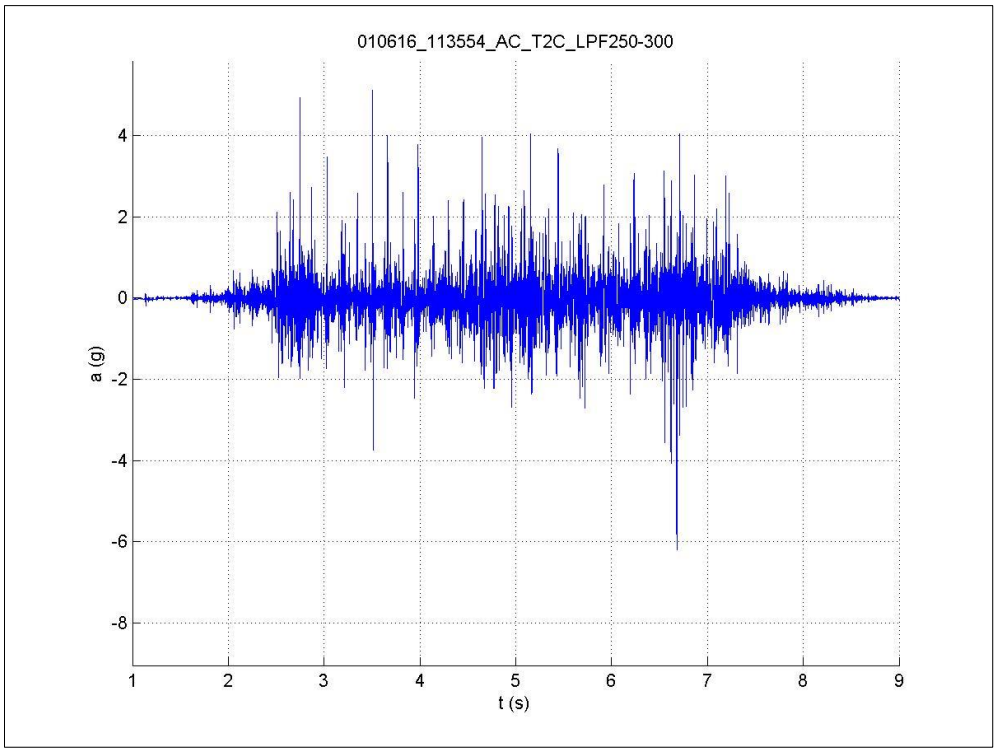

Figure 82: Sleeper acceleration signal in the center of sleeper T2 induced by 11:35:54 train.

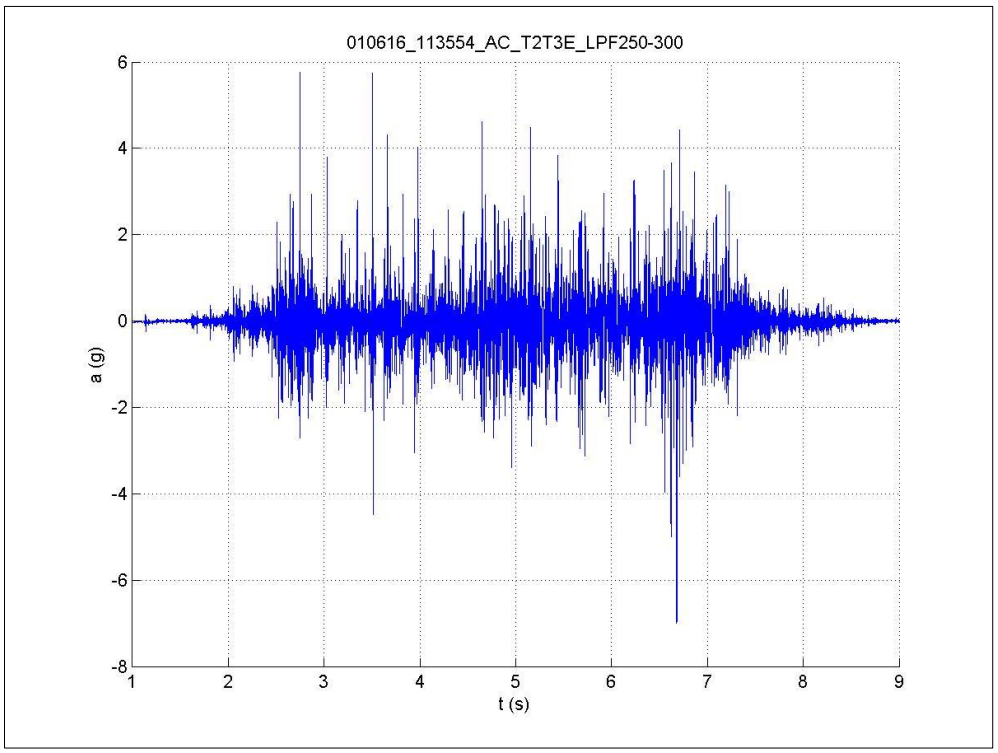

Figure 83: Rail acceleration signal in the outer rail between T2 and T3 induced by 11:35:54 train.

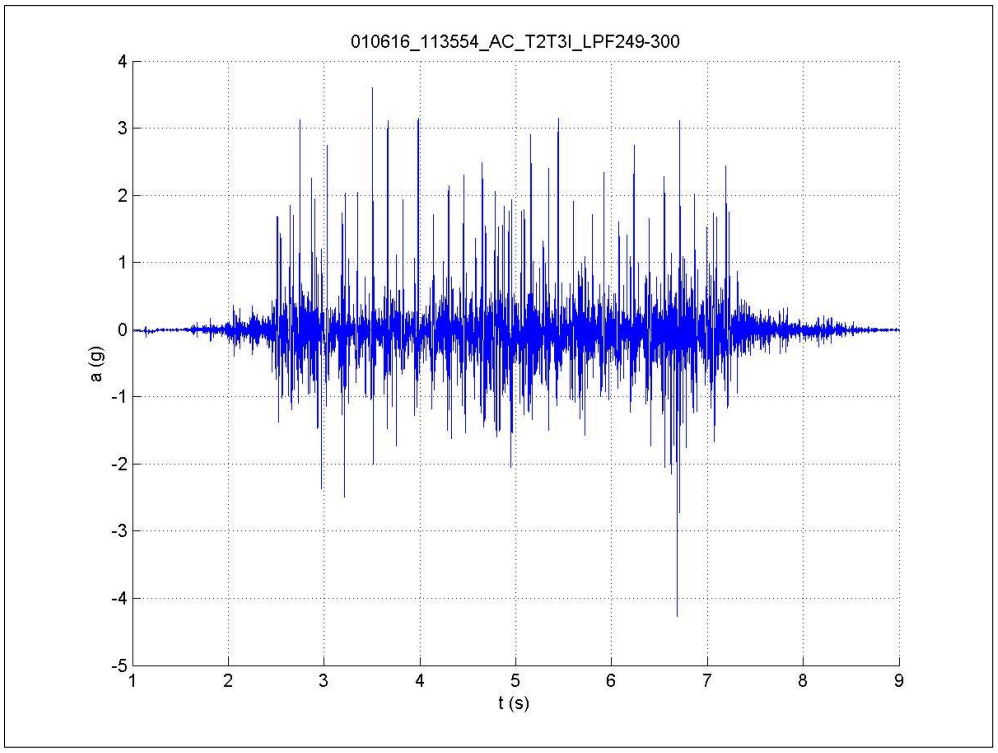

Figure 84: Rail acceleration signal in the inner rail between T2 and T3 induced by 11:35:54 train.

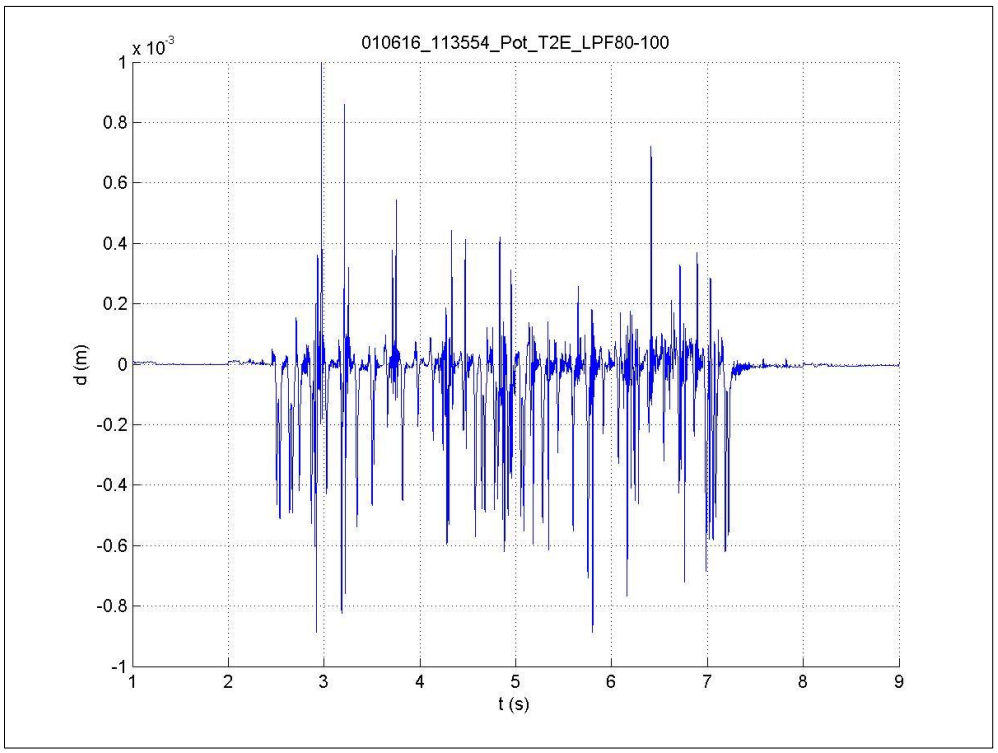

Figure 85: Relative displacement between outer rail and sleeper T2 induced by 11:35:54 train.

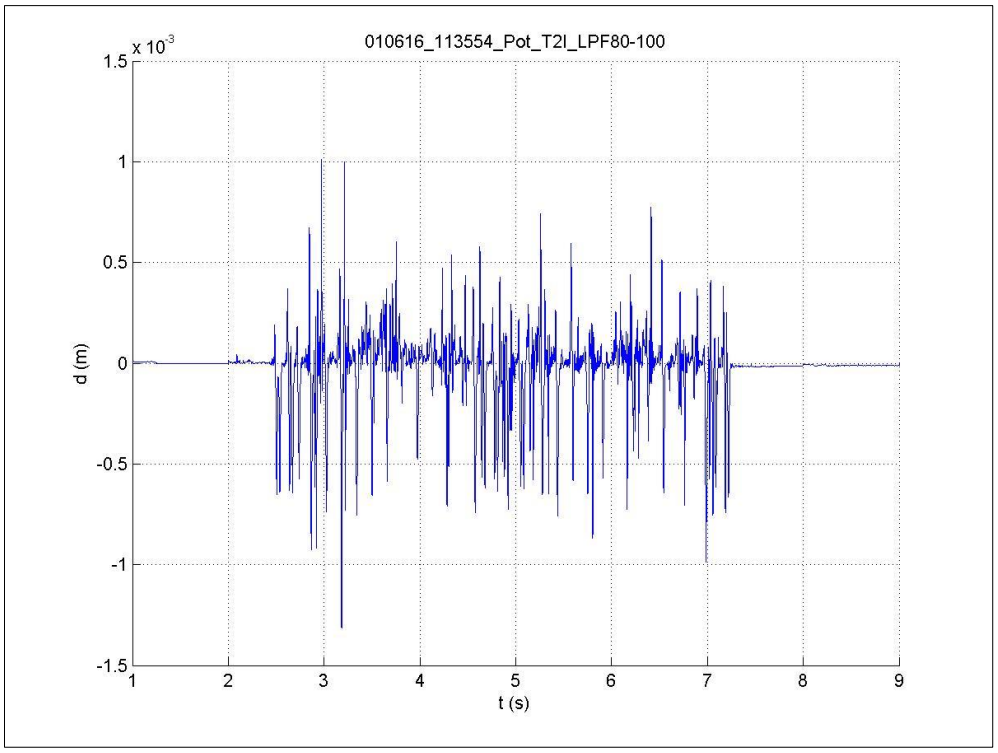

Figure 86: Relative displacement between inner rail and sleeper T2 induced by 11:35:54 train.

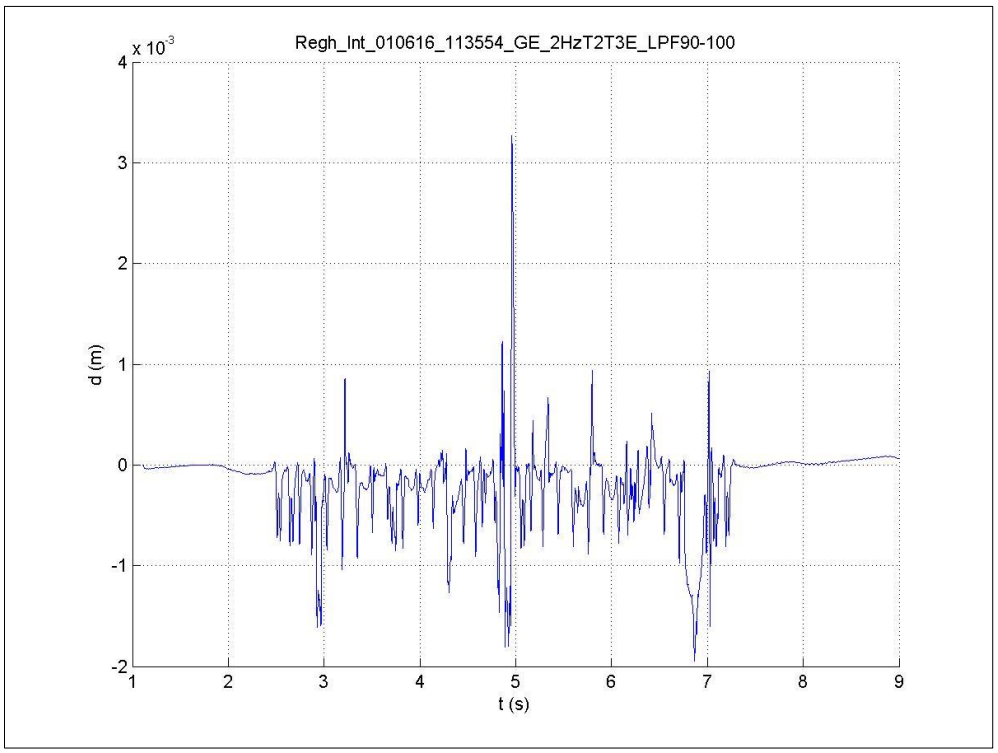

Figure 87: Rail deflection in the outer rail between T2 and T3 induced by 11:35:54 train.

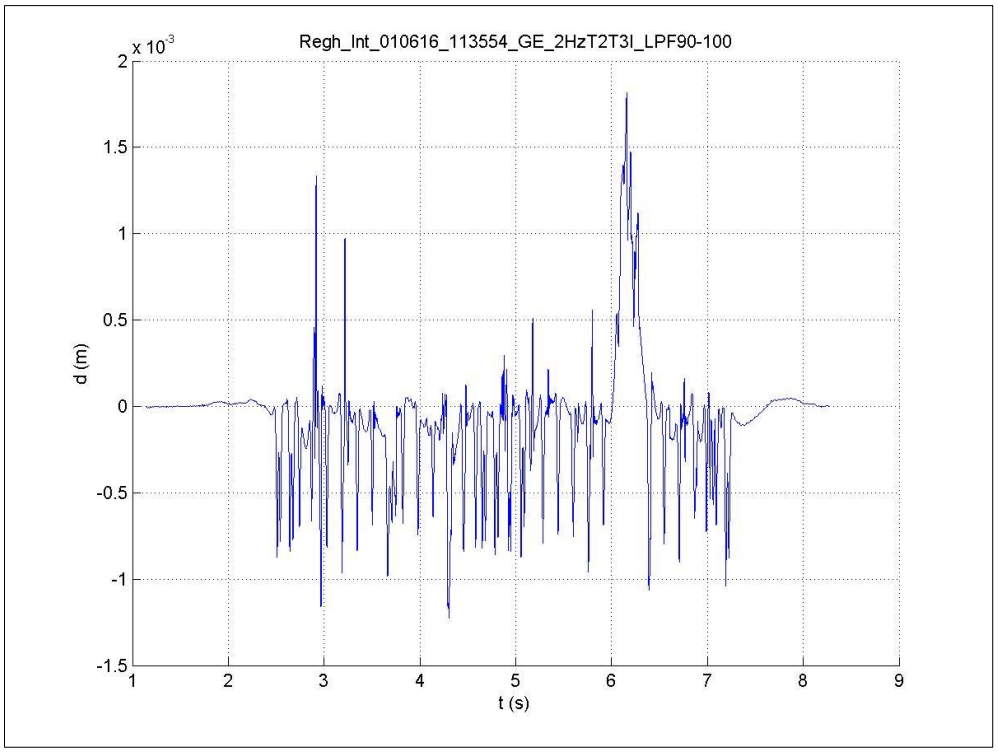

Figure 88: Rail deflection in the inner rail between T2 and T3 induced by 11:35:54 train.

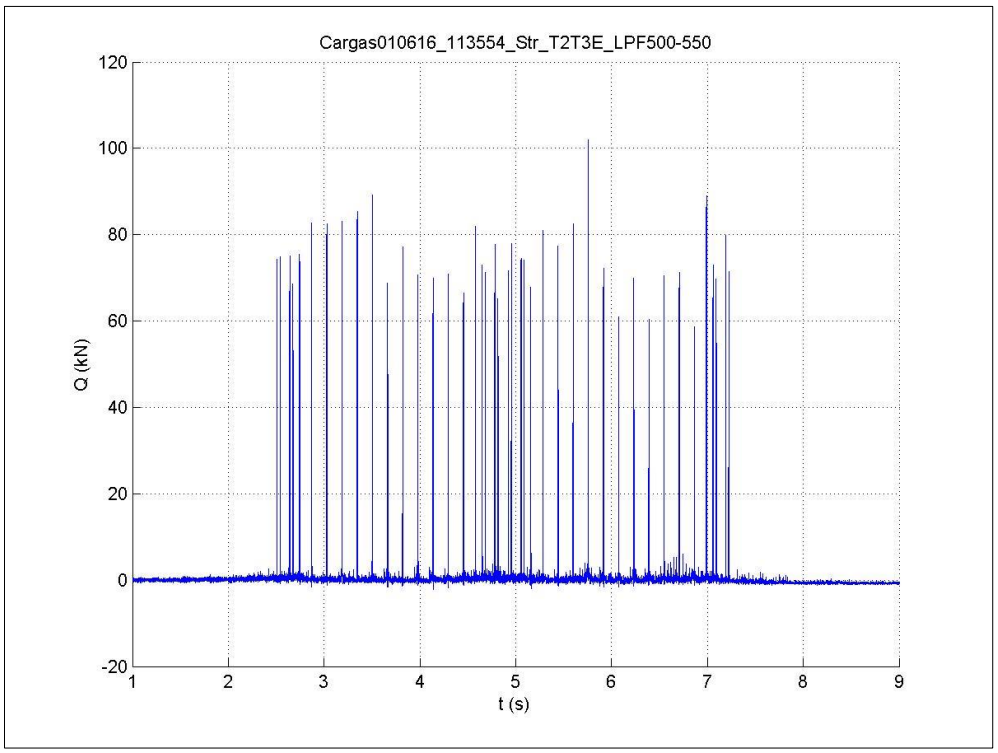

Figure 89: Loads in the outer rail between T2 and T3 induced by 11:35:54 train.

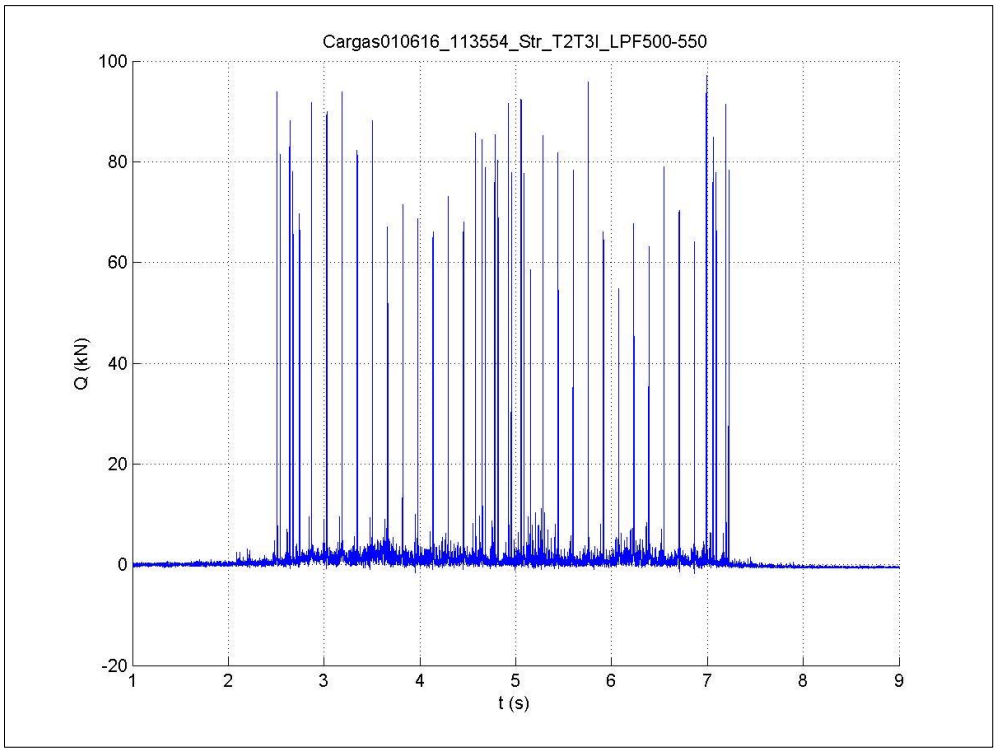

Figure 90: Loads in the inner rail between T2 and T3 induced by 11:35:54 train.

8 Train S120 (Time 12:07:44 / 16 axles / 226 km/h)

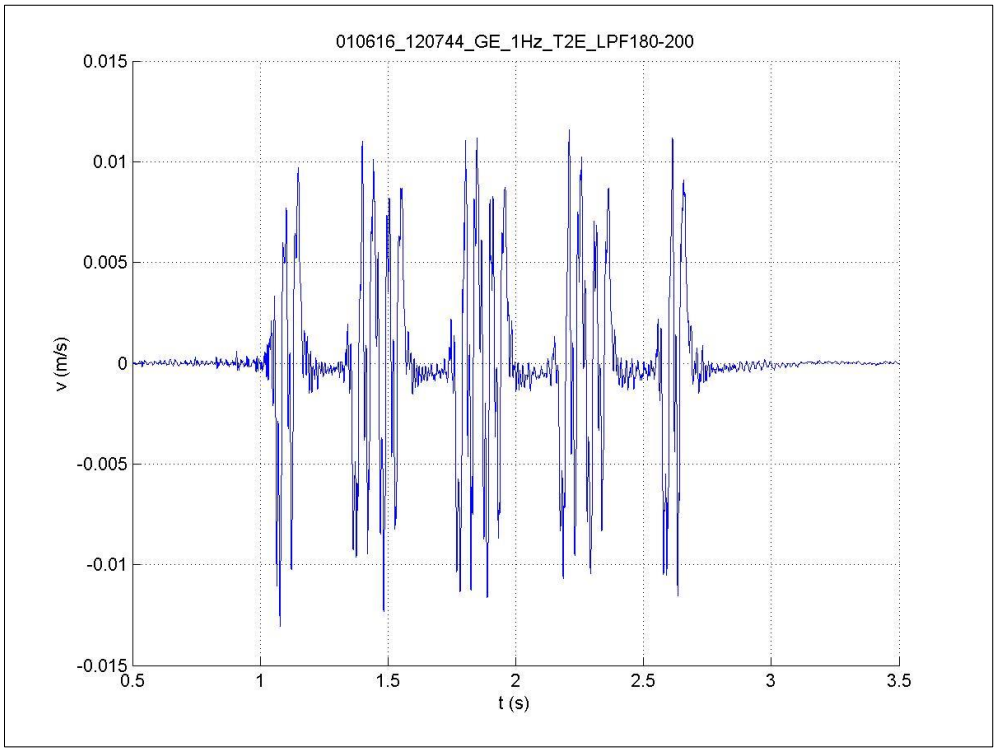

Figure 91: Sleeper velocity signal in the outer side of sleeper T2 induced by 12:07:44 train.

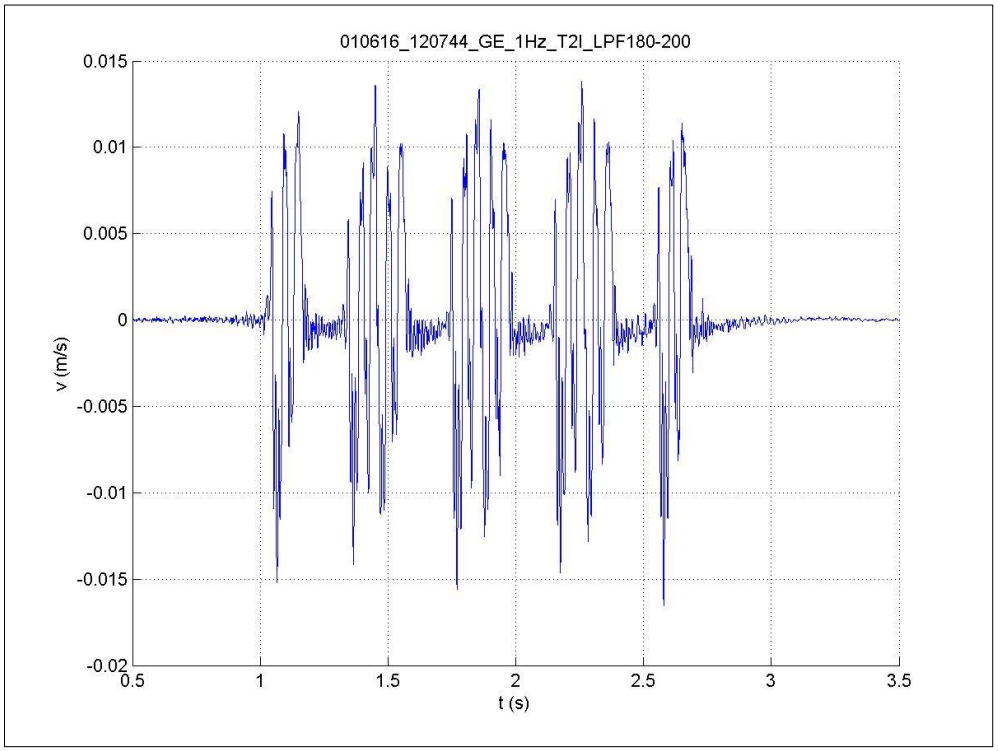

Figure 92: Sleeper velocity signal in the inner side of sleeper T2 induced by 12:07:44 train.

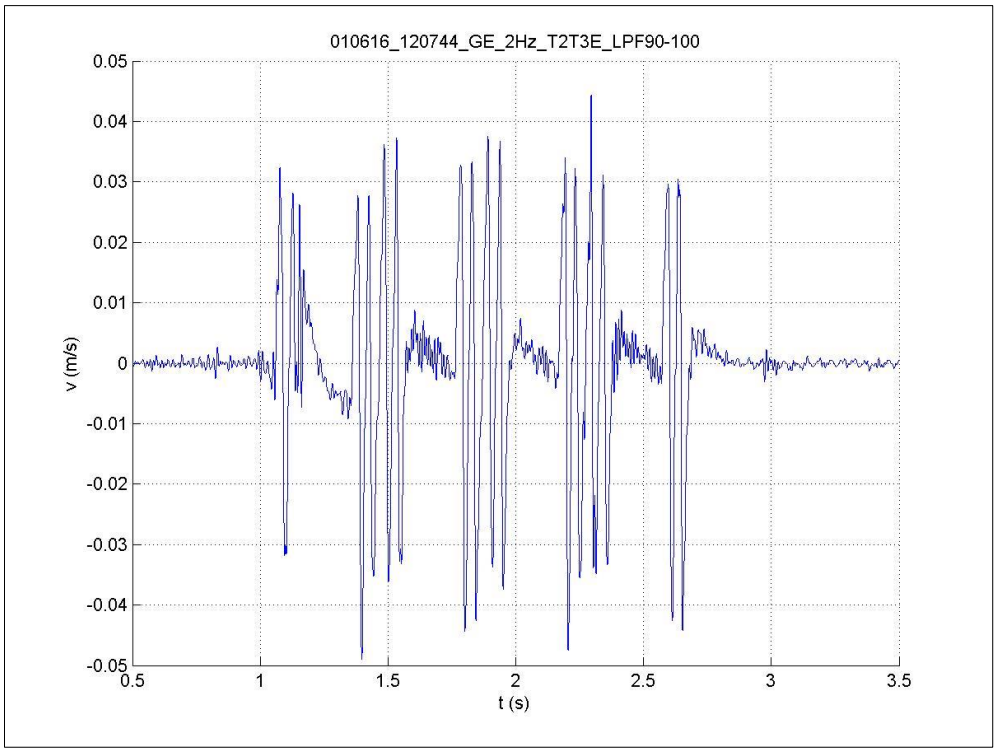

Figure 93: Rail velocity signal in the outer rail between T2 and T3 induced by 12:07:44 train.

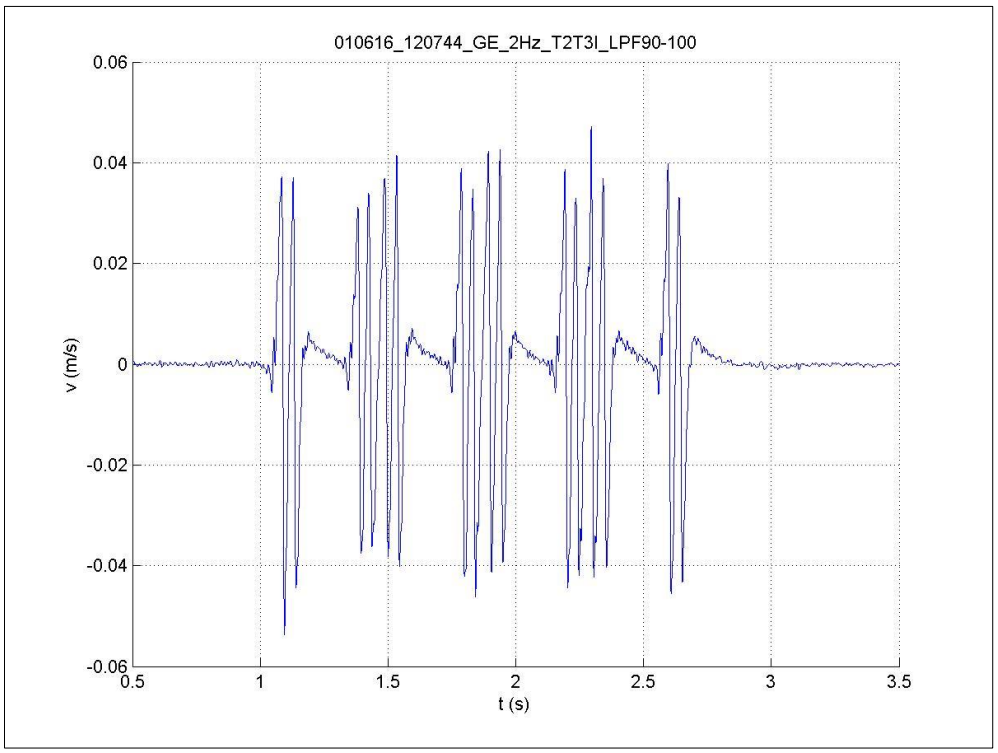

Figure 94: Rail velocity signal in the inner rail between T2 and T3 induced by 12:07:44 train.

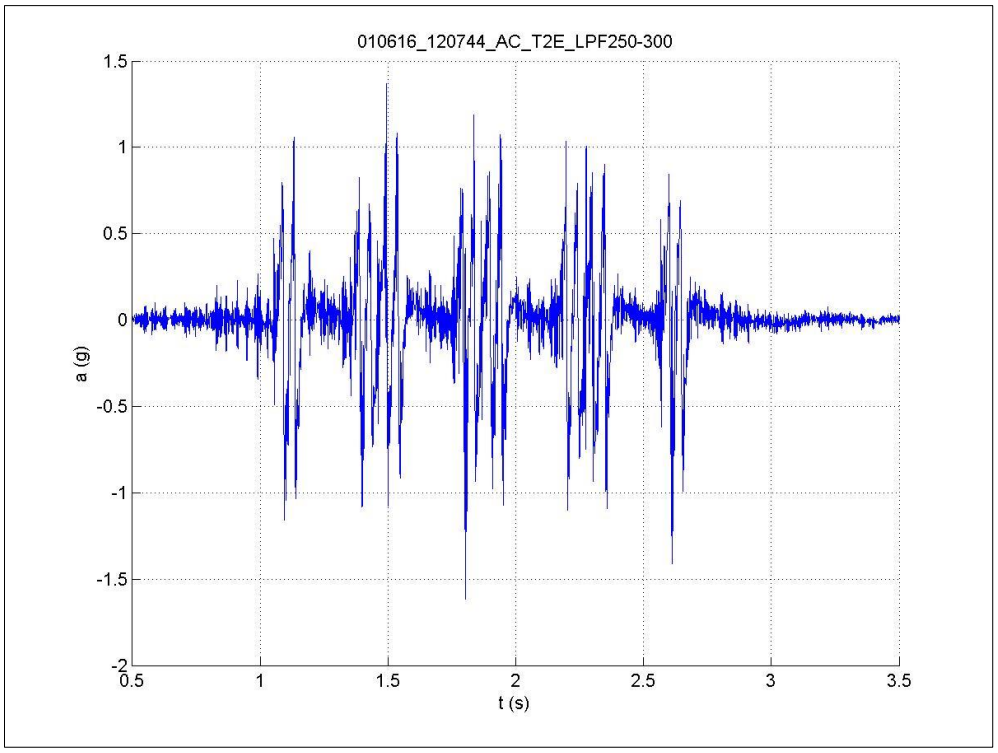

Figure 95: Sleeper acceleration signal in the outer side of sleeper T2 induced by 12:07:44 train.

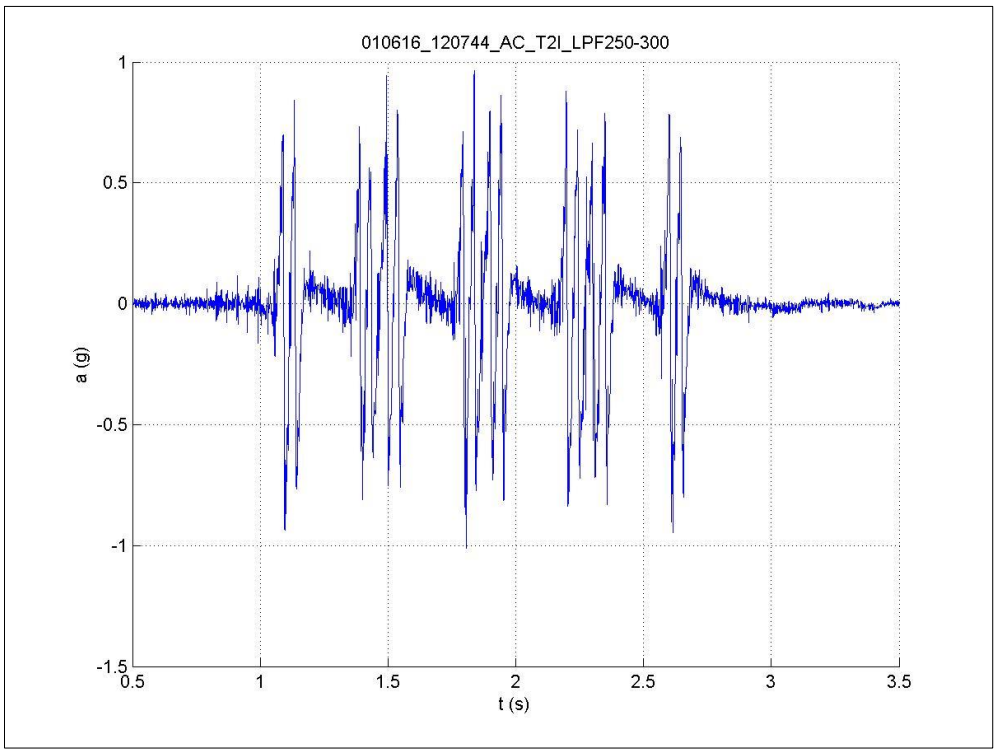

Figure 96: Sleeper acceleration signal in the inner side of sleeper T2 induced by 12:07:44 train.

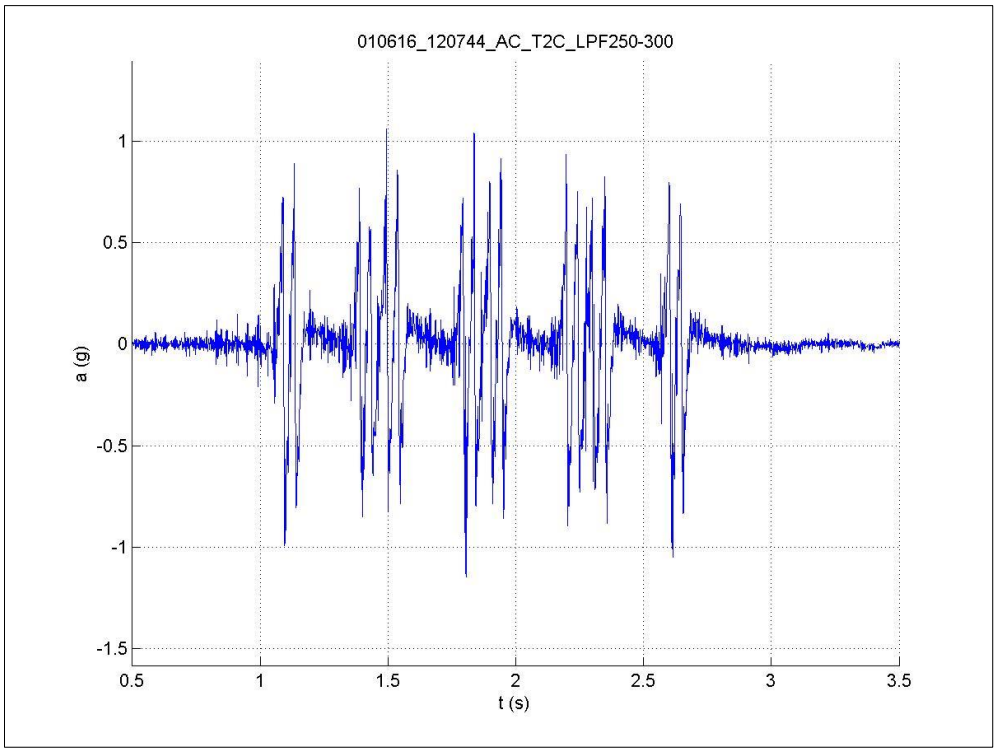

Figure 97: Sleeper acceleration signal in the center of sleeper T2 induced by 12:07:44 train.

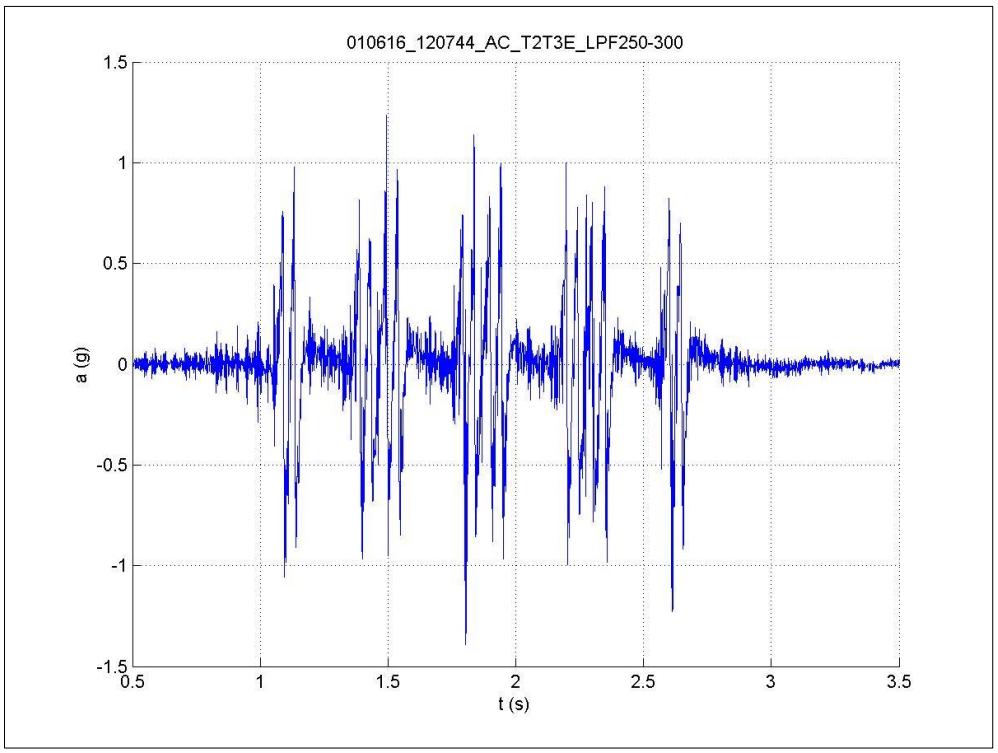

Figure 98: Rail acceleration signal in the outer rail between T2 and T3 induced by 12:07:44 train.

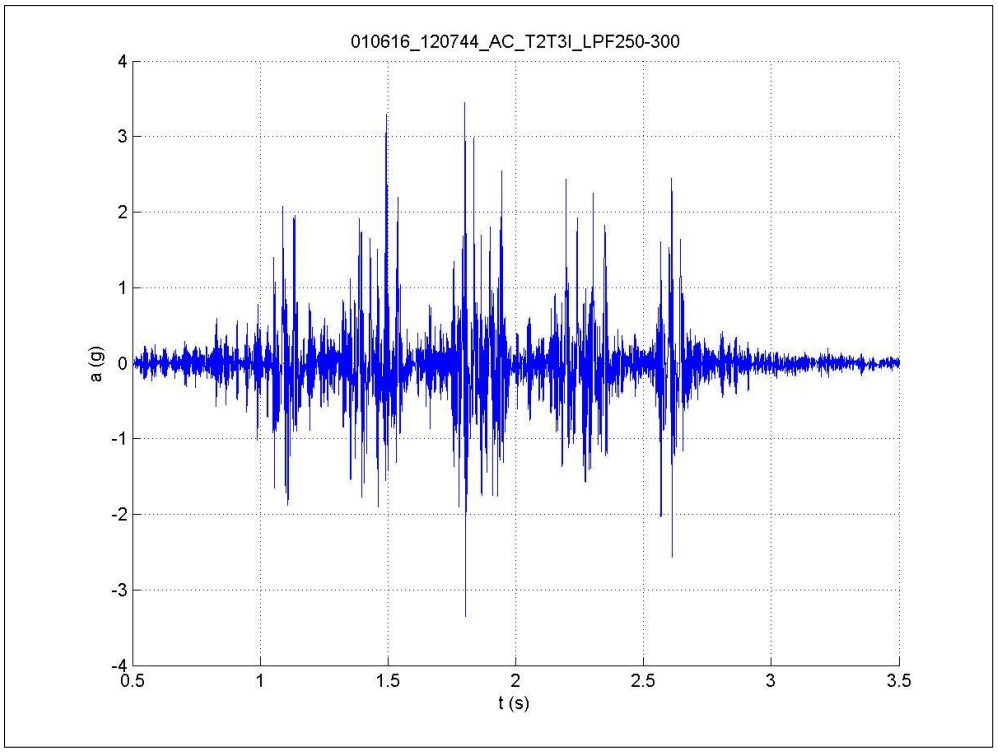

Figure 99: Rail acceleration signal in the inner rail between T2 and T3 induced by 12:07:44 train.

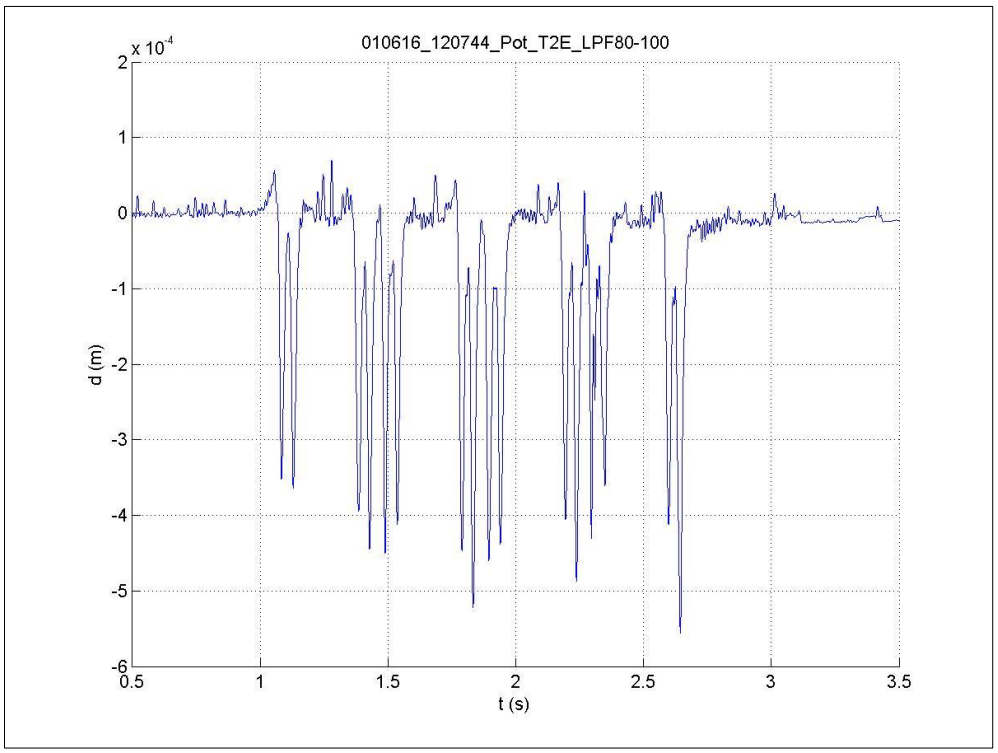

Figure 100: Relative displacement between outer rail and sleeper T2 induced by 12:07:44 train.

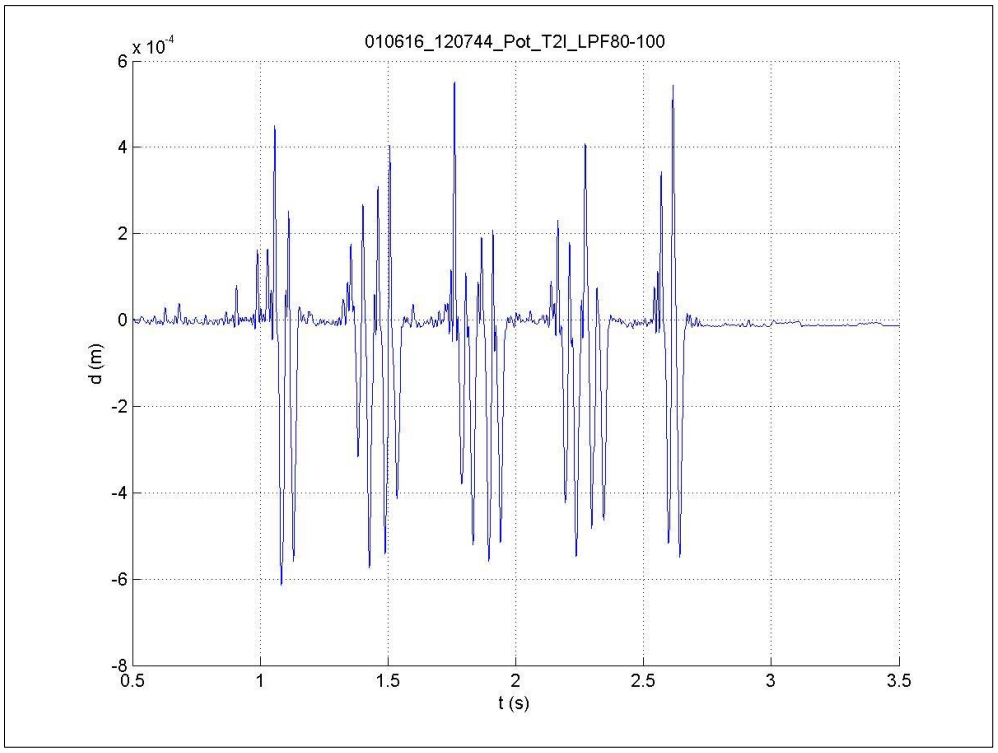

Figure 101: Relative displacement between inner rail and sleeper T2 induced by 12:07:44 train.

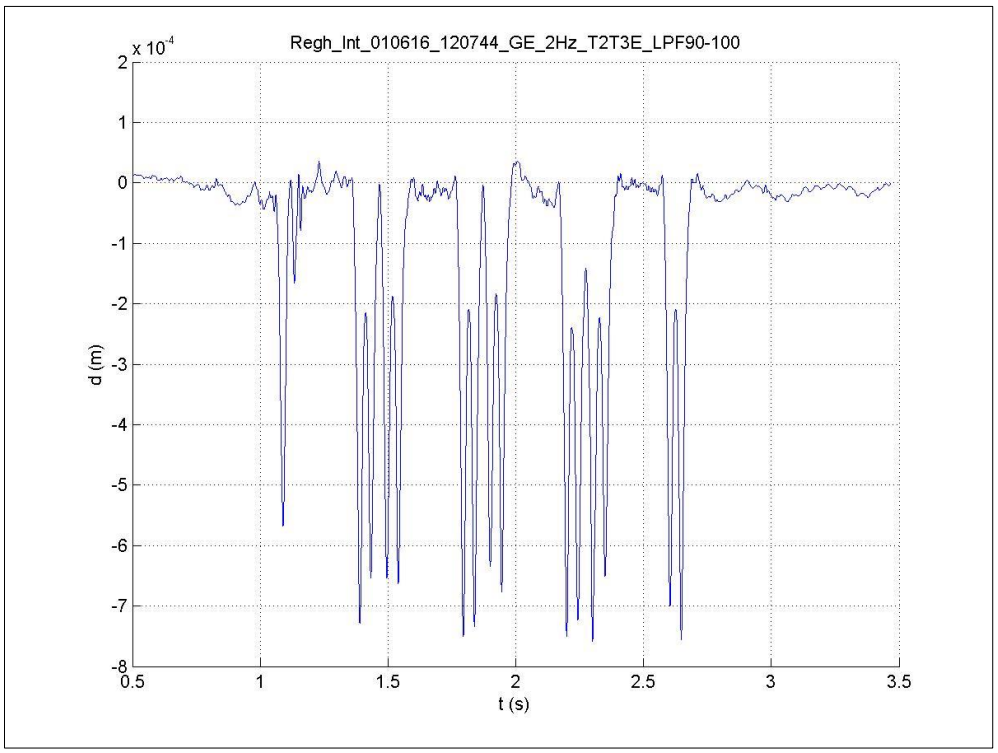

Figure 102: Rail deflection in the outer rail between T2 and T3 induced by 12:07:44 train.

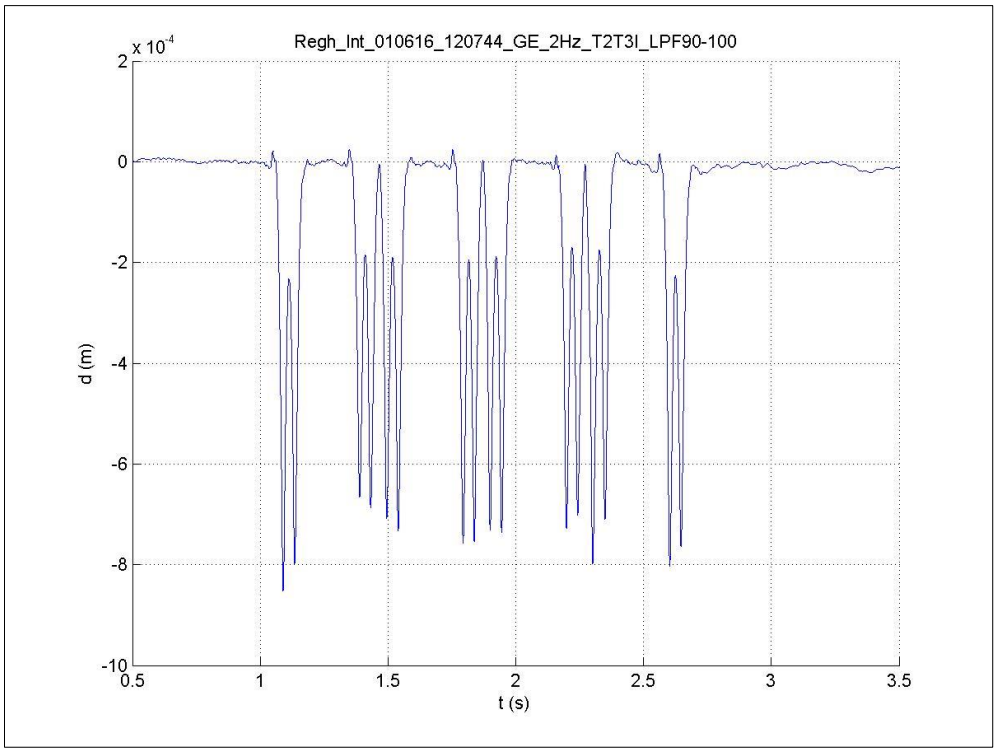

Figure 103: Rail deflection in the inner rail between T2 and T3 induced by 12:07:44 train.

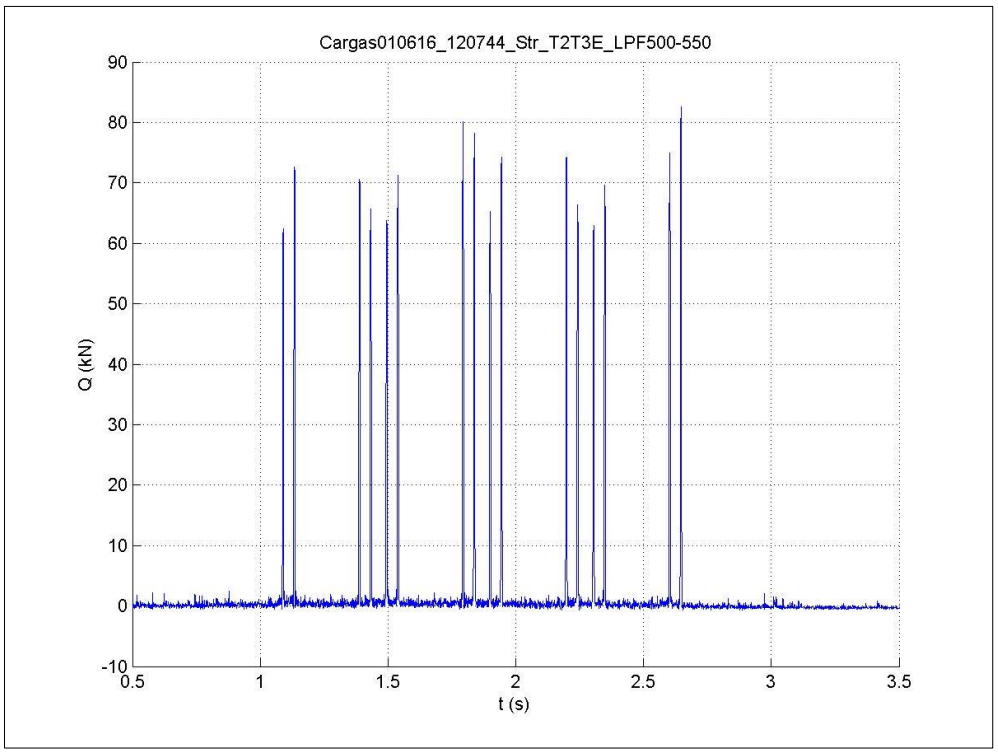

Figure 104: Loads in the outer rail between T2 and T3 induced by 12:07:44 train.

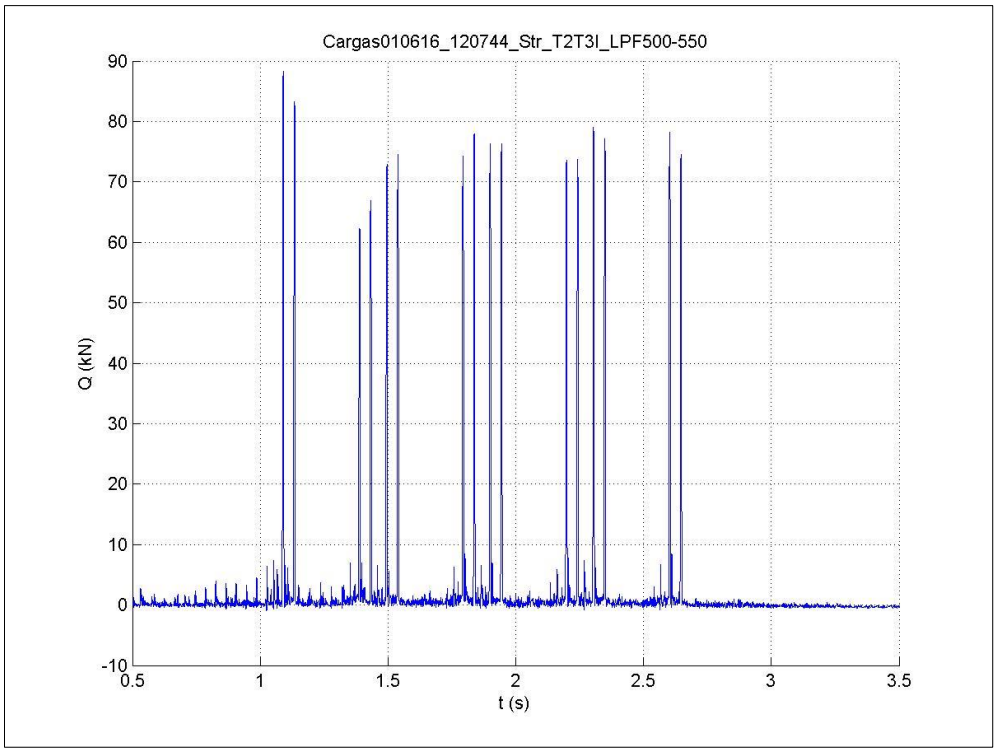

Figure 105: Loads in the inner rail between T2 and T3 induced by 12:07:44 train.

Collaborative project SCP3-GA-2013-60560

Increased Capacity 4 Rail networks through enhanced infrastructure and optimised operations

FP7-SST-2013-RTD-1

Deliverable D12.1

Innovative designs and methods for VHST (Intermediate)

Appendix 8.3

Track Design Optimization for Very High Speed

Dissemination Level		
PU	Public	PU
PP	Restricted to other programme participants (including the Commission Services)	
RE	Restricted to a group specified by the consortium (including the Commission Services)	
CO	Confidential, only for members of the consortium (including the Commission Services)	

Lead contractor for this deliverable: ADIF/CEDEX/IST

Document status		
Revision	Date	Description
0	2017/09/11	Preliminary version of Final Report –cap.5. Numerical estimations (IST) Authors: P. Ferreira, R. Maciel (IST)
1	2017/09/29	Final version of Final Report D12.1, IST – WP1.2.2
Reviewed	YES	

Table of contents

Abbreviations and acronyms

Abbreviation / Accronym	Description
C4R	Capacity for Rail Project
VHS	Very High Speed
CTB	CEDEX Track Box
USPs	Under sleeper pads
rp	Railpad

1 Introduction and Objectives

Having as major concern to attain a better performance of railway ballasted track for very high speed trains circulation, an upgrade of track design is envisaged in order to maintain vibration levels as well as track degradation rates within acceptable values. C4R Task 1.2.2 - "Track design for VHST" aims at proposing optimized innovative track design for very high speed on the basis of numerical simulation and real scale laboratory tests. While ADIF leading WP1.2 and contributing with its knowledge (for instance of real in situ tracks performance in Madrid – Barcelona HSL), CEDEX conducted tests in 1:1 scale laboratory CTB installation and IST made in parallel numerical estimations for preview of how certain track design solutions could undertake to increase in train speed above 300km/h up to 400km/h.

It is known that raising the elasticity of the superstructure (ballast layer and above) is a way to improve ballasted track dynamic behaviour at vhs. Track resiliency can be augmented through the insertion of high-damping materials. Three approaches would consist in: replacing former stiff railpads by softer ones, or introducing new resilient elements under sleepers, called under sleeper pads (USP), or thirdly applying simultaneously a combination of both softer railpads and USPs. This last approach was the track design solution which was to be tested at vhs both numerical and experimentally during WP1.2, not only in terms of track instantaneous behaviour (vibrations) but also in a lifetime perspective, studying fatigue and track degradation.

The inter-collaboration with CEDEX partner, which dealt with laboratory experimental tests (see Chapter 3 of this Deliverable and Appendix 8.1), was crucial to have a reference track to serve as basis for both model validation (CEDEX Track Box data results feed the model) and predictions to support decisions of which track design alternatives should be experimentally tested in the CTB (IST model results feed the CTB).

Mainly, the work was divided into the following parts:

- Numerical model validation based on the data provided by CEDEX from the tests conducted on the physical model of a ballasted track with granular subballast, CTB reference case (see Appendix 8.1);

- Evaluation of the predicted dynamic response of the reference railway track (CTB reference case) and the influence of train speed increase up until 400 km/h on its dynamic behaviour;

- Evaluation of the predicted dynamic response of different track design cases (having the CTB reference case as basis) when equipped with different combinations of railpads and undersleeper pads (USPs), including the study of the impact of increasing train speed;

- Optimization of track design (several specific combinations of railpad and USP stiffness) to improve dynamic performance at very high speeds (up to 400 km/h).

This report includes a sum-up of the previous work and the results achieved during the Capacity for Rail WP1.2.2, which have been reported internally in three intermediate reports, within Task 1.2.2 New track design and specifications for VHST. Sub-Task 1.2.2.1 Track design for VHST, namely: IR#1 - Preliminary draft report - Numerical modelling and validation of short term results at 300km/h (47 pags) - 17/06/2015, (IST - R. Maciel, P. Ferreira, 2015); IR#2 - Numerical simulations to study Track Box responses to the increase of train running speed (36 pags) - 17/12/2015, (IST - R. Maciel, P.

Ferreira, 2015); IR#3 - Track design solution for soft rail pads and under sleeper pads. Parametric study on train speed increase. (68 pags) - 30/05/2016, (IST - R. Maciel, P. Ferreira, 2016).

2 Brief notes on dynamic behaviour of vhs tracks

In what regards railway train/track dynamic behaviour at very high speeds (above 300km/h), intense research is still needed so as to assure a safe performance of the infrastructure, with reduced vibrations, by simultaneously maintaining its deterioration along time under reasonable levels. The subtask WP1.2.2 of the Capacity for Rail project intends to contribute for this scope.

It is known since very first experiments made in track by Prud'Homme in the 70's that increasing train speeds would imply a dynamic behaviour of track conducing to important increase in vibrations and consequent higher track deterioration rater (see (Ferreira, 2010) for further state-of-the art on the subject). Hence, it is already known that track geometry deterioration has been found to be primarily caused by degradation phenomena observed primarily within the ballast layer, where particle crushing resulting from cyclic loads plays a prominent role (Lobo-Guerrero & Vallejo, 2006). In addition to cyclic loading and ballast confining pressure, train speed has been found to be an important factor ((Sun, et al., 2015) among others). Frequency loading on granular media, such as high-speed traffic on ballasted tracks, has been linked to increased track deterioration rates, where particle acceleration plays a prominent role (Barke & Chiu, 2005). The influence of subsoil state on ballast behaviour has also received increased attention due to its influence on the "mud pumping" phenomena and higher track deterioration rates linked with ballast fouling and poor drainage conditions (Trinh, et al., 2012) (Nimbalkar, et al., 2015). It has also been suggested that environmental factors, such as changes in ground water level due to droughts or water infiltration resulting from heavy rain fall, also have a significant impact on settlement rates (Kang, 2016) (Bian, et al., 2016).

In what considers simulating this phenomenon, track settlement models can be classified into two categories: simulation-driven and empirical. Simulation-driven models, consist of simulation-based models which estimate settlement rates resulting from repeated train passages within the framework of viscoplasticity (Abdelkrim, et al., 2003). A number of papers on simulation-driven have been presented throughout the years (Suiker & de Borst, 2003) (Ishikawa, et al., 2014) (Nguyen, et al., 2015) (Sun, et al., 2017). The main drawback associated with simulation-driven models is its causal-descriptive nature. As they are implemented to reflect theories of how the real system operates, their accuracy is limited to the extent of which the theories used to build the model are capable of explaining the real-world phenomena. As simulation-driven models are unable to account for any behaviour which isn't reproduced by their underlying theories then the accuracy of their predictions, and consequently their usefulness in the design process of high-speed lines is limited. This is a major concern in high-speed rail applications, as simulation models are developed focused on the viscoplastic aspects of track degradation processes, driven by stress or strain-based measurements, and ignore vibration-driven degradation mechanisms, which become increasingly important with increasing train speed.

Empirical models are derived from the application of knowledge discovery and data mining techniques on collections of observational and experimental data collected in situ or on laboratory tests. An extensive review of empirical track degradation models was presented in (Dahlberg, 2001) (Dahlberg, 2004). More recently, an extensive review of empirical track geometry degradation and track condition models was presented in (Soleimanmeigouni, et al., 2016), and a review of ballast

settlement models that express expected degradation rates as a function of the number of load cycles was presented in (Abadi, et al., 2016).

Empirical models are the most popular choice of models employed in practical track design applications. Their main advantage is that, unlike simulation-based models, empirical models are able to provide accurate predictions of degradation rates for design cases that fall within their validity limit, and reflect contributions of degradation mechanisms that may not even be known at the time the model was proposed. There are, however, drawbacks to this approach. The main shortcoming of empirical models is that their estimates are tightly linked to the empirical data that was used to generate them. Therefore, the resulting data-driven models are bound to reflect relations between the set of attributes that were effectively measured, are implicitly bound to the characteristics of the observed subjects and experimental units.

In spite of the ongoing research effort and the wealth of settlement model proposed throughout the years, there is yet no consensus on which input parameters are necessary and sufficient to simulate settlement rates resulting from high-speed traffic, nor is there a widely accepted model capable of providing reliable predictions of the evolution of settlement rates for arbitrary combinations of track sections and railway traffic.

One of the approaches for railway track to cope with higher speeds and the vibrations and degradation these imply is to increase its resiliency through the insertion of high-damping materials. This would mean replacing former stiff railpads by softer ones or/and introducing new resilient elements under sleepers, called under sleeper pads (USP).

Rail pads increase axle load distribution to adjacent sleepers and reduce load concentrations resulting from rail-sleeper contact, thus reducing stresses on the sleepers as well as reducing track degradation rates (Sol-Sánchez, et al., 2015).Due to the influence exerted by rail pads on track degradation processes, as well as in important modes of failure, there has been an increase in research on the mechanical behaviour of rail pads to better understand specific aspects of degradation phenomena and improve simulation accuracy. Among the research areas explored, new constitutive models, such as fractional derivative viscoelastic models (Zhu, et al., 2015) and generalized Maxwell models (Oregui, et al., 2016), have been developed for railpad modelling and employed in train/track simulations to improve the accuracy of railway track dynamics simulations.

The introduction of new constitutive models has also paved the way to evaluate important design factors affecting the dynamic response, such as the combined influence of preload and usage of nonlinear rheological on track vibrations (Koroma, et al., 2015), frequency and rate-dependent behaviour (Fenander, 1997) (Wei, et al., 2016). Changes in mechanical properties due to aging and deterioration were also studied (Remennikov, et al., 2006), as well as the impact of temperature variations in the mechanical behaviour (Carrascal, et al., 2007) (Wei, et al., 2017).

The dynamic response of concrete sleepers has also been found to be an important factor in ballast degradation processes. A literature review was conducted to determine design requirements for precast concrete sleepers taking into account their dynamic response and associated failure modes (Taherinezhad, et al., 2013). Among the design requirements, the dynamic response was found to play an essential role in the dynamic response of global railway tracks. Although the link between traffic-induced sleeper vibrations and sleeper fatigue was already established (Salim, et al., 2012), the excitation of higher-frequency modes, induced by the passage of high-speed trains as well as rail corrugation, has been found to have a significant impact in particle wear, particle flow and lateral spreading (Aikawa, 2015).

To reduce degradation rates, under-sleeper pads (USPs) have been introduced to take advantage of their beneficial influence to the track system (Schilder, 2013). A literature review of the performance of USPs has been presented in (Kaewunruen & Remennikov, 2015). USPs play an important role in redistributing train loads to the ballast layer, reduce particle wear and breakage, as well as reducing noise emissions and track vibrations (Johansson, et al., 2008) (Sol-Sánchez, et al., 2015). Consequently, introducing USPs helps reduce degradation rates due to most of the degradation being caused by particle corner breakage and projections (Indraratna, et al., 2005). Laboratory tests have shown that the introduction of USPs result in a reduction of ballast settlement rates of over 25% (Sol-Sánchez, et al., 2016).

However, USPs must be selected based on a holistic approach to track design, which should takes into account not only the dynamic characteristics of a track solution, including the combined choice of rail pads and USPs, but also train traffic characteristics such as axle load and train speed (Schneider, et al., 2011). Otherwise, the introduction of USPs may result in increased rates of particle breakage and wear, sleeper cracking and ballast flow, as well as higher vibration and noise levels.

3 Computation model description

The numerical track model used in this project is a 3D elastodynamic finite element method model coupled with a discrete element model of the vehicle (Ferreira, 2010) (Ferreira & López-Pita, 2015). Sub-structuring and component mode synthesis techniques are employed to reduce the number of degrees of freedom of the global track model, thus reducing the computational workload while preserving the accuracy of the simulations. This implies very fast computing for each run, allowing to simultaneously estimate track instantaneous dynamic responses as well as to simulate millions of train passages in order to predict long term track settlement evolution.

The global track model is generated by synthesizing a superelement which will be used as a basic building block. The model-building process takes advantage of the translational symmetry of the railway track to synthesize a superelement comprising a section of the track that contains a single sleeper. Each superelement, henceforth referred to as *track slice*, is subjected to a model reduction process to reduce the number of degrees of freedom required to accurately represent the response of the railway track to the passage of a train. The global model of the railway track is assembled by coupling a predetermined sequence of track slices. A visual representation of a track slice and a global track model is shown in Figure 1.

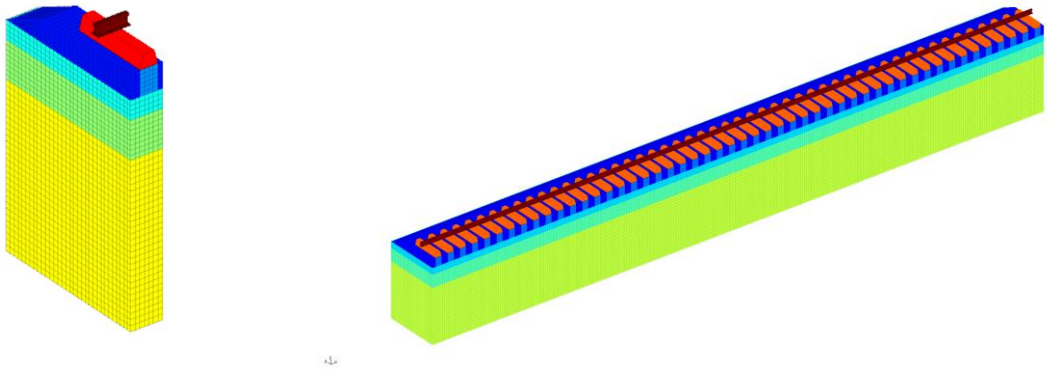

FIGURE 1 VISUAL REPRESENTATION OF THE COMPUTATIONAL MODEL: TRACK SLICE (LEFT) AND GLOBAL TRACK MODEL (RIGHT)

Once the global track model is built, an implementation of the Newmark time-stepping algorithm is used to obtain a time-domain response. The response outputted by the numerical model is represented by time series of kinematic fields taken at predetermined locations within the global track model. To draw a parallel between the numerical model and its physical counterpart, each location within the model adopted at a source of kinematic time series will henceforth be referred to as *sensor*.

Each numerical run performed by the computational model consists in the simulation of a passage of a vehicle model, in this case a single 2 axle bogie, which is made to circulate along the global track model. The interaction between the vehicle model running at a prescribed speed and the global track model leads the dynamic train/track system to output a response that is postprocessed to extract quantities of interest.

In this report, simulations made mostly asked for the response produced by the numerical model represented by time series of kinematic fields taken at predetermined locations within the global track model.

4 CEDEX Track box reference case

4.1 TRACK BOX CHARACTERISTICS AND MODEL

The reference case is represented by the physical model referred to as CTB Trackbox in the report (CEDEX, 2015), a full-scale physical model of a ballasted track with granular subballast built in the CEDEX Track Box testing facilities. The geometric parameters of the railway track are illustrated in the schematic cross-section diagram shown in Figure 2. The railway components used in the track and the material properties of the supporting layers are listed, respectively, in Table 1 and in Table 2. A thorough description of the CTB Trackbox physical model is provided in (CEDEX, 2015).

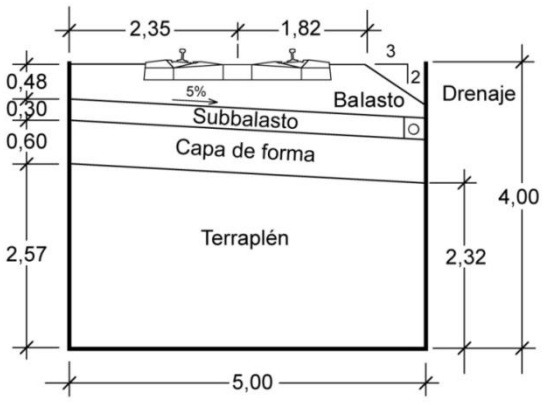

FIGURE 2 TRACK BOX: CROSS-SECTION SCHEMATIC DIAGRAM. SOURCE: (CEDEX, 2015).

TABLE 1 TRACK BOX: RAILWAY COMPONENTS. SOURCE: (CEDEX, 2015).

Component type	Description
Rails	UIC 60-E1
Rail pads	

Type	PAE2 (Adif, 2005)
Thickness	7 mm
Area	148×180 mm2
Nominal stiffness	Around 100 kN/mm
Secant stiffness	Between 20 kN/mm and 95 kN/mm
Sleepers	
Type	AI-99 (Monoblock) (Adif, 2014)
Mass	344 kg (average)

TABLE 2 MATERIAL PROPERTIES OF THE SUPPORTING LAYERS. SOURCE: (CEDEX, 2015).

	E_{v2} [MPa]	E_{max} [MPa]	ν [-]	Dry unit weight [kN/m^3]
Granular sub ballast	170	440	0,30	22,0
Form layer	165	400	0,30	21,5
Embankment	160	385	0,40	20,2

For the reference case, a reference model was defined based on the track properties listed in Table 1 and Table 2. The material property values of the supporting layers adopted for the CTB reference model are listed in Table 3.

TABLE 3 REFERENCE MODEL: PROPERTIES OF THE SUPPORTING LAYER.

	h [m]	E [MPa]	ν [-]	Density [kN/m^3]
Ballast (confined region)	0,40	230	0,20	17,0
Granular sub ballast	0,30	440	0,30	22,0
Form layer	0,60	400	0,30	21,5
Embankment	2,57	385	0,40	20,2

The CTB Trackbox physical model was also equipped with an array of sensors placed on the track superstructure and within the substructure. A thorough description of the sensor systems used in the CTB track is available in (CEDEX, 2015). The location of the sensors installed within the track substructure is represented in the schematic diagram shown in Figure 3.

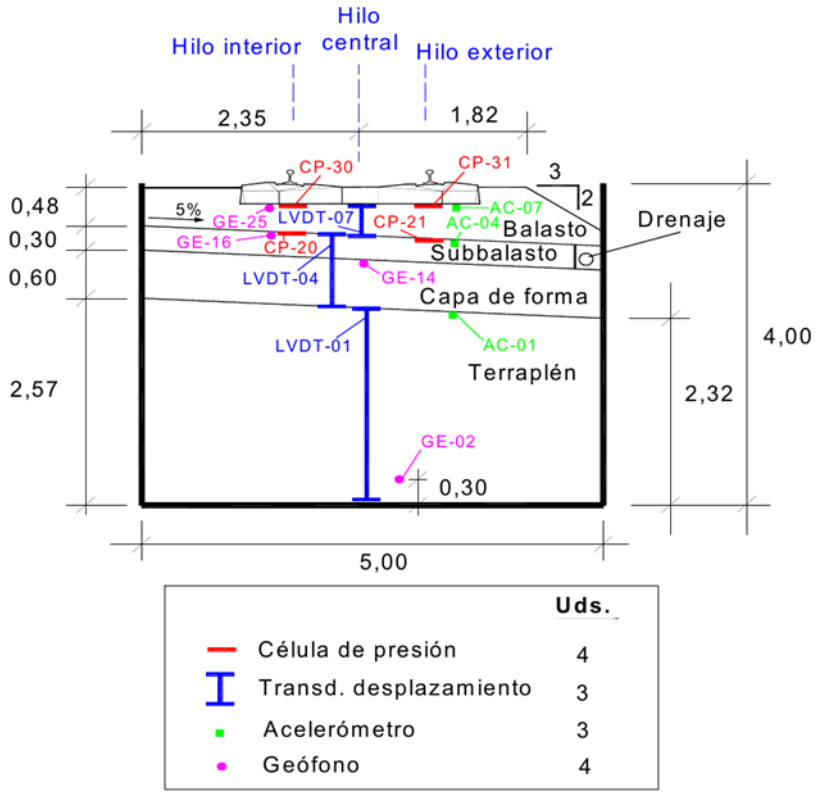

FIGURE 3 SENSOR PLACEMENT SCHEMATIC DIAGRAM. SOURCE: (CEDEX, 2015).

To draw a parallel between the numerical model and its physical counterpart, each location within the model adopted at a source of kinematic time series will henceforth be referred to as *sensor*.

Within the track supporting layers, a series of sensors were set bellow the 25th sleeper of the numerical model (approximately in half length of the model), each located at specific depths. The origin of the vertical axis is located in the boundary surface between the top of the ballast layer and the bottom of the sleeper/USP. Each sensor associated with the top or bottom of a supporting layer was placed 1cm inside the layer to avoid potential coupling and mesh-related issues and have accuracy on results. The list of sensors used in the railway track, as well as their depth, is presented in Table 4.

TABLE 4 NUMERICAL MODEL: SENSOR LAYOUT.

Supporting layer	Sensor name	Sensor depth [m]
Ballast	Ballast top	-0,01
	Ballast	-0,20
	Ballast bottom	-0,39
Sub-ballast	Subballast top	-0,41
	Subballast	-0,55
	Subballast bottom	-0,69
Form layer	Form layer top	-0,71
	Form layer	-1,00
	Form layer bottom	-1,29
Embankment	Embankment top	-1,31
	Embankment	-2,58

4.2 TRAIN MODEL

In the quasi-static test conducted by CEDEX in its Track Box testing facility, the train was modelled as an actuator force time series representing the wheel-rail contact force applied on the track by a Eurostar-type train circulating at 300km/h. The actuator force was applied on the railway track by feeding the time series to the CEDEX load system. The actuator force time series and resulting track deflection measured by CEDEX during a simulation run is represented in Figure 4.

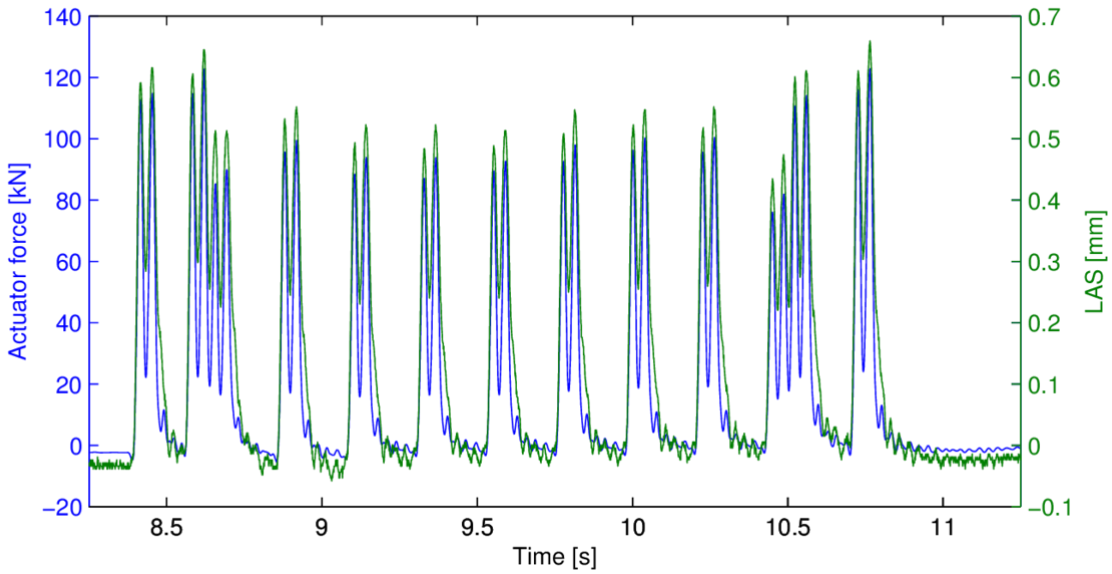

FIGURE 4 ACTUATOR FORCE TIME SERIES REPRESENTING A EUROSTAR-TYPE TRAIN CIRCULATING AT 300KM/H AND RESULTING TRACKDEFLECTION PROVIDED BY THE LASER SYSTEM.

The train model implemented in the in the computational model consists of a set of multi-body system designed to represent train bogies of a Eurostar-type trains. Each bogie model consists of mass-spring-damper elements connecting beam and mass elements representing the unsprung, semi-spring, and spring masses, calibrated to match the corresponding physical properties of the vehicle. A visual representation of a bogie model is shown in Figure 5.

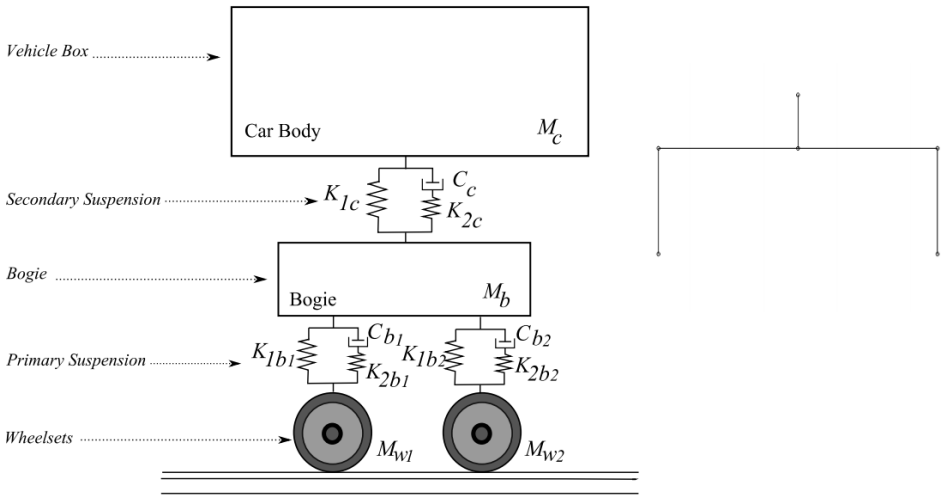

FIGURE 5 VISUAL REPRESENTATION OF A BOGIE MODEL. SOURCE: (FERREIRA, 2010)

Due to the negligible contribution by neighbouring bogies to the dynamic response and in order to reduce the computational cost of each simulation run, each simulation consisted of analysing the passage of a single bogie of the Eurostar train described in (CEDEX, 2015) along the global track. The resulting interaction between the multibody system representing vehicle model and the global track model leads the dynamic train/track system to output a response which is subsequently postprocessed to extract quantities of interest.

5 Model validation with CTB measurements

This section provides an overview of the results on the validation process, comparing results both from the model and from experimental measurements obtained on CTB in (CEDEX, 2015) already referred. Besides, a series of simulation experiments were performed throughout the project to analyse the responses of the reference track model to passages of high-speed trains.

Similarly to the order followed on execution, this section is organized this way: the model validation process based on results from static and quasi-static tests conducted on the Track Box test track are presented in chapter 5.1 and 5.2, as well as a parameter study of the effect of increasing train speeds (from 300 to 400km/h) on the dynamic response produced in the reference track model 5.3.

5.1 Model validation: static test

In the static test, the CTB Trackbox, described before, was subjected to two load/unload cycles of 200 kN. During the loading stage of each load/unload cycle; the track load was applied in increments of 20 kN. During the test, the resulting track deflection was recorded. A thorough description of the Static test performed on the Trackbox physical model is available in (CEDEX, 2015). The actuator force time series used in the test and resulting vertical rail displacement are shown in Figure 6.

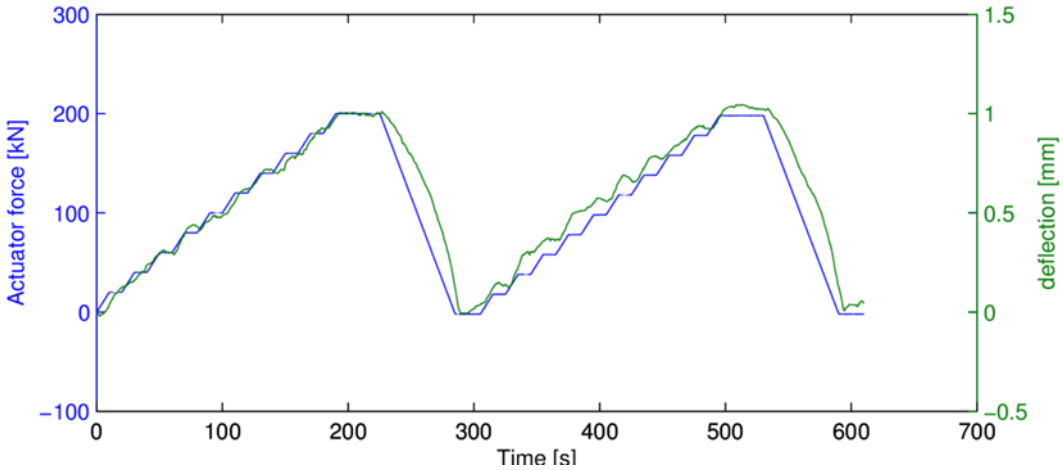

Figure 6 Static test: measured actuator force and vertical rail displacement time series. (CEDEX, 2015)

The inherent variability of the experimental measurements could be observed by contrasting the displacements time series induced by each load cycle. The superposition of the rail displacements obtained from each load cycle is shown in Figure 7.

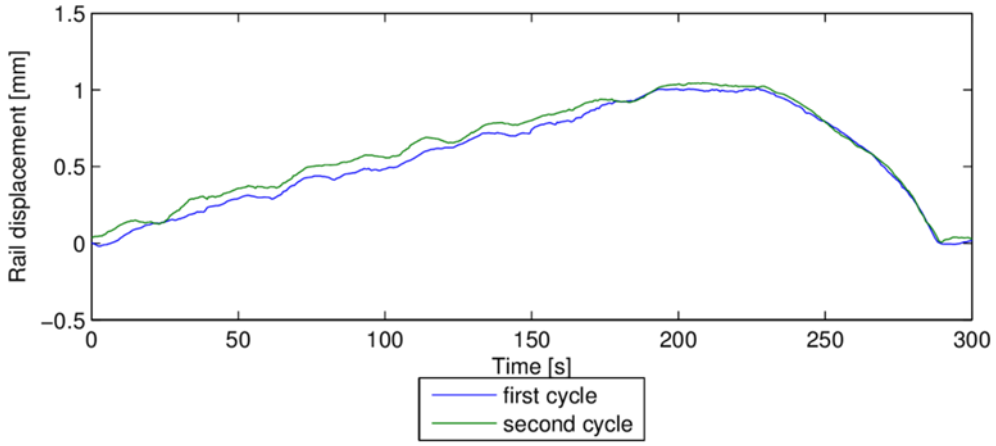

FIGURE 7 STATIC TEST: SUPERPOSED VERTICAL RAIL DISPLACEMENT TIME SERIES.

Due to the quasi-static nature of the track load used in the physical model, a static analysis was employed in the numerical model to simulate the experimental. To evaluate the influence that the uncertainty associated with the Young modulus of the supporting layer might exert on the computational results, two variants of the model were tested, adopting respectively the E_{v2} and E_{max} class of values. The parameters adopted for the E_{v2} and E_{max} model variants employed in this test are presented, respectively, in Table 5 and Table 6.

TABLE 5 STATIC TEST: SUPPORTING LAYER PROPERTIES: E_{v2} VARIANT.

	Layer depth	Young's modulus	Poisson ratio	Dry unit weight
	[m]	[MPa]	[-]	[kN/m3]
Ballast	0,40	230	0,20	17,0
Granular sub ballast	0,30	170	0,30	22,0
Form layer	0,60	165	0,30	21,5
Embankment	2,57	160	0,40	20,2

TABLE 6 STATIC TEST: SUPPORTING LAYER PROPERTIES: E_{MAX} VARIANT.

	Layer depth	Young's modulus	Poisson ratio	Dry unit weight
	[m]	[MPa]	[-]	[kN/m3]
Ballast	0,40	230	0,20	17,0
Granular sub ballast	0,30	440	0,30	22,0
Form layer	0,60	400	0,30	21,5
Embankment	2,57	385	0,40	20,2

The global track model used in the static test represented a section of track 13 sleeper spans in length, comprising totalling 7,8m. A visual representation of the global track model is shown in Figure 8.

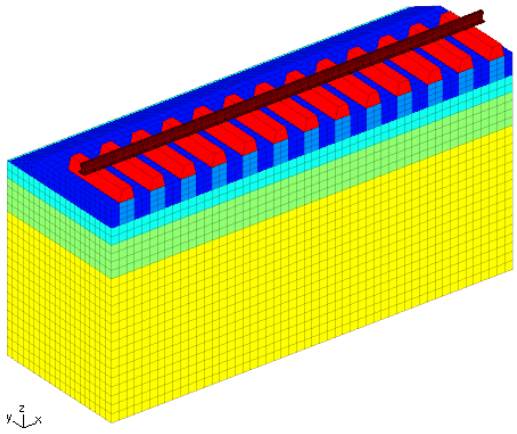

FIGURE 8 STATIC TEST: VISUAL REPRESENTATION OF THE GLOBAL TRACK MODEL.

The rail deflections produced by the numerical model in response to a 200 kN static axle load are shown in Figure 9.

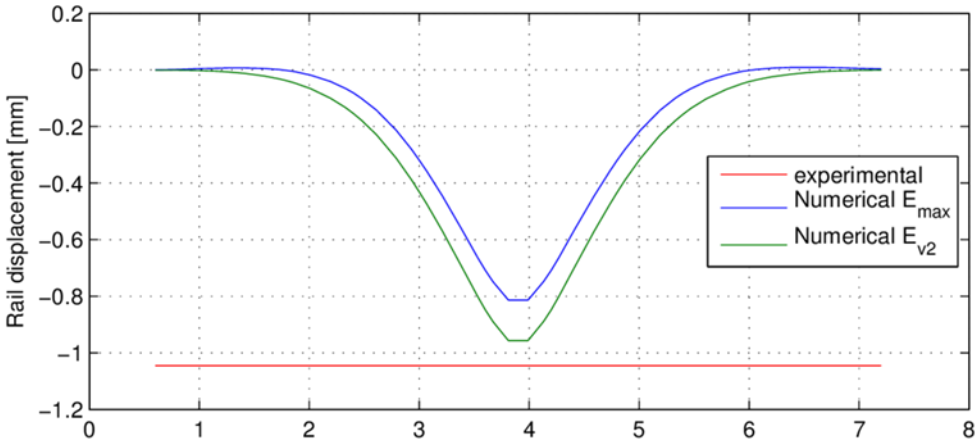

FIGURE 9 STATIC TEST: RAIL DEFLECTION CAUSED BY A 200 KN STATIC AXLE LOAD.

After comparing the deflections obtained from static analysis, it can be noted that the computational results agree with the reference experimental data.

TABLE 7 STATIC TEST: PEAK VERTICAL RAIL DISPLACEMENTS.

Source	Rail displacement [mm]
Experimental	1,05
E_{max}	0,81
E_{v2}	0,96

5.2 MODEL VALIDATION: QUASI-STATIC TEST

In the quasi-static test, the CTB laboratory track was subjected to a synthetic train load represented by a series of time-varying loads applied on the track through force actuators. The actuator force time series superposed with the resulting vertical rail displacements measured in situ are shown in Figure 10.

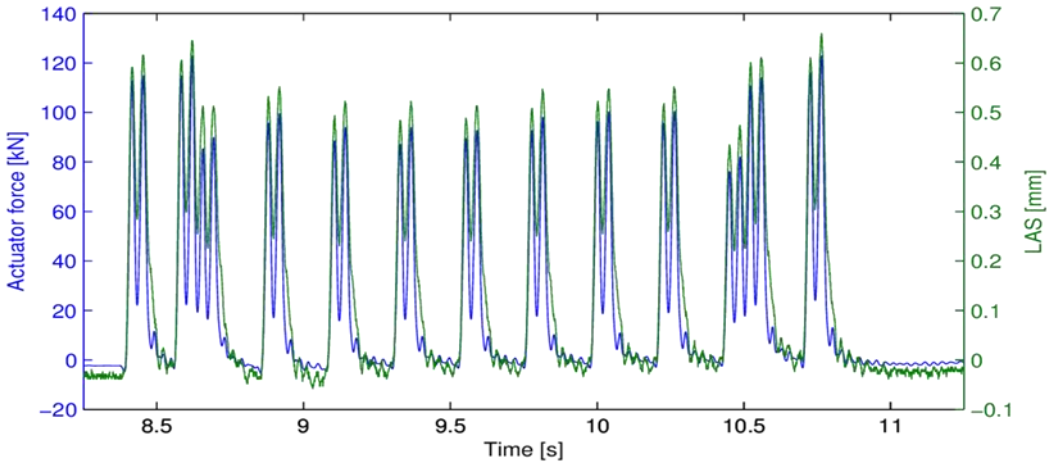

FIGURE 10 QUASI-STATIC TESTS: ACTUATOR FORCE AND VERTICAL RAIL DISPLACEMENT TIME SERIES. (CEDEX, 2015)

The peaks in the actuator force time series agree with the train's load distribution. The axle distances of the simulated train are represented in Figure 11.

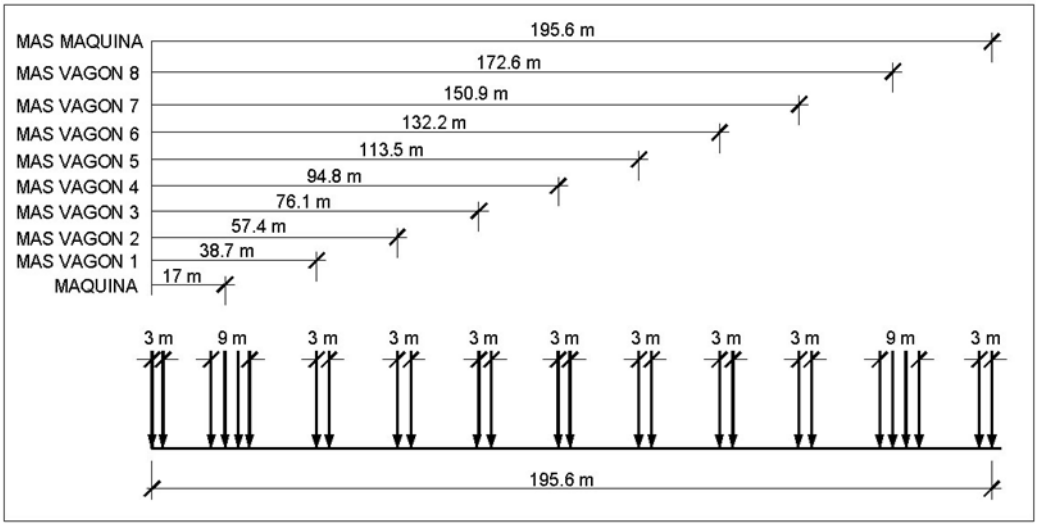

FIGURE 11 QUASI-STATIC TESTS: AXLE LOAD DISTRIBUTION. SOURCE: (CEDEX, 2015).

The inherent variability of the measured track response can be observed by superposing the rail displacements caused by similar loads. To illustrate the variability, the vertical rail displacements caused by the locomotive and coach bogies are shown, respectively, in Figure 12 and Figure 13.

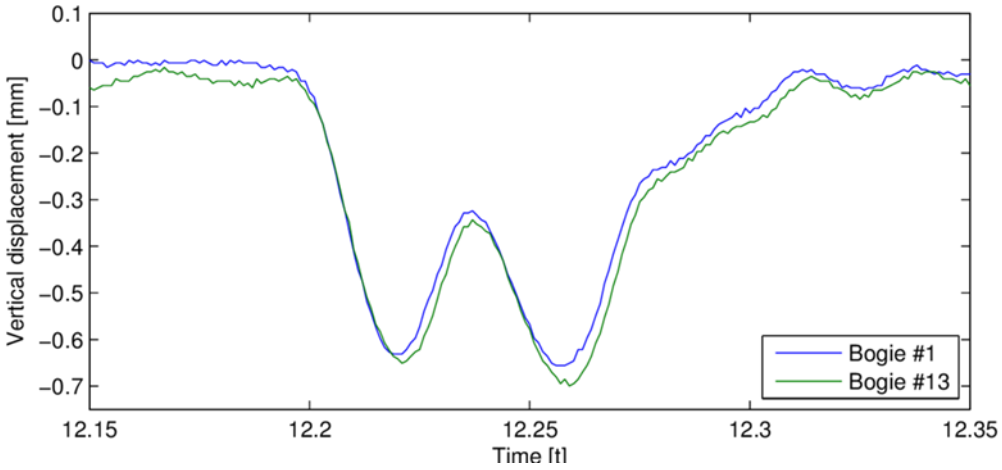

FIGURE 12 QUASI-STATIC TESTS: MEASURED RAIL DISPLACEMENT TO THE PASSAGE OF LOCOMOTIVE BOGIES.

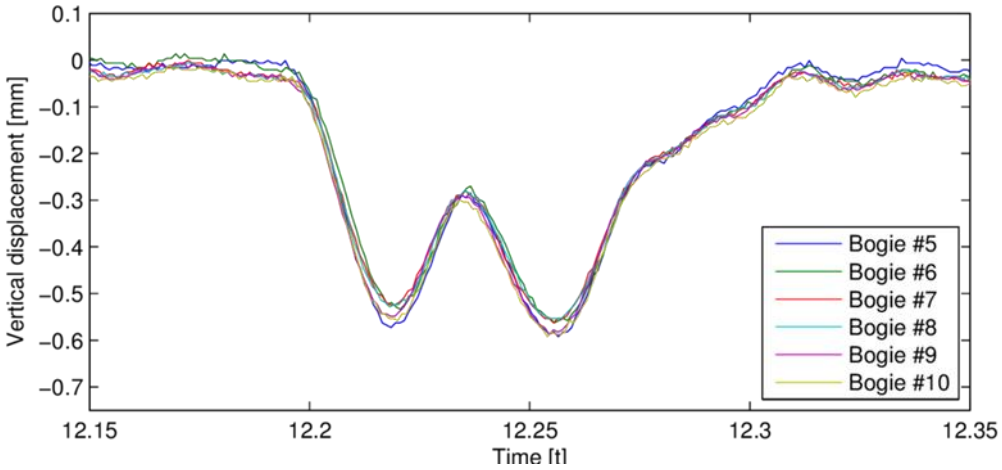

FIGURE 13 QUASI-STATIC TESTS: MEASURED RAIL DISPLACEMENT TO THE PASSAGE OF COACH BOGIES.

The frequency content of the input load should also be taken into account when comparing the output of different models. The magnitude spectrum of the actuator force time series is shown in Figure 14.

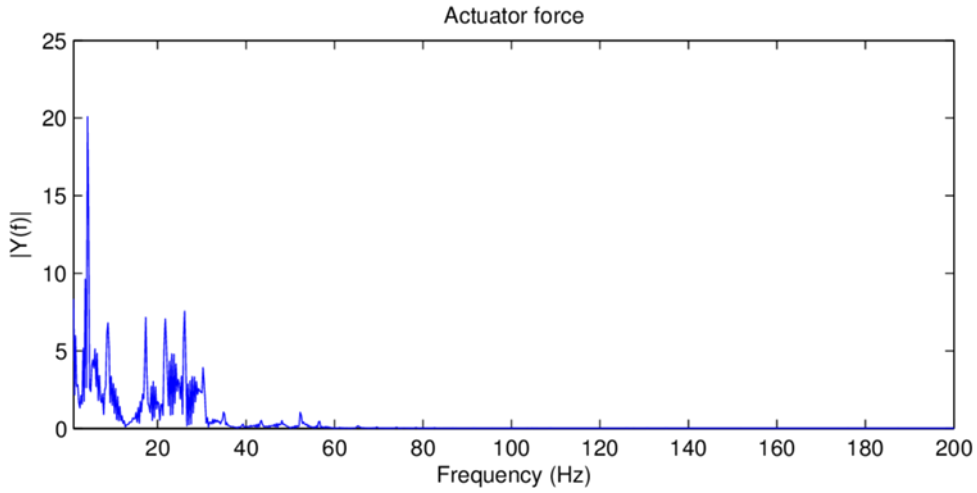

FIGURE 14 QUASI-STATIC TESTS: MAGNITUDE SPECTRUM OF ACTUATOR FORCE TIME SERIES.

It can be noted in the magnitude spectrum represented in Figure 14 that the frequency content of the actuator force signal is almost non-existent above 60Hz. This finding is consistent with the description of the force actuators used in the rail track testing facility at CEDEX included presented in (Moreno-Robles, 2008). The low frequency content of the actuator force signal affects the response exhibited by the track model. The magnitude plot of the vertical acceleration and velocity time series observed on the rail are shown, respectively, in Figure 15 and Figure 16.

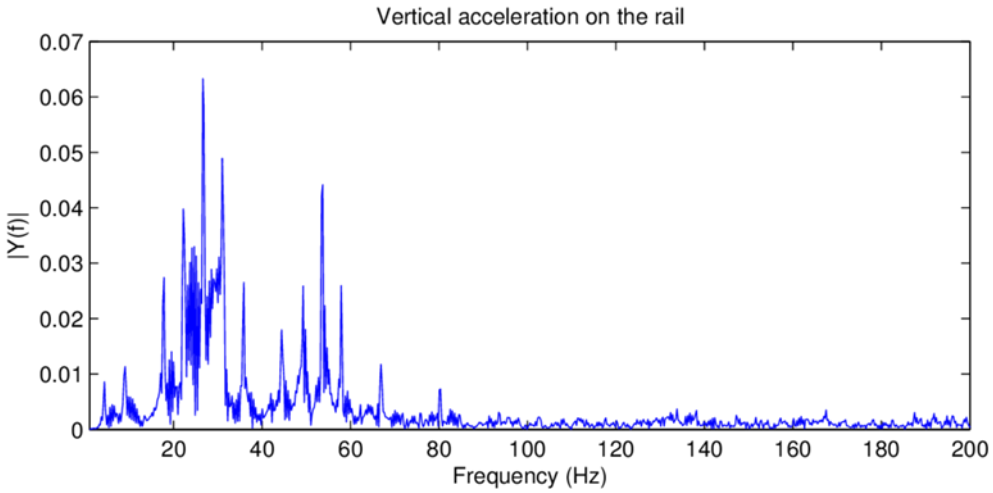

FIGURE 15 QUASI-STATIC TESTS: MAGNITUDE SPECTRUM OF THE MEASURED VERTICAL RAIL ACCELERATION TIME SERIES.

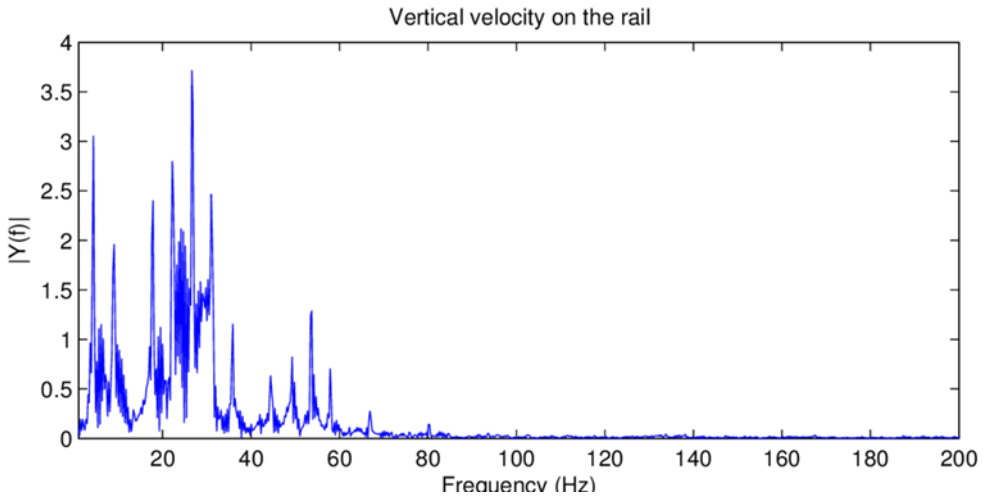

FIGURE 16 QUASI-STATIC TESTS: MAGNITUDE SPECTRUM OF THE MEASURED VERTICAL RAIL VELOCITY TIME SERIES.

The frequency content of the experimental measurements of the response induced by the actuator force indicates that, in order to compare the output of numerical models to the measured output of the physical model, comparisons should be limited to the frequency content that is possible to reproduce in the physical model. Therefore, throughout the validation procedure the contributions to the response coming from higher frequencies will be disregarded in order to make both responses comparable.

According to the information provided in CEDEX's technical report (CEDEX, 2015), the quasi-static test was conducted by subjecting each track model to actions that simulated the passage of a high-speed train circulating at 300km/h. The train model used in the test was described as "a Eurostar train of 195,6m with two locomotives and eight wagons having 13 bogies and 26 axles". The distances between axles are represented in Figure 11.

To corroborate the information made available through the report, the actuator and displacement time series were used to infer the train circulation speed. For this purpose, the actuator force and rail displacement time series represented in Figure 7 were used to estimate the duration between the passages of each axle of the simulated train. The speed estimates were then calculated based on the time intervals extracted from the time series data and the axle distances presented in Figure 2.6. The results are summarized in Table 8 and Table 9.

TABLE 8 QUASI-STATIC TESTS: TRAIN CIRCULATION SPEED ESTIMATES BASED ON WAGON DISTANCES.

		Force Actuator		LAS	
Description	dx [m]	dt [s]	Vel [km/h]	dt [s]	Vel [km/h]
'masvagon 1'	38,70	0,4640	299,71	0,4650	299,61
'masvagon 2'	57,40	0,6880	300,14	0,6910	299,04
'masvagon 3'	76,10	0,9130	300,04	0,9140	299,74
'masvagon 4'	94,80	1,1370	299,97	1,1380	299,89
'masvagon 5'	113,50	1,3610	300,15	1,3630	299,78
'masvagon 6'	132,20	1,5850	300,09	1,5880	299,70
'masvagon 7'	150,90	1,8100	300,04	1,8130	299,64
'masvagon 8'	172,60	2,0710	299,99	2,0720	299,88
'mas maquina'	195,60	2,3490	299,69	2,3500	299,64

TABLE 9 QUASI-STATIC TESTS: TRAIN CIRCULATION SPEED ESTIMATES BASED ON BOGIE DISTANCES.

		Force Actuator		LAS	
Description	dx [m]	dt [s]	Vel [km/h]	dt [s]	Vel [km/h]
'bogie'	3,00	0,0380	283,57	0,0370	291,89
'bogiex2'	9,00	0,1090	296,23	0,1090	297,25
'bogie'	3,00	0,0370	291,03	0,0380	284,21
'bogie'	3,00	0,0380	283,57	0,0350	308,57
'bogie'	3,00	0,0380	283,57	0,0370	291,89
'bogie'	3,00	0,0380	283,57	0,0360	300,00
'bogie'	3,00	0,0380	283,57	0,0350	300,00
'bogie'	3,00	0,0380	283,57	0,0350	300,00
'bogie'	3,00	0,0380	283,57	0,0340	317,65
'bogiex2'	9,00	0,1090	296,23	0,1070	300,00
'bogie'	3,00	0,0390	276,48	0,0380	284,21

From these results, it could be noted that, while the inferred train passage speed agreed with the expected results, there were some discrepancies in the signals generated by the passage of some bogies.

The dynamic nature of the experimental test required the usage of a dynamic train-track interaction analysis to simulate the physical experiment. Due to the negligible contribution by neighbouring bogies to the dynamic track response, the effect exerted on the track by the train was simulated by the passage of a single representative bogie circulating at 300km/h.

The material property values of the supporting layers adopted for this model correspond to the E_{max} values listed in Table 6.

The global track model adopted for this test consists of a 22,2 m section of track incorporating 37 sleepers. A visual representation of the global track model is shown in Figure 17.

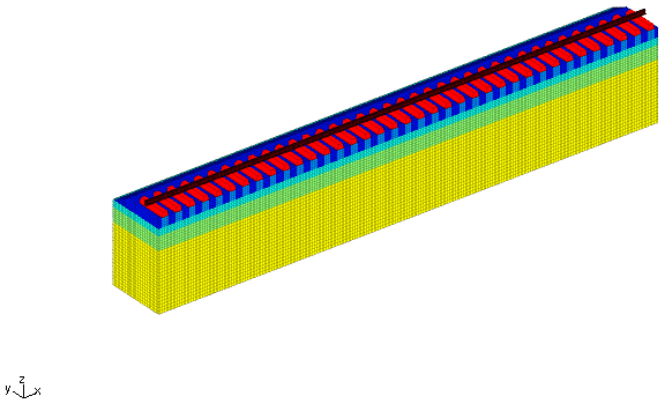

FIGURE 17 QUASI-STATIC TESTS: VISUAL REPRESENTATION OF THE GLOBAL TRACK MODEL.

A model of the Eurostar train circulating at 300km/h was used to reproduce the quasi-static test conducted on the physical test track.

The numerical model was subjected to a validation test based on the experimental measurements taken from the physical model described in Section previously which represents the case of a ballasted track subjected to a synthetic load designed to simulate the passage of a train circulating at 300km/h.

The dynamic response of the railway track was characterized by kinematic time series collected on points within the global track model matching the locations of each sensor installed in CEDEX's Track Box test track, already referred. A comparison between the vertical rail displacement produced by the numerical model and experimental measurements is shown in Figure 18.

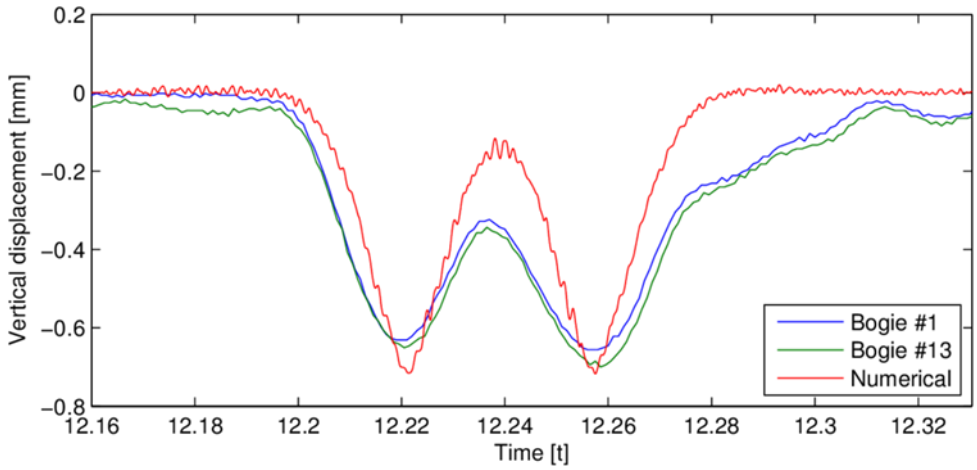

FIGURE 18 QUASI-STATIC TESTS: COMPARISON BETWEEN PHYSICAL MEASUREMENTS AND MODEL RESPONSE: VERTICAL RAIL DISPLACEMENT TIME SERIES.

Track dynamic responses inside the track could be also compared. A comparison of vertical acceleration time series on ballast and on subballast collected from the physical model and outputted by the computational model are shown in Figure 19 and Figure 20.

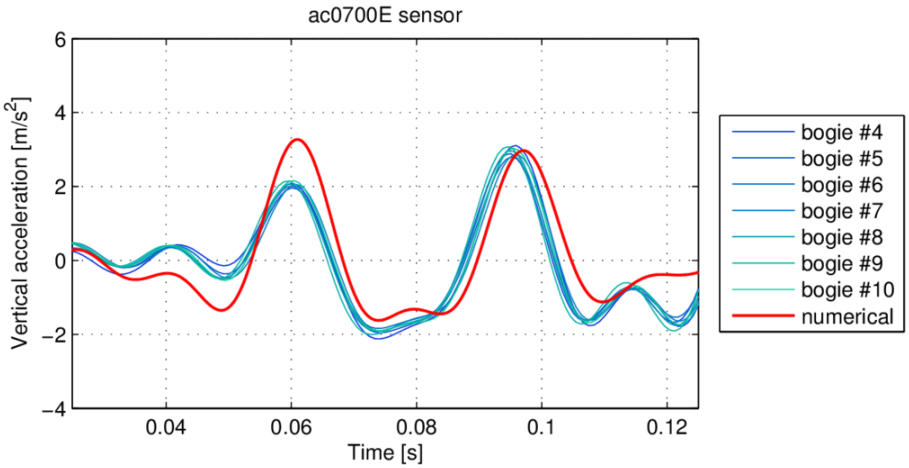

FIGURE 19 COMPARISON BETWEEN EXPERIMENTAL MEASUREMENTS AND COMPUTATIONAL RESPONSE: VERTICAL BALLAST ACCELERATION TIME SERIES GENERATED BY A EUROSTAR-TYPE TRAIN CIRCULATING AT 300KM/H.

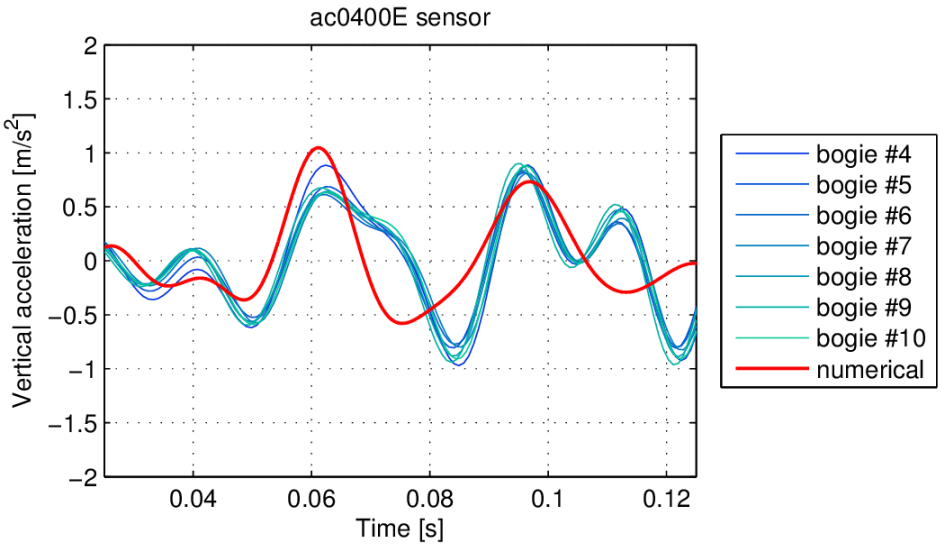

FIGURE 20 COMPARISON BETWEEN EXPERIMENTAL MEASUREMENTS AND COMPUTATIONAL RESPONSE: VERTICAL SUB-BALLAST ACCELERATION TIME SERIES GENERATED BY A EUROSTAR-TYPE TRAIN CIRCULATING AT 300KM/H.

Results show that in spite of the diverse nature of the obvious different methods used to simulate trains and track on the physical and computational models, the response measured on the physical model agrees well with the output of the computational model.

5.3 INFLUENCE OF TRAIN SPEED INCREASE

After validation test and process to which the numerical model was subjected to it must be said that confidence on the model for CTB track case was attained. So, the model certainty and accuracy is reinforced and it is considered as ready to be use further on to estimate other situations.

One of those situations is to evaluate the impact that the increase of train speeds above 300km/h would have on the dynamic performance of the CTB track reference case.

However, it must also be mentioned that, up to now, it wasn't possible to compare the output of the numerical model with field measurements collected on tracks subjected to the passage of trains circulating at speeds as high as 400 km/h, particularly on tracks equipped with USPs. Therefore, the responses produced by the numerical model for speeds around 400km/h should be analysed with caution.

In this subchapter are shown results obtained from a parametric study conducted to evaluate the response of reference CTB track model with regards to the train speed. The experiment consisted of simulating passages of a Eurostar-type train on the reference track model at speeds ranging from 300km/h to 400km/h. The train speed values used in this study were selected based also on other C4R partners regarding reference train speeds currently in use or of practical interest. The parameters used in the parametric study and the corresponding levels are listed hereafter.

TABLE 10 TRAIN SPEED PARAMETRIC STUDY: PARAMETERS AND CORRESPONDING LEVELS.

Parameter	Levels
Train speed [km/h]	{300, 320, 330, 340, 360, 380, 400}

Some of the results obtained for CTB track dynamic response are maximum values for track accelerations. Figure 21 shows peak vertical acceleration values resulting from train passages at varying speed levels observed inside ballast layer (at varying depths).

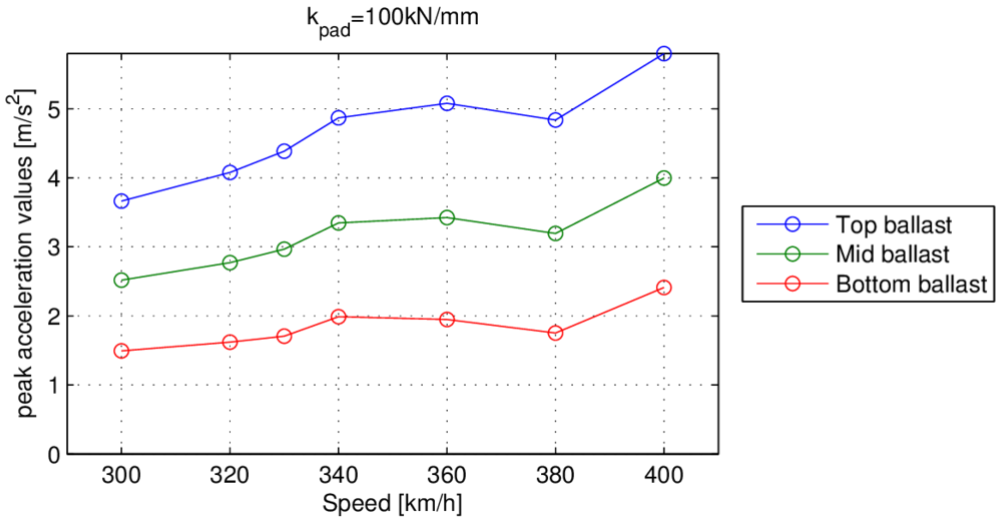

FIGURE 21 TRAIN SPEED PARAMETRIC STUDY: PEAK VERTICAL ACCELERATION VALUES WITHIN THE BALLAST LAYER.

Results show that peak vertical acceleration values observed near the top surface of the ballast layer exhibited a pronounced sensitivity to train speed increases, confirming that peak vertical accelerations increase with train speed. However, it may also be inferred that the amplitudes are rapidly attenuated in-depth of the ballast layer. Furthermore, peak vertical displacement values caused by each train speed level are shown in Figure 22.

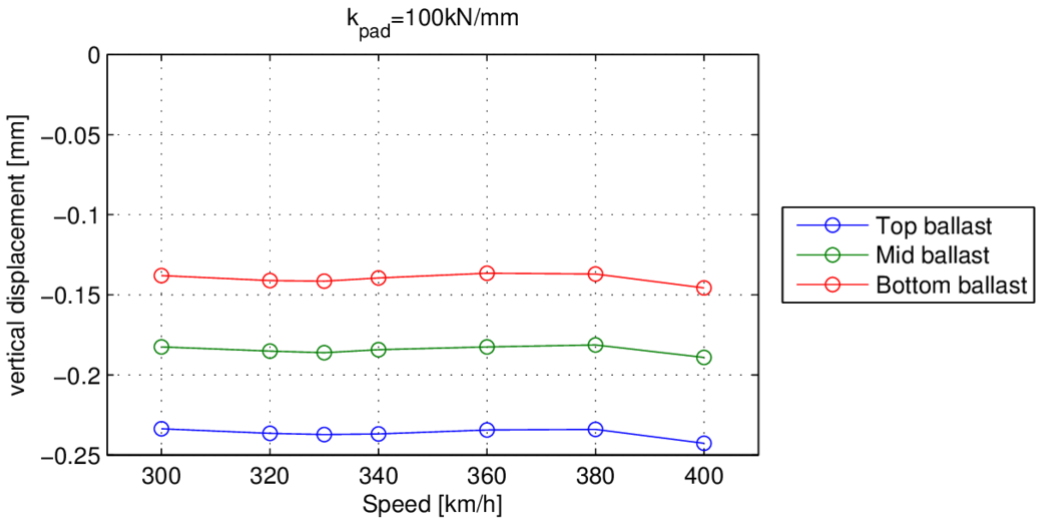

FIGURE 22 TRAIN SPEED PARAMETRIC STUDY: PEAK VERTICAL DISPLACEMENT VALUES WITHIN THE BALLAST LAYER .

Results indicate that peak vertical displacements outputted by the reference track model are practically insensitive to train speed.

6 Numerical estimations of track responses at vhs

Already in presence of a validated numerical model and having as main goal of Task 1.2.2 to propose optimized innovative track design for very high speed. As said before, it is intended to analyse in which measure the combination of different kind of railpads acting together with pads under sleepers would lead effectively to an enhanced dynamic track behaviour.

First of all, the idea was to use the model as a tool to provide as much information concerning track dynamic responses for as many different track design solutions as possible within the parameters of interest for railpads and USP.

In parallel, also many sensitivity analyses were carried out on the CTB case in order to test many different situations, varying design parameters and soil characteristics so as to assure some particular tendencies or influences seemed correct.

Hence, this chapter presents the main results of the computed estimations of different track responses at vhs and it is divided as follows:

- Evaluate the predicted dynamic response of the reference railway track when equipped with specific combinations of railpads and under-sleeper pads (USPs):
    - overview of track responses (response surfaces)
    - test plan 1
    - test plan 2
- Influence of train speed increase until 400 km/h on the dynamic behaviour of the railway track within the track supporting layers when subjected to the passage of a train.

During WP1.2.2, IST, together with partners CEDEX and ADIF, have been working in a parametric study to evaluate the predicted dynamic response of the reference railway track when equipped with specific combinations of railpads and under-sleeper pads (USPs). The numerical model used for the simulations was already validated based on the data provided by CEDEX from the tests conducted on the physical model of a ballasted track with granular subballast (chapter 5). Hence, the short term response of the test track, represented by experimental measurements collected on the CTB Track Box test track, were used as benchmark results.

6.1 Overview of track responses for track design variations

In order to guide the way to better discern which seemed the track solutions (rp/usp combinations on CBT) that conduced to better dynamic track behaviour, an algorithm was built to optimize the analysis. The goal was to obtain in the end, a space search of track response surfaces for certain ranges of design parameters. Hence, a multi-objective optimization problem was formulated to identify combinations of rail pads and USPs that minimized the predicted peak vertical acceleration levels observed on two points within the track: the sleepers and on top of the ballast layer. The design parameters adopted for this problem were the nominal vertical stiffness of the rail pads and USPs.

The resulting optimization problem, first presented in (Maciel & Ferreira, 2016), is characterized as an unconstrained global multi-objective optimization problem with computationally expensive “black-box” objective functions. Due to the characteristics of the optimization problem, the optimization algorithm adopted for this task was a multi-objective variant of the DIRECT algorithm,

developed in-house. As the algorithm was developed to solve bounds-constrained optimization problems, it was necessary to adopt bounds for the rail pad and USP's vertical stiffness values. The bounds adopted for each design parameter are listed in Table 11.

TABLE 11 DESIGN SPACE BOUNDS.

Design parameter	Lower bound	Upper bound
Rail pad vertical stiffness (k_{pad})	20 kN/mm	200 kN/mm
USP vertical stiffness (k_{usp})	20 kN/mm	500 kN/mm

Some values were exaggerated (comparing to what exists in railway practice) on purpose, as the idea was to have a generalised overview of what could be the responses in a broader perspective.

The application of the procedure guided the multiple simulations executed and interesting results could then be obtained. The data generated throughout the procedure was used to generate contour plots of the peak vertical acceleration values observed on sleepers and within the ballast layer, shown respectively in Figure 23 and Figure 24.

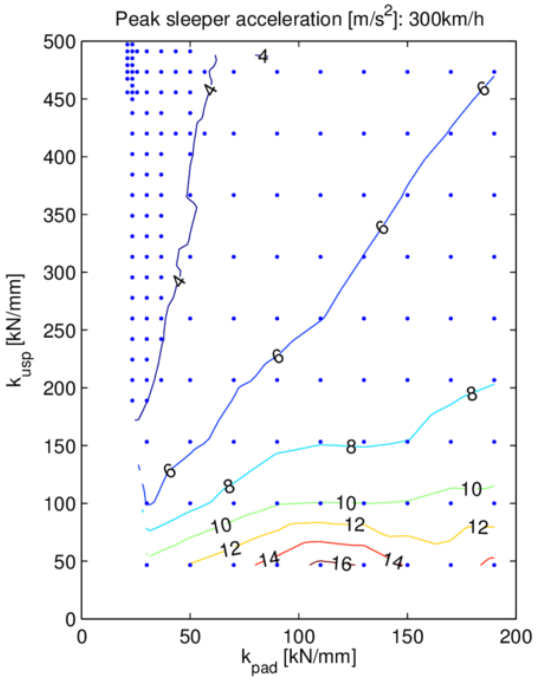

FIGURE 23 CONTOUR PLOT OF PEAK SLEEPER ACCELERATION VALUES: 300KM/H.

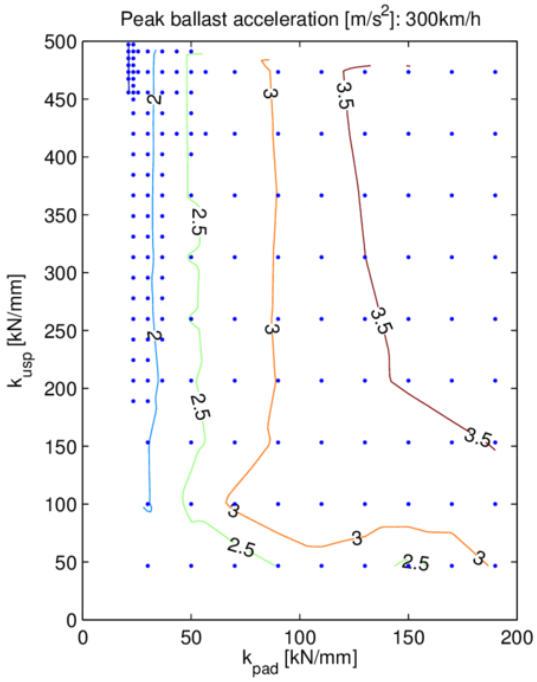

FIGURE 24 CONTOUR PLOT OF PEAK BALLAST ACCELERATION VALUES: 300KM/H.

In Figure 23 and Figure 24, each blue dot represents a sample point within the design space that was evaluated by the optimization algorithm. The evaluation of each sample point represents a simulation of a track design variant subjected to the passage of a train circulating at 300km/h. Each track variant is characterized by the combination of a rail pad and a USP, represented by their nominal vertical stiffness. The output of each simulation was subjected to a post-processing procedure to extract response quantities of interest, represented by peak vertical acceleration values observed on top of the ballast layer and on sleepers.

The concentration of sampling points, and resulting isocurves, indicate that, within the design space considered in this problem, the lowest acceleration levels observed not only on sleepers but also within the ballast layer were dictated by the activation of two arbitrary constraints: the lower bound of the rail pad vertical stiffness, and the upper bound of the USP vertical stiffness. Consequently, as there is no global minimum within the design space, optimal track solutions are dictated by specifying additional design constraints and requirements, such as specifying a target for the track's global track stiffness. From the peak acceleration isocurves, the following conclusions can be found:

- Qualitatively, the link between peak vertical stiffness levels and the design parameters (vertical stiffness of rail pads and USPs) is observed on all circulation speeds.
- Softer USPs lead to higher peak vertical sleeper acceleration level, particularly with vertical stiffness values lower than 150kN/m. Below this threshold, rail pads don't exert a significant influence on the response produced by railway sleepers. For stiffer USPs, increasing rail pad stiffness leads to an increase in peak vertical sleeper accelerations.
- USPs exert significant influence on peak vertical ballast accelerations when their stiffness falls below 100kN/mm. Above this threshold, results show that the dynamic response of railway is determined almost exclusively by the choice of rail pads.
- Results suggest that the simultaneous reduction of peak vertical acceleration levels observed on ballast and sleepers can be achieved by using soft rail pads, accompanied by the introduction of stiff USPs.

It should be stressed that, due to the limited availability of in-situ measurements of railway tracks equipped with USPs, the numerical model wasn't yet subjected to a validation process that covers this particular track solution. Therefore, results should be interpreted with care.

Previous results were discussed with other partners among the WP1.2. Crossing this with real/possibly existent USP and railpads and taking in consideration that results should support CEDEX to prepare the upcoming experimental tests, some particular track design variants stood out and were selected for further numerical tests. Further parametric studies were then carried out in order to examine closer different track responses enabling to have a benchmark of several track design solutions. In the following chapters are presented results obtained from two test plans undertaken.

6.2 TEST PLAN 1 – PARAMETRIC STUDY

As said before, the influence of changing properties of railpads and under-sleeper pads (USPs) is analysed using different track design cases. After the surface responses obtained previously and what was mentioned before, a first test plan consisting of a parametric study was conceived.

The parametric study was conducted to simulate the dynamic response of track design variants covered by the test plan when subjected to passages of trains circulating at high and very high speeds. Each variant is referred to as $M(k_{pad}, k_{usp})$.

The track design variants evaluated in this parametric study consisted of the following variants: M(100,-), M(40,-), M(60,-), M(40,80), M(60,80), M(80,80), M(100,80), M(80,50), M(100,50). Being M(100,-) in reality the same as CTB track reference case. The two last track variants M(80,50), M(100,50) represents track is equipped with softer USPs than the others. The complete list of track variants covered by the parametric study is presented in Table 12.

TABLE 12 TEST PLAN 1 TRACK DESIGN VARIANTS.

Test reference	Kpad [kN/mm]	Kusp [kN/mm]	Variant description	*Notes*
Test 1	100	-	M(100,-)	*CTB Track box Reference*
Test 2	40	-	M(40,-)	
Test 3	60	-	M(60,-)	
Test 4	40	80	M(40,80)	*Test 2 + USP*
Test 5	60	80	M(60,80)	*Test 3 + USP*
	80	80	M(80,80)	*Additional variant*
Test 1 + USP	100	80	M(100,80)	*Reference + USP*
	80	50	M(80,50)	*Additional variant*
	100	50	M(100,50)	*Additional variant*

6.2.1 INFLUENCE OF TRAIN SPEED INCREASE

As also the impact of increasing train speeds is to be tested, each track variant was subjected to the passage of a train circulating at high and very high speeds, from 300 to 400km/h. Consequently, the parametric study consisted of applying a full factorial design resulting from the combination of the set of track variants with the train speed levels. The full factorial design of the experiment is characterized by the parameter levels listed in Table 13.

TABLE 13 TEST PLAN 1 PARAMETRIC STUDY: PARAMETER LEVELS.

Parameter	Levels
Track variant	M(100,-), M(40,-), M(60,-), M(40,80), M(60,80), M(80,80), M(100,80), M(80,50), M(100,50)
Train speed [km/h]	300, 320, 330, 350, 360, 380, 400

To evaluate the impact of the train circulation speed on the dynamic response of each track variant, peak acceleration values were expressed with regards to train speed. The response within the ballast layer is represented in the graph shown in Figure 25.

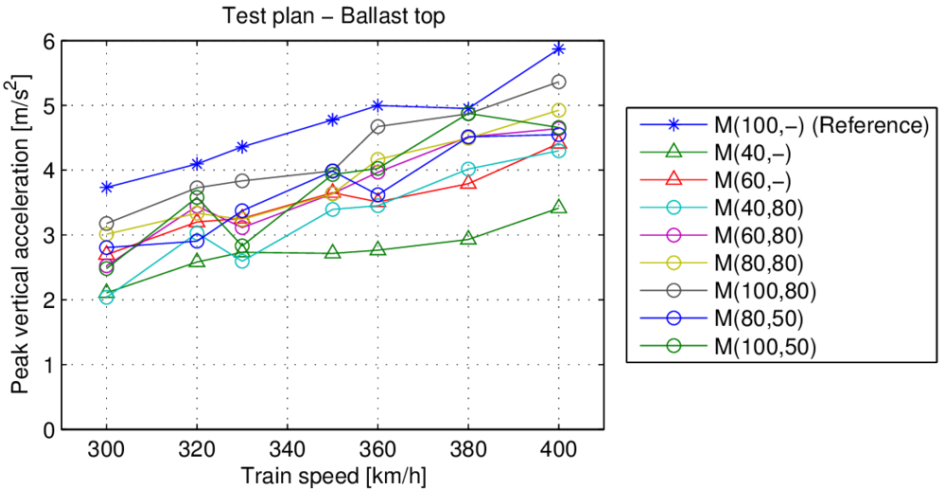

FIGURE 25 PEAK BALLAST ACCELERATION WITH REGARDS TO TRAIN CIRCULATION SPEED.

From the image shown above, it can be noted that, when compared with the CTB reference track, all track design variants covered by the parametric study lead to a reduction in peak vertical

acceleration levels within the ballast layer. This observation is consistent with two aspects of the test: incorporating softer rail pads to CTB (represented by M(40,-) and M(60,-)), and the introduction of USPs (the remaining tests, but in particular the M(100,80) variant representing CTB+USP variant. The same analysis was also applied to peak sleeper vibration levels, whose results are shown in Figure 26.

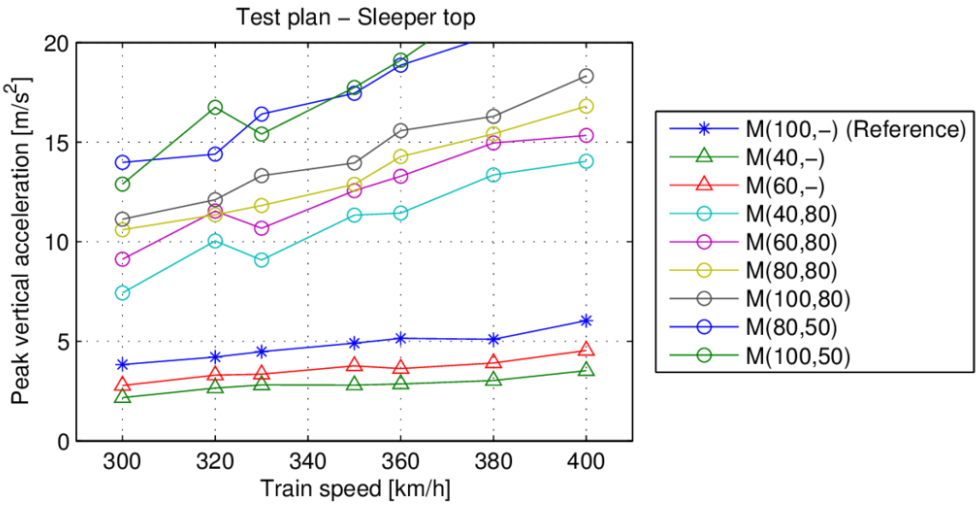

FIGURE 26TEST PLAN1: PEAK SLEEPER ACCELERATION WITH REGARDS TO TRAIN CIRCULATION SPEED.

The results show a stark contrast between the response obtained from track variants with and without USPs. This observation is consistent with the expected outcome of reducing the sleeper's support stiffness, as described in the general overview of the track response presented in Section 6.1. It should also be noted that reducing the rail pad's vertical stiffness also reduces the peak vertical sleeper acceleration levels.

The peak sleeper and ballast acceleration values obtained from the parametric study were used to compare each track variant in terms of dynamic behaviour. The peak acceleration levels obtained from simulations conducted with a circulation speed of 300km/h are shown in Figure 27.

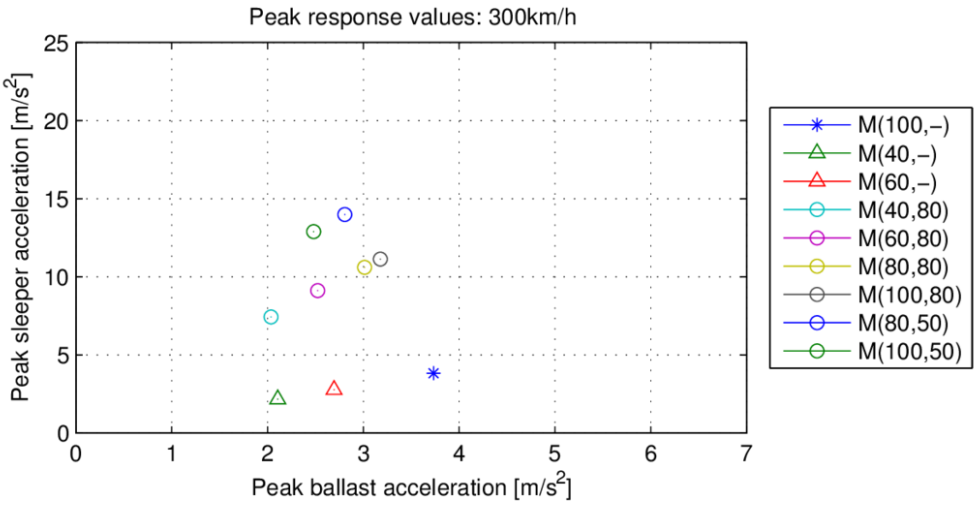

FIGURE 27TEST PLAN: PEAK ACCELERATION RESPONSES: 300 KM/H.

The results shown above in Figure 27 show that variants equipped with USPs lead to higher peak sleeper acceleration values when compared with the response produced by the reference track. Additionally, the results also show that adding USPs to the Test 2 and Test 3 variants, which is observed by comparing the response outputted by M(40,-) with M(40,80) and M(60,-) with M(60,80), results in a notable increase in peak sleeper acceleration levels, accompanied with a marginal reduction in peak ballast acceleration levels.

Qualitatively, the same conclusions can be drawn from the results obtained from all train speed evaluated in this parametric study, as can be noted from the peak response levels obtained from train circulation speeds of 350km/h and 400 km/h, shown respectively in Figure 28 and Figure 29.

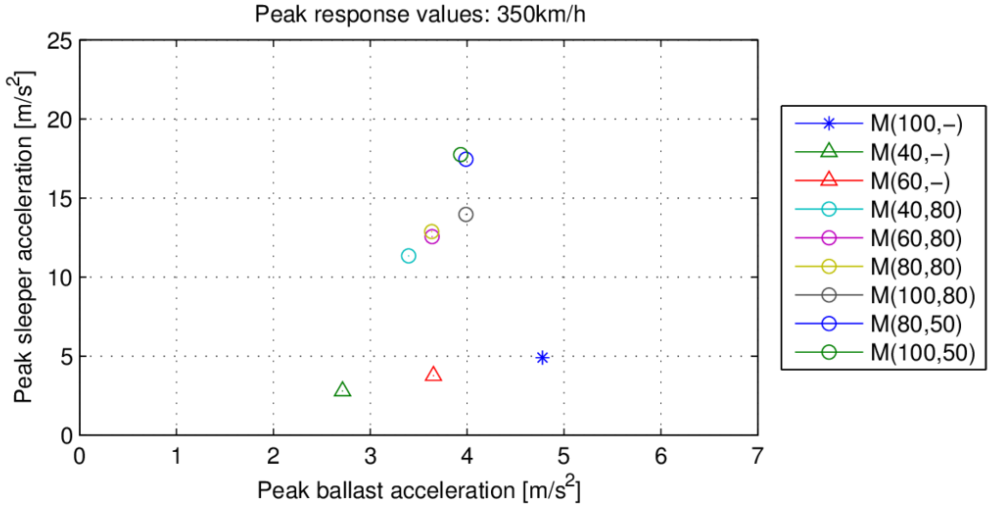

FIGURE 28 TEST PLAN: PEAK ACCELERATION RESPONSES: 350 KM/H.

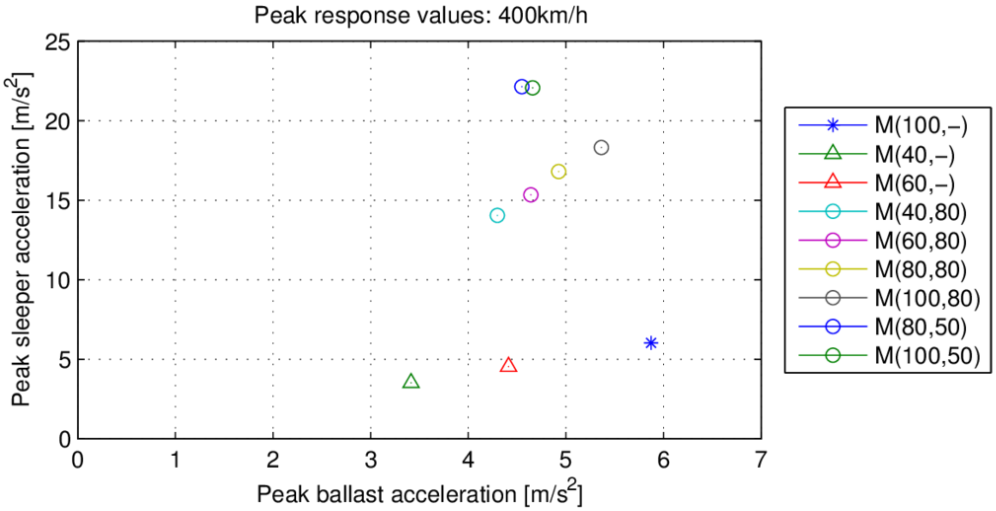

FIGURE 29 TEST PLAN: PEAK ACCELERATION RESPONSES: 400 KM/H.

6.3 TEST PLAN 2 – PARAMETRIC STUDY

Test plan 2 consists on a parametric study conducted to evaluate the performance of track design variants including this some solutions equipped with stiff USPs, instead. To help this benchmark and to analyse the performance, the variants with stiff USPs are compared with the output of the track variants included in the test plan covered in the previous section, taking out the ones with softer USPs to make graphics more clear. The track design variants equipped with stiff USPs covered in this study are the M(60,200) track variant and the M(60,500), which would mean a USP vertical stiffness of 200kN/mm and 500kN/mm respectively. It is known that in present such USP are still difficult to be built in industry, but even so, this hypothesis was tested numerically for comparison with the others. The complete list of track variants covered by the parametric study is presented in Table 14 .

TABLE 14 TEST PLAN2 WITH STIFF USPS: TRACK DESIGN VARIANTS.

Test reference	Kpad [kN/mm]	Kusp [kN/mm]	Variant description	*Notes*
Test 1	100	-	M(100,-)	*CTB Track box Reference*
Test 2	40	-	M(40,-)	
Test 3	60	-	M(60,-)	
Test 4	40	80	M(40,80)	*Test 2 + USP*
Test 5	60	80	M(60,80)	*Test 3 + USP*
	80	80	M(80,80)	*Additional variant*
Test 1 + USP	100	80	M(100,80)	*Reference + USP*
	60	200	M(60,200)	*Additional variant*
	60	500	M(60,500)	*Additional variant*

Each track variant was subjected to the passage of a train circulating at high and very high speeds. Consequently, the parametric study consisted of applying a full factorial design resulting from the combination of the set of track variants with the train speed levels. The full factorial design of the experiment is characterized by the parameter levels listed in Table 15.

TABLE 15 TEST PLAN 2 WITH STIFF USPS: PARAMETER LEVELS.

Parameter	Levels
Track variant	M(100,-), M(40,-), M(60,-), M(40,80), M(60,80), M(80,80), M(100,80), M(60,200), M(60,500)
Train speed [km/h]	300, 320, 330, 350, 360, 380, 400

6.3.1 INFLUENCE OF TRAIN SPEED INCREASE

To evaluate the impact of the train circulation speed on the dynamic response of each track variant, peak acceleration values were expressed with regards to train speed. The response within the ballast layer is represented in the graph shown in Figure 30

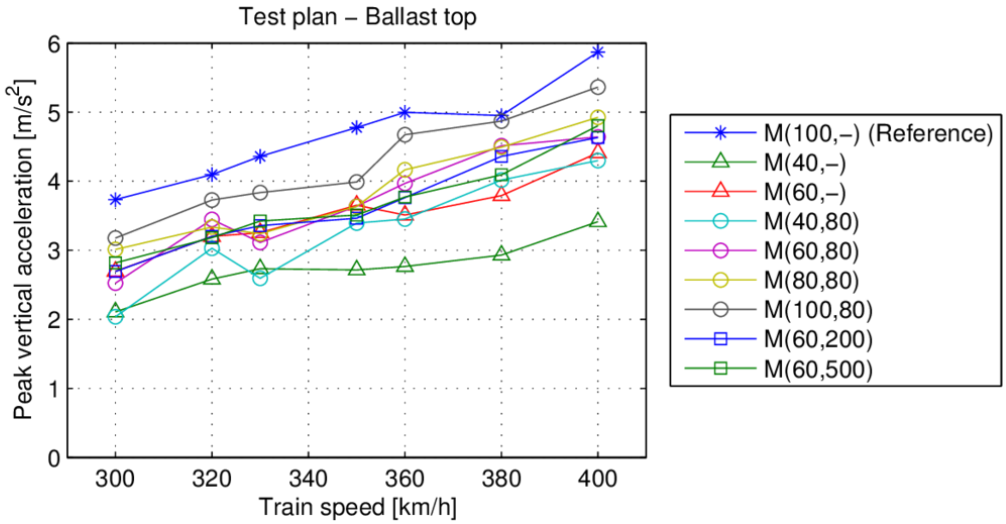

FIGURE 30 STIFF USPS: PEAK BALLAST ACCELERATION WITH REGARDS TO TRAIN CIRCULATION SPEED.

The results shown in Figure 30 indicate that peak vertical ballast acceleration levels outputted by design variants equipped with stiff USPs (i.e., M(60,200) and M(60,500) variants) are lower than the accelerations outputted by the reference track model. Additionally, the vertical ballast acceleration outputted by the variants equipped with stiff USPs are in line with the results outputted by other variants equipped with USPs. This result is consistent with the observation made previously on how introducing USPs invariably resulted in lower ballast accelerations with regards to the response outputted by the CTB reference track model.

To evaluate the impact of stiff USPs on sleeper vibration levels, peak vertical sleeper accelerations are shown in Figure 31.

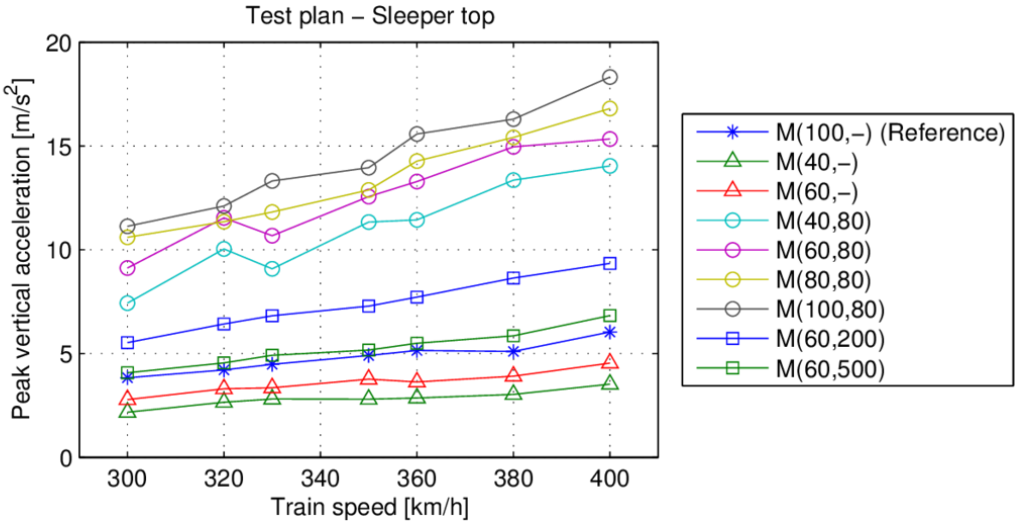

FIGURE 31 STIFF USPS: PEAK SLEEPER ACCELERATION WITH REGARDS TO TRAIN CIRCULATION SPEED.

Results show that peak vertical sleeper acceleration levels outputted by the design variants equipped with stiff USPs are higher than peak sleeper accelerations outputted by the reference track model. This observation is in line with the observation that introducing USPs reduces vibration levels within

the ballast layer at the expense of higher sleeper and rail vibration levels. However, unlike the responses outputted by other variants equipped with USPs, the stiff USP-equipped variants outputted peak sleeper accelerations which were comparable with the vibration levels of the CTB reference track model, albeit slightly higher peak acceleration levels outputted by the M(60,500) variant were marginally higher, almost coinciding.

To compare the performance trade-offs of each track design variant covered in this parametric study, peak sleeper and ballast accelerations of each track variant resulting from an train circulating at 300km/h are represented in Figure 32.

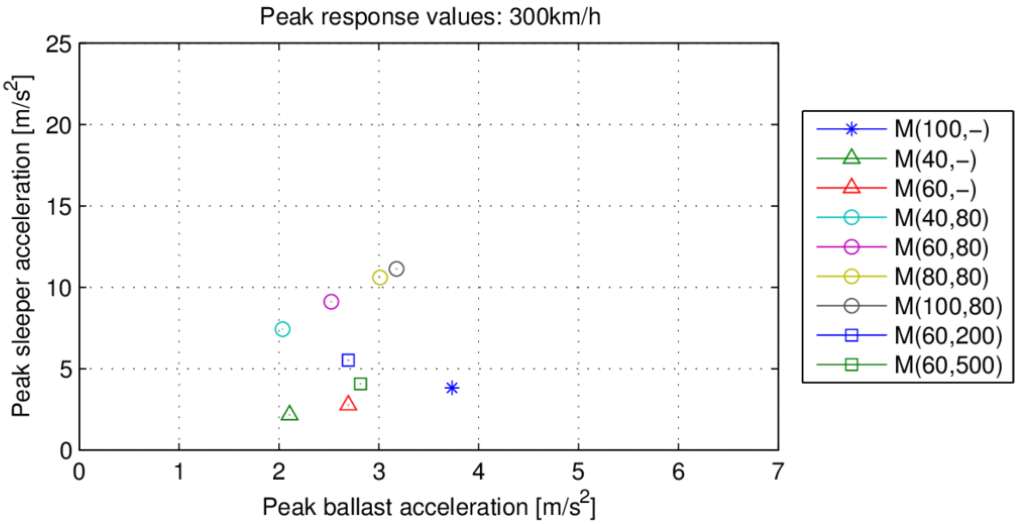

FIGURE 32 STIFF USPS: PEAK ACCELERATION RESPONSES: 300 KM/H.

As can be noted in the plot shown in Figure 32, both variants equipped with stiff USPs (i.e., M(60,200) and M(60,500)) output significantly lower peak ballast accelerations than the reference track model while increasing peak sleeper accelerations by a small margin. This trade-off between ballast and sleeper vibration levels presents itself as a better trade-off than the performance shown by other variants equipped with USPs. Moreover, both variants equipped with stiff USPs dominate the M(80,80) and M(100,80) track design variants by outputting slightly lower peak ballast accelerations while halving peak sleeper accelerations.

The same observations can be made based on the dynamic response of each track design variant when subjected to a train circulating at 350km/h, as shown in Figure 33.

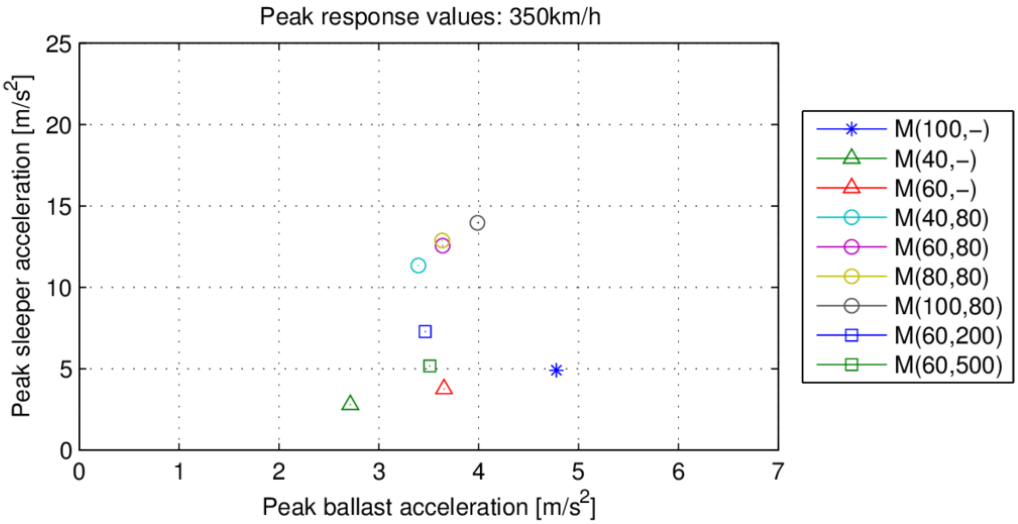

FIGURE 33 STIFF USPS: PEAK ACCELERATION RESPONSES: 350 KM/H.

As can be noted from the results shown in Figure 33, variants equipped with stiff USPs significantly reduce ballast vibration levels while slightly increasing peak sleeper accelerations. However, at 350km/h, variants with stiff USPs dominate all but one variant equipped with USPs while halving peak sleeper accelerations.

These results suggest that stiff USPs may attenuate ballast vibration levels at the expense of a more satisfactory trade-off in performance. However, it should be stressed out that these results should be interpreted with caution as, again, the computational model was not validated for designs equipped with USPs. Consequently, results should be interpreted with care.

7 Track design optimization process

As said before, it is intended to analyse in which measure the combination of different kind of railpads acting together with USPs would lead effectively to an enhanced dynamic track behaviour. The goal is to find the best combination(s) of both rp/USP to maintain track vibrations within acceptable levels, even for train speeds as high as 400km/h. The search for this ballasted track solution using the numerical model already presented is the target.

A track design optimization process was then conducted to identify railway track designs which lead to improvements in the performance of the track to the results produced by the reference track. Additionally, the track design optimization process was established to determine which design variants performed better on train speeds ranging from 300km/h to 400km/h.

The track design variants analysed in these numerical tests consisted of variants of the reference model which incorporate rail pads with lower vertical stiffness (softer rail pads), as well as USPs. The track performance was evaluated with regards to key dynamic track response quantities of interest derived from vertical displacement and acceleration time series taken inside the track within the supporting layers and also on sleepers and rails.

This consists on a track design optimization process that will take into account estimations done in the tests plan whose results were presented previously in chapter 6.

After results obtained in test plan 1 and 2 and to concentrate the review on the improvements that were obtained by using the combination of rail pads and USPs covered in the parametric study a selection process was implemented to pick a set of representative variants. As global track stiffness is a key factor in the design of railway tracks (Li & Selig, 1998) (Li & Selig, 1998) (López-Pita, et al., 2004), this factor was used to classify the variants analysed in the parametric study based in track stiffness levels.

The global track stiffness of each variant of the reference model was evaluated by applying a static axle load on the railway track (on the rail on the sleeper) and computing the relationship between this load and the corresponding rail vertical displacement. The resulting values of the global track stiffness of each variant are listed in Table 6.

TABLE 16 GLOBAL TRACK STIFFNESS DERIVED FROM A STATICALLY-APPLIED AXLE LOAD (IN KN/MM).

		K_{pad} [kN/mm]			
		40	60	80	100
K_{usp} [kN/mm]	20	40.6	44.0	46.1	47.4
	40	52.2	58.7	62.7	65.5
	60	58.1	66.6	72.2	76.1
	80	61.8	71.7	78.4	83.2
	100	64.2	75.2	82.8	88.3

As expected, the results indicate a high sensitivity of the global track stiffness with regards to the vertical stiffness of the rail pads and the USPs. It can also be noted that the global track stiffness exhibited by the track variants analysed in the parametric study are spread over a wide range of values.

To focus the analysis on variants which maximize the improvements obtained with regards to the reference model, track design variants were classified based on global track stiffness. Subsequently, the Pareto front of the members of each track stiffness class was determined for each train circulation speed. For each lower bound adopted for the global track stiffness, the Pareto fronts associated with each circulation speed were used to select a single variant that performed well throughout all circulation speeds. The variants selected based on this selection process are listed in Table 17.

TABLE 17 SELECTED TRACK DESIGN VARIANTS.

	Variant description	
Global track stiffness	Kpad [kN/mm]	Kusp [kN/mm]
> 50 kN/mm	40	60
> 60 kN/mm	40	80
> 70 kN/mm	60	80
> 80 kN/mm	80	100

Having these results and ideal global track stiffness in mind, the responses outputted by the track variants were grouped by ranges of global track stiffness values ranging from 50kN/mm to 90kN/mm.

In Figure 34, the peak response values outputted by the reference model and the model variants described in Section 6 when subjected to the passage of a train circulating at 300km/h are shown. The response values produced by the model variants are grouped by the corresponding global track stiffness values. Track designs which output lower values of both vertical ballast displacements and vertical ballast acceleration are represented by points in the output space closer to the graph's origin. The peak response values obtained for all train circulation speeds considered in the parametric study are available in (IST - R. Maciel, P. Ferreira, 2016).

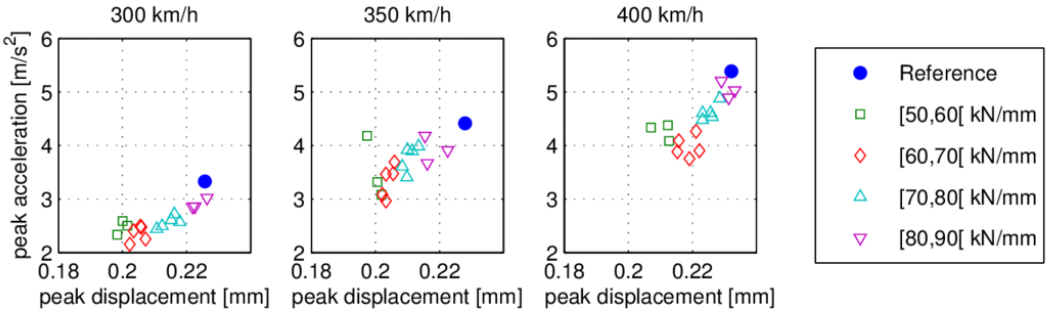

FIGURE 34 PEAK RESPONSE VALUES BY TRACK STIFFNESS.

The results presented in Figure 34 indicate that every variant analysed in the parametric study improves the responses within the ballast layer when compared with the results produced by the reference track model, either objectively (the response of the model variant dominates the response of the reference model) or subjectively (improves one indicator but worsens another). These results suggest that, for the track design variants analysed in this study, the introduction of USPs leads to significant improvements in the dynamic response of the track supporting layers, independently on the properties of the USPs.

Therefore it was decided to adopt and proceed with the following design parameters for the global track design optimization process, summarized in Table 18.

TABLE 18 TRACK DESIGN OPTIMIZATION PROCESS: PARAMETER LEVELS.

Parameter	Levels
Rail pad stiffness k_{pad} [kN/mm]	40, 60, 80, 100
USP stiffness k_{usp} [kN/mm]	40, 60, 80, 100
Train speed v [km/h]	300, 320, 330, 350, 360, 380, 400

The computational workload required by each train/track interaction simulation enabled the adoption of a full factorial design for the parametric experience. Consequently, the parametric study consisted of simulating the reference model and corresponding 16 variants subjected to the passage of a train travelling at 7 different speed levels, thus comprising the computation of a total of 112 train/track numerical simulations.

Having as global concern the long term degradation of the track (mostly related to track degradation mechanisms which take place on the ballast layer) and the global focus on the short and long-term behaviour of the track supporting layers, the quantities of interest considered in this parametric study were peak vertical displacements and accelerations observed within the ballast layer.

7.1 RESULTS AND DISCUSSION ON SELECTED TRACKS DESIGN SOLUTIONS

In this subchapter most interesting results and comparisons of track design optimization are shown for the track design solutions selected as representative to be further analysed and to support CEDEX on the forthcoming experimental tests, which are: M(40,60), M(40,80), M(60,80) and M(40,60).

To illustrate the differences in responses among the selected track solutions, peak response values outputted by each selected variant are shown in Figure 35.

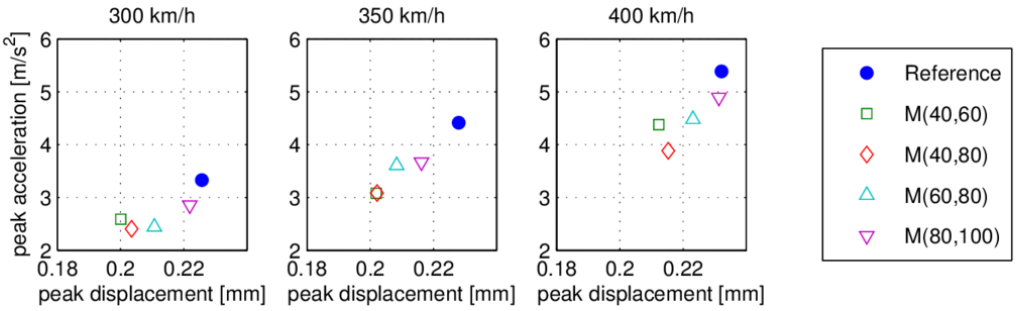

FIGURE 35 PEAK BALLAST RESPONSE VALUES OF THE SELECTED VARIANTS.

Both vertical maximum accelerations and displacements on top of the ballast layer outputted by the selected track variants are, expectedly, lower than those produced by the CTB reference track case. To illustrate the differences, a comparison of the vertical displacements time signals induced by a bogie circulating at 300km/h is shown in Figure 36.

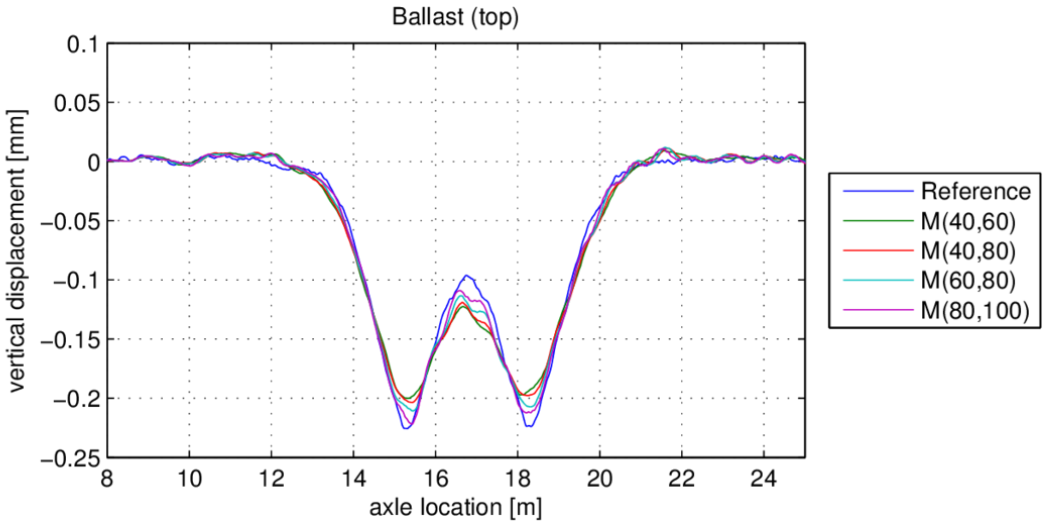

FIGURE 36 COMPARISONS OF VERTICAL BALLAST DISPLACEMENT TIME SERIES: 300KM/H.

The reduction in peak vertical displacements is an expected consequence of adding a flexible layer below the sleepers. Lowering the foundation medium's stiffness of each sleeper results in a redistribution of the train loads to adjacent sleeper. This redistribution results in lower stress concentrations observed on the top of the ballast layer. In lower depths within the track substructure, peak displacements exhibit equivalent levels, as can be noted in the vertical subballast displacement time series shown in Figure 37.

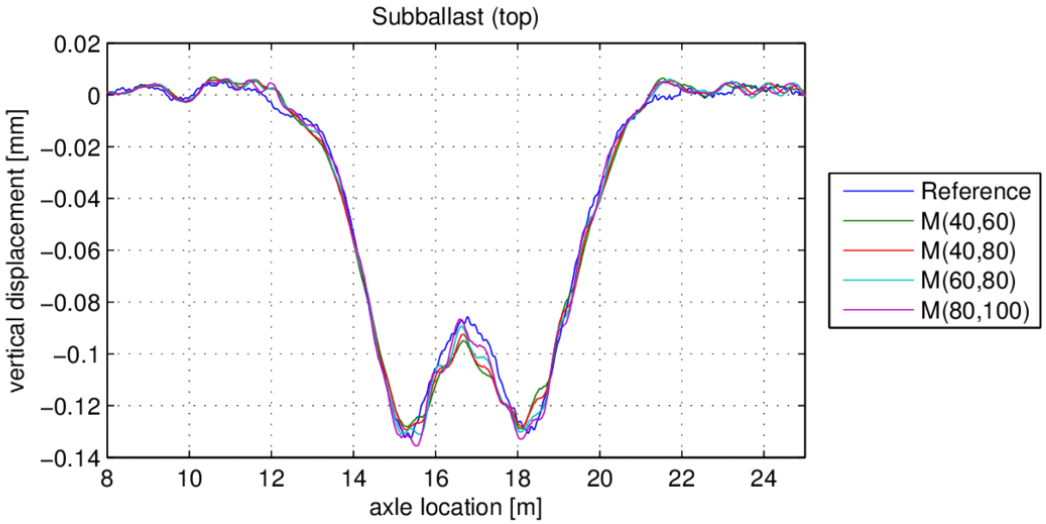

FIGURE 37 COMPARISONS OF VERTICAL SUBBALLAST DISPLACEMENT TIME SERIES: 300KM/H.

Results show that peak vertical displacement values near the ballast structure obtained from the variants are lower than the peak values outputted by the reference model. In general, this difference increases with the train circulation speed, but decreases with depth as peak displacements converge to a common value. The peak vertical displacement values obtained from simulations of a train circulating at 350km/h are shown in Figure 38.

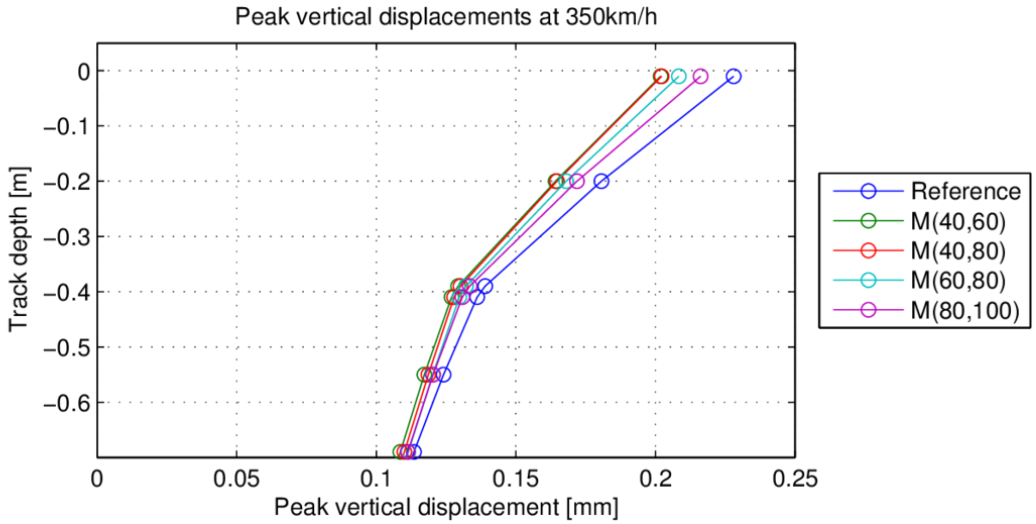

FIGURE 38 COMPARISON OF PEAK VERTICAL DISPLACEMENT VALUES THROUGHOUT THE TRACK'S DEPTH: 350KM/H.

With regards to the track superstructure, the addition of USPs resulted in an expected increase in the vertical displacements observed above the USP element. This result is a natural consequence of adding a resilient element, a track element whose stiffness, when compared with those of the ballast and remaining elements of the track substructure, is much lower. In Figure 39 the corresponding vertical displacements obtained on the rail support may be observed.

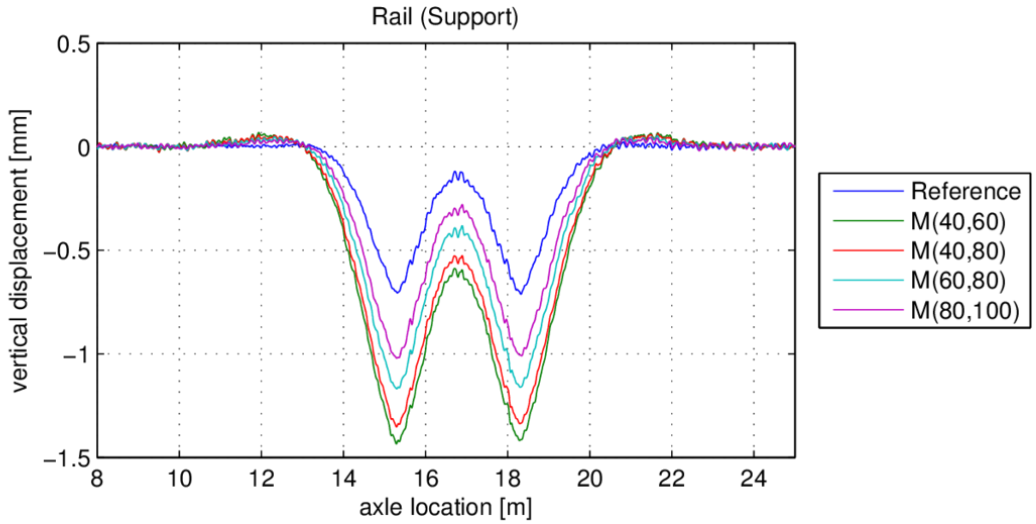

FIGURE 39 COMPARISONS OF VERTICAL RAIL SUPPORT DISPLACEMENTS TIME SERIES: 300KM/H.

The vertical displacements observed on the sleeper also increase greatly when compared with the reference case. This significant increase in vertical displacements is due to the drastic reduction in the stiffness of the medium on which the sleeper is placed. The vertical displacements observed on the sleeper are shown in Figure 40.

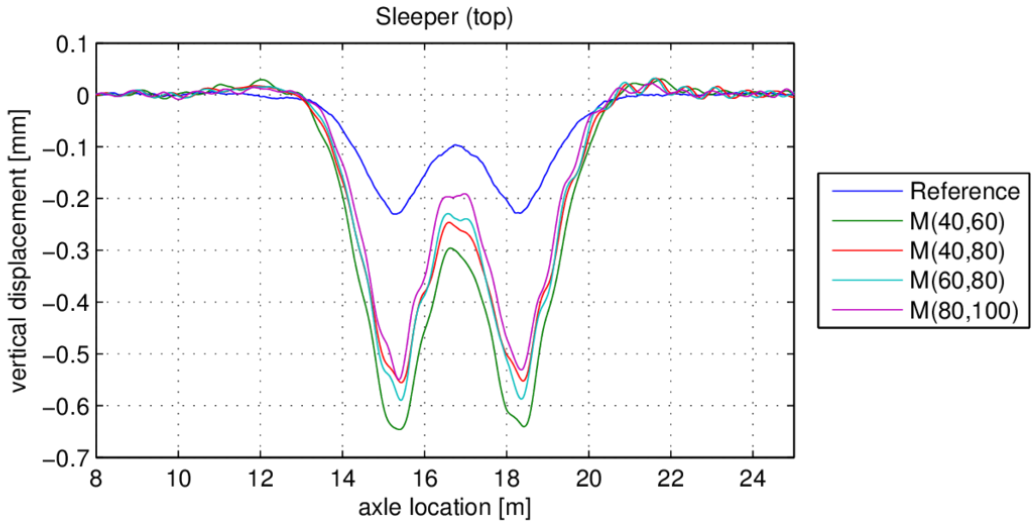

FIGURE 40 COMPARISONS OF VERTICAL SLEEPER DISPLACEMENTS TIME SERIES: 300 KM/H.

The same conclusions can be drawn with regards to peak vertical acceleration values. Responses obtained from the parametric study indicate that all variants lead to lower vertical acceleration levels than the reference model. Also, peak vertical acceleration values outputted by the selected variants remain lower than the results produced by the reference model throughout the substructure depth, and converge to a common with depth. The peak vertical acceleration values obtained from simulations of a train circulating at 350 km/h are shown in Figure 41.

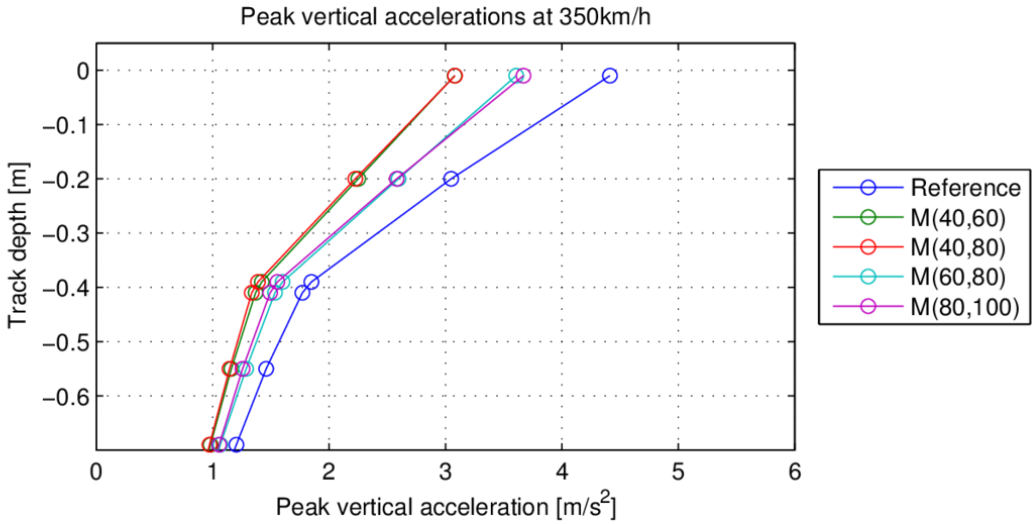

FIGURE 41 COMPARISON OF PEAK VERTICAL ACCELERATION VALUES THROUGHOUT THE TRACK'S DEPTH: 350 KM/H.

As expected, the introduction of USPs resulted in a reduction of the peak acceleration levels observed within the ballast and subballast layer. This effect is linked with the combined effect of adding a damping element to the track system, the reduction in concentration of the dynamic load applied to the track by the passing train, and the reduction of vibrations transferred from the superstructure to the substructure. The vertical acceleration time series taken from the top of the ballast layer are represented in Figure 42.

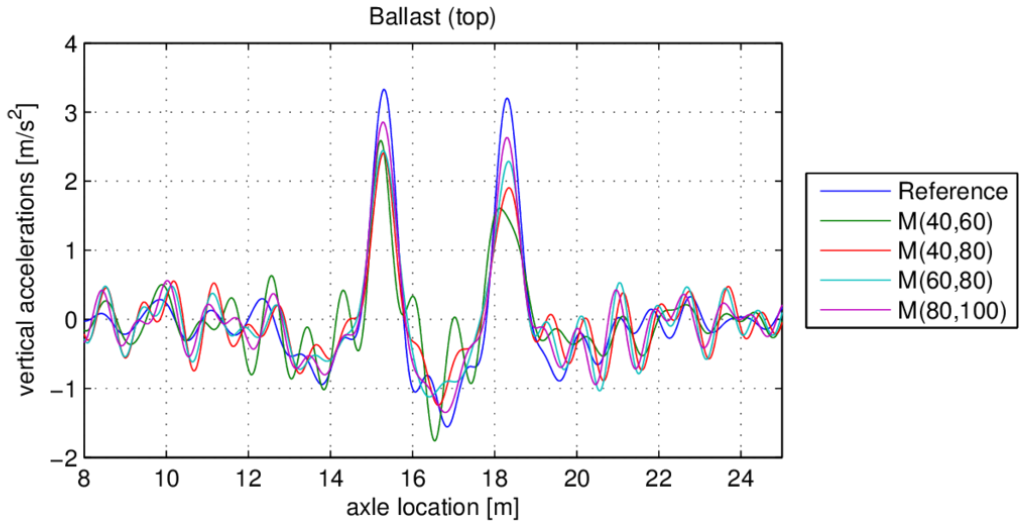

FIGURE 42 COMPARISONS OF VERTICAL BALLAST ACCELERATION TIME SERIES: 300 KM/H.

On the other hand however, the introduction of USPs has also lead to a significant increase in the vertical acceleration levels outputted by the numerical model on track components supported by USPs. The vertical acceleration time series observed on the rail support and on the top of the sleeper are shown, respectively, in Figure 43 and Figure 44.

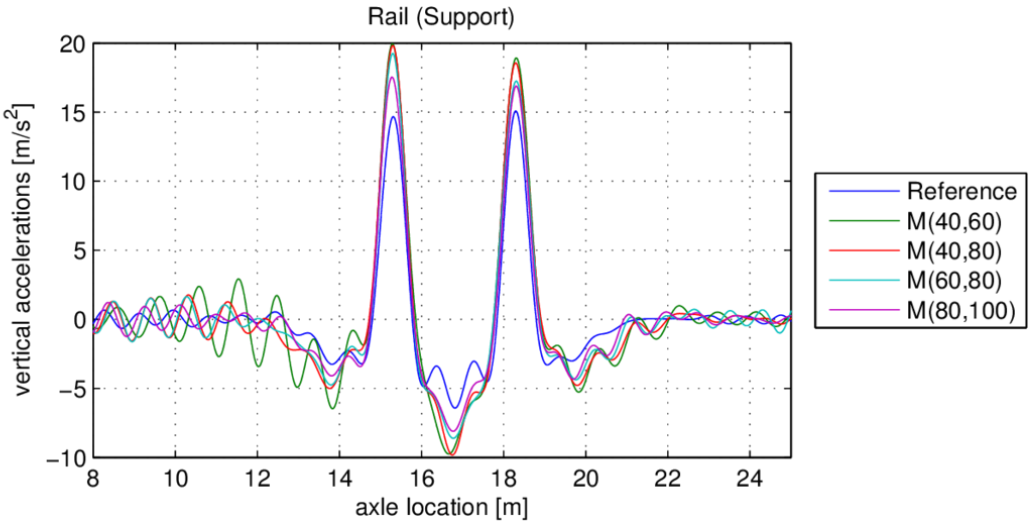

FIGURE 43 COMPARISONS OF VERTICAL RAIL SUPPORT ACCELERATION TIME SERIES: 300 KM/H.

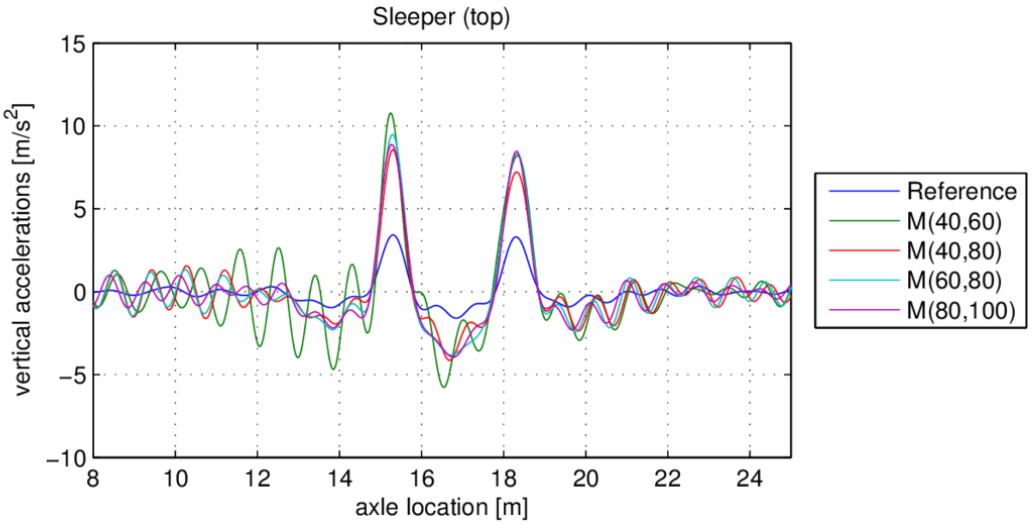

FIGURE 44 COMPARISONS OF VERTICAL SLEEPER ACCELERATION TIME SERIES: 300 KM/H.

As can be seen in the previous figures, the increase in peak vertical acceleration levels observed on the rail support is mild while on top of the sleepers the peak acceleration levels show a prominent increase. This is mainly due to the sleeper acting as a concentrated mass lodged between flexible supports (the rail pad above and the USP below). This pattern is common to all circulation speeds analysed in the parametric numerical study.

7.2 INFLUENCE OF TRAIN SPEED INCREASE

Once more the impact of increasing train speed was particularly studied and analysed. As expected, train speed has a significant influence on the response of all railway track variants. Peak vertical accelerations observed on top of the ballast layer with regards to train speed are shown in Figure 45. Peak vertical accelerations observed on sleepers with regards to train speed are shown Figure 46.

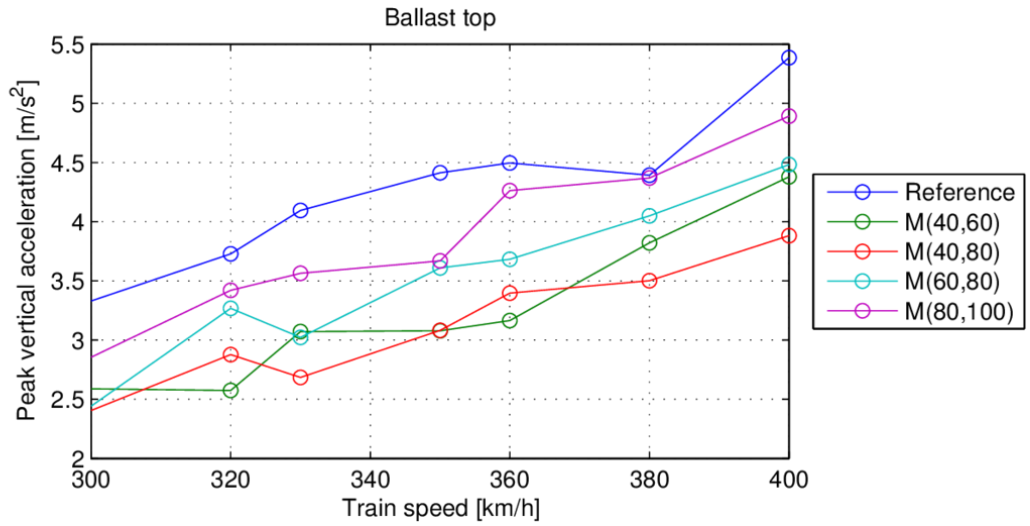

FIGURE 45 COMPARISONS OF PEAK VERTICAL BALLAST ACCELERATION VALUES WITH REGARD TO TRAIN SPEED.

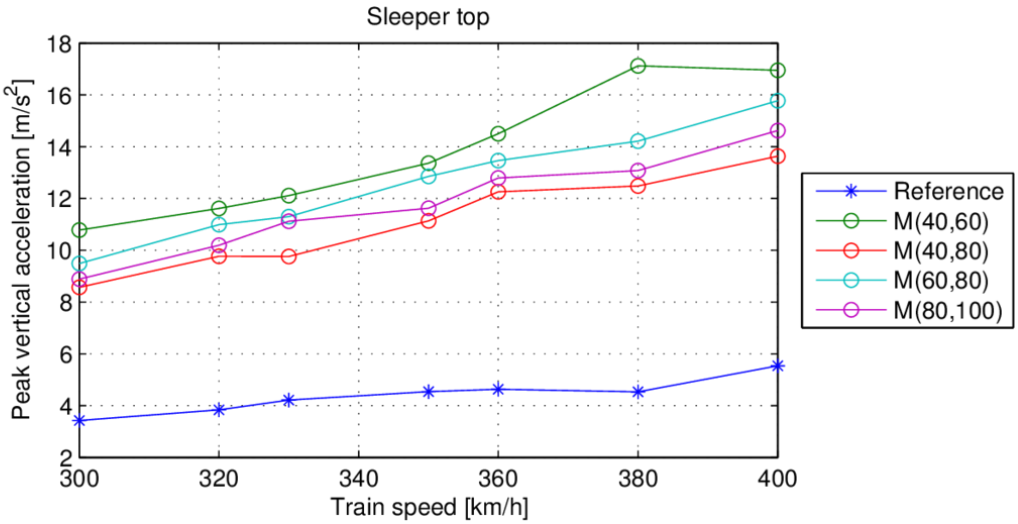

FIGURE 46 COMPARISONS OF PEAK VERTICAL SLEEPER ACCELERATION VALUES WITH REGARD TO TRAIN SPEED.

This result agrees with observations based on experimental measurements that indicate that increases in circulation speeds lead to higher vibration levels. The results also suggest a correlation between peak vertical accelerations and global track stiffness. A notable exception was found in the two variants with a lower global track stiffness, variant M(40,60) and variant M(40,80), where increasing the stiffness of the USPs from 60 to 80 kN/mm resulted in a reduction in peak vertical acceleration levels for some train running speeds.

Although the introduction of USPs resulted in lower peak vertical accelerations and displacements within the track substructure, it also resulted in higher sleeper and rail vibration levels. This trade-off between peak ballast and sleeper accelerations agrees with findings of other authors on the influence of USPs on the dynamic response of railway tracks, based on full-scale field tests (Schneider, et al., 2011) as well as computational experiments (Johansson, et al., 2008).

It must be also added that there are certain simplifying hypothesis in the numerical model which make it to not able to consider the following positive effects (most possibly) provided by the USPs: increase in the interface and load-distributing area between sleepers and ballast; embedding effect of the ballast stones by the USP elastic layer.

Another way to present results is shown in Figure 47 where to illustrate the improvements gained with the selected track design solutions, is presented a comparison of peak ballast acceleration values in terms of relative reduction (%) comparing to CTB track case.

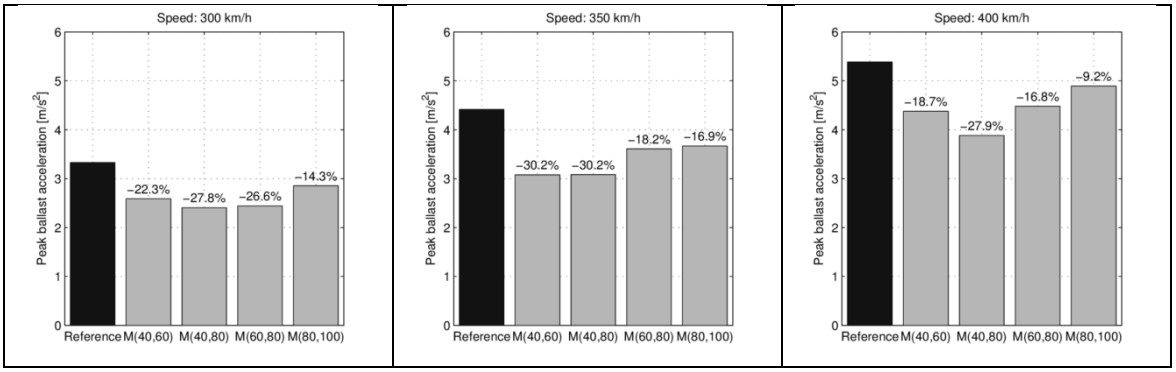

FIGURE 47 RELATIVE REDUCTIONS IN PEAK BALLAST ACCELERATIONS WITH REGARDS TO THE REFERENCE MODEL.

Among the selected track design variants, the M(40,80) variant stood out as the most promising track design, leading to reductions in peak ballast acceleration values of around 30% of the reference track design throughout all train speeds. These results suggest that potential improvements in track degradation rates may be achievable at the expense of trade-offs in other design requirements linked with the vibration of the track superstructure, such as rail degradation rates and sleeper fatigue (Schneider, et al., 2011)(Ferreira, et al., 2015).

8 Remarks on results

This report presented the work performed by IST within C4R SP1 in subtask 1.2.2.1 - "Track design for VHST". The work made by IST was mainly related to the numerical simulations part, that is, the development, validation and application of a numerical train/track FE model focused on estimations of track response to very high speed trains circulations.

The inter-collaboration with CEDEX partner, which dealt with laboratory experimental tests (see Appendix 8.1), was mandatory and crucial to have a reference track to serve as basis for both model validation and predictions to support decisions of which track design alternatives should be experimentally tested in the CTB.

Mainly the work was divided into the following parts:

- Numerical model validation based on the data provided by CEDEX from the tests conducted on the physical model of a ballasted track with granular subballast, CTB reference case (see chapter 3 and Appendix 8.1);

- Evaluation of the predicted dynamic response of the reference railway track (CTB reference case) and the influence of train speed increase up until 400 km/h on its dynamic behaviour;

- Evaluation of the predicted dynamic response of different track design cases (having the CTB reference case as basis) when equipped with different combinations of railpads and undersleeper pads (USPs); evaluation of train speed increase;

- Optimization of track design (several specific combinations of railpad+usp stiffness) to improve dynamic performance at very high speeds (up to 400 km/h).

The work reached to a track optimization procedure developed within the Capacity4Rail employed to select combinations of rail pads and USPs which improve the dynamic response of a reference high-speed railway track (subjected to train speeds ranging from 300km/h to 400 km/h). To do so, this report covered a series of parametric studies conducted to evaluate the differences in the dynamic response of a railway track incorporating different combinations of rail pads and USPs. The parametric study consisted in evaluating the response of several variants of the reference track case, each characterized by the combination of rail pads and USPs. The response of each variant was obtained when subjecting the track to the passage of a high-speed train circulating at different speed levels. The possible improvements (as vibrations attenuations) obtained from each case of the parametric studies tested were compared with those produced by a CTB reference track model (conventional ballasted track), based on a 1:1 physical model of a railway track analysed by CEDEX, previously used in the model validation (IST - R. Maciel, P. Ferreira, 2015).

Based on the numerical results of the parametric experience, it was possible to arrive to the following conclusions:

The introduction of USPs results in a significant reduction in peak vertical displacement and acceleration levels within the track supporting layers, ballast layer included. These peak response values (for the track design solutions tested) were found to be lower than the peak values outputted by the reference track case. However, it must be highlighted that these improvements in the response within the track supporting layers are accompanied by increases in peak vertical displacement and acceleration levels on track components supported by the USPs, as the rails and the sleepers. Nevertheless, the results also suggest that incorporating stiffer USPs may reduce peak acceleration levels within the ballast layer while preserving peak sleeper acceleration levels.

It should be stressed that, due to the limited availability of in-situ measurements of railway tracks equipped with USPs, the numerical model wasn't yet subjected to a validation process that covers this particular track solution. Therefore, results should be interpreted with care.

Also, in the interpretation and critical analysis of the results attention must be paid to the following:

- The numerical model is not able to consider the following positive effects (most possibly) provided by the USPs:
  - Increase in the interface and load-distributing area between sleepers and ballast;
  - embedding effect of the ballast stones by the USP elastic layer;
- Any results obtained for trains speeds of 400km/h must be taken with care as no validation with real measurements was made at these speeds;
- Post-processing of time signals, as filtering, was made and so, the conclusions withdrawn are made relatively to the frequency range used and they are linked to it.
- The numerical results here analysed are provided exclusively from short term computations, that is, only track instantaneous responses are obtained, so, conclusions cannot be directly extrapolated to track long-term performance nor within a life cycle analysis perspective.
- Computations to simulate cyclical effects as repeated train passages to produce track settlement and long term deterioration would have to be done.

USPs must be carefully selected taking into account the changes introduced in the dynamic response of the railway track. In fact, the process of designing high-speed track solutions which incorporate USPs needs to take into account the trade-off between ballast, sleeper and rail vibration levels, and resulting degradation processes.

References

Abadi, T., Le Pen, L., Zervos, A., and Powrie, W. (2016). A Review and Evaluation of Ballast Settlement Models using Results from the Southampton Railway Testing Facility (SRTF). *Procedia Engineering, 143*, 999-1006. doi:10.1016/j.proeng.2016.06.089

Abdelkrim, M., Bonnet, G., an de Buhan, P. (2003). A computational procedure for predicting the long term residual settlement of a platform induced by repeated traffic loading. *Computers and Geotechnics, 30*, 463-476. doi:10.1016/S0266-352X(03)00010-7

Adif. (2005). *Placas elásticas de asiento para sujeción VM.* Especificación técnica, Adif.

Adif. (2014). *Traviesas monobloque de hormigón prensado, 5ª Edición.* Especificación técnica, Adif.

Aikawa, A. (2015). Dynamic characterisation of a ballast layer subject to traffic impact loads using three-dimensional sensing stones and a special sensing sleeper. *Construction and Building Materials, 92*, 23-30.

Aikawa, A. (2015). Research on Vertical Natural Vibration Characteristics of Gravel Aggregate in Ballasted Track. *Quarterly Report of RTRI, 56*, 26-32. doi:10.2219/rtriqr.56.26

Al-Shaer, A., Duhamel, D., Sab, K., Nguyen, V. H., Foret, G., Merliot, E., and Schmitt, L. (2005). Dynamic design of a reduced-scale railway test bench using the CESAR-LCPC computation code. *Bulletin des laboratoires des ponts et chaussées*, 227-242.

Barke, D. W., and Chiu, W. K. (2005). A Review of the Effects of Out-Of-Round Wheels on Track and Vehicle Components. *Proceedings of the Institution of Mechanical Engineers, Part F: Journal of Rail and Rapid Transit, 219*, 151-175. doi:10.1243/095440905X8853

Bian, X., Jiang, H., and Chen, Y. (2016). Preliminary Testing on High-speed Railway Substructure Due to Water Level Changes. *Procedia Engineering, 143*, 769-781. doi:10.1016/j.proeng.2016.06.124

Bodin, V. (2001). *Comportement du ballast des voies ferrées soumises à un chargement vertical et latéral.* Paris: Ecole Nationale des Ponts et Chaussées.

Carrascal, I. A., Casado, J. A., Polanco, J. A., and Gutiérrez-Solana, F. (2007). Dynamic behaviour of railway fastening setting pads. *Engineering Failure Analysis, 14*, 364-373. doi:10.1016/j.engfailanal.2006.02.003

CEDEX. (2015). *Short and long term results obtained in the testing of high speed (300 kph) ballasted track with granular subbalast and ballasted track with bituminous subballast.* Technical report, CEDEX.

Corrêa, L., Quezada, J., Cottereau, R., d'Aguiar, S., and Voivret, C. (2017). Randomly-fluctuating heterogeneous continuum model of a ballasted railway track. *Computational Mechanics*, 1-17. doi:10.1007/s00466-017-1446-8

Dahlberg, T. (2001). Some railroad settlement models-A critical review. *Proceedings of the Institution of Mechanical Engineers, Part F: Journal of Rail and Rapid Transit, 215*, 289-300. doi:10.1243/0954409011531585

Dahlberg, T. (2004). *Railway track settlements - a literature review.* Linkoping University, Linkoping.

Fenander, Å. (1997). Frequency dependent stiffness and damping of railpads. *Proceedings of the Institution of Mechanical Engineers, Part F: Journal of Rail and Rapid Transit, 211*, 51-62. doi:10.1243/0954409971530897

Ferreira, L., and Murray, M. H. (1997). Modelling rail track deterioration and maintenance: current practices and future needs. *Transport Reviews, 17*, 207-221. doi:10.1080/01441649708716982

Ferreira, P. A. (2010). *Modelling and prediction of the dyamic behaviour of railway infrastructures at very high speeds.* PhD thesis, Instituto Superior Técnico, Lisbon.

Ferreira, P. A., and López-Pita, A. (2015). Numerical modelling of high speed train/track system for the reduction of vibration levels and maintenance needs of railway tracks. *Construction and Building Materials, 79*, 14-21. doi:10.1016/j.conbuildmat.2014.12.124

Guérin, N. (1996). *Approche Expérimentale et Numérique du Comportement du Ballsat des Voies de Chemins de Fer.* Paris: Ecole Nationale des Ponts ets Chaussées.

Guérin, N., Sab, K., and Moucheront, P. (1999). Identification expérimentale d'une loi de tassement du ballast. *Canadian Geotechnical Journal*, 523--532.

Indraratna, B., Lackenby, J., and Christie, D. (2005). Effect of confining pressure on the degradation of ballast under cyclic loading. *Faculty of Engineering - Papers (Archive)*. doi:10.1680/geot.55.4.325.65490

Ishikawa, T., Miura, S., and Sekine, E. (2014). Simple plastic deformation analysis of ballasted track under repeated moving-wheel loads by cumulative damage model. *Transportation Geotechnics, 1*, 157-170. doi:10.1016/j.trgeo.2014.06.006

Johansson, A., Nielsen, J. C., Bolmsvik, R., Karlström, A., and Lundéna, R. (2008). Under sleeper pads—Influence on dynamic train–track interaction. *Wear*, 1479-1487.

Johansson, A., Nielsen, J., Bolmsvik, R., and Karlstrom, A. (2008). Under sleeper pads—Influence on dynamic train–track interaction. *Wear*, 1479–1487.

Kaewunruen, S., and Remennikov, A. (2015). Under sleeper pads: field investigation of their role in detrimental impact mitigation. *Faculty of Engineering and Information Sciences - Papers: Part A*, 1-17. Obtido de http://ro.uow.edu.au/eispapers/5264

Kang, G. (2016). Influence and Control Strategy for Local Settlement for High-Speed Railway Infrastructure. *Engineering, 2*, 374-379. doi:10.1016/J.ENG.2016.03.014

Koroma, S. G., Hussein, M. F., and Owen, J. S. (2015). Influence of Preload and Nonlinearity of Railpads on Vibration of Railway Tracks under Stationary and Moving Harmonic Loads. *Journal of Low Frequency Noise, Vibration and Active Control, 34*, 289-306. doi:10.1260/0263-0923.34.3.289

Li, D., and Selig, E. T. (1998). Method for Railroad Track Foundation Design. I: Development. *Journal of Geotechnical and Geoenvironmental Engineering, 124*, 316-322. doi:10.1061/(ASCE)1090-0241(1998)124:4(316)

Li, D., and Selig, E. T. (1998). Method for Railroad Track Foundation Design. II: Applications. *Journal of Geotechnical and Geoenvironmental Engineering, 124*, 323-329. doi:10.1061/(ASCE)1090-0241(1998)124:4(323)

Lobo-Guerrero, S., and Vallejo, L. (2006). Discrete element method analysis of railtrack ballast degradation during cyclic loading. *Granular Matter, 8*, 195-204. doi:10.1007/s10035-006-0006-2

Lombard, P. C. (1978). Track structure - optimization of design. *Civil Engineering = Siviele Ingenieurswese, 1978*, 231-238.

López-Pita, A., Teixeira, P. F., and Robuste, F. (2004). High speed and track deterioration: The role of vertical stiffness of the track. *Proceedings of the Institution of Mechanical Engineers, Part F: Journal of Rail and Rapid Transit*, 31--40.

Maciel, R., and Ferreira, P. (2016). Optimization algorithm applied to VHS track design towards enhanced track dynamic performance and reduced settlement. *11th World Congress on Railway Research (WCRR 2016).* Milan.

Moreno-Robles, J. (2008). *Reproducción, mediante ensayos a escala real, del efecto en la vía de la circulación ferroviaria a alta velocidad.* PhD Thesis, Universidad Politécnica de Madrid, Madrid.

Moreno-Robles, J., Crespo-Chacón, I., and Garcia-de-la-Oliva, J. (2016). Instrumentation Techniques for Studying the. *Procedia Engineering*, 870-879.

Naudé, F. P., Fröhling, R. D., and Theron, N. J. (2005). Development of a Methodology to Calculate Stresses in Track Components. *Proceedings of the Institution of Mechanical Engineers, Part F: Journal of Rail and Rapid Transit, 219*, 213-224. doi:10.1243/095440905X8925

Nguyen, K., Villalmanzo, D. I., Goicolea, J. M., and Gabaldon, F. (2015). A computational procedure for prediction of ballasted track profile degradation under railway traffic loading. *Proceedings of the Institution of Mechanical Engineers, Part F: Journal of Rail and Rapid Transit, 230*(8), 1812-1827. doi:10.1177/0954409715615374

Nimbalkar, S., Tennakoon, N., and Indraratna, B. (2015). Effects of fouling and degradation on geotechnical behaviour of railway ballast. *Faculty of Engineering and Information Sciences - Papers: Part A*, 1-10. Obtido de http://ro.uow.edu.au/eispapers/4971

Oregui, M., Man, A. d., Woldekidan, M. F., Li, Z., and Dollevoet, R. (2016). Obtaining railpad properties via dynamic mechanical analysis. *Journal of Sound and Vibration, 363*, 460-472. doi:10.1016/j.jsv.2015.11.009

Oyarzabal, O., Gómez, J., Santamaría, J., and Vadillo, E. G. (2009). Dynamic optimization of track components to minimize rail corrugation. *Journal of Sound and Vibration, 319*, 904-917. doi:10.1016/j.jsv.2008.06.020

Profillidis, V. A. (1986). Applications of finite element analysis in the rational design of track bed structures. *Computers and Structures, 22*, 439-443. doi:10.1016/0045-7949(86)90049-0

Real, J. I., Gómez, L., Montalbán, L., and Real, T. (2012). Study of the influence of geometrical and mechanical parameters on ballasted railway tracks design. *Journal of Mechanical Science and Technology, 26*, 2837-2844. doi:10.1007/s12206-012-0734-7

Remennikov, A., Kaewunruen, S., and Ikaunieks, K. (2006). Deterioration of dynamic rail pad characteristics. *Faculty of Engineering - Papers (Archive)*. Obtido de http://ro.uow.edu.au/engpapers/320

Sadeghi, J., and Barati, P. (2010). Evaluation of conventional methods in analysis and design of railway track system. *International Journal of Civil Engineering, 8*(1), 44-56.

Salim, M. R., Bakar, A. A., and Shariff, A. A. (2012). Investigation on Simulation of Train Loading on Prestressed Concrete Sleepers. *Applied Mechanics and Materials, 157-158*, 666-670. doi:10.4028/www.scientific.net/AMM.157-158.666

Saltelli, A., and Annoni, P. (2010). How to avoid a perfunctory sensitivity analysis. *Environmental Modelling and Software, 25*(12).

Schilder, R. (2013). USP (Under Sleeper Pads): a contribution to save money in track maintenance. *AusRAIL PLUS 2013.* Canberra, Australia.

Schmitt, L., Létourneaux, F., De Keyzera, I., and Crompton, P. (2014). CAPACITY4RAIL: toward a resilient, innovative and high capacity European railway system for 2030/2050. *Transport Research Arena (TRA) 5th Conference: Transport Solutions from Research to Deployment.* Paris.

Schneider, P., Bolmsvik, R., and Nielsen, J. C. (2011). In situ performance of a ballasted railway track with under sleeper pads. *Proceedings of the Institution of Mechanical Engineers, Part F: Journal of Rail and Rapid Transit*, 299-309.

Shahu, J. T., Yudhbir, and Kameswararao, N. S. (2000). A Rational Method for Design of Railroad Track Foundation. *Soils and Foundations, 40*, 1-10. doi:10.3208/sandf.40.6_1

Soleimanmeigouni, I., Ahmadi, A., and Kumar, U. (2016). Track geometry degradation and maintenance modelling: A review. *Proceedings of the Institution of Mechanical Engineers, Part F: Journal of Rail and Rapid Transit*. doi:10.1177/0954409716657849

Sol-Sánchez, M., Moreno-Navarro, F., and Rubio-Gámez, M. C. (2015). The use of elastic elements in railway tracks: A state of the art review. *Construction and Building Materials, 75*, 293-305. doi:10.1016/j.conbuildmat.2014.11.027

Sol-Sánchez, M., Pirozzolo, L., Moreno-Navarro, F., and Rubio-Gámez, M. C. (2016). A study into the mechanical performance of different configurations for the railway track section: A laboratory approach. *Engineering Structures, 119*, 13-23. doi:10.1016/j.engstruct.2016.04.008

Steenbergen, M. J. (2013). Physics of railroad degradation: The role of a varying dynamic stiffness. *Computers and Structures*, 102-111.

Suiker, A. S., Chang, C. S., de Borst, R., and Esveld, C. (1999). Surface waves in a stratified half space with enhanced continuum properties. Part 1: Formulation of the boundary value problem. *European Journal of Mechanics - A/Solids, 18*, 749-768. doi:10.1016/S0997-7538(99)00108-4

Suiker, A., and de Borst, R. (2003). A numerical model for the cyclic deterioration of railway tracks. *International Journal for Numerical Methods in Engineering, 57*, 441-470. doi:10.1002/nme.683

Sun, Q., Indraratna, B., and Nimbalkar, S. (2015). Deformation and Degradation Mechanisms of Railway Ballast under High Frequency Cyclic Loading. *Journal of Geotechnical and Geoenvironmental Engineering, 142*, 04015056. doi:10.1061/(ASCE)GT.1943-5606.0001375

Sun, Y., Indraratna, B., Carter, J. P., Marchant, T., and Nimbalkar, S. (2017). Application of fractional calculus in modelling ballast deformation under cyclic loading. *Computers and Geotechnics, 82*, 16-30. doi:10.1016/j.compgeo.2016.09.010

Taherinezhad, J., Sofi, M., Mendis, P. A., and Ngo, T. (2013). A Review of Behaviour of Prestressed Concrete Sleepers. *Electronic Journal of Structural Engineering, 13*, 1-16.

Técnico, Universidade de Lisboa. (2015). *Capacity4Rail: Task 1.2.2 New track design and specifications for VHST. Sub-Task 1.2.2.1 Track design for VHST Numerical simulations to study Track Box responses to the increase of train running speed.* Internal report.

Técnico, Universidade de Lisboa. (2015). *Capacity4Rail: Task 1.2.2 New track design and specifications for VHST. Sub-Task 1.2.2.1 Track design for VHST Preliminary draft report - Numerical modelling and validation of short term results at 300km/h.* Internal report.

Técnico, Universidade de Lisboa. (2016). *Capacity4Rail: Task 1.2.2 New track design and specifications for VHST. Sub-Task 1.2.2.1 Track design for VHST Track design solution for soft rail pads and under sleeper pads. Parametric study on train speed increase.* Internal report.

Trinh, V. N., Tang, A. M., Cui, Y.-J., Dupla, J.-C., Canou, J., Calon, N., . . . Schoen, O. (2012). Mechanical characterisation of the fouled ballast in ancient railway track substructure by large-scale triaxial tests. *Soils and Foundations, 52*, 511-523. doi:10.1016/j.sandf.2012.05.009

Vincent, N., Bouvet, P., Thompson, D. J., and Gautier, P. E. (1996). Theoretical optimization of track components to reduce rolling noise. *Journal of Sound and Vibration, 193*, 161-171. doi:10.1006/jsvi.1996.0255

Wei, K., Liu, Z., Liang, Y., and Wang, P. (2017). An investigation into the effect of temperature-dependent stiffness of rail pads on vehicle-track coupled vibrations. *Proceedings of the Institution of Mechanical Engineers, Part F: Journal of Rail and Rapid Transit, 231*, 444-454. doi:10.1177/0954409716631786

Wei, K., Zhang, P., Wang, P., Xiao, J., and Luo, Z. (2016). The Influence of Amplitude- and Frequency-Dependent Stiffness of Rail Pads on the Random Vibration of a Vehicle-Track Coupled System. *Shock and Vibration*.

Zhu, S., Cai, C., and Spanos, P. D. (2015). A nonlinear and fractional derivative viscoelastic model for rail pads in the dynamic analysis of coupled vehicle–slab track systems. *Journal of Sound and Vibration, 335*, 304-320. doi:10.1016/j.jsv.2014.09.034